PIERS 2012 Kuala Lumpur

Progress In Electromagnetics Research Symposium

Abstracts

March 27–30, 2012
Kuala Lumpur, MALAYSIA

www.emacademy.org
www.piers.org

PIERS 2012 Kuala Lumpur Abstracts

Published by

The Electromagnetics Academy
777 Concord Avenue, Suite 207
Cambridge, MA 02138

www.emacademy.org
www.piers.org

ISSN: 1559-9450
ISBN: 978-1-934142-19-6

Progress In Electromagnetics Research Symposium

March 27–30, 2012

Kuala Lumpur, MALAYSIA

PIERS 2012 KUALA LUMPUR ORGANIZATION

PIERS Founding Chair

J. A. Kong, MIT, USA

PIERS Chair

L. Tsang, University of Washington, USA

PIERS 2012 Kuala Lumpur General Chair

H. T. Chuah, Universiti Tunku Abdul Rahman, Kuala Lumpur, Malaysia

PIERS 2012 Kuala Lumpur General Vice Chair

K. S. Chen, National Central University, Chung-Li, Taiwan

H. T. Ewe, Universiti Tunku Abdul Rahman, Kuala Lumpur, Malaysia

PIERS 2012 Kuala Lumpur Organization Committee Chair

F. A. Rahman, Universiti Tunku Abdul Rahman, Kuala Lumpur, Malaysia

PIERS 2012 Kuala Lumpur International Advisory Committee

S. Barmada
W. C. Chew
A. K. Fung
M. Hallikainen
E. Jakeman
I. V. Lindell
G. D. McNeal
A. C. Priou
M. Tateiba
K. Yasumoto
L. C. Botten
C.-K. Chou
Z.-H. Gu
Y. Hara
K. Kobayashi
S. Liu
K. K. Mei
K. D. Senne
P. M. van den Berg
W.-X. Zhang
C. H. Chan
S.-T. Chun
L. Gurel
H.-C. Huang
A. Komiyama
K. M. Luk
Y. Miyazaki
R. T.-K. Shin
D. Watts
D.-C. Chang
N. Engheta
T. M. Habashy
A. Ishimaru
L.-W. Li
S. Mano
P. Pampaloni
E. C. Slob
T. Yamasaki

PIERS 2012 Kuala Lumpur Technical Program Committee

S. J. Anderson
Z. Awang
A. Baghai-Wadji
G. Berginc
W.-M. Boerner
H. Braunisch
C. T. Chan
H.-W. Chang
H. S. Chen
P. K. Choudhury
B.-K. Chung
T. J. Cui
V. L. Druskin
Y. Du
A. Z. Elsherbeni
Y. J. Feng
H. Fernandes
J. C. Goswami
S. L. He
W. Hong
K. Iwatsuki
Y.-Q. Jin
J. Johnson
V. C. Koo
R. Kubacki
M. K. Li
Q. H. Liu
S. Lucyszyn
J. T. Lue
A. Massa
E. L. Miller
M. Moghaddam
Z.-P. Nie
Y. Okuno
D. Omeragic
M. Oristaglio
K. Ouchi
J. P. Pribetich
M. K. A. Rahim
T. A. Rahman
R. Ramer
L.-X. Ran
C. M. Rappaport
A. K. Sarychev
C. Seo
X.-Q. Sheng
Y. V. Shestopalov
J.-C. Shi
A. Sihvola
J. C. Souyris
M. S. Tong
R. Talhi
E. L. Tan
S. Y. Tan
S. Tjuatja
D. P. Tsai
J. Vrba
H. G. Wang
B.-I. Wu
C.-J. Wu
M. Y. Xia
G. Q. Xie
T.-S. Yeo
M. Zaslavsky
X. M. Zhang
J. Zhou

PIERS 2012 Kuala Lumpur Organizing Committee

A. Abdullah
M. F. Ahmad
B. M. Ali
K. Anuar
F. A. Bakhtiar
Y. K. Chan
Z. K. Chong
B. K. Chung
M. A. G. Ezra
A. S. Ganesan
K. S. Hon
A. A. Kadir
V. C. Koo
C. K. Lee
K. Y. Lee
Y. J. Lee
G. Y. Lim
T. S. Lim
J. Y. Loo
M. Masli
C. H. Ng
Z. M. Razak
M. Roslee
Z. M. Shari
H. T. Tan
S. N. Tan
C. H. Teh
P. C. Teh
H. T. Teng
F. M. Wong
K. H. Yeap
P. C. Yuen

PIERS 2012 KUALA LUMPUR SESSION ORGANIZERS

H. F. Abutarboush
S. J. Anderson
E. Audouard
A. Baghai-Wadji
G. Barbastathis
J. Berakdar
L. Capineri
X. D. Chen
Y. Cheng
S. W. Cheung
C.-K. Chou
U. A. K. Chude-Okonkwo
R. Doebbelin
Y. Du
H. T. Ewe
D. Felbacq
S.-W. Feng
G. Franceschetti
E. Gescheidtová
C. Gomes
B. Guizal
D. Gürsoy
F. K. Hann
S. Hantscher
M. Horibe
H. T. Hui
K. Iwatsuki
G. V. Jandieri
H. Jiang
S. G. Jin
K. Kobayashi
V. C. Koo
S. I. Kudryashov
Y.-C. Lan
D. Lesselier
J. Lettl
J. H. Li
Y. M. Li
X. H. Lu
B. Luk'yanchuk
C. Z. Ma
A. Massa
E. Mazur
A. E. Miroshnichenko
K.-H. Ng
S. X. (Michael) Ng
L. Nowosielski
H. Oraizi
M. Oristaglio
G. Pisano
R. Przesmycki
A. G. Radwan
S. H. S. Salleh
C. K. Seow
A. Shamim
Y. V. Shestopalov
A. K. Sinha
K. Stankovic
T. Takenaka
E. L. Tan
S. Y. Tan
D. P. Tsai
T. Wakabayashi
S. D. Wall
H.-C. Wang
C. G. Windsor
G. Q. Xie
T. Yakabe
T. J. Yang
T.-S. Yeo
N. Yoshikawa
B. L. Zhang
Q. Zhang

PIERS 2012 KUALA LUMPUR MAIN SPONSORS

- ☐ TELEKOM Malaysia — MALAYSIA
- ☐ TELEKOM Malaysia Research and Development — MALAYSIA
- ☐ Motorola Solutions — MALAYSIA

PIERS 2012 KUALA LUMPUR CO-SPONSOR

- ☐ Malaysia Convention and Exhibition Bureau (MyCeb) — MALAYSIA

PIERS 2012 KUALA LUMPUR EXHIBITORS

- ☐ TELEKOM Malaysia — MALAYSIA
- ☐ TELEKOM Malaysia Research and Development — MALAYSIA
- ☐ Motorola Solutions — MALAYSIA
- ☐ Kumpulan Abex Sdn. Bhd. — MALAYSIA
- ☐ Alliant Techsystems (ATK) — USA
- ☐ ATM Solutions (M) Sdn Bhd — MALAYSIA
- ☐ Computer Simulation Technlogy Malaysia Sdn Bhd — MALAYSIA

PIERS 2012 KUALA LUMPUR SUPPORTERS

- ☐ Ministry of Tourism, Malaysia
- ☐ Academy of Sciences Malaysia (ASM)
- ☐ Suruhanjaya Tenaga (Energy Commission), Malaysia
- ☐ The Institution of Engineers, Malaysia (IEM)
- ☐ ASEAN Academy of Engineering and Technology (AAET)
- ☐ ASEAN Federation of Engineering Organizations (AFEO)
- ☐ The Electromagnetics Academy
- ☐ The Electromagnetics Academy at Zhejiang University
- ☐ Multimedia University (MMU)
- ☐ Zhejiang University
- ☐ Universiti Tunku Abdul Rahman (UTAR)

PIERS 2012 SESSIONS

Session 1A1
Systems and Components, Electromagnetic Compatibility 1

Radiation and Temperature Effects on the Harmonic and Intermodulation Performance of Mach-Zehnder Optomodulator

Muhammed Taher Abuelma'atti
King Fahd University of Petroleum and Minerals, Box 203, Dhahran 31261, Saudi Arabia

Abstract— The transfer function of the Mach-Zehnder interferometric modulator shown in Fig. 1 can be modeled by Equation (1).

$$P_{out} = P_{in}(1 + \cos\phi) \tag{1}$$

In Equation (1), P_{in} is the optical input intensity, P_{out} is the output optical intensity, $\phi = \phi_{BIAS} + \phi_{RF}$ where ϕ_{BIAS} is the phase shift caused by the DC bias voltage V_{BIAS} and $\phi_{REF} = \frac{\pi V_{REF}}{V_\pi}$ is the phase shift caused by the modulating RF voltage, V_{REF}, and V_π is the voltage required to change the output light intensity from its maximum value to its minimum value. Equation (1) can be rewritten in the form

$$P_{out} = P_{in}\left(1 + \cos\left(\frac{\pi V_{REF}}{V_\pi} + \phi_{BIAS}\right)\right) \tag{2}$$

Experimental observations reported in the open literature show that ϕ_{BIAS} and V_π are strongly affected by radiation and temperature. Thus, the effect of temperature and radiation on the harmonic and intermodulation performance of the Mach-Zehnder interferometer of Fig. 1 can be investigated by studying the variation of harmonics and intermodulation products with ϕ_{BIAS} and V_π.

This paper presents closed-form expressions for the amplitudes of harmonic and intermodulation products resulting from driving a Mach-Zehnder optomodulator by a multisinusoidal RF voltage. These expressions are functions of the DC bias, ϕ_{BIAS}, and the voltage, V_π. Since ϕ_{BIAS} and V_π are strongly dependent on the radiation intensity and the temperature, these expressions can be used to study the variation of the harmonic and intermodulation performance of Mach-Zehnder optomodulator with irradiation intensity and/or temperature.

The special case of a driving two-tone equal-amplitude RF voltage is considered in detail. The results show that the harmonic and intermodulation perfomamce of the Mach-Zehnder optomodulator are strongly dependent on the parameters ϕ_{BIAS} and V_π and whence on the irradiation intensity and temperature variations. Using the results obtained in this paper, a data base can be established for the variation of the harmonic and intermodulation performance of the Mach-Zehnder optomodulators with the irradiation intensity and/or temperature. This would be interesting for any space applications using Mach-Zehnder optomodulators.

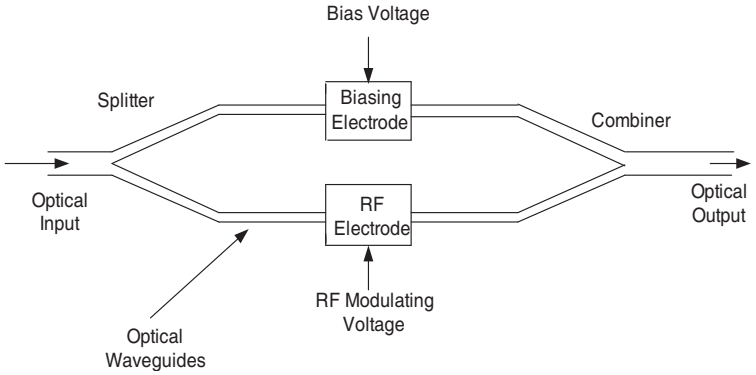

Figure 1: Mach-Zehnder interferometric modulator.

Experimental Investigation of the Shield Termination Effect on the Field-to-Cable Coupling Level

F. Üstüner[1], **N. Tarım**[2], **and E. Baran**[1]

[1]TUBITAK BILGEM UEKAE, Turkey
[2]Anadolu University, Turkey

Abstract— The field-to-cable coupling constitutes one of the fundamental electromagnetic interference coupling mechanisms that plays a central role in assessing the radiated immunity (or susceptibility) of the equipment under test. The theory that explains the field-to-cable coupling is well established and useful in the evaluation of simple cable structures [1, 2]. Although the cable shield characteristic (surface transfer impedance) plays the most important role in the coupling level, the type of the shield termination at the connector backshell is also important. In this work, a typical cable connection between two avionic equipments is considered and investigated experimentally in order to assess the effect of shield termination on the field-to-cable coupling level. Two shielded boxes are connected to each other with a 2 m long cable under test. For comparison purposes, the shield of the cable under test is terminated in five different configurations: no termination, 360° at one side, one pigtail at both sides, two pigtails at both sides, 360° at both sides. In order to illuminate the cable with a plane wave, GTEM cell environment is preferred. The boxes and the cable under test are placed on the bottom plate of GTEM cell in transverse position (see Figure 1). The coupling level is measured by a spectrum analyzer for each cable termination configuration. The first series of test is carried out on a coaxial cable of type RG-223. In the paper, the results of this test will be given and compared to each other assessing the influence of shield termination (see Figure 2). Moreover, the electric field over the cross section of the GTEM cell is estimated numerically and the theoretical coupling level is calculated for the simple wire case (no-termination configuration) in order to compare it with the experimental data. A second series of test is also carried out on a MIL-STD-1553 data bus cable which comprises of a shielded twisted pair. This second series test results will be given emphasizing the importance of the shielding integrity of the connectors in addition to the shield termination requirements.

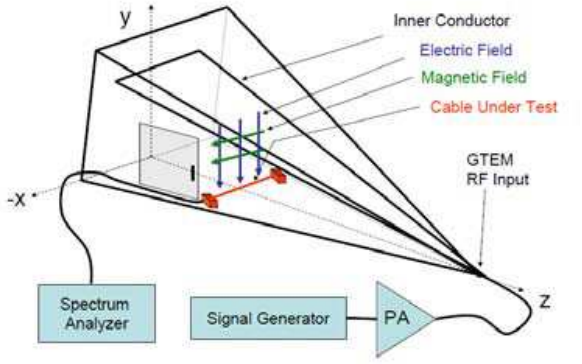

Figure 1.

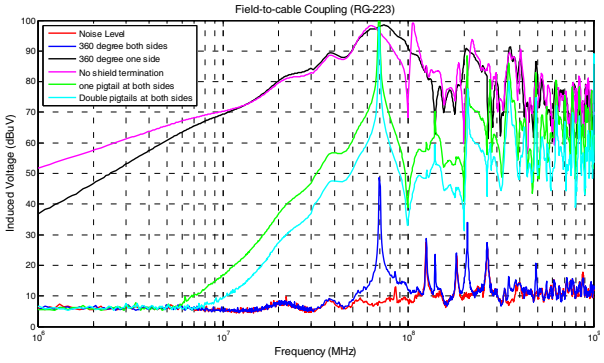

Figure 2.

REFERENCES

1. Smith, Jr., A. A., "Coupling of external electromagnetic fields to transmission lines," *Interference Control Technologies*, USA, 1989.
2. Paul, C. R., *Analysis of Multiconductor Transmission Lines*, Wiley, USA, 1994.

EMC in Malaysia: The First 10-Meter Semi-Anechoic Chamber (SAC) — Inception, Approach and Challenges

Lay Heng Chee and See See Cheng
EMC Testing Services and Solutions, Cisspr Sdn. Bhd., Malaysia

Abstract— In this paper, we provide an insight to the inception and approach used in the establishment of Malaysia's first public Electromagnetic Compatibility (EMC) Laboratory that is equipped with a 10-meter test range semi-anechoic chamber (SAC), and the challenges of EMC development in Malaysia. The PSDC EMC Laboratory, pioneered by Khazanah Nasional Berhad (a Government investment arm), PSDC (a non-profit society) and Cisspr Sdn. Bhd. (an entrepreneur enterprise), is a Malaysian government initiative to invest 30 million ringgit to establish a Shared Services Centre in Penang Skills Development Centre (PSDC). As the Electrical and Electronics (E&E) industry in Malaysia shifted from the lower value-added assembly and machining, to the higher value-added activities in test, manufacturing, and design and development (D&D), EMC test and measurement capability is vital to meet global regulatory compliance requirements in creating a situation of functional and safe operation in a common electromagnetic environment. A tri-partite approach was used to establish PSDC EMC Laboratory from concept to reality, based on well-defined objectives, voice of the industry, state-of-the-art test systems, competent people and internationally recognized ISO/IEC 17025 accreditation.

The Effects of End Plates on Coaxial Cable Coupling

Yu Xian Teo[1], **D. W. P. Thomas**[1], **and Christos Christopoulos**[2]

[1]University of Nottingham, UK
[2]George Green Institute in Electromagnetics, University of Nottingham, UK

Abstract— Coaxial cables are the most commonly used and a popular form of interconnect in the electronics industry. They are light and flexible but still possess a relatively high degree of shielding effectiveness. Much research has been done to measure as well as predict the crosstalk between two coaxial cables. In this work, the crosstalk between the cables is modelled as two coupled circuits using *TLM (Transmission Line Modelling)* technique [1]. The coupling path between the two cables is due to the current in the source cable circulating around a circuit composed of the braids of the two parallel cables that forms the coupling path, known as the tertiary circuit [2]. However, no research has been done to elaborate on the terminations of the tertiary circuit. It is often assumed that the tertiary circuit is terminated by an arbitrary impedance at each end. In this work, experimental measurements are performed on a representative termination using *TDR (Time Domain Reflectometry)*. The measured impedance is then incorporated into a complete system model and it is then shown that this enables the resonant frequencies in the coupling to be accurately predicted. Figure 1 shows that good agreement can be obtained between theory and measurement.

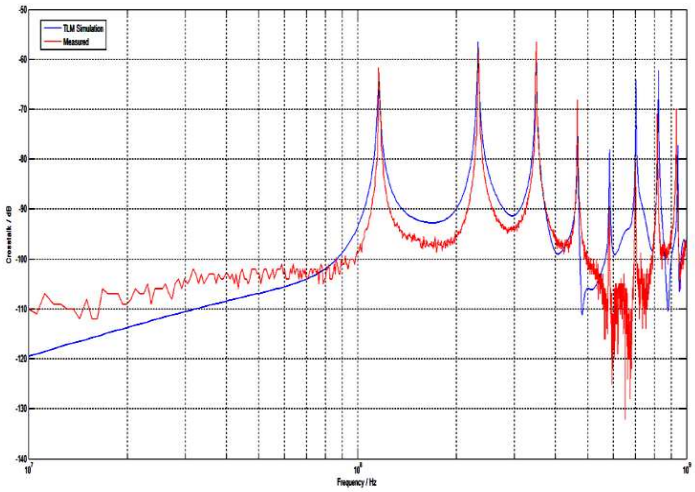

Figure 1: Crosstalk between two parallel RG-58 coaxial cables with separation of 2 cm.

REFERENCES

1. Christopoulos, C., *The Transmission-line Modelling Method: TLM*, John Wiley & Sons, Inc., 1995.
2. Thomas, D. W. P., C. Christopoulos, F. Leferink, and H. Bergsma, *Practical Measure of Cable Coupling*, IEEE Computer Science Press, Sep. 2005.

Development of RF Attenuation Standard in the Frequency Range of 100 kHz to 10 MHz

A. Widarta
National Metrology Institute of Japan (NMIJ)
National Institute of Advanced Industrial Science and Technology (AIST)
AIST Tsukuba Central, 1-1-1 Umezono, Tsukuba, Ibaraki 305-8563, Japan

Abstract— Attenuation is one of the fundamental measurement quantities that characterize electromagnetic waves propagating in transmission lines of radio frequency (RF) and microwave (MW) networks. At the National Metrology Institute of Japan (NMIJ, AIST), an accurate attenuation measurement system operated in the frequency range of 10 MHz to 40 GHz has been developed and used as a national standard of attenuation. The standard provides accuracy and traceability for measurements and calibrations of transfer standards used in a variety of applications such as communications, radar and navigation. On the other hand, the traceability of measurement to national standard is also required in recent electromagnetic compatibility (EMC) regulations for both national and global recognition purposes. However, since the EMC covers the electromagnetic measurements from several kilohertzs, it is necessary to extend the coverage frequency range of the standard.

This paper presents an improvement of the attenuation measurement system of the NMIJ, the dual channel intermediate frequency (IF) substitution method using an inductive voltage divider (IVD) as a reference standard, in order to establish the standard of attenuation in the frequency range of 100 kHz to 10 MHz. Higher dynamic range is obtained by placing toroidal ferrite chokes on the input and output ports of the device under test (DUT) to minimize the leakage effect which increases due to deterioration in the isolation of the skin effect of the coaxial transmission line used in the low frequency range. Sources of uncertainties of the system are discussed and the expanded uncertainties are expected to be less than 0.005 dB for attenuation range up to 20 dB and 0.01 dB for 80 dB.

Electromagnetic Shielding of Expanded Polystyrene Doped with Copper, Zinc and Graphite

E. Wiese and M. Yarlequé
Pontificia Universidad Católica del Perú, Sección Telecomunicaciones
Av. Universitaria 1801, Lima-32, Lima, Perú

Abstract— The continuous growth of the telecommunications has brought up more connectivity as well as interference, mainly electromagnetic. One way to reduce it is by employing metallic enclosure, which isolate a region from external EM interference. However, there are sceneries where metal shielding is not practical due to his weight, rigidity and proneness to corrosion. Conductive polymer has become a promising material to overcome these issues.

In this work, conductive polymers based on expanded polystyrene (EPS) doped with copper, zinc and graphite has been developed and evaluated at 9.6 GHz. The materials have been synthesized in the laboratory employing Dichloromethane. Samples of 30×30 cm for each type of dopant were obtained.

Conventionally, it can be expected that EPS doped with copper and zinc (high conductivity) would outperform the shielding features of the EPS doped with graphite (with lower conductivity). However, measurements show that latter exhibits the best shielding characteristics at 9.6 GHz. EPS doped with graphite provides 10 dB more shielding than EPS with copper, and 16 dB more than EPS with zinc. This can be understood since the presence of the delocalized π orbital of the graphite improves conductivity, like it was a soliton. Similarly, the graphite double bonds improve the transport of the electrons in the polymer while copper and zinc do not provide further bonds in the polymer structure.

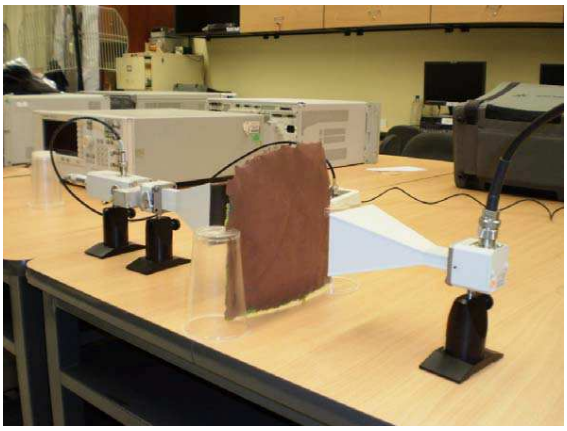

Measurement of EPS doped with copper.

Computation of Coupled Voltage to an Unshielded Cable Due to Transient EM Fields Radiated by ESD

Rajashree Narendra[1], **M. L. Sudheer**[2], **V. Jithesh**[3], **and D. C. Pande**[3]

[1]BNMIT, Bangalore, India
[2]UVCE, Bangalore, India
[3]EMI/EMC Group, LRDE, Bangalore, India

Abstract— The increasing development of dispersed but highly interconnected systems of telecommunication centers, computers and control equipments leads to an extensive use of cables to avoid interference problems. When an external electromagnetic field interacts with an imperfectly shielded cable, the interconnecting cables act as collectors of energy and considerable amount of energy can be coupled into the systems. The induced current and voltage transients may then cause damage or malfunction of sensitive electronic circuits. Simulation of structural current due to an Electrostatic discharge (ESD) event involves passing large transient currents through the object under test. This causes radiation of transient electromagnetic fields in the environment and induced transient voltages into the cables and equipments. A coupling model is developed to estimate the extent of coupling of transient EM fields to cables.

A coupling model is presented to predict induced terminal voltages on an unshielded cable placed above a ground reference plane due to transient electromagnetic fields radiated by Electrostatic discharge (ESD). The unshielded cable is exposed to the free space-radiating field due to IEC 61000-4-2 ESD waveform. The transient current is represented by Hertzian dipole elements and the time domain expressions for the resultant electric field intensity at any point are obtained. The frequency spectrum of the electric field is obtained using Discrete Fourier Transform. Assuming that the incident transient electric field is parallel to the cable termination, the frequency spectrum of the coupled voltage at the terminations is computed. The time domain representation of the terminal induced voltage is determined using Inverse Discrete Fourier Transform (IDFT). Computed results are presented for the contact discharge IEC 61000-4-2 ESD current waveform at 8 kV and air discharge IEC 61000-4-2 ESD current waveform at 16 kV. The coupled voltage into an unshielded cable is computed for resistive termination and RC shunt termination. The coupled voltage reduces from 6.25 V for ESD air discharge and 625 V for ESD contact discharge for a resistive termination to 0.325 mV for ESD air discharge and 7.8 mV for ESD contact discharge for a RC shunt termination.

Sampling Criterion for EMC Near Field Measurements

O. Franek[1], **M. Sørensen**[2], **H. Ebert**[1], **and G. F. Pedersen**[1]

[1]APNet Section, Department of Electronic Systems, Faculty of Engineering and Science
Aalborg University, Niels Jernes Vej 12, Aalborg 9220, Denmark
[2]Bang & Olufsen a/s, Peter Bangs Vej 15, Struer 7600, Denmark

Abstract— In the research field of electromagnetic compatibility (EMC), there has recently been a considerable interest in near field measurements of electronic modules. The idea of being able of predicting radiation levels of electronic devices without the need to use anechoic or semi-anechoic chambers seems certainly appealing. Another emerging application of near field measurements is characterization of electronic modules for the purpose of estimation of mutual coupling between the modules and/or a module and a chassis, which may result in unwanted radiation or intra-device electromagnetic interference.

In either case we need to know the appropriate sampling density of the near field measurement in order to accurately extrapolate the fields outside of the measured perimeter. While too low sampling density (large spatial step) leads to inaccuracies in the extrapolated field, too high density (small spatial step) results often in impractically long measurement times. Sampling theorem for near field measurements of antennas is available, having been derived from the plane wave spectra, and can be directly applied to the problem of radiation prediction. Nevertheless, if we want to use the near field measurements as a source to estimate near field coupling, validity of the antenna-based sampling theorem may be limited, because we are now interested in field values very close to the source, i.e., in the reactive near field.

In our paper, we propose an alternative, quasi-empirical sampling criterion for EMC near field measurements intended for close coupling investigations. The criterion is based on maximum error caused by sub-optimal sampling of near fields in the vicinity of an infinitely thin current trace, which is suggested as a worst-case representative of a signal trace on a typical printed circuit board. It has been found that the sampling density derived in this way is in fact very similar to that given by the antenna near field sampling theorem. The principal advantage of the proposed formulation is its parametrization with respect to the desired maximum error in measurements. This allows us to choose a suitable compromise between accuracy and measurement time.

Session 1A2
Biomedical Electromagnetic Instruments, EM Condensed Materials and Imaging

Contact-less Concentration Measurements in Aqueous Sodium-chloride Solutions Using Microwaves

Akio Oota and Tatsunori Uchida
Department of Electrical and Electronic Information Engineering, Toyohashi University of Technology
Tempaku-cho, Toyohashi, Aichi 441-8580, Japan

Abstract— Sodium chloride NaCl and its aqueous solutions have a wide variety of uses in foods, medicines, chemicals etc, because they are indispensable for supporting life of organisms. The NaCl concentration (c) therein is usually measured either by chemical methods such as a Mohr method and an ion chromatography, or by physical methods such as a conductivity measurement and an optical reflection method. However, contact-less measuring methods haven't been established yet.

Aqueous sodium-chloride solutions are well known to be one of the strong electrolyte solutions with both electrolytic ions Na^+ and Cl^-. These ions, together with H^+ and OH^- of water molecules, should cause a dramatic dielectric dispersion in the microwave range through complex interactions with each other by the following origins: One is a contribution from the electric conductivity (σ) of electrolytic ions in electric fields with frequency f, which is proportional to σ/f. Another is a dielectric relaxation phenomenon, mainly coming from rotational motions of water molecules and/or its macro-molecules via hydrogen bonds. Such phenomena cause a significant energy absorption in passing through microwaves therein, so that it should lead to developments of microwave contact-less testing (MCLT) system to determine the concentration c in aqueous sodium-chloride solutions.

For this purpose, we measure the complex dielectric constant $\varepsilon^* = \varepsilon' - j\varepsilon''$ as a parameter of the concentration c in aqueous sodium-chloride solutions in the microwave range using a network analyzer to obtain the basic data for MCLT. In parallel, we construct the experimental apparatus to measure the microwave transmission into the solutions, which is composed of a pair of monopole antennas, a signal generator with a power amplifier, a spectrum analyzer and a sample holder with a rotation mechanism by a stepping motor. Using this apparatus, we obtain the regression curve between the transmission loss P and the concentration c in aqueous sodium-chloride solutions crucial for developments of MCLT. We also elucidate the dominating factor of P based on an equivalent-circuit model of microwave transmission using the data of $\varepsilon^* = \varepsilon' - j\varepsilon''$.

FPCB RF Coil for Small Animal NMR Imaging at 3T MRI Systems

Sheikh Faisal Ahmad[1], **Son Hyeok Woo**[1], **Young Cheol Kim**[1], **Ick Chang Choi**[1], **Yongmin Chang**[2], **and Hyun Deok Kim**[1]

[1]School of Electronics Engineering, Kyungpook National University, South Korea
[2]Department of Molecular Medicine and Radiology, Kyungpook National University, South Korea

Abstract— Radio frequency (RF) coil is used to transmit an RF pulse and receive the weak nuclear magnetic resonance (NMR) signal in a magnetic resonance imaging (MRI) system. An RF coil is basically a RF resonator which has the ability to produce strong magnetic field in its coverage area. The NMR signal can be detected if the frequency of magnetic field produced by the RF coil is matched with the frequency of the NMR signal. There are available a number of different designs however the birdcage type RF coils because of their strong magnetic field development property are considered as the best candidate at medium and high field MRI systems.

In this paper we are presenting a method of implementation a birdcage coil in band pass configuration for NMR imaging in small animal as shown in Figure 1(a). The RF coil is designed for 3T MRI system and is able to resonate at 127.7 MHz resonance frequency as shown in Figure 1(b). The major difference between our implemented coil and the traditional birdcage coil is the utilization of flexible printed circuit board (FPCB) etched copper conductors as the legs and end rings of the RF coil. This introduction of FPCB improves the performance of the RF coil. The most important and desired parameter in the RF coil design is the magnetic field homogeneity inside the RF coil. It is observed that the utilization of FPCB in the RF coil improves the field homogeneity inside the RF coil. It also helps to suppress the undesired resonances which are a source of increasing SAR in the RF coil. The coil is implemented to perform the whole body NMR imaging of ^{1}H in small animal. The coil is composed of eight legs and two end rings with 4 cm internal diameter and 21.25 cm overall length. The coil dimensions were optimized with full wave 3D electromagnetic simulation software. The basic testing of the RF coil was performed with network analyzer. There is present a good agreement between the simulated and measured results. The NMR images of a small mouse were also obtained with the help of implemented RF coil.

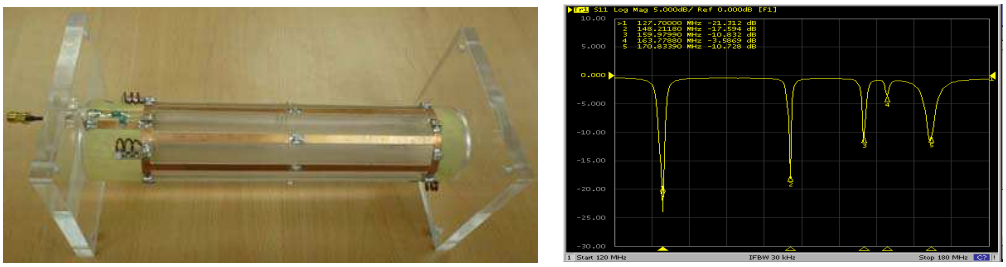

(a) (b)

Figure 1: (a) Implemented RF coil for ^{1}H NMR imaging at 3T. (b) Frequency response of RF coil.

ACKNOWLEDGMENT

This work was partially supported by the Grant of the Korea Ministry of Education, Science and Technology (The Regional Core Research Program/Anti-aging and Well-being Research Center) and the Korea Ministry of Education, Science and Technology under BK21 Program.

Point Spread Function for Optical Transillumination Imaging of Animal Body

Koichi Shimizu, **Hiroki Takahashi**, **Takeshi Namita**, **and Yuji Kato**
Graduate School of Information Science and Technology, Hokkaido University, Sapporo, Japan

Abstract— We can obtain transillumination images of an animal body using near-infrared light with a 700–1200 nm wavelength. However, the images are blurred by the strong scattering in the body tissue. If there is a light source at a specific depth inside the scattering medium, this blurring can be characterized by the point spread function (PSF) which is obtained as a solution of the diffusion equation for a point source case. The blurred transcutaneous image of a fluorescent source inside the body can be improved by the deconvolution with this depth-dependent PSF. We also attempted to apply this PSF to the transillumination image of a light-absorbing structure in a scattering medium. In a simulation, it was confirmed that the blurred transillumination images were effectively improved by the PSF for a fluorescent source. The effectiveness of the proposed technique was examined in an experiment using a tissue-simulated phantom. The transillumination image of an absorber (black-painted square metal plate, $10 \times 10 \times 2$ mm) appeared almost a black disc due to the strong scattering effect of the surrounding scattering medium (the reduced scattering coefficient and the absorption coefficient were 1.0/mm and 0.01/mm, respectively), when the depth of the absorber was 15 mm from the observing surface. The blurred image was significantly improved by the deconvolution with the PSF for 15 mm depth. These results suggested that the depth-dependent PSF we have derived for fluorescent imaging can be used to obtain a clear transillumination image of the internal structure of an animal body using near-infrared light.

Maxwell Sumudu Based Magnetic Solutions

Fethi Bin Muhammad Belgacem and Eman Al-Shemas
Department of Mathematics, Faculty of Basic Education, PAAET, Shaamyia, Kuwait

Abstract— The Dynamics of a planar, transverse electromagnetic (TEMP) wave propagating in the direction z in lossy media with constant permittivity ϵ, permeability μ, and conductivity $\sigma > 0$, are best described by Maxwell's equations.

$$\begin{cases} (i)\nabla \times \mathbf{E} = -\mu \frac{\partial \mathbf{H}}{\partial t} \\ (ii)\nabla \times \mathbf{H} = \epsilon \frac{\partial \mathbf{E}}{\partial t} + \sigma \mathbf{E} \end{cases} \tag{1}$$

Various forms of solutions for the electromagnetic couple solutions and profiles of (1) have been found, using various techniques, subject to distinct assumptions on the medium coefficients and fields initial directions.

In view of its advantageous attributes and many quantities preserving properties, the Sumudu turns out to be an ideal tool for many science applications and engineering. Without resorting to a new frequency domain, as in the case of Laplace or Fourier, having units and scale preserving properties, the Sumudu turns out to be the ideal tool, for engineering and many applied mathematics and physics problems. The Sumudu operator is defined by,

$$G(u) = \mathbb{S}[f(t)] = \int_0^\infty f(ut)e^{-t}dt, \quad u \in (-\tau_1, \tau_2) \tag{2}$$

over the set of functions,

$$A = \{f(t)/\exists\ M, \quad \tau_1, \tau_2 > 0 \quad |f(t)| < Me^{\frac{|t|}{\tau_j}}, \quad \text{if } t \in (-1)^j \times (0, \infty)\} \tag{3}$$

The function, $G(u)$, is then referred to as *the Sumudu of* $f(t)$. The Sumudu Operator is clearly linear since,

$$\mathbb{S}[af(t) + bg(t)] = a\mathbb{S}[f(t)] + b\mathbb{S}[g(t)] \tag{4}$$

Computationally, denoting the gamma function by, Γ, wherever, $\Gamma(\alpha+1)$ can be defined (classically for $\alpha > -1$), we then have,
$\mathbb{S}[t^\alpha] = \int_0^\infty (ut)^\alpha e^{-t}dt = u^\alpha \int_0^\infty t^\alpha e^{-t}dt = \Gamma(\alpha+1)u^\alpha$. So, $\mathbb{S}[1] = 1$, $\mathbb{S}[at+b] = au+b$, and $\mathbb{S}[t^n/n!] = u^n$, for any integer $n \geq 0$. Discretely, $\mathbb{S}[\exp(at)] = \mathbb{S}[\sum_0^\infty (at)^n/n!] = \sum_0^\infty (au)^n = 1/(1-au)$, for $a \in (-1/a,\ 1/a)$.

Consequently, for any frequency, w, $1/(1+(wu)^2)$, $(wu)/(1+(wu)^2)$, are the respective *Sumudi* of $\cos(wt)$, and, $\sin(wt)$, which may be obtained,

$$\mathbb{S}[\cos(wt) + j\sin(wt)] = \mathbb{S}[e^{jwt}] = 1/(1-jwu) = (1+jwu)/(1+(wu)^2).$$

Conversly, (with $w = 1$), $1/(1+u^2) = \sum_0^\infty (-1)^n u^{2n}$, with u in $(-1,\ 1)$, and applying the inverse operator, yields, with t in $\mathbb{R}$, $\mathbb{S}^{-1}\sum_0^\infty (-1)^n u^{2n} = \sum_0^\infty (-1)^n t^{2n}/(2n)! = \cos t$, & $\mathbb{S}^{-1}[u/(1+u^2)] = \mathbb{S}^{-1}\sum_0^\infty (-1)^n u^{2n+1} = \sum_0^\infty (-1)^n t^{2n+1}/(2n+1)! = \sin t$.

Furthermore, for $a \geq 0$, the Heaviside or unit step function, $H_a(t)$, any function shift, $f(t-a)$, has for sumudu,

$$\mathbb{S}[f(t-a)] = \mathbb{S}[H_a(t)f(t)] = e^{\frac{-a}{u}}\mathbb{S}[f(t)], \quad \text{for } u > a \tag{5}$$

The TEMP problem, like general field couple problems, can be considered in the Sumudu Transform frame work. Upon Sumudu transformation, Maxwells Equations are made to yield transient magnetic field solutions. In previous works, Sumudu based techniques were used to deliver transient electric field solutions for electromagnetic planar waves moving in the transversal direction of lossy media. Here we present a parallel treatment for the magnetic field, using Sumudu established properties. In this abstract, we first albeit briefly, state some Sumdu Convolution, Integration and Differentiation Properties whose application will help us solve the TEMP problem. The next theorem allows us to use the Sumudu transform efficiently to solve differential equations involving multiple integrals of the dependent variable as well, by rendering them into algebraic ones.

Cryptography of the Medical Images

Cherif Moumen[1], **Malek Benslama**[1], **and Mekhilef Saad**[2]

[1]Laboratoire d'Electromagnétisme et de Télécommunication, Université de Constantine, Algérie
[2]Department of Electrical Engineering, University of Malaya, Kuala Lumpur, Malaysia

Abstract— Nowadays, digital exchanges of medical images are frequently used throughout the world in a fraction of a second via the Internet. These data can be read or modified during their transmission via a non-controlled channel. Therefore, it becomes very important to protect this private information against unauthorized viewers by using cryptography.

Cryptographic techniques can be divided into symmetric encryption (with a secret key) and asymmetric encryption (with private and public keys).

In symmetric cryptosystems, the same key is used for the encryption or decryption and this key need to be secure and must be shared between the emitter and the receiver. These cryptosystems are very fast and easy to use.

In proposing specific algorithms for the transfer of medical data ensuring total privacy in parallel on the emission and receipt of data, by using 1D chaotic algorithms [5]: **BRIE** (Bit Recirculation Image Encryption), their basic ideas is the recirculation of bits (pixels) image in clear, so we resorted to study a simple logistic model: $x_{n+1} = rx_n(1 - x_n)$. This chaotic system is a deterministic nonlinear dynamic system which has an unpredictable long-term. This unpredictability is due to the sensitivity to initial conditions, the mixing property and the density of periodic points. This logistic model can generate chaotic binary sequences and pseudo-random, to manipulate of each pixels of the image, by the two properties "**confusion**" and "**diffusion**" in classical cryptography. It is a natural idea to use chaos to conceive new cryptosystems.

Indeed, the use of this new cryptosystems in the sector of the medical sciences, with evolves in the latter years in a remarkable way, generating applications related to the use of chaos in the security communication systems, for to realize the transfer of the medical data, is the object of this work.

Expandable Multi-frequency EIT System for Clinical Applications

H. Wi, **T. E. Kim**, **T. I. Oh**, **and E. J. Woo**
Department of Biomedical Engineering, Kyung Hee University, Korea

Abstract— An electrical impedance tomography (EIT) system can visualize conductivity and permittivity distributions inside the human body from measured boundary voltages induced byexternally injected currents. We have developed a fully parallel multi-frequency EIT system called the KHU Mark2.5. It is based on an impedance measurement module (IMM) comprising a current source, a voltmeter and a calibration circuit. Each IMM is independent and can calibrate its own current source and voltmeter through an automatic self-calibration procedure. We found thatthe output impedance values of all current sources are greater than 1M at the chosen frequencies. The CMRR is around 96 dB and the voltmeter SNR isbetween 80 and 85 dB depending. To increase spatial resolution of conductivity and permittivity images, we can cascade multiple EIT systems to form a system with a larger number of channels.They are synchronizedby clock synchronizationcircuits. Physiological events such as cardiac and respiratory functions alter electrical tissue properties. To correlate such events with EIT images, we can perform a biosignal-gated EIT imaging. We can improve interpretation of EIT images by incorporatingreal-time ECG and respiration signals into EIT images. This may allow us to separate fast cardiac events and slow respiratory events from reconstructed EIT images and also improve the SNR by signal-gated data averaging We present the performance of the KHU Mark2.5 system with experimental results of animal and human subjects.

Conductivity Imaging of Animal and Human Body Using 3T Magnetic Resonance Electrical Impedance Tomography (MREIT)

W. C. Jeong[1], **Y. T. Kim**[1], **H. J. Kim**[1], **C. Y. Lim**[2], **H. M. Park**[2], **and E. J. Woo**[1]

[1]Department of Biomedical Engineering, Kyung Hee University, Gyeonggi, Korea
[2]Department of Veterinary Internal Medicine, Konkuk University, Seoul, Korea

Abstract— Magnetic resonance electrical impedance tomography (MREIT) aims to produce cross-sectional images of conductivity distributions inside animal and human subjects. In this study, we validate its feasibility by performing conductivity imaging experiments of animal and human bodies. We attached four carbon-hydrogel electrodes on the imaging area and placed the imaging object inside our 3T MRI scanner. We injected imaging currents in a form of short pulses into a chosen imaging area, of which timing was synchronized with an MRI pulse sequence. Obtaining images of induced magnetic flux density distributions inside the imaging object, we reconstructed conductivity images using the single-step harmonic B_z algorithm based on the relation between the conductivity and the induced magnetic flux density. Reconstructed conductivity images of the canine heart, kidney, prostate, and other organs exhibit unique contrast information which is hardly observed in other imaging modalities. The conductivity images of the human lower extremity well distinguished different parts of the subcutaneous adipose tissue, muscle, crural fascia, intermuscular septum and bone. We could observe spurious noise spikes in the outer layer of the cortical bone primarily due to the MR signal void phenomenon there. Providing cross-sectional conductivity images with a spatial resolution of a few millimeters, MREIT may deliver unique new diagnostic information in its future clinical studies.

Microwave-heating for Liver Cancer Thermothrapy with Three Layer Tapered Coaxial Line Applicator

M. Urata, K. Wakino, and T. Kitazawa
Department of Electrical and Electronic Engineering, Ritsumeikan University, Japan

Abstract— The conventional applicators are slot type antennas which are made from commercially available semi rigid cables, therefore the impedance mismatching has occurred between the applicator and the liver tissue [1]. This mismatching causes unwanted heating of normal tissue and relatively large power (over 72 W) is required to get the proper operation temperature. The novel applicator structure is developed by inserting the impedance matching sections between the radiation port and the feeding coaxial line to ensure the better impedance matching with liver tissue. Reflection S_{11} can be reduced from −9.8 dB to −18.6 dB at 2.45 GHz by inserting intermediate material which has a proper selection of geometry and permittivity for impedance matching section [2]. In this study, we perform the finite element method (FEM) simulation to get the relationships between the power and temperature and obtain the detailed SAR (specific absorption rate) at 2.45 GHz. This optimized applicator can reach required temperature with smaller power 10 W with constantly feeding, and we can use the low power microwave source instrument which will provide safer environment for patient and operating staffs.

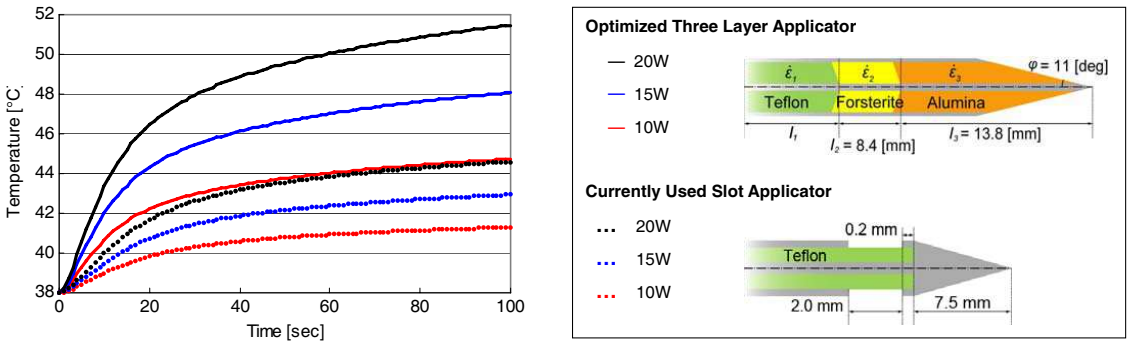

Figure 1: Time domain temperature of optimized three layer applicator and currently used slot applicator.

REFERENCES

1. Tumeh, A. M. and M. F. Iskander, "Performance comparison of available interstitial antennas for microwave hyperthermia," *IEEE Trans. on MTT*, Vol. 37, No. 7, Jul. 1989.
2. Urata, M., S. Kimura, K. Wakino, and T. Kitazawa, "Optimization of three layer tapered coaxial line applicator for cancer thermotherapy by impedance matching of transition layer sections," *The 2011 IEEE ISAP and USNC/URSI National Radio Science Meeting*, Jul. 2011.

Session 1A3
Inverse Scattering Problems: Theories, Computations, and Applications

Isoflux Beam Shaping Utilizing an Inverse Antenna Problem Approach

Kuiwen Xu, **Bo Lv**, **Lili Xu**, **Jianhua Shen**, **Jiangtao Huangfu**, **and Lixin Ran**
Department of Information and Electronic Engineering, Zhejiang University, Hangzhou 310027, China

Abstract— This paper presents an inverse antenna design approach to determine the optimal aperture distribution for an isoflux beam which is widely used in the satellite antenna in a fixed circularly symmetric aperture to fulfill constraints (sidelobe level, directivity and so on). In particular, it can illustrate the ultimate performances achievable by an aperture antenna of a given size and can serve as a reference source distribution for the synthesis of array antenna The approach is able to satisfy the given power pattern design constraints and adjust the beam shape properly by the optimization of various weighted functions as the aperture distribution. Although the approach does not apply to generic aperture and generic power pattern, it applies to a large number of satellite antennas and other some complex aperture antenna design. Preliminary results, supporting the effectiveness of the proposed strategies, are also presented.

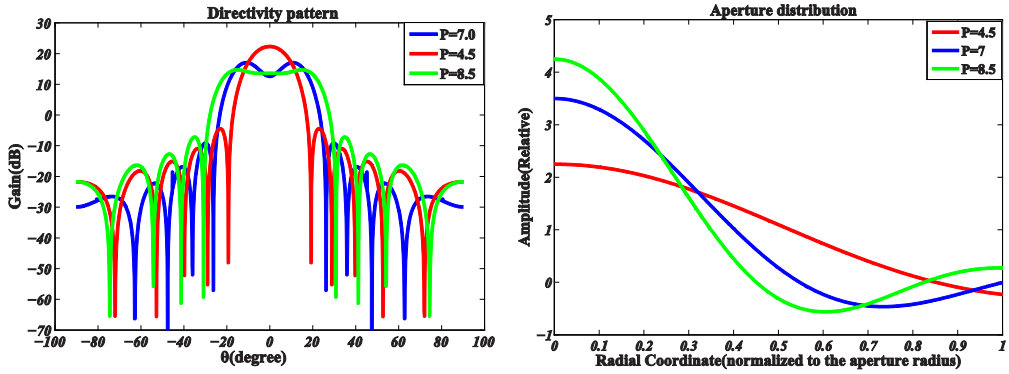

(a) (b)

Figure 1: (a) Farfield directivity pattern for the circular aperture distribution. The red curve, the blue, the green curve correspond to aperture distribution $J_1(x)/x$, $P = 4.5$, $P = 7$, $P = 8.5$, respectively as a function of radial coordinate (normalized to the aperture radius), having a Diameter of 6.5λ. (b) Aperture field distribution corresponding to the directivity pattern shown in (a).

Preliminary Assessment of the Iterative Multi-scaling Subspace Optimization Method in Three-dimensional Microwave Imaging

G. Oliveri[1], **Y. Zhong**[2], **K. Agarwal**[2], **X. Chen**[2], **and A. Massa**[1]

[1]ELEDIA Research Center at DISI, University of Trento, via Sommarive 5, I-38123, Trento, Italy
[2]Department of Electrical and Computer Engineering, National University of Singapore, 117583, Singapore

Abstract— Applications in non-destructive testing and evaluation, biomedical diagnostics, radar imaging, remote sensing, subsurface inspection, and material characterization often require the solution of challenging inverse scattering problems [1–6]. To this end, several deterministic [2] and stochastic [3] techniques have been proposed in the last years. Among the former, the so-called contrast source (*CS*)-formulation techniques have received much attention recently [3, 4] due to the higher reconstruction accuracies and robustness which they allow with respect to the "contrast field" (*CF*) formulations [3, 4]. However, CS techniques suffer from the non-uniqueness of the associated inverse source problem, which is caused by the *non-radiating* (or *non-measurable*) components of the unknown contrast source [3, 4].

To overcome this drawback, a subspace optimization method (*SOM*) has been recently introduced as a complement to the existing approaches [5]. In this technique, the contrast source is subdivided in a "deterministic" part, which is computed through singular value decomposition (SVD), and an "ambiguous" one [5], whose amplitude is determined by minimizing a cost functional including both "data" and "state" terms [5]. Despite the merits of the *SOM* method, such an approach presents also some limitations when dealing with large solution spaces, as a consequence of the 'local minima' issues [6]. To overcome these drawbacks, the integration of a multi-focusing strategy, namely the iterative multi-scaling approach (*IMSA*) [2], with the *SOM* method has been recently proposed and validated in a 2D scenario [6]. However, these issues can become even more restrictive when three-dimensional reconstructions are of interest, due to the intrinsically larger solution spaces at hand. Accordingly, an extended IMSA-SOM approach will be proposed in this work to enhance the effectiveness, efficiency, accuracy, and reliability of the subspace optimization method when dealing with 3D reconstructions.

REFERENCES

1. Rocca, P., M. Benedetti, M. Donelli, D. Franceschini, and A. Massa, "Evolutionary optimization as applied to inverse scattering problems," *Inverse Problems*, Vol. 25, No. 6, 1–41, art. No. 123003, Dec. 2009.
2. Caorsi, S., M. Donelli, D. Franceschini, and A. Massa, "A new methodology based on an iterative multiscaling for microwave imaging," *IEEE Trans. Antennas Propagat.*, Vol. 51, No. 4, 1162–1173, Apr. 2003.
3. Van Den Berg, P. M. and A. Abubakar, "Contrast source inversion method: State of art," *Progress In Electromagnetics Research*, Vol. 34, 189–218, 2001.
4. Rocca, P., M. Donelli, G. L. Gragnani, and A. Massa, "Iterative multi-resolution retrieval of non-measurable equivalent currents for the imaging of dielectric objects," *Inverse Problems*, Vol. 25, 1–15, 055004, 2009.
5. Zhong, Y., X, Chen, and K. Agarwal, "An improved subspace-based optimization method and its implementation in solving three-dimensional inverse problems," *IEEE Trans. Geosci. Remote Sens.*, Vol. 48, No. 10, 3763–3768, Oct. 2010.
6. G. Oliveri, Y. Zhong, X. Chen, and A. Massa, "Multi-resolution subspace-based optimization method for inverse scattering problems," *J. Opt. Soc. Am. A*, Vol. 28, No. 10, 2057–2069, 2011.

3D Microwave Imaging Using the Source-receiver Compression Scheme

Aria Abubakar, **Guangdong Pan**, **and Tarek M. Habashy**
Schlumberger-Doll Research, Cambridge, USA

Abstract— We apply a source-receiver compression approach to reduce the computational time and memory usage of the nonlinear inversion approaches for interpreting three-dimensional microwave data. By detecting and quantifying the extent of redundancy in the data, we assemble a reduced set of simultaneous sources and receivers that are weighted sums of the physical sources and receivers employed in the measurement setup. Because the number of these simultaneous sources and receivers can be significantly less than those of the physical sources and receivers, the computational time and memory usage of any inversion method such as steepest-descent, nonlinear conjugate-gradient, contrast-source inversion, and quasi-Newton can be tremendously reduced. The scheme is based on decomposing the data into their principal components using a singular value decomposition approach and the data compression is done through the elimination of eigenvectors corresponding to small eigenvalues. Consequently, this will also suppress the effect of noise in the data. As a concept demonstration we show that this approach has the potential of significantly reducing both computational time and memory usage of the Gauss-Newton inversion method by few orders of magnitude.

Comparison of Various Sparsity-regularized Gradient-based Algorithms for Solving 2D Electromagnetic Inverse Scattering Problem

A. Desmal and H. Bağcı
Division of Physical Sciences and Engineering
King Abdullah University of Science and Technology (KAUST)
KAUST 4700, Thuwal 23955-6900, Saudi Arabia

Abstract— The difficult of solving electromagnetic inverse problems stems from (i) the non-linearity of the scattering equations and (ii) the ill-conditioning of the problem. The former can be avoided via the use of Born iterations, which convert the non-linear inverse problem into a sequence of linear inverse problems. To alleviate the ill-conditioning, a regularization scheme has to be applied at each step of the Born iterations. For this purpose, L^2-norm regularizers have been used extensively, and the resulting optimization problem has been solved using Tikhonov- or conjugate gradient-based schemes. However, L^2-norm regularizers promote the smoothness in the solution; and will not produce sharp images when applied in domains with sharp variations and sparse content [1]. Such domains exist in many practical applications, such as see-through-the-wall and molecular imaging. In these applications, priori knowledge of the domain's sparseness could be used to alleviate the ill-conditioning.

In this work, we incorporate various gradient-based algorithms, with L^0- and L^1-norm regularizers, which promote the sparseness of the solution, into the Born iterations for solving the two-dimensional electromagnetic inverse problem. These algorithms are briefly described next: (i) Iterative Shrinkage Thresholding Algorithm (ISTA) employs Landweber iterations for the gradient step; and each of these iterations is followed by a thresholding/shrinkage operation [2]. Although ISTA has been proven useful for sparse optimization problems, it suffers from slow convergence rate, which gets worse with increasing ill-conditioning. (ii) Two-step IST (TWIST) and fast ISTA (FISTA) are increased-efficiency versions of ISTA, where thresholding/shrinkage operator is applied to a linear combination of current and previous gradient step updates [3, 4]. The two methods differ in the way they construct the linear combination. (iii) Split Augmented Lagrangian Shinkage Algorithm (SALSA) uses Tikhonov-based inversion with thresholding/shrinkage function at every iteration [5].

In our presentation, we will compare the performance of these algorithms, namely, ISTA, FISTA, TWIST, and SALSA, in terms of convergence and computational cost, when they are incorporated into the Born iterations for solving the two-dimensional electromagnetic inverse problem. Results of the algorithms for various scenarios, involving different sparseness levels, electrical sizes, and noise levels will be compared.

REFERENCES

1. Tropp, J. A. and S. J. Wright, "Computational methods for sparse solution of linear inverse problems," *Proc. IEEE*, Vol. 98, No. 6, 948–958, Jun. 2010.
2. Daubechies, I., M. Defriese, and C. de Mol, "An iterative thresholding algorithm for linear inverse problems with a sparsity constraint," *Commun. Pure Appl. Math.*, Vol. LVII, 1413–1457, 2004.
3. Bioucas-Dias, J. M. and M. A. T. Figueiredo, "A new TwIST: Two-step iterative shrinkage/thresholding algorithms for image restoration," *IEEE Trans. Image Process.*, Vol. 16, No. 12, 2992–3004, Dec. 2007.
4. Beck, A. and M. Teboull, "A fast iterative shrinkage-thresholding algorithm with application to wavelet-based image deblurring," *Int. Conf. Acoustics, Speech and Signal Process.*, 2009.
5. Afonso, M. V., J. M. Bioucas-Dias, and M. A. T. Figueiredo, "Fast image recovery using variable splitting and constrained optimization," *IEEE Trans. Image Process.*, Vol. 19, No. 9, 693–696, Sep. 2010.

On the Electromagnetic Response of Anisotropic Laminates

Yu Zhong[1], **Xudong Chen**[1], **Marc Lambert**[2], **and Dominique Lesselier**[2]

[1]Department of Electrical and Computer Engineering, National University of Singapore, Singapore
[2]Laboratoire des Signaux et Systèmes, Département de Recherche en Electromagnétisme
CNRS-SUPELEC, Univ Paris Sud, France

Abstract— Anisotropic laminates have many applications in aeronautic and automotive industries [1] but also for shieldings [2], machine cores [3], antenna substrates [4], optical films [5], etc., while geophysical surveying calls for anisotropic models [6]. They exhibit complex behaviors, due to various types of anisotropies (e.g., caused by fiber-reinforcements in artificial materials) and multi-layered geometries possibly involving many strata. Computation of the time-harmonic dyadic Green's functions (DGF) to model their response to given excitations (from kHz to GHz and beyond, depending upon material conductivities and applications envisaged) is challenging. Also, the DGF are a first step when aiming at the imaging of damaged laminates, at least if integral formulations and method of moments (MoM) are used, not only general finite-element or finite-difference schemes provided that they can indeed treat anisotropies properly.

Here, one will put in perspective a novel scheme of computation of the DGF dedicated to planar laminates — and further, of the field due to electrically active volumetric sources anywhere — with bi- and uni-axial electric and/or magnetic anisotropies in a frequency broad-band fashion (no approximation save allocating at each space point permittivity/permeability tensors). This scheme has been introduced in [7, 8], and its effectiveness illustrated from eddy-current to microwave frequencies.

Then, one will concentrate upon the case when defects affect a laminate, and illustrate their modeling and imaging via theoretical analysis and simulations. These defects can be voids or inclusions, some zone of the laminate exhibiting changes of bulk electromagnetic parameters due to changes in geometries and/or constituencies of the material in this zone. Such defects are 3-D bounded volumetric ones, and if small enough with respect to the wavelengths of the field, they can be modeled via depolarization tensors and are amenable to imaging via dedicated MUSIC-type methods, once those prolonged to anisotropic materials as doable since the DGF are available. But if volumes are too large, a contrast-source integral formulation has to be introduced and corresponding equations solved via a method of moments, here deployed in the spectral domain as it will be shown in a promising fashion.

REFERENCES

1. Heuer, H., et al., "High resolution inspection of carbon fiber materials by eddy current techniques," *2nd Intern. Symp. NDT Aerospace*, Proc. Mo.2.A3, 10, Hamburg Airport, 2010.
2. Chiu, H.-K., et al., "Near-field shielding and reflection characteristics of anisotropic laminated planar composites," *IEEE Trans. Electromagn. Compat.*, Vol. 39, 332–339, 1997.
3. Wang, J., et al., "A new formulation of anisotropic equivalent conductivity in laminations," *IEEE Trans. Magn.*, Vol. 47, 1378–1381, 2011.
4. Mehdipour, A., et al. "Reinforced continuous carbon-fiber composites using multi-wall carbon nanotubes for wideband antenna applications," *IEEE Trans. Antennas Propagat.*, Vol. 58, 2451–2456, 2010.
5. Hodgkinson, A., et al., "Eigenequations and compact algorithms for bulk and layered anisotropic optical media: reflection and refraction at a crystal-crystal interface," *J. Comp. Phys.*, Vol. 133, 75–83, 1997.
6. Løseth, L. O. and B. Ursin, "Electromagnetic fields in planarly layered anisotropic media," *Geophys. J. Intern.*, Vol. 170, 44–80, 2007.
7. Zhong, Y., et al., "On a new stable modeling of the dyadic Green's functions of an electrically uniaxial planar-layered medium and applications," *Int. Conf. Electromagn. Advanc. Applic.*, Turin, Sept. 2011 (in Proc. IEEE Explore, to appear).
8. Zhong, Y., et al., "On a novel computational scheme of dyadic Green's functions of electrically-uniaxial planar-layered composites," *15th Int. Symp. Appl. Electromagn. Mechan.*, Naples, Sept. 2011. (in JSAEM Studies in Applied Electromagnetics and Mechanics, Vol. 14, G. Rubinacci, et al., eds, 125–126, Tokyo.)

Twofold Subspace-based Optimization Methods for Solving Electromagnetic Inverse Scattering Problem

Yu Zhong and Xudong Chen
Department of Electrical and Computer Engineering
National University of Singapore, 117576, Singapore

Abstract— On the basis of the subspace-based optimization method (SOM), a twofold SOM (TSOM) and its variation, the FFT-TSOM, are proposed to solve in a more stable and more efficient manner the two-dimensional (2D) and three-dimensional (3D) electromagnetic inverse scattering problems. In the SOM, part of the induced current is found directly from the measured scattered fields while the remaining is searched within a current subspace, which has small contribution to the scattered fields, via optimization. By using the spectral property of the current-to-field operator, the TSOM further shrinks the dimension of the current subspace within which the induced current is optimized. Since the new current subspace is much smaller than the one used in the SOM, the TSOM shows better stability and better robustness against noise compared the SOM. However, in order to obtain the spectral property of the current-to-field operator, the singular value decomposition (SVD) of the operator is involved, and it is computationally burdensome, especially when dealing with problems with a large amount of unknowns. In order to decrease the computational complexity, the FFT-TSOM is proposed. In the FFT-TSOM, the discrete Fourier bases are used to construct a current subspace that is a good approximation to the original current subspace spanned by singular vectors. Such an approximation avoids the SVD and uses the FFT to accomplish the construction of the induced current, which reduces the computational complexity and memory demand of the algorithm compared to the original TSOM. By using the new current subspace approximation, the FFT-TSOM inherits the merits of the TSOM, better stability during the inversion and better robustness against noise compared to the SOM, and meanwhile has much lower computational complexity than the TSOM. Numerical simulations will be shown to validate the proposed TSOM and FFT-TSOM.

Linear Sampling in Transverse Electric Case

Krishna Agarwal, **Xudong Chen**, **and Yu Zhong**
Department of Electrical and Computer Engineering, National University of Singapore
#E4-05-45, 4 Engineering Drive 3, 117583, Singapore

Abstract— Linear sampling is well known for imaging extended scatterers. It uses the concept that if a point belongs to the scatterer support, we can use finite energy source distribution to create an induced source distribution whose radiation pattern is similar to a fundamental source at the point. In the transverse magnetic case with $\hat{z}$ as the longitudinal direction, the $\hat{z}$ directed line source is the fundamental induced source. On the other hand, in the transverse electric direction, two fundamental sources, $\hat{x}$ and $\hat{y}$ directed dipole sources are the fundamental sources. Usually, either an $\hat{x}$ or a $\hat{y}$ directed dipole source is used in linear sampling for imaging the scatterers. Thus, the image obtained is strongly directional.

It is worth considering if a combination of $\hat{x}$ and $\hat{y}$ directed dipole sources results in a better image. However, the main impediment for this approach is how to determine the appropriate combination. Another related issue is that should we use a fixed combination of the $\hat{x}$ and $\hat{y}$ directed dipole sources for all the points in the domain. It seems logical that the appropriate combination of $\hat{x}$ and $\hat{y}$ directed dipole sources varies from point to point.

In this work, we present a multipole based method of determining the most stable combination of the $\hat{x}$ and $\hat{y}$ directed dipole sources for each point. We show using some interesting examples that such automatic selection of the most stable combination results in better images for these examples. Two examples are presented in Fig. 1 and Fig. 2. For imaging the dielectric scatterers in Fig. 1(a) and Fig. 2(a), 30 turnstile antennas are used as transmitters as well as detectors. The results show that proposed variation of LSM that uses multipole theory and the most stable combination of the dipoles for each point provides superior results than LSM that uses only one fundamental dipole.

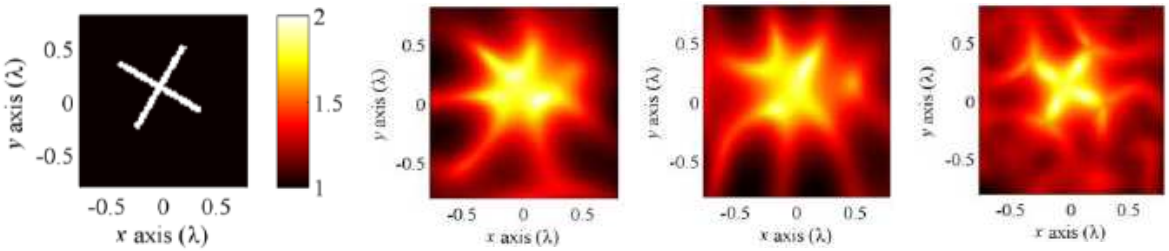

Figure 1: Example of a cross-structured dielectric scatterer. (a) Dielectric profile. (b) LSM with $\hat{x}$ directed dipole as the fundamental source. (c) LSM with $\hat{y}$ directed dipole as the fundamental source. (d) Proposed variation of LSM.

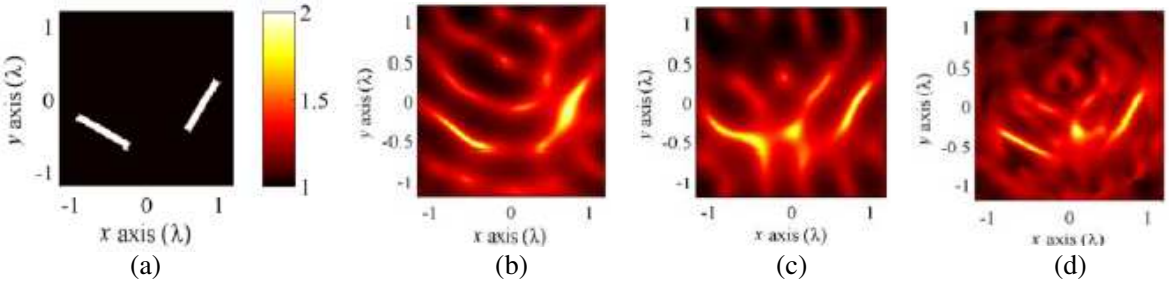

Figure 2: Example of two dielectric bars placed at right angles and not oriented exactly with the coordinate axes. (a) Dielectric profile. (b) LSM with $\hat{x}$ directed dipole as the fundamental source. (c) LSM with $\hat{y}$ directed dipole as the fundamental source. (d) Proposed variation of LSM.

Session 1A4
Antennas, Waves and Shielding

Dual Band Microstrip Antenna Working in the Frequency Bands 2.4 GHz and 5.8 GHz

R. Przesmycki, **M. Wnuk**, **L. Nowosielski**, **K. Piwowarczyk**, **and M. Bugaj**
Faculty of Electronics, Military University of Technology
Gen. S. Kaliskiego 2 Str., Warsaw 0-908, Poland

Abstract— The fast development technology of wireless internet access and the requirements to comply of the standards applied to the WLAN (Wireless Local Area Network) as well as the possibility of using the ISM (Industrial, Scientific, Medical) frequency bands in the ranges 2400–2500 MHz and 5725–5875 MHz has forced demand for dual-band antennas, which can be implemented in stationary and mobile devices. Using antennas in mobile devices provides to requirement for unidirectional radiation patterns. This requirement, and additionally requirements on the size and electrical parameters of antenna meets mostly built antenna in microstrip technology.

One of the ways implementation of dual-band microstrip antenna is a double T antenna, which composed of two radiators in the shape of the letter T. The double T antenna can be considered as two parts placed on one side of the laminate. They are supplied 50 Ω microstrip line placed on the same side of the laminate. On the second side dielectric is a ground plane (Fig. 1). One radiating element of antenna is operating in the lower frequency band. The second radiating element is designed for higher frequency band. Using different lengths of the horizontal line, and the thickness of the radiating elements allows for wider frequency bandwidth.

The paper shows the dimensional model of the antenna made in microstrip technology, working in two frequency bands −2.4 GHz and 5.8 GHz. This antenna can be used in mobile wireless networks. The paper shows the results of simulation of radiation characteristics and electrical parameters of designed antenna made in the software CST Microwave Studio and the measurement results performed in anechoic chamber in the Electromagnetic Compatibility Laboratory in Military University of Technology in Warsaw, Poland.

Analysis Different Methods of Microstrip Antennas Feeding for Their Electrical Parameters

Marek Bugaj, **Rafal Przesmycki**, **Leszek Nowosielski**, **and Kazimierz Piwowarczyk**
Faculty of Electronics, Military University of Technology
Gen. S. Kaliskiego 2 Str., Warsaw 00-908, Poland

Abstract— The paper describes problems related to antenna technology. The paper shows the construction of different microstrip antennas on a dielectric substrate operating on 1.8 GHz. Microstrip antennas in antenna technology appeared relatively late, but in recent years has been a very large development of the design of these antennas and the huge interest in their capabilities. Microstrip antennas are often used in all areas of radio communications. This is due to the simplicity of their design, ease of implementation and relatively low production costs. An important advantage of these antennas is their shape, small size, low weight and aesthetic appearance. Microstrip antennas also provide high repeatability parameters and high resistance to weather conditions.

The article presents four models of single-layer microstrip antenna operating on the same 1.8 GHz frequency. Each of antennas was feed in other ways. For each of the antenna models designer set parameters such as VSWR, input resistance, input reactance and radiation pattern. Antenna model that characterized the best parameters was constructed. The article presents the results of measurements of the antenna built in the anechoic chamber. The results were compared with those obtained in simulation using CST software. Also presents the detailed design of the antenna, which has been built. The article also analyzes the results of computer simulations and measurements, thereby demonstrating the advantages and disadvantages of microstrip antennas with different feeding.

Wearable Antenna Constructed in Microstrip Technology

Marian Wnuk, **Marek Bugaj**, **Rafal Przesmycki**,
Leszek Nowosielski, **and Kazimierz Piwowarczyk**
Faculty of Electronics, Military University of Technology
Gen. S. Kaliskiego 2 Str., Warsaw 00-908, Poland

Abstract— The paper describes problems related to antenna technology. The paper shows the construction of wearable microstrip antennas on a dielectric substrate. Microstrip antennas in antenna technology appeared relatively late, but in recent years has been a very large development of the design of these antennas and the huge interest in their capabilities. Microstrip antennas consist of a patch of metalization on a ground surface. These are low-profile, lightweight antannas, most suitable for aerospace and mobile applications. Microstrip antennas also provide high repeatability parameters and high resistance to weather conditions. Recently, the so-called body-centric communication (focused around the human body) has become a very big importance in the field of wireless communications. Typically, the requirements for this type of antennas used in modern solutions include small size and weight, low cost, virtually maintenance-free and no need to install. Communication-centric body type is of interest to areas such as emergency medical, firefighting, and above all military. However wearable antenna can also be used by athletes for example for monitoring.

The paper presents the design of the wearable antenna made in microstrip technique working at a frequency of 1.8 GHz. Presents the results of numerical analysis of the present antenna, and the results obtained by experimental measurement. The article presents the detailed dimensions of the created model. In the paper presented the results of measurements of the antenna in the anechoic chamber placed on free space and on human body. The article analyzes also the results of computer simulations and measurements, thereby demonstrating the advantages and disadvantages of microstrip antennas with different feeding.

Coaxial Cables Shielding Efficiency Measuring Methodology

L. Nowosielski, **M. Wnuk**, **R. Przesmycki**, **K. Piwowarczyk**, **and M. Bugaj**
Faculty of Electronics, Military University of Technology
Gen. S. Kaliskiego 2 Str., Warsaw 00-908, Poland

Abstract— The article concerns problems connected with electromagnetic compatibility (EMC). Its aim is to present a sample application of measuring position and methodology of measuring shielding efficiency of coaxial cables in the frequency range from 30 MHz to 950 MHz. In the article a description of the position for measuring shielding efficiency of coaxial cables on the basis of the documents: PN-EN 50080-2 and CISPR 16-2-2 Ed.2 has been presented. The aim of these studies is to obtain measuring data essential for calculation of shielding efficiency of coaxial cables. In the article sample results from measurements of shielding efficiency of two coaxial cables (coaxial cable with a constant shield of the Heliax ETS1-50T type and coaxial cable with a shield in the form of copper braid with impedance 50 Ω) in the frequency range from 30 MHz to 950 MHz have been shown. The above mentioned position is used for conducting research in the Laboratory of Electromagnetic Compatibility, Military University of Technology, which has accreditation granted by the Polish Accreditation Centre.

The Conducted and Radiated Emission Levels from IT Devices

Rafal Przesmycki, **Marian Wnuk**, **Leszek Nowosielski**,
Kazimierz Piwowarczyk, **and Marek Bugaj**
Faculty of Electronics, Military University of Technology
Gen. S. Kaliskiego 2 Str., Warsaw 00-908, Poland

Abstract— Telecommunications and data communications devices are integral part of complex systems, which determine the correct functioning of economy. Efficiency and reliability of the functioning of electric and electronic devices decide about the functioning and development of national economy. To a large extent it depends on hazards and the level of disturbances occurring in the environment surrounding us. Thus it is necessary not only to study sensitivity of electric and electronic devices to electromagnetic fields but also to control the level of electromagnetic disturbances emitted to the surrounding environment through different ways.

The article concerns problems of electromagnetic compatibility of contemporary IT devices. Particular attention was paid to undesirable emissions, which are by-products generated unintentionally during realization of basic functions of device. In the article the methodology of measuring conducted emission on supply terminals of IT devices according to the PN-EN 55022:2006 standard in the frequency range from 0.15 MHz to 30 MHz has been presented as well as the methodology of measuring radiated emissivity of IT devices in accordance with the norm: PN-EN 55022:2006 in the frequency range from 30 MHz to 6000 MHz. Also the results of measurements conducted on particular number of central processing units have been demonstrated along with keyboards and mice produced in the years 2007–2010 and next their analysis has been made.

EMC Filters Attenuation Measuring Method

Kazimierz Piwowarczyk, **Marian Wnuk**, **Leszek Nowosielski**,
Rafal Przesmycki, **and Marek Bugaj**
Faculty of Electronics, Military University of Technology
Gen. S. Kaliskiego 2 str., 00-908 Warsaw, Poland

Abstract— Electromagnetic compatibility (EMC) is the ability of an electronic system or subsystem to reliably operate in its intended electromagnetic environment without either responding to electrical noise or generating unwanted electrical noise. Electromagnetic interference (EMI) is the impairment of the performance of an electronic system or subsystem by an unwanted electromagnetic disturbance. In general the public mains power supply voltage waveform is sinusoidal, which means that it includes only the fundamental frequency (50 or 60 Hz) without any harmonic multiples of this frequency. Purely resistive circuits such as filament lamps or heaters, when powered from the mains, draw a current that is directly proportional to the applied voltage, and do not create any extra harmonic components. By contrast, non-linear circuits do draw a non-sinusoidal current, despite the applied voltage being sinusoidal. All non-linear currents, however, will cause harmonics currents, i.e., currents with frequencies that are integer multiples of the supply frequency. Traditionally, harmonic pollution was only a concern for larger installations, particularly for power generation and distribution and heavy industry. But the modern proliferation of small electronic devices, each drawing perhaps only a few tens or hundreds of watts of mains power, and usually single-phase (such as personal computers), has brought the problem of mains harmonics to the fore even in domestic and commercial applications. Of all the above examples, it is the electronic DC power supplies that are causing the most concern due to the increasing numbers of electronic devices such as TV sets in domestic premises, information technology equipment in commercial buildings and adjustable-speed drives in industry.

The aim of this work is to present the attenuation measurement procedure measurement and laboratory stand for filters used to interference suppression in power and telecommunication lines. The procedure is based on the CISPR 17 : 2000 standard. The article describes the attenuation measurement system for filter with impedance different then 50 Ω. The article presents the measured attenuation characteristics of set of EMC filters which are offered on the market. The calibration of measurement method is presented too.

The Absorption Effectiveness of Pulverized Metallic Glass at Microwaves

R. Kubacki[1], **J. Ferenc**[2], **R. Przesmycki**[1], **and M. Wnuk**[1]

[1]Faculty of Electronics, Military University of Technology, Warsaw, Poland
[2]Faculty of Materials Science and Engineering, Warsaw University of Technology, Warsaw, Poland

Abstract— The permittivity and permeability broadband measurements of solid materials are commonly performed with the use of coaxial fixtures. The basic measurements are based on scattering parameters of a sample. Coaxial line techniques allow to measure the constitutive parameters of materials over wide frequency. In the typical configuration of a solid material in coaxial line for measuring the permittivity and permeability, the sample completely fills the cross section of a holder.

For the measurements of powdered materials in coaxial lines, two additional walls have to be used. In such a case, the measured sample will be a composite material, consisting of powdered material and two walls. In fact, the walls can be made of any dielectric material, because the scattering parameters of wall are determined in additional measurements.

Using the graph method for network branch one can obtain formulas of resultant scattering parameters Sw_{ik} of the whole composite (material under test and 2 walls):

$$Sw_{11} = E_{11} + E_{21}\frac{(1 - E_{11}S_{11})\ S_{11} + E_{11}S_{21}^2}{(1 - E_{11}S_{11})^2 - E_{11}^2S_{21}^2} \tag{1}$$

$$Sw_{21} = \frac{E_{21}^2 S_{21}}{(1 - E_{11}S_{11})^2 - E_{11}^2S_{21}^2} \tag{2}$$

where:

Sw_{ik} – scattering parameters of the whole composite material

E_{ik} – scattering parameters of the wall

S_{ik} – scattering parameters of the powdered sample.

Equations (1) and (2) allow to obtain formulas for scattering parameters of a powdered sample in the following relationships:

$$S_{11} = \frac{\left(E_{21}^2 + E_{11}H\right)H - E_{11}Sw_{21}^2}{\left(E_{21}^2 + E_{11}H\right)^2 - \left(E_{11}\,Sw_{21}\right)^2} \tag{3}$$

$$S_{21} = \frac{E_{21}^2\,Sw_{21}}{\left(E_{21}^2 + E_{11}H\right)^2 - \left(E_{11}Sw_{21}\right)^2} \tag{4}$$

where:

$$H = Sw_{11} - E_{11}$$

Scattering parameters (3) and (4) are the functions of unknown parameters ε and μ of the specimen. Having the scattering parameters of the powder-sample (S_{ik}), it is possible to calculate the permittivity and permeability using the method proposed by Nicolson, Ross and Weir (NRW method). In their model, values of complex permittivity and permeability are determined according to the following formulas:

$$\mu = -j\frac{1+\rho}{1-\rho}\frac{\lambda}{2\pi L}\ln\left(\frac{1}{T}\right) \tag{5}$$

$$\varepsilon = -\frac{1}{\mu}\left[\frac{\lambda}{2\pi L}\ln\left(\frac{1}{T}\right)\right]^2 \tag{6}$$

In this paper the values of complex permittivity and permeability of powdered nanocrystallized $Fe_{73,5}Si_{13,5}B_9Nb_3Cu_1$ alloy (Finemet) versus frequency have been measured with the use of the proposed method.

Nanocrystalline powder was measured with the use of the proposed method. The nanocrystalline powder was sieved to obtain four groups with different particle size. In this study, the following groups of powders were investigated: group A – with particle size smaller than 25 µm, group B – (25–50) µm, group C – (50–100) µm and group D with particle sizes (100–200) µm. After the measurement, the density was determined for each group. The obtained densities are: group A – 3.1 (±0.05) g/cm^3, group B – 3.3 (±0.05) g/cm^3, group C – 3.2 (±0.05) g/cm^3 and group D – 2.6 (±0.05) g/cm^3. For comparison, the bulk density of the investigated alloy is 7.3 g/cm^3. Measurements of permittivity and permeability were performed for these four groups of powder with different particle sizes. Each investigation was conducted in the frequency range from 0.2 to 10 GHz.

Measurements of complex relative permittivity and permeability were carried out with using a vector network analyzer. This system consisted of a 7 mm coaxial air-line, equipped with measurement cables and LPC7 connectors. The center conductor of the coaxial air-line is 3.04 mm in diameter to receive the 50 Ω characteristic impedance of the holder. The system measures the magnitudes and phases of S-parameters of a sample. In this case, scattering parameters refer to the composite sample — Sw_{ik}. At first, the empty coaxial air-line was employed to calibrate the system. The additional tools consisted of auxiliary air-lines were used to obtain the calibration.

Using the described method values of complex permittivity and permeability and absorption effectiveness in function of frequency in the range from 0.2 to 10 GHz have been presented.

NO and N_2O Detection with CEAS Method

J. Wojtas[1], **Z. Bielecki**[1], **T. Stacewicz**[2], **J. Mikolajczyk**[1], **R. Medrzycki**[1], **and B. Rutecka**[1]

[1]Institute of Optoelectronics, Military University of Technology
2 Kaliskiego Str., Warsaw 00-908, Poland
[2]Institute of Experimental Physics, University of Warsaw
69 Hoza Str., Warsaw 00-068, Poland

Abstract— We present an application of quantum cascade lasers for NO and N_2O sensors. Operation of the system is based on cavity enhanced absorption spectroscopy (CEAS), which is one of the most sensitive optoelectronic technique of trace matter detection.

Vibronic molecular transitions are used for the detection of both nitric oxide and nitrous oxide. Wavelength of these transitions are situated in mid-infrared spectral range. Achievement of optimal sensitivity and selectivity requires avoiding of interferences by absorption lines from other trace gases which are commonly present in atmosphere (like H_2O or CO_2). Careful studies show that the best results can be achieved in spectral regions: 5.23 µm–5.29 µm for NO and 4.46 µm–4.54 µm for N_2O.

Setup of the sensor consists of pulsed laser source, optical cavity and a photodetector. As a radiation source single mode quantum cascade lasers (QCL) are applied (Alpes Laser SA). Their narrow emission lines could be precisely tuned to the wavlength of interest. The lasers pulses are characterized by high power and good spectral stability. Optical cavity is built with spherical mirrors of high reflectance. The optical signal from the cavity output is registered with a specially developed low noise detection module (VIGO System SA).

Detection limit of the sensors of single ppb was obtained at the wavelength 4.53 µm and 5.26 µm respectively. Therefore sensors can be applied to ambience monitoring and e.g., for the monitoring of luggage in ports, on airports, at entry points, in strategic for the state objects and rooms also in undertakings with the counteraction to terrorist attacks.

ACKNOWLEDGMENT

The researches were supported from the Ministry of Science and High Education of Poland (Projects No. OR00002807, No. ON515216839).

Asymmetric Coplanar Strip Semielliptical Dual Band Antenna

R. Dinesh, **D. Laila**, **V. P. Sarin**, **C. M. Nijas**, **V. A. Shameena**, **and P. Mohanan**
Centre for Research in Electromagnetics and Antennas (CREMA), Department of Electronics
Cochin University of Science and Technology, Cochin, Kerala 682022, India

Abstract— A novel compact dual band asymmetrical coplanar strip fed semi elliptical antenna is presented and discussed in this paper. The prototype is fabricated on a substrate of permittivity 4.4 with an overall dimension of 21 mm × 10 mm × 1.6 mm. The proposed antenna is designed to operate in DCS 1800/1900, 2.4 GHz (2400–2484 MHz) and 5 GHz (5150–5825 MHz) bands for WLAN applications in IEEE 802.11a/b and HIPERLAN2 systems. The antenna has a 2 : 1 VSWR bandwidth of 39% for the fundamental mode centered at 2.1 GHz and 35.5% for the first harmonics centered at 5.52 GHz.

The simulation and measurement are carried out using Ansoft HFSS and HP8510C network analyzer respectively. The agreement between the simulation and measurement is fairly good over the operating band. Compact dual band operation is achieved by folding the ground planes of the coplanar strip transmission line in a semi elliptic manner. The antenna consist of a semi elliptical ring of width 1.5 mm with major radius 10.5 mm and eccentricity 0.95. The inner semi ellipse of major radius 8.8 mm with eccentricity 0.8 is directly connected to inner conductor of SMA connector. It is found that the impedance matching for the lower band increases with decrease in eccentricity of semi ellipse. The Principal E and H plane patterns of the antenna for the two bands are also presented in this paper. The antenna exhibits good radiation patterns for both the bands. The antenna is compact and it exhibits high bandwidth, omni-directrional radiation pattern and moderate gain for both the operating bands. The uniplanar nature, simple feeding technique and compact structure make it easy for modular designs. Detailed parametric analysis of the proposed antenna is also presented.

Band Notched Ultra Wide Band Slot Antenna

V. A. Shameena, U. Deepak, R. Sujith, D. Laila, R. Dinesh, and P. Mohanan
Centre for Research in Electromagnetics and Antennas, Department of Electronics
Cochin University of Science and Technology, Cochin-22, India

Abstract— A compact printed CPW fed band notched ultra wideband (UWB) antenna is presented and discussed. The antenna comprises of a triangular slot loaded ground plane with a T shaped strip radiator. Two open ended slits are made at the top end of the T stub to reject 5–6 GHz frequency band. This compact antenna having a dimension of $26 \times 26\,\mathrm{mm}^2$ is printed on a substrate of dielectric constant 4.4 and thickness 1.6 mm. The simulation and measurement are carried out using Ansoft HFSS and HP8510C network analyzer respectively. The agreement between the simulation and measurement is fairly good over the operating band. The radiation patterns of the antenna in two principle planes are also measured and a monopole like pattern is obtained. An average gain of 3 dBi is noted throughout the operating band except at the notched frequency where a gain of -6 dBi is obtained. The antenna designed has a radiation efficiency of more than 70% in the pass band and a reduction in the rejected band.

Transient response of the antenna is studied by modeling the antenna by its transfer function. For this, the transmission coefficient S_{21} is measured in the frequency domain for the face-to-face and side-by-side orientations. The transfer function is computed from this. Fourth derivative of a Rayleigh pulse is selected as the transmitted pulse. The output waveform at the receiving antenna terminal can be expressed by convoluting the input signal and the transfer function. It is seen that the shape of the pulse is preserved very well in all the cases. Using the reference and received signals, it becomes possible to quantify the level of similarity between signals. The fidelity factor is a measure of the capability of an antenna to preserve a pulse shape. This factor is determined by the absolute value of the maximum of the cross correlation coefficient of the transmitted and received signals. Fidelity is found to vary from 0.8689 to 0.9687. These values for the fidelity factor show that the antenna imposes negligible effects on the transmitted pulses.Since FCC UWB operating bandwidth definition is based on power emission limits, investigation of the effective isotropic radiated power (EIRP) emission level of the antenna with a given excitation signal is essential. Measured EIRP emission level of the antenna excited with a fourth order Rayleigh pulse is plotted and EIRP of the antenna satisfies the FCC masks for the entire UWB band.

Broadband Circular Polarization Truncated Horn Antenna

T. H. Gan and E. L. Tan
School of EEE, Nanyang Technological University, Singapore

Abstract— Circular polarization horn antenna radiates two linear polarizations that are orthogonal and 90° out of phase. These circular polarization modes are usually obtained using complex feeding structures such as dual linear feed with 90° phase shifter or waveguide polarizers.

In this work, we present the design of a broadband circular polarization truncated horn antenna. The geometry of the truncated horn antenna is shown in Figure 1. It does not require any complex feeding structure and uses only a coaxial feed extended with a simple electric field coupling probe. The cross section of the truncated horn antenna is similar to a single feed truncated microstrip antenna. Therefore the basic operating principle of the truncated microstrip antenna can be used to describe the truncated horn antenna. The corners of the horn and feed waveguide are truncated to generate the circular polarization modes and a broad 3 dB axial ratio bandwidth which is insensitive to the probe feed dimension is achieved.

An S band Right Hand Circular Polarization (RHCP) truncated horn antenna was designed, simulated, fabricated and measured. The simulation was performed using HFSS ANSYS Inc. Figure 2 plots the simulated and measured axial ratio in the boresight direction. The measured axial ratio is better than 3 dB from 2.0 GHz to 2.6 GHz, thus the 3 dB axial ratio bandwidth is 26%. The agreement of the simulated and measured results for the gain, radiation pattern and return loss is good.

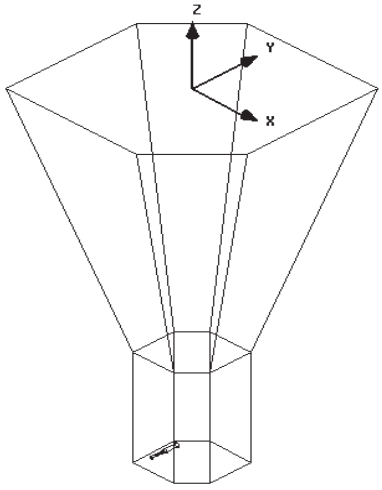

Figure 1: Geometry of truncated horn antenna.

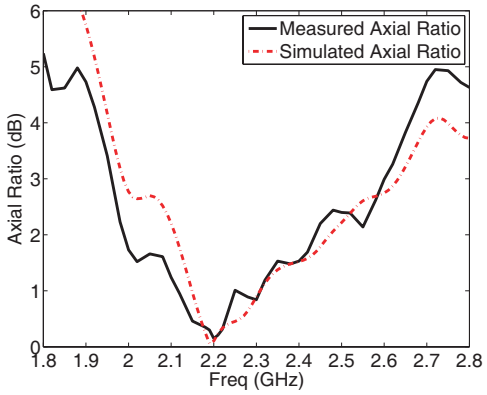

Figure 2: Simulated and measured axial ratio in the boresight direction.

Session 1A5
Next Generation Broadband Access

Estimation of Specific Attenuation Due to Scattering Points for Broadband PLC Channels

C. T. Mulangu, T. J. Afullo, and N. M. Ijumba
School of Electrical, Electronic and Computer Engineering
University of Kwazulu-Natal, Private Bag X54001, Durban 4000, South Africa

Abstract— The multipath propagation models in power-line communication channel (PLC) are some of the most successful models which are based mainly on scattering points located where impedance mismatch occurs. In such models, not only the desired signal, but also one or more delayed and attenuated versions of it get to the receiver. The attenuation is basically due to different routes that the signal will take before getting to the receiver hence at the end there are many signals that reach the load at different times. In this submission, we investigate the number of branches and the numbers of reflections that occur at each node; the Mie scattering theory is applied to nodes in the network in order to determine the resulting specific signal attenuation in the network. The proposed model is compared to theoretical model and the estimated error determined by root mean square and chi-square tests. Finally, a power law model is proposed where only the number of branches is needed to estimate the specific attenuation.

Transmission Analysis of Optical OFDMA-based Passive Optical Network Architecture Supporting Heterogeneous Services

Fan Bai, Peng Liu, and Mitsuji Matsumoto
Global Information and Telecommunication Studies, Waseda University, Japan

Abstract— The on-going surge in demand of high-speed broadband services such as Internet Protocol Television and High-Definition TV signals. For the next generation hybrid access networks, considering the increasing the bandwidth and data rate while keeping acceptable costs. Our research focus on orthogonal frequency division multiple access (OFDMA) technology over passive optical network (PON). Recently, optical OFDMA (O-OFDMA) research progress reviewed extensively in terms of adaptive transceiver design, intensity modulators, synchronisation techniques and network architectures. In this paper, we propose a novel architecture for Optical OFDMA over PON. We present the performance of this O-OFDMA PON system using IM/DD (intensity modulation/direct detection). Analyse the BER (bit error rate) through the simulation. Then, We give an overview on application of O-OFDMA over PON. Furthermore, compare the characteristics of O-OFDMA model with RF OFDMA model over PON. The obtained results can be useful for designing, predicting, and evaluating the O-OFDMA PON system.

Emerging Optical Broadband Access Networks from TDM PON to OFDM PON

Redhwan Q. Shaddad[1, 2], **Abu Bakar Mohammad**[1], **Sevia M. Idrus**[1], **Abdulaziz M. Al-hetar**[2], **and Nasir A. Al-geelani**[3]

[1]Photonic Technology Center, InfoComm Research Alliance, Universiti Teknologi Malaysia, Malaysia
[2]Communication and Computer Engineering Department
Faculty of Engineering and Information Technology, Taiz University, Yemen
[3]Institute of High Voltage and High Current, Universiti Teknologi Malaysia, Malaysia

Abstract— The bandwidth requirements of the telecommunication network users increased rapidly during the last decades. The emerging optical access technologies must provide the bandwidth demand for each user. The passive optical access networks (PONs) support a maximum data rate of 100 Gbps by using the orthogonal frequency division multiplexing (OFDM) technique in the optical access network. In this paper, the enabling optical broadband access networks with many techniques are presented and compared. The architectures, advantages, disadvantages, and main parameters of these access networks are discussed and reported. A combination of different techniques in a hybrid PON network introduces a cost-effective, reliable and efficient access network. The hybrid optical broadband access technologies are presented which have many advantages to become next-generation broadband access networks. The concept and architecture of the hybrid optical broadband access networks are discussed.

Over 300 km Repearterless Transmission Systems for Terrestial Applications in Malaysia

Zainuddin Lambak, **Kharina Khairi**, **Zulkifli Hamzah**,
Najib Abdul Rahman, **and Fong Kok Hann**
Next Generation Access, Malaysia

Abstract—

Introduction: Conventional repeaterless systems are typically installed as submarine transmission systems where stations separated by several hundreds of kilometers can be connected without inline amplifiers and the associated power and maintenance issues. With new technologies coming online, wavelength division multiplexing (WDM) transmission systems of up to 505 km have been demonstrated experimentally [1, 2].

As a consequence of the continued reduction of component costs, repeaterless transmission systems are now becoming attractive to terrestrial applications. One demonstration was the "hut-skipped" transmission system [3]. Moving forward, many terrestrial transmission systems will benefit from the long reach of such systems. A few examples of these applications are transnational transmission over land boundaries, rural broadband deployment and transmission across geographic areas where access for maintenance is limited and difficult. The availability of such repeaterless systems at reduced costs would encourage the increase of broadband penetration for pockets of population outside of major cities.

In this paper, we investigate the architecture and system design of repeaterless WDM transmission systems of over 300 km operating at 8×10 Gbps by simulating the feasibility and performance of such systems for terrestial applications using conventional G.652 fibers. The repeaterless system is simulated with 3 types of modulation format; Non-Return to Zero (NRZ), RZ (Return-to-Zero) and DQPSK modulation formats using a 10 Gb/s Pseudorandom Binary Sequence generator (PRBS).

System Design and Experimental Set-up: Figure 1 shows the schematic diagram of a 300 km repeaterless system under evaluation. The transmission sub-system consists of 10 Gb/s externally modulated transmitter, an 8-channel Array Waveguide (AWG), a pre dispersion compensation, Erbium doped fiber amplifier (EDFA) booster and a co-propagating polarization multiplexed Raman amplifier. The 300 km fiber route consists of 1 section of 300 km of standard G.652 fibers. At the receiving end, the incoming signal encounters a counter-propagating polarization multiplexed Raman pump, a low noise EDFA, a post dispersion compensation, an 8-channel AWG and a 10 Gb/s amplified photo receiver.

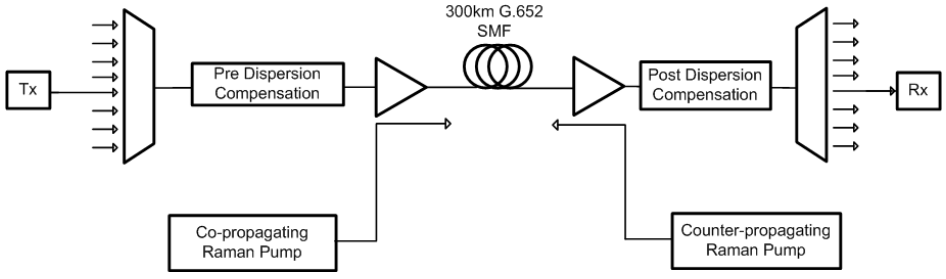

Figure 1: A simplified schematic diagram showing the 300 km repeaterless transmission system.

REFERENCES

1. Bakhshi, B., et al., "Ultimate capacity limitations in repeater-less WDM transmission up to 505 km," *OFC/NFOEC*, OThC4, 2009.
2. Golovchenko, E. A., et al., "Pushing the reach of repeaterless transmission systems," SubOptic, 2007.
3. Chen, D. Z., et al., "Long-haul "hut-skipped" transmission of mixed 10 & 40 Gb/s over deployed SSMF fiber in MCI's Dallas fiber loop using hybrid Raman-erbium doped fiber amplifiers," *Tech. Digest OFC/NFOEC*, Vol. 2, 3, 2005.

Scattering Points Size Distribution for Indoor Broadband PLC Channels

C. T. Mulangu, T. J. Afullo, and N. M. Ijumba
School of Electrical, Electronic and Computer Engineering
University of Kwazulu-Natal, Private Bag X54001, Durban 4000, South Africa

Abstract— The multipath propagation of the power-line communication channel (PLC) arises from the presence of several branches and impedance mismatches that cause multiple reflections. Each path comprises of scattering points that are reflected at specific number of times at specific points of discontinuityalong its routes. Scattering points are located where impedance mismatch occurs and can be seen as spherical pointswith approximate diameter sizes foreach branch. In such models, not only the desired signal, but also one or more delayed and attenuated versions of it get to the receiver. In [1], scattering points' spatial allocation, by which path amplitude distributions and path arriving time distributions are proposed to follow the lognormal distribution for different number of branches. Based on those findings in [1], we investigate the number of branches and the numbers of reflections that occur at each node. In this study, it is assumed that the scattering point for each diameter is dependent on the number of reflections. Thus, the scattering point diameter densityis derived in order to determine the scattering size distribution and the probability density distribution of the path. The proposed modelshows that there are more contributionsfrom branches with small diameters to the average attenuation in indoor PLC channel.

REFERENCES

1. Papaleonidopoulos, I. C., C. N. Capsalis, C. G. Karagiannopoulos, and N. J. Theodorou, "Statistical analysis and simulation of indoor single-phase low voltage power-line communication channels on the basis of multipath propagation," *IEEE Trans. Consumer Electronics*, Vol. 49, No. 1, 89–99, February 2003.

ONU Monitoring and Management Employing an In-band Ethernet Communication in FTTH/x System

Z. A. Manaf, **M. S. Salleh**, **K. Khairi**, **Z. Hamzah**, **M. N. Abd. Raman**, **D. A. M. Ssi**, **R. Mohamad**, **and Z. M. Yussof**
Next Generation Access Network Lab, TM Research & Development Sdn. Bhd.
Lingkaran Teknokrat Timur, Cyberjaya, Selangor 63000, Malaysia

Abstract— FTTH is an emerging technology with the capability to deliver a high speed broad band services to the subscribers. Its flexibility and reliability are among major factors that drive the implementation world wide. In relation to this matter, the technique for managing and monitoring the element is a crucial subject to look into in order to ensure smooth operation as well as network survivability. In principle, there are two major elements that will be monitored and managed in any FTTH system, namely, the Optical Line Terminal (OLT) and Optical Network Unit (ONU). The ONU can only be managed through the OLT utilizing data link layer (Layer 2 of the OSI Model), and using only a proprietary protocol and a dedicated software application from the Network Operation Center (NOC) office. Apparently, only the defined protocol, commands and messages between the OLT and ONU chipset will be handled. However, for Ethernet or Internet Protocol (IP) based management and communication, a suitable customer's device has to be connected to the ONU externally.

In this paper, an enhancement to the existing ONU management system is proposed, developed and demonstrated as a proof of concept solution. An in-band management technique has been developed by integrating a microprocessor and data switching chip with the ONU in a single board. The main idea is to provide an Ethernet or IP based management link for remote management from the NOC office rather than MAC based only. Consequently, the ONU could also be seen as a manageable IP node while the existence of the microprocessor and data switch would enable various types of monitoring agents and network application tools to be ported for remote monitoring as well as diagnostics purposes.

With this unique solution, it serve as a complimentary features to the existing ONU management and monitoring function and additional external managed devices could be eliminated for a cost effective and simpler FTTH deployment and maintenance process.

Implementing Multiple WiFi Hotspots Using One Single Embedded Platform

Chun Yeow Yeoh
Lab Next Generation Access, TM Research & Development Sdn. Bhd., Malaysia

Abstract— To offer the mobility to existing fixed broadband customers, Telekom Malaysia (TM) has opted to deploy the WiFi hotspot using the 2.4 GHz ISM band. The WiFi hotspot is basically based on the IEEE 802.11 standard. 802.11 is an increasing popular standard that can be easily found in smart devices. Mobile service providers in Malaysia are also tried to offload their mobile data from 3G to WiFi due to the traffic growth. The common problem for WiFi deployment is site acquisition, a time-consuming and costly process. WiFi hotspot is realized using an Access Point (AP) that allows the public users with client adapter to connect to it. Normally, user is required to go through the authorization and authentication process before gaining the access to Internet. The suitable sites for WiFi deployment are public places, such as shopping malls, coffee shops, school, parks and etc. Technically, placing many APs within a site creates the interferences amongst the APs since there are only 3 non-overlapping channels in 2.4 GHz. Thus, a single AP which can allow more than one hotspot services is an interesting solution to the service provider. The service provider that owns the infrastructure can then "lease" it to other operators as well. In TM R&D, we have successfully found out a way to implement more than one hotspot service using one single embedded platform. Our solution is based on the current open sources, such as OpenWRT. It only requires the firmware update to the existing embedded platform either with 802.11 chipset or without 802.11 chipset. In this paper, we discuss the technical approach for providing multiple wireless hotspot service using one single embedded platform and also the verification results. Lastly, we also discuss the technical challenges and issues while deploying the WiFi hotspot, especially for AP with multiple hotspot services.

Low Profile Monolithic Array Si Avalanche Photodiodes for Alignment Tracking Application

Mazlaini Yahya[1], **Zaiki Awang**[2], **and Mohd Khairil Azhar**[2]

[1]TM Research & Development, Malaysia
[2]Microwave Technology Centre, University Teknologi MARA, Malaysia

Abstract— Fabrication of low profile monolithic array Si avalanche photodiodes (APDs) is reported. Single element Si APD structure of p^+-i-p-n^+ has high gain and low injection noise. A monolithic multi element APD of similar structure can have two significant different element segmentation structures with individual advantages. The first segmentation structure has common avalanche region of p-substrate with segmentation p^+. The structure has zero dead space between adjacent elements and high element-to-element isolation. The second segmentation structure has common p^+ contact and separate avalanche region producing significant dead space and field-fringing effect. Large area 2×2 array APD devices of the two segmentation structures are developed for performance and fabrication complexity measurement.

Monolithic Double Quadrant Array Si Avalanche Photodiodes for High Performance Dynamic Alignment Tracking Application

Mazlaini Yahya[1], **Zulkalnain Mohd Yusof**[1], **Zaiki Awang**[2], **and Mohd Khairil Azhar**[2]

[1]TM Research & Development Sdn Bhd, Malaysia
[2]Universiti Teknologi Mara, Malaysia

Abstract— Single quadrant 2×2 array avalanche photodiode (APD) is commonly used for static position sensing, target tracking and ranging, fluorescence spectroscopy, scintillation detection and nuclear imaging. Double quadrant array Si APD offers high performance dynamic alignment tracking for airborne application. The double quadrant 2×4 array avalanche photodiode provides better accuracy aligment tracking data acquisition. Common p^+ contact with separate avalanche region is developed for such application. Performance of single and double quadrant APD is measured and compared on dynamic alignment tracking formulation and application.

Particle Swarm Optimization Based Reception Diversity in Rayleigh Fading Channel

M. Riahi Manesh, **M. Akbari**, **S. A. Rafiei Taba Zavareh**,
P. Shahabi, **and Z. Pouladmast Ghadiri**
Faculty of Engineering, Multimedia University, Cyberjaya, Malaysia

Abstract— The performance of wireless communication systems is considerably affected by the multipath propagation phenomena. Diversity techniques are one of the prominent ways to improve the reliability of wireless communication systems. The deleterious outcomes of fading can be mitigated by these techniques. The main idea of diversity methods is to extract information from received signals transmitted over multiple fading channels to improve the received signal to noise ratio (SNR). The commonly used diversity techniques are maximal ratio combining (MRC), equal gain combining (EGC), and selection combining (SC). The purpose of these techniques is to find a set of weights used to combine the received signals in different diversity branches. If the channel is perfectly estimated, the MRC can be applied to maximize the output SNR and minimize the bit error rate (BER). However, estimated channel is scarcely perfect in practice which degrades the system performance. In this work, a diversity combining technique based on particle swarm optimization (PSO) is proposed in which the received signals are weighted based on PSO algorithm. The proposed PSO based scheme opts for the best weighting coefficients vector, leading to improved performance of the system. The channel estimation error is considered as an additional source of noise with a parameter ρ which is the normalized estimation error correlation coefficient. Results indicate that the proposed method eliminates the need for channel estimation and outperforms the MRC when channel estimation is imperfect while it has approximately the same performance as MRC when channel is perfectly estimated.

Maximizing the Probability of Detection of Cooperative Spectrum Sensing in Cognitive Radio Networks

M. Akbari, **M. Riahi Manesh**, **S. A. Rafiei Taba Zavareh**, **and P. Shahabi**
Faculty of Engineering, Multimedia University, Cyberjaya, Malaysia

Abstract— To support the ever-increasing demand for radio spectrum, the cognitive radio (CR) is proposed as a solution to dynamically assign the spectrum based on certain observations. Weighting the coefficients vector is the principal factor influencing the detection performance of cognitive radio networks in soft-detection based cooperative spectrum sensing. Cooperative spectrum sensing can be classified into two main categories of hard-decision fusion (HDF) and soft-decision fusion (SDF). Equal gain combination (EGC) and maximal ratio combination (MRC) schemes have been investigated as a solution for weighting the coefficients vector of all CRs in a linear SDF-based system. However, these methods are not optimal since allocated weights to different users are all equal in the EGC method or are merely based on users' received signal-to-noise ratio (SNR) in the MRC technique. The idea of maximizing the normal deflection coefficient (NDC) and modified deflection coefficient (MDC) to optimize the weighting coefficients vector was also proposed in the literature. Nevertheless, the mentioned methods lead to sub-optimal results, imposing some performance deteriorations on the system. In addition, the SDF-based cooperative sensing using genetic algorithm (GA) was proposed to provide a good solution for weighting the coefficients vector. However the GA-based method suffers from slow convergence and sub-optimality due to its reliance on binary encoding of a naturally-continuous domain. In this paper, the use of particle swarm optimization (PSO) algorithm as a significant method is proposed to optimize the weighting coefficients vector. The proposed technique investigates the best weighting coefficients vector. The performance of the PSO-based proposed method is examined and compared with GA-based technique as well as other conventional SDF schemes through computer simulations. Simulation results confirm the strength of the proposed method compared to all other SDF-based schemes.

Session 1A6a
Metamaterials and Applications

Tuneable Metamaterials Containing Arrays of Magnetically Soft Microwires with GMI Effect

L. V. Panina[1,2], **M. Ipatov**[1], **V. Zhukova**[1], **J. González**[1], **and A. Zhukov**[1]

[1]Dpto. de Física de Materiales, Fac. Químicas, Universidad del País Vasco, San Sebastián 20018, Spain
[2]On leave from School of Computing and Mathematics, University of Plymouth
Plymouth, PL4 8AA, United Kingdom

Abstract— Metamaterials containing long parallel wires can be characterised by plasma-like dispersion of ε_{ef} [1] with a negative value of the real part of the permittivity below the characteristic plasma frequency, f_p. A number of experimental studies confirmed a negative permittivity in the GHz region for wire media. On the other handsurface impedance ζ_{zz} may change under applied magnetic field, H_{ex}, as a result of the MI effect [2]. In this case, the permittivity spectra will depend on H_{ex}.

Here we report on experimental studied of metamaterials containing amorphous ferromagnetic Co-rich microwires exhibiting large MI effect (about 300% at 300 MHz) by free space method. The S-parameters were measured at 0.9–17 GHz in the presence of external field ranging up to 3000 A/m. The effective permittivity spectra were deduced from S-parameters with the help of Reflection/Transmission Epsilon Fast Model.

We report on magnetic field tuneability of the dielectric response in metamaterials with arrays of parallel continuous and short-cut magnetic microwires in the frequency region of 0.9–17 GHz. Both the real and imaginary parts of ε_{ef} show strong variations with H_{ex} owing to the MI effect which controls the losses in the dielectric response. Long-wire metamaterials exhibit a plasmonic type dispersion of ε_{ef} with negative values of its real part below the plasma frequency (GHz range) for wire spacing of about 1 cm and wire diameter of few microns. The presence of H_{ex} suppresses low-frequency plasmons increasing the value of the real part of the permittivity. For cut-wire composites we observed a resonance type of ε_{ef} dispersion due to the dipole resonance in wires at half wavelength condition. Application of H_{ex}broadens the resonance and shifts it towards the higher frequencies. Therefore, both types of wire composites exhibit strong ε_{ef} (H_{ex}) dependence suitable for applications.

ACKNOWLEDGMENT

We acknowledge support under the MICINN project MAT2010-18914.

REFERENCES

1. Pendry, J. B., A. J. Holden, W. J. Stewart, and I. Youngs, "Extremely low frequency plasmons in metallic mesostructures," *Phys. Rev. Lett.*, Vol. 76, No. 25, 4773–4776, 1996.
2. Makhnovskiy, D. P. and L. V. Panina, "Field dependent permittivity of composite materials containing ferromagnetic wires," *J. Appl. Phys.*, Vol. 93, 4120, 2003.

Deformation of Surface Waves Propagating on 2-dimensional Metamaterial Structure

Osamu Sakai and Dae-Sung Lee
Kyoto University, Japan

Abstract— 2-Dimentional structure of metamaterials work as a supporter of surface waves as well as boundary of propagating waves. One of the popular research targets of metamaterials is a perforated metallic plate which can support a kind of surface waves, referred to as "spoof surface plasmons [1, 2]." It is well known that surface waves whose name is surface plasmon polaritons propagate on a metal surface in a certain condition. Since the electron plasma frequencies of ordinary metals are in or near the visible photon range, we cannot usually expect their propagation at microwaves. However, if holes are aligned in a metallic plate (or a perfect conductor), it can support surface waves similar to surface plasmon polaritons at much lower frequencies. In this structure, holes are arranged on its 2-dimensional plane, and each hole works as a small waveguide for microwaves; when the size of holes is much smaller than the wavelength, a microwave suffers a cutoff phenomenon inside a hole, in which similar features to surface plasmon polaritons are observed.

Such electromagnetic waves confined around a metamaterial structure are affected by a change of permittivity in or near the structure. One example is deformation by micro discharge plasmas occupying holes [3]. When we used a perforate metallic plate, whose inside periodic length was around 2 mm, as a discharge electrode at elevated gas pressures, we could successfully generate plasmas uniformly distributed in the holes. Here, the resonance frequency of the spoof surface plasmons without plasmas was at the sub-terahertz range, and the plasmas work as dielectrics at the corresponding frequency. Consequently, the resonance frequency shifted upwards, and we observed significant decrease and increase of transmitted and reflected sub-terahertz waves, respectively.

Another type of deformation is possible by formation of equivalent defect(s) on the metamaterial structure. Deformation of the propagating modes on 2-dimensional metamaterials will be much enhanced in comparison with the cases of propagation in free space, and its adjustable outputs may become interests in specific scientific and engineering fields.

REFERENCES

1. Pendry, J. B., L. Martin-Moreno, and F. J. Garcia-Videl, *Science*, Vol. 305, 847, 2004.
2. Miyamaru, F. and M. Hangyo, *Phys. Rev. B*, Vol. 71, 165408, 2005.
3. Lee, D.-S., O. Sakai, and K. Tachibana, *Jpn. J. Appl. Phys.*, Vol. 48, 062004, 2009.

A Bandwidth Enhanced Elliptical Metamaterial Antenna

K. L. Sheeja[1], **P. K. Sahu**[1], **and S. K. Behera**[2]

[1]Department of Electrical Engineering, N.I.T. Rourkela, Orissa, India
[2]Department of Electronics and Communication Engineering, N.I.T. Rourkela, Orissa, India

Abstract— In this paper, an elliptical Zeroth Order Resonant (ZOR) antenna based on composite right/left handed (CRLH TL) is proposed. ZOR antennas suffer from a negative drawback of being narrow bandwidth. In this paper, an effort is made to circumvent this negative effect by implementing a coplanar waveguide (CPW) fed elliptical unit cells without vias. The bandwidth, gain and radiation efficiency of the proposed antenna is about 5%, 2.1054 dB and 65.937% respectively at 4.88 GHz ($n = 0$ mode). Simulated results are presented and discussed. The antenna consists of 2 elliptical unit cells flanked symmetrically on both sides by open ended spiral and anti-spiral inductors. The antenna was designed to operate from (4.715 to 4.945) GHz with a reflection coefficient of −24.2836 dB at the zeroth mode (4.88 GHz). The proposed elliptical ZOR antenna serves another purpose of being a very low profile one, exhibiting an omni-directional radiation pattern in H-plane (phi = 0 deg) and a dumb-bell shaped radiation pattern in E-plane (phi = 90 deg). Hence the proposed antenna is aptly suited for wireless applications (IEEE 802.11a standards). All simulations were carried out by using Ansoft HFSS.

Perfect Invisibility Devices with Negative Refraction

J. C. Nacher[1] and T. Ochiai[2]

[1]Department of Complex and Intelligent Systems, Future University Hakodate
116-2 Kamedanakano-cho, Hakodate 041-8655, Hokkaido, Japan
[2]School of Social Information Studies, Otsuma Women's University
2-7-1 Karakida, Tama-shi, Tokyo 206-8540, Japan

Abstract— Recent works have highlighted the application of geometry and conformal mapping theory to meta-materials to guide electromagnetic fields. In anisotropic media, Pendry et al. proposed a coordinate transformation over the electromagnetic fields that allows to redirect them at will [1,2]. The distortion of the fields originated by the transformation media is used to generate the new values for ε and μ, defined in anisotropic media. As a result the electromagnetic waves follow the distorted space with newly generated ε and μ and go around the object and hide it from the sight. An alternative approach was introduced by Leonhardt, where a conformal mapping was used to design cloaking devices in isotropic media [3, 4].

Here, we present a novel method that uses a combination of positive and negative refraction indices, called plus-minus construction [5, 6], that enables us not only to enclose the trajectory of light, but also to achieve perfect invisibility in isotropic media, without both phase delay and reflection. In particular, we introduce a new construction of cloaking devices by performing three successive conformal maps on the space defined by a trivial flat metric. This operation results on a physical space R^2 with a non trivial refractive index. A technical advantage of using first a flat space metric is that the trajectory of light is trivial in the mathematical space and can be easily derived in the physical space through the conformal mappings. Hence, it is unnecessary to consider the motion equation for light rays a priori. The trajectory is readily obtained as the result of operating three successive conformal mappings that rotate the space. Interestingly, the proposed dielectric media leads to perfect invisibility with absence of both phase delay and reflection. These findings strongly highlight the role of the negative refraction in material sciences. Our proposed design has a discontinuity at each boundary between two media with different refractive indices. It is of common knowledge that discontinuities of refractive indices generate reflections leading to distortions. However, the invented method completely suppresses all reflections that occur at the boundary between two isotropic materials having different indices and readily leads to perfect invisibility.

REFERENCES

1. Pendry, J. B., D. Schuring, and D. R. Smith, *Science*, Vol. 312, 1780, 2006.
2. Schurig, D., J. J. Mock, B. J. Justice, S. A. Cummer, J. B. Pendry, A. F. Starr, and D. R. Smith, *Science*, Vol. 314, 977, 2006.
3. Leonhardt, U., *Science*, Vol. 312, 1777, 2006.
4. Leonhardt, U., *New. J. Phys.*, Vol. 8, 118, 2006.
5. Ochiai, T., U. Leonhardt, and J. C. Nacher, *J. Math. Phys.*, Vol. 49, 032903, 2008.
6. Nacher, J. C., T. Ochiai, *J. Math. Phys.*, Vol. 52, 012903, 2011.

Determination of Effective Constitutive Parameters, Material Boundaries and Properties of SRR-rod and Fishnet Metamaterials by Drude/Lorentz Dispersion Models

Feng-Ju Hsieh[1], **Cheng-Ling Chang**[1], **and Wei-Chih Wang**[1, 2, 3]

[1]Department of Mechanical Engineering, University of Washington, Seattle, Washington, USA
[2]Department of Electrical Engineering, University of Washington, Seattle, Washington, USA
[3]Medical Device Innovation Center, National Cheng-Kung University, Tainan, Taiwan

Abstract— Metamaterials (MMs) operated in quasi-optical or Terahertz (THz) frequency range have been attracting attention over the past several years due to their unique phenomena, such as the negative refractive index and strong resonance in THz range, lacking in naturally occurring media. In order to utilize these phenomena of MMs in applications for bio-chemical sensing, spectroscopy, bio-imaging, security and communications, the effective boundaries of MMs must be determined first, before the constitutive parameters and frequency-dependent material properties of MMs are characterized.

To meet this demand, we propose two optimization models to determine effective boundaries of split-ring-resonator (SRR)-based and fishnet MMs. The optimization models are defined based on the assumption of effective medium theory and characteristic of homogeneous media. The results are then compared with the traditional definition proposed by Kong.

Two proposed full extraction methods can retrieve effective refractive indices, impedances, and material properties, such as dielectric permittivity (ε) and permeability (μ) of MMs. The first full extraction method allows the determination of constitutive parameters and material properties over all frequencies including the strong resonant band, where the results are unavailable by a well-known method proposed by Cheng. The method based on the material continuity allows missing results in the strong resonant band where the imaginary part of permittivity or permeability is negative to be retrieved. The second method describes a genetic algorithm and optimization of properly defined goal functions to retrieve the parameters from Drude and Lorentz dispersion models for ε and μ, respectively. Proper initial values of the parameters of models and partial retrieved ε and μ are also derived for the second method in order to reduce the computation time and prevent the optimization solution from falling into local minimum. Finally, the refractive index, impedance, permittivity, and permeability of two slabs composed of SRR-based and fishnet MMs are retrieved and compared using the proposed methods. Retrieved material properties and parameters are then used to compute S-parameters and compared with the original transmission and reflection signals from the simulation.

A Compact Hilbert Curve Fractal Antenna on Metamaterial Using CSRR

S. Suganthi[1], **S. Raghavan**[2], **D. Kumar**[3], **and S. Hosimin Thilagar**[4]

[1]Shri Angalamman College of Engineering and Technology, Trichy, India
[2]National Institute of Technology, Trichy, India
[3]Periyar Maniammai University, Thanjavur, India
[4]College of Engineering Guindy, India

Abstract— Recent advances in metamaterial (MTM) research in the microstrip antenna design for various wireless applications have been attracting researchers for further improvement in the performances. Though there have been many MTM based small antennas proposed so far, the use of MTM structures in fractal shaped antennas have been less attempted. This paper proposes a compact and novel MTM loaded Hilbert Curve Fractal Antenna (HCFA) design. The conventional HCFA has been designed using copper on a 20 mm × 20 mm × 1.6 mm FR4 substrate ($\varepsilon_r = 4.4$) and simulated. A complementary slip ring resonator (CSRR) for μ negative (MNG) along with a rectangular slot for ε negative (ENG) has been designed using copper, to exhibit MTM properties (negative μ and negative ε). Later this structure has been used as a defected ground plane for the HCFA. The complete design and simulation have been performed using HFSS 3D EM simulator software and the MTM properties have been verified by a separate MATLAB coding developed for Nicolson-Ross-Weir technique. The MTM HCFA appearing as a simple and compact structure with double side printed substrate and resonating at multiple frequencies are the novelties in this paper. In the CSRR loaded HCFA, the μ negative property is found predominating and the structure exhibits appreciable improvement in gain, directivity, shaped radiation and down shifted resonant frequencies.

Session 1A6b
Microwave Energy Application for Materials and Environmental Processing

Fundamental and Application of Microwave Processing of Materials and Environmental Technology

Noboru Yoshikawa
Graduate School of Environmental Studies, Tohoku University, Japan

Abstract— Application studies of microwave heating to various fields have been performed in author's group, for which we understand it very important that the fundamental mechanisms and the related physical and chemical phenomena have to be elucidated. In this report, it is intended to demonstrate several recent findings and analyses on microwave heating and some attempts of application to metallic materials' processing and treatment of stainless steel pickling sludge.

Microwave heating mechanisms are classified into three contributions, which are described as the three terms related with the microwave power $P\,[\mathrm{W/m^3}]$ as written in the followings:

$$P = \frac{\sigma |E|^2 + \omega\varepsilon'' |E|^2 + \omega\mu'' |H|^2}{2},$$

where σ, ε, μ, ω are electric conductivity, permittivity and magnetic permeability, angular frequency, respectively. E and H are electric and magnetic field. The terms are corresponding to the induction, dielectric and magnetic mechanisms, however, the alternating electric (induction) current $J = \sigma E$ is raised by the magnetic field H and the high frequency electric conductivity of dielectrics is expressed as $\sigma = \omega\varepsilon''$, therefore it is not necessarily simple to discuss them with the separated manner.

In this report, it is intended to present some permittivity measurement of various materials and their mixtures, and to show some simulation studies on electromagnetic field analysis. Heating of metallic materials in microwave magnetic field is effective, and the microwave heating behavior of metallic thin films in different orientation with respect to the magnetic field will be discussed. Estimation of the microwave penetration depth into sludge/graphite mixture is important for the practical process for the dehydration. The experimental results and its analysis will be presented using the measured permittivity.

Study of the Heating Behavior of Fe_3O_4/Al Mixtures in Separated H and E Field and Heating of the Fabricated Porous Composite Body

Lee Chang Chuan[1, 2], **Noboru Yoshikawa**[1], **and Shoji Taniguchi**[1]

[1]Graduate School of Environmental Studies, Tohoku University, Japan
[2]School of Manufacturing Engineering, Universiti Malaysia Perlis, Malaysia

Abstract— Ceramic porous composites of Fe_3O_4/Al system had been fabricated by microwave-induce substitutional combustion reaction via controlling the reaction progress at the low temperature exotherm region. Prior to the fabrication of these porous composites, heating behavior of the Fe_3O_4 and Al powder mixtures is studied in advance in the separated electric (E) and magnetic (H) field. In addition, heating ability of the microwave fabricated porous products was also investigated. At the maximum H field, the powder mixture can be heated up easily as compared with those heated at maximum E field. Heating temperature of the Fe_3O_4 samples decreased sharply when Al powder was added in E-field. However, the same phenomenon was not observed in the maximum H field heating. Based on these results, Fe_3O_4/Al system of stoichiometric and non-stoichiometric ratio was heated in the maximum H field for the fabrication the porous composite body. Thru an adequate control of the reaction progress, products with desired phases and porous structure were obtained. Consequently, heating of the fabricated porous composite body was also been carried out successfully in the maximum H field. The heating ability of these products is mainly depended on the product microstructure. Products with a porous structure consisting of well-distributed metal particles in the alumina and/or hercynite matrix are preferable. For comparison, numerical simulation of the heating ability of the fabricated porous composite body was studied.

Effect of Coherency of Microwave on Non-thermal Reduction Process

Motoyasu Sato
National Institute for Fuson Science, Japan

Abstract— The coherency on frequency domains is the critical determinant of activation energy on chemical reactions under high intensity microwave irradiations. Reaction speeds of copper oxide were studied to the monochromatic-microwave heating, the amplitude modulated-microwave heating and the conventional infrared heating. The reduction speed was 5000 times larger by monochromatic microwave than the IR radiation heating. The activation energies showed 117 kJ/mol in monochromatic-microwave heating and 333 kJ/mol in IR heating. As the Gips free energy is estimated to 292 kJ/mol from CuO to Cu_2O, the energy must be given via another path to satisfy the energy conservation law. When the monochromaticity of microwave was disturbed by addition of amplitude modulations, it increased to 222 kJ/mol. The results suggest that microwaves are directly transformed into reduction energy of copper oxide. The results show the non-thermal effect to reduction depends on the quality of microwave.

A Simultaneous Cooling and Dielectric Heating: An Advanced Technology to Improve the Yield of Lactides

Ani Idris[1], **Attaullah Bukhari**[1], **Noordin Mohd Yusof**[2], **and K. G. Tan**[3]

[1]Department of Bioprocess Engineering, Faculty of Chemical Engineering
Universiti Teknologi Malaysia, 81310 UTM Johor Bahru, Johor, Malaysia
[2]Department of Manufacturing and Industrial Engineering, Faculty of Mechanical Engineering
Universiti Teknologi Malaysia, 81310 UTM Johor Bahru, Johor, Malaysia
[3]Synotherm (SEA) Pte. Ltd., Malaysia

Abstract— Lactides with improved yield are prepared by depolymerization of oligo (lactic acid) under simultaneous cooling and microwave heating. The influence of microwave power input and its non-thermal effects on the yield of lactides are investigated. By increasing microwave power input, increased yield of lactides is obtained at 180–220°C at reduced pressure. Combined application of simultaneous cooling with microwave heating further increased the lactides yield. The removal of lactides during reaction shifts the equilibrium to the right. Simultaneous cooling enhances the absorbance of microwave irradiation into reactants; though increased yield of lactides is not only due to thermal effects of microwave irradiation. Maximum 85% yield of lactides is obtained at 500 W microwave power at 180–220°C and < 20 torr.

Industrial Microwave Processing of Agri-food Products

K. G. Tan and Hu Peng
Synotherm (SEA) Sdn Bhd, No. 55, Jalan SG 8/7, Taman Sri Gombak
68100 Batu Caves, Selangor, Malaysia

Abstract— Microwaves cover a region of frequency range from 300 MHz to 300 GHz in the electromagnetic wave spectrum. Besides the applications of radar, navigation and communication equipment, microwave energy is widely applied at frequencies of 915 MHz and 2.45 GHz as an alternative method for thermal processing in view of its high energy efficiency. In microwave processing, energy is coupled directly and heat volumetrically with reduced thermal gradients throughout the total mass of materials. The conversion of microwave energy to heat depends upon the dielectric properties of materials. Agri-food products are basically containing water that becomes excellent dielectric materials to absorb microwaves. Industrial microwave processing of agri-food products offer advantages over conventional heat methods, in term of shortened processing time, energy efficiency, and end-product quality, has been gaining increasing attention. However, microwave processing has led to new challenges on knowledge of know-how that involves different mechanism of energy transfer, optimisation of various agri-food processing, and scale-up commercialisation. Some applications of microwave processing, such as rice disinfestation, herbs drying, etc. are reviewed in this presentation.

Session 1A7
Observing the Terrestrial Environment at HF

Propagation of HF Radar Signals through the Air-ground Interface

Stuart Anderson
Defence Science and Technology Organisation, Edinburgh SA 5111, Australia

Abstract— HF radar systems have been widely employed for the detection of aircraft, ships and other vehicles travelling on or above the earth's surface, and for remote sensing of ionospheric phenomena and sea surface conditions. In almost all cases, the radiowave propagation modes involved are (i) line-of-sight (space wave) within the neutral atmosphere, (ii) skywave via the ionosphere, or (iii) surface wave, especially across the sea surface; in some systems a combination of modes is used. These mechanisms of signal transport are effective because the propagation losses are acceptably low for the applications of interest.

Electromagnetic wave propagation in the solid earth is characterised by comparatively high losses, especially where there is appreciable water content, so few applications of HF radars to this domain have emerged. One of the rare exceptions is the deployment of HF radar systems or sounders aboard spacecraft placed in orbit around the moon, and Mars, probing the ground in search of water bodies or large-scale geological transitions. Yet, given the recent development of radar component technologies with extremely high dynamic range and sophisticated signal processing, we can start to envisage a broader range of possibilities that may be feasible in the terrestrial context.

In this paper, we examine some of the physical mechanisms and experimental configurations which may play an important role in prospective applications of HF radar looking through the air-ground interface:

- the role of surface topography on signal transmission through the surface
- lateral wave structure beneath the surface
- alternative techniques for measuring ground permittivity and conductivity
- properties of buried antennas
- scattering from buried inhomogeneities

Modelling results and experimental measurements will be used to illustrate these topics.

Monostatic and Bistatic Electromagnetic Signature of Sea and Ground Clutter in HF Band Estimated by Using SPM, TSM and SSA Models

Laurent Vaitilingom and Ali Khenchaf
Lab-Sticc UMR CNRS 6285, ENSTA Bretagne, France

Abstract— To cover a large area, the use of HF radars is preferred to classical radars one because HF radars are not limited by EM horizon. On counterpart, antennas of HF radars are huge and ionospheric and surface clutters disturb the use of such radars. In order to improve radar's performances, we will study, in this paper, electromagnetic signature of sea and ground clutter in HF band by means of radar cross section.

Among the calculation methods of radar cross section, we will define the use condition and the expression of radar cross section estimated by approximate methods which are Small Perturbation Method (SPM), Two Scale Model (TSM) and Small Slope Approximation (SSA). To implement the scattering coefficients using by those models, we need to know electrical permittivity, magnetic permeability, surface spectrum and surface slope distribution. In this paper, we will consider diamagnetic or paramagnetic surfaces so magnetic permeability is near to vacuum permeability.

Thanks to approximate methods we study in this paper, we will observe the effects of the polarization, of the parameters linked to sea (wind direction and wind speed, salinity and temperature of salt water) and ground (roughness and composition) surfaces, of the transmitter and receiver positions and of the transmitting frequency on the electromagnetic signatures of surface clutter.

Spatial Change of Normalized Radar Cross Section of Ocean Surface for HF Ocean Surface Radar due to the Wave-current Interaction Around Eddy

A. Nadai
National Institute of Information and Communications Technology, Japan

Abstract— HF ocean surface radar is one of the powerful tools to measure the ocean surface parameters. HF ocean surface radar transmits HF radio wave to the ocean and received the backscattered radio wave. The Doppler spectra of received signal include the information of backscattering processes. Because ocean surface waves having one-half the wavelength of the radar wave satisfy the Bragg resonant condition, two strong peaks, called first-order echoes, are appeared on the Doppler spectra. The Doppler velocity of each first-order echo is the relative radial phase velocity of the causal ocean waves to the radar. Because the theoretical phase velocity of the causal ocean waves is able to be calculated by the dispersion relation, the difference between the measured and theoretical velocities is the radial velocity of currents.

Because the phase velocity of the causal ocean waves is comparable with the current velocity, the influence of wave-current interaction cannot be ignored. By the wave-current interaction, the ocean waves changes its wavenumber vector and its spectral density. The HF ocean surface radar received backscattering signal by the influenced ocean wave. In this paper, the spatial change of normalized radar cross section around an ocean eddy with velocity change comparable with the phase velocity of causal wave is simulated using the ray-tracing method and the conservation of wave action along the wave ray. Then based on the simulation result, the influence on the current measurement is analyzed.

By the influence of wave-current interaction, the normalized radar cross section is not uniform around an eddy. One side of eddy in where the causal ocean waves propagate against the ocean current, the wave trains are compressed, and the wavenumber increased. Therefore, the wavenumber of the causal ocean waves before interaction with current is lower than that after the wave-current interaction. Considering the equilibrium region of ocean wave spectra, the lower wavenumber corresponds to the larger wave energy. Then, the normalized radar cross section in this side becomes larger by the wave-current interaction. In another side of eddy in where the causal ocean waves propagate along with currents, the normalized radar cross section becomes smaller by the wave-current interaction. As a result, the normalized radar cross section around the eddy represents the spatial variation.

Because the Doppler spectra measured by HF ocean surface radar are the spectra of current velocity weighted by the radar cross section, the spatial non-uniformity of normalized radar cross section influences the radial current measurement by the HF ocean surface radar. The momentum center of Doppler spectra of the first-order echo represents slower relative phase velocity to the radar than the eddy model. The measurement errors in radial current velocity appear as the artificial divergent/convergent field on 2D current field produced by combination of radial current fields measured by multiple HF ocean surface radars. In case of point source up-welling/down-welling, the errors appear as the artificial rotation field. These results of simulation are, in fact, recognized in the real observations by the HF ocean surface radar.

Novel Concept for Compact ULA Using MIMO Beamformer

T. Fickenscher and A. Gupta
Helmut Schmidt University/University of the Federal Armed Forces Hamburg, Hamburg, Germany

Abstract—

Summary: The investment for a coastal high frequency surface wave radar (HF SWR) is mainly driven by the huge beach property. Thus shortening the array length is of higher importance than reducing the hardware complexity in terms of number of channels/antennas. With a proper array arrangement Multiple-Input Multiple-Output (MIMO) beamforming can be used to keep the physical aperture of linear antenna array short. For a uniform linear N-element Rx array together with 2 Tx arrays and MIMO beamformer a virtual Uniform Linear Array (ULA) with $2N$ elements can be generated. Taking into account that compared to conventional beamformer MIMO concept requires an additional Tx array, the shortening of total antenna aperture of Tx and Rx arrays is $(N+1)/(2N+1/2)$. In case of FMCW waveform both Tx signals can be separated in each RX channel in the frequency domain in baseband when time or frequency staggered chirps are applied.

Motivation: HF SWR systems based on direction finding instead on beamforming rely on Rx antennas integrated at a single position. These systems are highly compact and are suitable for oceanographic measurements such as ocean current monitoring. On the downside direction finding algorithm does not allow for measuring second order sea clutter signal. Hence wave height cannot be measured by these systems. Furthermore, long range maritime surveillance using HF SWR — which is gaining more importance after establishing 200 nautical miles as the Exclusive Economic Zone (EEZ) — cannot be performed successfully by direction finding. The challenge of building a compact HF SWR system using beamforming is quite demanding as the investment for the system is mainly driven by the huge beach property necessary for the conventional large coastal receiver arrays. Superdirective arrays have been proposed as a solution but they inflict major problems as are low radiation resistance (hence low radiation efficiency), sensitivity to excitation and position tolerances, and narrow bandwidth. Multiple-input multiple-output (MIMO) beamformers enable to synthesize virtual antenna positions which result either in a larger number of effective virtual array elements for a given array length or in a reduced array length for a desired number of effective virtual array elements [1].

Concept: Figure 1 displays the geometry of physical Tx and Rx arrays for the example $N = 5$. Along the physical Rx aperture inter-element distances are uniformly distributed $\lambda/2$. Both elements of each Tx array are separated by $\lambda/2$ and are driven 180° out of phase resulting in a null in their respective radiation patterns along the receive array. Spacing between Tx phase centers and respective neighboring Rx element is half the inter-element spacing of Rx aperture.

The effective aperture (lower end of Figure 1) of the combination of a transmit and a receive array is the receive aperture that would produce the same two-way radiation pattern if the transmit antenna would be a point source. In conjunction with transmit array Tx_2 the elements Rx_1 ... Rx_5 provide the signals of elements EA_1 ... EA_5 of virtual effective aperture. In conjunction with transmit array Tx_1 the same elements provide the signals of elements EA_6 ... EA_{10}.

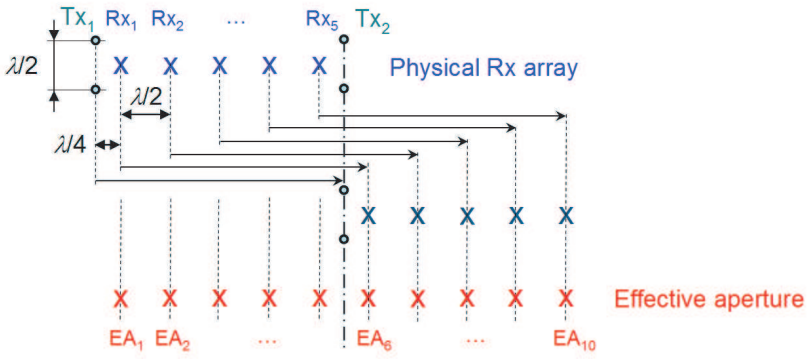

Figure 1: Uniform linear 10 element effective aperture generated by $N = 5$ element physical Rx array (spaced $\lambda/2$), 2 Tx arrays and MIMO beamformer. Equivalent conventional antenna array would require 10 Rx and 1 Tx channels.

REFERENCES

1. Frazer, G., Y. Ambramovich, and B. Johnson, "Spatially waveform diverse radar: Perspectives for high frequency OTHR," *IEEE Radar Conference 2007*, 385–390, Boston, USA, June 2007.

A Coordinate Registration Technique for OTH Sky-wave Radars Based on 3D Ray-tracing and Sea-land Transitions

A. Cacciamano[1], **A. Capria**[1], **D. Olivadese**[1, 2], **F. Berizzi**[1, 2], **E. Dalle Mese**[1, 2], **and F. Cuccoli**[1, 3]

[1]CNIT National Lab of Radar and Surveillance Systems (RaSS), Pisa, Italy
[2]Department of Information Engineering, University of Pisa, Pisa, Italy
[3]Department of Electron. & Telecommun., University of Florence, Florence, Italy

Abstract— Over-the-horizon (OTH) radars allow to reach distances well beyond the horizon by exploiting the effect of ionosphere refraction. In fact, in the 5–30 MHz frequency range (HF band), electromagnetic waves are gradually bended through the ionosphere until they are totally reflected back to the Earth [1].

In complex radar system like skywave OTH radars the scenario modelization is a key task in order to assess the system performance. In particular, the ionospheric propagation modeling is required to fulfill the coordinate registration (CR) requirement. CR is the process of target localization which is obtained by converting the slant coordinates R_g to ground coordinates R_{gr}. There is no simple method for translating from radar coordinates into geographic coordinates (longitude and latitude), and the necessary relationships can only be found by characterizing the propagation over the radar area of interest.

The CR method here presented is based on a 3D ray-tracing software which provides the reached ground range distance (R_{gr}) and corresponding time delay (τ_g) for a specific transmission frequency and elevation angle.

In particular, the ray-tracing code is based on numerically solving a system of differential equations firstly proposed by Haselgrove [2]. The ray-tracing algorithm is applied to a 3D electronic density data cube variable with height, latitude and longitude. The ionosphere characterization can be achieved by means of a network of ionosondes or by using worldwide recognized long term ionospheric model such as the International Reference Ionosphere (IRI).

Ionospheric abnormalities are difficult to model adequately during radar operation, furthermore the ray-tracing algorithm output is subject to errors due to the solver discretization step used to integrate the differential equations system, even though the latter has less impact than the former. Errors in the estimated down-range ionospheric parameters introduce, as a consequence, a degradation of the target localization accuracy. The inherent variability of the ionosphere and the inaccuracy of the related models brings to further degradation in the CR process [3–5].

The purpose of this paper is to provide a method able of achieving a coarse coordinate registration by means of a 3D ray-tracing and then refine the results by using sea-land transitions knowledge (geographic position and related radar time delay).

In [6], terrain features are used in order to determine position correction offsets, concluding that it can be used to provide coordinate registration benchmarks.

The proposed technique is finally tested by means of numerical simulations referred to a reference scenario.

REFERENCES

1. Headrick, J. M. and J. F. Thomason, "Application of high-frequency radar," *Radio Science*, Vol. 33, 1045–1054, Jul.–Aug. 1998.
2. Jones, R. M. and J. J. Stephenson, "A versatile three-dimensional ray tracing computer program for radio waves in the ionosphere," OT Report, 75–76, US Dept. of Commerce, Office of Telecomunications, Oct. 1975.
3. C.C.I.R./I.T.U., "C.C.I.R. Interim method for estimating sky-wave field strength and transmission loss at frequencies between the approximate limits of 2 and 30 MHz," Report 252-2, 1970.
4. Headrick, J. M. and J. F. Thomason, "Application of high-frequency radar," *Radio Science*, Vol. 33, 1045–1054, Jul.–Aug. 1998.
5. Kelso, J. M., *Radio Ray Propagation in the Ionosphere*, McGraw-Hill, New York, 1964.
6. Barnum, J. R. and E. E. Simpson, "Over-the-horizon radar target registration improvement by terrain feature localization," *Radio Science*, Vol. 33, No. 4, 1077–1093, Jul.-Aug. 1998.

Sea/Land Transition Identification for Coordinate Registration of OTH Sky Wave Radar: End to End Software Simulator and Performance Analysis

F. Cuccoli[1], **L. Facheris**[2], **and F. Sermi**[2]

[1]U.O. CNIT RaSS, c/o Dipartimento di Elettronica e Telecomunicazioni
Università di Firenze, via di Santa Marta, 3, Firenze 50139, Italy
[2]Dipartimento di Elettronica e Telecomunicazioni
Università di Firenze, via di Santa Marta, 3, Firenze 50139, Italy

Abstract— Recently we introduced a Coordinate Registration (CR) method for an Over The Horizon Sky Wave Radar (OTH SWR) sensor based on the identification of Sea/Land transitions (SLTI) over the Earth surface [1]. The method was outlined, implemented and tested in a simplified reference scenario and the requirements for its applicability, in terms of minimum Clutter-to-Noise Ratio (CNR) and of Sea/Land backscattering coefficients difference, were highlighted [2].

The SLTI method is based on the a priori knowledge of the displacement of the sea-land transitions within the radar coverage area through which a geographic reference mask for the received radar echo is defined. The CR is then provided by maximization of a time domain cross-correlation function between the received single frequency radar echo and the time mask that is obtained transforming the geographic reference mask in a time signal through a parametric ionospheric transformation.

In order to analyze the performance of the proposed SLTI method in realistic scenarios also a software tool for the simulation of the received echo of an OTH SWR in pulse mode has been developed [3]. The tool accounts for several models of the pulse radar Tx/Rx configuration, the antenna pattern, the electron ionospheric structure and the land/sea backscattering of the Earth's surface [4]. The tool is based on a numerical model of the OTH SWR monostatic equation that has been developed and already presented by the same authors of this work in [2].

In this paper we assume that the parametric ionospheric transformation is based on a look up table of 200 profiles of ionospheric equivalent reflection height in function of the elevation angle that are computed assuming 200 vertical profiles of electronic density. For a fixed frequency and a fixed aiming angle the ionospheric equivalent reflection is computed by means of a ray tracing procedure applied to the electron density profiles.

We recall the main characteristics of the SLTI method and we present some details of the end to end software simulator related to the core of the cross-correlation algorithm applied to the look up table of ionospheric equivalent reflection height.

Finally we present some simulation results assuming the Mediterranean scenario and some specific radar setup in order to discuss the CR performance of the SLTI for different configurations of the Sea/Land masks jointly with the ionospheric behavior.

REFERENCES

1. Cuccoli, F., L. Facheris, D. Giuli, and F. Sermi, "Over the Horizon sky-wave radar: Coordinate registration by sea-land transitions identification," *Progress In Electromagnetics Research Symposium Proceedings*, 21–25, Moscow, Russia, August 18–21, 2009.
2. Cuccoli, F., L. Facheris, and F. Sermi, "Coordinate registration method based on sea/land transitions identification for over the horizon sky-wave radar: Numerical model and basic performance requirements," *IEEE Transactions on Aerospace and Electronic Systems*, 2011, accepted.
3. Cuccoli, F., L. Facheris, and F. Sermi, "Over the Horizon sky wave radar simulator for ionosphere and earth surface sounding," *2011 IEEE International Proceedings of Geoscience and Remote Sensing Symposium (IGARSS)*, 2011.
4. Cuccoli, F., L. Facheris, D. Giuli, and F. Sermi, "OTHR-SW coordinate registration method based on sea-land transitions: Clutter model definition," *Proceedings of the 7th European Radar Conference (EuRAD)*, 101–104, Parigi, France, September 30–October 1, 2010.

Target Detection Based on Morphological Component Analysis of HFSWR Images for Maritime Surveillance

A. Baussard[1] and S. Grosdidier[2]

[1]ENSTA Bretagne (REMS), LabSTICC, 2 rue Francois Verny, 29806 Brest cedex 9, France
[2]LSEET, Université Sud Toulon Var, Btiment F, BP 20132, 83957 La Garde, France

Abstract— To supplement actual systems (like the Automatic Identification System-AIS) to monitor the maritime traffic in given areas within the Exclusive Economic Zone (EEZ-200 nm), High Frequency Surface Wave (HFSW) radar seem to be good candidates. Indeed recent works [1, 2] show that they can provide useful informations even if the spatial and temporal resolutions are weaks. A global surveillance system of the EEZ and harbor could also combine HFSW radar for the long range detection and X-band radar for short ranges (< 30 km). These last systems are more suitable for near area, which are more vulnerable, since they provide good spatial and temporal resolutions.

HFSW radars have been efficiently used these last three decades to remotely measure oceanographic parameters. They can provide surface currents, wave spectra, wind intensities and directions. In this contribution, as already introduced, these systems are considered for traffic surveillance. The used system is a WEllen RAdar (WERA), with a central frequency between 12 and 13 MHz, which provides Range-Doppler (RD) images to be processed for the detection part. These RD images, for the detection purpose, are strongly polluted by sea clutter and other interference leading to a challenging problem.

In the paper, a short review of previous works about simulating HFSW images [3] and the validation against real data will be given. Then the image processing approach will be detailed. The proposed method is based on the Morphological Component Analysis (MCA) [5, 6]. Due to HF image features, the method had required some adaptations and some first results have been already given in a previous work [4]. In this contribution, some new modifications of the MCA algorithm are introduced in order to enhance the extraction of the target signatures. The new algorithm includes some processing during the iterative MCA process against the multiscale coefficients (this will be detailed in the full paper). Some results from simulated and real data will be display to illustrate the efficiency of the proposed method.

REFERENCES

1. Gurgel, K. W. and T. Schlick, "HF radar wave measurements in the presence of ship echoes-problems and solutions," *OCEANS 2005-Europe*, Brest, France, 2005.
2. Ponsford, A. M., L. Sevgi, and H. C. Chan, "An integrated maritime surveillance system based on high-frequency surfacewave radars. Part 2: Operational status and system performance," *IEEE Antennas and Propagation Magazine*, Vol. 43, 52–63, 2001.
3. Grosdidier, S., A. Baussard, and A. Khenchaf, "HFSW Radar model: Simulation and measurement," *IEEE Trans. Geoscience and Remote Sensing*, Vol. 48, No. 9, 3539–3549, 2010.
4. Grosdidier, S., A. Baussard, and A. Khenchaf, "Morphological-based source extraction method for HFSW radar ship detection," *IEEE International Geoscience And Remote Sensing Symposium*, Honolulu, USA, July 2010.
5. Starck, J.-L., M. Elad, and D. Donoho, "Redundant multiscale transforms and their application for morphological component separation," *Advances in Imaging and Electron Physics*, Vol. 132, 288–348, 2004.
6. Starck, J.-L., F. Murtagh, and M.-J. Fadili, *Sparse Image and Signal Processing — Wavelets, Curvelets, Morphological Diversity*, Cambridge University Press, 2010.

Radiowave Depolarisation and Repolarisation During HF Skywave Propagation

Stuart Anderson
Defence Science and Technology Organisation, Edinburgh SA 5111, Australia

Abstract— Radiowave propagation through the inhomogeneous ionospheric magnetoplasma is characterised by a number of physical processes including linear and nonlinear coupling to various species of plasma waves, focussing at caustics and reflection points, deviative and non-deviative absorption, and continuous transformation of the local polarisation state. All of these processes have a direct bearing on the spatial and temporal behaviour of the oblique skywave propagation channels exploited by HF skywave radar systems, so much attention effort has been directed at understanding and exploiting the relevant physics so as to optimise radar performance.

The polarisation transformation properties of skywave channels are of particular interest because they impact on every stage of the radar process, from choice of waveform, through transmitting antenna design, scattering from the targets of interest, receiving antenna design and signal processing. Perhaps the most obvious signature of the transformation is the phenomenon of polarisation fading, where the time variation of the channel modulates the polarisation state of the signals arriving at the receiving antennas, each element of which acts as a projection operator. If all the antennas constituting the receiving system are identical and the spatial gradient of the transformation is not too great, any given echo will fluctuate, vanishing at times with serious implications for radar operations.

Despite this largely avoidable loss of information, no major skywave radar facility has incorporated polarisation diversity, let alone full polarimetric capability. Traditionally the arguments advanced to justify this decision were based on (i) the high cost of the additional receivers, which used to be the most expensive part of the receiving system, (ii) the complexity of dual polarisation antennas and, even more so, polarimetric antennas, and (iii) the fact that target echo fading was well understood in the wider radar domain, and tracking algorithms were able to deal with it effectively on time scales which did not seriously compromise surveillance capability. Yet, with the advent of cheap, compact, multi-channel, high performance digital receivers, the first argument loses its weight, while the second is of less consequence because of the development of highly accurate calibration techniques. Further, radar sensitivity should improve substantially with the increased signal dimensionality which affords new options for interference and clutter rejection, while there is some prospect of obtaining additional target information from polarimetric measurements.

Some of the spatial and temporal characteristics of the polarisation mapping between transmitter and receiver have been investigated previously by researchers concerned with OTH skywave radar performance, but in each case the nature of the measurements precluded complete characterisation of the channel. To determine the skywave channel polarisation transformation in its entirety, rather than by inference from partial information, we have conducted an experiment over a one-way skywave path. A transmitting complex consisting of two antennas, one vertically polarised, one horizontally polarised, was deployed near Woomera, South Australia, while a linear array of polarimetric antennas was constructed some 480 km south along the same magnetic meridian. Radar waveforms were radiated alternately, that is to say, pulses interleaved, from the two transmitting antennas, each signal being received on two orthogonal polarisations at the receiving site. This enabled the channel transfer function to be mapped in 7 dimensions: group delay, linear and quadratic variation of phase path, tilt and eccentricity of the polarisation ellipse, azimuthal angle of arrival, and slow time. This paper will present the results of the first experiments with this facility and discuss their implications for HF skywave polarimetry.

Session 1P1
Optics and Photonic Crystals

Photonic Crystal Based on Holographic Polymer Dispersed Liquid Crystal Films

Andy Ying-Guey Fuh[1], **Shing-Trong Wu**[2], **and Ming Shian Li**[3]

[1]Department of Physics, and Institute of Electro-optical Science and Engineering
National Cheng Kung University, Tainan 701, Taiwan, R.O.C.
[2]Department of Physics, National Cheng Kung University, Tainan 701, Taiwan, R.O.C.
[3]Institute of Electro-optical Science and Engineering, National Cheng Kung University
Tainan 701, Taiwan, R.O.C.

Abstract— Two unusual optical properties in photonic crystals (PCs) based on polymer-dispersed liquid crystal (H-PDLC) films are reported. They are the superprism and unsual refraction effects. The H-PDLC film is designed and fabricated using three coherent beams. The fabricated H-PDLC film contains two-dimensional ordered nano-sized LC domains (~ 150 nm in diameter) embedded in a polymer matrix; its periodicity is estimated using a scanning electron microscope to be $\sim$ 350 nm. The dispersion of white light from this H-PDLC superprism is $\sim 50^{\circ}$, and the deflection of light output from it is consistent with the theoretical value obtained by the plane wave expansion method. For the unusual refractive phenomena from a PC based on a H-PDLC film, the refracted collimated beams comprise positive and negative refractions, and can be switched to exhibit the negative refraction part only, by changing the incident angle or the wavelength of the incident beam. The equal frequency surfaces are adopted to analyze the refractions of light both inside and outside the HCP PC. The use of PCs based on H-PDLC for optical switch will be also reported.

REFERENCES

1. Li, M. S., S. T. Wu, and A. Y.-G. Fuh, "Superprism phenomenon based on holographic polymer dispersed liquid crystal films," *Appl. Phys. Lett.*, Vol. 88, 091109, 2006.
2. Wu, S. T., M. S. Li, and A. Y.-G. Fuh, "Unusual refreaction in holographic polymer dispersed liquid crystal films," *Appl. Phys. Lett.*, Vol. 91, 25117–9, 2007.
3. Li, M. S., A. Y.-G. Fuh, and S. T. Wu, "Optical switch of diffractive light from a BCT photonic crystals based on HPDLC doped with an azo dye," *Optics Letters*, 2011, accepted.

Photonic Quasi-crystal Research; Recent Theoretical Developments in Band Gap and Localized State Determination

R. C. Gauthier and S. Newman
Department of Electronics, Carleton University, Ottawa, Ontario K1S 5B6, Canada

Abstract— The rotational symmetry of photonic quasi-crystals renders the traditional plane wave expansion based on a translational symmetric structure inapplicable. To overcome these difficulties researcher resort to either the numerical techniques like FDTD of FEM or to experimental measurements. The focus of the paper is the recent development in solving Maxwell's equations for rotationally symmetric structures. We begin by putting forward the mathematical framework of the solution using Fourier-Bessel waves in a cylindrical coordinate environment. The derivation leads to an eigenvalue equation which can be solved for the frequencies of the supported modes. The array of frequencies obtained includes information on the presence, or absence, of optical band gaps in the structure and within the band gaps, the presence or absence of localized "defect" states about the rotational symmetry center. The accuracy and applicability of the Fourier-Bessel technique is verified by reproducing the band gap and defect state information of a central defect containing triangular lattice photonic crystal. The developed Fourier-Bessel technique is applied to several dielectric configurations. Traditional dielectric layouts such as the optical fiber, Bragg ring fiber and photonic crystal fiber are examined for in-plane modes. (Note: the theoretical framework for out-of-plane propagation is under development and will be presented if completed by the conference date.) The Fourier-Bessel technique is applied to a number of rotationally symmetric photonic crystals including the 8-fold, 10-fold and 12-fold quasi-crystals and now placed on the same theoretical level the traditional 4-fold (square) and 6-fold (hexagonal) photonic crystals.

Simultaneous Photonic and Phononic Band Gap, Defect States and Waveguides in Silicon-polymer Composite

Robert C. Gauthier and Mohammed A. Alzahrani
Department of Electronics, Carleton University, Ottawa, Ontario K1S5B6, Canada

Abstract— A silicon-polymer composite is presented which supports simultaneously a band gap for optical and acoustical waves, phoxonic crystal (band gap structure). A complete band gap for both optical polarizations at the same time in a phoxonic crystal is important in the design of polarization free devices. The typical low contrast in the optical and acoustical properties of the periodic material makes it a challenge to opening large and complete optical band gaps and at the same time an acoustic band gap. These optical based difficulties are overcome by using a composite unit cell composed of both high dielectric rods and low dielectric holes. The high dielectric regions are composed from silicon. The acoustical difficulties are overcome by filling the holes with a low dielectric polymer with low acoustical wave velocity to complement the high acoustical wave velocity in the silicon regions. Both square and triangular unit cell structures are examined but the bulk of the details are presented for the square array. The theoretical investigation is performed using the plane wave expansion method in both the optical and acoustical regime. Several design parameter sets are considered leading to the optical and acoustical band diagrams from which band gap maps are produced and permit the selection the optical structure dimensions. The phoxonic waveguide is introduced by increasing the local separation between adjacent unit cells along a lattice vector and filling with silicon. In the optical regime the plane wave expansion and FDTD are employed to examine the waveguide properties of the structure. The single mode optical waveguide width is selected and acoustical guidance is confirmed making the structure a phoxonic waveguide. The proposed structure is one which falls within the regime of nanofabrication and can be "easily" fabricated using conventional techniques.

Investigation of the Transmittance in Superconducting Photonic Crystal

Arafa H. Aly[1, 3], **Walied Sabra**[1], **and Ehab Abdel-Rahman**[2, 3]

[1]Department of Physics, Faculty of Sciences, Beni-Suef University, Egypt
[2]Department of Physics, The American University in Cairo
P. O. Box 74, New Cairo 11835, Egypt
[3]YJ-STRC, The American University in Cairo
P. O. Box 74, New Cairo 11835, Egypt

Abstract— We will investigate the optical properties of the high temperature superconducting photonic crystals (HTScPC) in the ultra-violet region by using the ($YBa_2Cu_3O_7$) as a superconductor layer with the dielectric material strontium titanite ($SrTiO_3$) as a dielectric layer. Also we will see the effect of the thicknesses of both the superconductor layer and the dielectric layer on the width of the photonic band gaps (PBGs).

Biaxial Anisotropy in Gradient Permittivity Dielectric Optical Instruments

Alireza Akbarzadeh, Cheng-Wei Qiu, and Aaron J. Danner
Department of Electrical and Computer Engineering
National University of Singapore, Singapore 117576, Singapore

Abstract— Light propagation in gradient anisotropic crystals can potentially lead to many interesting and unusual phenomena which cannot be observed in isotropic materials, and in this presentation, we will show some surprising results related to the optical functionality available in gradient biaxial dielectrics. Our interest is in designing such anisotropic permittivity profiles to perform useful tasks (dielectrics being the materials of choice when designing optical instruments) but unfortunately devices designed with transformation optics are unsuitable because they require $\mu = \varepsilon$. (In the past, if dielectrics are used, typically one polarization is sacrificed to allow $\mu = 1$). Designing devices with pure dielectrics thus necessitates a departure from transformation optics. Without that toolset available, ab initio device design becomes extremely challenging, especially in the biaxial case where a propagating ray can interact with multiple elements in the permittivity tensor along its trajectory. Fundamental limitations on device design with dielectrics beyond transformation optics are hence worth investigating.

Overcoming some drawbacks in a recently published paper [1], it has been shown that birefringence can be controlled in a way to design useful dielectric devices which offer multiple or identical functionalities for each polarization (Figure 1(a)). The discussion raised in this paper on controlling birefringence can be extended to the biaxial situation, though it is much more involved due to complexities in the Hamiltonian of a general biaxial media and the consequent restrictions on the design procedure. In this presentation, ray tracing in a general graded-index biaxial dielectric will be reviewed and fundamental limitations on what is and is not possible to do with biaxial dielectrics in various coordinate systems will be explored. It will also be shown that even with high symmetry, as many as four optical functions can be integrated into a single biaxial dielectric device. This is surprising, because there are only three elements along the permittivity tensor diagonal. Additionally, example devices will also be demonstrated through photorealistic animations that can "bring metamaterials to life" in educational settings. (Figure 1(b)).

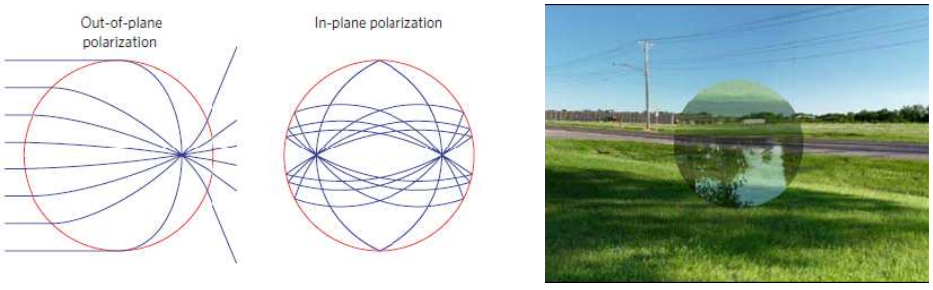

(a) (b)

Figure 1: (a) An example of a birefringent dielectric device designed in [1], an interior focusing potential for one polarization and a Maxwell fisheye for the other. (b) A photorealistic depiction of a spherical device which is an Eaton lens for one polarization and invisible for the other.

REFERENCES

1. Danner, A. J., T. Tyc, and U. Leonhardt, "Controlling birefringence in dielectrics," *Nature Photon.*, Vol. 5, 357–359, May 8, 2011.

Simulation of Reflection and Total Reflection of Optical Beams Using a Bidirectional Beam Propagation Method

Debjani Bhattacharya and Anurag Sharma
Indian Institute of Technology Delhi, New Delhi, India

Abstract— Analysis and modeling of reflections and transmissions are important for design of photonic structures. Numerical modeling of reflection requires methods, which can model both the forward and backward propagating fields. Methods like the finite difference time domain (FDTD) method are generally used for such modeling but these are computationally very extensive. On the other hand the beam propagation method (BPM) is a highly efficient method, but most of such methods solve the one-way wave equation and hence are not suitable for bidirectional propagation. We have recently developed a method, the split-step nonparaxial (SSNP), which is bidirectional and can be used for treating reflections in photonic devices [see, e.g., [1]]. We use here the finite difference implementation of the method. The method does not require any numerical matrix inversion or diagonalization (as these are done analytically) and only matrix multiplications are involved. We have used the method to model reflection at a simple dielectric interface as well as to model frustrated total reflection through an air gap between two glass slabs. The latter example shows that our method is capable of treating evanescent waves in the direction of propagation. We have also simulated the total internal reflection of a Gaussian beam. Such a beam undergoes the Goos-Hanchen shift, which is clearly shown in the simulation. In our formulation, it is rather simple to separate the forward and the backward propagating fields; this provides a simple means to compute the reflection coefficient at any given position during propagation.

REFERENCES

1. *Optical Quantum Electron.*, Vol. 39, 865–876, 2007.

Cancerous Cell Detection by Multi-spectral Imaging

Tsung-Chih Lin[1], **Ta-Wei Chien**[1], **Ju-Hsiu Hsiao**[2], **Ching-Te Huang**[2], **Hsiang-Chen Wang**[1], **and Chun-Ping Jen**[2]

[1]Graduate Institute of Opto-Mechatronics, National Chung Cheng University
168 University Rd., Min-Hsiung, Chia-Yi 62102, Taiwan, R.O.C.
[2]Department of Mechanical Engineering, National Chung Cheng University
168 University Rd., Min-Hsiung, Chia-Yi 62102, Taiwan, R.O.C.

Abstract— In the proposed cellular detection system, the analysis of optical micrographs taken using a CCD camera attached to an optical microscope. In this study, transmittance spectra were used as image data, because different cancer stages corresponding to transmittance spectra. With optical micrographs taken using a CCD camera, the use of principal component analysis, and chromatic adaptation transformation with the linear regression, the optical micrographs will transform into transmittance spectra. We can quickly help doctors diagnose patients with cancer through transmittance spectra of different cancer stages.

REFERENCES

1. Ortyn, W. E., D. A. Basiji, P. Morrissey, T. George, B. Hall, C. Zimmerman, and D. Perry, "Blood and cell analysis suing an imaging flow cytometer," US 2009/7,522,758 B2, 2009.
2. "Interactive transparent individual cells biochip processor," US 2005/0014201 Al, 2005.
3. Miyake, Y., "Applications of color image processing based on spectral information," Feb. 28, 2001.
4. Guo, N., L. Zeng, and Q. Wu, "A method based on multispectral imaging technique for White Blood Cell segmentation," *Elsevier Health Sciences*, Jun. 18, 2005.
5. Fauch, L., E. Nippolainen, V. Teplov, and A. A. Kamshilin, "Recovery of reflection spectra in a multispectral imaging system with light emitting diodes," *Optics Express*, Vol. 18, No. 22, 23394–23405, Oct. 21, 2010.

Efficiency Enhancement of CIGS Solar Cell with Nano-fabrication Technique

Guan-Huang Wu[1], **Xusn-Yu Yu**[1], **Hsiang-Chen Wang**[1], **Pei-Chang Tsai**[2], **Jian-Hung Lin**[2], **Chia-Chen Hsu**[1, 2], **and Raymond Chien-Chao Tsiang**[1, 3]

[1]Graduate Institute of Opto-Mechatronics, National Chung Cheng University, Chia-Yi 62102, Taiwan
[2]Department of Physics, National Chung Cheng University, Chia-Yi 62102, Taiwan
[3]Department of Chemical Engineering, National Chung Cheng University, Chia-Yi 62102, Taiwan

Abstract— When the incident light meets the interface between air and electrode layer, reflection occurs from difference of refractive indices. Reflection means the loss of the light, which is absorbed to solar cell and generates electric power. In order to prevent the reflection, some kind of anti-reflection methods need to be developed. Surface anti-reflection treatment can be categorized to 4 different techniques including surface texturing, single-layer interference coating, multi-layer coating and moth-eye structure forming. Among them, moth-eye effect, introduced by Bernhard, caused gradual change in refractive index by forming nano-sized patterns on the surface. Thus the reflection of incident light can be minimized over the whole spectra range. In this paper, for efficiency enhancement, polymeric moth-eye patterns were fabricated on the surface of CIGS solar cell by using laser interference lithography (LIL). Many technologies could be selected to fabricate the moth-eye pattern, such as E-beam lithography, photolithography and nano-sphere lithography. However, these conventional lithography technologies need more time and cost. Hence, faster and cheaper laser interference lithography processes are needed for photovoltaic devices.

REFERENCES

1. Shibata, N., *Jpn. J. Appl. Phys.*, Vol. 30, 997, 1991.
2. Sun, C. H., P. Jiang, and B. Jiang, *Appl. Phys. Lett.*, Vol. 92, 061112-1, 2008.
3. Hong, S. H., B. J. Bae, K. S. Han, E. J. Hong, H. Lee, and K. W. Choi, *Electron. Mater. Lett.*, Vol. 5, 39, 2009.

Plasmonic Effects in Organic Solar Cells

Wei E. I. Sha[1], **Wallace C. H. Choy**[1], **and Weng Cho Chew**[1, 2]

[1]Department of Electrical and Electronic Engineering, The University of Hong Kong
Pokfulam Road, Hong Kong, China
[2]Department of Electrical and Computer Engineering, University of Illinois
Urbana-Champaign, Illinois 61801, USA

Abstract— The work provides a systematic study on plasmonic effects in organic solar cells (OSCs). We first introduce the concepts, significance, and recent progress of OSCs incorporating plasmonic nanostructures. On the basis of unique features of OSCs, we exploit versatile resonance mechanisms acting on the absorption enhancement of OSCs; for example, Fabry-Pérot mode, quasi-guided mode, and plasmonic mode. Next, we present rigorous theoretical models to characterize optical properties of OSCs. The key physical quantities, as well as the pros and cons of different models, are described. After that, we show some theoretical results to unveil the fundamental and device physics of plasmonic effects in typical OSC structures. Finally, we conclude the paper and identify future opportunities in this field.

The following figures show the optical designs of plasmonic nanostructures for improving the optical absorption of OSCs.

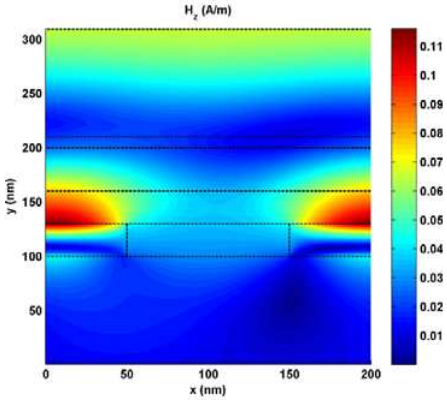

Figure 1: Surface plasmon resonance.

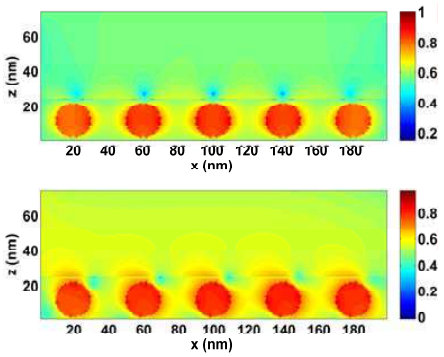

Figure 2: Local plasmon resonance.

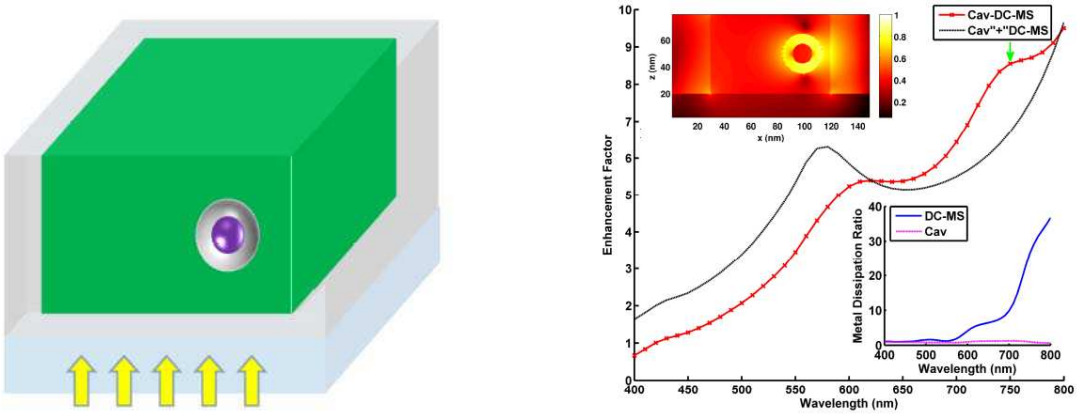

Figure 3: (a) Hybrid plasmonic system; (b) Near-field distribution and enhancement factors.

Optical Defect Modes in Spiral Media at Active Defect Layer

V. A. Belyakov
Landau Institute for Theoretical Physics, Russian Academy of Sciences
142432 Chernogolovka, Moscow Region, Russia

Abstract— An analytic approach to the theory of the optical defect modes in spiral media [1] for the case of an active defect layer is developed (under the term "active defect layer" is assumed a layer in which transformation of the light intensity or polarization occurs). The analytic study is facilitated by the choice of the problem parameters. Namely, a defect layer (with the averaged dielectric susceptibility equal to the average dielectric susceptibility of the spiral medium) sandwiched between spiral layers inserted in an isotropic medium with the dielectric constant equal to the average dielectric constant of the spiral medium is studied. The chosen model allows one to get rid off the polarization mixing at the external surfaces of the defect structure (DMS) and to reduce the corresponding equations to the equations for light of diffracting in the spiral medium polarization only. The dispersion equation determining connection of the defect mode frequency with the layer parameters and other parameters of the defect structure is obtained. Analytic expressions for the transmission and reflection coefficients of the defect mode structure (spiral medium layer-active defect layer-spiral medium layer) are presented and analyzed. To be specific as the defect layers were considered bierfringent, absorbing and amplifying defect layers in a perfect cholesteric structure. It is shown that the layer birefringence reduces the DM lifetime in comparison with the case of DMS with an isotropic defect layer and only at discrete values of DMS parameters it achieves the value of the corresponding DMS with an isotropic defect layer. Correspondingly, the effect of anomalously strong light absorption (and amplification) at the defect mode frequency and, consequently, the lowering of the lasing threshold are not so pronounced as in the case of the DMS with an isotropic defect layer. The case of DMS with low defect layer birefringence is studied in details. The effect of anomalously strong light absorption at the defect mode frequency for absorbing defect layer is discussed. It is shown that in DFB lasing at DMS with an amplifying defect layer an adjusting of the lasing frequency to the DM frequency results in a significant lowering of the lasing threshold and the threshold gain is lowering with increase of defect layer thickness. The options of effectively influence at the DM parameters by changing the defect layer birefringence are discussed.

REFERENCES

1. Belyakov, V. A. and S. V. Semenov, *JETP*, Vol. 112, 694, 2011.

Soliton Cryptography Using Dark-bright Conversion in a PANDA Ring Resonator

S. Songmuang[1], **X. Louangvilay**[2], **S. Mitatha**[3], **M. Yoshid**[4], **N. Komine**[4], **and P. P. Yupapin**[5]

[1]Faculty of Science and Technology, Kasem Bundit University, Bangkok 10250, Thailand
[2]International College, King Mongkut's Institute of Technology Ladkrabang, Bangkok 10520, Thailand
[3]Hybrid Computing Research Laboratory, Faculty of Engineering
King Mongkut's Institute of Technology Ladkrabang, Bangkok 10520, Thailand
[4]Department of Embedded Technology
School of Information Technology and Telecommunication Engineering, Tokai University, Japan
[5]Nanoscale Science and Engineering Research Alliance, Advance Research Center for Photonics
Faculty of Science, King Mongkut's Institute of Technology Ladkrabang, Bangkok 10520, Thailand

Abstract— We propose a concept of cryptography using dark-bright soliton conversion behaviors within a nonlinear ring resonator, in which the orthogonal soliton is established among the soliton conversion. A new model of add/drop filters is modified which is known as a PANDA ring resonator is proposed. The orthogonal solitons can be formed randomly within the system and detected simultaneously at the output ports. The entangled solitons(photons) can be formed in the same way of the entangled photons, but in this case the entangled soliton pair is gained more power that gives the advantage of long distance quantum communication. In application, the high capacity quantum communication is also available by using the multivariable entangled solitons. In this paper, we present the using optical randomly encoded techniques for communication security applications, in which the random signals can be generated and formed the security encoded signals. In the proposed system, firstly, a dark-bright soliton pair is input into a PANDA ring resonator, where the coincidence dark and bright soliton pair is occurred and obtained by using a $(\pi/2)$ phase retarder (i.e., a beamsplitter), which means that bit "1" and bit "0" states represent the orthogonal dark and bright soliton pulses. The signals from through (Th) port are formed and transmitted to the transmission line and finally to the end user. The add/drop filter is used to separate (filter) the required signal form the transmission link, in which the Th and drop port signals are formed as transmitted and referencing signals, respectively. Moreover, because of the lack of phase of $(\pi/2)$ between dark and bright solitons, the use of such behaviors can form in the same way as the entangled photon behaviors, in which the use of dark-bright soliton pairs for bit states. In this paper we also propose to transmit on the network applications that we will discuss after this.

THz Switching Generation Using a PANDA Ring Resonator for High Speed Computer Communication

Suphanchai Punthawanunt[1], **Saysamone Soysouvanh**[2, 3], **Khanthanou Luangxaysana**[2, 3], **Somsak Mitatha**[3], **Masahiro Yoshida**[4], **Noriyuki Komine**[4], **and Preecha Yupapin**[5]

[1]Faculty of Science and Technology, Kasem Bundit University, Bangkok 10250, Thailand
[2]International College, King Mongkut's Institute of Technology Ladkrabang, Bangkok 10520, Thailand
[3]Hybrid Computing Research Laboratory, Faculty of Engineering
King Mongkut's Institute of Technology Ladkrabang, Bangkok 10520, Thailand
[4]School of Information and Telecommunication Engineering, Tokai University, Japan
[5]Nanoscale Science and Research Alliance (N'SEAR), Faculty of Science
King Mongkut's Institute of Technology Ladkrabang, Bangkok 10520, Thailand

Abstract— A novel design of Terahertz (THz) switching generation for high speed computer used is proposed. The dense wavelength division multiplexing (DWDM) can be obtained by using a Gaussian or Soliton pluses propagating within a modified add-drop filter know as a PANDA ring resonator. The THz devices can made contributions to promising applications in high-speed switching, demultiplexing, and wavelength conversion of optical signals. Effective THz control is also essential for the potential application to ultrahigh-speed wireless digital interconnects for computer chips of the ultrahigh clock rates ($> 10\,\mathrm{GHz}$). In principle, the high density frequency (wavelength) can be generated and used to form the radio frequency identification (RFID), Ad-Hoc network and ubiquitous applications, moreover, the tiny device system is the another advantage, which can be constructed incorporating the available currently used system. In this paper is organized as follow: introduction, theory and the use of such a system in all proposed applications.

All Optical Logic NAND Gate Using Dark-Bright Soliton Conversion Control

Saysamone Soysouvanh[1,2], **Prapas Phongsanam**[2], **Khanthanou Luangxaysana**[1,2], **Somsak Mitatha**[2], **Komine Noriyuki**[3], **Masahiro Yoshida**[3], **and Preecha Yupapin**[4]

[1]International College, King Mongkut's Institute of Technology Ladkrabang, Bangkok 10520, Thailand
[2]Hybrid Computing Research Laboratory, Faculty of Engineering
King Mongkut's Institute of Technology Ladkrabang, Bangkok 10520, Thailand
[3]School of Information and Telecommunication Engineering, Tokai University, Japan
[4]Nanoscale Science and Research Alliance (N'SEAR), Faculty of Science
King Mongkut's Institute of Technology Ladkrabang, Bangkok 10520, Thailand

Abstract— In this paper, we present a new concept of all-optical gates using Dark-Bright soliton conversion behaviors within a nonlinear ring resonator, in which the orthogonal soliton is established among the soliton conversion. A new model of add/drop filters is modified which is known as a PANDA ring resonator is proposed. The entangled soliton/photon can work in the same way of the entangled photon, but in this case the entangled soliton is gained more power that can generate "1" and "0" for using optical gates. In application the logic bits can transport and process for long distance applications.

Session 1P2
Electromagnetic Theory and Design on the Optical Dispersive Materials, Invisible Cloak and Photonic Crystals

A New Novel GL Isotropic Invisible Cloak without Exceeding Light Speed Wave in Outer Layer of the Double Layer Cloak

Ganquan Xie, Jianhua Li, Lee Xie, and Feng Xie
GL Geophysical Laboratory, USA

Abstract— A more exciting breakthrough progress is that we discovered and propose a isotropic EM invisible cloak without exceeding light speed violation in this paper. The GL EM isotropic cloak is installed in outer layer of our double cloak. The GL isotropic invisible cloak in this paper and anisotropic invisible cloaks in our paper ArXiv 1050.3999 in May 2010 and paper in piers 2011 are complete new cloak and totally different from Pendry's cloak and Ulf's cloak in 2011. The dielectric and permeanbility of GL EM cloak in this paper are large than one. The refractive index of the GL cloak material, $n(r)$, is large than one or equal to one. The traditional geometry optical ray tracing method can not be used for explaining our GL isotropic and anisotropic cloak. When EM wave propagates in our GL cloak, an extensive Femate Principle is satisfied. Our GL isotropic cloak in this paper and anisotropic cloaks in ArXiv 1050.3999 in May 2010 are created from our unconventional GL EM cloak modeling and inversion that are proposed here. By searching in a distinctive class of the rational function of (h), $h = r - R_1$, the GL EM cloak modeling and inversion create GL EM isotropic invisible cloak class without exceeding light speed. The GL EM cloaks can be practicable by using conventional optical materials. The properties of our GL EM cloak and their proofs are presented by using GL modeling and inversion in this paper. The novel EM wave propagation and front branching in the GL cloak by GL EM modeling are presented in this paper. The EM wave front propagation in GL cloak is behind of the front in free space. At time steps $118dt$, in the GL cloak, the wave front is curved as a crescent like and propagates slower than the light in free space. At the time step $120dt$, the EM wave inside of the GL EM cloak propagates slower than light speed, moreover, its two crescent front peaks intersect at a front branching point. At the front branching point, the front is split to two fronts. The novel front branching and crescent like wave propagation are displayed in figures in this paper. We propose a new GL EM isotropic invisibility cloak as follows and its novel invisible properties without exceeding light speed are shown in references [1–3].

$$\varepsilon_r(r)=\mu_r(r)=\frac{R_2}{\sqrt{r-R_1}\sqrt{G_2\left(R_1,R_2,R_2-r\right)}}+\frac{4\left(R_2-2R_1\right)\sqrt{(r-R_1)}R_2}{\left(G_2\left(R_1,R_2,R_2-r\right)\right)^{\frac{3}{2}}F_2\left(R_1,R_2,(R_2-r)\right)}, \quad (1)$$

where

$$\begin{aligned} G_2(R_1,R_2,R_2-r) &= 3R_2-4R_1+\sqrt{R_2^2+16(R_2-R_1)(R_2-r)-8R_2(R_2-r)}, \\ F_2(R_1,R_2,R_2-r) &= \sqrt{R_2^2+16(R_2-R_1)(R_2-r)-8R_2(R_2-r)}, \end{aligned} \quad (2)$$

REFERENCES

1. Xie, G., J. Li, L. Xie, and F. Xie, arXiv:1005.3999.
2. Xie, G., J. Li, L. Xie, and F. Xie, "A new GL anisotropic and isotropic invisible cloak without exceeding light speed violation," *PIERS Proceedings*, 878–881, Suzhou, China, September 12–16, 2011; *Progress in Some Fields of Mathematical Sciences*, 56–69, Chinese Sciences Press, ISBN 9758-7-03-032787-1.
3. Li, J., G. Xie, L. Xie, F. Xie, and H. Zhou, "A new practicable GLLH EM invisible cloak without exceeding light speed wave," *PIERS Proceedings*, 18–26, Suzhou, China, September 12–16, 2011; *Progress in Some Fields of Mathematical Sciences*, 143–162, Chinese Sciences Press, ISBN 9758-7-03-032787-1.

Lossy Gradient Index Metamaterial with General Periodic Permeability and Permittivity: The Case of Constant Impedance throughout the Structure

M. Dalarsson[1], M. Norgren[1], and Z. Jaksic[2]

[1]Division of Electromagnetic Engineering, School of Electrical Engineering
Royal Institute of Technology, Stockholm SE-100 44, Sweden
[2]IHTM — Institute of Microelectronic Technologies and Single Crystals
University of Belgrade, Njegoševa 12, Belgrade 11000, Serbia

Abstract— We utilize an exact analytical approach to investigate the electromagnetic wave propagation across an infinite metamaterial composite with general periodic gradient effective permittivity and permeability. A remarkably simple direct solution for the field distribution is obtained for an arbitrary periodic variation of complex refractive index across the structure. The calculation is done for the case of constant impedance across the structure. Arbitrary temporal dispersion and losses are allowed and the model is generally applicable to inhomogeneous and anisotropic media simultaneously containing positive and negative refractive index constituents as long as the effective medium approximation is valid.

Electromagnetic metamaterials (MM) are a new paradigm in electromagnetics and (nano) plasmonics. They may be defined as artificial composites with electromagnetic properties not readily found in nature. A special class of MMs are the negative refractive index metamaterials (NRM or NIM), also known as the left-handed materials (LHM). LHM are typically produced using subwavelength "particles" or "atoms" with negative effective relative permittivity and permeability as their structural units. The novel and often counter-intuitive properties of the LHM, which include negative index of refraction (and, hence, negative phase velocity), inverse Doppler effect, radiation tension instead of pressure, etc. resulted in numerous proposed applications. These include superlenses and hyperlenses that enable imaging far below the diffraction limit, resonant cavities and waveguides with geometrical dimensions even orders of magnitude smaller than the operating wavelength, as well as invisibility cloaks and transformation optics.

A majority of cases considers structures with constant refractive index within the MM structure and abrupt interfaces with the surrounding positive index material ("right-handed" media, RHM). There is however a practical interest for metamaterials with spatially varying refractive index and with gradual transition from the RHM to LHM and vice versa, since many real-world applications would benefit from such structures. Graded refractive index is interesting for transformation optics and hyperlenses, and a class of the invisibility cloaks using spherically graded MM has been described. Various other proposed applications of graded metamaterials include beam shaping and directing, enhancement of nonlinear effects, superlenses, etc..

As far as the authors are informed, the first papers dedicated to gradient refractive index LHM were published in 2005. Exact analytical approaches to some special cases of graded index metamaterial structures have been developed by the present authors in a number of papers, and are of special interest, since they ensures fast, simple and direct route to the determination of the field distribution and the calculation of the scattering parameters within such materials. In this paper, we present an exact analytical solution of Helmholtz equation for the propagation of electromagnetic waves through a lossy gradient metamaterial structure with an arbitrary periodic permeability and permittivity for the case of constant impedance throughout the structure. We illustrate the obtained general results by considering a few special cases including the case of constant material parameters and abrupt transitions.

Monolithic Silicon-based Gauss to J_0-Bessel-Gauss Beam Converter

D. P. San Roman Alerigi, Y. Zhang, T. K. Ng, A. B. Slimane, and B. S. Ooi
Division of Physical Sciences and Engineering
King Abdullah University of Science and Technology (KAUST), Saudi Arabia

Abstract— We report on the first Si-based graded refractive index structure to realize conversion of Gaussian beams to J_0-Bessel-Gauss beams. Production of near-Bessel beams has been explored in recent years by different techniques like holograms, phase elements and plasmons (1; 2; 3). Although these methods yielded high quality beams they are potentially complicated when integrated with other photonic integrated circuits (PICs) elements. Hence, the need for an integrated and compatible solution to realize on-chip conversions of beam profiles. In our work we explore a theoretical device in which the refractive index profile and dimensions were tailored to produce silicon technology compatible near Bessel beam converter. Our device consists of a rectangular Si slab, width (w) and length (l) of 20 µm and 200 µm, respectively. The refractive index is tailored in both directions ranging from 1 (air) to 3.5 (Silicon) in controllable steps. To solve the inverse problem we implemented a hybrid technique based on transformation optics and variational methods. Two-dimensional Beam Propagation method (2D-BPM) was used to simulate the beam characteristics in the device. The near and far field studies showed that the proposed device transform an impinging Gauss beam with spot size of 10 µm into a J_0-Bessel-Gauss beam after 200 µm transmission, with 5% loss and a beam divergence of 2%. An optimization of the refractive index profile yielded a J_0-Bessel-Gauss beam coupling into a 0.5 µm wide waveguide with $n = 2.5$ at a coupling loss of 1%. Such self-healing beam, where the beam stays undisturbed after passing through nanoscopic objects, may be potentially useful in photonic-based microfluidic applications. Additionally, our technique can be extended to produce other non-linear beams. Further details will be presented in the final manuscript.

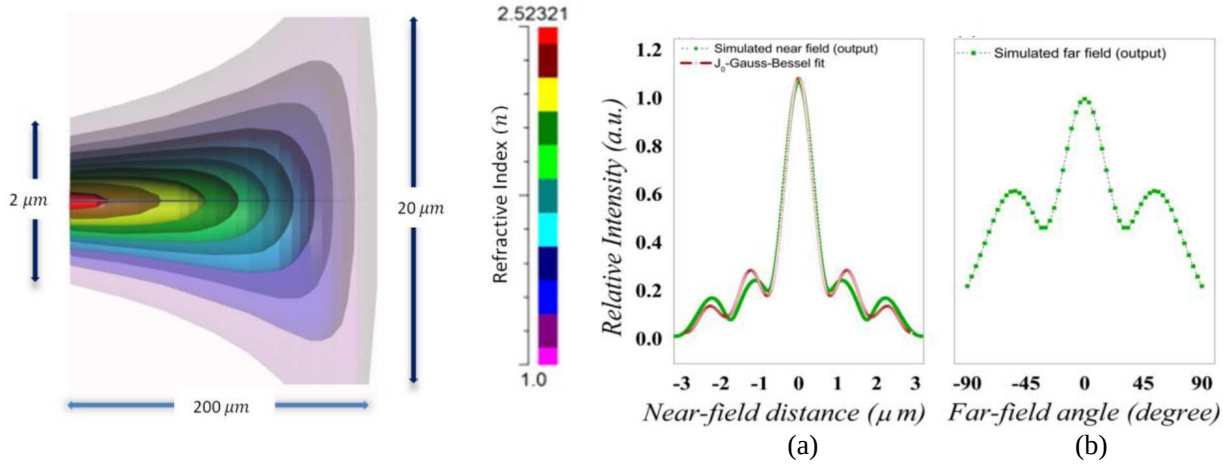

Figure 1: Proposed slab convertor structure (left), the device has 11 controllable refractive index steps. (a) The resulting beam (right) after a propagation of is a Bessel-Gauss beam, (b) the far-field profile is also of the Bessel-Gauss form.

REFERENCES

1. Méndez Otero, M. M., et al., ed., *OSA Technical Digest*, OSA, Rochester, New York, 2006; *Frointiers in Optics*, JWD129.
2. Cong, W., N. Chen, and B. Gu, *J. Opt. Soc. Am.*, Vol. 15, No. 9, 2362, 1998.
3. Zhan, Q., *Opt. Lett.*, Vol. 31, 1726–1728, 2006.

A New Tunable Metamaterial Using Low-loss Ferrofluid and Its Application on Lens Antenna

Haoxue Han, **Dichen Li**, **and Xiaoyong Tian**
State Key Laboratory of Manufacturing Systems Engineering
Institute of Advanced Manufacturing Technique
Xi'an Jiaotong University, Xi'an, Shaanxi 710049, China

Abstract— We present a new kind of tunable metamaterial using a low-loss ferrofluid, which is well suited for RF and microwave device applications. The ferrofluid is prepared by homogeneously dispersing magnetite (Fe_3O_4) nanoparticles in a low-loss mixture of organic solvents at microwave frequencies such as N, N-Dimethyl aniline, acetonitrile and benzene. Continuously tunable permittivity of the matrix can be achieved by controlling the concentration of different liquid components in the mixture. The impedance matching with free space and the loss tangent is substantially improved by the monodispersion of the magnetic nanoparticles with diameters between 10 and 20 nm. By using a dielectric probe kit and a network analyzer, the permittivity of the ferrofluid was retrieved in the range of 8 and 12 GHz. The measured data revealed a tunable range of permittivities from 2.3 to 25.8 with a loss tangent of 0.01 to 0.02 and an optimal relative characteristic impedance of 1.4. Based on the ferrofluid presented above, a low-loss lens antenna with a spacial refractive index distribution was designed to realize the tunable radiation angle of microwave beams.

Fabrication of Gradient index 3D Photonic Crystals Structure in Metamaterial

Ming Yin, **Dichen Li**, **and Xiaoyong Tian**
State Key Laboratory of Manufacturing Systems Engineering
Institute of Advanced Manufacturing Technique
Xi'an Jiaotong University, China

Abstract— A broadband and low-loss graded index (GRIN) 3D photonic crystals (PCs) structure in the metamaterial regime is proposed in the present research. The 3D isofrequency contours are approximately spherical in long-wavelength limit, which leads to nearly isotropic electromagnetic properties. By gradually varying the constitutive parameters of the PCs, the complex spatial distribution of the refractive index profile desgined for controlling electromagnetic fields can be fulfilled.

A carpetcloak and a 3D omnidirectional electromagnetic absorber (elctromagnetic blackhole), which employed the GRIN 3D PCs structure operating in the metamaterial regime were fabricated by stereolithography using photocurable resin. The nonresonant property of the sub-wavelength PCs unit cell resulted in a very broad bandwith and relatively low loss. Their eletromagnetic properties were stuied experimentally both in 2D and 3D cases, and agreed well with the simulation results, demonstrating a low-cost and rapid manufacturing method for the realization of pratical cloak and 3D "elctromagnetic blackhole".

Azimuthal Directive Emission Realized by Transformation Optics Concept

Xinying Wu, **Paul-Henri Tichit**, **Souad Kirouane**,
Shah Nawaz Burokur, **and André de Lustrac**
IEF, University of Paris-Sud, CNRS, UMR 8622, Orsay Cedex 91405, France

Abstract— Transformation optics is a mathematical tool that consists in generating a new transformed space from an initial one where solutions of Maxwell's equations are known. It offers an unconventional strategy to the design of novel class metamaterial devices, such as invisibility cloaks [1–3], waveguides transition and bends [4–8], Luneberg lenses [9] and ultra-directive antennas [10–12]. Using the idea of wave manipulation through transformation optics, we demonstrate numerically and experimentally a way to create an azimuthal directive emission from quasi omnidirectional sources such as microstrip patch antennas or monopoles. The manipulation is enabled by composite metamaterials that realize a space coordinate transformation in the radiation zone of the latter source. It is shown that a plane source radiating in the elevation plane can be transformed into an azimuthal radiative element by modifying the electromagnetic properties of the space around it. For a physical prototype fabrication, we have simplified the calculated material parameters through a parameter reduction procedure. The relevant electromagnetic parameters found are therefore μ_{zz}, $\varepsilon_{\theta\theta}$ and ε_{rr}. We maintained $\varepsilon_{\theta\theta}$ and μ_{zz} constant and hence the new set of coordinates is as follows:

$$\begin{cases} \varepsilon_{rr} = \left(\frac{1}{br}\right)^2 \div 1.7 \\ \varepsilon_{\theta\theta} = 2.8 \\ \mu_{zz} = 1.7 \end{cases}$$

The fabricated prototype is then composed of 30 identical layers where each layer is divided in 10 unit cells. The cells are composed of respectively SRRs [13] and ELCs [14] to secure μ_{zz} and ε_{rr}. $\varepsilon_{\theta\theta}$ is produced by a host medium, which is a commercially available resin. Near-field cartography and far-field pattern measurements performed on the fabricated prototype agree qualitatively with Finite Element Method (FEM) simulations. The results obtained confirm the bending of electromagnetic waves to create the azimuthal emission. This idea can find various applications in novel antenna design techniques for aeronautical and transport domains.

REFERENCES

1. Schurig, D., J. J. Mock, B. J. Justice, S. A. Cummer, J. B. Pendry, A. F. Starr, and D. R. Smith, "Metamaterial electromagnetic cloak at microwave frequencies," *Science*, Vol. 314, No. 5801, 977–980, 2006.
2. Liu, R., C. Ji, J. J. Mock, J. Y. Chin, T. J. Cui, and D. R. Smith, "Broadband ground-plane cloak," *Science*, Vol. 323, No. 5912, 366–369, 2009.
3. Kanté, B., D. Germain, and A. de Lustrac, "Experimental demonstration of non-magnetic metamaterial cloak at microwave frequencies," *Phys. Rev. B*, Vol. 80, 201104(R), 2009.
4. Rahm, M., D. A. Roberts, J. B. Pendry, and D. R. Smith, "Transformation-optical design of adaptive beam bends and beam expanders," *Opt. Express*, Vol. 16, No. 15, 11555–11567, 2008.
5. Rahm, M., S. A. Cummer, D. Schurig, J. B. Pendry, and D. R. Smith, "Optical design of reflectionless complex media by finite embedded coordinate transformations," *Phys. Rev. Lett.*, Vol. 100, No. 6, 063903, 2008.
6. Lin, L., W. Wang, J. Cui, C. Du, and X. Luo, "Design of electromagnetic refractor and phase transformer using coordinate transformation theory," *Opt. Express*, Vol. 16, No. 10, 6815–6821, 2008.
7. Huangfu, J., S. Xi, F. Kong, J. Zhang, H. Chen, D. Wang, B.-I. Wu, L. Ran, and J. A. Kong, "Application of coordinate transformation in bent waveguide," *J. Appl. Phys.*, Vol. 104, No. 1, 014502, 2008.
8. Tichit, P.-H., S. N. Burokur, and A. de Lustrac, "Waveguide taper engineering using coordinate transformation technology," *Opt. Express*, Vol. 18, No. 2, 767–772, 2010.
9. Kundtz, N. and D. R. Smith, "Extreme-angle broadband metamaterial lens," *Nat. Mater.*, Vol. 9, 129–132, 2010.

10. Tichit, P.-H., S. N. Burokur, and A. de Lustrac, "Ultradirective antenna via transformation optics," *J. Appl. Phys.*, Vol. 105, No. 10, 104912, 2009.
11. Tichit, P.-H., S. N. Burokur, D. Germain, and A. de Lustrac, "Design and experimental demonstration of a high-directive emission with transformation optics," *Phys. Rev. B*, Vol. 83, No. 15, 155108, 2011.
12. Tichit, P.-H., S. N. Burokur, D. Germain, and A. de Lustrac, "Coordinate transformation based ultra-directive emission," *Elec. Lett.*, Vol. 47, No. 10, 580–582, 2011.
13. Pendry, J. B., A. J. Holden, D. J. Robbins, and W. J. Stewart, "Magnetism from conductors and enhanced nonlinear phenomena," *IEEE Trans. Microwave Theory Tech.*, Vol. 47, 2075–2084, 1999.
14. Schurig, D., J. J. Mock, and D. R. Smith, "Electric-field-coupled resonators for negative permittivity metamaterials," *Appl. Phys. Lett.*, Vol. 88, 041109, 2006.

Quasi-perfect Isotropic Emission Realized by Coordinate Transformation

Paul-Henri Tichit, **Shah Nawaz Burokur**, **and André de Lustrac**
IEF, University of Paris-Sud, CNRS, UMR 8622, Orsay Cedex 91405, France

Abstract— Transformation optics is a mathematical tool that consists in generating a new transformed space from an initial one where solutions of Maxwell's equations are known. It offers an unconventional strategy to the design of novel class metamaterial devices, such as invisibility cloaks [1–3], waveguides transition and bends [4–8], Luneberg lenses [9] and ultra-directive antennas [10–12]. Using the idea of wave manipulation via transformation optics, we propose a way to create a quasi-perfect isotropic emission from a directional one. The manipulation is enabled by composite metamaterials that correspond to a space stretching around the source. The expansion procedure is further followed by a compression so as to secure a good impedance matching with free space. It is shown that the directive radiation of a plane source larger than the operating wavelength can be transformed into an isotropic one by modifying the electromagnetic properties of the space around it. A set of parameters allowing practical realization of the proposed device is defined. At the center of the transformed space, ε and μ present very low values ($\ll 1$). Consequently, light velocity and the corresponding wavelength are much higher than in vacuum. The width of the plane source then appears very small compared to wavelength and the source can then be regarded as a radiating wire, which is in fact an isotropic source. Numerical simulations using Finite Element Method (FEM) are performed to illustrate the proposed coordinate transformation. This idea, which consists in strongly reducing the apparent size of a radiating source, can find various applications in novel antenna design techniques.

REFERENCES

1. Schurig, D., J. J. Mock, B. J. Justice, S. A. Cummer, J. B. Pendry, A. F. Starr, and D. R. Smith, "Metamaterial electromagnetic cloak at microwave frequencies," *Science*, Vol. 314, No. 5801, 977–980, 2006.
2. Liu, R., C. Ji, J. J. Mock, J. Y. Chin, T. J. Cui, and D. R. Smith, "Broadband ground-plane cloak," *Science*, Vol. 323, No. 5912, 366–369, 2009.
3. Kanté, B., D. Germain, and A. de Lustrac, "Experimental demonstration of non-magnetic metamaterial cloak at microwave frequencies," *Phys. Rev. B*, Vol. 80, 201104(R), 2009.
4. Rahm, M., D. A. Roberts, J. B. Pendry, and D. R. Smith, "Transformation-optical design of adaptive beam bends and beam expanders," *Opt. Express*, Vol. 16, No. 15, 11555–11567, 2008.
5. Rahm, M., S. A. Cummer, D. Schurig, J. B. Pendry, and D. R. Smith, "Optical design of reflectionless complex media by finite embedded coordinate transformations," *Phys. Rev. Lett.*, Vol. 100, No. 6, 063903, 2008.
6. Lin, L., W. Wang, J. Cui, C. Du, and X. Luo, "Design of electromagnetic refractor and phase transformer using coordinate transformation theory," *Opt. Express*, Vol. 16, No. 10, 6815–6821, 2008.
7. Huangfu, J., S. Xi, F. Kong, J. Zhang, H. Chen, D. Wang, B.-I. Wu, L. Ran, and J. A. Kong, "Application of coordinate transformation in bent waveguide," *J. Appl. Phys.*, Vol. 104, No. 1, 014502, 2008.
8. Tichit, P.-H., S. N. Burokur, and A. de Lustrac, "Waveguide taper engineering using coordinate transformation technology," *Opt. Express*, Vol. 18, No. 2, 767–772, 2010.
9. Kundtz, N. and D. R. Smith, "Extreme-angle broadband metamaterial lens," *Nat. Mater.*, Vol. 9, 129–132, 2010.
10. Tichit, P.-H., S. N. Burokur, and A. de Lustrac, "Ultradirective antenna via transformation optics," *J. Appl. Phys.*, Vol. 105, No. 10, 104912, 2009.
11. Tichit, P.-H., S. N. Burokur, D. Germain, and A. de Lustrac, "Design and experimental demonstration of a high-directive emission with transformation optics," *Phys. Rev. B*, Vol. 83, No. 15, 155108, 2011.
12. Tichit, P.-H., S. N. Burokur, D. Germain, and A. de Lustrac, "Coordinate transformation based ultra-directive emission," *Elec. Lett.*, Vol. 47, No. 10, 580–582, 2011.

High Energy Particals and Nanostructures Physics

D. Bajalan
ret., Austria

Abstract— Demands for the continuous increase in the data storage density bring the challenge to overcome physical limits for currently used magnetic recording media. Magnetic nano structures are subjects of growing interest because of their potential applications in high density magnetic recording media and their original magnetic properties. Over the past several decades, amorphous and more recently nano-crystalline materials have been investigated for applications in magnetic devices. The benefits found in the nano-crystalline alloys is from their chemical and structural variations on a nano-scale which are important for developing optimal magnetic devices with high properties.

Research on Potential Use of Nanomaterials and Properties in Astrophysics

D. Bajalan
ret., Austria

Abstract— When the physical dimensions of a system become comparable to the interatomic spacing, strong modifications of the intrinsic magnetic properties (ordering temperature, magnetic anisotropy, spontaneous magnetization) are expected. Micromagnetic modeling of the behavior of a nanostructured film beautifully describes the magnetization process, but requires a high calculational effort and long computation times. Furthermore, it is difficult to predict changes of the macroscopic physical behaviour due to variation of parameters. Phenomenological models, on the other hand, are very useful to simulate the behaviour of the magnetic material under the influence of varying parameters, especially when the parameters are based on physical constants.

Nano Particle Thermal Stability and Natural Subnanostructures

D. Bajalan
ret., Austria

Abstract— Magnetic nano particle thermal stability calculation is essential for development of patterned ultra high magnetic storage media. The use of reliable model (like: Energetic Model (EM) in the predication of non linear ferromagnetic materials properties, wich may depend also on direction and history of magnetization) is very important. EM simulation of hysteresis opens a very big opportunities to calculate values of parameters which we then use directly for interpretation of the stability condition of stored information on a nano magnetic structure. The main idea behind that is to change the direction of the applied field H and then see the stability conditions on a given nano bit volume. The value of the fBS depends strongly on Ku and the volume of the nano structure which holds the stored magnetic information (a what socalled nano bit or nano dot). Research and development teams in companies implementing nano-technology are gaining more and more importance in the field of sensor systems and material science.

Session 1P3a
Microwave Remote Sensing

Physical Model for Radar Remote Sensing of Snow at X-band and Ku-band Based on Bicontinuous Medium

Xiaolan Xu[1], **Leung Tsang**[1], **Wenmo Chang**[1], **Simon Yueh**[2], **and Kung Hau Ding**[3]

[1]Department of Electrical Engineering, University of Washington, Seattle, WA 98195-2500, USA
[2]Jet Propulsion Laboratory, California Institute of Technology, Pasadena, CA 91109, USA
[3]Sensor Directorate, Air Force Research Laboratory, Wright-Patterson AFB, OH 45433, USA

Abstract— In this paper, we present forward models for microwave scattering by terrestrial snow. Snow is a dense medium with densely packed inhomogenieties. We used two models: densely packed particles, and bicontinuous medium. For the case of densely packed particles, we used the Metropolis shuffling method to simulate the positions of particles which can have adhesive properties. The Fold-Lax equations of multiple scattering are used to study scattering. For the case of bicontinuous media, the snow porous structures are generated according to a continuous representation of ice-air interfaces. A large number of the stochastic sinusoidal waves are used to construct the interfaces. Various snow structures are demonstrated by adjusting the probability density function of the wave amplitude. The extinction properties and phase matrix are studied through the Monte Carlo simulations. For each realization, the Maxwell Equation was performed and solved numerically using DDA/FFT to take into account the multiple scattering. We demonstrated the frequency dependence of the extinction coefficient. In different structure setting and fractional volume, the frequency dependent index can vary. The frequency dependence are compared with experimental measurements. The phase matrix calculated in the Bi-continuous model agree with analytical Quasi-crystalline Approximation (QCA) method in co-polarization. However, it shows significant large cross-polarization. The results are then combined in the dense media radiative transfer theory (DMRT). We obtain the 1st order solution by using the iterative method and full multiple solution through quadrature approach. The surface scattering from the snow-ground interface is included by searching the look up table. The lookup table is generated through performing large scale 3D simulations of numerical solutions of Maxwell equations of scattering by random rough surfaces. The model is applied to study the snow scattering characteristics at X-band and Ku-band which are the two frequencies proposed in the Cold Regions Hydrology High-resolution Observatory ($CoReH_2O$) mission by ESA and Snow and Cold Land process (SCLP) mission by NASA. The results are compared with the POSCAT Ku-band airborne data and X-band TerraSAR-X satellite data in Alaska region.

Physical Forward Models and Data Cubes for Radar Remote Sensing at L-band for SMAP Applications

Xiaolan Xu[1], **Leung Tsang**[1], **Tien-Hao Liao**[1], **Shaowu Huang**[1], **and Seung-Bum Kim**[2]

[1]Department of Electrical Engineering, University of Washington, Seattle, WA 98195-2500, USA
[2]Jet Propulsion Laboratory, California Institute of Technology, Pasadena, CA 91109, USA

Abstract— In this paper, we present forward models and data cubes of the microwave backscattering from a vegetated terrain at L band for application in the upcoming SMAP (Snow Moisture Active and Passive) mission. The vegetated surface model includes a layer of cylinders and disks to represent the branches and leaves of a vegetation layer on top of the soil surface. The data cubes are used in the active radar algorithm and in the active/passive algorithm.

In the scattering of waves by soil surfaces, we consider the soil to be a lossy dielectric medium. The random rough surface is characterized by Gaussian random process with exponential correlation functions. A hybrid UV/PBTG/SMCG method is developed to accelerate Method of Moment solution. Results are illustrated for bistatic scattering and backscattering. Both Co-polarization and Cross polarization have been calculated. Comparisons are made with experimental data. Lookup tables have been prepared for backscattering for a range of soil moisture, rms heights and correlation lengths.

For the case of vegetated surfaces, we have implemented the body of revolution (BOR) and the discrete dipole approximation (DDA) numerical solutions of Maxwell equations for scatterers of simple shapes including cylinders, ellipsoids, and disks. These are used to model branches, stalks and leaves in vegetation. Using the distorted Born approximation, the results are expressed in terms of volume scattering, surface scattering, and double bounce scattering. Data Cubes have been calculated for a variety of crop types. Studies are made on the dominant mechanism for each crop type. The models have been validated with HYDROS and SMAP field measurements.

Numerical Modeling to Analyze Effects of Mobile EM Source for Seafloor Exploration

Nazabat Hussain, **Norashikin Yahya**,
Noor Hazrin Hany Mohamad Hanif, **and Mohd Noh Karsiti**
Universiti Teknologi PETRONAS, Malaysia

Abstract— Electromagnetic (EM) geophysical surveys had been used to determine the spatial distribution of earth's physical properties from limited set of measurements which are conducted on earth surface. Whereas, marine controlled source electromagnetic (CSEM) method is used for seafloor exploration. This technique utilizes mobile EM source that is moved above the seafloor and fixed grounded receivers. In such scenarios, excited EM energy comes to the region of interest from a distant source and it terminates along the direction of propagation. Only reflected field would be received which contains information of earth interior. The procedure of converting received data into spatial distribution of earth's physical properties is known as modelling and the related mathematical process is called inversion. Marine CSEM has been fairly successful, however it still has fair amount of failure cases because of its limitations. The limitations are typically related to source-receiver geometry, source signal strength, seawater depth and geological complexities. These limitations can be resolved by implementing confidence modelling. This paper aims to find the optimum speed of mobile dipole source in marine CSEM survey. The changing of dipole speed during the survey can change the quality of survey data. Numerical solution is implemented by writing forward algorithm using staggered-grid finite difference solution in spatial domain and forward time central space in temporal domain. Solution is achieved through I) an optimal grid technique that extends the boundaries of the mesh outward from the region of interest using a minimal number of nodes, II) a direct matrix solution technique that allows for the simultaneous solution for all sources. This modelling provides what should be the optimal speed of EM source in marine CSEM survey and how to improve the quality of survey data.

Data collected from marine controlled-source electromagnetic (CSEM) survey has been used for hydrocarbon exploration in marine environment. Using the collected data, the spatial distribution of seabed layers can be mapped through inversion technique. However, the accuracy of the seabed mapping depends on the quality of the survey data. There are several factors affecting the survey data; such as source-receiver geometry, source signal strength, seawater depth and geological complexities. This paper presents a method of finding optimum speed of mobile dipole source in marine CSEM survey, one of the factor affecting the survey data. The technique involved numerical solution of forward modelling using staggered-grid finite difference in spatial domain and forward time central space in temporal domain. The results show that the optimal speed obtained from the forward model has significantly improve the quality of survey data.

Variation in Wireless-sensing of UHF-RFID Antennas with Insertion of Dielectric Material

S. D. Nawale[1] and N. P. Sarwade[2]

[1]Sinhgad Institute of Technology, Lonavala, Pune (MH), India
[2]Veermata Jijabai Technological Institute, Mumbai (MH), India

Abstract— Radiofrequency identification is growing technology in replacement of barcodes and optical character recognition. Wide range of applications including logistics, intelligent traffic, security, tale health made wireless RFID more popular. A passive tag, comprising of an antenna and a microchip transponder, is remotely interrogated by a reader. The contents stored in the internal memory of the tag are communicated to interrogating reader by modulated backscattering of the signal.

This work presents UHF RFID passive tag designed at 870 MHz, with the insertion of sensitive dielectric material placed at different portions of tag. Variation in position of dielectric, changes electrical properties of the tag whose consequence results in variation of tag response. The change in tag impedance and realized gain also can be remotely monitored.

The proposed device of the credit card size is simple in construction with folded planar antenna. Radiating H-shaped slot helps for impedance matching of antenna with the microchip. The integration of dielectric in open slot of antenna and even overlapping the slot is able to vary the read range 5–10 m. The idea of changing the material and its dielectric constant leads to develop RFID tag as a wireless sensor.

Here, set of experiments are performed, with the purpose to sense the variation of realized gain. Measurement is done with turn-on power method where minimum transmitted reader power is scattered back by the designed tag, placed at fixed distance. The results are compared to find the sensitivity with and without dielectric. It shows that tag becomes more sensitive and provides improved realized gain by 2 dB, when symmetrical dielectric is inserted in the H-slot. Variation in dielectric constant of material also results in dynamic variation of realized gain by 7 dB.

ACKNOWLEDGMENT

The authors would like to thank Board of Colleges and University Department, University of Pune, MH, India, for supporting this research with funding. (BCUD/OSD/390, Dated: 26/10/2010).

REFERENCES

1. Stockman, H., "Communication by means of reflected power," *Proceedings of the IRE*, Vol. 36, No. 10, 1196–1204, October 1948.
2. Marrocco, G., "The art of UHF RFID antenna design: Impedance-matching and size reduction techniques," *IEEE Antenna and Propagation Magazine*, Vol. 50, No. 1, 66–79, February 2008.
3. Marrocco, G., L. Mattioni, and C. Calabrese, "Multiport sensor RFID's for wireless passive sensing of objects — Basic theory and early results," *IEEE Transactions on Antennas and Propagation*, Vol. 56, No. 8, 2691–2702, August 2008.

Reflection Technique for the Determination of Moisture Content in Hevea Rubber Latex

Farizah Ansarudin[1, 2], **Zulkifly Abbas**[1], **Ali Hamad Ali**[1], **and Mohamad Aliff Ismail**[1]

[1]Department of Physics, Faculty of Science, Universiti Putra Malaysia, Serdang 43400, Selangor, Malaysia
[2]Department of Electrical, Electronic and Systems Engineering
Faculty of Engineering and Built Environment
Universiti Kebangsaan Malaysia, Bangi 43600, Selangor, Malaysia

Abstract— This paper presents a new technique for the determination of moisture content in hevea rubber latex using an insulated monopole antenna. The antenna was fabricated from a coaxial SMA stub contact panel. The reflection measurements of hevea rubber latex were carried out using an Agilent Professional Network Analyzer N5230A (PNA) in the frequency range from 0.1 to 4 GHz. The variations in magnitude and phase shift with moisture content were analyzed using regression analysis at several selected frequencies. These in turn were used to establish the relationship in magnitude and phase shift with moisture content. The actual moisture content was determined by the standard oven drying method and compared with predicted values of moisture content. The mean relative errors in the determination of moisture content range from 36.95% to 87.51% using magnitude and phase shift techniques were 0.0505 and 0.0144, respectively.

Session 1P3b
SAR/ISAR and Its Applications

SAR and ISAR for Diagnostic RCS Measurements

Christer Larsson[1, 2]

[1]Department of Electrical and Information Technology
Lund University, SE-221 00 Lund, Sweden
[2]Saab Dynamics, SE-581 88 Linköping, Sweden

Abstract— Synthetic Aperture Radar (SAR) and Inverse Synthetic Aperture Radar (ISAR) processing for diagnostic Radar Cross Section (RCS) measurements trace their roots back to the 1980's. The computers that were available then were slow, judging with present day standards, which meant that in order to do SAR/ISAR processing in reasonable times one used so called focused imaging that involved a 2D interpolation of the recorded RCS before the 2D FFT. This is a fast method but it introduces some error noise because of the interpolation and it is not that flexible. The algorithm for backprojection imaging, that in many ways is more straightforward, was too slow for practical work due to the computers used in those days. However, the tremendous advances that have been made in CPU processing power in addition to using multi core CPUs mean that these limitations no longer exist and that very accurate imaging can be performed, in close to real time, even on a low-end notebook computer. Furthermore, using the backprojection algorithm, it is straightforward to correct for geometric and amplitude aberrations that are caused by measuring in near field conditions. These corrections are important in order to obtain accurate RCS data.

The images obtained show the geometrically correct locations of the target scatterers with some exceptions for certain target features. Separate features in the images can be gated in the image domain and an inverse processing step can be performed to obtain the RCS of selected parts of the image, i.e., collections of scatterers on the target, as a function of frequency of angle and frequency. It is also possible to do an approximate near field to far field transformation of the RCS data using image gating.

The presentation will focus on two setups where image gating is used. The first one is an RCS near field broadband measurement range where a heavy duty turntable provides angular resolution for ISAR processing. The performance of image gating procedures will be shown using actual data from full scale objects over a wide frequency range. The second setup is a low cost transportable SAR for near field measurements. Image gating is used here to evaluate the effect of camouflage nets and the SAR signature of vehicles. The accuracy of the RCS obtained by the image gating process is evaluated for the two setups.

MIMO Radar 3D Imaging with Improved Rotation Parameters Estimation

Changzheng Ma[1], **Tat-Soon Yeo**[1], **Chin Yuan Chong**[2], **and Tao Zhang**[3]

[1]Department of Electrical and Computer Engineering, National University of Singapore, Singapore
[2]DSO, Singapore
[3]Xi'an Electronic Engineering Research Institute, China

Abstract— Multiple Input Multiple Output (MIMO) radar has received much attention in recent years. MIMO radar transmits multiple independent (orthogonal) signals from M transmitting antennas and receives the reflected signals from N receiving antennas. So Colocated MIMO radar can forms a larger virtual aperture and then has high cross-range resolution.

MIMO radar can be used to form 3D image of a target. Because the codes in MIMO radar cannot be orthogonal for all time shifts, cross-correlations and auto-correlations of these codes may have high values. This induces high range and cross-range sidelobes of the 3D image.

Inverse Synthetic Aperture Radar (ISAR) uses the rotation of the target relative to the radar to form 2D image of the target. Combined with ISAR and MIMO radar, low range and cross-range sidelobes may be obtained compared with only using MIMO radar techniques. In order to coherently combine the MIMO radar received signal, the rotation parameters of the target must be known. The 3D positions of some strong scatterers can be obtained by MIMO array, at the same time, the Doppler frequencies of these strong scatterers can also be obtained by ISAR technique. It is well know that $f_d = \frac{2}{\lambda}\omega \times r$, where ω is the rotation vector, r is the position of a scatterer. Then ω can be obtained by fitting technique.

Due to noise and interference, the estimate values of f_d and r may be wrong, which affect the estimation of ω. We know that the stronger a scatterer, the less probability of it's parameters (f_d, r) be wrongly estimated. So the amplitudes of the scatterers can be weight in the date fitting technique. This will improve the rotation parameters' estimation precision and then improve the 3D imaging quality. Detailed descriptions and discussion will be given in this paper.

High Performance Parallel Implementation of Compressive Sensing SAR Imaging

Jihua Tian, **Jinping Sun**, **Yuxi Zhang**, **and Najeeb Ahmad**
School of Electronic and Information Engineering, Beihang University, Beijing, China

Abstract— The compressive sensing (CS) theory has been applied to SAR imaging systems in many ways. And it shows a significant reduction in the amount of sampling data at the cost of much longer reconstruction time. In this paper, we investigate the development and optimization of Iterative Shrinkage/Thresholding (IST) algorithm applying to CS reconstruction of SAR images on two parallel architectures, standard vectorized multi-core processors (e.g., quad-core CPUs) and Graphics Processing Units (GPUs). Meanwhile, we modify the IST algorithm according to the characteristic of SAR images to obtain a faster recovery speed. The experiment results show that CS reconstruction of SAR images on parallel architecture has a significant speedup in comparison with implemented on conventional serial architectures.

Some main results of this paper:

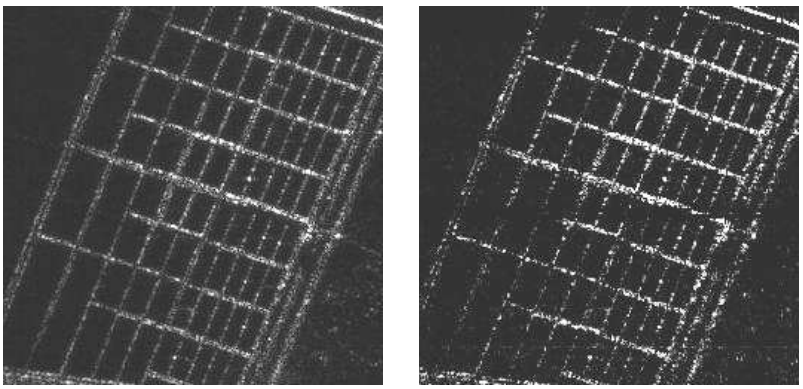

(a) (b)

Figure 1: (a) Conventional SAR imaging result with full samples. (b) Compressive sensing based SAR imaging result with 50% samples implemented on GPU.

Table 1: The average execution times on CPU and GPU.

	CPU	**GPU**	**Speedup**
Time/s	8.995	0.258	35

Spaceborne SAR Wide-swath Imaging Based on Poisson Disk-like Sampling and Compressive Sensing

Jinping Sun[1], **Yuxi Zhang**[1], **Jihua Tian**[1], **and Bingchen Zhang**[2]

[1]School of Electronic and Information Engineering, Beihang University, Beijing, China
[2]National Key Lab of MW Imaging Tech., Institute of Electronics, CAS, Beijing, China

Abstract— Due to the range swath width in the conventional single channel spaceborne SAR is restricted by the system parameters, there is a trade-off between the azimuth resolution and the swath width in order to satisfy the Nyquist sampling criterion. And the modern spaceborne SAR wide-swath imaging systems generally adopt the flexible digital beamforming (DBF) or waveform coding techniques of phased array radars, both of which increase the system complexity in various degrees and are still realized under Nyquist sampling criterion. However, the new concept of compressive sensing (CS) states that an unknown sparse (or sparse under transform-domain) signal can be recovered even from what appear to be highly sub-Nyquist-rate samples by solving a -optimization problem, which offers the possibility to realize wider swath for conventional single channel spaceborne SAR system. A novel spaceborne synthetic aperture radar (SAR) wide-swath imaging scheme based on compressive sensing (CS) for the sparse scene is presented. The proposed method designs a Poisson disk-like nonuniform sampling pattern along the azimuth direction, which meets the demand of wider swath by restricting the smallest time interval between any two azimuth samples. Experiment results validate the effectiveness of the proposed method via the Radarsat-1 raw data in F2 mode.

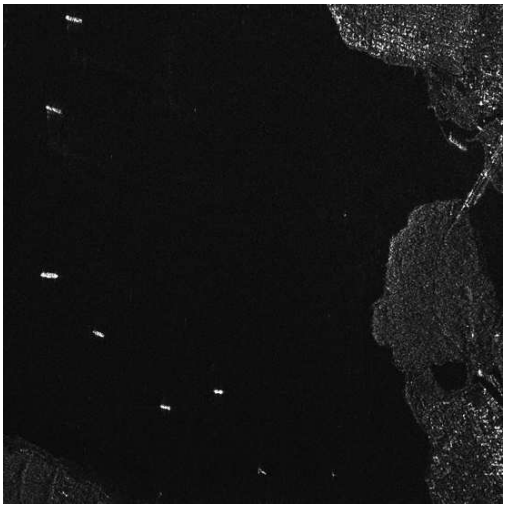

Figure 1: Imaging results with less than 50% samples of Radarsat-1 raw data.

Antenna Squint Effects on SAR Interferometric Requirements

Chih-Yuan Chu[1], **Chin-Fu Chao**[2], **Kun-Shan Chen**[1, 2], **and Chih-Tien Wang**[2]

[1]Communication Research Center, National Central University, Jhongli, Taoyuan, Taiwan
[2]Center for Space Science and Remote Sensing Research
National Central University, Jhongli, Taoyuan, Taiwan

Abstract— In this paper, the spatial decorrelation was evaluated with emphasis on antenna squint effect which is inherently produced by the non-orthogonality between the antenna beam and SAR flight track. For SAR image processing, Doppler centroid estimation is essential while correcting the squint effect. To improve the baseline estimation and proper selection for users, a new index Q, based on a differential squint angle, is introduced in this paper. In particular, a time-delay active radar calibrator was used to estimate the squint angles from SAR images. Over 36 SAR pairs from ERS-2 were used to test and to verify Q index as an InSAR pair selector. Comparing to refined Doppler centroid estimation, the accuracy is less than 0.03 degrees. It is demonstrated that the proposed Q index is very effective in selection of good InSAR pair with almost 100% successful rate. Hence, it is essential and convenient if index Q can be provided, in addition to baseline, so that interferometric can be readily determined.

High-resolution ISAR Imaging with Sparse-spectrum OFDM-LFM Waveforms

Ying Luo[1], **Qun Zhang**[1, 2], **You-qing Bai**[3], **and Yan-Li Duan**[1]

[1]Telecommunication Engineering Institute, Air Force Engineering University, Xi'an 710077, China
[2]Key Laboratory of Wave Scattering and Remote Sensing Information
Fudan University, Shanghai 200433, China
[3]Science Institute, Air Force Engineering University, Xi'an 710051, China

Abstract— High range resolution is achieved by transmitting broad-bandwidth waveforms in ISAR imaging techniques. Usually, bandwidth with several GHz is necessary to obtain a range resolution at centimeter level, where such a broad bandwidth may bring many difficulties to the A/D converter. For reducing the instantaneous bandwidth of radar system, the stepped-frequency signal (SFS) and stepped-frequency chirp signal (SFCS) were proposed and have been in wide applications. However, due to the frequency-stepped processing, both the SFS and SFCS are sensitive to the radial velocity of the target. Another disadvantage of this kind of signals is the relatively much long acquisition time for high resolution range profile (HRRP) synthesis, which maybe intolerable in certain applications such as multi-target imaging.

Recently, a new approach based on the orthogonal frequency division multiplexing (OFDM) technique is presented for improving target detection of radar systems. With the application in radar imaging, OFDM-LFM waveform is a kind of potential broad-bandwidth radar signals, due to the following reasons: 1) by taking the chirp signals as subpulses, many existing imaging algorithm can be easily extended to OFDM-LFM radar imaging; 2) insensitive to radial velocity between radar and target because all subpulses are transmitted at the same time; 3) much shorter acquisition time for HRRP synthesis compared with SFS and SFCS. However, different from SFCS, long enough frequency interval between each two subpulses is necessary to ensure perfect orthogonal performance of them. That's to say, the OFDM-LFM waveform is sparse-spectrum indeed, which brings difficulties to synthesize a total broad bandwidth.

Motivated by this, in the paper, based on the compressive sensing (CS) theory, an algorithm for high-resolution inverse synthetic aperture radar (ISAR) imaging with sparse-spectrum OFDM-LFM waveforms is proposed, which achieves high resolution of radar target and also much lower data rate of radar system. In the approach, the OFDM technique is utilized to overcome the velocity sensitivity in traditional broad-bandwidth radar waveforms such as stepped-frequency signals and stepped-frequency chirp signals, and greatly reduce the acquisition time for high resolution range profile (HRRP) synthesis. The simulations validate the effectiveness of the proposed algorithm.

SAR Imagery Compressing and Reconstruction Method Based on Compressed Sensing

F. Zhu, **Q. Zhang**, **J.-B. Yan**, **F. F. Gu**, **and M. Zhu**
Institute of Telecommunication Engineering, AFEU, Xi'an, Shaanxi 710077, China

Abstract— As the development of Synthetic Aperture Radar (SAR) imaging technology, the dimension of SAR imagery will become larger and larger. Thus some problems such as data processing and transmission in the real time would occur. Hence, how to compress and reconstruct SAR imagery data is an important problem, which is necessary to solve for the time being.

Compressive Sensing (CS), which is proposed by D. L. Donoho in 2006, is a new method of obtaining, compressing and reconstructing signals in Signal Processing field. Because of its special advantages, it will be applied in many different kinds of fields. It will provide a new idea and approach for many different kinds of data compressing and reconstruction.

In this paper, we intent to study SAR imagery data compressing and reconstruction based on CS theory. According to CS theory, there are three main steps should be carried out. One is the sparsity expression of the original signal. Second is the low-dimension measurement for the original signal. And third is effective reconstruction algorithm for recovering the original signal. In this paper, our research according to these three steps in CS theory can be revealed as follows. For the poor sparsity feature of SAR imagery data, the Discrete Wavelet Transform (DWT) which has a well time-frequency energy assembly character can be utilized to make SAR imagery data sparse. For the low-dimension measurement, the random Gauss matrix after approximate Orthogonal-matrix and Right-matrix (QR) decomposition can be employed, which perform better than the conventional random Gauss matrix. For the original data reconstruction, the modified Orthogonal Matching Pursuit (OMP) algorithm can be engaged for avoiding the sparsity degree estimation. In addition, compared with the traditional OMP algorithm, the convergency speed of the modified OMP algorithm is enhanced effectively. Finally, the simulation results suggest that by using the proposed method, the SAR imagery data can be compressed effectively, and the SAR imagery can be also reconstructed successfully.

This paper is organized as follows: Section 2 introduces the CS theory; and the SAR Imagery Compressing and Reconstruction Method Based on Compressed Sensing are stated step by step in Section 3, which contain our main work and innovations; finally, some computer simulations are given according to the method flow in the last Section.

Session 1P4a
The Biological Effects of Exposure to Extremely Low Frequency (ELF) Electromagnetic Radiation

Health Recovery Effect of Physiological Magnetic Stimulation on Elder Person's Immunity Source Area with Transition of ECG and EEG

K. Mohri[1], **Y. Inden**[2], **M. Yamada**[3], **and Y. Mohri**[4]

[1]Nagoya Industrial Science Research Institute (NISRI), Nagoya 464-0819, Japan
[2]Graduate School of Med., Nagoya University, Nagoya 466-0065, Japan
[3]Faculty of Sci. and Tech., Meijo University, Nagoya 468-8502, Japan
[4]Yamazaki Mazak Co., Oguchi, Aichi 480-0197, Japan

Abstract— We present an effective and safe health recovery method using a physiological magnetic stimulation based on the magneto-protonics [1, 2], in which the blood pressure and the body weight of an elder person both gradually decreased to a healthy stationary level during around two months. A vinyl pipe crammed with magnetized fayalite crashed stones which generates pulse distributed magnetic field useful for the arousal effect of elder persons during car driving [2] is vibrated on the body surface of the immunity source positions located at the thymus, the pit of the stomach, and the intestinal flora (the functional metabolic organ in Chinese medicine) for application of an extremely low frequency magnetic field to blood cells for their activation with the blood vessel smooth muscles using reinforced ATP.

We measured and analyzed the electro-encephalogram (EEG) for before and after the physiological magnetic stimulation (PMS) using the vibrated magnetized pipe. We found that a "flat frequency spectrum" (arousal frequency spectrum) with small magnitude of θ wave (drowsiness) and δ wave (sleep) components appeared even before the PMS for a 70 age man subject who had been stimulated everyday through around 4 months probably due to the accumulation of the PMS effect, while remarkable increase of the β wave (arousal) component appeared during the 20-min. PMS in the EEG of the same subject at the right head position.

REFERENCES

1. Mohri, K. and M. Fukushima, "Milligauss magnetic field triggering reliable self-organization of water with long range ordered proton transport through cyclotron resonance," *IEEE Trans. Magn.*, Vol. 39, No. 5, 3328–3330, 2003.
2. Mohri, K., T. Uchiyama, M. Yamada, T. Watanabe, Y. Inden, T. Kato, and S. Iwata, "Arousal effect of physiological magnetic stimulation on elder Person's spine for prevention of drowsiness during car driving," *IEEE Trans. Magn.*, Vol. 47, No. 10, 2011, in Press.

Arousal Effect of Physiological Magnetic Stimulation on Car Driver's Spine Evaluated with Electroencephalogram Using Driving Simulator

Y. Mohri[1], **M. Yamada**[2], **K. Endo**[2], **T. Suzuki**[2], **and K. Mohri**[3]

[1]Yamazaki Mazak Co., Oguchi, Aichi 480-0197, Japan
[2]Faculty of Science and Technology, Meijo University, Nagoya 468-8502, Japan
[3]Nagoya Industrial Science Research Institute (NISRI), Nagoya 464-0819, Japan

Abstract— We have proposed a new effective and safe method of arousal for car drivers with application of a physiological magnetic stimulation (PMS) to elder person's spine, for which a pulse distributed magnetic field is generated from a vinyl pipe crammed with magnetized fayalite crashed stones [1]. In this case, evaluation of the arousal level has been carried out analyzing the FFT frequency spectrum for detected electro-encephalogram (EEG) time series with considering mainly the relative magnitude of the θ wave (drowsiness) component. In this paper, we newly investigated the relationship between a transition of each EEG component wave of δ, θ, α, and β and the arriving time to sleep Ts at a driving simulator during the PMS on a driver's spine position. Condition of the driving simulator is set to a quiet night time high way driving on a simple slight curved road for easy going to sleep.

Three subjects out of five younger subjects (21–23 age men) showed longer Ts during the PMS with remarkable increasing of β wave although with decreasing of α wave. We may tentatively point out that a magnitude of the β wave should be an index of arousal concerning with car driving behavior although the number of subjects is small. We explain mechanisms of effect for the arousal using the PMS with the magneto-protonics [2].

REFERENCES

1. Mohri, K., T. Uchiyama, M. Yamada, T. Watanabe, Y. Inden, T. Kato, and S. Iwata, "Arousal effect of physiological magnetic stimulation on elder person's spine for prevention of drowsiness during car driving," *IEEE Trans. Magn.*, Vol. 47, No. 10, 2011, in press.
2. Mohri, K. and M. Fukushima, "Milligauss magnetic field triggering reliable self-organization of water with long range ordered proton transport through cyclotron resonance," *IEEE Trans. Magn.*, Vol. 39, No. 5, 3328–3330, 2003.

Characteristic of Human Arm Frequency Radiation

Siti Zura A. Jalil[1, 2], **Mohd Nasir Taib**[2], **Hasnain Abdullah**[2], **and Megawati Mohd Yunos**[2]

[1]Razak School of Engineering, Universiti Teknologi Malaysia, Malaysia
[2]Faculty of Electrical Engineering, Universiti Teknologi MARA, Malaysia

Abstract— Many studies have indicates that there are endogenous electromagnetic field generated by the human body. All the living body, especially the human being is believed to have their own radiation which the field radiates into space around on the body. With the advancement of science and technology, this radiation field can be described as the vibration of electromagnetic (EM) field generated by the human body. The field penetrates the physical body and emits their characteristics radiations of frequency. This works discusses the analysis of frequency radiation on human arm and classifies the characteristic of human arm radiation based on gender. The human radiation frequency is experimentally studied from 33 healthy human subjects of 17 males and 16 females. The frequency radiation is obtained from 6 points of human arm on left-side and right-side of human body. The statistical technique is used to examine the characteristic of radiation frequency. The multivariate analysis of variance (MANOVA) is employed to compare the characteristic of radiation frequency differences between genders. Prior to MANOVA analysis, several preliminary assumptions testing were performed, which it is confirmed that no serious violations noted in the tests and met the MANOVA assumptions. The results of MANOVA indicate there is statistically significant difference among gender of males and females on a linear combination of human arm frequencies radiation. It is confirmed that the population means on a set of human arm frequencies varies across gender. Then, k-nearest neighbor (k-NN) technique is employed for classification. The default neighborhood setting of Euclidean Distance is used to find nearest neighbors. The results show that the k-NN produced 89% of correctly classified, which suggested that the k-NN classifier is able to classify human arm radiation frequency.

Medical Imaging and Diagnostics Based on EM Field

J. Vrba, **J. Vorlíček**, **D. Vrba**, **J. Vrba (Jr.)**, **B. Vrbova**, **and T. Vydra**
Department of EM Field, Czech Technical University in Prague, Prague, Czech Republic

Abstract— Future trends in medical applications of microwave technique and technology can be seen in development of new diagnostic and imaging methods based on high frequency EM field. A significant importance for the future can be identified for the following methods: Microwave tomography, Microwave radiometry, Measurement of complex permittivity, Imaging in the Terahertz waves band and Microwave diagnostic radars.

Interactions of EM field with biological systems are utilised in the area of therapy (oncology, physiotherapy, urology atp.) from late seventieth of last century. Wideutilization of microwave thermotherapy can be observed in the countries of EU, USA and Japan. Our activities in microwave thermotherapy in former Czechoslovakia started in the year 1981. Since 1990 we are member of ESHO (European Society for Hyprthermia Oncology), which co-operates with NAHS (North American Hyperthermia Society) and ASHO (Asian Society of Hyperthermia Oncology).

Recent trends in microwave medical applications are to study the possibilities to develop new diagnostics based on EM field resp. on microwace technique. A significant importance for the future can be identified for the next methods:

- Magnetic resonance,
- Microwave tomography,
- Microwave radiometry,
- Measurement of complex permittivity,
- Imaging with terahertz waves,
- Microwave diagnostic radar.

We will not talk here about magnetic resonance, as it is just well known and broadly used application of EM field in medical diagnostics. We will focus here on other above mentioned methods (excluding microwave diagnostics radars).

ACKNOWLEDGMENT

This research is supported by Grant Agency of the Czech Republic, project: "Microwave Imaging for Biomedical Applications" (102/05/0959) and by the research program MSM6840770012 "Transdisciplinary Research in the Area of Biomedical Engineering II" of the CTU in Prague, sponsored by the Ministry of Education, Youth and Sports of the Czech Republic.

REFERENCES

1. Vrba, J., *Medical Applications of Microwaves*, 168, 1st Editon, Issued by CTU, Prague, 2003, ISBN 80-01-02705-8.
2. Semenov, S. Y., et al., "Three-dimensional microwave tomography, initial experimental imaging of animals," *IEEE Transactions on BME*, Vol. 49, No. 1, 55–63, Jan. 2002.
3. Gabriel, S., R. W. Lau, and C. Gabriel, "The dielectric properties of biological tissue — II. Measurements in the frequency range 10 Hz to 20 GHz," *Phys. Med. Biol.*, Vol. 41, 2251–2269, 1996.

Applicators with Optimized Effective Aperture

J. Vrba, **B. Vrbova**, **J. Vrba (Jr.)**, **J. Vorlicek**, **D. Vrba**, **and T. Vydra**
Department of Electromagnetic Field, FEE CTU in Prague
Technicka 2, 166 27, Czech Republic

Abstract— This contribution describes new types of applicators for microwave hyperthermia with large effective aperture, which are used for Head and Neck cancer treatment.

Introduction: The addition of Hyperthermia in the treatment of Head and Neck tumors has been shown in several randomized clinical studies. Because of specific tumor's localization, it is very convenient to have a small applicator with a large effective aperture. Goal of our project was to develop new types of applicators with a large effective aperture. Its effective aperture has been compared with cases of Waveguide and EMW (Evanescent Mode Waveguide) applicator.

We have compared four (2 new types and 2 well known) microwave applicators operating at frequency 434 MHz. 1) SH (Stripline Horn) applicator, 2) SME (Stripline with Magnetic Excitation) applicator, 3) EMW (Evanescent Mode Waveguide) applicator, 4) Waveguide applicator. We have designed and optimized these applicators by aid of numerical models based on FDTD. Vector analyzer based on sixport measured the radiation matching. The SAR distribution has been measured on muscle equivalent biological tissue by using the matrix of thermistory probes.

SH applicator is an applicator (Fig. 1) with aperture dimensions 10×12 cm, which is filled by distilled water. The impedance matching was performed by capacity screw and it is shown on the Fig. 2. Both lateral walls are made of dielectric material. It was studied that it increases the effective aperture.

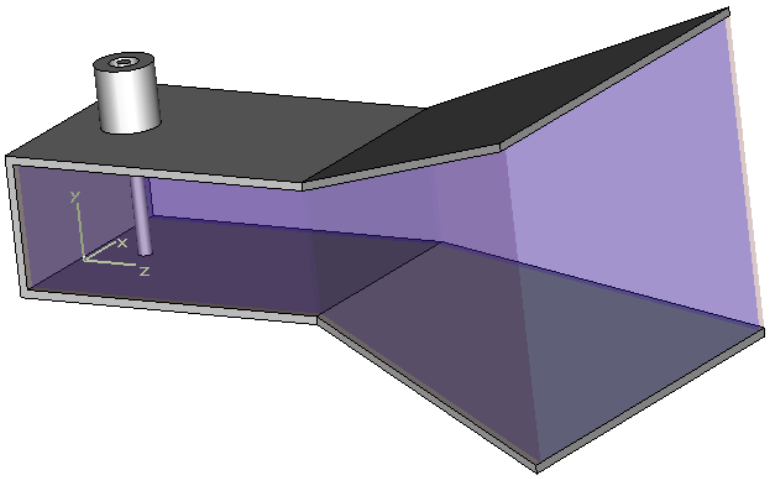

Figure 1: Stripline horn applicators, Prague, 2003.

Session 1P4b
RF Safety Issues

Influence of Shield Distance on RF Transmit Performance for a 7T Multi-channel MRI Loop Array

M. Kozlov and R. Turner
Max Planck Institute for Human Cognitive and Brain Sciences, Leipzig, Germany

Abstract— **Purpose:** Use of an RF shield is often proposed for minimization of RF coil array inter-element coupling and improvement of transmit performance. It is well known, nevertheless, that some unshielded 7T MRI coils still provide good transmit performance. For a single loop coil and a homogeneous phantom, the penetration depth is strongly influenced by the distance from coil to shield. However, there are no reliable transmit performance data for a loop-based array, loaded by a realistic head model, as a function of shield distance. Furthermore, it is difficult to compare literature values for transmit performance, because data for $\mathbf{B}_1+$ field versus array input power are rarely reported, and there are no reports of power balance. For an 8-channel loop based 7T RF coil array, we investigated the effect of shield distance on array power balance and performance (averaged over the entire brain volume and over a transverse slice).

Method: In the simulation, eight resonance coil elements were mounted on rectangular acrylic supports, assembled to give an octagonal cross section with extreme dimensions of 230 mm by 255 mm. The planar single loop elements were simulated for a range of sizes: width 85 mm; length 85, 150 mm. The realistic 3-D EM model included all coil construction details for the resonance elements, simulated with precise dimensions and material electrical properties. The loads utilized were the Ansoft human body models with different scaling factors: head #1 with scaling $X = 0.9$, $Y = 0.9$, $Z = 0.9$ simulating a small head, and head #2 with scaling $X = 0.95$, $Y = 0.975$, $Z = 0.9$ simulating large head, which practically fully occupied the coil volume.

Our investigation was performed using RF circuit and 3-D EM co-simulation [1]. The RF circuit simulator was Agilent ADS software, and Ansoft HFSS was chosen as the 3-D EM tool for its robustness in handling complex coil geometry. For all geometries the array was either tuned/matched/decoupled using capacitive and inductive decoupling networks, or alternatively tuned by minimization of the power reflected by the entire array ($\mathbf{P}_{array\_refl}$) without any dedicated decoupling network. We analyzed the power balance [2] as well as the transmit magnetic field performance and inhomogeneity (calculated as the ratio of standard deviation to mean $\mathbf{B}_1+$ over the entire human brain, or over the central transverse slice). The array was excited in circular polarization mode, applying the same power to each port, with a sequential 45 degree phase increment.

The scanner gradient shield (with diameter of 683 mm and length 1200 mm) was always included in the numerical domain for simulation of unshielded and shielded arrays. The distance between the shielded array and a 300 mm long local shield was varied between 10 mm and 80 mm.

Results: The influence of shield distance on array performance basically depends on the array tuning/decoupling approach, and for capacitor based decoupling it also depends on the decoupling capacitor position relative to the array feed point. For a decoupled array, the reflected power $\mathbf{P}_{array_refl}$ is large (up to 25% of transmit power) especially for a smaller head model (#1) positioned in a 150 mm array decoupled by capacitors placed at the coil middle position ($z = 0$). The larger the reflected power, the poorer the array coil performance. Relative to the decoupled array, tuning by minimization of $\mathbf{P}_{array\_refl}$ provides the best performance, for CP mode excitation, independently of the distance to the shield and the size of the head model. In

Table 1.

Coil length, mm	150												85											
Distance to local shield	no		60		40		20		15		10		no		60		40		20		15		10	
head	1	2	1	2	1	2	1	2	1	2	1	2	1	2	1	2	1	2	1	2	1	2	1	2
$\mathbf{P}_{radiated}$, W	0.63	0.43	0.08	0.06	0.05	0.04	0.02	0.02	0.02	0.02	0.02	0.02	0.42	0.26	0.05	0.03	0.02	0.02	0.01	0.01	0.01	0.01	0.01	0.01
$\mathbf{P}_{array\_internal}$, W	0.21	0.2	0.33	0.3	0.44	0.45	0.9	0.78	1.26	1.19	2.0	1.74	0.36	0.31	0.65	0.41	0.62	0.51	1.07	0.84	1.42	1.11	2.1	1.68
$\mathbf{P}_{load}$, W	7.16	7.37	7.59	7.64	7.51	7.51	7.08	7.20	6.72	6.79	5.98	6.24	7.22	7.43	7.30	7.56	7.36	7.47	6.92	7.15	6.57	6.88	5.89	6.31
$\mathbf{P}_{brain}$, W	2.67	2.73	2.78	2.74	2.71	2.67	2.53	2.51	2.39	2.27	2.19	2.13	2.54	2.52	2.72	2.50	2.50	2.43	2.28	2.23	2.14	2.11	1.90	1.92
$\mathbf{B}_1+_{brain}$, µT	1.57	1.47	1.62	1.50	1.61	1.48	1.56	1.44	1.52	1.40	1.43	1.33	1.59	1.47	1.61	1.48	1.60	1.46	1.50	1.41	1.50	1.37	1.41	1.31
Inhomogeneity brain, %	23	24	24	24	25	24	25	24	25	24	25	24	25	25	26	27	27	28	29	28	30	31	31	32
$\boldsymbol{B}_1+_{slice}$, µT	1.77	1.67	1.85	1.72	1.85	1.71	1.80	1.66	1.75	1.62	1.64	1.53	1.90	1.78	1.96	1.83	1.98	1.83	1.89	1.79	1.90	1.76	1.80	1.69
Inhomogeneity slice, %	23	23	24	23	24	23	24	23	24	23	24	23	18	17	18	17	18	17	17	16	16	16	16	17
$\mathbf{SAR}_{10\,g}$, W/kg	4.08	4.29	4.54	4.21	4.41	4.11	4.15	3.86	3.92	3.82	3.49	3.69	4.60	4.37	4.91	4.21	4.44	4.33	4.40	5.12	3.93	5.47	4.93	4.30

order to separate the shield distance effect from other effects, the data in Table 1 are provided only for tuning based on minimization of reflected power, where only losses due to radiation ($\mathbf{P}_{radiated}$) and array internal structure ($\mathbf{P}_{array\_internal}$) decrease the power delivered to load.

For the same head, $\mathbf{B}_1+$ averaged over the entire brain ($\mathbf{B}_1+_{brain}$) and its inhomogeneity vary little with coil length and distance to shield, when the shield distance is more than 20 mm. For smaller shield distances, $\mathbf{B}_1+_{brain}$ decreases, with a simultaneous decrease in homogeneity. $\mathbf{B}_1+$ averaged over the central transverse brain slice ($\mathbf{B}_1+_{slice}$) slightly increases for shield distances from 40 mm to 60 mm, while there is a rapid drop for distance less than 20 mm. In contrast with the inhomogeneity of $\mathbf{B}_1+_{brain}$, inhomogeneity of $\mathbf{B}_1+_{slice}$ is nearly constant for all shield distances. For 150 mm length coil, the 10-gram-average SAR ($\mathbf{SAR}_{10\,\mathrm{g}}$) approaches a maximum for a shield distance of about 60 mm. For 150 mm length coil, $\mathbf{SAR}_{10\,\mathrm{g}}$ is rather complicated and will be reported separately.

Conclusion: In the CP excitation mode with tuning by reflected power minimization, the transmit performance of a loop array is only weakly dependent on shield distance when it is greater than 20 mm. For array investigated performance is strongly affected by this distance only if it is less than 20 mm.

REFERENCES

1. Kozlov, M. and R. Turner, *Journal of Magnetic Resonance*, Vol. 200, 147–152, 2009.
2. Kozlov, M. and R. Turner, *Proc. ISMRM*, Vol. 18, 1445, 2010.

Duplication of in Vitro Experiments: Forgotten or Overlooked Factors

Quirino Balzano[1] and Asher R. Sheppard[2]

[1]Quirino Balzano University of Maryland
Kim Building, Rm 2135, College Park, MD 20742, USA
[2]Asher Sheppard Consulting, Santa Rosa, CA 95405, USA

Abstract— Over the last 50 years there have been a large number of in vitro experiments with RF energy whose results could not be replicated. This paper presents possible causes for the divergence of in vitro experimental results found in the extant literature [1]. The deposition of RF energy in the vessels used for in vitro exposure occurs with highly non-uniform patterns of SAR. In the 800–2400 MHz band, the main mechanism of RF energy deposition is through the magnetic field, especially for Petri dish exposures as the electric field does not couple efficiently with liquids only a fraction of a centimeter high. Heating patterns depend on the geometry of the container and the level of medium in the vessel [2]. If great enough, variations in temperature may influence diffusion rates of nutrients and growth factors to cells plated on Petri dishes and cause convection phenomena in test tubes. In Petri dishes, the locally-averaged SAR at the cell layer can be computed by straight application of Faraday's theorem [3]. In contrast, computation of SAR and temperature distributions in the volume of the liquid medium requires sophisticated computer tools, i.e., FDTD models of the entire exposed vessel. From the temperature pattern at steady state it is possible to identify regions where diffusion phenomena might be different for exposed and unexposed samples even if both samples are rigorously kept at the same environmental temperature using typical experimental methods (e.g., in incubators). If the steady-state temperature distribution is achieved slowlyor not at allRF-exposed cells might undergo a relatively long period when nutrient and growth factors availability is not the same as for unexposed samples. We present the dependence of average SAR at the bottom of a 35-mm diameter Petri dish vs. liquid volume to illustrate the magnitude of variations in local heating. Due to meniscus effects, there can be a nearly 2 : 1 variation in SAR values depending on how much liquid volume is taken up by the meniscus. SAR patterns in the liquid medium are far from simple and uniform. For example, we show that for an H-field parallel to the dish bottom, there are substantial variations from the center to the periphery along a radius parallel to the field. It may be very difficult, if not impossible, to show repeatable in vitro results unless the medium, vessel shapes, and medium heights are the same. For experiments where locally non-uniform heating is possible, the SAR distribution at the cell layer should be evaluated to discern possible liquid layer instability, convection, and other heat-driven phenomena that might influence the diffusion of nutrients to the exposed biological preparations. These analyses seldom have been performed in past research.

REFERENCES

1. Panafiel, L. M., et al., "Role of modulation on the effect of microwaves on ornithine decarboxylase activity in L929 cells," *Bioelectromagnetics*, Vol. 18, 132–141, 1997.
2. Schuderer, J. and N. Kuster, "Effect of the meniscus at the solid/liquid interface on the sar distributionin petri dishes and flasks," *Bioelectromagnetics*, Vol. 24, 103–108, 2003.
3. Balzano, Q. and A. Sheppard, "A simple method to estimate the SAR of cell preparations in petri dishes with meniscus," *33rd Annual Meeting of the Bioelectromagnetics Society*, paper 11-3, Halifax, Nova Scotia, Canada, Jun. 2011.

Estimation of Electromagnetic Exposure Level Based on a Multilayered Model of the Pelvic-hip Region

M. Macedo and M. Yarlequé
Pontificia Universidad Católica del Perú, Sección Telecomunicaciones
Av. Universitaria 1801, Lima-32, Lima, Perú

Abstract— Nowadays, there is a trend to place wireless device close to the hip-pelvic region, for instance, mobile phones inside the pants pockets, laptop computers on the lap, and so forth. The electromagnetic emission of this device is likely to make an impact on vital organs and other tissues that are around the hip. Then, it is important to assess the effect of this radiation.

To our best knowledge, explicit determination of SAR (Specific Absorption Rate) on the pelvic region of the body has not been developed yet, therefore the main aim of this paper is to determine SAR (W/kg) for the pelvic region and hip area through simulation software.

Knowing hip anatomy, we propose a seven-layer model for the pelvic and hip tissues plus internal organs. Based on this new model, the EM exposure level is determined for the following cases:

- Mobile phone radiation in the 900 and 1800 MHz bands.

- Laptop radiation in 2.4 GHz, through WiFi and Bluetooth wireless connection. Mobile phones also can establish connections through these technologies.

- Two-way radio handheld radiation in 150 MHz (VHF) and 450 MHz (UHF) band.

The maximum and average SAR value are obtained employing FDTD method. It is observed that most of the radiation is localized in the outer tissue layer, with minimum exposure within vital organs. The maximum SAR value was always lower than the exposure limit value specified by the ICNIRP (2 W/kg).

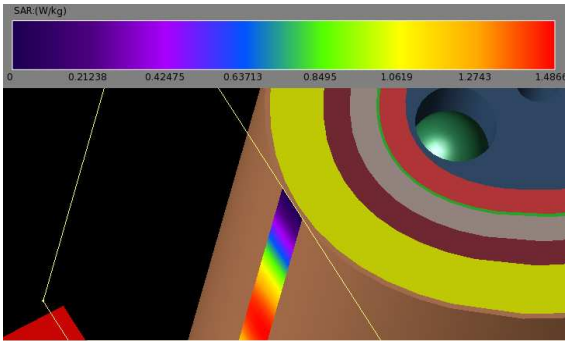

SAR distribution over tissues at 900 MHz.

An Investigation into the Effectiveness of Protective Clothing in the Presence of High Frequency Electromagnetic Fields

R. P. Findlay and P. J. Dimbylow
Health Protection Agency, Chilton, Oxfordshire OX11 0RQ, UK

Abstract— Protective suits, designed to reduce the absorption of electromagnetic fields in the body, are widely used by workers installing and maintaining radiofrequency (RF) antennas. However, these suits may not protect the user effectively if they are worn without a conducting screen to cover the face. The hood may act as a resonant cavity when exposed to RF fields in that particular case, resulting in higher field absorption in the head compared to when the protective suit is not worn.

The finite-difference time-domain (FDTD) method has been used to calculate the specific energy absorption rate (SAR) in a voxel model of a male adult enclosed in a protective suit. The model was derived from the anatomically realistic voxel phantom NORMAN. Vertically polarised plane-wave electromagnetic fields between 100 MHz and 3 GHz have been used in this study. The resolution of the voxel model was 2 mm.

SAR values are presented as a function of frequency. Results show that peak localised SAR in the hooded head are indeed higher compared to values calculated for a head without a protective hood at certain frequencies. Layer absorption plots and images of the SAR absorbed in individual voxels demonstrate the way in which the body absorbs the incident field when enclosed in a protective suit.

Figure 1: Tissue-enhanced view of the NORMAN voxel phantom with a protective suit.

An Overview of RF-EMF Health-related Activities in Malaysia

Kwan-Hoong Ng
Department of Biomedical Imaging, University of Malaya, Kuala Lumpur, Malaysia

Abstract— Malaysia has been very active in both regulatory, policy making, research and development, and risk management in radio frequency (RF). Some of the highlights are listed below.

The regulatory body Malaysian Communications and Multimedia Commission (MCMC) has been conducting RF safety awareness seminars and disseminating the necessary information to the general public. Their booklet, in three languages, "Radiation, mobile phones, base stations and your health" has been instrumnetal in educating the public and policy makers. They also published the mandatory standard on EMF emissions from radiocommunications infrastructure that came into effect in January 2011.

The Malaysia Nuclear Agency has been conducting RF radiation measurements for mobile telephone base stations and antennas throughout the country. They have also been engaging in various RF research activities.

The Minsitry of Health published a "Guidance to Safety and Health Aspects of Base Stations and Mobile Phones" in 2009. The Malaysian Standards also published "The Malaysian Standard Guidelines for Limiting Exposure to Time-varying Electric, Magnetic and electromagnetic Fields — Part 2: For Frequency from 3 kHz to 300 GHz (MS2232: Part 2 2010)" whcih is based on the International Commission on Non-Ionizing Radiation Protection 1998 guidelines.

In 2007, the University of Malaya along with World Health Organization and US Air Force (AFRL, AOARD) organized and hosted a very successful International EMF Conference: Electromagnetic Fields, Bioeffects Research, Medical Applications, and Standards and a short course on EMF Safety Management.

Three major projects initiated by local universities commenced in 2012, namely: (1) Researching the discourse representation of media texts when communicating scientific evidence regarding health effects of RF and EMF exposure and risk information to the public; (2) An Investigation into public perception of RF-EMF's effect on health risks and well-being; (3) Effects of short-term GSM and UMTS base station signal exposure on cognitive performance, well-being and physiological parameters.

Should Standards Be Revised Because There Are Reported Possible Biological Effects of RF Exposure?

C-K. Chou
Technical Committee 95, IEEE International Committee on Electromagnetic Safety
Piscataway, NJ, USA

Abstract— Currently there are more than 5000 papers in the IEEE International Committee on Electromagnetic Safety (ICES) Database concerning mainly radio frequency (RF) biological effect research results published since the 1950s. During the last 20 years, research has been focused on mobile telephony and there are now about 1000 publications describing experiments using frequencies at which mobile phones operate. According to the WHO, scientific knowledge on the effects of exposure to electromagnetic fields is now more extensive than for most chemicals. In 2004, Dr. John Osepchuk of ICES published a paper in which he categorized RF bioeffects-related papers into 6 groups from high to low scientific validity: A) confirmed or established science, B) unconfirmed science (could be useful), C) unconfirmed science (contradicts A), D) unconfirmed science with clear flaws and artifacts, E) junk science in peer-reviewed literature, and F) junk science in non-peer-reviewed literature. Only a portion of the published papers can be categorized as Group A papers. Like everything else in life, the literature on RF bioeffects varies in quality and this has contributed to current controversies on how best to protect against adverse effects in human beings associated with RF exposure.

The predecessor of ICES is the American Standards Association and its C95.1 Committee that began development of RF exposure standards in the 1960's. The first C95.1 RF safety standard, published in 1966, was based on possible thermal effects in human beings associated with whole-body exposure to RF energy. The standard was revised in 1974, 1982 and 1991 and the latest version, C95.1-2005, was published in April 2006. In the 2005 revision, recommendations were made to protect against established adverse health effects in human beings associated with exposure to electric, magnetic and electromagnetic fields in the frequency range of 3 kHz to 300 GHz. The established adverse effects are electrostimulation for the lower RF band and tissue and whole-body heating for the higher RF band. IEEE C95.1 RF standards are now available to the public without charge at http://standards.ieee.org/about/get/index.html#getC95.

The recommendations in both the IEEE C95 standards and the International Commission on Non-Ionizing Radiation Protection (ICNIRP) guidelines are based on established adverse biological effects. Following independent reviews of the literature, both organizations established the threshold for adverse health effects on the same set of research papers. Activist groups however, challenge the IEEE ICES standards and the ICNIRP guidelines as being too stringent in science quality because the limits for human exposure are based on established science and therefore are not protective of possible (unknown) biological effects. Some activist groups promote much lower exposure limits to protect against "possible biological effects" because of the precautionary principle. They acknowledge that these "possible biological effects" are not proven. As pointed out in my paper presented in the 2010 PIERS meeting [2], there are large differences between "possible biological effects" and "established adverse effects".

On May 31, 2011, the International Agency for Research on Cancer (IARC) classified radio frequency electromagnetic field exposure as a "possible" carcinogen (Group 2B). The WHO EMF Project and ICNIRP have published responses to this classification emphasizing that there is no established evidence that RF exposure causes cancer. In fact, IARC did not find sufficient evidence to assign RF fields to either of the two highest categories (Group 2A or Group1), i.e., RF fields were not found to be a "probable" human carcinogen (Group 2A) or a human carcinogen (Group1). The IARC classification of RF fields as a "possible" carcinogen, however, has led to a renewed effort by activists for precautionary measures and lower limits. The IEEE C95.1-2005[3] standard addresses the concerns of possible low level biological effects with the following statements: "*Further examination of the RF literature reveals no reproducible low level (non-thermal) effect that would occur even under extreme environmental exposures. The scientific consensus is that there are no accepted theoretical mechanisms that would suggest the existence of such effects.*", and "*Despite more than 50 years of RF research, low-level biological effects have not been established. No theoretical mechanism has been established that supports the existence of any effect characterized by trivial heating other than microwave hearing. Moreover, the relevance of reported low-level effects to health remains speculative and such effects are not useful for standard setting.*" Following the IARC classification of RF fields as a "possible" human carcinogen, the

ICES TC95 subcommittees and working groups responsible for reviewing the scientific literature and recommending exposure limits concluded that the IARC classification of RF energy as a possible carcinogen does not serve as a basis for a revision of IEEE/ICES C95.1.

REFERENCES

1. Osepchuk, J. M., "Environmental standards: The new concept and key to international harmonization of safety standards for the safe use of electromagnetic energy," *International Symposium on Technology and Society*, 165–173, 2004.
2. Chou, C-K., "Established adverse health effects versus possible biological effects of RF exposure," *Progress In Electromagnetics Research Symposium Abstracts*, Xi'an, China, 22–26, Mar. 2010.
3. IEEE C95.1-2005, "IEEE standard for safety levels with respect to human exposure to radio frequency electromagnetic fields, 3 kHz to 300 GHz," Piscataway, NJ, USA.

Session 1P5a
Radio Propagation, Ionospheric Propagation

Uncertainties in the Electromagnetic Field Environment around a Lightning Return Stroke

Robert L. Gardner
6152 Manchester Park Circle, Alexandria, VA 22310-4957, USA

Abstract— The lightning return stroke begins when a downward propagating leader (stepped or dart) reaches within a few meters of the ground and connects with an upward propagating leader. This joining of non neutral plasma columns is an extremely energetic and complex event requiring an understanding of the behavior of several charged and uncharged species at temperatures up to a few electron volts, rapidly changing electric fields of several megavolts/meter and charge transfer of several coulombs in a few microseconds. This region is important in understanding lightning because it is the source of much of the high frequency content of the radio-frequency emission of the return stroke. The evolution of the plasma channel also governs the propagation of the return-stroke current as it moves up channel. The fields around the lightning are determined by the current as predicted by Maxwell's Equations, but, in practice the currents have to be determined by the radiated fields because it is difficult to directly measure the current waveforms for a sufficient number of return strokes to determine the variation in the currents waveform. The process of determining the currents from fields is a difficult inverse theory so a very popular approximation using simple transmission line theory is used [1].

While we have not solved the full inverse theory problem, we have solved some other, somewhat less approximate problems in the forward direction. This paper is about the consequences of using the two complex models. Wait and Gardner [in separate chapters in Lightning Eletromagnetics] have discussed the effect of lossy ground on fields from lightning return stroke currents at length. In this case, we will only examine the effects of a simple vertical electric dipole model Such a model is appropriate for frequencies above a megahertz. This model predicts a preferential attenuation at frequencies above a few megahertz. The consequence of assuming a perfectly conduction ground in the inverse model (as is done in the transmission line model above) is to ignore that preferential attenuation and mask a possible faster rise time of the return-stroke current pulse.

The second model examines the consequences of using a lossy transmission-line model rather than the uniform model used in the transmission line model. The resistance per unit length of the transmission line is predicted from a nonlinear non-uniform analysis of the plasma column. This model predicts an attenuation of the leading edge of the current pulse confining the highest frequency (fastest) field effects to the joining point described in the first paragraph. Again, the consequence of this attenuation is to flatten the distant fields relative to the current waveform.

REFERENCES

1. Uman, M. A. and D. K. McLain, *J. Geophys. Res.*, Vol. 43, 33, 1969.

Investigation of Ionospheric Impacts on RF Propagation during Minimum Solar Activity

R. Talhi and G. Rogerie
C.N.R.S, LPC2E, University of Tours, Orleans 45071, France

Abstract— It is widely recognized that our current knowledge about ionosphere influence on radio systems, solar cycle phenomena and impact on operational systems, remains not sufficient to provide reliable and accurate predictions for the previous uncertainties [1–3]. This is mainly due to the interactions between solar wind, ionosphere and Earth, which are exceptionally complicated (with complex physical mechanisms), and cannot be -to date- easily described by any theoretical model [4–6]. Moreover, data from some satellite observations can be affected by the ionospheric irregularities (day-to-day variability, multiple scattering, nonlinearities phenomena, sporadic E, etc.), over a large range of spatial (few km to 1000 km) and temporal (1 to 15 mn) scales. These disturbances are often a major source of errors to data interpretation experts [7–10].

The aim of this contribution is to discuss some results of studies evaluating some ionospheric impacts on scattering and propagation conditions, during minimum solar activity period, with special emphasis on the crucial role of the electron density profile, the power spectrum of ionospheric irregularities, and the wave incidence angle, in presence of the terrestrial magnetic field. In order to characterize the distribution of energy over a receiver plane (grid size: 30×30 points, the vector radiative transfer equation, based on markovian jump processes, is used. The simulation results show, for HF frequencies (10 to 20 MHz) and for any incidence angle, a good concordance between zones of maximum scattered intensity and zones of high polarization rate. However, polarization rate presents some areas with random variations, which may be either due to multiple scattering effect (or mutual interaction phenomenon), or due to the weakness of scattered intensity. In addition, a fine analysis concerning the statistical behavior of the scattered intensity and the polarization rate for various incidences, is done. Moreover, to get more details regarding the spatial repartition of the incident wave, we defined an Energy Spatial Repartition Index (ESRI), which accounts for the global budget of reflected and transmitted energy. The ESRI index may take three values: -1 if the energy is totally reflected towards the earth, $+1$ if the energy is completely transmitted through the ionosphere (then "lost" in the space), and 0 if the energy is equally reflected and transmitted. The evolution of the ESRI index is studied versus the wave incidence angle, for a given frequency, for different values of the maximum electron density, and also for different strengths of the turbulence. The ESRI evolution shows, under certain conditions, the appearance of a critical zone characterized by ESRI ≈ 0, and corresponding to strong turbulence and weak to moderate electron density ($10 * *10$ to $10 * *11$ e/m**3). Some other results revealead by the behaviour of the ESRI index, and also some practical limitations, will be presented and discussed.

REFERENCES

1. Arbesser-Rastburg, B., "Ionospheric and tropospheric modelling and monitoring for GNSS at the European Space Agency," *URSI/GA*, Istanbul, Turkey, August 13–20, 2011.
2. Anderson, S. J, "Nonlinear scattering at HF: Prospects for exploitation in OTH radar systems," *Tübitak*, Vol. 18, No. 3, 2010.
3. Retterer, J., "Recent advances in ionospheric irregularity and scintillation forecasting," *Space Weather Workshop*, Boulder, Colorado, USA, April 26–29, 2011.
4. Rogers, N., et al., "Simulation of Ionospheric Effects and their mitigation for the ESA Biomass P-band space-based radar," *13th Int. Ionospheric Effects Symposium*, City of Alexandria, USA, May 17–19, 2011.
5. Cervera, M. A, et al., "Modelling the effects of ionospheric disturbances on vertically incident ionograms using 3D raytracing," *URSI/GA*, Istanbul, Turkey, August 13–20, 2011.
6. Maltseva, O. A., et al., "Comparison of various methods to control conditions of radiowave propagation in the ionosphere," *URSI/GA*, Istanbul, Turkey, August 13–20, 2011.
7. Galkin, I. A., et al., "Global ionospheric radio observatory (GIRO): Status and prospective," *URSI/GA*, Istanbul, Turkey, 2011.
8. Zabotin, N. A., et al., "Experiment on spatial effect of HF multiple scattering in the ionosphere," *URSI/GA*, Istanbul, Turkey, 2011.

9. Eccles, V., et al., "HF Propagation in real time GAIM ionosphere," *13th Int. Ionospheric Effects Symposium*, City of Alexandria, USA, May 17–19, 2011.
10. Zabotin, N. A., et al., "Effects of HF multiple scattering in the ionosphere: Experimental observations," *13th Int. Ionospheric Effects Symposium*, City of Alexandria, USA, May 17–19, 2011.

Temporal Backscattering of Tropical Forest at P Band with Ground Experiment

C. Albinet[3], **P. Borderies**[3], **T. Koleck**[1, 2],
F. Rocca[4], **S. Tebaldini**[4], **T. Le Toan**[2], **and L. Villard**[2]

[1]CNES, Toulouse, France
[2]CESBIO, Toulouse, France
[3]ONERA, Toulouse, France
[4]POLIMI, Milan, Italy

Abstract— This abstract deals with ground experiments related to the future spaceborne BIOMASS mission for global forest biomass estimation.

Tropical forests present the major part of the world forest biomass and their changes in biomass by deforestation and/or by forest regeneration affect strongly the terrestrial carbon budget. To measure with accuracy tropical forest biomass and its temporal change is one of the objectives of the BIOMASS mission [1], a candidate for the European Space Agency 7th Earth Explorer Mission.

The possible retrieval algorithms currently developed for BIOMASS are based on the use of backscatter measurements derived from intensity, polarimetry and interferometry. However, these quantities are subject to evolution with the life cycle and the meteorological conditions at very different time scales, ranging from a few minutes to days, months... with the possibility that their changes may affect the inversion algorithms. A ground experiment has been set up to follow systematically these evolutions. It has been installed over a temperate tree and also over a tropical forest in French Guiana. Based on the use of a Vector Network Analyzer and adequate antennas, it may deliver P band polarimetric, interferometric impulse responses and 2D (range/height) imaging.

In the presentation the full, actual system will be described. It permits impulse response measurements and tomographic images every 15 minutes. The results corresponding to the first months of measurements will be displayed and analyzed, both in intensity and in coherence.

REFERENCES

1. BIOMASS Phase 0 Report for Assessment, European Space Agency, Nov. 2008, ref. SP1313/2.

Comments on Some Radio Wave Propagation Mechanisms in the Amazon Region

Mauro S. Assis
Brazilian Committee of URSI, Brazil

Abstract— The Amazon region (Brazil) is covered by a dense rain forest, crossed by a large number of rivers and characterized by a hot and humid climate. The annual precipitation is of the order or higher than 2000 mm and the median temperature along the year is approximately constant between 25 and 28°C. In this scenario, depending on the frequency of operation, different propagation phenomena should be considered in the performance evaluation of a radio system. For instance, the following problems can be pointed out: a) Signal attenuation due to vegetation is higher as the frequency increases; b) Rain attenuation is a critical issue when using frequencies above 10 GHz, being particularly relevant for satellite communication in the Ku band; c) The knowledge of meteorological conditions of troposphere (turbulence and stratification), including super refraction and ducting, is quite important in the analysis of terrestrial VHF and UHF radio links covering long distances in this region. Based on theoretical considerations and experimental results, some of these problems are discussed in this paper.

1. HF band — In spite of limitations regarding the capacity of a radio system, the HF band can be used for covering different propagation conditions: a) Short distances when one or both terminals are inside the jungle; b) Medium distance ground wave propagation paths; c) Long distance ionospheric propagation paths. This paper emphasizes the radio wave propagation in a forest environment;
2. Radio wave propagation in VHF and UHF bands — The analysis of measurements carried out in long distance VHF and UHF links has shown that the behavior of the troposphere follows two different conditions: i) Turbulence in day hours; ii) Stratification during the night. In the first case, the main sources of this turbulence are probably the wind above forest top and the high temperature. On the other hand, the stratification is associated to a quiet state of troposphere;
3. Satellite Communications in the Ku band — In the planning of low availability satellite systems, an outage of 1 to 0.1% in the worst month is normally acceptable. In these systems the temporal variability of fading has a strong impact on system design. Consequently, the knowledge of rain dynamics is of fundamental relevance. It is recognized that the conversion of rain rate duration to slant path duration statistics is not an easy task. The main problems are the vertical non homogeneity of rain structure and the possibility of having more than one rain cell along the propagation path. However, if the vertical distribution of rain is uniform from the earth surface to a height near the 0° isotherm level and the elevation angle is higher than 30°, the measured rainfall rate threshold at a given probability level may be used to obtain information on the dynamics associated to the attenuation in slant paths.

Negative Power Law Attenuation Estimation for Rainy Earth-Space Radio Links

P. O. Akuon and T. J. O. Afullo
School of Electrical, Electronic and Computer Engineering
University of Kwa-Zulu Natal (UKZN), Durban 4041, South Africa

Abstract— The growth of rain attenuation is described by a power law model that is derived from rain cell diameter distribution, RCDD. The RCDD is determined from 1-minute integration time point rainfall rate data. To validate the proposed factor, the method of moments is used to evaluate the fractional area occupied by rain cells. Consequently, by the use of the given attenuation prediction equation, the expected attenuation values at 0.01% of time for five satellite links situated in tropical sites are obtained. The sampled links have varying elevation angles, frequencies and experience different rainfall types. This procedure is repeated for other two models used in attenuation prediction for satellite links: the ITU-R P.618-9 and Bryant et al. models. Comparison tests are then carried out using the RMS test variable, and the proposed model results in the lowest RMS value for the sites.

The sampled satellite links are situated in equatorial sites which include: Johor Bahru (Malaysia), Lae (Papua New Guinea), Suva (Fiji), Bangkok and Nairobi (Kenya).

The proposed attenuation growth is of the form:

$$\varsigma = 1 + R^{-\frac{1}{\lambda \sin\theta}}; \quad \lambda = 2.267$$

where R is the rainfall rate (mm/h) and θ is the link elevation angle.

This factor is applied in the attenuation equation that was earlier proposed by the authors and is described by:

$$\begin{aligned} A &= \frac{\gamma L}{\cos\theta} \cdot (r_{0.01}) \\ r_{0.01} &= \varsigma \frac{2}{\pi}\left(1 + \frac{1.047}{\xi_\theta}\right)\left(\frac{1}{\xi_\theta L_G/D + 1}\right) \\ \xi_\theta &= 1/\eta; \quad \eta = 1.0175 - 0.0029\theta - 0.0001\theta^2 \\ D &= 51R^{-0.46} \end{aligned}$$

where D is the equivalent rain cell diameter, γ is the specific attenuation and L_G is the slant path projected on the horizontal plane and is derived from the rain height, H_R: $H_R = 4.5{+}0.0005R^{1.65}$.

Session 1P5b
Distributed Coding and Cooperative Communications

A Simple Forwarding Technique for Two-way Relay Channels

Md Anisul Karim[1, 2], **Jinhong Yuan**[1], **Jun Li**[1], **and Zhuo Chen**[2]

[1]Wireless Communications Laboratory (WCL)
School of Electrical Engineering and Telecommunications
The University of New South Wales, NSW 2052, Australia
[2]Wireless and Networking Technologies Laboratory
CSIRO ICT Center, Marsfield, NSW 2122, Australia

Abstract— In this paper, we focus on soft forwarding schemes for two-way relay channels (TWRC). In specific, we propose two new soft information forwarding (SIF) schemes for TWRC, referred to as mutual information based forwarding with network coding (MIF-NC) and mutual information based forwarding with superposition coding (MIF-SC). In MIF-NC, the relay broadcasts the MIF based soft information to the sources using network coding, whereas in MIF-SC, the relay broadcasts the MIF based soft information to the sources using superposition coding. Simulation results reveal that when both the source-relay (S-R) channels are symmetric, the proposed MIF-NC scheme yields about 0.4–0.7 dB signal-to-noise ratio (SNR) gains compared to the existing schemes such as amplify-forward with network coding (AF-NC) and soft bit forwarding with network coding (SBF-NC). We then analyze the SIF schemes in both symmetric and asymmetric S-R channels. It is found that network coded SIF schemes perform better than superposition coded SIF schemes in symmetric S-R channels, albeit, the superposition coded SIF schemes outperform network coded SIF schemes in asymmetric S-R channels. All these results are verified by both the simulation and analysis.

BICM-ID for Relay System Allowing Intra-link Errors and a Similarity Constellation to ARQ Schemes

Meng Cheng[1], **Ade Irawan**[1], **Khoirul Anwar**[1], **and Tad Matsumoto**[1, 2]

[1]Japan Advanced Institute of Science and Technology (JAIST), Japan
[2]Center for Wireless Communication (CWC), University of Oulu, Finland

Abstract— In this paper, we propose an accumulator-assisted (ACC) relay system with bit-interleaved coded modulation using iterative decoding (BICM-ID) technique and apply the network topology to an Automatic Repeat Request (ARQ) scheme. Our code design is based on the analysis of the extrinsic information transfer (EXIT) chart. The ACC enables the convergence tunnel of the EXIT curves opening until almost the (1, 1) point of the mutual information, which avoids the error floor. The most advantageous point of the proposed technique is that even though errors may happen in the intra-link (source-relay), they can be corrected at the destination by exploiting the correlation knowledge between the source and the relay nodes. This technique significantly reduces the complexity of the relay where the source bits are simply extracted, even though errors may occur due to the imperfect channel. The error rate of the intra-link can be estimated at the destination node by using the a-posteriori Log likelihood Ratios (LLRs) of the two decoders. Then, it can be further utilised in the iterative processing. Since the relay location directly influences the quality of the intra-link, we change the relay locations, and provide the analysis of the performances corresponding to different relay locations. The theoretical background of this technique is the Slepian-Wolf/Shannon theorem for correlated source coding. The simulation results show that the bit-error-rate (BER) performances of the proposed system are very close to theoretical limits supported by the Slepian-Wolf/Shannon theorem. In this paper, it is also shown that if the intra-link is error free, the topology of the relay network is equivalent to an ARQ scheme that exploits Shannon's random coding theorem by utilising an interleaver in the framework of ARQ. Based on this observation, results of simulations conducted to evaluate the throughput of an ARQ scheme are presented.

Turbo-coded CDMA-based Two-way Relaying

Soon Xin Ng and Sha Sha Liao
School of Electronics and Computer Science, University of Southampton, UK

Abstract— We proposed a Turbo-coded Code-Division Multiple Access (CDMA) based two-way relaying scheme for cooperative communications with the aid of a relay node. More specifically, Turbo Codes (TCs) [1] are power-efficient channel coding schemes that can perform near Shannon's channel capacity. While CDMA [2] is an attractive multiple access scheme that allows multiple users to access the same frequency band at the same time. Both TC and CDMA schemes have been adopted in the current 3G mobile standard. By contrast, cooperative communications [3], [4] is a new paradigm where each mobile unit collaborates with one partner or a few partners for the sake of reliably transmitting its own information and of its partners jointly. More specifically, one or a few source nodes can transmit their signals to their destination nodes via one or a few relay nodes. Cooperative communications can increase the capacity, transmission reliability, energy efficiency and coverage area of the overall system. Due to these advantages, cooperative communication schemes based on relaying were considered in the recent LTE-Advance standard [5].

In this contribution, we studied the performance of the TC-CDMA scheme under the two-way relaying system based on the Decode-And-Forward (DAF) protocol. More explicitly, we employ a seven-user CDMA model, where two of the CDMA users are communicating with each other with the aid of an additional relay node, while the other five CDMA users are interferers. More explicitly, two CDMA users exchange their information frames within two timeslots. Note that the conventional one-way relaying system can only transmit one information frame within two timeslots because the relay node is half-duplex, where it cannot listen and transmit simultaneously. We found that our proposed TC-CDMA two-way relaying scheme is capable of attaining over 4 dB of SNR gain at a Bit Error Rate (BER) of 10^{-6} when compared to a conventional non-cooperative TC-CDMA system. We also found that there is about two dB of SNR loss at a BER of 10^{-6}, due to the error propagation from the relay node. The proposed scheme exploits the benefits of TC and CDMA schemes in order to assist the two-way relaying system to operate with a reduced transmit power. The reduction of the transmit power can also be exploited for increasing the coverage area of a cellular cell. Hence, the TC-CDMA two-way relaying scheme is a good candidate for future generation mobile systems.

REFERENCES

1. Hanzo, L., T. H. Liew, B. L. Yeap, R. Y. S. Tee, and S. X. Ng, *Turbo Coding, Turbo Equalisation and Space-Time Coding: EXIT-Chart-Aided Near-Capacity Designs for Wireless Channels*, 2nd Edition, John Wiley IEEE Press, New York, USA, March 2011.
2. Hanzo, L., L.-L. Yang, E. L. Kuan, and K. Yen, *Single- and Multi-Carrier CDMA*, John Wiley, IEEE Press, New York, USA, 2003.
3. Sendonaris, A., E. Erkip, and B. Aazhang, "User cooperation diversity part I: System description," *IEEE Transactions on Communications*, Vol. 51, No. 11, 1927–1938, 2003.
4. Laneman, N., D. N. C. Tse, and G. W. Wornell, "Cooperative diversity in wireless networks: efficient protocols and outage behavior," *IEEE Trans. on Information Theory*, Vol. 50, No. 12, 3062–3080, 2004.
5. Sesia, S., I. Toufik, and M. Baker, *LTE: The UMTS Long Term Evolution, from Theory to Practice*, 2nd Edition, John Wiley, 2011.

Differential Distributed Space-time Block Code for Two-way Relay Channel with Physical-layer Network Coding

Kai Zhu and Alister G. Burr
Communications Research Group, Department of Electronics
University of York, YO10 5DD, United Kingdom

Abstract— New applications of wireless communications in networked devices such as wireless sensor networks, body area networks, and the "smart grid" (sometimes referred to in general as "the Internet of Things") will result in networks containing much larger numbers of low powered communication nodes than current wireless networks. Networks of this sort are more likely to form a peer-to-peer or heterogeneous mesh topology, rather than the star topology more common today, and hence require data to be forwarded by relaying from node to node through the network.

However, since links in the network may be unreliable due to fading or node failure, diversity provided by cooperation between multiple relay nodes is very desirable to improve network robustness. Distributed space-time block coding (DSTBC) is one of the most popular cooperative MIMO techniques developed for multi-user communication environments. DSTBC is capable of offering similar temporal and spatial diversity gain as conventional MIMO systems employing multiple co-located antennas. In particular, in the context of large-scale shadow fading, conventional co-located STBC schemes would fail to provide full diversity gain because all the radio signals are likely to suffer from deep fading simultaneously rather than experiencing independent fading. Therefore, distributed or cooperative STBC seems likely to be a more effective solution in such systems.

DSTBC requires accurate estimation of the channel state information (CSI) for reliable detection at the receiver. However, the complexity of estimating the CSI generally increases exponentially as a function of the number of cooperating nodes, and is particularly difficult to coordinate in a mesh network with many active links. As a remedy, a differentially encoded non-coherently decodable STBC scheme was proposed (in [A]). By taking full advantage of the relationship between two successive transmitted symbols, the information conveyed by differential STBC signals can be recovered without the knowledge of CSI. Hence, compared with its coherently detected counterpart, differential STBC is appealing in saving power and bandwidth otherwise required for training symbols, as well as reducing implementation complexity.

The classic unidirectional cooperative communication has been recently extended to bidirectional or two-way relaying with the assistance of physical-layer network coding (PNC). Unlike other superposition coding techniques, the primary interest of PNC is to directly extract the network coded symbols from superimposed received signals at the relay nodes instead of explicitly detecting the individual symbols separately and independently. Therefore, the spectral efficiency as well as the achievable channel capacity is significantly increased by deploying PNC in the relaying protocol without additional power and any sacrifice in the bandwidth ([B]).

In this contribution, we combine the benefits of differential and distributed STBC with two-way relaying, and propose a differential distributed STBC scheme for the physical-layer network coded two-way relay channel using a "decode-and-forward" cooperative protocol. More specifically, we consider a four-node two-way relaying network, where two ordinary time-division half-duplex wireless terminals simultaneously exchange information with the assistance of two cooperating relay nodes. Note that each terminal node acts as a source node as well as a destination node. At time interval $\mathbf{T}$, a frame of information bits are encoded using differential M-PSK modulation and transmitted by two source nodes simultaneously. The received signals at two relay nodes are basically noisy version of superposition of two differentially-encoded and channel-corrupted M-PSK signals. Next, PNC is employed to decode this superimposed signal and extract the network coded (exclusive or-ed) symbols. Then, the resultant network coded symbols are re-encoded with differential DSTBC and broadcasted to the destination nodes at transmission period $\mathbf{T+1}$. At the destination, a conventional differential DSTBC decoder and M-PSK demapper are deployed to recover the network coded symbols. Eventually, each destination node is capable of recovering the information bits transmitted from corresponding source node by applying the exclusive or between the estimated network coded symbols and their local information.

REFERENCES

1. Tarokh, V. and H. Jafarkhani, "A differential detection scheme for transmit diversity," *IEEE Journal on Selected Areas in Communications*, Jul. 2000.

2. Cui, T., F. Gao, T. Ho, and A. Nallanathan, "Distributed space-time coding for two-way wireless relay networks," *IEEE Transactions on Signal Processing*, Vol. 57, 658–671, Feb. 2009.

Distributed Algorithm for Multiple Antenna Cooperative Cognitive Radio Networks with Multiple Primary and Secondary Users

S. Bayat[1], **R. H. Y. Louie**[1], **Y. Li**[1], **S. X. Ng**[2], **and B. Vucetic**[1]

[1]Centre of Excellence in Telecommunications, School of Electrical and Information Engineering
University of Sydney, Australia
[2]School of Electronics and Computer Science, University of Southampton, UK

Abstract— Cognitive radio has been proposed as a promising technology to improve the spectral efficiency of wireless networks. This is achieved by allowing unlicensed secondary users (SU) to coexist with licensed primary users (PU) in the same spectrum. This coexistence is facilitated by spectrum access techniques, such as those involving an agreement between the PUs and SUs on an acceptable spectrum access strategy. The key idea is that the PUs are motivated to lease spectrum bands to the SUs in exchange for some form of compensation.

To allow for high data rates, the use of cooperative relaying and multiple antenna technology has emerged as powerful techniques, due to their ability to provide diversity, high reliability and capacity in wireless networks. For cooperative relaying, this is achieved by the use of intermediate relay nodes to aid transmission between the source and destination nodes. The use of cooperative relaying is particularly advantageous when the direct link between the source and destination is weak, due to, for example, high shadowing. Multiple antennas can also be used to provide high capacity through spatial multiplexing techniques where separate data streams are transmitted through multiple transmit antennas, or reliability by diversity techniques where a single data stream is transmitted through multiple transmit antennas.

We consider a model where the SUs act as cooperative relays and utilize multiple antennas to assist the PUs' transmission in exchange for both spectrum access and monetary compensation, and thus the SUs are effectively providing both a *monetary and performance compensation* to the PUs. We consider a general cognitive radio relay network with multiple PUs and multiple SUs under the overlay model, which guarantees a minimum rate requirement for all matched PUs and SUs. We define a PU and SU as *matched* if the SU cooperatively relays the PU's data, in exchange for spectrum access and monetary compensation.

In particular, we propose a distributed matching algorithm which determines the matched pairings between PUs and SUs, such that the SU will provide monetary compensation, and relay its paired PU's data in exchange for spectrum access. The key idea behind the algorithm is that the PUs negotiate with the SUs on the amount of monetary compensation, in addition to the time the SUs are either (i) allowed access to the spectrum, or (ii) cooperatively relaying the PU's data, such that both the PUs' and the SUs' minimum rate requirement are satisfied. Again by using concepts from auction theory and matching theory, we then analyze the performance of the proposed algorithm, showing that it results in the best possible stable matching, and is weak Pareto optimal. We introduce a utility function, which incorporates both the rate and monetary factors. We demonstrate through numerical analysis that the algorithm can achieve utilities (i) comparable to the utilities achieved by an optimal centralized algorithm, and (ii) significantly greater than the utilities achieved by a random matching algorithm, while also being able to achieve a high number of matchings with low overhead and complexity.

We show that our algorithm is flexible in terms of prioritizing either the PUs or SUs, by a simple manipulation of global parameter values. We further demonstrate that the use of multiple antennas at the SUs can allow for a higher rate for both the PUs and SUs. This has the positive consequence of a longer spectrum access time for the SUs, or a higher utility for the PUs. Finally, we show that the PUs which utilize the SUs for cooperative relaying achieves a rate greater than what it would achieve without cooperative relaying, i.e., direct transmission, and thus motivates their participation in the proposed algorithm.

Distributed Allocation of the Spectrum Sensing Durations for Cooperative Cognitive Radios

O. van den Biggelaar, **J.-M. Dricot**, **P. de Doncker**, **and F. Horlin**
Université Libre de Bruxelles, Belgium

Abstract— The scarcity of available radio spectrum frequencies, densely allocated by the regulators, represents a major bottleneck in the deployment of new wireless services. Cognitive radios have been proposed as a new technology to overcome this issue [1]. For cognitive radio use, the assigned frequency bands are opened to secondary users, provided that interference induced on the primary licensees is negligible. Cognitive radios are established in two steps: the radios firstly sense the available frequency bands and secondly communicate using these bands.

One of the main challenges faced by wireless communication system designers is the fading phenomenon — an attenuation of the received power due to destructive interferences between the multiple interactions of the emitted wave with the environment. To tackle the fading problem when sensing the frequency spectrum, cooperative spectrum sensing has been proposed to take advantage of the spatial diversity in wireless channels [2–6].

In cooperative spectrum sensing, the secondary cognitive nodes send the results of their individual observations of the primary signal to a coordinator node through specific control channels. The coordinator node then combines the received information in order to make a decision about the primary network presence. Each cognitive node observes the primary signal during a certain sensing duration, which should be chosen high enough to ensure the correct detection of the primary emitter but low enough so that the node has still enough time to communicate. In literature [7, 8], the sensing durations used by the cognitive nodes are generally assumed to be identical and allocated by a central authority. In [9], the sensing performance of a network of independent cognitive nodes that individually select their sensing durations is analyzed using evolutionary game theory.

In this paper, a decentralized Q-learning algorithm is proposed to share the sensing duration among the cognitive radios in a way that maximizes the throughputs of the radios. The multiple cognitive radios (the agents) self-adapt by directly interacting with the environment in real time and by properly utilizing their past experience. They aim to distributively learn an optimal strategy to maximize their throughputs.

This distributed allocation of the sensing durations presents several advantages compared to a centralized allocation performed by the coordinator node [10]: 1) selfadaptability of the system to a variation of parameters (such as the gains of the sensing channels), 2) scalability of the system as the need for control communication is minimized and 3) maintainability of the system thanks to the modularity of the multiple agents.

Numerical results demonstrate the need for an exploration strategy for the convergence of the sensing duration allocation algorithm. It is furthermore shown that compared to a centralized allocation algorithm, the proposed allocation technique has a higher computational complexity but minimizes the need for exchange of control information between the cognitive nodes and the coordinator node. Finally, it is shown that there is an optimal tradeoff value for the frequency of execution of the learning algorithm.

REFERENCES

1. Jondral, F. K. and T. A. Weiss, "Spectrum pooling: An innovative strategy for the enhancement of spectrum efficiency," *IEEE Radio Communications*, Vol. 42, No. 3, s8–s14, 2004.
2. Aazhang, B., A. Sendonaris, and E. Erkip, "User cooperation diversity — Part i: System description," *IEEE Transactions on Communications*, Vol. 51, No. 11, 1927–1938, 2003.
3. Scuttari, G. and S. Barbarossa, "Cooperation diversity through virtual arrays in multihop networks," *Proceedings of the IEEE International Conference on Acoustics, Speech, and Signal Processing (ICASSP)*, 2003.
4. He, S. and C. Xiang, "A distributed cooperation spectrum sensing scheme in cognitive radio network," *4th International Conference on Wireless Communications, Networking and Mobile Computing, WiCOM '08*, October 2008.
5. Cabric, D. and A. Sahai, "Spectrum sensing: Fundamental limits and practical challenges," *Proceedings of the IEEE Conference on Dynamic Spectrum Access Networks (DySPAN)*, 2005.

6. Bazerque, G. B. and J. A. Giannakis, "Distributed spectrum sensing for cognitive radio networks by exploiting sparsity," *IEEE Transactions on Signal Processing*, Vol. 58, No. 3, 1847–1862, March 2010.
7. Peh, E., Y.-C. Liang, Y. Zeng, and A. T. Hoang, "Sensing throughput tradeoff for cognitive radio networks," *Proceedings of the IEEE International Conference on Communications (ICC)*, June 2007.
8. Stotas, S. and A. Nallanathan, "Sensing time and power allocation optimization in wideband cognitive radio networks," *GLOBECOM 2010, 2010 IEEE Global Telecommunications Conference*, 1–5, December 2010.
9. Wang, B., K. Liu, and T. C. Clancy, "Evolutionary game framework for behavior dynamics in cooperative spectrum sensing," *Proceedings of the Global Telecommunications Conference (GLOBECOM)*, November 2008.
10. Galindo-Serrano, A. and L. Giupponi, "Distributed q-learning for aggregated interference control in cognitive radio networks," *IEEE Transactions on Vehicular Technology*, Vol. 59, May 2010.

Collaborative Data Dissemination in Opportunistic Vehicular Networks

Yong Li[1], **Zhaocheng Wang**[1], **Depeng Jin**[1], **Lieguang Zeng**[1], **and Sheng Chen**[2, 3]

[1]Tsinghua National Laboratory for Information Science and Technology
Department of Electronic Engineering, Tsinghua University, Beijing 100084, China
[2]Electronics and Computer Science, Faculty of Physical and Applied Sciences
University of Southampton, Southampton SO17 1BJ, UK
[3]Faculty of Engineering, King Abdulaziz University, Jeddah 21589, Saudi Arabia

Abstract— Future opportunistic vehicular networks offers viable means for collaborative data dissemination by high- capacity device-to-device communication. This is a highly challenging problem because a) mobile data items are heterogeneous in size and lifetime; b) mobile users have different interests to different data; and c) dissemination participants have limited storages. We study collaborative data dissemination under these realistic opportunistic vehicular network conditions. We show that the optimal data dissemination can be formulated as a submodular function maximisation problem with multiple linear storage constraints. We propose a heuristic algorithm to solve this challenging problem, and provide its theoretical performance bound. The effectiveness of our approach is demonstrated through simulation using real vehicular traces.

Session 1P6
Millimetre and Submillimetre Wave Radar Systems — Theory and Applications

Ultra Thin Metamaterial Absorbers Using Electric Field Driven LC (ELC) Resonator Structure

Somak Bhattacharyya and Kumar Vaibhav Srivastava
Department of Electrical Engineering, Indian Institute of Technology, Kanpur, India

Abstract— Microwave absorbers play a crucial role in stealth technology [1], where reduction of Radar Cross-Section [2] is one of the major challenges. To make thin absorber at microwave frequencies, metamaterials [3] have been used where the thickness as well as size can be reduced significantly. SRR-based metamaterials are first used as absorbers [4], but the wave has to travel all along the length of the elements. Later, by using periodic metallic wires and SRRs, Landy et al. [5] proposed a structure where the wave has to travel much shorter distance. Li et al. [6] has suggested metamaterial absorbers using the Electric Field Driven LC (ELC) resonator structure, which is explained in [7].

The aim of this paper is to make ultra thin absorbers using metamaterials in C-band. The proposed ELC driven element structure and its equivalent L-C circuit combination are shown in Fig. 1(a) and Fig. 1(b) respectively. The structure is simulated in Ansoft HFSS software which shows that the absorption takes place at 6.46 GHz with absorbance of 98.24% as shown in Fig. 1(c) with S_{11} of -17.55 dB. Here the frequency of maximum absorption decreases as compared with [6] from 9.92 GHz to 6.46 GHz. The capacitor value can be changed by incorporating changes in the proposed structure as shown in Fig. 1(d), which shows that absorption occurs at 6.70 GHz with absorbance of 99.2%. This modified structure reduces the extra metallic strip in the outer side, and thus the size reduction of the ELC element is possible with slight increase of frequency at which absorption occurs.

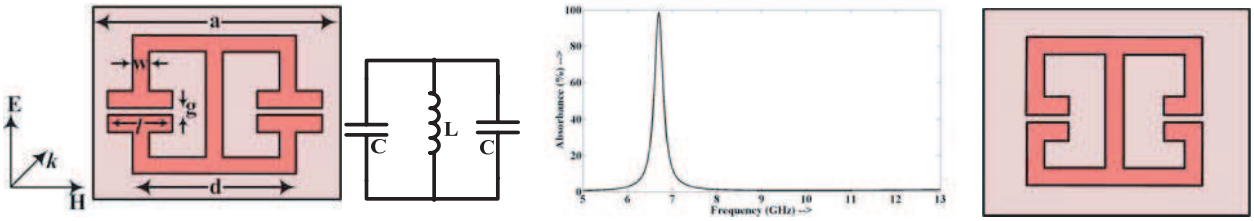

(a) (b) (c) (d)

Figure 1: (a) Proposed ELC structure (Dimension of the unit cell: $a = 5$ mm, $d = 3.6$ mm, $l = 1.5$ mm, $w = 0.4$ mm, $g = 0.2$ mm with FR-4 substrate). (b) Equivalent L-C circuit. (c) Absorbance plot. (d) The modified ELC structure.

REFERENCES

1. Bahret, W. F., "The beginning of stealth technology," *IEEE Transactions on Aerospace and Electronic Systems*, Vol. 29, No. 4, 1377–1385, Oct. 1993.
2. Skolnik, M., *RADAR Handbook*, Second Edition, 11.1–11.30, T McGraw Hill, 1990.
3. Smith, D. R., W. J. Padilla, D. C. Vier, S. C. Nemat-Nasser, and S. Schultz, "Composite medium with simultaneously negative permeability and permittivity," *Physical Review Letters*, Vol. 84, No. 18, 4184–4187, May 2000.
4. Bilotti, F., L. Nucci, and L. Vegni, "An SRR-based microwave absorber," *Microwave and Optical Technology Letters*, Vol. 48, No. 11, 2171–2175, Nov. 2006.
5. Landy, N. I., S. Sajuyigbe, J. J. Mock, D. R. Smith, and W. J. Padilla, "Perfect metamaterial absorber," *Physical Review Letters*, Vol. 23, 207402, May 2008.
6. Li, M. H., L. H. Yang, B. Zhou, X. P. Shen, Q. Cheng, and T. J. Cui, "Ultrathin multiband gigahertz metamaterial absorbers," *Journal of Applied Physics*, Vol. 110, 014909, 2011.
7. Schurig, D., J. J. Mock, and D. R. Smith, "Electric-field-coupled resonators for negative permittivity metamaterials," *Applied Physics Letters*, Vol. 88, 041109, 2006.

Moving Passenger Screening Using a Fast Millimetre Wave FMCW Radar

Sebastian Hantscher[1], **Beverly Schlenther**[1], **Stefan Lang**[1], **Manfred Hägelen**[1], **Helmut Essen**[1], **and Axel Tessmann**[2]

[1]Department of Millimetre Wave Radar and High Frequency Sensors
Fraunhofer Institute for High Frequency Physics and Radar Techniques
Neuenahrer Straße 20, Wachtberg 53343, Germany
[2]Department of High Frequency Devices and Circuits
Fraunhofer Institute for Applied Solid State Physics
Tullastraße 72, Freiburg 79108, Germany

Abstract— The currently developed scanners used for security checks on airports do not solve the task of handling increasing passenger flows. Moreover, they have a negative impact on the privacy of the persons to be screened. For this reason, a prototype of a person scanning system is introduced carrying out a full body scan of moving persons. The radar operates in the W band at 97 GHz providing an added value to existing security related systems as it supports them by detecting large and dangerous weapons (such as explosive belts) with low financial effort. However, the application is not restricted to the airport security checkpoint or the airport terminal but it can be further used for the protection of critical infrastructures with high passenger throughput, e.g., mass transport systems. The radar module contains a voltage controlled oscillator which is able to tune the frequency between 96 GHz and 99 GHz at a RF output power of 10 dBm. The conductor-backed coplanar waveguide technology in combination with metamorphic cascode HEMTs has been demonstrated to be highly suitable for the development of millimetre-wave low-noise heterodyne receiver MMICs. The radar consist of 5 receive channels in order to capture back scattered energy from different aspect angles. The presented 4 channel receiver operates between 84 GHz and 104 GHz and achieved a maximum conversion gain of 12 dB and an average noise figure of 3.5 dB. The developed radar front end uses an integrated FMCW radar chip with separated transmitter and receiver for increasing the dynamic range) and allows a coherent reception of all 5 receive channels. This coherence was obtained by using chirp signals which were derived by the same oscillator as well as by a precise chirp linearisation. Carrying out a full body measurement of a moving person, a stimulant of an explosive belt, a grenade and a gun worn concealed under a jacket could be detected and localized on the body without violating the privacy at any time.

ACKNOWLEDGMENT

The research leading to these results has received funding from the European TRANSPORT (including AERONAUTICS) Community's Seventh Framework Programme AAT.2008.5.2.2. under agreement of No. 234014.

Millimeter-wave Imaging System Using a One Dimensional Virtual Array for Stand-off Detection

V. Krozer and J. Moll
Goethe University Frankfurt, Germany

Abstract— Millimeter wave imaging has recently been considered for stand-off imaging in a number of applications, such as security and non-destructive testing (NDT). Millimeter waves penetrate most non-conducting materials and are reflected by conducting surfaces; interfaces of different refractive index reflect the beam partially. Real-time high resolution millimeter wave imaging is possible with array system. We report an active stand-off FMCW imaging system operating at 230–320 GHz for stand-off distances of 8 m. The instantaneous bandwidth is 100 GHz with around 100 frequency points and a sweep time of around 1 ms. Imaging is achieved by combining a line array consisting of 8 sources and 16 detectors with a scanning cylindrical mirror system. The optical design of the camera consists of a cylindrical optics which focuses on a horizontal slice. The height of this slice is adjusted by a planar triangular shaped rotating mirror. With a rotation of this mirror the target is vertically scanned, and a full 3D data set is created. For each slice a SAR reconstruction is performed. Range and intensity information of the object are obtained through an effective aperture of the 0.5×0.5 Meter. The system is currently working in two different experimental modes. The first mode employs a voltage controlled oscillator (VCO), delay line and a signal distribution network to feed all transmitters and provide LO to the receivers. The second mode substitutes the VCO unit with a vector network analyzer (Rhode&Schwarz ZVA 20 VNA) operating at 12–18 GHz stepping through in 201 steps and using 1 kHz resolution bandwidth. The mm-wave signals are generated using $\times 18$ frequency multiplication. Full 3D synthetic image reconstruction is achieved in real-time by an embedded GPU (Graphical Processing Unit) using back-projection algorithms. The data indicates a spatial resolution of about 2 cm and the range resolution of about 2 mm. A number of test objects have been reconstructed. We have also developed a new reconstruction algorithm based on fast factorized back-projection suitable for multi-static configurations.

Comparison of Ultra-wideband Radar Target Classification Methods Based on Complex Natural Resonances

M. Khodjet-Kesba, K. Chahine, K. El Khamlichi Drissi, and K. Kerroum
LASMEA UMR 6602 UBP/CNRS, 24 Avenue des Landais, 63177 Aubière Cedex, France

Abstract— The principal objective of automatic target recognition (ATR) is to identify the target from UWB radar returns. In intelligent vehicles, ATR can be a solution to identify pedestrians, vehicles, traffic signs, etc. Typically radar ATR relies on classifying the characteristics of the target obtained from the backscattered signal. In this paper, we apply Matrix Pencil Method (MPM) to extract complex natural resonances (CNRs) from the late time part of the field, which is characteristic of the studied target and can be used for its recognition and identification. Next, we compare three classification methods of CNRs: Support vector machine (SVM), K-nearest neighbor (KNN) and Naive Bayes classification, which are commonly used for classification.

The simulations are undertaken by using three metallic canonical objects: thin wire, sphere and cylinder. Different sizes are taken for these canonical objects. The backscattered fields of the targets are computed by using electromagnetic commercial simulation trial which is based on the method of moments (FEKO). The field is obtained in the time domain. A Gaussian pulse with duration of 0.45 ns is used as an excitation wave, which corresponds to a wideband frequency.

After assembling the CNRs extracted by the MPM into a database, we apply one of the three methods for classification. The comparison is made in terms of classification accuracy. Preliminary results indicate that target discrimination based on the natural frequencies of ultra wideband radar targets is a good solution to automatic target recognition. The extrapolation to real targets is expected to allow generation of a unique signature for each target.

The table below shows a part of the database. The values $P1, P2, \ldots, P5$ given below, correspond to the positive imagery part of the complex conjugate poles that we use as a feature for classification. As may be observed, different set of resonant frequencies correspond to different geometries.

Table 1: Natural frequencies of the canonical objects (l: length, r: radius).

	$P1$	$P2$	$P3$	$P4$	$P5$
Thin wire ($l = 1\,\mathrm{m}$)	4.5833e+009	2.7265e+009	8.7557e+008	0	0
Thin wire ($l = 2\,\mathrm{m}$)	4.1690e+009	3.2425e+009	2.3073e+009	1.3728e+009	4.4308e+008
Sphere ($r = 0.15\,\mathrm{m}$)	1.6171e+009	4.4744e+009	0	0	0
Sphere ($r = 0.30\,\mathrm{m}$)	8.4399e+008	1.7293e+009	4.5021e+009	0	0
Cylinder ($l = 0.5\,\mathrm{m}$, $r = 0.15\,\mathrm{m}$)	1.0597e+009	2.0566e+009	5.2131e+009	0	0
Cylinder ($l = 0.5\,\mathrm{m}$, $r = 0.25\,\mathrm{m}$)	1.0563e+009	2.1068e+009	5.0509e+009	0	0

Millimeterwave Synthetic Aperture Radar for UAV Applications

Winfried Johannes, **Helmut Essen**, **Stephan Stanko**, **Rainer Sommer**, **Alfred Wahlen**, **and Jörn Wilcke**
Fraunhofer Institute for High Frequency Physics and Radar Techniques, Wachtberg, Germany

Abstract— Airborne remote sensing is most important as well for civilian as for military applications. The inspection of disaster areas require very short reaction times to be able to take adequate means for recovering people or take other means of resilience. To get the necessary detailed information, high resolution multi parameter imaging of scenarios within limited area is necessary. It is, however, of importance to be able to operate day and night and under adverse weather conditions including smoke and dust. As the Fukushima nuclear accident shows, also unmanned operation over dangerous terrain can be essential. Unmanned aircraft systems (UAS) are presently discussed for such applications. To be able to operate under the conditions mentioned above and to maintain the capability to operate over medium range, medium sized airvehicles, fixed wing or rotary wing, may be employed, which allow to carry miniaturized synthetic aperture radar systems. Millimeterwave systems allow a very compact set-up, using MMIC technology and allow to use small antennas with adequate gain. Further, millimetre wave radar is very sensitive to small scale variations of the scattering surfaces and give information on small scale changes, which are not visible for classical radars at more traditional frequencies like X-band.

A miniaturised millimetre wave radar, MIRANDA, to be used as SAR onboard a small UAS was designed, built and tested onboard of an unmanned helicopter. The design followed the FM-CW principle, to get the highest possible average transmit power and thus the best range performance. An inertial system of high quality, based upon a fibre optic gyroscope maintained the necessary precision to allow high resolution SAR imaging. The raw data are transmitted to the ground station where they are preprocessed and finally undergo a realtime SAR-focussing algorithm. Additionally to the quick-look processing the data are stored to be able to apply further high quality SAR processing.

The system is developed to prototype status and can be produced to serve a wide range of applications. The paper describes the design details and discusses typical measurement results.

Millimeterwave SAR Monitoring for Precision Farming Applications

Helmut Essen[1], **Thorsten Brehm**[1], **Stefan Sieger**[1], **Rainer Sommer**[1], **Erich Meier**[2], **and Christophe Magnard**[2]

[1]Fraunhofer Intitute for High Frequency Physics and Radar Techniques, Wachtberg, Germany
[2]Remote Sensing Laboratories, University of Zurich, Switzerland

Abstract— With the background of the worldwide climatic change, stability or better increase of agricultural production is of worldwide importance. Precision farming is one means to increase quality and quantity of crops. This technique optimizes the production using agronomic management tools like fertilization or watering on a subfield scale. Current efforts integrate GPS and GIS technologies into farmwork. To be able to apply the necessary means of fertilization, the state of growth and ripeness state of crops have to be monitored within a short-term observation cycle.

Airborne radar, typically as one component of a multisensory suite, can give important information towards that aim. Synthetic aperture radar allows to survey a large terrain and thus to monitor different clutter characteristics, especially inhomogenities within this area. Millimeterwaves are especially sensitive upon small scale changes of scattering surfaces and can discriminate not only between different plants or soil by its varying roughness, but also between different conditions of specific plants. Synthetic aperture radar is an even more powerful tool, if the polarization state of the backscattered signal is evaluated.

Measurements were conducted with a full polarimetric millimeterwave SAR. The paper discusses the measurements and the evaluation methods and gives typical results.

Processing of COBRA FMCW SAR Data

M. Frioud[1], **A. Wahlen**[2], **H. Essen**[2], **and E. Meier**[1]

[1]Remote Sensing Laboratories, University of Zurich, Zurich, Switzerland
[2]Fraunhofer FHR, Wachtberg, Germany

Abstract— The experimental synthetic aperture radar COBRA, developed at the Fraunhofer Institute for High Frequency Physics and Radar Techniques (FHR), is a modular FMCW system with four front-end modules at 10 GHz, 35 GHz, 94 GHz and 220 GHz. The front-ends are coupled to common radar control and data acquisition electronics, identical to those used for the MEMPHIS pulsed radar system. COBRA was originally developed for ISAR applications, allowing high resolution imaging in a tower/turntable configuration.

In this paper, we report about the COBRA 35 GHz system operated in a standard SAR configuration, where the radar system was onboard a Transall C-160. With its unusually large bandwidth of 2 GHz, the theoretical image resolution falls to below 10 cm in both the range and azimuth dimensions.

The navigation data result from the integration of the data of 3 units, namely the on-board INS and GPS aircraft navigation units as well as an additional 20 Hz dGPS. Synchronization between the SAR and the navigational data is based on event markers and enables very accurate absolute positioning.

The transmitted signal consist of very long pulses. The received signal is de-chirped by mixing it with the transmitted signal, demodulated and AD-converted. The raw data are focused using a frequency scaling algorithm which accounts for the radar movement during the long pulse duration, i.e., without assuming the stop-and-go approximation. In addition the focusing chain integrates a two-steps motion compensation.

Results from measurement campaigns in 2010 and 2011 will be given. The single look complex images are geocoded using a lidar-based terrain model. These geocoded products are subsequently mosaicked. The geometric and radiometric characteristics are analysed based on corner reflectors deployed within the test site. Examples of change detection as well as moving targets signatures will be presented.

High Resolution MEMPHIS SAR Data Processing and Applications

C. Magnard[1], **T. Brehm**[2], **H. Essen**[2], **and E. Meier**[1]

[1]Remote Sensing Laboratories, University of Zurich, Switzerland
[2]Fraunhofer FHR, Wachtberg, Germany

Abstract— This paper focuses on MEMPHIS (Multi-frequency Experimental Monopulse High-resolution Interferometric SAR) data processing, possible applications using its various SAR modes, and the results obtained.

MEMPHIS is a millimeter-wave high-resolution SAR system, developed and operated by the German research institute Fraunhofer FHR. It operates at the 35 GHz and 94 GHz radar bands (Ka and W-bands respectively). It is an experimental, modular and removable system, typically mounted on a C-160 Transall airplane. Various antenna shapes and configurations can be used, making the following SAR modes possible: single-path multi-baseline cross-track interferometry with a four horn antenna, dual-pol circular or linear polarimetry and monopulse for MTI applications.

MEMPHIS was introduced at the end of the 90's and has significantly improved over the years, including enhancement of the bandwidth using a stepped-frequency chirp, addition of dGPS and precise INS systems, as well as the determination of the lever arms. This has led to a dedicated processing chain, whose features include navigation data processing, SAR data extraction and synchronization with the navigation data, range compression of the separate stepped-frequency raw data, reconstruction of the full bandwidth from the range-compressed data of each chirp and azimuth focusing using an Extended Omega-k algorithm.

The results of the focusing are presented. To demonstrate the focusing quality, the signatures of corner reflectors were analyzed, revealing not only a high resolution (better than 0.2 m in range and 0.1 m in azimuth), but also a very precise geometric positioning accuracy on the order of the resolution, in spite of MEMPHIS experimental and portable design.

Finally, applications and results using the various antennas are presented, such as the generation of digital surface models with the multi-baseline interferometric antenna along with its quality evaluation, and channel combinations of the polarimetric data.

A Highly-linear Low-power Down-conversion Mixer for Monostatic Broadband 80 GHz FMCW-radar Transceivers

Christian Bredendiek[1], **Nils Pohl**[1], **Timo Jaeschke**[1], **Klaus Aufinger**[2], **and Attila Bilgic**[3]

[1]Institute of Integrated Systems, Ruhr-Universität-Bochum, Germany
[2]Infineon Technologies AG, Germany
[3]KROHNE Messtechnik, Germany

Abstract— Recently, radar transmitters, VCOs and frequency multiplier in silicon-based circuits, which are well suited for mm-Wave applications have been published. This paper focuses on the design of highly-linear broadband mm-Wave down-conversion mixers for FMCW-Radar-Systems. The intended application is a single-channel monostatic transceiver with a high bandwidth of approximately 20 GHz.

While an output power of more than 10 dBm can easily be attained with VCOs and PAs around 80 GHz in SiGe-Technologies, a sufficient linearity of mixers can not be achieved that easily. Particularly in monostatic applications this is one of the most important requirements for SiGe-Radar-Frontends, due to possible strong reflections for instance at the antenna which could drive the frontend into saturation. Mixers with a 1-dB input referred compression point of around zero dBm in silicon technologies have been reported, while compromising with current-consumption and exhibiting higher noise. This compromise may not lead to an increase in dynamic range of the mixer depending on the amount of excess noise.

This paper investigates three techniques to improve the linearity of double-balanced Gilbert-Cell mixers on simulation level. The three techniques are the multi-tanh technique, resistive and inductive emitter degeneration. Using the inductive emitter degeneration the highest dynamic range can be obtained due to a slightly degenerated noise figure and a increased compression point. With this insight the paper proposes a mixer-design with inductive degeneration.

The developed direct-down-conversion mixer is fabricated in a SiGe:C bipolar production technology with a fT of 170 GHz and fmax of 250 GHz. The conversion gain of the mixer offers a 2 dB flatness over a 20 GHz frequency band with a peak conversion gain of 11 dB which is high enough for the targeted application. The mixer achieves a 1 dB-input-referred compression point of -1.2 dBm with a low current consumption of 13 mA from a 5 V supply. These results agree well with the simulated ones. The noise figure is approximately 12 dB in a wide frequency band around 80 GHz and the input matching for the LO- and RF-Ports is better than -13 dB over a 20 GHz band and -20 dB over a 30 GHz band, respectively. With these results the mixer is well-suited for an operation in a broadband monostatic FMCW-Radar-System with a high dynamic range.

Advantages of Using Broadband Millimeter Wave Radar Sensors for High Precision Distance Measurements and SAR Imaging

T. Jaeschke[1], **M. Vogt**[2], **C. Bredendiek**[1], **and N. Pohl**[1]

[1]Institute of Integrated Systems, Ruhr-Universität-Bochum, Germany
[2]High Frequency Engineering Research Group, Ruhr-Universität-Bochum, Germany

Abstract— Frequency modulated continuous wave (FMCW) radar systems are used in a large field of applications with different special requirements for the sensor. Radar sensors for high precision distance measurements, e.g., for use in industrial tank level probing radars, demand for small antenna beam widths and a good range resolution to guarantee reliable measurements in complex process tanks with many disturbing objects. For short range imaging applications with synthetic aperture radar (SAR) a sensor with a wide antenna beam and a good range resolution is needed.

However, all this applications benefit from using a higher modulation bandwidth which directly results in a better range resolution. Broadband FMCW radar sensors allow low jitter distance measurements with a very good repeatability and accuracy. A good range resolution enables the sensor for separating reflections of disturbing targets from the wanted signal. This leads to reliable measurements even in the ranges close to the antenna, where small bandwidth systems only have a very limited accuracy. For imaging applications the resolution in azimuth direction is given by half of the antenna aperture length, whilst the range resolution is determined by the used bandwidth of the FMCW ramp. So the image resolution and quality also directly benefit from using a higher bandwidth.

Higher modulation bandwidths in phase lock loop (PLL) stabilized radar systems can be achieved by using nested PLL concepts in combination with broadband voltage controlled oscillators (VCOs). Here, a single-chip SiGe 80 GHz FMCW radar transceiver with a bandwidth of 25.5 GHz is used to demonstrate the impact of increased bandwidth for different types of measurements. The results and advantages of using broadband radar sensors for high precision distance measurement systems and SAR imaging are discussed.

Dual-Frequency Laser Doppler Radar for Coherence Enhancement and Speckle Noise Reduction

Chih-Hao Cheng, **Jia-Wei Lee**, **Tzu-Wei Lin**, **and Fan-Yi Lin**
Department of Electrical Engineering, Institute of Photonics Technologies
National Tsing Hua University, Hsinchu 300, Taiwan

Abstract— We develop and investigate a dual-frequency laser Doppler radar based on an optically injected semiconductor laser. Under a period-one oscillation (P1) dynamical state, the laser emits light with two coherent frequency components separated by about 12 GHz at the range of the millimeter wave. In the dual-frequency laser Doppler radar, the velocity of the target is determined from the Doppler shift of the beat signals through optical heterodyning of the dual-frequency light. While it has the same advantages of good directionality and high intensity as in the conventional single-frequency laser Doppler radar, having an effective wavelength in the range of millimeter-wave greatly reduces the speckle noise caused by the random phase modulation from the rough surface of the moving target. Moreover, by applying a RF signal at the beat frequency, the coherence of the dual-frequency laser can be much enhanced to significantly improve the velocity resolution and detection range. To demonstrate the speckle noise reduction, the Doppler shifted signals from a moving target are measured both from the single- and the dual-frequency laser Doppler radars. The target is an aluminium scrapped with sand paper to form a rough surface. It is rotated to provide a transverse velocity and thus the phase variation, where the speckle noise increases as the transverse velocity increases. In the single-frequency laser Doppler radar, the bandwidth of the Doppler signal increases from 4.7 kHz to 7.5 kHz as the transverse velocity increases from 0 m/s to 5 m/s. On the contrary, the bandwidth maintains at about merely 26 mHz with or without the rotation for the dual-frequency laser Doppler radar phase-locked with a RF signal modulated at the beat frequency.

Session 1P7
Extended/Unconventional Electromagnetic Theory, EHD (Electro-hydrodynamics)/EMHD (Electro-magneto-hydrodynamics), and Electro-biology

Electromagnetic and Gravitational Equations of Rotational Objects

Zi-Hua Weng
School of Physics and Mechanical & Electrical Engineering
Xiamen University, Xiamen 361005, China

Abstract— The validity of Maxwell's equations and Newton's law of gravitation are being doubted all the time, when the charged objects rotate in the electromagnetic field in the presence of the gravitational field. This validity remains as puzzling as ever. The existing theories do not explain why the charged particles remain spinning and why the planets keep rotating, and then do not offer compelling reason for those special situations.

The algebra of quaternions was invented by W. R. Hamilton in 1843, and was first used by J. C. Maxwell to represent the properties of electromagnetic fields in 1861. Later the quaternion was divided into the scalar part and the vectorial part. In terms of vector terminology coming from the quaternion's vectorial part in 1884, O. Heaviside recast successfully Maxwell's equations into the four differential equations from the original twenty equations.

Making use of the scalar potential, S. D. Poisson reformulated the Newton's law of gravitation in 1812. Recently the quaternions can also be used to rephrase the features of gravitational fields. The quaternion space for the gravitational field is independent to that for the electromagnetic field. Those two quaternion spaces can be combined together to become one octonion space. The latter can be used to depict the gravitational field and electromagnetic field simultaneously.

Further the radius vector can be combined with the integral of field potential to become one compounding physical quantity in the octonion space, which is one kind of function space. With the algebra of octonions, the results claim that there exist some kinds of 'weightlessness' states in the two fields. The field potential will impact the 'weightlessness' states, and the variation of field potential may change the angular velocity or the spin velocity.

ACKNOWLEDGMENT

The author is grateful for the financial support from the National Natural Science Foundation of China under grant number 60677039.

The Active Filter for Use in Measurement of the Fast Moving Object

Martin Friedl, **Lubomír Fröhlich**, **and Jiří Sedláček**
Department of Theoretical and Experimental Electrical Engineering
Faculty of Electrical Engineering and Communication
Brno University of Technology, Kolejní 2906/4, 612 00 Brno, Czech Republic

Abstract— In the field of a measurement of the fast one shot processes there is necessary to use special frequency filters. This article deals about the synthesis and optimization of the ARC ladder filters with transmission zeros based on frequency dependent negative resistors (FDNR). Frequency filters designed using approximation functions with transfer zeros (like Inverse Tchebyschev or Cauer functions) exhibit in comparison to approximation functions with monotonic magnitude response in stop band essential higher steepness of magnitude response in area of transitive band of filter. Active RC filters synthesized using modern active elements grown from passive RLC filter prototypes with very small sensitivity on passive elements can be in comparison to their RLC prototypes realized relative easily. These filters designed using active FDNR blocks as LP (low pass) filters or using SI (Simulated inductors) active blocks in case of HP (high pass) filters can be designed with minimum active and passive elements. During resulting optimization filter design process must be an influence of real lossy active blocks (FNDR, SI) on resulting filter response respected. In contribution here are presented some possibilities of filter optimization from this point of view. There are also discussed and in some examples prescribed ways of filter synthesis with account of influence of lossy active blocks on resulting filter magnitude response in case of Inverse Tchebyschev and Cauer filter of LP and HP filters higher (from 3rd to 7th) filter orders.

ACKNOWLEDGMENT

The research described in the paper was financially supported by grant of Czech ministry of industry and trade no. FR-TI1/001, GACR 102/09/0314 and project of the BUT Grant Agency FEKT-S-11-15.

REFERENCES

1. Bruton, L. T., *RC-active Circuits Theory and Design*, Prentice-Hall, Inc., Englewood Cliffs, New Jersey, 1980, ISBN 0-13-753467-1.
2. Daryanani, G., *Principles of Active Network Synthesis and Design*, Library of Congess Cataloging in Publication Data, Canada, 1976, ISBN 0-471-19545-6.
3. Pactitis, S., *Active Filters: Theory and Design*, CRC Press, USA, 2008, ISBN 978-1-4200-5476-7.
4. Sedláček, J. and K. Hájek, *Kmitočtové Filtry*, 1. Vydání. Praha, BEN - Technická Literatura, 2002, ISBN 80-7300-023-7.

Electromagnetic Force and Velocity Curl

Zi-Hua Weng
School of Physics and Mechanical & Electrical Engineering
Xiamen University, Xiamen 361005, China

Abstract— The electromagnetic force can be represented with the algebra of quaternions, which was invented by W. R. Hamilton. The quaternion was first used by J. C. Maxwell to depict the electromagnetic theory. The radius vector can be combined with the integral of field potential to become one compounding radius vector in the quaternion space. And it deduces one relation formula between the field strength and the velocity curl.

The gravitational field can be described with the quaternions also. The quaternion space for the gravitational field can be combined with that for the electromagnetic field to become an octonion space, which was invented by A. Cayley etc.. Therefore the gravitational field and electromagnetic field can be depicted with the octonion simultaneously, including the electromagnetic force in the presence of the velocity curl and the gravitational field.

The force is defined from the octonion linear momentum, which is one function of field sources etc. And it includes the gravity, the inertial force, and Lorentz force, the interacting force between the magnetic strength with the magnetic moment etc. When the force is equal to zero, there are several kinds of 'weightlessness' states. The charged rotating objects in those states may occupy determinately the velocity, the angular velocity, and the spin velocity etc..

Similarly the radius vector and the integral of field potential can be combined together to become one compounding radius vector in the octonion space. When the field source does not equal zero, the field strength and the force may deviate from zeros, and the charged rotating objects will not stay on 'weightlessness' states. It causes the fields to exchange the angular momentum, the energy, and the torque etc with the charged rotating objects.

ACKNOWLEDGMENT

The author is grateful for the financial support from the National Natural Science Foundation of China under grant number 60677039.

Limiting Effects in the Application of Inductive Sensors for Measuring of Non-harmonic High-level Current Pulses

R. Myška, and P. Drexler
Department of Theoretical and Experimental Electrical Engineering
Brno University of Technology, Kolejni 2906/4, Brno 612 00, Czech Republic

Abstract— This article deals with description of limiting effect occurring by measurement of non-harmonical high-level current pulses by means of inductive sensors. These effects will described for the case of Rogowski coil application in current pulses measurement. The first is a fact that the sensor must be considered as a circuit with distributed parameters. For measuring of non-harmonic waveforms is necessary to ensure the Heaviside's condition for distortionless transmission line. The second factor is the Gibbs's effect which causes overshoots on the edges of a rectangular pulse. The third factor is the influence of wire position in the sensor on the character of output waveform. All of these factors which have been mentioned above cause a serious limitation of induction sensor application for non-harmonic current pulses measurement. Special precautions have to be ensured in order to attain of distortion-free measurement. The influence of precaution violation on the measured waveform will be shown.

ACKNOWLEDGMENT

The research described in the paper was financially supported by project of the BUT Grant Agency FEKT-S-10-13, by research plan No. MSM 0021630513 ELCOM and the grant of Czech ministry of industry and trade No. FR-TI1/001.

REFERENCES

1. Drexler, P., *Metody Měření Ultrakrátkých Neperiodických Elektromagnetických Impulsu: Doktorská Práce*, 92, Vysoké Učení Technické v Brně, Fakulta Elektrotechniky a Komunikačních Technologií, Brno, 2007.
2. Myška, R., *Měřicí Systém Impulzního Proudového Zdroje*, 79, Vysoké Učení Technické v Brně, Fakulta Elektrotechniky a Komunikačních Technologií, Vedoucí Diplomové Práce Doc. Ing. Petr Drexler, Ph.D., Brno, 2011.

Temperature Dependencies Measurement, Proposal and Preparing

J. Hrozek[1], **D. Nespor**[1], **and K. Bartusek**[2]

[1]Deptartment of Theoretical and Experimental Electrical Engineering
Brno University of Technology, Kolejni 2906/4, 612 00 Brno, Czech Republic
[2]Institute of Scientific Instruments, Academy of Sciences of the Czech Republic
Kralovopolska 147, 612 64 Brno, Czech Republic

Abstract— This paper contains two parts. The first one deals with measuring of bio-material thermal properties. The thermal properties of each matter are dependent on its own temperature. The measurement of heat conduction and specific heat of bio-material is described in this paper. Knowledge of these parameters is very important for the thermal processes computer simulation. However, these properties are very bad to find out. The bio-material will be used for a real experiment of the cryosurgery optimization. The second part of this paper deals with computer simulation of cryosurgery experiment. The new thermal properties are used in this computer model. The confrontation of computer simulation and real experiment will be provided in near future.

NMR Lens — Technological Limits

D. Nespor, **P. Drexler**, **K. Bartusek**, **and P. Fiala**
Department of Theoretical and Experimental Electrical Engineering
Brno University of Technology, Kolejni 2906/4, Brno 612 00, Czech Republic

Abstract— Electromagnetic field is possible to manipulate by means of dielectric materials. Electromagnetic field will be affected due to values of dielectric constant ε_r and permeability μ_r. The lens was constructed as periodic structure of single split ring resonators. A negative effective permeability μ_r can be imposed on this structure. The main problem is to set up the resonance frequencies of the resonators. The demand for the metamaterial structure is that the resonators size has to be much smaller than the length of electromagnetic wave. The intended application of the designed structure is the increasing of the magnetic resonance (MR) system sensitivity. The frequency of the MR system is 198,75 MHz. The resonator working frequency must be slightly higher than the frequency of the MR system because the effective permeability μ_r is negative in this area. But single split resonators for that frequency would be too big. That is why the constructed resonators with resonant frequency about 6 GHz has been modified by means of chip capacitors. Therefore, the ceramic chip capacitors have been assembled over the interspaces. But this solution is inconvenient in many aspects. The main inconveniency is the inaccuracy of capacitors and soldered pads. Next inconveniency is the need for the surface mount. Another solution is the spiral resonator. Spiral resonators are possible to manufacture as a planar types without the external component assembly. That is the main advantage of these resonators. But the problem of this solution is very high sensitivity on the technological accuracy of manufacturing. For example: resonant frequency of the particular resonators has very high scattering due the under-etching. The next step is to find an optimal technological process for the best resonator accuracy. Paper contains calculations and measuring of the basic resonators parameters for the different technological processes.

The Correction of B_1 Errors in Magnetization Transfer Ratio Measurements

M. Alkhaddour and P. Fiala
Department of Theoretical and Experimental Electrical Engineering
Brno University of Technology, Kolejni 2906/4, Brno 612 00, Czech Republic

Abstract— The paper presents the assessment and correction of B_1-induced errors in magnetization transfer ratio measurements, Where a new method is presented for fast and accurate large volumetric radio frequency (RF) field. This method is a modification of the double-angle method (DAM), which accelerates imaging speed and applies 3D.

Two main factors are releated with the B_1 errors, magnetizatoin transfer ratio (MTR) measurements, and radio frequency (RF) nonuniformity, wher MTR value is based on the amplitude of the magnetization transfer (MT) pulse. Non-uniform B_1 transmission (B_1+) produces spatially varying flip-angles, causing intensity and contrast to be non-uniform, and complicating quantitative imaging. Thus (RF) causes MTR histograms to be broadened. B_1 non-uniformity causes changes in intensity and contrast across MR images. RF field B_1 nonuniformity is the largest resours of error in the quantitative measurement of many relevant parametersin MR images. Radio frequency nonuniformity may cause MTR histograms to be broadened. The field strength B_1 of the of the saturation pulse affect on the magnetization transfer ratio histogram analysis, particularly if data from a large volume of interest are included.

The double angle method (DAM), with fast spin-echo (FSE) readout, are used in B_1 field mapping technique to quantify B_1 errors and correct MTR maps and histograms.

The aims of this Paper to describe B_1 errors in MTR and reduce MTR histogram dispersion using B_1 field mapping. The proposed B_1 field mapping sequence for the study is the DAM. In order to reduce acquisition time, an FSE sequence is used in this study. The FSE sequence is performed twice, with the excitation stage of the sequence altered.

REFERENCES

1. Kubásek, R., K. Bartušek, and P. Fiala, "Determination of pre-emphasis constants for eddy current reduction," *Measurement Science and Technology*, Vol. 21, No. 10, 2010, ISSN: 0957-0233.
2. Ropele, S., M. Filippi, P. Valsasina, T. Korteweg, F. Barkhof, P. S. Tofts, et al., "Assessment and correction of B_1 induced errors in magnetization transfer ratio measurements," *Magn. Reson. Med.*, Vol. 53, 134–140, 2005.
3. Stollberger, R. and P. Wach, "RF field mapping in vivo," *Proceedings of the International Society of Magnetic Resonance in Medicine*, 106, 1988.

Measurement of DWI and DTI Images of Isotropic and Anisotropic Materials by Using NMR Methods

P. Marcon[1], **K. Bartusek**[2], **and M. Cap**[1]

[1]Department of Theoretical and Experimental Electrical Engineering
Brno University of Technology, Kolejni 2906/4, 612 00 Brno, Czech Republic
[2]Institute of Scientific Instruments, Academy of Sciences of the Czech Republic
Kralovopolska 147, 612 64 Brno, Czech Republic

Abstract— The paper deals with measurement of DWI and DTI images of isotropic and anisotropic materials by using NMR methods. In tissues, such as brain gray matter, where the measured apparent diffusivity is largely independent of the orientation of the tissue (i.e., isotropic) at the voxel length scale, it is usually sufficient to describe the diffusion characteristics with a single (scalar) apparent diffusion coefficient (ADC). However, in anisotropic media, such as white matter or skeletal and cardiac muscle, where the measured diffusivity is how to depend upon the orientation of the tissue, a single ADC does not adequately characterize the orientation-dependent water mobility. The next most complex model that describes anisotropic diffusion replaces the scalar ADC with a symmetric effective or apparent diffusion tensor of water, **D**.

As a sample of isotropic material, we used a physiological solution. As a sample of anisotropic material we used plants — cabbage.

For measurement of DWI and DTI images, we used a widely used method of measuring — the Pulse Filed Gradient Spin Echo (PFGSE). The experiments were carried out on an MR tomograph system 4.7 T/120 mm (i.e., 200 MHz for 1 H nuclei). Actively shielded gradient coils yield a maximum gradient field magnitude of 180 mT/m. The data measured were processed in the MAREVISI and MATLAB programs.

REFERENCES

1. Johansen-Berg, H. and T. E. J. Behrens, *Diffusion MRI: From Quantitative Measurement to in Vivo Neuroanatomy*, Elsevier, China, 2009, ISBN 978-0-12-374709-9.
2. Bartusek, K. and E. Gescheidtova, "MR measurement technique of rapidly switched gradient magnetic fields in MR tomography," *Applied Magnetic Resonance*, Vol. 29, No. 12, 675–686, (IF 0,665), 2006, ISSN 0937-9347.
3. Mansfield, P. and B. Chapman, "Active magnetic screening of gradient coils in NMR imaging," *Journal of Magnetic Resonance*, Vol. 66, 1986.
4. Bartusek, K., "Special methods of diffusion coefficients measurement by use of nuclear magnetic resonance," *Inaugural Thesis*, Brno Univeristy of Technology, Brno, 2007, ISSN 1213-418X.
5. Bartusek, K. and E. Gescheidtova, "MRI method of diffusion measurement in heterogeneous materials," *Measurement Science and Technology*, Vol. 19, (IF 1,297), 2008, ISSN 0957-0233.
6. Gescheidtova, E., R. Kubasek, Z. Smekal, and K. Bartusek, "Digital filter banks in MR measurement of gradient magnetic fields," *Applied Magnetic Resonance*, Vol. 33, 399–417, (IF 0,706), 2008, ISSN 0937-9347.
7. Bartusek, K. and E. Gescheidtova, "Testing the quality of magnetic gradient fields for studying self-diffusion processes in biological specimens by magnetic resonance methods," *Measurement Science and Technology*, Vol. 17, 2256–2262, (IF1,118), 2006, ISSN 0957-0233.
8. Mikulka, J., E. Gescheidtová, and K. Bartušek, "Perimeter measurement of spruce needles profile using MRI," *PIERS Proceedings*, 1128–1131, Beijing, China, March 23–27, 2009.
9. Marcon, P. and K. Bartušek, "Errors in diffusion coefficients measurement," *PIERS Proceedings*, 1035–1039, Cambridge, USA, July 5–8, 2010.

The Determination of Function G and Air Ion Mobility Spectrum in an Aspiration Condenser with Segmented Inner Electrode

Z. Roubal[1] and K. Bartušek[2]

[1]Department of Theoretical and Experimental Electrical Engineering, Brno University of Technology
Kolejní 2906/4, Brno 612 00, Czech Republic
[2]Institute of Scientific Instruments, Academy of Sciences of the Czech Republic
Kralovopolska 147, Brno 612 64, Czech Republic

Abstract— It was confirmed that light air ions have positive influence on human health. For its appraisal it is necessary to know the concentration of air ions and air ion mobility spectrum. When we measurement spectrum of air ions by standard type of the Gerdien tube with non-segmented electrode we must change voltage in the time. The disadvantage of this method is impossibility of real-time measurement air ion mobility spectrum because it is time-consuming. If we use aspiration condenser with segmented inner electrode it is possible determination air ion mobility spectrum from current individual segments inner electrode. This is problem because it is necessary numeric modeling electrostatic field inside the aspiration condenser using FEM and in the next step determination trajectory of air ion in aspiration condenser. From this result it is possible determine function G. This function is used for determination of air ion mobility spectrum. This algorithm is showed in this paper.

ACKNOWLEDGMENT

The research described in the paper was financially supported by grant of Czech ministry of industry and trade No. FR-TI1/001, GACR 102/09/0314 and project of the BUT Grant Agency FEKT-S-11-15.

REFERENCES

1. Roubal, Z., M. Steinbauer, and Z. Szabó, "Modeling of saturation characteristic of an aspiration condenser," *PIERS Online*, Vol. 6, No. 1, 26–30, 2010.
2. Tikhonov, V. P., A. A. Temnov, V. A. Kushnir, T. V. Sirota, E. G. Litvinova, M. V. Zakharchenko, and M. N. Kondrashova, "Complex therapeutical effect of ionized air: Stimulation of the immune system and decrease in excessive serotonin. H_2O_2 as a link between the two counterparts," *IEEE Trans. Plasma Scien.*, Vol. 32, No. 4, 1661–1667, 2004.
3. Kondrashova, M. N., E. V. Grigigorreko, A. N. Tikhonov, T. V. Sirota, A. V. Temnov, I. G. Stavrovskaya, N. I. Kosyakova, N. V. Lange, and V. P. Tikonov, "The primary physicochemical mechanism for the beneficia biological/medical effects of negative air ions," *IEEE Trans. Plasma Scien.*, Vol. 28, No. 1, 230–237, 2000.
4. Tammet, H. F., *The Aspiration Method for Determination of Atmospheric-Ion Spectra*, IPST, Jerusalem, 1970.
5. Bartušek, K., P. Fiala, T. Jirku, and E. Kadlecová, "Experiments of accuracy air ion field measurement," *PIERS Online*, Vol. 3, No. 8, 1330–1333, 2007.
6. Bartušek, K., "Meření spektrálních charakteristik iontových polí," *Elektrorevue*, 2001, http://www.elektro-revue.cz/clanky/01038/index.html.
7. Roubal, Z. and M. Steinbauer, "Design of electrometric amplifier for aspiration condenser measurement," *PIERS Proceedings*, 1430–1434, Xi'an, China, March 22–26, 2010.
8. Steinbauer, M., P. Fiala, K. Bartušek, and Z. Szabó, "Experiments with accuracy of air ion field measurement," *PIERS Online*, Vol. 3, No. 8, 1330–1333, 2007 .

MR Perfusion Visualization in 3D Image

M. Cap[1], **E. Gescheidtova**[1], **P. Marcon**[1], **K. Bartusek**[2], **and E. Kroutilova**[1]

[1]Department of Theoretical and Experimental Electrical Engineering
Brno University of Technology, Kolejni 2906/4, 612 00 Brno, Czech Republic
[2]Institute of Scientific Instruments, Academy of Sciences of the Czech Republic
Kralovopolska 147, 612 64 Brno, Czech Republic

Abstract— MRI is a constantly developing region of medicine, which is suitable for the study of soft tissues. The current methodologies for obtaining images weighted by relaxation times give only an idea of the distribution of soft tissues. Differential diagnosis of a high-grade glioms and solitary metastases is in some cases inconclusive. Investigators in several studies have demonstrated that in perfusion MRI (magnetic resonance imaging) of high-grade glioms and solitary metastases are differences. Analysis of the peritumoral region could be more useful than the analysis of the tumor itself. Precise evaluation of mentioned differences in peritumoral region gives a hopeful chance for tumor diagnosis.

This article describes image processing and fusion of the MR images. T_2 weighted (T2W) images and perfusion weighted images are processed for creating a 3 dimensional image. System is designed for calculating slice from 3D image in any direction and position defined by user. Consequently, T2W and PWI are used for image fusion and to image perfusion in structural image in defined direction and position.

Calibration of the Apparatus for 3D Magnetic Measurement for EIT

Z. Roubal and T. Kříž
Department of Theoretical and Experimental Electrical Engineering, Brno University of Technology
Kolejní 2906/4, Brno 612 00, Czech Republic

Abstract— The paper deals about result measurement for designed apparatus 3D meter magnetic field. This apparatus allows measure direct or alternating magnetic field in environment with strong electromagnetic disturbance. In the case of measure alternating magnetic field is possible measure signal with lower amplitude than electromagnetic disturbance, concrete $S/N < 0.01$. The measurement was performing in workplace for mapping magnetic field. For determine suppression influence electromagnetic disturbance was measurement repeated for an environment with strong electromagnetic disturbance and environment without electromagnetic disturbance, Faraday chamber. In order to suppress these influences, the authors utilize the principle of synchronous detection in a lock-in amplifier; the amplifier facilitates the suppression of these spurious disturbing signals and enables the selection of the required ones. In the designed 3D magnetic field meter, Hall probes are used for the measurement of magnetic induction. For alternating measure, at the beginning of the measurement, the measuring device automatically corrects the reference signal phase shift for the maximum amplitude of the output direct voltage; also, the influence of Earth's magnetic field is compensated. The measurement result was compared with simulation result in program ANSYS. In this paper are discussing difference between measurement and simulation result and determine source systematic error. The magnetic field map measured using the calibration 3D meter is used for the reconstruction of material properties of the measured sample.

ACKNOWLEDGMENT

The research described in the paper was financially supported by grant of Czech ministry of industry and trade No. FR-TI1/001, GACR 102/09/0314 and project of the BUT Grant Agency FEKT-S-11-15.

REFERENCES

1. Kříž, T., K. Barušek, and J. Dědková, "Image reconstruction by EIT with usage NMR," *PIERS Proceedings*, 329–333, Marrakesh, Morocco, Mar. 20–23, 2011.
2. Dorrington, A. A. and R. Kunnemeyer, "A simple microcontroller based digital lock-in amplifier for the detection of low level optical signals," *IEEE Trans. Plasma Scien.*, Vol. 28, No. 1, 486–488, 2002.
3. Azzolini, C., A. Magnanini, M. Tonelli, G. Chiorboli, and C. Morandi, "Integrated lock-in amplifier for contactless interface to magnetically stimulated mechanical resonators," *3rd International Conference on Design and Technology of Integrated Systems in Nanoscale Era, DTIS 2008*, 1–6, Mar. 25–27, 2008.
4. De Marcellis, A., G. Ferri, and E. Palange, "A novel analog autocalibrating phase-voltage converter for signal phase-shifting detection," *Sensors Journal, IEEE*, Vol. 11, No. 2, 259–266, Feb. 2011
5. Roubal, Z. and M. Steinbauer, "Design of electrometric amplifier for aspiration condenser measurement," *PIERS Proceedings*, 1430–1434, Xi'an, China, Mar. 22–26, 2010.
6. Kříž, T., R. Kořínek, and K. Bartušek, *NMR Magnetic Field Measurement for EIT. Advanced Numerical Modelling*, 37–38, PL, EI, Warsaw, 2011, ISBN: 978-83-61956-02- 0.
7. Hájek, K. and J. Sedláček, *Kmitočtové Filtry*, Vydavatelství, BEN, Praha, 2002.

Detection of Skull Trauma Using Resistance Tomography

K. Ostanina and J. Dedkova
Department of Theoretical and Experimental Electrical Engineering
Brno University of Technology, Kolejni 2906/4, 612 00 Brno, Czech Republic

Abstract— In the article, the non-invasive way for reconstruction images of an internal conductivity distribution of the human head tissue is described. This approach is based on the uses of the current density distribution obtained from measurements of external magnetic flux density by using magnetic field measurement with the principles of conventional EIT imaging technique. The proposed algorithm enables the detection of biological tissue changes in a head with a high spatial resolution.

The algorithm was applied to the several computer simulations representing the detection of skull trauma to demonstrate its feasibility, and to assess the performance of reconstruction process in estimating head tissue conductivity values. Obtained conductivity reconstruction results will be presented and compared with reconstruction results. All reconstruction process properties will be also discussed.

ACKNOWLEDGMENT

The research described in the paper was financially supported by fund of university development, grant No. GACR 102/09/0314 and the project of the BUT Grant Agency FEKT-S-11-5.

REFERENCES

1. Lee, T. H., H. S. Nam, M. Lee, Y. J. Kim, E. J. Woo, and O. Kwon, "Reconstruction of conductivity using the dual-loop method with one injection current in MREIT," *Phys. Med. Biol.*, Vol. 55, 7523–7539, 2010.
2. Seo, J. K., O. Kwon, and E. J. Woo, "Magnetic resonance electrical impedance measurement tomography (MREIT): Conductivity and current density imaging," *Journal of Physics: Conference Series*, Vol. 12, 140–155, 2005.
3. Sikora, J. and S. Wójtowicz, *Industrial and Biological Tomography. Theoretical Basis and Applications*, Electro-technical Institute, Warsaw, 2010.
4. Sankowski, D. and J. Sikora, *Electrical Capacitance Tomography. Theoretical Basis and Applications*, Electro-technical Institute, Warsaw, 2010.
5. Ostanina, K., J. Dedkova, and T. Kriz, "Utilization of boundary conditions in MR image reconstruction," *PIERS Proceedings*, 661–664, Marrakesh, Morocco, March 20–23, 2011.

NMR Diagnostic and Brain Cancer Treatment

P. Fiala[1], **K. Bartusek**[1, 2], **and M. Cap**[1]

[1]Department of Theoretical and Experimental Electrical Engineering
Brno University of Technology, Kolejni 2906/4, Brno 612 00, Czech Republic
[2]Institute of Scientific Instruments, Academy of the Czech Republic
Kralovopolska 147, Brno 61264, Czech Republic

Abstract— Brain cancer can be threaded by several therapies. One of ways is killing of the cancer cells in targeted volume of the tumor by the influence of heat. In case of this therapy is necessary to know location and distribution of the tumor volume in surrounded tissue. Right precise tumor localization is one of the crucial parts of the brain tumor local hyperthermia which is necessary for corresponding adjustment of the local hyperthermia system. This method of cancer treatment requires observance of the temperature distribution in the threaded issue.

Authors are in this article focused on local hyperthermia for local increasing of the tumor tissue temperature and on minimizing of the treatment influence on the healthy tissue. In the article are presented simulations of the tumor tissue heating method based on utilization of the complex permeability and complex permittivity of the heated tissue. Authors also discuss adjustment of the local hyperthermia system, especially time of exposition needed to achieve required temperature distribution in tumor volume.

ACKNOWLEDGMENT

The research described in the paper was financially supported grant of Czech ministry of industry and trade No. FR-TI1/001, GACR 102/09/0314, project of the BUT Grant Agency FEKT-S-10-13, and EC and MEYS CR (project No. CZ.1.05/2.1.00/01.0017).

REFERENCES

1. Kubasek, R., K. Bartušek, and P. Fiala, "Determination of pre-emphasis constants for eddy current reduction," *Measurement Science and Technology*, Vol. 2010, No. 21, 1–9, 2010, ISSN: 0957- 0233.
2. Marcoň, P., K. Bartušek, and M. Čáp, "Modeling and measuring of the changes of the magnetic field next to non-ferromagnetic substances for magnetic susceptibility calculation," *Measurement*, 213–216, Institute of Measurement Sciences, Bratislava, 2011, ISBN: 978-80-969672-4-7.
3. Marcoň, P., K. Bartušek, M. Burdková, and Z. Dokoupil, "Magnetic susceptibility measurement using 2D magnetic resonance imaging," *Measurement Science and Technology*, Vol. 2011, No. 22, 1–8, 2011, ISSN: 0957- 0233.
4. Mikulka, J., E. Gescheidtová, and K. Bartušek, "Interpolation of 3D magnetic resonance data," *PIERS ONLINE*, Vol. 7, No. 1, 31–34, 2011.

X-ray Diagnostics of Non-homogeneous Material by Means of 2D Plane Transformation

P. Fiala[1], **P. Koňas**[1], **M. Friedl**[1], **E. Kroutilová**[1], **and P. Šmíra**[2]

[1]Department of Theoretical and Experimental Electrical Engineering
Brno University of Technology, Kolejni 2906/4, 612 00 Brno, Czech Republic
[2]Thermo Sanace s.r.o., Chamrádova 475/23, 718 00 Ostrava-Kunčičky, Czech Republic

Abstract— The issues of suitable diagnostic procedure for constructing material examination occur recently. The material of interest is the wood as a sort of heterogeneous materials. The important aspect of diagnostic procedure is the possibility of industrial application.

A new diagnostic method based on X-ray imaging has been proposed and examined. The method is based on imaging information reduction into the 2D planar projection. It allows clearly to image the rate of material damage by means of displaying the weighted damage rate.

ACKNOWLEDGMENT

The research described in the paper was financially supported grant of Czech ministry of industry and trade No. FR-TI1/368, project of the BUT Grant Agency FEKT-S-11-5.

REFERENCES

1. Prosser, V., *Experimentální Metody Biofyziky*, Academia Praha, 1989.

Session 1P8
Poster Session 1

Inhabitation of LPS-induced Brain Damage Using Static Magnetic Field

Che-Tong Lin[1], **Wei-Jen Chang**[1], **Po-Chieh Yang**[2], **Wei-Yi Lai**[2], **Kan-Shin Fan**[3], **and Haw-Ming Huang**[2]

[1]School of Dentistry, Taipei Medical University, Taipei, Taiwan
[2]Graduate Institute of Biomedical Materials and Engineering, Taipei Medical University Taipei, Taiwan
[3]Dental Department, En-Chu-Kong Hospital, Taipei, Taiwan

Abstract— It was reported that electromagnetic fields have positive effects on various neurodegenerative diseases, such as Parkinson's disease, Alzheimer's disease and multiple sclerosis. Since systemic lipopolysaccharide (LPS) causes chronic neuroinflammation and progressive neurodegeneration, the effects of electromagnetic on LPS-induced neurodegenerative diseases are still unclear. The aim of this study is to test the rationale that static magnetic fields has inhibitive effects on LPS-induced neural damages and thus provide a potential method for preventing neurodegenerative disease. In this study, BALB/cByNarl mice were used as test subject. The mice were challenged with high-dose endotoxin (LPS) and exposed to a static magnetic field (0.4 T). The survival rates of the mice were monitored and the changes in their body temperatures were recorded. In addition, Brain biopsy were performed to explain the mechanism of SMF effects on neurodegenerative damage. Our results showed that SMF significantly increases ($p < 0.05$) the survival rate of LPS-challenged mice, with a ratio of 1.5 fold. In addition, after 6 hours of LPS injection, the average body temperature of SMF exposed mice was 1.07°C lower than that of unexposed animal. Brain tissue biopsy results demonstrated that SMF exposure reduces the damage at cerebrum, cerebellum and midbrain in the LPS-challenged mice. Based on the results, it is suggested that SMF can be a potential tool for preventing LPS-induced neurodamage.

Static Magnetic Fields Increase Low-temperature Storage Efficiency of Human Blood Cells

Haw-Ming Huang[1], **Chun-Yen Lin**[2], **Wei-Jen Chang**[2], **Kuo-Ning Ho**[2], **Yuh-Yuan Shiau**[3], **and Che-Tong Lin**[2]

[1]Graduate Institute of Biomedical Materials and Engineering
Taipei Medical University, Taipei, Taiwan
[2]School of Dentistry, Taipei Medical University, Taipei, Taiwan
[3]School of Dentistry & Graduate Institute of Dental Sciences, Taichung, Taiwan

Abstract— The aim of this study is to evaluate the effect of static magnetic fields (SMF) on the cryopreservation of human blood cells (HBC). A customer-designed program freezer was established to perform the cryopreservation process. In the program freezer, NdFeB permanent magnets were used to supply strong SMF. During freezing process, the HBC samples were exposed to 20% (w/v) glycerol as well as a static magnetic field up to 8000 Gauss. The finial cryopreservation temperature was set at $-80°$C with a cooling rate of $-1°$C/min. After freezing for one day, the samples were thawing quickly in a 37°C water bath. In this study, survival rate and membrane structure of the HBC were tested by flowcytometry and fluorescence polarization technique, respective. Our results demonstrated that the survival rates of 8000 Gauss SMF-exposed HBC samples (50.14%) are significantly higher than the values of the SMF sham-exposed analogous (41.61%). In addition, the static magnetic field has a protective effect on the rigidity of cell membrane with a flux-intensity dependent manner. Fluorescence anisotropy of DPH and DMA-DPH tests in SMF-exposed RBC samples (0.2036 and 0.2123) are significantly higher compared with sham-exposed analogous (0.1701 and 0.1980) ($p < 0.05$). These results suggested that static magnetic field has potential to be a tool for low-temperature storage of human blood sample.

Biological Properties and Haemocompatibility Evaluation of a Novel Paramagnetic Nano-membrane via Electrospinning

Sheng-Wei Feng[1], **Ya-Hui Chan**[1], **Che-Tong Lin**[1], **Chien-Wu Yeh**[2], **Shu-Li Lin**[2], **and Haw-Ming Huang**[3]

[1]School of Dentistry, Taipei Medical University, Taipei, Taiwan
[2]Dental Department, Cathay General Hospital, Taipei, Taiwan
[3]Graduate Institute of Biomedical Materials and Engineering
Taipei Medical University, Taipei, Taiwan

Abstract— Artificial skin and wound dressing offer reliable methods for the treatment of chronic and extensively burned wound. Therefore, it is important to develop a functional and cheap artificial dressing. Besides, the effects of static magnetic fields (SMF) on wound healing have been reported in several studies. However, artificial dressing combined with SMF is still unavailable. With this regard, the aim of this study was to develop a novel magnetic dressing material. The Fe_3O_4 nano-particles with a size range of 2–12 nm were prepared by the chemical-precipitation method. Electrospinning method was carried out to manufacture Fe_3O_4-Polylactide membrane with nanofiber. The Biophysical properties of the nano-membrane were characterized by contact angle assay and haemocompatibility test. Our results showed that the diameter of the nano-fiber was lower than 10 nm. For the contact angle assay, no significant difference in surface wettability can be found between the newly-developed membrane and the nano-particle free membrane ($118 \pm 4^\circ$). However, the newly-developed nano-membrane demonstrated a better haemocompatibility than the Fe_3O_4 particle free membrane. These results of contact angle assay and blood coagulation tests demonstrated that our Fe_3O_4-Polylactide membrane has excellent biological compatibility and has potential to serve as a reference for future animal studies.

Analysis of SRR Metamaterials with Controllable Resonance Frequency

Shi-Quan Zhang[1], **Li-Jie Wang**[1], **Hui Zhang**[1], **and Bing Wei**[2]

[1]Physics Teaching and Research Office, Engineering University of CAPF
Xi'an, Shaanxi 710086, China
[2]Department of Physics, Xidian University, Xi'an, Shaanxi 710071, China

Abstract— In recent years, there has been a growing interest for the study of the special properties of left-handed metamaterials and their applications. Metamaterials are also referred to as double-negative media which behave as an effective medium with negative values of permittivity and permeability. In 1968 Soviet scientist Veselago V. G. indicated that media with negative permittivity ε and permeability μ would have distinct electromagnetic characteristics, such as negative refraction. Since Smith D. R. et al. fabricated metamaterials whose ε and μ are negative by using Pendry J. B. et al.'s theoretical results for the first time in 2001. The discovery of metamaterials was considered as one of the ten greatest scientific and technological breakthroughs in 2003 by the famous American Journal, *science*. It was once again regarded as one of the ten greatest scientific and technological achievements in 2006 by *science* due to its application in electromagnetic stealth. The study of metamaterials has become a hot topic in the international science field. Pendry J. B. and Koschny T. [7, 8] pointed out that both the effective permittivity and the effective permeability of split ring resonator (SRR for short) array of metamaterials can be negative, that is

$$\varepsilon_{\text{eff}}^{\text{SRR}}(\omega) = 1 - \frac{\omega_p^2 - \omega_0^2}{\omega^2 - \omega_0^2 + \mathrm{i}\omega\gamma};$$

$$\mu_{\text{eff}}^{\text{SRR}}(\omega) = 1 - \frac{\omega_m'^2 - \omega_m^2}{\omega^2 - \omega_m^2 + \mathrm{i}\omega\gamma}.$$

In this paper, simulations are made to three types of symmetric SRR including double-ring SRR, symmetric single-ring SRR and modified SSR by CST software. Comparison and analysis indicate that SRR with short metal rod can adjust the resonance frequency of the conventional SRR. It is also verified that the transmission zero points of the new type of SRR-based filter can be controlled by changing the distance between the short metal rod and the side of SRR with mouth. The above properties of the modified SRR are used to design a filter unit which shows an improved transmission characteristic and compact size.

Measurement of High Frequency Magnetic Radiation in Kuwait

Fuad Alkoot[1] and Rabie K. Dib[2]

[1]HITN, PAAET, P. O. Box 4575, Alsalmia 22046, Kuwait
[2]EE Department, CTS, PAAET, P. O. Box 4196, Hawalli 32072, Kuwait

Abstract— There has been an increase of mobile users accompanied by an expansion of mobile telephone networks. This has resulted in mounting community concern about health effects caused by radiation emissions from the mobile antennas mounted on base station towers. Whether this concern is justified or not depends on the level of radiation emitted from the towers. We aim to find the level of radiation emitted by all sources emitting at frequencies between 75 MHz to 3 GHz.

Based on the surveyed literature [1–6] we believe there is a health hazard associated with EMF and RF radiation. However, studies were not able to find and confirm the exact dangerous levels due to the complex nature of the problem. Many organizations [7, 8] have set limits for each frequency of the RF band. The limit changes with the change in the frequency.

This study aims at finding the degree of radiation available and compares it to the standard levels. Our aim is not limit our study to GSM bands and find the sum of all radiation existing due to many sources at one point covering the RF range of 75 MHz to 3 GHz. High frequency sources under investigation are GSM, UMTS, TV, FM, WLAN, satellite paging systems and private networks. The recorded levels are compared to limits set by ICNIRP. Based on this comparison we may conclude whether the radiation levels in Kuwait pose any health hazard, and which source is the main contributor to this sum. Using the ICNIRP limit we can sum radiation to all sources at one location and find the percentage each band contributes to this sum.

For each surveyed area we record location, position, meter readings, and time of measurement. Considering the sensitivity of this type of readings, and in order to incorporate any undesired enormous range of response that depend on the angle and direction in which the measurement device is held, many redundant readings are taken to consolidate our measurements. A selective radiation meter made by Narda is used to find the magnetic radiation level in units of power density and in percentage of the ICNIRP limit.

Results of several area will be made available to the scientific community for possible future use. Results show that none of the sources exceeds the maximum limit nor did the sum of the highest 100 sources. The main contributors at all surveyed areas were GSM900, UMTS and GSM1800. FM existed close to GSM900 at all areas except at one of the surveyed areas. WLAN existed at all areas except for area.

REFERENCES

1. Roosli, M., et al., "Symptoms of ill health ascribed to electromagnetic field exposure — A questionnaire survey," *Int. J. Hyg. Environ. Health*, Vol. 207, No. 2, 141–50, 2004.
2. Santini, R., et al., "Symptoms experienced by people in vicinity of base stations: II/Incidences of age, duration of exposure, location of subjects in relation to the antennas and other electromagnetic factors," *Pathol. Biol.*, Vol. 51, No. 7, 412–5, Paris, 2003.
3. Santini, R., et al., "Investigation on the health of people living near mobile telephone relay stations: I/Incidence according to distance and sex," *Pathol. Biol.*, Vol. 50, No. 6, 369–73, Paris, 2002.
4. Wolf, R. and D. Wolf, "Increased incidence of cancer near a cell-phone transmitter station," *International Journal of Cancer Prevention*, Vol. 1, No. 2, 2004.
5. Eger, H., et al., "The influence of being physically near to a cell phone transmission mast on the incidence of cancer," *Umwelt Medizin Gesellschaft*, Vol. 17, 4, 2004.
6. Carpenter, D. and C. Sage, "BioInitiative report: A rationale for a biologically-based public exposure standard for electromagnetic fields (ELF and RF)," http://www.bioinitiative.org, August 2007.
7. International Commission on Non-Ionizing Radiation Protection, "Guidelines for limiting exposure to time-varying electric, magnetic, and electromagnetic fields (up to 300 GHz)," *Health Physics*, Vol. 74, No. 4, 494–522, 1998.
8. F.C.C., "A local government official's guide to transmitting antenna RF emission safety: Rules, procedures, and practical guidance," June 2, 2000, available at http://wireless.fcc.gov/siting/FCC_LSGAC_RF_Guide.pdf.

Relative Cellular Energy Balance and Biometric Interaction

K. F. Kaspareck
CTE, Italy

Abstract— The human body has a mean requirement of c.a. 100 Kcal/hr, corresponding to about 3 kWhr of energy over the 24 hrs or 6×10^{25} electron volts. Cellular balance is function of energy intake and metabolic output, baseline energy, electrochemical/magnetization induced gradients.

Cellular energy controls ph and internal electrochemical exchanges, and vice versa, where differences in ph reflects on T over a thermodynamic loop. Changes in ph and, or T affect cellular energy balance and internal biometric gradients, including intracellular radiation re-radiation. Entropy shifts during the process as T, ph and electrochemical potential modifies ($\varepsilon = h\upsilon 2/4\pi - U$) and interrelate with molecular water. The shape of interaction surfaces, differential electromagnetic attenuation condition the process.

Biometric energy unbalance coincides with a yield point of cellular equilibrium, creating free energy available for additional thermo-electrochemical reactions and, or displacement of resident cellular energy. Protein acids are less than 2 orders of magnitude than cell size and activate/synthesize with relatively small free energy. Cellular vibration frequencies and feedback quality (RNA — ATPs) are also affected, so is the glycolic process.

The physics of reaction, linear over a wider internal loop, may be non-linear in the very near field. The process is inertial and progresses along sequential rebalancing or cumulative unbalancing. Trace elements with double asymmetric bonds such as aromatics contribute to unbalance, strongly electropositive elements provide inertial contribution.

This paper attempts to provide an integrated, perhaps viable, chemical and thermodynamic model for cellular energies and exchanges that drives biometric interactions.

Influence of Variations of Near Earth Electromagnetic Fields on Cerebrovascular System of the Person in Time of Heliogophysical Disturbances

Yu. Ya. Varakin[1], **V. G. Ionova**[1], **G. V. Gornostaeva**[1], **E. A. Sazanova**[2, 3], **and N. P. Sergeenko**[2]

[1]Scientific Center of Neurology RAMS, Moscow, Russia
[2]Pushkov Institute of Terrestrial Magnetism
Ionosphere and Radio Wave Propagation RAS, Troitsk, Moscow Region, Russia
[3]Clinical Hospital of Russian Academy of Sciences, Troitsk, Moscow Region, Russia

Abstract— During heliogeophysical disturbances many diseases (especially cardio-cerebrovascular, psychological, etc.) are aggravated up to lethal outcomes. Professional reliability of functioning of persons, labile to influence of heliogeophysical disturbances (that is especially importance — in systems and situations of extreme risk) is decreasing. Problems of adaptation of the person to influence heliogeophysical disturbances are actual at its life-support, both on the Earth, and in space. In this work properties cross-correlation between variations of number of the hospitalised people with defeats of vessels of a brain and indexes of heliogeophysical disturbances characterising various physical processes in near the Earth space are analyzed. It is supposed, that one of the internal reasons of observed effects are increases of levels catecholamins and deformability and aggregative ability of erythrocytes of blood. The found out effects are statistically authentic. and are consequence of direct influences of physical processes during disturbances on blood cells. The physical processes influencing on these shifts in an organism of people are discussed. It is supposed, that in a initial storm stage the stochastic resonance can be one of physical mechanisms of influence of external weak periodic signals against noise. External fluctuations can synchronize or desynchronize rhythms of electromagnetic fluctuations of cells of the central nervous system by external electromagnetic fields. At development of the resonant phenomena there is a stressful reaction that conducts to occurrence in blood of "stress hormones" — catecholamins which directly or indirectly influence on activation of curtailing system, increase of aggregation of cellular elements.

At the same time blood as electromagnetic system is sensitive to changes of external electromagnetic fields. Its main vulnerable link are membranes of cells. Influence of an electromagnetic field on membranes of cells and the subsequent changes of their electric mobility also can influence on dynamics of process of aggregation — disaggregation of erythrocytes in a blood stream.

Overview of Methods for Magnetic Susceptibility Measurement

P. Marcon and K. Ostanina
Department of Theoretical and Experimental Electrical Engineering
Brno University of Technology, Kolejni 2906/4, 612 00 Brno, Czech Republic

Abstract— Magnetic susceptibility is defined as ratio between magnetization **M** of material in magnetic field and this field intensity **H**. Today used methods of magnetic susceptibility measurement are based on many different principles. In this paper an overview of methods for magnetic susceptibility measurement is described. Older methods — Faraday's scale and Guoy's scale are based on force effects of magnetic filed to magnetized specimen. Another methods, Inductive methods, use change of coil inductance, when magnetically conductive specimen is embedded. Modern methods (SQUID magnetometer) benefits from quantum interference device, allowing such sensitive magnetic measurement, that magnetic quantum can be detected.

Magnetic resonance is another modern way, how to measure susceptibility and some of MR based methods were introduced. The authors of this article mainly focus on the measurement of magnetic susceptibility of non-ferromagnetic material by means of MRI methods. In this respect, three basic measurement techniques are known and covered in this article.

Algorithms for Electromagnetic Waves on Interface

R. Kadlec, **Z. Roubal**, **E. Kroutilová**, **and P. Fiala**
Department of Theoretical and Experimental Electrical Engineering
Brno University of Technology, Kolejní 2906/4, Brno 612 00, Czech Republic

Abstract— The paper presents the problem of algorithm design of propagation, reflection and refraction of the electromagnetic waves on a layered medium. The analytic solution of this issue is very intricate and time demanding. This method is suitable for specific purposes of the detailed analysis of the general issue. Numerical methods are more suitable for analysis of the reflection and refraction of electromagnetic waves on layered heterogeneous medium. Fundamental law for analysis of the reflection and the refraction of electromagnetic waves on the boundary line between two materials are Snell's law for electromagnetic waves. In some cases, the form of transfer matrices and wave impedances for perpendicular incidence is same as for oblique incidence. By selection transverse and longitudinal fields with respect to the direction the dielectrics are vertical. We show that the transverse components satisfy the identical transfer matrix relationships as in the case of perpendicular incidence. The paper deals with the problem of complex angle of refraction in the losing medium. In non-lossy environment, interpretation of Fresnel relations and Snell's law is simple. This phenomenon is occur in metamaterial. These materials with negative parameters constitute a group of media that possesses a negative value, relative permittivity or relative permeability or both.

ACKNOWLEDGMENT

The research described in the paper was financially supported by the research program MSM 0021630516 and research plan MSM 0021630513, Ministry of Defence of the CR, Ministry of Industry and Trade of the CR (Diagnostics of Superfast Objects for Safety Testing, FR-TI1/368), Czech Science Foundation (102/09/0314) and project of the BUT Grant Agency FEKT-S-11-5.

REFERENCES

1. Dedek, L. and J. Dedková, *Elektromagnetismus. 2*, 232, VITIUM, Brno, 2000, ISBN 80-214-1548-7.
2. Nešpor, D., *Electromagnetic Wave Propagation Study in Heterogeneous Structures*, 20, Pavel Fiala, Ph.D., 2009,
3. Fiala, P., "Finite element method analysis of a magnetic field inside a microwave pulsed generator," *2nd European Symposium on Non-Lethal Weapons*, Ettlingen, SRN, May 13–15, 2003.
4. Fiala, P., R. Kadlec, P. Drexler, and P. Dohnal, Tuned periodical structures — Model, experiments in thz band applied in safety application," *PIERS Proceedings*, 1022–1026, Cambridge, USA, July 5–8, 2010.
5. Orfanidis, S., *Electromagnetic Waves and Antennas*, 1031, 2008, Available from WWW: www.ece.rutgers.edu/∼orfanidi/ewa.

Comparison of Segmentation Methods in MR Image Processing

J. Mikulka[1], **E. Gescheidtová**[1], **K. Bartušek**[2], **and D. Nešpor**[1]

[1]Department of Theoretical and Experimental Electrical Engineering
Brno University of Technology, Czech Republic
[2]Institute of Scientific Instruments
Academy of Sciences of the Czech Republic, Czech Republic

Abstract— Image processing in biomedical applications is strongly developing issue. There were described many methods and approaches for image preprocessing, segmentation and visualization. It is necessary to choose suitable segmentation method to create a correct three-dimensional model. The accuracy of reconstruction depends on precision of regions boundary determining in MR slices. The very often application is sensing of soft tissues. To imaging mentioned soft tissues is usually used tomography by magnetic resonance. Ideally, several tissue slices in three orthogonal planes (sagittal, coronal, transverse) are acquired. With slices in three planes is following reconstruction of shape of examined tissues most accurate. In case of acquired slices only in one plane the high spatial information lost occurs by image acquisition. Then it is necessary the shape of tissue appropriately reconstruct. At first the images are segmented and with use of particular segments the three dimensional model is composed. This article compares several segmentation approaches of MR images and their results. The results of segmentation by active contour, thresholding, edge analysis by Sobel mask, watershed and region-based level set segmentation methods are compared. The results for different values of parameters of segmentation methods are compared. As the test image was chosen MR slice of human liver tumor.

Simulation and Experimental Measurements for Near Field Imaging

S. Adnan[1], **R. A. Abd-Alhameed**[1], **M. Usman**[2], **C. H. See**[1], **J. M. Noras**[1], **and M. B. Child**[1]

[1]Mobile and Satellite Communications Research Centre
University of Bradford, Bradford, UK
[2]Department of Electrical Engineering, University of Hai'l, KSA

Abstract— Active microwave imaging for breast cancer detection has gathered momentum in recent years because of the better tissue characterization in comparison to conventional mammographic techniques. For active microwave imaging for breast cancer detection many experimental prototypes were proposed [1–3].

This paper presents an experiment setup for breast cancer detection by using two proposed wideband planar inverted F-antennas. The performance of the prototype antenna is tested and analyzed experimentally and exhibits reasonable agreement with simulations.

In the simulation, a simple tissue is adopted and the interaction of the antenna (sensor) with the tissue is investigated, as depicted in Figure 1(a). This proposed electromagnetic model used to simulate the breast contains two layers: The first layer is the skin layer with thickness = 4 mm, dielectric constant = 36 and conductivity = 4 S/m. The second layer is the breast tissue, which extends to a width of 10 cm, with a dielectric constant = 9 and conductivity = 0.4 S/m [4, 5]. In order validate the results obtained from simulated model, an experimental model is setup, as shown in Figures 1(b) and 1(c). In the measurement, vegetable oil is used due to its dielectric properties are closely matched to the actual tissue.

The reflection coefficient obtained by placing the antenna on the wall of the container 0° apart. Figure 2(a) shows the two antenna array operates over extremely wide bands which cover the

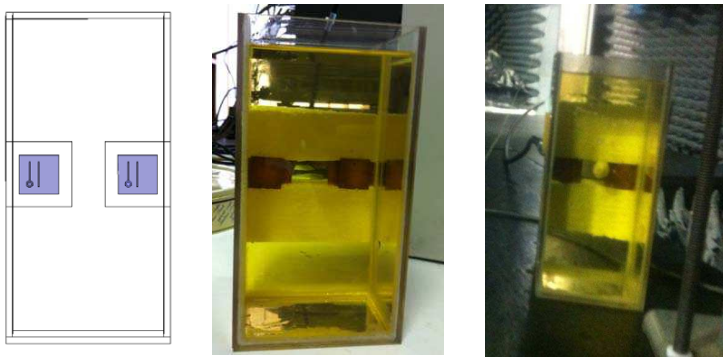

(a) (b) (c)

Figure 1: A two-element sensor array with oil apart 0°: (a) HFSS, (b) without tumor, (c) with the tumor cell.

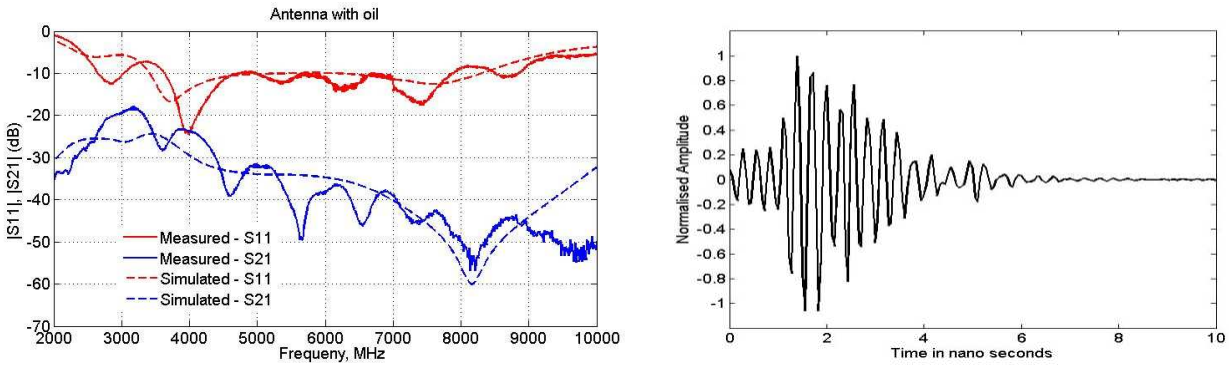

(a) (b)

Figure 2: (a) Scattering parameters for two element sensor array, (b) reflection from tumor.

frequency band from 4 to 8 GHz. As can also be noticed, the transmission coefficient (S_{21}) is as low as −23 dB across the operating frequency band when the two antennas are placed at 3 cm apart. Figure 2(b) illustrates the time domain normalised magnitude of the recorded signal when a tumor is presented in the tissue model.

REFERENCES

1. Meaney, P. M., M. W. Fanning, D. Li, S. P. Poplack, and K. D. Paulsen, "A clinical prototype of active microwave imaging of the breast," *IEEE Transactions on Microwave Theory and Techniques*, Vol. 48, 1841–1853, Nov. 2000.
2. Meaney, P. M., K. D. Paulsen, A. Hartov, and R. K. Crane, "An active microwave imaging system for reconstruction of 2-D electrical property distributions," *IEEE Transactions on Biomedical Engineering*, Vol. 42, 1017–1026, 1995.
3. Li, D., P. M. Meaney, T. Raynolds, S. Pendergrass, M. Fanning, and K. D. Paulsen, "A parallel-detection microwave spectroscopy system for breast imaging," *Review of Scientific Instruments*, Vol. 75, 2305–2313, 2004.
4. Sill, J. M. and E. C. Fear, "Tissue sensing adaptive radar for breast cancer detection: Study of immersion liquids," *Electronics Letters*, Vol. 41, 113–115, 2005.
5. Fear, E. C. and M. A. Stuchly, "Confocal microwave imaging for breast tumor detection: Comparison of immersion liquids," *IEEE APS*, 250–253, 2001.

Consideration of Metamaterial Transmission Line with Extended Constitutive Relationships by Using Circuit Theory

Toshikazu Sekine[1], **Yoshihiro Kawasaki**[2], **and Yasuhiro Takahashi**[1]

[1]Department of Electrical and Electronic Engineering
Gifu University, 1-1 Yanagido, Gifu-Shi 501-1193, Japan
[2]Graduate School of Engineering, Gifu University, 1-1 Yanagido, Gifu-Shi 501-1193, Japan

Abstract— The one dimensional propagation of Maxwell's equations with the constitutive relationships that there is coupling between the electric field and the magnetic field is analogized by the transmission line. An equivalent circuit representation in the minute section of this transmission line is presented. In addition, to examine whether such a constitutive relationships can be achieved by the transmission line that the medium consists of the metamaterials, the reciprocity, passivity, and reactivity are investigated by using the equivalent circuit. We have obtained analytically that this metamaterial transmission line is a non-reciprocal in general, but is a reciprocal when there is symmetry in strength of coupling the electric field and the magnetic field. And it is lossless when the coupling coefficients are imaginary. Moreover, the frequency response was calculated by cascade matrix of the equivalent circuit. We have confirmed the validity of our results. For example, it is shown that $S_{21} = -S_{12}$ is possible.

Equation (1) is usual constitutive relationships. Here, **D**, **E**, **B**, and **H** are electric flux density, electric field, magnetic flux density, and magnetic field respectively. ε and μ are permittivity and permeability respectively. Equation (2) is the extended constitutive relationships [1]. ζ and ξ are the coupling between the electric field and the magnetic field. From Equation (2), we obtain Equations (3) and (4). And, the equivalent circuit shown in Figure 1 is derived.

$$\mathbf{D} = \varepsilon\mathbf{E}, \qquad \mathbf{B} = \mu\mathbf{H} \tag{1}$$

$$\mathbf{D} = \varepsilon\mathbf{E} + \xi\mathbf{H}, \qquad \mathbf{B} = \zeta\mathbf{E} + \mu\mathbf{H} \tag{2}$$

$$-\frac{\partial E_x}{\partial z} = \mu\frac{\partial H_y}{\partial t} + \zeta\frac{\partial E_y}{\partial t}, \qquad -\frac{\partial H_y}{\partial z} = \varepsilon\frac{\partial E_x}{\partial t} + \xi\frac{\partial H_x}{\partial t} \tag{3}$$

$$\frac{\partial E_y}{\partial z} = \mu\frac{\partial H_x}{\partial t} + \zeta\frac{\partial E_x}{\partial t}, \qquad \frac{\partial H_x}{\partial z} = \varepsilon\frac{\partial E_y}{\partial t} + \xi\frac{\partial H_y}{\partial t} \tag{4}$$

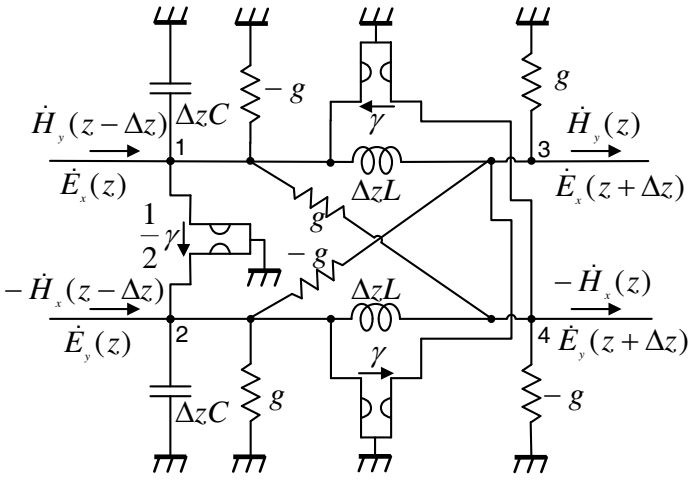

Figure 1: Equivalent circuit representation of minute section for metamaterial transmission line with coupling between dielectric and magnetic flux density.

REFERENCES

1. Krowne, C. M., "Electromagnetic theorems for complex anisotropic media," *IEEE Trans. Antennas Propag.*, Vol. 32, No. 11, 1224–1230, Nov. 1984.

The Measurement of Diffusion in Plants Tissue Culture

M. Burdková, **P. Marcon**, **E. Gescheidtová**, **and M. Cap**
Department of Theoretical and Experimental Electrical Engineering
Brno University of Technology, Kolejni 4, 612 00 Brno, Czech Republic

Abstract— For monitoring of tissue structures of Euphorbia plants is used magnetic resonance imaging (MRI). In contrast with CT the MRI does not emit any harmful radiation. The images are obtained without any deformation or destruction of the plant. The principle of MRI technique is based on the measurement of the interaction of the electromagnetic waves with nuclei placed in the strong magnetic fields. Diffusion is random translational motion of molecules from a place of higher concentration to a location with lower concentrations, arising due to their thermal energy. The diffusion coefficients measured by MRI method are describing the degrees of mobility of nuclei. Measurements of these coefficients is performed by measuring the PFGSE sequence, it is a normal spin-echo sequence extended by two identical rectangular diffusion gradients. During measurements there are distinguished three time intervals. In the first interval the nuclei are dephased, in the next interval the nuclei diffuse (relaxation time). In the last interval the nuclei are phased in by gradient pulses. When not all magnetization vectors are phased, diffusion is non-zero, otherwise diffusion is zero and the maximum MRI signal is obtained. During the measurement of the diffusion coefficient the static gradient is manifested as a result of magnetic properties of the substance. There are four gradients used for measurement for each axis. Evaluation of acquired images was performed in the program Marevisi. The images were evaluated separately for positive gradient ones and negative gradient ones. To obtain more accurate values in all directions averaged values were calculated.

Waves and Signals

S. L. Vesely[1], **A. A. Vesely**[2], **and C. A. Dolci**[3]

[1]I.T.B. — C.N.R., Italy
[2]Via L. Anelli 13, Milano, Italy
[3]Politecnico, Milano, Italy

Abstract— Maxwell's equations are in the first place about the induction of electric currents within circuits due to relative motions of magnets, and the mechanical effects on magnets due to electric current. That is, electromagnetism was not originally conceived as a theory of communication of information. However, Maxwell himself noted that his theory lends itself to applications in optics. Later on, H. Hertz showed that "Hertzian waves" exhibit refraction and reflection phenomena too. Yet later, O. Wiener delved into the reason why metal mirrors work as optical signals *decoders*; that is to say, they convert light into visible images. Actually, he had a different attitude: even if images correspond to the observed phenomenon, he explained his experiments by saying that the presence of stationary light waves can be captured by a photographic film slightly tilted with respect to a flat mirror. His interpretation is consistent with the mainstream physical conceptions of 1800s, involving the dynamics of aether. Nowadays, in classical physics electromagnetic waves are just the solutions of Maxwell's equations, and the description of perceptible effects requires considering the energy associated with them. The emphasis on energy leans toward reproducing the traits of a signal $s(x)$ by calculating the statistical moments M_k in the expansion of its characteristic function[1]. However, disregarding small energy fluctuations is different from poor signal reception: For example, while using a different sampling window doesn't change the average energy content too much, signals reconstructed using data from different samplings may differ in information content well beyond what a variation of signal strength might justify. In spite of information being *inhomogeneously* distributed across the signal traits, received signals can be considered linear as long as receiving circuits are so. Thus, describing perceived signals directly is a viable approach, and is alternative to approaches that associate signals with power spectra.

In the beginning, when telegraph experience was being extended to broadcasting, optimal sampling conditions were determined under the assumption that continuous messages consist of wavelets emitted by stationary Gaussian sources, and that statistical treatment of information allows to process those messages independently of the kind of receiver. This means assuming that radiation from a source with random features is frequency-encoded, and that bandwidth limited radiation is always faithfully reproduced provided that it is sampled at the Nyquist frequency. Shannon distinguishes the channel's capacity from the intelligibility of the transmission. His work hinges on the hypotheses that transmitters and receivers have linear performances, and use a common set of symbols and codes that they established out-of-band. Radar echoes, for a contrasting example, carry ambiguous information content even in the linear detection region. The responses of each target depend on its surface conditions, on the channel, and on the system type and configuration... in short, they are non-linear. This entails that, while we cannot make stringent assumptions on a returned echo, such as expecting given electromagnetic wave parameters, each receiver's output — the received signal — has a well defined, measurable information content, independently of any further interpretation. In addition, pursuing signal compression, the relevance of non-linear processes in sensorial perception was recognized, thus noting they play a role also in object recognition, and identification. We consider the signal received by an imaging system an image of the subject in its own right, without investigating the nature of radiations per se, although detection may affect the intelligibility of the information contained therein. In the linear reception case, the transfer function becomes the (known) receiver's response, which can be taken into account when rendering the received signal. We think that such an approach may allow, in general, to consider the information contained in a received signal without the need to model the source. Rather than attributing a power spectrum to noise, which is the core of N. Wiener's interpretation, we face experimental errors in the signal acquisition [1]. In conclusion, we think that the *detected* radiations have no energetic meaning, but rather carry some encoded information that, in the case of passively diffusing subjects, we can cast in a spatiotemporal frame. The detection process doesn't necessarily decode radiations diffused by a scenery so as to produce a 1-1 correspondence with the subject like ordinary photographic images.

[1]If $s(x) = \int_{-\infty}^{+\infty} S(\varsigma) e^{i\varsigma x} d\varsigma$ the function is $\ln s(x) = \Sigma_{k=1}^{+\infty} (M_k/k!)(ix)^k$.

REFERENCES

1. Kolmogorov, A. N., "Logical basis for information theory and probability theory," *IEEE T. Inform. Theory*, Vol. 14, No. 5, 662–664, 1968.

Effects of Multipath Propagation and Measurement Noise in IEEE 802.11g WLAN Beacon for Indoor Localization

C. Sapumohotti, **M. Y. Alias**, **and S. W. Tan**
Multimedia University, Malaysia

Abstract— GPS technology has become the de-facto standard for outdoor localization. However, GPS requires line of sight satellite signal which does not function well in indoor environment due to multipath signals. Indoor location information is highly useful for context aware applications. Recent proliferation of WLAN devices gives an opportunity to provide indoor localization by using radio maps generated from WLAN access point beacons.

Indoor localization based on IEEE 802.11 Wireless Local Area Network (WLAN) beacon measurement was first introduced in RADAR system [1]. In RADAR, the information about the propagation environment was not considered and localization was done by matching the online measurements with offline calibration data using a variant of nearest neighbour classification. The evolution of this approach, which is named as location fingerprinting, was done by considering probabilistic models [2] for the radio fingerprint measurements and by considering motion models [2, 3] to capture the user movement in a constrained map.

The propagation information was only used in cases where simple indoor propagation models were used for generating the offline radio map. However, the beacon measurement is not similar to narrow band measurements which were used to generate the propagation models and such systems do not have high accuracy. Apart from the complexity in radio propagation, the beacon measurement also contains noise. The usefulness of WLAN beacon based localization techniques depends on the correlation of beacon strength with the propagation environment. Apart from the propagation related issues, measurement noise may present in WLAN beacon measurement. It is necessary to identify random processes that affect the beacon measurement and to determine how the propagation environment affects the beacon measurement.

In this paper, we simulate beacons in IEEE 802.11g network and evaluate how the beacons response to the changes in propagation environment. We also present results from experimental data collected in an anechoic chamber for modelling the noise process in an IEEE 802.11g network due to beacon measurement noise. Understanding the effects of measurement noise and multipath propagation in WLAN beacon measurement will significantly improve the efficiency of indoor localization systems.

REFERENCES

1. Bahl, P. and V. N. Padmanabhan, "RADAR: An in-building RF-based user location and tracking system," *Proc. IEEE Conf. Comput. Commun.*, 775–784, 2000.
2. Honkavirta, V., T. Perala, S. Ali-Loytty, and R. Piche, "A comparative survey of WLAN location fingerprinting methods," *6th Workshop on Positioning, Navigation and Communication*, 243–251, Mar. 19–19, 2009.
3. Lim, Y.-X., "Efficient wireless location estimation through simultaneous localization and mapping," Ph.D. Thesis, Georgia Institute of Technology, May 2009.

Correlation Analysis on the Specific Absorption Rate (SAR) between Metallic Spectacle and Pins Exposed from Radiation Sources

M. H. Mat, **M. F. B. A. Malek**, **S. I. Syed Hassan**, **M. S. Zulkefli**, **and S. H. Ronald**
School of Electrical Systems Engineering
Universiti Malaysia Perlis, Kangar, Perlis 01000, Malaysia

Abstract— In this paper, the Specific Absorption Rate (SAR) inside the head due to metallic straight pins and spectacles is investigated. Nowadays, with more open source for mobile applications listed in market, mobile communication equipment (MCE) used in frontal of the face is becoming increasing significantly. Numerous studies have examined the interaction between the electromagnetic fields radiated by the antenna that may also couples with metallic objects and the results seem to suggest that metallic objects could increase the SAR [1–4]. The finite integration in time domain technique (FIT) computer simulation using CST Microwave Studio was used in this investigation. Two sets of dipole antennas operated at 900 MHz and 1800 MHz for GSM application were used in the simulation model represent as radiation sources from MCE. The head model is irradiated by dipole sources in front of the face in different orientations. In parametric studies the optimum dipole location is selected for all simulations and only varying both of the pin length and its horizontal separation distance between the head. The results compared on both of SAM head phantom and voxel head model. The shell with a fixed relative permittivity and electrical conductivity of 3.5 and 0.0016 S/m filled with Tissue Stimulant Liquid (TSL). There is a correlation between dielectric properties of SAM model and muscle of voxel model. The presented analysis studies show that 1 gram SAR at 900 MHz is slightly reduced. However at 1800 MHz, it decreased if pin lengths were varied longer than dipole and it can increase if pin is shorter or both has the same length. The results presented may find great potential awareness in wireless communication design and evaluating the power absorption in a bio-medium due to the antenna.

REFERENCES

1. Panagamuwa, C. J., et al., "A study of the effects of metallic pins on sar using a specific anthropomorphic mannequin (SAM) head phantom," *The Second European Conference on Antennas and Propagation*, 2007.
2. Whittow, W. G. and R. M. Edwards, "A study of changes to specific absorption rates in the human eye close to perfectly conducting spectacles within the radio frequency range 1.5 to 3.0 GHz," *IEEE Transactions on Antennas and Propagation*, Vol. 52, No. 12, 3207–3212, 2004.
3. Stergiou, K., et al., "Effects of metallic semi-rimmed spectacles on SAR in the head from a 900 MHz frontal dipole source," *Antennas & Propagation Conference*, Loughborough, 2009.
4. Whittow, W. G., et al., "Effect of tongue jewellery and orthodontist metallic braces on the SAR due to mobile phones in different anatomical human head models including children," *Antennas and Propagation Conference*, Loughborough, 2008.

Active Basestation Antenna for 4G Mobile Service

Young-Bae Jung
Hanbat National University, San 1 Duckmyong-dong, Yusung-gu, Daejeon 305-719, South Korea

Abstract— In this paper, we proposed a multi-band basestation reconfigurable antenna which can electrically control the antenna beam direction and radiating power. Thus mobile communications service providers can reduce the cost of infrastructure and operating expenses. Besides, the multiband basestation antenna can solve the human hazard problem of RF signal, thus it will be a key engineering issue in next generation mobile service for eco-friendly green environment

The antenna can be mainly divided by 4 parts. First, the multiband array antenna is composed of two types of array. The array for $B_1 + B_2$ is operated in two bands of B_1 and B_2, and the other is operated in B_1 and B_3. This structure was designed to minimize the array size using the optimal arrangement of individual radiators operated in single band considering the radiator size. Next, the active channels are connected with the B_2- and B_3-band radiators and composed of several components written below to control the frequency band selection, the antenna beam direction and the pattern shape.

From the results, it was confirmed that the minimum gain of the fabricated antenna is 16.5 dBi (HPBW = $65^\circ \sim 68^\circ$), 16.2 dBi (HPBW = $61^\circ \sim 69^\circ$) and 16.4 dBi (HPBW = $60^\circ \sim 63^\circ$) for B_1, B_2 and B_3 respectively. The SLL is 17.5 dB for B_1, 14.0 dB for B_2 and 13.2 dB for B_3.

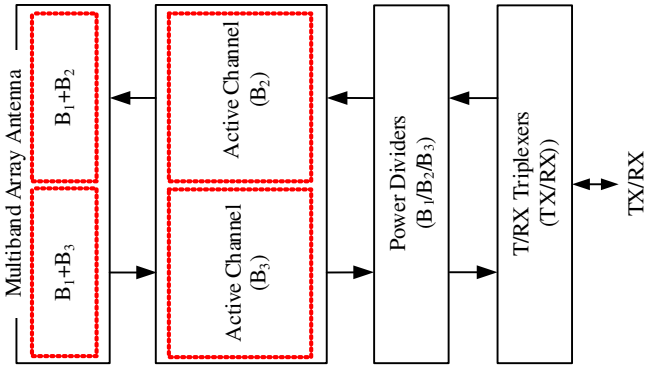

Figure 1: Block diagram of the proposed multiband antenna.

ACKNOWLEDGMENT

This research was supported by Basic Science Research Program through the National Research Foundation of Korea (NRF) funded by the Ministry of Education, Science and Technology (2011-0013213).

REFERENCES

1. Jung, Y. B., "Dual-band reconfigurable antenna for base-station applications," *IEE Electronics Letters*, Vol. 46, No. 3, 195–196, 2010.

Q-factors of Weakly Deformed Optical Resonators

Michael White and Stephen C. Creagh
School of Mathematical Sciences, University of Nottingham, Nottingham NG7 2RD, UK

Abstract— Light emission from whispering gallery modes in optical cavities can show strong directionality even for small deformations from perfect circular or spherical symmetry. This shape sensitivity and the resulting emission patterns can be explained using a perturbation theory of the underlying ray dynamics, which is then extended to the complex domain to account for evanescent escape. An important practical consideration in exploiting directionality resulting from deformation is the extent to which deformation effects the resonator's Q-factor. In this poster we exploit the methodology of perturbative complex ray theory to develop analytical models of the degradation in Q-factor that occurs when a resonator is deformed.

A general calculation is first presented which allows us to approximate the Q-factor analytically for arbitrary perturbations of a two-dimensional cavity of the form $r(\theta) = R_0(1+\epsilon f(\theta))$. Although this approximation is simple to evaluate, it is restricted to relatively weak deformations, where, formally, ϵk is of order unity.

In the important special case of an elliptical cavity, a better approximation is derived which, in particular, is valid for significantly stronger deformations. For sufficiently strong deformations, this allows the Q-factor to be expressed simply in terms of intrinsic geometrical properties of the underlying ray families. In particular, the degradation of the Q-factor depends on a canonically-invariant measure of the degree to which a symmetry of the escaping rays under complex conjugation is broken. In the limit of small deformations we recover the generic perturbative result derived earlier. A single uniform approximation is presented which unites these two limits.

Self-field Theory — A Biophotonic Model of Cellular Replication

A. H. J. Fleming
Biophotonics Research Institute, Melbourne, Australia

Abstract— This paper presents a model for cellular replication based on the biophysics of self-field theory (SFT) with its photon chemistry, a recently discovered level of organization below atomic chemistry resulting from the non-zero mass of the photon. Like bubbles that form into foam, cells occur in large populations known as colonies that cooperate amongst themselves to achieve replication. Overall (1) the cells interact via cell-cell signaling of electric and magnetic fields (termed biophotons) and (2) the chromosomes emit biophotons of specific frequencies within the UV range related to the continuously changing molecular state of the chromosomes as replication proceeds. The various states of the chromosomes are controlled by their photonic states. The states result from cell-cell interactions of first electric and then magnetic fields arising from the diffusion of dipolar proteins within the plasma membranes of various sectors of the colony. These two processes couple inducing metaphase and anaphase. Dipolar proteins diffuse within the membrane of cells in response to intra or extracellular endogenous or exogenous E- and H-fields. These diffusive processes involve two feedback loops (1) electrical feedback between membrane proteins of a fertilized cell and those of surrounding cells in a north south orientation; (2) magnetic feedback between biophotons emitted by chromosomes and proteins diffusing within the plasma membranes of neighbouring cells in an east-west orientation. Experimental observations including Gurwitsch's work in the 1920–1930's, cytoplasmic 'stirring' just before metaphase, and dielectric theory within the extremely low frequency range support the hypothesis. The UV frequencies inherent in the photonic states of the DNA may have first originated from energy cycles such as the seasons available within the proto solar system, while the ELF signals are biogenic in origin. Life may have first been a way of incorporating cyclic energy changes within a small body of tissue. In this early period, cooperation to establish life rather than competition for available food may have been a modus operandi within unicellular species. Cooperation was necessary since the available energy was dropping as cosmic expansion continued. Biophotonics research continues within areas of growth and development, repair and maintenance, genetics and evolution.

REFERENCES

1. Fleming, A. H. J., "Electromagnetic self-field theory and its application to the hydrogen atom," *Physics Essays*, Vol. 18, No. 3, 265–285, 2005.
2. Fleming, A. H. J. and E. B. Bauer, "A predicted photon chemistry," BEMS-26, Washington DC, 2004.
3. Fleming, A. H. J., "Analytic estimate for the mass of the photon," *PIERS Proceedings*, 1604–1607, Moscow, Russia, Aug. 18–21, 2009.
4. Fleming, A. H. J., *Self-field Theory: A New Mathematical Description of Physics*, Pan Stanford Publishing, 2011.
5. Fleming, A. H. J. and E. B. Bauer, *Inside the Photon: A Journey to Health*, Pan Stanford Publishing, 2011.
6. Fleming, A. H. J., "Self-field theory-biodiversity may be a resonance process," *PIERS Proceedings*, 828–831, Cambridge, USA, Jul. 5–8, 2010.

A Compact Internal Antenna Design for 3G and 4G Mobile Handset

Cheng-Hung Lin[1], **Chih-Liang Cheng**[1], **Kwong-Kau Tiong**[1], **and Guan-Yu Chen**[2]

[1]Department of Electrical Engineering, National Taiwan Ocean University, Taiwan
[2]Department of Electronic Engineering, National Taipei University of Technology, Taiwan

Abstract— In this paper, a high performance planer inverted F-antenna (PIFA) structure is presented for the radiators for 3G/4G wireless communication system. The proposed antenna with a compact area of 60 mm × 30 mm × 6 mm is implemented. And the PCB is FR4 substrate of the dimension 120 mm × 60 mm × 0.8 mm. The antenna shows a wide bandwidth of about 200 MHz and 500 MHz for low and high band respectively, making it easy to cover the LTE700 (Long term evolution), CDMA800/1900 (Code Division Multiple Access), and WCDMA2100 (Wideband Code Division Multiple Access) bands for 3G/4G wireless communication system. Of course, the antenna design can cover the GSM850 (Global System for Mobil Communication), DCS1800 (Digital communication system) and PCS1900 (Personal Communication Service) as well.

The multi-path fading is a critical issue in the wireless communication systems. In order to solve the problem, the multiple-input and multiple-output (MIMO) technique is considered. Therefore, a secondary antenna design is studied for the MIMO system. The compact area of the secondary antenna is 60 mm × 20 mm × 6 mm. The secondary antenna shows the bandwidth of about 80 MHz and 300 MHz for low and high band respectively. It can support to the application of the LTE700, CDMA1900, and WCDMA2100 bands.

The study mainly focuses on the current trends in development of compact, slim and low profile mobile handset, and provides antennas design which is suitable for application in 3G/4G wireless communication system. The proposed antennas are easily fabricated by the flex-film antenna at low cost and embedded into the mobile handset. A 50 ohms micro-strip line is used to excite the two antennas. The data of return loss, efficiency, and radiation pattern are performed. The SAR results of the proposed antenna are also analyzed. The antenna design can have the high efficiency and low SAR value. All of the performances tell that the proposed antenna is acceptable in the 3G/4G wireless communication system.

A Internal Planar Antenna Design for WiMAX Mobile Handset

Cheng-Hung Lin[1], **Wei-Hung Liu**[1], **Kwong-Kau Tiong**[1], **and Guan-Yu Chen**[2]

[1]Department of Electrical Engineering, National Taiwan Ocean University, Taiwan
[2]Department of Electronic Engineering, National Taipei University of Technology, Taiwan

Abstract— In recent years, a multiple-input multiple-output (MIMO) technique is utilized to enhance the performance of wireless communication systems. To design multiple antennas in the same ground plane for getting the benefit from MIMO technology are required to have high isolation property. Moreover, the antennas are strongly coupled with each other. It is quite challenge for antennas to obtain good isolation when the two antennas are located closely due to the limited antenna space in a mobile handset.

In this paper, we propose the compact antennas design for WiMAX mobile handset application. The proposed antennas are using the printed inverted F antennas (PIFAs). In the first study, the locations of two antennas are at the difference sides on the top of the mobile handset. The compact area of the proposed antenna is 20 mm × 10 mm × 6 mm. And the PCB is FR4 substrate and the dimension is 120 mm × 60 mm × 0.8 mm. The two antennas show the operating bandwidth of about 200 MHz in 2.6 GHz respectively for covering the WiMAX bands.

To miniaturize the antenna area in a mobile handset, the two antennas are placed at the same side on the top of the mobile handset. In these circumstances, the two antennas have poor isolation with each other. In order to enhance the performance, the two PIFAs with a common grounding pad structure are studied.

The L-type area of the proposed antenna is used on the top side of the mobile handset. The two WiMAX antennas are PIFAs with a common grounding pad which is capable of covering the bandwidth of 2.5–2.7 GHz. The common grounding pad design effectively reduces the mutual coupling between the two antennas. A good isolation and low correlation coefficient between the antennas are obtained by utilizing the common grounding design. All of the performances including return loss, antenna gain, current distribution and radiation patterns tell that the proposed antenna is proper to applied in the WiMAX wireless communication system.

A Novel on-glass DVB-H Antenna Design for Mobile Handset

Cheng-Hung Lin[1], **Li-Gang Lai**[1], **Kwong-Kau Tiong**[1], **and Guan-Yu Chen**[2]

[1]Department of Electrical Engineering, National Taiwan Ocean University, Taiwan
[2]Department of Electronic Engineering, National Taipei University of Technology, Taiwan

Abstract— The Digital Video Broadcasting- Handheld (DVB-H) is commonly used for terrestrial digital TV broadcasting. The mobile handset with DVB-H system can makes it receive digital video broadcast type services. The previously popular antenna design in the mobile handset for DVB-H is using the external helix or retractable rod type. The external antenna can have the advantage for the signal covering, but the cost is high. As in any consumer product, price is one of the most important parameters.

In the current commercial market, the size of the mobile handsets has become progressively smaller and slimmer. The internal flex-film antenna design can have the lower cost than the external antenna, but it is still a challenge to design the DVB-H internal antenna in the mobile handset which is leading very small height above ground plane. In order to solve the problem, a novel antenna covering frequencies of 470–750 MHz of digital video broadcasting band for mobile handheld is presented.

The proposed antenna is a multi-turn loop type which is placed along the frame of the display on the front side of the device. The antenna is easily fabricated by the flex film antenna at low cost and embedded into the mobile phone. To paint the radiator is studied as well for reducing the thickness. Additionally, the handheld condition of the mobile handset is considered in the design. The performance of the proposed antenna has the signification improvement than the internal antenna placed on the backside of the mobile handset.

A 50 ohms micro-strip line is used to excite the proposed antenna. The performed data including return loss, antenna gain, current distribution and radiation patterns are measured in an anechoic chamber. The antenna design can have the high efficiency and fit in a slim device. All of the performances show that the proposed antenna is proper to the DVB-H communication system.

A New Proof of the Non-constancy of Speed of Light in Vacuum and a Simple Solution for the Damped Wave Equation with a Moving Mirror Boundary (Part I)

Namık Yener
Technical Education Faculty, Kocaeli University, Izmit, Kocaeli 41380, Turkey

Abstract— A new proof of the non-constancy of speed of light in vacuum is obtained in the process of solving the damped wave equation with a mirror boundary in uniform rectilinear motion with respect to a simple, lossy medium and with specific conditions for the other boundary, using Laplace transform. Lorentz transformation is also needed in the proof. However because of the need to assign different speeds of light in vacuum to the two moving media, the resulting solution has further to be stretched in time, in addition to the hyperbolic rotation of the Lorentz transformation. The existing methods in literature to solve the involved damped wave equation are employed and a simple solution is proposed when the boundary conditions are of a special class. In the solution Laplace transform technique is used to convert the partial differential equation into an ordinary one. The uniform rectilinear motion of the mirror boundary and the particular type of conditions treated for the other boundary, permit a solution by this technique. The presentation of the work is organized as a series of three papers with the same title but with an extension in the title as Part (I), Part (II) and Part (III). In Part (I) which is the present paper, the moving mirror boundary condition is imposed and the new proof for the non-constancy of speed of light in vacuum is introduced. In Part (II), different speeds of light in vacuum for K and K' are incorporated in the differential equation. In Part (III), an example is worked out that illustrates the ideas developed in the first two parts.

A New Proof of the Non-constancy of Speed of Light in Vacuum and a Simple Solution for the Damped Wave Equation with a Moving Mirror Boundary (Part II)

Namık Yener
Technical Education Faculty, Kocaeli University, Izmit, Kocaeli 41380, Turkey

Abstract— A new proof of the non-constancy of speed of light in vacuum is obtained in the process of solving the damped wave equation with a mirror boundary in uniform rectilinear motion with respect to a simple, lossy medium and with specific conditions for the other boundary, using Laplace transform. Lorentz transformation is also needed in the proof. However because of the need to assign different speeds of light in vacuum to the two moving media, the resulting solution has further to be stretched in time, in addition to the hyperbolic rotation of the Lorentz transformation. The existing methods in literature to solve the involved damped wave equation are employed and a simple solution is proposed when the boundary conditions are of a special class. In the solution, Laplace transform technique is used to convert the partial differential equation into an ordinary one. The uniform rectilinear motion of the mirror boundary and the particular type of conditions treated for the other boundary, permit a solution by this technique. The presentation of the work is organized as a series of three papers with the same title but with an extension in the title as Part (I), Part (II) and Part (III). In Part (I), the moving mirror boundary condition is imposed and the new proof for the non-constancy of speed of light in vacuum is introduced. In Part (II) which is the present paper, different speeds of light in vacuum for K and K' are incorporated in the differential equation. In Part (III), an example is worked out that illustrates the ideas developed in the first two parts. In the present paper, we discuss a simple general solution of the differential equation involved making use of a simplification that applies when the boundary conditions for the non-moving boundary are of a special class. In particular we assume $E_x|_{z'=0}$ and $\frac{\partial E_x}{\partial z'}|_{z'=0}$ have no essential singularities or branch points and furthermore the former tends to zero while the latter remains bounded as s' tends to infinity. $E_x(z',\, t')$ is the unknown function of the differential equation, s' is the complex frequency, z' is the space coordinate and t' is the time variable, the last three of which are measured in K'.

A New Proof of the Non-constancy of Speed of Light in Vacuum and a Simple Solution for the Damped Wave Equation with a Moving Mirror Boundary (Part III)

Namik Yener
Technical Education Faculty, Kocaeli University, Izmit, Kocaeli 41380, Turkey

Abstract— A new proof of the non-constancy of speed of light in vacuum is obtained in the process of solving the damped wave equation with a mirror boundary in uniform rectilinear motion with respect to a simple, lossy medium and with specific conditions for the other boundary, using Laplace transform. Lorentz transformation is also needed in the proof. However because of the need to assign different speeds of light in vacuum to the two moving media, the resulting solution has further to be stretched in time, in addition to the hyperbolic rotation of the Lorentz transformation. The existing methods in literature to solve the involved damped wave equation are employed and a simple solution is proposed when the boundary conditions are of a special class. In the solution Laplace transform technique is used to convert the partial differential equation into an ordinary one. The uniform rectilinear motion of the mirror boundary and the particular type of conditions treated for the other boundary, permit a solution by this technique. The presentation of the work is organized as a series of three papers with the same title but with an extension in the title as Part (I), Part (II) and Part (III). In Part (I), the moving mirror boundary condition is imposed and the new proof for the non-constancy of speed of light in vacuum is introduced. In Part (II) different speeds of light in vacuum for K and K' are incorporated in the differential equation. In Part (III), which is the present paper, an example is worked out that illustrates the ideas developed in the first two parts. The result of the solution takes into account different speeds of light for the two reference frames involved.

ARC-phobic and Other Characteristics of Surface Flashover

Halimatusaadiah Binti Rusli, **Chandima Gomes**, **and Zainal Kadir**
Department of Electrical and Electronics Engineering
Universiti Putra Malaysia, Serdang, Selangor 43400, Malaysia

Abstract— High voltage systems should be design to operate under stresses associated not only with normal operating power frequency voltage but also those caused by transient over voltages. Between the spacing in the HV circuits or setups, arc or flashover can occur along the surface if the two conducting parts meets each other and will lead to destructive damage. Thus insulation materials medium can be used to reduce the spacing between two points that has different voltage level. On the other hand, insulation materials such as isolators, spacers, bushing and etc. can also deteriorate faster if the flashover follows the surface. Detailed investigations are required to be conducted in this regard for better understanding of conditions under which discharges adheres the surface.

The previous studies have focused extensively on developing and understanding the flashover characteristic in vacuum and atmospheric conditions and these studies have shown that the breakdown voltage in both air and vacuum is influence by the presence of insulating surfaces. Once breakdown occur the discharge channel may either follow of the insulator or repelled from the surface. Hence, investigation is required to know whether the materials surface are either arc-phobic or not.

The flashover (electric breakdown) strength of a given system significantly depends on gap parameters, temperature, humidity, pressure, nature of applied voltage, surface condition of electrodes and atmospheric pollutants. Thus, the breakdown strength of a system is highly complex and it is a function of numerous interrelated variables and parameters.

Experiments have been conducted to investigate the flashover characteristic of rod-plane gaps of length 10 cm under lightning (1.2/50 μs) voltage impulses of both polarities. The impulses have been applied for an air gap and repeated with the insertion of Perspex and polyethylene rods of diameter 2 cm for the same gap. Photographs of the discharge channels were taken during the experiments. The photographic details revealed that for Perspex rod, in the case of positive polarity, the breakdown channels take paths away from the insulation surface in most of the cases while in negative polarity, the breakdown channel follow the surface. In the presence of the polyethylene rod, inverse results were observed. For 10 cm gaps, the insertion of Perspex and polyethylene rods has not change the 50% breakdown voltage. However, the insertion of Perspex rod has changed the time to breakdown at 95% confidence level while the presence of polyethylene rod does not make such significant change. Thus, information provides important insight to the degradation properties of materials under surface arcing.

Optical Properties of Photo-induced Metallic Structure in Terahertz Frequency Region

Takanori Okada
Pioneering Research Unit for Next Generation, Kyoto University, Japan

Abstract— Artificial periodic metal/semiconductor or dielectric structures, such as photonic crystals and metamaterials, have peculiar optical properties determined by their characteristic periodicities. In addition to such "static" structures, dynamic optical responses have also been achieved through photo-carrier injection or the application of a bias voltage in so-called active structures. The dynamic control of metamaterials has great potential for use in applications that involve time and space variation, for example, the active control of optical filters, optical switches, and waveguides. However, active metamaterials currently require time-consuming micro-fabrication processes, such as photolithography. Therefore, their spatial or temporal design has thus far been rigidly fixed and of limited flexibility. In this study we propose a photo-induced active structure and report on its optical characteristics in the terahertz frequency region. We created a periodical corrugation namely, the wire grating pattern on a semiconductor surface by illumination with a femtosecond laser in combination with a spatial light modulator. The surface optical properties of the structure were investigated by attenuated total reflection measurements. We also studied the spatial evolution of the photo-induced carrier layer by varying the power of the irradiation and using time-domain spectroscopy. A characteristic minimum due to the excitation of surface waves is observed in the attenuated total reflection spectrum. We confirm that the photo-induced structure at the surface of the semiconductors has metallic properties. This technique enables us to investigate the various shapes of the structures by changing the pumping intensity, timing, and patterns. This technique can be also used in the realization of ultrafast optical devices.

Indoor Positioning Based on IEEE 802.15.4a Standard Using Trilateration Technique and UWB Signal

Jirapat Sangthong[1], **Prakaidao Dokpikul**[2], **and Sathaporn Promwong**[2]

[1]Department of Electrical Engineering, Faculty of Engineering
King Mongkut's Institute of Technology Ladkrabang, Bangkok 10520, Thailand
[2]Department of Telecommunication Engineering, Faculty of Engineering
King Mongkut's Institute of Technology Ladkrabang, Bangkok 10520, Thailand

Abstract— Nowadays, The indoor positioning technology is becoming the essential applications such as such as emergency services, home-entertainment applications or smart home, equipments control in industrial, surgical navigation in the operating room and patient tracking in hospital and so on. There have been many position estimation techniques that can be proposed such as geometric technique, statistical technique, mapping technique and many others. These position estimation techniques is related on signal parameters: received signal strength (RSS), angle of arrival (AOA), time of arrival (TOA) and time difference of arrival (TDOA). Trilateration technique is the one technique of geometric technique. This technique can be estimate the target position by using the intersection of circle that can be obtained from a set of reference positions. For low-rate communication, the IEEE 802.154a standard is proposed. The IEEE 802.15.4a standard has two optional signaling formats that are IR-UWB and chirp spread spectrum (CSS). The IR-UWB is an optional ranging capability which has three optional bands: sub-gigahertz band uses frequencies ranging between 250–750 MHz, low band uses frequencies ranging between 3.244–4.742 GHz and high band uses frequencies ranging between 5.944–10.234 GHz; whereas the CSS can be used for communication purposes only which uses frequencies ranging between 2.4–2.4835 GHz. This paper studies on indoor positioning based on IEEE 802.15.4a standard in IR-UWB option. All of measurements using vector network analyzer (VNA) to measure the channel frequency transfer functions. The biconical antennas were used as both transmitter (Tx) antenna and receiver (Rx) antenna with vertical polarization. Trilateration technique will be use to estimate position related parameter RSS and TOA. Finally, the accuracy and precision of estimated distances are studied and shown in the terms of cumulative distribution function (CDF).

Session 2A1
Microwave/Terahertz Photonics Technologies and Their Applications

Design of Terahertz Quantum Cascade Lasers for High Temperature Operations Using Non-equilibrium Green's Function Method

Hiroaki Yasuda[1], **Tillmann Kubis**[2], **Iwao Hosako**[1], **and Kazuhiko Hirakawa**[3]

[1]National Institute of Information and Communications Technology, Japan
[2]Network for Computational Nanotechnology, Purdue University, USA
[3]Institute of Industrial Science and INQIE, University of Tokyo, Japan

Abstract— Remarkable progress on terahertz quantum cascade lasers (THz-QCLs) has been made since their first demonstration in 2002. However, operation temperatures of THz-QCLs tend to be limited by hf/k (h: the Planck constant, f: frequency, k: the Boltzmann constant). Room-temperature operation of THz-QCLs has not been realized yet. In this presentation, we clarified the degradation mechanisms for population inversion in THz-QCLs at high temperatures using the non-equilibrium Green's function (NEGF) method and proposed new THz-QCL schemes for further improvement.

First, we revealed with the NEGF calculations that one of the major degradation mechanisms is the thermally-activated longitudinal optical (LO) phonon scattering, where electrons in the upper lasing level acquire sufficient in-plane kinetic energy to emit LO phonons and relax to the lower lasing level in a non-radiative manner.

We investigated two candidates for reduction of the thermally-activated phonon scattering. First, we calculated performance of GaN-based THz-QCLs because the large LO phonon energy of 90 meV might suppress the thermally-activated phonon scattering at room temperatures. However, contrary to the expectations, the calculated gain was significantly low. This is due to subband broadenings caused by the large Frohlich interaction between electrons and LO phonons in GaN. The other candidate is the diagonal transition design of active regions. The thermally-activated phonon scattering depends on the overlap of the wavefunctions of the upper and lower lasing states, whereas the optical transition is proportional to the dipole moment, that is, the overlap of the lower lasing state, the position z, and the upper state. We found that the gain at high temperatures improved by optimizing the overlap of the wavefunctions.

Furthermore, we calculated performance of the novel scattering injection scheme THz-QCLs where electrons are injected to the upper lasing level by LO phonon scattering. The gain was larger than that of the conventional THz-QCLs. This is mainly because a larger number of electrons contribute to lasing in the scattering injection scheme. In contrast, a half of electrons contribute to lasing in the conventional THz-QCLs that use resonant tunneling for electron injections.

Using the achievements, we proposed a novel and simple two-well THz-QCL structure that has the scattering injection and diagonal transition schemes. The NEGF calculations showed that the gain at high temperatures improved and the thermally-activated phonon scattering was suppressed. Furthermore, we found that terahertz optical gain still exists below the threshold electric field and the peak frequency of the gain moves with the electric field. This would lead to a realization of wavelength-tunable THz-QCLs, which are not realized in the conventional THz-QCLs.

Optical Pulse Generation from Quantum Dot Optical Frequency Comb Laser

Naokatsu Yamamoto[1], **Kouichi Akahane**[1], **Tetsuya Kawanishi**[1], **Hideyuki Sotobayashi**[2], **Yuki Yoshioka**[3], **and Hiroshi Takai**[3]

[1]National Institute of Information and Communications Technology
4-2-1 Nukui-kita, Koganei, Tokyo 184-8795, Japan
[2]Aoyama Gakuin University, 5-10-1 Fuchinobe, Sagamihara, Kanagawa 229-8558, Japan
[3]Tokyo Denki University, 2-2 Nishiki, Kanda, Tokyo 101-8457, Japan

Abstract— Self assembled quantum dot (QD) structure has been investigated globally for developing attractive optical gain devices. We previously demonstrated a fine teeth optical frequency comb generation with a broadband wavelength tunability from a newly developed the quantum dot optical frequency comb laser (QD-CML). In this paper, we successful demonstrate a short optical pulse (< 15-ps) generation from the QD-CML with a GHz-order high-repetition and wavelength tunability. To fabricate the QD-CML operating in a 1.3-μm waveband, we also proposed a useful growth method of a sandwiched sub-nano separator (SSNS) growth technique. Using this technique, the high-density ($8.2\times1010/cm^2$) and high-quality InAs/InGaAs QD optical gain media operating in an over 1.3-μm wavelength are effectively obtained on a GaAs substrate. The QD-CML was fabricated using the multi-stacked InAs/InGaAs QD with SSNS technique on GaAs substrate. An external cavity laser system was constructed using the QD-CML and optical band-pass filters. The optical pulse generation with a 1.0-GHz high-repetition can be simply obtained, when the 1.0-GHz rf-voltage (approx. 18-dBm) was applied to the QD-CML. It is considered that the optical pulsation of the QD-CML is based on a hybrid mode-locking operation of a semiconductor laser. Therefore, we can obtain the synchronized optical short pulse with an external reference clock. In addition, it is confirmed that the optical pulse generation with a wide wavelength tuning range between 1263-nm and 1295-nm can be achieved from the QD-CML. From these experimental results, it is expected that the QD-CML will become an attractive photonic device for the optical frequency comb generation and the high-repetition and short optical pulse generation.

Mode-locked Yb-doped Fiber Ring-Laser for Use as a Pump Pulse Source of THz-TDS

J. Hamazaki, **N. Sekine**, **and I. Hosako**
National Institute of Information and Communications Technology, Japan

Abstract— Terahertz time-domain spectroscopy (THz-TDS) provides a powerful tool to examine optical properties of materials in 0.1–3 THz. Generally, photoconductive antennas (PCAs) based on LT-GaAs substrates are used as THz emitter and detector, and recently second harmonic generation (SHG) of Er-doped fiber lasers (EDFL) is used as a pump femto-second (fs) pulse, in place of Ti:Al_2O_3 laser pulse due to a lot of advantages of fiber lasers.

For efficient THz-TDS, using fundamental FL pulse is preferred as pump pulse, rather than its SHG pulse. This is because pulse energy decreases and pulse width becomes longer due to SHG process. However, optical energy of pump pulse is required to be higher than bandgap energy of the substrates of PCA. Note that, optical energy of EDFL and bandgap energy of GaAs are 0.8 and 1.5 eV, respectively. Therefore, pulsed fiber laser with higher optical energy and substrate of PCA with lower energy are required, for efficient THz-TDS.

Yb-doped fiber laser (YDFL) operates at wavelength of 1.0–1.1 μm. Its optical energy (1.0–1.1 eV) is about 1.5 times higher than that of EDFL. Moreover, high-intensity ultra short pulse oscillation is expected due to large gain and broad gain spectrum of YDF. Therefore, YDFL attracts much attention as a promising candidate for pump pulse sources of THz-TDS.

In this paper, we investigate ring-type mode-locked YDFL by nonlinear polarization rotation technique. In this cavity, various types of mode-locked pulses are observed, depending on cavity condition. Each type of mode-locked pulse was well characterized individually in various reports. However, detailed comparative study of these is not well investigated. We characterize various types of mode-locked pulses from our ring YDLF cavity and compare them, and also we mention suitable type for THz-TDS.

Terahertz Negative Dynamic Conductivity in Optically Pumped Graphene

A. Satou[1], **T. Otsuji**[1], **V. Ryzhii**[2], **and F. T. Vasko**[3]

[1]Research Institute of Electrical Communication, Tohoku University, Japan
[2]Computational Nanoelectronics Laboratory, University of Aizu, Japan
[3]Department of Electrical Engineering, University at Buffalo, USA

Abstract— Graphene has been investigated extensively for a variety of device applications. Recently, we have proposed a terahertz (THz) laser utilizing optically pumped graphene [1, 2]. Under (pulse or cw) optical pumping, photogenerated carriers experience the quasi-equilibration by carrier-carrier (CC) scattering and the energy relaxation and recombination by intraband and interband optical-phonon (OP) scattering, and the population inversion near the Dirac point, i.e., in THz region, can take place at sufficiently strong pumping. Then the amplification of THz wave and, hence, the lasing of THz wave can be achieved when the dynamic conductivity of graphene accounting for both the intraband (Drude) and interband contributions becomes negative.

As reported by several groups [3–5], at room temperature or strong pumping, the CC scattering quasi-equilibrates carriers before the energy relaxation/recombination by OP emission. However, an interplay between CC and OP mechanisms has still been unclear (e.g., for the case of the transient saturation of absorption [6, 7]), and it is crucial to reveal the effect of the CC scattering quantitatively for the realization of the graphene-based THz laser.

In this paper, we theoretically study the carrier relaxation dynamics in graphene under pulse excitation in two limiting cases: (1) where the CC scattering always quasi-equilibrates carriers and (2) where the energy relaxation by intraband OP emission is dominant. In the latter case, we assume that carriers are quasi-equilibrated after all the possible intraband OP emission finishes. We develop rate equations for the quasi-Fermi level and carrier temperature and calculate their time evolution. From these quantities the dynamic conductivity are calculated. As a result, it has been shown that much lower pulse intensity is necessary in the case (2) to achieve the population inversion; e.g., the population inversion at $\varepsilon = 5\,\mathrm{meV}$, corresponding to the stimulated emission of photons at 2.43 THz, is achieved at $I_{pump} \sim 2 \times 10^7\,\mathrm{W/cm^2}$ and at $2 \times 10^6\,\mathrm{W/cm^2}$ in the cases (1) and (2), respectively. This demonstrates that the population inversion is degraded by the effect of the CC scattering.

We also investigate the effect of the CC scattering by developing the collision integral for the CC scattering with the unscreened Coulomb potential. We reveal that the quasi-equilibration takes place during the time scale of 10–100 fs, and that the effect of the CC scattering on the population inversion can be reduced by the dielectric screening if employing high-k dielectric layer and/or substrate.

REFERENCES

1. Ryzhii, V., M. Ryzhii, and T. Otsuji, *J. Appl. Phys.*, Vol. 101, 083114, 2007.
2. Ryzhii, V., et al., *J. Appl. Phys.*, Vol. 106, 084507, 2009.
3. Dawlaty, J. M., et al., *Appl. Phys. Lett.*, Vol. 92, 042116, 2008.
4. Sun, D., et al., *Phys. Rev. Lett.*, Vol. 101, 157402, 2008.
5. Breusing, M., C. Ropers, and T. Elsaesser, *Phys. Rev. Lett.*, Vol. 102, 086809, 2009.
6. Bonaccorso, F., Z. Sun, T. Hasan, and A. C. Ferrari, *Nature Photonics*, Vol. 4, 611, 2010.
7. Vasko, F. T., *Phys. Rev. B*, Vol. 82, 245422, 2010.

Electromagnetic Beam Steering Based on Nonreciprocal Metamaterials

Tetsuya Ueda and Yuichi Kado
Department of Electronics, Kyoto Institute of Technology
Matsugasaki, Sakyo-ku, Kyoto 606-8585, Japan

Abstract— Nonreciprocal phase-shift metamaterials are reviewed. The artificial structures can support electromagnetic wave propagation with positive refractive index in a propagation direction whereas they also provide negative refractive index in the anti-parallel direction at the same frequency. The interesting propagation characteristics are expressed in terms of the equivalent circuit model. It is a ladder network including transmission line sections and is periodically loaded with series capacitance and shunt inductance in order to achieve negative permeability and negative permittivity, respectively. The nonreciprocal transmission characteristics are achieved by using gyrotropic materials, such as magnetized ferrite in microwave region. A new type of traveling-wave resonator can be constructed by using the nonreciprocal phase-shift metamaterials. The resonant condition automatically holds independently of the resonator's size, but is determined by configuration parameters of the unit cell. The field profiles have a uniform magnitude distribution and linearly-varying phase distribution along the resonator. The phase gradient of the resonator can be controlled by the nonreciprocal phase characteristics of the transmission lines. The traveling-wave resonator can be implemented into beam steering antennas. The beam angle is determined by the gradient of the phase distribution on the resonator. When the soft magnetic medium is employed as the ferrite, the nonreciprocal phase gradient of the resonator as well as the beam direction of the antenna can be varied with an externally applied dc magnetic field to the ferrite. The antenna directivity and gain can be enhanced by making the size of the resonator larger.

REFERENCES

1. Ueda, T., K. Horikawa, M. Akiyama, and M. Tsutsumi, *IEEE Trans. on Antennas Propag.*, Vol. 57, No. 7, 1995–2005, July 2009.
2. Kishimoto, H., T. Ueda, and Y. Kado, *IEEE Trans. on Mag.*, Vol. 47, No. 10, 3724–3727, October 2011.
3. Ueda, T. and H. Kishimoto, *2010 IEEE MTT-S Int. Microw. Symp. Dig.*, 41–44, May 2010.
4. Ueda, T., S. Yamamoto, and Y. Kado, *2011 IEEE Int. Symp. Antennas Propag. Proc.*, 1058–1061, July 2011.

Millimeter-wave Generation and Modulation Techniques Based on Photonics for Wired and Wireless Convergence

Tadao Nagatsuma[1], **Daisuke Asa**[1], **Naoto Yoshimoto**[2], **and Katsumi Iwatsuki**[3]

[1]Graduate School of Engineering Science, Osaka University
1-3 Machikaneyama, Toyonaka, Osaka 560-8531, Japan
[2]NTT Access Network Service Systems Laboratories, NTT Corporation, Japan
[3]NTT Service Integration Laboratories, NTT Corporation, Japan

Abstract— Recently, there has been an increasing research and development towards convergence of broadband wired (fiber-optic) and wireless communications particularly in access network systems. A radio-on-fiber (RoF) technique, where radio-frequency (RF) signals are controlled in the optical domain and delivered through optical fibers, plays a key role for generation, modulation and distribution of broadband signals. In this paper, we propose a novel system concept of wired and wireless convergence to enable us to employ common components for wired and wireless systems, and show some results on proof-of-concept experiments in the W-band (75–110 GHz).

RoF-DAS over WDM-PON Using Bandpass-sampling and Optical TDM Techniques as Universal Entrance Network for Broadband Wireless Access

Katsutoshi Tsukamoto[1], **Tatsuhiko Iwakuni**[1], **Kenji Miyamoto**[1], **Takeshi Higashino**[1], **Shozo Komaki**[1], **Takayoshi Tashiro**[2], **Youichi Fukada**[2], **Jun-Ichi Kani**[2], **Naoto Yoshimoto**[2], **and Katsumi Iwatsuki**[3]

[1]Graduate School of Engineering, Osaka University, Japan
[2]NTT Access Network Service Systems Laboratories, Japan
[3]NTT Service Integration Laboratories, Japan

Abstract— Under the situation of mobile traffic explosion, air interfaces of mobile services are rapidly improved and new ones are being provided in new radio frequency bands. Also in order to effectively use frequency or network resources and avoid their bottleneck, the use of femto-cell or pico-cell architectures have been started. Backhaul networks accommodating a huge number of these pico- and femto-cell stations become more important issue. Broadband fixed access networks like FTTH systems will play a important roll as a entrance network for broadband wireless access. Radio on Fiber (RoF) technologies are able to transparently transmit various types of radio services, and its operation on the entrance network realize an effective universal platform for newly coming air interfaces. RoF-DAS over WDM-PON using bandpass-sampling and optical TDM techniques has been proposed as a universal entrance network for broadband wireless access. This paper introduces its proposed architecture and reports the latest results of experimental investigation of RoF transmission performance.

Toward 100 G High-speed Wireless Communication by Coherent RoF Technique

Atsushi Kanno[1], **Toshiaki Kuri**[1], **Iwao Hosako**[1], **Tetsuya Kawanishi**[1], **Yuki Yoshida**[2], **Yoshihiro Yasumura**[2], **and Ken-ichi Kitayama**[2]

[1]National Institute of Information and Communications Technology
4–2–1 Nukui-kitamachi, Koganei, Tokyo 184–8795, Japan
[2]Graduate School of Engineering, Osaka University, 2–1 Yamadagaoka, Suita, Osaka 565–0871, Japan

Abstract— To meet various requirements for enhancement of the quality of life and economic activity, defeat of energy consumption issue and realization of link robustness against critical disasters, access network infrastructure should be evolved to be dynamic and adaptive, so that it can provide a seamless connection of wired and wireless signals over a physical layer.

We have presented the concept of coherent wired/wireless seamless network, where optical digital coherent baseband systems and the radio-over-fiber (RoF) systems coexist. Key techniques in the concept are digitally-supported optical baseband modulation and demodulation, and RoF signal generation by the direct photonic up-conversion. The RoF signals generated by the technique will be simultaneously received with optical coherent receiver and digital wireless receiver.

In this paper, we report a W-band high-speed wireless transmission using RoF and digital signal processing techniques on the proposed system. Transmission over the air with the data rates greater than 20 Gb/s were successfully demonstrated at the center frequency of around 90 GHz. Direct photonic up-conversion technique using high-speed photomixer and digitally coherent detection with analogue heterodyning technique will provide high-speed wireless transmission.

Development of Heterogeneous Radio Access Network Using Radio on Fiber and Its Field Trial

T. Higashino, **S. Okumura**, **K. Hayasaka**, **K. Tsukamoto**, **and S. Komaki**
Division of Electric, Electronic and Information Engineering
Graduate School of Engineering, Osaka University, Japan

Abstract— As for nationwide progressing the digital terrestrial broadcasting and high-speed Internet such as the Fiber-To-The-Home (FTTH) with the optical fiber network and the Common Antenna Television (CATV) network. Recently, the equipment of the broadcasting and communication infrastructure is spread in Japan. Meanwhile, various radio services like the one segment broadcasting, and a high-speed mobile communication are provided in the urban area. Especially in mobile Internet access service for the smart phone and tablet terminal, wireless traffic is growing rapidly which is over the tethering to the WWAN and WMAN such as 3G cellular and WiMAX. The traffic demand will be increased next few years. Thus, traffic management will be important role of taking traffic load off the congested network. As for the cellular system, a lot of radio base stations are installed with overlapping in order to make a huge coverage area. Plural network-operator independently provides and maintains radio services and its access network with compete against each other. In other case, a network-operator provides and maintains plural radio services. Behind this background, heterogeneous radio network and its control technique is required in order to the traffic management and vertical handover. To construct heterogeneous radio network, the Radio on Fiber (RoF) technologies originally proposed to establish a radio access link that can make convergence of the various kind of radio access and radio broadcasting. In urban area, radio repeaters for dead zone and the Gap filler for the Digital Terrestrial Television (DTTV) are installed in building. On the other hand, the mountainous area and isolated islands, where the equipment of the broadcasting and communication infrastructure is few than urban area despite there are much people who wants to access to the Internet. The rural area have a serious problem so called "digital divide". The ICT strategy in Japan can treats to solve these digital divides. It is preferable for such a digital divide region to install the general-purpose network infrastructure that doesn't depend on the waveform formats of radio service. This paper describes on application of RoF technology, for the digital divide solution. We have been developed heterogeneous radio access network utilizing RoF and conducted field trial under the experimental bureau. The radiation inspection have been done in the mountainous area at the Nosegawa village in Nara prefecture, Japan aiming evaluating the correspondence with the link budget design. The RoF transmission of multiple radio services and result of the field trial is reported.

Next Generation Free-space Optical System by System Design Optimization and Performance Enhancement

Mitsuji Matsumoto
GITS/GITI, Waseda University, Japan

Abstract— Free-Space Optical (FSO) communication has been receiving considerable attention recently to provide broadband communications due to its remarkable advantages including flexibility, easy-to-install, and license-free. Conventional FSO systems operate at 800 nm wavelength band, and need to use O/E and E/O conversions before emitting/coupling optical signals from/into an optical fiber. They have been used for data transmission, but due to power and bandwidth limitation of optical devices in this wavelength band, they are not possible to operate above 2.5 Gbps. The use of 0.8 m wavelength optical devices also makes those FSO systems incompatible with current high capacity optical fiber systems. Because of this, it is not being considered as a suitable and practical solution for very high-speed communications, such as terrestrial WDM optical networks.

ext generation FSO technology has been developed in order to overcome the limitations of conventional FSO systems. Unlike conventional FSO systems, in the next generation FSO systems the necessity of converting signal from electrical to optical and vice versa before transmitting or receiving through free-space is eliminated. In this configuration, the signal is emitted directly to the free-space from the fiber termination point and at the receiving end focused directly into the fiber core. Therefore, a protocol and data rate transparent FSO link is achieved. The seamless interconnection of standard single mode fiber (SMF) and FSO links, whereby an optical signal is coupled from one media to another without any optical-electrical conversions, creates an opportunity for cost savings and other remarkable merits. However, in these systems, the impact of phase fluctuations is particularly severe due to the use of direct coupling the received signal into a fiber cable at the receiver. The systems thus need specially designed terminals and precisely coupling techniques. In practical communication systems, various techniques have been developed and applied to mitigate atmospheric effects such as adaptive optics (AO), use of large receive apertures (aperture averaging), diversity techniques and fast tracking antennas.

To improve performance of a next-generation FSO system under effects of strong atmospheric turbulence or long transmission ranges, in this paper we introduce a spatial diversity scheme in which many receivers are used to receive the signal. In this scheme, the incoming optical signal is collected by multiple receiving apertures, optically combined, amplified by an optical pre-amplifier and finally detected by a photo-detector. This helps to reduce the receiver complexity, system cost and noises. We mathematically model and numerically evaluate the performance of the proposed system. Based on the model, optimal values of system parameters such as receiving aperture size, pre-amplifier gain, transmitting power are derived for different operation conditions and requirements. Furthermore, to compare more accurately the performance of systems employing different numbers of receivers, we introduce a new analysis considering the impact of receiving aperture size on both signal fading and received power. Numerical results demonstrate that the system performance can be significantly improved when multiple receiver apertures are employed, especially under strong atmospheric turbulence conditions. The use of reception diversity also helps to lessen each aperture size and pre-amplifier gain.

λ-tunable WDM/TDM-PON Using DWBA towards Flexible Next-generation Optical Access Networks

Hirotaka Nakamura
NTT Access Network Service Systems Laboratories, NTT Corporation, Japan

Abstract— Broadband optical access systems based on passive optical network (PON) are rapidly being installed in the world. Gigabit Ethernet-PON(GE-PON) system has been first commercially installed in Japan in 2004 and the number of subscribers of FTTH was over 20 million in March, 2011. 10-Gbit/s-class PON systems, namely 10G-EPON and XG-PON, have been standardized in IEEE in 2009 and ITU-T in 2010, respectively. Requirements of next-generation-PON2(NG-PON2) over 40 Gbit/s as post 10-Gbit/s-class PON are being now discussed. This paper introduces its requirements from the telecom operator's viewpoint and proposes the best technological solution for the next-generation optical access networks.

In the next-generation optical access networks, the flexibility of the bandwidth assignment to the user and the migration from the existing system is needed in addition to the cost effectiveness and the high capacity. This paper proposes the λ-tunable wavelength-division-multiplexing/time-division-multiplexing-PON (WDM/TDM-PON) using dynamic wavelength and bandwidth assignment/allocation (DWBA). The WDM technology can incrementally and cost-effectively upgrade the total bandwidth by adding the wavelength, because devices used in the 40-Gbit/s-class TDM-PON is too expensive. This incremental upgradability can realize the smooth migration from the existing system. Moreover, the wavelength tunablity in the OLT and ONU realizes to change their sending and receiving wavelengths dynamically according to the utilization of the wavelength, so the bandwidth which the user demands can efficiently be allocated. This paper reports results of the transmission experiment that uses 10-Gbit/s-class burst-mode receivers, fast-switching tunable laser diode and fast-switching tunable filters to emulate the proposed system and DWBA operation.

Session 2A2
Laser-induced Periodic Surface Nanostructures: Fundamental Fabrication Mechanisms, Nanoscale-dominated Physical and Chemical Properties 1

New Regimes of Sub- and Near-threshold Femtosecond Laser Nanostructuring of Solids

Sergey Kudryashov[1], **Eugene Golosov**[2], **Ol'ga Golosova**[2], **Andrey Ionin**[1], **Yuriy Kolobov**[2], **Alexander Ligachev**[3], **Sergey Makarov**[1], **Leonid Seleznev**[1], **and Dmitry Sinitsyn**[1]

[1]P. N. Lebedev Physical Institute, Russian Academy of Sciences
Leninskiy Prospect 53, Moscow 119991, Russia
[2]Belgorod State University, Victory Prospect 1, Belgorod 308015, Russia
[3]General Physics Institute, Russian Academy of Sciences, Vavilova str. 38, Moscow 119991, Russia

Abstract— Two new regimes of sub- and near-threshold 744-nm femtosecond laser nanostructuring of solids were revealed.

In the first regime, superimposed one-dimensional periodic gratings with multiple sub-wavelength periods (down to 80 nm) and trench orientations perpendicular to the linear polarization of the laser pulses were fabricated in ambient air after multiple near-threshold laser shots on different solid surfaces. The broad range of the grating periods corresponds to the large number of spatial Fourier harmonics of the final nanorelief, representing the non-sinusoidal profile of the laser-induced intermediate surface relief (the set of periodical, broadly spaced narrow nanotrenches), which provides the corresponding multi-angle diffraction of the incident femtosecond laser pulses. Experimental measurements and modeling of the transient optical constants of the photo-excited materials justify the excitation, at the first stage, of the near-wavelength surface plasmon-polaritonic (SPP) wave on the photo-excited initial planar surface. Such SPP wave provides the intermediate nanorelief in the form of the non-sinusoidal surface grating via its interference with the incident laser wave, resulting under the near-threshold irradiation conditions in the highly-localized surface ablation of the material in the interference maxima. During the next stage, the multi-period sub-wavelength nanogratings are developing through the multi-angle diffraction of the multiple incident laser pulses on the intermediate non-sinusoidal surface grating.

In the second (sub-threshold) regime, the topology of the near-wavelength SPP-laser interference gratings is found to be periodically modulated along their ridges with even shorter period about 200 nm, through incomplete nanoscale spallation of the material becoming molten in the interference maxima stripes.

Formation Dynamics of Ultrafast Laser-induced Periodic-surface Structure

J. P. Colombier[1, 2], **F. Garrelie**[1, 2], **R. Stoian**[1, 2], **M. Bounhalli**[1, 2], **S. Reynaud**[1, 2], **N. Faure**[1, 2], **E. Audouard**[1, 2], **and F. Pigeon**[1, 2]

[1]Laboratoire Hubert Curien (UMR 5516 CNRS), Université de Lyon, France
[2]Université de Saint-Etienne, 42000 Saint Étienne, France

Abstract— Ultrafast laser radiation has a strong potential for surface structuring on ultimate scales due to a strongly localized character of energy deposition. Depending on laser parameters and material properties, these self-formed structures develop with varying periodicities and amplitudes. We propose here a study concerning the effects of surface plasmon coupling and electron-phonon relaxation on laser-induced periodic surface structure (LIPSS) formation. Plasmonic effects are identified as a key parameter for ultrafast laser energy coupling and explanation of LIPSS orientation with laser polarization. A set of gratings with different periods has been exploited to investigate the correlation between ripples formation under ultrashort laser exposure and surface plasmon generation conditions. For TM irradiation conditions and a well-defined period of grating, ripples formation occurs [1]. Apart from the comprehension effort related to laser excitation mechanisms, the objective is to design user-defined nanostructuration with predictable properties for a wide range of metals by taking advantage of their behavior under nonequilibrium conditions. In this context, we have generated LIPSS on various materials with different electronic configuration in order to investigate the influence of the electron-phonon coupling strength and the effective thermal diffusion length on the specific contrast of LIPSS. Representative metals (transition, noble) with a large range of coupling strengths were exposed to ultrafast laser excitation and the patterning surface was investigated ex-situ by atomic force microscopy and scanning electron microscopy. It appears that the LIPSS contrast is correlated to the constant of electron-phonon coupling determining the initial energy redistribution, and to the amount of material experiencing solid-to-liquid transitions. Time history of ripples formation and growth is discussed in this context of transient phase transition using an hydrodynamic approach.

REFERENCES

1. Garrelie, F., J. P. Colombier, F. Pigeon, S. Tonchev, N. Faure, M. Bounhalli, S. Reynaud, and O. Parriaux, "Evidence of surface plasmon resonance in ultrafast laser-induced ripples," *Optics Express*, Vol. 19, No. 10, 9035, 2011.

Femtosecond Laser-induced Subwavelength Ripples on Various Materials (Al, Si, CaF_2 and CR-39)

Wolfgang Husinsky[1], **Shazia Bashir**[1, 2], **and M. Shahid Rafique**[1, 3]

[1]Institute for Applied Physics, Vienna University of Technology, A-1040 Vienna, Austria
[2]Centre for Advanced Studies in Physics, GC University Lahore, Pakistan
[3]Department of Physics, University of Engineering and Technology Lahore, Pakistan

Abstract— The formation of self-organized sub-wavelength ripples on Al, Si, CaF_2, and CR-39 induced by 25 fs laser pulses at central wavelength of 800 nm has been observed under certain experimental conditions. In case of Al sub wavelength gratings with periodicities ranging from 20 nm to 220 nm are reported. For CaF_2 the periodicity goes up to 625 nm. In case of Si, nano-gratings have the periodicity of 10 nm to 100 nm. The interspacing of these gratings is 60 nm in case of CR-39. These features, which are significantly shorter than the incident laser wavelength, are observed for an irradiation fluence slightly higher than the ablation threshold, regardless of the target material. In addition to these nano-ripples, classical or micro ripples with an average spacing of 1–2 µm have also been observed on irradiated surfaces of Al and Si. These micro ripples typically appear at fluences higher than that those required for nano-ripple formation. It has been found that the formation of the laser-induced ripples is strongly dependent and quite sensitive on the incident laser fluence and the material itself.

The results will be correlated and put into perspective with investigations of other processes characteristic for fs-laser irradiation of the materials, as, i.e., particle emission. This allows a much better understanding of the processes involved.

Femtosecond-laser-induced Nanostructuring on Si Surface through the Excitation of Surface Plasmon Polaritons

Kenzo Miyazaki and Godai Miyaji
Institute of Advanced Energy, Kyoto University, Japan

Abstract— We report an experimental study of femtosecond (fs)-laser-induced periodic nanostructure formation on Si surface, where the growth mechanism of nanostructures can be explained well with the model based on the excitation of surface plasmon polaritons (SPPs) [1, 2].

Linearly polarized, 800 nm, 100 fs laser pulses were focused on Si surface immersed in water at fluence F smaller than the single-pulse ablation threshold, where the focal spot size on the target was 200 μm in radius. The morphological change of surface was carefully observed as a function of F and the superimposed shot number N at a repetition rate of 10 Hz.

We have observed that two kinds of periodic nanostructures are formed on the surface: one is fine with the period of $d \sim 150$ nm, and the other is coarse with $d \sim 400$ nm. The fine structure was formed in a range of $F = 60$–$70\,\mathrm{mJ/cm^2}$, being preceded by the coarse structure formation with increasing N. The observed period sizes in fine and coarse structures were almost constant for different F and N under the present conditions.

The results have demonstrated that the coarse structure or the surface corrugation is crucial for the formation of the fine structure, and then the nanostructuring can be illustrated well by using a model target that consists of the upper amorphous Si (a-Si) layer and the lower Si substrate. The nanostructures with the coarse and fine periods can be formed by the excitation of SPPs at the corrugated interface A between water and the thin a-Si layer and the interface B between the a-Si and Si, respectively. The calculated periods of near-field at the interfaces A and B are in good agreement with those observed.

REFERENCES

1. Miyaji, G. and K. Miyazaki, *Appl. Phys. Lett.*, Vol. 91, 123102, 2007.
2. Miyaji, G. and K. Miyazaki, *Opt. Express*, Vol. 16, 16265, 2008.

The Role of Anisotropic Excitation in Self-organized Nanostructure Formation upon Femtosecond Laser Ablation

O. Varlamova[1, 2], **S. Varlamov**[3], **M. Bestehorn**[3], **and J. Reif**[1, 2]

[1]Exp. Physics II/Materials Science, BTU Cottbus, Cottbus, Germany
[2]Cottbus JointLab, Cottbus, Germany
[3]Statistical Physics and Nonlinear Dynamics, BTU Cottbus, Cottbus, Germany

Abstract— Surface pattering upon multi-pulse femtosecond laser ablation (formation of ripples, LIPSS) is attributed to nonlinear self-organized structure formation from laser-induced surface instability. However, this model does, so far, not account for an experimentally observed strong influence of the laser polarization on the nanostructure features. On the other hand, this influence is very surprising that the laser electric field is already off when the initial electronic excitation is transferred to the target lattice and transformed into particle emission (ablation) and subsequent structure formation.

In this work, we present an adopted surface erosion theory for the ablation dynamics. Exploiting the similarity to ion-beam sputtering, we extend a corresponding model for laser ablation by including the influence of laser polarization. This provides an accordant dependence of coefficients in a nonlinear equation of the Kuramoto-Sivashinsky type. We show that the directional anisotropy in the pattern formation may result from a spatial anisotropy of the initial excitation process, such as the presence of directional surface plasmons/polaritons [1] or even an anisotropic collision probability of excited electrons.

We present, then, numerical simulations of the (ablated) surface morphology for different values of the incident angle and polarization of the laser beam and compare those to experimental results for similar conditions.

The numerical results are in a good agreement with our experimental data. The theoretical model further predicts the time evolution of the surface morphology and some new features of nanopatterns that can be checked experimentally.

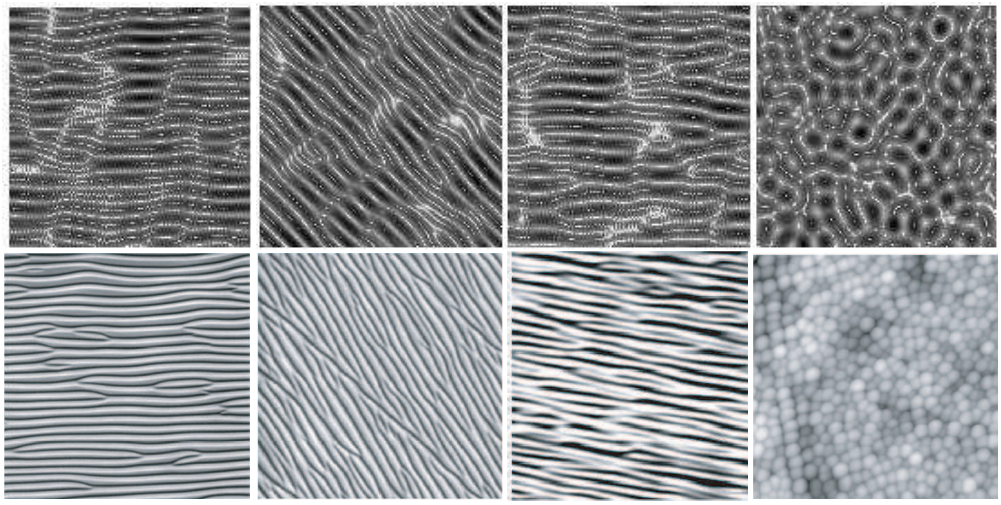

Figure 1: Numerical (upper row) and experimental (lower row) surface patterns for different laser polarization: linear horizontal (left column), linear 45° (second column), elliptical (third column), circular (right column).

REFERENCES

1. Miyaji, G. and K. Miyazaki, "Origin of periodicity in nanostructuring of thin film surfaces ablated with femtosecond laser pulses," *Opt. Express*, Vol. 16, 16265–16271, 2008.

Femtosecond Laser Ablation from Silicon and Ripples Formation: Evolution of Surface Excitation

Mourad Bounhalli[1,3], **Marco Muth**[1], **Olga Varlamova**[1,2], **and Juergen Reif**[1,2]

[1]Brandenburg Technical University BTU Cottbus, Universitätsplatz 1, 03046 Cottbus, Germany
[2]JointLab Cottbus, Cottbus, Germany
[3]Laboratoire Hubert Curien, Université Jean Monnet, St. Etienne, France

Abstract— We report on pump-probe experiments to study the time evolution of surface excitation during femtosecond laser ablation from silicon and its influence on self-organized ripples formation.

When measuring the ablation yield by monitoring the Si^+-ion signal in a Time-of-Flight spectrometer, we find that in addition to the coherence peak at complete overlap of pump and probe pulse a strong revival of ablation efficiency occurs for pump-probe delays of several picoseconds (Fig. 1), similar to previous observation on dielectrics [1], but significantly stronger, reaching almost the zero-delay yield. Subsequently, we investigated in detail the correlation between this revival and the self-organized nanostructure formation (ripples) at the irradiated spot. For this purpose, we irradiated a series of spots ($\varnothing \approx 100\,\mu m$) on Si(100) by 50 pulse-pairs of $3.5\,TW/cm^2$ each, with a series of delays between the two pulses ranging from a few 100 fs to about 100 ps.

As can be seen from the exemplary SEM pictures in Fig. 2, the affected area of the delayed pulse pairs is smaller than for zero delay, slightly decreasing with increasing delay. More significant, however, is the apparent change of surface morphology: while at zero delay the spot seems to follow the beam profile and the pattern exhibits the well known features of fine ripples at the edge and increasingly more complex structures towards the center (Fig. 2(a)), already at a moderate delay of four picoseconds (cf. the rise of the revival in Fig. 1) the morphology at the spot center is completely different (Fig. 2(b)): it is not simply depressed but even can rise *above* the pristine sur-face level (cf. left panels in Fig. 3). At longer delay between the pulses (Figs. 2(c), (d)), the spot center appears almost unaffected, though slightly below the pristine level. Only fine ripples are seen in this area, similar to the low intensity structures at the spot edge for zero delay. Around this "eye", however, the surface modulation is extremely strong, with amplitude of more than one m, oscillating around the original surface level (middle and right rows of Fig. 3).

A combination of all observations leads us to suggest the following scenario: The excitation of the surface produced by the pump pulse reproduces the Gaussian beam profile and is strongest at the center. Assuming a certain build-up time for the structure formation after energy input [2, 3], the weaker excitation in the annulus around the central "eye" has already relaxed and formed ripples when the probe pulse arrives. In the central region of the spot, however, the relaxation is not yet completed, and the second pulse interacts with still "soft" matter. While, there, the total excitation becomes weaker with increasing delay, the coupling in the annulus becomes stronger and stronger with increasing surface modulation. Thus, the increase in total ablation yield should be mainly the result of this annular "rough" surface.

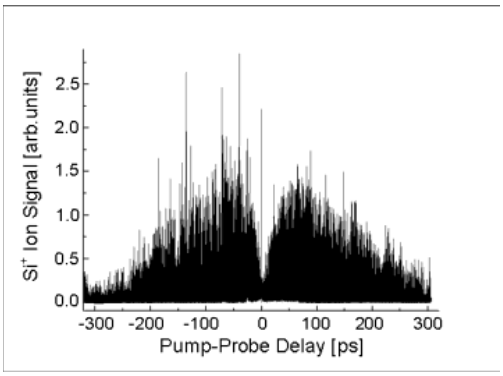

Figure 1: Pump-probe femtosecond laser ablation from Silicon: Ablated Si^+ ion yield vs. p-p delay.

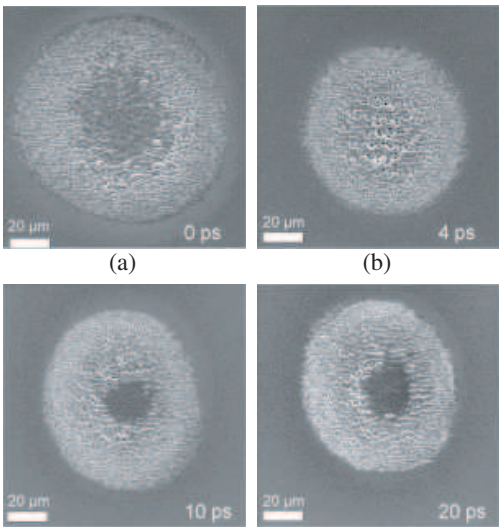

Figure 2: Surface patterns for selected p-p delays (SEM).

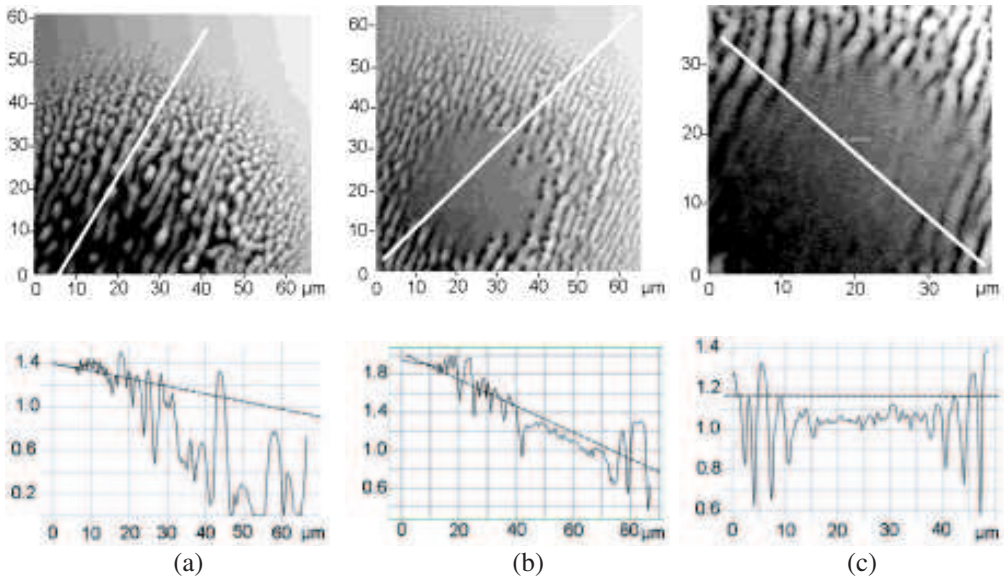

Figure 3: AFM analysis of ablation patterns for three different p-p delays (a) 4 ps; (b) 10 ps; (c) 20 ps; the dashed line in the lower panels indicates the pristine Si surface).

REFERENCES

1. Reif, J., F. Costache, and S. Eckert, "The role of energy and phase relaxation (T_1 and T_2) in ultrafast laser ablation," *J. Phys.: Conf. Series*, Vol. 59, 1–4, 2007.
2. Reif, J., O. Varlamova, M. Bounhalli, Tz. Arguirov, M. Schade, and H. S. Leipner, "Long-time feedback in self-organized nanostructures formation upon multi-pulse femtosecond laser ablation," *Proc SPIE*, Vol. 7586, 75860H, 2010.
3. Reif, J., O. Varlamova, M. Ratzke, M. Schade, and H. S. Leipner, Tz. Arguirov, "Multipulse feedback in self-organized ripples formation upon femtosecond laser ablation from silicon," *Appl. Phys. A*, Vol. 101, 361–365, 2010.

Selected Studies of Laser-induced Periodic Surface Structures on Synthetic Single-crystal Diamond

J. A. Z. Brawley-Hayes[1], **E. M. Hsu**[1], **and H. K. Haugen**[1, 2]

[1]Department of Engineering Physics, McMaster University, Canada
[2]Department of Physics and Astronomy, McMaster University, Canada

Abstract— In this presentation we will discuss studies of the formation of periodic structures on the surfaces of synthetic single-crystal diamond.

Experiments are conducted using a femtosecond Ti:sapphire laser typically operating at a central wavelength of 800 nm and at a 1 kHz repetition rate. Ancillary equipment, including an optical parametric amplifier, facilitates nonlinear optical conversion of the laser pulses. Sample irradiation is typically performed under rough vacuum conditions. Analysis of the samples is conducted using scanning electron microscopy, high-resolution optical microscopy, atomic force microscopy, and combined focused ion beam and transmission electron microscopy (FIB/TEM) techniques.

We will first briefly present selected highlights of earlier studies on the formation of laser-induced ripples in our laboratory, in particular on indium phosphide and gallium phosphide as well as from our first experiments on synthetic single-crystal diamond. In particular, the utilization of FIB/TEM techniques, facilitating cross sectional studies on the laser-induced ripples, will be highlighted. This offers complementary information to that obtained through other approaches. In particular, analysis of the crystalline nature of the final state of the target in conjunction with the morphology of the ripples in cross section can provide unique insights into the mechanisms of their formation.

Our recent studies on single crystal diamond have been directed to exploring a broader range of parameters including the laser wavelength and the angle of incidence. Experiments involving the removal of substantial amounts of material have led to very fine structuring of the diamond surfaces, down to periodicities ~ 60 nm.

We would like to thank the Natural Sciences and Engineering Research Council of Canada (NSERC) for financial support. The technical support of the Brockhouse Institute for Materials Research (BIMR) and the Canadian Centre for Electron Microscopy (CCEM) is gratefully acknowledged. Several students and collaborators have made contributions to the work discussed in this presentation, including the earlier work which is highlighted briefly. In particular,we would note the efforts of Andrzej Borowiec, Martin Couillard, Nick Mailman, Mariana Budiman, and Professor Gianluigi Botton.

Selected Studies of Laser-induced Periodic Surface Structures on Silicon

E. M. Hsu[1], **B. Liu**[1], **A. P. Knights**[1], **and H. K. Haugen**[1, 2]

[1]Department of Engineering Physics, McMaster University, Hamilton, Ontario, Canada
[2]Department of Physics and Astronomy, McMaster University, Canada

Abstract— In this presentation we will discuss studies of the formation of periodic structures on silicon surfaces.

Experiments are conducted using a femtosecond Ti:sapphire laser typically operating at a central wavelength of 800 nm and at a 1 kHz repetition rate. Ancillary equipment, including an optical parametric amplifier, facilitate nonlinear optical conversion of the laser pulses. Sample irradiation is typically performed under rough vacuum conditions. Analysis of the samples is conducted using scanning electron microscopy, high-resolution optical microscopy, atomic force microscopy, and combined focused ion beam and transmission electron microscopy (FIB/TEM) techniques.

We will review briefly our previous results on ripple formation on silicon in the nominal transparency wavelength regime where a variety of morphologies has been observed. More recently, we have undertaken a range of studies of femtosecond laser interactions with silicon, including incubation mechanisms, ablation of SiO_2/Si samples, threshold properties of ion-implanted samples, and light absorption properties of silicon which has been both laser processed and ion-implanted. In parallel with these efforts, new experiments on ripples have been undertaken. Our recent studies have concentrated on investigations of ripple formation on silicon and SiO_2/Si at wavelengths of 800 nm and 400 nm. In addition, a series of experiments is being undertaken on silicon in the temperature range from room temperature to 600°C. Following the current survey of ripple formation on these materials, we plan to conduct selected FIB/TEM based investigations on the samples.

We would like to thank the Natural Sciences and Engineering Research Council of Canada (NSERC) for financial support. The technical support of the Brockhouse Institute for Materials Research (BIMR) and the Canadian Centre for Electron Microscopy (CCEM) is gratefully acknowledged. Several students and collaborators have made contributions to the work discussed in this presentation, including the earlier work which is highlighted briefly. In particular, we would note the efforts of Travis Crawford, Andrew Walker, Nikola Maric, Tara Power, and Professor Gianluigi Botton.

Fabricating Nanostructured TiO_2 by Femtosecond Laser Irradiating Titanium

Eric Mazur[1], **Katherine C. Phillips**[1], **Elizabeth C. Landis**[2], **and Cynthia M. Friend**[1, 2]

[1]School of Engineering and Applied Sciences, Harvard University
9 Oxford Street, Cambridge, Massachusetts 02138, USA
[2]Department of Chemistry, Harvard University
12 Oxford Street, Cambridge, Massachusetts 02138, USA

Abstract— Femtosecond laser pulses provide a precise and clean way to form nanoscale surface structures on many materials including titanium.Laser structuring of titanium surfaces has been investigated for a variety of applications, including biocompatibility and solar energy harvesting.We use femtosecond laser irradiation of titanium to create nanometer scale laser-induced periodic surface structures and study the influence of atmospheric composition on these surface structures. Altering the gas composition and pressure does not change the surface morphology, but it does impact the chemical composition of the surface. We demonstrate that irradiation of titanium in oxygen containing atmospheres forms a highly stable surface layer of nanostructured amorphous titanium dioxide(TiO_2).We find that the resultingsurface structures do not depend on gas chemical composition and pressure, which is in contrast to earlier work using nanosecond pulses.

In addition, we present a novel method for femtosecond-laser doping of TiO_2 for above bandgap absorptance by irradiating titanium metal in the presence of oxygen and dopants. With a bandgap of 3.2 eV for the anatase crystalline phase, TiO_2 most strongly absorbs in the UV range ($\lambda <$ 387 nm). However, doping with metals and nitrogen has been shown to create intermediate states in the bandgap. We present compositional data from x-ray photoelectron and Raman spectroscopy and structural data from scanning electron microscopy.

In conclusion, we form nanostructured and doped TiO_2 and non-stoichiometric TiN films by femtosecond laser irradiation in controlled atmospheres. We show that oxygen and nitrogen incorporation occurs in these films when the laser fluence exceeds the ablation threshold. Our research offers an innovative approach using laser scanning techniques to alter the surface and structure of $TiO_2$to generate new materials with applications in biomedical devices and for visible-light watersplitting.

Orientation Controlling of Femtosecond Laser-induced Subwavelength Ripples on Metal Surfaces by the Light Helicity

Jianjun Yang, **Yanfu Tang**, **Bo Zhao**, **Mingwei Wang**, **and Xiaonong Zhu**
Institute of Modern Optics, Nankai University
Key Laboratory of Optical Information Science and Technology, Education Ministry of China, China

Abstract— We report on the formation of subwavelength ripple structures on metals such as Cu and W under the irradiation of elliptically-polarized femtosecond lasers with the central wavelength of 800 nm and the pulse time duration of 50 fs. It is shown that the spatial alignment of the laser-induced ripples tends to change for different degrees of laser ellipticity, but it always remains perpendicular to the larger axis of the elliptical laser beam. In particular, the slantwise orientation angle with respect to the incident plane of the beam can be only varied periodically from -45° to 45° when a quarter-wave plate inserted in the incident beam is continuously rotated. Theoretical analysis reveals that the phase retardation of femtosecond laser pulses introduced by the quarter-wave plate no longer equals to $\pi/2$ owing to the wide spectrum components of the incident femtosecond laser pulses, which makes the axis of the ellipse slant as a function of the plate rotation angle. As a result, the observed periodic change of the ripple orientation can be interpreted with the help of the optical interference. Our simulation results agree well with the experimental measurements. It is expected that a new method to control the subwavelength ripples formation by the laser helicity can be obtained through this study.

Experimental and Theoretical Investigations of Laser-induced Periodical Structures Main Parameters in Femtosecond Regime

Sergey Makarov[1], **Andrey Ionin**[1], **Sergey Kudryashov**[1], **Alexander Ligachev**[2], **Leonid Seleznev**[1], **and Dmitry Sinitsyn**[1]

[1]P. N. Lebedev Physical Institute, Russian Academy of Sciences
Leninskiy Prospect 53, Moscow 119991, Russia
[2]General Physics Institute, Russian Academy of Sciences, Vavilova Str. 38, Moscow 119991, Russia

Abstract— As is known, calculation of a LIPSS period in the context of interference model for ns-regime laser action requires consideration of various thermal surface processes (e.g., capillary or acoustic waves) during the pulse absorption by medium. However, for the fs-regime the LIPSS formation single-shot threshold for fluence below the homogeneous melting threshold of the surface layer, moreover pulse duration is less than the characteristic times of various thermal processes. Thus, the value of the LIPSS period in fs-regime depends on the medium characteristic mainly through the optical properties, which change dramatically during the laser pulse.

According to results of our experiments the interference model is correct, because the orientation of LIPSS perpendicular to polarization, LIPSS period is directly proportional to a laser wavelength, and a period dependence on incident angle is similar to the interference theory prediction with some deviations. For confirmation of the last requirement a correct calculation of the instantaneous complex permittivity of a photoexcited material was done.

In our work, we have done simulations in the context of the interference model (plasmon-polariton model) with our experimental data for Al, Si and Ti with taking into account the instantaneous optical characteristics.

Session 2A3
Solution Strategies for Inverse Scattering Problems

Reconstruction of a Layered Dielectric Cylinder Using a Split Particle Swarm Optimization

K. Ishida
Kyushu Sangyo University, Japan

Abstract— Electromagnetic inverse scattering problem of evaluating properties of an object from its scattered electromagnetic waves is interesting in a variety of application such as medical diagnostics, nondestructive testing, and underground prospecting. For a strongly scattering object the problem reduces an optimization problem to minimize a cost function that relates differences between the measured and the calculated scattered-waves. It is difficult in general to search for the minimum point of the cost function in terms of a gradient-based optimization method because of existence of local minimum points.

To avoid traps at local minimum points two strategies are being considered. One is use of a stochastic nonlinear optimization algorithm such as particle swarm optimization (PSO). In PSO, multiple particles (candidate points) change their positions (the coordinates) in solution space according to their own experience and experience of the swarm. PSO requires as many evaluation of the cost function at each iteration as the number of particles.

The other is use of multiple cost functions. In inverse scattering problems, it is likely that data of different measurements, such as multi-frequency data, is utilized in order to obtain detailed information of the object. In those cases it is natural that we should introduce a cost function as a sum of squared errors of the different measurements. Summing the cost functions would reduce rises and falls, emphasize its global minimum point, and facilitate the search for the global minimum point to some extent. There probably remain local minimum points, however, and evaluation time of the cost function is increased.

In the present study a split PSO, which is a blending of the above strategies and has been proposed by the author [1], is applied to reconstruction of a layered dielectric cylinder. In the split PSO, particles are split into, say, two groups. Particles of a group evaluate a cost function and those of the other group do another cost function. Particles change their positions according to experience of their own and both groups to search the common minimum point of both cost functions. Solution might not be trapped at a local minimum point unless the minimum points lie at the same point.

In order to clarify effectiveness of the split PSO, we will apply PSO to a simple inverse scattering problem of evaluating a few parameters of a layered dielectric cylinder from scattered waves. Numerical examination will be done and comparison of the split PSO with the basic PSO will be presented.

REFERENCES

1. Ishida, K., "An application of particle swarm optimization to reconstruction of a homogeneous dielectric circular cylinder," *Proceedings of the 2011 International Symposium on Antennas and Propagation*, Jeju, Korea, 2011, to appear.

PSO-FBTS Approach to Microwave Breast Imaging

Toshifumi Moriyama[1], **Zhiqi Meng**[2], **Kismet Anak Hong Ping**[3], **and Takashi Takenaka**[1]

[1]Nagasaki University, Nagasaki 852-8521, Japan
[2]Fukuoka University, Fukuoka 814-0180, Japan
[3]Universiti Malaysia Sarawak, Sarawak 94300, Malaysia

Abstract— In this paper, a combination of the forward-backward time-stepping (FBTS) algorithm and a particle swarm optimization (PSO) is introduced as a time-domain inversion method for breast cancer detection. We have proposed a time-domain inverse scattering imaging technique referred to as FBTS based on a gradient optimization to reconstruct the electrical parameters profiles of scattering objects and applied it to breast cancer detection. When inverse scattering problems are solved using optimization techniques, it is important to choose a proper initial guess to avoid the local minima problem and obtain the solution with less computation time. PSO is used to find a rough geometrical data about the size and location of a fibroglandular tissue region inside a breast by assuming that both fibroglandular and fat tissue regions are homogeneous and a shape of fibroglandular is ellipse in the first step. This greatly reduces the number of parameters to be estimated. Before the second step, the roughly estimated fibroglandular tissue region was enlarged a little bit, followed by filtering to smooth the abrupt change at the boundary of the region. After obtaining rough image of the breast inside, detailed reconstruction in the second step is efficiently carried out applying the FBTS method. The proposed PSO-FBTS reconstruction algorithm was applied to imaging of 2D breast numerical phantom based on a MR image and was shown to successfully detect 5 mm diameter tumor in the breast model.

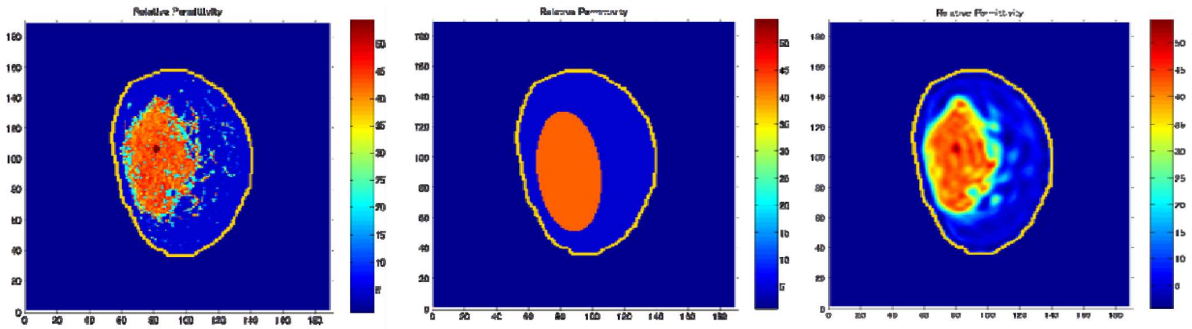

(a) (b) (c)

Figure 1: Reconstructed results. (a) is relative permittivity image of a numerical breast model derived from MR images. (b) is rough reconstructed image by PSO. (c) is fine reconstructed image by FBTS.

REFERENCES

1. Johnson, J. E., T. Takenaka, and T. Tanaka, "Two-dimensional time-domain inverse scattering for quantitative analysis of breast composition," *IEEE Transactions on Biomedical Engineering*, Vol. 55, No. 8, 1941–1945, 2008.
2. Lazebnik, M., L. McCartney, D. Popovic, C. B. Watkins, M. J. Lindstrom, J. Harter, S. Sewall, A. Magliocco, J. H. Booske, M. Okoniewski, and S. C. Hagness, "A large-scale study of the ultrawideband microwave dielectric properties of normal breast tissue obtained from reduction surgeries," *Physics in Medicine and Biology*, Vol. 52, 2637–2656, 2007.
3. Kennedy, J. and R. Eberhart, "Particle swarm optimization," *Proceedings of IEEE International Conference on Neural Networks*, IV, 1942–1948, 1995.

Imaging of 3D Anisotropic Inclusions in Multi-layered Medium by MUSIC with Enhanced Resolution

Rencheng Song, **Rui Chen**, **and Xudong Chen**
Department of Electrical and Computer Engineering, National University of Singapore, Singapore

Abstract— Subsurface imaging to detect the buried object has wide applications in demining, archaeology and mineral exploration etc. In this paper, the MUltiple SIgnal Classification (MUSIC) algorithm for the retrieval of small dielectric inclusions in free space is extended to multi-layered medium. Our paper has three contributions compared to the standard MUSIC methods. Firstly, the exact Foldy-Lax equation is employed to build the multi-static response (MSR) matrix. Since multiple scattering is considered, it avoids the assumption that inclusions should be well separated as requested in those methods based on Born approximation. Secondly, we consider the very general 3D anisotropic dielectric inclusions in multi-layered medium. Most known MUSIC papers focus on the isotropic inclusions in half space. Thirdly, the degenerate scatterers can also be imaged by choosing the optimal test dipole direction. In comparison, the standard MUSIC can't deal with this case. Numerical simulations show our method has wider applicability, better resolution, and more robust in presence of noise than the standard MUSIC methods.

Time-domain Inverse Scattering through the Filtered IMSA-FBTS Strategy: A Numerical Assessment

F. Caramanica[1], **T. Moriyama**[2], **G. Oliveri**[1], **A. Massa**[1], **and T. Takenaka**[2]

[1]ELEDIA Research Center at DISI, University of Trento, via Sommarive, I-38123, Trento, Italy
[2]Department of Electrical and Electronic Engineering, Nagasaki University, 852-8521, Japan

Abstract— Microwave non-destructive testing/evaluation applications including biomedical diagnosis, subsurface imaging, and material probing require efficient and reliable imaging strategies. Unfortunately, the development of these techniques is a challenging task because of the intrinsic features of the associated inverse problems, which turn out ill-posed and strongly non-linear. Accordingly, several methodologies have been developed in the last years either considering the frequency-domain [1] or the time-domain formulation of the scattering problem itself.

In this framework, a powerful approach, namely the Forward-Backward Time Stepping (FBTS) method, has been introduced to effectively exploit the large amount of information collected by broadband probing fields and achieve good resolutions and accuracies [2]. However, these interesting features have been achieved at the cost of a large computational complexity for the inversion [2]. To overcome this drawback, the integration of the FBTS with iterative multi-scaling methodologies has been recently proposed. Such approaches have been shown to yield interesting features in terms of resolution, efficiency, and accuracy if low noise conditions are at hand. Accordingly, in this work an improved IMSA-FBTS approach will be proposed which will integrate a multi-step time-domain filtering procedure during the inversion process to effectively tackle also the high noise case (Fig. 1).

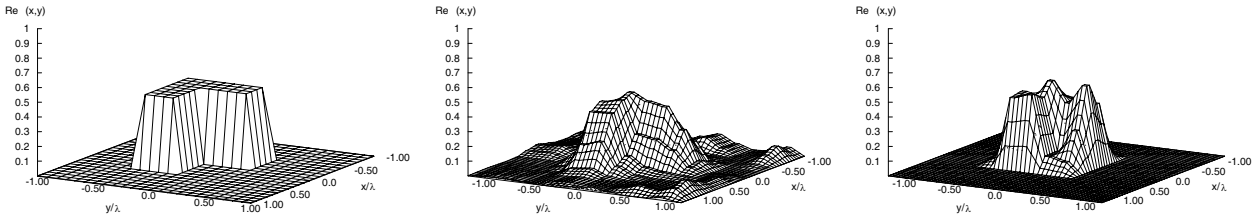

Figure 1: Reconstruction of a dielectric L-shaped cylinder with $\tau = 0.5$ illuminated by band-pass Gaussian incident pulse with center frequency $f_0 = 2\,\text{GHz}$ and bandwidth $1.3\,\text{GHz}$ [$SNR = 0\,\text{dB}$]. (a) True object; retrieved profiles by (b) BARE-FBTS and (c) IMSA-FBTS when using a multi-filtering strategy [3-step filter, cut-off frequencies: $1.43\,\text{GHz}$, $1.79\,\text{GHz}$, $2.71\,\text{GHz}$].

REFERENCES

1. Donelli, M. and A. Massa, "A computational approach based on a particle swarm optimizer for microwave imaging of two-dimensional dielectric scatterers," *IEEE Trans. Microwave Theory Techn.*, Vol. 53, No. 5, 1761–1776, May 2005.
2. Takenaka, T., H. Jia, and T. Tanaka, "Microwave Imaging of electrical property distributions by a forward-backward time-stepping method," *Journal of Electromagnetic Waves and Applications*, Vol. 14, No. 12, 1609–1626, 2000.
3. Caorsi, S., M. Donelli, D. Franceschini, and A. Massa, "A new methodology based on an iterative multiscaling for microwave imaging," *IEEE Trans. Antennas Propagat.*, Vol. 51, No. 4, 1162–1173, Apr. 2003.
4. Caorsi, S., M. Donelli, and A. Massa, "Detection, location and imaging of multiple scatterers by means of the iterative multiscaling method," *IEEE Trans. Microwave Theory Techn.*, Vol. 52, No. 4, 1217–1228, Apr. 2004.

On Using Multiple Modes to Reconstruct Conductor Locations in a Power Transformer Winding

M. Dalarsson, A. Motevasselian, and M. Norgren
Division of Electromagnetic Engineering, School of Electrical Engineering
Royal Institute of Technology, Stockholm SE-100 44, Sweden

Abstract— The power transformer is one of the most critical components in the electric power grid and a failure may result in large consequences. While in operation, power transformers are subject to several degradation mechanisms, e.g., thermal degradation at hot spots, partial discharges due to local over-stress, deformations of the windings caused by mechanical forces from short circuit currents, and increased levels of moisture in the cellulose insulation due to decomposition.

In this paper we present a preliminary study for a project, in which we will investigate a new proposed principle to diagnose power transformers while in operation. The existing methods are either coarse methods or off-line methods that require disconnection from the grid, which imply a non-service stress of the transformer.

The new principle is to insert antennas inside the transformer tank to radiate and measure microwave fields that interact with the metallic structure and the insulation. The responses from the radiated waves are supposed to be sensitive to material properties that reflects ageing, e.g., moisture in the electrical insulation, local over-heatings, contaminations and mechanical deformations — all signatures of a harmful deterioration process. The analysis of the measured signals and their complex relations to the material and structure parameters that are critical signatures of deterioration is an inverse electromagnetic problem that requires development of advanced algorithms.

As a very simplified model for initial studies, we model the transformer as a two-dimensional parallel plate waveguide where one plate represents the wall of the transformer tank and the other plate represents the iron core that conducts the magnetic flux. In between there are a set of parallel conductors representing the windings. The propagation problem is solved accurately and efficiently by conventional waveguide theory, including modematching and cascading techniques.

Assuming that waves may be launched at both ends of the waveguide, the inverse problem is to determine the locations of the individual conductors, from measurements of the scattered fields at both ends. Using a waveguide environment, the cut-off frequencies of the modes imply restrictions on how much information that can be obtained from measurements at various frequencies. The dominant TEM-mode yields information at all frequencies, while the higher order modes enter as the frequency increases. Hence, an important question is whether we can utilize multiple modes to improve the reconstruction.

We envisage optimization as a suitable method for solving the inverse problem. From a parametric study of the cost-function, we have found that wide band data are needed for stable reconstructions and that information from multiple modes are likely to decrease the occurrence of local minima. Hence, it is important that several waveguide modes can be transmitted and received with high accuracy, which implies that many antennas will be needed in the measurement system.

Shape Reconstruction of a Buried Perfectly Conducting Cylinder by Inverse Schemes

Wei Chien[1], **Chi-Hsien Sun**[2], **Chien-Ching Chiu**[2], **Szu-Chi Shen**[2], **and Chung-Hsin Huang**[3]

[1]Electronic Engineering Department
De Lin Institute of Technology, Tu-Cheng, Taipei, Taiwan, R.O.C.
[2]Electrical Engineering Department
Tamkang University, New Taipei City, Taiwan, R.O.C.
[3]Department of Computer and Communication Engineering
Taipei College of Maritime Technology
Danshui Town, New Taipei City, Taiwan, R.O.C.

Abstract— Dynamic differential evolution (DDE) for shape reconstruction of perfect conducting cylinder (PEC) buried in a half-space is presented. Assume that a conducting cylinder of unknown shape is buried in one half-space and scatters the field incident from another half-space where the scattered filed is measured. Based on the boundary condition and the measured scattered field, a set of nonlinear integral equations is derived and the imaging problem is reformulated into an optimization problem. The inverse problem is resolved by an optimization approach, and the global searching scheme DDE is then employed to search the parameter space. Numerical results demonstrate that even when the initial guess is far away from the exact one, good reconstruction can be obtained by using DDE.

A Multiplicative Regularization Scheme for Three-dimensional Shape-based Inversion

Maokun Li and Aria Abubakar
Schlumberger-Doll Research, Cambridge, USA

Abstract— We present a multiplicative regularization scheme for a three-dimensional (3D) shape-based inversion algorithm for inverting microwave data. In this algorithm, the shapes of targets are described by sampling points and the interpolation is carried out by using radial basis functions (RBFs). The usage of RBFs renders the surface of the target intrinsically smooth. Moreover, it eliminates the need for connecting information among the sampling points to describe a surface, which greatly simplifies the shape-based inversion algorithm. During the inversion process, the coordinates of the nodes and the material properties of the targets are reconstructed so that the modeled responses match the measurement data. In the 3D shaped-based inversion, the number of nodes can still be large, e.g., hundreds or thousands of nodes. Therefore, the use of a regularization scheme is necessary. In our algorithm we apply the multiplicative regularization scheme with the L2-norm or the weighted L2-norm regularization function, which is usually employed in the tomographic-based inversion. This regularization scheme constrains the curvature of the surfaces of the targets and further smooths the target surfaces. Similar as in the tomographic-based inversion, the L2-norm regularization scheme favors a smooth profile while the weighted L2-norm regularization scheme promotes sharp edges. We tested these two regularization schemes using both synthetic and experimental data sets. The results demonstrate that both shapes and material properties of the targets are well reconstructed. These two regularization schemes make the inversion more robust. We also show that the weighted L2-norm regularization scheme performs better for the shape reconstruction than the L2-norm regularization scheme.

Reconstruction of Perfectly Electric Conductors under TE Wave

Jianhua Shen[1], **Xudong Chen**[2], **and Lixin Ran**[1]

[1]Department of Information and Electronic Engineering
Zhejiang University, Hangzhou 310027, China
[2]Department of Electrical and Computer Engineering
National University of Singapore, 117576, Singapore

Abstract— This paper deals with the two-dimensional inverse scattering problem of perfectly electric conductors (PEC) under transverse electric (TE) wave illumination by using the subspace-based optimization method (SOM). The PEC scatterers under investigation can be of arbitrary contour, location and quantity. Moreover, both closed contour and infinitesimally thin structure are studied in this paper. The proposed SOM requires no prior information of the scatterers, such as the approximate location or quantity, and is able to generate good reconstruction results that agree well with the original PEC boundary. The proposed method is well robust against noise and the reconstruction result under 50% noise-to-signal level is still satisfactory.

Figure 1 shows the reconstruction result for a rectangle cylinder under 50% noise level. The rectangle is centered at (0, 0) and with a size of $1\lambda \times 1\lambda$. Since the PEC scatterer is impenetrable for electromagnetic wave, only the reconstruction result for the boundary is critical. In Figure 1, the reconstruction result marked by $\triangle$ shows good agreement with the original contour marked by the red lines.

Figure 2 shows the reconstruction result for multiple scatterers under 10% noise level. The PEC scatterers are composed of one rectangle centered at $(-0.6\lambda, 0)$ with a size of $0.4\lambda \times 0.4\lambda$ and one L shape thin metal with a 0.3λ length for both arms. The reconstruction obtains the correct boundary for both the closed-contour scatterer and the line-shape scatterer.

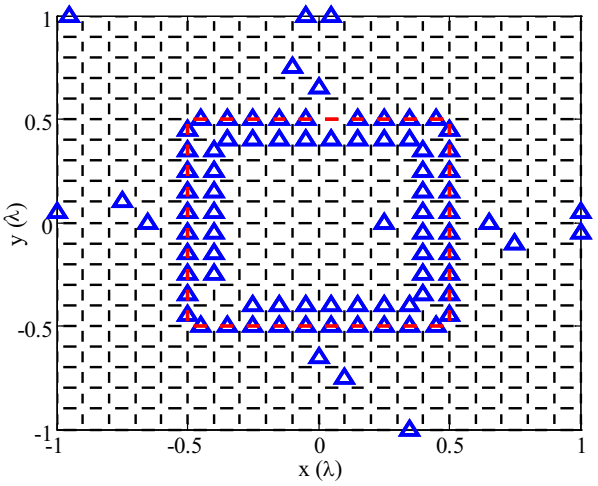

Figure 1: Reconstruction result of rectangle.

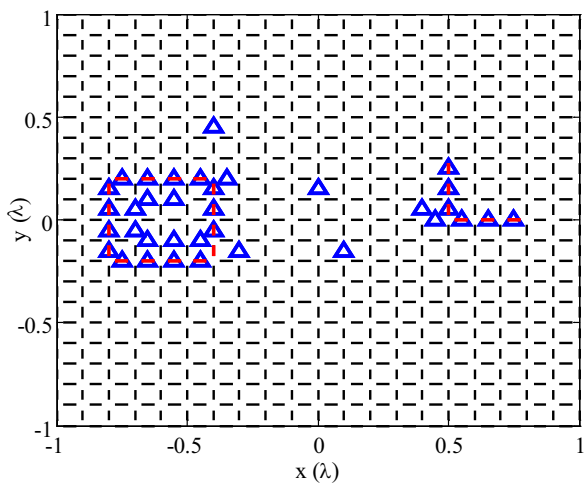

Figure 2: Reconstruction result of multiple scatterers.

Session 2A4
Antennas for Mobile Communication 1

Study of Compact Thin-film UWB Antenna with Dual Band-notched Characteristics

M. Tangjitjetsada[1], **P. Rakluea**[2], **and C. Benjangkaprasert**[1]

[1]Faculty of Engineering, King Mongkut's Institute of Technology Ladkrabang
Ladkrabang, Bangkok 10520, Thailand
[2]Department of Electronic and Telecommunication Engineering, Faculty of Engineering
Rajamangala University of Technology Thanyaburi, Pratumthani 12110, Thailand

Abstract— A study of compact thin-film ultra-wideband (UWB) antenna with dual band-notched characteristics is presented. The proposed antenna operated in the frequency range 2.9–11.3 GHz with 10 dB impedance bandwidth, and reasonable radiation properties. It also exhibit dual band-notched characteristics, one notch frequency band at 3.3–3.7 GHz (WiMax band), and the other at 5.1–5.8 GHz (WLAN-WiMax band). This antenna is printed on Mylar® Polyester Film substrate with thickness of 0.4 mm, and dielectric constant of 3.2. The antenna also demonstrates very compact dimensions, 27.3 × 34.5 mm in physical size. The antenna is designed for dual band-notched by embedding two separated slots on ground plane. The main aim behind the design methodology of the notch function is to tune the total length of the U-like slot and rectangular slot approximately equal to the half guided wavelength (λ_g) of the desired notch frequency. The antenna is determined using design equation, and simulated the commercial IE3D software, which is based on the method of moments. Good agreement is obtained between simulated and measured antenna characteristics. The results show that proposed antenna is very suitable for various portable UWB applications.

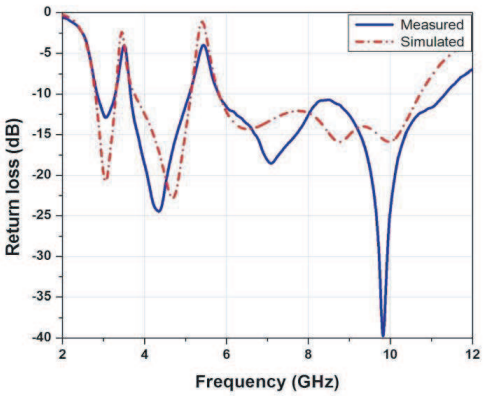

Figure 1: Simulated and measured return loss curves.

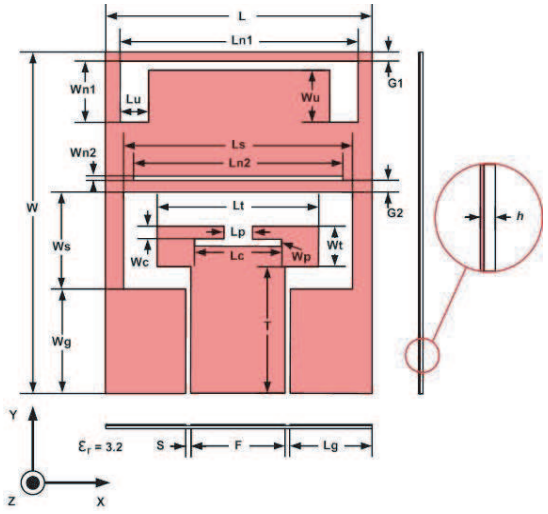

Figure 2: Geometry of proposed compact UWB antenna.

High-gain Antenna for Base Station Using MSA and Triangular EBG Cavity

P. Kamphikul, **P. Krachodnok**, **and R. Wongsan**
School of Telecommunication Engineering, Institute of Engineering
Suranaree University of Technology, Nakhon Ratchasima, Thailand

Abstract— This paper presents a high-gain antenna using microstrip antenna (MSA) with triangular Electromagnetic Band Gap (EBG) cavity for mobile base station. The advantages of this proposed antenna are light weight, easy fabrication and installation. Moreover, it provides the moderately high gain compare to the other antennas in the cellular phone system at present. The paper also presents the procedures of 3-element MSA and triangular EBG cavity design. A Computer Simulation Technology (CST) software has been used to compute the return loss, VSWR, radiation pattern, and gain of the antenna. The azimuth patterns of the proposed antenna can cover 360 degree of user's areas according to our requirement. The bandwidth, at S_{11} (-10 dB), is between 1920 to 2170 MHz with a gain more than 10 dB of each element.

A Dual-band Single-feed Planar Antenna for WLANs

Herman Hideyuki Uchida[1] **and Toshio Wakabayashi**[2]

[1]Tokai University, 4-1-1 Kitakaname, Hiratsuka, Kanagawa, Japan
[2]Malaysia-Japan International Institute of Technology (MJIIT)
University of Technology Malaysia(UTM), Jalan Semarak, Kuala Lumpur 54100, Malaysia

Abstract— Portable devices such as mobile phone and laptop computer are developed rapidly. These devices contain many wireless applications like WLAN(IEEE802.11a, b, g), Bluetooth, ZigBee, and WiMax. In relation to this, the numbers of antenna of a device are increasing. However, portable devices need low-profile, low-volume, and conformal design for portable use.

Therefore, multi-frequency antennas have been proposed in order to receive at two or more frequencies in a device. It is focused on reducing the numbers of antenna to lighten the devices. Many antennas are studied such as an antenna which has several elements to resonate at the frequencies corresponding to the element lengths and which is a type of inverted F with slots in the ground conductor.

In this study, a single-feed planar antenna which has a line element and a slot in the ground conductor are proposed in order to resonate at the frequencies of WLAN; IEEE802.11a(5.15–5.725 GHz), b(2.4–2.5 GHz), g(2.4–2.5 GHz). It has an advantage in the shape that the line element and the ground conductor with a slot are printed on the same plane of the dielectric substrate. This point leads devices to a low-profile and a conformal design. Moreover, the line element and the slot have independent resonance; therefore, it is easy to tune the frequencies and fabricate the antenna.

In this presentation, simulated reflection coefficient and current distribution of the dual-band antenna are shown. The simulated reflection coefficient represent that the antenna has two independent resonant frequencies, and the current distribution indicate that the line element and the slot resonate at each frequency.

Statistical Analysis of Microwave Scattering and Attenuation in Randomly Distributed Rainfalls Using Parallel Computation

Yasumitsu Miyazaki[1], **Koichi Takahashi**[1], **and Nobuo Goto**[2]

[1]Department of Media Informatics, Aichi University of Technology
50-2 Manori, Nishihasama-cho, Gamagori 443-0047, Japan
[2]Institute of Technology and Science, The University of Tokushima
2-1 Minamijosanjima-cho, Tokushima 770-8506, Japan

Abstract— Rain measurement system using propagation characteristics of microwave and millimeter wave is very effective for disaster prevention system for local strong rainfalls. Measurement technique of electromagnetic scattering and attenuation characteristics by rain is one of useful evaluation methods of rainfall rate [1], as shown in Fig. 1. A parabolic antenna with diameter $2a = 0.5\,\mathrm{m}$ is used to transmit and receive microwave of 10–20 GHz. Gaussian beam with beam spot $r_0 = 0.15\,\mathrm{m} \cong 5\lambda \sim 10\lambda$ is transmitted. Attenuations of Gaussian beam with 20 GHz carrier frequency in random media of rainfall rate $10 \sim 40\,\mathrm{mm/h}$ are evaluated by three-dimensional FDTD method [2]. To obtain accurate relationship between rainfall rate and rain attenuation, analysis of propagation for the incident wave with relatively small beam spot is considered. For the analysis of large area, parallel computing is studied [3, 4]. Calculation model for attenuation divisions of the calculation region are shown in Fig. 2.

Firstly, we show comparison of scattering fields of single raindrop by numerical FDTD method in small area with theoretical results derived by Rayleigh scattering theory For single raindrop, scattering properties of cubic and non-cubic raindrop models are evaluated. An example of comparison of numerical FDTD calculations and theoretical analysis for scattering field by single raindrop is shown. Secondly, scattering and attenuation in two raindrop are discussed as in Fig. 3. Lastly, the field in the large area which contains hundred raindrops is calculated using parallel and successive FDTD method. Scattering of Gaussian beam mainly depends on spatial

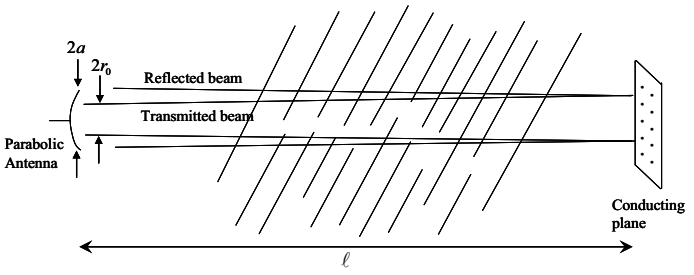

Figure 1: Measurement system of rain attenuation.

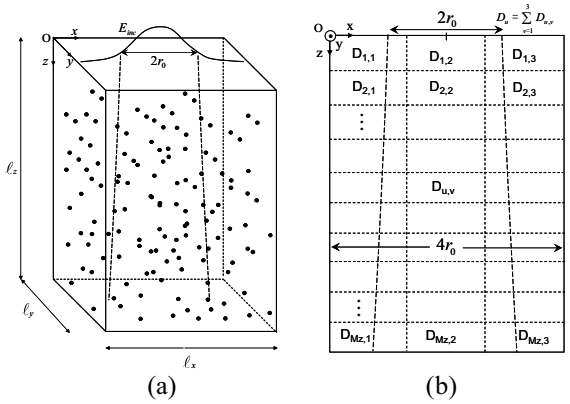

Figure 2: Analysis model for rain attenuation and division of calculation region.

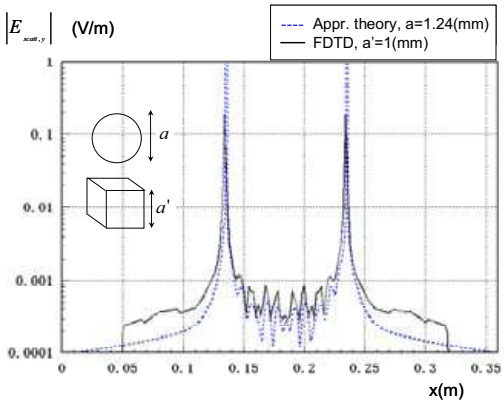

Figure 3: Comparison of scattering field in two raindrops. a: side length of a cube, a': diameter of a sphere ($y = 0.18\,\mathrm{m}$, $z = 0.07\,\mathrm{m}$).

rain densities and the ratio of the correlation length of random media to the wavelength [5]. Forward scattering intensity obtained by FDTD method is compared with statistical theory of electromagnetic scattering in random media. The comparison of numerical calculations of specific attenuation with the experimental results is also considered. Based on these computer simulations, the optimum measurement systems of raindrops using microwave techniques may be accomplished.

REFERENCES

1. Oguchi, T., *IEEE Proc.*, Vol. 71, 1029–1078, 1983.
2. Miyazaki, Y., K. Takahashi, and N. Goto, "Electromagnetic smart screen for tunable transmission and reflection applications," *PIERS Online*, Vol. 4, No. 2, 251–254, 2008.
3. Rodriguez, G., Y. Miyazaki, and N. Goto, *IEEE Trans. Antennas & Propagat.*, Vol. 54, No. 3, 785–796, 2006.
4. Takahashi, K., Y. Miyazaki, and N. Goto, *IEEJ Trans. EIS*, Vol. 127, No. 12, 1973–1981, 2007.
5. Miyazaki, Y., *Jpn. Jour. Appl. Phys.*, Vol. 13, No. 8, 1238–1248, 1974.

Calculation of Circular Microstrip Antenna Parameters with a Single Artificial Neural Network Model

S. S. Gultekin[1], **D. Uzer**[1], **and O. Dundar**[2]

[1]Department of Electrical and Electronics Engineering
Faculty of Engineering and Architecture, Selcuk University, Konya, Turkey
[2]Electronic Communication Technology Department
Eregli Kemal Akman Vocational High School, Selcuk University, Turkey

Abstract— A model for the design of circular microstrip antennas, based on Artificial Neural Networks, is presented. The multiple output design parameters are calculated by using a neural network. This neural model is simple and useful for the computer-aided design (CAD) of microstrip antennas. A distinct advantage of neural computation is that, after proper training, a neural network completely bypasses the repeated use of complex iterative processes for new cases presented to it. For engineering applications, this simple model is very usable. Thus the neural model given in this work can also be used for many engineering applications and purposes. In this study, for this neural network model, patch radius, radiation resistance, directivity, total quality factor, bandwidth, efficiency and gain are calculated as output parameters against input parameters as dielectric constant, resonant frequency, dielectric substrate thickness and tangent loss. Extended Delta-Bar-Delta training algorithm by Multilayer Perceptron structure that used popular in literature and gives good approaches is used for training the network. The design results obtained by using the neural model are in very good agreement with the results available in the literature.

Estimation and Design of U-slot Physical Patch Parameters with Artificial Neural Networks

D. Uzer[1], **S. S. Gultekin**[1], **and O. Dundar**[2]

[1]Department of Electrical and Electronics Engineering
Faculty of Engineering-Architecture, Selcuk University, Konya, Turkey
[2]Electronic Communication Program
Eregli Kemal Akman Technical Vocational School of Higher Education
Selcuk University, Konya, Turkey

Abstract— In this study, physical U slot parameters of rectangular microstrip patch antennas as vertical and horizontal slot lengths and widths with the patch lengths and widths are determined by the help of Artificial Neural Networks. The aim of the study is calculation of physical U slot patch parameters without any mathematical expressions or long and complex numeric calculations with a eural network model. Experimental results in the literature are used as the training data for the network by using Gradient Descent with Adaptive Learning Rate Back Propagation learning algorithm. The resonant frequency, dielectric constant of the substrate and the dielectric substrate thickness values are the inputs of the neural network and the patch length, patch width, the lengths and widths of the vertical and horizontal slots are the network outputs. The test output data of the network are used for simulations and the results are confirmed by these simulations. S_{11} responses, resonant frequency, impedance bandwidth, directivity, gain and radiation efficiency values of the antennas are investigated by HFSS. Simulation results are compatible with test outputs. The high training success of the network and R_2 values very close to 1 show that physical patch parameters of U-slot rectangular microstrip antennas can be calculated with this Artificial Neural Network model with high accuracy.

Effect of U-slot Applications on Circular Microstrip Patches Modeling with Artificial Neural Networks on Impedance Bandwidth

D. Uzer, **M. S. Uzer**, **S. S. Gultekin**, **and N. Yilmaz**
Electrical and Electronics Engineering Department
Faculty of Engineering and Architecture, Selcuk University, Konya, Turkey

Abstract— In this study, effects of etching U-slot on circular patches on their bandwidths are investigated. The study is carried out by etching U-slots on the present microstrip patches in the literature by simulating them with HFSS. Simulation results are used for training and testing of an Artificial Neural Network model for different microstrip patches' bandwidth predictions. The obtained simulation results are compared with Artificial Neural Network results. Comparison of the simulation and Artificial Neural Network results, accuracy rates of training and testing were found to be 93.28% and 94.19%, respectively. It is obtained that by etching U-slot, the bandwidths can be enhanced for the present circular microstrip patches. It is shown that possible the bandwidth behavior of U-slot circular microstrip disc antenna with this Artificial Neural Network model is powerfully estimated.

Bandwidth Modeling of U-slot Rectangular Microstrip Antennas with Artificial Neural Networks

M. S. Uzer, **D. Uzer**, **N. Yilmaz**, **and S. S. Gultekin**
Electrical-Electronics Engineering Department
Faculty of Engineering and Architecture, Selcuk University, Konya, Turkey

Abstract— In this study, rectangular U-slot microstrip antennas are modeled by an Artificial Neural Network structure and their bandwidth values are calculated with the model. The antenna parameters are taken from in the literature. The experimental results are compared with Artificial Neural Network results. Comparison of the experimental and Artificial Neural Network results, accuracy rates of training and testing were found to be 96.6% and 91.3%, respectively. It is obtained that ANN results are compatible with experimental bandwidth results from the literature. It is shown that possible bandwidth behavior of U-slot rectangular microstrip patch antennas with this Artificial Neural Network model is powerfully estimated.

A Metamaterial Antenna with Reduced Radiation Hazards towards Human Head

D. Laila, **R. Sujith**, **C. M. Nijas**, **V. A. Shameena**, **R. Dinesh**, **and P. Mohanan**
Centre for Research in Electromagnetics and Antennas(CREMA), Department of Electronics
Cochin University of Science and Technology, Cochin, Kerala 682022, India

Abstract— The use of cellular phones and mobile wireless communication systems has been growing rapidly during the past few years. And, there is public concern for safety exposure from these devices. Therefore, it is necessary to decrease the interaction of electromagnetic energy towards human head when mobile handset in use.

A modified coplanar wave guide (CPW) fed printed monopole antenna with reduced radiation hazards for mobile application is presented and discussed. Directional radiation pattern of a CPW fed monopole antenna in the elevation plane is modified with a single null in the azimuth plane by using metamaterial substance like Split Ring Resonator (SRR). The SRR with resonance frequency 2.04 GHz is printed at back side of the monopole antenna at the optimum position to modify the radiation pattern. By properly choosing the geometrical parameters of monopole antenna and SRR, the stop band can be shifted to GSM band of the cellular phone. Experimental and simulation studies of the proposed antenna are considered using HP8510C Net work Analyser and Ansoft HFSS respectively. A 25 dB reduction of radiated power in one quadrant of the radiation pattern offers a reduction of radiation towards the users head. This resultant antenna resonates at 1.8 GHz, when printed on a substrate of dielectric constant (ε_r) 4.4 and thickness 1.6 mm with an overall dimension of 42 mm × 14 mm × 1.6 mm.

Since this printed metamaterial based antenna is used to reduce EM interaction between antenna and human head, study of Specific Absorption Rate (SAR) is also performed. The simulation model of SAM phantom head model is used for SAR calculation. Simulated SAR value of the proposed antenna is also compared with monopole antenna of same dimension. It is observed that SAR value for the proposed antenna is 1.32 W/kg which is less than the FCC recommended value of (1.6 W/kg).

Polarization Diversity Unidirectional Antenna for IEEE 802.11a Applications

S. Vongsack[1], **C. Phongcharoenpanich**[2], **S. Kosulvit**[2], **K. Hamamoto**[3], **and T. Wakabayashi**[4]

[1]International College, King Mongkut's Institute of Technology Ladkrabang, Thailand
[2]Faculty of Engineering, King Mongkut's Institute of Technology Ladkrabang, Thailand
[3]School of Information and Telecommunication Engineering, Tokai University, Japan
[4]Malaysia-Japan International Institute of Technology (MJIIT)
University of Technology Malaysia (UTM), Jalan Semarak, Kuala Lumpur 54100, Malaysia

Abstract— This paper introduces the polarization diversity unidirectional antenna for wireless LAN applications by using two-probe excited circular ring antenna above square reflector. The purpose of this investigation is to design a polarization diversity unidirectional antenna to resonate at the center frequency of 5.5 GHz to cover the frequency range from 5.2 to 5.8 GHz for wireless LAN system following IEEE 802.11a standard. The performances of the antenna such as the return loss, the isolation between two-probes, the radiation pattern and the gain, were analyzed by using Computer Simulation Technology (CST) Microwave Studio. For the specified operating frequency, the dimension of circular ring is first chosen to achieve the condition that only the dominant mode TE_{11} can be propagated inside the circular ring for a single probe antenna. Then, the suitable probe length and ring length are determined for the two-probe antenna. Finally, isolation between two probes is enhanced by insertion of an linear isolator between the probes. Besides, this antenna structure radiates unidirectional pattern. It is obvious that the beam peak directs along the circular ring aperture in $+x$ direction. The antenna consists of two parts of circular ring fed by two probes and square reflector. The two probes are perpendicular to each other and are located at the center of the circular ring of the length l aligned along the z and y axes. The first probe will be active while the second probe is terminated with 50 Ω load resulting in horizontal polarization, and on the other hand resulting in vertical polarization. The simulated results of the return loss, the isolation between two-probes and the radiation pattern are presented. The proposed antenna has a polarization diversity unidirectional pattern with maximum gain of 8.34 dBi. Moreover, the proposed antenna yields the front-to-back ratio better than 20 dB and the isolation between the two-probes better than 20 dB as well. Furthermore, the prototype of the antenna was fabricated and measured to confirm the simulated results. Besides, the proposed antenna is useful for wireless local area network (WLAN) communication systems.

A New Seljuk Star Shape Microstrip Antenna Design

D. Uzer and S. S. Gultekin
Electrical and Electronics Engineering Department, Faculty of Engineering and Architecture
Selcuk University, Turkey

Abstract— A new star shape microstrip patch antenna in the form of Seljuk star is designed on a circular shape Foam substrate that has a thickness of 5 mm. It is simulated using by HFSS simulator. Electrical parameters of the antenna like bandwidth, radiation pattern, and return loss, exc. are investigated. The relationship between geometric sizes of the patch and the electrical parameter specifications of the antenna is researched. It is concluded that this new antenna design can be used for different applications and widespread bandwidth enhancement techniques can be adapted to this type of patch antenna.

Session 2A5
Wireless Network and Applications 1

A Novel Radiation Enhancement Technique for Multilayer Microwave Circuits

K. M. Lum
University of Surrey, Guildford, Surrey, GU2 7XH, United Kingdom

Abstract— Design and measurement data are presented that shows how a single strip of low permittivity, thick film dielectric material beneath the radiating edges of the microstrip patch antenna can be employed to improve the fringing field of the radiating edges and thus the efficiency of radiation. Design and practical data are provided for two prototype antennas working at 5 GHz. The radiation enhanced patch antennas demonstrated return loss below −30 dB and improvement in radiation efficiency. This simple yet efficient technique is particularly suitable for use with patch antenna under consideration, because of the general suitability of the whole structure for implementation in multilayer thick film, or LTCC formats.

Novel M-shaped Defected Ground Structure for Spurious Suppressed Dual Mode Bandpass Filter Design

J. W. Lau and K. M. Lum
School of Electrical Engineering and Computer Science
University of Newcastle, Callaghan, NSW 2308, Australia

Abstract— This paper presents a spurious suppressed microstrip dual mode bandpass filter (BPF). High selectivity and good adjacent channel interference rejection are required of modern transmitting and receiving devices. Conventionally, square resonator with orthogonal input and output feedlines is employed to achieve a quasi-elliptic type of bandpass response with two transmission zeros near its passband edges. However, this resulted in spurious response of unwanted harmonics at higher frequencies. The proposed spurious suppressed dual mode BPF utilized novel M-shaped defected ground structures (DGS) etched in the ground plane beneath a square resonator input and output feedlines to attain spurious suppressed bandpass responses. The presence of DGS leads to the increment in the current path and effective permittivity, and also the decrement of effective phase velocity and effective wavelength. In addition, DGS of different sizes, patterns and positioning, equivalent L-C ratio, coupling coefficients and other electrical parameters will result in various spurious suppression responses. It can be represented by a parallel tuned circuit arranged in series with the main circuit transmission line to which it is coupled. The prototyped BPF is fabricated on a Ro4003C substrate with relative permittivity of 3.38 and loss tangent of 0.0021. The center frequency is 2.55 GHz. The best measured S_{11} is obtained at 2.58 GHz with a value of -23.76 dB and the corresponding S_{21} is -3.7 dB which is slightly lower as compared to the simulated response. This is mainly due to fabrication tolerance and misalignment loss. One transmission zero is obtained at 2.25 GHz and 2.85 GHz respectively. The lower and upper stopband attenuation is greater than 20 dB/GHz. The bandwidth of the passband response at -3 dB level is 3.2%. Validation of the BPF design is obtained via good agreement between the simulated and measured results.

Stepped Impedance Key-shaped Resonator for Bandpass and Bandstop Filters Design

K. C. Lek and K. M. Lum
School of Electrical Engineering and Computer Science
University of Newcastle, Callaghan, NSW 2308, Australia

Abstract— In this paper, a bandpass filter (BPF) and bandstop filter (BSF) designs using Key-shaped resonators are presented. The filter designs comprise stepped impedance resonators (SIR) and by utilizing defective ground structure (DGS), a coupling capacitor is inserted in the ground plane. The capacitor provides a filtering channel for improving the insertion loss and bandwidth performances of the bandpass and bandstop filters. The filters were fabricated on FR4 substrate having a thickness of 1.6 mm and relative permittivity of 4.7. The dimensions of the prototyped BPF and BSF are 23.5 mm by 25.2 mm and 25.5 mm by 22.5 mm respectively.

Multilayered Miniaturized Hairpin Resonator for Bandpass Filter Design

M. L. Lee and K. M. Lum
School of Science and Technology, SIM University, Singapore

Abstract— This paper present a multilayered bandpass filter (BPF) operating at 3 GHz. Four miniaturized hairpin resonators are positioned in pairs, laid on two different conductor layers to obtain the BPF response. The multilayer configuration allows more flexibility in controlling the variation on the coupling effect of the resonators, namely the horizontal coupling effect between resonators on the same layer and vertical coupling effect between the top and bottom overlaid resonators. The overall dimensions of the prototyped BPF are 6.5 cm by 2.6 cm. It is fabricated on two FR4 substrates with relative permittivity, $\varepsilon_r = 4.7$. Validation of the BPF design is obtained via good agreement between the simulated and measured results.

A Stepped Impedance Comb-line Filter Design Using Defective Ground Structure for Wireless Applications

Y. T. Lim and K. M. Lum
School of Science and Technology, SIM University, Singapore

Abstract— This paper presents a novel bandpass filter (BPF) design using stepped impedance comb-line resonator and defected ground structure (DGS) for S-band application. Two microstrip stepped impedance resonators (SIR) lay on the top conductor layer, are grounded using VIA hole. A 50 Ω microstrip line is connected to each resonator to act as the input and output feedlines respectively. DGS is widely and commonly exploited for its advantage of producing compact and simple design procedures, as well as mutual coupling between elements of the arrays. The proposed DGS is implemented by using a square-shaped capacitor represented by slots into the ground plane. The coupling effect of the slot to the microstrip stepped impedance resonators laid above it is further enhanced by adding stub and cavity structures around the border. Charges are accumulated within the slots which will in turn increases the effective capacitance of the microstrip resonators. Two prototyped BPF are fabricated using FR4 substrate with a relative permeability of 4.7, loss tangent of 0.027 and thickness of 1.6 mm. The center frequency of the designed BPF is 3 GHz and the dimensional size is 2.56 cm by 2.56 cm. The best match for the first BPF is obtained at 2.7 GHz with a S_{11} value of less than −35 dB. In the passband response, the corresponding S_{21} is approximately −4 dB with rejection rate at 10 dB/GHz. In addition, the second BPF is best matched at 3.3 GHz with a S_{11} value of less than −20 dB. The corresponding S_{21} is approximately −4 dB with rejection rate at above 10 dB/GHz. Both simulation and measurement results are presented and discussed for the two proposed BPF, which are designed using different DGS topologies to validate the new concept.

Miniaturized Multilayered Bandpass Filter Using Microstrip Hairpin Resonator for C-band Application

C. Y. Wong and K. M. Lum
School of Science and Technology, SIM University, Singapore

Abstract— This paper presents a miniaturized multilayered bandpass filter (BPF) using U-shaped and W-shaped hairpin resonators. The proposed BPF consisted of five microstrip hairpin resonators arranged on two separate conductor layers and being placed by design to control the vertical and horizontal coupling effect in order to obtain the desired bandpass filter performance. Resonator 1, 2 and 3 are arranged on the top conductor layer of the substrate. Resonator 4 and 5 are buried between the first and second substrate with a 180 degree change in the orientation of the position. In addition, the buried U-shaped resonators are attached together which result in the implementation of a unique W-shape resonator structure. 50 Ω microstrip input and output feedlines are joined together with resonator 1 and 3 on the top conductor layer respectively. The proposed BPF is fabricated on two FR4 substrates with a dielectric constant of 4.7, loss tangent of 0.027 and thickness of 0.8 mm. Epoxy adhesive loss is used to laminate the two substrates collectively. The dimension of the prototyped BPF is 33 mm by 21 mm. The best matching return loss S_{11} is observed at 5.18 GHz with a value less than −15 dB. The corresponding passband response S_{21} is approximately −4 dB with an upper and lower stopband attenuation rate of about 8 dB/100 MHz. Both simulation and measurement results are presented and discussed.

Compact Lowpass Filter Design Using Cavity Resonator and Ladder-shaped Defected Ground Structure

K. X. Ng and K. M. Lum
School of Science and Technology, SIM University, Singapore

Abstract— A compact lowpass filter (LPF) design using cavity resonator and ladder-shaped defected ground structure (DGS) is presented in this paper. A cavity resonator is implemented on the top conductor layer with orthogonally oriented input and output feedlines for the proposed LPF filter. The cavity resonator has identical electrical function as of a square resonator. By proper design of the cavity structure, coupling coefficients and electrostatics parameters which influence the cutoff frequency can be controlled. The ladder-shaped DGS is etched on the ground plane directly beneath the 50 Ω input and output feedlines in order to manipulate the filter response. The DGS structure is effective for accurate transmission cutoff values, which ensure proper multiple spurious suppressions. The proposed LPF is prototyped using FR4 substrate with a dielectric constant of 4.7, loss tangent of 0.027 and thickness of 0.8 mm. The prototyped LPF has a compact dimensional size of 26 mm by 26 mm. The observed measured stopband attenuation rate is 8dB/GHz. Both simulation and measurement data are presented and discussed for the proposed LPF with and without the novel ladder-shaped DGS.

A Novel Bandpass Filter Design Using E-shaped Resonator and Dual Square-loop Defected Ground Structure

P. L. Lim and K. M. Lum
School of Science and Technology, SIM University, Singapore

Abstract— This paper presents a second-order chebyshev bandpass filter (BPF) using two E-shaped microstrip resonators and a dual square-loop defected ground structure (DGS). The proposed novel DGS structure is realized by implementing two opened square loop topologies on the ground plane. The etched structure interfers with the shield current distribution in the ground plane which affects the characteristics of the two E-shaped resonators laid above it. This disturbance creates beneficial capacitance and inductance effect on the filter design, which results in the desired filter response. Two E-Shaped resonators are laid on the top conductor layer. The behavior of the E-shaped resonators can be represented using even and odd mode analysis. For odd mode analysis, an electric wall is inserted between the two E-Shaped resonators to enable a quasi quarter wavelength to be extracted. In the case of even mode analysis, a magnetic wall is added in between the two E-Shaped resonators. Thus the resonators can be associated with a folded quasi half wave resonator. By manipulating the E-shaped resonator and dual square-loop DGS designs, the desired BPF response can be achieved. The proposed BPF is fabricated on FR4 substrate with a relative permittivity of 4.7 and thickness of 0.8 mm. The center frequency is 2.5 GHz and the dimensions of the prototyped BPF are 12.41 mm by 13.70 mm. The best matching return loss S_{11} response is obtained at 2.2 GHz with a value less than -10 dB. The corresponding insertion loss S_{21} is -2.2 dB. The lower and upper stopband attenuation is 5 dB/GHz and 7 dB/GHz respectively. Both simulation and measurement results are presented and discussed for the proposed BPF.

Study on New Ultrasonic Positioning and Movement Detection Installed in Sensor Network

Mitsutaka Hikita, **Akira Nakano**, **and Natsuki Tobita**
Faculty of Global Engineering, Kogakuin University, Shinjuku-Ku, Tokyo 163-8677, Japan

Abstract— Cellular-phone systems have spread all over the world and their technologies continue to be developed during the first half of the twenty-first century. On the other hand outstanding technical innovations have been observed in a sensor area. A new concept called "Sensor Network" has been proposed recently by combining sensor technologies together with such mobile communications system as cellular-phone, radio LAN and Bluetooth. Sensing signals from many sensor nodes distributed in a certain area such as home, office and public places are collected to a center node by the technology similar to that used in mobile communications. Sensor network enables home/office circumstance control, environment monitoring and protection based on the collected data. It is also thought to have a big impact on our lives and to grow to be a giant industry like the cellular-phone systems in the future. In our laboratory, we have been studying the sensor network to achieve comfortable living circumstances by home/office sensing and control.

We have proposed an accurate novel ultrasonic positioning method and based on it invented a new movement detection technique which can be installed in sensor network. Sensor nodes require long-term operation with extremely low-power supply, such as several-year operation with a single battery. However, such conventional accurate ultrasonic positioning methods as a code-division method and a chirp-signal method require complicated and heavy signal processing procedures for both the transmitter and receiver. Therefore, their devices cannot be included in sensor nodes due to the power consumption. Our proposed method can provide not only the low-power consumption but also removal of the complicated signal processing procedures, which overcomes the limitation for use as sensor-node devices. Ultrasonic continuous waves (CWs) at discrete frequencies within the transducer bandwidth which correspond to those of the Inverse Fast Fourier Transform (IFFT) procedure are transmitted. Based on the relative amplitudes and phases between the received and transmitted CWs, the impulse response can be calculated in the center node, which can provide accurate distance information without any sophisticated procedures such as the pulse compression or the correlation between the received and replica signals. If we subtract the impulse responses at present from those at the preceding time, we can obtain the change of distances between objects and nodes at two different points in time. By this procedure, we can exclude effects of inactive objects and can emphasize only moving objects. Therefore the sensor network including our positioning and movement detection devices will possibly be applied not only to home/office monitoring but also to care for old people, prevention of crime and watch in hospitals. In this paper, both theoretical investigation and experimental results will be presented.

Evaluation of Site Diversity Effectiveness Using Weather Radar Data for Singapore

See Chuan Leong, **Wan Jing Loh**, **Yanjuan Chen**, **Peng Hon Yip**, **and Boon Tiong Koh**
Defence Science & Technology Agency, Singapore

Abstract— Long term weather radar data from open source are used for the determination of rainfall exceedance distributions for Singapore. Using an empirical model and methodology, the τ-min to 1-min time sampling of rainfall values is achieved so that accurate and high spatial resolution rain rate, attenuation maps and site diversity measurements can be computed in accordance to ITU-R recommendations. Rainfall contour maps within Singapore show a difference of about 40 mmhr^{-1}. Site diversity gain dependence with distance shows a different relationship as compared to ITU-R Hodges model for Singapore. Site diversity methodology provides at least 10 dB of gain at 99.99% availability Ku band frequencies. The diversity gain is also highly dependent on the combination of site used in addition to the site separation distances.

REFERENCES

1. Leong, S. C. and Y. C. Foo, "Singapore rain rate distributions," *6th Int. Conf. on Information, Comms and Signal Processing*, 1–5, Dec. 2007.
2. Timothy, K. I., J. T. Ong, and E. B. L. Choo, "Performance of the size diversity technique in Singapore: Preliminary results," *IEEE Communications Letters*, Vol. 5, No. 2, 49–51, Feb. 2001.
3. Yeo, J. X., Y. H. Lee, and J. T. Ong, "Performance of site diversity investigated through radar derived results," *IEEE Trans. on Antennas and Propagation*, Vol. 59, No. 10, 1–9, 2011.
4. ITU-R, "Propagation data and prediction methods required for the design of Earth-space telecommunication systems," *Recommendation ITU-R P.618-10*, Geneva, 2009.
5. Hodge, D. B., "An improved model for diversity gain in earth-space propagation paths," *Radio Science*, Vol. 17, No. 6, 1393–1399, 1982.
6. Marshall, J. S. and W. Palmer, "The distribution of raindrops with size," *Journal of Atmospheric Sciences*, Vol. 5, No. 4, 165–166, 1948.
7. http://www.weather.gov.sg/wip/c/portal/layout?p_l_id=PUB.1023.5, Meteorological Service Singapore, 2011.
8. "Regional Weather Radar Information," http://www.ulfp.com/ulfp/mod_animate/view.asp?ID=1, Ulfpettersson.com, 2011.
9. "Summary of observations," Meteorological Service Singapore, 1993.
10. Chebil, J., "Rain rate and rain attenuation distribution for microwave propagation study in Malaysia," Ph.D. Thesis, Universiti Teknologi Malaysia, 1997
11. ITU-R, "Specific attenuation model for rain for use in prediction methods," *Recommendation ITU-R P.838-3*, Geneva, 2007.

An Assessment of ZigBee Wireless Communications in Aircraft

Anthony Centeno and Neil Alford
Department of Materials, Imperial College London
Exhibition Road, London SW7 2AZ, United Kingdom

Abstract— It is increasingly desirable to continuously monitor the structural health of an aircraft using a wireless sensor network. Key to the sensor network is the reliability of a suitable wireless channel in the various enclosed structures found within an aircraft. This paper will report on the ongoing work that is being undertaken for the SHEMS consortium (www.shemsproject.co.uk) in testing and evaluating the 2.4 GHz ZigBee wireless protocol in various aircraft enclosures. Previously we have reported on Measurement of ZigBee wireless communications in mode-stirred and mode-tuned reverberation chamber [1] and showed that even for very low loss enclosures wireless communications is possible, but only under very specific conditions. A higher loss chamber has more reliable communication channels, but even with loading there are large variations in packet error rates even between adjacent ZigBee channels. In this paper we will report on testing of the ZigBee wireless channels in structures found within actual aircraft. The structures used for testing are all fully or partially enclosed and are of different sizes with various amounts of loading. In most cases reliable communications with a low BER is obtained, but in enclosures with large amounts of equipment and wiring bundles we find that attenuation even over quite short distances, less than 2 m for example, can be very high (> 90 dB). In large unloaded cavities the BER is high, as in the reverberation chamber, but we find that in most practical locations there is sufficient loading, primarily due to cable bundles.

Session 2A6
Filter, Transmission Line and Waveguide

Realization and Characterization of a High-performance SOA-based Multi-wavelength Fiber Ring Laser

Peng-Chun Peng[1], **An-Li Tsou**[2], **Hoshin H. Yee**[2], **and Hai-Han Lu**[1]

[1]Department of Electro-Optical Engineering
National Taipei University of Technology, Taipei 106, Taiwan, R.O.C.
[2]Department of Electrical Engineering
National Taipei University of Technology, Taipei 106, Taiwan, R.O.C.

Abstract— In this report, we will demonstrate a stable multiwavelength fiber ring laser with ultra-narrow wavelength spacing using a semiconductor optical amplifier (SOA). In the laser configuration, the delay interferometer and the mirror play the role as a double-pass interferometer which greatly improves the signal-to-noise ratio in this experiment. Up to 181 stable lasing wavelengths, from 1574.91 to 1591.25 nm, with a wavelength spacing of 10.7 GHz and a signal-to-noise ratio of over 24 dB, as well as a relatively small power variation below 0.5 dB are achieved at room temperature.

Besides traditional DFB or DBR diode lasers, it is believed that this sort of high-performance fiber laser will be a very promising alternative as the light source in large-capacity optical communications.

Design and Implementation of Asymmetric Coupled SIR Dual-band Bandpass Filter

Wen Ko and Man-Long Her
Ph. D. Program in Electrical and Communications Engineering, Feng Chia University, Taiwan

Abstract— The paper proposed an available structure that applies asymmetrical coupling SIR to make the 2.6/5.2 GHz dual-band bandpass filter. The filter used the principle of microstrip line and coupling to control the center frequency of the first and the second passband by the way of the impedance ratio of the stepped impedance resonator.

The basic construction of filter is constituted by the LCL series resonance bandpass filter. It can be divided into two sets of SIR coupling, the low frequency of 2.6 GHz passes the upper half of high impedance SIR, and high frequency of 5.2 GHz passes the lower part of low impedance SIR. The entity circuit structure is made by FR-4 that contains two-sided plate microstrip line as shown in Figure 1. The frequency response is presented by the software of electromagnetism simulator (IE3D) that shows the scattering parameters $|S_{11}|$, $|S_{21}|$ as you see in Figure 2.

This structure of circuit is simple and the board size is small, the center frequency can be easily controlled. The center frequency f_1 of the first passband with 2.6 GHz is tunable by adjusting the upper half SIR impedance and changing the gap distance. The center frequency f_2 of the second passband with 5.2 GHz is also tunable by adjusting the lower part SIR impedance and changing the gap distance.

This research discusses the relationship between the used microstrip line asymmetric SIR impedance and the gap distance to create the fabrication of the dual-band bandpass filter. The process is simple and the effect is good. The electric entity circuit layout and the measured results are shown in Figure 3 and Figure 4.

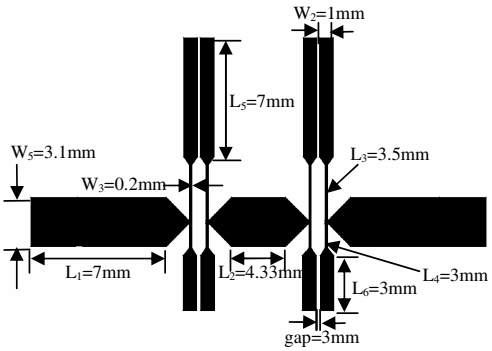

Figure 1: The circuit configuration.

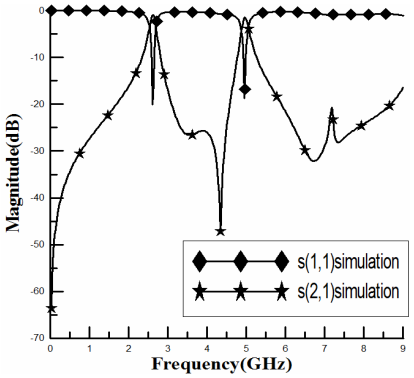

Figure 2: The simulated results.

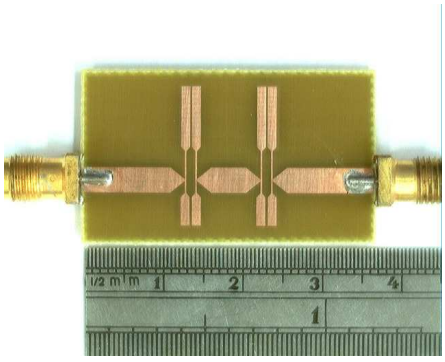

Figure 3: The circuit layout.

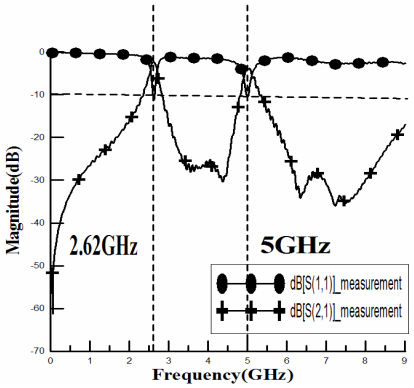

Figure 4: The measured results.

Realization of Compact Dual-band Band Pass Filter with Transmission Zeros and Wide Bandwidth Using Low-temperature Co-fired Ceramic

Li Ju Chen and Ken-Huang Lin
National Sun Yat-Sen University, Taiwan

Abstract— This investigation proposes a novel and compact dual-band band pass filter design with a multilayer structure, formed in a low-temperature co-fired ceramic. Widening the tunable bandwidth, improving the arbitrary frequency ratio, having transmission zero at the stop band and making the design of dual-band filters compact are continuing challenges The proposed dual-band band pass filter not only exhibits a dual-band response, but also has a wide second bandwidth and external transmission zeros. This topology introduces transmission zeros at the out band and improves the isolation between the two passbands to provide high selectivity. The bandwidth ratio of the first and the second band is about 1 : 4 and the compact size makes the filter suitable for wireless communication applications. A 2.4/5.5 GHz dual-band bandpass filter for 802.11n is designed and implemented in LTCC substrate in this investigation. The semi-lumped prototype enables the integration of the filter in a multilayer circuit for miniaturized implementation. This new method for realizing dual-band filters is based on the use of coupled semi-lumped quarter-wave filters. One of the important components of this circuit design is a coupled strip-line. The strip-line structure is highly suitable for implementing millimeter-wave passive components in a highly integrated multifunctional module, because of its symmetrical structure, high isolation, and low loss characteristics.The proposed circuit is composed ofa coupled line (TL1 $\sim$ TL2), three capacitors (C1 $\sim$ C3), two stub-lines to ground (TL3 $\sim$ TL4), one serial stub-line (TL6) and two shunt open stub-lines (TL5, TL7). Finally, simulated and measured results are presented.

A Compact Aperture-backed Square Ring UWB Bandpass Filter

A. S. H. Kuek, H. T. Su, and M. K. Haldar
School of Engineering, Computing and Science
Swinburne University of Technology (Sarawak Campus), Malaysia

Abstract— Ultra-wideband (UWB) radio frequency (RF) technology, which operates on low energy and high bandwidth, has gained tremendous research interest in recent decade. UWB bandpass filter (BPF) is essential to tap the unlicensed use of the frequency range covering from 3.1 GHz to 10.6 GHz, which is the UWB spectrum released by US Federal Communications Commission [1]. 3.1 GHz and 10.6 GHz are the lower and upper frequencies, respectively, where attenuation is 10 dB providing fractional bandwidth of 1.095. This paper presents a compact quintuplet-mode aperture-backed square ring UWB BPF. Firstly, a one-wavelength square ring resonated at 6.85 GHz centre frequency is coupled with interdigital line at both sides to produce a triple-mode filter characteristic as discussed in [2]. To increase the modes of the filter to five, stepped-impedance feed lines are then implemented to introduce two extra poles at each side of the centre frequency as described in [3]. The drawback of interdigital line coupling is that it requires very narrow coupling gaps. Wide aperture is then etched on the ground plane directly below each interdigital line to achieve strong coupling by effectively weakening the coupling between each conductor strip and the ground plane [4]. This results in wider coupling gaps to enable in-house fabrication. A floating strip conductor is then added at the centre of each ground aperture to suppress the spurious harmonic appearing at twice the central frequency of the ring resonator [5]. The physical layout of the proposed filter designed with Sonnet Suite TM is shown in Figure 1(a). The simulated frequency responses of S_{21}- and S_{11}-magnitudes as shown in Figure 1(b) exhibit low insertion loss below 1 dB within UWB passband. The proposed filter will be fabricated with RT/Duroids 6010 to experimentally validate that it is in good agreement with the simulated results. This paper will discuss on the analysis and design of the proposed filter as well as performance measurement of the fabricated filter.

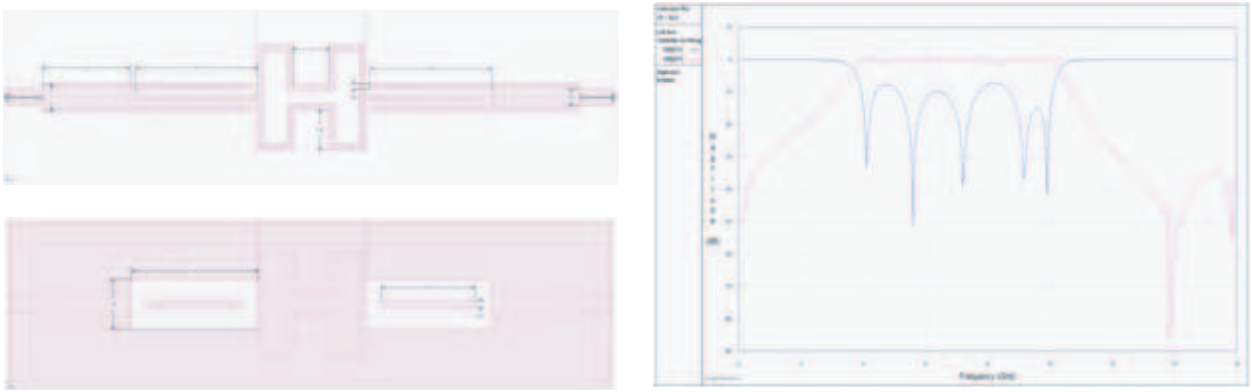

(a) (b)

Figure 1: (a) Physical layout of the proposed bandpass filter. (b) Simulation results of S_{21} and S_{11} of the proposed bandpass filter.

REFERENCES

1. FCC, "Revision of part 15 of the commission's rules regarding ultrawideband transmission system first report and order," F. C. Commission, Ed., 98–153, February 2002.
2. Wong, S. W., et al., "A stopband-enhanced UWB bandpass filter using short-/open-stubs embedded ring resonator," *Microwave Conference, 2009. APMC 2009. Asia Pacific*, 913–916, 2009.
3. Watanabe, K., et al., "A microstrip UWB bandpass filter using a stub-loaded dual-mode ring resonator and a step impedance two-mode resonator," *Microwave Conference, 2008. APMC 2008. Asia-Pacific*, 1–4, 2008.

4. Zhu, L., et al., "Aperture compensation technique for innovative design of ultra-broadband microstrip bandpass filter," *2000 IEEE MTT-S International Microwave Symposium Digest*, Vol. 1, 315–318, 2000.
5. Velazquez-Ahumada, M. C., et al., "Parallel coupled microstrip filters with floating ground-plane conductor for spurious-band suppression," *IEEE Transactions on Microwave Theory and Techniques*, Vol. 53, 1823–1828, 2005.

180 GHz Microstrip Ring Resonator Bandpass Filter on Micromachined Silicon Substrate

H. R. Lin[1], **K. B. Ng**[2], **C. H. Chan**[3], **E. Y. B. Pun**[3], **F. J. Hsieh**[1], **and W. C. Wang**[1, 4, 5]

[1]Department of Mechanical Engineering, University of Washington, Seattle, Washington, USA
[2]State Key Laboratory of Millimeter Waves, City University of Hong Kong, China
[3]Department of Electrical Engineering, City University of Hong Kong, China
[4]Department of Electrical Engineering, University of Washington, Seattle, Washington, USA
[5]Medical Device Innovation Center, National Cheng-Kung University, Tainan, Taiwan, R.O.C.

Abstract— A 180 GHz bandpass filter utilizing dual mode stepped impedance ring resonator is reported. A monolithic integrated microstrip design is proposed and fabricated on a silicon substrate. To excite appropriate resonant mode and to alleviate difficulties in micro-machining process, the second-order resonance of the circular ring resonator is adopted in the filter design. The whole design includes a conductor-backed coplanar waveguide (CBCPW) to guide signals into and out of the filter. Coplanar waveguide (CPW)-microstrip transition structure between CBCPW and central ring is also considered to avoid having via metal layers bridging the top and bottom electrodes. This design also eliminates the need for wire bonding. A capacitive coupling gap design is used between the microstrip and ring resonator for its simple design and easy to modify for different frequency operation. Aluminum is used for the top and bottom electrodes and the thickness is controlled at 600 nm. A (110) p-type 150 µm double side polished silicon wafer is used as the substrate. The thickness of the wafer is etched down to 100 µm by inductively coupled plasma (ICP) dry etching to insure optimal waveguide transmission at the operation frequency. Since the surface roughness of substrate is shown to be less than 50 nm, the subsequent metal deposition of bottom electrode will be affected. The result from the CST simulation shows that a 3.5 dB insertion loss at 181 GHz and 3 dB passband from 176 to 186 GHz can be obtained.

Wide Band Harmonic Suppression Bandpass Filters Using Coupled Open- and Short-ended Resonators

Homayoon Oraizi and Mahdi Zoghi
Department of Electrical Engineering, Iran University of Science and Technology
Narmak, Tehran 1684613114, Iran

Abstract— Various types of resonators in the form of closed or open loop and hairpin configurations have been used as the main components for the design of filters. However, such filters mostly suffer from the generation of harmonics in their frequency response. Various techniques have been proposed to suppress such spuriuos harmonics. A procedure is developed for the suppression of harmonics for the cases composed of short- and open-ended resonators [1]. In this paper, we propose to select the coupled sections of resonators in such a way as to enhance the suppression of the specified harmonics. The various line sections are made into step-lines to provide more degrees of freedom for the filter design. By the variation of width of line sections at various locations of the loop resonators, the filter bandwidth has increased considerably compared to the conventional design with uniform line sections. Furthermore, the level of harmonics have drastically decreased. The diagram of a second order coupled open- and short-ended filter with stepped-line sections is drawn in Fig. 1, which is designed for the suppression of second harmonic. The center frequency is 1 GHz. The frequency response of the filter is drawn in Fig. 2. Note that the achieved bandwidth is about 40% and the second harmonic is reduced to −30 dB.

Table 1: Geometrical dimensions of the proposed filter (millimeter).

L_1	L_2	L_3	L_4	L_5	L_6	L_7	L_8	L_9	L_{10}	$L11$
1	25.1	4.17	60.259	17.94	17.94	41.2	16.55	1	5	1
L_{12}	L_{13}	L_{14}	L_{15}	L_{16}	L_{17}	W_1	W_2	W_3	W_4	W_5
48.63	48.63	27.78	27.78	41.1	50	5.49	3.64	0.96	1.52	0.2
W_6	W_7	W_8	W_9	W_{10}	W_{11}	W_{12}	g	s		
2.4	5.5	0.2	2.65	1.86	0.55	2.4	2.43	0.11		

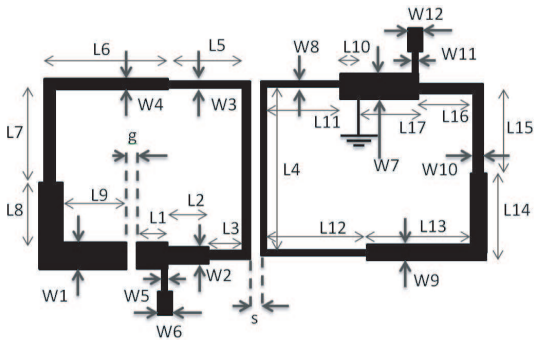

Figure 1: A second order filter using open- and short- ended loops with stepped- line sections.

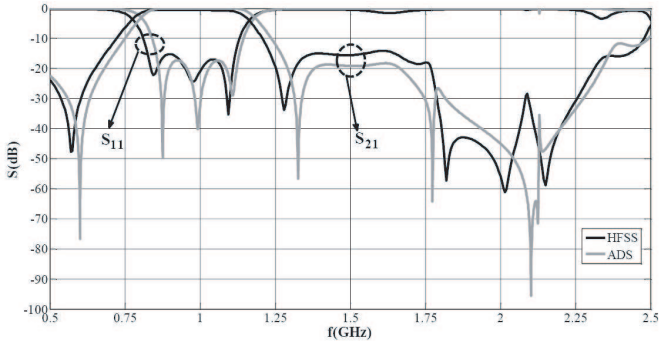

Figure 2: Frequency response of propesd filter.

REFERENCES

1. Dai, G. L., X. Y. Zhang, C. H. Chan, Q. Xue, and M. Y. Xia, "An investigation of open- and short-ended resonators and their applications to bandpass filters," *IEEE Transactions on Microwave Theory and Techniques*, Vol. 57, No. 9, 2203–2210, Sep. 2009.

Novel Tunable Band-reject Filter Using Modified C-shaped Defected Ground Structure

Rajab M. Begenji and M.-H. Neshati
Department of Electrical Engineering, Ferdowsi University of Mashhad, Iran

Abstract— In this paper, a novel tunable DGS filter is proposed to provide a frequency-rejection property at 2.4 GHz. The new structure has a simple and compact shape and its rejection characteristic is very sharp at top band. Different parameters of the DGS have been adjusted for the best frequency response to reject the centre frequency. Moreover, using a variable capacitor, the resonance frequency of the proposed filter is varied and a tunable band reject filter is obtained.

Figure 1(a) shows the 2-D view of the proposed DGS filter. Rogers RO3003 with dielectric constant of 3.5 and height of 60 mil is used as the substrate of the filter. A 50 Ω line, a feed line, is designed by line width of $W = 3.44$ cm. The C-shaped DGS is etched at the backside of the PC-board and its size are $l_1 = 14.4$ cm, $l_2 = 4$ cm, $t = g = 0.2$ cm and $b = 0.4$ cm as shown in Fig. 1(a). A parasitic patch with size of 5×0.6 cm^2 is also added at the proper place to ease adding of electronically variable capacitance using varactor diode.

The proposed filter is numerically simulated using HFSS. Results show that for a 6 pF to 0.4 pF variation of the capacitor, the centre frequency is varied from 1.9 GHz to 2.8 GHz. Fig. 1(b) shows the transmission coefficient of the DGS filter versus frequency. Also filter characteristics such as resonance frequency, rejection bandwidth and its Q-factor is summarized in Table 1. It can be seen that the proposed filter provide a very high Q-factor, and as a result the variable center frequency is effectively rejected.

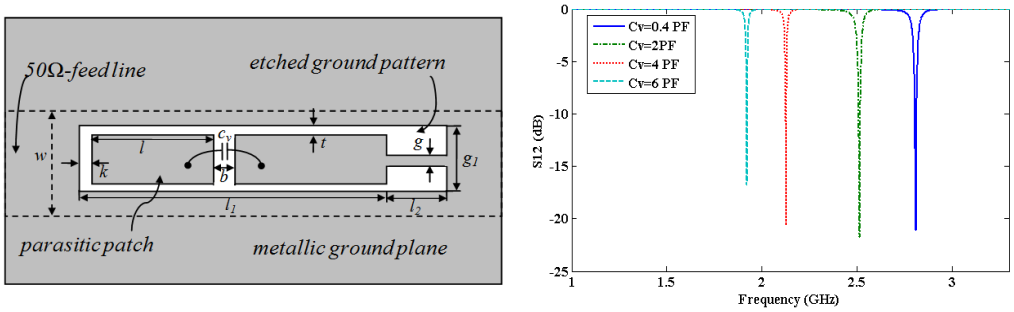

(a) (b)

Figure 1: (a) 2-D bottom view of microstrip filter with a variable capacitor (b) frequency response for different C_V values.

Table 1: Characteristics of band-reject filter for various values of capacitor.

C_v (PF)	f_0 (GHz)	BW (MHz)	Q	S_{12} (dB)	S_{11} (dB)
0.4	2.811	28	100	−21.15	−0.814
2	2.514	27	93	−21.74	−0.815
4	2.127	14	152	−20.64	−0.781
6	1.922	12	160	−16.83	−0.893
without C_v	2.309	28	82.5	−21.78	−0.793

Miniaturization and Harmonic Suppression of a Novel Rat-race Coupler

Wei Song, Hiroyuki Deguchi, and Mikio Tsuji
Department of Electronics, Doshisha University, Kyotanabe, Kyoto 610-0321, Japan

Abstract— Rat-race coupler is a basic component in modern microwave systems. In Fig. 1, we can see that a rat-race coupler consists of three $1/4\lambda$ microstrip-line segments and one $3/4\lambda$ microstrip-line segment. Rat-race coupler has two functions. When port 1 is the input port, port 2 and port 4 are the output ports with port 3 as the isolation port. The voltage in port 2 and port 4 is equal but out of phase. When port 2 is the input port, port 1 and port 3 are the output ports with port 4 as the isolation port. The voltage in port 1 and port 3 is identical. However, it suffers not only large volume but harmonic problem.

To overcome the two shortages, a novel rat-race coupler first introduces the structure shown in Fig. 2, which consists of three $1/6\lambda$ microstrip-line segments and one $2/3\lambda$ microstrip-line segment. This is the first step of miniaturization. In order to realize further miniaturization and harmonic supression, the $2/3\lambda$ microstrip-line segment is equally divided into four microstrip-line segments. Then, each of the seven $1/6\lambda$ microstrip-line segments is replaced by T-shape structure which has a $1/16\lambda$ stub which can be used to suppress the fourth harmonic.

Finally, two spiral asymmetric defected ground structures (DGS) are added to both ends of the T-shaped structure. Each asymmetric DGS can provide two resonance frequencies, which can suppress second and third harmonics. It can further reduce the volume due to slow-wave effect. This novel coupler is designed at the centre frequency 0.9 GHz, and its top view and back view is shown in Fig. 3. The volume of the present coupler is just 25% of a conventional rat-race coupler. Meanwhile, the second, third and fourth harmonics are suppressed below -15 dB. The detailed calculation results and the measurements for the designed coupler will be presented at the talk.

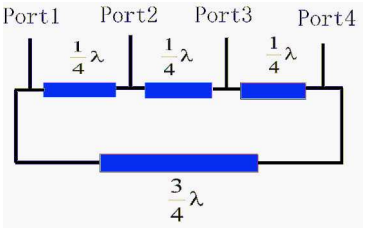

Figure 1: onventional coupler constructed by the $1/4\lambda$ segment.

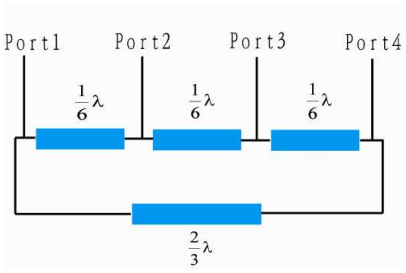

Figure 2: Proposed coupler constructed by the $1/6\lambda$ segment.

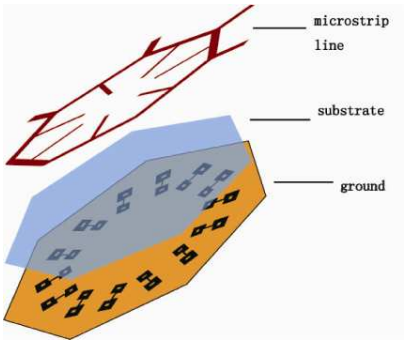

Figure 3: Proposed rat-race coupler.

A New Method for Detection and Characterization of Electrical Cable Aging

L. El Sahmarany[1], **F. Auzanneau**[1], **and P. Bonnet**[2]

[1]Embedded Systems Reliability Laboratory, CEA, LIST, Gif-sur-Yvette, France
[2]LASMEA, Clermont University, Blaise Pascal University, Clermont-Ferrand, France

Abstract— Cables are omnipresent in all electrical systems for power and information transfer. They are subjected to the same constraints as the systems to which they are connected and may suffer from failures or slow degradation (aging) as well. The knowledge and evaluation of cable aging can help anticipate the maintenance of degraded cables. Therefore, it is necessary to test the cable state and to provide information on its degradation.

Several methods exist to test cables, one of the best one being reflectometry [1]. This method is well suited to detecting and locating defects along the cable, but in the case of an overall aging of the cable, it does not provide relevant information.

To overcome these limitations, we propose a new approach based on time reversal [2] applied to the fundamental principle of reflectometry (i.e., injection of a high frequency signal in one end of the cable). This new method uses an adapted signal that adds value and allows us to more precisely characterize the modifications of the electrical parameters (RLCG) due to aging of the cable.

In order to investigate the feasibility of this method, numerical simulation and experimental measurements are performed. The simulation is done by using a frequency model of a cable in MATLAB (Fig. 1). To verify the results, we apply the method to a real case of identical new and aged cables. The goal is to analyze the response of the cable to the injected adapted signal in order to verify the status of the cable.

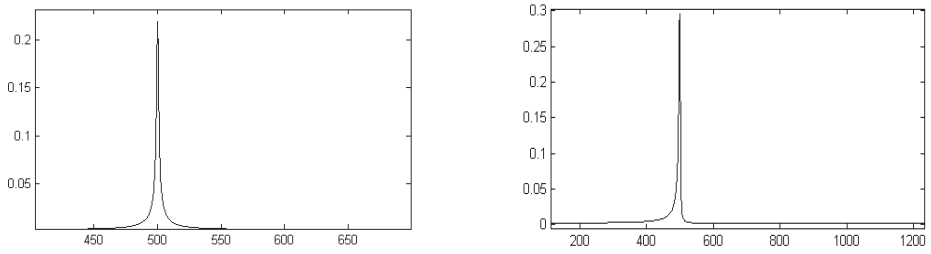

(a) (b)

Figure 1: The response of (a) new and (b) aged cable.

REFERENCES

1. Auzanneau, F., M. Olivas Carrion, and N. Ravot, "A simple and accurate model for wire diagnosis using reflectometry," *PIERS Proceedings*, 232–236, Prague, Czech Republic, August 27–30, 2007.
2. Fink, M., Time reversal of ultrasonic fields Part 1: Basic principles," *IEEE Transactions on Ultrasonics, Ferroelectrics, and Frequency Control*, Vol. 39, No. 5, 555–566, September 1992.

A Dynamic Low-pass Transmission Line and Resonant Power Transmission and Reflection

P. Halevi, U. Algredo-Badillo, and O. M. Becerra-Fuentes
Instituto Nacional de Astrofísica, Óptica y Electrónica
Apdo. Post. 51, Puebla, Pue. 72000, México

Abstract— A low-pass transmission line (TL) with all the capacitors replaced by identical and simultaneously pumped varactors has unusual properties [1]. The dispersion relation $\omega(k)$ displays a double band structure, being periodic in both the circular frequency ω (period Ω, equal to 2π times the modulation frequency of the varactors) and in the phase advance ka (period 2π, a being the size of the unit cell). Moreover, $\omega(k)$ can exhibit astonishing "topologies", depending on the parameter $\bar{\omega}_N = 1/(\Omega\sqrt{L\bar{C}})$, where L is the inductance of the inductors and $\bar{C}$ is the *average* capacitance of the varactors in a unit cell. These band structures may display frequency band gaps $\Delta\omega$, wave vector band gaps Δk, or neither. A source emitting a monochromatic wave of frequency $\omega/2\pi$ excites in the TL harmonics of all the frequencies $(\omega - n\Omega)/2\pi$ with $n = 0; \pm 1; \pm 2; \ldots$ and, moreover, it is a superposition of plane waves with wave vectors $k_1(\omega), k_2(\omega), \ldots$.

It turns out that, in the long-wavelength limit ($ka \ll 1$) the dynamic low-pass TL can be represented by an effective medium. Namely, the electromagnetic properties of the TL are identical to those of a uniform medium with permeability $\mu = L/a$ and a time-periodic permittivity $\varepsilon(t) = C(t)/a$; actually a *temporal* photonic crystal! Thus, the instantaneous effective permittivity is, simply, the instantaneous distributed capacitance of the TL [1].

Two recent papers [2] develop the electromagnetic theory of a dielectric slab characterized by a permittivity $\varepsilon(t)$ that is periodic in time. We can expect all the results of these papers to carry over to our dynamic TL provided that the phase advance ka is sufficiently small. In particular, we have predicted parametric resonances in the transmission and reflection coefficients of the dynamic-periodic slab [3]. These occur for special values of the signal frequency, given by $\omega_i = \Omega/2 = \nu_i(M)/(2D\sqrt{\bar{\varepsilon}\bar{\mu}})$, $i = 1; 2; \ldots$; where D is the slab thickness and the $\nu_i(M)$ are a series of "magic" (fractional) numbers whose values depend on the modulation strength M. For these values of the frequency, standing waves form within the slab for all wave vectors $k_1(\omega), k_2(\omega), \ldots$.

We have performed simulations of transmission and re ection by a TL of length D, with all the capacitors replaced by varactors whose capacitance $C(t)$ is a periodic function with period $2\pi/\Omega$. This TL is terminated at both extremes by impedances $Z_0 = 376.73\,\Omega$hm, representing vacuum. Then, as expected, resonant power transmission and re ection occurs whenever the signal frequency is $\omega_i = \Omega/2 = \nu_i(M)/(2D\sqrt{(\bar{C}/a)(L/a)})$ with the same "magic numbers" $\nu_i(M)$ that have been found for the uniform, dynamic slab [3]. Such transfer of energy from the pump source that modulates the varactors could have important applications.

REFERENCES

1. Halevi, P., U. Algredo-Badillo, and J. R. Zurita-Sánchez, *Appl. Phys. Lett.*, submitted.
2. Zurita-Sánchez, J. R., P. Halevi, and J. C. Cervantes-González, *Phys. Rev. A*, Vol. 79, 053821, 2009.
3. Zurita-Sánchez, J. R. and P. Halevi, *Phys. Rev. A*, Vol. 81, 053834, 2010.

Inverse Scattering Experiments for Electric Cable Soft Fault Diagnosis and Connector Location

Florent Loete[1], **Qinghua Zhang**[2], **and Michel Sorine**[3]

[1]LGEP-SUPELEC, 11 rue Joliot Curie 91192 Gif sur Yvette, France
[2]INRIA, Campus de Beaulieu, 35042 Rennes Cedex, France
[3]INRIA, Domaine de Voluceau, 78153 Le Chesnay, France

Abstract— The fast development of electronic devices in modern engineering systems comes with more and more connection cables, and consequently, the reliability of electric connections becomes a crucial issue. This fact has motivated research projects on methods for the diagnosis of faults in electric transmission lines. In this context, a promising technology for transmission line fault diagnosis is the reflectometry, which consists in analyzing the reflection and the transmission of electric waves observed at the ends of a cable. It has been reported that this technology is able to easily detect and locate hard faults (open circuit or short circuit) up to an accuracy of about 10 cm. For soft faults, the problem is much more complicated. Although it has been shown that a degraded connector can influence the reflection coefficient [1], no satisfactory experimental result has been reported for the detection of soft faults in electric cables, to our knowledge.

Recently, the inverse scattering theory has been applied to the reflectometry technology [2, 3]. After completing the theoretic studies initiated by [4], these recently published results show, by numerical simulation, the ability of the method based on the inverse scattering theory to diagnose soft faults in electric cables. The considered soft faults are modeled as spatially smooth variations of the characteristic parameters of electric cables governed by the telegrapher's equations.

The purpose of the present paper is to report the experiments made with laboratory equipments confirming the previously reported theoretic results and numerical simulations. To physically produce a smooth variation of the characteristic impedance of a twisted-pair cable simulating a soft fault, the two wires of the cable are untwisted and separated by 1 cm over a portion of 20 cm. In the real life, untwisted wires are often observed at connector locations because the wires need to be soldered to the connector's pins. In our experiments a real truck electric cable with several connectors is used. With the aid of a standard network analyzer and by analyzing the reflection coefficient with the inverse scattering-based method, it is possible to detect and to locate the untwisted portion of the cable, as well as the connectors, distant of about 10 meters from the end of the cable connected to the network analyzer. The shape of the smoothly untwisted and separated portion is also reasonably estimated.

REFERENCES

1. Loete, F., S. Noël, R. Meyer, M. Olivas, F. Auzanneau, and D. Chandon, "Feasability of the detection of vibration induced faults in connectors by reflectometry," *24th Int. Conf. on Elec. Contacts ICEC*, 440–443, St Malo, France, June 2008.
2. Zhang, Q., M. Sorine, and M. Admane, "Inverse scattering for soft fault diagnosis in electric transmission lines," *IEEE Trans. on Antennas and Propagation*, Vol. 59, No. 1, 141–148, 2011.
3. Tang, H. and Q. Zhang, "An inverse scattering approach to soft fault diagnosis in lossy electric transmission lines," *IEEE Trans. on Antennas and Propagation*, Vol. 59, No. 10, 3730–3737, 2011.
4. Jaulent, M., "Inverse scattering problems in absorbing media," *J. Math. Phys.*, Vol. 17, 1351–1360, 1976.

Session 2A7
Electromagnetic Modeling, Inversion and Applications

MAGIC2D Implicit Particle Pusher Description and Test

Andrew J. Woods and Lars D. Ludeking
Alliant Techsystems (ATK), 8560 Cinderbed Road, Suite 700, Newington, VA 22122, USA

Abstract— MAGIC2D [1] has been upgraded to include an implicit particle-in-cell (PIC) update scheme (particle "pusher") for increased time steps Δt and stability in beam-plasma simulations. The adjustable damping implicit update method of Friedman [2] allows selectable attenuation of modes in a plasma.

Our approach has been to first develop a simple particle pusher one-dimensional (1D) finite-difference code model, named PPUSH1, which incorporates implicit PIC as outlined in [2]. Particles are started with initial energy and applied electric field, and the motion computed with an adjustable damping parameter. We have replicated the electron motion reported in [2] for a potential well with electric field linear in excursion distance. This model represents the simplest form of plasma oscillation. The essential result is that for a given $\omega_0 \Delta t$ (= 0.42 in the test case) where ω_0 is the frequency of oscillation, the damping parameter θ can be chosen between 0 (no damping) to 1.0 (10× damping in 16 periods for our test problem). Hence, for a mix of frequencies in a complex many-particle system, unwanted higher frequency oscillations can be adjustably diminished while preserving the lower values of greater interest.

Subsequent to verification against [2], the implicit PIC routine was extended to three dimensions and relativistic dynamics, tested for magnetic field effects, and incorporated into MAGIC2D. The Lorentz equation particle update code closely resembles the 1D subroutine checked out previously. Additional successful tests included particle deceleration in self fields to analytically solvable positions, and acceleration through known potentials to relativistic levels. The new method agrees with the previous explicit treatment in these simple tests where both have sufficiently small time step.

A more rigorous example test problem showing the benefits of the implicit treatment is given in Fig. 1. Electron temperature versus time is shown for an initial population of charged particles of density 3.3×10^{13} #/cc. The implicit curve reaches steady state at $T_e \sim 7.5$ keV reasonably close to the expected range of 4 and 6 keV. The artificial heating of the explicit results is $\sim 100\times$ the desired value in the short simulation time.

The new implicit particle pusher in MAGIC2D enables the user to select damping of high-frequency modes thus concentrating on plasma fundamental frequencies of interest. This additional user tool, to be available in MAGIC version 3.2.0, can prevent instabilities resulting from ionization growth beyond the time step limit for explicit particles.

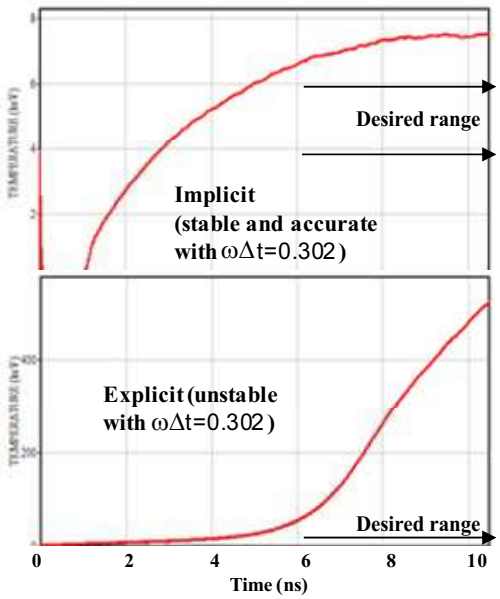

Figure 1: MAGIC2D plasma temperature results showing stability of implicit particle update (top) compared to unphysical values from the explicit model (bottom).

ACKNOWLEDGMENT

Work supported by ATK.

REFERENCES

1. Goplen, B., et al., "User-configurable MAGIC for electromagnetic PIC calculations," *Computer Physics Communications*, Vol. 87, 1995, http://www.magictoolsuite.com.
2. Friedman, A., "Implicit multiscale PIC and related topics," *Workshop on Multiscale Processes in Fusion Plasmas*, UCLA, Jan. 2005, http://hifweb.lbl.gov/public/slides/.

A New GL Visible and Controlling EM Stirring for Steel and Meta Casts

Ganquan Xie[2, 1], **Jianhua Li**[1, 2], **Qing Xie**[1], **Feng Xie**[2], **and Lee Xie**[2]

[1]Hunan Super Computational Science Center, China
[2]GL Geophysical Laboratory, USA

Abstract— In this paper, we proposed a new visible and controlling electromagnetic stirring (EMS) for steel and metal casts. Our GL EM modeling and inversion software and a new special radar are key technology. In international and China, the EMS are installing and running in most steel casts lines with blind operation. The visible and controlling EMS is not practicable. Our visible controlling EMS will be practicable. The copyright and patent of our visible controlling EMS are belong to Professor Jianhua Li in GL Geophysical Laboratory in USA.

Application of Digital Filtering Techniques in Field Solvers to Represent Small Embedded Features in a Coarse Mesh

Vongurai Rawin, **Christos Christopoulos**, **Dave Thomas**, **and Steve Greedy**
University of Nottingham, UK

Abstract— Differential techniques for full field solutions to electromagnetic problems such as TLM&FDTD usually involved iteration of a mesh of discrete points in the problem space. In general, fine embedded object requires high computational costs as a large number of nodes or fine mesh is needed. The Digital Filtering (DF) technique is introduced for the Transmission-Line Modelling (TLM) technique in which first the DF parameters from a fine mesh simulation around a fine object are extracted and then these parameters are embedded into a coarse mesh for large scale simulation. As a result, the coarse TLM mesh can then give comparable accuracy to a fine mesh and a significant saving in computation. The weakness of this technique is the coarse mesh with embedded digital filters is unable to give accurate results at high frequency.

This paper describes a technique for the 3D TLM method which uses with the digital filters. The Fast Fourier Transform (FFT), Bilinear-Z-transform and Prony's method [1] are employed to estimate the DF parameters. It is shown how the digital filters are derived for an embedded object using a fine meshed simulation of the object. The digital filters are then used in a special node of a coarser mesh to represent the embedded object. In the way a significant computational saving can be made. Moreover, the comparisons in time-domain, frequency-domain and computational costs are given.

The technique is illustrated by an example of a metal conductor in a TLM model as shown in Fig. 1. In the example, the digital filters of the objects are individually obtained. It is shown how these can be combined to provide a complete representation of the object comprising joined individual objects. The accuracy and computational efficiency of this approach is then assessed.

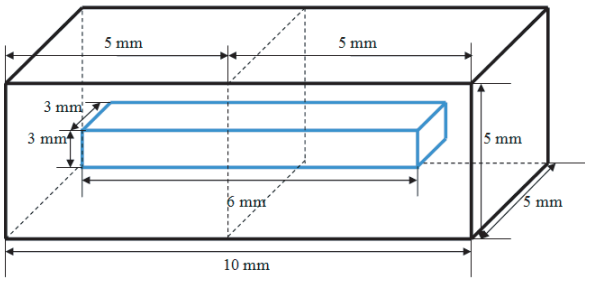

Figure 1: A metal conductor (blue box) in the fine mesh model with space-step of 1 mm $\Delta l = 1$ mm.

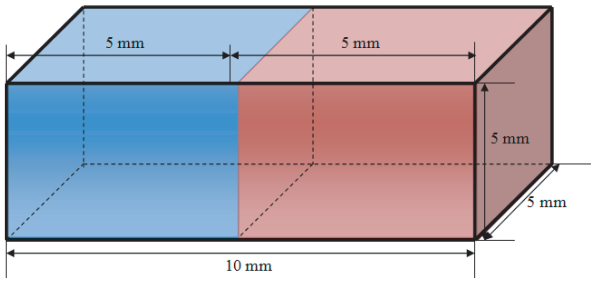

Figure 2: Two different coarse mesh nodes embedded with digital filters (blue and red boxes) in the coarse mesh model with space-step of 5 mm $\Delta l =$ 5 mm.

REFERENCES

1. Brittingham, J. N., E. K. Miller, and J. L. Willows, "Pole extraction from real-frequency information," *Proc. IEEE*, Vol. 68, 263–273, Feb. 1980.

Synthesis of Composite Materials with Conductive Aligned Cylindrical Inclusions

M. H. Nisanci, F. de Paulis, D. Di Febo, and A. Orlandi
UAq EMC Laboratory, University of L'Aquila, L'Aquila, Italy

Abstract— Many of our modern technologies today require materials with complex performances in terms of both electric and mechanical properties. These features can be achieved with unusual combinations of properties that cannot be met by conventional homogeneous materials, but they are rather obtained combining different materials together, obtaining the so called composite structures. These materials have many advantages allowing for high design flexibility, since they can be adapted to achieve complex shapes and ad-hoc strength levels, providing sound and heat isolations, as well as achieving electromagnetic protection. Electromagnetic shielding is one of the main concerns for electrical engineers designing enclosures containing complex electronic systems. The electronics, in fact, can be sensible to the surrounding EM environment, and also because it can act as noise source, to be dampened for avoiding EM interference toward other systems around it.

Previous studies are focused on analyzing the EM properties of composites getting the electrical permittivity ε_{eff} of an equivalent homogeneous medium from their physical dimensions and electrical properties by using some mixing rules (i.e., Maxwell Garnett approximation). Then the frequency dependent ε_{eff} can be employed in numerical 3D EM simulators to compute the shielding performances of such materials. [1,2].

This work is focused on the synthesis of composites consisting of a host material with aligned cylindrical inclusions. The aim of this study is to extract the physical dimensions of the composite constituents such as inclusion diameter and length, starting from the shielding effectiveness performance related to a known homogeneous material, and from additional constrains in terms of host and inclusion materials to be employed. The step-by-step procedure is summarized in Fig. 1.

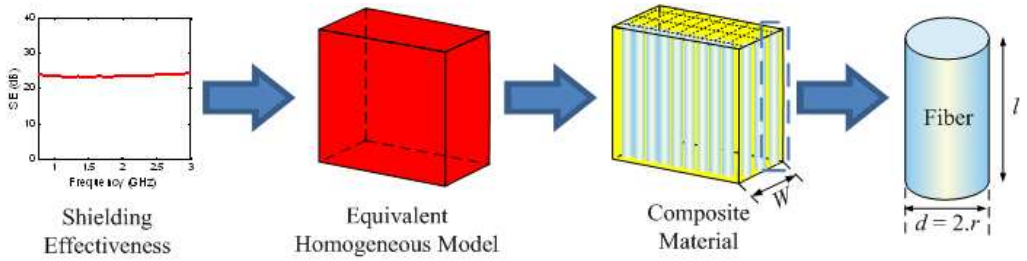

Figure 1: Flowchart for synthesis of aligned cylindrical composite slabs.

REFERENCES

1. Koledintseva, M. Y., J. L. Drewniak, R. E. DuBroff, K. N. Rozanov, and B. Archambeault, "Modeling of shielding composite materials and structures for microwave frequencies," *Progress In Electromagnetics Research B*, Vol. 15, 197–215, 2009.
2. Xu, X., A. Qing, Y. B. Gan, and Y. P. Feng, "Effective properties of fiber composite materials," *Journal of Electromagnetic Waves and Applications*, Vol. 18, No. 5, 649–662, 2004.

Efficient Embedding of Thin Sheet Models in TLM Simulations

Xuesong Meng, Phillip Sewell, Ana Vukovic, and Trevor M. Benson
The University of Nottingham, UK

Abstract— Carbon fibre composite (CFC) materials have received considerable recent attention in the spacecraft and aircraft industries due to their high strength-to-weight ratio and ease of fabrication [1]. Since CFC panels are very thin ($\sim 1\,\text{mm}$) in comparison to wavelengths of interest, a very fine mesh is required when performing electromagnetic simulation using traditional numerical methods. This incurs large runtime and memory usage. This paper presents a new approach for embedding the thin sheet models in an otherwise coarse grid, thus relaxing the mesh requirements. This is done in the numerical Transmission Line Modelling (TLM) method [2] and uses a digital filter theory approach. The method is suited for single and multiple CFC panels.

In this model, a one-dimensional (1D) CFC single- or multi-layered panel is inserted into the TLM mesh as a section of transmission line, see Fig. 1, with the aim to get the relations between incident and reflected voltages at the input and output of the panel. Known analytical expansions for the cosecant and cotangent terms in the CFC admittance matrix are implemented using digital filter theory, and the transition to the time domain is obtained using a Z-transform. The final matrix is solved using a Gauss-Seidel method which is suitable for large matrix problems. As an example, Fig. 2 shows reflection and transmission coefficients for a three-layered CFC panel for different numbers of expansion terms in the digital filters, N, and compares them with exact results obtained from a network approach in the frequency domain. The TLM results show excellent agreement with the exact ones, especially when higher order filters are used.

The model implementation and the impact of model parameters on accuracy will be discussed in the presentation.

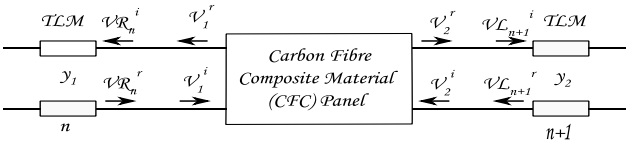

Figure 1: Single layered CFC model.

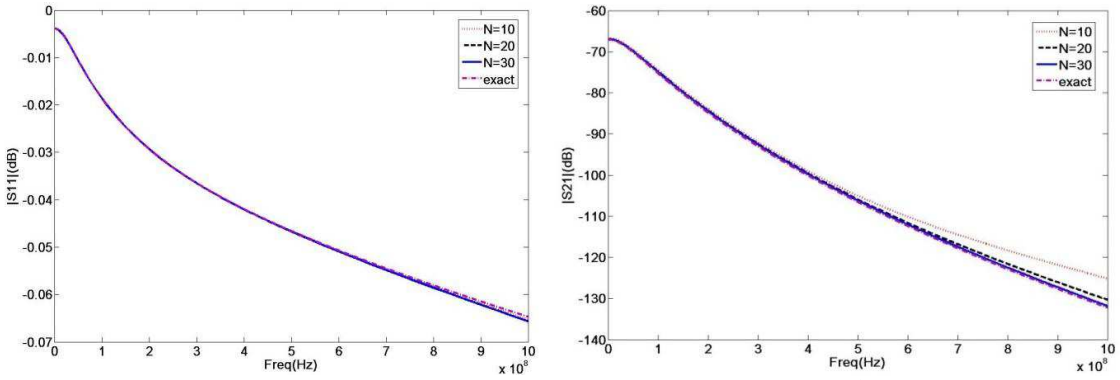

Figure 2: (a) The reflection coefficient (b) the transmission coefficient of three layered CFC panel. The first layer and third layer have the same parameters with $\varepsilon_{r1} = 4.56$, $\sigma_{e1} = \frac{2kS}{m}$, $d = 1\,\text{mm}$ and the parameters of the second layer are $\varepsilon_{r2} = 4.56$, $\delta_{e2} = \frac{8kS}{m}$, $d = 1\,\text{mm}$.

REFERENCES

1. Sarto, M. S., "A new model for the FDTD analysis of the shielding performances of thin composite structures," *IEEE Transactions on EMC*, Vol. 41, No. 4, 298–306, November 1999.
2. Christopoulos, C., *The Transmission-line Modeling Method TLM*, IEEE Press, New York, 1995.

Analyzing Effects of Mobile Dipole Speed on Survey Data via Forward Modeling Technique

Nazabat Hussain, Norashikin Yahya, M. N. Karsiti, and Zainal A. Burhanuddin
Department of Electrical and Electronic Engineering, Universiti Teknologi Petronas
Bandar Seri Iskandar, Tronoh 31750, Perak, Malaysia

Abstract— Controlled-source electromagnetic (CSEM) survey has be used for hydrocarbon exploration in marine environment. This technique utilizes a mobile EM transmitter that is moved above the seafloor and fixed grounded receivers. In such scenarios, excited EM energy comes to the region of interest from a distant source and it terminates along the direction of propagation. Only reflected fields would be received at receivers which contain information of earth interior. Using electric and magnetic fields value collected from an EM survey, the spatial distribution of seabed layers can be mapped through inversion technique. However, the accuracy of the seabed mapping depends on the quality of the survey data. There are several factors affecting the survey data; such as source-receiver geometry, source signal strength, seawater depth and geological complexities. This paper presents a method of finding optimum speed of a mobile dipole source in marine CSEM survey, one of the factor affecting the survey data. The technique involved numerical solution of forward modelling using staggered-grid finite difference in spatial domain and forward time central space in temporal domain. Solution is achieved through a) an optimal grid technique that extends the boundaries of the mesh outward from the region of interest using a minimal number of nodes, b) a direct matrix solution technique that allows for the simultaneous solution for all sources. The simulation results from 1D model indicates that the speed of a mobile dipole source should be set at a 10 nautical mile ($\approx 18.52\,\mathrm{km}$) or less in order to get high quality data. Increasing the dipole speed will cause the dipole position to change more rapidly and hence, gives poor quality survey data.

Numerical Solution of BLT Equation for Inhomogeneous Transmission Line Networks

M. Oumri, Q. Zhang, and M. Sorine
INRIA Paris-Rocquencourt, France

Abstract— The Baum-Liu-Tesche (BLT) equation [1] is widely used for the modeling and analysis of complex transmission line networks, such as wired telecommunication networks and power lines in automotive vehicles, railway infrastructures, aircrafts, etc.. The original BLT equation for networks with homogeneous transmission lines has been generalized to the case of inhomogeneous transmission lines in [2]. This generalized BLT equation is parameterized by the propagation matrices of inhomogeneous transmission lines and by the scattering matrices at network nodes. However, it is not indicated in [2] how these propagation and scattering matrices can be computed from the structural specification of a network and from the inhomogeneous characteristic parameters of the transmission lines constituting the network. For the purpose of numerical simulation and analysis, a *fully automatized method* is proposed in the present paper to solve the non trivial problem of the computation of the propagation and scattering matrices. The existence and uniqueness of a solution to the generalized BLT equation are also studied. A new convention for the notations involved in the generalized BLT equation is also introduced to facilitate the implementation of the automatized approach to network simulation through the construction and numerical solution of the generalized BLT equation.

On each transmission line connecting two nodes of a network, two waves of opposite directions are defined as linear combinations the voltage and the current along the line. The BLT equation is the collection of wave propagation equations on each line and of wave scattering equations at each node, usually written in a compact form with super wave vectors, super propagation and scattering matrices.

In this paper, a fully automatized method is presented for the computations of the propagation matrices and of the scattering matrices from the specification of the topological structure of a network and from the *inhomogeneously* distributed resistance, inductance, capacitance and conductance (RLCG) characteristic parameters of all the transmission lines. It is shown that the propagation and scatterig matrices are independent of the choice of the directions of the currents in transmission lines, despite the fact that the definition of the two opposite waves on each line (as linear combinations of voltage and current) depends on the chosen current direction. It is then possible to compute the propagation and scatterig matrices with some local convention for current directions on each line and at each node, without taking care of the consistency between all the local choices in a network. The automatized computation method is greatly simplified thanks to these well defined local conventions. The computation of the scattering matrices has been partially inspired by the results reported in [3].

REFERENCES

1. Baum, C. E., T. K. Liu, and F. M. Tesche, "On the analysis of general multiconductor transmission line networks," *Interaction Notes*, Vol. 350, November 1978.
2. Baum, C. E., "Generalization of the BLT equation," *Interaction Notes*, Vol. 511, April 1995.
3. Parmantier, J.-P., "An efficient technique to calculate ideal junction scattering parameters in multiconductor transmission line networks," *Interaction Notes*, Vol. 536, February 1998.

Quasi Dispersion Curve And Its Bandwidth in Coupled Resonator Optical Waveguides

Chih-Hsien Huang[1, 2], **Wei-Shuo Li**[1], **Jing-Nuo Wu**[3], **Wen-Feng Hsieh**[1], **and Yia-Chung Chang**[2, 1]

[1]Department of Photonics, National Chiao Tung University, Hsinchu 300, Taiwan
[2]Research Centre for Applied Sciences, Academia Sinica, Taipei 115, Taiwan
[3]Department of Physics, Chinese Culture University, Taipei 111, Taiwan

Abstract— The dispersion relation of the coupled resonator optical waveguide (CROW) made in a photonic-crystal slab (PCS) is not well-defined due to the leakage of the electromagnetic wave into the air. (i.e., it has finite lifetime) By using the stabilization method, we obtain the finite spectral width of the CROW guided mode, which typically has a high quality factor, so the EM wave can still propagate in the CROW with low leakage into the air. When properly choosing the simulation cell to avoid strong interaction with the unconfined modes, the dispersion curve of the guided mode become less sensitive to the simulation cell dimension and its approximate dispersion curve can be obtained. For the CROW made of dielectric rods, the dispersion curve of the guided mode is nearly parallel to the 2D counterpart. However, for the CROW made of air holes, it is no longer the case due to different localization of the EM wave in the defects. When the defect holes are shrunk or replaced by a dielectric rod, the CROW becomes a double-mode waveguide with different group velocities for the two guided modes (one longitudinal and one transverse). The longitudinal mode is found to have larger group velocity because of the stronger coupling between two adjacent defects. These simulation results for the PCS CROWs provide important information for designing practical devices such as slow-light optical waveguides and nonlinear photonic devices.

ACKNOWLEDGMENT

Work support in part by X-Photonics Interdisciplinary Center of National Chiao Tung University and the National Science Council of the Republic of China under grants NSC99-2112-M006-017-MY3, NSC99-2221-E009- 095-MY3, and NSC 98-2112-M- 001-022-MY3.

Improvised PEEC Method in the Modeling of the Near-field Coupling with Electrical Cable

E. R. Rajkumar, **M. Bensetti**, **B. Ravelo**, **and M. Kadi**
Institut de Recherche en Systèmes Electroniques Embarqués (IRSEEM)
EA 4353, 76801 Saint Etienne du Rouvray, France

Abstract— In the modern automotive electronic system cables play a major role for the reliability due to the integration density [1, 2]. In power electronic system transmission and energy conversion, electrical cabling is an indispensable part. To study the susceptibility of these cables due to external electromagnetic (EM) perturbation, several numerical methods have been developed. This paper describes a technique for obtaining integrated near-field (NF) coupling Partial Element Equivalent Circuit (PEEC) model for the electromagnetic compatibility (EMC) issues. It incorporates EM coupling due to electronic components and cables with/without ground plane along with its capabilities of transforming field based problem into the circuit domain. Elementary dipoles are used to calculate the EM field, which represents modeling of electronic components radiation [3]. The proposed approach is demonstrated by analyzing a cable above the ground plane and with elementary dipoles as source of disturbances. It is being carried over with Finite Element Method (FEM) and then Finite Integration Technique (FIT). The results obtained by both the methods are in good agreement. In order to validate the obtained results, the test set up is being built by analytical TLM models [4, 5]. The developments of 2D and 3D dimensional dipole are being integrated into the PEEC method.As perspective, coupling PEEC [6] model could be developed considering inductive and capacitive coupling between the cable, ground plane and devices.

REFERENCES

1. Shin, J., "Automotive EMC standards and testing," *Tutorial Workshop Digests on "Introduction to Automotive EMC Testing" at the 2011 APEMC*, Jeju, S. Korea, May 2011.
2. Liu, K., "An update on automotive EMC testing," *Microwave Journal*, Vol. 54, No. 7, 40–46, Jul. 2011.
3. Fernández López, P., A. Ramanujan, Y. Vives Gilabert, C. Arcambal, A. Louis, and B. Mazari, "A Radiated emission model compatible to a commercial electromagnetic simulation tool," *20th Int. Symp. EMC*, 369–372, Zurich, Switzerland, Jan. 2009.
4. Atrous, S., D. Baudry, E. Gaboriaud, A. Louis, B. Mazari, and D. Blavette, "Near-field investigation of the radiated susceptibility of printed circuit boards," *2008 Int. Symp. EMC Europe*, Hamburg, Germany, Sep. 8–12, 2008.
5. Leseigneur, C., P. F. Lopez, C. Arcambal, D. Baudry, and A. Louis, "Near-field coupling model between electronic systems and transmission line," *IEEE Int. Symp. EMC*, 22–27, Fort Lauderdale, FL, USA, Jul. 25–30, 2010.
6. Ekman, J., G. Antonini, and A. E. Ruehli, "Toward improved time domain stability and passivity for full-wave PEEC models," Special Session at the *IEEE Int. Symp. on EMC*, Portland, USA, 2006.

Session 2A8
Poster Session 2

The Scattering Property Analysis of Metamaterials-coated Object Based on FDTD

Shi-Quan Zhang
Engineering University of CAPF, Xi'an, Shaanxi 710086, China

Abstract— In recent years, there has been a growing interest for the study of target stealth technique, while the special properties of left-handed metamaterials with negative values of permittivity and permeability exhibit brilliant prospect for applications in target stealth. In this paper, the electromagnetic scattering properties of the object such as metamaterial-coated metallic circular cylinder are analyzed and discussed by using finite-difference time-domain method (FDTD) based on Drude model.

The constitutive parameters of metamaterials are the function of frequency, hence, metamaterials are surely dispersive media. Their effective permittivity and permeability can be expressed in terms of lossy Drude model as follows:

$$\varepsilon(\omega) = \varepsilon_0\varepsilon_r(\omega) = \varepsilon_0\left(1 - \frac{\omega_{pe}^2}{\omega(\omega + \mathrm{j}\Gamma_e)}\right),$$
$$\mu(\omega) = \mu_0\mu_r(\omega) = \mu_0\left(1 - \frac{\omega_{pm}^2}{\omega(\omega + \mathrm{j}\Gamma_m)}\right).$$

The following electromagnetic field equations are derived and obtained by applying Maxwell's vortex equations and time-frequency relation:

$$\nabla \times H = \varepsilon_0\frac{\partial E}{\partial t} + J_e,$$
$$\nabla \times E = -\mu_0\frac{\partial H}{\partial t} - J_m,$$
$$\frac{\partial J_e}{\partial t} + \Gamma_e J_e = \varepsilon_0\omega_{pe}^2 E,$$
$$\frac{\partial J_m}{\partial t} + \Gamma_m J_m = \mu_0\omega_{pm}^2 H.$$

The above equations are discretized, two-dimensional recursive formulas are derived, and FDTD programs for both the metallic and metamaterial-covered targets are compiled. The radar cross sections (RCS) for metallic and metamaterial-coated metallic circular cylinders are computed. It is demonstrated that the backward scattering is reduced greatly within a wide range of frequency band when the target is coated with metamaterials. Therfore, it is obvious that the metamaterials take an active role in stealth applications.

Multilayered Periodic Structures — Tunneling and Electromagnetic Curtain Effects

R. Lech, **A. Kusiek**, **and J. Mazur**
Gdansk University of Technology, Poland

Abstract— The scattering and tunneling properties of multilayered periodic arrangement composed of frequency selective surfaces (FSS) is presented. The structure under investigation is composed of a multilayered arrays of uniformly spaced identical sections situated in a free space and illuminated by a plane wave. Such structures possess a stop band in their transmission characteristics and therefore are called electromagnetic band gap (EBG) or photonic band gab (PBG) structure. The constructive elements of these structures are comparable in size to the operation wavelength and may be composed of different media. In the presented approach the unit cell contains cylindrical metallo-dielectric objects of arbitrary cross section or a set of objects each of which is described by its isolated **T**-matrix. In the case of multiple objects in a unit cell we use the ISP procedure [1] to calculate the aggregated $\mathbf{T}_{\mathrm{a}}$-matrix which then represents the whole unit cell. Assuming the direction of electromagnetic plane wave incidence to be normal to the cylinder axis, the problem is reduced to a two-dimensional one and therefore the incident polarization may be decomposed into the two fundamental polarizations: TM and TE relative to the posts axis. In order to calculate a multimodal scattering matrix of a periodic array of cylindrical scatterers we utilize an efficient numerical technique described in [2] which is based on the transmission matrix approach and uses the lattice sums technique [3]. In our approach, we calculate the scattering matrix of N-layered structure by cascading the scattering matrices of each periodic array and the scattering matrices of free space, defined utilizing the decaying space harmonic components, which include the spacing between the layers.

In a layered system, the multiple interaction of space harmonics scattered from each of the array layers modifies the frequency response, and bandgaps or stopbands in which any electromagnetic wave propagation is forbidden are formed. With the layered medium composed of irregular cross-section posts we obtained the effect called an electromagnetic curtain by rotating the posts in the stack. This effect allows to control the transmission of polarized wave of one kind though the periodic structure, while the wave with orthogonal polarization is blocked. Another interesting case of band shifting can be observed for the structures with the whole layers rotated with respect to each other. For the same plane wave illuminating both configurations, they produce stop bands which only slightly overlap. When half of the structure are being rotated with respect to the other half one obtains the effect of stop band shifting. The stop bands, which are almost identical in width, can be shifted from one bandwidth to another.

An interesting effect of wave tunneling can be obtained in the structure under investigation. This effect, along with the "growing evanescent envelope" for field distributions, was previously observed in metamaterial medium and a structure composed of a pair of only-epsilon-negative and only-mu-negative layers. It can be seen that a complete electromagnetic wave tunneling may be achieved through a pair of different stacked FSSs which are characterized by dual behaviors, even though each stack is completely alone opaque (operates in its stop band). The effect can be obtained for the structure composed of a pair of identical stacks of periodic arrays of cylindrical posts rotated by 90° with respect to each other. This effect can also be controlled by introducing a gap between the stacks.

ACKNOWLEDGMENT

This work was supported by the Polish Ministry of Science and Higher Education under Contract N515 501740, decision No. 5017/B/T02/2011/40.

REFERENCES

1. Polewski, M. and J. Mazur, "Scattering by an array of conducting, lossy dielectric, ferrite and pseudochiral cylinders," *Progress In Electromagnetics Research*, Vol. 38, 283–310, 2002.
2. Kushta, T. and K. Yasumoto, "Electromagnetic scattering from periodic arrays of two circular cylinders per unit cell," *Progress In Electromagnetics Research*, Vol. 29, 69–85, 2000.
3. Yasumoto, K. and K. Yoshitomi, "Efficient calculation of lattice sums for freespace periodic greens function," *IEEE Trans. Antennas Propag.*, Vol. 47, No. 6, 1050–1055, 1999.

Mutual Impedance Probes as Diagnostic Tools for Space Plasmas

J. G. Trotignon and J. L. Rauch
LPC2E/CNRS, 3A av. de la Recherche Scientifique, 45071 ORLEANS Cedex 2, France

Abstract— A technique, used in geophysical prospection to measure the ground permittivity, has been successfully transposed to space plasmas. The basic principle is to measure the self impedance of a single electric antenna or the mutual impedance between two sets of Hertz dipoles. Since the impedance of the probe depends on the dielectric properties of the medium in which the probe is immersed, characteristics of this medium such as the density and temperature of thermal electrons can be determined. As a bonus, natural waves are also investigated in a large frequency range.

The quadripole probe technique has been used for many years on sounding rockets and spacecraft (GEOS-1, GEOS-2, VIKING, ARCAD/AUREOL-3, MARS-96). Electric-field impedance measurements will also be made on ROSETTA and BepiColombo and have been proposed as part of the Radio and Plasma Waves Investigation for the EJSM/JGO Cosmic Vision mission candidate.

To illustrate the capabilities of this technique, results obtained by the Mutual Impedance Probe, MIP, onboard ROSETTA will be shown. MIP and the 4 other instruments of the ROSETTA Plasma Consortium, RPC, were switched on during the three Earth swingbys, in early March 2005, mid-November 2007, and mid-November 2009. Calibration and general testing were the main objectives, nevertheless valuable observations of the Earth's space environment have actually been made, in particular by the MIP, in the plasmasphere, the cold and high electron-density region dominated by the Earth's magnetic field.

Measurement of the Electric Thunderstorm Lightnings and TLEs Signatures by IME-HF Instrument on Board TARANIS Satellite

J. L. Rauch[1], **O. Santolik**[2], **I. Kolmasova**[2], **J. Chum**[2], **F. Hruska**[2], **and L. Uhlír**[2]

[1]LPC2E, 3A av. de la Recherche Scientifique, 45071 Orléans Cedex 2, France
[2]Institute of Atmospheric Physics AS CR, Prague, Czech Republic

Abstract— The observations of red sprites, blue jets, elves, sprite halos, gigantic jets, etc, named Transient Luminous Events (TLEs) and the observations of Terrestrial Gamma ray Flashes (TGFs) have pointed out the existence of impulsive transfers of energy between the Earth atmosphere and the space environment. Possible electromagnetic signatures of electron acceleration processes have been investigated. Many authors have shown that relativistic runaway electron beams driven by intense lightning-generated Quasi-Electrostatic (QE) fields may undergo intense interactions with the background magnetospheric plasma, leading to rapid nonlinear growth of Langmuir waves. Intense radio emissions in the range of several MHZ up to tens of MHZ are predicted to be produced by runaway electrons or by a simultaneous effect of runaway breakdown and extensive atmospheric showers. Plasma physics offer other interactions and so other potential signatures like the production of lower hybrid waves. TIPPs (Trans Ionospheric Pulse Pairs) have been frequently observed by the FORTE satellite.

TARANIS is a satellite of the french space agency (CNES) dedicated to study the thunderstorm lightings and TLEs to have a comprehensive understanding of the energy transfer between atmosphere-ionosphere and magnetosphere region. TARANIS scientific payload consists in a complex package of instruments, in particular the (Instrument de Mesure Electrique Haute Frequence) IME-HF experiment proposed to measure the wave electric field in the frequency range from 100 kHz up to 35 MHZ. The aim of IME-HF experiment is to characterize the properties of lightnings and TLEs signatures. The experiment is composed of electric sensors and on board analyzer. Several kinds of signals can be recorded as waveform and filters bank. In this presentation, we propose to described the capability of the IME-HF experiment and the strategy of measurement and how TARANIS payload is integrated taken as a whole.

Analysis of Near-field Optical Disk with a Circular Aperture

T. Kitamura
Faculty of Engineering Science, Kansai University, Japan

Abstract— The capacity of optical storage system has been improved by shortening wavelength, or increasing the numerical aperture of an objective lens. However, the recording density of conventional optical recording systems has a limitation due to optical diffraction limit. Recording methods based on near-field optical principles have stimulated much interest in optical storage technologies because they have potential to overcome the limitation by writing and reading recording marks using a localized optical near-field. In order to achieve high throughput of optical near field many types of nano-apertures and nano-antennas have been considered. For example, a triangular bulge-shaped antenna for granular recording media, an aperture with periodic metal gratings, and a metallic slit aperture with rectangular holes have been investigated. Figure-eight, bow-tie and cross shaped apertures have been studied. Nano-rings made of silver spheres have also been proposed.

In this paper, a phase change disk illuminated by near-field optical light through a circular nano-aperture is analyzed by using three-dimensional FDTD method into which motion equations of free electrons are installed to analyze a metallic material. We consider installing metal ridges into the circular aperture in order to enhance transmission of optical near field. Electromagnetic field distributions of optical near-field around the aperture and far-field scattering patterns from the phase change disk are analyzed. Cross-talk characteristics between plural recording marks are also investigated.

GMI Effect in Thin Amorphous Microwires for Sensors and Tuneable Metamateriales Applications

A. Zhukov[1,2], **M. Ipatov**[1], **and V. Zhukova**[1]

[1]Dpto. Fís. Mater., Fac. Químicas, UPV/EHU, San Sebastián 20018, Spain
[2]IKERBASQUE, Basque Foundation for Science, Bilbao 48011, Spain

Abstract— Giant magneto-impedance effect (GMI) consisting of large sensitivity of the impedance of soft magnetic conductor on applied magnetic field attracted great attention owing to possibilities of application in magnetic sensors and smart metamateriales [1-3]. Most attractive feature of GMI effect is enhanced magnetic field sensitivity suitable for low magnetic field detection. Highest GMI effect is observed in ferromagnetic magnetically soft wires (especially of amorphous and nanocrystalline origin) [1–3].

It is worth mentioning, that in most of recent applications an enhanced frequency range, high linearity of MI dependence and low hysteresis are required [4, 5]. Anti-symmetrical MI curve with linear region has been obtained in current pulsed excitation scheme of wires using detection of off-diagonal GMI component and quite useful for real GMI sensors development [4, 5]. At the same time we have recently showed, that linearity and shape of off-diagonal component in microwires can be tailored by thermal treatment [3]. Considerable GMI hysteresis has been observed and analyzed in microwires possessing helical anisotropy [6], although enhanced magnetic field sensitivity of the GMI effect in amorphous wires is related to specific outer domain structure in the surface area [1–3]. On the other hand, stress-impedance effect is quite useful for applications in tuneable metamateriales [7].

In this paper we studied the GMI effect (GMI ratio, $\Delta Z/Z$, diagonal Z_{zz} and off-diagonal impedance tensor $\zeta_{\phi z}$ components) at elevated frequencies and it correlation with hysteretic magnetic properties in ultra-thin amorphous glass-coated microwires with vanishing magnetostriction constant. The origin of the MI hysteresis and the method of its suppressing are discussed.

REFERENCES

1. Panina, L. V. and K. Mohri, *Appl. Phys. Lett.*, Vol. 65, 1189, 1994.
2. Beach, R. and A. Berkowitz, *Appl. Phys. Lett.*, Vol. 64, 3652, 1994.
3. Zhukova, V., M. Ipatov, and A Zhukov, *Sensors*, Vol. 9, 9216, 2009.
4. Mohri, K. and Y. Honkura, *Sensors Letters*, Vol. 5, 267, 2007.
5. Sandacci, S. I., D. P. Makhnovskiy, L. V. Panina, K. Mohri, and Y. Honkura, *IEEE Trans Magn.*, Vol. 35, 3505, 2004.
6. Ipatov, M., V. Zhukova, A. Zhukov, J. Gonzalez, and A. Zvezdin, *Phys. Rev. B*, Vol. 81, 34421, 2010.
7. Zhukov, A., *Adv. Func. Mat.*, Vol. 16, 675, 2006.

Effect of Ionospheric Macroscale Inhomogeneities on Radiosignals under Conditions of High-frequency Oblique Heating

Yu. K. Kalinin[1] and N. P. Sergeenko[2]

[1]Fedorov Institute of Applied Geophysics, Moscow, Russia
[2]Pushkov Institute of Terrestrial Magnetism
Ionosphere and Radiowaves Propagation, Moscow, Troitsk, Russia

Abstract— The basic properties of macroscale ionospheric inhomogeneities with horizontal sizes of the order of 1 thousand km and lifetime of more than 10^4 s, traveling over a distance of up to 10 thousand km at a nearly sonic velocity, are considered. The occurrence frequency of such objects varies from 0.05 to 0.3 and is characterized by the Poisson law. The results characterizing the effect of macroscale inhomogeneities on various radiosignals during sounding of the ionosphere in the HF ranges are presented. In the present paper, we mainly considered the radiophysical effects of the presence of macroscale inhomogeneities in the ionosphere using, as an example, vertical sounding, under natural conditions and under conditions of disturbance by oblique HF heating.

Under the oblique action of a narrow powerful high-frequency (HF) radiowave beam on the ionosphere, several new features of the listed signals may arise. These features can be interpreted in terms of macroscale inhomogeneities in the ionosphere. What we mean here are the series of unique experiments carried out in 1971–1973. Thus, the hypothesis of a macroscale instability of the ionosphere takes hold; i.e., the ionosphere can form macroscale long-living inhomogeneities of the electron density spontaneously and under the action of "shock" external sources. For oblique HF heating of the ionosphere, it should be stressed that the ionogram deformations take place also after chemical explosions in the ionosphere and after earthquakes. In all cases, the ionospheric critical frequency varies. Some results of high-frequency oblique heating of the ionosphere are interpreted in terms of macroscale inhomogeneities originating as a result of anthropogenic effects on near-Earth space.

Spectral Switches of a Circular Aperture with Pockels Effect

Hsun-Ching Hsu and Pin Han
Graduate Institute of Precision Engineering, National Chung Hsing University
250 Kuo Kuang Road, Taichung 402, Taiwan, R.O.C.

Abstract— In this work, we show that the spectral switches of a circular aperture can be controlled by the so call Pockels effect (Electro-optic effect), which has the advantage of high speed compared with traditional ways (e.g., aperture control mechanism or light source property control mechanism). First the Fresnel diffraction integral is used to derive the analytic expression for the diffracted spectral intensity. Then the numerical results illustrate the effect of Pockels effect on the spectral switches, which includes the red shift and blue shift of the spectrum maximum. It is also shown that this electro-optic way can be developed into a data transmission scheme in free space.

Background Field Modeling for Ionospheric Ion Temperature Based on DEMETER Satellite Data

Lingli Tang[1], **Chuanrong Li**[1], **Xianfeng Song**[2], **Bo Yuan**[1], **Lingling Ma**[1], **and Xinhong Wang**[1]

[1]Academy of Opto-Electronics, CAS, China
[2]Graduate University of Chinese Academy of Sciences, China

Abstract— With the development of earth observing remote sensing techniques, it has been becoming a novel way to do the short-term/impending earthquake prediction that capture ionospheric abnormalities from electromagnetic satellite data and then extract earthquake precursory information. However, the ionosphere is heavily affected by solar radiation and Earth magnetic field. Only after removing those background signals away from satellite observed physical abnormal signal, true abnormalities related to seismic activities can be obtained. So, it is an essential work to establish a background field reflecting the changes of various seismic unrelated features in the ionosphere. This paper presents an advanced time-series analysis approach to modeling the background filed of ionospheric ion temperature (Ti) using DEMETER (Detection of Electro-Magnetic Emission Transmitted from Earthquake Regions) earth-observing dataset. First, by analyzing the relationship between DEMETER satellite's revisit interval and the modeling longitude/latitude grid size, the $1.75^\circ \times 1.75^\circ$ grid is selected to divide the longitude/latitude range, which corresponds to nearly a 14-day revisit interval for the latitude 38°N regions. Then, the seasonal ARIMA (AutoRegressive Integrated Moving Average) model is applied to model the background field of ionospheric ion temperature. By making stationarity analysis and autocorrelation analysis of the time-series data, the period and other parameters of ARIMA prediction model are determined, and the prediction model of ionospheric ion temperature is established. The time-series is produced using the ionospheric ion temperature data between 2006 and 2008, and the data of 2009's first 16 weeks is used to validate the model. Final results indicate that the maximum relative error is less than 4.5% between predicted values and actual values, which indicates the proposed time-series model could well simulate the natural changing trend of ionospheric ion temperature through time, and can generate reliable ionospheric ion temperature background field.

UHF Propagation Prediction in Smooth Homogenous Earth Using Split-step Fourier Algorithm

Seyyed Reza Hosseini[1], **Reza Sarraf Shirazi**[1], **A. Kiaee**[1], **P. Pahlavan**[2], **and M. Sharifi Sorkherizi**[3]

[1]Wave Propagation & Microwave Measurement Research Lab., Department of Electrical Engineering Amirkabir University of Technology, 424 Hafez Avenue, Tehran 15914, Iran
[2]Sharif University of Technology, Iran
[3]Khajenasir University of Technology, Iran

Abstract— The electromagnetic wave propagation prediction in smooth homogenous earth is studied. This estimation employs Fourier Split-Step algorithm. The process of how parabolic equation and Fourier Split Step algorithm achieved, is investigated. Error resulted from this approximation is studied. Source modeling is analyzed. Simulations based on this method are illustrated on different values of frequency, range and antenna height.

Radio-frequency Spectrum of Radar Return Signal from Extended Targets

B. S. Yurchak
Goddard Earth Sciences & Technology Center
University of Maryland, Baltimore County, USA

Abstract— Remote sensing application for retrieving physical information about state and features of spatially extended geophysical target (SEGT) such as atmospheric clouds/rain and deep snow covers of polar terrains is of great importance in geophysics. Although the radar remote sensing reached significant progress, known kinds of analyzing of radar return signals from SEGT do not include an analysis of their radio-frequency spectrums (RFS). Radar return signal from the SEGT is a convolution of the radar probing pulse with the radial distribution of Slice Equivalent Length (SREL) of the SEGT. The SREL is the arithmetic sum of square roots of radar cross section of scatterers located close to the spherical wavefront of radar irradiance within a so-called "slice" at a given moment of time. Thus the return signal from spatially bounded SEGT is a group of overlapping RF-pulses each of which is caused by a reflection from a slice. The features of such signals are studied in the theory of communication and statistical radio-engineering. The aim of the paper is to show the primarily features of RFS and its possible application in remote sensing issue. The measurements were carried out by X-band weather radar and analog dispersive spectrum analyzer. The RFSs were observed from broad class of meteorological targets, which included clouds of different forms and rain of different intensities. The results indicate, on average, that RFSs have a bandwidth usually equal to the bandwidth of the probing pulse, independently on the spatial extension of meteorological object (duration of return signal). Simulation procedure included a generation of random spatial distribution of the SREL and probing pulse, calculations their convolution and the spectrum of a "return signal". The phase structure of simulated return signals was analyzed as well. Simulation of RF-spectrums verified the theoretical assessment of the cause of spectrum envelope oscillations as due to the intersignal phase statistics. On average, the envelopes and bandwidth of RFSs of meteorological echo-signals and probing radar pulse are coincided roughly, although individual spectrum envelopes of return signals demonstrate significant oscillations. A qualitative interpretation of the RFS shows that oscillations are caused by the correlation between the phases of the carrier wave over intervals equal to the probing pulse duration. Thus an individual meteorological echo-signal can be represented as a group of adjoining radio frequency pulses of the probe pulse duration with random initial phases. The depth and pattern of the oscillations depend on the rate and interval of the phase correlation and can be used as indicators of the spatial homogeneity of a meteorological target. It can be assumed that similar features are also inherent to the other kinds of the SEGT such as a thick snow slab, for instance. Since the base calibration principal requires the same distortion for a test-signal as for a real signal, the features of the RFSs obtained were used to calculate calibration errors for X-band weather radar and several kinds of calibration signals. The approach developed can be used for instrumental calibration of different kinds of geophysical radar as well.

Specular Radar Backscatter from a Planar Surface

Boris S. Yurchak
Goddard Earth Sciences & Technology Center
University of Maryland, Baltimore County, MD 21228, USA

Abstract— There are several altimeter backscatter models from a planar surface in incoherent approach. Nevertheless, the return signal often contains also the specular component then should be estimated under coherent (i.e., physical optics) approach. This paper presents an assessment of specular radar backscatter from a smooth and planar surface with arbitrary distributed Fresnel reflection coefficient taking into account the spherical nature of an incident electromagnetic wave. To calculate specular backscatter, an illuminated area on a surface is represented as a circular surface "aperture" excited by irradiation of elevated radar. Using such technique, the radar equation was derived in general form for an arbitrary distributed Fresnel reflection coefficient across a geophysical surface and Gaussian main lobe of antenna pattern. In particular case of constant reflection coefficient, the equation is represented in closed-form and coincides with the classical radar equation. Based on the general solution, we obtained the customary form of the equation specified for calculation the radar backscatter from an infinite surface and also from such spatially finite targets as a large disk and an annulus (their radii are compared or greater than the radius of the First Fresnel Zone). Formulas obtained can be applied to analyze the specular component of altimeter return signal. Since the solution takes into account an antenna size, it allows applying the results to real radar systems. Particular result for a large disk coincides with known field measurements. Certainly, the closed form of the equation for the spherical wave cannot be obtained for all possible spatial patterns of reflection coefficient distribution. However, basing on the evaluation undertaken in the work, the backscatter calculation can be completed numerically for any given distribution of reflection coefficient. The calculation technique of an area primarily contributed into specular backscatter is shown and illustrated with the example of a homogeneous planar surface. Contemporary characterization of the specular scattering properties with the backscatter coefficient, based on far field Radar Cross Section (RCS) concept, meets difficulties since RCS is defined only for point targets and assumed plane wave approach. It turns out to confusing result that RCS depends on the distance. Moreover, a size of an area, primarily contributed to the backscatter, depends on a pattern of spatial distribution of the reflection coefficient. The final conclusion drawn from this work is that the only Fresnel reflection coefficient is the correct parameter for describing specular scattering property of a geophysical surface. Basing on radar equation obtained, the methodological approach measuring the reflection property of a surface with unknown reflection capabilities by comparison with a reference surface was suggested and illustrated by exploring experimental data reported in the literature. The result obtained can be used as a base for further improvement of surface backscatter models.

A New Compact Size Fractal Based Microstrip Slot Antenna for GPS Applications

Jawad K. Ali[1], **Zaid A. Abed AL-Hussain**[2], **Ammer A. Osman**[2], **and Ali J. Salim**[1]

[1]Department of Electrical and Electronic Engineering, University of Technology, Baghdad, Iraq
[2]Department of Electrical Engineering, Al-Mustansiriya University, Baghdad, Iraq

Abstract— A circularly polarized single feed microstrip slot antenna has been introduced in this paper as a candidate for use in GPS applications. The slot structure of the proposed antenna has been created on the radiating patch in two steps. At first, a 45 degree rotated square has been etched at the center of the patch, and then a Sierpinski gasket type of the 3rd iteration occupies the resulting slot. The presented antenna has been fed with a single 50 Ohm probe. The position of the feed has been allocated in such away to produce the dual orthogonal modes required to produce the circular polarization radiation. The antenna has been designed to resonate at 1.575 GHz, L1 GPS band. Finite element simulations have been carried out to evaluate the performance of the modeled antenna using the HFSS v.11 EM simulator, from Ansoft. The resulting antenna has a slotted square patch with side length of about 40 mm. Simulation results show that it possesses impedance and axial ratio bandwidths of about 27 MHz and 22 MHz respectively, which meet the GPS L1 band requirement. Furthermore, the proposed antenna possesses satisfactory circular polarization radiation characteristics and gain. The antenna can be used for a wide variety of communication applications adopting circular polarization.

Simulation and Verification of Methods for Partial Discharge Source Localization

R. Myška and P. Drexler
Department of Theoretical and Experimental Electrical Engineering
Brno University of Technology, Kolejni 2906/4, Brno 612 00, Czech Republic

Abstract— This article deals with possibilities of localization of the partial discharges (PD) in oil power transformers. Localization can be performed on the basis of measured UHF waveforms analysis during activity of the partial discharges. The time-shifts of the waveforms related to transient process occurrence in the signals are the main input parameters for localization methods. In order to estimate the position of the signal source in the 3D space a minimum of four antennas has to be used, since the time of the PD is unknown. For localization purposes the system of nonlinear equations has to be solved. It can be performed by means of analytical or numerical methods. Both of the methods have their own advantages and disadvantages. The application of both approaches for signal source localization in measurement model will be presented in the paper. The methods will be compared in view of their suitability for a given configuration of antenna system.

ACKNOWLEDGMENT

The research described in the paper was financially supported by project of the BUT Grant Agency FEKT-S-10-13, by research plan No. MSM 0021630513 ELCOM and the grant of Czech ministry of industry and trade No. FR-TI1/001.

REFERENCES

1. Tang, J. and Y. Xie, "Partial discharge location based on time difference of energy accumulation curve of multiple signals," *IET Electric Power Applications*, Vol. 5, No. 1, 175–180, 2011, ISSN: 1751-8660.
2. Markalous, S. M., S. Tenbohlen, and K. Feser, "Detection and location of partial discharges in power transformers using acoustic and electromagnetic signals," *IEEE Transactions on Dielectrics and Electrical Insulation*, Vol. 15, No. 6, 1576–1583, 2008, ISSN: 1070-9878.

The Development of Methods for Estimation of Time Differences of Arrival of Pulse Signals

R. Myška and P. Drexler
Department of Theoretical and Experimental Electrical Engineering
Brno University of Technology, Kolejni 2906/4, Brno 612 00, Czech Republic

Abstract— This article deals with possibilities of detection of the impulse signals which are produced by partial discharges in oil power transformers. Possible methods of signal detection and their next processing are solved in the paper. One of the possibilities is electromagnetic waves sensing due partial discharges in UHF range. Suitable sensor can be realized in a form of antenna. It is important to determine the front transient process in analyzed signals. The basic method for transient identification is to track the crossing of threshold level. However, this method may fail in case when obtained waveform doesn't contain expressive front transients. One of the solutions can be the modification of the basic method which consists in the observation of immediate power waveform of the signal. The second possibility is to calculate rate of energy accumulation waveform. The energy of the signal is transferred from the sensing space through the antenna on the input impedance of the recording instrument. Another group of method is based on the signals cross-correlation which can also to indicate the relative time shift of signal waveforms. The work in the paper is focused on the application of suitable methods on data, which were acquired in the model of partial discharge detection system. The methods will be compared in view of their reliability and accuracy.

ACKNOWLEDGMENT

The research described in the paper was financially supported by project of the BUT Grant Agency FEKT-S-10-13, by research plan No. MSM 0021630513 ELCOM and the grant of Czech ministry of industry and trade No. FR-TI1/001.

REFERENCES

1. Yang, L., M. D. Judd, and C. J. Bennoch, "Time delay estimation for UHF signal in PD location of transformers," *Proceedings of Annual Report Conference on Electrical Insulation and Dielectric Phenomena*, Boulder, USA, 2004, ISBN: 0-7803-8584-5.
2. Tang, J. and Y. Xie, "Partial discharge location based on time difference of energy accumulation curve of multiple signals," *IET Electric Power Applications*, Vol. 5, No. 1, 175–180, 2011, ISSN: 1751-8660.

A Time Domain Analytic Solution for Finite and Perfectly Conducting Ellipsoidal Surface Illuminated by Transient Impulsive Plane Wave

Shih-Chung Tuan[1] **and Hsi-Tseng Chou**[2]

[1]Department of Communication Engineering, Oriental Institute of Technology, Pan-Chiao, Taiwan
[2]Department of Communication Engineering, Yuan Ze University, Chung-Li 320, Taiwan

Abstract— This paper presents an analytical and closed-form solution, based on a time domain (TD) physical optics (PO) approximation, for the fast analysis of transient scattering from a finite and perfectly conducting ellipsoidal surface when it is illuminated by a transient impulsive plane wave. An ellipsoidal surface is selected because it may resemble a variety of realistic surface such as spherical or parabolic surfaces. The integration of various finite ellipsoidal surfaces may be used to model a realistic scattering object such as an aircraft, which makes this solution more applicable to treat realistic problems in an effective fashion. This TD-PO solution can be further applied via a convolution to derive the early time transient fields scattered from the same scatterer that is illuminated by a realistic astigmatic finite-energy pulse. Physical appealing interpretation of wave phenomena in terms of reflection and diffraction mechanisms is also provided in the solution. Numerical examples are presented to demonstrate its physical phenomenon of the scattering mechanisms.

Omega-K Algorithm for Bistatic SAR Image Formation

C. Y. Dai and X. L. Zhang
University of Electronic Science and Technology of China, China

Abstract— Comparing to the common monostatic synthetic aperture radar (SAR), the bistatic SAR data are more challenging to process because of its complicated flight geometry. Although several bistatic SAR image formation algorithms have been presented, most of them are only able to handle azimuth-invariant bistatic configuration where the transmitter and receiver platforms are moving in parallel tracks with identical velocities. This paper proposes an Omega-K algorithm to handle a general case of bistatic SAR data. The two-dimensional frequency spectrum expression derived by the method of series reversion is rewritten to a new form with explicit geometric significance. Based on this new frequency spectrum expression, the frequency mapping function can be derived by making use of the multi-variable Taylor's theorem. After data mapping operation, the coupling between the range and azimuth can be eliminated, and the final focused image can be obtained using FFT technology. Numerical simulations are performed to validate the proposed algorithm.

The Object Position Detection and Tracing Using Bistatic Radar Network and Modified Hyperbolic Positioning Method

Tadeusz Nowak, **Mateusz Mazur**, **Andrzej Nalewaja**, **and Jarosław Pędziwiatr**
Przemysłowy Instytut Telekomunikacji S.A., Poland

Abstract— In that work, authors describe the bistatic receivers network's architecture and performance. The architecture of the system is presented focusing on main parameters of the system units like ATC (Air traffic Control) radar, synchronization receiver, bistatic receiver and functions of supervisory systems that collects, groups and process data obtained from all individual receivers. The architecture of recivers may vary, it may be low cost one channel receiver with omni or sector antenna or high end multichannel/multibeam solution both may find their utilization in bistatic radar network. The main aim of that paper is to describe modified hyperbolic positioning method (TDOA — time difference of arrival) used to estimate targets positions and trace them in case when three or more receivers detect object. In that method the time of receiving signal reflected from object illuminated by ATC radar is recorded. Such information from three or more receivers is processed to achive target location. Hyperbolic set of equations is solved in optimization process, where starting point is a mean value of obiect location obtained for all receivers in monopulse method. That allows for fast convergence in calculating target position. Simulation results obtained for bistatic receivers network and different scenarios prove that using TDOA method, the errors in position estimation are significantly reduced comparing to single bistatic receivers capabilities. The advantages of bistatic radar network are depicted. The most important are ability to extend range of ATC/PRS radar, increase sensitivity in restricted areas, ability to detect "stealth" objects and no electromagnetic emission of receiver. These advantages makes bistatic receivers a cheap and functional alternative comparing to other systems allowing to cover "blind zones" and sensitive areas.

The Effective 3D Modeling of Electromagnetic Waves' Evolution in Photonic Crystals and Metamaterials

A. V. Zakirov[1] and V. D. Levchenko[2]

[1]Moscow Institute of Physics and Technology, Russia
[2]Keldysh Institute of Applied Mathematics, Russia

Abstract— Up-to-date artificial optical devices and materials such as photonic crystals, metamaterials (Left-Handed Materials), streamlined surfaces are usually very complicated structures. Analytical calculations for propagation of electromagnetic waves in this media are possible only in simplest cases. On application of computational algorithms the difficulties appear due to large dimensions of calculation area. It results in necessity of effective algorithm development and realization for this calculations. "Effective" algorithm means such one, that has real rate coming up to theoretical. In the work the implementation of such algorithm is offered for Maxwell's equations' modeling.

In the capacity of difference scheme the Finite-difference time-domain method (FDTD) is used. For method of cell rounding (sequence of calculations) the Local-recursive nonlocal-anisochronous algorithm (LRnLA) is used, which makes possible to reach the high rate of program's effectiveness. The computational area contains of many Yee cells, that form the rectangular parallelepiped. This area is rounded from 5 faces by Perfectly Matched Layer (PML). So we can set absorbtion boundary conditions. In many cases, it is the necessary requirement for limited areas studying. At the 6th face there are the source and reflecting boundary conditions. In addition, the reflecting or periodic boundary conditions are available to set at the any face. It is developed the methods for modeling of the following media:

- The simple undispersion materials with real permittivity ε and magnetic permeability μ, which are depended only on the position in space.
- The media with dispersion described by Drude model.
- Anisotropic media.
- Nonlinear media.

The optimization the software package makes possible to use the advantages of modern processors for acceleration of calculations and allows to use many cores or processors in single calculations without descending of rate. The rate of calculations in all cases is nevertheless than 40% beside the theoretical estimation on the assumption of CPU clock and doesn't depend on capacity of analyzed data that is the computational area. Due to the such results we can use the existent program for modeling of many electrodynamics problems of today.

Implementation of Space-time Adaptive Processing (STAP) for Target Detection in Passive Bi-static Radar

Zia Ul Mahmood[1], **Mubashir Alam**[1], **Khalid Jamil**[2], **and Mohammed Elnamaky**[2]

[1]Department of Electrical Engineering, King Saud University, Riyadh, KSA
[2]Prince Sultan Advanced Technologies Research Institute (PSATRI)
King Saud University, Riyadh, KSA

Abstract— Target detection and tracking in passive bi-static radars (PBR) using Illuminators of opportunity have received significant interest mainly due to its covert operation and freedom in choosing from the available illuminators of opportunity. The major disadvantages of passive radar is the lack of control over transmitters and its parameters, and the presence of interferences such as direct path and multipath signals, due to which it requires advanced and sophisticated signal processing for the detection of targets. One way to effectively cancel these interferences is in the adaptation of Space Time Adaptive Processing (STAP) algorithm. STAP algorithm has been extensively applied to signals from pulse-Doppler active radars. This work explores the possibility of using STAP algorithm for target detection in passive bi-static radar, and specifically the FPGA implementation of STAP algorithm for real-time applications.

The feasibility of STAP for passive bi-static radar is first verified by using actual FM data captured with an array of eight sensors. Then a simulated target is inserted in the captured array data, and all the steps of STAP algorithm for bi-static passive radar are verified. These steps include mixing for STAP data cube formation, matched filtering and optimal match filtering, all in Matlab environment. Then all these algorithm steps will be implemented in FGPA environment using Viretx-6 platform, and specifically for real-time applications.

Fusion of Radar and Optical Images for Person Screening in Security Sensitive Environments

Nadia Fatihi, **Sebastian Hantscher**, **Stefan Lang**, **and Helmut Essen**
Fraunhofer Institute for High Frequency Physics and Radar Techniques, Germany

Abstract— Recent terror attacks showed the vulnerability of our public life. That is why, a lot of security systems have been developed; especially for person screening on airports. However, sometimes images with anatomic details are produced violating the human privacy rights. To avoid it, mostly stylised avatars are shown on which the locations of the detected prohibited items on the body are marked. This, however, gives only a coarse orientation. In this paper, a better way is proposed by fusing the images of a radar sensor and an optical sensor. The radar image is generated by a rotating millimetre wave FMCW radar operating between 96 GHz and 99 GHz. It consists of a one transmitter and five receivers in order to scan the person from different aspect angles. The RF front end consists of a monolithic microwave integrated circuit with a chip size of 2×3 mm. The circuit features coplanar technology and cascode HEMTs for compact size and low cost. The optical image is generated by a time of flight (ToF) camera system which is able to measure the distance between the camera and a reflecting point by measuring the elapsed time. Hence, the ToF principle is quite similar to a radar (active ranging system), that needs an illumination source. To measure the distances, the light has to be modulated adequately. Then, it is possible to evaluate it as the modulation of the back-scattered signal differs from that of the emitted one. Mostly, the near infrared area is used for this purpose, because it is invisible and simultaneously not harmful for the human eye. Both, optical and radar image are superimposed showing the exact location of concealed objects worn under the cloths. For this purpose, perspective distortions are removed by a complex mathematic model considering the dimensions and the physical inner structure of the CMOS ToF chip array.

A Study on Recognition of Similar Wire Targets Using E-pulse Technique

In-Sik Choi[1], **Seung-Jae Lee**[1], **Se-Hoon Park**[1], **and Edward J. Rothwell**[2]

[1]Department of Electronic Engineering, Hannam University, Daejeon, Korea
[2]Department of ECE, Michigan State University, MI, USA

Abstract— The complex natural resonance (CNR) frequencies can be used for radar target recognition. By SEM (singularity expansion method), the late-time measured response of a conducting radar target can be represented as a sum of natural resonance modes. An extinction-pulse (E-pulse) waveform is defined as a finite duration waveform which upon excitation of a particular radar target extinguishes a pre-specified portion of the target's natural mode spectrum. In this paper, we will show the results for target recognition of wire targets using E-pulse technique. Figure 1 shows the target geometry used for the simulations. As you can see, target

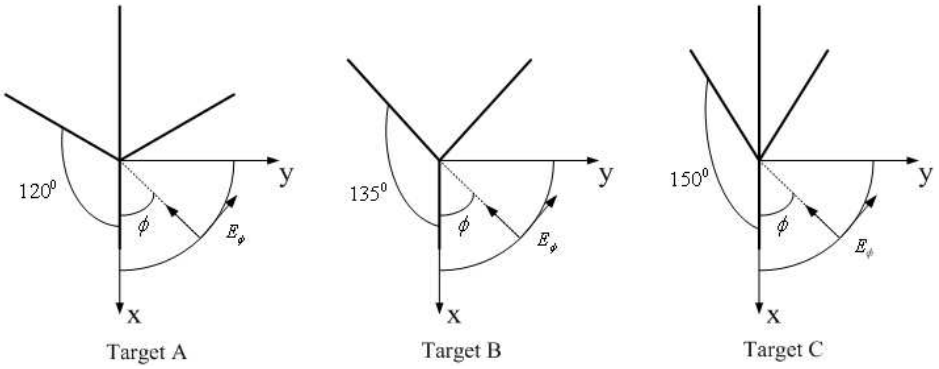

Figure 1: Wire targets used for simulations.

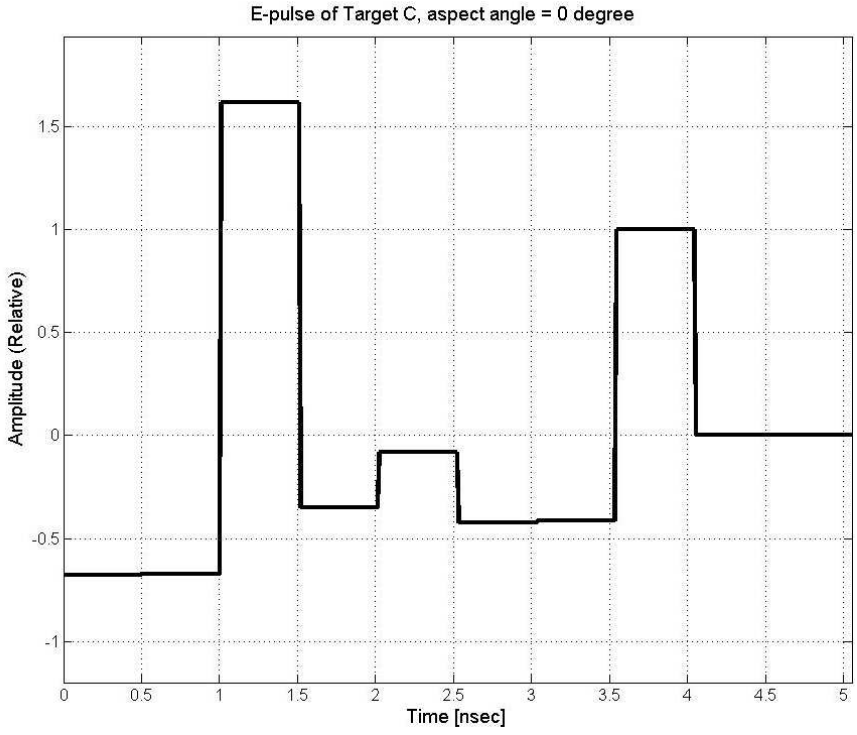

Figure 2: E-pulse waveform generated by Target C, aspect angle = 0°.

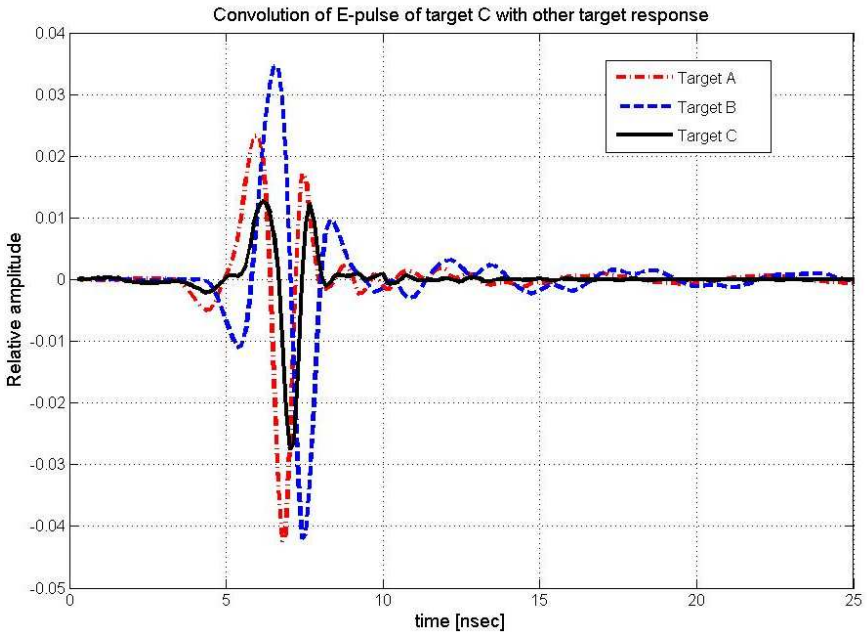

Figure 3: Convolution of E-pulse of target C with three target responses.

geometry is very similar with each others. Figure 2 shows the E-pulse generated by target C at the aspect angle of 0 degree. Figure 3 shows the convolution of E-pulse of target C with other target responses. The convolution of target C's waveform with E-pulse of Figure 2 is zero at the late-time region, but are not zeros for other target's waveform at late-time region. Results show that E-pulse technique can discriminate similar target at same aspect angle for three targets, but cannot discriminate targets at different aspect angles with the aspect angle of E-pulse.

ACKNOWLEDGMENT

This work was supported by the Basic Science Research Program through the National Research Foundation of Korea (NRF) funded by the Ministry of Education, Science & Technology (No. 2011-0003209). Corresponding author: In-Sik Choi (recog@hnu.kr).

Performance Improvement of a Switched Reluctance Motor

Jawad Faiz[1], **F. Tahvilipour**[2], **and G. Shahgholian**[2]

[1]Center of Excellence on Applied Electromagnetic Systems, School of Electrical and Computer Engineering
University College of Engineering, University of Tehran, Tehran, Iran
[2]Department of Electrical Engineering, Islamic Azad University, Najafabad Branch, Isfahan, Iran

Abstract— This paper analyzes and enhances the torque, torque ripple and radial forces in a typical switched reluctance motor (SRM) based on circuit coupled time stepping finite element method. Flux pattern in the SRM for a given excitation used in the computations has been shown in Fig. 1.

The impact of rotor and stator poles arc is investigated and the optimum arc is achieved for a certain excitation pattern regarding the motor torque as shown in Fig. 2.

The radial force of the optimized motor may be reduced using a circular hole in its rotor teeth. Previously the impact of a rectangular hole in the radial force reduction has been demonstrated [1]. However, the circular hole has some advantages such as simplicity of manufacturing, structural satiability and preventing from the local saturation in sharp corners.

The effect of holes inserted in the pole (Fig. 3) in a reduction of radial forces is also investigated and the holes radius, r_h, is optimized based on finite element method. These improvements can

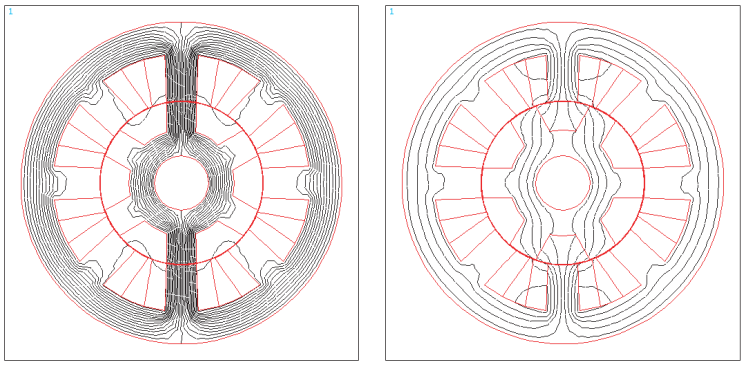

Figure 1: Flux pattern of the SRM in aligned and unaligned positions with phase A excitation.

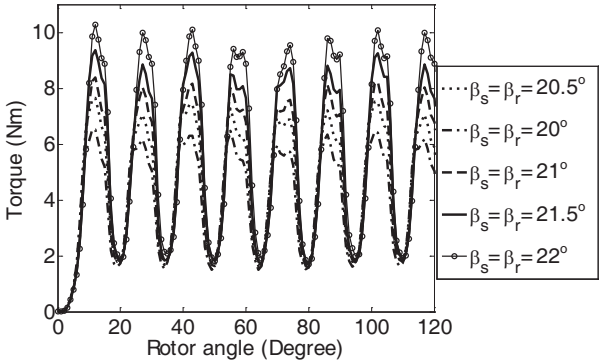

Figure 2: Torque of the SRM for different pole arcs.

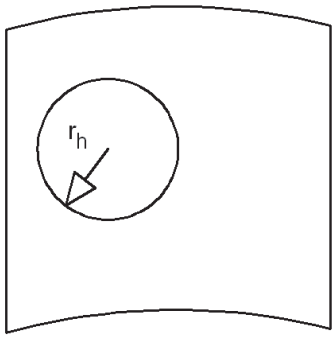

Figure 3: Pole with circular hole.

Table 1: Rotor iron loss.

Case	Rotor iron loss (W)
Without holes	8.34
With holes ($r_h = 2\,\text{mm}$)	8.84
With holes ($r_h = 2.5\,\text{mm}$)	9.15

decrease the motor vibration significantly. As shown in Table 1 these holes do not increase the loss significantly.

REFERENCES

1. Sanada, M., et al, "Radial force and acoustic noise reduction for switched reluctance motor with hole inside pole," *Transactions of the Institute of Electrical Engineers of Japan*, Vol. 123, No. 12, 1438–1445, 2003.

Monitoring of Mid-ocean Eddies in the Northeastern Atlantic

Shigehisa Nakamura
Kyoto University, Japan

Abstract— This work concerns on mid-ocean eddies in the North Atlantic. The author notes that the eddies in the ocean are frequently found as a result of an undulation of the ocean western boundary current though the other local case of a smaller scale is possible referring to his understanding of hydrodynamics. Eddies in the ocean have been seen though no observation had been considered in the early stage of oceanography. It was in the NW Pacific that a ring is formed as a result of an undulation of the ocean current extension on the bases of the oceanographic surveys. In the Atlantic, eddies in the ocean was noticed as an extension of the Gulf Stream by 1983. Meddy as mid-ocean eddy has been surveyed in the ocean. Several contributions on meddy in the North Atlantic in the 1990s to suggest a more time in need to realize the details of physical aspect of meddy. The author would introduce his note about a meddy could be formed by the contact of the water of the Gulf Stream and the Mediterranean water in the area around the Azores. Then, the author has to notice about the ocean front formed by the two water masses with his understanding of problems on the primary productivity of zoo-plancton.

Satellite Monitoring in Relation to Ekman Transport and Kelvin-Helmholz Billows in Ocean

Shigehisa Nakamura
Kyoto University, Japan

Abstract— As for the water motion in the upper layer of the ocean, there are two kinds of the water flows. These two flows are known as "geostrophic current" as a part of ocean circulation and "currents" found around an ocean front which could be an evolution of a Kelvin-Hellnholtz instability in the field of physical ocean science. In this work, an outline of these two flows is introduced in relation to the existing satellite monitoring of the earth surface. A brief review note is given for helping a dynamical understanding of these historical backgrounds with the striking pattern found alter the observation during the oceanographic expeditions in the early age of the ocean science. After a review of the two flows in the ocean, it might be found a key to introduce the existing satellite monitoring in order to promote research works on the motions of the ocean flows as inertia motion in a global scale with a polar orbital path.

Satellite Monitoring of the Ocean in Relation to Structure of the North Atlantic

Shigehisa Nakamura
Kyoto University, Japan

Abstract— Ocean front which can be monitored by the existing satellite is a glimpse of the two water masses in the ocean. In this work, a basic problem about the ocean front in relation to the density of the ocean water. The typical ocean water motion is geostrophic under the effect of the earth's rotation. The ocean water is essentially stratified in densimetric stratification. The density of the ocean water is determined by salinity, temperature and depth under the ocean surface. In brief, the water is specified by a function of salinity, temperature and depth. For demonstrate the waters in the ocean surface layer, intermediate layer and deep water layer (abyssal layer). For the author's convenience, a special reference is taken for the structure of the North Atlantic.

Improvement of Signal Integrity with Active Metamaterial for Microwave Applications

B. Ravelo and E. R. Rajkumar
IRSEEM, EA 4353, Graduate School of Engineering ESIGELEC, Av. Galilée, BP 10024
76801 Saint-Etienne-du-Rouvray Cedex, France

Abstract— Because of the operating speed and integration density increases, the reliability and the integrity of modern electronic components used in the measurement become less and less efficient [1]. These limitation effects can be investigated with the spectral analysis of the interaction between the operating signals and the electronic systems used. The basic parameters considered for such investigation are based on the gain and the phase qualities. In the microwave frequency bands, the S-parameters are generalized used to interpret the different behaviors of the structures. The correction techniques of these microwave parameters are always one of the most attractive topics of the researchers working in the electronic and microwave instrumentations. In [2, 3], an innovative technique based on the use of the negative group delay (NGD) was proposed. The NGD circuits present a particular function enabling to compensate the delay in the electronic systems [4–6]. But in this case, the behaviors of the phase remains degraded. So, it seems interesting to exploit the concept of the metamaterial (MM) or left-handed (LH) passive devices [7–11] which are capable to generate phase in opposite sign to the classical circuit like the interconnect lines. The MM concept was introduced in 1968 by Veselago [12] and validated fifty years later by Pendry and Smith with 3D artificial material [13, 14]. Then, 2D- and 1D-circuits were implemented thanks to the analogy between the frequency responses of the structures.

But these passive circuits [4–7] present significant losses due to the absorption phenomenon linked to the LH effect. To overcome such an effect, the use of active MMs can be a good solution in the future. In this letter, innovative concept of microwave device integrity corrections is introduced by using the active MM circuits. To illustrate the feasibility of the principle, one focuses on the association of the LH cell proposed in [7, 8] and a field effect transistor (FET). An analytical approach for the synthesis of the circuit is established knowing the characteristics of the FET transconductance and the Drain-Source resistance. Then, numerical analyses performed with the Advance Design System electronic microwave circuit simulators were realized to explain the validity of the principle. The results from the analyses realized around some GHz confirm the effectiveness of the principle.

REFERENCES

1. http://www.itrs.net/links/2010itrs/2010Update/ToPost/2010_Update_Overview.pdf.
2. Ravelo, B., A. Perennec, and M. Le Roy, "New technique of inter-chip interconnect effects equalization with negative group delay active circuits," *VLSI, INTECH Book*, Chap. 20, 409–434, Edited by Pr. Zhongfeng Wang, Feb. 2010, ISBN: 978-953-307-049-0.
3. Ravelo, B., A. Perennec, and M. Le Roy, "Equalization of interconnect propagation delay with negative group delay active circuits," *11th IEEE Workshop on Signal Propagation on Interconnects*, 15–18, Genova, Italy, May 2007.
4. Ravelo, B., "Demonstration of negative signal delay with short-duration transient pulse," *Eur. Phys. J. Appl. Phys. (EPJAP)*, Vol. 55, 1–8, 10103, 2011.
5. Ravelo, B., "Baseband NGD circuit with RF amplifier," *Electronic Letters*, Vol. 47, No. 13, 752–754, Jun. 23, 2011.
6. Ravelo, B., "Investigation on microwave NGD circuit," To be published in *Electromagnetics Journal*, Edited by Taylor & Francis.
7. Caloz, C., A. Sanada, and T. Itoh, "A novel composite right/left-handed coupled-line directional coupler with arbitrary coupling level and broad bandwidth," *IEEE Trans. MTT*, Vol. 52, 980–992, Mar. 2004.
8. Lai, A., C. Caloz, and T. Itoh, "Composite right/left-handed transmission line metamaterials," *IEEE Microwave Magazine*, Vol. 5, 34–50, Sept. 2004.
9. Islam, R. and G. V. Eleftheriades, "Phase-agile branch-line couplers using metamaterial lines," *IEEE MWC Lett.*, Vol. 14, No. 7, 340–342, Jul. 2004.

10. Eleftheriades, G. V., O. Siddiqui, and A. K. Iyer, "Transmission line for negative refractive index media and associated implementations without excess resonators," *IEEE MWC Lett.*, Vol. 13, No. 2, 51–53, Feb. 2003.
11. Veselago, V., "The electrodynamics of substances with simultaneously negative values of ε and μ," *Soviet Physics Uspekhi*, Vol. 10, No. 4, 509–514, 1968.
12. Pendry, J. B., "Negative refraction make a perfect lens," *Phys. Rev. Lett.*, Vol. 85, 3966–3969, 2000.
13. Shelby, R. A., D. R. Smith, and S. Schultz, "Experimental verification of a negative index of refraction," *Science*, Vol. 292, 77–79, Apr. 2001.

Radar and Optical Parallel Remote Sensing Modelling of Forest: Soil and Leaves Moisture Content Effect

C. Albinet[1], **P. Borderies**[1], **and S. Fabre**[2]

[1]Département Electromagnétisme et Radar
Office National d'Études et de Recherches Aérospatiales, ONERA, Toulouse, France
[2]Département Optique Théorique Appliquée
Office National d'Études et de Recherches Aérospatiales, ONERA, Toulouse, France

Abstract— Retrieval of bio-physical parameters of forests with remote sensing is nowadays a challenge. A focus is done in this paper on a parallel direct modelling approach in which the same forest scenario is simulated in polarimetric P band backscattering and in optics (visible and NIR).

A ground representation of a maritime pine forest as a function of growing age and consequently growing biomass is obtained thanks to a growth model depicted in [1], which delivers the statistical parameters of the trunks and branches in terms of sizes, locations and orientations. It is then used for MIPERS [2] computation of backscattering matrix and the position of all scatterers is then re-used as input for the optical model DART [3], with soils input data from [4]. The optical model has been coupled with an internally developed soil reflectance model as a function of moisture content and with commonly used PROSPECT model for leaves as a function of leaves moisture content. The influence of moisture in leaves is only significant in infrared, whereas the influence of smc is all the more significant as the biomass is higher.

REFERENCES

1. Saleh, K., A. Porte, D. Guyon, P. Ferrazzoli, and J. P. Wigneron, "A forest geometric description of a maritime pine forest suitable for discrete microwave models," *IEEE TGARS*, Vol. 43, No. 9, 2024–2035, September 2005.
2. ESA contract No. 20449/06/NL/LvH, "Rigorous numeric techniques applied to microwave interaction with natural targets: Volume scattering," CCN, 2010.
3. Martin, E., "DART: Modèle 3D multispectral et inversion d'images optiques de satellite — Application aux couverts forestiers," Ph.D. dissertation, Université Paul Sabatier, July 25, 2006.
4. Lesaignoux, A., "Estimation de l'humidité de surface des sols nus à partir de l'imagerie hyperspectrale sur le domaine optique 0.4–14 µm," Ph.D. dissertation, Institut Supérieur de l'Aéronautique et de l'Espace, December 16, 2010.

Signal Processing for High Resolution RCS Measurement

E. S. Kashani and Y. Norouzi
Electrical Engineering, Amirkabir University of Technology, Tehran, Iran

Abstract— The interfering signal is the main difficulty in high resolution RCS measurement. Besides, using the network analyzer with a limited output power as the signal source reduces the attainable SNR. In this paper we have examined several different signal processing methods that can cure both above problems. Our proposed signal processing methods are based on some famous radar signals such as LFM, Non Linear FM and Costas.

Introduction: Radar Cross Section (RCS) of a radar target is a presumed area with isotropic scattering pattern which its scattered power equals that of the radar target. Before designing any radar system it is quit necessary to know the RCS of the objects that system encounters. So, over time many methods for measuring and estimating radar cross section have developed. Despite several methods have been considered for measuring RCS in lab, each of these methods have some disadvantages. Modern radio frequency generation technology available in network analyzers makes it possible to synthesize high resolution measurements using frequency-stepping techniques. In this method, the radiated frequency is stepped across a specified band at specified intervals. At each frequency received signal is sampled and its phasor relative to transmitted sinusoid is calculated.

Network analyzers have limited output power in usually between 10 and 20 dBm. So a short duration pulse produced by these systems cannot provide enough SNR necessary for RCS measurement. As a result long pulses should be transmitted by the system. These long pulses reduce the range resolution of the measurement which is a necessity for today's high resolution RCS measurement.

As was mentioned earlier to cure this problem usually stepped frequency waveform is applied by the network analyzer. After the phasor of the received signal at each frequency step is determined, inverse Fourier Transform is used to convert the signal to the frequency domain. Nevertheless, the important matter in laboratory methods is separation of real reflected signals from disturbing signals. However simple Fourier Transform produces signals with great side lobes which forbid detection of a small scattering centre in vicinity of a greater one.

In this paper we will examine different signal processing methods to find which method is more suitable when fine range resolution is the goal and which one is more suitable when higher dynamic range is required. The proposed methods are based on the radar signal design mainly linear and non-linear frequency modulation as well as Costas Signals.

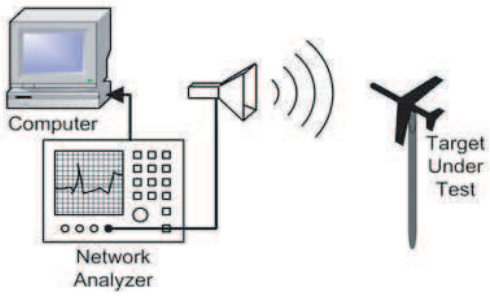

Figure 1: RCS measurement using network analyzer.

The Pancharatnam-berry Phase for Non-cyclic Polarization Changes: Theory and Experiment

Thomas Van Dijk[1], **Hugo F. Schouten**[1], **Wim Ubachs**[1], **and Taco D. Visser**[1,2]

[1]Free University, Amsterdam, The Netherlands
[2]Delft University of Technology, Delft, The Netherlands

Abstract— In a seminal paper Berry [1] showed that when the Hamiltonian of a quantum mechanical system is adiabatically changed in a cyclic manner the system acquires, in addition to the usual dynamic phase, a so-called geometric phase. It was soon realized that such a phase is in fact quite general: it can also occur for non-adiabatic state changes and even in classical systems. One of its manifestations is the *Pancharatnam* phase in classical optics [2]. The polarization properties of a monochromatic light beam can be represented by a point on the Poincaré sphere [3]. When, with the help of optical elements such as polarizers and phase plates, the state of polarization is made to trace out a closed contour on the sphere, the beam acquires a geometric phase. This Pancharatnam-Berry phase, as it is nowadays called, is equal to half the solid angle of the contour subtended at the origin of the sphere [4, 5].

We study the geometric phase for *non-cyclic* polarization changes, i.e., polarization changes for which the initial state and the final state are different (see also Refs. [6, 7]). Such changes correspond to non-closed paths on the Poincar sphere. The geometric phase can depend in a linear, a nonlinear or in a singular fashion on the orientation of the optical elements. We present a novel interferometric setup that allows the observation of these three types of behavior. The observed singular behavior may be applied in the design of fast optical switches.

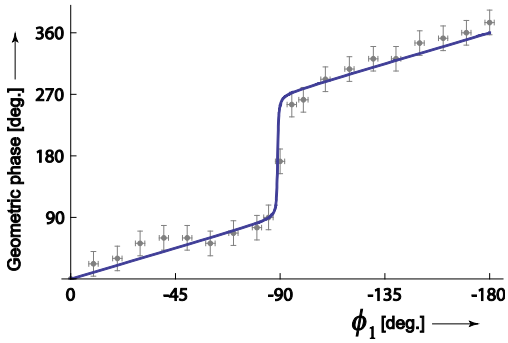

Figure 1: Singular behavior of the geometric phase of the final polarization state as a function of the orientation angle ϕ_1 of a linear polarizer in a Mach-Zehnder interferometer. The solid curve is the theoretical prediction, the dots and error bars represent measurements.

REFERENCES

1. Berry, M. V., *Proc. R. Soc. Lond. A*, Vol. 392, 45–57, 1984.
2. Pancharatnam, S., *Proc. Indian Acad. Sci. A*, Vol. 44, 247–262, 1956.
3. Born, M. and E. Wolf, *Principles of Optics*, 7th Edition, Cambridge University Press, Cambridge, 1999.
4. Bhandari, R., *Phys. Rep.*, Vol. 281, 1–64, 1997.
5. Hariharan, P., "The geometric phase," *Progress in Optics*, E. Wolf, Ed., Vol. 48, 149–201, Elsevier, Amsterdam, 2005.
6. Van Dijk, T., H. F. Schouten, W. Ubachs, and T. D. Visser, *Opt. Express*, Vol. 18, 10796–10804, 2010.
7. Van Dijk, T., H. F. Schouten, and T. D. Visser, *J. Opt. Soc. Am. A*, Vol. 27, 1972–1976, 2010.

Experimental Demonstration of an Intensity Minimum at the Focus of a Laser Beam Created by Spatial Coherence

Shreyas B. Raghunathan[2], **Thomas van Dijk**[1], **Erwin Peterman**[1], **and Taco D. Visser**[1,2]

[1]Free University, Amsterdam, The Netherlands
[2]Delft University of Technology, Delft, The Netherlands

Abstract— The intensity distribution of a wave field in the focal region of a lens is a classical subject of physical optics. One can manipulate this distribution by employing phase or amplitude masks. Recent theoretical studies showed that the state of spatial coherence of the field can also be used for this goal. It was found, for example, that partially coherent, Gaussian-correlated beams produce a focal intensity distribution that is more spread out than that of a fully coherent beam [1]. Two studies of Bessel-correlated fields yielded the surprising prediction that it is possible to change the maximum of intensity at the geometric focus into a minimum, in a continuous manner by simply changing the size of an iris [2, 3]. In this talk we discuss an experimental setup with which these predictions have been verified. Having the ability to tailor the focal intensity distribution allows one, for example, to switch from trapping high-index particles to trapping low-index particles [4].

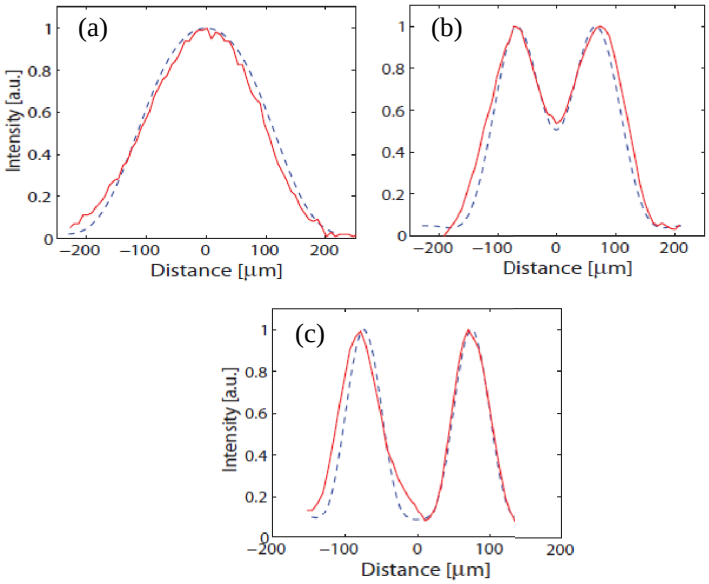

Figure 1: Transforming the intensity in the focal plane from a maximum into a minimum by varying the radius of an aperture from (a) 0.25 mm to (b) 0.75 mm and to (c) 1.2 mm. The dotted curves are theoretical predictions, the solid curves represent experimental results.

REFERENCES

1. Visser, T. D., G. Gbur, and E. Wolf, *Opt. Commun.*, Vol. 213, 13–19, 2002.
2. Gbur, G. and T. D. Visser, *Opt. Lett.*, Vol. 28, 1627, 2003.
3. Van Dijk, T., G. Gbur, and T. D. Visser, *J. Opt. Soc. Am. A*, Vol. 25, 575, 2008.
4. Raghunathan, S. B., T. van Dijk, E. J. G. Peterman, and T. D. Visser, *Opt. Lett.*, Vol. 35, 4166–4168, 2010.

Coherence Effects in Mie Scattering

David G. Fischer[1], **Thomas Van Dijk**[2], **Emil Wolf**[3], **and Taco D. Visser**[2, 4]

[1]NASA Glenn Research Center, Cleveland, OH, USA
[2]Free University, Amsterdam, The Netherlands
[3]University of Rochester, Rochester, NY, USA
[4]Delft University of Technology, Delft, The Netherlands

Abstract— When considering the scattering of light by spherical particles (so-called Mie scattering), it is usually assumed that the incident field is spatially completely coherent [1]. However, in practice this assumption is not always justified. Examples of partially coherent fields include those generated by multi-mode lasers, and beams that have passed through a random medium e.g. the turbulent atmosphere. Such more general situations have only recently begun to attract attention [2].

In the present contribution we consider scattering of partially coherent light (specifically, scattering of Gaussian Schell-model beams) by deterministic, spherical particles. In particular, we determine the influence of the degree of coherence of the incident beam on the total amount of scattered power (the extinction for non-absorbing particles) and the angular distribution of the scattered power.

We use a recently developed formalism [3] to study the total scattered power. We find that it is independent of the degree of coherence of the incident beam. We also investigate the angular intensity distribution of the scattered light (the radiant intensity). We find that the radiant intensity does depend on the degree of coherence of the incident beam, most strongly when the effective transverse coherence width is comparable to the size of the scatterer. Finally, we calculate the encircled energy of the scattered radiation in the far-zone of the scatterer for different detector geometries, as a function of the degree of coherence of the incident beam.

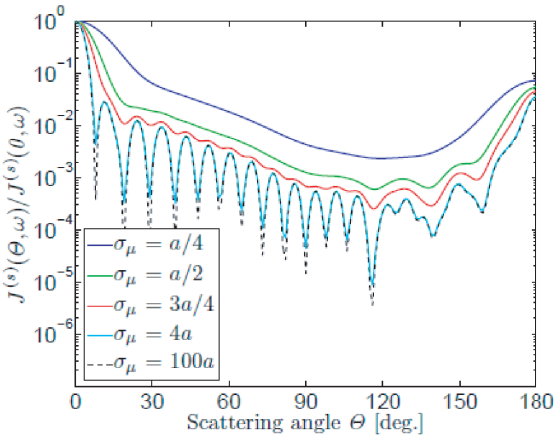

Figure 1: Angular distribution of the radiant intensity generated by scattering a partially coherent beam by a sphere, shown on a logarithmic scale, for various values of the transverse coherence length σ_μ. In this example the sphere radius $a = 4\lambda$, and the refractive index $n = 2$.

REFERENCES

1. Van De Hulst, H. C., *Light Scattering by Small Particles*, Wiley, New York, 1957.
2. Gbur, G. and T. D. Visser, "The structure of partially coherent fields," *Progress in Optics*, E. Wolf, Ed., Vol. 55, 285–341, Elsevier, Amsterdam, 2010.
3. Van Dijk, T., D. G. Fischer, T. D. Visser, and E. Wolf, *Phys. Rev. Lett.*, Vol. 104, 173902, 2010.

L-band H Polarized Microwave Emission during the Corn Growth Cycle

A. T. Joseph[1], **R. Van Der Velde**[2], **P. E. O'Neill**[1], **E. Kim**[1], **R. H. Lang**[3], **and T. Gish**[4]

[1]Faculty of Geo-Information Science and Earth Observation (ITC)
University of Twente, Hengelosestraat 99, P. O. Box 6, AA 7500, Enschede, The Netherlands
[2]Hydrological Sciences Branch/614.3, Hydrospheric and Biospheric Sciences Laboratory
NASA/Goddard Space Flight Center, Greenbelt, MD 20771, USA
[3]Department of Electrical and Computer Engineering
George Washington University, Washington, DC 20052, USA
[4]Hydrology & Remote Sensing Lab, USDA-ARS, Beltsville, MD 20705, USA

Abstract— Hourly L-band (1.4 GHz) horizontally (H) polarized brightness temperatures (T_B's) measured during five episodes (more than two days of continuous measurements) of the 2002 corn growth cycle are analyzed. These T_B measurements were acquired as a part of a combined active/passive microwave field campaign, and were obtained at five incidence and three azimuth angles relative to the row direction. In support of this microwave data collection, intensive ground sampling took place once a week. Moreover, the interpretation of the hourly T_B's could also rely on the data obtained using the various automated instruments installed in the same field.

In this paper, the soil moisture and temperature measured at fixed time intervals have been employed as input for the tau-omega model to reproduce the hourly T_B. Through the calibration of the vegetation and surface roughness parameterizations, the impact of the vegetation morphological changes on the microwave emission and the dependence of the soil surface roughness parameter, h_r, on soil moisture are investigated. This analysis demonstrates that the b parameter, appearing in the representation of the canopy opacity, has an angular dependence that varies throughout the growing period and also that the parameter h_r increases as the soil dries in a portion of the dry-down cycle. The angular dependence of the b parameter imposes the largest uncertainty on T_B simulations near senescence as the response of b to the incidence is also affected by the crop row orientation. On the other hand, the incorporation of a soil moisture dependent h_r parameterization was responsible for the largest error reduction of T_B simulations in the early growth cycle.

Session 2P1
Quantum and Classical Aspects of Novel Photonic Materials

Analysis of Diffraction Gratings via Their Resonances

B. Vial[1,2], F. Zolla[1], A. Nicolet[1], M. Commandré[1], G. Demésy[1], and S. Tisserand[2]

[1]Institut Fresnel UMR CNRS 6133, Aix-Marseille Université, École Centrale de Marseille
Campus de Saint-Jérôme, Marseille F-13013, France
[2]Silios Technologies, France

Abstract— The field of application of diffraction gratings has been extended over the past decades. For spectral filtering applications, for instance, one should determine the line shape of the transmission or reflection spectra in order to fit the required features. To avoid the calculation of diffracted efficiencies for a wide range of wavelengths, it is by far more efficient to search out the resonances. These are obtained directly **by determining the eigenvalues of the scattering operator discretized by a Finite Element Method (FEM):** the real parts of the complex eigenfrequencies correspond to the resonant frequencies and the imaginary parts are related to the damping factors. This FEM can be applied to one-and two-dimensional gratings. The originality of our approach is that it works irrespective to the geometry and material properties. We use an orthogonal co-ordinate system $Oxyz$. We deal with time-harmonic fields, so that the electric and magnetic fields are represented by complex vector fields $\mathbf{E}$ and $\mathbf{H}$ with a time-dependence in $\exp(-i\omega t)$. The grating is illuminated by an incident plane wave of wave vector defined by the angles θ and ϕ: $\mathbf{k}^+ = k^+(\sin\theta\cos\phi, \sin\theta\sin\phi, \cos\theta)^T = (\alpha, \beta, \gamma)^T$. Its electric field $\mathbf{E}^0$ is linearly polarized along the direction defined by the unit vector $\mathbf{A}^0$: $\mathbf{E}^0 = \mathbf{A}^0 \exp(i\mathbf{k}^+ \cdot \mathbf{r})$, with $\mathbf{r} = (x, y, z)^T$ and $\mathbf{A}^0 = (\cos\varphi\cos\theta\cos\phi - \sin\varphi\sin\phi, \cos\varphi\cos\theta\sin\phi + \sin\varphi\cos\phi, -\cos\varphi\sin\phi)^T$. The problem of diffraction is to find Maxwell's equation solutions in harmonic regime such that the diffracted field satisfies an Outgoing Wave Condition and where $\mathbf{E}$ is quasi-periodic with respect to x and y coordinates, i.e.:

$$\mathbf{E}(\mathbf{r} + \mathbf{d}) = \mathbf{E}(\mathbf{r}) \exp\left(i\mathbf{k}^+ \cdot \mathbf{d}\right) = \mathbf{E}(\mathbf{r}) \exp(i(\alpha d_x + \beta d_y)) \tag{1}$$

with $\mathbf{d} = (d_x, d_y, 0)^T$.

A method [1–4] based on the resolution of the diffraction problem and adapted to the FEM, allows us to extract the transmission, reflection, Joule losses and to obtain a global energy balance.

The eigenvalues of the structure are denoted $\omega_n = \omega_n' + i\omega_n''$. We then define the quality factor of the resonance as $Q_n := \omega_n'/(2\omega_n'')$. *These eigenvalues are also the poles of the reflection coefficient of the device [5].*

The eigenvalue problem we are dealing with consists in finding the solutions of fMaxwell's equations without sources. We want to find the complex eigenvalues ω_n and the non-zero fields $\mathbf{E_n}$ which are bi-quasi-periodic on a basic cell, such that:

$$\epsilon_r^{-1}\mathbf{curl}\left(\mu_r^{-1}\mathbf{curlE_n}\right) = c^{-2}\omega_n^2\mathbf{E_n}. \tag{2}$$

In fact, there is no incident plane wave, but nevertheless the coefficients of quasi-periodicity α and β are parameters of the eigenproblem given above (via the quasi-periodicity conditions given in Eq. (1)) and are forced to be real valued. Note that giving α and β do not allow to recover θ and ϕ since k^+ is not known but can be easily derived thanks to the eigenvalues ω_n: if ω_n'' is small enough, we can set $k_n^+ \simeq \sqrt{\epsilon^+\mu^+}\omega_n'/c$, where ϵ^+ and μ^+ are the permittivity and the permeability of the superstrate. We then deduce the corresponding angles for which a resonance may occur from $\alpha = k_n^+(\sin\theta_n\cos\phi_n)$ and $\beta = k_n^+(\sin\theta_n\sin\phi_n)$.

We will present a validation of our method together with applications to mono-and bi-gratings corresponding to 2D and 3D practical geometries and possibly dispersive materials.

REFERENCES

1. Demésy, G., F. Zolla, A. Nicolet, M. Commandré, and C. Fossati, "The finite element method as applied to the diffraction by an anisotropic grating," *Opt. Expree*, Vol. 15, No. 26, 18089–18012, Dec. 2007.
2. Demésy, G., F. Zolla, A. Nicolet, and M. Commandré, "Versatile full-vectorial finite element model for crossed gratings," *Opt. Lett.*, Vol. 34, No. 14, 2216–2218, Jul. 2009.

3. Demésy, G., F. Zolla, A. Nicolet, and M. Commandré, "All-purpose finite element formulation for arbitrarily shaped crossed-gratings embedded in a multilayered stack," *J. Opt. Soc. Am. A*, Vol. 27, No. 4, 878–889, Apr. 2010.
4. Demésy, G., F. Zolla, A. Nicolet, and M. Commandré, "An all-purpose three-dimensional finite element model for crossed-gratings," *Proceedings SPIE*, Vol. 7353, 73530G, Prague, Czech Pepublic, 2009.
5. Zolla, F., G. Renversez, A. Nicolet, B. Kuhlmey, S. Guenneau, D. Felbacq, A. Argyros, and S. Leon-Saval, *Foundations of Photonic Crystal Fibres*, 2nd Edition, Imperial College Press, 2012.

Efficient Light Coupling into Retinal Rods: Towards Single Photon Detection?

Guillaume Vienne, **Nigel Sim**, **Ying Lin**, **and Leonid Krivitsky**
Data Storage Institute, Agency for Science Technology and Research (A-STAR)
Singapore 117608, Singapore

Abstract— We investigate a new and simple scheme for delivering laser light to retinal rod cells. In contrast to delivery methods previously employed, we focus light along the length of the cell. To this avail we couple light to an optical fiber which is tapered and rounded at its extremity to act as a lens, so that the light is focused on a rod cell held by a recording electrode and placed a few tens of microns away from the fiber tip. Both the fiber tip and the cells are immersed in a ringer solution. The system is observed through an optical microscope and cell response is measured by patch clamp electrophysiology. This scheme considerably increases the light coupling efficiency since it is wellsuited to the geometry of rod cells, which are typically cylindrical in shape with a diameter of 4–5 µm and a length of around 40 µm. In addition, a rod cell in aqueous solution acts as an optical waveguide. Its main structures are on the nanometer scale. Therefore they are not resolved by visible light, and an effective refractive index applies. Its value is around 1.40, about 0.07 above the refractive index of the ringer solution, so that a rod cell acts as a multimode waveguide. We will show how the technique is implemented experimentally together with the results from FDTD simulations for analysis and optimization. This scheme will be used to understand how rod cells detect low intensity light down to a few photons, and perhaps even down to a single photon.

Random Dielectric Fibers and Resonances

G. Bouchitté, C. Bourel, and L. Manca
Institut de Mathématiques IMATH, Université de Toulon, BP 20132, La Garde Cedex 83957, France

Abstract— In [1–4], a theory for artificial magnetism in two-dimensional photonic crystals was developed for large wavelength (homogenization) and more recently in a full three dimensional setting in [5], where a rigorous justification for effective tensors of negative permeability is given. Here we would like to present a random counterpart of the latter results in order to test the robustness of the micro-resonance phenomena from which artificial magnetism arises.

In this work, we consider randomly disposed parallel dielectric fibers each of them having, up to a large scaling factor, a random permittivity $\varepsilon^r(\omega)$ whose law is represented by a density on a window $\Delta_\delta = [a,b]\times[0,\delta]$ of the complex plane. The key point is that, when the photonic crystal is illuminated at a given frequency, it happens that some values in interval $[a,b]$ are associated with internal resonances of the inclusions. The homogenization process is therefore difficult to handle if one starts with a law of ε^r concentrated on the real axis (i.e., $\delta = 0$).

We determine conditions on the probability law of ε^r on Δ_δ under which the homogenization process can be identified and leads to a deterministic effective permeability of the same kind as the one found in [1, 5]. Subsequently a limit analysis is performed when the law for ε^r depends on δ and concentrates on the real axis as $\delta \to 0$.

Then we evidence that the limits in the homogenization process and as $\delta \to 0$ cannot be commuted. Diverse related open issues will be addressed.

REFERENCES

1. Bouchitté, G. and D. Felbacq, "Homogenization near resonances and artificial magnetism from dielectrics," *C. R. Math. Acad. Sci. Paris*, Vol. 339, No. 5, 377–382, 2004.
2. Felbacq, D. and G. Bouchitté, "Left handed media and homogenization of photonic crystals," *Optics Letters*, Vol. 30, 10, 2005.
3. Felbacq, D. and G. Bouchitté, "Homogenization of wire mesh photonic crystals embdedded in a medium with a negative permeability," *Phys. Rev. Lett.*, Vol. 94, 183902, 2005.
4. Felbacq, D. and G. Bouchitté, "Negative refraction in periodic and random photonic crystals," *New J. Phys.*, Vol. 7, 159, 10.1088, 2005.
5. Bouchitté, G., C. Bourel, and D. Felbacq, "Homogenization of the 3D Maxwell system near resonances and artificial magnetism comptes rendus mathematique," Srie A, Vol. 347, Nos. 9–10, 571–576, 2009.
6. OBrien, S. and J. B. Pendry, "Magnetic activity at infrared frequencies in structured metallic photonic crystals," *J. Phys. Condens. Mat.*, Vol. 14, 6383–6394, 2002.

Tamm Surface Plasmon Laser

C. Symonds[1], **S. Aberra-Guebrou**[1], **A. Lemaitre**[2], **P. Senelart**[2], **and J. Bellessa**[1]

[1]Laboratoire de Physique de la Matière Condensée et Nanostructures, Université Lyon 1
CNRS, UMR 5586, Domaine Scientifique de la Doua, F-69622 Villeurbanne Cedex, France
[2]Laboratoire de Photonique et de Nanostructures, CNRS, Route de Nozay, F-91460 Marcoussis, France

Abstract— Plasmonic Tamm states are interface modes formed at the boundary between a photonic structure and a metallic layer. These modes present both the advantages of surface plasmons and of microcavities photonic modes. Tamm plasmons can be spatially confined by structuring the metallic part of the system, thus reducing the size of the mode and allowing various geometries. They are very good candidates for optimizing the emission properties of semiconductor nanostructures. Very recently the extraction of single photon emitted by a quantum box has been evidenced [1] in a Tamm plasmon structure. Due to the relatively low damping and the versatility of the Tamm geometries, these modes are also good candidate for new type of lasers.

We will show that lasing can be obtained for InGaAs semiconductor quantum wells embedded in a GaAs/AlAs Bragg mirror covered by silver or gold. For this purpose the sample is optically excited with a pulsed laser. For low excitation power a strong coupling regime is observed, with formation of hybrid Tamm/plasmon exciton states. When the excitation power increases a modification of the emitting diagram appear with a strong emission at $k = 0$ at the energy of the bare Tamm mode. The typical threshold in the emitted power and the modification of the emission diagram is observed.

Due to the large variety of geometries of confined lasers which can be obtained with Tamm structures and the compatibility of these types of devices with electrical excitation, the Tamm laser can represent a promising type of new confined lasers.

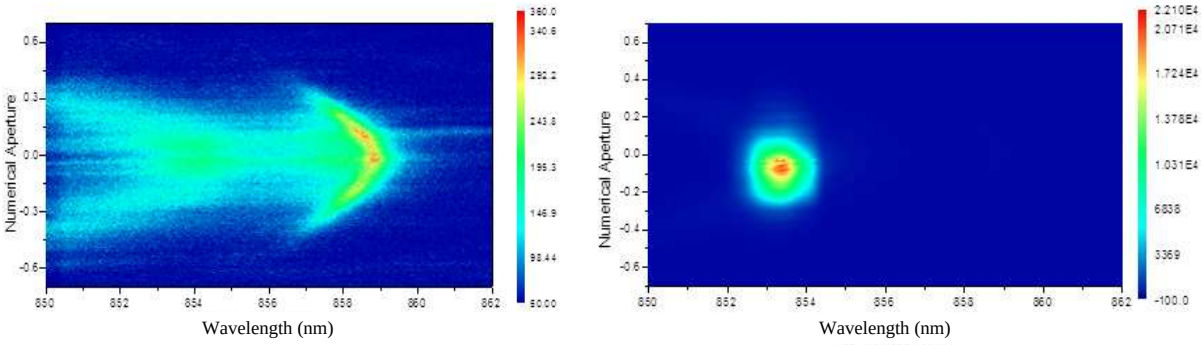

Figure 1: Emission as a function of the wavelength and the numerical aperture for excitation power of (a) 40 mW and (b) 180 mW.

REFERENCES

1. Full Control of Spontaneous Emission in Confined Tamm Plasmon Structures, arXiv:1106.4437v2.

Numerical Studies in Nanoplasmonics: Local vs Non-local Response

G. Toscano[1], **S. Raza**[1], **A. P. Jauho**[2], **M. Wubs**[1], **and N. A. Mortensen**[1]

[1]DTU Fotonik, Department of Photonics Engineering, Technical University of Denmark
Ørsteds Plads, Building 343, DK-2800 Kongens Lyngby, Denmark
[2]DTU Nanotech, Department of Micro- and Nanotechnology, Technical University of Denmark
Ørsteds Plads, Building 344, DK-2800 Kongens Lyngby, Denmark

Abstract— The study of the free-electron optical response of metallic nanostructures is usually based on the classical Drude model. The ongoing miniaturization of nanoplasmonic structures down to sizes comparable to the Fermi wavelength of the electrons, calls for a description that captures the emerging quantum effects. To this end, we propose the use of the hydrodynamical Drude model, a semiclassical model that describes the free-electron gas in a metal as a Fermi gas subject to the electromagnetic force, as described by the Navier-Stokes like equation. New in this description are for example the presence of pressure waves, analogous to sound waves, that give rise to a spatially nonlocal optical response.

Here I will survey our recent investigations of the scattering properties of metallic nanostructures within the linearized hydrodynamical Drude model. We implement this model in the frequency domain, as an add-on to standard commercial software (COMSOL 4.1) [1, 2]. We analytically solve the scattering problem for a cylindrical metallic nanowire [3]. Unlike what is known from the standard Drude theory, we show that in the hydrodynamical model light *does* couple to discrete bulk plasmons for frequencies above the plasma frequency ω_p. Our numerical implementation accurately describes the new scattering resonances to within promilles. A blueshift of the surface plasmon resonances is also observed in such nanowires, and we numerically investigate blueshifts of more general structures such as dimers [2]. We also find that the field enhancement of dimers is sensibly affected by the nonlocal response: The diminution of the enhancement can reach one order of magnitude for small gaps (see Fig. 1).

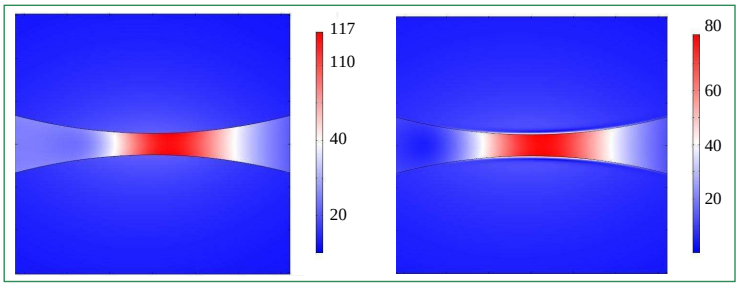

(a) local (b) non-local

Figure 1: Electric field distribution E/E_0 in the gap area between two cylindrical nanorods of radius $a = 25\,\text{nm}$ at frequency $\hbar\omega = 3.28\,\text{eV}$. The gap size is $d = 1\,\text{nm}$. The electric field in the non-local case (b) spreads over a wider area than in the local case (a). The maximum amplitude is also different.

REFERENCES

1. Toscano, G., M. Wubs, S. Xiao, M. Yan, F. Öztürk, A.-P. Jauho, and N. A. Mortensen, "Plasmonic nanostructures: Local versus nonlocal response", *Proceedings of SPIE, The International Society for Optical Engineering*, Vol. 7757, San Diego, CA, USA, August 2010.
2. Toscano, G., S. Raza, A.-P. Jauho, M. Wubs, and N. A. Mortensen, "Reduction of field enhancement in plasmonic nanowire dimers due to non-local response," (to be submitted).
3. Raza, S., G. Toscano, A.-P. Jauho, M. Wubs, and N. A. Mortensen, "Unusual resonances in nanoplasmonic structures due to nonlocal response," *Phys. Rev. B Rapid Commun.*, 2011 (in press), see preprint ArXiv:1106.2175.
4. David, C. and F. J. Garcia de Abajo, "Spatial nonlocality in the optical response of metal nanoparticles," *J. Phys. Chem. C*, 2011 (Just Accepted), DOI: 10.1021/jp204261u.
5. McMahon, J. M., S. K. Gray, and G. C. Schatz, "Nonlocal optical response of metal nanostructures with arbitrary shape," *Phys. Rev. Lett.*, Vol. 103, 097403, 2009.

Spontaneous Radiation in Hyperbolic Media

A. N. Poddubny[1,2], **I. Iorsh**[1], **A. A. Orlov**[1], **P. A. Belov**[1,3], **and Yu. S. Kivshar**[1,4]

[1]National Research University for Information Technology, Mechanics and Optics, Russia
[2]Ioffe Physical-Technical Institute, Russia
[3]Queen Mary University of London, UK
[4]Australian National University, Australia

Abstract— Hyperbolic medium is an uniaxial medium where the transverse and longitudinal dielectric constants have opposite signs. For such medium the isofrequency surface in the wavevector space is a hyperboloid. Hyperbolic regime has been realized in plasma, subjected to the external magnetic field [1], and, recently, in metamaterials. In such system the density of photonic states at the given frequency, proportional to the surface area of the hyperboloid, is infinite. Thus, one can expect [2] huge spontaneous decay rate of the light source, placed in the hyperbolic medium, or, in another words, huge Purcell effect.

In our theoretical work [3] we have considered the light source placed in the hyperbolic medium and have taken into account the finite spatial extent of the real source. We have studied the Purcell effect for arbitrary values of the longitudinal and transverse dielectric constants. Rigorous analytical answers have been obtained within the framework of the Green function technique. We have demonstrated, that the radiative rate is greatly enhanced, but remains finite and strongly depends on the size of the source. The maximum enhancement of the radiative rate is on the order of the cube of the ratio of the light wavelength and the source size.

Purcell factor strongly depends on the dipole orientation with respect to the axis of the system and on the ratio of longitudinal and transverse dielectric constants. It reaches maximum when one of the dielectric constants is negative but close to zero. The growth of Purcell factor in epsilon-near-zero regime is explained by the suppression of the screening of the local electric field.

The hyperbolic metamatetials can be realized either as a grid of parallel metallic wires or as a periodic layered metal-dielectric nanostructure. In such systems we can uncover two independent regimes for spontaneous emission enhancement: (i) hyperbolic regime, where the structure behaves as a homogeneous effective medium and the enhancement is limited by the finite period of the structue, playing the role of the effective source size, and (ii) nonlocal regime, where the homogenization fails but the Purcell factor can be still enhanced due to the excitation of plasmons [4].

REFERENCES

1. Fisher, R. K. and R. W. Gould, "Resonance cones in the field pattern of a short antenna in an anisotropic plasma," *Phys. Rev. Lett.*, Vol. 22, 1093, 1969.
2. Jacob, Z., I. Smolyaninov, and E. Narimanov, "Broadband purcell effect: Radiative decay engineering with metamaterials," ArXiv:0910.3981.
3. Poddubny, A. N., P. A. Belov, and Yu. S. Kivshar, "Spontaneous radiation of a finite-size dipole emitter in hyperbolic media," *Phys. Rev. A*, Vol. 84, 023807, 2011.
4. Iorsh, I., A. N. Poddubny, A. Orlov, P. Belov, and Yu. S. Kivshar, "Spontaneous emission enhancement in metal-dielectric metamaterials," *Phys. Lett. A*, ArXiv: 1108.2128, in press.

Quasi-normal Modes and Strong Coupling in a Plasmonic Nanocavity

A. Castanié and D. Felbacq
Laboratoire Charles Coulomb UMR-CNRS 5221, Université de Montpellier 2
34095 Montpellier Cedex 05, France

Abstract— Quasi-normal modes in a perfectly conducting waveguide coated with a layer of lossy metal are considered. The completeness of these modes is proven and a quantization scheme is proposed. Several applications are given.

Surface Plasmons can be coupled to photons in layered structures [1, 2]. In this work, we consider a waveguide with infinitely conducting walls. It is well known, that field inside this waveguide can be expanded on a set of complete modes and that the second quantization can be performed straighforwardly. It is the basic model of cavity quantum electrodynamics. When a wall is coated with a layer of lossy metal, new modes appear. Indeed, the plasmons living on the metal can be coupled to the guided modes of the waveguide forming new hybrid modes. The new band structure is studied as a function of the width of the coating. Various regimes ranging from weak coupling to strong coupling are exhibited. The new dispersion curves are fully computed, which imply to obtain the imaginary part of the propagation constants of the modes. This is done by means of Cauchy integrals. The strong coupling can then be fully characterized by showing the anti-coupling of the real parts of the propagation constants and the crossing of the imaginary parts. The modes are lossy, in the space variables, but still form a complete family in the L^2 meaning. This set of functions, or quasi-normal modes, can thus be used to perform a second quantization of the modes of the cavity. A comparison with a method based on fictitious Langevin currents and Green functions is performed. These results are then applied to the computation of relevant physical quantities: the Purcell effect, the Casimir effect in the waveguide [3], the possibility of designing a spaser [4].

REFERENCES

1. Bellessa, J., et al., "Giant Rabi splitting between localized mixed plasmon-exciton states in a two-dimensional array of nanosize metallic disks in an organic semiconductor," *Phys. Rev. B*, Vol. 80, 033303, 2009.
2. Bellessa, J., C. Bonnand, J. C. Plenet, and J. Mugnier, "Strong coupling between surface plasmons and excitons in an organic semiconductor," *Phys. Rev. Lett.*, Vol. 93, 036404, 2004.
3. Antezza, M., L. P. Pitaevskii, S. Stringari, and V. B. Svetovoy, "Casimir-Lifshitz force out of thermal equilibrium," *Phys. Rev. A*, Vol. 77, 022901, 2008.
4. Bergman, D. J. and M. I. Stockman, "Surface plasmon amplification by stimulated emission of radiation: Quantum generation of coherent surface plasmons in nanosystems," *Phys. Rev. Lett.*, Vol. 90, 027402, 2003.

Photon-plasmon Strong Coupling in a Layered Structure

B. Guizal and A. Castanié
Université de Montpellier 2, Laboratoire Charles Coulomb UMR CNRS-UM2 5221
34095 Montpellier Cedex 05, France

Abstract— The strong coupling of a guided mode with a surface plasmon in a waveguide coated by a lossy metal is numerically demonstrated. We first developped effective numerical tools able to find the dispertion relation of the multilayered structure. It is based on the use of the S matrix of the structure and on trackig the poles of its determinant $\det(S)$. This is achieved through the use of the well known Cauchy theorem applied to $\det(S(k_{//}))$ where $k_{//}$ is the complex tangential component of the wave vector. It is shown that the original states give rise to two new mixed states exhibiting a Rabi splitting; as has been shown by Bellessa et al. in [1]. In the present study, we focus on the (i) the spatial structure of the new modes and show that one of them exhibits low losses as copared to the original surface plasmon; and (ii) the temporal aspect of the modes that is related to Rabi oscillations [2]. From the point of view of applications, the possibility of amplication of a plasmon [3] is investigated in the situation when the waveguide is flled with quantum dots. Various models are used: a classical simple one using a permittivity with an imaginary part properly chosen and a more realistic semi-classical model based on the Maxwell-Bloch system.

REFERENCES

1. Bellessa, J., et al., "Giant Rabi splitting between localized mixed plasmon-exciton states in a two-dimensional array of nanosize metallic disks in an organic semiconductor," *Phys. Rev. B*, Vol. 80, 033303, 2009.
2. Centeno, E. and D. Felbacq, "Rabi oscillations in bidimensional photonic crystals," *Phys. Rev. B*, Vol. 62, 10101, 2000.
3. Bergman, D. J. and M. I. Stockman, "Surface plasmon amplification by stimulated emission of radiation: Quantum generation of coherent surface plasmons in nanosystems," *Phys. Rev. Lett.*, Vol. 90, 027402, 2003.

Session 2P2a
Laser-induced Periodic Surface Nanostructures: Fundamental Fabrication Mechanisms, Nanoscale-dominated Physical and Chemical Properties 2

Ripples Formation under Femtosecond Laser Irradiation: Actual and Potential Applications

E. Audouard
Université Jean Monnet, Laboratoire Hubert Curien, CNRS UMR 5516, Université de Lyon
18, rue du Pr Benoit Lauras, Saint Etienne 42000, France

Abstract— Femtosecond lasers have proved to be great tools for precise, accurate and high quality micro- but also nano-machining. Numerous works have been carried out to study laser-matter interaction mechanisms on the one hand, and laser machining processes on the other hand. Periodic surface structures, usually named ripples, are often presented in machined samples, either on the surface itself, or on the walls of grooves or holes [1, 2]. Such structures have to be controlled with accuracy to improve processing quality. Sub wavelength ripples can be obtained both on metallic or dielectric samples. The control of sample marking requires a good understanding of laser matter interaction mechanisms and many works are under progress in this field [3].

Such periodic nanostructures can be used for surface functionalization and "smart" marking. Applications can be found in various field. For instance, nanostructures can be obtained with ultrafast laser pulses precisely controlled, and used to obtain optical diffractive effects also precisely controllable. Color effect due to the diffraction of light by periodic structures on metallic surfaces has been evidenced [4], the image is obtained with a usual reading scanner, and the technique can be used to transfer information on a metallic surface.

The modifications of solid surfaces for tribological applications are also of great technological importance, especially for energy saving and eco-friendly technologies. Processes like adhesion, friction, lubrication, coating and de-icing can be optimized for nowadays challenges through surface modifications [5]. A control of laser parameters can help to create a multi-scale topography on metallic surfaces. For instance, initially hydrophilic materials are made hydrophobic without a subsequent chemical coating. The switch from hydrophilicity to hydrophobicity is due to some chemical reaction initiated by the laser action on the irradiated surfaces and not to the surface roughness. However, the effect of surface roughness is visible and predominant in the extreme wetting behaviors.

For practical applications, we have to pay attention to typical parameters of industrial development, such as the processing time [6]. For instance, the physical time can be easily calculated, using the total length of the machining, speed and laser parameters. This calculated physical process time can be compared to the effective time needed to machine the sample. The ability of performing nanostructures with only one pulse open the way to use the ripples for structuring large areas with reasonable time process.

Dedicated or specific tools can be also used for process control. Beam shaping (temporal and/or spatial) is a key tool to understand the influence of time duration on the processes but also to find solutions to speed them [1, 7]. For instance, A strong influence of different pulse durations and double pulse delay times on the formation of periodic surface structures on polyimide were observed employing ultrashort laser pulses tailored on a sub-picosecond and picosecond time scale. Multi-photon, defect-related excitation mechanisms and thermal expansion of the polymer lattice correlated to a loss of long range order and polarisation memory has to be considered [8].

Finally, several applications can be found in the medical field. For instance Titanium and Ti-alloys are widely used for dental and orthopedic implants. Several methods of surface treatments have been developed to make this metal bioactive and/or to improve biological fixation to bone tissue. The ultra fast laser pulse enabled to process micrometeric and sub-micrometeric scales. These hierarchical features consisted of a combination of microgrooves and oriented nanostructures. The femtosecond laser allows to control the width of the microgroove and the orientation of the nanostructures (parallel or perpendicular to the microgrooves) by adjusting its polarization. Mesenchymal stem cells (MSCs) can be cultured on these different topographies to investigate the changes in the development of focal contacts, in cell morphology and orientation as well as in the organization of the extracellular matrix. The development of this innovative method of multi-scale texturing is promising for the development of structured surfaces which could be able to accelerate osteogenesis and improve osseointegration of metal implants [9].

REFERENCES

1. Sanner, N., H. Huot, E. Audouard, C. Larat, and J.-P. Huignard, "Direct ultrafast microstructuring of materials using programmable beam shaping," *Optics and Lasers in Engineering*, Vol. 45, 737–741, 2007.
2. Guillermin, M., F. Garrelie, N. Sanner, E. Audouard, and H. Soder, "Mono- and multi-pulse formation of surface structures under static femtosecond irradiation," *Appl. Surf. Sc.*, Vol. 253, 8075–8079, 2007.
3. Colombier, J. P., F. Garrelie, N. Faure, S. Reynaud, M. Bounhalli, E. Audouard, R. Stoian, and F. Pigeon, "Effects of electron-phonon coupling and electron diffusion on ripples growth on ultrafast-laser-irradiated metals," *J. Appl. Phys.*, to be published.
4. B. Dusser, Z. Sagan, H. Soder, N. Faure, J. P. Colombier, M. Jourlin, and E. Audouard, "Controlled nanostructrures formation by ultra fast laser pulses for color marking," *Optics Express*, Vol. 18, 2913, 2009.
5. Bizi-Bandoki, P., S. Benayoun, S. Valette, B. Beaugiraud, and E. Audouard, "Modifications of roughness and wettabilit properties of metals induced by femtosecond laser treatment," *Applied Surface Science*, Vol. 257, 5213–5218, 2011.
6. Bruneel, D., G. Matras, R. Le Harzic, N. Huot, K. Koenig, and E. Audouard, "Micromachining of metals with ultra-short Ti-Sapphire lasers: Prediction and optimization of the processing time," *Opt. Las. Eng.*, Vol. 48, 268, 2010.
7. Mauclair, C., A. Mermillod-Blondin, S. Landon, A. Rosenfeld, I. V. Hertel, E. Audouard, I. Myiamoto, and R. Stoian, "Single pulse multipoint ultrafast laser photoinscription of axial dot arrays in bulk glasses," *Opt. Lett.*, Vol. 36, 325, 2011.
8. Forster, M., W. Kautek, N. Faure, E. Audouard, and R. Stoian, "Periodic nanoscale structures on polyimide surfaces generated by temporally tailored femtosecond laser pulses," *Phys. Chem. Chem. Phys.*, Vol. 13, 4155, 2011.
9. Dumas, V., A. Rattner, E. Audouard, P. Bertrand, J.-C. Dumas, J. Vidal, and I. Smurov, "Improved biomedical titanium alloys using ultrafast laser-induced multi-scale surface texturing," to be published.

Harnessing Ultrafast Laser-induced Subwavelength Structures for Liquid Crystal Photonics Application

Ya Cheng[1], **Yang Liao**[1], **Min Huang**[1, 2], **and Zhizhan Xu**[1]

[1]State Key Laboratory of High Field Laser Physics, Shanghai Institute of Optics and Fine Mechanics
Chinese Academy of Sciences, P. O. Box 800-211, Shanghai 201800, China
[2]State Key Laboratory of Optoelectronic Materials and Technologies
Sun Yat-Sen University, Guangzhou 510275, China

Abstract— Over the past decade, the field of Lab-on-a-Chip (LOC) has undergone a tremendous growth, because it offers the possibilities for downsizing of both biological and chemical analysis. Liquid crystals (LCs), due to their liquid-like behavior, large birefringence, extreme sensitivity to external field and surface interactions, offer great flexibility for photonics applications. For traditional LC devices, LCs are generally sandwiched between two glass plates coated with transparent Indium-Tin-Oxide (ITO) films as electrodes and alignment layers for orientating the LC molecules, in which homogeneous LC alignment can usually be achieved on topographic surface created by mechanical rubbing or lithography processes. Although the multilayer structuring technologies are well-established and widely used in the field of LC display, it is difficult to fabricate integrated individual LC cell for miniature opto-electronic devices.

As a direct, maskless fabrication technique, femtosecond (fs) laser micro- and nano-fabrication provides a new approach for local modification inside transparent materials through nonlinear optical processes, thus allowing for flexible construction of various 3D functional structures inside transparent substrates. Here, we demonstrate that subwavelength periodic surface structures (nanoripples) can be produced on the sidewalls of a micro-cell vertically embedded in a fused silica glass substrate by fs laser ablation, and homogeneous LC alignment with different azimuthal angles can be achieved in the LC micro-cell. Furthermore, we demonstrate an integrated LC electro-optic phase modulator embedded in fused silica glass by integrating a micro-LC cell, optical waveguides, and microelectrodes in a single substrate using fs laser micromachining.

Hyperdoped and Microstructured Silicon for Solar Energy Harvesting

Eric Mazur, **Meng-Ju Sher**, **Benjamin Franta**, **Yu-Ting Lin**, **and Katherine C. Phillips**
School of Engineering and Applied Sciences, Harvard University
9 Oxford Street, Cambridge, Massachusetts 02138, USA

Abstract— We have developed a unique technique to significantly change the optoelectronic properties of silicon through hyperdoping and texturing. By irradiating silicon with a train of amplified femtosecond laser pulses in the presence of a wide variety of dopant precursors, we can hyperdope silicon to > 1 at .% in a 300-nm thin layer. In addition, laser-induced semi-periodic surface textures have excellent anti-reflection and light-trapping properties. The technique is robust: it is effective on both crystalline and amorphous silicon and for both thin films and thick substrates. When the dopant is chosen from the heavy chalcogen (sulfur, selenium, tellurium), fs-laser doped silicon exhibits near-unity light absorptance from the ultraviolet ($\lambda > 0.25\,\mu\text{m}$) to the near infrared ($\lambda < 5\,\mu\text{m}$), which is far beyond silicon's bandgap at $1.1\,\mu\text{m}$.

Femtosecond laser hyperdoping achieves dopant concentrations higher than the equilibrium solubility limit through a process called solute trapping. Femtosecond laser pulses with energy greater than the melting threshold transform the surface into a molten layer, enabling dopant precursors in the vicinity to diffuse in. As the deposited energy diffuses into the substrate, the molten layer resolidifies with a speed faster than the rate at which thermodynamic equilibrium can be established ($> 1\,\text{m/s}$), thus trapping the dopants in their hyper-concentrated state. The dopant precursors can be in the gas phase (such as SF_6) or the solid phase (such as a thin film of Se or Te thermally deposited onto a Si substrate). Femtosecond laser texturing, on the other hand, originates from the formation of laser induced period surface structures (LIPSS), and consists of semi-periodic nanometer- and micrometer-scaled structures. Recently, we identified laser parameters for independently tuning the hyperdoping and texturing processes.We envision the fs-laser technique being used to produce new materials for many applications, especially in the area of solar energy.

The femtosecond laser hyperdoping technique endows silicon with remarkable optoelectronic properties, such as near unity absorption and a strong sensitivity to infrared wavelengths of light that pass through a standard silicon wafer. Laser hyperdoping creates defect- and bandgap engineered semiconductors, and laser texturing further enhances the optical density through excellent light trapping. Hyperdoped silicon devices represent the fruit of a novel fabrication technique for Earth-abundant, semiconductor-based solar energy harvesters with the potential for both low cost and high photoconversion efficiency.

Laser Fabrication of Large-scale Nanoparticle Arrays and Their Application to Plasmonic Sensing

Arseniy I. Kuznetsov[1, 2], **Andrey B. Evlyukhin**[2], **Carsten Reinhardt**[2], **Manuel R. Gonçalves**[3], **Othmar Marti**[3], **Guillaume G. Vienne**[1], **Boris Luk'yanchuk**[1], **and Boris N. Chichkov**[2]

[1]Data Storage Institute, DSI Building 5, Engineering Drive 1, 117 608, Singapore
[2]Laser Zentrum Hannover e.V., Hollerithallee 8, Hannover D-30419, Germany
[3]Institute of Experimental Physics, Ulm University, Ulm D-89069, Germany

Abstract— A novel method for high-speed fabrication of large-scale periodic arrays of spherical metal and dielectric nanoparticles (diameters of 40–200 nm) has been developed. This method is based on a combination of lithographic techniques with laser-induced transfer (Fig. 1(a)) [1–3]. First, nanosphere and e-beam lithography are applied to fabricate arrays of triangular prism- or disk-shape nanostructures. Then these nanostructures are melted by femtosecond laser irradiation and transferred towards a different (receiver) substrate. Millions of identical nanoparticles can be transferred simultaneously by a single laser pulse. The transferred particles have spherical shape, which makes them suitable for plasmonic applications. They are arranged in high-quality arrays corresponding to the template structures fabricated on the donor substrate by lithography (Fig. 1(b)). At some specific sets of parameters, these nanoparticle structures possess very narrow dips in their transmission spectra. These spectral features appear due to diffractive coupling of localised surface plasmons of the nanoparticles and are very sensitive to the refractive index of local environment. We experimentally demonstrate sensors based on these nanoparticle arrays with the sensitivity of 365 nm/RIU and the figure of merit (FOM) of 21.5 in the visible spectral range. This high sensing performance together with the fast and cheap fabrication procedure makes these nanoparticle array sensors promising for biomedical applications. Other applications of this novel method for fabrication of 2D and 3D metamaterials and nanophotonic devices will be discussed.

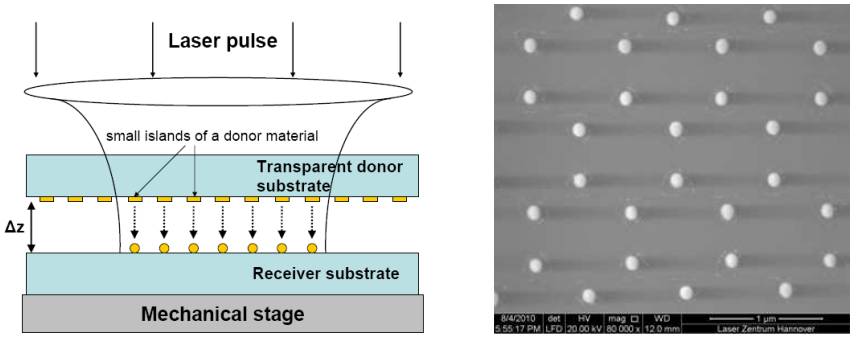

Figure 1: (a) Laser-induced transfer (LIT) scheme; (b) An array of nanoparticles fabricated by a combination of the LIT approach and the nanosphere lithography [4].

REFERENCES

1. Kuznetsov, A. I., J. Koch, and B. N. Chichkov, "Laser-induced backward transfer of gold nanodroplets," *Opt. Express*, Vol. 17, 18820, 2009.
2. Kuznetsov, A. I., A. B. Evlyukhin, C. Reinhardt, A. Seidel, R. Kiyan, W. Cheng, A. Ovsianikov, and B. N. Chichkov, "Laser-induced transfer of metallic nanodroplets for plasmonics and metamaterial applications," *J. Opt. Soc. Am. B*, Vol. 26, B130, 2009.
3. Kuznetsov, A. I., R. Kiyan, and B. N. Chichkov, "Laser fabrication of 2D and 3D metal nanoparticle structures and arrays," *Opt. Express*, Vol. 18, 21198, 2010.
4. Kuznetsov, A. I., A. B. Evlyukhin, M. R. Gonçalves, C. Reinhardt, A. Koroleva, M. L. Arnedillo, R. Kiyan, O. Marti, and B. N. Chichkov, "Laser fabrication of large-scale nanoparticle arrays for sensing applications," *ACS Nano*, Vol. 5, 4843–4849, 2011.

Preparation of Nanostructured Ag Substrate with Femtosecond Laser as Surface-enhanced Raman Scattering Substrates

H. W. Chang[1], **C. Y. Lin**[2], **C. W. Cheng**[2], **Y. W. Lin**[3], **T. M. Wu**[3], **and Y. C. Tsai**[1]

[1]Department of Chemical Engineering, National Chung Hsing University
250 Kuo Kuang Road, Taichung 402, Taiwan
[2]ITRI South, Industrial Technology Research Institute
No. 8, Gongyan Road, Liujia Shiang, Tainan County 734, Taiwan
[3]Department of Materials Science and Engineering
National Chung Hsing University, 250 Kuo Kuang Road, Taichung 402, Taiwan

Abstract— The surface-enhanced Raman scattering (SERS)-active nanostructured Ag substrate were fabricated using femtosecond laser technique. After the femtosecond laser pulses, the surface morphology of the substrates was analyzed by field emission scanning electronic microscope (FESEM) and atomic force microscopy (AFM). Chemical compositions of the prepared SERS-active substrate were using X-ray photoelectron spectroscopy (XPS) patterns. FESEM images indicated the formation of periodic structures on Ag substrate with a spacing of approximately 500–600 nm. The AFM images of the resultant products showed that the root of mean squared (RMS) roughness of the nanostructured Ag substrate was larger than the untreated Ag substrate. The XPS spectras demonstrated no impurities of Ag oxide species. The produced nanostructured Ag surface in SERS was evaluated by using rhodamine 6G (R6G) as a probe molecule. The nanostructured Ag surface exhibits a higher SERS intensity by 15-fold, as compared with the SERS intensity of untreated Ag substrate. The Results demonstrated an increase of SERS enhancement that follows the nanostructured Ag surface roughness. This result reveals that the nanostructured Ag surface could be very useful for analytical applications of the SERS.

Photonic Applications of Femtosecond Laser-induced Surface Nanogratings

S. V. Makarov[1], **A. A. Ionin**[1], **S. I. Kudryashov**[1], **A. E. Ligachev**[2], **L. V. Seleznev**[1], **D. V. Sinitsyn**[1], **R. V. Samsonov**[3], **A. I. Maslii**[4], **A. Zh. Medvedev**[4], **B. G. Gol'denberg**[5], **and V. P. Korol'kov**[6]

[1]P. N. Lebedev Physical Institute, Russian Academy of Sciences
Leninskiy Prospect 53, Moscow 119991, Russia
[2]General Physics Institute, Russian Academy of Sciences, Vavilova Str. 38, Moscow 119991, Russia
[3]Novosibirsk State University, Novosibirsk, Russian Federation
[4]Institute of Solid State Chemistry and Mechanochemistry
Siberian Branch of the Russian Academy of Sciences, Novosibirsk, Russian Federation
[5]G. I. Budker Institute of Nuclear Physics, Siberian Branch of the Russian Academy of Sciences
Novosibirsk, Russian Federation
[6]Institute of Automation and Electrometry, Siberian Branch, Russian Academy of Sciences
Novosibirsk, Russian Federation

Abstract— We investigate the effect of diffraction color marking of Si, Al, Ti and Cu using femtosecond laser pulses ($\lambda \approx 744\,\text{nm}$, $\tau \approx 100\,\text{fs}$). Laser-induced surface gratings (LIPSS) have well-defined relief with nonsinusoidal profile that gives diffraction colorizing of surface. The period of such surface laser-induced grating can be estimated by using the plasmon-polariton model and additional calculated instantaneous optical characteristics of the surface photoexcited by fs-irradiation. This method of metal and semiconductor colorizing allows creating spots (the parts of the picture) very fast with any color and with different brightness (possibility to creating black and gray points).

We also examined whether the LIPSS on Ni/Cu bilayer foil could be used to produce an anti-reflective coating on polymer replicas of the Ni/Cu surface relief pattern. The polymer surface with the characteristic nanostructure periods obtained in this study $\Lambda \approx 400$–$450\,\text{nm}$ may show up anti-reflective behavior in the near-IR spectral region. Indeed, in our experiments the polymer with modificated surface by discussed technic shows increasing of 20% of light transmission at wavelengths above 2250 nm.

Consequently, the advantages of the femtosecond laser lithography (inexpensively, high speed of writing and ability to create surface with unique chemical characteristics) can be used successfully in applications where requirements of relief precision characteristics are not very high.

Rapid Prototyping of Three-dimensional Microfluidic Mixers in Glass by Femtosecond Laser Direct Writing

Yang Liao, **Jiangxin Song**, **Ya Cheng**, **and Zhizhan Xu**
State Key Laboratory of High Field Laser Physics
Shanghai Institute of Optics and Fine Mechanics, Chinese Academy of Sciences
P. O. Box 800-211, Shanghai 201800, China

Abstract— The creation of complex three-dimensional (3D) microfluidic systems has attracted significant attention from both scientific and applied research communities. However, it is by now still a formidable challenge to build 3D microfluidic structures with arbitrary configrations using conventional planar lithographic fabrication methods. Here, we demonstrate rapid fabrication of high-aspect-ratio microfluidic channels of various 3D configurations in glass substrates by femtosecond laser direct writing. As a maskless fabrication technique, femtosecond laser direct writing can directly form 3D microfluidic structures embedded in glass materials without using extra stacking and bonding procedures, offering several distinct advantages in terms of fabrication precision and efficiency, flexibility, and cost-effectiveness. Based on this new approach, we demonstrate a 3D passive microfluidic mixer and characterize its functionalities. Both the numerical simulations and mixing experiments show that the 3D mixer can offer far more superior mixing performance than its 1D counterpart. This technology will enable rapid constrcution of complex 3D microfluidic devices for a wide array of lab-on-a-chip applications.

Session 2P2b
Nano Scale Electromagnetics

Resonant Magnetoplasmonic Core-shell Nanostructures for Biosensing Applications

M. Essone Mezeme, **S. Lasquellec**, **and C. Brosseau**
Lab-STICC, Université de Bretagne Occidentale
CS 93837, 6 Avenue Le Gorgeu, 29238 Brest Cedex 3, France

Abstract— We present a numerical model for characterization of the frequency dependence of the effective magnetic permeability and permittivity of a core-shell (CS) nanostructure composed of a magnetic core and a plasmonic shell with well-controlled dimensions for different geometries and polarizations. Our model has two principal features: (i) we consider two-dimensional three-phase heterostructure (or cross sections of infinite three-dimensional parallel, infinitely long, identical, cylinders, where the properties and characteristics are invariant along the perpendicular cross sectional plane). (ii) While strictly valid only in a dc situation, our analysis can be extended to treat electric fields that oscillate with time provided that the wavelengths associated with the fields are much larger than the microstructure dimension in order that the homogeneous (effective medium) representation of the composite structure makes sense. Such nanostructures simultaneously possess both magnetic (GYR) and plasmonic (PLR) resonances. To illustrate the effects of shape anisotropy of the CS structure, we analyze several possible shell shapes involving sharp edges and tips. Geometric parameters of the CS nanostructures and excitation polarized parallel and perpendicular to the antenna axis permit fine tuning of the PLR. Changing the internal geometry of the nanostructure not only shifts its resonance frequencies, but can also strongly modify the relative magnitudes of the electric field enhancement, independently of nanoparticle shape. The model sets the foundation of quantitatively determining the spatial confinement of the electric field in regions $\approx 20\,\text{nm}$ in linear dimension. Because of its resonant nature, we found nanolocalized THz fields corresponding to large electric field enhancement two orders of magnitude higher in amplitude than the excitation optical field. The simulations in this paper are important because magnetoplasmonic CS nanostructures are currently being explored as candidates for resonant optical nanoantennas for biosensing applications.

Exchange Splitting of Backward Volume Spin Wave Configuration Dispersion Curves in a Permalloy Nano-stripe

G. Venkat[1], **A. Prabhakar**[1], **M. Franchin**[2], **and H. Fangohr**[2]

[1]Department of Electrical Engineering
Indian Institute of Technology, Madras, Chennai 600036, India
[2]Engineering and Environment, University of Southampton, Southampton, UK

Abstract— Micromagnetic simulations can now yield information on the dispersion relation of spin waves in nano-stripe geometries. We excited backward volume spin waves (BVSW) in a permalloy film (1000 nm × 50 nm × 1 nm), assuming a sinc excitation pulse applied to a current carrying wire placed above the nano-stripe. An external bias field of 10 kOe ensured that the magnetization was in its ground state. We then applied an excitation pulse, with a peak amplitude of 5 kOe at the circumference of the wire. Although the wire was not included in the micromagnetic geometry, the Oersted fields were calculated for each finite element cell in the geometry based on its distance from the axis of the wire. The spatial and temporal variation in the excitation field excited only the dominant lowest order BVSW, which is easily visible as a parabola in Figure 1(a).

We also observe a number of horizontal lines in Figure 1(a), a manifestation of the exchange splitting of the dispersion relation due to interactions between the lowest and higher order longitudinal modes [1]. We plotted $\omega(k)$ for $k \approx 0.55\,\mathrm{rad/nm}$, shown by the vertical dotted line in Figure 1(a) to quantify the inter-mode interactions. The resulting resonance peaks in power are shown in Figure 1(b). However, we observe the existence of multiple spin wave resonances in the dispersion curve due to the possibility of longitudinal modes which cause an exchange splitting of the dispersion curve. Resonances due to longitudinal modes would follow a relation of the form [2]

$$\omega_n = \omega_0 + \omega_M \lambda_{ex} \left(\frac{(2n+1)\,\pi}{d} \right)^2$$

such that there is a linear increase in frequency separation with mode order number n. We fit the spin wave resonances to a straight line $\Delta f = mn + b$ with $m = 57.53 \pm 0.76\,\mathrm{MHz}$ and $b = 523.88 \pm 32.61\,\mathrm{MHz}$ and extract an effective exchange length for BVSW excitations in such a geometry.

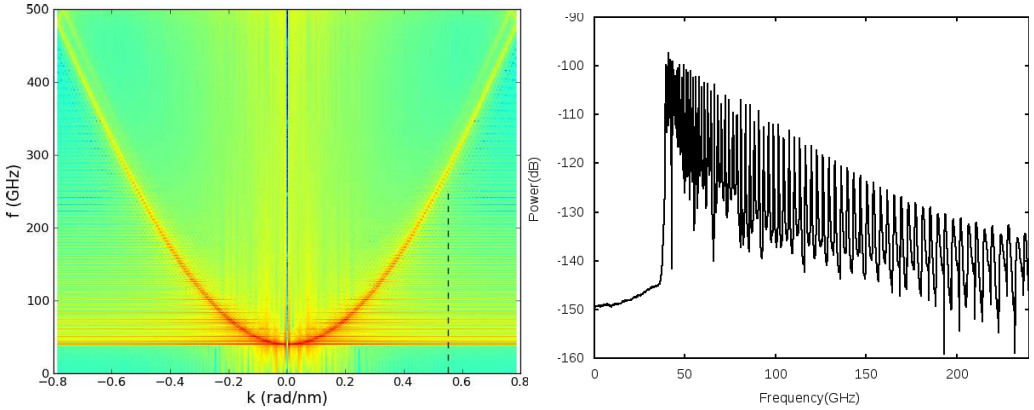

(a) (b)

Figure 1: (a) Dispersion curve for BVSWs in a permalloy nano-stripe excited by Oersted fields from a current carrying wire. (b) Corresponding power spectrum at $k = 0.55\,\mathrm{rad/nm}$.

REFERENCES

1. Kalinikos, B. and A. N. Slavin, "Theory of dipole-exchange spin wave spectrum for ferromagnetic films with mixed exchange boundary conditions," *J. Phys. C: Solid Sat. Phys.*, 19, 1986.
2. Stancil, D. D. and A. Prabhakar, *Spin Waves Theory and Applications*, 1st Edition, Springer, New York, 2008.

A Computational Study of the Coupled Emissions between Flurophores and Gold Triangular Prism Bow Tie

A. Centeno, **F. Xie**, **and N. Alford**
Department of Materials, Imperial College London, SW7 2AZ, United Kingdom

Abstract— In this work, we report on calculations using the Finite Difference Time Domain (FDTD) method that investigates how radiated emissions are modified if the fluorophore is located between the tips of two Au triangular prisms in a bow-tie configuration. The triangles considered in the calculations have equilateral sides of 60 nm and a height of 30 nm. The Au is modelled using a Drude-Lorentz model, with one Drude and two Lorentz terms. The radiated emissions are found by considering the power flow through a three-dimensional closed surface around the bow-tie. The distance of this surface from the nanoparticles is determined by convergence testing. The fluorophore is considered to be a point dipole where its orientation is determined by its polarization. The tip-to-tip separation considered between the triangles is 10 nm and 20 nm respectively with the fluorophore placed mid-way in the gap. The emissions are normalised to that of an uncoupled fluorophore. If the normalised emissions are greater than 1 enhancement has occurred whilst if less than 1 quenching has taken place. When the fluorophore is orientated such that it is perpendicular to the tips of the triangles there is an enhancement in the radiated emissions for all wavelengths between 300 nm and 1000 nm, when compared with that of just the point source. When the fluorophore is orientated tangential to the tip, that is the source is rotated by 90 degrees from the previous case, then an enhancement is seen between 500 and 600 nm but significant emission quenching occurs above 630 nm. The significance of these results to fluorescent enhancement or quenching by metal nanoparticles will be discussed. The near-fields around the nanoparticles due to both the fluorophore and incident light will be presented and the significance shown.

Blocking Oscillation Due to Combination of Discrete and Continuous Charge/Flux Transfer in Systems Including Nano/Josephson Tunnel Junctions

Yoshinao Mizugaki
The University of Electro-Communications (UEC Tokyo), Japan

Abstract— Nanotechnology enables us to manipulate a single electron in solid-state circuits. Single-electron tunneling is known to transfer electric charge in units of the fundamental charge e through tiny (nano-scale) tunnel junctions. So far, many single-electron devices, such as a single-electron transistor, a single-electron turnstile, and a single-electron pump, have been proposed and demonstrated. The author proposes a blocking oscillator composed of tiny tunnel junctions and a dissipative element (resistor). The key is the combination of the discrete and continuous charge transfer. Monte-Carlo simulation demonstrates blocking oscillation of an island charge. Similar blocking oscillation occurs in a superconducting loop including Josephson junctions and a resistor. Electromagnetic duality between single-electron devices and superconducting Josephson devices are observed in these results. In this paper, the author numerically demonstrates these blocking oscillation phenomena and discusses the possibility of experimental observation.

ACKNOWLEDGMENT

This work was partially supported by the Asahi Glass Foundation.

REFERENCES

1. Mizugaki, Y., "Numerical demonstration of relaxation oscillation in a resistive superconducting quantum interference device with two nonhysteretic Josephson junctions," *IEEE Trans. Appl. Supercond.*, Vol. 20, No. 5, 2322–2326, 2010.
2. Mizugaki, Y., "Blocking charge oscillation in a series array of two tiny tunnel junctions with a resistive ground path from its island electrode," *IEEE Trans. Nanotechnol.*, Vol. 11, No. 1, 194–199, 2012.

Derivative-free Optimization of Nano-plasmonic Structures

Mohamed H. El Sherif, **Osman S. Ahmed**, **and Mohamed H. Bakr**
The Department of Electrical and Computer Engineering, McMasterUniversity
Hamilton, Ontario L8S4K1, Canada

Abstract— Sub-wavelength operation at the optical frequency range has recently witnessed the introduction of metallic plasmonic structures. The introduction of the slit array in a metallic film has attracted tremendous attention due to its extraordinary transmission as well as its beaming effect. This ability to confine light in a sub-wavelength manner led to a diverse number of applications for optical interconnects, CMOS image sensors, and lens effect [1]. However, optimizing nano-plasmonic structures has always been a challenge, and very few publications have worked on it. For plasmonic structures that operate in the optical range, the electrical size of the structures is large, thus requiring arduous simulations. In [2], a Genetic Algorithm (GA) is proposed for the optimization of metalic slit arrays. A large number of time-consuming initial simulations are needed. Also, as the array increases in dimensions, the optimization parameters increase as well, requiring more time and computations.

In this paper, we demonstrate an efficient method for the design of plasmonic slit array structures. These arrays are electrically large with many designable parameters. Our methodology converts this computationally-intensive design problem into a simpler problem with only two variables. The approach takes advantage of a parabolic phase profile to determine the optimal values of the different parameters. We demonstrate this approach by optimizing different arrays of slits using a derivative-free pattern search solver. The goal of our formulation is to obtain the furthest focal point without deteriorating the beam width. Our approach is successfully demonstrated through many design problems. The accuracy of our designs is verified using Lumerical's FDTD Solutions software.

REFERENCES

1. Verslegers, L., P. B. Catrysse, Z. Yu, J. S. White, E. S. Barnard, M. L. Brongersma, and S. Fan, "Planar lenses based on nanoscale slit arrays in a metallic film," *Nano Lett.*, Vol. 9, 235–238, 2009.
2. Choi, D., Y. Lim, S. Roh, I.-M. Lee, J. Jung, and B. Lee, "Optical beam focusing with a metal slit array arranged along a semicircular surface and its optimization with a genetic algorithm," *Appl. Opt.*, Vol. 49, A30–A35, 2010.

Calculation of the Acoustomagnetoelectric Field in a Rectangular Quantum Wire with an Infinite Potential in the Presence of an External Magnetic Field

N. V. Nghia, **N. Q. Bau**, **N. V. Nhan**, **and D. Q. Vuong**
Department of Physics, College of Natural Sciences, Hanoi National University, Hanoi, Vietnam

Abstract— The acoustomagnetoelectric (AME) effect in a rectangular quantum wire with an infinite potential is investigated in the presence of an external magnetic field. The analytic expression for the AME field in a rectangular quantum wire with an infinite potential is calculated by using the quantum kinetic equation for the distribution function of electrons interacting with external phonons. The dependence of AME field on the acoustic wave number q, the temperature of the system T and the intensity of the external magnetic field H are obtained. The analytic expression for the AME field is numerically evaluated, plotted and discussed for the specific rectangular quantum wire with an infinite potential GaAs. The dependence of the AME field on the temperature of the system is significantly reduced in the low temperature region and it is approximately constant in the high temperature region. In the dependence of the AME field on the intensity of the external magnetic field, the AME field can get the small peaks corresponding to the resonance frequency of the cyclotron-electron-acoustic phonon. The results are compared with those for normal bulk semiconductors and superlattices to show the difference.

Sensitive Surface Plasmon Sensors Using Hot Embossing Gold Nanostructures on Plastic Films

Kuang-Li Lee[1], **Shu-Han Wu**[2], **and Pei-Kuen Wei**[1, 2, 3]

[1]Research Center for Applied Sciences, Academia Sinica, Taipei, Taiwan
[2]Institute of Biophotonics, National Yang-Ming University, Taipei, Taiwan
[3]Department of Optoelectronics, National Taiwan Ocean University, Keelung, Taiwan

Abstract— Nanostructure-based sensors are capable of sensitive and label-free detections for biomedical applications. However, high-throughput sensitivity and low-cost fabrication are the main issues which should be addressed. The majority of the fabrication techniques for gold nanostructures utilize focused ion beam milling to directly pattern gold films or electron-beam lithograthy combined with a dry etching method or lift-off process to generate nanostructure on a substrate. These writing techniques are not suitable for massive production. Besides, the surface plasmon loss is high due to electron scattering on the grain boundaries. In this study, chip-based nanostructures for intensity-sensitive sensors were fabricated and tested using a thermal annealing-assisted template stripping method. Large-area uniform nanoslit arrays with 500 nm period and various slit widths, from 30 nm to 165 nm, were made on polycarbonate films. Transverse-magnetic polarized wave in these gold nanostructures generated shape and asymmetric Fano resonant spectra. The full width at half maximum bandwidth decreased with the decrease of slit width. The narrowest bandwidth was down to 6 nm. Compared to nanoslit arrays using electron beam lithography on glass substrates, the proposed chip has a higher intensity sensitivity up to 9260%/RIU (refractive index unit) and reaches a figure of merit up to 49. The higher intensity sensitivity for the template-stripped nanostructure is attributed to smoother gold surface and larger grain size on plastic film which reduce the surface plasmon propagation loss. In the applications, we demonstrate real-time, high-throughput sensing arrays for studying antibody-antigen interactions and living cells secretions.

Session 2P3a
Ground Penetrating Radar Methods for Subsurface Investigations

Ground Penetrating Radar Detection of Human Vital Signals in Complex Environments

Lanbo Liu[1,2], **Zijian Liu**[1], **Hao Xie**[1], **Benjamin Barrowes**[2], **and Amvrossios Bagtzoglou**[1]

[1]Department of Civil and Environmental Engineering
University of Connecticut, Storrs, CT 06269-2037, USA
[2]USACE Engineering Research and Development Center
Cold Regions Research and Engineering Laboratory, Hanover, NH 03755, USA

Abstract— Using finite difference time domain numerical simulation approach we investigate the use of ground penetrating radar techniques for human vital signal detection in some complex ambient environments including concrete debris caused by collapsed building at an earthquake disaster site, and some highly reverberating chambers and hallways. The model consists of two or more persons with different vital signals, i.e., with different cardio-respiration features, posed in different position, and placed at different distances to the antennas. We model the situation with different setups including single source multiple receiver, single-source and single receiver profiling, and time lapse vital signal detection. This paper will present the simulation and imaging results and recommend the appropriate practice and procedure for improving the accuracy for the detection and monitoring of life humans behind obstacles using ground penetrating radar.

Microwave Reflectometry for the Diagnostic of Cultural Heritage Assets

L. Capineri[1], **P. Falorni**[1], **C. Frosinini**[2], **M. Mannucci**[3], **N. Macchioni**[4], **R. Olmi**[7], **S. Palanti**[4], **S. Penoni**[5], **S. Pieri**[7], **S. Priori**[7], **C. Riminesi**[6], **A. Santacesaria**[2], **and C. Todaro**[5]

[1]Dipartimento Elettronica e delle Telecomunicazioni, Università di Firenze, Firenze 50139, Italy
[2]Opificio delle Pietre Dure, Via degli Alfani 78, Firenze 50100, Italy
[3]LegnoDOC, Via Pier della Francesca, b39, Prato 59100, Italy
[4]CNR, IVALSA, Via Madonna del Piano 10, Sesto Fiorentino 50019, Italy
[5]Faberestauro, piazza Ginori 13, Sesto Fiorentino 50019, Italy
[6]ELab Scientific, 17 Fra' D. Bartolomeo Street, Firenze 50132, Italy
[7]CNR, IFAC, Via Madonna del Piano 10, Sesto Fiorentino 50019, Italy

Abstract— The research work on a new Microwave Reflectometry system is presented for the diagnostic of Cultural Heritage assets. This new system allows to investigate in depth several materials like stone, plaster and wood. The depth analysis is performed thanks a modulated continues wave operating in the 1 GHz–5 GHz frequency range. The electromagnetic wave penetration in the medium depends on the physical characteristics of the material: moisture, presence of cavities and hole, and differences between the constituent materials. The specifications of the system should take into account the application requirements in not easy areas, such as restoration sites, including: portability (weight and reduced size) autonomy (battery operation). These features should be added to the responsiveness, reliability and, possibly, the low cost.

The implementation of the the Microwave Reflectometer prototype consists of:

(1) The development of a generator/receiver that complies with electromagnetic compatibility issues; the subsystem will be based on a commercial Vectorial Network Analyzer.
(2) An optical compact low cost system for tracking the scan head with accuracy better than 1 cm that takes into account different environmental illumination conditions.
(3) The development of models to study the interaction between the electromagnetic signal and the different media — e.g., wood, stone, plaster.
(4) The development of software for signal analysis and imaging of the reflectometric response.

The results of the prototype applied on several case studies will be presented for two areas of interest on cultural heritage:

- With regard to the study of wall paintings and other artistic means to verify, through the images obtained by scanning, non-contact capacity detect the presence of heterogeneity and moisture changes in materials to support and assess the feasibility of detecting the underlying layer texture painting.
- Regarding wooden artefacts, will be considered two types: structural elements and panel paintings. For structural elements (beams) are simulate the presence of fungal decay and pockets of moisture, while for the paintings on wood are simulated xylophages insect attacks.

These activities should lead to the creation of a database of "signatures" that will later be used to interpret the results of campaigns in situ diagnostic case studies that will be discussed in the presentation.

Investigation of Holographic Radar Capabilities for the Detection of Shallow Buried Plastic Antipersonnel Landmines

T. Bechtel[1], **L. Capineri**[2], **P. Falorni**[2], **M. Inagaki**[3], **S. Ivashov**[4], **and C. Windsor**[5]

[1]Department of Earth and Environment, Franklin & Marshall College, Lancaster, PA, USA
[2]Department of Electronics and Communications, University of Florence, Florence 50139, Italy
[3]Walnut Ltd., 1-19-13, Saiwaicho, Tachikawa, Tokyo 190-0002, Japan
[4]Remote Sensing Laboratory, Bauman Moscow State Technical University, Moscow, Russia
[5]116, New Road, East Hagbourne, OX11 9LD, UK

Abstract— The holographic subsurface radar (HSR) of RASCAN type has been investigated for detection of small plastic antipersonnel landmines buried at shallow depth in natural soil. The investigation consists of the comparison of data obtained by surface scans in an outdoor test bed with two HSR operating at different discrete frequencies near 2 GHz and 4 GHz, each with receiving antennae both parallel and perpendicular to the polarization of the transmitter. The two systems have different signal penetrations (up to 20 cm in dry soil for the 2 GHz), different antenna radiation patterns and different sensitivities for the parallel and perpendicular polarization images. The HSR has the capability to record small phase changes in the received signals due to electromagnetic impedance discontinuities. This high sensitivity is an advantage to detect small (5 cm diameter) plastic targets but introduces also clutter signals due to surface irregularities and other clutter objects commonly found in battlefield. The choice of the operating frequency, the coupling of the antenna with soil surface and the scanning spatial sampling is important to get enough information for an efficient detection of small plastic targets. Thanks to high spatial resolution of the HSR images, the detection of targets by direct image interpretation is still possible, but is time consuming, is limited to sensitivity of the human eye grey scale variations, and is may be subjective based on different operators' experience and level of expertise. Therefore, pre-processing software has been developed to correct images to a common background level, and to detect objects that stand-out from this background using scanned scanned receptive fields. These objects can then be identified by a trained neural network. Training data HSR images have been collected in test beds around the world for soils with different mineralogies, moisture content, grain size distribution and organic content in order to identify geomorphological settings where this method would be applicable for field use.

Microwave Imaging System for the Detection of Buried Objects Using UWB Antenna — An Experimental Study

Elizabeth Rufus and Zachariah C. Alex
School of Electronics Engineering, VIT University, Vellore, India

Abstract— The studies conducted in the past have proved the potential of microwave imaging technique for many applications in the field of non destructive evaluation. Different types of microwave imaging systems are currently being used for imaging in areas such as Ground Penetrating Radar and Remote Sensing. Depending on the objects to be imaged, different antennas are needed; these range from small antennas used for near field measurements in ground penetrating radar to large airborne system used in remote sensing.

There are two key issues to address when designing a microwave imaging system. One is the increase of the signal to noise ratio in the system and the other is to assure that the system has a large dynamic range. This is important because of the fact that the scattered signal is often weak in comparison with the transmitted signal. This implies that any noise in the system will have large impact on the image quality and then the system must be able to distinguish even small difference in the received signals.

In this paper, we present the development of an experimental set up of a radar based microwave imaging system using 1-D beamforming algorithm to detect the buried object using a UWB antenna operating between 1–11 GHz (Xu Li et al. 2003) and its experimental validation.

The experimental set up consists of a mechanical scanner with 3.6 mm in the X and Y directions, UWB horn antenna whose height is 1.3 cm, and aperture dimesions are 2.5 cm and 2 cm, and a network analyzer PNA N5230A. The ultra wideband (UWB) antenna is mounted on the scanner. At each position, the antenna sweeps over a frequency range from 1 GHz to 11 GHz. This antenna transmits the microwave signal and receives the backscatters from all the objects. These backscatters are passed through the 1-D beam former designed to image the backscatter energy as a function of location. Even millimeter sized embedded objects have relatively large microwave scattering cross-sections due to their significant dielectric property contrast. Therefore they produce localized region of large backscatter energy levels in the beamformer image. We have found from the experimental study that the objects of size of up to 4 mm embedded in the sand bath could be detected using the developed microwave imaging setup.

Detection, Identification and Localization of Underground Objects via Continuous Wave GPR

Hülya Şahintürk[1], **and İbrahim Akduman**[2]

[1]Mathematical Engineering Department, Yıldız Technical University
34210 Davutpaşa, Istanbul, Turkey
[2]Electrical and Electronics Engineering Faculty, Istanbul Technical University
34469 Maslak, Istanbul, Turkey

Abstract— One of the main applications of the GPR systems is the detection, localization and identification of underground objects such as landmines, pipelines, cracks etc. Although there has been a significant development in this direction, the problem is still open and more robust and reliable systems and methodologies have to be investigated.

Along this line, the main objective of this work is to give a new approach and related measurement system whose aim is to detect, locate and identify the objects buried under a rough surface. The proposed system is a continuous wave Ground Penetrating Radar operating in the frequency range of 1–4 GHz. The system carries two modified Vivaldi antennas which are located with an offset of 10 cm. One of the antennas operates as transmitter while the other works as the receiver. By moving this transmitter and receiver system on a line as parallel to the mean plane of the rough interface the scattered data is collected.

The detection, localization and identification of the buried objects are achieved by reconstructing the equivalent surface impedance of the bodies on the rough surface. To this aim, the measured data is analytically continued to the rough surface where the equivalent impedance is located through the representation of scattered field in terms of plane waves in the spectral domain. Then the equivalent surface impedance is calculated directly from the standard impedance boundary condition (IBC) which requires to know the total field and its derivative on the rough interface [1]. The objects make strong contributions to the impedance function both in amplitude and phase and by observing these contributions one can detect and locate them. In the presence of buried objects, the surface impedance contains jumps at the surface points just above the bodies. The sizes of these jumps are proportional to the sizes of the bodies. Thus these results can directly be used to detect and locate the objects, as well as to get information about their sizes. By repeating this procedure for a number of frequencies one can obtain the variation of the surface impedance with respect to frequency. Every material has its own surface impedance variation and it can be used as a signature to identify the material properties of the objects. The system has been realized and tested with several object contributions and it is observed that it gives very accurate results.

REFERENCES

1. Sahinturk, H., A. Yapar, and İ. Akduman, "On the use of the surface impedance in the detection and location of buried objects," *AEU-Int. J. Electronics and Communications*, Vol. 58, 249–255, July 2004.

A Review on the Migration Methods in B-scan Ground Penetrating Radar Imaging

Caner Özdemir[1, 2], **Sevket Demirci**[2], **and Enes Yiğit**[2]

[1]Department of Electrical and Electronics Engineering, Zirve University
Kızıllhisar Campus, Gaziantep 27260, Türkiye
[2]Department of Electrical-Electronics Engineering, Mersin University
Yenişehir, Mersin 33343, Türkiye

Abstract— Ground penetrating radar (GPR) has been a pioneering electromagnetic tool for detecting and locating subsurface objects with good imaging fidelities [1, 2]. The main defocusing effect in the GPR imagery is occurred due to the well-known hyperbolic distortion of the subsurface scatterers in the resultant space-time B-scan GPR image [1–3]. Although many migration/focusing methods have been proposed by various researchers, the focusing problem in the measured GPR images remains to be a challenging task. In this work, we review the recent migration methods of the B-scan GPR images that are popular among the GPR researchers. These methods are the hyperbolic summation, the Kirchhoff migration, the phase-shift migration, the f-k migration and the SAR-based focusing techniques. The brief formulation of these methods together with their algorithms is presented. The applications of the algorithms to both the numerical and the measurement data are provided and the corresponding B-scan focused GPR images are presented. The comparison of the methods is also presented by pointing out the advantages and the shortcomings of the algorithms.

ACKNOWLEDGMENT

This work is supported by the Scientific and Research Council of Turkey (TUBITAK) under grant No. EEEAG-104E085.

REFERENCES

1. Daniels, D. J., *Surface-penetrating Radar*, IEE Press, London, 1996.
2. Peters, Jr., L., D. J. Daniels, and J. D. Young, "Ground penetrating radar as a subsurface environmental sensing tool," *Proc. IEEE*, Vol. 82, No. 12, 1802–1822, 1994.
3. Ozdemir, C., S. Demirci, E. Yigit, and A. Kavak, "A hyperbolic summation method to focus B-Scan ground penetrating radar images: An experimental study with a stepped frequency system," *Microwave Opt. Tech. Letters*, Vol. 49, No. 3, 671–676, 2007.

Session 2P3b
EM Scattering Models and Applications

Topology Optimization Procedure to Minimize Radar Cross Section of Perfectly Electric Conductive Structures

H. Yigit
Gebze Institute of Technology, Turkey

Abstract— A new approach to achieve optimum radar cross section (RCS), based on level-set based topology optimization will be introduced throughout this work. Limited studies in this area [1, 2] shows, finding optimum RCS from initial geometries are struggled from some restrictions(volume/surface constraint, aerodynamics vs.) and large number of parameters which should be considered. In addition not only minimization of RCS, in some applications maximization can be also desired (ex. RFID tags).

Pioneering studies about level-set based topology optimization in electromagnetics shows us method itself gives promising opportunity to design electromagnetic materials [3, 4]. Flexibility in handling geometric changes, focus on final design, avoiding numerous sensitivity evolutions respect to all design variables ... level-set based topology optimization method has become attractive tool in engineering applications on electromagnetic material design.

Subject to our study, free space and perfectly electric conductive(PEC) mediums implicitly expressed by zero-level contour of a higher dimensional level set function. Following proper sensitivity analysis of electric field integral equation (EFIE) [5], objective function related to optimization procedure is constructed. Here objective can be either surface current or scattered field. For each optimization iteration EFIE problem is solved via MOM analysis and this continues till desired minimal value reached. Within the aspects of this paper, first method will be introduced briefly, after that general algorithm on RCS optimization will be described and finally some graphical results will be demonstrated about RCS optimized PEC surfaces under various electric field illuminations.

REFERENCES

1. Bondeson, A., Y. Yang, and P. Weinerfelt, "Optimization of radar cross section by a gradient method," *IEEE Transactions on Magnetics*, Vol. 40, No. 2, 1260–1263, 2004.
2. Lee, D. S., L. F. Gonzalez, K. Srinivas, and J. Periaux, "Robust evolutionary algorithms for UAV/UCAV aerodynamic and RCS design optimisation," *Computer and Fluids*, Vol. 37, 547–564, 2007.
3. Hokyung, S., H. Vinh, W. Semyung, and T. Daniel, "Level-set based topology optimization for electromagnetic systems," *IEEE Transactions on Magnetics*, Vol. 45, No. 3, 1582–1585, 2009.
4. Zhou, S. W., W. Li, Y. H. Chen, G. Y. Sun, and Q. Li, "Topology optimization for negative permeability metamaterials using level-set algorithm," *Acta Materialia*, Vol. 59, 2624–2636, 2011.
5. Zhou, S. W., W. Li, Y. H. Chen, and Q. Li, "Sensitivity analysis for electromagnetic topology optimization problems," *WCCM/APCOM*, Sydney, Australia, Jul. 2010.

An Extended Study on an Inverse Model for the Retrieval of Sea Ice Parameters

Y. J. Lee[1], **Y. F. Chan**[1], **W. K. Lim**[2], **and H. T. Ewe**[1]

[1]Universiti Tunku Abdul Rahman, Malaysia
[2]Multimedia University, Malaysia

Abstract— Recently, an inverse model for the retrieval of sea ice thickness using Radiative Transfer Theory had been developed. The model incorporates the Dense Medium Phase and Amplitude Correction Theory for better accuracy in the calculation and the Levenberg-Marquardt Optimization for estimating the required information. Previous research showed that the model is able to estimate sea ice thickness from the use of single polarization radar backscatter data (HH) successfully. However, several shortcomings were also revealed during the study. In this paper, the results of the simulations to retrieve sea ice thickness using ground truth measurement data from 2008 shall be presented. Next, the use of the model is extended towards the use of multipolarization data to retrieve sea ice thickness. Previous analysis with the model had shown that the use of multipolarization data to estimate sea ice thickness from radar backscatter data may be more effective compared to single polarization data. In addition, the model will be improvised to cater for the retrieval of some other sea ice parameters.

The Physical Interpretation of Complex Angles of Refraction in DZR Metamaterials

A. Abdolali[1], **H. Oraizi**[1], **S. Hashemi**[2], **A. Mohtadi**[2], **N. Vaseghi**[3], **H. Mirzaei**[1], **and M. Aghajani**[4]

[1]Department of Electrical Engineering, Iran University of Science and Technology (IUST), Iran
[2]Department of Electrical and Computer Engineering, Tehran University, Iran
[3]Department of Electrical Engineering, K. N. Toosi University of Technology, Tehran, Iran
[4]Department of Computer Eng. and IT, Amirkabir University of Technology, Tehran, Iran

Abstract— A plane wave with arbitrarily polarization obliquely incident onto a half space composed of DZR metamaterials. In such materials the real parts of the permittivity and permeability are both equal to zero. The angle of refraction in the DZR metamaterials becomes complex. In this paper we investigate this complex angle of refraction and its physical interpretation.

REFERENCES

1. Veselago, V. G., "The electrodynamics of substances with simultaneously negative values of ε and μ," *Soviet Physics Uspekhi*, Vol. 10, No. 4, 509–514, Jan.-Feb. 1968.
2. Caloz, C. and T. Itoh, *Electromagnetic Metamaterials, Transmission Line Theory and Microwave Applications*, Wiley — IEEE Press, Hoboken, NJ, 2005.
3. Pendry, J. B. and A. MacKinnon, "Calculation of photon dispersion," *Phys. Rev. Lett.*, Vol. 69, No. 3, 2772–2775, 1992.
4. Pendry, J. B., A. J. Holden, D. J. Robbins, and W. J. Stewart, "Low-frequency plasmons in thin wire structures," *Phys. Condens. Matter*, Vol. 10, 4785–4809, 1998.
5. Kong, J. A., "Electromagnetic wave interaction with stratified negative isotropic media," *Progress In Electromagnetics Research*, Vol. 35, 1–52, 2002.
6. Oraizi, H. and A. Abdolali, "Analytical determination of zero reflection conditions for oblique incidence on multilayer planar structures," presented at *IEEE Mediterranean Microwave Symposium*, 196–199, Damascus, Syria, 2008.
7. Oraizi, H. and A. Abdolali, "Mathematical formulation for zero reflection from multilayer metamaterial structures and their notable applications," *IET Microwaves, Antennas & Propagation Journal*, Vol. 3, No. 6, 987–996, Sep. 2009.
8. Kong, J. A., *Theory of Electromagnetic Waves*, EMW Pub., New York, 2005.
9. Oraizi, H. and A. Abdolali, "Combination of MLS, GA & CG for the reduction of Rcs of multilayered cylindrical structures composed of dispersive metamaterials," *Progress In Electromagnetic Research B*, Vol. 3, 227–253, 2008.
10. Oraizi, H. and A. Abdolali, "Design and optimization of planar multilayer antireflection metamaterial coatings at Ku band under circularly polarized oblique plane wave incidence," *Progress In Electromagnetics Research C*, Vol. 3, 1–18, 2008.
11. Oraizi, H. and A. Abdolali, "Some aspects of radio wave propagation in double zero metamaterials having the real parts of epsilon and mu equal to zero," *Journal of Electromagnetic Waves and Applications*, to be published.

A Preconditioned GMRES Method for EM Scattering from Dielectric Rough Surfaces

Guangdi Yang and Yang Du
Department of Information and Electronical Engineering, Zhejiang University, Hangzhou 310027, China

Abstract— We propose a generalized minimal residual (GMRES) procedure which is right preconditioned with the forward-backward method (FBM) for the analysis of electromagnetic scattering from one-dimensional (1D) dielectric randomly rough surfaces. The spectral acceleration (SA) technique is also combined to expedite the computation of matrix-vector product. The applied preconditioning transforms the original linear system from near singular to stable with a good condition number. The spectrum of the preconditioned matrix is found condensed in the vicinity of the point 1 in the complex plane, which speaks of the good approximation quality of the preconditioner to the original matrix. Moreover, the construction of the preconditioner does not require the knowledge of the distribution of the impedance matrix spectrum, which means that the proposed method can be used as a general purpose iterative solver. The proposed method has demonstrated the desirable properties of a numerical algorithm: robustness and efficiency. Regarding robustness, the proposed method significantly improves convergence over the FBM-SA, in particular for exponentially correlated rough surfaces. Regarding efficiency, the proposed method runs 2–4 times faster than the FBM-SA for horizontal (HH) polarization, and is about twice faster for vertical (VV) polarization. These features indicate that the proposed method can be effectively used to analyze electromagnetic scattering from 1D dielectric Gaussian surfaces with both Gaussian and exponential spectra.

Radar Cross Section Analysis of a Square Plate Modeled with Triangular Patch

N. Altın[1] and E. Yazgan[2]

[1]Turkish Aerospace Industries, Inc., Fethiye Mah., No. 17 Havacılık Bulvarı, Kazan Ankara 06980, Türkiye
[2]Electrical & Electronics Engineering Department, Hacettepe University, Beytepe, Ankara 06532, Türkiye

Abstract— In this study, monostatic Radar Cross Section (RCS) of targets which are modeled with different number of triangular patches were analyzed Shooting and Bouncing Ray (SBR) method based on geometric optics which is one of the high frequency techniques. Numerical results obtained by SBR method are compared with Physical Optics (PO) results. As a result of study showed that monostatic RCS value is not changed when smooth-surface targets are modeled with different number of triangular patches but computation time increased with increasing the number of triangular patch.

Session 2P4a
Antennas for Mobile Communication 2

Feeding Techniques to Excite Slot on an Open Ended Coplanar Waveguide Transmission Line

R. Sujith, D. Laila, C. M. Nijas, U. Deepak, R. Dinesh, and P. Mohanan
Centre for Research in Electromagnetics and Antennas (CREMA), Department of Electronics
Cochin University of Science and Technology, Cochin, Kerala 682022, India

Abstract— Compact antennas with excellent radiation characteristics are good candidates for modern wireless communication gadgets. Coplanar waveguide (CPW) fed antennas are compact, uniplanar and hence can be easily integrated with Monolithic Microwave Integrated Circuits (MMIC). Researchers have explored a lot on the applications of coplanar waveguide structures for the last few decades. The investigations on the power leakage of coplanar waveguide with width of lateral strip, signal strip and gaps were carried out. By properly adjusting the feed point, lateral ground plane and signal strip dual band antenna for WLAN applications can be achieved. Signal strip and ground plane are also modified by researchers to get good antenna performance. However, most of the published papers are either complex in structure or large in size for practical applications.

In this paper centre fed slot dipole antennas with Coplanar Waveguide Feed are presented. The slot on the lateral ground plane of a coplanar waveguide transmission line is to be excited properly to convert it to a good antenna. Different method to excite the slots efficiently to achieve the required impedance characteristics is discussed. The very high impedance of an open ended coplanar waveguide (CPW) is made lower by off centering the feed position, optimizing the feed length and by using a T-shaped feed. The advantage and disadvantage on these three new feeding techniques are discussed in detail.

The radiation behavior and evolution of the antenna from a normal open ended coplanar waveguide transmission line with proper radiation patterns and gains are presented. The frequency of the antenna can be controlled by changing the slot length. The signal strip is mainly contributing to the real part of impedance and the slot width to the imaginary part. Thus it is easy to control the resonance by simply trimming these three parameters. The radiation pattern is omnidirectional in one plane and figure of eight in other plane, like a standard dipole antenna. All the prototypes are fabricated on a substrate of dielectric constant 4.4 and thickness 1.6 mm. The simulations are carried out using Ansoft HFSS and experimental studies using HP8510C Vector Network analyzer.

A Three Element Handheld, Mobile Communication Antenna for MS Space Diversity

A. R. Lwin Maw[1], **P. R. P. Hoole**[2], **R. Harikrishnan**[1], **K. Jeevan**[1], **and S. R. H. Hoole**[3]

[1]Department of Electrical Engineering, University of Malaya, Malaysia
[2]School of Engineering, Taylor's University, Malaysia
[3]Department of Electrical and Computer Engineering, Michigan State University, USA

Abstract— Space diversity, where antennas separated in space at the receiver, is considered one of the most effective ways of either eliminating unwanted signals in order to maximize the signal to noise ratio of the desired signal. Moreover it may be used to receive a signal that has gone through less fading when the direct path signal may have undergone deep fade. In this paper we use analytical electromagnetic solutions for the radiate signals to implement antenna space diversity on small handheld receiver units of mobile stations. While using the standard time difference of arrival method to obtain a first approximation of the mobile station position, the electromagnetic model is used to determine a more accurate position of the mobile station. The performance of a multi element mobile station antenna is shown to give good position estimation in the presence of various noises. A three element mobile station receiver is for the first time reported to be able to simultaneously null a deeply faded signal in the Rayleigh fading environment, and maximize the signal that has a strong signal. It is shown that a three element antenna may be used to both eliminate an undesired signal, while it may maximize the reception of a desired signal. The transmitter does not require a training sequence, as in the case of an equalizer, since entire signal processing of the electromagnetic signal is done at the mobile receiver.

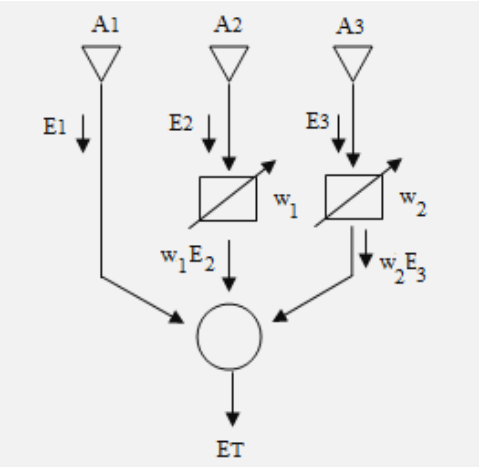

Figure 1: Configuration of the new MS three element array antenna.

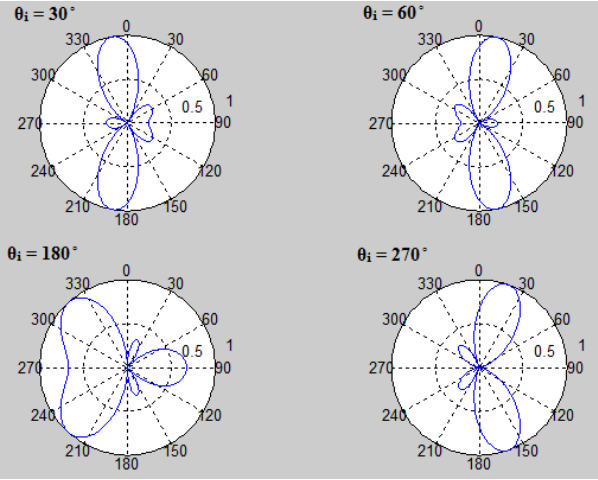

Figure 2: Three element array antenna beam nulling to interference direction while MS moves in the horizontal plane.

Dual Wideband CPW Fed Dieletric Resonator Antenna

Sriparna Bhattacharya (Mitra)[1] **and Bhaskar Gupta**[2]

[1]Department of Electronics and Communication Engineering
Heritage Institute of Technology, Kolkata 700107, India
[2]Department of Electronics and Tele-Communication Engineering
Jadavpur University, Kolkata 700 032, India

Abstract— Dielectric resonator antenna has received much attention as an effective radiating element since last three decades. DRA has become very popular because of many attractive features like low loss, light weight, compact size, high radiation efficiency and good compatibility with other structures. Moreover, a DRA can be excited by many methods like using a probe, a slot coupled microstrip or CPW. The coplanar waveguide fed slot antenna has become a promising candidate due to its uniplaner structure, wide bandwidth, and easy integration with RF front-end circuitry. Recently much focus has been given on the band width enhancement of DRA and many techniques have been proposed to broaden their operational bandwidth. One type of effective methods uses some special composite DR structures such as stacked DRs with different materials and embedded DRs. Other types of methods adopt special feeding mechanisms or utilize multisegment DRAs or use parasitic elements, or air gap in DRA. However all of these either include complex design or a combination of different dielectric materials.

In this paper, a very simple and novel design is proposed for dual wideband operation. The antenna is a hybrid structure consisting of a CPW slot and a dielectric resonator antenna placed on the loop shaped slot (Fig. 2). A substrate with $\varepsilon_r = 2.5$ has been chosen for etching the slot on it with $LS = WS = 120\,\text{mm}$. The DRA consists of material with $\varepsilon_r = 6$ and is parallelepiped in structure. The dimension of the loop shaped CPW are as follows: $S = 0.3\,\text{mm}$ and $G = 7.8\,\text{mm}$. The slot is designed with $V = 10.525\,\text{mm}$, $W = 29.4\,\text{mm}$ and $P = 46.075\,\text{mm}$. After thorough parametric studies, the DRA dimensions are optimized as $a = 28\,\text{mm}$, $b = 15\,\text{mm}$, $c = 12\,\text{mm}$ as shown in Fig. 2.

The loop and the DRA are designed in such a way so that they have closely placed but staggered resonating frequencies thereby giving broadband performance. Two different modes are further excited to give rise to dual band operation.

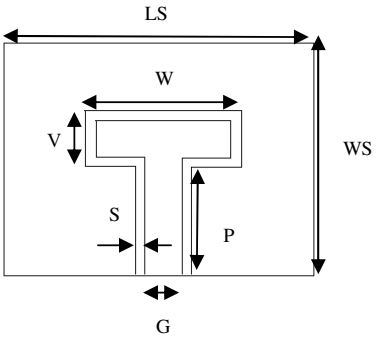

Figure 1. The loop shaped slot.

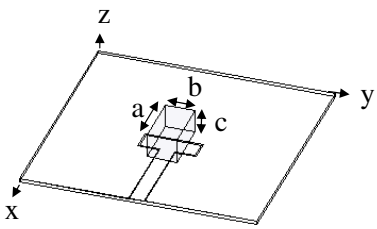

Figure 2. The Loop with the DRA.

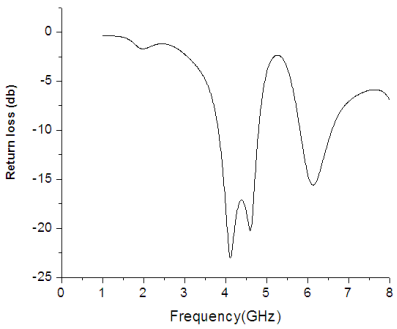

Figure 3.

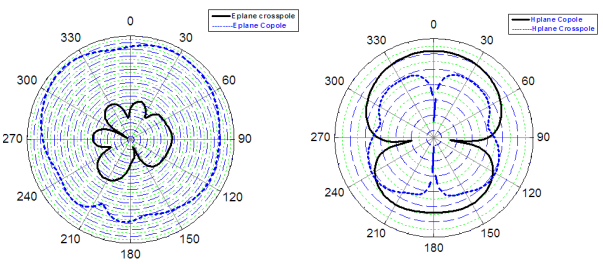

Figure 4. Radiation patterns at 4.3 GHz,

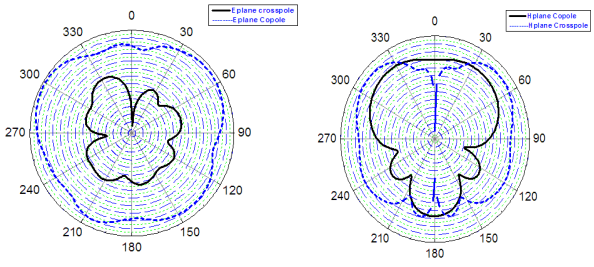

Figure 5. Radiation patterns at 6.2 GHz,

Dual wideband operation has been observed through simulation using HFSS, one ranging from 3.8 GHz to 4.8 GHz and another ranging from 5.8 GHz to 6.6 GHz. The 10-dB simulated return loss band widths are 23% (3.8–4.8 GHz) and 12.9% (5.8–6.6 GHz). A very good impedance match has been obtained in both bands as is evident from the simulated return loss plot (Fig. 3). Both bands satisfy the Ultra Wide Band (UWB) requirements according to IEEE definition.

The radiation patterns at centre frequencies of the two bands are shown in Fig. 4 & Fig. 5. The radiation patterns are Omnidirectional in E plane and monopole like in H plane. The antenna has been fabricated and measured results are awaited for.

Design of a Wide Dual-band Microstrip Antenna for WLANs Applications

Abdulkareem S. Abdullah and Nabil E. Abdulhussein
Department of Electrical Engineering, College of Engineering
University of Basrah, Basrah, Iraq

Abstract— A wide dual-band microstrip antenna is proposed in this paper as shown in Fig. 1. The patch has a width of 13 mm and length of 10 mm. The patch is fabricated on $(23 \times 20)\,\text{mm}^2$ FR4 substrate with a thickness of 1.6 mm, a relative permittivity of 4.4 and a loss tangent of 0.02. A 2 Ω chip resistor is connected between the patch and ground plane at 1 mm above patch center. The chip resistor presence causes the antenna to operate at two frequencies with wide bandwidth. Two cross-slots in ground plane are existed to control the two resonant frequencies and to reduce the antenna size. The vertical arm of the lower cross-slot has a length of (L) mm and the vertical arm of the upper cross-slot has a length of $(L-2)$ mm. The horizontal arms of upper and lower cross-slot have lengths of $(d\,\text{mm})$. The width of all arms is 1 mm. A 50 Ω probe feed is used for feeding the antenna. The optimal feed position is found to be 3 mm left of the chip resistor along x-axis to ensure acceptable values of return loss at the two bands.

3-D FDTD method is used for the simulation of the complete structure of the antenna including the resistive load. The FDTD problem space is composed of cells with $\Delta x = 0.5$ mm, $\Delta y = 0.5$ mm and $\Delta z = 0.533$ mm, which are selected to be smaller than (1/20) wavelength of maximum frequency (6 GHz) in order to ensure the accuracy of the computed results. These cell sizes make the volume of object to be ($40^{\Delta x}$, $46^{\Delta y}$ and $3^{\Delta z}$).

The effects of the length of the two arms for two cross-slots in the ground plane are studied. To find the effect of the vertical arms of the two cross-slots on the two operating frequencies, the length of the two vertical arms (L) and $(L-2)$ is varied at fixed length of horizontal arms of the two cross-slots ($d = 8$ mm). Fig. 2 shows the calculated return losses for two frequencies at different values of L.

The results clearly show that, upon the increasing of the slot length L, the lower frequency f_{r1} is not affected by the variation of L and it remains at 2550 MHz. On the other hand, the higher frequency f_{r2} is decreased and is lower than 6000 MHz. Also, from the results, it is found that the optimal feed positions for the present design are almost about the same, which indicates that the feed position is not affected by the variation of L. At $L = 9$ mm, the lower mode of the proposed design has a 10 dB bandwidth of 307 MHz (2398–2705 MHz), and the upper mode has a bandwidth of 332 MHz (5097–5429 MHz). The obtained bandwidths cover WLANs operations in two bands, the first band is ISM band (2400–2483.5 MHz) required by WLAN IEEE 802.11b,g and Bluetooth standards, and the second band is U-NII1 (5150–5350 MHz) required by IEEE 802.11a and HiperLAN2 standards.

The horizontal arms length d is varied with fixed L ($L = 8$ mm). Fig. 3 shows the calculated return losses for two frequencies at different values of d.

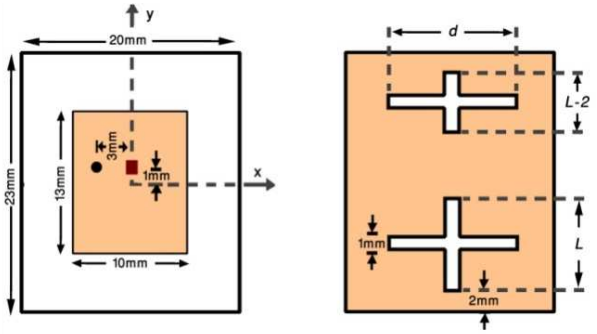

(a) Patch side wiew (b) Ground plane view

Figure 1: Proposed configuration for dual-band microstrip antenna.

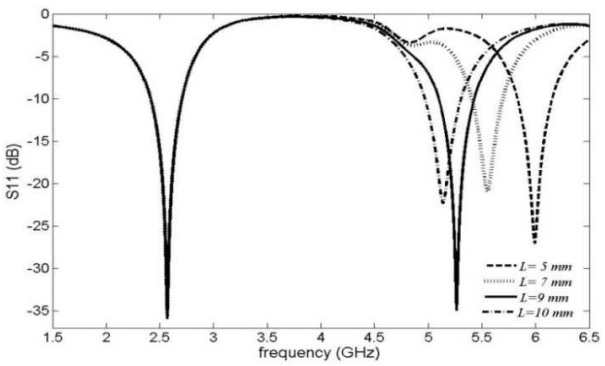

Figure 2: Return losses for different value of L at $d = 8$ mm and $R = 2\,\Omega$.

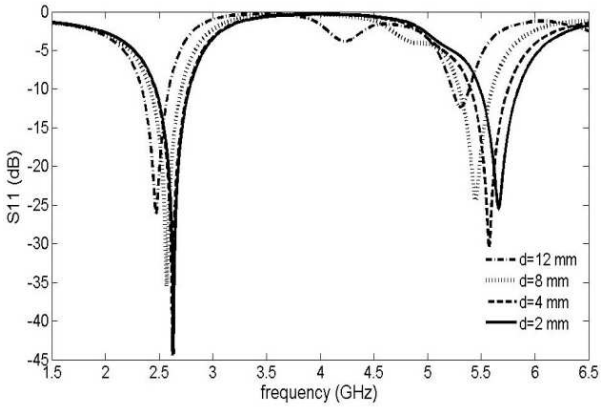

Figure 3: Return losses for different value of d at $L = 8\,\text{mm}$ and $R = 2\,\Omega$.

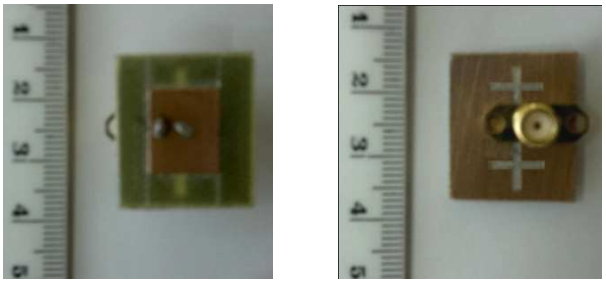

(a) Patch side view (b) Ground plane view

Figure 4: The fabricated dual-band microstrip antenna.

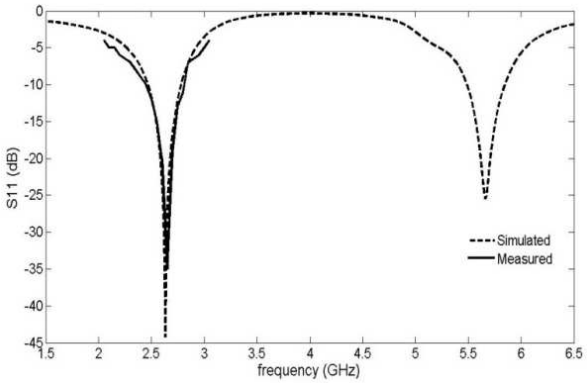

Figure 5: Measured (2–3 GHz) and simulated return losses for $L = 8\,\text{mm}$, $d = 2\,\text{mm}$ and $R = 2\,\Omega$.

From the above results, the increasing in slot length d has same effect on two resonant frequencies and causes decreasing in both resonant frequencies, so that the frequency ratio approximately remains constant compared with the case of varying L. It is clear that, the increasing in d causes longer paths for two modes. By setting $d = 2\,\text{mm}$, the lower mode of the proposed design has a bandwidth of 319 MHz (2394–2713 MHz), and the upper mode has a bandwidth of 362 MHz (5467–5829 MHz). The obtained bandwidths cover WLANs operations in two bands, the first band is ISM band (2400–2483.5 MHz) required by IEEE 802.11b,g and Bluetooth standards and the second band is U-NII2 (5470–5725 MHz) and U-NII3/ISM (5725–5825 MHz) required by IEEE 802.11a standard.

The fabricated proposed design with $L = 9\,\text{mm}$, $d = 8\,\text{mm}$ and $R = 2\,\Omega$ is shown in Fig. 4. The measured and simulated return losses of this antenna are as shown in Fig. 5. There is a good agreement between measured and simulated results.

Relevant Electromagnetic Details for a Couple Antenna-vehicle

M. Sossouhounto and Thierry Gilles
Royal Military Academy of Brussels, Belgium

Abstract— To study the electromagnetic behavior of an antenna mounted on a vehicule, a geometrical modelling is the first unavoidable step. Two strategies share the preference of the electromagnetic community. The first option is to acquire and simplify a Computer Aided Design (CAD) model containing many unnecessary details and possibly omitting the electrical continuity of some parts of the vehicule. The second option is to manually enter surface and volume primitives that will form the desired electromagnetic model. Both methods require a large amount of work, that can be greatly reduced if only the important elements and details are included in the geometrical model with the appropriate accuracy.

In the next step of the analysis, the electromagnetic storage requirement and simulation time will also greatly benefit from a simpler geometrical model. To determine which details are electromagnetically relevant or significant, we analyzed in detail the case of a monopole antennna mounted on the roof of a Light Multipurpose Vehicule (LMV) of the Belgian Defense. The far field, outdoor near field and antenna impedance have been considered.

Our study shows and quantifies how the electromagnetic relevance of every individual outdoor vehicule elementary part depend on the application, the location of the antenna and the frequency of interest.

Session 2P4b
UWB and Reconfiguration Antennas

Reconfigurable E-shaped Antenna with Bandwidth Control for Wideband Applications

Hattan F. Abutarboush[1] **and R. Nilavalan**[2]

[1]Electrical Engineering, Physical Science and Engineering
King Abdullah University of Science and Technology (KAUST), Saudi Arabia
[2]School of Engineering and Design, Electrical and Electronics Engineering
Brunel University, London, UK

Abstract— A reconfigurable antenna is proposed in this paper for controlling the bandwidth of an E-shaped Antenna. The bandwidth of the antenna can be increased and controlled from 2% to 29% by varying the capacitance of the varactor diodes. The antenna consists of four E-shaped connected to 50 ohm GCPW line, varactor diodes and 10 pF ship capacitance. Simulated and measured results are in good agreements.

Introduction: An increasing demands for Wideband antennas which can be easily integrated in a wireless device supporting multiple standards. The printed antenna has become one of the most commonly used antenna types in the last 20 years for a broad assortment of applications, including hand-held, automotive and aircraft applications. Its popularity is due to a number of factors unobtrusive and low profile shape, rugged form factor, and low construction cost. The printed antenna is a resonant antenna, and in its basic form has only a few precent bandwidths.

Antenna Design and Results: In this paper, varactor diodes are used to control the bandwidth of the antenna. The bandwidth can be controlled from 2% to 29% by varying the voltage from 20 V to 7 V.

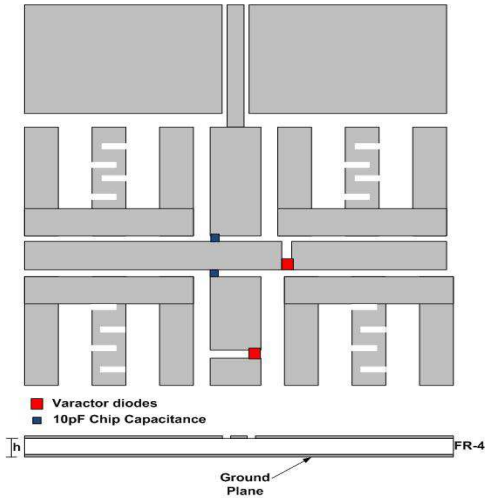

Figure 1: Layout of the proposed antenna.

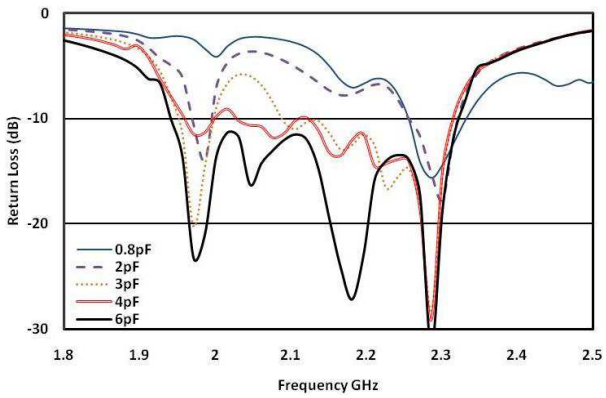

Figure 2: Measured S_{11}.

Table 1:

Varactor diodes	Bandwidth (−10 dB)
0.8 pF	2%
2 pF	4%
3 pF	5%
4 pF	8%
6 pF	20%

Frequency-tunable Antenna for Dual-band WLAN Applications

X. L. Sun, **S. W. Cheung**, **and T. I. Yuk**
Department of Electrical and Electronic Engineering
The University of Hong Kong, Hong Kong, China

Abstract— In this paper, a frequency-tunable dual-band antenna for WLAN applications is proposed. The antenna consists of two microstrip branches serving as radiating elements for two frequency bands at 2.4 and 3.5 GHz and two variable capacitors on the radiating elements for individually tuning the frequency bands. The antenna is designed on a 40 mm × 40 mm substrate with a thickness of 0.8 mm, relative permittivity of 3.5 and loss tangent of 0.02. The reflection coefficient S_{11} of the antenna with different capacitance values is studied. Simulation results suggest that the two frequency bands have a tuning range of 2.4–3.5 GHz and 3.5–5.9 GHz separately. Moreover, simulated radiation patterns, efficiencies and gains of the proposed antenna are also presented.

CPW-coupled-fed Elliptical Monopole UWB Antenna with Dual-band Notched Characteristic

J. Zhang, **S. W. Cheung**, **and T. I. Yuk**
Department of Electrical and Electronic Engineering
The University of Hong Kong, Hong Kong, China

Abstract— This paper presents the results of a coplanar-waveguide (CPW)-coupled-fed elliptical monopole UWB antenna (CCFEMUA) with a dual band-notched characteristic. The antenna has a large bandwidth covering the frequency band from 2.4 GHz to 15.2 GHz with the return loss larger than 10 dB. Two band notches at 3.7 GHZ and 4.8 GHz are realized by cutting two half-elliptical-arc slots on the radiation patch. The return loss, radiation pattern, peak gain and efficiency of the antenna are studied using computer simulation.

Deep Band-notched Characteristic Using Meander Lines for UWB Monopole Antennas

L. Liu[1], **Y. F. Weng**[1], **S. W. Cheung**[1], **T. I. Yuk**[1], **and T. Peter**[2]

[1]Department of Electrical and Electronic Engineering
The University of Hong Kong, Hong Kong, China
[2]Department of Electronics and Computer Engineering
Brunel University, Kingston Lane, Uxbridge, UB8 3PH, UK

Abstract— The paper proposes to use two meander-line structures to design a deep single-band notch for planar-monopole ultrawide band (UWB) antennas. The center frequency and bandwidth of the deep notch in the characteristic of the UWB antennas can be adjusted by using the dimensions of the meander-line structures. For illustration, the single-band notch is designed in the wireless area network (WLAN) band from 5.15 GHz to 5.825 GHz. Results of parametric studies on the meander structures are presented. The band-notched characteristics such as radiation patterns and peak gains of the antenna are studied using computer simulation.

Planar UWB Monopole Antenna with Tunable Notch Band

X. L. Sun[1], **C. Wang**[1], **S. W. Cheung**[1], **T. I. Yuk**[1], **and H. F. Abutarboush**[2]

[1]Department of Electrical and Electronic Engineering
The University of Hong Kong, Hong Kong, China
[2]Electrical Engineering, King Abdullah University of Science and Technology (KAUST)
Saudi Arabia

Abstract— In this paper, a planar monopole antenna with a tunable notch band for ultra-wideband (UWB) applications is proposed. The antenna consists of an elliptical radiator, a microstrip-feed line and a ground plane. A meander-defected-ground structure (meander-DGS) etched on the ground plane is used to create a notch. A variable capacitor placed on the meander-DGS structure is used to tune the frequency of the notch band. The antenna is designed on a $30\,\text{mm}\,(W) \times 39.1\,\text{mm}\,(L) \times 0.762\,\text{mm}\,(h)$ substrate with a relative permittivity of 3.48 and a loss tangent of 0.004. The antenna is studied by using computer simulation. The results show that the notch band can be tuned from 5.5 to 9.6 GHz by varying the capacitance from 1.7 to 0.07 pF, respectively.

A Novel Transparent TSA for Laptop and UWB Applications

T. Peter[1], **R. Nilavalan**[1], **and S. W. Cheung**[2]

[1]Brunel University, Uxbridge, Middlesex, UK
[2]The University of Hong Kong, Pokfulam Road, HK, China

Abstract— A novel transparent Tapered Slot Antenna is proposed in this paper. Since the approval by the FCC in 2002, much research has been undertaken on UWB especially for wireless communications. Often times especially for devices where internet services are required, UWB is complemented with the 2.4 GHz WLAN service like in Laptops or notebooks instead of being filtered out. In this paper, a transparent Tapered Slot Antenna (TSA) covering the frequency range from 2.1 GHz to 10.8 GHz is designed and fabricated using AgHT-8 for use in Laptop applications. The antenna provides sufficient gain, reasonable efficiency and a good return loss.

Planar Monopole Ultra-wideband Antennas with Different Radiator Shapes for Body-centric Wireless Networks

Y. Y. Sun, **S. W. Cheung**, **and T. I. Yuk**
Department of Electrical and Electronic Engineering
The University of Hong Kong, Pokfulam Road, Hong Kong, China

Abstract— This paper is a further study on the performances of planar UWB monopole antennas using a radiator of different shapes such as triangle, rectangle, square, circle, annual ring, ellipse (both horizontal and vertical), pentagon and hexagon, for body-centric wireless networks. The planar antennas consist of a radiator and a microstrip-feed line on one side of the substrate and a ground plane on the other side. Previous simulation studies showed that the elliptical and hexagonal antennas appeared to have the best performances in terms of bandwidth, gain, efficiency and radiation pattern. Studies using measurements of these two antennas on a liquid-body phantom are presented in this paper. Results show that the elliptical antenna achieves a wide impedance bandwidth of 3.1–12 GHz, an average peak gain of nearly 2.3 dBi and good radiation patterns, making it a good candidate for UWB body-centric wireless networks.

Session 2P5
Wireless Network and Applications 2

Energy Consumption Reduction by Multi-hop Transmission in Cellular Network

Pengty Ngor, Siya Mi, and Peter Han Joo Chong
School Electrical and Electronic Engineering, Nanyang Technological University, Singapore

Abstract— As wireless communication develops, higher requirements of wireless networks are demanded. In 2003, the International Telecommunication Union Radio communication sector (ITU-R) proposed that next generation networks should achieve a total cell capacity of up to 1 Gbps for slow-moving users and 100 Mbps for fast moving mobile stations. However, the limitation on radio resource is the real bottleneck for developing higher-speed wireless networks. Research on future wireless system to provide higher capacity, yet retaining efficient use of energy is challenging. This paper focuses on new cellular network architecture by adding relaying stations between base stations and mobile stations to reduce energy consumption.

Adding relay stations between base stations and mobile stations in a cellular system can extend network coverage, overcome multi-path fading and increase the capacity of the system. In this paper, a two-hop relay network consisting of a source, a destination and multiple relay nodes is investigated. With the increase of data traffic, more and more energy is needed to support communication. Hence, it is imperative to design an optimal relay network that minimizes the average energy consumption. We propose an improved architecture of TDD-CDMA multi-hop cellular networks, named Multi-Tier Architecture (MTA), which can decrease the consumed energy for a given QoS requirement.

Based on investigation of system performance and energy consumption of the fixed relay station and random relay station, the optimal structure of MTA intern of the influenced area of base station and relay station is designed and analyzed. Fig. 1 to Fig. 4 show the simulation results of consumed energy per mobile station and per link station in low and high traffic for fixed switching

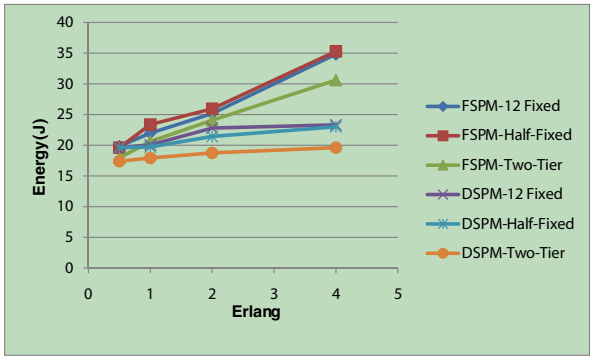

Figure 1: Consumed energy per mobile station for low traffic class.

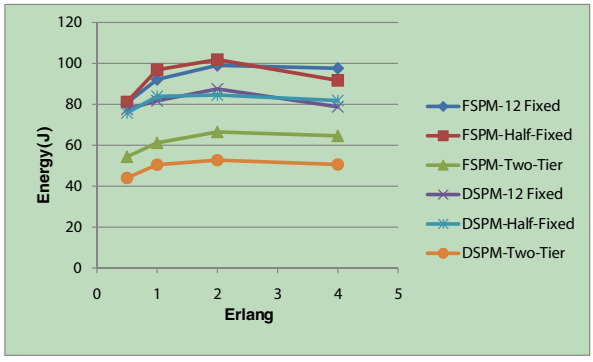

Figure 2: Energy per mobile station for high traffic class.

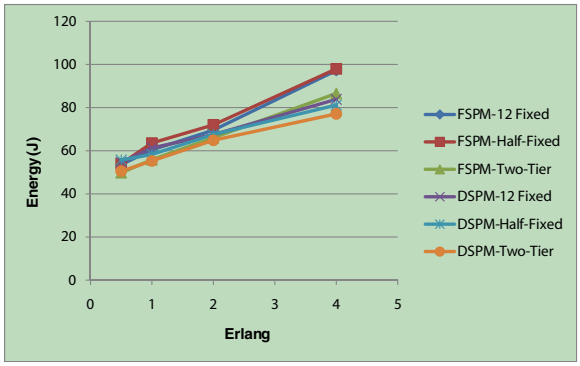

Figure 3: Consumed energy per link station for low traffic class.

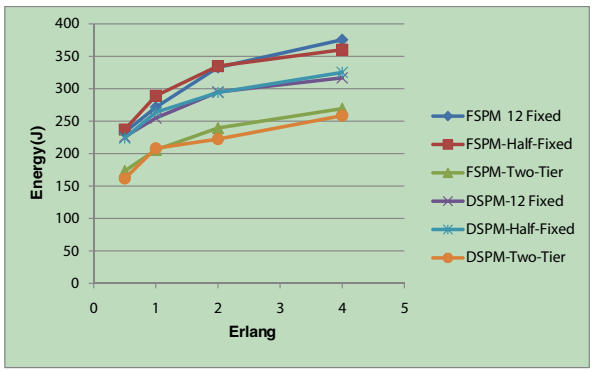

Figure 4: Consumed energy per link station for high traffic class.

point with multi-hop (FSPM) and dynamic switching point with multi-hop (DSPM) in Two-Tier Architecture (TTA). There are two observations from the simulation results. First, by comparing the cases using FSPM and DSPM, it can be seen that DSPM costs less than FSPM. Second, our TTA consumes the least energy at all cases and it can save up to 45.3% energy for one mobile station and 27.6% for one call. Hence, there is a huge improvement for TTA for both energy per mobile and energy per link.

Routing Performance of Mobile Ad Hoc Network in Urban Street-grid Environment by Using Peer-to-Peer Propagation Model

Pengty Ngor and Peter Han Joo Chong
School of Electrical and Electronic Engineering, Nanyang Technological University, Singapore

Abstract— Mobile ad hoc network (MANET) is a self-organizing and self-creating network which requires no fixed infrastructure. Due to this nature, MANET is currently attracted to many applications such as home networking, search and rescue operation, battlefield communication and inter-vehicular communication system. Many network simulation tools have been used to analyze the routing performance of MANET by assuming that the link between two nodes is in line of sight (LOS). However, this LOS assumption is not valid especially in an urban environment where received signals in non line-of-sight (NLOS) region are dominated by multiple reflections along the street referred to as NLOS propagation. However, most of MANET papers reported in

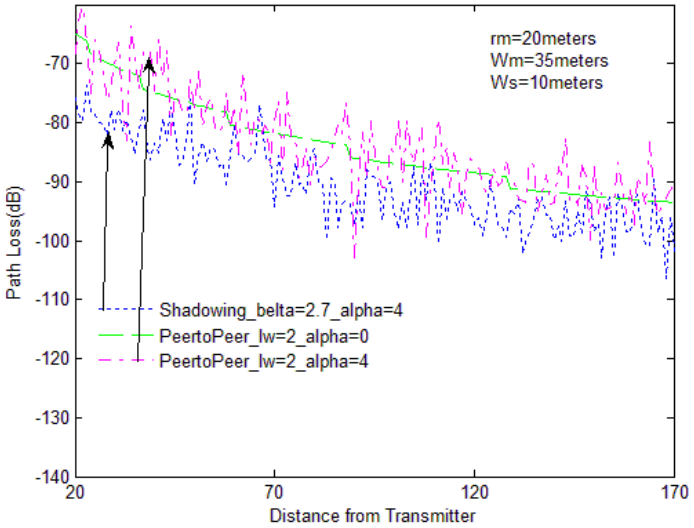

Figure 1: Path loss along tokyo street.

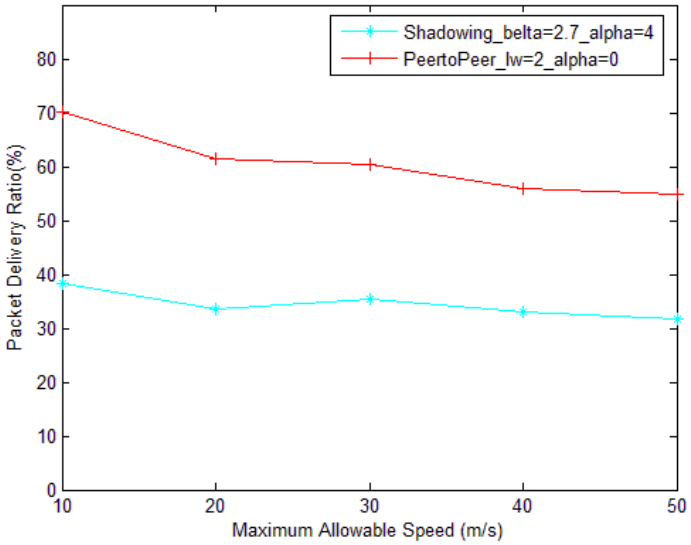

Figure 2: Comparison between peer-to-peer and shadowing models of packet delivery ratio.

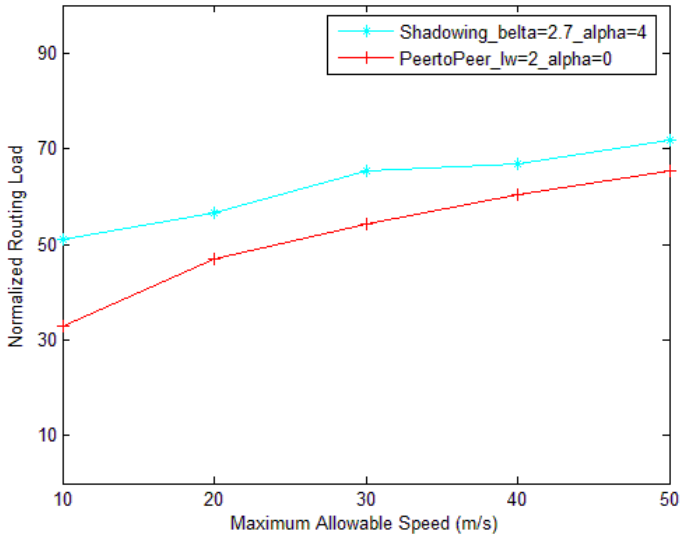

Figure 3: Comparison between peer-to-peer and shadowing models of normalized routing load.

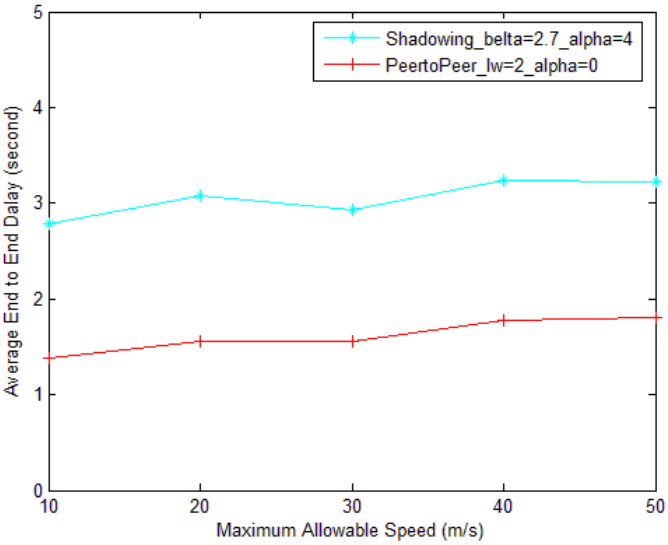

Figure 4: Comparison between peer-to-peer and shadowing models of Average end to end delay.

the literature ignored such propagation. Hence routing protocol with realistic propagation model that takes into account geometry of the environment is imperative and challenging for MANET in dense urban environment such as urban street grid environment. In this report, we propose a realistic propagation model so called peer-to-peer to propagation model which takes into account the multiple reflected signals along the street in an urban street grid environment to be integrated in Network Simulation 2 (NS2) provided the environment's geometry is known. To investigate the effects the NLOS propagation on MANET routing performance, routing metrics of AODV protocol are examined by using our peer-to-peer propagation model compared with modified shadowing model. Fig. 1 shows the path loss of our peer-to-peer propagation and shadowing model. It can be observed that the received power strength of shadowing model is underestimated compared to that of peer-to-peer propagation model in our street grid environment. From Fig. 2 to Fig. 4, the routing performance of AODV is higher when peer-to-peer to propagation model is used. For example, in Fig. 2 the packet delivery ratio increases from around 39% to 70% when modified shadowing and peer-to-peer propagation model are used respectively. Hence the NLOS propagation has a significant impact on MANET routing performance and received signal strength cannot be arbitrarily chosen.

Observations of the Effect of Temperature upon Stability of Resource-constrained, Embedded Clocks

M. A. Collett and T. H. Loh
National Physical Laboratory, Teddington, Middlesex, UK

Abstract— Wireless Sensor Networks (WSNs) are being increasingly sought after for critical applications such as security and health care. This is leading to an increased need to understand and quantify the reliability and stability of WSN-based systems when deployed in real environments. Timing synchronization is a vital capability for many WSN functions such as robust communications, stable sampling, data combining and location finding. This paper presents measured results of the frequency output of a WSN node clock. The clock incorporates several layers of software and hardware components, which need to function robustly together. We observe that there is a strong relationship between the standard deviation in clock frequency and temperature variation; with the standard deviation varying between 1×10^{-5} Hz and 10×10^{-5} Hz (the standard deviation in the mean of 10 minute rolling window of frequency measurements) as the ambient temperature crosses a threshold of approximately 23.5 degree Celsius. Quantification of the stability of a clock output is an important factor in any subsequent synchronization, affecting decisions such as the employment of hibernation for energy saving, sensor sample rates and time division multiple access communications. This is an important consideration for system designers and end users, who may experience unexpected system behavior in real deployments, or who may be unable to make reliable meaningful design choices.

There are a number of factors which affect the frequency of a resource constrained, embedded clock system. These include manufacturing tolerances of the governing quartz oscillator and ambient temperature. The stability of such clocks can also be affected by many factors. As wireless sensing systems become increasingly complex, both in terms of capability and requirements, it will be increasingly important to optimise every element. When synchronising clocks it is important to make judgements about the optimum intervals over which to carry out synchronisation and to be able to estimate the accuracy achieved. The observations presented here have highlighted that temperature is an important factor in determining both of these.

On a Useful Tool to Localize Jacks in Wiring Network

M. Franchet[1], **N. Ravot**[1], **and O. Picon**[2]

[1]CEA, LIST, Embedded Systems Reliability Laboratory
Point Courrier 94, Gif-sur-Yvette, F-91191 France
[2]Université Paris-Est; ESYCOM, Marne-La-Vallée, France

Abstract— In many fields such as automobile, aeronautics or robotics the current trend is to develop X-by-wire systems. Although this enables to decrease their load, the complexity of their wiring network increases in the meantime. This makes them more prone to electrical failures. This emphasizes the need for reliability of the wiring networks. To ease and speed up their maintenance and monitoring, a good knowledge of their topology is needed. Most of the time these networks aren't made of a single wire but of several cables linked to each others with jacks. Knowing where these jacks are is a first step to identify the topology of the network. Besides as they can be damaged too, monitoring them is also important.

One way to localize them is to use reflectometry which consists in injecting a signal into the wiring network and analysing the reflected signals at the injection point. One method, called Time Domain Reflectometry (TDR) (cf. [1–3]) uses a step or a pulse. This method works quite well for detecting hard faults such as open or short circuits. However the reflections on jacks are of low amplitude (as they are not perfectly matched to the line) and TDR may be not efficient enough to detect them. For doing so, some further signal processing tools can be used. In [4–6], a method, called Joint Time Frequency Domain Reflectometry (JTFDR), based on the Wigner Ville Transform (WVT) and a normalized Time Frequency Function (TFC) has been proposed. It has shown promising results concerning soft faults detection (cf. [7, 8]).

We show that thanks to the WVT and the TFC, it is possible to localize a jack in a line. The WVT and the TFC will be defined in the first part. Then it will be applied on experimental data. The second part exposes the measurement setup. The first line under test is made of two identical coaxial wires linked with a jack. The results are presented in part 4. The second type of line to be tested is made of two identical aeronautic wires (embedded in a set of several other wires) linked with a jack.

REFERENCES

1. Pan, T.-W., C.-W. Hsue, and J.-F. Huang, "Time-domain reectometry using arbitrary incident wave-forms," *IEEE Transactions on Microwave Theory and Techniques*, Vol. 50, No. 11, 2558–2563, Nov. 2002.
2. Auzanneau, F., M. Olivas Carrion, and N. Ravot, "A simple and accurate model for wire diagnosis using reflectometry," *PIERS Proceedings*, 232–236, Prague, Czech Republic, Aug. 27–30, 2007.
3. Ravot, N., F. Auzanneau, Y. Bonhomme, M. O. Carrion, and F. Bouillault, "Distributed reflectometry-based diagnosis for complex wired networks," *EMC: Safety, Reliability and Security of Communication and Transportation Syst.*, Jun. 2007.
4. Shin, Y. J., "Theory and application of time-frequency analysis to transient phenomena in electric power and other physical systems," Ph.D. dissertation, University of Texas, 2004.
5. Wang, J., P. Stone, Y.-J. Shin, and R. Dougal, "Application of joint time-frequency domain reflectometry for electric power cable diagnostics," *IETt Signal Processing*, Vol. 4, No. 4, 395–405, Aug. 2010.
6. Kwak, K. S., T. S. Yoon, and J. B. Park, "Load impedance measurement on a coaxial cable via time-frequency domain reectometry," *SICE-ICASE International Joint Conference 2006*, Oct. 2006.
7. Wang, J., P. Crapse, J. Abrams, Y. J. Shin, and R. Dougal, "Diagnostics and prognostics of wiring integrity via joint time-frequency domain reectometry," *10th Joint FAA/DoD/NASA Conference on Aging Aircraft*, Apr. 2007.
8. Franchet, M., N. Ravot, and O. Picon, "The use of the pseudo wigner ville transform for detecting soft defects in electric cables," *IEEE/ASME International Conference on Advanced Intelligent Mechatronics*, Budapest, Hungary, Jul. 3–7, 2011.

Deterministic Chanel Modeling for the White-Space TV-Band in Real-World Indoor Environments Considering Antennas Effects

M. El-Hadidy[1], **M. Fahmy**[2], **M. Ibrahim**[2], **and T. Kaiser**[1]

[1]The University of Duisburg-Essen, Germany
[2]The German University in Cairo, Egypt

Abstract— The enormous development of wireless communication increased the limitation of frequency resources. This force the researchers to direct their attentions and activities to the field of Cognitive Radio (CR) and to make use of the White-Space spectrum in the TV-Band from 470 MHz to 862 MHz. Main objective of this work is to present a deterministic channel model in the TV-Band for a real-world indoor environment. This deterministic channel model based on hybrid EM Ray-Tracing technique which includes both the characteristics of the antennas and the multipath propagation through the channel. The characteristics of the antennas would be investigated and considered based on EM simulation tool as CST-Microwave Studio, while the multipath propagation in the spatial channel between the transmitter and the receiver would be computed using a ray-tracing tool as Wireless-Insite from Remcom. Main characteristics of the TV-Band indoor channel model as the Delay Profile (CDP), Pathloss, Delay Spread (DS) would be investigated and computed in this work. Furthermore, the influence of the antennas directivity, orientation, polarization and frequency dependence on the channel parameters would be presented and investigated. In this work, the concert hall in the city of Hannover of "Niedersachsenhalle" has been considered as an indoor-environment, while Vivaldi patch antennas have been considered to be the transmitting and receiving ones. Fair comparison between the channel characteristics in the case of using either Vivaldi antennas or circular array with respect to the isotropic antennas would be illustrated as well. This work gives the opportunity to the CR researchers to examine their systems and designs on deterministic real-world channels.

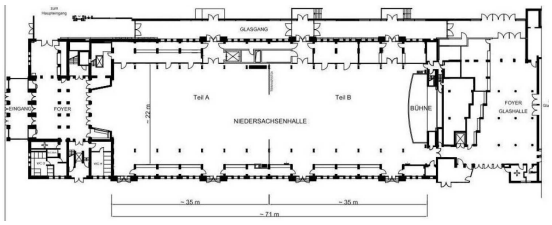

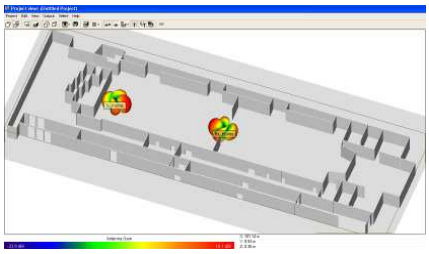

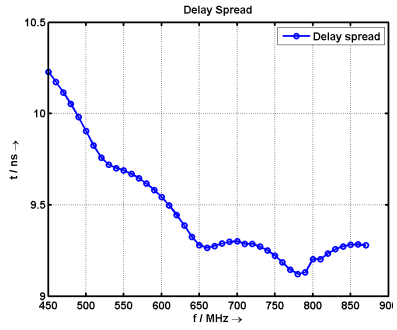

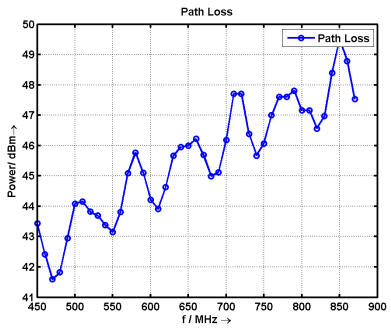

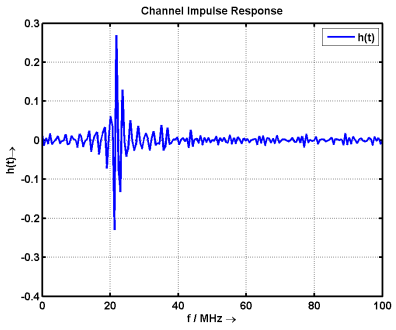

Shadowing Effect Analysis at Multiple Moving Persons Tracking by UWB Radar

Daniel Urdzík[1], **Rudolf Zetík**[2], **Dušan Kocur**[1], **and Jana Rovňáková**[1]

[1]Technical University of Košice, Košice, Slovak Republic
[2]Ilmenau University of Technology, Ilmenau, Germany

Abstract— Ultra wideband (UWB) radars appear as the suitable technology for detection and tracking of moving people in critical situations and hazardous environments. Our experiences with such applications of UWB radar systems have shown that at multiple moving person scenarios, a single radar with a small antenna array is able to detect very often the person moving closest to the radar antennas only, whereas the other target (persons) are also detected but usually with a small reliability. This negative effect can be explained in such a way that the person located in front of the radar antenna array acts as an obstacle and creates an area with high attenuation of the energy of the electromagnetic waves behind his/her. This area is referred to as the shadow zone. The shadowing person absorbs and reflects the energy of electromagnetic waves transmitted by the radar transmitting antenna and/or reflected by the other targets and hence, only a negligible part of the energy of the electromagnetic waves reflected by the other targets can be received by the radar. This effect is referred to as shadowing effect. The outlined problem of due to shadowing effect has been addressed for firstly in [1], where a qualitative analysis of shadowing effect has been described. The main contribution of this paper is the quantitative analyses of shadowing effect based on the measurement of the additional attenuation within the shadow zone due to the person localized in front of the radar transmitting antenna (so-called shadowing person).

In order to analyze shadowing effect, the measurement campaign with M-sequence UWB radar was realized. The scheme of the measurement is outlined in Fig. 1. The radar system was equipped with one transmitting and one receiving omnidirectional antenna. Shadowing person was standing in the fixed position in front of the transmitting antenna. The shape of the shadow zone and the level of additional attenuation behind shadowing person were measured by using the radar receiving antenna. The radar receiving antenna was localized subsequently in the different positions within the investigated area. At each position, the additional attenuation due to shadowing person was evaluated.

The experimental results obtained by the measurement are given in Fig. 1. It can be seen from this figure that the shadow zone has approximately a shape of a trapezoid. The additional attenuation

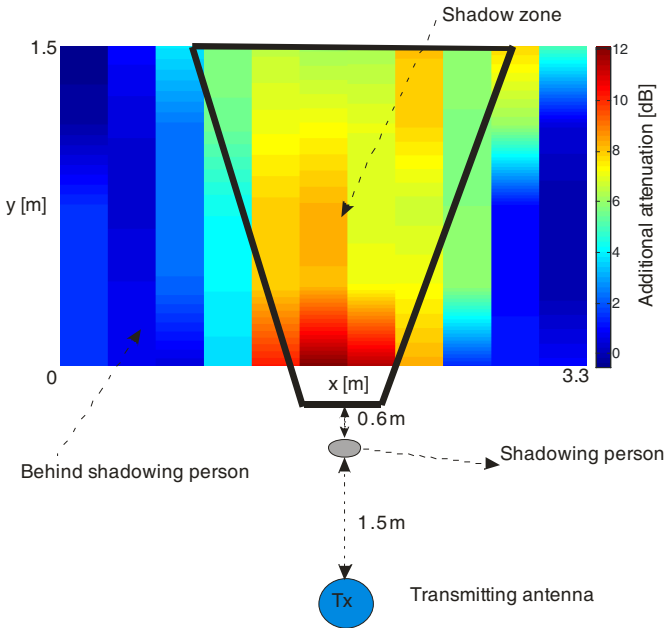

Figure 1: Experimental results of the shadowing effect.

within the shadow zone due to shadowing person can take on values from 4 to +12 dB. With regard to the requested ratio of signal to noise at the radar receiver input, it can be concluded that the additional attenuation due to shadowing person results in a limited detection of the other moving person within the shadow zone. With regard to that fact, shadowing effect has to be taken into account in the case of the design of radar systems for multiple moving person detection and tracking.

REFERENCES

1. Kocur, D., J. Rovňáková, and D. Urdzík, "Mutual shadowing effect of people tracked by the short-range UWB radar," *The 34th International Conference on Telecommunications and Signal Processing (TSP)*, 302–306, Budapest, Hungary, August 2011.

Human Shadow Effect Assessment when Integrating Inertial Navigation System with Signal Strength Measurements for Pedestrian Dead Reckoning

A. Bahillo[1], **J. Prieto**[1], **S. Mazuelas**[2], **P. Fernández**[1], **R. J. Durán**[1], **R. M. Lorenzo**[1], **and E. J. Abril**[1]

[1]Department of Signal Theory and Communications and Telematic Engineering
University of Valladolid, Spain
[2]Laboratory for Information and Decision Systems
Massachusetts Institute of Technology, USA

Abstract— The ability to locate the position of the user is an essential part of many applications: electronic travel aids for the visually impaired, context-aware guidance systems for exhibition touring, spatially based applications for a wearable computer, and public and private safety services. The problem of positioning in an open environment is relatively easy to solve using a Global Navigation Satellite System (GNSS). However, GNSS is limited because its inability to provide static heading and its lack of availability due to its signal outages when used in harsh urban areas, and indoors. Existing indoor navigation solutions complement GNSS in GNSS-compromised areas. Usually, they relay on pre-installed wireless sensor networks (WSN) (beacon-based solutions) where signal strength (SS) based techniques are the most spread due to their availability and cost [1]; whereas several applications such as emergency ones are interested in beacon-free solutions where an inertial navigation system (INS) framework is the closest solution to these requirements since it follows the user movements from a known start position independently from the building infrastructure [2]. Unfortunately, on the one hand, INS achieves high precision within short time periods but, it has the inconvenient of accumulating errors that grow rapidly. On the other hand, the positioning error of beacon-based positioning is not increasing with time but, less shortterm accurate with an absolute error in the range of several meters [3]. Therefore, SS based positioning techniques have a clear benefit to compensate INS when finding a reliable, continuous and accurate indoor positioning solution for large routes [4]. However, neither of the SS based positioning techniques take into account the shadow effect of the human body who carries the SS meter since the presence of the human body alters the pattern of wave propagation in its immediate proximity [5]. Hence, there are several problems that remain unsolved related to correctly interpret the SS readings when the SS meter is carried by a pedestrian and this information is wanted to be used for positioning [6]. The aim of this paper is to assess the SS errors caused by the presence of the human body in a theoretical and experimental approach to weight the SS information that feeds the INS-SS framework based on the human body attitude. The assessment takes advantage of the fact that the body itself is the only element for sure will be present in the environment. As magnetic disturbances can be severe and permanent indoors, only the accelerometer and gyroscope sensors (without a compass) will be used to estimate the pedestrian attitude and thus to assess the human body shadow effect. Finally, the positioning system coupled with measurements performed in an indoor environment demonstrates that taking into account the human body shadow effect from its attitude outperforms the conventional INS-SS frameworks [7].

REFERENCES

1. Mazuelas, S., A. Bahillo, R. M. Lorenzo, P. Fernández, F. A. Lago, E. García, J. Blas, and E. J. Abril, "Robust indoor positioning provided by real-time RSSI values in unmodified WLAN networks," *IEEE Journal of Selected Topics in Signal Processing, Special Issue on Advanced Signal Processing for GNSS and Robust Navigation*, Vol. 3, No. 5, 821–831, October 2009.
2. Renaudin, V., O. Yalak, P. Tomé, and B. Merminod, "Indoor navigation of emergency agents," *European Journal of Navigation*, Vol. 5, No. 3, July 2007.
3. Lei, F., P. J. Antsaklis, L. A. Montestruque, M. B. McMickell, M. Lemmon, Y. Sun, H. Fang, I. Koutroulis, M. Haenggi, M. Xie, and X. Xie, "Design of a wireless assisted pedestrian dead reckoning system — The Navmote experience," *IEEE Trans. on Instrumentation and Measurement*, Vol. 54, No. 6, Dec. 2005.
4. Retscher, G. and Q. Fu, "Integration of RFID, GNSS and DR for ubiquitous positioning in pedestrian navigation," *Journal of Global Positioning Systems*, Vol. 6, No. 1, 56–64, 2007.

5. Blas, J., F. A. Lago, P. Fernández, R. M. Lorenzo, and E. J. Abril, "Potential exposure assessment errors associated with body-worn RF dosimeters," *Bioelectromagnetics*, Vol. 28, No. 7, 573–576, 2007.
6. Bahillo, A., J. Prieto, S. Mazuelas, P. Fernández, R. M. Lorenzo, and E. J. Abril, "*E*-field assessment errors caused by the human body on localization systems," *Proceedings of the IEEE Vehicular Technology Conference (VTC)*, Taipei, Taiwan, May 2010.
7. Woodman, O., "An introduction to inertial navigation," Tech. Rep., No. 696, University Cambridge, Cambridge, UK, 2007.

A Novel 3D Ray-tracing Model for Precise Mobile Localization Application

Chee Kiat Seow, **Teng Wah Ang**, **and Kai Wen**
School of Electrical and Electronic Engineering, Nanyang Technological University, Singapore

Abstract— Recent year has seen the need for precise localization for both commercial and government applications. The underlying building block for accessing the performance of the localization algorithm is either the channel measurement data or ray-tracing algorithms that are highly correlated to the empirical channel measurement data. However, the accuracy of ray tracing algorithm is highly related to the simulation of all possible propagation paths traversing through various structures in the realistic environment. Traditionally, most of the rays tracing algorithms have been well researched for planar structures. This paper presents a novel three-dimensional ray-tracing model for building structures with non-planar or curved surfaces. Methodology to overcome the problem in modeling scatterers with non-planar surfaces has been proposed. It takes into all possible propagation paths from any combinations of reflections, diffractions and transmissions from/through planar and non-planar/curved surfaces. Comparisons between proposed model and the measured power delay profile in an environment containing building structure with curved surfaces has shown good agreement and articulate the impact of including scattering phenomenon from curved surfaces on the power delay profile.

Peer-to-peer Non-line-of-sight Localization in Multipath Environment

Si Wen Chen, **Chee Kiat Seow**, **and Kai Wen**
School of Electrical and Electronic Engineering, Nanyang Technological University, Singapore

Abstract— Current bidirectional localization schemes are able to locate a mobile device using Line-of-Sight (LOS) or Non-Line-of-Sight (NLOS) Time-of-Arrival (TOA) and Angle-of-Arrival (AOA) information measured at both the mobile device and reference device. This information is used to derive line of possible mobile device position (LPMD). The intersection points of LPMDs are used to estimate mobile position. However these algorithms do not work well in a dense multipath environment with high levels of TOA and AOA measurement noise. In addition, these techniques require at least two single bounce reflection paths to locate the mobile position. This paper presents novel methods based on multiple image theory and area of possible mobile device position to overcome the abovementioned limitations. Furthermore, the proposed technique is able to determine mobile device using one single bounce scattering path without the need of any mitigation techniques. Simulation results show that our proposed scheme outperforms previous bidirectional NLOS localization schemes by a significant margin especially for dense multipath environment and at high levels of TOA and AOA measurement noise.

PAPR Reduction in OFDM Signals via Combination of Active Constellation Extension and Genetic Algorithm

Seyed Ahmad Rafiei Taba Zavareh[1], **Paria Shahabi**[1], **Mohsen Akbari**[1], **Mohsen Riahi Manesh**[1], **and Ayman A. El-Saleh**[1, 2]

[1]Faculty of Engineering, Multimedia University
Jalan Multimedia, Cyberjaya, Selangor 63100, Malaysia
[2]Faculty of Engineering & Built Environment
Universiti Kebangsaan Malaysia, Bangi, Selangor 43600, Malaysia

Abstract— An efficient technique for transmitting signals in multipath and fading channels is multi carrier modulation (MCM). Orthogonal frequency division multiplexing (OFDM) as one the MCM techniques suffers from the high peak-to-average power ratio (PAPR) which can significantly decreases power efficiency and performance of wireless communication systems. Therefore, reducing the PAPR is highly considerable and lots of existing methods were proposed to modify or introduce new signal constellations to fight large signal peaks. One of the fast and reliable methods to reduce PAPR is active constellation extension — approximate gradient project (ACE-AGP) algorithm. This algorithm does not require side information like other methods and provides no loss in data as well. On the other hand, ACE-AGP lightly diminishes the bit error rate (BER) at the same time. However, a very high computational complexity and consequently a large convergence time are the main drawbacks of ACE-AGP. In this paper, use of genetic algorithm (GA) is proposed to overcome this complexity by searching and reducing the PAPR with respect to ACE-AGP. GA is a search technique which is widely used to find true or approximate solutions for optimization problems in different application fields of communication engineering such as modulation for wireless transmission, network design, etc. The robustness of the proposed GA-based method is investigated by eliminating and reinstating pilots. Results indicate that the proposed combination of ACE-AGP and GA reduces the envelope fluctuations in OFDM signals for any number of subcarriers and enhances the performance of ACE-AGP system for PAPR reduction at a very low complexity.

Multi-user MC-CDMA Using Pseudo Noise Code for Rayleigh and Gaussian Channel

M. F. Ghanim and M. F. L. Abdullah
Department of Communication Engineering, Faculty of Electrical and Electronic Engineering
University Tun Hussein Onn Malaysia, Johor, Malaysia

Abstract— The conventional code division multiple access (CDMA) technique used in third generation system faced serious limitations by channel dispersion, causing inter symbol interference (ISI), and it requires advanced signal processing algorithms to contain it. Therefore, multi carrier code division multiplexing (MC-CDMA) employing multiple stream of data channel can combat channel dispersion, hence ISI, thereby increasing system capability to accommodate a higher number of users. This paper presents simulation for the MC-CDMA system using pseudo noise code as spreading code (PN code) to spread data over channel. In this system instead of applying spreading sequences in the time domain, they are applied in the frequency domain, mapping a different chip of a spreading sequence to an individual OFDM subcarrier. The MC-CDMA system is applied in two channel cases, the first one when the used channel is Additive white Gaussian noise (AWGN) channel: the relationship between bit error rate and signal to noise ratio is discussed when the number of the users is increased from 4 to 64 users. Then Rayleigh fading which has four taps with different powers is added to the channel and its effect is simulated. The simulation shows that the fading affects the characteristics of the system sharply and clearly. The best values of signal to noise ratio for the system to work with minimum bit error rate are extracted and compared through the figures of SNR with BER in the case of 4, 16, 32 and 64 users. For each SNR between 0 dB and 50 dB the BER value showed an effect of AWGN and Rayleigh fading channel on the multi user MC-CDMA system.

Session 2P6
Microwave and Millimeter Wave Circuits and Devices

Medium Power Amplifiers: A Review

Arjuna Marzuki
Advanced Integrated System Device Group, School of Electrical and Electronic Engineering
Universiti Sains Malaysia, Nibong Tebal 14300, Malaysia

Abstract— This paper relook at the current work of medium power amplifiers (MPA) on four areas namely circuit technique, design methodology, modelling and application. More than 20 latest papers have been reviewed. Medium power amplifier is defined as device before the power amplifier, it normally has lower power output than the power amplifier. It is found there are many works on 60 GHz application such as radio over fiber, wireless digital communications and numerous others. These amplifiers employ broadband approach such as wideband matching techniques, parallel/series amplifier with different bands, distributed and other methods. It is still crucial for MPAs to achieve high efficiency with low distortion, various techniques such as such as dynamic biasing, envelope-tracking, tunable matching networks and Doherty amplifiers are employed to achieve this desired performance. As the cost of the MPAs are expensive, the first time right concept should be seriously considered in the development of these MPA. The parasitic aware approach in the design and simulation is famously used and employed in this new concept. Finally the process or technology used in designing these MPAs are also reviewed.

Analysis and Design of Triple-band Input Matching for CMOS Low-noise Amplifier

Chun-Yi Lin, **Ching-Piao Liang**, **Pei-Zong Rao**, **and Shyh-Jong Chung**
Institute of Communication Engineering, National Chiao Tung University, Hsinchu, Taiwan

Abstract— This paper presents the analysis and design of a triple-band low-noise amplifier (LNA) fabricated in a 0.18 µm CMOS process. The triple-band operation is achieved by adding a switch component in a dual-band input network of an LNA, so that it can function at 2.5, 3.5, and 5.2 GHz. The proposed method can effectively decrease the chip area as compared to conventional designs. In addition, based on the design procedures provided in this paper, the component values of the triple-band input network can be accurately calculated to reduce the complication of the circuit design.

A 24 GHz Low-power and High-gain Low-noise Amplifier Using 0.18 μm CMOS Technology for FMCW Radar Applications

Chun-Yi Lin, **Ming-Wei Lin**, **Ching-Piao Liang**, **and Shyh-Jong Chung**
Institute of Communication Engineering, National Chiao Tung University, Hsinchu, Taiwan

Abstract— In this paper, a low power and high gain low-noise amplifier (LNA) is presented for 24 GHz FMCW applications, fabricated in a 0.18 μm RF CMOS process. The proposed LNA is with the characteristics of the source inductive degeneration type, the current reuse technique, and the invariance of current density in CMOS process. The proposed LNA with a compact size has a gain of 18.95 dB and a noise figure of 5.8 dB, while consuming 11.3 mW. The measured input 1-dB compression point (IP1dB) and an input third-order intercept point (IIP3) are −26 dBm and −16.5 dBm, respectively.

Design of High Resolution MEMS Accelerometer Using Interdigital Bandpass Filter

Chandan Sharma[1], **Chandra Charu Tripathi**[2], **Santosh Bhagat**[3], **and Harpreet Singh**[4]

[1]Department of Electronics & Communication, Indus International University
Una, Himachal Pradesh, India
[2]Department of Electronics & Communication, Kurukshetra University, Haryana, India
[3]Department of Electronic Science, South Campus, University of Delhi, India
[4]Solid State Physics Laboratory, Defence Research & Development Organisation
Timarpur Lucknow Road, Delhi, India

Abstract— Interdigital band pass filters have been widely used in to the microwave industry because they provide reasonably good pass band characteristics, moderate loss and fairly high attenuation in the stop bands. Now with the advantage of bulk micromachining used in the MEMS fabrication technology, an interdigital band pass filter simultaneously can also be realized as an MEMS accelerometer with a very high capability of finding small changes in the acceleration in comparison to the conventional MEMS based accelerometer. Taking the advantage of a simple arc-length expression commonly used in the mathematics, acceleration is measured as change in the value of central cut off frequency due to the change in coupling of the microstrip resonators by applying the acceleration. Working on X-band region, an interdigital band pass filter of order four with the central pass frequency of 9 GHz is designed. Various structural parameters of the intedigital band pass filter are extracted from the mathematical calculations. As a starting material which should work for both microstrip resonator and also the sensor, Nickel, gold, copper and combination of these three with different thickness is used. Gold has the higher density as compared to nickel and copper and more ductile so it is mechanically more robust for behaving as a cantilever therefore fulfilling the criteria for cantilever based MEMS accelerometer, moreover due to its high conductivity value, in most of RF device metallization is done with gold with ensuring the minimum thickness of 2 µm. Therefore gold with the minimum thickness of 4 µm is optimized for both microstrip resonator as well as accelerometer and shows the best displacement and sensitivity with the applied acceleration as compared to other two materials used. In the normal operation this kind of device will behave as a filter but on applying the acceleration it will behave as a MEMS accelerometer, so it can be used in small g RF-MEMS applications and also for reliability test for the cantilevers. CST MWS-9 tool is used for the RF-part whereas mechanical simulation is carried out in the ANSYS tool. Cost of gold is the factor that plays an important role, so instead of using gold, composites that give sensitivity as comparable to the gold and have high ductile strength will be used for the future analysis.

Tuning Space Mapping: The State of the Art

Qingsha S. Cheng[1], **John W. Bandler**[1], **and Slawomir Koziel**[2]

[1]Department of Electrical and Computer Eng., McMaster University
Hamilton, ON L8S 4K1, Canada
[2]School of Science and Engineering, Reykjavik University
Menntavegur 1, Reykjavik 101, Iceland

Abstract— The space mapping approach to electromagnetics-based optimal design is based on aligning a fine model (high-fidelity electromagnetic simulation) with a suitable physics-based companion coarse model or surrogate. Space mapping facilitates efficient design while avoiding direct simulation and optimization of the detailed fine model. Tuning within an electromagnetic simulator (simulator-based tuning or "tuning space mapping") is inspired by the idea of the operation of mechanical tuning screws in microwave filter realizations. It combines EM accuracy with circuit-design speed to achieve fast design closure and typically offers satisfactory results after one or two iterations, a small number of full-wave electromagnetic simulations of the optimized microwave structure. As in any space mapping algorithm, tuning space mapping exploits a fast, physically-based surrogate of the fine model under consideration. A difference from conventional space mapping techniques is that tuning space mapping uses a tuning model as its surrogate. The tuning model is developed from a so-called auxiliary fine model (a fine model with "cuts" and corresponding tuning ports) that is augmented with circuit-based tuning elements. A "Type 0" tuning model uses an auxiliary fine model that has infinitesimal cuts (with corresponding ports) reserved for small tuning elements. A "Type 1" tuning model uses an auxiliary fine model that has larger cuts prepared for larger tuning elements. A fast "Type 1" tuning model uses an auxiliary fine model with collapsed cuts of a "Type 1" tuning model and a reduced number of tuning ports to save simulation time. A co-simulation-based ("Type 2") tuning model makes use of sections of the auxiliary fine model reconnected by tuning elements. Once the tuning model is constructed, we proceed with the standard space mapping procedure. Our tuning space mapping approaches are demonstrated using several microwave design optimization problems.

Advances in Automatic Model Generation for Microwave Modeling

Chuan Zhang[1], **Qijun Zhang**[1, 2], **and Jianguo Ma**[1]

[1]School of Electronic Information Engineering, Tianjin University
92 Weijin Road, Nankai District, Tianjin 300072, China
[2]Department of Electronics, Carleton University, Ottawa K1S 5B6, Canada

Abstract— Artificial neural networks (ANN) have been used for microwave/Electromagnetic (EM) modeling due to its accuracy and faster computation. In this paper we review advances in neural model development with automatic model generation (AMG) algorithms. AMG has emerged to convert human based modeling into a CAD process, which uses adaptive data sampling algorithm to automatically drive the EM/physics/circuit simulators to generate new samples required by ANN training. High ANN model generating accuracy is achieved by more searching of different ANN structures. However, the CPU expensive EM/physics/circuit simulations and the iterative training process are the most computationally intensive parts in AMG. To improve AMG efficiency, the parallel automated model generation (PAMG) approach exploits parallelism to split the processes of the data generation and the training into smaller sections which are simultaneously executed on parallel processors in a multi-processor environment to speed up the computation. AMG includes three key parts: adaptive sampling and data generation, training and validation. Parallel adaptive-sampling/data-generation is to drive several data generators simultaneously to generate multiple training data on parallel processors. To avoid the interference of input/output files during processing we set independent simulation environment in each processor. While in ANN training, the parallel processing technique can perform the training error computation and back propagation (BP) in multiple processors at the same time. Both of them improve the speed of the ANN procedure. We also use a parameter Sp to measure the performance of PAMG. It concludes that high speed parallel modeling efficiency can be achieved. Data in the examples of driving a physics-based device simulator for MESFET modeling and driving a circuit simulator for power amplifier (PA) behavior modeling shows that the PAMG highly shortens the model development time with parallel efficiency above 90%. So it is very efficient method in automatic model development for microwave applications.

A Novel Defected Microstip Structure (DMS) for Microstrip Gaps

S. R. Hosseini, **R. Sarraf Shirazi**, **and Gh. Moradi**
Wave Propagation & Microwave Measurement Research Lab., Department of Electrical Engineering
Amirkabir University of Technology, 424 Hafez Avenue, Tehran 15914, Iran

Abstract— Planar structures have been found useful various applications in microwave instruments fabrication and generally microwave engineering producing different types of antennas, filters, couplers and etc are simple models of this increasing interest.

One of bold features of these structures is Flexibility and using changes in their structures to achieve better performance. In this regard, new structures such as defected ground structures (DGS), coupled resonators, defected microstrip structures (DMS) and etc have been developed.

Microwave discontinuity like gap, T-shape, bend, step and etc are some common changes that apply to microwave structures for leading to specific design performances.

In this paper, gap structure studying in microstrip and presenting new structure using defected mirostrip structures (DMS) will be discussed.

Microstrip gap is a common discontinuity in planar structures. Circuit modeling of gap as capacitances convert microstrip line to a high pass transmission line. Novel defected microstrip structure (DMS) is presented to model gap discontinuity. 3D full wave simulations show the presented model is valid up to near 30 GHz until higher order modes features will appear.

A very WB band pass filter using DMS present to model microstrip gap structure. This behavioral adaption continue to approximately 30 GHz where higher order modes eliminate high pass features.

Frequency Selective Surfaces Based Planar Microwave Absorber

F. Che Seman[1] and R. Cahill[2]

[1]Radio Communication and Antenna Design Laboratory, Faculty Electrical and Electronics Engineering
University of Tun Hussein Onn Malaysia, 86400 Batu Pahat, Johor, Malaysia
[2]The Institute of Electronics, Communications and Information Technology
Queen's University Belfast, Northern Ireland Science Park, Queen's Road, Queen's Island
Belfast BT3 9DT, Northern Ireland, UK

Abstract—

Introduction: Modern communications technology employs radio frequency absorbing surfaces for a diverse range of applications, for example to create isolation between antennas and to reduce radar visibility of platforms in military scenarios. For the latter, the absorber material must be placed on or integrated into the surface of the stealthy platform so there is much interest in developing thin, lightweight, RF absorbers which are capable of broadband operation. As is well known, this imposes conflicting requirements on the design because thin stealthy structures normally give narrowband performance and vice versa [2.1, 2.2]. The simplest classical structure is the Salisbury screen which is a quarter wavelength thick [2.3]. Configurations incorporating Frequency Selective Surface (FSS), known as Circuit Analogue (CA) absorbers, have received significant interest due to their ability to reduce the thickness of the screen and/or increase functionality. Research has recently been undertaken to use lossy FSS as planar microwave absorbers [x-y].

Performance Analysis of Complementary and Non-complementary EBG Geometries

Gnanam Gnanagurunathan and Krishnasamy T. Selvan
Department of Electrical and Electronic Engineering
The University of Nottingham, Malaysia Campus
Selangor Darul Ehsan 43500, Malaysia

Abstract— This paper analyses the bandgap occupancy of the Electromagnetic Bandgap (EBG) structures. These structures are currently of interest in the electromagnetic fraternity. These structures are periodic in nature and are able to prevent the propagation of surface electromagnetic waves in a specified band of frequency hereby known as the bandgap.

In this work, a performance analysis on the bandgap of complementary form of various EBG geometries is undertaken. The transmission line analysis method is used for this purpose and the bandgap is observed based on S_{11} and S_{21} measurements across a 2 port transmission line. The transmission line is modelled on one side of the planar board while the other side is lined with a single row of EBG units. Decay on the S_{21} measurement below $-20\,\mathrm{dB}$ and S_{11} above $-10\,\mathrm{dB}$ indicates the surface wave bandgap. This would be the region over which the surface waves will be substantially attenuated.

Five fundamental geometries namely, square, circle, cross, spiral and hexagon are analysed in both the complementary and non-complementary forms. The filling ratio, r/a (where r is the EBG size and a is the periodicity of the EBG units backing the transmission line) is maintained at about 0.5 for all the five geometries.

In each of the EBG geometries analysed, except square, it emerges that the complementary form sees a significant shift in the bandgap to lower frequencies and wider bandgap widths when compared to the non-complementary form.

Preliminary simulations are carried out on a commercial simulator, the CST Microwave Studio. Based on the results, the models are fabricated and measurements carried out with a Scalar Network Analyser for verification. Both simulation and experimental results are in good agreement.

Design a Broadband 50 W Power Amplifier with Large Signal Stability Verification

Kumar Narendra[1], **Juan-Mari Collantes**[2], **and Mohamad Noorazuan**[1]

[1]Research & Development Center, Motorola Technology, Penang 11800, Malaysia
[2]Department of Electronics Engineering, University Basque County, Bilbao 48080, Spain

Abstract— This work describes a strategy and methodology for eliminating oscillation in broadband high power amplifier (PA). Large signal stability verification based on system pole-zero identification techniques under varying of load termination are proposed to guide designer towards a stable broadband PA. An example design of dual-LDMOS transistor with splitting/combining scheme is used. Oscillation is eliminated in prototype measurement level while maintaining optimum circuit performance. The performance of the PA is recorded, where output power of 50 W, PAE more than 45% and gain of 13 dB for frequency range of 750 to 860 MHz.

Session 2P7a
Power Electronics

Simulation of Sensorless Control of Induction Motor Using HIL Method

P. Brandstetter, M. Dobrovsky, and P. Krna
Department of Electronics, VSB-Technical University of Ostrava, Czech Republic

Abstract— The paper deals with simulation of sensorless control of the induction motor using hardware in the loop simulation method (HIL) in Matlab-Simulink. The first part of the paper deals with the description of vector control of the induction motor with the sensorless control using the structure MRAS. The second part describes HIL method and its implementation using modern digital signal controller. In the last part, simulation results for different speed changes and torque changes of the induction motor are shown.

MRAS observer structure is shown in Figure 1. In this system, induction motor state variables evaluated in the reference model based on the measured variables (stator voltages, stator currents). The reference model is independent of the speed and uses the voltage machine model. Adaptive model uses the current model of the machine and the mechanical angular speed of the machine is one of the input variables of this model.

The difference between state variables is adaptive signal (AS) $\Phi_{(e)}$, which is evaluated and minimized most often by the PI regulator in the block of the adaptation mechanism, which performs the estimate value of the mechanical angular speed ω_m and adapts adaptive model until the desired behavior. With feedback, the observer is able to limit the impact of changes in machine parameters on the accuracy of the calculation.

The error signal $\Phi_{(e)}$ corresponding to the deviation of rotor fluxs (Equation (1)) enters to the PI controller, after processing by PI controller, we get estimated angular speed ω_m (Equation (2)). The adaptation algorithm is described with the following equations:

$$\Phi(e) = \hat{\bar{\Psi}}^S_{R(AM)} \times \bar{\Psi}^S_{R(RM)} = \hat{\Psi}_{R\alpha(AM)}\Psi_{R\beta(RM)} - \hat{\Psi}_{R\beta(AM)}\Psi_{R\alpha(RM)} \tag{1}$$

$$\hat{\omega}_m = K_1\Phi(e) + K_2\int_0^t \Phi(e)\,\mathrm{d}t \tag{2}$$

where $K_1 > 0$, $K_2 > 0$.

Hardware in the Loop (HIL) simulation is a technique that is used in the development and testing of complex real-time systems. It is a tool that connects the hardware (controller) with a mathematical model (managed system) in a closed feedback loop. To simulate this method a real control system and a mathematical model is required.

The mathematical model is used to configure the control system. The control system generates an actuator variable dependent on the control deviation, which is the difference between desired and actual quantity. The control variable enters to the model, then output variable (actual value) gets off from the mathematical model, and than gets back to the control system. This simulation works in real time.

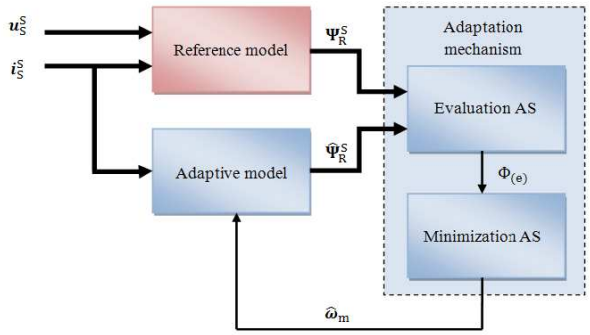

Figure 1: MRAS — basic scheme for the estimation of mechanical angular speed.

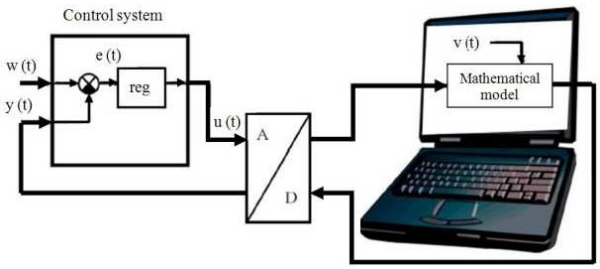

Figure 2: Diagram of hardware in the loop simulation.

Results of this simulation approach to reality, because the control system with sensors and actuators is implemented as close as it would be in real. To the fact that the results would match the reality, we need a sufficiently accurate mathematical model, on which simulation accuracy dependents most. As soon as the control system is set up according to the requirements, the mathematical model can be replaced by the real system and the results can be compared.

Figure 2 shows a general diagram of the simulation using method hardware in the loop. The meaning of values in this picture: $y(t)$ — process value, $w(t)$ — reference quantity, $e(t)$ — control error, $u(t)$ — control variable, $v(t)$ — fault value, reg — regulator.

Optimization of Indirect Space Vector Modulation Strategy for Matrix Converter

D. Kuzmanovic and J. Lettl
Faculty of Electrical Engineering, Czech Technical University in Prague, Czech Republic

Abstract— Due to the absence of energy storage elements, conventional modulation strategies cannot be used for the matrix converter. A range of modulation strategies have been developed for the matrix converter. They can be classified into the Modulation Duty-Cycle Matrix (MDCM) based strategies, and the Space Vector Modulation (SVM) based strategies. MDCM strategies calculate individual bi-directional switches duty cycles by solving the matrix converter input-output equations. SVM strategies can be direct and indirect. The Direct SVM strategy combines all matrix converter switching combinations (vectors) to generate the reference output voltage and the input current vectors. The Indirect SVM (ISVM) observes the matrix converter as an equivalent combination of an input virtual rectifier and an output virtual inverter, connected by a virtual DC-link. The virtual rectifier is then controlled as the classical current source rectifier, and the virtual inverter as the classical voltage source inverter. The selection of the virtual rectifier and the virtual inverter stages switching combinations for each combination of the input current vector and the output voltage vector sectors is illustrated in Table 1. However, unlike the classical AC/AC converters, where the energy storage element in the DC link enables independent operation of the input rectifier and the output inverter, in the case of the matrix converter the operation of the input and output stages has to be precisely coordinated. That is achieved by synchronizing the input and output SVM, and by choosing a suitable switching pattern. The selection of the modulation strategy and the switching pattern does not impact only the quality of the input and output quantities, but also the switching losses. In this paper, the analysis of the matrix converter switching losses, when the ISVM is used, is presented. It was shown, how a simple modification of the modulation strategy can lead to a significant decrease in the switching losses. A special software tool for the evaluation of the matrix converter losses was designed. The numerical simulations have shown that the use of the optimized modulation strategy decreases the switching losses by up to 20%.

Table 1: Virtual rectifier and inverter stages switching states lookup table.

		OUTPUT SECTOR					
		1	2	3	4	5	6
Input Sector	1	ab, ac 100,110,111	ab, ac 110, 010, 000	ab, ac 010, 011, 111	ab, ac 011, 001, 000	ab, ac 001, 101, 111	ab, ac 101, 100, 000
	2	ac, bc 100,110,111	ac, bc 110, 010, 000	ac, bc 010, 011, 111	ac, bc 011, 001, 000	ac, bc 001, 101, 111	ac, bc 101, 100, 000
	3	bc, ba 100,110,111	bc, ba 110, 010, 000	bc, ba 010, 011, 111	bc, ba 011, 001, 000	bc, ba 001, 101, 111	bc, ba 101, 100, 000
	4	ba, ca 100,110,111	ba, ca 110, 010, 000	ba, ca 010, 011, 111	ba, ca 011, 001, 000	ba, ca 001, 101, 111	ba, ca 101, 100, 000
	5	ca, cb 100,110,111	ca, cb 110, 010, 000	ca, cb 010, 011, 111	ca, cb 011, 001, 000	ca, cb 001, 101, 111	ca, cb 101, 100, 000
	6	cb, ab 100,110,111	cb, ab 110, 010, 000	cb, ab 010, 011, 111	cb, ab 011, 001, 000	cb, ab 001, 101, 111	cb, ab 101, 100, 000

Comparison of Gamma and T Models for Convector Controlled Induction Machine Drives

J. Lettl[1], **S. Fligl**[1], **J. Bauer**[1], **and M. Vlcek**[2]

[1]Faculty of Electrical Engineering, Department of Electric Drives and Traction
Czech Technical University in Prague, Czech Republic
[2]Faculty of Nuclear Sciences and Physical Engineering, Department of Mathematics
Czech Technical University in Prague, Czech Republic

Abstract— Nowadays in variable speed drives induction machines are widely used. For the understanding and clear specification of the electromagnetic processes in the induction machines different equivalent circuits can be employed. Traditionally, in order to reduce the complexity of the mathematical model the resistances and inductances are represented as concentrated components and 3 phase winding is assumed to be symmetrical.

These equivalent circuits are also used as a starting point for the design of the drive controller. For the satisfactory function of a controller or model of the machine designed on the basis of the machine's equivalent circuit the parameters of the equivalent circuit must be known with the sufficient accuracy.

In most papers that deal with the problematic of the IM drive control representations based on the Park's equations or T-form of the equivalent circuit are used. These models are adequate in many situations. Even though they can seem to be overly simplified, they can serve as a solid basis for an advanced motor control. However other authors tend to use gamma models and there are approaches using both. This paper examines and compares some of the issues of adequate machine modeling and attempts to provide a firmer basis for selection of an appropriate model and to confirm or disprove the equivalence of different approaches.

Simulation of the Matrix Converter Drive with Sliding Mode Control

J. Lettl[1], **S. Fligl**[1], **J. Bauer**[1], **and S. Ryvkin**[2]

[1]Department of Electric Drives and Traction, Faculty of Electrical Engineering
Czech Technical University in Prague, Czech Republic
[2]Trapeznikov Institute of Control Sciences, Russian Academy of Science, Russia

Abstract— Beginnings of the Matrix Converter go to late seventies. Nowadays, the name "Matrix Converter" is used to label any power topology that is possible to organize into sub blocks placed in a matrix shape. In this contribution the name "Matrix Converter" means the symmetrical 3×3 topology made by nine bidirectional switches. Such converter belongs to the direct frequency converter category. Output voltage is made by direct switching of input phases to output phases. This fact means that converter does not need DC-link capacitor, which increases the costs of the converter and volume requirements of the converter. The absence of DC-link capacitor is one of the main advantages of the matrix converter. On the other hand it means that output voltage amplitude is limited to 86.6% voltage amplitude on input. Higher voltages can be achieved with over modulation, which causes input current distortion. The other advantages of the converter compared to conventional indirect frequency converter are power factor regulation; work in all four quadrants; its high dynamic; sinusoidal current consumption; nearly sinusoidal output voltage waveform, with low harmonic content and high efficiency. To the main disadvantages belongs: amount of semiconductors device, limited output voltage amplitude and complicated regulation algorithm. The matrix converter is therefore suitable to replace the indirect frequency converter in the area of the compact induction machine drives.

Very important parts of the converter's controller are used modulation strategy and control algorithm. The common modulation strategies from the area of the indirect frequency converters can not be used because of the absence of the DC-link. Therefore the modulation strategies based on virtual DC-link space vector modulation were developed. Such approach helps to reduce the modulation complexity and enables to reuse classical modulation strategies (after a slight modification). At the same time, it works as a dependency injection. That is why different approaches can be used to control both the output voltage and the input current at the same time. In this paper the phase control of the input current in the combination with the sliding mode control of the output voltage is presented. This enables us to overcome the traditional limitation of the output voltage without resigning from the input current control.

Voltage Converters with Switched-capacitor

V. Sladecek, **P. Palacky**, **P. Vaculik**, **and J. Oplustil**
Faculty of Electrical Engineering and Computer Science
Department of Electronics, VŠB — Technical University of Ostrava,
17, Listopadu 15, Ostrava-Poruba 70833, Czech Republic

Abstract— Switched-capacitor converters are an alternative to the DC-DC converters with accumulation inductance. Using the switched-capacitor converters leads to a substantial increase in efficiency switching power supply. Switched-capacitor power converters are often used to provide simple power-conversion functions at low power levels. These functions include doubling, halving and inverting the input voltage, and can be combined to achieve other conversion ratios. Typical applications include RS232 level converters and FLASH memory programming voltage generators. These standard converters are often unregulated or supplemented with a linear regulator for voltage regulation.

Switched-capacity converters slowly come to the front in the field of power converters, which promise greater efficiency than previously used DC-DC converters, which use the energy storage inductance.

Getting the output voltage (U_{OUT}), which corresponds to n - multiple voltage input is the basic function of increasing the inverter.

For inverters with switched-capacitor creates the n — multiple generally parallel charging n — internal capacitor converters. These capacitors are then connected in series to the load. Custom converter topology then determines the combination of these connections.

Internal resistance R_i is a very important property of the inverter. It represents the sum of all losses that are parasitic properties of components. Reducing internal resistance (impedance) leads to the use of capacitors with low series resistance (low ESR). It is also necessary to use switching elements with a small unipolar character of the impedance in the closed state.

The paper provided theoretical and practical results obtained in the design of medium power converters. The following are the different topologies used in the design and their possible applications.

Modern Control Strategies for Power Active Filter

P. Simonik, **D. Slivka**, **P. Hudecek**, **and L. Odlevak**
VSB-Technical University of Ostrava, FEI, 17. listopadu 15, Czech Republic

Abstract— The paper deals with possibilities for currents regulation methods of parallel active power filter and also with applicable techniques for acquisition of referential current value. For example in our case was necessary to evaluate performances of a new hysteresis current control strategy for autonomous three phase parallel active filter for harmonic currents elimination. Hysteresis control strategy, is based on the currents errors and their derivatives calculation each time the zero voltage vector is set at the AC side of the inverter of the active filter.

There are presented results which were confirmed by theoretical analyses, where the reasonable methods and techniques were analyzed with real sample testing. The filter was designed as laboratory sample which can work as hard or soft (ZVS — Zero Voltage Switching) switched device. For regulation methods authentication was designed special control unit which will be described in the paper. The unit was designed on the base of demands from the area of future usage — control unit of power converters, three level inverters, pulse rectifiers, power active filters and so on. These applications require high-power control system and on the base of good previous experience with the development kit eZdsp TMS320F2407A was selected the new line with the F2812. For this application is important that the selected DSP was developed for power electronics applications and has implemented all important peripheries which are required for power converter control.

This research is realized within the research activity in the branch of power electronics in the Department of Electronics, Technical University of Ostrava.

Session 2P7b
Microwave and Millimeter-wave Measurements

Accurate Measurement Standards and Calibration Techniques for S-parameter Measurements in Coaxial Line System at Millimeter Wave Frequency

M. Horibe and R. Kishikawa
National Metrology Institute of Japan
National Institute of Advanced Industrial Science and Technology, Japan

Abstract— S-parameter measurements are usually established by the vector network analyzers (VNAs) and reference standards. An air dielectric coaxial line is usually used as a reference standard in the VNA measurements. High accurate and precise mechanical tolerance is required in the reference standard air line. The tolerance must be comparable or smaller than wave length at measuring frequency. This means tolerance should be getting smaller at the millimeter wave frequency. The causes of tolerance are coming from manufacturing tolerance and dimensional measurement accuracy. We improve both manufacturing tolerance and dimensional measurement accuracy for air line as the reference standard at millimeter wave frequency. As a result of this, uncertainty of an S-parameter standard (i.e., approximately 0.005 at 110 GHz) is becoming a half of uncertainty of previous standards (i.e., 0.012 at 110 GHz) in NMIJ.

Establishment of S-parameter Standards of Rectangular Waveguide at Millimeter-wave and THz Frequencies

R. Kishikawa and M. Horibe
National Metrology Institute of Japan
National Institute of Advanced Industrial Science and Technology, Japan

Abstract— Precise S-parameter measurements in the vector network analyzers (VNAs) are established by reference standards with small uncertainty. A standard line section is usually used as a VNA's reference standard. High precise mechanical tolerance of waveguide aperture is required in the reference standard in waveguide system. The tolerance must be smaller than wave length at measuring frequency. This means tolerance (i.e., a few micro meters) should be achieved at the sub-millimeter wave and THz frequencies. The causes of tolerance are coming from manufacturing tolerance and dimensional measurement accuracy. We have already developed the evaluation scheme of dimensions of WR-3 (WM-864) waveguide apertures by three dimensional coordinate measuring machine (3DCMM). However, it is impossible that 3DCMM measures the aperture of THz waveguide (WR-1, WM-250). We developed new dimensional measurement system for small size aperture. As a result of this, an S-parameter standard is established in the frequency range from 110 GHz to 1 THz.

A Calibration Method without a Matched Load for a Six-port Wave-correlator Based VNA

N. Akutsu, **R. Matsuguma**, **N. Iwaki**, **and T. Yakabe**
The University of Electoro-Communications, Tokyo, Japan

Abstract— The six-port technology and its many useful applications are now being recognized once again in modern society [1], and are published in book form [2]. Since the six-port wave correlator (SPC) technology is well known for its unique ability to accurately measure the complex two waves ratio (amplitude and phase deference), many applications of the SPC have been extensively investigated, such as beam direction finding [3], Doppler frequency measurement [4], and vector network analyzer (SPC-VNA) [5].

In this paper, to improve both measurement accuracy and dynamic range, a new calibration method without ideal matched loads for the prototype MMIC SPC-VNA is proposed.

The proposed calibration method has been evaluated with several two-port passive components, and the validity and utility are confirmed compared with previous one.

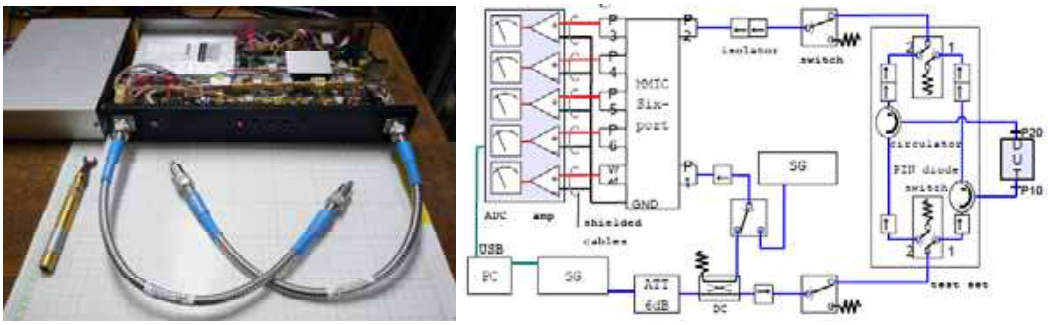

Figure 1: Scheme of a prototype MMIC SPC-VNA.

REFERENCES

1. Loelpin, A., G. Vinci, B. Laemmel, D. Kissinger, and R. Weigl, "The six-port in modern society," *IEEE Microwave Magazine*, Vol. 11, No. 7, S35–S43, Dec. 2010.
2. Ghannouchi, F. M. and A. Mohammadi, *The Six-port Technique with Microwave and Wireless Applications*, Artech House, Sep. 2009, ISBN-13: 978-1-60807-033-6.
3. Yakabe, T., F. Xiao, K. Iwamoto, F. M. Ghannouchi, K. Fujii, and H. Yabe, "Six-port based wave correlator with application to beam direction findig," *IEEE Trans. Instrum. Meas.*, Vol. 50, No. 2, 377–380, Apr. 2001.
4. Xiao, F., F. M. Ghannouchi, and T. Yakabe, "Application of six-port wave-correlator for a very low velocity measurement using the Doppler effect," *IEEE Trans. Instrum. Meas.*, Vol. 52, No. 2, 297–301, Apr. 2003.
5. Yakabe, T., K. Hirose, H. Matsuura, K. Fujii, and F. Xiao, "Evaluation of prototype MMIC six-port wave correlator based VNA," *2010 Asia-Pacific Radio Science Conference*, AB-3, Sep. 2010.

Estimation of Terrestrial Rain Attenuation at Microwave and Millimeter Wave Signals in South Africa Using the ITU-R Model

P. A. Owolawi[1], S. J. Malinga[1], and T. J. O. Afullo[2]

[1]Department of Electrical Engineering, Mangosuthu University of Technology
Umlazi, KwaZulu-Natal 0002, South Africa
[2]Department of Electrical, Electronic, and Computer Engineering, University of KwaZulu-Natal
Durban 4000, South Africa

Abstract— The interest of many telecommunications companies to provide high speed wireless internet access, broadcast multimedia information, multimedia file transfer, remote access to local network, interactive video conference and Voice-Over-IP has forced migration from lower frequency bands which are already congested to higher frequency bands such as microwave and millimetre bands. The choice of these bands became the key solution to today's request because of large bandwidth availability, small device size and wide range of spectrum availability. Although with all the inherent advantages, rain is the major offender to optimum performance and usage of these bands. Rain attenuation results in outages that compromise the quality of signals and link availability, making it the prime factor to be considered in designing both terrestrial and satellite links. This means that the designing of any communication device at this spectrum range requires knowledge of rain fade in order to provide optimum link availability and robust and reliable link to telecommunication systems that offer the aforementioned benefits.

The most important performance metric considered in link analysis is the system availability. That is, the time percentage the link is providing service either at or below the specified given bit error rate. It was confirmed that at frequencies just above 5 GHz, the rain fade depth becomes noticeable and it is severe at frequencies above 10 GHz. Rain rate measurement is one of the active components needed to estimate the amount of rain fade, which is frequency and location dependent. The extensive work carried out on the rainfall characteristics at different locations in South Africa has confirmed a dynamic distribution of rain rate in the region.

This paper presents the application of results found in rain rate characteristics study in South Africa and their application to terrestrial links. It provides an analysis on rain fade in the light of the link distance chart and how it relates to the link budget. The outcomes are incorporated into the link budget to determine the maximum link distance and other performance parameters.

In summary, the paper presents the rain rate experimental measurements with the application of International Telecommunication Recommendations (ITU-R) on the rain attenuation model in South Africa. The nineteen chosen sites, at least one from each province in South Africa, are considered for this study. The parameters presented in this paper are specific attenuation and total path attenuation due to rain at horizontal, circular, and vertical polarizations at frequencies ranging from 1 GHz to 400 GHz. The implications of rain attenuation to the system designers are evaluated by finding the link distance chart, and designing the link-budget at the chosen frequency range. The results of this work can be used in planning links for both microwave and millimetre broadband wireless networks in South Africa such as Local-Multipoint-Distributed-Services (LMDs).

The paper is organized as follows. Section 1 introduces the concept of higher frequency ranges, advantages, disadvantages inherent in them and applications to the modern wireless communication. Section 2 deals with the mathematics of rain fade modelling using the ITU-R method while Section 3 presents the cumulative distribution of rain rate as peculiar with each province in South Africa at 0.01% of exceedence. Section 4 and Section 5 of the paper focus on an assessment of specific attenuation and its distribution in the South African context respectively. Section 6 deals with statistical analysis of the model and Section 7 demonstrates its applications using 19.5 GHz links within five campuses of the University of KwaZulu-Natal, Durban South Africa. Finally, the link resources analysis is carried out using the link distance chart.

Computational Design and Performance Evaluation of Green Painting Absorbing Material

Hasnain Abdullah[1], **Mohd Nasir Taib**[1], **Ida Rahayu Mohamed Noordin**[1], **Norhidayah Saad**[1], **Wan Khairuddin Wan Ali**[2], **Rusnani Ariffin**[1], **Ahmad Takiyuddin Abdullah**[3], **and Siti Zura A. Jalil**[1]

[1]Faculty of Electrical Engineering, Universiti Teknologi MARA, Malaysia
[2]Faculty of Mechanical Engineering, Universiti Teknologi Malaysia, Malaysia
[3]Industrial Automation Section, UniKL MFI, Malaysia

Abstract— Microwave absorbing materials have received great attention from recent years in both civil and military fields due to various applications in communications, radar, satellite systems, and anechoic chambers. Wireless communication is currently the fastest growth of telecommunication technology. Many studies have indicated that there are harmful radiations produced by transmitting telecommunications structures. Effects on human exposure include dizziness, nausea, vomiting and loss of breath. A way to reduce strong microwave radiations for human is by applying a microwave absorbing paint coating to the wall of the built spaces. The green painting mixed with ingredients from coconut shells is the main material that is analyzed in this research. The findings show that material applied with the green painting can readily absorb the microwave radiations. The wave-absorbing materials are designed by using Computer Simulation Technology (CST) Microwave Studio simulation software. The goal of this simulation is to find the best performing absorber. From dielectric constant value, the modeling and simulation stage of microwave absorber are executed to obtain the reflectivity or S_{11} result using CST Microwave Studio software. Analysis of the S_{11} results and measurement of absorber performance are evaluated to define the microwave absorber performance. A free space measurement setup operating in the frequency of Ku Band is employed to measure absorption. The results show that the green painting with coconut based carbon can be used as coating absorbing material. Each material applied with the green painting shows excellent absorption at 3 to 6 dB range. The most excellent result is shown by double layer coating absorption up to 17 dB.

Measurements and Analysis of Terrain Clutters at Ku-band

Chih-Yuan Chu[1], **Kun-Shan Chen**[1, 2], **and Wei-An Chuang**[2]

[1]Communication Research Center, National Central University, Jhongli, Taoyuan, Taiwan
[2]Center for Space Science and Remote Sensing Research
National Central University, Jhongli, Taoyuan, Taiwan

Abstract— Terrain clutter is essential for radar detection performance and image interpretation. Understanding the clutter under different land cover has been studied by conducting field measurements, numerical simulation, and theoretical modeling. Though a historically long subject of research, still limited databank are only available to selected cases of radar parameters (look angle, frequency, polarization, etc.) and terrain types. This paper is to expand our database by extensive field measurement at Kun-band to include 7 terrain types at different polarizations (HH, HV, and VV) were characterized with look angles from 5 to 85 degrees: grass land, herbaceous plant, woody plant, buildup, waterbody, asphalt road, and concrete road. Backscattering coefficients were derived from a scatterometer system carefully calibrated in anechoic chamber and open site with known RCS man-made targets. Comparisons with existing reported data wherever is available was also made to radiometrically confirm the measured data. Statistical analysis was then followed to characterize the clutter under different terrain types for stationary case and Doppler effects were also examined for trees.

Design of High Performance Low Pass Filter Using Neural Network and Simulated Annealing

Bhabani Sankar Nayak[1], **Subhendu Behera**[1], **Pradyumna Ku Patra**[1], **and R. K. Mishra**[2]

[1]Department of ECE, NIST, Berhampur, Orissa, India
[2]Berhampur University, India

Abstract— A low pass filter using defected ground with multiple numbers of scaled down complementary split ring resonators (CSSR) structures of a micro strip line is designed. The introduction of CSSR unit results in interesting filtering characteristics, like very high attenuation rate, couple of the dimension dependent finite attenuation poles and a very low-pass band ripple level. The scaling of CSSR unit cells is made in a systematic way optimizing the LPF performance. The frequency responses in terms of pass band as well as the stop band are investigated with the simultaneous change of length and gap as variable and the effect on insertion loss is studied. A neural network model is applied for the modeling of frequency response of filter with SSR and CSSR defects. Simulated annealing method is also used for the modeling of frequency response to further minimize the error. The obtained results are compared. The size of split ring resonator is optimized in order to obtain the minimum error in the frequency response. Incremental back propagation learning approach is followed in the training of neural network.

Session 2P8
Poster Session 3

FDTD Study on Permittivity and Permeability Adapted to Noise Suppression Sheet

Y. Kawamura[1], **T. Suzuki**[2], **T. Ohno**[2], **K. Ishii**[2], **and O. Hashimoto**[3]

[1]Chiba University, Japan
[2]Kisarazu National College of Technology, Japan
[3]Aoyama Gakuin University, Japan

Abstract— Recently harmonic electromagnetic noise from transmission lines and devices is increasing, so that a noise suppression sheet (NSS) is frequently used to improve the problem above. However, there are not so many papers dealing with the relationship among an NSS, permittivity and permeability. Therefore, a microstrip line (MSL) based on IEC standard (IEC62333-2) is fabricated, and a transmission characteristic of the MSL attached with an NSS is simulated and measured. Then, we will examine material constant for NSS having a good lowpass characteristic.

Figure 1 shows a simulation model of the MSL attached with an NSS. The model shown in Fig. 1 assumes DiClad522 manufactured by ARLON ($\varepsilon_r = 2.55$, $\tan\delta = 0.0022$). Input and output power are supplied to the rectangular coaxial lines connected to the back of the substrate. Fig. 2 shows the simulated and measured results of Fig. 1. As shown in Fig. 2, the maximum difference of transmitted electric power between measured and simulated results is 1.86% in Sample 1, and 1.45% in Sample 2 respectively. Therefore, the simulation model shown in Fig. 1 is verified from the above results. Fig. 3 shows the simulation results of the MSL with the NSS which have five types of material constants. The attenuation band shown in Fig. 3 is shifted to a low frequency

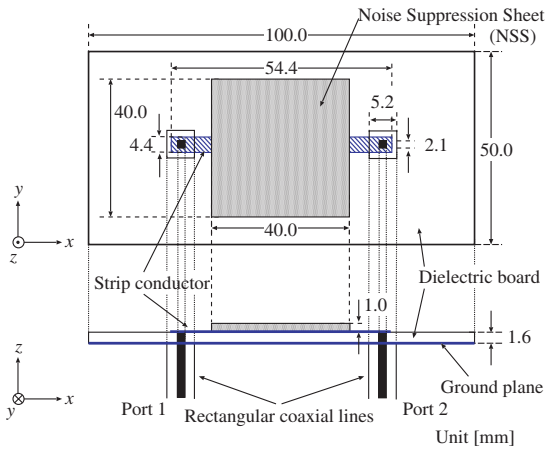

Figure 1: Simulation model of MSL with NSS.

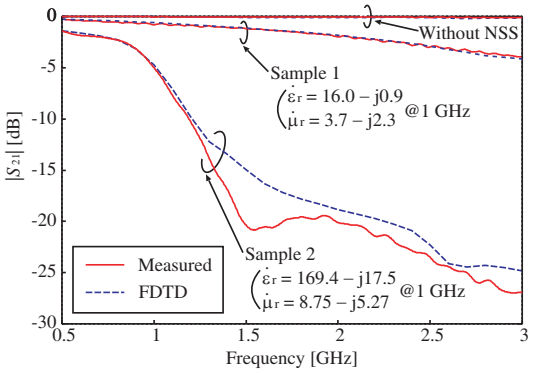

Figure 2: Simulated and measured results of Fig. 1.

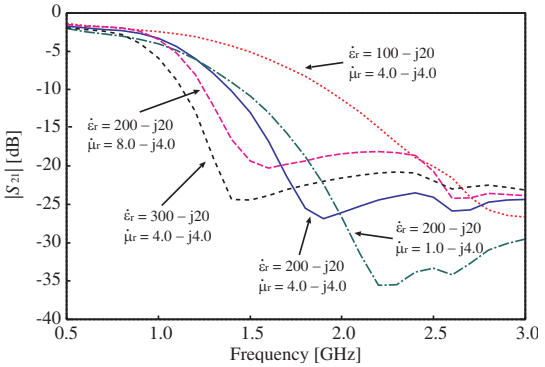

Figure 3: Simulation results of NSS with different material constant.

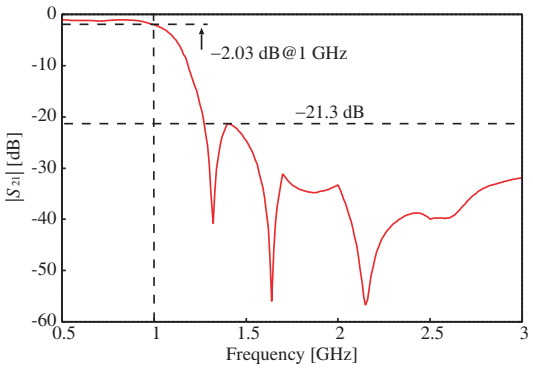

Figure 4: Simulation results of NSS with frequency dependence of permeability.

with high real parts of permittivity and permeability. Moreover, the low frequency characteristic less than 1 GHz is improved by a high real part of permeability. Fig. 4 shows the result of the NSS which has frequency dependence of permeability considering the tendency of Fig. 3 mentioned above. As a result, a good transmission characteristic is obtained that is more than −2.03 dB at the frequency of up to 1 GHz and is less than −21.3 dB at more than 1.26 GHz.

ACKNOWLEDGMENT

We appreciate the support of the Futaba Electronics Memorial Foundation.

Numerical Design of Matching Structures for Characteristic Improvement of Finite Periodic Structures

H. Sanada[1] and J. Ren[2]

[1]Hokkaido Institute of Technology, Japan
[2]Hokkaido University, Japan

Abstract— This study describes how to design matching structures for characteristic improvement of finite periodic structures based on numerical optimization methods. Especially this paper deals with one-dimensional semiconductor superlattices and one-dimensional left-handed circuits. It is well known that infinite superlattice structures have energy-bands and infinite periodic left-handed circuits have pass-bands. We can control the position and the band width of those bands by adjusting structural parameters or circuit element parameters. These characteristics are effectively used in the fields of semiconductor engineering and microwave engineering. However, we need to utilize finite periodic structures instead of infinite periodic structures in real situations. Finite periodic structures have different energy (frequency) characteristics from those of infinite periodic structures. For example, Finite superlattice structures have many sharp transmission peaks instead of energy bands. As a result, we cannot often obtain performance being up to our expectations. In this study, we show a new approach based on numerical optimization methods, which can be used for characteristic improvement of finite periodic structures. We propose to place matching structures at both sides of finite periodic structures and to improve energy (frequency) characteristics by adjusting many parameters of matching structures. The numerical optimization methods we adopted were a downhill simplex method and a genetic algorithm. Judging from results of numerical experiments, we concluded that our method is effective for improve the energy (frequency) characteristics of finite periodic structures.

Investigation of Spectrally Efficient Transmission in Mixed WDM Systems

V. Bobrovs, A. Udalcovs, and I. Trifonovs
Institute of Telecommunications, Riga Technical University, Latvia

Abstract— The authors have investigated the minimal allowed channel spacing for developed mixed wavelength division multiplexing (WDM) systems in order to obtain maximal spectral efficiency for system's channels. These fiber optic transmission systems can be considered under the concept of next generation optical networks and is offered as a model for the future design of backbone optical networks. In a case of different telecom operators' optical networks convergence a necessity to transmit differently modulated optical signals over a single optical fiber even with different per channel bitrates may occur in the soon future. Authors have revealed the optimal parameter configuration for developed mixed transmission systems and obtained in system's channels detected signals bit-error-rate (BER) correlation diagrams. They represent BER as a function from different system's parameters such us channel output power level, optical amplifier fixed output power level and system's channels allotment in C-band of ITU-T recommended spectral grid. As a model of developed combined WDM systems that is offered for the future design of backbone optical networks, is considered WDM system with the following configuration: [1st channel: NRZ-OOK (10 or 40 Gbit/s)] — [2nd channel: 2-POLSK (10 or 40 Gbit/s)] — [3rd channel: NRZ-DPSK (10 or 40 Gbit/s)]. It is also found out that minimal channel spacing for differently modulated optical signals in investigated mixed data rates WDM system is equal to 75 GHz if optical signals are transmitted with 10 Gbit/s and 40 Gbit/s per channel bitrates. As well as, system's average spectral efficiency depends not only from the minimal allowable channel spacing but also from mixed system's configuration if equal frequency intervals are used for channels separation.

Investigation of External Electromagnetic Disturbance in HDWDM System

J. Porins, G. Ivanovs, V. Bobrovs, and A. Supe
Institute of Telecommunications, Riga Technical University
12 Azenes Street, Riga LV-1010, Latvia

Abstract— Fiber optics telecommunication systems (FOTS) are developing at a very high rate. The reasons for this steady growth include the availability of optical fibers with small attenuation and dispersion characteristics, invention of powerful and narrow band lasers, development of high-speed optical modulators and use of very sensitive optical receivers. Due to rapidly growing capacity requirements for FOTS high-speed high-density wavelength division multiplexing (HDWDM) systems are advancing into high data transmission rate and narrow channel spacing is used to utilize the available bandwidth more effectively [1]. In HDWDM communication systems optical wave's polarization becomes the main effect. In principle, external electric, magnetic and electromagnetic (EM) fields can affect light transmission in optical fibers through Kerr effect, Faraday effect and Pockels effect. As it is well known, Kerr effect is based on the material refractive index changes depending on the electromagnetic field strength. According to [2], external electric field can effectively rotate the polarization plane of light in the fiber due to the Kerr effect by the angle φ. In our experiments, influence of external electromagnetic disturbance in HDWDM communication system (see Fig. 1.) with the minimum allowed channel spacing in wavelength nm range 1546 nm–1554 was studied. Our polarization rotation studies show BER changes from 10^{-12} to 10^{-9} which is close to critical value by ITU-T recommendations.

The results indicate that for 10 Gbit/s HDWDM transmission with suitable channel interval 37.5 GHz between adjacent channels BER changes from 10^{-12} to 10^{-6} due to the change plane of polarization which is critical for system performance. In the case when the polarization is rotated by 45° when using HDWDM with 37.5 GHz spacing between the channels it is necessary to increase the spacing up to around 50 GHz.

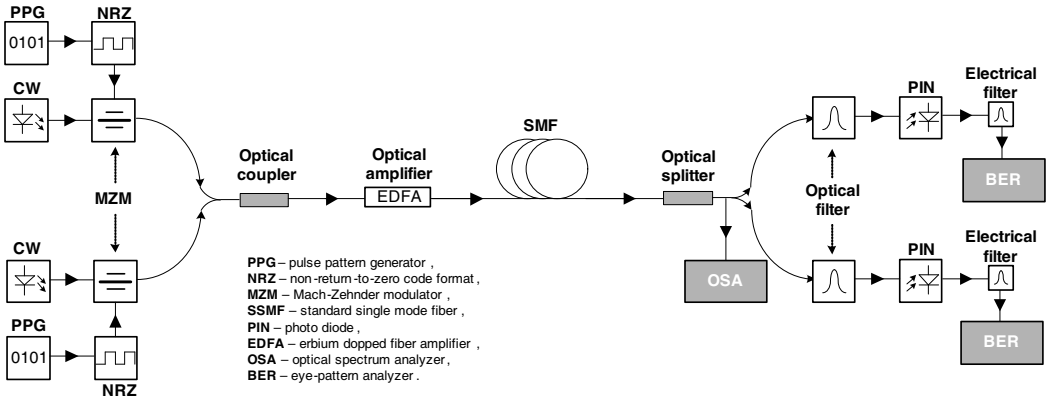

Figure 1: The setup used for investigation of HDWDM transmission.

REFERENCES

1. Ivanovs, G., V. Bobrovs, O. Ozolins, and J. Porins, "Realization of HDWDM transmission system," *International Journal of the Physical Sciences*, Vol. 5, No. 5, 452–458, 2010.
2. Sokolov, S. A., "Features of polarization mode dispersion in optical cable with a wave seal from lightning," *The First Russian Conference on Lightning Protection, Book of Abstracts*, 111–114, 2007 (in Russian).

The Design of HEV Drive Unit with an Axial Flux Rotary Converter

P. Chlebis, **A. Havel**, **and P. Vaculik**
Department of Electronic, VSB — TU Ostrava, 17, 15 Listopadu, Ostrava 70800, Czech Republic

Abstract— This paper describes an efficient axial flux arrangement of the four quadrant rotary converter for hybrid electric vehicles. The main task of here presented axial flux rotary converter (AFRC) is to keep the internal combustion engine (ICE) working in the area of its maximal efficiency during all possible driving conditions to satisfy minimal fuel consumption. In other words, the AFRC have to convert the optimal torque-speed operation point of the ICE on the input shaft to the required variable torque and speed on the output shaft, which is through the final gear connected to the wheels.

The AFRC is supplied by the three phase voltage inverter from the DC power source, which can be realized as a combination of two autonomous power sources — $LiFePO_4$ battery pack delivering nominal current and ultracapacitor pack for peak power supplying. Whole system is controlled by the DSP TMS320F28335 with implemented direct torque control algorithm to satisfy sufficient computing power and dynamics of the four quadrant rotary converter (4QRC) drive system.

The proposed solution combines two known principles of electric rotating machines together in one unit, which is composed from synchronous and asynchronous machine having two rotors affixed to the input and output shaft, one wound stator and two axial air gaps δ_1 and δ_2. Due to selected double rotor arrangement it is possible to vary both the speed and the torque between the input and output shaft, hence the transferred power. The input and output power difference is possible to supply or consume by the stator winding, so only a part of the total vehicle drive energy is transferred across the electromagnetic coupling.

The design of the axial flux wound stator and both axial flux squirrel cage rotors is based on the arrangement of radial air gap induction motor and permanent magnet synchronous motor. The method of constant magnetic circuit volume is utilized for dimensions conversion, which results into basic dimensions of stator and rotor discs in axial flux conception. This allows the creation of real 3D models in the CAD application. Finally, the finite element simulations of electromagnetic induction in the axial flux stator pack are presented in the concluding part of this paper.

Absorption Enhancement of Multiple Junction Solar Cells by an Intermediate Reflection Mirror

Ming-Jer Jeng and Liann-Be Chang
Department of Electronic Engineering, Green Technology Research Center
Chang Gung University, Taiwan

Abstract— Multiple junction solar cells can absorb the large parts of full optical spectrum and result in an increase of solar efficiency. However, current matching is an important issue to design a high efficiency multiple junction solar cells due to series connection of individual solar cells. The photocurrent is limited by the small one among these junction solar cells. Generally, the top cell will generate a small photocurrent and limit the whole cell current due to high energy bandgap. One can increase an optical absorption of the top cell. It can effectively enhance the photogenerated current and then increase the solar efficiency. In this work, we focus on the characteristics of three junction (InGaP/GaAs/Ge) solar cells by a reflective Bragg mirror. We insert the Bragg mirror between the top and middle cells to reflect the short wavelength light and enhance the top cell photocurrent. The Bragg mirror consists of alternating quarter wavelength optical thickness with high and low refractive index materials. We can control the stopband width by the index ratio of high and low refractive index materials. The resonance wavelength is determined by optical thickness of layers and the height of reflectance stopband is increased by an increasing the number of periods. For example, AlAs and GaAs thin films were used as low and high index materials. Five periods of Bragg mirror can achieve the reflectance of 75%. It can increase the optical absorption more than 30% in the top cells. Therefore, solar efficiency can be significantly increased. The further detailed study is under progress.

Characterization of the Cerenkov Radiations Generated in Optical Fibers Irradiated by Co-60 Isotope

K. W. Jang[1], W. J. Yoo[1], J. Moon[1], K. T. Han[1], D. Y. Jun[1], S. H. Shin[1], J.-Y. Park[1], B. G. Park[2], S. Kim[3], Y.-H. Cho[4], and B. Lee[1]

[1]School of Biomedical Engineering, Research Institute of Biomedical Engineering
Konkuk University, Korea
[2]Department of Energy & Environmental Engineering, Soonchunhyang University, Korea
[3]Department of Nuclear & Energy Engineering, Applied Radiological Science Research Institute
Cheju National University, Korea
[4]Department of Radiological Science, Catholic University, Korea

Abstract— Optical fibers have been widely used as sensing elements or a means of relaying signals. General method for measuring physical fluctuations with fiber-optic sensors is to measure light intensities or wavelength shifts of incident lights. Here, the optical fibers can transmit light signals, which are related to physical fluctuations, to light measuring devices without experiencing external influences such as pressure, temperature, and humidity. In hazardous nuclear reactor environments, especially, the radiation sensors using optical fibers have a number of advantages such as high spatial resolution, availability in narrow spaces, and real-time measurement.

The fiber-optic Cerenkov radiation sensor which is one of the fiber-optic radiation sensors is composed with optical fibers and light measuring devices. Generally, the Cerenkov radiation is produced by a charged particle traveling through some transparent mediums at a velocity greater than that of light in the same medium. In the case of spent fuel storage pool in a nuclear power plant, the Cerenkov radiations could be generated in the optical fibers by Compton electrons produced by gamma-ray interactions. Therefore, these signals depend on the burn-up of the fuel assembly in the spent fuel storage pool.

To develop the fiber-optic Cerenkov radiation sensor, in this study, we characterized the Cerenkov radiations generated in optical fibers irradiated by a Co-60 isotope. We measured the amounts of Cerenkov radiations as a function of lengths and diameters of optical fibers. Also, the amounts of Cerenkov radiations are measured according to irradiated locations of the optical fiber.

A Study on Surge Immunity of the 77 GHz Radar System

Soon-Mi Hwang, **Chul-Hee Kim**, **and Kwan-Hun Lee**
Korea Electronics Technology Institute (KETI), Korea

Abstract— Radar system is a core product of vehicle safety system and the Europe and North America are the leading developers [1]. This paper evaluates surge resistance, the primary failure factor of vehicles, of latest radar system and analyzes its result.

Close-range radar and long-range radar are merged and miniaturized into a single 77 GHz multi-mode radar system and it covers wide azimuth and produces a large output at the same time [2, 3]. The radar's module consists of millimeter wave bandwidth antenna and RF Transceiver H/W, Electronic Control Unit (ECU), radome and instrumental parts including housing, Detection S/W for mid-long range detection, Tracking S/W, TJA, CDM, ACC Stop & Go, and FCW interface.

Surge is one of the major causes of failure in vehicle parts. It refers to the movement of high electricity caused by electrical or mechanical switching. When such high electricity moves to other device for an instant, it damages the device's IC.

Surge test was done on ARS308 model of Continental from Germany, according to the international standard, IEC61000-4-5 standard (1.2/50 µs, Open Circuit Voltage type, ∼ 8/20 µs, Short Circuit current waveform) [4]. Starting from 1 kV, the test began by adding 200 V until the failure occurred. CANanalyzer V7.5 (Vector coperation, Germany) was used to measure before/after performance. As a result, input of 4 kV disturbed transmission of radar module signal, increased current, and unstable power.

Examining the failed sample from Surge test, we found there was a change in power input pin's resistance and capacitance of the sample. The power input's standard resistance is 1000 MΩ, but the failed sample had resistance of 141.7 Ω. Also its capacitance changed from its original range, 12 pF ∼ 13 pF, to 1,000 pF.

Looking closely at the internal circuit with an optical microscope showed us trace of burning in the circuit's capacitor and chip-type inductor. Surge caused sudden rush of high electricity, which led to failure of the power part circuit's insulation.

REFERENCES

1. Wenger, J., "Automotive mm-wave radar: Status and trends in system design and technology," *IEE Colloquium on Automotive Radar and Navigation Techniques*, 1–7, Feb. 9, 1998.
2. Klotz, M. and H. Rohling, "A 24 GHz short range radar network for automotive applications," *Radar, CIE International Conference on Proceedings*, 115–119, Oct. 15–18, 2001.
3. Tullsson, B. E., "Alternative applications for a 77 GHz automotive radar," *Radar Conference*, 273–277, May 07–12, 2000.
4. IEC 61000-4-5, Electromagnetic Compatibility (EMC) Test, Surge Test, 2001.

Active Charging Stations for Electric Vehicles Charging

P. Simonik, **A. Havel**, **M. Hromjak**, **and P. Chlebis**
VSB — TU Ostrava, Katedra Elektroniky, 17, 15 Listopadu, Ostrava 70800, Czech Republic

Abstract— Currently is the electromobility one of the most discussed issues in the automobile technology field. The intent of electric vehicles diffusion assumes that electromobiles will relive extreme ecological situation in cities and especially in their centres and also enables occasional connection between distant locations as well. The Czech Republic is in this branch still distinctive, because electromobilism is rather activity of amateur enthusiasts and the corresponding number of operating electric vehicles is still low. The low number of electric vehicles corresponds to the low density of charging network, which is run mostly by amateurs. In order to make sense to deal with both positive ecological and energy use impacts of electric cars, the electric cars should constitute at least 10–15% of total number of cars driving on our roads. In the Czech Republic on the 31.12.2010 registered total number of 4 515 885 passenger cars and buses, i.e., to fulfil the requirement of 10–15% of electric cars means to put into operation about five hundred thousand electric passenger cars, and buses particularly for the public transport. The average stored energy of 40 kWh per one vehicle generate the accumulation element with instantaneous energy up to 20 MWh (according to the current electric vehicles operation) located apparently to the metropolitan distribution networks. Therefore, the expansion of electric cars goes along the claim to build an adequate network of charging stations and the group of users create a significant market segment for suppliers of electricity. The concept of active charging station has to ensure, that the energy needed for electric vehicles charging will be available regardless network options, e.g., at the time of vehicle shut down period and its charging also at the time of maximum power consumption. Therefore, the station has to be equipped by own accumulation source, which is able to cover the reductions of network supply by accumulated energy and also use energy from various types of renewable sources attainable in given location.

Estimation of Induction Machine Electrical Parameters Based on the Genetic Algorithms

P. Simonik, **P. Hudecek**, **P. Palacky**, **and Slivka David**
Department of Electronics, Faculty of Electrical Engineering and Computer Science
VSB Technical University of Ostrava, 17.listopadu 15, Ostrava 708 00, Poruba, Czech Republic

Abstract— This article shows one of many ways how identify the parameters of the IM in real time. For identification is used theory of genetic algorithms. The Genetic Algorithms (GA) is a search technique used in many fields, like in computer science, to find accurate solutions to large optimization and search problems. The advantage of GAs is flexible and intuitive approach to optimization and demonstrates a higher probability of not converging to local optima solutions compared to traditional gradient based methods. More recently, methods which have appeared in the scientific literature about general GAs become popular and can be successfully ported to power electronics and drives. This article deals with the possibilities to improve dynamics and other properties of the drive with using online parameters estimation integrated in main control algorithm. In this paper at the first there is presented an analysis of the current state of the investigated problem and there is also explained why the problem is discussed. Following chapters show induction machine dynamic model the principles and ways of implementation the IM parameters identification. Theory of used genetic algorithm and experimental results are demonstrated in the end of this article. The conclusion describes the potential use of this method and discusses further development in the real time estimation of induction machines parameters.

PCB Power Plane with Wideband Noise Suppression by Embedding High Permeability Material between the Substrate and Power Plane

Hui Fen Huang and Wei Guo
School of Electronic and Information Engineering, South China University of Technology, China

Abstract— In today's high-speed electronic systems, the simultaneous switching noise (SSN) or ground bounce noise (GBN) is one of the major unavoidable problems. There are two classical ways to suppress SSN: decoupling capacitors and electromagnetic band-gap (EBG) structures. Using decoupling capacitors is limited in low frequency. EBG structure is usually used in GHz frequency range, but it has large size and the IR-drop is not optimized. A compact power plane with wideband noise suppression and low voltage drop is necessary [1].

In this paper, a novel compact power plane for optimized direct current property based on constructal theory is proposed. This power plane has the properties of compact size, low voltage drop and wideband noise suppression. Three classic tree structures (H-shaped tree, spider tree and disc tree) are optimized by minimizing the overall resistance when the entire area and the structure of the tree are given. From the optimized results, we know that the disc tree has the best direct current (DC) performance among the three trees. Then a disc power plane based on the disc tree is developed for printed circuit board (PCB). Patches with high impedance lines are assembled into the disc tree grid and the disc power plane is obtained. The disc tree distributes overall direct current for the power plane for optimized DC performance. Capacitors are added on the edge of the power plane, and magnetic material with high permeability is embedded between the substrate and power plane. The capacitors and magnetic material with high permeability form a very low cut-off frequency and wide band-gap so that the noise from 50 MHz to GHz in the power system can be suppressed. Simulated and measured results show that this novel power plane' suppression bandwidth over than 20 dB is from 50 MHz to GHz. The power plane has the properties of compact size, low voltage drop and wideband noise suppression.

ACKNOWLEDGMENT

This project is supported by the Science Fund of China (No. 61071056) and the Doctoral Program of Higher Education of China (No. 20090172120009).

REFERENCES

1. Rao, P. H., "Multi-slit electromagnetic bandgap power plane for wideband noise suppression," *IEEE Transactions on Components, Packaging and Manufacturing Technology*, Vol. 1, No. 9, September 2011.

Equivalent Parallel Capacitance Cancellation Utilizing Coupling between Integrated EMI Filter Components

Hui-Fen Huang, **Mao Ye**, **and Liang-Yong Deng**
School of Electronic and Information Engineering
South China University of Technology, Guangzhou 510641, China

Abstract— Due to the existence of equivalent parallel capacitance (EPC) of inductors, the effective filter frequency range is usually limited. The problem can become even worse when planar cores replace toroidal cores to realize low-profile structure in an integrated form. This paper introduces a technique for improving the high-frequency performance of integrated CM filter by effectively cancelling the parasitic winding capacitance. Other than implementation in [1], where an embedded conductor layer is inserted into the inductor winding and grounded to obtain ideal inductor characteristics, the added conductor layer is moved outside and served for CM capacitor here, which results in improved filtering performance with a smaller size and less fabrication time.

To achieve EPC cancellation, besides the required capacitance, the winding structure of CM capacitor layer also needs to be carefully designed so that the negative coupling between inductor winding and capacitor can be utilized. At initial stage, a simple strategy is to make the direction of capacitor winding and inductor winding opposite. However, because of non-unity coupling coefficient and relatively small CM capacitance, the performance over several MHz suffers notable degradation.

In order to overcome limitations brought by the simple implementation, a bi-direction windings structure is then developed with somewhat increased CM Capacitance as compared to the uni-direction case. Thus attenuation in the frequency range between 10 MHz to 30 MHz can be further improved. To demonstrate this, a simplified equivalent circuit model is derived and main influence factors in implementation are investigated. Simulations and experimental results show the performance of newly proposed filter could be as good as former integrated CM filter [1].

ACKNOWLEDGMENT

This project is supported by the Science Fund of China (No. 61071056) and the Doctoral Program of Higher Education of China (No. 20090172120009).

REFERENCES

1. Chen, R., J. D. van Wyk, S. Wang, and W. G. Odendaal, "Improving the characteristics of integrated EMI filters by embedded conductive layers," *IEEE Trans. Power Electronics*, Vol. 20, No. 3, 611–619, 2005.

A Novel Integrated EMI Filter Based on Interleaved Planar PCB Windings and Flexible Foils

Huifen Huang and Liangyong Deng
School of Electronic and Information Engineering
South China University of Technology, Guangzhou, China

Abstract— More and more power conversion systems use the switching mode power supply (SMPS) for high efficiency and high power density. The switching operation of these systems becomes the potentially large source of the electromagnetic interference (EMI). EMI filters are necessary to insure the electromagnetic compatibility. The conventional discrete EMI filter occupied a large room of the whole converter, and its high frequency performances are discounted by parasitic of components and layout. There are many integrated EMI filters are proposed based on planar PCB integrated L-C windings to overcome the shortcomings mentioned above. However, on one hand, its the difference mode (DM) inductor depends on the leakage of the common mode (CM) choke, which is difficult to control. Inserting I core can enhance the leakage but also increase the profile, weight and cost of the EMI filter. On the other hand, because of the unavoidable structural parasitic parameters of the distributed components, such as the equivalent parallel capacitance (EPC) of CM choke windings and equivalent series inductance (ESL) of capacitors, the high frequency attenuation is affected. Although EPCs of the integrated EMI filter was greatly reduced by using a staggered and interleaved winding structure, it complicates the manufacturing processes and increases the total thickness.

In this paper, a novel integrated EMI filter structure is proposed, based on the planar and flexible PCB integrated L-C winding. Overlapped and interleaved planar PCB windings with proper coupling distance are introduced which greatly reduces EPC of CM choke and the total thickness. Using the Finite Element Analysis (FEA) software, the calculated EPC of the integrated EMI filter is less than 10 pF. In addition, FML foils are rolled around E core side legs to enhance DM inductance. Compared with the previous Integrated EMI filters, it can reduce total profile by 40%. And the parameter n (turn numbers of Flexible foils) makes the design of DM inductance more flexible. The effectiveness of these technologies has been evaluated by FEA simulation results.

ACKNOWLEDGMENT

This project is supported by the Science Fund of China (No. 61071056) and the Doctoral Program of Higher Education of China (No. 20090172120009).

Asymmetric Y-branch Plastic Optical Fiber Coupler

A. A. Ehsan[1], **S. S. Shaari**[1], **and M. K. Abd Rahman**[2]

[1]Institute of Microengineering & Nanoelectronics
Universiti Kebangsaan Malaysia, Bangi, Selangor, Malaysia
[2]Faculty of Applied Science, Universiti Teknologi MARA
Shah Alam, Selangor, Malaysia

Abstract— Asymmetric Y-branch plastic optical fiber (POF) coupler based on metal- and acrylic-based substrates have been developed. The POF coupler devices utilized two optical designs: a Y-branch structure and an attenuation technique based on lateral displacement of two fibers. The Y-branch designs are based on two waveguide taper structures namely the hollow waveguide taper and the high index contrast waveguide taper. The non-symmetrical coupling ratios are obtained by attenuation due to the lateral displacement of two adjoining fibers at the output port. In the asymmetric coupler mode, the output fiber is laterally displaced from 0 mm to 4.4 mm with a 0.1 mm step. Fabrication of the device is done by producing the device structures on a metal and acrylic blocks using high speed CNC machining tool. In the 3 dB coupler mode, the metal-based fabricated device has an excess loss of 6.3 dB while the coupling ratios are 46.27% and 53.73%. The coupling ratio ranges from 46.27% down to 14.23% for port 1 and from 53.73% to 85.77% for port 2. The excess loss of this device varies from 6.3 dB to 8.33 dB. Similarly, the acrylic-based fabricated device has an excess loss of 5.85 dB with coupling ratios of 56.86% and 43.14% when operating as a 3 dB coupler. The coupling ratio ranges from 44.84% down to 8.01% for port 1 and 55.16% to 91.99% for port 2. The excess loss of this device varies from 5.42 dB to 7.64 dB.

Optimization of the Femtosecond Laser Pulses for Micromachining Processes

Hoon Jeong[1], **Dongjoo Lee**[2], **Seungtaek Kim**[1], **Jongseok Kim**[1], **and Hyoyeong Park**[1]

[1]Manufacturing System R&D Department, Korea Institute of Industrial Technology, South Korea
[2]Swamp Optics, Atlanta, GA, USA

Abstract— There are many optics elements used in the laser micromachining system, which can introduce some distortions in the pulse. Recent research has shown that distortions of the femtosecond pulses used for machining adversely affect micromachining performance because the pulse should not be optimized on the sample and the system cannot perform tasks with an expected resolution. Also, the pulse distortions can make unwanted pattern on the sample. This paper presents the optimization of the femtosecond laser pulses using pulse characterization and control techniques in order to obtain the best resolution and the highest performance in the micromachining process. After measuring the temporal chirp and the pulse front tilt introduced by the optical elements in the micromachining system, we designed and built a device with two prism pairs to compensate the distortions. By adjusting the distance between two prisms and the angle of the last prism we can control the temporal chirp and the pulse front tilt continuously. With optimized pulses in a micromachining system, we can not only achieve the best resolution possible but also avoid unwanted inner structures in the patterns on the sample.

Enhanced Sensitivity of Surface Plasmon Resonance Phase-interrogation Biosensor by Using Oblique Angle Deposited Silver Nanorods

Chih-Chia Chen[1], **Wen-Chi Lin**[1], **Chih-Wei Chen**[1], **Hsiang-Lin Huang**[1], **Heng-Chuan Kan**[2], **Din Ping Tsai**[3, 4], **and Hai-Pang Chiang**[1, 4, 5]

[1]Institute of Optoelectronic Sciences
National Taiwan Ocean University, Keelung, Taiwan, R.O.C.
[2]National Center for High-Performance Computing
National Applied Research Laboratories, Hsinchu, Taiwan, R.O.C.
[3]Department of Physics, National Taiwan University, Taipei, Taiwan, R.O.C.
[4]Instrument Technology Research Center
National Applied Research Laboratories, Hsinchu, Taiwan, R.O.C.
[5]Institute of Physics, Academia Sinica, Taipei, Taiwan, R.O.C.

Abstract— Since the accomplishment of various optical methods in the excitation of the surface plasmon resonance (SPR) at a metal-dielectric interface, it has been well-known that such an excitation can be utilized to achieve sensing of various interfacial phenomena with ultrahigh sensitivity. These include, for example, chemical and biological sensing, film-thickness sensing, temperature sensing and angular measurement. Recently we observed that high resolution angular measurement and biological sensing can be achieved by SPR phase interrogation at optimized incident wavelength [1, 2].

It was theoretically reported that metallic nanoparticles dispersed over metallic film could enhance the sensitivity of SPR sensor. Recently, we have demonstrated that the sensitivity of surface plasmon resonance (SPR) biosensor can be enhanced by using silver nanoparticles [3]. In this paper, it is demonstrated that the sensitivity of surface plasmon resonance (SPR) biosensor can also be enhanced by using oblique angle deposited silver nanorods. Silver nanorods are thermally deposited on silver nano-thin film by oblique angle deposition (OAD). The length of nanorod can be tuned by controlling the deposition parameters of thermal depostion. By using surface plasmon resonance heterodyne interferometey to measure the phase difference between the p and s polarization of incident light, we have demonstrated that sensitivity of glucose detection with values down to the order of 10^{-8} refractive index units (RIU) can be obtained with optimal deposition parameters of silve nanorods.

REFERENCES

1. Chiang, H. P., J. L. Lin, R. Chang, and S. Y. Su, "High-resolution angular measurement using surface-plasmon-resonance via phase interrogation at optimal incident wavelengths," *Opt. Lett.*, Vol. 30, 2727–2729, 2005.
2. Chiang, H. P., J. L. Lin, and Z. W. Chen, "High sensitivity surface plasmon resonance sensor based on phase interrogation at optimal incident wavelengths," *Appl. Phys. Lett.*, Vol. 88, 141105, 2006.
3. Peng, T.-C., W.-C. Lin, C.-W. Chen, D. P. Tsai, and H.-P. Chiang, "Enhanced sensitivity of surface plasmon resonance phase-interrogation biosensor by using silver nanoparticles," *Plasmonics*, Vol. 6, 29, 2011.

All-optical Switches for Transparent Networks: The Problem, Available Technologies, New Implementations

J. Tioh, **M. Mina**, **and R. J. Weber**
Department of Electrical and Computer Engineering, Iowa State University, Ames, IA 50011, USA

Abstract— The past decade has seen a paradigm shift from connection-oriented communications to high-bandwidth IP-centric packet switched data traffic, driven by the influx of high bandwidth applications. Due to the huge volume of data that is transmitted on these networks, there is a need for high-speed switching with effective switching in the ns regime or better. While such switches exist for electronic media, they have been challenging for optical applications. An overview of the trends and issues of modern optical communications systems is reported. Transparent network components that perform its basic functions (routing, switching and multiplexing) are the key to enabling more reliable, scalable and richly connected optical networks. Some of the latest developments in small-scale high-speed switching for all-optical lightpath applications are also presented and discussed along with experimental results of the newly implemented switches in Iowa State University's High-speed Systems Engineering program.

On the Improved Characterization of the Faraday Effect

J. Tioh, **R. J. Weber**, **and M. Mina**
Department of Electrical and Computer Engineering, Iowa State University, Ames, IA 50011, USA

Abstract— The Faraday effect produces a rotation of the plane of polarization of light passing through magnetized media arising from the interaction between light passing through or reflecting from a medium and electron spin. It has found a great many scientific and practical applications, including optical networking where it is a potential enabler of better scaling, transparent networks that are bit-rate, protocol and format insensitive. In order to analyze an optical network device or system consisting of fibers, films, birefringent, and magnetic materials, it is helpful to have an analysis structure. Often Jones Calculus is employed to perform such an analysis, with the effect of reflections being neglected for the sake of simplicity in standard analyses. This discourse expounds on the improved characterization of Faraday rotation using the formalism of matrix notation that alleviates the shortcomings of standard Jones Calculus. The two representations applied to characterizing structures at optical frequencies are the scattering and transmission matrices, which are more commonly and conventionally used in mm wave analyses. This formalism is essential for the proper analysis of magneto-optic devices.

PV Carbon Emissions Baseline Study

K. F. Kaspareck[1] and Elio Poggiagliolmi[2]

[1]CTE, Italy
[2]Entec Integrated Technology, UK

Abstract— Carbon dioxide (CO_2) emissions are climate critical because of their greenhouse power. Renewable energy is considered emission free or close to zero environmental footprint, thus the recent deployment of large-scale photovoltaic (PV) generation systems.

Photovoltaic systems, do not generate emissions while operating, but require energy for manufacturing, thus generate emissions upfront. In this case, these are "anticipated emissions" and substantial with a mean well over 50 GJ per kWp-installed. Nominal life cycle emissions break even happens around the fourth-fifth year of operations.

On the other hand, the final PV emission footprint per MWh basis, when all other manufacturing steps, process chemicals, process wastes and decommissioning are accounted, is larger and, on a per generated electric unit base, higher than for a nuclear power station or a dam, the most energy intensive power plant constructions.

A different viewpoint may also contend that the refining of silicon (Si) from silica (SiO_2) generates almost half the equivalent amount of CO_2 of raw input material weight. Because of the strong affinity of carbon to oxygen and similar atomic dimension of silicon, two oxygen atoms freed by one molecule of silica will bond to a carbon atom to form a molecule of CO_2.

Finally, the reduced earth cover metabolic effect for ground PV installations averages 10 standard conditions Tons of CO_2 per Hectare per year.

In recent years, due to the constantly increasing PV power base in certain areas, hydrocarbon related emissions emerge comparable to emissions linked to PV deployment in the same areas.

This study compares analytically all emissions contributions of commercial PV life cycle starting from the mining of raw silica up to decommissioning, integrating an intelligent weighted assessment of existing estimates and statistics. Ultimately, it performs a comparative analysis with other energy generation sources.

Interband Detectors of Terahertz and Infrared Radiation Based on Graphene p-i-n Structures

M. Ryzhii[1], **V. Ryzhii**[1, 2], **N. V. Baryshnikov**[2], **V. E. Karasik**[2], **and T. Otsuji**[3]

[1]Computational Nanoelectronics Laboratory, University of Aizu
Aizu-Wakamatsu 965-8580, Japan
[2]Center for Photonics and Infrared Engineering
Bauman Moscow State Technical University, Moscow 105005, Russia
[3]Research Institute for Electrical Communication
Tohoku University, Sendai 980-8577, Japan

Abstract— Different graphene structures based on signle graphene layers (SGLs), non-Bernal stacked multiple graphene layers (MGLs), graphene bilayers (GBLs), and graphene nanoribbons (GNRs) have atracted much attention due to their prospects in terahertz (THz) and in- frared (IR) applications. This in part is due to the gapless energy spectrum (in SGLs and MGLs) or controlled narrow gap spectrum (in GBLs and GNRs) that allows to exploit the interband transitions assicted with relatively low energy photons.

In this communication, we consider the concepts of THz/IR photodetectors utilizing MGL and GNR structures: the MGL p-i-n photodiode considered previously [1] and the newly proposed GNR p-i-n photodiodee [2]. The detector structures under consideration are shown in figure: (a) and (b) correspond to MGL photodiodes with chemically and electrically doped p- an n-regions, respectively, whereas (c) and (d) correspond to GNR photodiodes with different doping. We develop the device models for MGL and GNR photodiodes and compare their characteristics. As shown, the MGL and GNR photodiodes under consideration can surpass, particularly at elevated temperatures, quantum-well and quantum-dot photodetectors as well as photodetectors made of more customary narrow gap semiconductors in speed, responsivity, detectivity, and broad-band functionality The MGL and GNR p-i-n photodiodes can essentially supplement a wide wariety of existing THz and IR detectors.

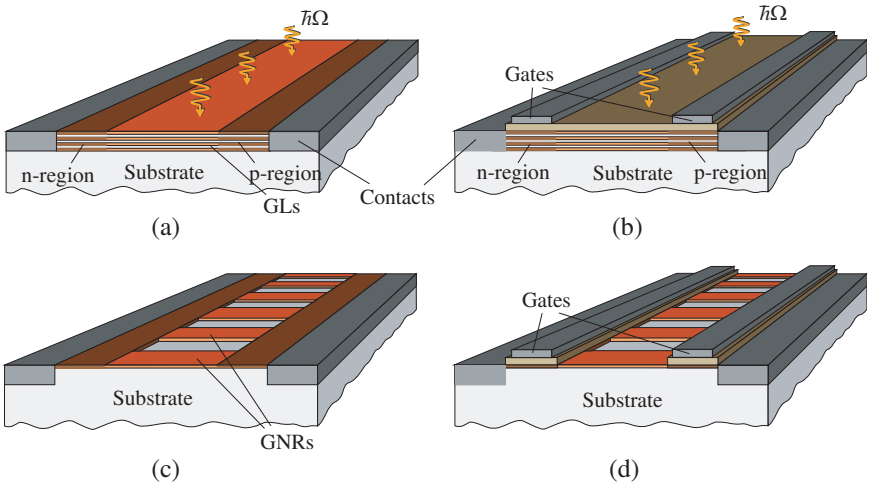

Figure 1.

REFERENCES

1. Ryzhii, V., M. Ryzhii, M. Mitin, and T. Otsuji, *J. Appl. Phys.*, Vol. 106, 084512, 2009.
2. Ryzhii, V., N. Ryabova, M. Ryzhii, N. V. Baryshnikov, V. E. Karasik, V. Mitin, and T. Otsuji, *Optoelectronics Review*, 2011, in press.

The Intensity Modulation of THz-quantum Cascade Lasers by NIR Optical Pulse Injection

S. Saito[1], **Y. Sakasegawa**[1], **N. Sekine**[1], **M. Ashida**[2], **and I. Hosako**[1]

[1]National Institute for Information and Communications Technology, Japan
[2]Graduate School of Engineering Science, Osaka University, Japan

Abstract— In daily life, the electromagnetic wave of GHz frequency is widely used as a carrier of the personal communication, mobile phone or wireless network and the demand for high-speed communications is increasing day by day. THz electromagnetic wave is desired as a carrier for the high-speed wireless communication. THz quantum cascade lasers (THz-QCLs) [1] are expected as light sources for short-range high-speed wireless communications, because it is predicted that the THz-QCLs are able to have the modulation bandwidth more than 100 GHz by theory [2].

By electrical method, it was reported that the modulation bandwidth of THz QCLs was approximately 13 GHz [3]. The bandwidth in the research is limited by parasitic circuit components, therefore the intrinsic properties of THz QCLs have not been clarified. Measurement with external optical injection is a suitable way to obtain the high-speed modulation characteristics of THz-QCLs [4].

We have built the modulation measurement system for THz-QCLs with NIR optical pulse. The optical pulse was injected to the front cleaved facet of the THz QCL operated at 15 K. When the 770 nm optical pulse injected into THz-QCL before the current pulse injection, it was observed that output intensity from the THz-QCL was reduced. And it depended on the intervals between optical and current pulse injection. This reduction by injection of optical pulse agrees with the precedent study in quality [4]. The reduction time was about 1000 nsec and may correspond to the revival time of the reflectivity of the cavity that is disturbed by modulation optical pulse.

REFERENCES

1. Kohler, R., et al., *Nature*, Vol. 417, 156, 2002.
2. Mustfa, N., et al., *IEEE Photon. Tech. Letter*, Vol. 11, 527, 1999.
3. Barbieri, S., et al., *Appl. Phys. Lett.*, Vol. 91, 143510, 2007.
4. Sekine, N. and I. Hosako, *Appl. Phys. Lett.*, Vol. 95, 201106, 2009.

Phononic Band Gaps in One Dimensional Mass Spring System

Arafa H. Aly, **Ahmed Mehaney**, **and Hassan S. Hanafey**
Physics Department, Faculty of Sciences, Beni-Sef University, Egypt

Abstract— In this work, we have studied theoretically the band gap effect in 1D mass spring system, As well as the mechanical vibrations (longitudinal waves) in infinite periodic lattice subjected to periodic force loading. We have investigated how the number of unite cells affected on the band structure, and on the number of frequency band gaps. We have investigate also how the arranging of the mass that subjected to force loading (i.e., vibrations) affected on creation of band gaps, therefore we have treated the homogenous lattice as a special case approximation. In 1D mass spring system the band structure response and band gaps number were shown to be insensitive to damping force and small imperfections. One dimensional mass spring system can be use as a filter to longitudinal waves and other applications like sound transducer and micromechanical resonators.

The Influence of the Electromagnetic Wave on the Nonlinear Acoustoelectric Effect in a Superlattice

N. V. Hieu, **N. Q. Bau**, **and N. V. Nhan**
Faculty of Physics, Hanoi University of Science
Vietnam National University, Hanoi, Vietnam

Abstract— The acoustoelectric effect (AE) in a superlattice (SL) is investigated for an acoustic wave whose wavelength $\lambda = 2\pi/q$ is smaller than the mean free path l of the electrons and hypersound in the region $ql \gg 1$ (where q is the acoustic wave number). The dependence of the AE current j^{ac} on the acoustic intensity Φ, the acoustic wave number q, the intensity E and frequency Ω of the electromagnetic wave are obtained by using the Boltzmann kinetic equation in the case of relaxation time of momentum τ constant approximation, and the degenerate electron gas. Numerical calculation is done, and the result is discussed for a typical GaAs/AlAs SL. At $\omega_q = 10^{11}\mathrm{s}^{-1}$, $\Omega\tau = 10^{-1}$, $\Delta = 1.6 \cdot 10^{-20}J$ (here ω_q is frequency of sound wave, 2Δ is the width of the lowest energy miniband), the acoustoelectric current behaviour in the same manner as the constant electric field. At this frequency $\omega_q = 10^{11}\,\mathrm{s}^{-1}$ the graph is symmetrical about the origin. As ω_q increases the symmetry breaks down and at $\omega_q = 10^{13}\,\mathrm{s}^{-1}$ we obtaine that the absolute value of the maximum peak $|j_z^{ac}/j_0^{ac}|_{\max}$ is smaller than the absolute minimum value $|j_z^{ac}/j_0^{ac}|_{\min}$.

Ability to Increase a Weak Electromagnetic Wave by Confined Electrons in Quantum Wells in the Presence of Laser Radiation

N. V. Nhan[1], **N. T. T. Nhan**[2], **N. V. Nghia**[2], **S. T. L. Anh**[2], **and N. Q. Bau**[2]

[1]Department of Physics, Academy of Defence Force — Air Force, Hanoi, Vietnam
[2]Department of Physics, College of Natural Sciences, Hanoi National University, Hanoi, Vietnam

Abstract— The analytic expressions for the absorption coefficient of a weak electromagnetic wave caused by confined electrons in the presence of laser radiation in quantum wells are obtained by using the quantum kinetic equation for electrons in the case of electron-optical phonon scattering. The dependence of the absorption coefficient of a weak electromagnetic wave on the intensity E_{01} and frequency Ω of the external laser radiation; the intensity E_{02} and frequency ω of the weak electromagnetic wave; the temperature T of the system are analyzed. The results are numerically calculated, plotted, and discussed for AlAs/GaAs/AlAs quantum well. The numerical results shows that absorption coefficient of a weak electromagnetic wave in a quantum well can get negative values. So, by the presence of laser radiation, in some conditions, the weak electromagnetic wave is increased. The results are compared with those for normal bulk semiconductors.

Optical Bistability in a V-type System in the Presence of an Additional Field

R. Doustkam[1], **M. Mahmoudi**[1], **and M. Sahrai**[2]

[1]Department of Physics, University of Zanjan, P. O. Box 45195-313, Zanjan, Iran
[2]Research Institute for Applied Physics and Astronomy, University of Tabriz, Tabriz, Iran

Abstract— We investigate the optical bistability (OB) in a V-type system in the presence of an additional field. The interest is that OB can be induced in a V-type system by adjusting additional field intensity. The additional field is applied on system in three configurations. First, the additional field driven transition shares an excited state level with the coupled transition, in the second system it shares an excited state level with the probed transition, finally in third one, the additional field is applied on the ground state level. We study the optical bistability behavior in these systems and investigate the system response to increasing of additional and coupling field intensity. It is shown that when the coupling field has high value, in the first and second systems OB behavior can be induced by increasing of the additional field intensity. While the third system shows OB behavior for low intensity of the coupling field. In the following we fix intensity of the additional field and investigate OB behavior of systems related to the increasing of intensity of the coupling field. In the first system by increasing intensity of coupling field the threshold of the OB reduces and the OB disappear. It can be seen the second system shows OB behavior for specific values of intensities. But this work has no effect on the OB behavior of third system.

Controlling the Optical Bistability via Electromagnetically Induced Absorption in a Three-level Λ-type System

E. Sadati Nosrat Abad[1], **M. Mahmoudi**[1], **and Mostafa Sahrai**[2]

[1]Department of Physics, University of Zanjan, P. O. Box 45195-313, Zanjan, Iran
[2]Research Institute for Applied Physics and Astronomy, University of Tabriz, Tabriz, Iran

Abstract— Optical bistability (OB) has been extensively studied both experimentaly and theoretically in two_ level atomic systems due to its wide applications such as optical transistors, memory elements, and optical switches. In this paper, we investigate the OB behavior of a three-level Λ-type quantum system in electromagnetically induced absorption (EIA) condition. It is shown that in the presence EIA peak due to the spontaneous emission quantum interference, the system shows the OB behavior and in the absence of EIA peak the OB behavior disappeared. Moreover, by increasing the detuning of pumping field, the width of EIA peak is reduced and then the OB threshold is decreased.

NMR Measurement of the Relaxations and Conductivity of Gel Electrolytes

R. Korinek[1, 2], K. Bartusek[1, 2], K. Ostanina[2], and M. Musil[3]

[1]Institute of Scientific Instruments of the ASCR, v.v.i.
Kralovopolska 147, 612 64 Brno, Czech Republic
[2]Department of Theoretical and Experimental Electrical Engineering
Brno University of Technology, Kolejni 2906/4, 612 00 Brno, Czech Republic
[3]Department of Electrotechnology
Brno University of Technology, Technicka 10, 602 00 Brno, Czech Republic

Abstract— There are other methods for evaluating properties of conducting gels, but NMR spectroscopy offers a deeper insight into the behavior of polymer gels during the UV polymerization proccess. Mainly we are able to relatively exactly determine when the polymerization proccess is completed. The relaxation times T_1 and T_2 can better define the behavior of the structure of polymer gels during the UV polymerization process. Advantage over liquid gel electrolytes is their higher safety. Liquid electrolytes are now very widespread and we want to replace them with safer solid electrolytes. There is a direct proportionality between MR relaxation and conductivity of the electrolyte. Along with the relaxation times T_1 and T_2 we also interested in the course of conductance changes during the UV polymerization process. To measure of relaxation times T_1 and T_2, the basic NMR methods was used. For measuring the spin-lattice relaxation T_1, we used the Inversion Recovery (IR) method. To measure spin-spin relaxation time T_2 was used Hahn echo method. For approximation, we used two-exponential function (equation for inversion recovery and hahn echo techniques). The calculation was performed using genetic algorithm (GA). Gel polymer electrolytes are based on inorganic salt $NaClO_4$. The aim is to find a suitable solid electrolyte for use in electrochemical industry and especially to improve their safety. In the paper a methodology of NMR relaxation times measurement is presented. The results are compared with measurements of conductivity gel during polymerization. The experiment was performed on the 4.7 T NMR system at the Institute of Scientific Instruments of the ASCR in Brno.

ACKNOWLEDGMENT

The research described in the paper was financially supported by EC and MEYS CR (project No. CZ.1.05/2.1.00/01.0017) and a research project of the Czech Science Foundation, Grants No. P102/10/2091 and project of the BUT Grant Agency FEKT-S-11-5.

REFERENCES

1. Korinek, R., J. Vondrak, and K. Bartusek, "Relaxation time study of gel electrolytes during polymerization by MR methods," *ECS Transactions — Advanced Batteries, Accumulators and Fuel Cells (ABAF 11)*, Vol. 32, 2011, (in press).
2. Reiter, J., J. Vondrak, J. Velicka, and Z. Micka, "Nové elektrolyty nejen pro chemické zdroje elektrické energie," *Chem. Listy*, Vol. 100, 133–139, 2006.
3. Thomas, L. H., J. Noggle, and J. Noggle, *Proc. Natl. Acad. Sci.*, Vol. 62, 644–649, USA, 1969
4. Every, H. A., F. Zhou, M. Forsyth, and D. R. MacFarlane, *Electrochim Acta*, Vol. 43, 1465–1469, 1998.
5. Judson, R. S., "Genetic algorithms," *Encyclopedia of Optimization*, 1254–1257, 2009.

Phase and Amplitude Control of Optical Bistability in the Closed-loop Three-coupled Quantum Wells

M. Mahmoudi and N. Heidari
Department of Physics, University of Zanjan, P. O. Box 45195-313, Zanjan, Iran

Abstract— The coherence and quantum interference have important role in controlling the optical properties of quantum systems. Semiconductor quantum well is a two-dimensional electron gas device which the quantum mechanical properties of such system can be considered as the atomic system. The nonlinear quantum optical phenomena based on the quantum coherence in the semiconductor quantum wells have been extensively studied.

On the other hand, control of light by light is important in all-optical switching and optical computing. optical transistors, all-optical switching and all-optical storage devices based on optical bistability (OB). Such bistable behavior is the result of nonlinearity of the interactivity atomic medium and feedback of the optical interactivity field from the cavity mirrors. Atomic coherence effects provide a useful mechanism for an optical bistable device.

The relative phase of applied laser fields is an important parameter for controlling the atomic coherence. It is well known that the optical properties of a closed quantum system interacting with laser fields are completely phase dependent.

In this paper, we investigate the optical properties of a weak probe field in a closed-loop ladder-type configuration in an asymmetric semiconductor three-coupled quantum well system. It is shown that, the dispersion, absorption and optical bistability behavior of the system can be controlled by both of the amplitude and relative phase of applied fields. The phase dependence arises from a scattering of the pumping and signal fields into the probe field mode at a frequency which in multi-photon resonance condition is same as the probe field frequency. Moreover, it is demonstrated that in the gain region of the absorption spectrum, the considerable output is obtained for zero input.

Theoretical Study of Negative Refraction in Pseudochiral Media

Ruey-Lin Chern
Institute of Applied Mechanics, National Taiwan University, Taipei, Taiwan

Abstract— The author investigates the features of negative refraction in pseudochiral media characterized by anisotropic magnetoelectric coupling parameters. In these media, electric fields give rise to magnetic dipoles (and magnetic fields to electric dipoles), but oriented in a perpendicular direction. The chirality parameters are indeed tensors with zero diagonal entries, showing the pseudo nature of a distinct chiral medium. In practice, the magnetoelectric coupling in a perpendicular direction can be achieved by surface currents induced on Ω-shaped metal wires [1].

With suitable arrangement of the chirality parameters, strong magnetoelectric couplings occur and lead to a special form of dispersion relation. In particular, the equifrequency contours on the wave vector domain represent four inclined lobes for TM polarization. Due to the phase matching at the interface between an ordinary and a pseudochiral medium, negative refraction will occur for a range of angle of incidence. This feature is indicated by the tangential component of the group velocity, which points in the opposite direction of the tangential incident wave vector.

For illustration, a Gaussian beam is obliquely incident upon a semi-infinite pseudochiral medium. The refraction beam bends toward the same side of the incident beam with respect to the surface normal, showing the feature of negative refraction. Here, the Gaussian beam is formulated as an integral of plane waves, with amplitudes varied as a Gaussian function, over the tangential wave number component [2]. The reflection and transmission coefficients associated with each wave component are derived from the boundary conditions. By expanding the wave number component to first few orders, an approximate solution of the Gaussian integral can be analytically obtained. This formula explicitly demonstrates the negative refraction of Gaussian beams in pseudochiral media.

ACKNOWLEDGMENT

This work was supported in part by National Science Council of the Republic of China under Contract No. NSC 99-2221-E-002-121-MY3.

REFERENCES

1. Saadoun, M. M. I. and N. Engheta, "A reciprocal phase shifter using novel pseudochiral or ω medium," *Microwave and Optical Technology Letters*, Vol. 5, 184–188, 1992.
2. Kong, J. A., B.-I. Wu, and Y. Zhang, "A unique lateral displacement of a Gaussian beam transmitted through a slab with negative permittivity and permeability," *Microw. Opt. Technol. Lett.*, Vol. 33, 136–139, 2002.

Recovery of Electron-photon Interaction Time τ_{eph} Using the Quasi-particle Tunnelling Heating Effect in a Niobium SIS Mixer

B.-K. Tan and G. Yassin
Department of Physics (Astrophysics), University of Oxford, UK

Abstract— It is well known that quasi-particle tunnelling in a Superconductor-Insulator-Superconductor (SIS) tunnel junction is influenced by local oscillator (LO) power heating when it is used as an SIS mixer at millimetre and sub-millimetre wavelengths [1, 2]. When the DC current-voltage (IV) curve of the junction is pumped hard, it is easy to notice that the superconducting gap is suppressed by a significant amount depending on the frequency. This effect has been investigated previously in view of its effect on the mixer sensitivity, in particular above the superconducting gap.

In this paper, we describe a new method for recovering the electron-phonon interaction time (τ_{eph}) using the junction heating effect from the measured pumped and un-pumped IV curves of an SIS device under the irradiation of an LO source. Experimental investigation in this paper was carried out using a Niobium (Nb) SIS mixer which was designed to operate in the frequency range of 600–700 GHz.

A key feature of our method is that it doesn't require the assumption of a particular power dependence between the received power and the temperature of the electrons in order to calculate the value of the electron-phonon interaction constant τ_{eph}. Instead, the power law, n, which describes the dependence of the heat transfer equation on temperature, is deduced together with τ_{eph} of the superconducting material at various bath temperatures by comparing the theoretical model that describes photon-assisted tunnelling with the measured results. The tunnelling currents in the theoretical model are calculated using Werthamer [3] method and BCS theory [4].

The coupled LO power, the embedding impedance of the SIS device and the local effective junction temperature are then recovered by matching the measured IV curves with those computed theoretically. From the BCS equations and the recovered LO power, the total power at each bias point, both DC and RF, dissipated in the junction are found. We start by an initial guess value of τ_{eph} and n, which yields an effective temperature at that particular bias point. A new gap voltage is recalculated using standard temperature dependent expression. The junction model is called again to find the current. This process is repeated throughout the full range of bias voltage. The generated IV curve is then compared to the measured curve, and the parameters are optimised until both theoretical and measured curves are matched.

The above method has been used successfully by several investigators to recover the embedding impedance seen by the tunnel junction in SIS mixer circuits. To the best of our knowledge this is the first time it has been used to obtain physical constants of the device superconductors that cannot easily be obtained by other methods.

REFERENCES

1. Leone, B., B. D. Jackson, J. R. Gao, and T. M. Klapwijk, "Geometric heat trapping in niobium superconductor-insulator-superconductor mixers due to niobium titanium nitride leads," *Applied Physics Letters*, Vol. 76, 780, Feb. 2000.
2. Leone, B., J. R. Gao, T. M. Klapwijk, B. D. Jackson, W. M. Laauwen, and G. de Lange, "Electron heating by photon-assisted tunneling in niobium terahertz mixers with integrated niobium titanium nitride striplines," *Applied Physics Letters*, Vol. 78, 1616, Mar. 2001.
3. Werthamer, N. R., "Nonlinear self-coupling of josephson radiation in superconducting tunnel junctions," *Physical Review*, Vol. 147, 255–263, Jul. 1966.
4. Bardeen, J., L. N. Cooper, and J. R. Schrieffer, "Theory of superconductivity," *Physical Review*, Vol. 108, 1175–1204, Dec. 1957.

Measurement of Dielectric Parameters of Biological Tissue

Jaroslav Vorlíček and Jan Vrba
Department of Electromagnetic Field, Czech Technical University, Czech Republic

Abstract— The goal of hyperthermia cancer treatment is to raise the temperature of the targeted tissue area. Thus, temperature can be maintained above 43°C for up to one hour. To evaluate the expositions of microwave radiation from thermo therapeutical microwave applicators, we need to know the dielectric properties of the tissues. This can be performed using measure of the complex permittivity of the tissues in the desired area of the treatment. For this purpose, we constructed a sensor based on the coaxial transmission line for measuring the complex permittivity. Measurement method on an open-ended coaxial line is based on the reality that the reflection coefficient of an open-ended coaxial line depends on dielectric parameters of material which is attached to the coaxial line.

For calculation of biological tissue dielectric parameters from the measured reflection coefficient, it is ne-cessary to use an equivalent circuit of an open-ended coaxial line. The values of elements in the equivalent circuit depend on the dielectric properties of the material attached to the end of coaxial line.

To determine the values of elements in an equivalent circuit, we use calibration by means of material with known dielectric properties. Open-ended coaxial probe has a capability of broadband measurements and simple sample preparation. Also, its nondestructive nature and capability for in-vivo measurements provide open-ended coaxial probes with a significant advantage over other techniques for biological applications. There have been many techniques to correlate the measured input admittance to the complex permittivity of the sample material, which resulted in significant improvement in the extraction process. Accurate measurements of the complex permittivity of biological tissues gain great importance in both basic and applied research.

The performance of this system was evaluated by measuring of the deionized water. The measured data were compared with the value calculated by Debye's model. The relative errors between the measurement and the calculation were less than ±4%. The reliability of this method was confirmed by the measurement of deionized water in wide frequency range.

ACKNOWLEDGMENT

This research is supported by Grant Agency of the Czech Republic, project: "Non-standard application of physical fields — analogy, modeling, verification and simulation" (102/08/H081).

Amorphous Silicon-based Thin Film Solar Cells

Shokri Alforgani[1], **M. Sbeta**[2], **and A. Abugalia**[2]

[1]Plasma Research Laboratory, Libya
[2]Center for Solar Energy Studies oe, Libya

Abstract— The electric and the photo characteristics of solar cells were studied at TU-Delft (Holland). The deposition technique that was used is an rf PECVD AMOR deposition system "radiofrequency Plasma Enhanced Chemical Vapor Deposition" on an amorphous thin films that has been deposited on a supporting substrate made from glass. High quality thin films were deposited at temperature of 180°C and an rf power of 4 watts, while CVD "Chemical Vapor Deposition" techniques require higher temperature range to produce similar quality films. Another system is used (Leybold deposition system CVD) for depositing metallic contacts from either silver (Ag) or aluminum (Al). AMOR and Leybold systems were used to deposit devices and layers with different specifications. Two substrates were used for layer; glass-based and c-Si wafer-based while TCO-coated glass substrate was used for devices. Three types of glass-based layers; p, n and i were deposited with 300 nm thickness each. Three 300 nm intrinsic layers of c-Si based-wafer were deposited at three different rf powers; 3 W, 4 W and 5 W. On the other hand three devices with three different thicknesses; 150 nm, 300 nm and 450 nm were deposited on TCO-coated substrate. The measured performances of solar cells.

Session 3A1
Optics, Photonics, and Biophotonics for Young Scholars and Researchers 1

Self-field Theory: Faster Than Light Neutrino

A. H. J. Fleming
Biophotonics Research Institute, Melbourne, Australia

Abstract— Recently scientists at CERN reported measuring neutrino speeds marginally faster than light. The photons traveled a distance of ~ 730 km in $4 \sim 2.4$ ms while the neutrino did the same distance 60 ns quicker. Conventional relativity maintains nothing can go faster than light. General relativity like the various quantum theories depends on a zero mass photon. By balancing Planck's constant within a cycle of the hydrogen atom self-field theory estimated the mass of the photon to be $\sim 0.221 \times 10^{-19}$ eV. There is a collision mechanism within the atom where two photons transit between the electron and the proton. There are an integer number of coherent collisions each atomic cycle where the photon mean free path is the Bohr radius, 0.529×10^{-10} m. Neutrino mass was recently reported to be around ~ 0.28 eV. If it weighs more than a photon can a neutrino possibly travel at speeds faster than light? We need to be careful since speed depends on the particle, the medium in which it travels, and the physics. For example the speed of an electron moving in a metal and another moving in an atom can be very different. If the neutrino has a small cross section it might burrow through the medium easier than the photon even if it has more mass. While the photon is buffeted around in relative terms, the heavier neutrino just bores through the medium without being as impeded. The neutrino may be very compact compared to the photon. This is similar to a heavy metal having a small nucleus where the strong nuclear forces are greater compared with a hydrogen atom that is physically much larger. Part of the standard Big Bang theory is a period of early inflation when the Universe inflated at superluminal speeds to around its current size. The neutrino may have evolved some time before the nucleosynthesis of nucleons and a corresponding boson decay after the Big Bang. The neutrino, like a fossilized ancient relic, remains captured inside the nucleus until it is released in electroweak reactions involving the neutron. Thus the neutrino has much more energy than the photon and is likely to be more compact in size. Being smaller than the photon the neutrino may move at superluminal speeds. In the present case as measured by CERN the photon collisions are not random but form a coherent process that rotates the photon in the gravitational field both near the surface of the Earth and more generally throughout the universe. Thus SFT suggests the fractal nature of the photon and other forms of matter plays an important role within the physics of the universe.

REFERENCES

1. Ereditato, A., et al., "Measurement of the neutrino velocity with the OPERA detector in the CNGS beam," http://static.arxiv.org/pdf/1109.4897.pdf.
2. Fleming, A. H. J., "Electromagnetic self-field theory and its application to the hydrogen atom," *Physics Essays*, Vol. 18, No. 3, 265–285, 2005.
3. Fleming, A. H. J., "Self-field theory, analytic spectroscopy of the ordinary photon," *Proc. 2nd Electromagnetics Health and Environment Intl. Conf.*, 18–23, Wroclaw, Poland, 2007
4. Fleming, A. H. J., "Analytic estimate for the mass of the photon," *PIERS Proceedings*, 1604–1607, Moscow, Russia, August 18–21, 2009.
5. Fleming, A. H. J., "Self-field theory, general relativity and quantum theory," *PIERS Proceedings*, 1444–1447, Suzhou, China, September 12–16, 2011.
6. Fleming, A. H. J., *Self-field Theory — A New Mathematical Description of Physics*, Pan Stanford Publishing, 2011, to be published.
7. Guth, A. H., *The Inflationary Universe, Reading*, Perseus Books, Massachusetts, 1997.
8. Thomas, S. A., F. B. Abdalla, and O. Lahav, "Upper bound of 0.28 eV on neutrino masses from the largest photometric redshift survey," *Physical Review Letters*, 105, 031301.

Theoretical Simulations of the Performance of InGaN*p*-*n* Junction Solar Cells

Shih-Wei Feng[1], **Yu-Ru Su**[1], **Chih-Ming Lai**[2], **and Li-Wei Tu**[3]

[1]Department of Applied Physics, National University of Kaohsiung, Kaohsiung, Taiwan, R.O.C.
[2]Department of Electronic Engineering, Ming Chuan University, Taoyuan, Taiwan, R.O.C.
[3]Department of Physics and Center for Nanoscience and Nanotechnology
National Sun Yat-Sen University, Kaohsiung, Taiwan, R.O.C.

Abstract— We conduct theoretical simulations to design the device structure for the optimized performance of InGaN*p*-*n* junction solar cells. Operation mechanisms of InGaN*p*-*n* junction solar cells with indium composition and width dependences of upper *p*-InGaN and lower *n*-InGaN junctions are explored through the calculation of characteristic parameters such as the short circuit current density, open circuit voltage, fill factor, and conversion efficiency. An $In_{0.6}Ga_{0.4}N$ solar cell with *p*-InGaN width less than 1,000 nm can exhibitan ∼22% conversion efficiency, demonstrating that medium-indium-content InGaN is an appealing candidate to realize a high efficiency solar cell. Also, InN and high-indium-content InGaN solar cells could be useful for fabricating tandem cells with other materials. Simulation results help us to better understand the operation mechanisms of InGaN*p*-*n* junction solar cells and can be utilized for efficiency enhancement through the optimization of thedevice structures.

Crystallinity Improvement of ZnO Thin Film on Different Buffer Layers Grown by MBE

Shao-Ying Ting[1], **Po-Ching Chou**[2, 3], **Jeng-Jie Huang**[1], **Che-Hao Liao**[1], **Wen-Ming Chang**[1], **Hsiang-Chen Wang**[2, 3], **and C. C. Yang**[1]

[1]Institute of Photonics and Optoelectronics
National Taiwan University, Taipei 10617, Taiwan
[2]Graduate Institute of Opto-Mechatronics
National Chung Cheng University, Chia-Yi 62102, Taiwan
[3]Advanced Institute for Manufacturing with High-Tech Innovations (AIM-HI)
National Chung Cheng University, Chia-Yi 62102, Taiwan

Abstract— The material and optical properties of ZnO thin film samples grown on different buffer layers on sapphire substrates through a two-step temperature variation growth by molecular beam epitaxy were investigated. The thin buffer layer between the ZnO layer and the sapphire substrate decreased the lattice mismatch to achieve higher quality ZnO thin film growth. A GaN buffer layer slightly increased the quality of the ZnO thin film, but the threading dislocations still stretched along the c-axis of the GaN layer. The use of MgO as the buffer layer decreased the surface roughness of the ZnO thin film by 58.8% due to the suppression of surface cracks through strain transfer of the sample. From deep level emission and rocking curve measurements it was found that the threading dislocations play a more important role than oxygen vacancies for high quality ZnO thin film growth.

High-excitation Effects on Photoluminescence of ZnMgO Alloys

C. H. Chia, **T. C. Han**, **and Y. M. Hu**
Department of Applied Physics, National University of Kaohsiung, Kaohsiung 81148, Taiwan, R.O.C.

Abstract— We studied the photoluminescence of ZnMgO thin film, grown by the radiofrequency sputtering method, as a function of excitation intensity and temperature. As the excitation intensity increases, a nonlinear emission band caused by the radiative recombination of the inelastic exciton-exciton scattering was detected at low temperature. We found that the inelastic exciton-exciton scattering process can only persist up to $T \sim 260\,\mathrm{K}$. The nonlinear emission band observed at room temperature is due to the radiative recombination of the electron-hole plasma. We also studied the power-dependent photoluminescence of $Zn_{1-x}Mg_xO$ nanopowders grown by sol-gel method, at temperature $T = 100\,\mathrm{K}$. At moderate optical pumping intensity, a nonlinear emission band due to the radiative recombination of free biexcitons was detected. We found that the free biexciton binding energies of $Zn_{1-x}Mg_xO$ nanopowder ($0.01 \leq x \leq 0.05$) are nearly constant ($13.5 \pm 1.5\,\mathrm{meV}$).

Suppression of Surface Recombination in an InGaN/GaN Multiple Quantum Well Sample by Surface Plasmon Coupling

Xusn-Yu Yu[1, 2], **Hsiang-Chen Wang**[1, 2], **Yu-Lun Chueh**[3], **Tadas Malinauskas**[4], **Kestutis Jarasiunas**[4], **and Shih-Wei Feng**[5]

[1]Graduate Institute of Opto-Mechatronics, National Chung Cheng University
168 University Rd., Min-Hsiung, Chia-Yi 62102, Taiwan
[2]Advanced Institute for Manufacturing with High-Tech Innovations (AIM-HI)
National Chung Cheng University, 168 University Rd., Min-Hsiung, Chia-Yi 62102, Taiwan
[3]Department of Materials Science and Engineering, National Tsing-Hua University
101 Sec. 2, Kuang-Fu Road, Hsinchu 30013, Taiwan
[4]Institute of Applied Research, Vilnius University, LT-10222 Vilnius, Lithuania
[5]Department of Applied Physics, National University of Kaohsiung, Kaohsiung 81148, Taiwan

Abstract— Temperature-dependent picosecond non-degenerate four-wave-mixing experiments were performed to explore the carrier dynamics in an InGaN/GaN multiple quantum well sample, in which light emission enhancement with surface plasmon (SP) coupling has been identified. In the time-resolved photoluminescence results, we can identify the faster carrier decay time of the sample with surface plasmon coupling. The faster decay time is due to this sample's ability to create additional channels for effective carrier recombination. In the four-wave-mixing results, a slower grating decay time of the sample with surface plasmon coupling was measured. The diffusion coefficients and surface recombination velocities of photo-created carriers were estimated by modeling the decay rate of transient grating signals. For the sample for which surface plasmon coupling exists, smaller diffusion coefficients and slower surface recombination velocities can be estimated when the temperatures are above 150 K. The carriers coupling with some SP modes is not the only mechanism contributing to emission enhancement. In the InGaN/GaN multiple quantum well sample, surface recombination suppressed by SP coupling is another factor for increased light emission efficiency.

Speckle Reduction Based on EMD Database

Chen-Wei Lee[1], **Wei-Hung Su**[2], **and Chao-Kuei Lee**[1]

[1]Department of Photonics, National Sun Yat-Sen University
No. 70, Lienhai Rd., Kaohsiung 80424, Taiwan, R.O.C.
[2]Department of Material and Optoelectronic Science, National Sun Yat-sen University
No. 70, Lienhai Rd., Kaohsiung 80424, Taiwan, R.O.C.

Abstract— In this paper, we introduce an automatic speckle-reduction approach for interference patterns based on the empirical mode decomposition (EMD). The relationships of the number of removed intrinsic mode function (IMF), period of fringes and signal-to-noise ratio are analyzed and discussed. Based on these, a database system based on the EMD was built to assist the denoise process. With this database, speckles on an interference pattern can be efficiently and robotically reduced. By using proposed procedure, up to 80% of speckles on fringe patterns can be efficiently and robotically reduced.

Determination of Moisture Content of Maize Kernel (*Zea mays L.*) by Reflectance Measurement at Wavelengths 300 nm to 800 nm Using Optical Technique

A. M. Norimi, **Z. Abbas**, **A. Jusoh**, **and M. A. Ismail**
Faculty of Science, Department of Physic, Universiti Putra Malaysia
43400 UPM Serdang, Selangor Darul Ehsan, Malaysia

Abstract— This paper presents a method to determine moisture content of single maize kernels based on optical reflectance measurement at wavelengths from 300 nm to 800 nm. The method provides a simple, fast, non-destructive and accurate technique to establish the relationship between reflectance and moisture content. The actual amount of moisture content was determined by standard oven drying method. The optical measurement setup consists of a UV-VIS-NIR light source, an integrated set of seven 440 µm diameter fibers with six illumination fibers encircling one detection fiber, a spectrometer, and a sample holder ensuring that the direction of the incident beam was normal to the sample surface. The results suggest that the percentage of reflectance decreases with moisture content. Calibration equations were established at wavelengths 380 nm, 450 nm and 590 nm corresponding to UV-VIS boundary, carotenoid pigment absorption and yellow colour wavelengths. The lowest mean relative error of the optical fiber technique to determine moisture content based on reflectance measurements was 0.037 at 590 nm.

High Resolution Image Synthesized by Using Multiple Low-resolution CCD

Chen-Wei Lee[1], **Jhao-Yu Zeng**[1], **Wei-Hung Su**[2], **Chao-Kuei Lee**[1], **and Tsong-Ru Tsai**[3]

[1]Department of Photonics, National Sun Yat-Sen University
No. 70, Lienhai Rd., Kaohsiung 80424, Taiwan, R.O.C.
[2]Department of Material and Optoelectronic Science, National Sun Yat-Sen University
No. 70, Lienhai Rd., Kaohsiung 80424, Taiwan, R.O.C.
[3]Institute of Optoelectronic Sciences, National Taiwan Ocean University
Keelung 20224, Taiwan, R.O.C.

Abstract— Image with high resolution (HR) are required in many application, such as medical resonance image, satellite image and surveillance image. With a higher spatial sampling density, an HR image can offer more detail of the object information. In this paper, we provide a novel approach to improve the image quality by reassembling images obtained from multiple low resolution cameras. Experimental results have shown that accuracy better than sub-pixel of the low resolution camera can be achieved.

Ultrafast Ablation Dynamics in Fused Silica with a White Light Beam Probe

Guan-Huang Wu[1, 2], **Ping-Han Wu**[3], **Xuan-Yu Yu**[1, 2], **Chung-Wei Cheng**[3], **Che-Hao Liao**[4], **Shih-Wei Feng**[5], **and Hsiang-Chen Wang**[1, 2, 3]

[1]Graduate Institute of Opto-Mechatronics, National Chung Cheng University
168 University Rd., Min-Hsiung, Chia-Yi County 62102, Taiwan
[2]Advanced Institute for Manufacturing with High-Tech Innovations (AIM-HI)
National Chung Cheng University, 168 University Rd., Min-Hsiung, Chia-Yi County 62102, Taiwan
[3]ITRI South, Industrial Technology Research Institute
No. 8, Gongyan Rd., Liujia District, Tainan County 73445, Taiwan
[4]Institute of Photonics and Optoelectronics, National Taiwan University
1 Roosevelt Rd., Section 4, Taipei 10617, Taiwan
[5]Department of Applied Physics, National University of Kaohsiung
700 Kaohsiung University Rd., Nanzih District, Kaohsiung 81148, Taiwan

Abstract— This study demonstrates a non-degenerate pump-probe spectroscopy with a white light beam probe based on a regenerative, amplified, mode-locked, Ti:sapphire laser. This white light beam probe is produced by supercontinuum generation of sapphire crystal after ultra-short pulse excitation. To implement the pump-probe experimental operation, the ablation dynamics with and without fresh spot measurements in fused silica samples are demonstrated. Combining the time-resolved differential reflection profiles in the white light range and X-ray photoelectron spectroscopy spectra of fused silica, the following ablation dynamics processes can be observed: Without fresh spot measurements, once carriers are excited, first, the three absorption bands of the intrinsic defect sites are observed within 750 fs. Then, a fast recovery is observed. This recovery comes from defect-trapped carriers excited to conduction bands through hot-carrier-phonon interactions. In the final step, a rapidly rising signal is observed after 800 fs. This signal rise comes from the creation of free-electron plasma, the density of which increases with increasing excitation energy accumulation. With fresh spot measurements, time delay of carrier dynamics among the three bands can be identified clearly within 750 fs. The intrinsic defect sites of fused silica play the key role during the ultrafast laser ablation process.

Optical Frequency Conversion: Novel Integrated Devices and Applications

R. Morandotti[1, 2], L. Razzari[1, 2], M. Ferrera[1, 2], D. Duchesne[1, 2], M. Peccianti[1, 2], A. Pasquazi[1, 2], S. Chu[3], B. E. Little[3], and D. J. Moss[4]

[1]INRS-EMT, 1650 Boulevard Lionel Boulet, Varennes, Québec J3X 1S2, Canada,
[2]Dipartimento di Elettronica, Università di Pavia, via Ferrata 1, 27100 Pavia, Italy
[3]Infinera Corp., 9020 Junction Dr, Annapolis, Maryland 94089, USA
[4]CUDOS, School of Physics, University of Sydney, New South Wales 2006, Australia

Abstract— Until today, the world of electronics has always been an inexhaustible source of resources to satisfy the continuous request for larger bandwidths in communication systems. Unfortunately the bit rate limit of electronic devices (around 50 Gb/s) will soon be reached, and scientists and engineers are now struggling for alternative solutions. Among them, all-optical signal processing appears to be one of the most viable approaches since it brings the promise to drastically increase the performances of transmission networks and, at the same time, to keep the associated costs low. However, in order to fulfill the goal of realizing all-optical agile communications systems and improve overall all-optical devices performances, it is mandatory to efficiently perform fundamental network operations such as optical switching, data storage, ultrafast modulation, etc. In particular, wavelength conversion is required to realize wavelength division multiplexing systems capable of substantially increasing the bit rate by channeling the information on different frequency carriers. Recently ultra-low CW pump power (5 mW) wavelength conversion based on Four Wave Mixing (FWM) has been reported in silicon micro-ring resonators. Nevertheless, it is of paramount importance to study other material systems, since silicon is well known to suffer from two-photon absorption (TPA) that in turn induces free carrier losses and may affect the performance of silicon based devices. In this work we first demonstrated, by means of C-MOS compatible high index glass based micro ring resonators, efficient wavelength conversion by FWM using ultra-low continuous-wave pump power (< 5 mW, @1553.38 nm).

Our results are comparable to the highest values reported to date in silicon ring resonators, and in addition they combine the advantages of ultra-low optical loss (0.06 dB/cm) with the absence of two-photon absorption (near $\lambda = 1.5\,\mu$m). We believe that these achievements may bring us a step forward in the quest to create very efficient all optical communication networks.

Furthermore, the possibility of creating novel frequency at very affordable power levels could open up an host of different applications beyond their use in telecommunication networks. For example, integrated multiple wavelength laser sources may be considered of great importance for applications as high-precision broadband sensing and spectroscopy, molecular fingerprinting, optical clocks, and attosecond physics. Even if they have recently been demonstrated in silica and single crystal micro-toroid resonators using parametric gain, for applications in telecommunications and optical interconnects, analogous devices in a fully integrated, CMOS compatible platform still do not exist. While approaches such as silicon micro-ring resonators have been shown not to be ideal, other materials, such as Silicon nitride, have recently been proven to be a promising alternative platform for nonlinear optical on chip applications since they exhibits negligible saturation effects due to multi-photon absorption, and this enabled the demonstration of efficient multi-wavelength optical parametric oscillation in integrated ring resonators.

By using rings with a Q factor higher than 1000000, we succeeded in realizing a fully integrated, CMOS compatible, multiple wavelength source. We achieve CW optical "hyper-parametric" oscillation with a differential slope efficiency above threshold of 7.4% for a single oscillating mode out of a single port, a CW threshold power as low as 54 mW, and a controllable range of frequency spacing from 200 GHz to more than 6 THz. The low loss, design flexibility, and CMOS compatibility of this device will enable multiple wavelength sources for telecommunications, computing, sensing, metrology and other areas.

Session 3A2a
Optics, Quantum-well Devices, Optical Soliton

Entanglement Creation by the Dipole-dipole Blockade Effect

Khulud Almutairi[1], **Ryszard Tanaś**[2], **and Zbigniew Ficek**[3]

[1]Institute for Quantum Information Science, University of Calgary, Alberta T2N 1N4, Canada
[2]Nonlinear Optics Division, Faculty of Physics, Adam Mickiewicz University, Poznań 61-614, Poland
[3]The National Centre for Mathematics and Physics, KACST, P. O. Box 6086, Riyadh 11442, Saudi Arabia

Abstract— The dipole-dipole blockade mechanism is developed for the study of a controlled generation of pure Bell state in a two-atom system. The proposed blockade mechanism inhibits transitions into either singly or doubly excited collective states of a two-atom system by shifting them from their unperturbed energies. The shift is accomplished by the short range dipole-dipole interaction between the atoms. When the double-excitation states are shifted form their resonances, the two-photon excitation of the system by a resonant laser field becomes suppressed. The two-photon excitation is suppressed without destroying the one-photon excitation. The blockade effect is a simple process for creation of single-excitation entangled states. When single-excitation states are shifted a two-photon dipole-dipole blockade takes place that allows simultaneous absorption of two photons by inhibiting one-photon absorption in the system. Specifically, we analyze the blockade effect for both, a pure state of the system isolated from a dissipative environment and for a mixed state resulting from the coupling of the system to the environment. We find that the two-photon blockade effect reduces the collective four level system to an effective two-level two-photon system. The state of this reduced system is then obtained analytically and the nature of the state is fully analyzed. We show that this technique might be useful in achieving entangled two-photon Bell states. We follow the temporal evolution of the Bell states and find that the concurrence can be different from zero only in the presence of the dipole-dipole interaction. Furthermore, in the limit of a large dipole-dipole interaction, the concurrence reduces to that predicted for an X-state of the system. A general inequality is found which shows that the concurrence of an X-state system is a lower bound for the concurrence of the two-atom system. With the relaxation present, the general state of the system is a mixed state that under a strong two-photon dipole blockade reduces to an X-state form. A simple analytical expression is obtained for the steady-state concurrence which shows that there is a threshold value for the dipole-dipole interaction relative to the Rabi frequency of the driving field above which the atoms can be entangled over the entire time of the evolution.

Gaussian Optical Solitons for the Biswas-Milovic Equation

Chaudry Masood Khalique
International Institute for Symmetry Analysis and Mathematical Modeling
Department of Mathematical Sciences, North-West University, Mafikeng Campus
Private Bag X2046, Mmabatho 2735, Republic of South Africa

Abstract— In this talk we obtain the 1-soliton solution of the nonlinear Biswas-Milovic's equation in a log law media. Biswas-Milovic equation is the generalized version of the nonlinear Schrodinger's equation that governs the propagation of solitons through optical fibers. Biswas-Milovic equation is in general a better and improved model as compared to the nonlinear Schrodinger's equation as it accounts for imperfections in an optical fiber, thus affecting pulse evolution in the temporal domain. Therefore a generalized evolution is considered. The dispersion and nonlinearity, that could also possibly vary due to these imperfections or laser injection error into an optical fiber, is also generalized to account for these detrimental factors.

The technique that is used to obtain the solution for the Biswas-Milovic equation in a log law media is the Lie symmetry method. This method is one of the most powerful methods to determine solutions of nonlinear partial differential equations. It is based upon the study of the invariance under one parameter Lie group of point transformations. Lie symmetry method was developed by Sophus Lie (1842–1899) in the latter half of the nineteenth century and is highly algorithmic. These methods systematically unify and extend well known ad hoc techniques to construct explicit solutions for differential equations, especially for nonlinear differential equations. A closed form soliton solution for the Biswas-Milovic equation in a log law media is obtained.

Simulation of High Power GaInNAs-GaNAs Double Quantum-well Laser Diodes for Raman Amplifier Pumping

M. Faiez Ali[1], **M. Kamil Abd-Rahman**[1], **M. Salleh Mohd Deni**[1], **and M. S. Alias**[2]

[1]Faculty of Applied Science, Universiti Teknologi MARA, Shah Alam 40450, Malaysia
[2]Advance Physical Technologies Laboratory, Telekom Malaysia Research & Development (TMR&D)
Lingkaran Teknorat Timur, Cyberjaya Selangor 63000, Malaysia

Abstract— We present theoretical analysis via simulations on high power GaInNAs-GaNAs quantum-well (QW) broad area laser diode operated in the 1.204–1.242 µm wavelength regime. The structure is based on previous other group experimental work. Simulation design is based on 2D cross section which is treated as perpendicular to the optical axis and lasing direction. We strongly believed that the increased number of quantum wells has leading effects on the increment of the optical confinement factor (OCF) as compared to increment of nitrogen doping. A maximum total power output of more than 4.5 W and lasing spectrum around 1242 nm is obtained for the proposed structure. The device shows potential application to be used as pumping source for Raman amplifiers.

Fidelity of Classical and Quantum Measurements

Thomas B. Bahder
Charles M. Bowden Research Facility
Aviation and Missile Research, Development, and Engineering Center
US Army RDECOM, Redstone Arsenal, AL 35898, USA

Abstract— The goal of any experiment is to determine some physical quantity. However, in most cases, the quantity that is directly measured is not the quantity that we intend to determine through the experiment. For example, we may want to determine a wavelength of an atomic optical transition, however, the quantity that we directly measure may be a voltage. The question arises: how good is our measurement of the wavelength? To answer this question, I propose the use of Shannon mutual information (calling it fidelity) between the directly measured quantity, the voltage, and the quantity that we seek, the wavelength. Another important question is: given two different experiments that attempt to determine the wavelength, which experiment is better? The experiment with the highest Shannon mutual information (fidelity) provides, on average, the best measurement of the wavelength. The fidelity also takes into account our prior information about the wavelength through a prior probability distribution. Historically, the quality of measurements has been discussed in terms of parameter estimation, through the use of the Fisher information, to provide an upper bound on the variance of an unbiased estimator through the Cramer-Rao inequality. I argue that there are two objections against using the Fisher information as a measure of the quality of measurements. First, the Fisher information may depend on the unknown physical quantity (parameter to be determined), which may occur when dissipation is present. Second, the Fisher information does not take into account prior information about the parameter (as does the fidelity). Consequently, I proposed the use of fidelity (Shannon mutual information between measurements and physical quantities) as a quantitative measure of the quality of physical measurements. The fidelity is sufficiently general that it allows the comparison of classical and quantum measurement experiments, to determine which one is a better measurement. As an example, I compute the fidelity of a classical and quantum Mach-Zehnder interferometer, to determine which provides a better measurement of phase shift in one arm of the interferometer.

Session 3A2b
Plasmonic Nanophotonics I - Experiment

Surface Plasmon Modulation in Silver Nanowires Revealed by Quantum Dot Fluorescence Imaging

Hong Wei and Hongxing Xu
Institute of Physics, Chinese Academy of Sciences, Beijing 100190, China

Abstract— Plasmonic nanostructures show many interesting and valuable properties due to surface plasmon (SP) resonances, and are extensively investigated for their potential applications in different fields. Recently, the propagation of SPs in Ag nanowires (NWs) has received increasing attention. We have shown the remote excitation of Raman scattering and quantum dot (QD) fluorescence by using the propagating SPs in Ag NWs.

For Ag NWs coated by a layer of semiconductor QDs with dielectric spacer layer between them, the QDs will be excited when plasmons propagate along the NW. Excitation of the QDs is proportional to the local electric field intensity, allowing us to clearly visualize the plasmon-induced field distribution at every point along the NW. Quasi-periodic spatial modulation is observed for the near field of propagating SPs (Fig. 1) [1]. The spatial modulation is formed by the interference of different plasmon modes excited on the NW, and can be controlled by tuning the incident polarization.

In simple NW networks, the QD imaging method can provide us a clear picture of how plasmons can be redirected by and to additional proximal NWs at specific points along a primary NW. Interference between SPs launched at different positions along a primary NW can turn on or off emission paths, resulting in combinations of optical signals that execute specific interferometric Boolean logic operations. This primary NW can thus be viewed as the plasmonic equivalent of a bus in a central processing unit. In addition, a plasmonic NOR gate, one of the so-called "universal logic gates", is demonstrated by cascading OR and NOT gates in four-terminal plasmonic NW networks [2]. These findings shed new light onto fundamental understanding of propagating plasmons in complex networks, and may advance the development of novel nanophotonic on-chip processor architectures for future optical computing and information technologies.

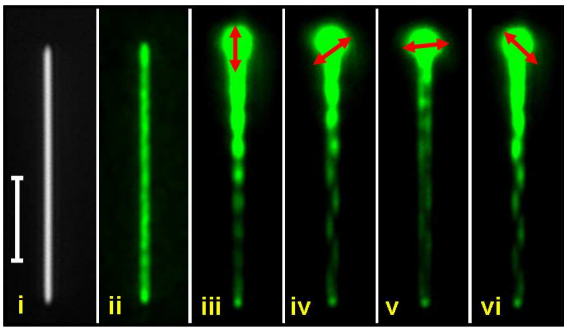

Figure 1: (i) Optical image of a NW. (ii) The QD emission image with wide field excitation. (iii–vi) QD emission images for different incident polarizations. The scale bar is 5 μm. The red arrows show the polarization of excitation light.

REFERENCES

1. Wei, H., et al., *Nano Lett.*, Vol. 11, 471–475, 2011.
2. Wei, H., et al., *Nat. Commun.*, Vol. 2, 387, 2011.

Hybrid Plasmonic Structures Design and Fabrication by Laser Means

M. H. Hong, **L. Xu**, **N. T. V. Thanh**, **M. Tang**, **and Z. C. Chen**
Department of Electrical and Computer Engineering
National University of Singapore, 10 Kent Ridge Crescent, 117576, Singapore

Abstract— Surface plasmon resonance (SPR) is a powerful means to achieve the localized enhancement of the optical field by forming "hot spots" on the metallic nanostructures to increase signal detection sensitivity. SPR peak wavelength can be flexibly tuned by manipulating metallic nanoparticles or nanostructures' sizes, shapes, thin film materials, and their inter-coupling. Optical signal is increased greatly near or at the SPR peak wavelength with a sharp peak distribution. By coupling the molecules on the plasmonic structures, the resonance peak shift due to the surrounding medium refractive index change can be used to characterize the molecules properties. However, this high Q resonance is typically corresponding to only one specific wavelength, which limits its applications for wideband spectrum response devices, such as for high efficiency solar cells in which Sunlight covers a light spectrum from 300 nm to 3 μm. It is an inevitable need to design and fabricate hybrid plasmonic structures, which can work in a broadband. In this talk, the synthesis of $Ag:TiO_2$ nanocomposites by pulsed laser ablation in liquid is carried out. By coupling in Ag nanoparticles, TiO_2 optical properties can be modified with an additional resonance peak at visible light range to enhance the light absorption for photo-catalyst and solar cell applications. Meanwhile, SPR can be tuned as well by modifying single-element metallic thin film patterns from nanodots, to nanorods, and to nanodiamonds shapes by laser interference lithography. Bio-sensing of DNA molecules on large area Au nanorods surfaces shows an amplified Fano-like shape resonance. Meanwhile, multi-element metallic alloy (Ag/Au and Ag/Au/Cr) thin films and their nanostructures are fabricated to achieve multi-peak SPR. These hybrid plasmonic structures can be used to make wideband anti-reflection black Si surfaces to increase Sunlight absorption. Furthermore, laser micro-lens array (MLA) lithography is also applied to make arbitrary plasmonic structures from optical, NIR to THz spectra. To further reduce the metallic nanostructures down to 50 nm over a large area, thermal de-wetting of the laser nanopatterned periodic structures is also carried out, which leads to better optical sensing performance.

Localized Surface Plasmon Resonance of Arrayed Metallic Nano-structures Fabricated by Metal Contact Printing Lithography

Hao-Yuan Chung, **Chun-Ying Wu**, **Chun-Hung Chen**, **and Yung-Chun Lee**
Department of Mechanical Engineering, National Cheng-Kung University, Tainan, Taiwan, R.O.C.

Abstract— In this study, we demonstrate a rapidly, low-cost, large-area, and mass productive fabrication process to obtain arrayed metallic nanostructures on a variety of substrates. The key element in this fabrication method is to combine an innovative metal contact printing lithography with conventional lifting-off and thermal annealing processes. Hexagonal arrays of metallic nano-particles with sub-micron periodicity are successfully deployed on an ITO/glass substrate. The dimensions, shapes, and arrangements of these arrayed metallic nano-structures and nano-particles can be easily adjusted by using different pattern designs in the imprinting molds. The sizes and material compositions of the obtained metal nano-particles can be easily controlled by the deposition thicknesses and material varieties of films deposited during the sample preparation process.

Optical transmittance measurements show that certain kinds of noble metallic arrayed nanoparticles deployed on an ITO/glass substrate can result in a phenomenal narrowband of extinction in spectral range of visible light. Theoretical analysis indicates this narrowband extinction spectrum is associated with electromagnetic field coupling between the arrayed metallic nanostructures and the underlying ITO layer. Numerical simulation based on finite-difference time-domain method (FDTD) is carried out to demonstrate the electromagnetic field distributions of the localized surface plasmon resonance of arrayed metallic nanostructures and the excited waveguide modes within the ITO layer. This electromagnetic field coupling induces significant plasmon resonance in the ITO layer underneath the arrayed metallic nanostructures. A further evidence is attained by comparing the measured transmittance spectrum of a similar noble metallic arrayed nanoparticles deployed on a glass substrate. Experimental results show that the narrowband extinction in visible spectrum is vanished since there is no ITO layer to support guided modes resonance. Based on this observed phenomenon and our innovative large-area nano-fabrication processes, optoelectronic devices with arrayed metallic nanostructures can be easily designed and developed in the future.

Speed-up the Nanoelectronics with Plasmonics Technology

Er Ping Li[1, 2] **and Ping Bai**[1]

[1]Department of Electronics and Photonics, A*STAR-IHPC, Singapore
[2]Department of Information Technology and Electronic Engineering, Zhejiang University, China

Abstract— The integration of optical devices into electronic circuits can achieve both the advantages of ultra-compactness in electronics and super-wide bandwidth in optics. However, the dimensions of traditional optical devices are fundamentally limited by the law of diffraction and consequently limit the progress of merging photonic circuits with electronics. Plasmonics emerges as a promising technology platform towards deployment of small-footprint integrated-circuitry for chip-scale and high density integration, and could bridge the gap between the conventional optics and nanoelectronics. In this talk, I will present the latest progress in the Institute of High Performance Computing (IHPC) on plasmonics applications for optic data transmission in electronic integrated circuits. A waveguide platform based on a hybrid plasmonic waveguide has been demonstrated with CMOS-compatible technology, and used as a building block to build high-performance plasmonic devices, including bends, filters, splitters, and modulators. Plasmonic detectors based on antennas and resonant cavities will also be discussed. With the developed plasmonic devices, plasmonic circuits could be implemented to transmit signals optically on a chip.

ACKNOWLEDGMENT

This work was supported by the A*STAR Metamaterials-Nanoplasmonics research programme under grant A*STAR-SERC 0921540098.

Session 3A3
SAR Systems and Signal Processing

Dual Band Antenna with Paired Excitation for Reduced Cross-polarisation

Gobi Vetharatnam, **Koo Voon Chet**, **and Fabian Kung Wai Lee**
Multimedia University, Malaysia

Abstract— Dual L- and C-band antenna with single polarisation is designed for application in synthetic aperture radar (SAR). Shared-aperture antenna systems are increasingly preferred in modern SAR systems. One key requirement in a SAR antenna is low cross-polarisation. In a probe-fed patch, the cross-polarisation reduction depends on the cancellation of fields by adjacent patches. An analysis of the field cancellation with equal-power, unequal-power and different phases was carried out. Good cancellation may be achieved if the adjacent powers are the same. The phases of the adjacent patches do not have significant effect on the cross-field cancellation. Paired excitation may not be immediately possible in a shaped pattern. Modification to the array excitation coefficient must be performed so that adjacent powers in an array are the same even for a shaped beam pattern. Then, the cross-polarisation may be controlled and suppressed to meet the SAR requirements. In this work, the C-band array is made up of three paired radiators in the elevation plane. The azimuth plane has four elements. The L-band patch is made up of two patches placed above the C-band array. The prototype is fabricated with three GML1032 laminates, with two of them being the thicker substrate (1.52 mm) and the other 0.76 mm. A layer of 4 mm low-loss Rohacell HF51 foam separates the radiating layers from each other. The C-band array achieved a cross-polarisation level of 31 dB in the main beam, while the L-band achieved a cross-polarisation level of 25 dB. The C-band achieves a bandwidth of 220 MHz centred at 5.3 GHz. The return loss is about −20 dB. The L-band return loss is about −20 dB at centre frequency with a bandwidth of about 120 MHz. Good radiation pattern was achieved for both the frequency bands.

Three Layers Configuration Microstrip Patch Antenna for Unmanned Aerial Vehicle Synthetic Aperture Radar

P. N. Tan[1], **V. Gobi**[2], **Y. K. Chan**[1], **T. S. Lim**[1], **and V. C. Koo**[1]

[1]Faculty of Engineering and Technology, Multimedia Media University
Jalan Ayer Keroh Lama, Bukit Beruang, Melaka 75450, Malaysia
[2]Faculty of Engineering, Multimedia University
Jalan Multimedia, Cyberjaya, Selangor 63100, Malaysia

Abstract— A C-band microstrip patch antenna for Unmanned Aerial Vehicle Synthetic Aperture Radar (UAVSAR) has been designed and developed. The antenna operates at 5.3 GHz with a required minimum bandwidth of 80 MHz in order to match with the design specification of the UAVSAR sensor. Probe fed method and three layers configuration have been adopted for the ease of feeding network design. The top layer consists of radiating elements; the feeding network is fabricated on the bottom layer while the ground plane is located at the middle. The antenna has an incident angle of 30° away from center with elevation beamwidth of 24° to offer a wider swath range. As the UAVSAR applies side-looking scan method, the sidelobes power level has been suppressed with achieved maximum power level of −15 dB to overcome left-right ambiguity issue. The measured return loss result of the antenna shows a return loss of −32.381 dB achieved at 5.3 GHz. Multiple feeding ports are utilized in elevation array to avoid undesired power loss due to extremely long microstrip transmission line in feeding network. The microstrip patch antenna is divided into 3 sub panels with each panel consist of 6×8 radiating elements and the sub panels are joined by power dividers. This configuration offers flexibilities to the UAVSAR system as both monostatic and bistatic antenna systems are possible to achieve by modifying the feeding layout. Moreover, the azimuth resolution of the UAVSAR system can also be adjusted by deciding the total sub-panels in use. The radiation pattern of the UAVSAR antenna has been measured in anechoic chamber and the measured radiation pattern is matched with simulation radiation pattern. Several UAVSAR flight measurements have been conducted by using both monostatic and bistatic antenna system in 2010. The flight measurement result proved that the developed microstrip patch antenna with UAVSAR system is able to produce SAR image of the imaging area.

The Design and Development of Unmanned Aerial Vehicle Synthetic Aperture Radar for Environmental Monitoring

Y. K. Chan and V. C. Koo

[1]Faculty of Engineering & Technology, Multimedia University, Malaysia
[2]Jalan Ayer Keroh Lama, Bukit Beruang, 75450 Melaka, Malaysia

Abstract— The principle of synthetic aperture radar (SAR) was discovered nearly 40 years ago. It becomes a main tool of microwave remote sensing because of its capability to operate in nearly all weather condition and operates during day and night. As the radar platform flies over an observation area, the doppler spread of the echo signal can be processed using a digital signal processing method. This reduces the number of hardware components for doppler filtering as well as range gating.

Microwave remote sensing is one of the major research areas conducted by a research group in Multimedia University, Malaysia, for the past 10 years or so. Theoretical modelling and image processing technique on SAR images have been developed. However, the main limitation is the dependence on overseas institution to supply the measurement data and SAR images. For national monitoring and management of earth resources, limited number and timely supply of the required SAR images have been a major problem. Therefore, there is an urgent need to develop our own SAR sensor system.

In late 2007, the project to develop a UAVSAR system was initiated with joined collaboration with Agency Remote Sensing of Malaysia. The main objective of this project is to design and construct an imaging radar system with UAV as the platform. The SAR system is a C-band, single polarization, linear FM pulse radar system. This SAR system is designed to operate at low altitudes with low transmit power and small swath width in order to optimize the development cost and operating cost. The system will be used for monitoring and management of earth resources such as paddy fields, oil palm plantation and soil surface. This paper describes the design and development of the SAR sensor as well as the current status of the development.

Design and Development of a Miniature C-band RF Transceiver for Synthetic Aperture Radar

Kuo Shen Yee, **Yee Kit Chan**, **Wai Lee Fabian Kung**,
Voon Chet Koo, **and Ming Yam Chua**
Faculty of Engineering & Technology, Multimedia University
Jalan Air Keroh Lama, Melaka 75450, Malaysia

Abstract— Synthetic Aperture Radar is an effective tool for Earth's resource monitoring. Typical SAR systems are operated on satellites, spacecrafts or airplanes. Recently, unmanned aerial vehicle (UAV) has become an alternative flying platform for SAR system. The main reason of choosing UAV is due to its capability to fly and operate remotely without the crew or pilot on the flying platform. Besides, a small UAV can operate at lower power and fuel consumption, hence reducing the overall operating cost. However, due to its space and weight constraints, it is a challenging task to design a UAV-based SAR sensor. Most of the commercially available RF components are in standard sizes and some are too bulky to be fit into the flying platform. Thus, the design of a miniature RF transceiver is of great interest. Main components of the RF transceiver include an up-convert mixer, a power amplifier, a low noise amplifier, a down-convert mixer, a band-pass filter and a low-pass filter. The RF transceiver will operate in C-band, with more than 30 dB gain in total. This paper highlights the design of a miniature RF transceiver module for UAV-based SAR.

Design of a Digital Synthetic Aperture Radar

W. G. Cheaw, **Y. K. Chan**, **and V. C. Koo**
Multimedia University, Malaysia

Abstract— Synthetic Aperture Radar is rapidly becoming a popular choice for aerial imaging due to the fact that it does not require any form of lighting and can operate in adverse weather conditions. We propose the design of a software based approach to a digital Synthetic Aperture Radar (SAR) processor. We also propose a system where the digital signals are fed to a computer and can be processed in real-time. This processor system allows for a modular approach to the research and development of newer algorithms SAR systems. We attempt to mitigate the specific requirements of processing a radar signal in real-time, direct from the analog return by applying some changes to typical signal flow. A typical digital SAR system requires the combination of a complex system comprising of an analog system, an analog to digital interface, storage and a processor system. This system is usually a form hard-coded for of digital logic designed to meet strict timing requirements. The recent advent of high speed ADCs and DAC as well as the recent increase in Ethernet technologies allow for a system that is capable of transferring data through an industrial standard and common form of connection. Our current demands of a digital SAR system also gives us some headroom in term of processing power enabling us to perform relatively fast processing of signals using a typical PC. The taxation of the program complexity is also reduced by using various forms of hardware processing such as GPGPU processing. Existing algorithms have to be modified to run GPGPU and fine tuning required for better efficiency. This system should allow for faster development of SAR systems as the input and output signals can be defined via software thus reducing the need for major reengineering.

FPGA-based Pre-processing Unit for Real-time Synthetic Aperture Radar (SAR) Imaging

Y. C. Lee, **V. C. Koo**, **and Y. K. Chan**
Multimedia University, Melaka, Malaysia

Abstract— Synthetic Aperture Radar (SAR) is a powerful and well established microwave remote sensing technique which is capable in producing high resolution images from the measurements of the earth surface independent of weather conditions. The potential of SAR applications led to the development of a large number of airborne and space-borne SAR systems. Range-Doppler algorithm is commonly used for the processing of SAR data by achieving range and azimuth compression via matched filtering. The algorithm massively utilizes Fast Fourier Transform (FFT) and Inverse Fast Fourier Transform (IFFT) operations. Therefore, the majority of computation time in SAR image formation is occupied by FFTs and IFFTs. SAR processing system by using Field-Programmable Gate Array (FPGA) gives a useful approach to the real-time process of SAR data. This is due to FPGA-based system able to exploit pipelining and massively parallel processing resulting in faster and cost effective designs. Hence, this system is ideal for the realization and implementation of real-time algorithm in hardware through Hardware Description Language. This system offers the flexibility in perform different algorithms in the same hardware platform and adaptable for different implementation strategies due to its reconfigurable computing, high parallelism and pipelining capability. On board storage of SAR data is often not feasible due to quick response demands, power consumption and limitations in space of the carrier system such as Unmanned Aerial Vehicle (UAV). Therefore, real-time processing capability is one of the desired and demanded abilities in the SAR imaging systems. This paper highlights the design and development of a FGPA-based pre-processing unit for real-time SAR imaging. Particularly, an efficient FFT processing module has been developed. The proposed architecture significantly reduced the hardware resources while achieving the reasonably high processing speed and throughput rate.

Performance Evaluation of Modified MLCC Dopple Centroid Estimator

S. B. Cheng, Y. K. Chan, and T. S. Lim
Faculty of Engineering & Technology, Multimedia University
Jalan Ayer Keroh Lama, Bukit Beruang, Melaka 75450, Malaysia

Abstract— Radar is a very important system in the field of military and non-military for the purpose of monitoring and positioning. The imaging resolution is governed by the size of antenna aperture. In fact, due to limitation of the radar platform body size, the design of the antenna aperture is always restricted into certain range. Therefore, Synthetic Aperture Radar (SAR) is designed and developed. SAR is a remote sensing which gives better resolution image by utilizing advance signal processing technique to 'systhesize' a very long antenna. To produce a high-quality image, accurate parameters are required for signal processing work. In the azimuth matched filtering processing of SAR data, Doppler centroid is an important azimuth parameter that helps to focus the image intensity.

The estimation work for Doppler centroid parameter used to isolate by researcher. It is because the estimation work involved complicated steps and increased the signal processing time. Therefore, researcher used to apply only the approximate Doppler value which is not precise enough and possibly causes defocus image generated. In this work, we review and develop several conventional Doppler centroid estimation algorithms by using Matlab software. We also introduce a modified MLCC algorithm which is suitable for all sorts of SAR data. This modified MLCC dividing the range compressed spectrum into four looks instead of two looks which given better sensitivity to the change of phase information of adjacent signals. In addition, we evaluate the performance of each estimator by indicators of signal-to-noise ratio, 3 dB resolution and image entropy. Experimental result showed that modified MLCC managed to extract precise Doppler value and gives the best focused images.

Geometric Correction on SAR Imagery

A. L. Choo, Y. K. Chan, and V. C. Koo
Multimedia University, Melaka, Malaysia

Abstract— SAR also known as synthetic aperture radar is an advanced side looking radar which utilizes the flight path of the platform to simulate an extremely large antenna or aperture electronically. It continuously transmitting the generated chirp signals to a target scene which perpendicular to the flight direction then received and stored the echo backscattered from the target scene. The data collected contain the earth surface information of the target scene are processed into a SAR image. However the SAR images generated through signal processing contain errors or distortions which cause the data in the present image to be inaccurate. These errors or distortions present in the SAR image also known as geometric distortion. Geometric distortions exist in all remote sensing images and broadly related to the target, sensor and platform. The objective of this research project is to reduce the error of SAR images through implementation of geometric correction on SAR. Geometric correction can be done by reposition of pixels form the uncorrected image location to the reference grid through geometric operations. There are few types of geometric correction such as registration, rectification, geocoding and orthorectification. The three main process of geometric correction are mathematical distortion model, coordinate registration and resampling. These three components also known as warping process. Mathematical distortion model such as polynomial distortion model has been generated using MATLAB for the geometric correction purpose. Experiments have been done using a few generated images and polynomial distortion model to prove its usability. After coordinate registration the SAR image will be resampled. The result images of different type of resampling methods have been observed to obtain good quality images. The geometric correction will help to improve the data accuracy of the SAR Image.

Session 3A4
Design and Mathematical Modeling of Wide band Antennas

A 60 GHz Wideband and Miniaturized CMOS Fractal Antenna

F. A. Ghaffar and A. Shamim
King Abdullah University of Science and Technology (KAUST), Saudi Arabia

Abstract— In recent years the interest in the 60 GHz band has increased significantly due to the availability of 7 GHz unlicensed band. This band is ideally suitable for high data rate applications such as WPAN, HD video streaming and wireless ethernet. CMOS based transceivers operating in the 60 GHz band have been reported, but there are only a few with integrated on chip antennas. Incorporating the antenna on-chip greatly simplifies its integration with the active circuits, eliminating the need of bond-wires, and off-chip components. However, the challenging part is to design an on-chip antenna, which can cover the entire 7 GHz bandwidth with reasonable radiation pattern and efficiency. This work, for the first time, reports the design of a wide-band on chip fractal antenna in standard 65 nm CMOS technology.

The term fractal was introduced by 'Madelbrot' to propose new shapes, which can be defined as complex structures and have self similarity. Fractals are composed of numerous small units non-integer dimensions stack up together form a complete structure similar shape that the unit structure. This distinctive characteristic fractals has been exploited antenna designers demonstrate antennas compact in size large bandwidth. bandwidth is due their geometry, multi-resonant structures. In addition, self-affine space filling properties increases effective electrical length reduce hence, making them compact.

The fractal structure used in this design is a third order Sierpinski carpet antenna. The antenna has a size of 0.6 mm by 0.6 mm, which is 25% smaller than a conventional patch antenna. The antenna demonstrates an impedance bandwidth of 10 GHz. An omni-directional radiation pattern with a maximum gain of -5 dB has been achieved. The large bandwidth and compact size of the antenna makes it extremely suitable for integration with circuits implemented in CMOS technology.

LCP-based Half Circle Fractal Patch Antenna for Wide Band Applications

M. Sabeh and A. Shamim
King Abdullah University of Science and Technologh (KAUST), Saudi Arabia

Abstract— Recent years have seen rapid growth in wireless communication area where emerging devices like smart phones are providing an integrated solution for a number of wireless applications like personal communication services (PCS) 1.8 GHz, Global Positioning System (GPS) 1.575 GHz, Bluetooth 2.4 GHz, and Wi-Fi 5 GHz on miniaturized platforms. To reduce the overall size of such multi-function modules, it is important to reduce the number of antennas required. The ideal solution is if one antenna can cover all these bands. This paper presents the design of a wideband fractal antenna that can operate for all the above-mentioned bands. The design has been realized in an innovative medium called Liquid Crystal Polymer (LCP) that is a new organic, thin and flexible substrate with superb high temperature, and high frequency performance. Due to its lightweight and flexible nature the design is also well suited for the futuristic wearable wireless applications.

Microstrip patch antennas have many advantages such as their low profile, lightweight and low cost, however the major limitation is their narrow bandwidth. One solution to their narrow bandwidth is the use of fractal structures. A fractal structure is composed of numerous self-similar small units of non-integer dimensions. Due to unique self-similar shapes, they provide a good platform for antennas that are compact in size and possess multiple resonances. The fractals provide larger bandwidths because of their space filling nature.

A half circle fractal patch antenna fed through coplanar waveguide (CPW) is chosen for this work. Using coplanar waveguide (CPW) feed makes antennas more suitable for compact wireless communication devices, due to its features like uniplanar structure, easy fabrication and circuit integration. The antenna is realized on a single layer LCP substrate (100 µm thick) with relative permittivity of 2.9. The antenna demonstrates a return loss below 10 dB for the entire bandwidth ranging from 1.5 GHz till 6 GHz. It also maintains a good radiation pattern with a maximum gain of approximately 3 dBi. From the results above, the design is well suited to a number of applications within the operating bandwidth of the antenna.

Design and Analysis of a High Performance Triband 20/30/44 GHz Corrugated Horn

K. K. Chan
Chan Technologies Inc., 15 Links Lane, Brampton, Ontario L6Y 5H1, Canada

Abstract— For future communication satellites, multiple frequency bands may be combined together and radiated through a common aperture. This will reduce the number of antennas on board the satellite. The antenna of choice is typically an offset reflector fed by a single high performance horn. The work reported here is on the development of a single tri-band corrugated horn as feed for a reflector antenna. The three frequency bands are Band 1: 20.2–21.2 GHz, Band 2: 30.0–31.0 GHz and Band 3: 43.5–45.5 GHz. The challenging requirements are the return loss and the peak cross-polar level, both of which are critical for a frequency reuse feed. Such a horn has been designed to use with a dual polarized 6-port feed network to illuminate a reflector located on a spacecraft platform. Its return loss is better than 30 dB, 33 dB and 27 dB at K, Ka, and EHF bands respectively and the corresponding worst-case cross-polar levels relative to the co-polar peak are −33 dB, −40 dB and −26 dB. The slot and tooth widths are designed for manufacturability and the number of corrugations is minimized so that the horn can be fabricated at a low cost while still meeting the stringent electrical specifications. A limit on the level of the next higher order symmetric TE_{31} mode that can be present at the horn input from the feed network without deteriorating the cross-polar performance is examined.

A literature survey of the state-of-the-art in multi-band horn design was carried out. The horn type that is frequently used to provide dual or tri-band capability is the corrugated horn with dual depth slots [1] or slots with special shapes such as ring loaded slots or stepped slots. Horns with dual depth slots typically show −25 to −30 dB peak cross-polar responses in two bands and −20 to −25 dB in the third band. This is expected since the slots can be made to exhibit approximately balanced hybrid condition in two bands. While at the third band, if present, the corrugated surface impedance should hopefully still remain capacitive. Otherwise, the dual depth slots will not give good tri-band performance. Ring loaded horns can cover a wide bandwidth with frequency ratio of not more than 1.7 : 1 for peak cross-polar level below −30 dB and return loss level greater than 30 dB. They do not perform well when the bands are widely separated. Recently, a paper by Granet and James had stated that a corrugated horn could not be easily designed to meet low cross-polarization requirement in the three bands of interest, i.e., 20/30/44 GHz regardless of the type of corrugations used. They then introduced two optimized smooth-walled horns with computed peak cross-polar levels in the three bands as −28.7/−25/−26 dB and −21/−27/−27.5 dB respectively, but there is no mention of the return loss performance of the horn. Such a claim is proven to be false. The dual-depth corrugated horn design presented here not only shows much better cross-polar performance but is also about 38% shorter in axial length than that of the smooth-walled horn. A compact horn is an important attribute on a satellite platform.

Micro Strip Line Fed I-shaped Dielectric Resonant Antenna for Millimeter Wave Applications

Chandra Kandula, Prasanna Kumar Sahu, Prakash Kumar Panda, and K. L. Sheeja
Department of Electrical Engineering, NIT Rourkela, Orissa, India

Abstract— This paper proposes for a broadband and high gain dielectric resonator antenna applicable in millimeter-wave wireless networks at Ka-band. Here the design of a simple and a generic transmission line (T.L.) circuit approach along with a fast and generic formulation for the novel antenna model is developed. The proposed antenna is modeled as an I-shape and is placed on a material of dielectric constant of ε equal to 2.2 (Teflon material) and size of 15 mm × 11 mm. The ε (epsilon) value of dielectric resonator is taken to be 10.2 (material: Rogers RO3010). A simple micro strip line feeding of novel design has been used to feed the antenna. The ground plane is considered to be 10 mm × 11 mm in size. The width of the resonator has been changed to get optimum results. Different values for width are 2.4, 2.0, 1.6 and 1.4. A good return loss is found at 2.0 mm. The proposed antenna is simulated and a return loss of −10 db below is obtained which is in the range of 30.58 GHz to 39 GHz. Here a good return loss is obtained at two peaks whose values are −21 db at 31.54 GHz and a value of −22 db at 35.39 GHz. In this paper a bandwidth improvement of 24.36% has been achieved. In addition to that a total efficiency of 72.88% is found at 35.39 GHz and 69% is found at 31.54 GHz. A directivity of 10.2 dbi at 35.39 GHz and a 7.61 dbi at 31.54 GHz have been claimed, besides that a significant gain of 10.59 db at a frequency of 35.39 GHz and 8.34 db at 31.54 GHz. The designed antenna is proposed for applications in the area of satellite communications, radio location, and imaging systems for weapon and hazardous material detection.

Fractional-order Equivalent Circuit Models of UWB Omnidirectional Small Antennas

A. G. Radwan
Department of Applied Engineering Mathematics, Faculty of Engineering, Cairo University, Egypt

Abstract— In ultra-wideband antennas, the relationship between the transmitter and the receiver acts as a frequency dependent filter response such as in omnidirectional small antennas. Recently, a circuit methodology to model the UWB omnidirectional small antennas system using the circuit fundamentals such as canonical forms and equivalent circuits have been introduced and validated with experimental results. Both electrical and magnetic antennas are introduced based on five circuit elements which are two capacitors, two inductors and a single resistor (represents radiation). In this paper we will study analytically the frequency response for each circuit, critical frequencies and quality factor.

In the last few decades, many scientific papers have discussed the existence and fabrication of the fractional-order element ($Z(s) = ks^{\alpha}$) which span all the conventional elements (R, L, C) when the fractional-order α equals (0, 1, -1). Many fundamentals and theorems are converted from integer order systems into fractional ones through using the extra fractional-order variables which provide more flexibility, freedom, best fit, and aid in optimization techniques. Several physical, biomedical phenomena and industrial applications have been restudied in fractional-order domain showing great improvement than the traditional analysis. For example in the industrial field, practically, by studying the behaviour of Coilcraft RF inductors in high frequencies it shows that the skin effect losses are proportional to $\sqrt{jf}$ which can be modelled as a fractional element. In addition, the characteristic impedance of a lossy transmission line was modelled as half order element. The second part of this paper will discuss the effect of the fractional-order parameters on the system response and the critical frequencies as compared to the integer-order circuit model.

On the Mathematical Analysis of Broadband Equivalent Circuit Model Suitable for Mobile Terminal Antenna

A. G. Radwan
Department of Applied Engineering Mathematics, Faculty of Engineering, Cairo University, Egypt

Abstract— During the last few decades, many circuit models for different antennas were introduced. These models are based on capacitors, inductors and resistors which represent the radiation power. Recently, the ultra-high frequency band of a capacitive coupling element based mobile terminal antenna was modelled as circuit blocks that represent chassis, capacitive coupling element and matching circuitry. It was shown that this equivalent circuit model expands the basic understanding of antenna structure. In this paper we will investigate by analytical and numerical solutions the frequency response for the capacitive coupling element with and without the effect of the chassis two lowest order wave modes. In addition, the critical frequencies and the sensitivity analysis with respect to each parameter of the circuit elements, and the quality factor will be introduced with numerical examples.

Modeling the Transmit and Receive Antenna Impulse Responses for UWB Systems and Increasing the Effective Channel Gain

M. El-Hadidy and T. Kaiser
The University of Duisburg-Essen, Germany

Abstract— Main objective of this work is to determine the transfer functions of the Ultra-Wideband (UWB) antennas either in time domain or in frequency domain based on EM-Simulation tools as CST-Microwave Studio. The UWB Antenna Impulse Response (AIR) has to consider the whole antennas properties as polarization, angular gain, matching, efficiency and the operating phase (Transmitting/Receiving). Since the operating bandwidth of the UWB antennas has been defined by Federal Communications Commission (FCC) from 3.1 to 10.6 GHz, the AIRs have to consider the frequency dependence of the antennas characteristics through the whole bandwidth.

The AIR would be later embedded in a ray-tracing tool as Wireless-Insite from Remcom for computing the multipath channel considering the reflections, diffractions and transmission from and through the objects in the environment. In the ray-tracing tool, the frequency dependence, polarization and material characteristics of the scattering objects would be considered as well. In the transmitting and receiving nodes, several UWB directional antennas as Vivaldi antennas would be used in an indoor office environment for LoS and NLoS scenarios. Antenna selection technique would be applied to select the best scenario achieves the maximum effective channel gain. UWB smart antennas could be used by designing an UWB beamformer for rotating the main lobe and fetching the maximum channel gain in the environment for specific positions of the transmitting and receiving nodes. This can enhance the overall performance of the UWB communication system. From the other hand, modeling the UWB antennas in the channel can also provide practical solutions for applying Interference Alignment (IA) in UWB multiuser communication systems. Mathematical framework and the simulation results would be illustrated in the full version of this paper.

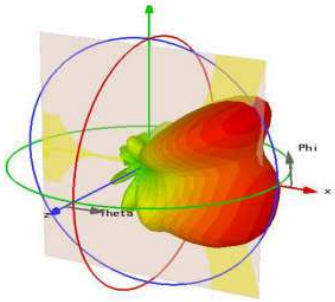

Figure 1: Vivaldi Antenna radiation pattern at 6 GHz.

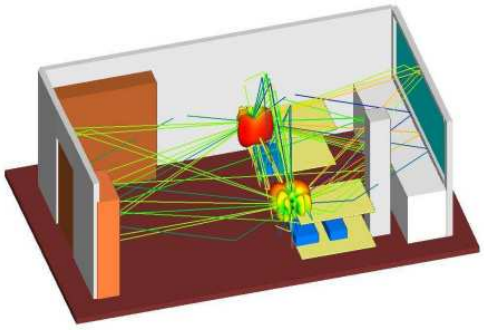

Figure 2: Indoor office environment.

Wideband Isosceles 75°-30°-75° Triangular Dielectric Resonator Antenna

S. Maity, S. Dasgupta, and B. Gupta
Department of Electronics and Tele-Communication Engineering
Jadavpur University, Kolkata, India

Abstract— Dielectric Resonator Antenna (DRA) made up of low loss dielectric material is a potential candidate for high frequency application. Its inherent wide band nature, compact size, ease of fabrication, light weight, low cost etc. make DRAs attractive to antenna engineers. DRAs come in different shapes and sizes of which the most common are cylindrical, cylindrical ring, hemispherical, rectangular, equilateral triangular, hexagonal and/or trapezoidal DRAs.

Triangular shape is the simplest geometry among polygonal (except rectangular) resonators. Literature survey shows that only equilateral triangular resonators have been analyzed. Some simulated and/or practical measurements can be found on isosceles right angled or 30°-60°-90° triangular resonators. Compared to other resonating geometries, the triangular resonator antenna is physically smaller having radiation properties similar to rectangular resonator but has a lower radiation loss. In recent year, it is found that triangular resonator is used as broad band radiator, circularly polarized antennas, dual-triple and/or multi band antennas, arrays etc..

In this paper, a simple probe fed Isosceles 75°-30°-75° triangular DRA having median (M) 19 mm, height 5 mm and permittivity 10 is designed using FEM based HFSS software. First two board side modes are merged to get a wide band covering 4.21 GHz to 6.76 GHz. The simulated return loss is shown in Fig. 1. Radiation patterns at 5.2 GHz, 5.3 GHz and 5.8 GHz are shown in Figs. 2, 3 and 4 respectively. This antenna can be used for IEEE 802.11a/h/j/n, HiperLAN, U-NII bands.

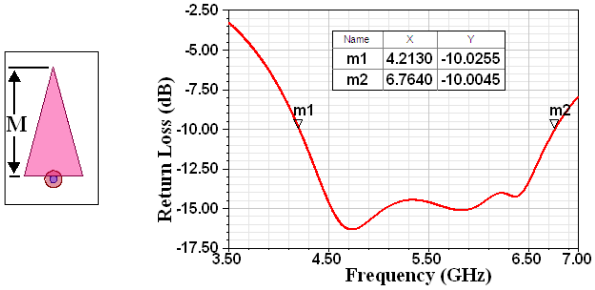

Figure 1: Frequency vs return loss.

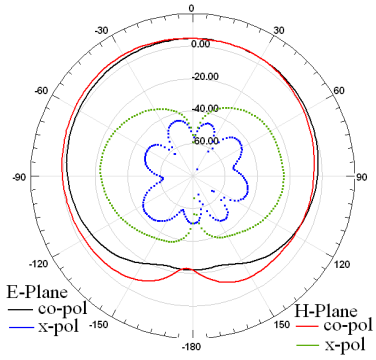

Figure 2: Radiation pattern at 5.2 GHz.

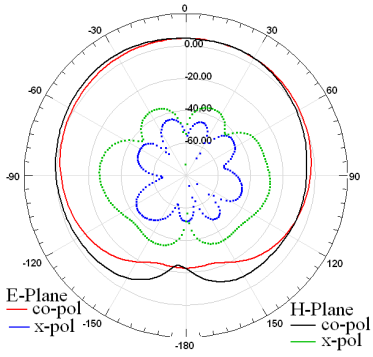

Figure 3: Radiation pattern at 5.3 GHz.

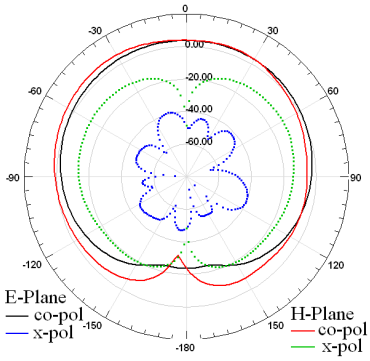

Figure 4: Radiation pattern at 5.8 GHz.

Resonant Frequency and Field Solution of Isosceles Triangular Dielectric Resonator Antenna

S. Maity, S. Dasgupta, and B. Gupta
Department of Electronics and Tele-Communication Enggineering, Jadavpur University, Kolkata, India

Abstract— Dielectric Resonators (DRs) have been widely used in shielded microwave circuits such as cavity resonators, filters and oscillators. As the frequency range increases gradually to millimeter and sub-millimeter region (100 GHz–300 GHz), conductor loss limits the use of metallic antennas. On the other hand, Dielectric Resonator Antenna (DRA) made up of low loss dielectric material is a potential candidate for high frequency application. Its inherent wide band nature, compactness in size, ease of fabrication, light weight, low cost etc. make DRAs very attractive. A recent, up to date, good survey of theoretical and experimental investigations have been reported by Petosa and Ittipiboon on cylindrical, cylindrical ring, hemispherical, rectangular, equilateral triangular, hexagonal and/or trapezoidal DRAs.

Triangular shape is the simplest geometry among polygonal (except rectangular) resonators. Schelkunoff first summarized all the results for symmetrical mode of an equilateral triangular wave guide with metallic walls in 1943. Most researchers have used Schelkunoff's result to analyze equilateral triangular resonator. Field solution of right angled triangular resonator can be found from the knowledge of rectangular resonator as analyzed by Overfelt and White but with hugely inaccurate results. In this paper, isosceles -120° Triangular DRA (TDRA) is analyzed theoretically. An accurate expression for resonant frequency is given here using trilinear transformation, waveguide model and transverse resonance technique.

The TM-mode field solutions for an isosceles -120° TDRA are given by:

A. Field Components for TM^z Even (TM^z_S) Mode

$$\begin{aligned}
E_x &= -\left(\frac{jk_z}{\omega\mu\varepsilon}\right) A_s \left[\sum_{i=1}^{3}(-\alpha_i)\sin[\alpha_i(x+R)]\cos[\beta_i(2qy)]\right] \times \cos(k_z Z)\\
E_y &= \left(\frac{jk_z}{\omega\mu\varepsilon}\right) A_s \left[\sum_{i=1}^{3}(-2q\beta_i)\cos[\alpha_i(x+R)]\sin[\beta_i(2qy)]\right] \times \cos(k_z Z)\\
E_z &= -\left(\frac{j\chi^2}{\omega\mu\varepsilon}\right) A_s \left[\sum_{i=1}^{3}(-2q\beta_i)\cos[\alpha_i(x+R)]\cos[\beta_i(2qy)]\right] \times \sin(k_z Z)\\
H_x &= \left(\frac{1}{\mu}\right) A_s \left[\sum_{i=1}^{3}(-2q\beta_i)\cos[\alpha_i(x+R)]\sin[\beta_i(2qy)]\right] \times \sin(k_z Z)\\
H_y &= -\left(\frac{1}{\mu}\right) A_s \left[\sum_{i=1}^{3}(-\alpha_i)\sin[\alpha_i(x+R)]\cos[\beta_i(2qy)]\right] \times \sin(k_z Z)\\
H_z &= 0
\end{aligned} \tag{1}$$

B. Field Components for TM^z odd (TM^z_A) Mode

$$\begin{aligned}
E_x &= -\left(\frac{jk_z}{\omega\mu\varepsilon}\right) A_a \left[\sum_{i=1}^{3}(-\alpha_i)\sin[\alpha_i(x+R)]\sin[\beta_i(2qy)]\right] \times \cos(k_z Z)\\
E_y &= -\left(\frac{jk_z}{\omega\mu\varepsilon}\right) A_a \left[\sum_{i=1}^{3}(2q\beta_i)\cos[\alpha_i(x+R)]\cos[\beta_i(2qy)]\right] \times \cos(k_z Z)\\
E_z &= -\left(\frac{j\chi^2}{\omega\mu\varepsilon}\right) A_a \left[\sum_{i=1}^{3}\cos[\alpha_i(x+R)]\sin[\beta_i(2qy)]\right] \times \sin(k_z Z)\\
H_x &= \left(\frac{1}{\mu}\right) A_a \left[\sum_{i=1}^{3}(2q\beta_i)\cos[\alpha_i(x+R)]\cos[\beta_i(2qy)]\right] \times \sin(k_z Z)\\
H_y &= -\left(\frac{1}{\mu}\right) A_a \left[\sum_{i=1}^{3}(-\alpha_i)\sin[\alpha_i(x+R)]\sin[\beta_i(2qy)]\right] \times \sin(k_z Z)
\end{aligned} \tag{2}$$

$$H_z = 0$$

where A_s, A_a are constants for even and odd mode respectively, k_z denotes the wave number in z-direction into the resonator and χ is composite wave number along x and y-direction togetherly and

$$\begin{aligned}
&\alpha_1 = \frac{\pi l}{H}, \quad \beta_1 = \frac{\pi}{2}\left[J(m-l) + \frac{(m+l)}{G}\right], \quad r = \left(\frac{b}{2}\right)\tan\left(\frac{\pi}{12}\right)\\
&\alpha_2 = \frac{\pi m}{H}, \quad \beta_2 = \frac{\pi}{2}\left[J(n-m) + \frac{(n+m)}{G}\right], \quad R = r/\sin\left(\frac{\pi}{3}\right)\\
&\alpha_3 = \frac{\pi n}{H}, \quad \beta_3 = \frac{\pi}{2}\left[J(l-n) + \frac{(n+l)}{G}\right], \quad p = \left(\sqrt{6}-\sqrt{2}\right)/4\\
&l+m+n = 0, \quad \{l,m,n\} = 0, \pm 1, \pm 2, \pm 3 \ldots\\
&q = \left(\sqrt{6}+\sqrt{2}\right)/4, \quad Q = 2+\sqrt{3}, \quad S = 2-\sqrt{3}, \quad t = \sqrt{3}/2\\
&g = \frac{1}{2p}, \quad G = (gr+2tR), \quad H = (gr+R), \quad J = \frac{SG}{H^2 Q}\\
\text{and} \quad &\chi^2 = \frac{2}{3}\pi^2\left[\frac{S}{H^2} + \frac{Q}{4}\left(3J^2 + \frac{1}{G^2}\right)\right](m^2+mn+n^2)
\end{aligned} \tag{3}$$

Resonant frequency can be found by solving $\chi^2 + k_z^2 = \varepsilon_r k_o^2$, and $k_z \tan(k_z h - \pi/2) = \sqrt{(\varepsilon_r - 1)k_o^2 - k_z^2}$ togetherly where k_o denotes the free space wave number.

The ratio of theoretical resonant frequency of semicircular and circular tube is 1.4 but the exact value is 1.6. This is because of the magnetic lines avoid corners in semicircular tube which makes the effective area small than the actual area. Using this concept and assuming that maximum energy passes through the in-circle of isosceles 120° triangle, the effective base (opposite side of ∠120° and effective median length is

$$b_{eff} = b - (b - 2r)/A \tag{4}$$

$$M_{eff} = M - (M - 2r)/A \tag{5}$$

$$h_{eff} = h(1 - 1/\varepsilon_r) \tag{6}$$

where b, M, h, r are base, median, height and in-radius respectively and

$$A = 1.5 \tag{7}$$

Table 1 shows simulated (fr_{sim}) and computed resonant frequency using above theory (fr_{the}) of isosceles ∠120° triangle.

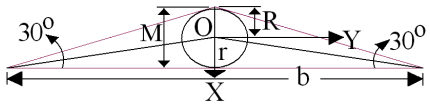

Figure 1: Geometry of isosceles ∠120° triangle.

Table 1: Comparison of resonant frequency TM^z_{101} mode.

ε_r	M (mm)	h (mm)	Resonant Frequency (GHz)			Error (%)	
			fr_{sim}	Overfelt	fr_{the}	Overfelt	Theory
10	5	5	11.5	9.5460	11.57	−16.9913	0.6087
10	7	7	8.15	6.8190	8.2630	−16.3313	1.3865
10	9	9	6.35	5.3030	6.4270	−16.4882	1.2126
10	11	11	5.2	4.3390	5.2580	−16.5577	1.1154
10	13	13	4.4	3.6720	4.4490	−16.5455	1.1136
10	15	15	3.8	3.1820	3.8560	−16.2632	1.4737

Study and Analysis of GUNN Loaded Active Microstrip Patch Antenna

Sanghamitra Dasgupta and Bhaskar Gupta
Department of Electronics and Tele-Communication Engineering
Jadavpur University, Kolkata-700 032, India

Abstract— An antenna with some active processing elements before intercepting or producing electromagnetic wave is called an active antenna. But since the active element should have an impact on the interception of the radiation of the electromagnetic waves, an active fully integrated antenna can be defined as "an antenna whose radiation properties are intimately associated with an active element or elements behavior". Active antennas reduce size, weight and cost over conventional designs which are very useful in microwave systems.

Gunn diode is a two terminal device, which like a normal diode exhibits non linear I-V characteristics but has a negative resistance region. GUNN diode must be biased within the negative resistance region to produce a RF output signal. DC voltage is applied to the diode along a path known as the radial line transformer which is a complex device that acts as the bias circuitry for the diode; the components and their magnitudes therein are crucial. The negative differential impedance of the Gunn diode is modeled by a complementary pair of JFETs in Ansoft Designer and the GUNN diode I-V characteristics plot is done showing the negative resistance region as shown in Figs. 1 and 2. Using the GUNN diode model, Gunn relaxation oscillator is designed as shown in Fig. 3 and the Oscillator response using GUNN diode is shown in Fig. 4. This circuit will operate properly if the DC source resistance is less than the diode negative impedance and also if the load-line intersects the active characteristic in the negative impedance region. The AC impedance of the DC source should be very high in order to ensure that the bias point becomes astable. The first and last conditions can be met by the transforming properties of a quarter-wavelength transmission line.

Here an active microstrip patch antenna design has been presented which is simulated and analyzed at 9.5 GHz (experimental results awaited). This active antenna is designed integrating a GUNN diode, by connecting it to the patch through a microstrip transformer. *S*-parameter

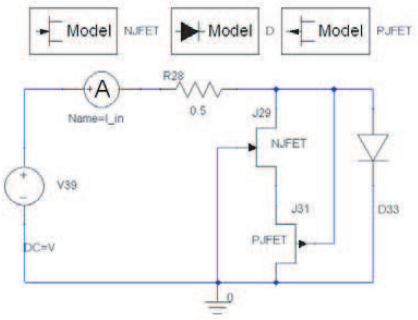

Figure 1: GUNN diode modeled using FET.

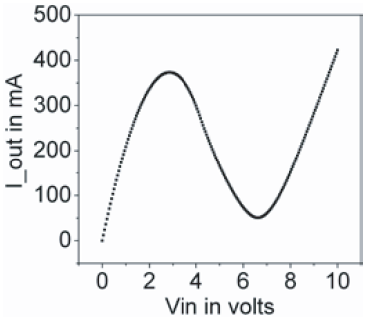

Figure 2: GUNN diode I-V characteristics plot.

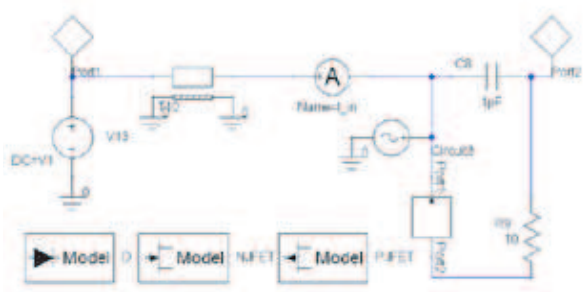

Figure 3: GUNN diode relaxation oscillator modeled using FET.

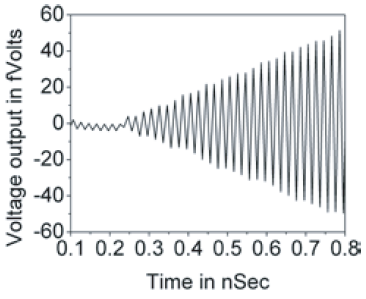

Figure 4: Oscillator response using GUNN diode.

plots for both the passive and active antenna has been done. Comparing active and the passive antenna system BW has been increased by 10.9% which is predicted by analyzing the Q-value of the system. In this work the active device and the patch has been considered as a composite unit instead of taking them as independent units whereas in conventional wireless or radar systems antenna and circuit are being considered as separate. The main disadvantage of antenna circuit integration is contradictory requirements of systems. Thick, low dielectric constant substrates are required to enhance microstrip antenna efficiency but thin, high dielectric constant substrates are needed for good circuit action. Also since efficiency of a single Gunn diode is very low proper heat sink design is very important. However this limitation can be avoided if we design large phased arrays where transmit-receive function is distributed across the array. Personal communications and vehicle telematics are areas where future requirements may be fulfilled with integrated circuit-antenna modules. Also one of the applications of this technology is single chip transceiver where antenna, transmitter and receiver are made on a single semiconductor substrate. The purpose of the active antenna design is to obtain maximum radiated power from the antenna so that the antenna developed can be applied in the field of transfer of DC power through wireless links to construct X-band link. The design and simulation results of this paper will be used to develop a practical active rectenna system to make a wireless DC charger.

Session 3A5
FDTD Methods and Applications

Comprehensive Comparison of FDTD Algorithms for Kerr Nonlinearities

Ivan S. Maksymov[1], **Andrey A. Sukhorukov**[1], **Andrei V. Lavrinenko**[2], **and Yuri S. Kivshar**[1]

[1]Nonlinear Physics Centre, Research School of Physics and Engineering
Australian National University, Canberra ACT 0200, Australia
[2]Department of Photonics Engineering, Technical University of Denmark
2800 Kongens Lyngby, Denmark

Abstract— Accurate finite-difference time-domain (FDTD) modeling of optical pulse propagation in nonlinear media usually implies the use of auxiliary differential equation (ADE) techniques. The updating of electric field in full-vectorial 3D ADE FDTD modeling of the optical Kerr effect and two-photon absorption in optical media is proceeded conventionally through the iterative solution of nonlinear algebraic equations. We study three approaches for the field update including simple non-iterative explicit schemes. By comparing them with the analytical results for optical pulse propagation in long nonlinear media (nonlinear phase incursion for the pump wave of about π radians), we demonstrate convincingly that simple non-iterative FDTD updating schemes, which are commonly believed to be inaccurate and unstable, produce accurate results and drastically speed up the computation as compared with ADE approaches. Such schemes can significantly reduce the CPU time for nonlinear computations, especially in 3D models.

The capability of an FDTD method to solve problems of electromagnetic wave interactions with materials having frequency-dependent nonlinear optical properties [1] keeps this method among the most universal and powerful numerical tools for optics, electrodynamics, antennas, and waveguides theory. An essential part of every modern FDTD simulator is the implementation of auxiliary differential equation (ADE) FDTD techniques that drastically broaden the use of the FDTD method and its calculation accuracy. Recently, Dissanayake et al. [2] proposed an extended 3D FDTD scheme for modeling optical phenomena in silicon waveguides, which takes into account material anisotropy of the third-order electronic and Raman susceptibilities.

ADE FDTD schemes for materials with multiple-pole linear Lorentz, instantaneous Kerr, two-photon absorption-induced and Raman nonlinear polarizations require to find solution of a system of nonlinear coupled equations at every time step. In the case of anisotropic media the coupled update equations for the electric field components involve three auxiliary variables [2] that, in turn, are nonlinear functions of all three electric field components. Additionally, the denominators of two out of three auxiliary variables contain electric field terms that can in principle diverge if corresponding field values approach to zero. Therefore, general 3D FDTD modeling of nonlinear waves in Si waveguides might encounter numerical problems with the proposed iterative algorithm.

We perform a comprehensive comparison of alternative non-iterative approaches [3, 4] against the iterative one [2] and the approximate analytical solution to clarify their constraints and limits in applications. The findings support our hypothesis that the non-iterative schemes are stable and reasonably accurate. They can be recommended for a broad range of problems especially addressing the designs with complex 3D topology, where iterative solutions of coupled nonlinear equations can be unstable and resource-claiming.

REFERENCES

1. Greene, J. H. and A. Taflove, *Opt. Express*, Vol. 14, 8305–8310, 2006.
2. Dissanayake, C. M., M. Premaratne, I. D. Rukhlenko, and G. P. Agrawal, *Opt. Express*, Vol. 18, 21427–21448, 2010.
3. Maksymov, I. S., L. F. Marsal, and J. Pallares, *Opt. Commun.*, Vol. 239, 213–222, 2004.
4. Maksymov, I. S., A. A. Sukhorukov, A. V. Lavrinenko, and Yuri S. Kivshar, *Ant. Wireless Propagat. Lett.*, Vol. 10, 143–146, 2011.

BPM and FDTD Analyses of a Metal-insulator-metal-type Terahertz Waveguide

J. Shibayama, **Y. Uchizono**, **J. Yamauchi**, **and H. Nakano**
Faculty of Science and Engineering, Hosei University, Tokyo 184-9594, Japan

Abstract— A metal-insulator-metal-(MIM-) type waveguide is numerically analyzed for the transmission of a terahertz wave, in which the metal dispersion is taken into account. The eigenmode of the MIM waveguide is calculated using the imaginary-distance technique with the Yee's-mesh-based BPM (YM-BPM) [1]. The skin depth from the silver/air surface is found to be about 70 μm, where the width of the air core is 1 μm. As a result, the spatial sampling widths Δx should be quite small, e.g., 62.5 nm. In this case, the mesh density $\lambda/\Delta x$ is 4800, which may impose a considerable burden on the FDTD analysis.

The eigenmode obtained from the YM-BPM is next used as an input field for the frequency-dependent finite-difference time-domain (FDTD) analysis. The trapezoidal recursive convolution (TRC) technique is used for the convolution calculation, in which the metal dispersion of silver is expressed by the Drude model. Unfortunately, the computation time is quite long, because of the extremely small time step resulting from the small spatial sampling widths.

Then, the implicit locally one-dimensional (LOD) FDTD [2–5] is introduced for efficient calculations. The LOD-FDTD, a simple type of the split-step approach [6], yields a quite simple algorithm compared to the ADI counterpart. Taking advantage of the unconditional stability, we can adopt a large time step beyond the stability limit. Consequently, the propagating field obtained from the TRC-LOD-FDTD [7] agrees well with that from the explicit FDTD. It is worth mentioning that the computational time is significantly reduced, due to the use of a time step 50 times as large as the explicit counterpart.

REFERENCES

1. Yamauchi, J., T. Mugita, and H. Nakano, "Implicit Yeemesh-based finite-difference full-vectorial beam-propagation method," *J. Lightw. Technol.*, Vol. 23, No. 5, 1947–1955, 2005.
2. Shibayama, J., M. Muraki, J. Yamauchi, and H. Nakano, "Efficient implicit FDTD algorithm based on the locally one-dimensional scheme," *Electron. Lett.*, Vol. 41, No. 19, 1046–1047, 2005.
3. Do Nascimento, V. E., B.-H. V. Borges, and F. L. Teixeira, "Split-field PML implementations for the unconditionally stable LOD-FDTD method," *IEEE Microw. Wireless Compon. Lett.*, Vol. 16, No. 7, 398–400, 2006.
4. Tan, E. L., "Unconditionally stable LOD-FDTD method for 3-D Maxwell's equations," *IEEE Microw. Wireless Compon. Lett.*, Vol. 17, No. 2, 85–87, 2007.
5. Ahmed, I., E. K. Chua, E. P. Li, and Z. Chen, "Delvelopment of the three-dimensional unconditionally stable LOD-FDTD method," *IEEE Trans. Antennas Propagat.*, Vol. 56, No. 11, 3596–3600, 2008.
6. Fu, W. and E. L. Tan, "Development of split-step FDTD method with higher order spatial accuracy," *Electron. Lett.*, Vol. 40, No. 20, 1252–1254, 2004.
7. Shibayama, J., A. Nomura, R. Ando, J. Yamauchi, and H. Nakano, "A frequency-dependent LOD-FDTD method and its application to the analyses of plasmonic waveguide devices," *IEEE J. Quantum Electron.*, Vol. 46, No. 1, 40–49, 2010.

An Explicit Fractional Step Scattered Field Formulation for Modeling General Lossy Media in the FDTD Technique

H. H. Abdullah[1] and A. Mohsen[2]

[1]Microwave Department, Electronics Research Institute (ERI), Dokki, Giza, Egypt
[2]Faculty of Engineering, Cairo University, Giza, Egypt

Abstract— During the last two decades, the finite difference time domain (FDTD) method becomes one of the most efficient and flexible electromagnetic numerical techniques. The accuracy of the technique is the main concern of many researchers since it is a key issue in modeling real life problems. In this paper, a formulation based on dividing the computational time step in two fractional steps to solve the scattering from a general lossy media will be presented. From Maxwell equations, every field components has variations only with the two directions perpendicular to each field component. Thus, the computational time step will be splitted into two fractional steps. In the first fractional step, each field component will be allowed to vary in only one of the two directions perpendicular to the direction of this field component. In the next fractional step, the variations in the remaining direction will be allowed. So, instead of updating the fields in the two perpendicular directions at one step, they will be updated in two fractional steps. This will provide more accurate computations of the fields without the need for more memory storage or additional computational time. Another important parameter in the accuracy of computations is the method of computing the incident field. The incident field may be computed in a total field formulation or in a scattered field formulation. In the total field formulation, the incident field will propagate in the FDTD lattice which may add some error due to numerical computations. In this paper, the scattered field formulation will be adopted where the incident electric field will be computed analytically at each spatial cell which results in no error in the incident field computations and thus yielding more accurate computation of the scattered fields. The proposed method is tested for 3D problems and the accuracy is proved.

Unified Efficient Fundamental ADI-FDTD Schemes for Lossy Media

Ding Yu Heh and Eng Leong Tan
School of Electrical and Electronic Engineering, Nanyang Technological University, Singapore

Abstract— This paper presents the unified efficient fundamental alternating-direction-implicit finite-difference time-domain (ADI-FDTD) schemes for lossy media. A novel exponential time differencing scheme for ADI-FDTD is introduced. Other existing schemes include averaging, forward-forward and forward-backward. Unifications of these schemes in both conventional and efficient fundamental forms of source-incorporated ADI-FDTD are provided. In the latter, they are formulated in the simplest, most concise, most efficient, and most fundamental form of ADI-FDTD. The unified update equations and implementation of the efficient fundamental ADI-FDTD schemes are provided. Such efficient fundamental schemes have substantially less right-hand-side update coefficients and field variables compared to the conventional ADI-FDTD schemes. Thus, they feature higher efficiency with reduced memory indexing and arithmetic operations. A Table is provided to show the comparisons of number of arithmetic operations per grid between conventional and efficient fundamental forms of ADI-FDTD schemes for lossy media over one complete time step. The table clearly indicates that the efficient fundamental form of ADI-FDTD schemes have lesser multiplications/divisions (M/D) and additions/subtractions (A/D) operations compared to the conventional form of ADIFDTD schemes. Numerical results show that the efficient fundamental ADI-FDTD schemes can achieve efficiency gain as high as 2.5 over the conventional ADI-FDTD schemes in terms of Central Processing Unit (CPU) run time. In terms of accuracy, the proposed exponential time differencing scheme of ADI-FDTD exhibits the lowest numerical error in both time and frequency domains among all other schemes. For forward-backward scheme, numerical results show that it exhibits significant perfect electric and magnetic conductors field leakage, and has the highest asymmetry and numerical errors among all other schemes. It shall be pointed out here that while it was shown in past literatures that the forward-backward scheme of an *independent* source, J is accurate and has lower electric field asymmetry error, similar argument cannot be applied here if the source is *dependent* on electric field, such as in the case of lossy media where $J = \sigma E$.

An Unconditionally-stable FDTD Method with Low Anisotropy in Three-dimensional Domains

Yong-Dan Kong[1] **and Qing-Xin Chu**[1, 2]

[1]School of Electronic and Information Engineering
South China University of Technology, Guangzhou, Guangdong 510640, China
[2]The State Key Laboratory of Millimeter Waves, Nanjing, Jiangsu 210096, China

Abstract— Recently, to remove the Courant-Friedrichs-Lewy (CFL) limitation on the time step size of the FDTD method, an unconditionally-stable FDTD method based on the alternating direction implicit (ADI) technique was developed. The ADI-FDTD method has second-order accuracy both in time and space. However, it presents large numerical dispersion error with large time steps. Subsequently, other unconditionally-stable methods such as spit-step and locally-one dimensional (LOD) FDTD methods were developed. The LOD-FDTD method can be considered as split-step approach (SS1) with first-order accuracy in time, which consumes less CPU time than that of the ADI-FDTD method. Subsequently, to improve the accuracy, unconditionally-stable split-step FDTD methods with high-order accuracy and low dispersion were proposed. However, these methods are proposed in two-dimensional (2-D) domains.

To achieve high-order accuracy and low anisotropy, a novel unconditionally-stable FDTD method in 3-D domains is proposed in this paper, which is based on the split-step scheme and has four sub-steps. The 3-D Maxwell's equations can be written in a matrix form as $\partial\vec{u}/\partial t = [M]\vec{u}$. Firstly, symmetric operator and uniform splitting are adopted simultaneously to split Maxwell's matrix $[M]$ into four sub-matrices, $[A]/2$, $[B]/2$, $[B]/2$, and $[A]/2$, respectively. Accordingly, the time step is divided into four sub-steps. After some manipulations, four sub-procedures are generated as follows,

$$\begin{aligned}
([I] - \Delta t/4 \cdot [A])\vec{u}^{n+1/4} &= ([I] + \Delta t/4 \cdot [A])\vec{u}^{n} \\
([I] - \Delta t/4 \cdot [B])\vec{u}^{n+2/4} &= ([I] + \Delta t/4 \cdot [B])\vec{u}^{n+1/4} \\
([I] - \Delta t/4 \cdot [B])\vec{u}^{n+3/4} &= ([I] + \Delta t/4 \cdot [B])\vec{u}^{n+2/4} \\
([I] - \Delta t/4 \cdot [A])\vec{u}^{n+1} &= ([I] + \Delta t/4 \cdot [A])\vec{u}^{n+3/4}.
\end{aligned}$$

Then, the proposed scheme is generalized. Secondly, the proposed method is proven to be unconditionally-stable by using the Fourier method. In addition, the dispersion relation of the proposed method is carried out.

Thirdly, the numerical dispersion and the anisotropy performances of the proposed method have been studied for different parameters such as the propagation angle, the mesh size and the time step. Specifically, with CFLN = 2, CPW = 10, $\theta = 0^\circ$, the normalized numerical phase velocity error of the proposed method is reduced by more than 53% in comparison with the ADI-FDTD method and the LOD-FDTD method. Moreover, the dispersion errors of three unconditionally-stable FDTD methods increase as CFLN increases. Nevertheless, the increase of the dispersion error of the proposed method is much less pronounced than those of the ADI-FDTD method and the LOD-FDTD method. Furthermore, the proposed method with the coarsest mesh leads to the same level of accuracy as the ADI-FDTD method with the finest mesh. Such an improvement of the accuracy, which is realized by the proposed method with the coarsest mesh, lead to other advantages, such as higher computational efficiency and lower memory requirements. The normalized phase velocity anisotropic errors increase as CFLN increases. However, the normalized phase velocity anisotropic error of the proposed method is lower than the other two methods. Particularly, for the proposed method, corresponding to a certain CPW, there is a CFLN value causing the numerical phase velocity anisotropic error to be zero. The normalized phase velocity anisotropic errors decrease as CPW increases, and similarly, the normalized phase velocity anisotropic error of the proposed method is lower than the other two methods. Specifically, for the proposed method, corresponding to a certain CFLN value, there is a CPW value making the normalized phase velocity anisotropic error to be zero.

SAR Computation of a Human Head Exposed to Different Mobile Headsets Using FDTD Method

Reza Aminzadeh[1, 2], **Mehrangiz Ashiri**[1, 2], **and Ali Abdolali**[1, 3]

[1]Bioelectromagnetics Research Group
Iran University of Science and Technology, Tehran, Iran
[2]School of Science and Engineering
Sharif University of Technology, International Campus, Kish Island, Iran
[3]Department of Electrical Engineering
Iran University of Science and Technology, Tehran, Iran

Abstract— Many standards are not considering Specific Absorption Rate (SAR) measurements with the use of mobile headsets. In this paper a simulation of mobile headset effects on a human head is done using FDTD-based platform, SEMCAD-X software. We designed two headset models with different case materials to observe their interaction with a Specific Anthropomorphic Mannequin (SAM) phantom as a human head model. Both headset models are installed in the left ear and the human head is rotated by 30°. As headset communicates via Bluetooth at the frequency of 2.4 GHz, we chose a suitable planar inverted F antenna (PIFA) to use with both the headset models. Spatial peak SAR values averaged over 1g and 10g for each model in both the environments and compared to each other. The results confirm that the value of SAR in a car is lower than free space due to the presence of dielectric materials in the car. We conclude that headset case material has a high impact on SAR changes in different environments.

FDTD Simulation of an Arbitrary Shape in Google SketchUp

Yong-Gu Lee
Gwangju Institute of Science and Technology, South Korea

Abstract— Although in practice only simple shapes are being used, Finite-Difference Time-Domain (FDTD) simulation can be applied for arbitrary geometry. This requires a preprocessing tool that can input a designed shape and generate the discretized grid data where permittivity and permeability are enumerated on structured three-dimensional array of space-mapped cells. The tool needs to efficiently process the location of each cell and decide the point location queries with respected to the shape boundary. There are tools that exist in many commercially available Computer-Aided Design and Analysis software who can do this for numerical simulation methods such as Finite Element Methods. However such tools are not widely available for FDTD methods. Rather, most FDTD design tools only support primitive shapes such as spheres, cylinders or cones and in some cases support two and half-dimensional shapes that are not true three-dimensional shapes.

In this paper, we describe the design and implementation of a FDTD grid model generation tool utilizing the Application Procedural Interface (API) offered by free shape design software called Google SketchUp. Although SketchUp does not support free-form surfaces and only support polygonal surfaces, it can model arbitrary polyhedral shapes that are two-manifold. And this representation is precise enough for modeling shapes that will eventually be discretized. This grid generation tool is offered as a part of BeaconFDTD, a plug-in for Google SketchUp that can do optical simulation based on FDTD method. The result is a fully functional shape modeling and optical simulation package that works on an advanced and free shape modeling environment.

ACKNOWLEDGMENT

This research was supported by Basic Science Research Program through the National Research Foundation of Korea (NRF) funded by the Ministry of Education, Science and Technology (grant number (2011-0027395) and by a grant from the institute of Medical System Engineering (iMSE) in the GIST, Korea.

Transient Electromagnetic Response of a Coaxial Feeding Monopole Antenna Mounted on a Rectangular Metallic Enclosure Illuminated by Electromagnetic Pulses (EMP)

Qingqing Zhang[1], **Jian Wang**[1], **and Wen-Yan Yin**[1, 2]

[1]Center for Microwave and RF Technologies
Key Lab of Ministry of Education of EMC and High-Speed Electronic Systems
Shanghai Jiao Tong University, Shanghai 200240, China
[2]Center for Optical and EM Research (COER), State Key Lab of MOI
Zhejiang University, Hangzhou 310058, China

Abstract— It is well known that feed networks of antennas in most information systems can be interfered by external electromagnetic pulses (EMPs), and under such circumstances, source integrity problem will be caused and the system performance will be degraded obviously. Thus, it is essential to investigate the transient electromagnetic responses of these systems so as to guide our electromagnetic compatibility (EMC) design and take electromagnetic protection against electromagnetic interference (EMI).

Transient electromagnetic coupling responses of a coaxial feeding line for a monopole antenna mounted on a rectangular metallic enclosure with a window are investigated in this presentation, as shown in Fig. 1. The electromagnetic fields in the environment will produce induced current on the antenna and it couples into the coaxial feeding cable through the interaction at the connection point between the coaxial cable and the monopole antenna. On the other hand, the electromagnetic fields penetrating into the shielding enclosure through the window also have an impact on the coaxial cable due to the transfer impedance. Both coupling paths above provide directive electromagnetic energy coupling on the coaxial feeding line when there are incident external intentional or non-intentional electromagnetic pulses illuminating the structure.

The mathematical treatment is based on the hybrid FDTD method with coaxial feed model, transfer impedance coupling model, and thin wire antenna model integrated together for handling such a complex three-dimensional (3D) composite structure. The modified monopole antenna coupling model will be verified by comparing our calculated terminal voltage and current responses of the coaxial feeding cable in the enclosure with that of the direct transmission line coupling method. The incident EMPs can be the Gaussian pulse or double-exponential pulse with very high field strength and different incident directions and polarization states. Some regularity conclusions and suggestions for EMC design will be presented after the calculation results analysis.

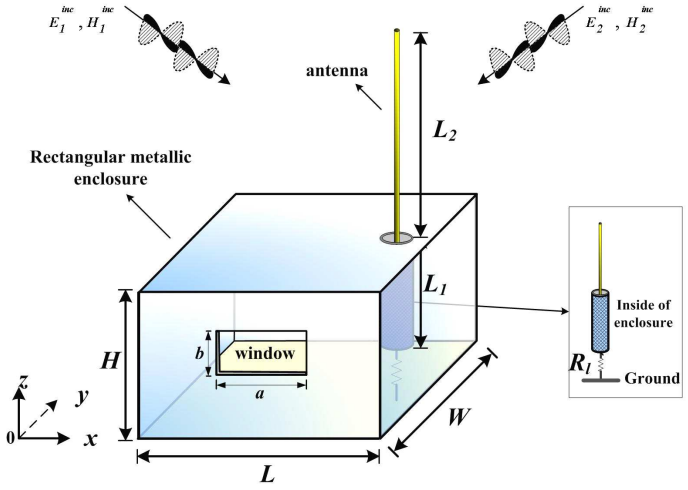

Figure 1: Geometry of a coaxial feeding monopole antenna mounted on a metallic rectangular enclosure with one window illuminated by external EMPs.

Session 3A6
Systems and Components, Electromagnetic Compatibility 2

Effect of Electromagnetic Interference (EMI) on the DC Shift, Harmonic and Intermodulation Performance of NMOSFET Current Mirror

Muhammad Taher Abuelma'atti[1] and Ali M. T. Abuelmaatti[2]

[1]King Fahd University of Petroleum and Minerals, Box 203, Dhahran 31261, Saudi Arabia
[2]RFMD (UK) Ltd., Millennium Way, Newton Aycliffe, County Durham DL5 6JW, UK

Abstract— At present there is a growing interest in designing current-mode circuits; where the input is a current and the output is a current. This is attributed to their simple structures, wider bandwidth and larger dynamic range compared to the voltage-mode circuits; where the input is a voltage and the output is a voltage. Current-mirrors using NMOSFET transistors play a crucial part in the design of current-mode circuits.

The NMOSFET current-mirror is inherently nonlinear. This nonlinearity manifests itself in generating unwanted DC components; which may alter the correct biasing and may therefore prohibit the circuit from functioning correctly. Moreover, in addition to the unwanted DC, unwanted harmonics and intermodulation products may be generated when a multisinusoidal electromagnetic interfering (EMI) signal is superimposed on the DC biasing current. These effects have been extensively studied for MOSFET and bipolar transistors and operational amplifiers. However, only very little has been written about these effects in NMOSFET current-mirrors assuming that the amplitude of the EMI signal is relatively small [1]. This assumption paves the way for using a Taylor series expansion for approximating the nonlinearity of the NMOSFET current-mirror, thus, restricting the validity of the results to relatively small EMI signals only. No attempt has been reported for studying the DC shift, the harmonic and intermodulation performance of the NMOSFET current-mirror under relatively large EMI signal.

In this paper, a new approximation is presented for the input current-output current nonlinear relationship of the NMOSFET current-mirror. Using this expression closed-form expressions are obtained for the DC and the amplitudes of the fundamental, second- and third-harmonic and intermodulation components of the output current resulting from exciting the NMOSFET current-mirror by a DC biasing current plus a superimposed multisinusoidal EMI. Comparison between calculated and simulated results is included.

REFERENCES

1. Redoute, J.-M. and M. Steyaert, *EMC of Analog Integrated Circuits*, Springer Sciences + Business Media, 2010.

Near-field Characterization of a Printed Circuit Board in the Presence of a Finite-sized Metallic Ground Plane

O. Franek[1], **M. Sørensen**[2], **H. Ebert**[1], **and G. F. Pedersen**[1]

[1]APNet Section, Department of Electronic Systems, Faculty of Engineering and Science
Aalborg University, Niels Jernes Vej 12, Aalborg 9220, Denmark
[2]Bang & Olufsen a/s, Peter Bangs Vej 15, Struer 7600, Denmark

Abstract— An electronic apparatus consisting of one or several modules may often not fulfil requirements on electromagnetic compatibility (EMC) in terms of radiation, in spite of the fact that the particular modules may pass the requirements. There has been a growing interest in the possibility of identifying such situations early in development stage of the modules, since later changes in the design of the apparatus are costly. Electromagnetic simulations of the interaction between the modules and the apparatus have been instrumental to achieve this goal. As it is not always possible to simulate a full model of the electronic module, designers often resort to characterizing the module by the near fields it produces, whereas these fields are obtained by measurement.

According to Love's equivalence theorem, an arbitrary source of electromagnetic field (the module, in our case) can be replaced by electric and magnetic currents running over a surface entirely enclosing the source, whereas the currents are uniquely determined by electric and magnetic fields tangential to the surface (and obtained by measurement, in our case). For this theorem to hold, linearity must be ensured, and the sources have to be placed in a free space. However, it is the latter condition that cannot be fulfilled in practice, since we desire to use the currents to characterize the module in the presence of other objects belonging to the apparatus enclosing the module, not in free space. In our study, we focused on this problem, and attempted to quantify the disturbance of the equivalence theorem by a finite-size metallic ground plane placed near the equivalent sources, which we see as a common example occurring in real conditions.

First, a generic printed circuit board (PCB) with dimensions $150 \times 100\,\mathrm{mm}$ is introduced as a representative of a typical electronic module. Then we use the well-established finite-difference time-domain (FDTD) method to obtain distribution of electromagnetic fields in three distinct situations:

(1) Generic PCB in free space;
(2) Generic PCB in the presence of the metallic ground plane;
(3) Equivalent field sources (obtained from (1)) in the presence of the metallic ground plane.

By comparing (2) and (3) we arrive at maximum errors in electric and magnetic fields surrounding the equivalent sources, while the simulations are performed for various sizes and distances of the ground plane. While at the lower end of the investigated frequency range, at 100 MHz, error of only 14% has been found, at 1 GHz the error reaches 84% due to resonant nature of the field distribution. Since the errors are caused by the absence of the re-scattered fields from the PCB itself, we propose to include the ground plane of the PCB as its major feature inside the equivalent surface. In this arrangement, the peak error drops to acceptable 33% (i.e., at most $-3.5\,\mathrm{dB}$ drop in magnitude).

We conclude that the near-field characterization of a common printed circuit board using Love's equivalence theorem is a feasible technique, even though the conditions for the theorem are not entirely fulfilled. Resulting errors can be mitigated by including major features of the substituted object, without the need to use a full model. In the perspective, it appears to be possible to simulate an apparatus consisting of modules modeled only by their near-field representations, plus a few major features, and estimate unwanted radiation with a high degree of reliability.

Improvement of Absorbing Frequency Bandwidth of Composite Electromagnetic Wave Absorber Made of Granular Sendust Particles Dispersed in Polystyrene Resin

Y. Hongo[1], **K. Sakai**[2], **Y. Sato**[1], **and S. Yoshikado**[1]

[1]Graduate School of Engineering, Doshisha University, Japan
[2]Graduate School of Natural Science and Technology, Okayama University, Japan

Abstract— Development of an electromagnetic wave absorber suitable for frequencies above 10 GHz is required because of the increasing use of wireless telecommunication systems. Composite electromagnetic wave absorber made of sendust dispersed in resin is low-cost and contains no rare metal. The frequency dependences of the relative complex permeability μ_r^*, the relative complex permittivity ε_r^* and the absorption characteristics for composite electromagnetic wave absorbers made of sendust particles dispersed in polystyrene resin were investigated in the frequency range from 100 MHz to 20 GHz. In this study, spherical shaped sendust particles with the average particle size of approximately 5 and 20 µm were dispersed in polystyrene resin with the volume ratio of 20–40 vol% in order to broaden the absorbing frequency bandwidth. To design an absorber, the control of the frequency dependences of μ_r^* and ε_r^* is important because the absorption of an electromagnetic wave is mainly determined by μ_r^* and ε_r^*. The non-reflective condition is satisfied at a desired frequency range is important to design an absorber. Value of μ_r^* can be controlled by changing the volume ratio of sendust in resin. When an electromagnetic wave of high frequency enters sendust particle, eddy current flows on the surface, and a reverse magnetic moment appears in the frequency range from above 10 GHz similar to aluminum particle. Thus, to examine this phenomenon, qualitative theoretical calculation was carried out. The frequency dependence of the relative complex permeability μ_r^* is one factor that improving of absorbing frequency bandwidth in the frequency range from 10 and 20 GHz. Experimental results reveal that the optimal volume mixture ratio of sendust is approximately 30 vol% for the average particle size of approximately 5 µm in order to broaden the absorbing frequency bandwidth.

Delay Response of Gas Discharge Tubes

Milic Pejovic[1], **Momcilo Pejovic**[1], **Radeta Maric**[2], **Ljubinko Timotijevic**[3], **and Koviljka Stankovic**[3]

[1]Faculty of Electronic Engineering, University of Nis
Aleksandra Medvedeva 14, Nis 18000, Serbia
[2]Electric Power Industry of Serbia
Masarikova 1-3, Belgrade 11000, Serbia
[3]Faculty of Electrical Engineering, University of Belgrade
Bulevar kralja Aleksandra 73, Belgrade 11000, Serbia

Abstract— Transient surge voltages, either conducted or coupled, are a rather common occurrence in all electronic circuits, which makes efficient transient voltage suppression (TVS) a primary design requirement. Efficient protection against transient voltages, also called over-voltages, has two aspects: protection of integrity (no permanent damage of the protected device) and maintenance of operational functionality (operation reliability in the event of an over-voltage). Both power systems (providing energy generation, transmission and distribution) and low-voltage electronic systems are susceptible to transient voltages. The widespread use of gas discharge tubes (GDT) for over-voltage protection has been justified, since it has several advantages comparing to the other over-voltage protection components, such as the ability to conduct high currents, low intrinsic capacity, high insulating resistance, broad range of voltage protection, etc. But, the main problem in GDT application is its relatively high response time. Electrical breakdown time delay is often refereed as delay response and it is also very important parameter of gas filled devices. The aim of this paper is to investigate dependence of the GDT delay response on the relaxation time, as well as the to determine the voltage range within which the GDT operate reliably.

Radiation Induced Noise Level in Solar Cells

Milos Zdravkovic[1], **Aleksandra Vasic**[2], **Bojan Cavric**[1], **Radovan Radosavljevic**[1], **and Koviljka Stankovic**[1]

[1]Faculty of Electrical Engineering, University of Belgrade
Bulevar Kralja Aleksandra 73, Belgrade 11000, Serbia
[2]Faculty of Mechanical Engineering, University of Belgrade
Kraljice Marije 16, Belgrade 11000, Serbia

Abstract— One of main characteristics of all detectors is energy resolution which primarily depends on noise. Negative influence of noise on the detector functioning is in widening of the spectral line of the impuls signal and rasing the detection threshold, and that is main limiting factor for detector functioning. That is the reason why lowering noise level is very important precondition for obtaining a good quality detectors, so investigation of physical basis of different types of noise is necessary for their optimization. It could be said that regardless of the detector quality, noise is present in all detectors and it depends on fundamental physical processes during fabrication and operation of these devices. The most common source of noise that is connected to the hostile working conditions is radiation. During the interaction with the material, radiation could deposit large amount of energy that could induce various effects. Due to their wide range of application, solar cells are exposed to various kinds of radiation in working environment. From the technological point of view it is very important to establish changes in output characteristics of the device (current, voltage, and efficiency) induced by the radiation that affect their operation. The aim of this paper is to investigate increased noise level in solar cells due to radiation in order to facilitate the production of more reliable devices.

Radiation Effects in Cooper Pair Insulating Thin Films

Djordje Lazarević[1], **Edin Dolićanin**[2], **Bratislav Iričanin**[2], **Miloš Vujisić**[2], **and Koviljka Stankovic**[2]

[1]Radiation Protection Department, Institute of Nuclear Sciences Vinca
Mike Alasa 12-14, Belgrade 11000, Serbia
[2]Faculty of Electrical Engineering, University of Belgrade
Bulevar kralja Aleksandra 73, Belgrade 11000, Serbia

Abstract— Cooper-pair insulators are materials that exhibit superconducting behavior, but under specific conditions, regarding film thickness, bias voltage, applied magnetic field, and presence of magnetic impurities, act as insulators with thermally activated Cooper pairs as charge carriers. This paper investigates possible radiation effects in thin films of such materials. Radiation effects are predicted on the basis of Monte Carlo simulations, using 2D Josephson junction array as a model of material structure. Results of a combined theoretical and numerical analysis suggest that radiation-induced change of the Josephson junction charging energy could significantly affect the current-voltage characteristics of a Cooper-pair insulator, and that a transition to a metallic state is possible, due to radiation-induced disruption of the fine-tuned granular structure. The breaking of Cooper pairs, caused by incident and displaced ions, can also destroy the conditions for this specific insulating state to exist.

Expressing the Measurement Uncertainty of the Non-ionizing Radiation Survey in the Vicinity of GSM Base Stations

Branislav Vulevic[1], **Dragan Kovacevic**[2], **and Predrag Osmokrovic**[3]

[1]Public Company Nuclear Facilities of Serbia, Belgrade, Serbia
[2]Institute of Electrical Engineering "Nikola Tesla", Koste Glavinića 8a, Beograd 11000, Serbia
[3]Faculty of Electrical Engineering, University of Belgrade, Belgrade, Serbia

Abstract— The use of wireless communications devices has been increasing rapid over the past decades. Simultaneously with development of these technologies, increase public concerns about health risks of exposure to RF radiation for people residing in the vicinity of the GSM BS antennass. The public concern about the adverse effects has grown in the past ten years. The increasing number of cellular telephony subscribers has led an expansion of networks, with the installation of more base stations. This paper presents a summary values for broadband measurements of the radiofrequency (RF) radiation in the vicinity of GSM base stations (GSM BS). It will be useful for determination of non-ionizing radiation exposure levels of the general public in future. The purpose of the paper is an appropriate representation of the basic information on the expresing of measurement uncertainty.

Uncertainty Evaluation of Conducted Emission Measurement by the Monte Carlo Method and the Modified Least-squares Method

Aleksandar Kovačević[1], **Dragan Kovačević**[2], **and Predrag Osmokrović**[3]

[1]Department of Electromagnetic Compatibility and Environmental Conditions
Technical Test Centre, Vojvode Stepe 445, Belgrade 11000, Serbia
[2]Institute of Electrical Engineering Nikola Tesla
Koste Glavinića 8a, 11000 Belgrade 11000, Serbia
[3]Faculty of Electrical Engineering, University of Belgrade
Bulevar kralja Aleksandra 73, P. O. Box 3554, Belgrade 11000, Serbia

Abstract— This paper presents a new model which uses mixed distribution for evaluation of conducted emission measurement. Evaluation of PDF (probability density function) for the measurand has been done by using a Monte Carlo method and a modified least-squares method. For illustration, the evaluation is applied in three cases for two independent input quantities. Namely, the combined method is used for the evaluation of PDF for the output quantity (mixed distribution) according to PDF from two independent input quantities, i.e., two independent input quantities assigned by the normal distributions, in the second case from two independent input quantities where the first quantity is assigned a normal distribution and the second is assigned a rectangular distribution and in the third case from two independent input quantities where the first quantity is assigned a normal distribution and the second is assigned a triangular distribution. The results obtained by the Monte Carlo method and the modified least-squares method are compared to the corresponding results when applying the standard GUM (Guide to the Expression of Uncertainty in Measurement) procedure.

Radiation Induced Change of Serial PNP Power Transistor's Dropout Voltage in Voltage Regulators

Vladimir Vukić[1] and Predrag Osmokrović[2]

[1]Institute of Electrical Engineering "Nikola Tesla", University of Belgrade, Belgrade, Serbia
[2]Faculty of Electrical Engineering, University of Belgrade, Beograd, Serbia

Abstract— Previous examinations of voltage regulators "National Semiconductor" LM2940CT5 and "STMicroelectronics" L4940V5 in γ radiation field pointed on similar influences of geometry of serial pnp transistor and its perimeter-to-area ratio on degradation of the transistor's forward emitter current gain. It was also perceived that even drastic fall of forward emitter current gain does not necessary lead to significant decrease of integrated circuit's radiation hardness, especially in the case of voltage regulators, devices with the negative feedback loop. In the previous papers were presented results of change of the maximum output current and its influence on serial transistor's forward emitter current gain. In this paper were presented new results on this topic, but the main examined value was the serial transistor's dropout voltage.

Foregoing results pointed on high radiation hardness of BiCMOS voltage regulators "STMicroelectronics" L4940V5 with vertical pnp transistors, also as very low radiation tolerance of conventional monolithic bipolar devices "National Semiconductor" LM2940CT5 with round lateral pnp transistors. Presented results related on data of maximum output current indicated on high possibility of making an error in detemination of device's radiation hardness based on experiments that only analyze a change of the forward emitter current gain, particulary in electron devices with negative feedback loop. On the other hand, results on the maximum output voltage gave much more reliable results on voltage regulator's radiation tolerance. During the maximum output current examination was noticed that bias conditions had the great influence on measured values of forward emitter current gain.

In this paper, were presented results related to the change of the serial transistor's dropout voltage and the forward emitter curent gain in a function of absorbed total dose of gamma radiation. Lateral serial transistor's dropout voltage of LM2940CT5 voltage regulators decreased up to 12%, while dropout voltage of vertical serial devices in voltage regulators L4940V5 increased up to 70%. On the other hand, measured values of serial transistor's forward emitter current gain of radiation sensitive devices LM2940CT5 decreased 20–40% after the absorption of ionizing dose of 500 Gy(SiO_2), while on the radiation hard voltage regulators L4940V5 was observed decrease of forward emitter current gain (without data of serial transistor's voltage base-emitter) by 30–80 times! This was a consequence of abrupt rise of the serial transistor's base current and operation with low current of 100 mA during the examination, that altogether caused a significant shift of voltage regulator's serial transistor's operation point toward the left part of the characteristic $\beta(V_{BE})$, and not almost hundredfold degradation of forward emitter current gain. This is the sharp illustration of deceptive conclusions that may be extricated from the isolated data related to the electron device's radiation tolerance, without seeing the entire collection of data. As was previously published, voltage regulators L4940V5 operated correctly and reliably after the absorption of total ionizing doses exceeding 10 kGy(SiO_2), while, on the other hand, devices LM2940CT5 became completely mulfunctional after total doses of 300 Gy(SiO_2).

Session 3A7
Electromagnetic Waves Propagation in the Atmosphere and Remote Sensing

Seismo-Electromagnetics: GNSS Observations and Implications for Recent Earthquakes

Shuanggen Jin
Shanghai Astronomical Observatory, Chinese Academy of Sciences
Shanghai 200030, China

Abstract— Understanding and prediction of Earthquake are still challenging issues from current seismometer or ground surface observations. It may help from non-seismic measurements, e.g., atmospheric, ionospheric or electromagnetic observations. Although electromagnetic field disturbances implied a possible consequence of crustal failure processes by historic recording data, much of the earliest works are needed to further validate. In this paper, GNSS seismo-ionosphere and some recent progresses are presented and discussed, particularly for recent bigger earthquakes. The pre-seismic and coseismic ionospheric disturbances are investigated from continuous GPS measurements during the 2004 Mw 9.1 Sumatra, 2008 Mw 8.0 Wenchuan and 2011 Mw 9.1 Tohoku Earthquakes. Significant atmospheric seismic disturbances are observed from GPS measurements. The co-seismic atmospheric disturbances are mainly driven by the ground-coupled air waves from ground vertical motion of seismic waves propagating. The coupling processes and mechanism between the atmosphere and solid Earth need to be further investigated in the future.

Special Beam Arrays for Scintillation Reduction in Atmospheric Turbulence

Greg Gbur and Yalong Gu
Department of Physics and Optical Science, University of North Carolina at Charlotte, USA

Abstract— The scintillation of optical beams is one of the most fundamental limitations in the development of free-space optical communication systems. These fluctuations of beam intensity due to turbulence-induced distortion increase the bit error rate of such systems, and work has been ongoing since at least the 1970s to understand and mitigate the effects of atmospheric turbulence.

One solution that has shown much promise is the use of partially coherent (PC) fields as the information carrier in communications. It has been demonstrated numerous times over the past fifty years that the scintillation of a partially coherent field can be lower than that of its fully coherent counterpart. However, a partially coherent beam has a comparatively larger angular spread and forms a larger spot at the receiver plane, which results in a smaller proportion of the transmitted energy being received by the on-axis detector. In general, the use of partially coherent beams for communications involves a trade-off, sacrificing signal strength for improved scintillation characteristics.

Though significant reductions in scintillation have been shown for partially coherent beams, a true optimization of the effect has proven elusive. In recent years, arrays of incoherent beamlets have been studied as simpler class of partially coherent beams that can be used for scintillation reduction. These arrays are a more restrictive class, but have the advantage of being easier to construct than a general PC beam.

In this paper, we consider the propagation of several special classes of incoherent beam arrays in atmospheric turbulence, including pseudo-Bessel correlated beam arrays, Airy beam arrays and arrays of nonuniformly polarized beamlets. Pseudo-Bessel correlated beam arrays are used as an approximate representation of a partially coherent field with Bessel function spatial correlation. Airy beam arrays use the properties of Airy beams to "curve" spatially separated beamlets towards the detector. Nonuniformly polarized beams, beams whose state of polarization varies in the transverse plane, will be shown to act effectively as a simple partially coherent field.

Simulation and analytic results demonstrate that such arrays can be used to reduce scintillation to near the theoretically predicted minimum. Furthermore, the results indicate that under many if not most cases, the scintillation of a general partially coherent beam can be reproduced by an appropriately chosen finite array of beamlets. In other words, a finite array of incoherent beamlets is sufficient to reproduce the scintillation reduction properties of almost any partially coherent beam.

A Radiometeorological Study Based on Data from Malaysia and Amazon Region (Brazil)

Kesavan Ulaganathen[1], **Tharek A. Rahman**[1], **Jorge L. Cerqueira**[2], **and Mauro S. Assis**[3]

[1]Wireless Communication Centre, Electrical Engineering Faculty
University Technology Malaysia, Malaysia
[2]Department of Electrical Engineering, Military Institute of Engineering, Rio de Janeiro, Brazil
[3]Brazilian Committee of URSI, Rua Coelho Neto, 17 Apt. 301, 22231-110 Rio de Janeiro, Brazil

Abstract— The problem of rain attenuation prediction has been studied along the years. In spite of the effort developed in different parts of the world, there are yet some points to be clarified. This problem is quite difficult to be solved, mainly due to the complexity of rain structure. Rain varies randomly both in time and space, and the accuracy of a prediction model depends on its capacity to describe these variations. Usual prediction models are based on meteorological parameters like cumulative distribution of precipitation rate and rain cell shape and dimension. This problem is particularly critical in regions characterized by severe precipitations, such as low latitude areas. In this context, a radio meteorological study based on rainfall rate and rain attenuation data from Malaysia and Amazon Region (Brazil) was carried out. The first step in this investigation was the comparison between climates taking into account the Köppen classification and the annual rainfall rate statistical distribution measured in different sites in the areas under study. This classification was adopted because its structure depends on temperature, precipitation and vegetation, factors that can be related to the cumulative distribution of rainfall rate in a given area. It was shown that the Köppen climate Rainy Equatorial (A_f) prevails in both areas. Once demonstrated the climate similarity, the paper discusses the following problems: a) Worst month characteristics; b) Path length reduction factor; c) Dynamic aspects of rainfall rate and rain attenuation; d) Diurnal variability of rainfall rate; e) The performance of low availability satellite systems in the Ku band. Although both in Malaysia and Brazil different approaches are used in the analysis of these problems, the final results lead essentially to the same conclusions.

Microwave Absorption in Nonuniform Plasma with Different Magnetic Field Configurations Using the Magneto-ionic Appleton-Hartree Theory

M. S. Bawa'aneh[1, 2], **Ahmed M. Al-Khateeb**[3], **Sayeed Makkiyil**[1], **Saud Al Awfi**[4], **Ibrahim Abualhaol**[1], **and Ghada Assayed**[2],

[1]Khalifa University of Science, Technology and Research, P. O. Box 573, Sharjah, United Arab Emirates
[2]Department of Physics, The Hashemite University, P. O. Box 150459, Zarqa, Jordan
[3]Department of Physics, College of Science, King Faisal University, P. O. Box 400, Al-Hufof, Saudi Arabia
[4]Department of Physics, Faculty of Science, Taibah University, P. O. Box 30002, Madina, Saudi Arabia

Abstract— Electromagnetic wave reflection, absorption and scttering in plasma has attracted much attention lately because of the special opprotunities that plasma stealth technology offers, where by changing different plasma parameters one can control the absorption rates of microwaves in plasma. In this work, microwave propagation in a nonuniform, collisional, and magnetized plasma slab with different magnetic field configurations is investigated. To simplify the study of the EM wave interaction with the nununiform plasma, the plasma slab (with a certain density profile) is divided into uniform layers, and the propagation constant for the mth layer is given by $ck^{(m)} = \omega\sqrt{\epsilon_r^{(m)}}$, where c is the speed of light in vacuum, ω is the EM wave frequency and $\epsilon_r^{(m)}$ is the dielectric function for the mth layer obtained using the magneto-ionic Appleton-Hartree theory (AHT). This theory was developed to describe electromagnetic wave propagation in ionized media in the presence of static magnetic fields. Magneto-ionic and optical-ray theories lead to useful and satisfactory description of wave propagation and reflection. Within the magneto-ionic theory combined with the optical ray theory, waves are assumed to be of a plane wave nature with a complex propagation constant, namely, vary as $e^{i\omega t - Kx}$. All dynamical effects are included in the complex propagation constant K. For the zero B-field case, a narrow stealth band is obtained, while for parallel and perpendicular propagation with respect to the B-field, results show a wider stealth band in the vicinity of ω_{ce}. An electron cyclotron frequency of about 4 GHz could result in almost total absorption of the C-band. The results also show higher maximum absorption and wider peak for parallel propagation compared to perpendicular propagation.

The Statistical Character of Atmospheric Noise Temperature Induced by Rain at Millimeter Wave Band in Xi'an, China

Shuhong Gong, **Meng Wei**, **Tiancheng Zheng**, **and Xiangdong Li**
School of Science, Xidian University, Xi'an 710071, China

Abstract— The mechanism of producing noise to communication systems by troposphere is investigated, and the importance of the effects is analyzed. The contribution of rain and other sedimentation particles to antenna noise temperature is discussed. The annual CDFs (Cumulative Distribution Functions) of noise temperature and the reduction of G/T induced by rain at millimeter wave band in Xi'an, China are discussed under the link parameters of the satellites of Xinnuo-No.1 etc. The possible effects induced by atmospheric noise on MIMO system at millimeter wave band are analyzed, some examples are given and discussed. The results show that the contribution of rain to noise temperature can not be neglected. It is necessary to invested in detail the effects of weather phenomena on antenna noise temperature, for instance rain, snow, dust-storm and so on.

ACKNOWLEDGMENT

This work has been supported by "the National Natural Science Foundation of China (61001065)" and "the Fundamental Research Funds for the Central Universities".

Far Field of a Electric Dipole Located above Layered Half Space

Bing Wei and Debiao Ge
Department of Physics, Xidian University, Xi'an 710071, China

Abstract— Usually, the far field of a electric dipole located above layered half space can be obtained by Green function method. But the Green function of the layered half space often very complexity. In this paper, the radiation far field of a electric dipole located above layered half space is obtained by the reciprocity theorem. First, the far field formula of an arbitrary direction electric dipole in free space is deduced. And the far field characteristics of the dipole are analyzed. Then, the far field of an electric dipole located at the origin point (a point of the interface of layered half space) are deduced by the reciprocal theorem. To obtain the far field of E_φ and E_θ, the electric dipoles $\hat{\boldsymbol{\varphi}} I_{\varphi b} l_{\varphi b}$ and $\hat{\boldsymbol{\theta}} I_{\theta b} l_{\theta b}$ are put at the observation point P along the $\hat{\boldsymbol{\varphi}}$ and the $\hat{\boldsymbol{\theta}}$ direction, respectively. The field of the origin point is compose of the direct incident wave and the wave reflected by the layered half space. The direct incident wave is the radiation field of the dipole in the free space, and the reflected field can be calculated by the Fresnel formula. And then, the radiation field of dipole located above the interface of the layered half is considered. The formula of the optical path difference of the direct incident wave and the reflected wave is derived. At last, the radiation far field of a electric dipole located above layered half space is obtained. Fig. 1 and Fig. 2 show the far-field pattern of a electric dipole located perpendicular and parallel to the interface of the half space. The far-field pattern of a electric dipole in free space are also given for comparison.

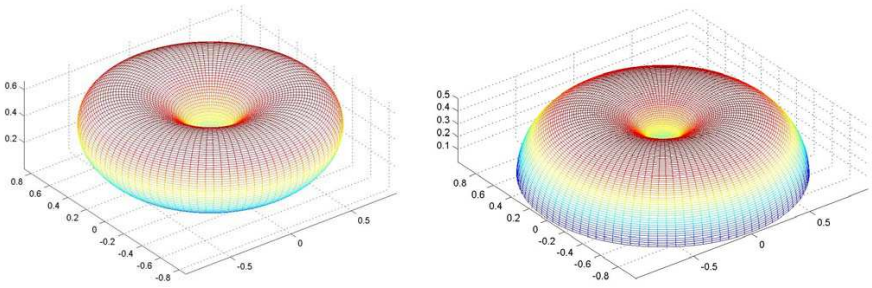

(a) (b)

Figure 1: The far-field pattern of a electric dipole. (a) Perpendicular to the interface of the half space, (b) in free space.

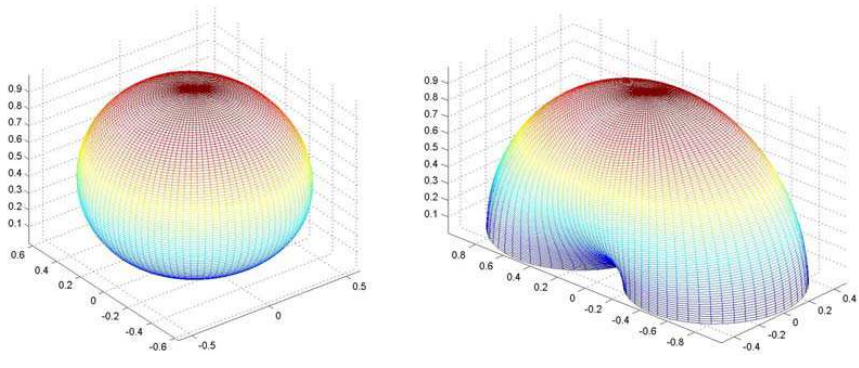

(a) (b)

Figure 2: The far-field pattern of a electric dipole. (a) Parallel to the interface of the half space, (b) in free space.

On the Influence of Spatial-temporal Fluctuations of Electron Density and Magnetic Field Fluctuations on the Angular Power Spectrum of Scattered Electromagnetic Wave by Magnetized Plasma Slab

G. V. Jandieri[1], **A. Ishimaru**[2], **and K. Yasumoto**[3]

[1]Department of Physics, Georgian Technical University, Georgia
[2]Department of Electrical Engineering, University of Washington, USA
[3]Department of Computer Science and Communication Engineering, Kyushu University, Japan

Abstract— Influence of temporal fluctuations of both electron density and external magnetic field fluctuations on scattered ordinary and extraordinary waves by magnetized plasma slab is investigated using the ray-optics method. Transport equation for frequency fluctuations of scattered radiation has been derived. Amplification of frequency fluctuations in the collisional magnetized plasma slab is possible due to temporal fluctuations of plasma parameters and depends on the anisotropy factor and the direction of wave propagation with respect to the imposed magnetic field. Correlation functions of the phase and frequency fluctuation are obtained for arbitrary correlation functions of fluctuating plasma parameters. Broadening of the angular power spectrum is analyzed analytically and numerically for the anisotropic Gaussian correlation function using the remote sensing data.

Statistical Characteristics of Scattered Radiation by Collisional Magnetized Turbulent Plasma Slab

G. V. Jandieri[1], **A. Ishimaru**[2], **and K. Yasumoto**[3]

[1]Department of Physics, Georgian Technical University, Georgia
[2]Department of Electrical Engineering, University of Washington, USA
[3]Department of Computer Science and Communication Engineering, Kyushu University, Japan

Abstract— Peculiarities of electromagnetic waves propagation and scattering in magnetized plasma slab taking into account collision of electrons with ions and neutral particles are investigated in this paper. The set of stochastic differential equations for scattered electric field satisfying the boundary conditions has been obtained using the perturbation method. Correlation functions of scattered fields have been calculated in the principal and perpendicular planes for arbitrary correlation functions of electron density fluctuations and correlation tensor of second rank for an external magnetic field. External magnetic field varies in both value and direction. Stokes parameters are calculated and depolarization degree of scattered radiation is estimated for both weak and strong external magnetic field. Numerical calculations have been conducted for anisotropic Gaussian correlation function of electron density fluctuations taking into account anisotropy degree and angle of inclination of prolate irregularities with respect to the external magnetic field. Gaussian model is used for the correlation function of an external magnetic field. The curves of the normalized correlation functions of the phase; phase portraits of both phase and amplitude correlation functions have been constructed taking into account absorption caused by collision of electrons with other plasma particles in turbulent magnetized plasma slab.

Stochastic differential equation for fluctuating frequency of scattered electromagnetic waves has been obtained in absorptive chaotically inhomogeneous non-stationary medium with smooth spatial-temporal electron density and external magnetic field fluctuations on the basis of eikonal equation using the geometrical optics method. Correlation function of frequency fluctuation is calculated for arbitrary two-dimensional spectral density of randomly fluctuating medium parameters. Frequency fluctuations are amplified at small damping even in absorptive medium with complex refractive index. Amplification effect is caused by electron density and magnetic field fluctuations. In medium with a complex refractive index frequency perturbations are not only transferred with a group velocity, but also are amplified. Amplification can be simulated by parameters of a randomly-inhomogeneous non-stationary medium. Correlation function taking into account diffusion of irregularities in weakly ionized plasma is utilized in analytical and numerical analysis. In medium without dispersion, in the absence of absorption, maximum of the power spectrum is shifted to the higher frequency region.

Session 3A8
Poster Session 4

An Ultra-wideband CMOS LNA for 3–10 GHz with Low Power Consumption

Chien-Hua Lai and Jeng-Rern Yang
Microwave Laboratory, Department of Communication Engineering
Yuan Ze University, Jhongli City, Taoyuan Country 320, Taiwan

Abstract— The Low-Noise Amplifier (LNA) was used for an Ultra-Wide-Band (UWB) application with low power consumption. The low power consumption UWB LNA was designed with standard 0.18 µm CMOS technology. Low power consumption was achieved through the use of the inter stage technique, and current reused topology, with a peaking inductor. The input matching stage used an improved Chebyshev filter to achieve the input return loss, and inductive shunt-peaking was applied to the output matching. The LNA exhibited the maximum S_{21} of 14.6 db. The power consumption was 5.95 mW at $V_{dd} = 1.2$ V.

Suitable Thickness of Material in Determination of Complex Permittivity from Transmission Measurements

T. Suzuki[1], **Y. Kawamura**[2], **T. Ohno**[1], **K. Ishii**[1], **and O. Hashimoto**[3]

[1]Kisarazu National College of Technology, Japan
[2]Chiba University, Japan
[3]Aoyama Gakuin University, Japan

Abstract— The transmission method using rectangular waveguides is commonly used to measure complex permittivity of dielectric materials. We examine the relationship between complex permittivity and thickness of a material in rectangular waveguides.

The transmission method using waveguides is a way to determine the complex permittivity ($\dot{\varepsilon}_r = \varepsilon'_r - j\varepsilon''_r$) of a material from transmission coefficient $\dot{S}_{21}$. Fig. 1 shows a photograph of measurement system for determining complex permittivity of a material from the magnitude and phase of $\dot{S}_{21}$ by using X-band waveguides and a vector network analyzer. Table 1 shows the measured results of thickness of a material (d), ε'_r and $\tan\delta$ under the system of Fig. 1. As shown in Table 1, it is confirmed that some of measured $\tan\delta$ are differ from reference values. Therefore, we investigate the relationship between ε'_r and magnitude of transmission characteristic $|S_{21}|$. Fig. 2 shows theoretical results of the relation above when $\tan\delta$ is 0.002. The symbols ($\square$, $\triangle$, $+$, $\triangledown$, $\Diamond$) in Table 1 and Fig. 2 correspond with each other. The measured $\tan\delta$ at the points of $\triangle$ and $\triangledown$ is similar to reference values, and the others which have high insertion loss indicate poor results. These errors are caused by $|S_{21}|$ expressed in a logarithmic scale.

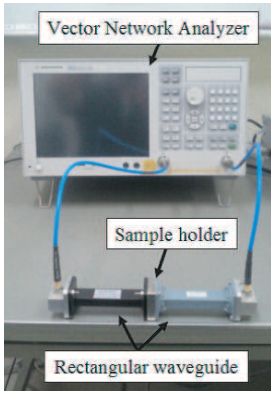

Figure 1: Photo of measurement system.

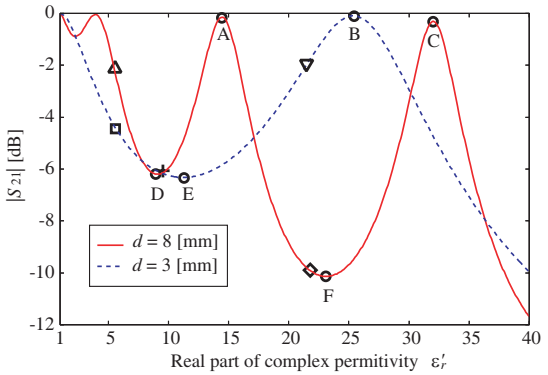

Figure 2: Theoretical results of $|S_{21}|$ versus ε'_r ($\tan\delta = 0.002$).

Table 1: Measured results of 5-type mateials.

Reference (3 GHz)		Measured (10 GHz)			Symbol in Fig. 2
ε'_r	$\tan\delta$	d [mm]	ε'_r	$\tan\delta$	
6	0.002	2.98	5.71	0.073	$\square$
		7.91	5.56	0.001	$\triangle$
9	0.002	7.85	9.21	0.028	$+$
22	0.006	3.08	21.5	0.005	$\triangledown$
		8.04	22.13	0.173	$\Diamond$

Table 2: Simulated results of samples.

Type	Test parameters			By FDTD	
	ε'_r	$\tan\delta$	d [mm]	ε'_r	$\tan\delta$
A	14.44	0.0020	8.0	14.48	0.00199
B	25.42	0.0020	3.0	25.51	0.00202
C	32.00	0.0020	8.0	32.13	0.00206
D	9.11	0.0020	8.0	9.15	0.00067
D′			5.0	9.12	0.00197
E	11.16	0.0020	3.0	11.01	0.00186
E′			4.6	11.21	0.00193
F	23.09	0.0020	8.0	22.96	0.00281
F′			9.4	23.18	0.00206

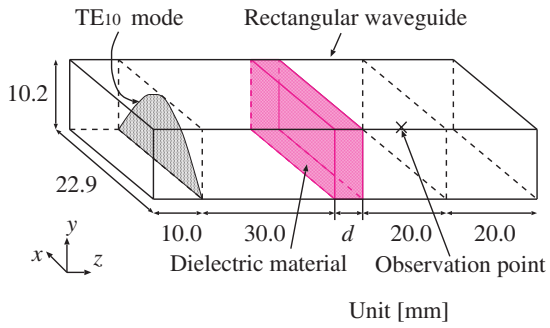

Figure 3: FDTD model for transmission method.

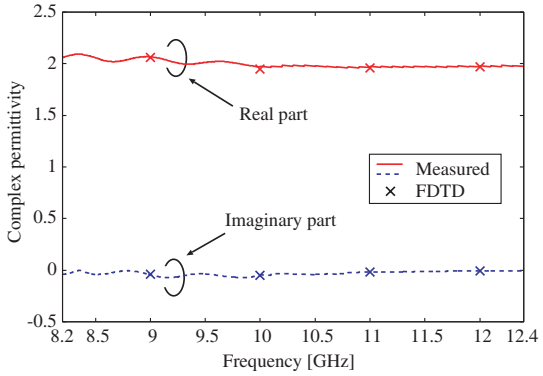

Figure 4: Simulated and measured results of Fig. 3.

An FDTD model for validating the relation above is shown in Fig. 3. Fig. 4 shows the simulated and measured results of a PTFE. As a result, the FDTD model shown in Fig. 3 is verified with a good agreement between simulated and measured results. Table 2 shows the simulated results of the points from A to F in Fig. 2. As shown in Table 2, $\tan\delta$ is obtained a good result in the case of types A, B and C which have low insertion loss, whereas types D, E and F is confirmed with poor $\tan\delta$. Hence, the types D, E and F adjusted their thickness for getting low insertion loss are recalculated as types D′, E′ and F′. From Table 2, $\tan\delta$ of types D′, E′ and F′ are obtained good results in comparison with test parameters. We conclude that an accurate determination of $\dot{\varepsilon}_r$ needs for low insertion loss that depends on d.

ACKNOWLEDGMENT

We appreciate the support of the Futaba Electronics Memorial Foundation.

A Multi-band Magnetic Metamaterial Structure Using the Three Split Ring Resonators

Jeong-Geun Park, **Kyung-Soo Kim**, **and Che-Young Kim**
School of Electronics Engineering, Kyungpook National University
Sankyuk-dong, Buk-gu, Daegu 702-701, South Korea

Abstract— In this study, a multi-band magnetic metamaterial structure is presented. To obtain a multi-band magnetic resonance operation, the new type of three split ring resonator structures (SRRs) is proposed. This SRR behaves like the LC resonator as seen in the conventional SRR, but the shape of metal ring is different from conventional one. The SRR is made of conducting strip printed over a square shaped Rogers 4003 substrate. The proposed metamaterial structure has three resonances in a frequency range of 2.5 to 4 GHz. Furthermore, the three distinct negative effective permeability regions also exist at the referred frequency band. In order to demonstrate the magnetic resonance phenomena, transmission and reflection characteristic of the proposed metamaterial structure are simulated by using full-wave electromagnetic solver (Ansoft HFSS). In addition, electric and magnetic field intensity and surface current densities are calculated at these resonance frequencies. From these results, the nature of resonance is fully explained during the descriptive illustrations. The complex-valued effective medium parameters having the effective permeability and the effective permittivity are retrieved from the simulated complex scattering parameters to verify the existence of fully developed -negative regions. Finally, the transmission characteristic obtained by the parallel-plate waveguide measurement system effectively reveals that three resonances are caused by magnetic modes.

Balanced UWB BPF Design Using Slotline Resonator

Chung-Jung Chen[1], **Ching-Her Lee**[1], **Chung-I G. Hsu**[2], **and Jhih-Hong Chang**[1]

[1]Graduate Institute of Communications Engineering
National Changhua University of Education, Changhua, Taiwan
[2]Department of Electrical Engineering
National Yunlin University of Science and Technology, Yunlin, Taiwan

Abstract— This paper presents a new balanced ultra-wideband (UWB) bandpass filter (BPF), which is designed using a slotline multi-mode resonator (SLMMR). The SLMMR is deployed symmetrically across the plane of symmetry (POS) of the balanced filter circuit. Due to this circuit symmetry, the BPF will exhibit distinct differential-mode (DM) and common-mode (CM) resonant characteristics and the DM and CM analyses can be carried out by considering only half of the balanced BPF circuit. The SLMMR is fed with orthogonally crossed microstrip feed-lines, and both of the SLMMR and the microstrip feed-lines are made extending beyond the microstrip-slotline junction by a quarter-wavelength around the passband center frequency (around 6.85 GHz) of the BPF to ensure good DM signal transmission. For DM operation, the POS can be replaced with an electric wall, and the SLMMR half circuit works as a uniform slotline resonator (USLR) which resonates at the frequencies such that the length of the USLR is integral multiples of a half-wavelength. The design strategy of this work is to allocate the first three resonant frequencies of the USLR inside the UWB passband to achieve a favorably uniform UWB passband response. Furthermore, the next higher mode with its resonant frequency just beyond 10.6 GHz, the upper-edge frequency of the UWB passband, should not be excited so as to have a wider upper stopband.

On the other hand, to obtain good CM performance, the SLMMR is bent at both ends such that the quarter-wavelength resonances occurring near the input and output sides of the resonator are well decoupled so as to enhance the CM signal rejection. In particular, resonant CM signals excited by the input feed-lines on the part of the SLMMR near the input side will little excite those near the output side of the SLMMR, thus reducing the CM signals transmitted to the output feed-lines. The measured minimum DM insertion loss is 0.92 dB in the DM passband, in which the measured CM suppression is larger than 17.1 dB.

Design Investigation of a Novel Bandpass Filter Using Trisection Open Loop Resonator

Hossein Saghlatoon and Mohammad H. Neshati
Department of Electrical Engineering, Ferdowsi University of Mashhad, Iran

Abstract— With the rapid development of wireless communication systems, there is an increasingly demand for high quality components at microwave frequencies. Filters are one of the most important components in wireless systems. So, high performance band pass filters with small size and low cost are highly demanded in microwave circuits.

In this paper, a novel band pass microwave filter is designed and numerically investigated. A trisection open loop resonator filter is used to provide a narrow band pass filter at 2.4 GHz. The three-pole trisection filter is not only the simplest filters by itself, but also it is the basic unit for construction of higher-degree complicated filters. Microstrip trisection filters with different resonator shapes, such as open-loop resonators and triangular patch resonators, can produce asymmetric frequency responses with an attenuation pole at finite frequency on either side of the pass band. This structure has a simple and compact shape and useful for narrow band usage.

The proposed filter is shown in Fig. 1 consist of three open resonator. A three-pole band pass filter with an attenuation pole at finite frequency on the high side of the pass band is designed and simulated using ADS. The band pass filter is designed on the TLY 5A031 substrate with dielectric constant of 2.2 and 31 mil heights. The simulation result of transmission coefficient is shown in Fig. 2. It can be seen that the obtained resonance frequency is 2.4 GHz, while impedance bandwidth is 100 MHz which provide a high Q-factor of 24.

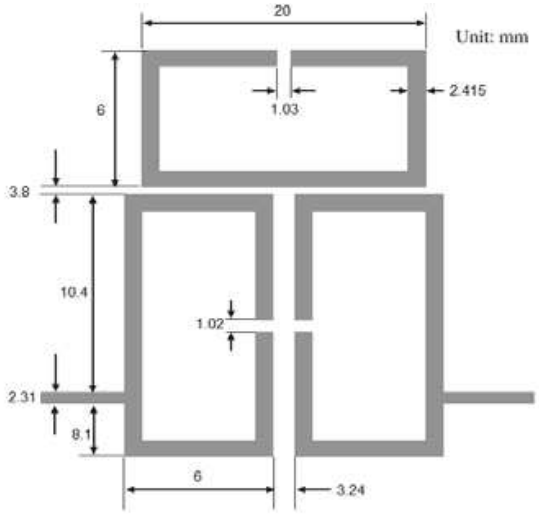

Figure 1: Trisection open loop resonator band pass filter.

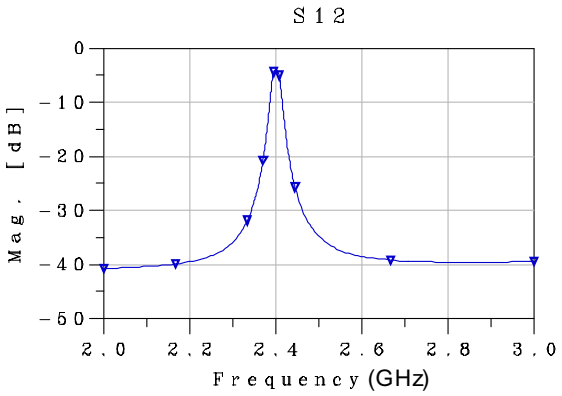

Figure 2: Simulated transmission coefficient of the propped filter.

Application of Cylindrical Ferrite Coupled Line Junction to Nonreciprocal Devices

A. Kusiek, W. Marynowski, R. Lech, and J. Mazur
Gdansk University of Technology, Poland

Abstract— Nonreciprocal devices have been extensively used in modern microwave and millimeter systems. In order to obtain the nonreciprocal effects one needs to utilize the ferrite materials or active elements such as amplifiers. Recently, the longitudinally magnetized ferrite coupled strip [1–3] or slotlines [4, 5] are being developed and employed to realize integrated nonreciprocal devices. Significant interest in these devices results from their advantages which are weak biasing magnetic field and wide operation bandwidth. The basic part of ferrite coupled line (FCL) devices is longitudinally magnetized FCL section obtained as a section of two coupled lines placed on ferrite substrate.

So far, studies concerning FCL devices have been focused mainly on structures realized in planar line technology [1–5]. Such structures allow one to obtain fully integrated FCL devices. However, due to the significant length of ferrite section, the main drawbacks are high insertion losses occurring in ferrite material and large dimensions of the structure. Also due to the geometry of line in planar junction it is difficult to obtain a linear polarization of the wave and to eliminate the isotropic coupling which results in significant deterioration of isolation.

In this paper, a novel cylindrical ferrite coupled line (CFCL) junction is proposed and applied to realization of longitudinally magnetized isolator and circulator. In comparison to planar ferrite coupled line configurations, which are well known in literature, proposed CFCL ensures higher gyromagnetic coupling. This gives possibility to use in CFCL junction shorter ferrite rods made of material with lower value of saturation magnetization. As a result the total insertion losses in the ferrite section can be reduced using the proposed topology.

In the analysis of considered CFCL junction the hybrid technique combining method of moments (MoM) and coupled-mode method (CMM) was applied. Utilizing this approach the four port CFCL junction operating at frequency $f_0 = 10\,\mathrm{GHz}$ was designed. For the designed four-port junction the total insertion losses were about 0.2 dB and were much lower than in planar structures for which insertion losses are about 1.2 dB [3]. Also, in comparison to the planar structures operating in similar frequency band, the length reduction of a junction by a half was obtained. The designed CFCL junction was applied to realization of circulator and isolator. The obtained results were compared with commercial software and a good agreement was achieved.

ACKNOWLEDGMENT

This work was supported in part by Polish Ministry of Science and Higher Education from sources for science in the year 2011 under Contract No. 0215/T02/2010/70 and in part by the Polish Ministry of Science and Higher Education from sources for science in the years 2010-2012 under COST Action IC0803, decision No. 618/N-COST/09/2010/0.

REFERENCES

1. Yang, L.-Y. and K. Xie, "Design and measurement of nonuniform ferrite coupled line circulator," *Journal of Electromagnetic Waves and Applications*, Vol. 25, No. 1, 131–145, 2011.
2. Cao, M., R. Pietig, H. C. Wu, and R. G. Gossink, "Perturbation theory approach to the ferrite coupled stripline," *IEEE MTT-S International Microwave Symposium Digest*, Vol. 3, 1903–1906, May 2004.
3. Marynowski, W. and J. Mazur, "Study of nonreciprocal devices using three-strip ferrite coupled line," *Progress In Electromagnetics Research*, Vol. 118, 487–504, 2011.
4. Kusiek, A., W. Marynowski, and J. Mazur, "Investigations of the circulation effects in the structure using ferrite coupled slot-line section," *Microwave and Optical Technology Letters*, Vol. 49, No. 3, 692–696, January 2007.
5. Abdalla, M. A. and Z. Hu, "Multi-band functional tunable LH impedance transformer," *Journal of Electromagnetic Waves and Applications*, Vol. 23, No. 1, 39–47, 2009.

Novel Structures of Circulator and Isolator Employing Ferrite Coupled Line Section

W. Marynowski, **A. Kusiek**, **R. Lech**, **and J. Mazur**
Gdansk University of Technology, Poland

Abstract— This paper presents the investigations of nonreciprocal devices employing a novel ferrite coupled line (FCL) junction. The structures were designed using different configurations of coupled three-strip lines. The first one is similar to the coplanar slot line with two ground half-planes reduced to the strips [1] . The second one is similar to the two microstrip coupled lines with reduced ground-plane. The investigated junctions are composed of one ferrite section placed between two dielectric sections. In the ferrite section the longitudinally magnetized ferrite slab is located at the top or bottom of the strips and is covered with the dielectric layers. The ports of the junctions are located in the dielectric sections. The wave parameters and field distributions of the modes propagated in the dielectric and ferrite sections are obtained from spectral domain approach. In order to determine the scattering matrix of the junction the mode matching method is utilized. The results of the simulations were verified by the use of HFSS. The proposed approach allows to obtain the results faster then by using commercial simulators and therefore can be utilized in optimization process to design sections of various nonreciprocal devices. The obtained S-matrices were used to design the circulators and the double isolators. Predicted performance of the designed devices was verified experimentally.

For the devices using the proposed coplanar FCL junction the measured average insertion losses of the circulator were about 2.7 dB and isolations were about 12 dB in the frequency range 10–14 GHz. The compact structure of the integrated planar double isolator in the experiment showed average reflection losses better than 10 dB in the frequency range from 11 to 14 GHz. The average insertion losses were about 4.5 dB and isolation better than 16 dB. For the devices utilizing the proposed microstrip FCL junction the measured average insertion losses of the circulator were about 3.5 dB and isolations were about 12 dB in the frequency range 11–15 GHz. The structure of the double isolator containing SMA-broadband loads in the experiment showed average reflection losses better than 14 dB in the frequency range from 11 to 20 GHz. The average insertion losses were about 4.5 dB and isolation better than 16 dB. The insertion losses obtained for all measured devices are better than the results found in literature [2–5].

ACKNOWLEDGMENT

This work was supported in part by Polish Ministry of Science and Higher Education from sources for science in the year 2011 under Contract No. 0215/T02/2010/70 and in part by the Polish Ministry of Science and Higher Education from sources for science in the years 2010-2012 under COST Action IC0803, decision No. 618/N-COST/09/2010/0.

REFERENCES

1. Marynowski, W. and J. Mazur, "Treatment of the three strip coplanar lines on the ferrite," *XVII International Microwaves, Radar and Wireless Communications Conference*, Vol. 1, 135–138, Wroclaw, Poland, May 2008.
2. Ch. K. Q. and L. E. Davis, "Microstrip and stripline ferrite-coupled-lines (FCL) circulators," *IEEE Transactions on Microwave Theory and Techniques*, Vol. 50, No. 12, 2910–2917, Dec. 2002.
3. Queck, C. K. and L. E. Davis, "Broad-band three-port and four-port stripline ferrite coupled line circulators," *IEEE Transactions on Microwave Theory and Techniques*, Vol. 52, No. 2, 625–632, February 2004.
4. Cao, M. and R. Pietig, "Ferrite coupled-line circulator with reduced length," *IEEE Transactions on Microwave Theory and Techniques*, Vol. 53, No. 8, 2572–2579, Aug. 2005.
5. Kusiek, A., W. Marynowski, and J. Mazur, "Investigations of the circulation effects in the structure using ferrite coupled slot-line section," *Microwave and Optical Technology Letters*, Vol. 49, No. 3, 692–696, Jan. 2007.

Remotely Controllable Robotic System to Detect Shallow Buried Objects with High Efficiency by Using an Holographic 4 GHz Radar

I. Arezzini[1], **M. Calzolai**[1], **L. Lombardi**[1], **L. Capineri**[1], **and Y. Kansal**[2]

[1]Dipartimento Elettronica e Telecomunicazioni, Università di Firenze, Firenze 50139, Italy
[2]Birla Institute of Technology and Science, Pilani, India

Abstract— The ambit of non-destructive testing has several diagnostic methods, each with its own characteristics. The microwave high resolution imaging methods allows the detection of shallow buried objects with high plane resolution.

The diagnostic method that uses the holographic subsurface radar up to 4 GHz (RASCAN 4/4000) allows obtaining images of the dielectric contrast at a high spatial resolution (about 1 cm).

The scanning of large areas of several square meters with a subsurface radar requires an automatic scanning tool that must also associate the obtained dielectric contrast data with the relative position of measurement.

The necessity of an automated scanning system has led to the creation of a robotic platform, equipped with a wireless remote connection, with a high degree of expandability and flexibility, also for use with other types of sensors (acoustic, ultrasonic, ...).

The mechanical part of the robotic system consists of a motorized platform, which is entrusted with the advancement; and of a system for the scanning motion of head, transverse to the direction of advancement.

The electronic part consists of several modules connected together by a bus 485 and connected remotely to a computer by a Bluetooth wireless connection. The developed computer software sends control instructions to the robot and plots the obtained dielectric contrast data along with the relative position of measurement to obtain a picture of the scan.

The holographic radar can be programmed to scan the surface with up to 10 discrete frequencies in order to get high phase contrast for objects buried at different depths. It can also do a frequency sweep to automatically scan the surface with the entire range of frequencies available.

The developed robotic system successfully scans large areas of land with high accuracy to detect shallow buried objects, while being remotely controlled through a computer.

The trajectory control was carried out on Flex board, with dsPIC processor onboard and programmed with Scicoslab, an integrated development environment equipped with visual programming tools.

The position of robotic platform, is measured with optical position sensors and used also in the trajectory control system.

High-Q Transmission Line Stub Resonators Using Interdigital Capacitor Loading for MMIC Applications

T. Katayose[1], **M. Okunogi**[1], **K. Hosoya**[2], **and S. Tanaka**[1]

[1]Shibaura Institute of Technology, Japan
[2]NEC Corporation, Japan

Abstract— Transmission line (TL) resonators are critical elements in MMIC low phase-noise oscillators. Previously, we proposed TL resonators that are directly coupled to the main signal line and yet can yield high Q (loaded Q) by using open stubs with length close to $\lambda/4$ [1]. The mechanism of such high-Q resonator can be explained by coupling coefficient analysis [1] and attenuation poles approaching the resonant frequency. The large footprint of the resonator, however, hinders shrinking of MMIC chip size. Slow-wave TL is one approach to miniaturizing such TL-based passive elements, but the complicated structure and relatively high insertion loss still remains issues for this technique to be widely used for high-Q resonators in MMICs.

In this paper, we demonstrate compact stub resonators using interdigital capacitor (IDC) which is compatible with most MMIC fabrication process. The basic concept of using external capacitors to reduce the size of TL resonator in the UHF bands was reported [2], but there are two major concerns that need be addressed in order to apply this method to the above-mentioned type of high-Q stub resonators in MMICs. First, the amount of capacitance required for sufficient reduction of the stub length may cause self-resonance in such high frequencies as in microwave bands. Second, the difference between attenuation pole and resonance frequency tends to increase with increasing capacitance, resulting in Q-factor deterioration.

To cope with these issues, analytical calculations were performed to obtain design guidelines of resonators shrunk with minimum impact on the performance. It was found that by using high impedance TLs the stub length can be effectively reduced with modest capacitance, i.e., with no self-resonances in the frequency of interest. We fabricated 2.5 GHz TL resonators on FR4 and achieved 50% reduction in size while maintaining the self-resonance frequency above 6 GHz.

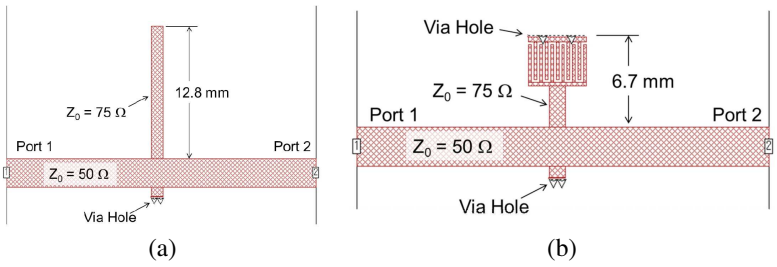

Figure 1: Directly coupled microstrip line resonators for (a) before and (b) after interdigital capacitor loading.

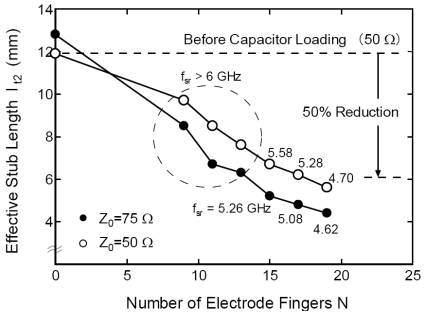

Figure 2: Effective stub length as a function of the number of IDC electrode fingers (measured).

REFERENCES

1. Hosoya, K., et al., "RF HBT oscillators with low-phase noise and high-power performance utilizing a $(\lambda/4 \pm \delta)$ open-stubs resonator," *IEEE Trans. Circuit and Systems-I*, Vol. 53, No. 8, 1670–1682, 2006.
2. Henkes, D. D., "Designing short high Q resonators," *Microwaves & RF*, 75–109, Dec. 2003.

Non-bias Inspection of Electrical Failures in LSI Chips Using Laser Terahertz Emission Microscope

Masatsugu Yamashita[1], **Chiko Otani**[1], **Toru Matsumoto**[2], **Yoshihiro Midoh**[3] **Katsuyoshi Miura**[3], **Kiyoshi Nikawa**[3], **Koji Nakamae**[3], **and Masayoshi Tonouchi**[4]

[1]RIKEN Advanced Science Institute, Miyagi 980-0845, Japan
[2]Hamamatsu Photonics, Shizuoka 431-3196, Japan
[3]Graduate School of Information Science and Technology
Osaka University, Osaka 565-0871, Japan
[4]Institute of Laser Engineering, Osaka University, Osaka 565-0871 Japan

Abstract— Recently, we have developed a prototype system of laser terahertz emission microscope (LTEM) to localize the position of electrical failures in LSI chip without electrical probing for LSI failure analysis. By exciting p-n junctions in LSI chips with ultrafast laser pulses with the wavelength of 1.06 μm, the transient photocurrents in p-n junctions flow into the interconnections and emit the THz waves through the silicon substrate into the free space. The generated THz waveforms are strongly affected by the structures of the interconnections connected to the photo-excited p-n junctions, which means that THz waveforms depend on the electrical failure positions in interconnects. The system provides the backside observation of LSI chips with multilevel interconnection from the silicon substrate side with the rapid image acquisition time (Approx. 5 min. for 512×512 pixels with lock-in time constant 1ms) and the high spatial resolution ($\sim 0.35\,\mu$m) by means of a solid immersion lens.

In this study, logic LSI chips fabricated by 180 nm process were measured. By comparing the LTEM images between a normal circuit and a defective one as shown in Fig. 1, p-n junction connected to the interconnection with an open defect can be successfully determined under non-bias measurement condition. This result indicates that LTEM can be a useful tool which realizes the electrode less measurement for the defect localization in LSI failure analysis. The localization of the defect position in the interconnection can be realized by comparing the THz waveform with the numerical simulation. The improvement of the spatial resolution and detection sensitivity of the system is underway to apply the system for LSI chips with more advanced process node.

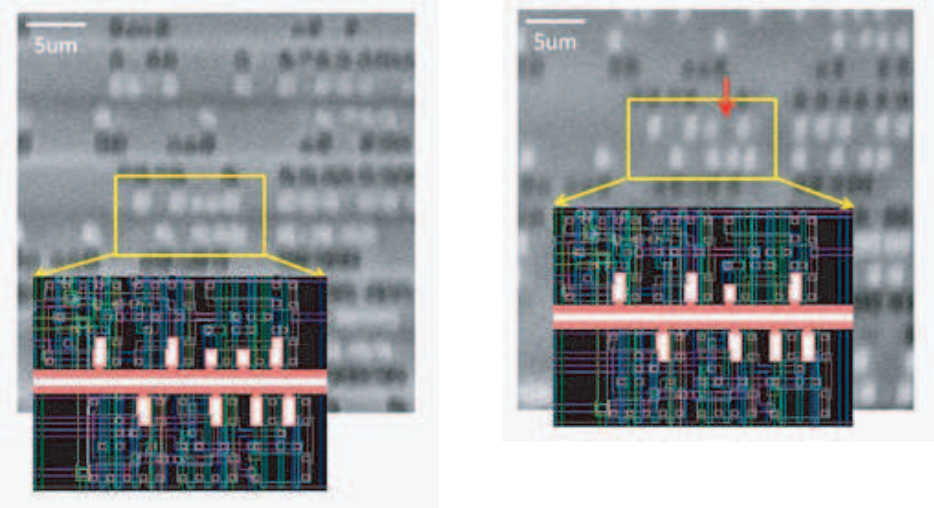

(a) Normal (b) Open circuit

Figure 1: Comparison of LTEM image between (a) the normal circuit and (b) the open circuit. White and black areas show the positive and negative amplitude of THz emission. The red arrow indicates the p-n junction connected to the interconnection with open defect.

Design of ARC Filters by Leap-Frog Method

L. Fröhlich, J. Sedláček, and M. Friedl
Brno, FEEC BUT, UTEE, Kolejni 2906/4, Brno 612 00, Czech Republic

Abstract— The sphere concerning frequency filters is constantly developing and there are many principles of non-cascade synthesis method which can be used for the design and optimisation of ARC filters. Usually, due to a very difficult design of some kinds of filters, certain types of synthesis method are not properly described and there is no detailed description of their usage in practice. One of this is the Leap-Frog method, which can be successfully used in area of filter design and optimisation.

The article describes the method of the design of ARC filters growing from the LCR ladder filter prototype. This method of the frequency filter synthesis is not used very often due to higher amount of active elements (OAs), relatively difficult design and relatively pure prescribed synthesis method in literature. But on the other hand, this method has a considerable advantage as very little sensitivity and excellent filter dynamic qualities. Thus, it is ideal for realization with switching capacitors and their following usage in integrated circuits. The aim will be following — from the created complete analysis of filters realizing LP, HP, BP, BR, LP_N and HP_N with either ending T or PI, make their analysis and comparison with other filters and create a suitable description for the usage of certain circuits. Some circuits were realized physically for the evaluation of the wider frequency usage by using of the modern OAs.

ACKNOWLEDGMENT

The research described in the paper was financially supported by grant of Czech ministry of industry and trade No. FR-TI1/001, GACR 102/09/0314 and project of the BUT Grant Agency FEKT-S-11-15.

REFERENCES

1. Sedláček, J. and K. Hájek, *Kmitočtové Filtry. 1. Vydání*, 535, Echnická Literatura, BEN, Praha, 2002, ISBN 80-7300-023-7.
2. Dimopoulos, H. G. and A. G. Constantinidis, "Linear transformation active filters," *IEEE Trans. CAS*, Vol. 25, No. 10, 845–852, 1978.
3. Ghausi, M. S. and K. R. Laker, *Modern Filter Design*, Practice Hall, New Jersey, 1981.
4. Kapustin, V. I., "Aktivnye RC-filtry vyskovo porjadka," *Radio i Svjaz*, Moskva, 1985.
5. Sedra, A. and K. Martin, "Design of signal-flow graph (SFG) active filters," *IEEE Trans. CAS*, Vol. 25, No. 4, 185–195, 1978.

Programme for Synthesis of ARC Leap-frog Filters

L. Fröhlich, **J. Sedláček**, **and M. Friedl**
FEEC, BUT, UTEE, Kolejní 2906/4, Brno 612 00, Czech Republic

Abstract— Due to the fact that the method of the frequency filter synthesis methods of ARC filters (with the help of non-cascade realization Leap-Frog which combines method of blocked filter realizations and method based on RLC ladder filter prototypes) is very complicated, the program for a complete synthesis of these filters was created.

The article deals with a complete frequency filter design and description of the program, coming out of suitable set developing diagram. From the option of input values, enabling the choice of approximations with or without notch transfer, choice of transfer function LP, HP, BP, BR to kinds of ending T or PI. The output of the program is the display of the circuit and values of the components according to input parameters and the display of transfer characteristics with the possibility of control and change of dynamic behaviour of the circuit.

The program should serve mainly and enable wider using of this Leap-Frog method synthesis in area of filter design and optimisation in practice, when the user can compare several designs of ARC filters designed by different method and compare which of the stated applications will be the most suitable.

ACKNOWLEDGMENT

The research described in the paper was financially supported by grant of Czech ministry of industry and trade No. FR-TI1/001, GACR 102/09/0314 and project of the BUT Grant Agency FEKT-S-11-15.

REFERENCES

1. Sedláček, J. and K. Hájek, *Kmitočtové Filtry. 1. Vydání*, 535, Echnická Literatura, BEN, Praha, 2002, ISBN 80-7300-023-7.
2. Dimopoulos, H. G. and A. G. Constantinidis, "Linear transformation active filters," *IEEE Trans. CAS*, Vol. 25, No. 10, 845–852, 1978.
3. Ghausi, M. S. and K. R. Laker, *Modern Filter Design*, Practice Hall, New Jersey, 1981.
4. Kapustin, V. I., "Aktivnye RC-filtry vyskovo porjadka," *Radio i Svjaz*, Moskva, 1985.
5. Sedra, A. and K. Martin, "Design of signal-flow graph (SFG) active filters," *IEEE Trans. CAS*, Vol. 25, No. 4, 185–195, 1978.
6. Sedláček, J. *Optimalizace v Syntéze Filtru RLC*, Habilitační práce, VA Brno, 1994.
7. Hájek, K., *Optimalizovaný Návrh Filtru ARC s Využitím Počıtače*, Habilitační práce, VA Brno, 1994.

Novel Compact Triple-bandpass Filter Using $\lambda/4$ Resonator Pairs with Common via Ground

Fei Liang[1], **Hongwen Gan**[2], **Zhiyong Wang**[2], **and Wenzhong Lu**[1]

[1]Department of Electronic Science and Technology
Huazhong University of Science and Technology, 1037 Luoyu Road, Wuhan 430074, China
[2]Base Station Supporting Products Division
Wuhan Hongxin Telecommunication Technologies Co., LTD, China

Abstract— Multi-band multi-standard wireless communication systems have been gaining much attention in recent years. These systems prefer multi-band transceivers to several single-band ones. In tri-band transceivers, tri-band bandpass filters are important building blocks and thus heavily demand. In response to this need, a number of design methodologies have been studied to realize filters with tri-passband responses. However, in those design methodologies, the degrees of design freedom are still limited or the design process is a little complicated or the size of the filter is still large.

In this paper, a compact planar tri-band BPF is presented. The filter employs the novel structure called $\lambda/4$ resonator pairs with common via ground which is basically composed of a $\lambda/4$ SIR and a $\lambda/4$ UIR with common via ground. The former resonates at the first and third passbands and the latter at the second passband. The three passband frequencies can be easily adjusted to desired values by changing the dimensions. In addition, it not only can fit easily the specific coupling coefficients at each band simultaneously, but also achieve compact size. For demonstration, a filter with triple-band Chevbyshev response is implemented. An example of filter with a tri-band chebyshev response operating at 2.4, 3.6, and 5.2 GHz was designed and fabricated. Finally, the circuit size of the proposed filter occupies only $22 \times 22\,\mathrm{mm}^2$. The design methodology is described and the experimental results are presented. The measured results are in good agreement with the full-wave simulation results.

An Efficient Method for Analyzing Microwave Polarizer with Finite Grid Thickness

Teng Wah Ang[1], **Kwok Kee Chan**[2], **and Tat Soon Yeo**[3]

[1]National University of Singapore, 21 Lower Kent Ridge Road, 119077, Singapore
[2]Chan Technologies Inc., 15 Links Lane, Brampton, Ontario L6Y 5H1, Canada
[3]Temasek Defence Systems Institute, Block E1, #05-05, 1 Engineering Drive 2, 117576, Singapore

Abstract— Polarizers are used in practice to convert electromagnetic waves from one polarization state to another. In the microwave region, polarizers are employed in systems such as Cassegrain antennas to reduce aperture blockage and feed mismatch and conversion of linear to circular polarization for satellite communications.

Analysis of microwave polarizer can broadly be divided into two categories: Network Model based technique [1], and Floquet Mode Expansion Moment Method [2]. While Floquet Mode Expansion have shown good accuracy compared to the Network Model, it does not take into account the grid metallization thickness — which can be problematic in multi-grid low axial ratio design.

The proposed method in this work models the space between two parallel grids in a unit cell as a form of step waveguide. The transverse resonance technique is used to set up the characteristics equation. Singular value decomposition is then applied to solve for the mode cutoff wave numbers efficiently. Finally, the generalized scattering matrix of the polarizer is obtained by field matching the waveguide and Floquet modes.

Figure 1 shows the differential transmission phase shift results for two meanderline polarizers published by Terret et al. [3]. The accuracy of this proposed method is validated by the good agreement with both measurement data and finite element method calculations. Compared to the finite element method, the proposed method in this paper is approximately an order of magnitude faster.

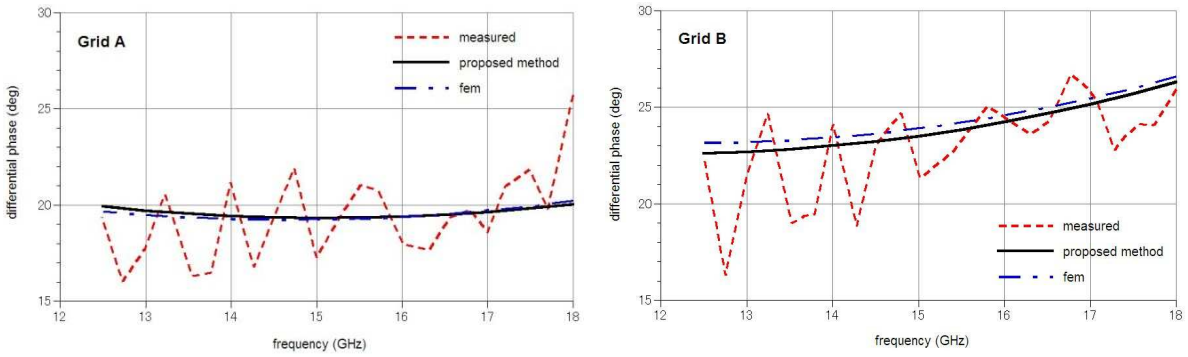

Figure 1: Comparison of differential phase shift for Grid A and B.

REFERENCES

1. Chu, R. S. and K. M. Lee, "Analytical model of a multilayered meander line polarizer plate with normal and oblique plane-wave incidence," *IEEE Trans. Antennas and Propagat.*, Vol. 35, 652–661, 1987.
2. Chan, K. K., S. R. Gauthier, and G. Dinham, "A broadband and wide angle meanderline polarizer," *Proceedings of the 3rd Int. Conf. on Electromagnetics in Aerospace Applications*, 171–174, 1993.
3. Terret, C., J. Levrel, and K. Mahdjouubi, "Susceptance computation of a meanderline polarizer layer," *IEEE Trans. Antennas Propagat.*, Vol. 32, No. 9, 1007–1011, 1984.

Failure Analysis of LTCC Coupler Using Microwave

Soon-Mi Hwang, **Yong-Baek Jung**, **and Sung-Dae Noh**
Korea Electronics Technology Institute (KETI)
#68 Yatap-Dong, Bundang-Gu, Sungnam-Si, KyungGi-Do, Korea

Abstract— As the component for dividing and sampling the high frequency signal of high frequency coupler, it is used in the mobile communication repeaters and transmitter-receivers. With the application of laminated LTCC processing on coupler, further miniaturization and reduced cost can be achieved [1–3], however, LTCC coupler is more fragile compared to the existing Microstrip or Waveguide structures. This paper analyzes the primary failure mode and the failure mechanism of LTCC coupler using microwave.

LTCC coupler used in high frequency is formed by plating green sheet, composed of glass and ceramic, with metallic conductor, which will function as transmitting line, then piling the green sheets according to the circuit's structure to co-fire ceramic and metal. It has multiple layers and ceramic exists inside the top and bottom metal layers to form strip path.

LTCC coupler's primary failure mode and failure mechanism are the followings: First, deformation of the inside strip path and damaged ceramic, caused by high humidity, high temperature or drastic change of temperature. Second, ceramic damaged by mechanical vibration or impact. High temperature and humidity, or sudden change of temperature may cause damage to the inside ceramic, which then may deform or cut strip path, changing the coupler's high frequency property. Instant high temperature may also cause deformation of strip line, resulting in the same changed high frequency property [4]. Also manufacturing process may cause crack between via hole and stripline, depending on the calcination temperature [5].

Mechanical vibration or impact can damage ceramic and this causes changed frequency property as well.

To verify aforementioned reasons for the failure of LTCC, a temperature change test was carried out according to RS C0087. Coupler has been put into high temperature ($125 \pm 2°C$), and low temperature ($-55 \pm 2°C$) and run for 30 minutes. The coupler failed sporadically after 2000 cycles. Figure 1 shows the failed coupler. In case of a hybrid coupler which forms its circuit by soldering to PCB, being exposed to drastic change of temperature for a long time accumulated thermomechanical fatigue damage, which cracked PCB coupler's soldering part and disconnected the circuit.

REFERENCES

1. Wu, K.-L. and Y. Huang, "LTCC technology and its applications in high frequency front end modules, antennas," *6th International Symposium on Propagation and EM Theory Proceedings*, 730–734, Oct. 28–Nov. 1, 2003.
2. Consolazio, S., K. Nguyen, D. Biscan, K. Vu, A. Ferek, and A. Ramos, "Low temperature cofired ceramic (LTCC) for wireless applications," *IEEE MTT-S Symposium on Technologies for Wireless Applications*, 201–205, 21–24, Feb. 1999.
3. Vendik, I. B., D. V. Kholodnyak, A. V. Simine, P. V. Kapitanova, P. A. Turalchuk, and I. A. Fischuk, "Passive microwave devices based on LTCC and sandwich multilayer technologies," *5th International Conference on Microwave Electronics: Measurements, Identification, Applications*, 70–75, 13–15, Dec. 2005.
4. Pietrikova, A., "Thermal shock reliability test of multilayer LTCC modules with thick film conductors," *26th International Spring Seminar on Electronics Technology*, 485–488, May 8–11, 2003.
5. He, X. Q., X. Ma, and Y. Zhang, "Elimination of opens failure between via holes and traces in LTCC multilayer substrate by coherent shrinkage," *Proceedings of the 8th International Symposium on the Physical and Failure Analysis of Integrated Circuits*, 138–141, Jul. 9–13, 2001.

A New Tunable Dual-mode Bandpass Filter Design Based on Fractally Slotted Microstrip Patch Resonator

Jawad K. Ali[1], **Nasr N. Hussain**[2], **Ali J. Salim**[1], **and Hussam Alsaedi**[1]

[1]Department of Electrical and Electronic Engineering, University of Technology, Baghdad, Iraq
[2]Communication Engineering Department, Technical College of Najaf, Najaf, Iraq

Abstract— A dual-mode slotted microstrip patch resonator is introduced in this paper for use in wireless communication applications. The slot structure, etched inside the patch resonator, is in the form of the 2nd iteration Koch fractal curve; using the conventional square microstrip patch resonator as the initiator. Modeling and performance evaluation of the proposed filter design have been carried out using a method of moment based EM simulator, IE3D. Simulation results show that the resulting resonator filter has good transmission and return loss responses. The modeled resonator has been found to possess a side length of about 0.22 the guided wavelength, which represents a size reduction of about 81% as compared with that based on the conventional square microstrip patch without slot. In addition, slits have been symmetrically etched in the external edges of the patch structure, in an attempt to provide the resonator with tuning facility. Besides the tuning possibility, these slits have been found to offer further size reduction without worsening the resulting filter performance; providing the designer with more degrees of freedom.

The Design of Wideband DC-35 GHz IF Modules for 78–113 GHz Receiver Array

Hsiao-Feng Teng[1], **Jing-Cheng Wu**[1], **Tzi-Hong Chiueh**[1], **and Robert Hu**[2]

[1]National Taiwan University, Taipei 100, Taiwan, R.O.C.
[2]National Chiao Tung University, Hsinchu 300, Taiwan, R.O.C.

Abstract— To facilitate simultaneous detection of the 78–113 GHz millimeter-wave electromagnetic spectra, compact DC-35 GHz IF modules have been designed where the down-converted signals will be divided and further transformed into four 8.7 GHz bands, thus suitable for fiber-optics signal transfer and digital-signal processing. This paper will detail the design methodology and related microwave circuits that constitute the wideband modules; measured results will also be presented. In additional to the intended radio-astronomical instrumentation, this work can be used in applications such as geographical remote sensing and human biological sensors.

A New High-Q Resonator Using Combination of D-SR and S-SRR with μ-near Zero Metamaterial

H. Lee[1], **K. C. Yoon**[2], **D. K. Lee**[1], **T. S. Jung**[1], **and J.-C. Lee**[1]

[1]Department of Wireless Communications Engineering, Kwangwoon University, South Korea
[2]Energy-Display R&D Center, Korea Electronics Technology Institute, South Korea

Abstract— It is suggested that a new high-Q_L resonator using a combination of double spiral resonator (D-SR) and single split ring resonator (S-SRR) with μ-near zero metamaterial. S-SRR is applied to a resonator to get high-Q_L performance and D-SR is used to obtain μ-near zero characteristic for size reduction. The resonator is designed to operate at 9.2 GHz. Also, the proposed resonator has positive phase response due to zero-value permeability, which means that it has MNZ metamaterial structure. The experimental result shows the Q_L value of 140 at the resonant frequency of 9.17 GHz. It can be fabricated with MEMS (Micro-electro mechanical systems), NEMS (Nano-electro mechanical systems) and HMIC (Hybrid Microwave Integrated Circuits) or MMIC technique due to its entirely planar structure.

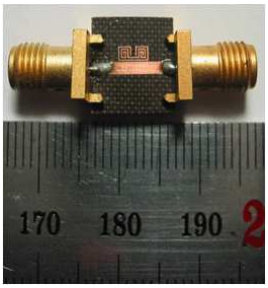

Figure 1: A photograph of the new resonator with MNZ metamaterial.

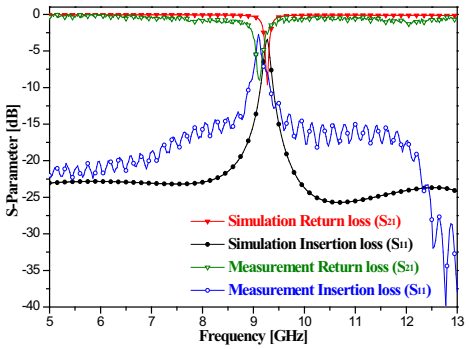

Figure 2: Simulation and measurement results for the new resonator with MNZ metamaterial.

A Differential-mode Wideband Band-pass Filter for UWB Application

M. Li, **F. Zhang**, **Kyosoon Choi**, **Jaeyeong Lee**, **and J. C. Lee**
Department of Wireless Communications Engineering, Kwangwoon University
447-1 Wolgye-Dong, Nowon-Ku, Seoul 139-701, Korea

Abstract— A different-mode wideband bandpass filter with good common-mode suppression is designed in this paper for Ultra-Wideband (UWB) application.

UWB system transmits information though duration pulses and spread over a large bandwidth, which is different from traditional radio system. UWB technology has been developed in radar imaging, local area networks, locating and tracking applications for its advantages of low energy levels, low cost and high date rate transmission.

On the other hand, balanced circuits play an important role in modern communication systems for their higher immunity to the environment noise when compared with that of the single-end signaling. Many amplifiers, mixers and oscillators have been developed as balanced components.

Therefore, the wideband bandpass balanced filter is essential in a UWB system.

In this study, we propose a wideband differential-mode BPF on microstrip line. The proposed structure is divided into two parts with a perfect electric or magnetic wall at the symmetrical plane, under differential-mode or common-mode excitation Under the differential-mode operation, the equivalent circuit is a wideband BPF, but under the common-mode operation, the equivalent circuit is a wideband bandstop filter. Two open stubs in bandstop filter are used to control the 3 dB bandwidth of bandpass filter with reducing the 3 dB cutoff bandwidth of bandstop filter slightly, resulting the common-mode stopband cover the entire differential-mode passband. And as a four-port balanced device, the two-port differential- and common-mode S-parameters can be deduced from the standard four-port S-parameters. Finally, a differential-mode bandpass filter centered at 4 GHz with a 3-dB factional BW of 55% and near 30 dB common-mode suppression is designed and fabricated.

Design of Double-Pole-Double-Throw Bandpass Filter-Integrated Switches

S. F. Chao and M. W. Shih
National Kaohsiung Marine University, Taiwan

Abstract— In this paper, a double-pole-double-throw (DPDT) filter-integrated switch is proposed. The circuit integrates a DPDT switch and a microwave bandpass filter into a single circuit component. The circuit consists of four switchable feed lines and four hairpin resonators. The feed lines are connected via p-i-n diodes to the two symmetric taped points of each I/O halfwavelength resonator. Therefore, the I/O signal paths can be selected by applying different bias voltages to the p-i-n diodes. Moreover, the defected-ground-structure (DGS) is also adopted to improve the stopband rejection. At the thru port, the measured insertion loss is about 3.0 dB at the center frequency of 1.5 GHz with a 3 dB fractional bandwidth of 7%. The isolations are 29 dB and 36 dB at the center frequency and higher than 23 dB from dc to 8 GHz at the two isolated ports. The proposed circuit successfully increases the level of integration of the RF front end, and the circuit size is also reduced.

Measurement of the Temperature by FSS Structures

A. Abdolali, A. Emami, and S. Moinzad
Department of Electrical Engineering, Iran University of Science and Technology (IUST)
Narmak, Tehran 1684613114, Iran

Abstract— In this paper, a new instrument is suggested for measuring the temperature by using a FSS structure.

We know that a patch-type frequency selective surfaces (FSSs) has S parameters in the form of a band-stop filters. Furthermore, resonant frequency and bandwidth of this filter is dependent on dimensions and physical specifications of this patch. Accordingly, once physical dimensions of the patch are altered by the changes in the temperature, the resonant frequency will be shifted. Therefore, having volume expansion pattern of the patch, we can calculate resonant frequency shifts during a temperature interval.

Hence, we may find out the temperature of the furnace by measuring resonant frequency of the FSS structure and comparing it with the results achieved by simulation of the patch.

Sensitivity of this instrument is strongly dependent on the intensity of the changes in physical dimensions affected by the temperature and on the intensity of the resonant frequency shifts caused by the changes in physical dimensions.

As the free-standing aperture-type and patch-type FSSs are completely supplementary, we can also use an aperture-type Instead of patch-type FSSs.

In this article, volume expansion pattern is measured by Abaqus software and the S parameters are calculated by CST software.

E-band Transmitter Module Using a LCP Substrate

Young Chul Lee[1], **Salizul Jaafar**[2], **Mohd. Fadzil Amiruddin**[2], **Suhandi Bujang**[2], **and Azzemi Ariffin**[2]

[1]Division of Marine Electronics and Communication Engineering
Mokpo National Maritime University (MMU), Korea
[2]System Technology, Telecom Malaysia Research & Development (TMR&D), Korea

Abstract— We present a 70 GHz Amplitude-Shift-Keying (ASK) transmitter module based on a systemon-package (SoP) technology using a liquid-crystal polymer (LCP) substrate for point-topoint wireless communication applications. Four monolithic microwave integrated circuits (MMICs), which are two frequency multipliers (MTLs), a driver amplifier (DA), and a ASK modulator, are used in the metal-backed LCP SoP module. Its size is $15.8 \times 13.0 \times 2.2\,\mathrm{mm}^3$ and output power is -10.2 dBm at the local oscillation (LO) frequency of 12.017 GHz with 5 dBm, intermediate frequency (IF) of 20 MHz with ± 25 mV and -0.7 V for off-set.

Effect of Finger-patterned Electrodes on Tunability of Tunable Capacitors

Young Chul Lee[1], **Baek Ju Lee**[2], **and Kyung Hyun Ko**[2]

[1]Division of Marine Electronics and Communication Engineering
Mokpo National Maritime, University (MMU), Korea
[2]Department of Materials Science and Engineering, Ajou University, Korea

Abstract— In this paper, effect of the finger-patterned electrodes on tunability of tunable capacitors using multi-layer thin-film dielectrics is presented, compared with a conventional metalinsulator-metal (MIM) and inter-digital tunable capacitor. Type 1 and 2 capacitor with the finger-patterned electrode on the top metal and both top and bottom ones, respectively, were designed and fabricated on a quartz wafer employing a low-loss and high-tunability para/ferroelectric multi-layer thin film dielectric. At 2 GHz, the type 1 and 2 capacitor show tunability improvement of 3% and 26%, compared to the conventional MIM and inter-digital one, respectively.

Dumbbell Resonators to Reduce Crosstalk on Slotted Ground Plane

Ding-Bing Lin[1], **Chen-Kuang Wang**[1], **Chi-Hao Lu**[1], **and Jui-Hung Chou**[2]

[1]Graduate Institute of Computer and Communication Engineering
National Taipei University of Technology, Taiwan
[2]Graduate Institute of Communication Engineering, National Taiwan University, Taiwan

Abstract— By placing dumbbell resonators with different length on the slotted ground plane, the crosstalk noise can be decreased. The dumbbell resonators can be implemented on printed circuit board without additional cost by just designing length of resonators to improve crosstalk.

Introduction: Nowadays, the fabrication technology for integrated circuit (IC) is improved, million transistors are integrated into one chip and the numbers of transistor are increased rapidly. As to suppress power/ground coupling noise between different parts on the PCBs, using the etched slot on the power or ground planes is effective method since lower manufacture costs.

Dunbbell Resonators: Figure 1 shows the concept of the dumbbell resonators structure on slotted ground plane. A coupled microstrip lines can perpendicularly cross the slotted ground plane (36×2 mm). Dumbbell resonators are placed in PCB which consists of four symmetrically located at two sides of the coupled microstrip lines and one located between coupled microstrip lines.

Experimental Results: To verify the proposed methodology for NEXT and FEXT improvement, the waveforms of the NEXT and FEXT on victim line are measured. We chose the parameter values as follows: the thickness of the FR4 with dielectric constant 4.4 was 1.6 mm, copper thickness was 0.035 mm, width of microstrips was 3 mm, board width was 40 mm, and trace length 80 mm.

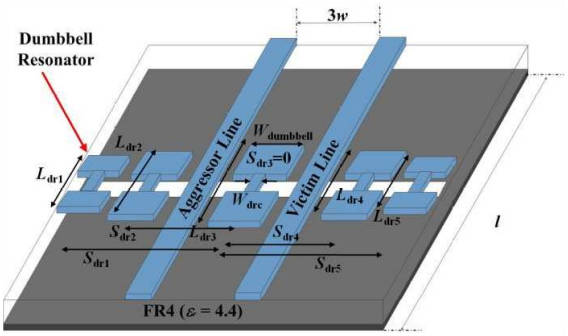

Figure 1: Physical structures of dumbbell resonators.

An Ultra-low-voltage CMOS VCO Using Parallel Capacitor for Phase Noise Reduction

Chun-Yi Lin, **Pei-Zong Rao**, **Hsen-Hung Chiu**, **and Shyh-Jong Chung**
Institute of Communication Engineering, National Chiao Tung University, Hsinchu, Taiwan

Abstract— In this work, a 0.62 V low-voltage VCO with 7.92 GHz output is introduced. The developed VCO uses LC tank with NMOS cross-coupled pair and cross-paralleled capacitor improving the phase noise. The phase noise at 600 kHz frequency offset is −98 dBc/Hz, at 1 MHz offset is −108 dBc/Hz, and the frequency tuning range is 300 MHz. This developed circuit can be applied to UWB system. The power consumption of VCO core circuit draws only 0.87 mW and FOM value is −187 dBc/Hz. This circuit is designed and implemented in TSMC 0.18 µm 1P6M CMOS technology.

Investigation of Zeros and Poles Properties for Filter Tuning Procedures

Mateusz Mazur and Jerzy Michalski
TeleMobile Electronics Ltd., Poland

Abstract— Tuning filters is time consuming procedure. Many approaches were proposed to reduce filters or diplexers production costs related to final trimming. For example, in [1] author describes implementation of artificial neural network with improved efficiency in filter tuning process, in [2] utilization of coupling matrix in that purpose is proposed. To utilize that method the structure of filter must be known, nevertheless, depending on structure, there may be more than one set of theoretical coupling matrix coefficients obtained from determined rational polynomials coefficients. The choice of proper one may be achieved by investigating resonant element properties [3].

The aim of that work was to investigate the behavior of physical filter's zeros and poles (z&p) on complex plane, find their sensitivity vs. trimming and define zones where they should be located to retain proper filter parameters. Convergence of z&p not to individual points on complex plane, but to defined, predicted zones should allow to improve trimming procedures.

Authors investigated behavior of filter scattering characteristics versus change of its ze&p values. They may be obtained theoretically from filter design or from measurements of tuned filter. The interpolation algorithm was used to obtain polynomial coefficients from measured data. Set of equations for rational polynomial is defined like in [4] and solved numerically. Next the coefficients were used to calculate zeros and poles. That method is fast, but accuracy of interpolation is limited. To achieve better results the optimization methods may be implemented. Standard optimization procedures were tested. As they are time consuming, especially for higher filter orders, it is hard to implement them directly in real time tuning system. A main afford was put to define the sensitivity of scattering parameters to its z&p movement on a complex plane. The Monte Carlo method was used to evaluate the characteristics of the filter when their localization change. Z&p new positions are defined as no farther then defined by radius R from origin ones. Simulating the behavior of scattering parameters versus different values of R allowed to define the areas in a complex plane, where z&p must be located to allow proper scattering characteristics of investigated device.

Also investigations related to change of z&p positions versus tuning elements set were proceeded. It allowed to define z&p traces on complex plane related to individual element trimming. That may be directly utilized in tuning procedures. Utilization of z&p on this stage of art will not give ability to tune high order filters due to small distances between them on complex plane that may cause problems with assigning dynamically z&p to trimming elements and traces. But for medium order filter it may be efficient to make first tuning steps before final optimization. Disadvantages of this approach are accuracy and speed in calculations. So further work will be focused on developing better and faster algorithms More detailed investigation of traces vs. different tuning elements sets are also required and will be proceeded.

ACKNOWLEDGMENT

This work is supported by National Ministry for Science & Higher Education (Decision nr. 736/N-COST/2010/0), under the project name "New optimization methods and their investigation for the application to physical microwave devices that require tuning" performed within the COST Action RFCSET IC0803.

REFERENCES

1. Michalski, J. J., "Artificial neural networks approach in microwave filter tuning," *Progress In Electromagnetics Research M*, Vol. 13, 173–188, 2010.
2. Cameron, R. J., "Advanced coupling matrix synthesis techniques for microwave filters," *IEEE Trans. Microwave Theory Tech.*, Vol. 51, No. 1, 1–10, January 2003.
3. Atia, A. E. and H.-W. Yao, "Tuning and measurements of couplings and resonant frequencies for cascaded resonators," *IEEE MTT-S Int. Microwave Symp. Dig.*, Vol. 3, 1637–1640, 2000.
4. Walsh, J. L., "Interpolation and approximation by rational functions in the complex domain," *Amer. Math. Soc.*, Vol. XX, Chapter IX, 1969.

Research for RFID Tag Implementation in Vehicle Environments

Shih-Chung Tuan[1], **Hsi-Tseng Chou**[2], **and Shih-Peng Liang**[2]

[1]Department of Communication Engineering, Oriental Institute of Technology, Pan-Chiao, Taiwan
[2]Department of Communication Engineering, Yuan Ze University, Chung-Li 320, Taiwan

Abstract— In this paper we study UHF RFID for applications under the vehicle environment and faced problems characteristic. RFID applications for the vehicle identified and electronic charging system in the expressway, pass in and out administrative system, number plate management and parts of car such as burglar-proof system have extensive using and develop prospectively. In above described to consider on the basis of convenience and cost down, the passive tag in vehicle environment are adopted. For example: number plate on the vehicle body's location that is in large-scale metal environment. Inside windshield of the car that is semi-closed metal environment. These environments for propagation characteristic of RFID system are damaging and interfere with and then will influence the range employed. The solution proposed simulation and measurement analyzing and according with the industry technical application of current RFID then developed the applicable products (Tag). To reach static and dynamic behavior detected for vehicle environment that the application category of RFID increased.

Terahertz High-pass Filter Fabricated by Imprinting Pd-based Bulk Metallic Glass

Tsong-Ru Tsai[1], **H. Sung**[1], **Y. C. Chen**[2], **and J. P. Chu**[2]

[1]Institute of Optoelectronic Sciences
National Taiwan Ocean University, Keelung City, Taiwan
[2]Department of Materials Science and Engineering
National Taiwan University of Science and Technology, Taipei City, Taiwan

Abstract— The authors have demonstrated an imprint process to create a two-dimensional (2D) wire array structure on a Pd-based bulk metallic glass (BMG) surface for filtering the terahertz (THz) radiation. By the simplified imprinting process, a 10×10 straight wire array with a wire height of $\sim 320\,\mu m$ and a diameter of $100.6\,\mu m$ is produced. After imprinting fabrication, a thin film of gold is electroplated on the BMG to ensure adequate conductivity. Transmission properties of the filter are measured and a turn-on frequency of 0.4 THz is observed.

Second Harmonic Reduction of Miniaturized Dual-mode Microstrip Bandpass Filters Using Fractal Shaped Open Stub Resonators

Jawad K. Ali and Hussam Alsaedi
Department of Electrical and Electronic Engineering, University of Technology, Baghdad, Iraq

Abstract— Higher harmonics normally accompany the performance of bandpass filers; and the miniaturized microstrip dual mode bandpass filters are not an exception. The use of the conventional open stub resonator to reduce such harmonics is not a practical solution since it has a length of a quarter the guided wavelength at the harmonic frequency. This will make the miniaturized filter larger. In this paper, the use of a fractal based open stub, with high space filling property, has been investigated as a more practical solution of the 2nd harmonic reduction of the miniaturized dual mode bandpass filters. The proposed stub has the Peano fractal shape geometry which is characterized by its high space-filling property. The Peano based stub has been applied to many miniaturized filter reported in the literature. Modeling and performance evaluation of the presented filters have been carried out using a full-wave electromagnetic EM simulator, from Sonnet Software Inc. Simulation results show that the introduction of the proposed stub maintains the physical size of the filter under test and improves the filter performance by reducing the harmonics to satisfactory levels. This might presents a solution for second harmonic reduction of a wide variety of miniaturized dual mode bandpass filters with different miniaturization levels.

Coupled-line Bandpass Filters Using Mixed Half-wave and Quarter-wave Resonators with Improved Out-of-band Response

Shih-Cheng Lin and Chi-Wen Hsieh

Department of Electrical Engineering, National Chiayi University, Chiayi City 60004, Taiwan, R.O.C.

Abstract— Parallel coupled-line microstrip filters (PCMF) feature easy design procedure, the feasibility of accomplishing wide factional bandwidth, and uni-planar structure. Over the past several decades, the design approach of PCMF has been well established. However, filters which fall into conventional catalog utilized half-wavelength ($\lambda/2$) resonator as fundamental resonators (i.e., the coupled-line section of $\lambda/4$ long) thus occupy large circuit size. In comparison with the spurious-suppression method employed so far, in this research, this study presents a thorough design methodology, including the concept discussion and detailed design formulas to design stopband-extended coupled-line filters utilizing both $\lambda/2$ and $\lambda/4$ stepped-impedance resonators (SIRs). The schematic layout of 3rd-order filter is depicted in Fig. 1 in advance. With careful derivations of the design equations, open-ended parallel coupled line (PCL) in Fig. 2(a) and short-ended anti-parallel coupled line (APCL) in Fig. 2(b) may be used with arbitrary coupled lengths. Specifically, a 3rd-order bandpass filter centering at 1 GHz with fractional bandwidth 10% is designed and implemented for validating the described concept. The alternative utilization of open-ended PCL and short-ended APCL provides the design flexibility when using different types of transmission line resonators as resonating components. Benefiting from the simultaneous use of $\lambda/4$ and $\lambda/2$ SIRs, the electromagnetic coupling at those spurious harmonics are significantly reduced. The proposed approach can be extended to higher-order filter design since the given design concept are general.

Without losing the simple design procedure of classical PCL filters, the complete design formulas are derived to facilitate the procedure. Since the harmonic resonances of $\lambda/2$ and $\lambda/4$ SIRs except for the fundamental one are well misaligned, the stopband is extended up to $8.69f_0$ without demanding SIRs possessing large impedance difference. The stopband with satisfactory rejection level of 33 dB up to $8.69f_0$ has been accomplished. This is a good achievement in improving out-of-band response with such simple filter structure. The presented filter may find application in modern microwave communication systems which demand wide out-of-band rejection for suppressing the unwanted interferences.

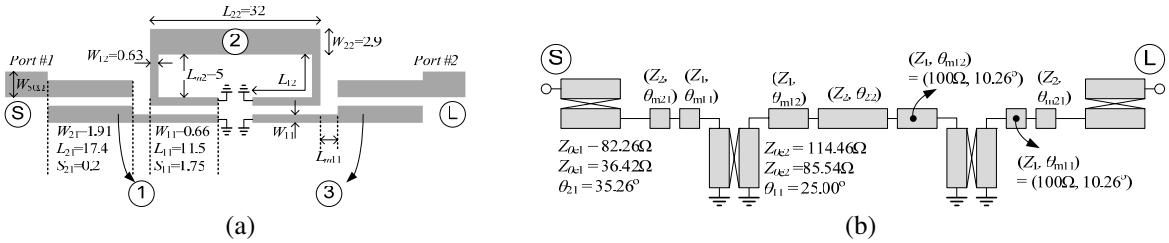

Figure 1: Proposed PCL filter using mixed $\lambda/2$ and $\lambda/4$ SIRs. (a) Schematic view. (b) Its corresponding equivalent circuit.

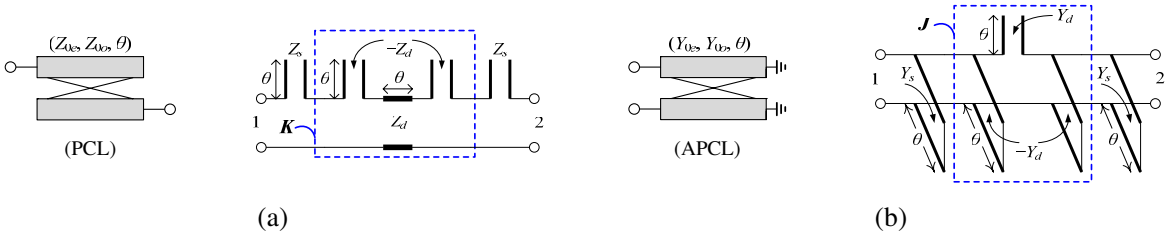

Figure 2: The main building blocks of the filter: (a) Open-ended PCL. (b) Short-ended APCL.

Design of K-band CMOS Frequency Divider Integrating a Marchand-type Transformer

Sen Wang and Chen-Chin Lin
Department of Electronic Engineering, National Taipei University of Technology, Taipei, Taiwan

Abstract— In this paper, a design of K-band frequency divider integrating a Marchand-type transformer based on 0.18-μm RF CMOS process is presented. The edge-coupled transformer is used to characterize and to provide differential signals for the CML frequency divider. The amplitude imbalance between S_{21} and S_{31} of the transformer is negligible below 35 GHz, and the phase imbalances are within 2° from 5 GHz to 33 GHz. Moreover, the insertion losses of the transformer are less than 6 dB from 21 GHz to 34 GHz. The 16 : 1 frequency divider formed by four 2 : 1 CML stages work correctly at entire K band with a total power consumption of 25 mW.

Compact MEMS Based Tunable Bandstop Microstrip Filter Using Defected Ground Structure (DGS)

Sajjad Ur Rehman, **Abdel Fattah A. Sheta**, **and Majeed A. S. Alkanhal**
Department of Electrical Engineering, King Saud University, Riyadh, KSA

Abstract— The paper presents a new compact tunable MEMS-based bandstop filter. The proposed tunable bandstop filter is constructed by employing coupled DGS resonators etched in the ground plane. The bandstop filter consists of symmetrical DGS resonators with a microstrip excitation to obtain a bandstop filter response. The coupling between the resonators is adjusted by placing a strip with width S between the two DGS resonators. The bandwith of the bandstop filter can be controlled by changing the strip width S. A bandstop tunable filter is achieved by short circuiting part of the slots etched in the ground plane using RF MEMS switches. The RF-MEMS switches placed at appropriate position across the slots of the DGS cells etched in the ground plane. Commercially available RF-MEMS switches (Radant MEMS RMSW101 SPST) are used for integration with the microstrip bandstop filter.

The paper first introduces a DGS cell based bandstop resonator. The DGS resonator dimensions are selected in order to allow place the MEMS switches at appropriate positions and implementing the bias strips. The tunability of the resonator is examined by placing short bridges across the DGS slot at various positions. The short bridges are placed at various positions in order to reduce the length of the DGS slot, which causes increase in the resonance frequency. The concept is then utilized to construct a compact tunable bandstop filter employing two coupled DGS resonators. For experimental verification, a tunable bandstop filter is designed, analyzed and implemented on Duroid dielectric substrate with 2.2 dielectric constant and 0.78 mm thickness. The tunable bandstop filter is implemented by actuating two RF MEMS switches, located at appropriate position on the slots etched in the ground plane. The ON and OFF states of the MEMS switches causes variation in center frequency of the bandstop filter. The tunable bandstop filter is designed to achieve about 830 MHz tuning range. The proposed filter has the ability to switch between the two center frequencies 1.42 GHz and 2.25 with approximately 150 MHz rejection bandwidth under the condition of 15 dB rejection.

In the past few years there are various techniques proposed for microstrip tunable bandstop filters filters using DGS. Tunability of the filters can be achieved using various devices such as: varactor diodes [1] and RF MEMS switches [2]. MEMS based tunable EBG bandstop filter with low insertion loss and miniatured size has been proposed in [2] to achieve tunability from 19 GHz to 17.3 GHz.

ACKNOWLEDGMENT

This work is supported by the National Plan for Science and Technology Program, Kingdom of Saudi Arabia, Research Grant: 08-ADV210-2.

REFERENCES

1. Wang, X. H., B. Z. Wang, H. Zhang, and K. J. Chen, "A tunable bandstop resonator based on a compact slotted ground structure," *IEEE Transactions on Microwave Theory and Techniques*, 1912–1918, 2007.
2. Karim, M. F., A. Q. Liu, A. B. Yu, and A. Alphones, "MEMS-based tunable bandstop filter using electromagnetic bandgap (EBG) structures," *Asia-Pacific Microwave Conference Proceedings*, Vol. 3, 4–7, 2005.

Broadband Resistive Active Power Combiner

B. Ravelo and E. R. Rajkumar
IRSEEM, EA 4353 at the Graduate School of Engineering ESIGELEC
Av. Galilée, BP 10024, 76801 Saint-Etienne-du-Rouvray Cedex, France

Abstract— Till now, most of the power combiners used in microwave engineering is designed with passive circuits [1–11]. Due to the losses, the application of these passive power combiners is limited. For this reason, our attention is attracted by the development of active power combiner based on the use microwave transistors. This letter addresses an investigation of an active power combiner susceptible to operate in very wide frequency band. Analytical approach illustrating the functioning principle of the active power combiner understudy is established and practical results from a proof of concept were proposed. The theory is mainly focused on the S-parameter analysis and followed by synthesis process enabling to determine the power combiner parameters. This latter is based-on the use of simple active cell comprising field effect transistor (FET) in cascade with shunt resistor similarly to resistive amplifier topology. Detailed S-parameter theoretic analysis of innovative two-way power combiner is provided. Moreover, according to basic characteristics of used FET, mathematical formulas illustrating how to synthesize each element of power combiner are established. Then, design of broadband active in-phase power combiner capable to operate with unequal gain is performed. For the validation of theoretical prediction, two-way power combiner containing three FETs was designed and simulated by using Advanced Design System (ADS) microwave circuit simulator from Agilent^{TM}. According to the employed PHEMT FET-EC-2612 bias regime, for 3-V DC supply voltage, the simulated power combiner consumes 90 mA. Therefore, interesting results showing insertion gains $|S_{31}|_{\mathrm{dB}}$ and $|S_{32}|_{\mathrm{dB}}$ above 6 dB with very good flatness accompanied by excellent return- and isolation-losses respectively, better than -10 dB and below -20 dB at all three accesses are obtained from 1 GHz to 9 GHz. Furthermore, by tuning an element of simulated active power combiner, gain control according to proposed analytic formulas is evidenced. In addition, in the indicated frequency range, a good flatness constant ratio, $\lambda = |S_{32}|/|S_{31}| = 1.050 \pm 0.002$ was also found between the two input accesses. Finally, potential applications of the active power combiner proposed are discussed.

REFERENCES

1. Joardar, S., M. Jaint, V. Bandewar, and A. B. Bhattacharya, "An innovative portable ultra wide band stereophonic radio direction finder," *Progress In Electromagnetics Research*, Vol. 78, 255–264, 2008.
2. NASA's Jet Propulsion Laboratory, Pasadena, CA, USA, "Four-way Ka-band power combiner. A prior X-band design has been adapted to Ka band," *NASA Tech. Briefs*, 13, Dec. 2007.
3. Chen, H. and Y. X. Zhang, "A novel compact planar six-way power divider using folded and hybrid-expanded coupled lines," *Progress In Electromagnetics Research*, Vol. 76, 243–252, 2007.
4. Wu, Y., Y. Liu, S. Li, C. Yu, and X. Liu, "Closed-form design method of an N-way dual-band Wilkinson hybrid power divider," *Progress In Electromagnetics Research*, Vol. 101, 97–114, 2010.
5. Catoiu, M., "A novel 3-way hybrid combiner/divider for high power C-class microwave amplifiers," *Proc. of IEEE MTT-Symposium IMS 2001*, Vol. 1, 31–34.B, Phoenix, AZ, USA, 2001.
6. Li, L. A., B. J. Hilliard, J. R. Shafer, J. Daggett, E. J. Dickman, and J. P. Becker, "A planar compatible traveling-wave waveguide-based power divider/combiner," *IEEE MTT*, Vol. 56, No. 8, 1889–1898, Aug. 2008.
7. Lin, Z. and Q.-X. Chu, "A novel approach to the design of dual-band power divider with variable power dividing ratio based on coupled-lines," *Progress In Electromagnetics Research*, Vol. 103, 271–284, 2010.
8. Li, X., Y.-J. Yang, L. Yang, S.-X. Gong, X. Tao, Y. Gao, K. Ma, and X.-L. Liu, "A novel design of dual-band unequal Wilkinson power divider," *Progress In Electromagnetics Research C*, Vol. 12, 93–100, 2010.
9. Wilkinson, E. J., "An n-way power divider," *IRE Trans. on MTT*, Vol. 8, 116–118, Jan. 1960.
10. Pozar, D. M., *Microwave Engineering*, 3rd Edition, John Wiley & Sons, New York, 2005.
11. http://www.microwaves101.com/encyclopedia/Resistive_splitters.cfm.

Triple Band Fractal Koch Antenna for Wearable Application

M. E. Jalil, M. K. A. Rahim, N. A. Samsuri, and N. A. Murad
Radio Communication Engineering Department, Faculty of Electrical Engineering
University Technology Malaysia, Skudai 81310, Johor, Malaysia

Abstract—

Introduction: Wearable antenna are important for the wireless devices on the medical and military communication system [1]. A compact size, flexible structure, comfortable to the user and low cost are the main requirement of antenna on this system. A number of researchers have studied on designing a various type of antenna for wearable application [2–4]. The size of the antenna has becomes the main issue on the wearable antenna. The antenna must have a compact size while maintaining the antenna's performance. In order to produce a compact size antenna, fractal antenna is introduced, which able to reduce the size of antenna [5]. In this paper, Koch fractal geometry for first iteration is designed with dipole antenna structure. The flare angle parameters of Koch fractal which involved 30 degree, 45 degree and 60 degree are investigated and analyzed. The antennas are optimized to perform at desired frequencies. The antenna performances such as return loss, gain and radiation pattern are determined. The proposed antenna cover three Industrial Scientific and Medical ISM band (0.902 GHz $\sim$ 0.928 GHz, 2.4 GHz $\sim$ 2.45 GHz and 5.725 $\sim$ 5.875 GHz).

Antenna Design Consideration: In this paper, a triple arm dipole antenna is employed to perform at triple-band operation. In order to obtain the design an antenna, a few parameters needed to be calculated such as the length of main arm.

These parameters were calculated according to Equation (1).

$$l = 0.5 \times \frac{c}{f\sqrt{\varepsilon_r}} \tag{1}$$

l = length of total dipole arm; c = velocity of speed; f = determined resonant frequency; ε_r = dielectric constant of material.

The main first arm dipole antenna is added with other two arm length to resonate at three frequency band. To get a 50 ohm impedance matching, the 4 mm of width main radiating element is calculated based on the substrate used. The combination of three arm length is carried out to perform at three different resonant frequencies (0.915 GHz, 2.45 GHz and 5.8 GHz).

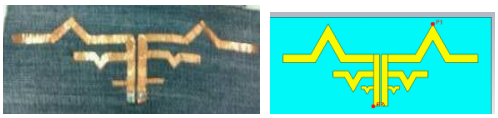

Figure 1: Prototype of multiband wearable antenna and simulation design.

Result and Discussion:

Table 1: The percentage of size reduction compared with the straight dipole length arm antenna.

Flare angle	Types of arm	height	Arm length
30	**1st**	**38.39 mm**	**63 mm**
	2nd		**27.3 mm**
	3rd		**8.55 mm**
45	**1st**	**42.94 mm**	**59.4 mm**
	2nd		**26.7 mm**
	3rd		**8.4 mm**
60	**1st**	**50.84 mm**	**56.7 mm**
	2nd		**25.2 mm**
	3rd		**7.65 mm**

Conclusion: The 60 degree flare multiband can reduced the size for all the arm antenna which consist of first arm length (56.7 mm), second arm (25.2 mm) and third arm (7.65 mm) compared

with other dipole antenna. The frequency range, return loss at determined frequency, gain and efficiency are presented in the full paper. The measurement and simulation results are described on the full paper.

REFERENCES

1. Winterhalter, C. A., J. Teverovsky, P. Wilson, J. Slade, W. Horowitz, E. Tierney, and V. Sharm, "Development of electronic textiles to support networks, communications, and medical applications in future U.S. military protective clothing system," *IEEE Transaction on Information Technology in Biomedicine*, Vol. 9, No. 3, September 2005.
2. Matthews, J. C. G., B. P. Pirollo, A. J. Tyler, and G. Pettittt, "Wide-band body wearable antennas," BAE Systems & Defence Science and Technology Laboratory.
3. Osman, M. A. R., M. K. A. Rahim, M. Azfar, N. A. Samsuri, F. Zubir, and K. Kamardin, "Design, implementation and performance of ultra wideband textile antenna," *Progress In Electromagnetics Research B*, Vol. 27, 307–325, 2011.
4. Ma, L., R. M. Edwards, S. Bashir, and M. I. Khattak, "A wearable flexible multiband antenna based on a square slotted printed monopole," *Loughborough Antennas & Propagation Conference*, 2008.
5. Karim, M. N. A., M. K. A. Rahim, T. Masri, and O. Ayop, "Analysis of fractal koch dipole antenna For UHF band," *IEEE International RF and Microwave Conference Proceeding*, 2008.

Session 3P1a
Optics, Photonics, and Biophotonics for Young Scholars and Researchers 2

Determination of Moisture Content of Hevea Rubber Latex Using a Microstrip Patch Antenna

N. Z. Yahaya[1], **Z. Abbas**[1], **M. A. Ismail**[1], **and B. Mohd Ali**[2]

[1]Department of Physic, Faculty of Science, Universiti Putra Malaysia
43400 UPM Serdang, Selangor Darul Ehsan, Malaysia
[2]Faculty of Engineering, Universiti Putra Malaysia
43400 UPM Serdang, Selangor Darul Ehsan, Malaysia

Abstract— The development of an accurate and low cost microstrip patch sensor for determination of moisture content in Hevea Rubber Latex is presented in this paper. The microstrip patch sensor was designed to operate at microwave frequency range from 0.1 to 5 GHz on a RT/Duroid substrate with 6.15 ± 0.015 permittivity and 1.27 mm thickness. The width and length of the rectangular patch antenna was 18 mm and 38 mm, respectively. The reflection coefficient of the sensor loaded with hevea latex at various percentages of moisture content from approximately 42.47% (fresh latex) to 77.57%. Calibration equations have been established between moisture content and magnitude of reflection coefficient at several selected frequencies. These equations were used to predict the amount of moisture content on hevea latex based on the measured reflection coefficient values. The actual values of moisture content were obtained using standard oven drying method. The lowest mean relative error between actual and predicted moisture contents was 0.06 at 3 GHz.

Synthesis of CIGS Absorber Layer by Solvothermal Route

Chao-Chi Wang[1, 2], **Pei-Chang Tsai**[3], **Jian-Hung Lin**[3],
Hsiang-Chen Wang[1, 2], **Chia-Chen Hsu**[1, 2, 3], **and Raymond Chien-Chao Tsiang**[1]

[1]Graduate Institute of Opto-Mechatronics
National Chung Cheng University, Chia-Yi 62102, Taiwan
[2]Advanced Institute for Manufacturing with High-Tech Innovations (AIM-HI)
National Chung Cheng University, Chia-Yi 62102, Taiwan
[3]Department of Physics
National Chung Cheng University, Chia-Yi 62102, Taiwan

Abstract— We use the selenide compounds and the nitrate compound of copper, indium, and gallium which were dissolved in alcohol then mix them well as a precursor. Then add the appropriate bonding agent and dispersing agent for viscosity adjustment, so that it can be uniform and complete coating on the glass substrate. By using this method, we have fabricated thin film of copper indium gallium selenide successfully. And we found that as annealing temperature increases, the XRD diffraction peak intensity increasing trend and the location will be slightly shift. Therefore, the lattice constant will be different as well. Experimental results show that after adding the dispersant agent in the precursor, its XRD diffraction intensity increase after annealing. In addition, the right amount of hydrogen gas in annealing process will be available to obtain larger grain size.

REFERENCES

1. Chuna, Y.-G., K.-H. Kim, and K.-H. Yoon, *Thin Solid Films*, Vol. 480–481, 46–49, 2005.
2. Lee, E., J. W. Cho, J. Kim, J. Yun, J. H. Kimc, and B. K. Mina, *Journal of Alloys and Compounds*, Article in press.

Optimal Visual Perception and Detection of Oral Cancer by Multi-spectral Imaging

Ta-Wei Chien[1, 2], **Yung-Tsan Chen**[1, 2], **Hsiang-Chen Wang**[1, 2], **Meng-Tsan Tsai**[3], **and Chun-Ping Chiang**[4]

[1]Graduate Institute of Opto-Mechatronics, National Chung Cheng University, Chia-Yi, Taiwan
[2]Advanced Institute for Manufacturing with High-Tech Innovations (AIM-HI)
National Chung Cheng University, Chia-Yi, Taiwan
[3]Department of Electrical Engineering, Chang Gung University, Tao-Yuan, Taiwan
[4]Department of Dentistry, National Taiwan University, Taipei, Taiwan

Abstract— A color reproduction system based on the multi-spectral imaging technique (MSI) for estimating reflection spectra of camera images is proposed. Images from an oral cancer patient were taken as the experimental sample, and spectrum differences between precancerous and normal oral mucosal tissues, were calculated after three times of the 5-Aminolevulinic acid photodynamic therapy (ALA-PDT) to analyze whether they were consistent with disease processes. The experimental results show that this system makes the estimated reflection spectra consist with treatment of the ALA-PDT. The decreased reflection in the blue-green wavelength range (430–575 nm) caused by the increased amount of hemoglobin of inflammation can be observed. This system can also reproduce images under different light sources. By using RGB LEDs with various correlated color temperatures (CCTs) for color difference comparison, the light source with CCT of about 4500 K was found that it has the best ability to enhance the color difference between cancerous and normal oral mucosal tissues in oral cavity.

Discrimination of Precancerous Stages with Optical Coherence Tomography

Hong-Li Jin, **Meng-Tsan Tsai**, **and Jainn-Der Lee**
Department of Electrical Engineering, Chang Gung University
259 Wen-Hwa 1st Road, Kwei-Shan, Tao-Yuan 33302, Taiwan

Abstract— Optical coherence tomography (OCT) has been widely used for biomedical applications due to noninvasive, depth-resolves, and high imaging speed natures. Compared with ultrasound technique, OCT provide much higher resolutions including the longitudinal and lateral resolutions. Here, a swept-source optical coherence tomography (SS-OCT) is used for cancer studies. A swept-source centered at 1310 nm with a full width at half maximum of 90 nm was used as the light source. This OCT system can provide a frame rate of 30 frames/s and each frame consists of 1000 A-scans. The longitudinal and transverse resolutions of our OCT system are approximately 11 µm and 20 µm, respectively. In this study, oral mucosa samples from the patients in the different stages of oral precancer were scanned with OCT system *ex vivo*. In precancerous stages, the boundaries between the epithelium and lamina propria layers gradually disappeared, which can be a useful indicator to identify the existence of dysplasia. From the OCT images, this phenomenon also can be found. Aside from the acquisition of OCT structural images to discriminate the different precancerous stages, a new approach is proposed to analyze the optical path difference (OPD) in the epithelium layer, which is related to the change of refractive index of the epithelium layer. Based on the proposed approach, the different stages of precancer can be discriminated.

Optimal Illumination for the Direct Visualization of Oral Cavity

Tsung-Chih Lin[1, 2], **Yung-Tsan Chen**[1, 2], **and Hsiang-Chen Wang**[1, 2]

[1]Graduate Institute of Opto-Mechatronics
National Chung Cheng University, Chia-Yi, Taiwan
[2]Advanced Institute for Manufacturing with High-Tech Innovations (AIM-HI)
National Chung Cheng University, Chia-Yi, Taiwan

Abstract— A color reproduction system based on the multi-spectral imaging technique (MSI) for estimating reflection spectra of camera images is proposed. Images from an enterovirus-infected child were taken as the experimental sample, and spectrum differences between normal and abnormal oral tissues were calculated for three days of the infection to analyze whether they were consistent with disease processes. The experimental results show that this system makes the estimated reflection spectra consist with development of the disease. The decreased reflection in the blue-green wavelength range (430–575 nm) caused by the increased amount of hemoglobin of inflammation can be observed. This system can also reproduce images under different light sources. By using RGB LEDs with various correlated color temperatures (CCTs) for color difference comparison, the light source with CCT of about 4500 K was found that it has the best ability to enhance the color difference between normal and inflamed tissues in oral cavity.

Session 3P1b
Generation, Transform, Propagation and Applications for Laser Beams

Experimental Study of the Coupling of a Stochastic Beam into a Single-mode Optical Fiber

Chengliang Zhao and Yangjian Cai
School of Physical Science and Technology, Soochow University, Suzhou 215006, China

Abstract— Coherence and polarization are two important properties of light beam, and were studied separately in the past decades. It is conventionally assumed that the degree of polarization of light wave remains invariant on propagation in free space. Recent research results show that the degree of polarization of a stochastic electromagnetic beam (i.e., partially coherent and partially polarized beam) may change on propagation in free space, and such change depends closely on the initial coherence. Electromagnetic Gaussian Schell-model (EGSM) beam was introduced as a natural extension of the scalar GSM beam. On the other hand, in 1972, Cohen carried out experimental study of the coupling GaAs injection lasers into optical fibers. Since then, the coupling of light into optical fibers has been investigated extensively due to its wide applications in optical communications, biomedical optics, lidar, stellar interferometry, and wavefront sensing. Most of previous literatures were published on the coupling of coherent laser beams into optical fibers, and only few theoretical efforts were paid to the coupling stochastic scalar and electromagnetic beams into optical fibers. Recently, Salem et al. theoretically studied the effects of coherence and polarization on the coupling of an EGSM beam into optical fibers, and found that the coupling efficiency are closely related with the coherence and polarization. In this paper, we report the experimental study of the coupling of a stochastic electromagnetic Gaussian Schell-model (EGSM) beam into a single-mode optical fiber. It is found that the coupling efficiency depends closely on the coherence and polarization properties of the EGSM beam. Our results are consistent with the theoretical predictions reported in previous literatures.

The Optical Airy Transform and Its Application in Generating and Controlling the Airy Beam

Yunfeng Jiang, Kaikai Huang, and Xuanhui Lu
Department of Physics, Institute of Optics, Zhejiang University, Hangzhou 310027, China

Abstract— We propose an optical Airy transform and obtain the analytical expressions for the Airy transform of fundamental Gaussian beams and finite energy Airy beams. The setup for performing the optical Airy transform is presented. The Airy transform for Gaussian beams and finite energy Airy beams are theoretically calculated and analyzed. The numerical results show that through the optical Airy transform, the Airy beam can be easily and conveniently generated and controlled. It is also found that the two dimensional Airy beams can even be transformed into fundamental Gaussian beams with the Airy transform.

Generation and Propagation of a Stochastic Electromagnetic Gaussian Schell-model Beam

Yahong Chen, Fei Wang, and Yangjian Cai
School of Physical Science and Technology, Soochow University, Suzhou 215006, China

Abstract— Stochastic electromagnetic Gaussian Schell-model (EGSM) beam has important applications in free-space optical communication, optical imaging, laser radar and particle trapping. In this paper, we report experimental generation of a stochastic electromagnetic Gaussian Schell-model (EGSM) beam. The beam parameters of the generated EGSM beam are measured. Furthermore, the propagation properties of a stochastic EGSM beam through a thin lens are studied theoretically with the help of the tensor method, and are compared with the experimental results. Our experimental results agree well with the theoretical predictions.

Experimental Generation of a Partially Coherent Vortex Beam

Fei Wang, **Shijun Zhu**, **and Yangjian Cai**
School of Physical Science and Technology, Soochow University, Suzhou 215006, China

Abstract— In many applications, such as optical trapping, free-space optical communication and material thermal processing, laser beams with special beam profiles are required. Recently, more and more attention is being paid to partially coherent dark hollow (DH) and flat-topped (FT) beams, and it is found that partially coherent DH or FT beam has advantage over corresponding coherent beam for applications in optical trapping and free-space optical communications. Experimental generations of those beams have been reported, respectively. We usually use either focused Gaussian or FT beams to trap a particle with a refractive index larger than that of the ambient, and focused DH beam to trap a particle with refractive index smaller than that of the ambient. Thus it would be convenient for us to trap two types of particles with different refractive indices if we can generate focused DH, FT and Gaussian beam spots using one optical setup. Vortex beam whose phase has a spiral structure exhibits many new phenomena and has important applications in singular optics, optical trapping and free-space optical communication. Partially coherent vortex beam attracts increased attention recently. In this letter, we report experimental generation of a partially coherent vortex beam, and study its focusing properties both experimentally and theoretically, and we find that it is possible to obtain focused DH, FT and Gaussian beam spots by varying the initial coherence. The experimental results agree well with the theoretical results. Our results will be useful for trapping two types of particles with different refractive indices using one optical setup.

Session 3P2
Plasmonic Nanophotonics II - Theory, Design and Simulation

Electromagnetic Forces in Metallic Cavity

S. B. Wang[1], **Jack Ng**[1], **H. Liu**[2], **H. H. Zheng**[1], **Z. H. Hang**[1], **and C. T. Chan**[1]

[1]Department of Physics and William Mong, Institute of Nano Science and Technology
The Hong Kong University of Science and Technology, Clear Water Bay, Hong Kong, China
[2]Department of Physics, National Laboratory of Solid State Microstructures
Nanjing University, Nanjing 210093, China

Abstract— Particles can be trapped or manipulated using light [1] through light-induced forces. After the invention of the laser,optical forces have been extensively studied and find useful applications in various sub-fields in physics and beyond. Optical tweezers, as an example, have been widely used in atoms cooling and biologic cell/molecule (e.g., DNA) manipulations. Using a boundary element method, we studied the forces induced by electromagnetic waves in a metal-air-metal sandwich structure, which forms a metallic cavity under certain polarization of the incident wave [2, 3]. Different frequency regimes are considered, from the plasmonic regime with nano-scale structures down to the microwave regime, which involves millimeter-scale structures. We found that at both length scales, electromagnetic-wave-induced forces can be significantly stronger than the usual photon pressure exerted by a laser beam if the cavity is excited at resonance, although the mechanisms that underlie the strong force are very different at different length scales. In the plasmonic regime, the strong force is induced by field penetration into the metal and the dominance of the internal inductance, whereas in the microwave regime, the electromagnetic force is induced by the leakage of electric field at the edges. We showed that a transmission line model can give simple expressions that can capture the essence of the physics. The effects of surface corrugation and surface roughness are also investigated, and we find that corrugation/roughness generally induces attraction between the plates as a consequence of spoof surface plasmon effect.

REFERENCES

1. Ashkin, A., *Phys. Rev. Lett.*, Vol. 24, 156–159, 1970.
2. Liu, H., J. Ng, S. B. Wang, Z. F. Lin, Z. H. Zhang, C. T. Chan, and S. N. Zhu, *Phys. Rev. Lett.*, Vol. 106, 087401, 2011.
3. Wang, S. B., J. Ng, H. Liu, H. H. Zheng, Z. H. Hang, and C. T. Chan, *Phys. Rev. B*, Vol. 84, 075114, 2011.

Plasmonic Metamaterials: From Total Absorption to High Tunneling

Jiaming Hao, **Laurent Santandrea**, **and Said Zouhdi**
Laboratoire de Génie Electrique de Paris (LGEP)
Supélec, Plateau de Moulon, Gif-sur-Yvette 91192, France

Abstract— Plasmonic metamaterials are artificial materials composed by subwavelength local resonance structures. Much attention has been attracted recently due to which display fascinating physical properties and promise many potential applications involving waves and energy (e.g., negative refraction, the superlensing effect, polarization control and invisibility cloaking). However, the existences of intrinsic material losses would greatly detrimental to their performance. In this paper, we firstly apply the concept of plasmonic metamaterials to design perfect optical absorption devices, in which the loss properties of the materials have been sufficiently exploited rather than avoiding them. On the other hand, in comparison with total absorption, systems with greatly transparent properties based on plasmonic metamaterials are also studied. Theoretical analyses and Numerical efforts are preformed for both cases around optical communication frequencies. The potential impact of our proposed systems in the field of photonics and nanoscience are discussed also.

REFERENCES

1. Smith, D. R., J. B. Pendry, and M. C. K. Wiltshire, *Science*, Vol. 305, 788, 2004.
2. Atwater, H. A. and A. Polman, *Nature Mater.*, Vol. 9, 205, 2010.
3. Hao, J., Y. Yuan, L. Ran, T. Jiang, J. A. Kong, C. T. Chan, and L. Zhou, *Phys. Rev. Lett.*, Vol. 99, 063908, 2007.
4. Leonhardt, U., *Science*, Vol. 312, 1777, 2006.
5. Pendry, J. B., D. Schurig, and D. R. Smith, *Science*, Vol. 312, 1780, 2006.
6. Landy, N. I., S. Sajuyigbe, J. J. Mock, D. R. Smith, and W. J. Padilla, *Phys. Rev. Lett.*, Vol. 100, 207402, 2008.
7. Chen, H. T., J. F. Zhou, J. F. O'Hara, F. Chen, A. K. Azad, and A. J. Taylor, *Phys. Rev. Lett.*, Vol. 105, 073901, 2010.

Engineering of Radiation of Optically Active Molecules with Chiral Nano-meta-particles

Vasily Klimov
Lebedev Physical Institute, Russian Academy of Sciences, Russia

Abstract— It is well known that nanoparticles influence substantially both fluorescence of molecules and Raman scattering of light by molecules. These effects are especially strong in the case of metallic nanoparticles where plasmon resonances can be excited. When investigating such processes it is usually assumed that only electric dipole transitions are important. However, both electric and magnetic dipole momenta of transitions are important in chiral biomolecules. The goal of present work is to investigate influence of nanoparticles made of metamaterial on spontaneous emission of chiral molecules. We have built general theory, where decay rate was expressed through Green's function of Maxwell equations in presence of nanoparticle. Then we apply our general theory to spontaneous emission of chiral molecule placed near nanosphere made of different materials, including chiral "left-handed" metamaterial. We have found general conditions when radiation of right or left molecules can be fully suppressed. It paves the way to control radiation of chiral molecules. In Fig. 1, the example of our calculations is shown.

From this figure one can see the substantial (by a factor of fifty at $\varepsilon = -0.75$, see right panel of Fig. 1) influence of nanoparticles on spontaneous emission of chiral molecules with different chiralities ("right" and "left" molecules) due to appearance of interference between radiation of electric and magnetic dipoles. Let us stress that "left-handedness" of chiral sphere is of crucial importance for such discrimination.

An application of results obtained to separate racemic mixtures of drug enantiomers is suggested.

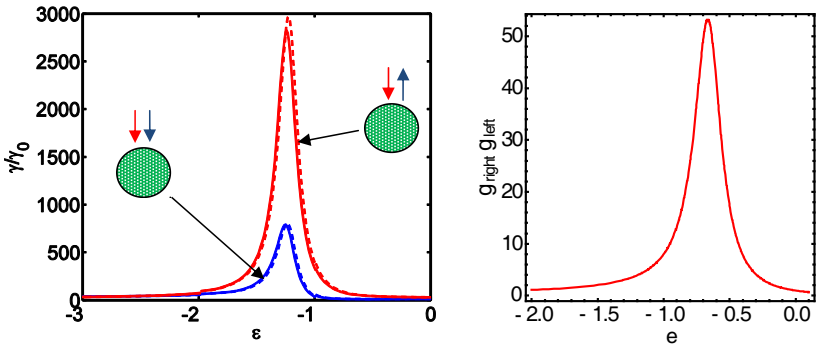

Figure 1: Relative decay rates of chiral molecules placed near chiral nanosphere. Blue curve corresponds to parallel orientation of electric and magnetic dipole moments of chiral molecule, while red curve corresponds to antiparallel orientations. (a) Dashed lines correspond to quasistatic approximation. (b) Ratio of decay rates of right and left molecules as function of sphere dielectric constant ε. Sphere parameters: Magnetic permeability $\mu = -1.9$, dimensionless chirality parameter $\kappa = 0.1$, size parameter $kR_0 = 0.1$. Electric and magnetic dipole momenta of chiral molecules are oriented along radius and their ratio is equal to $m_{or}/d_{or} = \pm 0.1$.

ACKNOWLEDGMENT

The author thanks the Russian Foundation for Basic Research (grants ## 11-02-01272, 11-02-91065, 11-02-92002) for financial support of this work.

Plasmonic Toroidal Metamaterials at Optical Frequencies

Yao-Wei Huang[1], **Wei Ting Chen**[1], **Pin Chieh Wu**[1], **You Zhe Ho**[1], **Yuan-Fong Chau**[2], **Nikolay I. Zheludev**[3], **and Din Ping Tsai**[1, 4, 5]

[1]Department of Physics and Graduate Institute of Applied Physics
National Taiwan University, Taipei 106, Taiwan
[2]Department of Electronic Engineering, Ching Yun University, Jung-Li 320, Taiwan
[3]Optoelectronics Research Centre and Centre for Photonic Metamaterials
University of Southampton, Southampton SO17 1BJ, UK
[4]Instrument Technology Research Center
National Applied Research Laboratories, Hsinchu 300, Taiwan
[5]Research Center for Applied Sciences, Academia Sinica, Taipei 115, Taiwan

Abstract— Toroidal dipole is created by currents flowing on a surface of a doughnut-shaped structure along its meridians first considered by Zel'dovich in 1957 [1]. Toroidal metamaterials were first theoretically proposed in 2007 [2]. In 2010, the toroidal metamaterials consisted by four three-dimensional resonant split rings show toroidal response in microwave region [3].

In this paper, we study the optical responses by integrating four U-shaped split-ring resonators (SRRs) together. The resonances of the four U-shaped SRRs array with magnetic field of incident light passing through the resonant rings was numerically investigated by using commercial software COMSOL 3.5a based on finite-element method (FEM). The permittivity of gold was described by the Lorentz-Drude model [4]. The size of a single U-shaped SRR is 250 nm (arms) $\times$300 nm (bottom) and 50 nm line width wire loop. Simulation results shows toroidal and magnetic dipole resonance at free space wavelength 2520 nm and 2620 nm respectively. Incident light induced magnetic dipoles point in the same direction produced magnetic resonance. In contrast, four magnetic dipoles form a head-to-tail configuration which concentrates toroidal resonance.

ACKNOWLEDGMENT

The authors thank the research support from National Science Council un-der grant number 99-2120-M-002-012, 99-2911-I-002-127, 100-2923-M-002-007-MY3 and 100-2120-M-002-008. D. P. Tsai thanks National Center for Theoretical Sciences, Taipei Of-fice and National Center for High-Performance Computing.

REFERENCES

1. Zel'dovich, I. B., "The relation between decay asymmetry and dipole moment of elementary particles," *Soviet Physics — JETP*, Vol. 6, 1184, 1958.
2. Marinov, K., A. D. Boardman, V. A. Fedotov, and N. Zheludev, "Toroidal metamaterial," *New Journal of Physics*, Vol. 9, 324, 2007.
3. Kaelberer, T., V. A. Fedotov, N. Papasimakis, D. P. Tsai, and N. I. Zheludev, "Toroidal dipolar response in a metamaterial," *Science*, Vol. 330, No. 6010, 1510–1512, 2010.
4. Chen, W. T., P. C. Wu, C. J. Chen, H. Y. Chung, Y. F. Chau, C. H. Kuan, and D. P. Tsai, "Electromagnetic energy vortex associated with sub-wavelength plasmonic Taiji marks," *Optics Express*, Vol. 18, No. 19, 19665–19671, 2010.

Generalization of Superscatterer Design and Photorealistic Raytracing Thereof

Alireza Akbarzadeh, **Tiancheng Han**, **Aaron J. Danner**, **and Cheng-Wei Qiu**
Department of Electrical and Computer Engineering
National University of Singapore, Singapore 117576, Singapore

Abstract— Enhancement of light scattering and absorption by optically small particles is of fundamental interest in both theoretical and experimental physics. It is known that the energy of light incident into a small particle is mostly stored in the near field and the radiation efficiency of such a particle is extremely low. In order to overcome this undesirable near field storage, different techniques have been proposed. Recently the concept of complementary media has been invoked to enrich the scattered or absorbed energy by a small particle, though the suggested approaches rely on initial knowledge of the spatial transformation [1, 2].

In this presentation, an inverse method based on the spatial transformation will be proposed to design a general superscatterer. In fact it will be shown that any well defined function can act as a generating function to produce the required parameters for the superscatterer profile. Accordingly the complementary media can be uniquely determined without having prior knowledge of the corresponding spatial transformation. However, the superscatterer profile is not unique and this inverse recipe is inclusive of all possible parametric profiles and hence leads to preferred field patterns in the complementary media. This concept provides a straightforward way to investigate the parameters of the superscatterer, which will be employed to obtain an isotropic retro-reflecting superscatterer with inhomogeneous negative refractive index. The mathematical formulation will be presented in a regressive manner in both 2D and 3D. Along with these calculations, several full wave simulations of the designed superscatterers will be provided, in which different generating functions will be examined. The required parameters for the design of an isotropic superscatterer will be driven and imaging characteristics of that will be studied. In addition to the full wave simulations, ray tracing analyses will be conducted to provide a better estimation on how the designed superscatterers actually work (Figures 1(a), (b)). On the basis of the given ray trajectories, time-flying animations will be illustrated to give an idea of how the superscatterers may look like in real life (Figures 1(c), (d)).

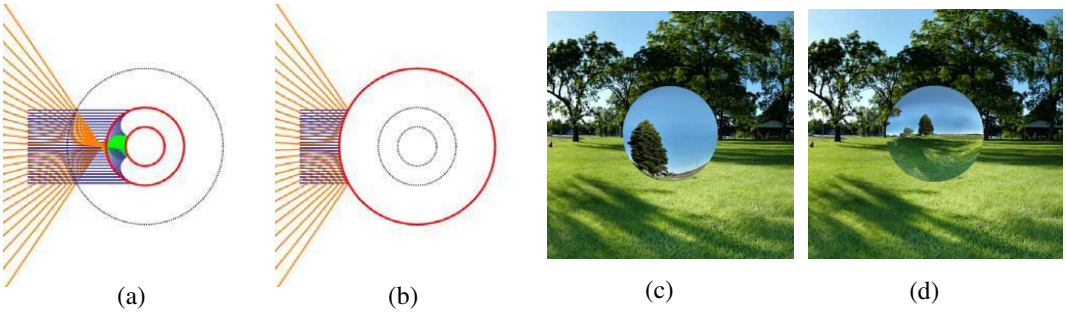

Figure 1: (a) Ray trajectories of a superscatterer. (b) Ray trajectories of a bare mirror which shows equivalence with the outgoing rays in (a). (c) A snapshot of the coated mirror (the superscatterer). (d) A snapshot of the bare mirror.

REFERENCES

1. Wee, H. and J. B. Pendry, "Shrinking optical devices," *New J. Phys.*, Vol. 11, 073033, 2009.
2. Yang, T., H. Chen, X. Luo, and H. Ma, "Superscatterer: Enhancement of scattering with complementary media," *Opt. Exp.*, Vol. 16, 18545–18550, 2008.

Subwavelength Modulational Instability And Plasmon Oscillons in Arrays of Metal Nanoparticles

Roman E. Noskov[1], **Pavel A. Belov**[1], **and Yuri S. Kivshar**[1, 2]

[1]St. Petersburg University of Information Technologies, Mechanics and Optics (ITMO)
St. Petersburg 197101, Russia
[2]Nonlinear Physics Centre, Research School of Physics and Engineering
Australian National University, Canberra ACT 0200, Australia

Abstract— Nonlinearity-induced instabilities are observed in many branches of physics, and they provide probably the most dramatic manifestation of strongly nonlinear effects that can occur in Nature. Modulational instability in optics manifests itself in a decay of broad optical beams or quasi-continuous wave pulses into optical filaments or pulse trains [1], and such effects are well documented in both theory and experiment. It is expected that the study of subwavelength nonlinear systems such as metallic nanowires or arrays of nanoparticles will bring many new features to the physics of modulational instability and the scenarios of its development, however such effects were never studied before.

Over the past decade, surface plasmon polaritons were suggested as the mean to overcome the diffraction limit in optical systems. In particular, by using plasmons excited in a chain of resonantly coupled metallic nanoparticles [2], one can spatially confine and manipulate optical energy over distances much smaller than the wavelength. In addition, strong geometric confinement can boost efficiency of nonlinear optical effects, including the existence of subwavelength solitons [3, 4].

In our work, we study modulational instability in nonlinear arrays of subwavelength metal nanoparticles, and analyze numerically nonlinear scenarios of the instability development. We demonstrate that modulational instability can lead to the formation of regular periodic or quasi-periodic modulations of the polarization. We reveal that such nonlinear nanoparticle arrays can support long-lived standing and moving oscillating nonlinear localized modes which can be termed *plasmon oscillons*, in analogy with the similar localized modes excited in driven granular materials [5] and Newtonian fluids [6].

ACKNOWLEDGMENT

The authors acknowledge a support from the Australian Research Council and a mega-grant of the Ministry of Education and Science of Russian Federation, as well as fruitful discussions with A. A. Zharov.

REFERENCES

1. Bespalov, V. I. and V. I. Talanov, "Filamentary structure of light beams in nonlinear liquids," *JETP Lett.*, Vol. 3, 307, 1966.
2. Takahara, J., S. Yamagishi, H. Taki, A. Moromoto, and T. Kobayashi, "Guiding of a one-dimensional optical beam with nanometer diameter," *Opt. Lett.*, Vol. 22, 475, 1997.
3. Liu, Y., G. Bartal, D. A. Genov, and X. Zhang, "Subwavelength discrete solitons in nonlinear metamaterials," *Phys. Rev. Lett.*, Vol. 99, 153901, 2007.
4. Ye, F., D. Mihalache, B. Hu, and N. C. Panoiu, "Subwavelength plasmonic lattice solitons in arrays of metallic nanowires," *Phys. Rev. Lett.*, Vol. 104, 106802, 2010.
5. Umbanhowar, P. B., F. Melo, and H. L. Swinney, "Localized excitations in a vertically vibrated granular layer," *Nature*, Vol. 382, 793, 1996.
6. Arbell, H. and J. Fineberg, "Temporally harmonic oscillons in newtonian fluids," *Phys. Rev. Lett.*, Vol. 85, 756, 2000.

Study of Transformation Optics with Uniform and Non-uniform Grid in Electro-optical Simulation

Jian-Shiung Hong[1], **Wei-Ming Cheng**[2], **Ruei-Cheng Shiu**[1], **Yung-Chiang Lan**[1], **and Kuan-Ren Chen**[1, 3, 4, 5]

[1]Institute of Electro-Optical Science and Engineering
National Cheng Kung University, 1 University Road, Tainan 70101, Taiwan, R.O.C.
[2] Institute of space, Astrophysical and Plasma Sciences
National Cheng Kung University, 1 University Road, Tainan 70101, Taiwan, R.O.C.
[3]Department of Physics
National Cheng Kung University, 1 University Road, Tainan 70101, Taiwan, R.O.C.
[4]Advanced Optoelectronic Technology Center
National Cheng Kung University, 1 University Road, Tainan 70101, Taiwan, R.O.C.
[5]Research Center for Energy Technology and Strategy
National Cheng Kung University, 1 University Road, Tainan 70101, Taiwan, R.O.C.

Abstract— We employ the parallel 3D finite-difference time-domain (FDTD) method to simulate the enhanced transmission of electromagnetic wave through a rectangle subwavelength slit in an infinite film of perfectly electric conductor (PEC). Since the slit is much smaller than the wavelength, high resolution is required for the simulation so that the computation can be extremely large. The technique of transformation optics is applied to simulate a system with non-uniform cell size and thus to reduce significantly the computation requirement. It offers the possibility of realizing the coordinate mapping of light between physical and numerical system by changing the material properties, ε and μ, with a designed transform function. In the point view of simulation, the advantage of this technique can be taken so that the resolutions of both systems can be tuned. We design a physical system that has a higher resolution around the slit area as required while the resolution is lower at other areas so that the overall cell number is greatly reduced. With the use of transformation optics, the non-uniform physical cell system is transformed into a uniform numerical cell system while the uniform material properties become non-uniform. The Courant condition for numerical stability is also derived. The numerical cell system is then simulated by a FDTD code, MEEP. The numerical result yielded is then transformed back to physical system and is found to be consistent with a large computation with uniform physical cells and with the analytical result.

Coherence-converting Plasmonic Hole Arrays

Greg Gbur[1], **Choon How Gan**[2], **Yalong Gu**[1], **and Taco D. Visser**[3,4]

[1]Department of Physics and Optical Science, University of North Carolina at Charlotte, USA
[2]Institute of High Performance Computing, Agency for Science, Technology and Research, Singapore
[3]Department of Physics and Astronomy, Free University, Amsterdam, The Netherlands
[4]Department of Electrical Engineering, Delft University of Technology, Delft, The Netherlands

Abstract— It has been known for some time that the presence of surface plasmons on a metal plate can influence the amount of light transmitted through an array of subwavelength-size holes, in a phenomenon now referred to as "extraordinary optical transmission". This transmission is typically larger than that predicted by classical theoretical optics, though under certain circumstances it can also be smaller. Both enhanced and suppressed transmission has been shown to be the result of plasmon-mediated coupling of light emitted from different holes; this was demonstrated in a simple manner both theoretically and experimentally using a plasmonic version of Young's double slit experiment. In this experiment, a pair of slits were etched in a metal screen that supports plasmons at optical frequencies. The transmission showed strong oscillations as a function of wavelength, readily interpreted as interference between light directly transmitted through a hole with light coupled from the other hole via surface plasmons.

More recently, it has been shown that this coupling can also affect the spatial coherence of light in a Young-type interferometer with two or three slits [1]. The spatial coherence of light can be enhanced or suppressed on transmission through the interferometer, depending on the wavelength of light, the slit separation, and the light-plasmon coupling. This modification of spatial coherence is created by the plasmon-mediated mixing of light between apertures, and the modification can often range from complete spatial coherence to complete incoherence of the emerging wavefield.

Spatial coherence is an important characteristic of a light field, and can influence its propagation characteristics, spectral properties, polarization, and interference-causing capability. The existence of plasmon-induced coherence changes suggests that it may be possible to use an array of holes in a metal plate to change the global state of coherence of an optical beam, and could be extremely useful in applications where variable coherence is necessary.

In this paper, we extend the plasmon coherence results for the Young interferometer and consider the effect of surface plasmons on the spatial coherence of light on transmission through an array of holes in a metal plate. Simulations suggest that the overall global state of spatial coherence of a light beam can be modified on transmission, making a plasmonic hole array a "coherence-converting" optical device.

REFERENCES

1. Gan, C. H., G. Gbur, and T. D. Visser, "Surface plasmons modulate the spatial coherence in Young's interference experiment," *Phys. Rev. Lett.*, Vol. 98, 043908, 2007.

Design of Optical Hybrid-Hyperlens for Go beyond the Diffraction Limit

B. H. Cheng[1], **Y. Z. Ho**[2], **Y. C. Lan**[1], **and D. P. Tsai**[2, 3, 4, 5]

[1]Department of Photonics, National Cheng Kung University, Tainan 701, Taiwan, R.O.C.
[2]Department of Physics, National Taiwan University, Taipei 10617, Taiwan
[3]Graduate Institute of Applied Physics, National Taiwan University, Taipei 10617, Taiwan
[4]Instrument Technology Research Center, National Applied Research Laboratories, Hsinchu 300, Taiwan
[5]Research Center for Applied Sciences, Academia Sinica, Taipei 115, Taiwan

Abstract— We proposed a new design device called "*Hybrid Hyperlens*" which is capable of overcoming the diffraction limit. This device is composed of two anisotopic metamaterials that possess opposite signs of the two permittivity tensor component in each constituent. The upper part is a planar layered metal-dielectric system proposed by Pendry et al. [1]. The lower part, "hyperlens" [2–4] takes a form of cylindrical metamaterial comprising periodic metal and dielectric layers. Both upper part and lower part which are the anisotropy medium have interesting properties. The subwavelength details of the object which are the high-spatial-frequency component are enhanced and transmitted through the upper hyperlens at certain frequencies [1]. Then the lower hyperlens form a magnified optical image of subwavelength object in the far field [3].

In this paper, we reported 150 nm resolution at 410 nm working wavelength with the flat object plane which is convenient for placing object.

ACKNOWLEDGMENT

The authors thank the research support from National Science Council un-der grant number 99-2120-M-002-012, 99-2911-I-002-127, 100-2923-M-002-007-MY3 and 100-2120-M-002-008. D. P. Tsai thanks National Center for Theoretical Sciences, Taipei Of-fice and National Center for High-Performance Computing.

REFERENCES

1. Wood, B., J. B., Pendry, and D. P. Tsai, "Directed subwavelength imaging using a layered metal-dielectric system," *Phys. Rev. B*, Vol. 74, No. 11, 115116, 2006.
2. Jacob, Z., L. V. Alekseyev, and E. Narimanov, "Optical Hyperlens: Far-field imaging beyond the diffraction limit," *Optics Express*, Vol. 14, No. 18, 8247–8256, 2006.
3. Lee, H., Z. W. Liu, Y. Xiong, C. Sun, and X. Zang, "Development of optical hyperlens for imaging below the diffraction limit," *Optics Express*, Vol. 14, No. 18, 8247–8256, 2006.
4. Liu, Z. W., H. Lee, Y. Xiong, C. Sun, and X. Zang, "Far-field optical hyperlens magnifying sub-diffraction limited objects," *Scienece*, Vol. 315, No. 5819, 1686–1686, 2007.

Design of a Castle-like Shape Plasmonic Nanoantenna with Wavelengths Ranging from UV, Visible Light and IR Light

Yuan-Fong Chau
Department of Electronic Engineering, Ching Yun University, Jung-Li 320, Taiwan, R.O.C.

Abstract— A plasmonic nanoantenna is proposed and investigated numerically by using the three-dimensional finite element method. The influence of the dielectric hole in nanoshell on the antenna field enhancement and spectral response is discussed. Results show that the resonant wavelength of the proposed nanoantenna may be tuned over a broad spectral by considering the contour of a castle-like shape core antenna and introducing the design parameters, the gap distance and contour thickness. These new antennas allow for a threefold reduction in the antenna footprint and increase in the gap enhancement.

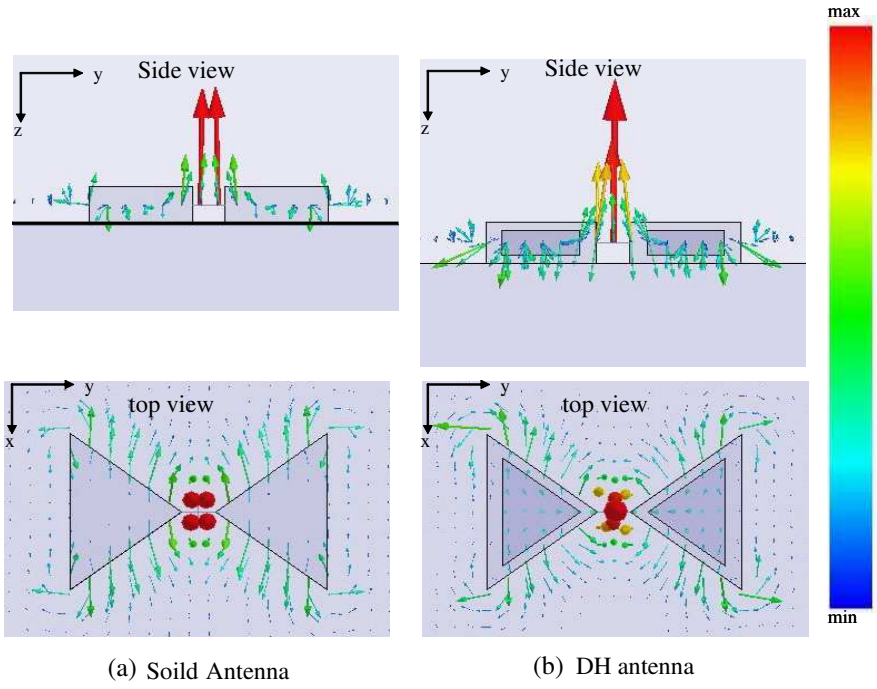

(a) Soild Antenna (b) DH antenna

Figure 1: Corresponding power flow on side view and top view: (a) for solid case and (b) for DHs cases.

ACKNOWLEDGMENT

The authors are grateful for the financial support from the National Science Council, Taiwan, R.O.C., under Grant numbers NSC 99-2112-M-231-001-MY3, NSC-100-2120-M-002-008, and NSC-100-2632-E-231-001-MY3.

Electromagnetic Field Confinement in Self-similar Chains of Magnetoplasmonic Core-shell Nanostructures

M. Essone Mezeme, **S. Lasquellec**, **and C. Brosseau**
Lab-STICC, Université Européenne de Bretagne, Université de Brest
CS 93837, 6 Avenue Le Gorgeu, 29238 Brest Cedex 3, France

Abstract— We apply first-principles methodology to study the spatial localization of electric field enhancement at plasmonic resonance and magnetic field enhancement at gyroresonance in a self-similar chain of magnetoplasmonic core-shell nanostructures (MCSN). Localized regions of high electric and magnetic fields in the vicinity of metal nanostructures can be created in a controlled manner by adjusting the physical parameters characterizing this system and the polarization of the external harmonic excitations. We demonstrate the high degree of control achieved on electric field confinement, of the order of 10^3, down to a feature size of $\lambda/1000$ in self-similar chains of MCSN, where λ denotes the free space wavelength of the resonant excitation. We also compare our findings with recent investigations in related plasmonic nanostructures.

Plasmonic Roche Limit in Metal-Dielectric-Metal Structure

Ruei-Cheng Shiu and Yung-Chiang Lan
Department of Photonics, National Cheng Kung University, Taiwan, R.O.C.

Abstract— Roche limit, an astronomy phenomenon observed in a two-star system, defines the trajectories within which a celestial body will be disintegrated by the gravitational fields of the two stars. Roche limit can be mimicked by the coupled surface plasmon that propagates in a designed Metal-Dielectric-Metal (MDM) structure. When the MDM structure contains two neighboring circle regions in which the refraction index of dielectric layer has the same function form as the gravity potential (i.e., $n(r) \propto 1/r$), a Gaussian beam that moves in the plasmonic Roche limit will also be disintegrated by the optical force. This phenomenon has never been proposed and observed in the literature. In this work, plasmonic Roche limit is investigated by using both FDTD simulations and theoretical analyses. The simulation results exhibit that the relative magnitude of the refraction index gradients between the first and second circles strongly modulated the motion of the incident beam. That the beam will rotate around the first circle or disperse and approach the second circle depends on its incident position being within or outside the plasmonic Roche limit. The beam's trajectories forecasted by ray optics method and Newton's law of motion closely correspond to the simulation results.

Session 3P3a
Electromagnetic Inverse Problems in Medicine and Biology

Image Reconstruction in Electric Field Tomography (EFT)

A. Korjenevsky and T. Tuykin
Kotel'nikov Institute of Radioengineering & Electronics of the RAS, Russia

Abstract— The electric field tomography is relatively new imaging method applicable for biomedical applications. It uses interaction of alternating electric field with the conducting media to obtain information about the spatial distribution of its conductivity without electrical contact with the object. The method is based on the Maxwell-Wagner relaxation phenomenon, i.e., finite relaxation time of the nonequilibrium free charges in the conductor. This phenomenon leads to the phase shift of the alternating electric field outside the object depending on its internal electrical properties and geometry. Measuring such phase shifts using multiple transmitting and receiving electrodes enables to reconstruct internal structure of the object. Mathematically such reconstruction procedure consists of solving the inverse problem for Laplace equation with inhomogeneous complex permittivity. While this inverse problem is ill-posed and nonlinear in general, fast and robust linearized algorithms are most interesting for the practical system implementation. Forming of the appropriate reconstruction matrix converting measured phase shifts into image is possible in various ways. One of them is single step regularized Gauss-Newton method. Another is least squares optimization using extensive training data sets comprised of different distributions of properties and corresponding simulated results of measurement with appropriate noise added. Such approach is known as linear artificial neural network also. One of the popular heuristic algorithms is back projection. It is based on known spatial localization of the most sensitive areas for each transmitter-receiver pair. We have implemented successfully the back projection method for EFT taking into account that sensitivity is localized near the line of electric field connecting the active and sensing electrodes. Corresponding results of numerical simulation and applying the algorithm to the experimental data are demonstrated. The linear neural networks are considered also as very promising for EFT image reconstruction.

Overview of Electric Field Tomography Experiments in Russia

Vladimir A. Cherepenin, **Alexander V. Korjenevsky, and Timur S. Tuykin**
The Institute of Radioengineering and Electronics of Russian Academy of Sciences
Street Mokhovaya 11-7, Moscow 125009, Russia

Abstract— The paper introduces EFT operational principal briefly and overviews EFT experiments in Russia.

EFT based on the Maxwell-Wagner relaxation phenomenon accompanying redistribution of nonequilibrium free charges carriers inside the inhomogeneous conductive object. It is a new kind of quasistatic electro-magnetic tomography suitable for contactless imaging of biological objects.

The first single-channel measuring EFT system and set of experiments are discussed. Single channel experiments proved EFT theory and shown possibility to obtain data required for EFT realization.

The first multi-channel measuring system for EFT is described. Experiments on imaging of a test objects with different geometry and electrical properties are presented. The first EFT images obtained experimentally are given and discussed.

Using Memristive Elements for Modeling Electrical Properties of Biological Tissue

Ørjan G. Martinsen[1, 2], **Sverre Grimnes**[1, 2], **Carsten A. Lütken**[1], **and Gorm Krogh Johnsen**[1]

[1]Department of Physics, University of Oslo, N-0316 Oslo, Norway
[2]Department of Clinical and Biomedical Engineering
Oslo University Hospital, Rikshospitalet, N-0372 Oslo, Norway

Abstract— The memristor was predicted by Leon O. Chua to exist on purely theoretical grounds many years ago [1], but was not realized in the laboratory as a physical, electronic nano-component until 2009 [2]. The memristor is treated as an elementary passive circuit element, complementing resistors, coils, and capacitors (RLC), whose memristance $M(q) = d\phi/dq = v/i$ is defined by how the magnetic flux $\phi = \int v(t)dt$ responds to the charge $dq = idt$ transported by the electrical current $i(t)$.

Later the concept was expanded to memristive systems [3], which are generalizations of the memristor concept where the memristance is controlled by a number of state variables. Furthermore, in 2009 the theory was further expanded by Di Ventra et al. to memcapacitance and meminductance [4].

We show that electro-osmosis in human sweat ducts is of memristive nature and that memristors therefore will be important when modeling electrical properties of human skin. We also show that dielectric dispersion in biological tissue is of memcapacitive nature and that nonlinear phenomena probably play a significant role in the overall electrical properties of biomaterials.

Numerical Reconstruction of Perfectly Conducting Inclusions from One Electrostatic Boundary Measurement

Mirza Karamehmedović[1], **Kim Knudsen**[2], **and Thomas Wriedt**[1]

[1]Department of Process and Chemical Engineering, University of Bremen, Germany
[2]Department of Mathematics, Technical University of Denmark, Denmark

Abstract— Electrical Impedance Tomography (EIT) aims to reconstruct inhomogeneities or inclusions in the interior of a medium based on current and voltage measurements at the boundary of the medium. In many practical applications of EIT, the efficiency of the employed numerical inversion scheme is an essential parameter.

The inversion methods typically evaluate an indicator function in order to estimate whether or not a given point is in the interior of the sought inclusion. The so-called sampling methods do not assume any à priori knowledge about the boundary condition valid at the inclusion boundary, but the evaluation of their indicator functions can be numerically expensive. On the other hand, decomposition methods express the solution of the Laplace equation in the medium in terms of layer potentials and estimate the inclusion using boundary value error minimisation. However, matching the sources in the potentials with the measured current or voltage at the medium boundary can be numerically costly.

We describe a novel method for the reconstruction of perfectly electrically conducting inclusions in arbitrary homogeneous, simply connected media of finite conductivity and with sufficiently smooth boundary. Similarly to the decomposition methods, our approach is based on a boundary layer representation of a solution of the Laplace equation in the medium, and it uses à priori knowledge of the boundary condition satisfied at the interface between the inclusion and the medium. However, both of these developments occur at the analytic stage only, and the actual numerical computation involves neither forward-model sources nor boundary-error minimisation. The method requires inclusions to be placed relatively close to the boundary of the medium, and it is well-suited for detection of small inclusions and for detection and partial shape estimation of large inclusions.

We give a mathematical justification for the indicator function used in the inversion method. Also, we illustrate the performance of the method using several numerical examples involving different medium geometries, as well as single and multiple inclusions of different shapes and positions within the medium. Finally, we compare the efficiency and accuracy of the method to a decomposition scheme based on the Method of Auxiliary Sources.

The Impact of Model Mismatch Errors on Magnetic Induction Tomography Inverse Problem

D. Gürsoy and H. Scharfetter
Graz University of Technology, Austria

Abstract— Magnetic induction tomography (MIT) is a non-invasive and non-contact imaging modality that attempts to reconstruct the internal conductivity distribution of the human body. It promises to facilitate diagnosis of several physiological disorders such as edema or internal hemorrhage and has the potential to be used for continuous monitoring of physiological uids. Several features of the device such as high-speed data acquisition, portability and comparably inexpensiveness make the proposed modality attractive.

In MIT, an array of coils is used to induce eddy-currents inside the body and the magnetic fields are recorded outside using an array of magnetic sensors. The corresponding inverse problem is defined as the reconstruction of conductivity distribution from the measured magnetic fields and is generally stated based on the minimization of the Euclidean norm of the data misfit term. Therefore, small differences between the modeled and true coil geometry induce errors in the data misfit and generate artifacts in images. In this study, we performed a simulation study to analyze the impact of modeling errors on measured data and corresponding conductivity reconstructions.

For the analysis, we considered two different cases of coil geometry distortions: the displacement of coils from ideal positions and rotation of coils. We generated synthetic data by using a typical 16-channel MIT system coil arrangement. We indexed the worst receiver channels in terms of susceptibility to distortion errors in data and in the corresponding reconstructed images. It was found that slight geometrical distortions of the coils may cause significant deviations in the data considering local and small perturbations in conductivity. It was showed that the imaging artifacts appear on the proximity of the boundary of the conducting object.

A Software Based Framework for Estimating Patient Displacement in Magnetic Induction Tomography

Mamatjan Yasin[1], **Ali Roula**[2], **Doga Gürsoy**[3], **and Andy Adler**[1]

[1]Carleton University, Ottawa, K2E7E8, Canada
[2]University of Glamorgan, Pontypridd, CF371DL, UK
[3]Graz University of Technology, Graz, A-8010, Austria

Abstract— Magnetic Induction Tomography (MIT) is a contactless, inexpensive and non-invasive technique for imaging the conductivity distribution inside volume conductors. Time-difference imaging can be used for the monitoring of patients in critical care. This includes monitoring of cerebral strokes and breathing (aeration and ventilation of the lung), as well as continuous screening of oedema. However, MIT signals are much more sensitive to body movements than to the conductivity changes inside of the body. This is because small movements during MIT measurements can overwhelm the signals of interest and cause significant image artefacts. Thus, it is crucial to accurately estimate and factor body movements into image reconstruction. Movement estimation is nonetheless a challenging problem due to 3 possible translations (along x, y and z axis) and rotations which can cause significant signal magnitude changes as well as phase shifts.

Methods: We proposed algorithmic methods for identifying and estimating object movements from simulated MIT data prior to the image reconstruction step. A simulation was performed based on a 16 channel MIT system where a finite-difference based MIT software package was used to (i) generate reference data without a target and movement, and (ii) simulate whole tank movement with a target placed close to edge of the tank. The homogenous tank (radius of 13.5 cm and height of 20 cm) has the conductivity of $1\,\mathrm{Sm}^{-1}$, and the small cubic target has the conductivity of $3\,\mathrm{Sm}^{-1}$. The movement was estimated using frequency domain analysis (FFT and Wavelet), and statistical approaches (Independent Component Analysis (ICA)) that used training data on various displacements. Once movements are identified, images are reconstructed by (i) minimizing movement artefacts for small movements; (ii) compensating for the movements if these are accurately estimated, or (iii) taking a new MIT measurement if movements are too severe.

Results: Results show that movements of 1% of the radius of the tank cause image blurring but the artifacts can be minimized by regularization. Higher movements totally distorted images which require artifact compensation or acquisition of new measurements.The percentage errors for FFT based movement estimation were 35%, 0.3% and 6% for a displacement of 1% (1.3 mm), 5% (6.7 mm) and 10% (13.5 mm) respectively where the displacement was chosen relative to the radius of the tank. ICA and wavelet approaches also produced similar results to the FFT based approach. It was also found that the accuracy of movement estimation was found to be related to the size of the background in real measurements.

Session 3P3b
Advanced Artificial Materials for Sensing and Imaging

Spatial-spectral Optical Imaging and Sensing

Yuan Luo[1, 2, 3] **and George Barbastathis**[3, 4]

[1]Center for Optoelectronic Biomedicine, College of Medicine
National Taiwan University, 10051, Taiwan, R.O.C.
[2]Molecular Imaging Center, National Taiwan University, 10055, Taiwan R.O.C.
[3]Singapore-MIT Alliance for Research and Technology (SMART) Centre
Block S16-06-17, 3 Science Drive 2, 117543, Singapore
[4]Department of Mechanical Engineering
Massachusetts Institute of Technology, Cambridge, MA 02139, USA

Abstract— Advances in three dimensional imaging systems are of vital importance in many areas of scientific research including microscopic imaging applications. Conventional optical imaging systems such as confocal microscopes have been applied to obtain three-dimensional information from an object, and these systems have shown great promise for monitoring and detecting cancer cell structures. However, all the existing systems acquire three-dimensional image data of interest by either time-consuming scanning schemes or intensive computational techniques. Microscopy based on volume hologram has been developed as a new microscopic instrument for spatial-spectral imaging of biological samples with scanning.

The holographic grating formed in the volume recording material can be considered a Bragg filter, which is capable of selecting very narrow angular and wavelength information from an object. In addition, holographic gratings can be used to discriminate wavefronts originating from different depths within a volumetric object. If the gratings are multiplexed in the same recording material, several depths within the object can be sampled simultaneously. A phenanthrenquinone (PQ)-doped poly (methyl methacrylate) (PMMA) polymer material is used to make very thick recording samples. For our experiments, the recording material is approximately 2 mm thick and is recorded using an argon ion laser operating at a wavelength of 488 nm. With proper fabrication the gratings can operate at wavelengths much longer than the recording wavelength, allowing greater imaging depths within biological tissue samples. Our experimental results demonstrate the ability of the volume holographic filters in an imaging system to reconstruct depth-resolved three dimensional images of tissue samples without the need for scanning.

Z-shaped LC Resonator for Producing Negative Permittivity

Abdallah Dhouibi[1], **Shah Nawaz Burokur**[1], **André de Lustrac**[2], **and Alain Priou**[1]

[1]LEME, University of Paris-Ouest, EA 4416, Ville d'Avray 92410, France
[2]IEF, University of Paris-Sud, CNRS, UMR 8622, Orsay Cedex 91405, France

Abstract— Metamaterials have recently attracted considerable interests [1–3] because of their capabilities which go beyond conventional materials [4] and because of their applications in novel class coordinate transformation based devices such as invisibility cloaks [5–9], rotators [10], retroreflectors [11], Luneburg lenses [12, 13] and directive antennas [14–16]. A typical metamaterial is an artificial composite material made of a periodic array of sub wavelength inclusions called meta-atoms. These inclusions are equivalent to LC resonant elements with the inductance and capacitance greatly influenced by the geometrical shape and dimensions. We present in this communication a printed Z-shaped electric meta-atom as an alternative design to the conventional electric-LC (ELC) resonator [17]. We propose an easy way to redesign the ELC footprint to get a compact and a low cost electric resonator exhibiting a strong electric response. Our approach involves, in the effective medium regime, redressing the resonator shape to accommodate higher inductance and lead to a lower resonance frequency without being limited by fabrication tolerances. The electromagnetic behaviour of the meta-atom has been investigated through both simulations and experiments in the microwave regime. Our results show that the Z meta-atom exhibits an electric response to normally incident radiation and can be used very effectively in producing materials with negative permittivity. The proposed planar meta-atom can find various applications in high frequency passive circuits which are designed in planar technology. Moreover the proposed structure can be scaled to much higher frequencies via appropriate lithographic scaling.

REFERENCES

1. Shelby, R. A., D. R. Smith, and S. Schultz, *Science*, Vol. 292, 77, 2001.
2. Yen, T. J., W. J. Padilla, N. Fang, D. C. Vier, D. R. Smith, J. B. Pendry, D. N. Basov, and X. Zhang, *Science*, Vol. 303, 1494, 2004.
3. Smith, D. R., J. B. Pendry, and M. C. K. Wiltshire, *Science*, Vol. 305, 788, 2004.
4. Veselago, V. G., *Sov. Phys. Usp.*, Vol. 10, 509, 1968.
5. Leonhardt, U., *Science*, Vol. 312, 1777–1780, 2006.
6. Pendry, J. B., D. Schurig, and D. R. Smith, *Science*, Vol. 312, 1780, 2006.
7. Schurig, D., J. J. Mock, B. J. Justice, S. A. Cummer, J. B. Pendry, A. F. Starr, and D. R. Smith, *Science*, Vol. 314, 977, 2006.
8. Cai, W., U. K. Chettiar, A. V. Kildishev, and V. M. Shalaev, *Nat. Photonics*, Vol. 1, 224, 2007.
9. Kanté, B., A. de Lustrac, J.-M. Lourtioz, and S. Burokur, *Opt. Express*, Vol. 16, 9191, 2008.
10. Chen, H., B. Hou, S. Chen, X. Ao, W. Wen, and C. T. Chan, *Phys. Rev. Lett.*, Vol. 102, 183903, 2009.
11. Ma, Y. G., C. K. Ong, T. Tyc, and U. Leonhardt, *Nat. Mater.*, Vol. 8, 639, 2009.
12. Kundtz, N. and D. R. Smith, *Nat. Mater.*, Vol. 9, 129, 2010.
13. Ma, H. F. and T. J. Cui, *Nat. Commun.*, Vol. 1, 21, 2010.
14. Tichit, P.-H., S. N. Burokur, and A. de Lustrac, *J. Appl. Phys.*, Vol. 105, 104912, 2009.
15. Tichit, P.-H., S. N. Burokur, D. Germain, and A. de Lustrac, *Phys. Rev. B*, Vol. 83, 155108, 2011.
16. Tichit, P.-H., S. N. Burokur, D. Germain, and A. de Lustrac, *Elec. Lett.*, Vol. 47, 580, 2011.
17. Schurig, D., J. J. Mock, and D. R. Smith, *Appl. Phys. Lett.*, Vol. 88, 041109, 2006.

Smooth-interfaces-induced High Contrast Superlens Lithography

H. Liu[1], **B. Wang**[1], **L. Ke**[1], **J. Deng**[1], **C. C. Chum**[1], **L. Shen**[1], **S. A. Maier**[2], **and J. Teng**[1]

[1]Institute of Materials Research and Engineering
Agency for Science, Technology and Research (A*STAR), 3 Research Link, 117602, Singapore
[2]Department of Physics, Imperial College London, London SW7 2AZ, UK

Abstract— Thin slab silver superlens has been transformed from splendid ideas [1, 2] into reality in recent years under an enormous research effort driven by not only its fascinating physics but also ability of real-time sub-diffraction-limit imaging. Superlens has been experimentally demonstrated in various frequencies and optical frequency has been predicted as one of its promising application areas [3]. At UV regime, photoresist has been commonly employed in experiments as the medium to record the near-field optical imaging. Unfortunately, the achieved photoresist contrasts were very poor through AFM characterization although sub-diffraction-limit features were resolvable [4–7]. On the other hand, drastically increasing demand on creating ultrasmooth silver thin films has been driven by the development of plasmonic nanodevices and metamaterials in recent years [8]. Silver has been the most-commonly used noble metal as a superlens material because of its excellent optical properties. However, Ag films fabricated by convention methods exhibit a relatively rough and inhomogeneous surface, which is accountable for remarkable surface plasmon polaritons (SPPs) scattering loss and insensitive surface plasmon resonance (SPR) resulting in the performance degradation [9–12].

In this work, we report high imaging contrast and sub-diffraction-limited resolution obtained by a silver superlens at UV region. Utilizing the flat optical superlens comprising of the smooth dielectric-Ag-photoresist structure, we have experimentally demonstrated sub-50 nm (about one-eighth of illumination wavelength) superresolution imaging with high contrast. The step-by-step characterization of the interfacial roughness indicates that the roughness effect plays an essential role in the quality of the sub-diffraction-limit imaging in terms of the contrast and resolution. It unveils the promising applications of superlens for sub-diffraction-limit photolithography.

REFERENCES

1. Pendry, J. B., "Negative refraction makes a perfect lens," *Physical Review Letters*, Vol. 85, 3966–3969, 2000.
2. Veselago, V. G., "The electrodynamics of substances with simultaneously negative values of ε and μ," *Soviet Physics Uspekhi-USSR*, Vol. 10, 509–514, 1968.
3. Zhang, X. and Z. W. Liu, "Superlenses to overcome the diffraction limit," *Nature*, Vol. 7, 435–441, 2008.
4. Fang, N., H. S. Lee, C. Sun, and X. Zhang, "Sub-diffraction-limited optical imaging with a silver superlens," *Science*, Vol. 308, 534–537, 2005.
5. David, O. S. M. and J. B. Richard, "Super-resolution imaging through a planar silver layer," *Optics Express*, Vol. 13, 2127–2134, 2005.
6. Jeppesen, C., R. B. Nielsen, A. Boltasseva, S. Xiao, N. A. Mortensen, and A. Kristensen, "Thin film Ag superlens towards lab-on-a-chip integration," *Optics Express*, Vol. 17, 22543–22552, 2009.
7. Chaturvedi, P., W. Wu, V. J. Logeeswaran, Z. N. Yu, M. S. Islam, S. Y. Wang, R. S. Williams, and N. Fang, "A smooth optical superlens," *Applied Physics Letters*, Vol. 96, 043102, 2010.
8. Valentine, J., S. Zhang, T. Zentgraf, E. Ulin-Avila, D. A. Genov, G. Bartal, and X. Zhang, "Three-dimentional optical metamaterial with a negative refractive index," *Nature*, Vol. 455, 376–379, 2008.
9. Yuan, H. K., U. K. Chettiar, W. S. Cai, A. V. Kildishev, A. Boltasseva, V. P. Drachev, and V. M. Shalaev, "A negative permeability material at red light," *Optics Express*, Vol. 15, 1076–1083, 2007.
10. Jing, F., H. Tong, L. Kong, and C. Wang, "Electroless gold deposition on silicon (100) wafer based on a seed layer of silver," *Appl. Phys. A*, Vol. 80, 597–600, 2005.
11. Chi, Y., E. Lay, T. Y. Chou, Y. H. Song, and A. Carty, "Deposition of silver thin films using the pyrazolate complex $[Ag(3,5\text{-}(CF_3)_2C_3HN_2)]_3$," *Chem. Vap. Deposition*, Vol. 11, 206–212, 2005.

12. Yin, L. L., V. K. V. Vlasko, J. Pearson, J. M. Hiller, J. Hua, U. Welp, D. E. Brown, and C. W. Kimball, "Subwavelength focusing and guiding of surface plasmons," *Nano Lett.*, Vol. 5, 1399–1402, 2005.

Analytical Approach for Design of Thin-film Photonic Lüneburg Lens

Hanhong Gao[1], **Baile Zhang**[2, 3], **Steven G. Johnson**[4], **and George Barbastathis**[2, 5]

[1]Department of Electrical Engineering and Computer Science
Massachusetts Institute of Technology, Cambridge, USA
[2]Singapore-MIT Alliance for Research and Technology (SMART) Centre, Singapore
[3]Division of Physics and Applied Physics, School of Physical and Mathematical Sciences
Nanyang Technological University, Singapore
[4]Department of Mathematics, Massachusetts Institute of Technology, Cambridge, USA
[5]Department of Mechanical Engineering
Massachusetts Institute of Technology, Cambridge, USA

Abstract— Since at least Maxwell's time, GRadient INdex (GRIN) media, e.g., the Lüneburg lens, have been known as a good candidate for light manipulation. Arbitrary GRIN lens is difficult to implement with bulk materials; however, in optics-on-a-chip or integrated optics applications, effective refractive index distribution can be realized with subwavelength structures patterned on a substrate. The effective index for a certain unit cell structure is commonly estimated with a 2D model, where the height in the 3rd dimension is assumed to be infinity. However, most of such structures are placed on the substrate and their height is comparable or even smaller than the optical wavelength; therefore the 2D assumption is questionable. This thin-film problem has been discussed in literature on photonic crystals, using a numerical 3D band diagram; but little attention has been received for periodic/aperiodic dielectric metamaterial devices.

We designed an all-dielectric finite-thickness aperiodic nanostructured Lüneburg lens. In order to compensate for the thin-film effect, an all-analytical approach is proposed. Our method estimates the effective refractive index of the infinite-height lattice from the second-order effective medium theory, then we replace this lattice with a continuum medium of the same effective index. In this way the structure becomes one of the asymmetric waveguide, and a new effective index explicitly accounting for the thin-film effect can be derived from the waveguide dispersion relation. The results agree with those calculated using the conventional numerical treatment — a direct 3D unit cell band diagram calculation; but our method avoids 3D numerical calculation and provides more physical intuition. The performance of the Lüneburg lens has been verified with 3D finite-difference time-domain (FDTD) method. It can also be shown that the performance of the thin-film lens is quite different than the estimates obtained assuming infinite height.

ACKNOWLEDGMENT

This work is supported by Singapore's National Research Foundation through the Singapore-MIT Alliance for Research and Technology (SMART) Centre and the Air Force Office of Scientific Research MURI program on Nanomembranes under contract No. FA9550-08-1-0379. The authors thank Lei Tian for useful discussions and Justin W. Lee for setting up the computation server.

Classical Imaging Theory of a Microlens with Super-resolution

Baile Zhang[1, 2] **and George Barbastathis**[2, 3]

[1]School of Physical and Mathematical Sciences
Nanyang Technological University, Singapore
[2]Singapore-MIT Alliance for Research and Technology Centre, Singapore
[3]Department of Mechanical Engineering
Massachusetts Institute of Technology, United States

Abstract— Recently, there has been some exciting progress towards super-resolution in imaging through a transparent microlens. For example, a new record of 50 nm lateral resolution has been reported for real-time imaging through a dielectric micro-lens. This breakthrough will definitely bring out a profound impact on related disciplines, such as biological studies and photolithography industry. However, the mechanism underlying this high resolution still remains unclear in the sense that it is counterintuitive according to traditional imaging theory, which usually exploits scalar wave diffraction as a proper approximation.

Here we adopt vectorial electromagnetic diffraction analysis to better emulate the real imaging procedure. We find that the calculation does not lead to the 50 nm lateral resolution reported previously, which means that there must be some other mechanism, that hasn't be discovered yet, to support this phenomenon.

Session 3P4
Antenna Arrays in Wireless Communications and Biomedical Applications

Effects of Loop Shape, Size and Filling Factor on RF Transmit Performance for a 7 T Multi-channel Loop Array

M. Kozlov and R. Turner
Planck Institute for Human Cognitive and Brain Sciences, Leipzig, Germany

Abstract— Purpose: For a single loop coil the excitation profile is strongly influenced by the distance from array to load. However, there are no reliable transmit performance data for a loop-based array, loaded by a realistic head model, as a function of array to load distance (filling factor), or array shape. Furthermore, it is hard to compare literature values for transmit performance, because data for $\mathbf{B}_1+$ field versus array input power ($\mathbf{P}_{transmit}$) are rarely reported, and there are no reports of power balance. Using two types of 8-channel loop based 7T array, we investigated the effect of array shape and its distance to load on array power balance and performance (averaged over the entire brain volume and over a transverse slice). While parallel transmission and RF shimming are hot topics, for many practical applications so far the workhorse for driving a multi-channel transmit RF coil has been a single power amplifier followed by a power splitter and phase shifter. The arrays investigated were accordingly excited in circular polarization mode, applying 1 W power to each port ($\mathbf{P}_{transmit} = 8$ W), with a sequential 45 degree phase increment. Data obtained after performing simulated RF shimming will be reported separately.

Method: Our investigation used RF circuit and 3-D EM co-simulation [1]. In the simulation, for array type #1, eight rectangular planar resonance coil elements were mounted on rectangular acrylic supports, assembled to give an octagonal cross section with extreme dimensions of 230 mm by 255 mm (Fig. 1). The single loop elements were simulated with width 85 and length 120 mm. RF array type #2 comprised 8 channels with identical rectangular loops (length 120 mm, angular size 37.5 degree), mounted on a cylindrical acrylic former with diameter ranging from 220 mm to 300 mm. The realistic 3-D EM model of both arrays included all coil construction details for the resonance elements, simulated with precise dimensions and material electrical properties. The load utilized was the Ansoft human body (head, shoulders, torso) with scaling factor: $X = 0.9$, $Y = 0.9$, $Z = 0.9$.

For all geometries the array was either tuned/matched/decoupled using an inductive decoupling network, or alternatively tuned by minimization of the power reflected by the entire array ($\mathbf{P}_{array\_refl}$) without any dedicated decoupling network. We analyzed the power balance as well as the transmit magnetic field performance and inhomogeneity (calculated as the ratio of standard deviation to mean $\mathbf{B}_1+$ over the entire human brain ($\mathbf{B}_1+_{brain}$), or over the central transverse slice ($\mathbf{B}_1+_{slice}$)).

The scanner gradient shield (with diameter of 683 mm and length 1200 mm) was always included in the numerical domain for simulation of unshielded and shielded arrays. The distance between the shielded array and a 300 mm long local shield was varied to maintain approximately the same ratio of the distances of coil to load center and shield to load center.

Results: For all arrays investigated, there is no striking difference in $\mathbf{B}_1+$ distribution within the central transverse slice, when the data are rescaled to the maximum value calculated in the brain. The simulated slice and whole brain inhomogeneity also varies only slightly (Table 1). Increasing

Table 1: Array performance for different shapes and diameters.

Coil shape	∅300 mm				∅280 mm		∅250 mm		∅220 mm		∅230 mm by 255 mm			
Shield	No		Yes		Yes		Yes		Yes		No		Yes	
Tuning	R	I	R	I	R	I	R	I	R	I	R	I	R	I
$\mathbf{P}_{reflected}$, W	0	1.12	0	0.60	0	0.51	0	0.28	0	0.21	0	0.51	0	0.25
$\mathbf{P}_{radiated}$, W	1.34	1.33	0.23	0.26	0.12	0.12	0.09	0.09	0.02	0.02	0.42	0.53	0.03	0.03
$\mathbf{P}_{array\_internal}$, W	0.42	0.44	0.76	0.89	0.64	0.76	0.52	0.68	0.32	0.40	0.28	0.29	0.47	0.58
$\mathbf{P}_{body}$, W	6.24	5.11	7.01	6.25	7.24	6.61	7.38	7.04	7.66	7.37	7.30	6.67	7.50	7.14
$\mathbf{P}_{brain}$, W	2.14	1.75	2.53	2.30	2.63	2.42	2.70	2.61	2.75	2.71	2.58	2.39	2.62	2.47
$\mathbf{B}_1+_{brain}$, µT	1.47	1.32	1.62	1.53	1.66	1.59	1.69	1.66	1.72	1.70	1.57	1.51	1.61	1.56
Inhomogeneity brain, %	23	23	23	23	23	23	24	24	24	25	24	24	25	25
$\mathbf{B}_1+_{slice}$, µT	1.64	1.48	1.83	1.73	1.89	1.81	1.93	1.89	1.99	1.97	1.83	1.75	1.91	1.85
Inhomogeneity slice, %	18	18	18	18	18	18	18	18	18	19	21	22	20	20

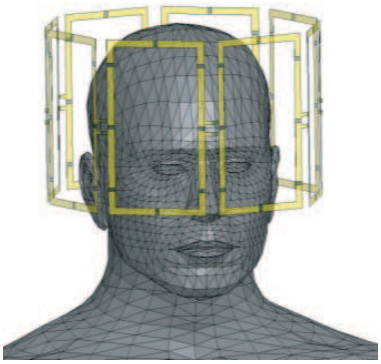

Figure 1: Human head inside array type #1.

the array diameter from 220 to 300 mm results in a decrease of both $\mathbf{B}_1+_{brain}$ and $\mathbf{B}_1+_{slice}$, by as much as 6 and 8% correspondingly. Thus in order to excite the same brain with the same $\mathbf{B}_1+_{brain}$, the 300 mm diameter array utilizes 12% more power. $\mathbf{B}_1+_{brain}$ and $\mathbf{B}_1+_{slice}$ for array type #1, with rectangular elements, are lower, as compared with the 250 mm diameter array type #2, by as much as 5% and 1% correspondingly. For all arrays, the ratio of $\mathbf{B}_1+_{brain}/\sqrt{\mathbf{P}_{brain}}$ is equal to $1.0\,\mu\mathrm{T}/\sqrt{\mathrm{W}}$ with only $+/-3\%$ variation. As an important result, analysis of the power balance is clearly to be regarded as key for understanding the relative improvement or degradation of array performance.

The $\mathbf{Q}_{load}/\mathbf{Q}_{unload}$ ratios are not tabulated, because at 300 MHz they are not useful in calculating inherent coil losses for the array ($\mathbf{P}_{array\_internal}$), nor the power absorbed by the entire human body ($\mathbf{P}_{body}$). This is because a) both for unloaded and loaded coils, radiation losses and the coupling between array elements differ significantly; b) the coupling between power supply and coil is altered by coil loading, which can invalidate the general requirement of critical coupling that enables calculation of **Q**-factor; c) the reflected power $\mathbf{P}_{array\_refl}$ is not taken into account. For an unshielded array, the sum of $\mathbf{P}_{reflected}$ and $\mathbf{P}_{radiated}$ is generally larger than $\mathbf{P}_{array\_internal}$.

Relative to the decoupled array, tuning by minimization of $\mathbf{P}_{array\_refl}$ increases the coupling between elements. However, because this strategy maximizes $\mathbf{P}_{brain}$, it is a solution for obtaining the best CP mode excitation performance, independently of the distance to the load and the shape of the array.

The influence of shield distance on array performance depends both on the array tuning/decoupling approach and the filling factor. For a 300 mm diameter inductively decoupled array, S_{21} and S_{31} for the shielded/unshielded array are equal to $-15.3/-10.7$ dB and $-14.0/-9.8$ dB respectively. This relatively small increase of coupling for the unshielded array results in a 100% rise of $\mathbf{P}_{array\_refl}$, which increases to 14% of the $\mathbf{P}_{transmit}$. Simultaneously the radiated power ($\mathbf{P}_{radiated}$) increases to 16% of $\mathbf{P}_{transmit}$. The larger the $\mathbf{P}_{array\_refl}$ and $\mathbf{P}_{radiated}$, the poorer the array coil performance. Therefore, taking into account the much smaller $\mathbf{P}_{radiated}$ and $\mathbf{P}_{array\_refl}$ (despite the same relative increase of $\mathbf{P}_{array\_refl}$) the performance of the array type #1 drops relatively less when unshielded than the 300 mm diameter array.

Conclusion: For an array excited by a single power source, followed by a power splitter and phase shifters operating in the CP mode, there is no advantage to use an array with shape adapted to the human head. With tuning by reflected power minimization, the transmit performance of a loop array is only weakly dependent on filling factor when its diameter is less than 280 mm. Performance is strongly affected by filling factor only if the diameter is more than 280 mm and the array is unshielded. The results obtained assist the design of transmit-only/receive-only (TORO) arrays, because a TX-only coil of 280 mm diameter provides adequate space for an RX-only coil.

REFERENCES

1. Kozlov, M. and R. Turner, *Proceedings of the 40th European Microwave Conference*, 328–331, 2010.

Radiation Pattern Decoupling for Compact Transmitting Antenna Arrays

C. H. Niow and H. T. Hui
Department of Electrical and Computer Engineering, National University of Singapore, Singapore

Abstract— An effective method is proposed to compensate for the coupled array patterns of the compact antenna arrays due to mutual coupling. By using the mutual impedances of the antenna elements and the principle of pattern multiplication, it is possible to design compensation networks remove the distortion in the coupled array patterns. Equations to realize the compensation networks are derived. Numerical examples on the dipole and monopole arrays are discussed to demonstrate the validity and accuracy of the compensation method.

The proposed compensation method is able to decouple the coupled the radiation patterns in the transmitting compact antenna arrays due to mutual coupling so that the radiation patterns of the individual antenna element effectively appear as isolated element patterns. The distortion of the radiation pattern of the antenna array caused by the coupled voltages can be expressed using the mutual impedances of the array. By exciting the antennas with the compensated voltages derived using the compensation method, the antenna array is able to produce the isolated radiation patterns without the effects of mutual coupling. This compensation method can also accommodate another matching circuit in the feeding network such as a conventional port-decoupling network.

Various monopoles and dipoles arrays at less than half a wavelength separations are used to demonstrate the effectiveness of the proposed compensation method. The results are compared with the array patterns obtained using the excited voltages and using the principle of pattern multiplication. From the simulation examples, it is found that the main beam and side lobes are accurately restored using the compensation method.

Wideband Beamforming for Compact Receiving Antenna Arrays

C. H. Niow, H. T. Hui, and T. S. Yeo
Department of Electrical and Computer Engineering
National University of Singapore, Singapore 117576, Singapore

Abstract— An effective compensation method is proposed to eliminate the beamforming distortions in compact antenna arrays due to the effects of mutual coupling. By using the receiving mutual impedances with the optimal Riblet-Chebyshev weights, it is possible to restore the distorted antenna array patterns for effective beamforming. Equations are derived to determine the compensated Riblet-Chebyshev weights used to restore the distorted antenna array patterns. Numerical examples using a compact antenna array are discussed to demonstrate the effectiveness of the proposed compensation method.

The optimal Riblet-Chebyshev weights used for beamforming at element spacings smaller than half a wavelength cannot be applied directly in practical compact antenna arrays due to the effects of mutual coupling which is not present in these weights. By using the receiving mutual impedance to compensate the Riblet-Chebyshev weights, the distortions in the beamforming pattern in compact antenna arrays can be effectively restored. The compensation method can also be applied over the usable bandwidth using the transfer function which is derived using the system identification method. The transfer function is determined using the complex curve fitting method.

To demonstrate the effectiveness of the proposed compensation method, a compact antenna array at element spacings smaller than half a wavelength is used and results are compared with the theoretical and the uncompensated antenna array patterns over the usable bandwidth. It is found that the antenna array pattern is fully restored using the compensation method. The restored antenna array patterns match exactly to the theoretical antenna array patterns using the optimal Riblet-Chebyshev weights over the usable bandwidth.

A Simple Channel Simulator for Multiuser MIMO Broadcast Channel Systems

Chong Pei Ho, **Hieu Duy Nguyen**, **Xuan Wang**, **and Hon Tat Hui**
Department of Electrical and Computer Engineering, National University of Singapore, Singapore

Abstract— In this paper, our effort will be focused on modelling the MU MIMO BC system. Efficient and accurate channel modeling is important to help predict the performance of MIMO communication systems. However, due to the large number of parameters that are involved in channel modeling, an analytical approach is usually too difficult. This leads to the use of computer simulations. The challenge is to employ a method that is able to take all the parameters into account, and is also able to apply to most applications. Various methods are available for the simulation of the capacity of single user MIMO systems however such simulation is lacking in MU MIMO system where extensive researches on its performance are still very much ongoing.

The method of modelling a single user MIMO system was proposed by by having scatterers around both the transmitting and receiving antennas to introduce random scattering events. This work is extended in this paper to include the MU MIMO system, where instead of only one single user in the receiving end, two users were implemented. This paper presents an effort to construct a multiuser (MU) multiple-input multiple-output (MIMO) broadcast channel (BC) model. Our method is able to adequately build in the correlation and mutual coupling, which are important factors affecting the multi-antenna arrays. This helps to decrease the need for complex mathematical analysis and allows an easy simulation of the MU MIMO BC performance. Based on our model, the characterizations of MU MIMO systems are done and the impact of varying the number of transmitting and receiving antennas is explored. These insights are useful in physical realization of the systems.

Influence of the Position of Decoupling Capacitors on RF Transmit Performance for a 7 T MRI Loop Array

M. Kozlov and R. Turner
Planck Institute for Human Cognitive and Brain Sciences, Leipzig, Germany

Abstract—

Purpose: Use of capacitive decoupling is often proposed for coupling minimization within MRI RF loop based arrays. There are three typical capacitor placements: the middle ("**M**" position) of the long leg [1]; just above the first capacitor and just below the third capacitor of the long leg ("**E**" position) [2], or between each end of the long leg ("**S**" position). How the decoupling capacitor position influences the array's transmit performance has not been explored systematically up to now. For an 8-channel loop-based 7 T RF coil array, we investigated the effect of decoupling capacitor position on array transmit performance and safety excitation efficiency.

Method: In the simulation, eight resonance coil elements were mounted on rectangular acrylic supports, assembled to give an octagonal cross section with extreme dimensions of 230 mm by 255 mm. The planar single loop elements were simulated for a range of sizes: width 85 mm; length 85, 150 mm. The realistic 3-D EM model included all coil construction details for the resonance elements, simulated with precise dimensions and material electrical properties. The loads utilized were the Ansoft human body models with different scaling factors: head #1 with scaling $X = 0.9$, $Y = 0.9$, $Z = 0.9$ simulating a medium-size head, and head #2 with scaling $X = 0.95$, $Y = 0.975$, $Z = 0.9$ simulating a large head, which occupied most of the coil volume.

Our investigation was performed using RF circuit and 3-D EM co-simulation [3]. The RF circuit simulator was Agilent ADS software, and Ansoft HFSS was chosen as the 3-D EM tool for its robustness in handling complex coil geometry. For each geometry, the array was tuned, matched and decoupled, using capacitive decoupling networks placed in three different positions. We analyzed the array power budget, the transmit magnetic field performance, and the inhomogeneity (calculated as the ratio of standard deviation to mean B1+ over the entire human brain). The array was excited in circular polarization mode, applying the same power to each port, with a sequential 45 degree phase increment.

The scanner gradient shield (with diameter of 683 mm and length 1200 mm) was always included in the numerical domain for simulation of unshielded and shielded arrays. The distance between the shielded array and a 300 mm long local shield was varied between 10 mm and 80 mm.

Results and Discussion: For an array of length 150 mm, a relatively small adjustment of the distributed capacitor values ($\mathbf{C_d}$) results in significant variation of the power reflected by the entire coil ($\mathbf{P_{refl}}$) (e.g., for an array with distance to shield = 60 mm, $\mathbf{C_d} = 5.5\,\mathrm{pF} -> \mathbf{P_{refl}} = 2/1.4\,\mathrm{W}$, $\mathbf{C_d} = 5.15\,\mathrm{pF} -> \mathbf{P_{refl}} = 1/0.7\,\mathrm{W}$, $\mathbf{C_d} = 5\,\mathrm{pF} -> \mathbf{P_{refl}} = 0.4/0.3\,\mathrm{W}$ for middle and large head sizes respectively), and thus improvement of the array performance can be obtained. This effect is most pronounced for the "**M**" position, about half as much for the "**E**" position, and relatively small for the "**S**" position.

For a locally shielded array with the capacitor in "**E**" position, the array internal loss significantly increases (compared to the unshielded case) due to a large increase of current through the long leg. This results in an increase of both copper and distributed capacitor losses.

For an array of length 85 mm, adjustment of $\mathbf{C_d}$ results in a relatively smaller variation of $\mathbf{P_{refl}}$ (e.g., for an array with distance to shield = 60 mm, $\mathbf{C_d} = 10\,\mathrm{pF} -> \mathbf{P_{refl}} = 0.85\,\mathrm{W}$, $\mathbf{C_d} = 9\,\mathrm{pF} -> \mathbf{P_{refl}} = 0.37\,\mathrm{W}$ for middle size head), for all capacitor position.

The safety excitation efficiency $\mathbf{B_1+_{brain}}/\sqrt{\mathbf{SAR_{10\,g}}}$, which defines MRI scanner performance, and the brain excitation efficiency $\mathbf{B_1+_{brain}}/\sqrt{\mathbf{P_{brain}}}$ are nearly equal for a given head model, in all arrays investigated. Differences in array transmit excitation efficiency

For the same head, $\mathbf{B_1}+$ inhomogeneity calculated over the entire brain varies little with coil length, distance to shield, or position of decoupling capacitor, when the shield distance is more than 20 mm. For smaller shield distances, $\mathbf{B_1+_{brain}}$ decreases, with a simultaneous decrease in homogeneity.

Conclusion: Given the assumptions of ideal common-mode current suppression and idealized array design conditions (specifically: fixed capacitors not restricted to commercially available values, zero component value tolerance, all tuning/matching/decoupling optimizations reaching

their global minima), the transmit performance and safety excitation efficiency of the arrays investigated are similar for three typical decoupling capacitor positions, in the CP excitation mode. However, different capacitor positions entail different sensitivities to distributed capacitor values, changes of load, etc, and these sensitivities also depend nonlinearly on the distance to the local shield and the length of the array. In a given configuration, the reflected power provides an excellent figure-of-merit for array decoupling and transmit performance. Multi-parameter complex sensitivity analysis for the desired excitation mode should be performed before final coil design decisions are made.

REFERENCES

1. Gilbert, K. M., A. T. Curtis, J. S. Gati, L. M. Klassen, and R. S. Menon, "A radiofrequency coil to facilitate B(1) (+) shimming and parallel imaging acceleration in three dimensions at 7 T," *NMR Biomed.*, Dec. 8, 2010. [Epub ahead of print].
2. Kim, K., N. Darji, T. Herrmann, J. Mallow, Z.-H. Cho, O. Speck, and J. Bernarding, "Improved B1 + field using a 16-channel transmit head array and an 8-channel pTx system at 7 T," *Proc. ISMRM*, Vol. 19, 3829, 2011.
3. Kozlov, M. and R. Turner, *Journal of Magnetic Resonance*, Vol. 200, 147–152, 2009.

Side Lobe Level Reduction of Linear Antenna Arrays Using a Hybrid Approach Based on MoM/GA Algorithms

Amr H. Hussein[1], **Haythem H. Abdullah**[2], **Salah Khamis**[1], **Ahmed M. Attiya**[2], **and Mohammed Nasr**[1]

[1]Faculty of Engineering, Tanta University, Tanta, Egypt
[2]Electronics Research Institute, Cairo, Giza, Dokki, Egypt

Abstract— Side lobe level (SLL) reduction has a great importance in recent communication systems. It is considered as one of the most important applications of digital beamforming since it reduces the effect of interference arriving outside the main lobe. This interference reduction increases the capacity of the communication systems. In this paper, our home made synthesis scheme that is based on the Method of Moments and the Genetic Algorithm to synthesize linear antenna arrays is utilized. The algorithm accepts a desired radiation pattern and provides the excitation coefficients that realize the required pattern. If the desired pattern is set to have zero side lobes, the resulting array will have large number of array elements. So, it is proposed a new procedure to get the desired pattern. If this pattern is applied to the synthesis scheme, it results in excitation coefficients that lead to minimum SLL with minimum number of array elements. The procedure starts by generating a pattern of a known uniform equispaced linear array that achieves the required beamwidth. This pattern will be multiplied by a rectangular function of the same beamwidth in order to remove the side lobes. The resulting pattern will be raised by a certain level h allowing the smooth extension of the pattern to the zero level. The resulting pattern values will be raised to an exponent in order to keep the desired beamwidth that is changed slightly by raising the pattern by the level h. This process contributes greatly in smoothing the desired pattern in such a way that prevents the appearance of the undesired harmonics that affect the SLL when applied to the synthesis scheme. The proposed MoM/GA synthesis scheme is utilized to estimate the optimum level h, exponent, element spacing and excitation coefficients required to minimize the designed cost function to achieve minimum SLL at the desired number of antenna elements. The MoM/GA scheme provides SLL reduction with exactly the same half power beamwidth as the original array pattern. The MoM provides a deterministic solution for the excitation coefficients. Several examples are considered to verify the validity of this method compared with those obtained from other techniques.

Fixed Beamwidth Electronic Scanning Antenna Array Synthesis and Its Application to Multibeam Pattern Synthesis

Amr H. Hussein[1], **Haythem H. Abdullah**[2], **Mohammed Nasr**[1], **Salah Khamis**[1], **and Ahmed M. Attiya**[1]

[1]Faculty of Engineering, Tanta University, Tanta, Egypt
[2]Electronics Research Institute, Dokki, Giza, Egypt

Abstract— The synthesis of fixed beamwidth scanning antenna arrays with optimum number of antenna elements is of main concern in many applications such as radar systems, tracking systems, and satellite communications. In some applications, where, the scanning rate is not a critical factor, mechanically rotating system is sufficient to do fixed beamwidth scanning. In mechanical systems, a directive antenna array of a specific beam is mounted on a mechanically rotating system that directs the array to the desired direction keeping its beam unchanged such as rolling radar.

The electronic scanning is an optimum solution to the high scanning rate applications, but it suffers from the beamwidth broadening with steering angles. The broadening of the beam width at some scanning angles allows interfering signals to disrupt the scanning system.

In this paper, a fixed beamwidth electronic scanning algorithm is proposed. The proposed algorithm is based on designing a linear antenna array that has optimum number of array elements and elements spacing. The excitation coefficients will be the steering parameters. The algorithm is based on synthesizing sets of excitation coefficients to direct the main beam at some scanning angles. The synthesis takes into consideration the fixation of the beamwidth at different angles. The synthesis of the excitation coefficients will be done using a scheme based on the moment method due to its accuracy in solving such a problem. The optimum spacing between elements will be determined using the genetic algorithm. Due to the fact that the excitation coefficients are complex values, each excitation coefficient value at different angles will be fitted using two Nth order polynomials. One of the polynomials is set to the real part while the other is set to the imaginary part. So, once the steering angle is set, the suitable excitation coefficients will be generated in away to direct the beam at the specified angle. As a result the proposed algorithm provides easy, accurate, continuous scanning, and high scanning rate approach. One of the main advantages of the proposed algorithm is the applicability of synthesizing multibeam antenna array of fixed beamwidths using the superposition principle. One can synthesize beams at different scanning angles and by adding the corresponding excitation coefficients; the multibeam pattern will be generated. Some representative results are applied to assess the effectiveness of the algorithm.

Mutual Coupling Compensation for a Compact Array in Direction Finding

Yantao Yu[1], **Choon Hock Niow**[2], **and Hon Tat Hui**[2]

[1]College of Communication Engineering, Chongqing University, Chongqing, China
[2]Department of Electrical & Computer Engineering
National University of Singapore, Singapore

Abstract— Multiport antenna arrays are more and more widely used in wireless communication systems. The strong mutual coupling effect between the elements of compact arrays may cause significant system performance degradation. Recently, a method using receiving mutual impedances has been proposed for mutual coupling compensation. In this paper, a compact monopole array is constructed and used in direction finding. For comparison, experiments are conducted with mutual coupling compensated by using the conventional mutual impedances and the receiving mutual impedances, respectively. The measured results show that the mutual coupling effect can be effectively removed using the receiving mutual impedances and the performance of direction finding can be greatly improved.

Effects of Microstrip Feed Line Width on 1×4 Rectangular Microstrip Antenna Array Electrical Parameters and Estimation with Artificial Neural Networks

O. Dundar[1], **D. Uzer**[2], **S. S. Gultekin**[2], **and M. Bayrak**[3]

[1]Electronic Communication Program
Eregli Kemal Akman Technical Vocational School of Higher Education
Selcuk University, Konya, Turkey
[2]Department of Electrical and Electronics Engineering
Faculty of Engineering-Architecture, Selcuk University, Konya, Turkey
[3]Department of Electrical and Electronics Engineering
Faculty of Engineering, Mevlana University, Konya, Turkey

Abstract— In this study 1×4 rectangular microstrip array antennas are designed at 16 GHz resonant frequency for KU Band usage on Duroid 5880 substrates that has a thickness of 0.254 mm and a dielectric constant of 2.2. Designs are simulated using HFSS v12. At these designs, by changing the feed line widths systematically, for each antenna, electrical parameters like S_{11} response, directivity, gain, radiation efficiency etc. are investigated for 26 array antennas in simulation media. Also, directivity and gain values are predicted with an Artificial Neural Network model. The network has four inputs as dielectrik substrate thickness, resonant frequency and dielectric constant of the substrate and three outputs as directivity, gain and radiation efficiency. Multilayer perceptron structure for Artificial Neural Network model and Levenberg-Marquart learning algorithm for training the network are used. The network model is trained with 20 of 26 design data and is tested with the rest 6 ones. It is seen that the results from simulations and the neural network model are compatible with similar studies in the literature.

Fractal Inspired Patch Antenna on Metamaterial

S. Suganthi[1], **S. Raghavan**[2], **and D. Kumar**[3]

[1]Shri Angalamman College of Engineering and Technology, Trichy, India
[2]National Institute of Technology, Trichy, India
[3]Periyar Maniammai University, Thanjavur, India

Abstract— This paper proposes a novel design of a compact microstrip antenna on a metamaterial (MTM) substrate. This antenna is composed of a fractal outlined square patch as the main radiating element. The MTM used is a combination of multiple slip ring resonators (MSSR) along with a Wire Strip on a FR4 substrate. Another novelty in this design is that the structure utilizes co-planar waveguide (CPW) system and a microstrip feed. Hence, the ground plane lies along the antenna plane which makes fabrication easier. The design and simulation have been carried out using HFSS 3D electromagnetic simulation software. Initially an investigation has been made to confirm that the preferred MSRR and Wire structure exhibit metamaterial property. With a separate coding written in MATLAB for Nicolson-Ross-Wier method, the negative permeability and negative permittivity have been verified to be present. The magnetic permeability is found to be more predominant in large frequency ranges. Then square fractal antenna has been designed and simulated separately and it resonates at multiple frequencies. Finally with MTM loading, this antenna was found to resonate at multiple frequencies with a comparatively reduced return loss, improved gain and focused radiation.

CPW-fed Slot Patch Antenna for 5.2/5.8 GHz WLAN Application

Vepuri Niranjan, **Alok Kumar Saxena**, **and Kumar Vaibhav Srivastava**
Department of Electrical Engineering, Indian Institute of Technology, Kanpur, India

Abstract— In microwave and millimeter wave applications, slot antennas fed by coplanar waveguide (CPW) are receiving increasing attention [1]. These antennas have several useful properties, such as a wider impedance bandwidth compared to microstrip patch antennas and easier integration with solid state devices [2–4]. In this paper, a CPW-fed patch antenna with slots is presented. The antenna consists of patch structure with two rectangular slots on it. The physical size of the proposed antenna is 30 mm × 24 mm. Antenna was de signed on a polyflon polyguide substrate with parameters = 2.32 and = 0.0016 and a thickness of 1.59 mm.

The characteristics of the design structure are investigated by using FEM based electromagnetic solver Ansoft HFSS. The impedance bandwidth of the proposed antenna is 4 GHz ranging from 4.8 GHz tto 8.8 GHz aand has a fractional bandwidth of 58%. The proposed CPW-fed slot patch antenna produces a 30% higher bandwidth compared to the CPW-fed patch antenna [5]. The antenna is resonating at 5.5 GHz and gives monopolar radiation pattern at this frequency. This antenna can bee used in 5.2 GHz/5.8 GHz WLAN application. The variation of the resonant frequency with slot width has been studied. The antenna produces a gain of 3.8 dBi at the resonant frequency and the radiation efficiency of antenna is in the order of 90%. The other advantage of this antenna is simple in configuration which leads to easy fabrication and can be built in any wireless wideband device applications.

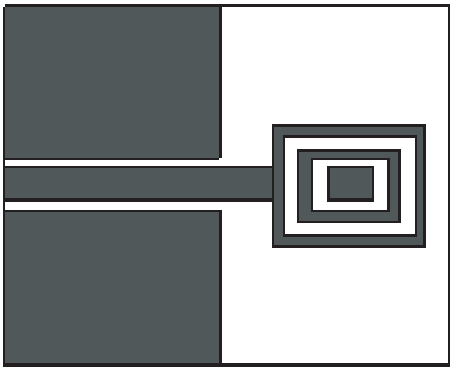

Figure 1: Proposed CPW-fed slot patch antenna.

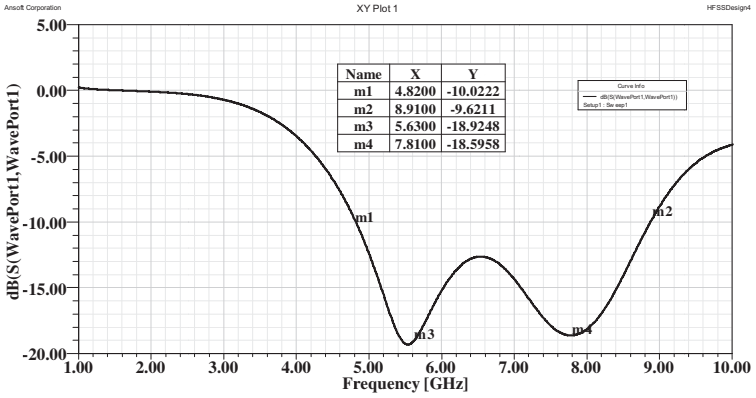

Figure 2: Simulated return-loss characteristics of proposed slot patch antenna.

REFERENCES

1. Deng, S.-M., M.-D. Wu, and P. Hsu, "Analysis of coplanar waveguide-fed microstrip antennas," *IEEE Trans. Antennas Propagation*, Vol. 43, 7734–737, July 1995.
2. Giauffret, L. and J.-M. Laheurte, "Theoretical and expiremental characterisation of CPW-fed microstrip antennas," *IEEE Proc.-Microw. Antennas Proppag.*, Vol. 143, No. 1, Februaary 1996.
3. Wu, C.-M., "Dual bannd CPW-fed cross-slot monopole antenna for WLAN operation," *IET Microwave Antennas Propogation*, Vol. 1, No. 2, 542–546, 2007.
4. Liu, W.-C. and C.-M. Wuu, "Broadband dual-frequency CPW-fed planar monopole antenna with rectangular notch," *Electronic Letters*, Vol. 40, No. 11, May 27, 2004.
5. Antoniades, M. A. and G. V. Eleftheriades, "A broadband dual-mode monopole antenna using NRI-TL metamaterial Loading," *IEEE Antennas and Wireless Propagation Letters*, Vol. 8, 2009.

E-shaped Reflectarray Antenna with Radar Cross Section Reduction

N. H. Sulaiman and M. Y. Ismail
Radio Communications and Antenna Design (RACAD), Department of Communication Engineering
Faculty of Electrical and Electronics Engineering, Universiti Tun Hussein Onn Malaysia
Parit Raja 86400, Johor, Malaysia

Abstract— The demand for low cost and lighter weight antenna with compact broadband features and dual frequency in communication system is rapidly increasing. Radar cross section (RCS) is one of the considerations for designing a radar antenna. A larger RCS indicates that an object can more easily be detected by other radar detectors. To reduce any detection from other radar antenna RCS should be minimized. The radar systems require two different frequencies which are used for detection and tracking applications. Based on the current demands, dual frequency reflectarray antenna with radar cross section reduction is presented in this paper. In order to realize dual frequency with RCS reduction, the simulation work has been carried out by using commercially available computer software of CST MWS. The simulated results show that the proposed design can be operated in X-band (8–12 GHz) frequency band. Dual frequency has been achieved by integrating dual gap on the patch element (E-shaped) of reflectarray antenna. The simulated results demonstrated a reflection loss of 0.684 dB at 8.21 GHz and a reflection loss of 1.44 dB at second resonant frequency of 11.82 GHz. By introducing dual gap on the patch element, it is shown that the radar cross section is significantly reduced from $-8.43\,\mathrm{dBm}^2$ to $-3.84\,\mathrm{dBm}^2$. In this work, far field radiation pattern of 10×10 element of (E-shaped) element of reflectarray antenna has been generated to observe gain performance. By using gain and aperture size of the E-shaped element radar cross section has been calculated. Moreover $4.59\,\mathrm{dBm}^2$ reduction of radar cross section is achieved by introducing dual gap on the patch element of reflectarray antenna. Simulated results show that the reduction of radar cross section gives significant advantages for tracking radar application particularly for defense systems and military system. The proposed design can be useful for radar application which requires dual frequency operation simultaneously.

Analytical Model of Progressive Phase Distribution of Reflectarray Antenna

M. Inam and M. Y. Ismail
Radio Communications and Antenna Design Laboratory
Faculty of Electrical & Electronic Engineering
University Tun Hussein Onn Malaysiaa, Parit Raja, Johor 86400, Malaysia

Abstract— A novel technique for the analysis of the required reflection phase properties from individual reflectarray elements to form a planar wavefront of the periodic aperture is presented. A unit cell patch element representing an infinite reflectarray modeled based on FEM using the waveguide simulator demonstrates that there is no significant influence on the scattering parameters of reflectarray resonant elements until the angle of incidence is increased up to 40 degrees. An algorithm for the progressive phase distribution is developed and different substrate materials have been employed to investigate the scattering parameter behavior of the S-shaped reflection phase curves for a reflectarray antenna design. A Figure of Merit (FoM) has been defined for the comparison of the reflection phase curves of reflectarrays modeled with different dielectric substrates and the results are compared in terms of bandwidth performance and static linear phase range. It has been demonstrated that the bandwidth of the reflectarray increases from 218 MHz to 540 MHz with decrease in the dielectric permittivity value of the substrate within the range $\varepsilon_r = 13$ and $\varepsilon_r = 2.08$. However there is a tradeoff between the bandwidth performance and linear static phase range as a maximum linear static phase range of 355° is achieved for Gallium Arsenide ($\varepsilon_r = 13$) as compared to minimum linear static phase range of 300° achieved by Teflon ($\varepsilon_r = 2.08$). Furthermore reflectarray unit cell patch elements have been fabricated in X-band frequency range using different substrate thicknesses of Roger's RT/d 5880 dielectric material. Vector network analyzer has been used for the waveguide scattering parameter measurements of unit cell reflectarray elements. The measured results demonstrated an improvement in FoM and reflectarray bandwidth performance with an increase in substrate thickness.

Session 3P5
Computational Electromagnetics, Spectra, Time, and Frequency Domain Techniques

MAGIC3D EM-PIC Code Implicit Particle Pusher Description and Test

Andrew J. Woods and Lars D. Ludeking
Alliant Techsystems (ATK), 8560 Cinderbed Road, Suite 700, Newington, VA 22122, USA

Abstract— The MAGIC3D [1] electromagnetic (EM) particle-in-cell (PIC) code has been upgraded to include an implicit update scheme (particle "pusher") for increased time steps Δt and stability in beam-plasma simulations. The adjustable damping implicit update method of Friedman [2] allows selectable attenuation of modes in a plasma.

Our approach has been to first develop a simple one-dimensional (1D) particle pusher finite-difference code model which incorporated implicit PIC and replicated the electron motion reported in [2]. Then we upgraded the method for the MAGIC2D PIC code including magnetic field and relativistic effects [3]. Now we present the method as implemented in MAGIC3D with example problems of interest, focusing on low energy plasmas. The new capability provides a damping parameter θ which can be chosen between 0.0 (no damping) to 1.0 (10× damping in 16 periods for an example test problem). Hence, for a mix of frequencies in a complex many-particle system, unwanted higher frequency oscillations can be adjustably diminished while preserving the lower values of greater interest.

The new method agrees with the previous explicit treatment in MAGIC3D for test cases where both have sufficiently small time step. The implicit approach shows stability for a longer time in rigorous example plasma test problems with larger time steps. As an example, a simple rectangular plate configuration containing a gas at 0.001 atmospheres is subjected to a short ionizing 500 eV electron beam pulse. Much of the resulting population of charged particles is swept out by an applied 250 V potential. The electron average energy at late time long after the beam is off is shown in Figure 1. The implicit case is on the left and the standard explicit results on the right. The curves demonstrate reduced artificial heating of the electrons with the new capability.

The new implicit particle pusher in MAGIC3D enables the user to select damping of high-frequency modes thus concentrating on plasma fundamental frequencies of interest. This additional user tool, to be available in MAGIC version 3.2.0, can prevent instabilities resulting from ionization growth beyond the time step limit for explicit particles.

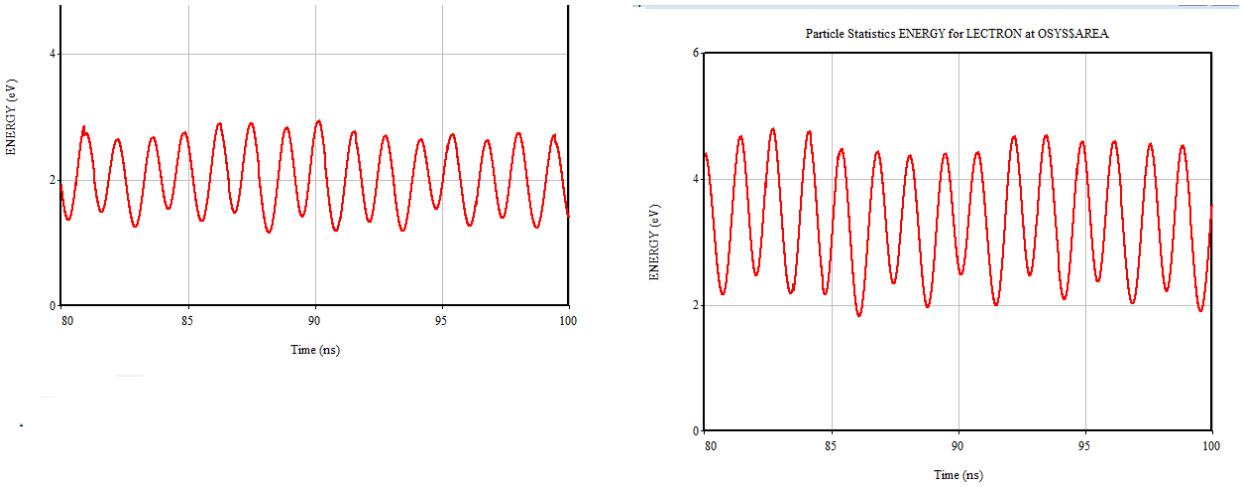

Figure 1: Average energy of electrons contained by ionized gas showing reduced artificial heating for implicit model with $\theta = 1.0$ (left) compared to the explicit model (right) for identical numerical grids.

ACKNOWLEDGMENT

Work supported by ATK.

REFERENCES

1. Goplen, B., et al., "User-configurable MAGIC for Electromagnetic PIC Calculations," *Computer Physics Communications*, Vol. 87, 1995, http://www.magictoolsuite.com.
2. Friedman, A., "Implicit multiscale PIC and related topics," *Workshop on Multiscale Processes in Fusion Plasmas*, UCLA, January 2005, (http://hifweb.lbl.gov/public/slides/).
3. Woods, A. and L. Ludeking, "MAGIC2D implicit particle pusher description and test," abstract prepared for *Progress in Electromagnetics Research Symposium*, Kuala Lumpur, Malaysia, March 27–30, 2012.

An Efficient Method for Computing Highly Oscillatory Physical Optics Integral

Yumao Wu[1], **Lijun Jiang**[1], **and Weng Cho Chew**[1, 2]

[1]Department of Electrical and Electronic Engineering
The University of Hong Kong, Pokfulam Road, Hong Kong, China
[2]Department of Electrical and Computer Engineering
University of Illinois, Urbana-Champaign, USA

Abstract— When the electrical size of objects are on the order of hundreds or even larger compared with the incident wavelength λ, the physical optics (PO) approximation has been accepted as an efficient approach for analyzing the scattering and radiation electromagnetic problems. However, the PO integral kernels will always get more highly oscillatory as the ratio of objects size and wavelength λ becomes larger. In this sense, the computation cost by a direct numerical integration scheme for the PO integral will be extremely high. The only frequency-independent approach for analyzing the highly oscillatory PO integral is via the traditional asymptotic expansion approximation. However, it will evaluate the PO integral with limited accuracy since the traditional asymptotic approximation procedure is used.

In this work, we use the steepest descent path (SDP) technique to calculate the highly oscillatory PO integral with a quadratic phase variation on quadratic patches. Stokes phenomenon will occur due to different asymptotic behaviors on different domains. The stationary phase points contributions are carefully studied by the SDP and complex variables theory using contour deformation, which agree quite well with the leading terms by the traditional asymptotic expansion. Furthermore, we extract other contributing terms for the PO integral, including the resonance points and vertex points contributions. Compared with traditional approximate asymptotic expansion approach, our method has significantly improved the accuracy for evaluating the PO integral. Moreover, the computation effort for the highly oscillatory integral is frequency-independent.

Method of Moments Analysis for Antenna Arrays with Optimum Memory and Time Consumption

Kamel S. Sultan, **Haythem H. Abdullah**, **and Esmat A. Abdallah**
Electronics Research Institute, Dokki, Giza, Egypt

Abstract— For some applications, single element antennas are unable to meet the gain or radiation pattern requirements. Combining several single antenna elements in an array can be a possible solution. In order to get accurate analysis of the antenna arrays, full wave analysis methods such as the method of moments (MoM), the finite difference time domain (FDTD), etc are required. Unfortunately, these methods are heavy computational methods that consume long time and large computational resources. Even with the appearance of the high performance parallel processing resources, the computational time and memory usage still large due to the nature of the problem. So, in this paper, the MoM is chosen to analyze large problems such as antenna arrays taking into consideration the reduction of its needed computational resources and time consuming. The MoM is a well-established and an accurate full wave analysis method. In this paper, the MoM is applied to solve the electric field integral equation (EFIE) on conducting objects with the use of RWG basis function that is used with triangular segmentation of the scatterer surface. The triangular segmentation is used because it is the geometry that is best fit arbitrarily shaped objects. The MoM solves the EFIE for the current distribution by converting it to a system of linear equations in the form $[Z][I] = [V]$. The main parts of the MoM that consume memory and time are the filling of the Z-matrix and the inverse matrix to get the current on the scatterer surface.

Consider N element array synthesis using the MoM and assume that M discretization segments per array element are used. In order to take the mutual coupling between the array elements into consideration, it is required to have a $[Z]$ matrix with $(M \times N) \times (M \times N)$ elements. But in fact, the mutual coupling between array elements decreases with the increase of the distance between elements, e.g., the base station antenna arrays. In this paper, the solution domain is decomposed into N domains, one for each array element. Since the incident wave is the field that exists in the absence of the scatterer, each element will be analyzed using its own excitation in conjunction with the scattered waves from the preceding analyzed element. The analysis over all elements will be repeated for each element from two to three times according to the distance between elements until steady state solution is reached. In this way the memory requirement will be $M \times (N \times N) \times 3$ at maximum which is efficient when the number of elements M exceeds three. By reducing the $[Z]$ matrix, not only its computational time will be reduced but also the computational time of the inverse matrix will also be reduced.

Simulation results for arrays of linear dipoles at different distances are tested and compared to the conventional MoM procedure.

Development of a Symplectic Scheme with Optimized Numerical Dispersion-relation Equation to Solve the Maxwell's Equations in Dispersive Media

Tony W. H. Sheu[1, 2], **R. Y. Chung**[1], **and J. H. Li**[1]

[1]Department of Engineering Science and Ocean Engineering, National Taiwan University
No. 1, Sec. 4, Roosevelt Road, Taipei, Taiwan, China
[2]Taida Institute of Mathematical Science (TIMS), National Taiwan University, Taiwan, China

Abstract— In this paper an explicit finite-difference time-domain scheme is developed in non-staggered grids for solving the Maxwell's equations. We are aimed to preserve discrete zero-divergence for the electrical and magnetic fields. The inherent local conservation laws in Maxwell's equations are also discretely preserved all the time using the explicit second-order accurate symplectic partitioned Runge-Kutta temporal scheme. The remaining spatial derivative terms in the semi-discretized Faraday's and Ampere's equations are then discretized to provide an accurate mathematical dispersion relation equation that governs the numerical angular frequency and the wavenumbers in two space dimensions. To achieve the goal of getting a best dispersive characteristics, we propose a fourth-order accurate space centered scheme which minimizes the difference between the exact and numerical dispersion relation equations. In this newly proposed FDTD context, both frequency-independent and dispersive media are investigated. Emphasis is placed on the accurate modelling of EM waves in the vicinity of interface, across which there is a jump of medium permittivity, through the use of matching interface conditions. Through the current computational exercises, the proposed dual-preserving solver is computationally demonstrated to be efficient for use to predict the long-term accurate Maxwell's solutions for media of frequency independence and frequency dependence types.

Eigenproblem Approach for Analysis of Microwave Filters Using Finite Element Method

A. Lamecki, **M. Rewienski**, **and M. Mrozowski**
Gdansk University of Technology, Poland

Abstract— Ability to model high frequency devices with arbitrary, complex geometry is a key advantage of finite element method. It is the main reason for FEM's popularity in computational electromagnetics, including design of high power filters and multiplexers for modern communication systems.

A classic approach for computation of scattering/impedance parameters for a structure using FEM leads to a linear system $A \cdot x = b$ that has to be solved anew at each frequency point for a collection of excitations at the feeding ports (for the N-port device one gets N right hand sides at each frequency). Since matrix A is usually large, sparse and frequency-dependent, the numeric cost of solution procedure (using either direct or iterative methods) is high, especially if response at tens or hundreds frequency points needs to be computed.

In this contribution an alternative approach is proposed. It allows one to replace the repeated solutions of linear problems with a defined set of eigenproblems. The new formulation binds the eigenvalues of the predefined eigenproblems with zeros and poles of the rational representation of impedance parameters $z_{ij(s)} = \frac{P(s)}{Q(s)}$ of the analyzed structure. Additionally, it is shown that the resulting eigenproblems can be efficiently solved using iterative eigensolvers, such as shift-and-invert Lanczos methods. The proposed formulation is particularly well suited for analysis of high frequency filtering devices, since their responses are commonly described by zeros and poles of the transfer function.

The technique is applied to model high frequency filtering structures and initial results show that one can get full information about admittance parameters in the band of interest with numeric cost competitive with classic frequency-by-frequency analysis.

Frequency Sensitivity of Lossless Planar Devices by FEM

A. Kiaee, **R. Sarraf Shirazi**, **and S. R. Hosseini**
Department of Electrical Engineering, Amirkabir University of technology, Tehran, Iran

Abstract— In this paper numerical calculation of frequency sensitivity of a lossless planar device using finite element is presented. The finite element method has been shown to be an efficient and flexible way of computing the equivalent circuit parameters of N-port planar devices (microstrip, stripline, rectangular waveguide, etc.). In addition, the sensitivity of admittance parameters can be provided at little extra cost for changing in operating frequency. This way, frequency sensitivity of the equivalent circuit parameters can be found by two dimensional finite element method. This approach has been implemented by triangular finite elements and the sensitivity was computed for microstrip bend: the agreement with previously published result was excellent.

Analysis of Waveguide with Arbitrarily Shaped Cross-section and Its Application to Circular Polarizer

M. Tanigawa[1], **Y. Urano**[1], **K. Wakino**[1], **T. Kitazawa**[1]
S. Imai[2], **K. Taguchi**[2], **T. Kashiwa**[2], **M. Suzuki**[3], **and K. Fujii**[3]

[1]Department of Electrical and Electronic Engineering, Ritsumeikan University, Japan
[2]Department of Electrical and Electronic Engineering, Kitami Institute of Technology, Japan
[3]Section of FBR fuel production, Division of Advanced Nuclear System
Japan Atomic Energy Agency, Japan

Abstract— Spectral domain approach is extended to analyze the propagation characteristics of waveguides with an arbitrarily shaped cross-section (Fig. 1). Accurate and efficient numerical procedure is developed to design a circular polarizer for uniform microwave heating, which consists of a circular waveguide with the conductor fin. The extended version of spectral domain approach [1] takes the effect of the thickness of the conductor fin and the field singularity near the conductor edge into consideration, and determines the proper choice of the TwidthT, height and length of the conductor fin to generate the circular polarized wave. The horn antenna with the prototype circular polarizer radiates the circular polarized wave with the axial ratio 2.04 dB at 2.45 GHz (Fig. 2).

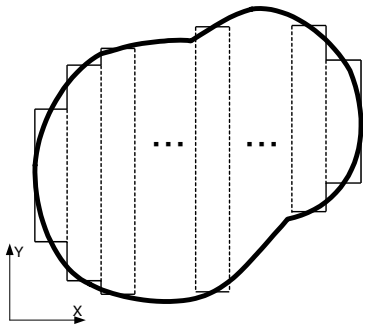

Figure 1: Waveguide with arbitrarily shaped cross-section.

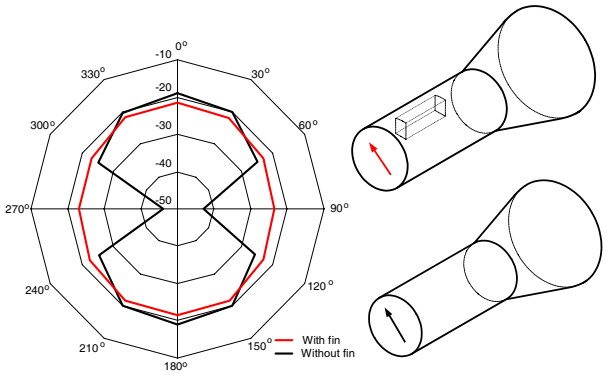

Figure 2: Measured polarization pattern of horn antenna with circular polarizer.

REFERENCES

1. Kitazawa, T., *IEEE Trans. on MTT*, Vol. 43, 445–451, 1995.

Determination of Complex Permittivity of Materials with High or Low Losses

R. Yokoyama, **Y. Konishi**, **K. Wakino**, **and T. Kitazawa**
Department of Electrical and Electronic Engineering, Ritsumeikan University, Japan

Abstract— A hybrid numerical method developed by the authors [1] is based on the extended spectral domain approach combined with the mode-matching method and does not include any approximate perturbational scheme. The method can be applied to evaluate the scattering parameter of obstacles located arbitrarily in waveguide. The obstacle may be made of the wide variety of materials and be electrically large or small. The hybrid electromagnetic method is applied to evaluate the complex permittivity of materials with high or low losses. The sample material with the proper size is situated at the proper position in the waveguide to achieve the adequate scattering parameters S_{21} for the material estimation. For example, the smaller sample should be prepared for the material with high permittivity and/or high loss and it should be placed near the waveguide wall where the electric field is weaker than that in the center for TE_{01} mode.

REFERENCES

1. Miyagawa, H., et al., *IEEE Trans. MTT*, Vol. 57, 2249–2256, 2009.

Classification of Multi-rate CDMA Signals Using Compressed Cyclostationary Features

Said E. El Khamy[1], **Amr El Helw**[2], **and Azza Mahdy**[2]

[1]Department of Electrical Engineering, Faculty of Engineering
Alexandria University, Alexandria, Egypt
[2]Department of Communication & Electronics Engineering
Arab Academy for Science and Technology and Maritime Transport, Cairo, Egypt

Abstract— Spectrum sensing is considered as a promising technology for open-spectrum sharing scenarios which enables cognitive radio networks to adapt their parameters according to channel status variations. Many spectrum sensing techniques were introduced such as matched filter detection, energy detection, and cyclostationary feature detection. Cyclostationary detection is one of the spectrum sensing types which is used to solve weak signal detection. By exploiting the cyclic properties presented in modulated or coded signals, classification of signals became adequate and clear. The main advantage of cyclic feature detection is that it discriminates the noise energy from modulated signal energy. However, cyclostationary detectors require also long observation times that is why it is not suitable for online signals detections or real-time applications. Accordingly, compressed features are required to increase features detectors performance in real time. In this paper, we introduce a method classify multi-rate CDMA signals using compressed cyclic features by Wavelet Transform. Our studies show that the cyclostationary features of the CDMA signals become completely different as the processing gain is changed. It was noticed that the detailed wavelet coefficients have no significant information and hence compression was performed using the approximation coefficients only. The result is a 2-D matrix with one dimension indicating scales in the direction of the cycle frequency and the other dimension indicating the scales in the direction of the traditional frequency. Then we choose the peak values of these coefficients that correspond to certain range of cycle frequencies. Finally, Features are generated for each type of signals and ready to be applied to the input of a Neural Network classifier. Calculations of the average classification error is performed using 10-folds cross validation method. In particular it is found that the number of the generated peaks in the cyclic spectra increases as the processing gain increases. This increase affects the classification performance. By varying the code rate we notice that each rate identifies distinguished cyclic spectrum of the spread spectrum signal.

Solving the Electric Field Integral Equation Using Markov Chain Monte Carlo Method

Mrinal Mishra
Department of Electronics & Communication Engineering
Birla Institute of Technology, Mesra, Ranchi, India

Abstract— In this paper, a new Markov Chain Monte Carlo method for solving the Electric Field Integral Equation (EFIE) is proposed for the problem of scattering of a plane wave by an infinite dielectric cylinder. A transverse magnetic plane wave is incident on a dielectric cylinder of infinite length along one direction. The problem is posed in form of a volume integral equation, the solution for which is is to obtain the unknown current that is induded over the cross section of the cylinder. Conventionally, the EFIE is solved by techniques like the method of moments (MoM) which involves a basis function expansion of the unknown current. This requires a judicious choice of the basis functions depending upon the geometry and dimensionality of the problem. Also, the singular kernel of the EFIE poses a major problem for which it has to be approximated to remove the singularity appearing in the MoM matrix element integrals. In the present work, the Monte Carlo method performs a Markov Chain estimatin of the unknown current over the cross section. This does not require any basis function expansion and is independent of the dimensionality of the problem. Also, the singularity issue is resolved without any approximation. To test the correctness of the problem, a standard problem of known frequency of the incident wave and known dielectric constant and dimension of the cylinder is solved. The results for the scattering cross section by proposed method are compared with standard results obtained by MoM.

3D LFE-27 Formulae for the Method of Connected Local Fields

Hung-Wen Chang and Sin-Yuan Mu
Department of Photonics, National Sun Yat-Sen University, Taiwan

Abstract— Following our previous work on the method of connected local field [1, 2], we present the derivation of 3D local field expansion (LFE) formulation for obtaining semi-analytical solutions of the Helmholtz equation. Figure 1 illustrates a basic cube in a 3D network of equally spaced points containing 26 points on the faces and a point inside the cube. The EM field within a cube can expanded as a truncated spherical Fourier-Bessel series. The end result is the LFE-27 formulae which is a FD-like twenty-seven coefficients for the three-dimensional Helmholtz equation in a homogeneous medium. We shall study the truncation and dispersion errors for the novel LFE-27 stencils. Numerical results of computation of the 3D free space Green's function using LFE-27 equation will also be discussed.

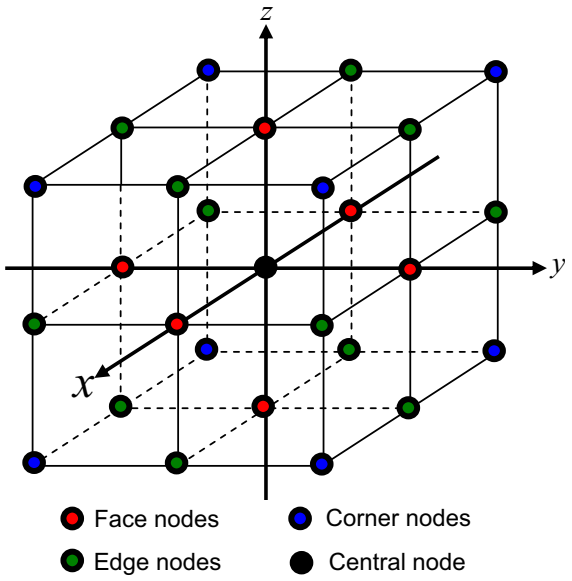

Figure 1: The unit cube and the twenty seven nodes for the 3D theory of connected local fields.

REFERENCES

1. Chang, H.-W. and S.-Y. Mu, "Semi-analytical solutions of Helmholtz equation by the method of connected local fields," *Progress In Electromagnetics Research*, Vol. 109, 399–424, 2010.
2. Mu, S.-Y. and H.-W. Chang, "Theoretical foundation for the method of connected local fields," *Progress In Electromagnetics Research*, Vol. 114, 67–88, 2011.

Implementation of Second-order Accurate Engquist-Majdat Absorbing Boundary Condition for the Helmholtz Equation

Hung-Wen Chang and Chun-Yu Lian
Department of Photonics, National Sun Yat-Sen University
70 Lien-Hai Rd. Kaohsiung 80424, Taiwan, R.O.C.

Abstract— We present the frequency-domain version of the well-known time-domain Engquist-Majdat absorbing boundary condition (EM-ABC) for the Helmholtz equation. While the time-domain implementation of the one way equation is only first-order accurate in both temporal and spatial step size, in frequency-domain realization we are able to keep every finite-difference operator accurate to the second power of the grid spacing for both the edge and corner points [1]. We derive the plane wave reflection coefficients of as function of the incident angle and grid size. Numerical results of computation of the 2D free space Green's function using EM-ABC will also be discussed.

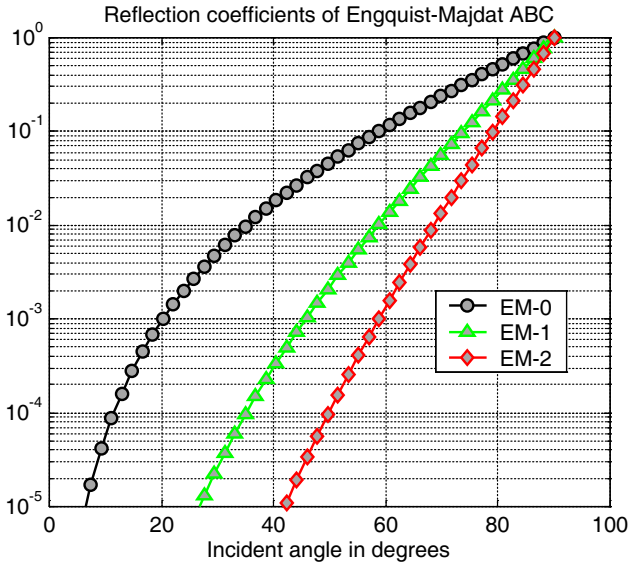

Figure 1: Plane wave power reflection coefficients of Engquist-Majdat ABC. The black, green or red line is the 0/1/2th-order approximation to the one way equations.

REFERENCES

1. Chang, H.-W. and C.-Y. Lian, "Engquist-Majdat absorbing boundary condition for the Helmholtz equation," *International Photonics Conference 2011*, Tainan, Taiwan, 2011.

New Numerical Method for Solving Maxwell Equations with Strong Singularity

V. A. Rukavishnikov and A. O. Mosolapov
Computing Center of Far-Eastern Branch, Russian Academy of Sciences
Kim-Yu-Chen Str. 65, Khabarovsk 680000, Russia

Abstract— Maxwell equations are used in mathematical models of electromagnetic fields, for example, in plasma physics, electrodynamics and engineering of high-frequency devices. As a rule, in practical problems the computational domain is nonconvex with reentrant corners or edges on its boundary. Such geometry singularities leads to strong electromagnetic fields in their neighborhood, and a solution of Maxwell equations is strongly singular, i.e., it does not belong to the Sobolev space.

In the present talk we develop the weighted edge finite element method (FEM) based on the conception of R_v-generalized solution (see, example, [1]) of the Maxwell equations with strong singularity due to a reentrant corner on the boundary. Numerical experiments of model problems showed that the rate of convergence of the numerical solution to the exact one is more than one and a half times better in comparison with the results established in papers of other mathematicians. Another advantage of this method is simplicity of the solution determination which is an additional benefit for numerical experiments.

REFERENCES

1. Rukavishnikov, V. A., "Methods of numerical analysis for boundary value problem with strong singularity," *Russ. J. Numer. Anal. Math. Model.*, Vol. 24, No. 6, 565–590, 2009.

Design of Rectangular Cavity by Extended Spectral Domain Approach

Mohamad Shaiful Bin Abdul Karim[1], **Kikuo Wakino**[2], **Toshihide Kitazawa**[3], **Hsin-Hsiang Su**[4], **and Chih-Wen Kuo**[4]

[1]Electrical and Electronic Engineering, Ritsumeikan University, Japan
[2]Institute of Science and Technology, Ritsumeikan University, Japan
[3]Electrical and Electronic Engineering, Ritsumeikan University, Japan
[4]National Sun Yat-San University, Taiwan

Abstract— The extended spectral domain approach (ESDA) [1] is applied to design the rectangular cavity resonator. An accurate and efficient numerical method is developed considering the thickness of the input and output windows of the resonator and the singularities near the conductor edge. An X-band resonator is designed with the optimized coupling aperture between the cavity and waveguides. The measured frequency dependent scattering parameter S_{21} of the prototype resonator is in excellent agreement with the numerical result by ESDA and the high Q of 9011 is obtained. This resonator will be useful to evaluate the material constants of the sample placed in the resonator.

REFERENCES

1. Shiraishi, T., et al., *IEICE Trans. Electron.*, Vol. E86-C, 2184, 2003.

Session 3P6
Microwave and Millimeter Wave Circuits and Devices, CAD

Characteristic Impedance of a Defected Microstrip Line Structure

Jongsik Lim[1], **Yuckhwan Jeon**[1], **Kyunghoon Kwon**[1], **Jaehoon Lee**[1], **Yongchae Jeong**[2], **Sang-Min Han**[1], **and Dal Ahn**[1]

[1]Soonchunhyang University, Republic of Korea
[2]Chonbuk National University, Republic of Korea

Abstract— Recently a defected microstrip structure (DMS), of which microstrip line pattern is modified for additional equivalent inductance and capacitance, has been proposed in order to replace the previous DGS (defected ground structure) microstrip lines. Geometric patterns should be realized on the bottom ground plane in DGS microstrip lines, and this is one of drawbacks of DGS microstrip lines. In order to solve the problem, additional patterns are realized in the signal line on the top planes in DMS microstrip lines, while the advantages of DGS are being kept such as slow wave effect, longer electrical length for the same physical length and higher characteristic impedance. In addition, the ground plane of DMS microstrip lines is untouched, so the packaging problem does not arise while it is serious in DGS microstrip lines. The additional inductance and capacitance exist due to the DMS patterns, and they play a role to increase slow wave effect and change the characteristic impedance. In this work, the new characteristic impedance is calculated with an analytic method from the S-parameters of the DMS microstrip lines. For an example, a T-shaped DMS patterns are inserted into a microstrip line (Fig. 1) and its S-parameters are obtained by electromagnetic simulation (Fig. 2). The practical example of DMS line is fabricated for the verification of transmission properties (Fig. 3), and its measured S-parameters are shown and compared to simulation (Fig. 4). By applying the analytic method to the DMS microstrip line, the new characteristic impedance of the DMS microstrip line is calculated (Fig. 5). For the same line width, 2.38 mm, the characteristic impedance of a normal microstrip line is 50 Ω, while it is 78 Ω at 1 GHz for the DMS microstrip line for the given substrate with 2.2 of dielectric constant and 31mils of thickness.

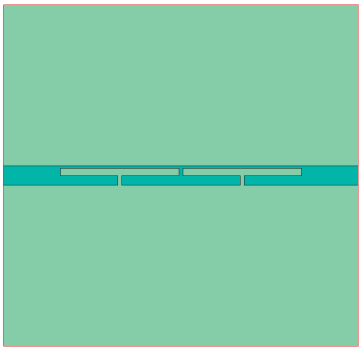

Figure 1.

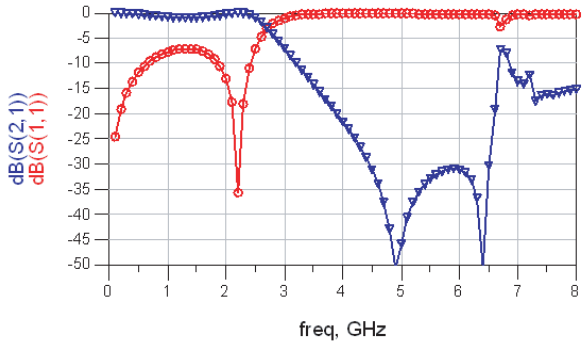

Figure 2.

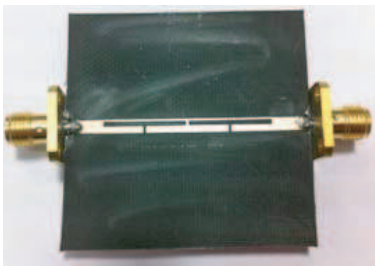

Figure 3.

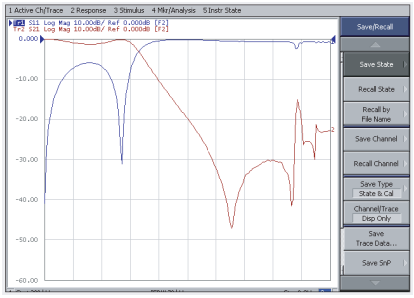

Figure 4.

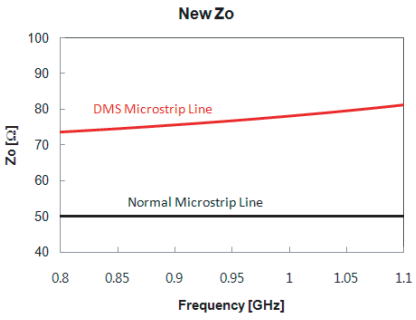

Figure 5.

Efficiency Enhancement by Harmonic Phase Tuning in Class-F Amplifiers

Ken Hiraga and Toshio Nojima
Hokkaido University, Sapporo 060-0814, Japan

Abstract— Power efficiency in power amplifiers has long been a major issue in the field of radio transmitters. accordingly, many techniques that reduce the power dissipation in active devices have been proposed. load impedance at harmonic frequencies has been considered to be one of the most important factors in decreasing the power dissipation of power amplifiers for radio transmitters. however, some packaged high-frequency power devices have electric length and parasitic components. moreover, there are individual differences among each of these devices. these factors limit harmonic phase precision, which deteriorates efficiency in class-F operation. therefore, to realize precise harmonic phases, load circuits should have a fine tuning mechanism. to address this issue, harmonic matching and reflection amplifiers (HMRAS) include a mechanism to optimize the second harmonic phase condition. however, no consideration has been given to third harmonic phase tuning in HMRAS.

In this paper, we used numerical analysis to clarify the negative effects on class-F operation efficiency produced by second and third harmonic phase errors. when the third harmonic error is more than 20 degrees, the third harmonic cannot contribute to efficiency improvement if the phase error of the third harmonic takes such a value.

Figure 1 shows the relationship of the drain efficiency to second- and third- harmonic phase errors, ϕ_2 and ϕ_3, respectively. When the third harmonic phase error ϕ_3 is more than 20 degrees, drain efficiency does not depend on ϕ_3. This means that the third harmonic cannot contribute

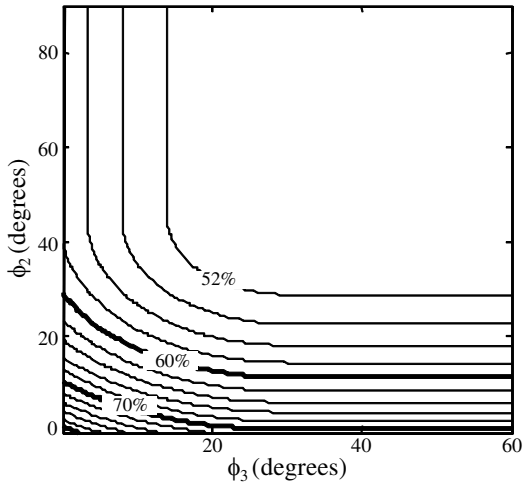

Figure 1: Drain efficiency with harmonic phase errors.

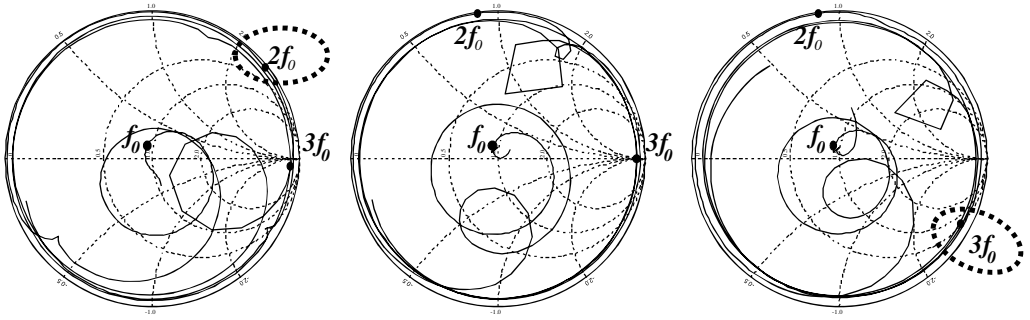

(a) $L_2 = 2$ mm $L_3 = 0$ mm (b) $L_2 = 0$ mm $L_3 = 0$ mm (c) $L_2 = 0$ mm $L_3 = 1.33$ mm

Figure 2: Input impedance transition of the harmonic filter.

to efficiency improvement if its phase error takes such a value. The same can be said when ϕ_2 is more than 40 degrees. Second and third harmonic phase errors significantly deteriorate efficiency.

Hence, precise harmonic phase conditions in both second and third harmonic are very important in class-F amplifiers. To realize them, it is preferable that the phase conditions are tunable independently without influencing the impedance at the fundamental frequency. Conventional circuits did not have such tuning functions.

As a solution to handle this issue, we introduced a harmonic reflection filter circuit for class-F amplifiers that can provide tunable phases for the second and third harmonics independently. the harmonic filter reflects the second and third harmonics at the appropriate phase and has no effect on the fundamental frequency. the filter simplifies the precise phase tuning for the second and third harmonics and promises to enable the achievement of highly efficient class-F operations.

By making use of these characteristics, we can easily tune the harmonic load condition by tuning the second and third harmonic tuners in sequence. This circuit simplifies the precise phase tuning for the second and third harmonics for the achievement of highly efficient class-F operations.

Compact Microstrip Bandstop Filter with Controllable Triple Stopband Response

Shry-Sann Liao[1], **Shih-Yi Yuan**[1], **Yu-Lun Wu**[2], **and Ting-Yao Huang**[1]

[1]Department of Communication Engineering, Feng-Chia University
100, Wen-Hua Rd., Taichung 407, Taiwan, R.O.C.
[2]Ph.D. Program in Electrical and Communications Engineering, Feng-Chia University
100, Wen-Hua Rd., Taichung 407, Taiwan, R.O.C.

Abstract— Recently, microwave passive components and devices with multi-band operation become more and more important in modem communication systems and have been focused much attention for the miniaturization and multifunction requirement of the portable equipments [1–3]. Multiple band microwave components with compact size and low cost are required and studied. On the other hand, multi-bandstop filters are desired for their effective suppression of spurious signals in wireless communication systems. Other advantage is its low passband insertion loss and group delay due to its resonators resonates in the stopband rather than in the passband.

There are few papers about multiband bandstop filter. The paper [4] proposed one equilateral triangle to get the tri-band stopband performance. Y. Wang proposed single ring resonator structure [5] to get three bandstop responses by changing the gap of ring resonator. In this study, a general design methodology of triple bandstop filter with compact and controllable triple stopband response is proposed.

The design and implementation of a tri-band bandstop filter by using microstrip lines to validate the design method for center frequencies are 0.9, 1.57 and 2.1 GHz, respectively. The three transmission zeros are −38.66 dB at 0.9 GHz, −40.36 dB at 1.59 GHz, and −39.92 dB at 2.15 GHz. The stopband for less than −20 dB are 0.86 to 0.93 GHz, 1.53 to 1.66 GHz, and 2.04 to 2.23 GHz, respectively. Simulated and measured results are in good agreement. Also the size of the prototype filters has been reduced to 20% in the circuit area compared to the conventional design and still has good performance.

REFERENCES

1. Chen, J., C.-H. Liang, J.-Z. Chen, and B. Wu, "Analytical design of triple passband of microwave filters using frequency transformations method," *Microwave and Optical Technology Letters*, Vol. 53, No. 10, 2199–2201, Oct. 2011
2. Wang, C., P. Xu, B. Li, and Z.-H. Yan, "A compact and multiband antenna for WLAN and WiMAX applications," *Microwave and Optical Technology Letters and EMC Technologies for Wireless Communications*, Vol. 53, No. 9, 2016–2018, Sep. 2011.
3. Lung, C.-K., K.-S. Chin, and J. S. Fu, "Tri-section Stepped-impedance resonators for design of dual-band bandstop filter," *2009 Proceedings of 39th European Microwave Conference*, 771–774, Sep. 2009.
4. Xiao, J.-K., X.-P. Lu, H.-F. Huang, and W.-L. Dai, "Muti-mode band stop filter using defected equilateral triangular patch resonator," *2010 International Symposium on Antennas Propagation and EM Theory (ISAPE)*, 1252–1255, Nov. 2010.
5. Wang, Y., J. Zhou, and W. Hong, "A multiband bandstop filter using a single ring resonator for a wireless access communication system," *Microwave Journal*, Vol. 54, No. 3, 102, Mar. 2011.

The Design of 40 GHz Active Power Splitter

Ching-Ying Huang[1], **Dow-Chih Niu**[2], **Robert Hu**[1], **and Christina F. Jou**[1]

[1]School of Electrical Engineering, National Chiao Tung University, Hsinchu, Taiwan
[2]Chun Shan Institute of Science and Technology, Taoyuang, Taiwan

Abstract— Based on the idea of distributed amplifier, a wideband active power divider is designed using 90 nm RF-CMOS process to provide moderate gain and superb output-port isolation from quasi-DC up to 40 GHz. The requirement of good input matching over the whole bandwidth poses a severe constraint in the development of 40 GHz active power splitter than in our previously reported 20 GHz one, as the tradeoff between gain and bandwidth becomes more intricate now. Partially coupled inductors are therefore adopted inside the circuit's artificial transmission line to improve both the return loss and allow the use of larger transistors in the gain stage. The fabricated circuit exhibits good input and output return losses and has 10 dB output-port isolation across the whole band; the bias is 1.8 V and 190 mA. Related circuit theories and mathematics will also be analyzed in this paper.

Dielectric Measurement Using a Planar Ring Sensor for Low-loss Powder Form Materials

K. Y. You and H. K. Mun
Radio Communication Engineering Department, Universiti Teknologi Malaysia
UTM Skudai 81310, Malaysia

Abstract— This paper uses planar ring sensor for dielectric measurements of low-loss powder materials by applying conversion of measured reflection coefficient to relative dielectric constant via a lumped-element model. The ring sensor has been fabricated using 1.58 mm thickness of FR4 substrate and designed to operate at frequency range between 1 GHz to 3 GHz at room temperature. This sensor was tested on free space and various types of powder. In this study, the predicted dielectric constant is in good agreement with the results obtained using commercial dielectric probe.

Linearized 2.4 GHz Power Amplifier

Bilge Türkel and Mehmet Fatih Çağlar
Department of Electronics and Communication Engineering, Faculty of Engineering & Architecture
Süleyman Demirel University, Isparta, Turkey

Abstract— The RF power amplifiers (PA) are the critical units in the IEEE802.11 standardized transceivers, and they are expected to provide a suitable output power at sufficient gain level with high efficiency and linearity. High power added efficiency (PAE) and high linearity are two key factors for power amplifier (PA) applications. However, these are contrasting requirements and a typical power amplifier design would require a certain level of compromise. Linearity plays an even more important role in wireless communication. High linearity is necessary for efficient bandwidth modulations. Linear power amplifiers (PAs) are becoming widely used in modern wireless communication systems. The envelope of the signals in these systems is typically not constant, so that the PA design must address the issue of device nonlinearity in order to limit the amount of spectral re-growth, which can cause unacceptable levels of interference mostly in the adjacent channels. In this study, our aim is to design a highly linear power amplifier without reducing efficiency and gain; we also desire to meet 802.11b Wi-Fi specifications of the designed power amplifier. Linearity design parameters are 1 dB compression point, IIP3 (third order input intercept point), OIP3 (third order output intercept point) and ACPR (adjacent channel power ratio).

There are several techniques to enhance the linearity of the power amplifiers. In this work, optimum linear power amplifier will be achieved using methods like as optimum gate biasing, analog pre-distortion (using series diode, shunt diode, diode in a bias feed, active bias, shunt active FET, series passive FET), post-distortion, derivative superposition, nonlinear feedback. Selected best simulation results which are performed by these methods are compared and competed with each other. Nonlinear Advanced Curtice2 Model of PHEMT transistors and Advanced Design System (ADS) simulation program are used. Consequently the method of linearity improvement which could be performed for designed 802.11b Wi-Fi power amplifier is obtained.

Sequential Tuning of Waveguide PIN Diode Limiters

T. Kacmajor, **J. J. Michalski**, **and M. Mazur**
TeleMobile Electronics Ltd., Poland

Abstract— Many microwave devices like filters, antennas or amplifiers require, due to their imperfections, the postproduction process of tuning. There has been a lot of effort put in order to improve this process, especially in large-scale production of microwave filters. Recently, methods using Artificial Intelligence have been proposed [1], where, parallel[1] filter tuning is performed with the use of Artificial Neural Networks. The ANN training is based on patterns consisting of physical reflection characteristics (input vectors) and corresponding positions of the tuning elements (output vectors). Neuro-Fuzzy concept was described in [2], which employed fuzzy logic and was another multidimensional approximator of the relation between scattering characteristics and tuning screws. In contrast to the parallel tuning approach, novel sequential tuning of microwave filters with use of ANN was proposed in [3]. It is the procedure that we mostly benefit from in the process of tuning a waveguide PIN diode limiters presented here.

A new method of tuning waveguide PIN diode limiters is presented in the paper. It is based on the use of Artificial Neural Network (ANN), which models the relationship between physically measured scattering characteristics in the frequency domain and the positions of limiter tuning elements. The limiter is treated as a device consisting of R subsections. Each subsection is associated with one tuning screw and is obtained by successive removal of tuning elements. The ANN builds R inverse models of these subsections which are used for calculating proper positions of tuning element. These methods relieve humans of the challenging task and the necessity of having knowledge about certain devices. The tuning experiment was conducted on limiter built as a cascade of 3 PIN diode sections (6 tuning elements). The conducted experiments have indicated that a 3-diode limiter can be easily tuned using this method.

REFERENCES

1. Michalski, J. J., "Artificial neural networks approach in microwave filter tuning," *Progress In Electromagnetics Research M*, Vol. 13, 173–188, 2010.
2. Kacmajor, T. and J. J. Michalski, "Neuro-Fuzzy approach in microwave filter tuning," *IEEE International Microwave Symposium*, Baltimore, 2011.
3. Michalski, J. J., "Inverse modeling in application for sequential filter tuning," *Progress In Electromagnetics Research*, Vol. 115, 113–129, 2011.

[1] In parallel tuning, the algorithm generates corrections for all tuning elements simultaneously.

Dynamics of a System of Bilaterally Coupled Chaotic Gunn Oscillators

B. C. Sarkar[1], **D. Ghosh**[1], **C. Koley**[1], **A. Guin**[1], **and S. Sarkar**[2]

[1]Department of Physics, Burdwan University, India
[2]Electronics Department, Burdwan Raj College, India

Abstract— In the recent years, the coupled oscillations of periodic as well as chaotic oscillators have become a problem of active research in several branches of physical, biological and social sciences. Since a Gunn Oscillator (GO) is an important source of microwave frequency (because of its application in low noise coherent receivers, active transmitting antennas, locking amplifier etc.), the dynamics of a system of two bilaterally coupled GOs (BCGOs) is a problem of both academic and practical interest. In bilaterally coupled oscillators, two oscillators are mutually coupled in the sense a fraction of the output power of one oscillator is applied at the input of second oscillator through an attenuator and a circulator and vice-versa. The effects of coupling factors between two periodic oscillators on the dynamics of the BCGO have been reported earlier. In present paper we have studied the dynamics of a bilaterally coupled chaotic GOs. Here in this experiment in order to get the chaotic oscillations in a GO, it operated in the under-biased (at a voltage less than the voltage at which the GO becomes oscillating) condition and a weak external RF field is injected into the cavity of a GO. At this conditions broad band continuous spectrum (BBCS) output is found at the output of two GOs indicating their chaotic mode of oscillation. The nature of the chaotic oscillation in a GO may be varied by the variation of the dc bias and the external RF signal frequency. The GO outputs are multiplied in a microwave mixer and the low pass filtered version of the product is examined. For a range of coupling parameters a dc voltage is obtained at the filter output. This indicates phase synchronization between two chaotic GOs. Further changes in the dc voltage level are noted as the frequency of the external signal is varied. The similar nature of spectrum output of the GOs and the constancy of the averaged product prove that the bilaterally coupled chaotic GOs are in synchronized state for some values of coupling parameters. The study reported in the paper is of importance in the field of chaos synchronization in microwave frequency range.

Application of PSO Algorithm for Optimizing the Dimensions of Tunable Interdigitated Capacitor

G. Lakshmi Narayana Rao, **Sravan Kumar**, **Samrat L. Sabat**, **and K. C. James Raju**
School of Physics, University of Hyderabad
Central University PO, Hyderabad, Andhra Pradesh 500046, India

Abstract— Interdigitated capacitors (IDC) employ coupled "fingers" to form a horizontal, rather than vertical capacitor structure. One can easily make a tunable capacitor using the Barium Strontium Titanate $(Ba_{0.5}Sr_{0.5})TiO_3$(BST) thin film material deposited on a dielectric substrate because the dielectric constant of BST is a function of applied electric field. The planar IDC got the advantage that it can be deposited even on top of the packaging say in a low temperature co-fired ceramic (LTCC) case. Since there is no buried electrode for an IDC, the chances of breakdown or shorting through pin holes can be avoided at the cost of miniaturization.

In this paper, we describe an approach to optimize the dimensions of a tunable interdigitated capacitor using particle swarm optimization (PSO) algorithm. PSO algorithm is inspired by the social behavior of bird flocking or fish schooling developed by Kennedy in 1995. In PSO, a set of particles (N_P) in the swarm is defined. Each particle represents a potential solution in the solution space and is characterized by its position and velocity. Analytical model of an interdigitated capacitor (IDC) is developed using conformal mapping method (CMM) and partial capacitance technique (PCT). The dimensions of IDC operating at 1 GHz frequency with capacitance values of 1 pF to 5 pF are extracted using PSO algorithm. The structural dimensions of tunable IDCs are simulated using finite difference time domain (FDTD) based software (IMST's Empire). The designed IDC shows approximately 20% tunability with 30% variation in dielectric constant of the tunable BST thin film on which the modeled IDC structure is patterned. An IDC is patterned with the structural parameters extracted using PSO algorithm.

The simulated results are verified with measured results of IDCs fabricated on different single crystal substrates. The obtained results from structural optimization of IDCs and fabricated IDCs are shown in the Table 1, which reveal that, PSO algorithm is able to calculate the dimensions

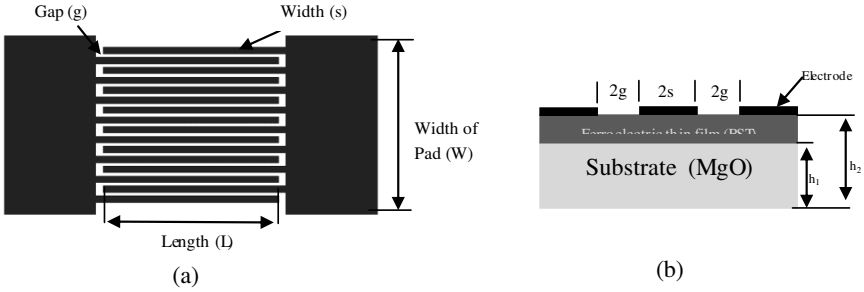

Figure 1: (a) Tunable interdigitated capacitor layout and its (b) cross sectional diagram.

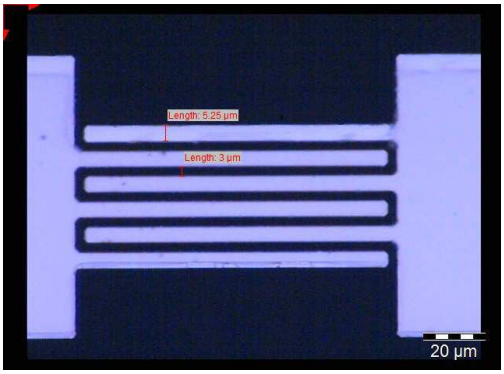

Figure 2: IDC structure fabricated on BST coated over single crystal substrates.

Table 1: Verification of modeled IDC dimensions with fabricated IDC dimenstions.

S. No	Substrate	Dimensions of Fabricated IDC (μm)			Capacitance of IDC (pF)		Dimensions of IDC from PSO (μm)			Capacitance of an IDC from 3D EM simulation (pF)
		Gap	Width	Length	VNA Characterization	3D EM simulation	Gap	Width	Length	
1	MGO	3	5	100	0.5387	0.5387	3	5	121	0.5535
2	ALO	3	5	100	0.5169	0.4763	3	5	121	0.5242
3	LAO	3	5	100	0.9112	0.92410	3	5	129	0.9942

of tunable IDCs fairly accurately and successfully and hence this technique can be applied to extract the dimensions of any planar microwave device.

A Novel Passive Dual-band Bandpass Microwave Filter Using Microstrip Loop Resonators

Sholeh Jahani Maleki[1], **Samaneh Sadi**[2], **Kambiz Sadat Najafi**[3], **and Massoud Dousti**[1]

[1]Department of Electronic Engineering, Islamic Azad University (IAU)
Science and Research Branch, Tehran, Iran
[2]Department of Electrical Engineering
Islamic Azad University (IAU), South Tehran Branch, Tehran, Iran
[3]Departement of Electrical Engineering
Islamic Azad University (IAU), Islamshahr Branch, Tehran, Iran

Abstract— In this paper, a dual-band bandpass microwave filter using two loop resonators with square patches is proposed, which needs only single input and output. These resonators play a major role in reducing the size of the filter, since each of these resonators provides two return loss poles. This type of filter is used in Wireless LAN protocols, such as IEEE 802.11 and Some mobile phone networks, like GSM. However, there is need for further work since the communications development requires low loss filters with compact size.

This filter is designed at 1.8 GHz and 2.4 GHz frequencies. The patches used in resonators are called perturbation element. The strength and nature coupling between the degenerate modes of the dualmode resonators is mainly determined by perturbation's size and shape. These resonators can produce an elliptic characteristic. A square substrate without metallic plane is stacked on the one of the microstrip loops, which increases ε_{eff} effectively. One of the substrates without ground plane at in bottom side is stacked on the mid-layer loop, and bottom side of other substrate is ground plane. The two substrates materials for design and simulation are RT/Duroid6010 with permittivity of 10.8 and thickness of 1.27 mm. The feed-line using microstrip line type gives the convenience to connect with other circuits in system. The two resonators located on mid-layer and top-layer provide two transmission patches to RF signal. The proposed filter generates to separeted passbands by using square loop and meander loop resonating different frequency, mid-layer loop for higher passband, and top-layer loop, for lower passband. This can provide convenience to easily change on passband frequency. In addition, Several finite attenuation poles in stopbands are realized to improve the good selectivity of proposed bandpass filter and isolation between the two passbands. The proposed filter has a compact size, high quality factor, low losses, high selectivity characteristics and good rejection between the two bands.

A Miniaturized Dual-narrowband Bandpass Filter Using Microstrip Open-loop and Complementary Split Ring Resonators (CSRRs) for Personal Communication Systems (PCS's)

S. Sadi[1], **M. Dousti**[2], **and A. Moradikordalivand**[3]

[1]Department of Electrical Engineering
Islamic Azad University (IAU), South Tehran Branch, Tehran, Iran
[2]Department of Electrical Engineering
Islamic Azad University (IAU), Science and Research Branch, Tehran, Iran
[3]Faculty of Electrical Engineering, University Technology Malaysia, Malaysia

Abstract— The demands for smaller and low-cost microwave components are increased by the rapid growth of modern satellite microwave communication systems more and more. To design compact dualband band-pass filters, several communication systems such as personal ones operate in dual bands which necessary narrow-band kinds of such components. Dual-narrowband band-pass filters (BPF) are one of the most popular components increasingly investigated in the most recent studies. Many dual-band BPFs have been introduced by different topologies in several investigations: however, they still occupy a relatively large area on their substrates and often with complicated structures.

This paper introduces a new kind of dual-band BPF developed using a combination of μ-Strip open-loop and complementary split ring resonators. This structure consists of four μ-Strip open-loop resonators which have been somehow arranged to provide electrical, magnetic and mixed couplings among these resonators.

To develop this compact filter to that provides dual-band behavior, the gaps in its structure can be provided by a complementary split ring resonators (CSRRs). The two coupled gaps for the electrical coupling are supported with a CSRR together and other two ones are provided by a CSRR each one. The frequency response of the filter is simulated using an EM simulation tool where transmission zeroes of the proposed structure have created the sharpness the skirts of scattering parameters of dual-band BPF. Simulated central frequencies are 2530 MHz and 5680 MHz with 3-dB bandwidths of 3.9% and 4.1%, respectively, making this compact dual-band BPF very attractive and suitable for applications in the mobile and personal communication systems (PCS's). Besides, the maximum insertion losses are reported to be 0.05 dB and 1.3 dB in the first and second bands, respectively. The return losses for these two bands are better than −20 dB and −10 dB, respectively. The active area occupied on the substrate is about $16 \times 16\,\mathrm{mm}^2$ for this filter in comparison with that of the conventional one which has been reported about $26 \times 28\,\mathrm{mm}^2$ where a size reduction about 64% is obtained with this proposed filter. It is designed and simulated on a 50-miles-thickness substrate with a constant dielectric of 10.8.

A Novel Miniaturized Narrow Band Bandpass Filter Utilizing Microstrip Open-loop Ring Resonators for Narrow-band Applications

Massoud Dousti[1], **Parisa Taheri**[2], **Samaneh Sadi**[2], **and Majid Zamani**[1]

[1]Department of Electronic Engineering
Science and Research Branch, Islamic Azad University (IAU), Tehran, Iran
[2]Department of Electronic Engineering
South Tehran Branch, Islamic Azad University, Tehran, Iran

Abstract— In this paper, a novel compact topology of microstrip open-loop ring resonator is introduced to design narrowband bandpass filters with better performance in making tradeoff between insertion loss and bandwidth. By consulting the design procedure of the conventional microstrip open-loop ring resonators which has been established, it is revealed that in fact, their structures have utilized three types of couplings including electrical, magnetic and mixed ones. Ignoring the mixed coupling which is created between loops; other ones have an inevitable role in realizing this kind of NB BPF. The proposed structure comprises of two microstrip open-loop ring resonators only with magnetic coupling instead of electrical, magnetic and mixed ones in the conventional ones.

The performance of this novel bandpass filter is simulated using an EM simulation tool and simultaneously compared with the conventional one which confirms the priority of this filter to them. The proposed NB BPF provides a narrowband bandpass filter with a bandwidth of 0.91% and better insertion and return losses in comparison with the conventional ones. Additionally, a size reduction about 36% is also reported by this novel layout.

Session 3P7
RF and Wireless Communication, Multipath

A New Wavelet Space Time Coding Technique Designed for UWB MISO Systems

Said E. El-Khamy[1], **Ehab Farouk Badran**[2], **and Amira Ibrahim Zaki**[2]

[1]Department of Electrical Engineering, Faculty of Engineering
Alexandria University, Alexandria, Egypt
[2]Department of Electronics and Communication Engineering
Arab Academy for Science and Technology, Alexandria, Egypt

Abstract— A new Multi input single output space time coding (MISO-STC) scheme designed specifically for Ultra-Wideband (UWB) systems is introduced in this paper. The proposed scheme is based on multiplexing multiple symbols in the wavelet domain of the UWB pulses in addition to the spatial multiplexing offered by using multiple transmitting antennas. Rake receivers are used to collect the energy in the dense multipath channel components. The suggested technique is referred to as the wavelet space time coding scheme (WSTC). In WSTC four symbols are transmitted on the same UWB transmission pulse with the same bandwidth, symbol duration, and number of transmitting antennas of the conventional MISO-STC scheme. The used mother wavelet (MW) in the symbol multiplexing process is selected to be highly correlated with transmitted pulse shape and such that the multiplexed signal has almost the same spectral characteristics as those of the original UWB pulse. The simulation results show that the proposed WSTC scheme has better performance than the conventional STC scheme. This is in addition to increasing the data rate to four times that of the conventional STC scheme. In this paper the performance of the WSTC scheme is compared to the conventional STC scheme using a figure of merit which is the ratio between the bit error rate and the bandwidth efficiency. The simulations and comparisons are performed for different channel models. The simulations are also performed for different number of Rake fingers showing that the introduced WSTC scheme also reduces the system complexity when compared to a conventional STC scheme. The paper illustrates the transmitter, the receiver, and the analytical description of the WSTC system.

Linear Regression Route Roughness Parameter to Correct Hata Path Loss Prediction Formula for 1800 MHz

Mahdi A. Nisirat[1], **Mahamod Ismail**[1], **Liyth Nissirat**[1], **and Salim Alkhawaldeh**[2]

[1]Department of Electrical, Electronics and System Engineering
Universiti Kebangsaan Malaysia, 43600 UKM Bangi, Selangor Darul Ehsan, Malaysia
[2]Department of EE, Faculty of Engineering Tech., Al-Balqa' Applied University, Jordan

Abstract— Propagation path loss models are going under intensive improvement to allow for more accurate predictions. Such improvements should include terrain areas that are not been exposed extensively in most of the earlier models. In this paper the main equation of Hata urban model is modified by a relation that includes the standard deviation of the measuring campaign route elevations (σ). This relation is consisting of two regression formulas, as a function of $\log(\sigma)$, modifying both the intercept point (DC value) and the slope of Hata urban model. Root Mean Square Error (RMSE) difference between this model and the measured filtered raw data path loss has overcome RMSE calculated for Hata suburban model, by up to 13 dB. Areas where data are collected would be assumed suburban by Hata model. Data were obtained from mobile service providers in Amman city and Madaba city, Jordan for the frequency band of 1800 MHz.

Performance Analysis of a Simple Coordinated and Distributed MIMO Network

G. G. Borg[1] and A. Khandaker[2]

[1]Research School of Physics and Engineering, The Australian National University
Canberra, 0200 Australian Capital Territory, Australia
[2]College of Engineering and Computer Science, The Australian National University
Canberra, 0200 Australian Capital Territory, Australia

Abstract— Although wireless networking technology continues to progress at a frantic pace, we are fast approaching the point where performance will be bounded by fundamental limits. Co-channel interference, fixed antenna radiated power, limited battery power, fixed spectrum, rank of the channel matrix and signal processing overhead are among the fundamental impairments to increased capacity, range and coverage of wireless networks. Most wireless networks nowadays are either Single Input Single Output (SISO) or single and multi-user MIMO (SU/MU-MIMO) systems. The reason these approaches to wireless networking have been adopted is probably due to the simplicity of their implementation. However if we take the view that the aforementioned impairments are unavoidable consequences of SISO based architectures then an appropriate paradigm shift may allow us to step into a new regime of network performance. Coordinated and Distributed Multiple Input Multiple Output system (CD-MIMO) is a radically different approach to wireless communications that promises improved coverage and unprecedented spectral efficiency.

In this research paper, we propose a CD-MIMO network that employs a vast array of coordinated and distributed base stations. Our analysis shows that replacing the single or co-located base stations used in conventional cellular networks with multiple coordinated and distributed sources substantially overcomes the above impairments. The concept was first proposed in general form by S. Zhou et. al. [1]. Since then there has been much work on the subject in which numerous sub-problems have been considered. Most intense has been the introduction of multi-user MIMO (MU-MIMO) into LTE (Long-Term Evolution)-Advanced in 3GPP (3rd Generation partnership Project) and IEEE802.16m [2]. MU-MIMO by itself is little more than an infrastructure SU-MIMO system. However cooperative MIMO (CO-MIMO) goes a step further and is currently being applied to alleviate inter-cellular co-channel interference in mobile phone networks by allowing base stations to cooperate in their signaling.

In this work, we consider a CD-MIMO network in which independent remote or mobile users are served by a distributed array of base stations. The base stations operate as a coordinated MIMO array for remote/mobile users. Under the assumption that all MIMO processing is done at the bases, we provide an analysis of performance limits and a short discussion of implementation issues. We show that the proposed network significantly outperforms current infrastructure technologies with respect to coverage and capacity.

REFERENCES

1. Zhou, S., M. Zhao, X. Xu, J. Wang, and Y. Yao, "Distributed wireless communication system: A new architecture for future public wireless access," *IEEE Communications Magazine*, Vol. 41, No. 3, 108–113, 2003.
2. Sungjin, K., H. Kim, Y. Zhou, and J. Li, "Multimode multiuser MIMO system with finite rate feedback," *Proceeding of 3rd International Symposium on Wireless Communications Systems (ISWCS)*, 219–222, Valencia, Italy, September 2006.

Impact of Wireless Channel Modeling on SAR Estimation in Indoor Environment

O. Jawad[1], **D. Lautru**[2], **J. M. Dricot**[1], **F. Horlin**[1], **and P. De Doncker**[1]

[1]OPERA Departement, Université Libre de Bruxelles (ULB)
avenue F.D. Roosevelt 50 1050 Bruxelles, Belgium
[2]UPMC Univ Paris 06, UR 2, L2E F-75005, Paris, France

Abstract— The study of whole-body exposure to electromagnetic fields emitted by mobile terminals and base stations led to the development of standards and guidelines proposed by the International Commission on Non-Ionizing Radiation Protection (ICNIRP) [1]. Nowadays, numerical dosimetry took an important place into assessing compliance with these guidelines. Specific Absorption Rate (SAR) calculation is a target of numerical dosimetry. The improvement of human body models, and the development of numerical methods taking into account accurate propagation modelling have fostered this domain of research.

Currently, propagation modelling for wireless channels is based on the *cluster* concept. It has been experimentally proven that waves propagate in wireless channels as packets referred to as clusters [2]. Inside each cluster, the waves, which are also called MultiPath Components (MPCs), are grouped in the angular and delay domains. Internal characteristics of clusters are defined in a statistical way based on experimental data.

The aim of this paper is to study the impact of cluster's parameters on SAR. As a first step towards exposure assessment in realistic channels, this study is based on the exposure of a 2D human body model to clusters as shown in Figure 1.

The cluster parameters that have been taken into account are presented in Table 1. Most of these parameters are chosen randomly following a probability density function that has been defined thanks to channel measurement campaign [3]. In the full paper, the relative impact on SAR of each cluster parameter has been assessed.

The results show that the standards deviations of SAR are of the same order as its mean value. The cluster angular spread has been specifically found to have a strong impact on SAR standard deviation, due to interference mechanisms between multipath components.

Table 1: Cluster parameters.

Symbol	Description	Probability Density Function	Unit
α_k	k-th MPCs Complex Amplitude	Complex Normal	complex
θ_k	k-th MPCs azimuthal angle of incidence	Normal	rad
μ_θ	Angle of incidence of the cluster	Experimental distribution	rad
σ_θ	Angular spread of the cluster	Lognormal	rad
P_{cl}	Power of the cluster		watt
N_{MPCs}	Number of MPCs		1

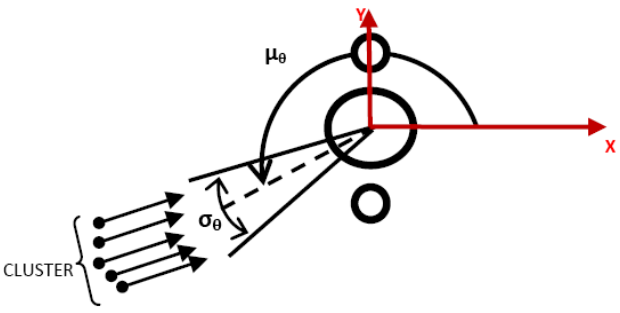

Figure 1: 2D Human body model exposed to a cluster.

It appears thus mandatory to study SAR in a statistical way because its variability can be significant in a given exposure scenario. In the full paper, detailed results on SAR distribution will be presented following the proposed methodology.

REFERENCES

1. ICNIRP, "Guidelines for limiting exposure to time-varying electric, magnetic, and electromagnetic fields (up to 300 GHz)," *Health Physics*, 1998.
2. Quitin, F., C. Oestges, F. Horlin, and P. De Doncker, "A polarized clustered channel model for indoor MIMO systems at 3.6 GHz," *IEEE Trans. Vehic. Tech.*, 3685–3693, Oct. 2010
3. Jawad, O., D. Lautru, S. Van Roy, J.-M. Dricot, F. Horlin, and P. De Doncker, "Statistical study of SAR in clustered wireless channels," *Antennas and Propoagation (Eucap)*, 2580–2584, 2011.

Analytical and Experimental Study of Spatial Focusing by UWB Time-Reversal in Indoor Environment

T. Mavridis[1,2], **F. Bellens**[1,2], **F. Quitin**[1], **A. Benlarbi-Delaï**[2], **and P. De Doncker**[1]

[1]OPERA Wireless Comm. Group, Université Libre de Bruxelles, Belgium
[2]Université Pierre et Marie Curie, L2E, France

Abstract—

Introduction: The popularity of wireless communication technologies has increased the need for reliable, high-speed communications. To cope with the need for high-data rate transmission, new technologies have been proposed that use large bands of the RF spectrum, such as ultra-wideband (UWB) or 60 GHz communications. Time Reversal focusing technique permits to concentrate the transmitted power on a certain area, where the receiver is located. This focusing technology presents multiple advantages: a reduction of the amount of electromagnetic power absorbed by peoples bodies, an increase of the reliability of the communication by decreasing the rate of interference, etc.

In this paper a new analytic formalism is developed which allows to characterize the quality of spatial focusing techniques. MISO and MIMO experiment are presented to assess the validity of the theoretical results.

Time Reversal: The Time Reversal (TR) method is a two-step transmission method. First, the receiver sends a pilot broadcast signal to the transmitter. The transmitter deduces the channel impulse response $h(\tau)$ by sampling the received (known) signal. The second step consists of the transmission itself: the transmitter filters its transmitted signal with the filter $h^*(-\tau)$. In that case, and if the channel remains static, the receiver will receive the transmitted signal through the equivalent channel $h(\tau) \otimes h^*(-\tau)$. If the transmitted signal has a unit energy, the energy of the received signal will be the following:

$$E(\vec{r}) = \int |h(r,\vec{r}) \otimes h^*(-\tau,\vec{r_0})^2 d\tau = \int |H(f,\vec{r}) H^*(f,\vec{r_0})^2 df \tag{1}$$

where $\vec{r}$ is the position where the energy is evaluated, and $\vec{r_0}$ is the position where the energy is being focused (the receiver's position). The transfer function, in a local area, can be developed as follows:

$$H(f) = \sum_{i=0}^{N} a_i e^{j\phi_i} e^{-j\omega\tau_i} e^{-j\vec{\beta}_i \cdot \vec{r}} \tag{2}$$

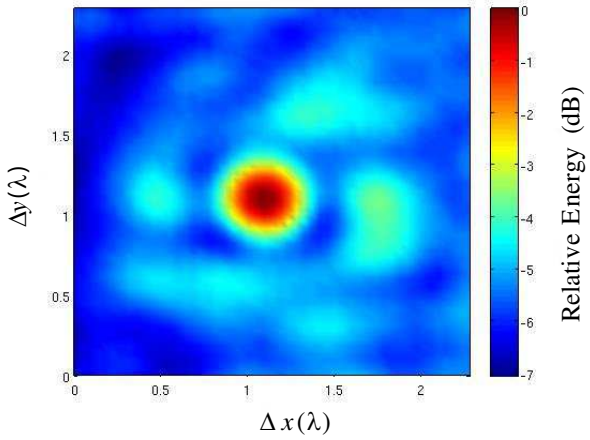

Figure 1: Relative energy received for three base stations and $f_c = 6.85$ GHz and $\Delta f = 7.5$ GHz. The focal spot has a radius of about 0.2λ.

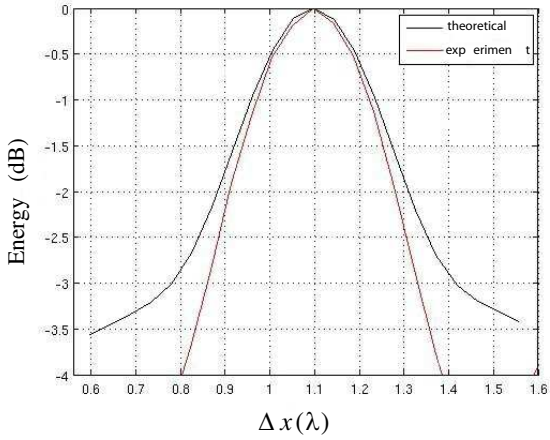

Figure 2: Relative energy received for three base stations. Comparison between the experiment result and the theoretical calculations.

In the full paper, it will be shown that by using the Parseval equality and by integrating the energy over the band $[f_c - \Delta f/2, f_c + \Delta f/2]$, a closed-form expression can be obtained for the spatial distribution of the energy. It will be shown that the focal spot depends on the number of waves N, their angle of incidence and their magnitude, the carrier frequency and the frequency band. It will be shown that this closed-form solution permits to define the best combination of parameters to improve the focusing skills of the TR.

Measurement Campaign: Experimental measurements were performed to assess the performances of the TR method. The channel frequency responses were measured with a four-port VNA. Three transmit base station were considered, and the receiver was moved on a 10 cm square grid with an automatic positioning device. Since all base stations are in line-of-sight, the channel can be reduced to a channel composed of three waves incident on the receiver. The TR is applied as a posteriori treatment. An example of the spatial distribution of the energy is given in Fig. 1.

As can be seen on Fig. 2, the theoretical results and the experimental measurements are compared by showing the energy distribution in a random direction.

The validity of the method has been verified in a spatial zone depending on the $f_c/\Delta f$ ratio.

Conclusion: In the full paper, a closed-form solution for the spatial energy of a time-reversed channel will be developed. The theoretical results will be compared with experimental measurements to assess the validity of the TR modelling. Also a parameter study has been done to determine the influence of the delay spread and angular spread on the TR energy distribution. It will be shown how the obstruction of the line-of-sight can reduce the size of the focal spot.

Characterization of the Polarization of Received Electromagnetic Waves in Indoor Communication Channels

Ali Panahandeh[1,2], **François Quitin**[3], **Jean-Michel Dricot**[1], **François Horlin**[1], **Claude Oestges**[2], **and Philippe De Doncker**[1]

[1]OPERA Department, Université Libre de Bruxelles (ULB), Belgium
[2]ICTEAM Electrical Engineering Department, Université Catholique de Louvain (UCL), Belgium
[3]Electrical and Computer Engineering Department, University of California, Santa Barbara, USA

Abstract— Polarized MIMO systems have been proposed as a space- and cost-effective alternative to classical co-polar MIMO systems. By using perpendicularly polarized colocated antennas, the inter-antenna correlation remains low, while maintaining a compact antenna system [1].

Let's consider a MIMO system where the receive antenna is a tri-polarized antenna system made of three colocated perpendicular omnidirectionnal antennas. In an idealistic case where there are no Interacting Objects (IOs) in the environnement surrounding the transmitter and the receiver, the polarization of the wave transmitted from the transmitter antenna stays the same at the receiver side. However in a realistic scenario where the environnement is made of many IOs, the polarization of the transmitted wave will change. The multi-path components at the receiver will in this case, each have different polarization properties. A fraction of a linearly polarized wave will for instance be depolarized, into its perpendicular components leading to an elliptical polarization [2].

The superposition of the different multi-path components having each a different elliptical polarization scheme will lead to another elliptical polarization scheme. In a dynamic scenario, the IOs could change their position and/or shape over time, leading to a more dynamic receive scheme where the global receive polarization ellipse also changes over time.

Previous works have been done in order to model the multi-polarized MIMO channel for different sources (spatial/temporal) and scales of variation [3, 4]. While these works tend at characterizing the signals received at one vertical and two horizontal perpendicular antennas, no work has been done in order to model the polarization of the received waves from an electromagnetic point of view. The aim of this paper is to dynamically characterize the receive polarization ellipse for a particular scenario. This approach has the advantage to be transposable to any orientation of a receiver with multi-polarized co-located antennas. An elliptically polarized wave may be resolved in two linearly polarized waves having different phase and amplitude and being perpendicular to each-other. Based on the signals received on one vertical and two horizontal perpendicular antennas, the elliptical polarization parameters in the three dimensional (3D) space are obtained. A measurement campaign has been performed in an indoor-to-indoor scenario and at a frequency

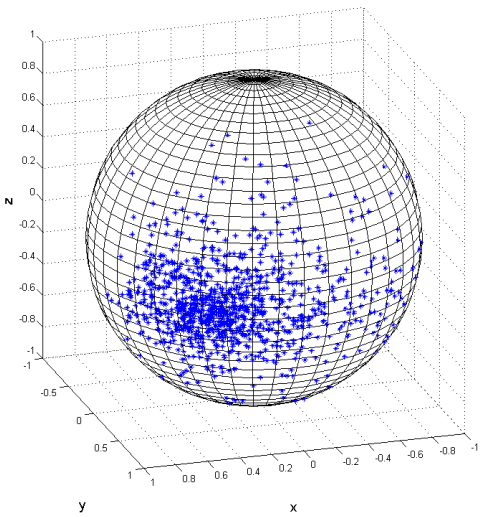

Figure 1: The directions of the normal to the polarization plane in 3D space.

of 3.6 GHz. Based on these measurements and the proposed theoretical formulation, the time-variation of the parameters describing the polarization ellipse is analyzed and a time-variant statistical model is proposed. The statistical distribution that follows each parameter is obtained. In order to study the time-variant dynamics of the channel, the autocorrelation functions of all the parameters defining the elliptical polarization in the 3D space have been analyzed. Except for one of the parameters which has no temporal correlation in the time-resolution used for the measurement, exponential models were proposed for the autocorrelation functions of the other parameters. A discussion then follows on the behavior of the polarization of electromagnetic waves in an indoor-to-indoor wireless communication. In Figure 1, the directions of the normal to the polarization plane are presented in 3D space for different temporal samples. We notice the concentration of these vectors in a privileged direction which corresponds to the direction of incidence of the main beam.

The paper is organized as follow: Section 2 gives the theoretical formulation in order to obtain a 3D representation of the polarization wave. Section 3 shows the experimental measurement campaign. Section 4 presents the results derived from the measurement. Section 5 concludes the paper.

REFERENCES

1. Lindmark, B. and M. Nilsson, "On the available diversity gain from different dual-polarized antennas," *IEEE Journal on Selected Areas in Communications*, Vol. 19, No. 2, 287–294, Feb. 2001.
2. Oestges, C. and B. Clerckx, "MIMO wireless communications: from real-world propagation to space-time code design," *Electronics & Electrical*, Academic Press, 2007.
3. Quitin, F., F. Bellens, A. Panahandeh, J.-M. Dricot, F. Dossin, F. Horlin, C. Oestges, and P. De Doncker, "A time-variant statistical channel model for tri-polarized antenna systems," *PIMRC*, 64–69, 2010.
4. Panahandeh, A., F. Quitin, J. M. Dricot, F. Horlin, C. Oestges, and Ph. De Doncker, "Multi-polarized channel statistics for outdoor-to-indoor and indoor-to-indoor channels," *71st Vehicular Technology Conference (VTC2010-Spring)*, May 15–19, 2010.

Genetic Algorithm Optimization Tool for Multi-user Detection of SDMA-OFDM Systems

M. A. Alansi, I. M. Elshafiey, and A. M. Al-Sanie
Electrical Engineering Department, King Saud University, Riyadh 11421, P. O. Box 800, Saudi Arabia

Abstract— Space division multiple access (SDMA) enables support of multiple users within the same time and frequency slots, implementing user-specific channel impulse responses (CIRs) as shown in Fig. 1. Moreover, SDMA have been combined with orthogonal frequency division multiplexing (OFDM) in order to mitigate the technical challenges of channel impairments and enhance the spectral efficiency. The non-orthogonality nature of the CIRs, however, raises a challenge to the process of multi-user detection (MUD). Maximum likelihood (ML) methods are known as an optimum tool for multi-user detection, but they are associated with high computational complexity that grows exponentially with the increase of the number of simultaneous supported users.

Genetic algorithms (GAs) are proposed in this work as a powerful optimization tool that allows restricting the search space and maximizing the number of users. The objective is to investigate an over-loaded scenario, in which the number of users exceeds the number of receiver antennas at the base station. In the implementation of GAs, the output of simple minimum mean squared error (MMSE) detector is used to create the GAs initial population, and initial range for the individuals as shown in the flowchart of Fig. 2. Reduction of the search space of GAs and thus the convergence time is achieved by defining a sphere in the signal space that encompass the transmitted symbol vector.

Simulation implements 16-QAM modulation. The standard ITU-vehicular channel model is adopted. FFT size is set to 512 along with 5-MHz bandwidth in the OFDM system. Results are presented that investigate the performance of SDMA-OFDM system considering hard- and soft decoders for the MMSE, ML, as well as GAs. GAs performance is found to lie between those of the simple MMSE and the optimum ML detectors. GAs tool provided results close in performance to that attained using optimum soft ML detector particularly in the over-loaded scenario. The tradeoff between the complexity and performance of the developed system is presented. Computational complexity is investigated considering various scenarios of number of simultaneous users.

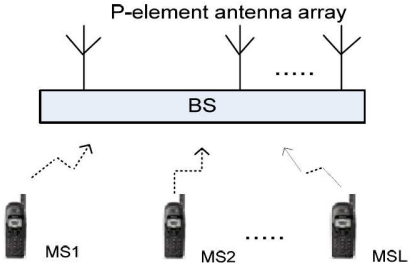

Figure 1: Uplink SDMA system.

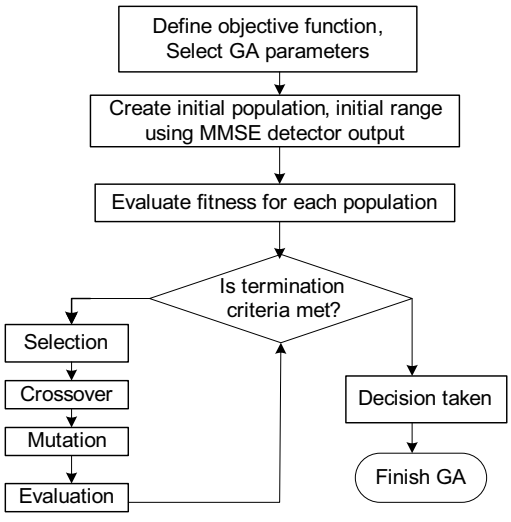

Figure 2: Flowchart for optimization MUD using GA.

Methods for the Assessment of the Performance of Short-range Multi-hop Wireless Network Communications

M. A. Collett and T. H. Loh
National Physical Laboratory, Teddington, Middlesex, UK

Abstract— Wireless Sensor Networks (WSNs) are envisaged to perform critical monitoring for applications such as healthcare, security and industrial monitoring, resulting in ever increasing demands for understanding and quantification of the reliability and stability of WSN-based systems when deployed in real environments. This can be challenging as real environments are rapidly changing with a range of scattering and interference effects which can have a significant effect upon the communications performance. WSNs rely on their communications for sending data and responding to commands. They typically employ multi-hop wireless communications, where messages are routed through the network using paths determined by continuous link quality estimation and complex routing algorithms. The complexity and autonomy of such systems makes defining repeatable and reliable performance measurement techniques challenging. But without such tests users will be unable to make informed decisions about their procurement choices, and designers will be unable to reliably see the impact of changes to their system.

In this paper, we propose one method for assessing the performance of a WSN in establishing and maintaining communications in a highly multi-path environment. By deploying a network of SunSPOT wireless sensor nodes within an electromagnetic reverberation chamber, the effect of chamber configuration such as absorber volume and reflective stirrer position was observed. A simple metric of network coverage was used that was based upon the number of visible nodes at any given time. This allowed the rapid repeatable and reproducible characterization of WSN systems, allowing meaningful comparisons of performance to be made. It was found that the network coverage was highly sensitive to stirrer position and for the SunSPOT system, in the reverberation chamber only a 50% average network coverage was achievable.

A Rigorous Measurement Technique for Radiation Pattern Characterisation of Embedded Wireless Communication Systems

T. H. Loh and M. A. Collett
The National Physical Laboratory, Teddington, Middlesex, United Kingdom

Abstract— There has been a proliferation of wireless communication systems such as mobile phone handsets and wireless sensor network (WSN) platforms to meet existing and future demands for compact designs, higher data-rates and greater capacity. Electronic components, antennas and devices embedded within wireless system are continually decreasing in size, resulting in highly complex structures and that operate in close proximity. However, the operating environment, including casing, nearby object etc., can have a significant effect on the antenna radiation pattern, which causes deviation of the antenna performance from the ideal, and can lead to unforeseen behaviour and loss of communications. Furthermore, when testing a prototype antenna, a coaxial feed cable is often employed even though such a cable may not be present in the final design of the wireless communication system and, for a poorly balanced antenna, can result in common mode currents that radiate and distort the true radiation pattern of the antenna under test. There is an increasing need to understand the performance of whole wireless communication systems, and to give advice to those deploying wireless sensing systems. This makes the testing of whole systems and configurations necessary despite the measurement challenge that the embedded radios within these systems are often only capable of emitting a modulated, bursty and intermittent signal.

Accurate radiation pattern characterisation for wireless communication systems requires a rigorous measurement technique within a reflectionless environment. We present and validate a rigorous measurement technique carried out at the UK National Physical Laboratory for radiation pattern characterisation of wireless communication systems, which is based on a single receiving antenna connected to a spectrum analyser. A pattern measuring process that is robust to modulated and bursty signals is presented and validated against a traditional vector network analyser (VNA) pattern measuring method using a monopole antenna element extracted from a MICAz sensor mote, fed by a signal generator with an emulated Bluetooth signal. It was found that this method shows good agreement with traditional radiation pattern measurement techniques using a VNA. Following the rigorous assessment of the technique it is applied to a commonly employed WSN platform, the MICAz sensor mote. The measurement repeatability is investigated, where the results show good repeatability and demonstrated that the technique is robust and would be valuable for assessing the performance of embedded radio systems designs.

Characterization of Indoor 30 GHz Bandwidth Multipath Channel Propagation

W. N. W. Ibrahim, M. El-Hadidy, and T. Kaiser
The University of Duisburg-Essen, Germany

Abstract— Nowadays, the demand of wireless communication especially in indoor environment has increased rapidly in order to provide high speed digital transmission between two terminals for multimedia applications. Furthermore, if the wireless medium needs to be shared among many users in the same network system, the aggregate network capacity of hundreds of megabits per second or even up to gigabits per second may be needed. One solution in order to achieve such considerably high capacity is to use an extremely large bandwidth which is basically related to small wavelength concept. Thus, it leads to the invention of small size antennas and other device which could be used as portable device such as hand phone, tablet pc, laptop and others.

The use of 30 GHz bandwidth communication system from 10 GHz to 40 GHz is a very promising candidate for high-data-rate and short-range indoor wireless communications. Thus, many important aspects of the 30 GHz bandwidth wireless system have not yet been thoroughly investigated. To our knowledge, no literature review on characterizing 30 GHz bandwidth propagation channel is available at the moment. Some research work on both deterministic [1] for 40–60 GHz and statistical modeling [2] at 20 GHz and 40 GHz have been reported. Previous studies on propagation related to the Extremely High Frequency (EHF) range such as at 27 GHz to 40 GHz in outdoor environment [3], the 40 GHz range in indoor environment [4] where else [5] is about statistical parameters for frequency at 30 GHz.

Main objective of this work is to obtain a better assessment of the potential of 30 GHz bandwidth indoor communication system by characterizing the propagating channel from 10 GHz to 40 GHz. Channel characterization refers to extracting the channel parameters from a deterministic channel

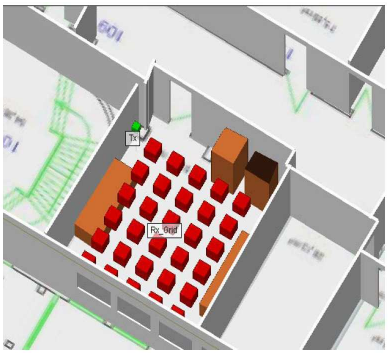

Figure 1: LoS scenario in the ray-tracer.

Figure 2: NLoS scenario in the ray-tracer.

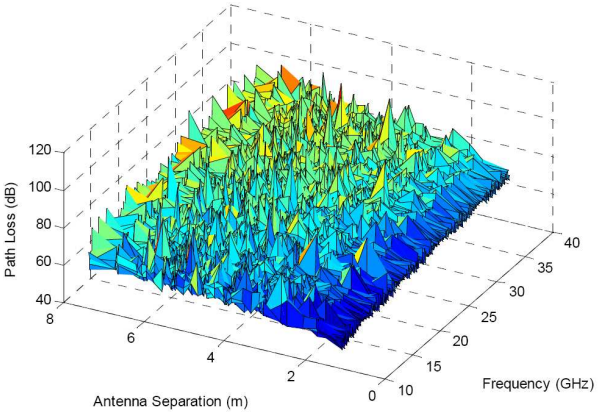

Figure 3: Path Loss of LoS 30 GHz bandwidth considering multipath propagation.

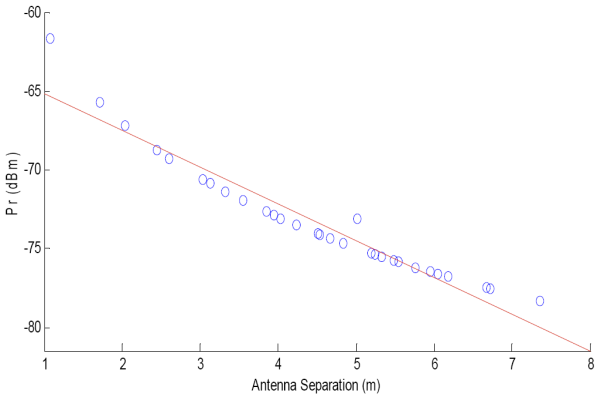

Figure 4: Received power of first path at 40 GHz.

modeling for an indoor real-world environment. Simulation of 30 GHz bandwidth communication has been performed based on a ray-tracing tool "Wireless Insite" from Remcom [6]. A typical real-world indoor environment considering Line of Sight (LoS) and Non Line of Sight (NLoS) scenarios have been explored. For LoS scenario, a grid of (6×5) points of receives antenna with sub-distance of 1 m and a grid of (5×3) points with the same sub-distance for NLoS scenario had been considered as shown in Figures 1 and 2 respectively. Results for indoor propagation simulations which consist of path loss exponent, mean excess delay, rms delay spread and cumulative distribution function (cdf) would be presented in the full paper. Constructive conclusions and guidelines will be offered for the 30 GHz bandwidth communication system designers.

REFERENCES

1. Smulders, P. F. M., "Deterministic modelling of indoor radio propagation at 40–60 GHz," *Wireless Personal Communications*, Vol. 1, No. 3, 127–135, 1995.
2. Muhi-Eldeen, Z., J. Richter, M. Al-Nuaimi, and L. Ivrissimtzis, "Statistical modelling of building scatter in metropolitan cells at 20 and 40 GHz for fixed wireless access links," *Proc. International Conference on ITS Telecommunications*, 358–361, Chengdu, Jun. 2006.
3. Roche, J. F., H. Lake, D. T. Worthington, C. K. H. Tsao, and J. T. Bettencourt, "Radio propagation at 27–40 GHz," *IEEE Trans. Antennas Propag.*, Vol. 18, No. 4, 452–462, 1970.
4. Talbi, L. and G. Y. Delisle, "Experimental characterization of EHF multipath indoor radio channels," *IEEE J. Sel. Areas Commun.*, Vol. 14, No. 3, 431–440, 1996.
5. Beauvarle, D. and K. L. Virga, "Indoor propagation characteristics for wireless communications in the 30 GHz range," *Proc. Antennas and Propagations Society International Symposium*, 288–291, Aug. 2002.
6. El-Hadidy, M., *Realistic UWB MIMO Channel Model Considering Analogue Aspects and Antennas Effects*, DruckTeam, Druck und Verlag, Hanover, Germany, 2009, ISBN 978-3-925658-10-5.

RFID and Bluetooth Technology for Tagging and Transmission of Data to POS (Point of Sale)

R. Mardeni and T. W. Lee
Faculty of Engineering, Multimedia University
Jalan Multimedia, Cyberjaya, Selangor 63100, Malaysia

Abstract— This work describes a study on wireless technology which involve on RFID and Bluetooth technology for tagging and transmission of data to point of sale in Malaysia. The objective of this study is to using RFID and Bluetooth technology for item tagging and data transmission. The expectation of this project study is to allow certain item to be tag that easily to be identified and localized by using RFID technology which will communicate with personal computer. Besides, data encryption for Bluetooth was pairing with personal computer need to perform to achieve secure and simple pairing feature when customer transaction is done. It did involve hardware and software. Moreover, from the simulation result, there will be using double side band modulation to design on RFID reader for better item tagging.

LTE-FDD and LTE-TDD for Cellular Communications

A. Z. Yonis[1], **M. F. L. Abdullah**[1], **and M. F. Ghanim**[2]

[1]Faculty of Electrical and Electronic Engineering, Department of Communication Engineering
University of Tun Hussein Onn Malaysia, Johor, Malaysia
[2]Computer Engineering Department, College of Engineering, University of Mosul, Mosul, Iraq

Abstract— LTE-Advanced (Long Term Evolution-Advanced) is used on fourth generation (4G) in mobile phone technology as many providers are beginning to augment their networks with LTE. As known, mobile phone traffic is divided into two parts: an uplink and a downlink. This paper presents the LTE two duplexing modes: LTE-TDD (Time Division Duplexing) and LTE-FDD (Frequency Division Duplexing).

Where LTE-TDD favored by a majority of implementations because of flexibility in choosing uplink to downlink data rate ratios, ability to exploit channel reciprocity, ability to implement in non-paired spectrum and less complex transceiver design.

In the case of FDD operation there are two carrier frequencies, one for uplink transmission (f_{UL}) and one for downlink transmission (f_{DL}). During each frame, there are thus ten uplink subframes and ten downlink subframes, so uplink and downlink transmission can occur simultaneously within a cell.

LTE-FDD implies that downlink and uplink transmission take place in different, sufficiently separated, frequency bands, while TDD implies that downlink and uplink transmission take place in different, non overlapping time slots. Thus, TDD can operate in unpaired spectrum, whereas FDD requires paired spectrum. Also the required flexibility and resulting requirements to support LTE operation in different paired and unpaired frequency arrangements are discussed in this Paper.

This paper focuses on the main difference between LTE-FDD and LTE-TDD in how they divide the single channel to provide paths for both uploading (mobile transmit) and downloading (base-station transmit). FDD does this by dividing the frequency band allotted into two discrete smaller channels. TDD uses the entire channel but alternates between uploading and downloading and in the case of TDD uplink and downlink communication taking place in the same frequency band but in separate non-overlapping time slots; there is typically a high fading correlation between the downlink and uplink.

A RFID Reader Suppressive Interferences Due to Multipath

S. Duangsuwan and S. Promwong
Faculty of Engineering, King Mongkut's Institute of Technology Ladkrabang
Chalongkrung Road, Ladkrabang, Bangkok 10520, Thailand

Abstract— The radio-frequency identification (RFID) is growing rapidly for wireless communications, at 2.45 GHz is very speed transmission signal in their applications. Multipath fading has been leading to bandwidth limited and channel interfered, following, RFID reader could be still lacks the demands on improvement. Therefore, RFID reader suppressive interferences is proposed. In this paper, we investigates the signal-to-interference plus noise (SINR) of resolve convergence, order-suppressive interference cancelation (OSIC), second orders is considered includes the constant modulus algorithm (CMA). As the results, we also compared as the ZF and MMSE equalization, and will be seen that the OSIC receiver requires of iterative less than traditional. This techniques is very useful for adaptive beamforming algorithm in RFID signal detection and interferences cancelation.

Measurement and Parameter Description of Time-varying Ultra-wideband Infostation Channel

U. A. K. Chude-Okonkwo, **R. Ngah**,
Yasser K. Zahedi, **S. M. Zaid**, **and T. A. Rahman**
Wireless Communication Center, Universiti Teknologi Malaysia, Malaysia

Abstract— The concept of infostation presents a new way to look at the problem of providing high data rate wireless access. It is an isolated pocket area with small coverage (hundreds of meters) of high bandwidth connectivity that collects information requests from mobile users and delivers data while users are going through the coverage area. Infostations can be located in heavily populated areas such as airports, shops, pubs, hotels, and along highways. To cover larger area in the case of the highway, the infostation is positioned at intervals along the path. Consider a scenario in which a user moving along the highway desires to receive/transmit large chunk of data from/to an infostation network located along the highway. This will require a technology that will be able to handle high data rate information transfer. Since, the infostation technology is designed for small area of coverage, low power transmission requirement is necessary in order to avoid interference with other existing services. One of the technologies that have the potential to deliver the envisaged high-data rate infostation services is the UWB signalling. The UWB has the basic attributes of extremely low transmission power, operating at unlicensed frequency, high data rate, multipath immunity and low cost. Existing channel characterization and measurement for the UWB channel have been limited to the case where the channel is assumed to be fixed over the transmission duration. However, for many infostation scenarios, time variation is expected due to the mobility of one of the communication terminals/scatterers. Hence, the existing channel models cannot be used to describe this new target scenario where terminal mobility is expected. In this paper, we present the measurement and the descriptions of design parameters for the time-varying Infostation UWB channel. We also consider how such parameters can be used to improve system performance in terms of combating inter-channel interference (ICI) in the case of multiband OFDM and mismatch in channel estimation.

Session 3P8
Poster Session 5

Small Loop-type Mobile Antenna with Less Interference of Nearby Conductors for Wi-Fi Application

Hyunmin Jang, Yang Liu, Jongin Ryu, and Hyeongdong Kim
Hanyang University, Seoul, Korea

Abstract— A small loop-type mobile antenna with less sensitivity to near field conductors for Wi-Fi application is proposed. The proposed antenna has a small volume of $8 \times 4 \times 3\,\text{mm}^3$ to be easily implemented within mobile devices and a simple structure using lumped elements without any extra matching network. In this paper, we place a LCD under the proposed antenna to discuss the effects of conductors. The proposed antenna has less effect to the LCD and radiates efficiently over Wi-Fi band. The $-6\,\text{dB}$ bandwidth was measured as 120 MHz from 2.38 to 2.5 GHz, and the measured antenna efficiency is 50.2%.

Analysis of Cable Effects in Portable Antennas

Xinxin Lu, **Yang Liu**, **and Hyeongdong Kim**
Department of Electronics and Computer Engineering, Hanyang University, Seoul, Korea

Abstract— Ground plane may act as a main radiator in most portable antennas. Various cables connected with the ground plane, such as FPCB, speaker wire, and coaxial cables for measurement, can affect the radiation performances of the antenna significantly. In this paper, we use a loop-type ground antenna to examine the cable effects and analyze the effects by an EM simulator HFSS. The loop-type ground antenna is printed on a ground plane that measures 50×20 mm and is required a ground clearance of 4×6 mm. The antenna is operated at Wi-Fi (2.4–2.5 GHz) band. Without any extra cable effects, the resonant frequency is at 2.46 GHz. With extra cable connected to the different points on the ground plane, simulation results show that the resonant frequency and input impedance varies. Based on analysis, we demonstrate that the cable near the electric field maxima on the ground plane has strong influence on the resonant frequency and impedance of the ground antenna.

Size Reduction of Patch Antenna Array Using CSRRs Loaded Ground Plane

H. A. Jang, D. O. Kim, and C. Y. Kim
School of Electronics Engineering, Kyungpook National University, South Korea

Abstract— Recent theoretical and experimental studies have shown that microstrip patch antennas loaded by ground plane partially filled with a negative permeability metamaterial may in principle provide a resonant radiating mode, even if the size of the patch antenna is smaller than the wavelength of operation. However, those studies have investigated only a single microstrip patch antenna. To extend the research for patch antenna with metamaterial, this paper offers a novel patch array antenna mounted with the rectangular complementary split ring resonators (CSRRs). The antenna consists of two patch arrays, and they are constructed on Rogers4003 substrate with the thickness of 0.812 mm and relative permittivity of 3.38. The CSRRs are arranged on area of the ground plane surrounding the radiating patch. The designed and fabricated antenna has the operating frequency of about 3.8 GHz, whereas the resonant frequency of an ordinary array antenna having the same patch size without the CSRRs is about 5.1 GHz. It means that the occupied area of our suggested array antenna can be reduced by 44.5% to that of the ordinary one. The miniaturized antenna maintains the high directivity performance required by an array antenna, which are confirmed by both simulation and measurement.

Design of Internal Multi-band Mobile Antenna for LTE700/WCDMA/UMTS/WiMAX/WLAN Operation

D.-G. Yang, D.-O. Kim, and C.-Y. Kim
School of Electronics Engineering, Kyungpook National University, South Korea

Abstract— In this paper, an internal multi-band antenna is proposed for use with the LTE700/WCDMA/UMTS/WiMAX/WLAN bands. The proposed antenna was configured to have three radiating elements. These elements were the folded loop line, rectangular patch inserting meandered slit, and L-shaped ground branch closely coupled to the feeding line. The antenna was constructed on a substrate FR4 with a relative permittivity of 4.5. The antenna operated at a lower band to cover the LTE700 operations and at a wide upper band to cover the WCDMA/UMTS/WLAN operations. In addition, this antenna could also provide another upper band at about 3.5 GHz to cover WiMAX operations. By inserting the folded loop line and L-shaped ground branch, the LTE700 operations had VSWR ≤ 2.5 and RL ≤ -8 dB, while the WiMAX operations had VSWR < 2 and RL < -10 dB. By adding the rectangular patch with a meander slit, WCDMA/UMTS/WLAN band operations had VSWR < 2 and RL < -10 dB. The return loss and radiation patterns of the suggested antenna were simulated by commercial EM tool software by SEMCAD X. The computed results show both a good omni-directional radiation pattern and a moderate amount of radiation gain. According to the results mentioned, the proposed antenna can be applied to mobile handset using the LTE700/WCDMA/UMTS/WiMAX/WLAN bands.

Planar UWB Antenna with WLAN/WiMAX Dual Band-notched Characteristics Using the Hilbert-curve Slots

D. O. Kim and C. Y. Kim
School of Electronics Engineering, Kyungpook National University, South Korea

Abstract— In this paper, a compact ultra-wideband (UWB) antenna with dual band-notched design is proposed. The antenna consists of a rectangular metal patch and a 50 ohm coplanar waveguide (CPW) transmission line. By etching both the first iteration and the third iteration Hilbert-curve slots on the radiating patch, band-rejected filtering properties in the WiMAX/WLAN bands can be obtained. Furthermore, each notched band can be easily tuned by adjusting the length of each Hilbert-curve line segment because the sum of whole line segment controls the corresponding resonance frequency. The proposed antenna is simulated, designed, and measured showing a broadband matching and a stable radiation performance over the entire UWB frequency range, which prospects the deployment in the UWB system. As will be seen, the operation bandwidth of the antenna is from 2.5 to 10.6 GHz for VSWR < 2, in which two frequency rejection bands from 3.3 to 3.7 GHz and from 5.4 to 6 GHz for VSWR > 2 can be achieved. The measured results agree well with the simulation by the Microwave Studio of the CST. Based on the simulated and measured results, the newly proposed antenna by this paper can be found its application on the design of multi-band rejection characteristics with broadband antenna technology.

Reconfigurable Omnidirectional Loop Antenna with Left-handed Loading for RFID Applications

E. Serrano[1], **E. Diaz**[2], **A. Belenguer**[1], **J. Cascón**[1], **H. Hesteban**[2], **and A. L. Borja**[1]

[1]E. Politécnica de Cuenca, Universidad de Castilla-La Mancha, Campus Universitario 16071 Cuenca, Spain
[2]Instituto de Telecomunicaciones y Aplicaciones Multimedia, Universidad Politécnica de Valencia
Camino de Vera s/n 46022 Valencia, Spain

Abstract— This letter presents an omnidirectional horizontally polarized planar printed loop antenna using left handed CL loading with 50 Ω input impedance. The antenna gives an omnidirectional pattern in the plane of the loop, whilst working in an $n = 0$ mode at 868 MHz. In addition, reconfigurable responses can be achieved by using hard wire switches or diode varactor components. Finally, the antenna is compared with other right-handed conventional antennas i.e., a straight dipole, a folded dipole and a microstrip patch antenna working at the same frequency. Design details, simulated results and a fabricated prototype are presented. The concept significantly extends the design degrees of freedom for RFID antennas.

Millimeter-wave Design of Broadband Active Integrated Microstrip Patch Antenna

Mohammad Mahdi Honari, **Abdolali Abdipour**, **and Gholamreza Moradi**
Microwave/Millimeter Wave and Wireless Communication Research Lab
Department of Electrical Engineering, Amirkabir University of Technology
Tehran 15914, Iran

Abstract— In this paper, a broadband active integrated antenna (AIA) in millimeter wave frequency band is presented. For the direct integration, the output matching network is omitted so the microstrip antenna operates as an output matching network of the power amplifier and radiator.

Introduction: The amplifier-type active antenna has been a main issue in recent researches. In recent years, a novel fully integrated active antenna using the direct integration between power amplifier and antenna is proposed to obtain high PAE and compact RF-front end because of omitting interconnecting elements between the amplifier and antenna. On the other hand, there is a growing interest in communication systems that operates in the millimeter wave frequency band in order to take advantage of the wider bandwidth that is accessible at the high frequencies. In a broadband AIA, the antenna design in wide bandwidth as well as the amplifier. Using the aperture-stacked patch (ASP) antenna in this paper increases bandwidth because it utilizes a resonant aperture with stacked patches.

In this paper, we design a broadband AIA in millimeter wave frequency band. In our design, without any output matching network, the transistor of the power amplifier is connected to the antenna directly. The both of power amplifier and antenna are designed to operate in wide bandwidth. The harmonic balance analysis by ADS simulator is used for designing the power amplifier. The input impedance of the ASP antenna is adjusted to be optimized output impedance of power amplifier, obtained by load pull analysis. The input matching network designs base on load sensitivity analysis for power amplifier. Finally, the simulation of the ASP antenna by HFSS simulator are done that it shows good cross polarization and radiation pattern.

Configuration: *The power amplifier:* To achieve the maximum PAE and output power, we do load pull analysis at centre frequency of 28 GHz then we optimize input matching network and load impedance for broadband operation. Also, we do load sensitivity analysis for the amplifier. In this analysis, we optimize input matching network so that, in the broad bandwidth, we reduce load sensitivity over frequency range. By reducing the load sensitivity, we can design the antenna so much easier than before because, input impedance of the antenna can change more much range in the bandwidth.

The Antenna: In the aperture-stacked patch antenna, the aperture is employed as a radiator so its size cannot be varied alone and the coupling to the feed line must be controlled in other method. To achieve this, we use feed line shaping under aperture. It must be notice that the antenna is designed for the optimized load of power amplifier in addition to the adequate gain, radiation efficiency, radiation pattern and, cross-polarization over the bandwidth.

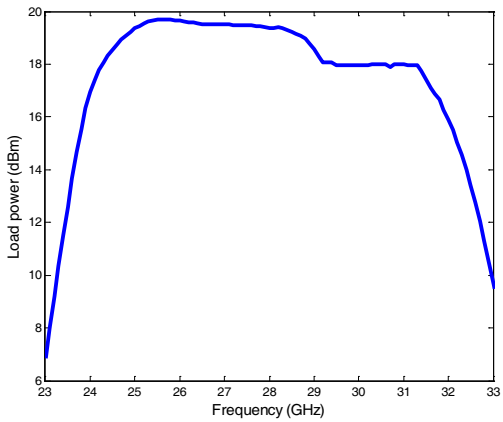

Figure 1: The output power of AIA.

The Aia: The AIA consists of the designed power amplifier and antenna. We do load sensitivity analysis thus design the antenna so easier and so the bandwidth of the AIA is improved. Fig. 1 shows the output power of AIA. A 2-dB ripple bandwidth of 25% is achieved. The maximum output power of the amplifier is obtained about 19.9 dBm.

Phase Only Optimization for Omni-directional Radiation Pattern with Constrained Amplitude

Lili Xu, **Qingqing Song**, **Jianhua Shen**, **Jiangtao Huangfu**, **and Lixin Ran**
Department of Information and Electronic Engineering
Zhejiang University, Hangzhou 310027, China

Abstract— This paper discusses the optimization for antenna array with variable phases and constrained amplitude to get good omni-directional pattern. We present the uniform circular array with cells of rectangle dual-pin fed circularly polarized patch antennas and calculate respective pattern of each element in CST Microwave Studio including mutual coupling. Based on the symmetry phases and constrained amplitude, Steepest Descent Method (SDM) is introduced to get maximum beamwidth by optimizing phases of antennas. The amplitude of center element is times as amplitudes of the other elements while the other elements have the same amplitude. The center element plays an important role in the optimization and the effect of center element's amplitude is also presented. The optimization results show the availability of the optimization technique, using which antenna array can get better omni-direction compared to the array excited by the same phase.

Such optimized array has good tracing ability for wide angle, especially the signals from low elevation. It is able to apply in the transmitter, to send signals in arbitrary direction.

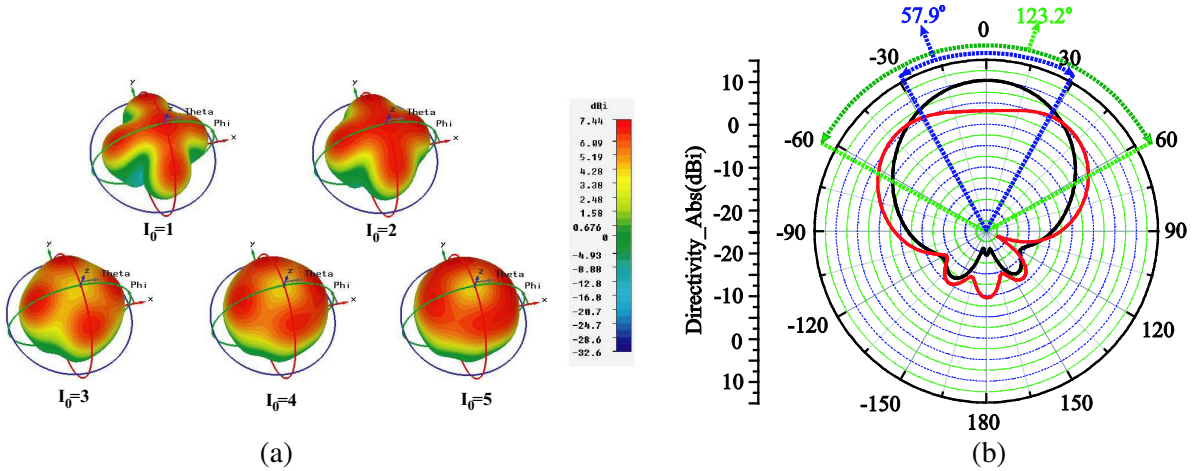

Figure 1: (a) Optimized farfield directive patterns corresponding to different excitation amplitudes (I_0) of center element. (b) Radiation patterns of optimized array and initial array. The red curve represents the optimized array with excitations of amplitude $I_0 = 4$ and optimized phases, while the black curve represents initial array with excitations of same amplitude and same phase. Blue curve and green curve show the 3-dB beamwidth of corresponding arrays.

A Dual Bevel Compact Planar Monopole Antenna for UHF Application

M. Jusoh[1], **M. F. Jamlos**[1], **M. R. Kamarudin**[2], **Z. A. Ahmad**[1], **M. A. Romli**[1], **and Naseer Sabri**[1]

[1]School of Computer and Communication Engineering
Universiti Malaysia Perlis (UniMAP), Malaysia
[2]Wireless Communication Centre, Faculty of Electrical Engineering
Universiti Teknologi Malaysia, Malaysia

Abstract— Cognitive Radio (CR) technology approach has ability to overcome the spectrum allocation congestion with reflect to the rapid wireless communication growth. The CR antenna system must be able to sense, adapt and communicate without interrupting the primary user. Yet, no CR antenna standard and guideline released. Paper [1] discussed a wideband CR antenna is necessary for the spectrum scanning purpose. Hence, this paper presented a novel dual bevel planar monopole antenna with the ability to operate from 470 MHz to 1100 MHz. The planar monopole antenna consists of radiating element perpendicular to ground plane with dimension of 148 mm × 64 mm and 80 mm square respectively. The proposed antenna can be considered compact compared to the conventional antenna [2, 3]. The presented monopole antenna which is fabricated of FR4 substrate leads to the low cost while implementation of beveling technique generates a higher bandwidth performance. By introducing a dual bevel, an enhancement of 100% impedance bandwidth can be achieved compare to a single bevel with the same bevel angle of 10°, 20°, 30°, 40° and 50°. Moreover, the dual bevel antenna capable in producing divisive radiation patterns with linear polarization at three different frequencies: 500 MHz, 700 MHz and 900 MHz. The measured outputs have shown the same behaviour with the simulation results. A prototype antenna was designed, fabricate and the measured performance is presented. All designs and simulations have been done using CST Microwave Studio and the measurements performed by ZVL Rohde & Schwarz Network Analyzer. The proposed antenna has a great potential as a spectrum sensing device for cognitive radio application in the future.

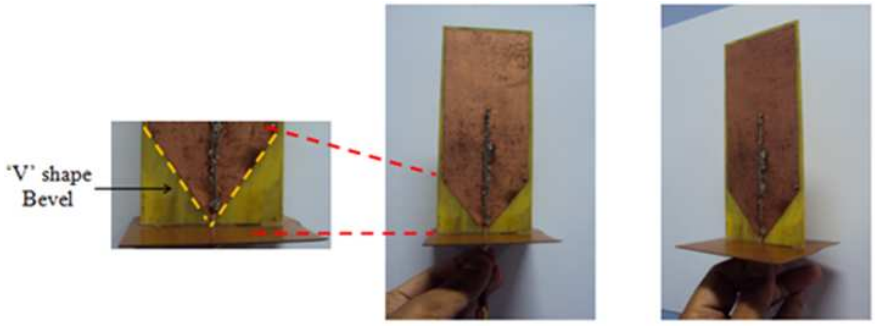

(a) (b)

Figure 1: The structure of the fabricated antenna. (a) Front view. (b) Side view.

Table 1: Comparison of single and dual bevel techniques.

Bevel Technique	A (bevel angle)	BW (MHz, %)	f_r (MHz)
Single	10	180, 28.7	626
	15	228 , 36.8	620
	20	250, 40.5	618
Dual	10	336, 53.8	624
	15	450, 71.5	629
	20	522, 82.1	636

REFERENCES

1. Kelly, J. R., E. Ebrahimi, P. S. Hall, P. Gardner, and F. Ghanem, "Combined wideband and narrowband antennas for radio applications," *Cognitive Radio and Software Defined Radios: Technologies and Techniques*, 2008.
2. Chu, J., C. Ruan, X. Liao, and Y. Cui, "A small size broadband antenna used in VHF/UHF band," *8th International Symposium IEEE Antennas, Propagation and EM Theory*, 2008.
3. Kyi, Y. Y., L. Jianying, and G. Y. Beng, "Study of broadband small size conical antenna," *IEEE Antennas and Propagation Society International Symposium*, 2006.

A UWB MIMO Spatial Design Effect on Radiation Pattern

M. Jusoh[1], **M. F. Jamlos**[1], **M. R. Kamarudin**[2], **Z. A. Ahmad**[1], **M. A. Romli**[1], **and S. H. Ronald**[3]

[1]School of Computer and Communication Engineering
Universiti Malaysia Perlis (UniMAP), Malaysia
[2]Wireless Communication Centre, Faculty of Electrical Engineering
Universiti Teknologi Malaysia, Malaysia
[3]School of System Electrical Engineering, Universiti Malaysia Perlis (UniMAP), Malaysia

Abstract— Attractive features of emerging Ultra-wideband (UWB) and Multiple-Input Multiple-Output (MIMO) technique are outlined and special design effects are described. The proposed antenna is a compact co-located MIMO antenna with two symmetrical antennas on the same substrate. The MIMO antenna has successfully functioned for UWB operating frequency of 2.8 GHz to 8 GHz with good impedance matching of −54 dB. Besides, the attainable UWB-MIMO's gain of 6 dBi is considered high compared to the conventional antenna [1]. Moreover, UWB-MIMO antenna with advantageous of high bandwidth, handy and small in size (91 mm × 38 mm) is accessible for wireless communication system [2]. To the author's knowledge, the MIMO antenna's reflection coefficient, mutual coupling and correlation coefficient need to be analyzed collectively as there are intimately engaged to each other. Hence, this research focuses on the minimization of the mutual coupling effects and the correlation coefficient since a lower mutual coupling increases radiation efficiency while a lower correlation coefficient improves antenna diversity. In the sense of the ultimate antenna configuration, this paper presented a parametric studies on the inter element spacing (IES) varying from 0 mm to 40 mm to obtain an optimize reflection coefficient, mutual coupling and correlation coefficient. Furthermore, the research focuses on the antenna's spatial design effect towards radiation pattern at three different frequencies points of $f_1 = 3$ GHz, $f_2 = 6$ GHz and $f_3 = 10$ GHz. As illustrated in Figure 4, the UWB-MIMO antenna has relative stable radiation patterns that functioned at three particular frequencies with linear polarization capability. Therefore, the proposed antenna is potential for point-to-point and point-to-multipoint wireless communication.

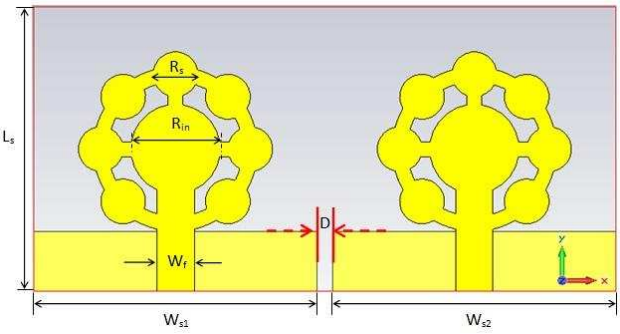

Figure 1: The simulated geometry of the proposed UWB MIMO antenna.

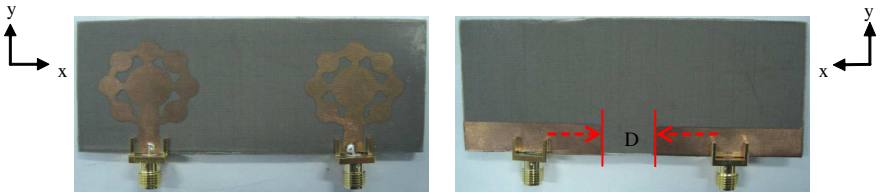

Figure 2: The fabricated geometry of the proposed UWB MIMO antenna. (a) Front view. (b) Back view.

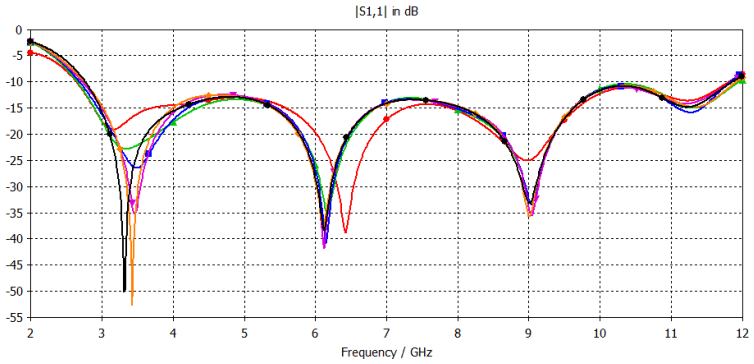

Figure 3: The reflection coefficient of the proposed antenna.

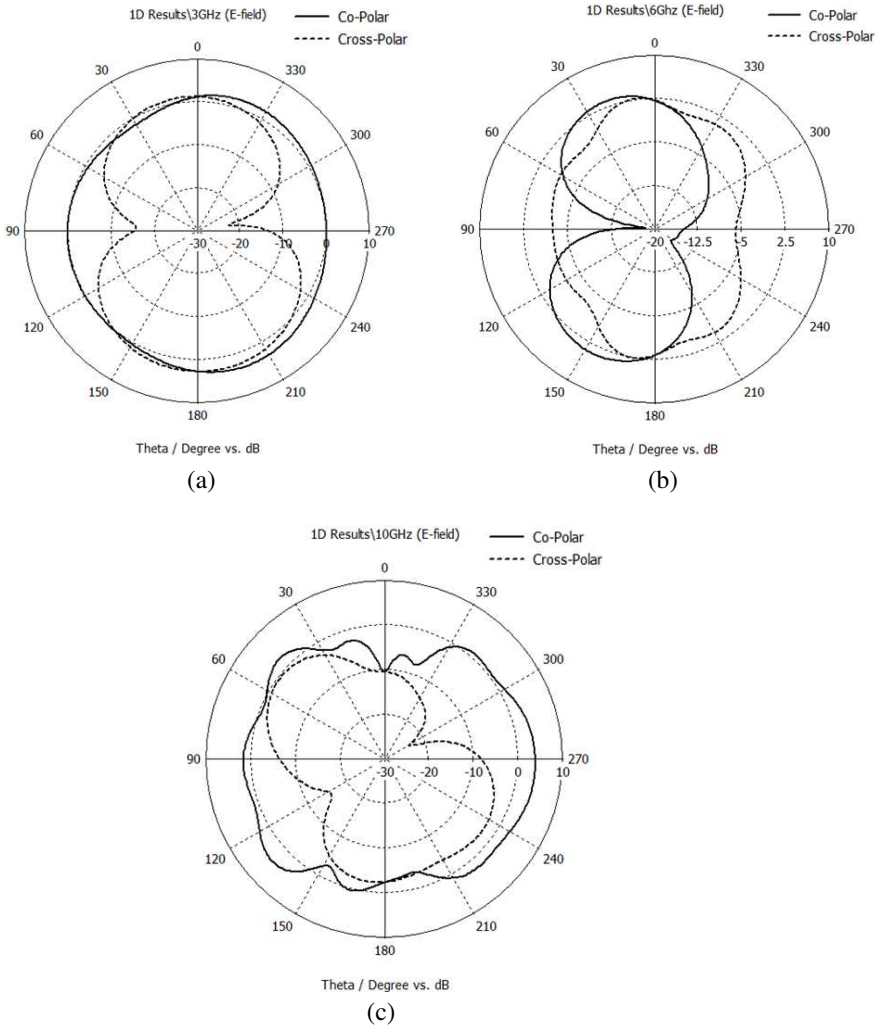

Figure 4: The simulated radiation pattern of the presented antenna on E-plane (y-z plane). (a) 3 GHz. (b) 6 GHz. (c) 10 GHz.

REFERENCES

1. Najam, A. I., Y. Duroc, and S. Tedjni, "UWB-MIMO antenna with novel stub structure," *Progress In Electromagnetics Research C*, Vol. 19, 245–257, 2011.
2. See, T. S. P., A. M. L. Swee, and Z. N. Chen, "Correlation analysis of UWB MIMO antenna system configurations," *Proceedings of the 2008, IEEE International Conference on Ultra-Wideband*, Vol. 2, 2008

Modal Study of a Via-hole in a Planar Circuit

Sameh Toumi, **Fethi Mejri**, **and Taoufik Aguili**
Syscom Laboratory, Engineers' National School of Tunis, Tunisia

Abstract— In recent years, the applications of hyperfrequency and microelectronics are in continuous expansion. General public applications such as mobile communications, local radio loops LMDS. It is the same applications in the domain of millimeter wave such as the radar automobile anticollision, the communication between satellites, pico-cellular networks and microwave imagery. We are interested in this work to the via-hole planar technology that allows better use of both sides of the printed substrate. The structure microstrip is a planar circuit, single layer, consisting of a metallic conductor connected to ground through a via-hole. In our work we use the iterative method FWCIP to see the influence of via-hole in the structure study. FWCIP is a mathematical tool powerful enough for the characterization of microwave circuits. The convergence and the speed of convergence of our iterative method (F.W.C.I.P) gives a robustness with regard to the other numeric methods used to resolve the problems of electromagnetism. In this paper we present the propagation of the fundamental mode: presentation modal of the Virtual source Je, presentation of the field via-hole following axes (ox) and (oy) and then determination of the propagation constant for all modes TEM, TE and TM. The determination of the propagation constant multiple modes give as the opportunity to add other modes to the fundamental mode and see the influence in the structure of study.

Harmonic Rejection Triangle Patch Antenna

M. S. Bin-Melha[1], **R. A. Abd-Alhameed**[1], **C. H. See**[1], **M. Usman**[2], **I. T. E. Elfergani**[1], **and J. M. Noras**[1]

[1]Mobile and Satellite Communications Research Centre, University of Bradford, Bradford, UK
[2]Department of Electrical Engineering, University of Hai'l, KSA

Abstract— Due to the low-profile, low manufacturing cost and easy to integrating with the electronic circuit, microstrip patch antennas have increasing gained its popularity for use in wireless handheld devices [1]. In this paper, a harmonic rejection triangular patch antenna is presented. This antenna is proposed to suppress power radiation at harmonic frequencies from active integrated antennas. This antenna is very similar to [2], but it performance has been optimised to serve its application.

The geometry of the proposed antenna is shown in Fig. 1. This triangle patch is designed on a FR4 substrate of thickness 1.6 mm and relative permittivity of 4.4 mounted over the ground plane. The sizes of the printed antenna patch and the ground plane are $90 \times 25\,\text{mm}^2$ and $135 \times 65\,\text{mm}^2$ respectively. The co-axial or probe feed technique is adopted on this antenna owing to the feed point can be placed at any place in the patch to match with its 50 ohm input impedance.

Figure 2 shows the simulated reflection coefficient of the proposed antenna. As can be seen, the antenna is designed to operate at 700 MHz and its corresponding second and third harmonics which are 1400 MHz and 2100 MHz were eliminated. It should be noted that the simulations were carried out by using HFSS simulator.

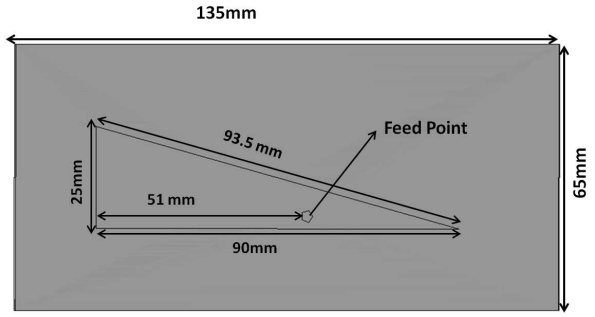

Figure 1: Basic geometry of the proposed antenna.

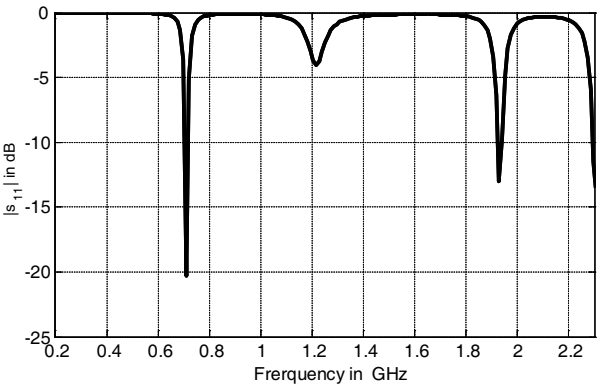

Figure 2: Refection coefficient of the proposed antenna and its harmonics.

REFERENCES

1. James, J. R. and P. S. Hall, *Handbook of Microstrip Antennas*, Vol. 1, Peter Peregrinus, Ltd., London, 1989.
2. Olaimat, M. M. and N. I. Dib, "A study of 15°-75°-90° angles triangular patch antenna," *Progress In Electromagnetics Research Letters*, Vol. 21, 1–9, 2011.

A New Fractal Based Printed Slot Antenna for Dual Band Wireless Communication Applications

Jawad K. Ali and Emad S. Ahmed
Department of Electrical and Electronic Engineering
University of Technology, Baghdad, Iraq

Abstract— Different fractal based structures have been widely used in numerous antenna designs for various applications. In this paper, a printed slot antenna has been introduced as a candidate for use in the dual band wireless communication applications. The antenna slot structure is in the form of a Sierpinski gasket of the first iteration. The antenna has been fed with 50 Ohm microstrip transmission line, and the slot structure is to be etched on the reverse side of the substrate. Performance evaluation of the proposed antenna design has been carried out using a method of moments based EM simulator, IE3D. Simulation results show that the resulting antenna exhibits an interesting dual frequency resonant behavior making it suitable for dual band communication systems including the dual band WLAN applications. Parametric study has been carried out to explore the effects of antenna parameters on its performance.

Performance Evaluation of Three Rectangular Patch Element Array Antenna Conformed on Small Radius Cylindrical Surface

Emad S. Ahmed and Jawad K. Ali
Department of Electrical and Electronic Engineering, University of Technology, Baghdad, Iraq

Abstract— The cylindrical geometry can offer certain desirable antenna characteristics that are not provided by planar elements. In this paper, a three-element cylindrical conformal array antenna has been presented as a candidate for operating in wireless communications and Radio Frequency Identification (RFID). Each element in the array is a microstrip fed rectangular patch antenna designed to resonate at 2.4 GHz. Once the desired results were obtained for a single element, each element in the conformal cylindrical array was then designed using the same dimensions and parameters. Modeling and performance evaluation of the array has been carried out using the commercially available electromagnetic software CST Studio Suite^{TM} 2009. Simulations were conducted to study the performance of the proposed conformal array as well as the effects of small radius cylinder on mutual coupling and the radiation pattern of the array. The cylindrical radii in consideration are of about one quarter wavelengths or slightly more. The radius of cylinder used in simulation is taken to be 0.24λ and 0.32λ. Compared with the existing cylindrical conformal antenna, the proposed array antenna possesses a reduction in cylindrical structure radius with acceptable ominidirectionality and gain needed for wireless communications and RFID applications.

A New Fractal Based PIFA Antenna Design for MIMO Dual Band WLAN Applications

Ali J. Salim[1], **Raad S. Fyath**[2], **Adil H. Ahmad**[1], **and Jawad K. Ali**[1]

[1]Department of Electrical and Electronic Engineering, University of Technology, Baghdad, Iraq
[2]Department of Electronic and Communication Engineering, University of Nahrain, Baghdad, Iraq

Abstract— This paper introduces the design of a dual-band internal F-PIFA (Fractal Planar Inverted F-antenna) as a candidate for use in the dual band WLAN (wireless local area network) MIMO (multi-input multi-output) applications. At first, the 4th iteration Koch's fractal geometry has been applied to the edges of the conventional rectangular patch structure to design a single compact antenna with a dual band resonant behavior. The radiating fractal based patch has been printed on a substrate with relative permittivity of 4.1 and thickness of 0.9 mm, and the antenna has been fed with 50 Ohm probe. This antenna is located at the corner of a copper ground plane of 0.05 mm thickness and dimensions of $110 \times 70\,\text{mm}^2$. It has been found that the resulting F-PIFA has the dimensions of about 21 mm × 15 mm × 6.2 mm, making it suitable for mobile terminal applications. Furthermore, the proposed antenna offers a dual band resonance with a frequency ratio of about 2.41; resulting in bandwidths, for return loss ≤ -10 dB, covering the two WLAN band standards. Modeling and performance evaluation of the proposed antenna have been carried out using the CST Microwave Studio. The modeled antenna has been applied to a 4 by 4 MIMO system suggested for use in dual band WLAN applications. Simulation results show that the suggested system offers −10 dB impedance bandwidths of about 300 MHz with an isolation of about 12 dB, for the lower band, and 570 MHz with an isolation of higher than 22 dB, for the upper band. This makes the proposed system suitable for use in MIMO dual band WLAN applications.

A New Compact Ultra Wideband Printed Monopole Antenna with Reduced Ground Plane and Band Notch Characterization

Jawad K. Ali, **Mahmood T. Yassen**, **Mohammed R. Hussan**, **and Mohammed F. Hasan**
Department of Electrical and Electronic Engineering, University of Technology, Baghdad, Iraq

Abstract— In this paper, a printed monopole antenna with reduced ground plane has been presented as a candidate for use in ultra-wideband applications. The monopole antenna structure is a nearly square shaped with m-slot embedded in it. A 50 Ω microstrip line is used to feed the proposed antenna. The proposed antenna has been supposed to be etched using a substrate with relative permittivity of 4.6 and thickness of 1.6 mm. Modeling and performance evaluation of the proposed antenna design have been carried out using a method of moments based EM simulator, IE3D. Results show that the proposed antenna has a compact size of 20 mm × 25 mm. The resulting antenna has been found to possess an impedance bandwidth, for voltage standing-wave ratio less than 2, exceeding what is required for UWB applications. Simulation results show that the lower frequency is primarily determined by the monopole square perimeter, while the slot has an effective role to allocate the position of the band notch. A parametric study has been conducted to provide more understanding of the effects of antenna parameters on its performance. Besides the reasonable performance, the simple structure of the proposed antenna will make it an attractive choice for the antenna designers.

Experimental Studying the Nonlinearity Effects on Adaptive Nulling

Cheng-Nan Hu, **Jing-Wei Huang, and Kevin Peng**
Communication Research Center (CRC), Oriental Institute of Technology
No. 58, Sec. 2, Sihchuan Rd, Ban-Ciao City, Taipei County, Taiwan, R.O.C.

Abstract— "Beam forming architecture", used in conjunction with an array of sensors to provide a versatile form of spatial filter for space-division multiple accesses (SDMA), becomes one of the enabling technologies to the 4G LTE network [1–3]. This approach features multiple users within the same radio cell to be accommodated on the same frequency and time slot by using internal feedback controlling the amplitude/phase weighting of the adaptive array [4] to modify its time, frequency, and spatial response. However, realization of the beam-forming techniques poses high linearity demands on RF/IF up-/down-conversion chain because nonlinear distortion will degrade the radiation pattern, resulting in the poor signal quality [5, 6]. This study employs a two-element antenna array incorporated with two amplifiers for experimental studying the nonlinearity effects on adaptive pattern nulls shift. Measured results validate the effective proposed method for further analysis on the performance degradation of adaptive array due to multicarrier power amplifiers (MCPA) nonlinearity.

REFERENCES

1. Tsoulos, G., M. Beach, and J. McGeehan, "Wireless personal communications for the 21th century: European technological advances in adaptive antennas," *IEEE Communication Magazine*, Vol. 35, No. 9, 102–109, Sep. 1997.
2. Parkvall, S., A. Furuskar, and E. Dahlman, "Evolution of LTE toward IMT-advanced," *IEEE Communication Magazine*, Vol. 49, No. 2, 84–91, Feb. 2011.
3. Park, C. S., Y.-P. E. Wang, G. Jongren, and D. Hammarwall, "Evolution of uplink MIMO for LTE-advanced," *IEEE Communication Magazine*, Vol. 49, No. 2, 112–121, Feb. 2011.
4. Widrow, et al., "Adaptive antenna system," *Proceeding of IEEE*, Vol. 55, No. 12, 2144–2159, Dec. 1967.
5. Laperle, C., T. Lo, J. Litva, and R. Turner, "Modeling of nonlinearity and their effects on digital beamforming," *IEEE AP-S*, Vol. 1, 124–127, Seattle, USA, Aug. 20–24, 1994.
6. Shimbo, O., "Effects of intermodulation, AM-PM conversion, and additive noise in multicarrier TWT systems," *Proceedings of IEEE*, Vol. 59, No. 2, 230–238, 1971.
7. Schneider, W. K. W., "Efficient simulation of multicarrier digital communication systems in nonlinear channel environments," *IEEE Journal on Selected Areas in Communications*, Vol. 11, 328–339, 1993.
8. http://www.acxc.com.tw/products.php.

Circular Switched Parasitic Patch Antenna Array for Unmanned Aerial Vehicle

M. H. Mat[1], **M. F. B. A. Malek**[1], **and M. Jusoh**[2]

[1]School of Electrical Systems Engineering, Universiti Malaysia Perlis (UniMAP)
Kangar, Perlis 01000, Malaysia
[2]School of Computer and Communication Engineering, Universiti Malaysia Perlis (UniMAP)
Kangar, Perlis 01000, Malaysia

Abstract— A circularly polarized smart antenna array which uses switched parasitic patch antenna with circular elements for WLAN 2.4 GHz frequency band was designed as an unmanned aerial vehicle (UAV). Paper [1] discussed hexagonal shape can be applied for designing microstrip patch element to effectively increase the bandwidth thus overcome the inherent defect of narrow bandwidth of microstrip patch antenna. The technique of parasitic switching is used in order to enable steering of the beam in 6 locations on azimuth plane with an elevation angle between 20° to 60°. The beam-steering of this antenna which is fabricated of TLY-5 substrate can be achieved in two ways where the parasitic antenna element is short-circuited or open-circuited using switches. The parasitic element becomes a director when open-circuited or simply transparent when close-circuited. One parasitic element will be isolated and others are short-circuited to ground. All designs and simulations have been done using CST Microwave Studio and the measurements performed by ZVL Rohde & Schwarz Network Analyzer. The low profile and low cost characteristics along with the simplistic beam control system of these smart patch antennas are ideal prototypes for commercialization. The proposed antenna can be considered compact compared to the [2, 3]. The proposed antenna has a great potential as a commercial antenna for UAV and ground station. Since its ability to function at 802.11 b/g for WLAN this is also a good a replacement for new smart router's antenna. Moreover it is possible to be implementing in future laptop design to more save energy.

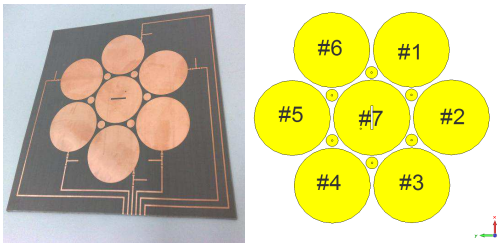

(a) (b)

Figure 1: Switched parasitic patch antenna, (a) fabricated antenna, (b) configuration of 6 elements.

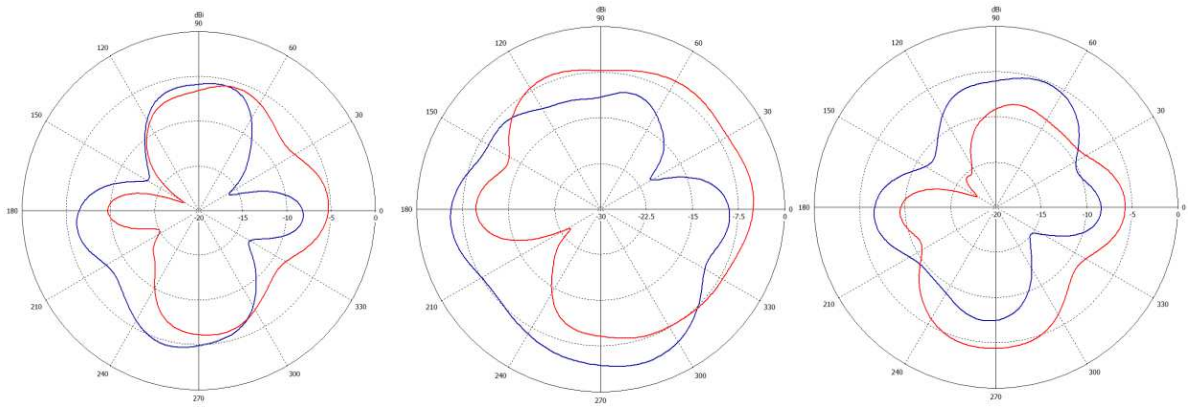

(a) (b) (c)

Figure 2: Radiation pattern in azimuth plane for configuration switch, (a) #2 (red) and #5 (blue), (b) #1 (red) and #4 (blue), (c) #3 (red) and #6 (blue).

REFERENCES

1. Min, S., L. Junwei, and D. J. Ireland, "Smart patch antenna for indoor mobile wireless computing," *Asia-Pacific Microwave Conference Proceedings, APMC*, 2005.
2. Junwei, L., A. Stark, and D. Thiel, "Switched parasitic patch antenna array using thirteen hexagonal shaped elements," *8th International Symposium on Antennas, Propagation and EM Theory, ISAPE*, 2008.

Wideband Circularly Polarized Antenna Using Two Linked Loops

The-Nan Chang
E. E. Dept., Tatung University, Taipei, Taiwan

Abstract— There are many techniques involving the perturbation of a ring-slot to generate circular polarized waves. In this paper, we share a new idea to design wide-band circularly polarized antennas using two linked loops. The two loops could be two annular-slots or two square slots fed by a 50 Ω microstrip line as shown in Fig. 1.

On the left-hand side of Fig. 1, two center points of the circular rings, "*a*" and "*b*", are lined at 45° with respect to the horizontal reference line. On the right-hand side of Fig. 1, the 45° inclined line is also seen to pass through 8 diagonal-points.

The achievable axial-ratio bandwidth of either structure is largely dependent on the shift distance between the two loops. For the annular-slot rings, the shift distance is determined by the parameter "*d*". For the square-slot rings, the shift distance is determined by the parameter "L_4". In this simulation, each annular-slot has an equal inner radius, $R_i = 6.5$ mm, and an outer radius, $R_o = 9.5$ mm. The side-lengths of the two square-slot rings may be different to get better tuning. The outer side-length of the square-slot ring ranges between 15 mm and 19 nn.

The measured 3 dB axial-ratio bandwidth is 1.4 GHz (46.7%) centered at 3 GHz for the annular-slot rings and is 1.05 GHz centered at 3.1 GHz for the square-slot rings.

In summary, the linked structure can be viewed as a combination of two perturbed slot-rings. The perturbation causes the generation of a circularly polarized wave.

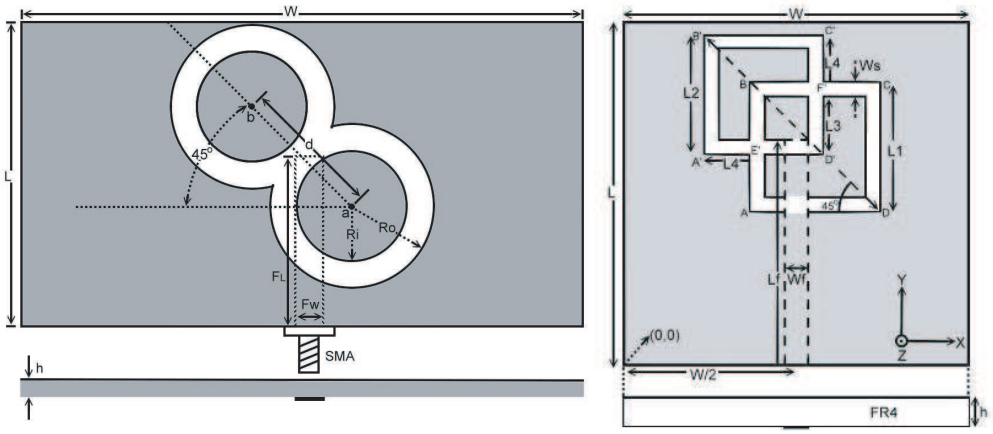

Figure 1: Wideband CP design using linked loops.

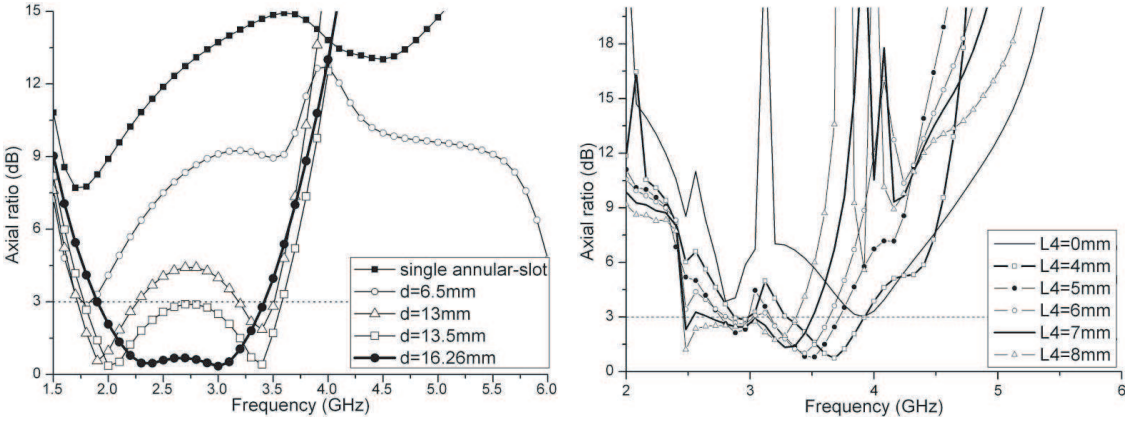

Figure 2: The shift distance, d or L_4, is used to control the axial-ratio bandwidth of each structure.

A Broadband Dipole Antenna for DTV and GSM850/900 Applications

I-Tseng Tang[1], **Ding-Bing Lin**[2], **Simon Li**[3], **Wen-Fan Chang**[3], **and Kuan-Ting Lin**[3]

[1]Department of Greenergy, National University of Tainan, Tainan, Taiwan
[2]Institute of Computer and Communication Engineering
National Taipei University of Technology, Taipei, Taiwan
[3]Department of Electrical Engineering, National University of Tainan, Tainan, Taiwan

Abstract— A simple planar broadband dipole antenna for both digital television signal (DTV) reception in UHF band and mobile communications in the GSM850/900 band is presented. Broadband operation of the proposed dipole antenna is obtained by successfully exciting its half- and one-wavelength modes which are further adjusted to be at close frequencies to form a broadband characteristic. The simulated impedance bandwidth defined by return loss $S_{11} \leqq -8$ dB is from 460 to 980 MHz. This proposed antenna with broadband matched impedance, stable radiation patterns and good antenna gains can be suitable for communication products of DTV and GSM850/900 applications.

Introduction: Recently, digital video broadcasting-handheld (DVB-H) has made it possible to deliver broadcast television or other multimedia services to a mobile or handheld device. The DVB standard is designed to operate in UHF bands of IV and V (470–862 MHz). Some promising designs of the broadband planar dipole antenna suitable for DTV (Digital Television) signal reception in the UHF band has recently been reported [1, 2]. This paper proposed a simple idea of printed broadband dipole antenna for DTB (470–862 MHz) and GSM850/900 applications.

Antenna Design: A dipole antenna with asymmetric configuration is able to generate tthree resonant modes, it could be exhibited a much wider bandwidth than a conventional symmetric dipole to cover the DTV signal reception within 470–862 MHz and GSM850/900 bands. Figure 1 shows the geometry and configuration of the proposed simple broadband dipole antenna for DTV and GSM850/900 applications. This antenna has been printed on FR4 substrate with the relative permittivity (ε_r) of 4.4, loss $\tan\delta = 0.02$ and the substrate thickness of 0.8 mm, and is fed by a 50-Ω transmission line. The antenna is separated into two asymmetric radiating portions of right C-shaped strip (length 145 mm or about 0.375λ) and left reverse-C-shaped strip (length 115 mm or about 0.25λ). Figure 2 shows the simulated return loss for the proposed antenna. The simulated impedance bandwidth defined by return loss $S_{11} \leqq -8$dB is from 460 MHz to 980 MHz. The radiation patterns are displayed with traditional 8-shape in E-plane, and omni-directional in H-plane.

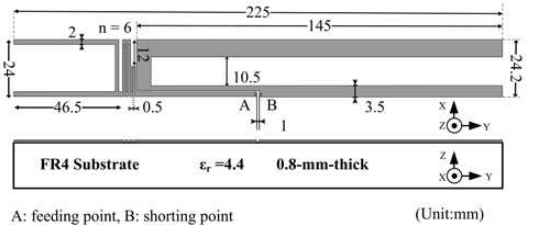

Figure 1: Geometry and configuration of the proposed antenna.

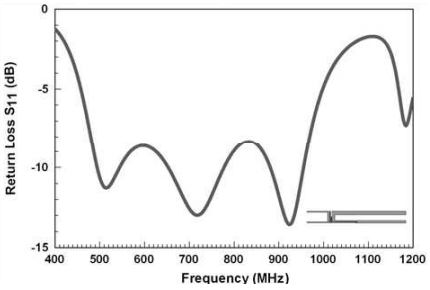

Figure 2: Simulated return loss S_{11} for the proposed antenna.

REFERENCES

1. Lee, C. T. and K. L. Wong, "Broadband planar dipole antenna for DTV/GSM operation," *Microwave Opt. Technol. Lett.*, Vol. 50, 1900–1905, 2008.
2. Tang, I.-T., C.-M. Li, and C.-Y. Lin, "Printed dipole antenna with back to back asymmetric dual-C-shape uniform strips for DTV applications," *Progress In Electromagnetics Research C*, Vol. 22, 73–83, 2011.

A Planar Monopole Antenna for DTV/GSM850/900 Applications

I-Tseng Tang[1], **Ding-Bing Lin**[2], **Chi-Min Li**[3], **Sin-Siang Wang**[1], **and Tony Su**[1]

[1]Department of Greenergy, National University of Tainan, Tainan, Taiwan
[2]Institute of Computer and Communication Engineering
National Taipei University of Technology, Taipei, Taiwan
[3]Department of Electrical Engineering, National University of Tainan, Tainan, Taiwan

Abstract— This paper is to design the miniaturized digital video broadcasting (DVB) and GSM850/900 antenna. The proposed planar monopole antenna consists of the oval-shaped and dual-L shape strips. The simulated impedance bandwidth defined by return loss $S_{11} \leq -8$ dB is from 460 to 1120 MHz. The antenna bandwidth includes DVB-H (470–862 MHz), GSM 850 (824–894 MHz), and GSM 900 (880–960 MHz) GSM850/900 bands. The antenna characteristics including return loss and radiation patterns were analyzed and discussed.

Introduction: The rapid progress of personal wireless communications has made it possible for a multimedia mobile handset to cope with both the digital video broadcasting and global system for mobile communication. Some promising designs of the broadband planar monopole antenna suitable for DTV (Digital Television) signal reception in the UHF band has recently been reported [1–3]. Owing to covering wideband bandwidth (460–1120 MHz), we propose a novel antenna structure to satisfy this issue.

Antenna Design: Antenna structure and design: Figure 1 shows the geometry and configuration of the proposed antenna. The proposed antenna is to fabricate on a low-cost FR-4 substrate with dielectric constant $\varepsilon_r = 4.4$, loss $\tan\delta = 0.02$, and thickness $h = 0.8$ mm, and fed by a 50-Ω microstrip line of width 1.5 mm. The antenna consists of the oval-shaped and two L-shape strips connected the oval-shaped. The oval-shaped has the outer ellipse radius 18 mm and the inner ellipse radius 12 mm. Two circles yield two different electric paths to satisfy the bandwidth requirements. Figure 2 show that the simulated return loss of the proposed monopole antenna. The input impedance is well matched as the −8-dB return loss bandwidth covers the DVB-H band (470–862 MHz) and GSM850/900 bands (824–960 MHz).

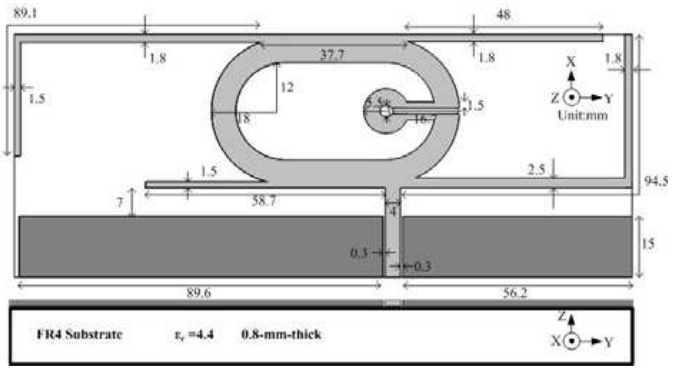

Figure 1: Geometry and configuration of the proposed antenna.

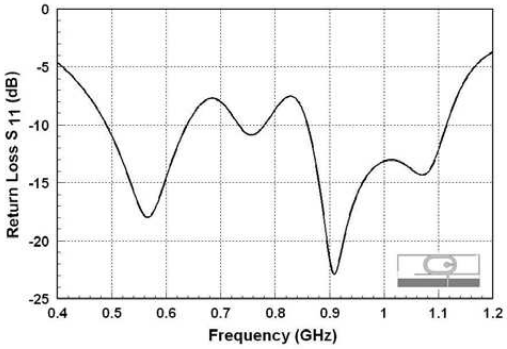

Figure 2: Simulated return loss S_{11} for the proposed antenna

REFERENCES

1. Li, R. L., B. Pan, J. Papapolymerou, J. Laskar, and M. M. Tentzeris, "Low-profile broadband planar antennas for DVB-H, DCS-1800, and IMT-2000 applications," *IEEE Antennas 2nd Propagation Society International Symposium*, 4729–4732, 2007.
2. Zhou, S., J. Guo, Y. Huang, and Q. Liu, "Broadband dual frequency sleeve monopole antenna for DTV/GSM pplications," *Electronics Letters*, Vol. 45, 766–768, 2009.
3. Liu, H., X. Chen, and K. Huang, "A novel wideband cylinder conformal microstrip antenna," *Journal of Electromagnetic Waves and Applications*, Vol. 22, Nos. 14–15, 1955–1964, 2008.

The Antenna Feed Structure with the Wide Impedance Bandwidth

Sinhyung Jeon, **Yang Liu**, **Jaeseok Lee**, **Hyunmin Jang**, **and Hyeongdong Kim**
Hanyang University, Republic of Korea

Abstract— This paper proposes a novel antenna design for achieving wide bandwidth in the lower frequencies bands. The antenna is realized by adding a branch line in the feed structure of a conventional planar inverted-F antenna (PIFA). Such a modification significantly enhances the impedance bandwidth while maintaining the size of the antenna element. In the lower frequency bands, the proposed antenna possesses a very wide impedance bandwidth, 245 MHz, from 730 MHz to 975 MHz, under a voltage standing wave ratio (VSWR) of 3 : 1 with a good realized antenna efficiency. A comparative analysis on both the reference antenna and proposed antenna characteristics are conducted to verify the improved bandwidth and efficiency of the proposed antenna. The proposed antenna fully covers Long Term Evolution (LTE) 13 band, Global System for Mobile communications 850 and 900 bands (GSM850/ GSM900). The average realized antenna efficiency over the LTE 13, GSM850 and GSM900 bands are about 55%. In addition, good radiation patterns are obtained for mobile services at the desired frequency bands.

A New CPW-Fed C-slot Based Printed Antenna for Dual Band WLAN Applications

Jawad K. Ali[1], **Ali J. Salim**[1], **Zaid A. Abed AL-Hussain**[2], **and Hussam Alsaedi**[1]

[1]Department of Electrical and Electronic Engineering
University of Technology, Baghdad, Iraq
[2]Department of Electrical Engineering, College of Engineering
Al-Mustansiriya University, Baghdad, Iraq

Abstract— The C shaped structures and alike have been widely used in numerous antenna designs for various applications. In this paper, a printed slot antenna has been introduced as a candidate for use in the dual band wireless communication applications. The antenna slot structure is to be composed of two or more C shaped slots with different lengths combined together to form a single slot structure. The antenna has been fed with 50 Ohms CPW, and the slot structure is to be etched on the ground plane. Performance evaluation of the proposed antenna design has been carried out using a method of moments based EM simulator, IE3D. Simulation results show that the resulting antenna possesses a dual frequency resonant behavior covering the 2.45/5.8 GHz WLAN applications. The resulting percentage impedance bandwidths of the modeled antenna at the center frequencies of 2.51 GHz and 5.21 GHz are 22.70 (2.29 GHz to 2.86 GHz), and 4.80 (5.11 GHz to 5.36 GHz) respectively. In addition, the antenna with three C-slot structure possesses a dual frequency resonant behavior covering the 2.45/5.8 GHz WLAN applications. The resulting percentage impedance bandwidths at the center frequencies of 2.45 GHz and 5.71 GHz are 11.80 (2.32 GHz to 2.61 GHz), and 7.2 (5.53 GHz to 5.94 GHz) respectively. Parametric study has been carried out to explore the effects of antenna parameters on its performance. Besides the satisfactory radiation characteristics, the simple structure of the proposed antenna makes it an attractive choice for antenna designers.

Analysis and Simulation of Electric Field Intensity from a Half-wave Dipole Antenna in Open Area Test Site

I. A. Wibowo, M. Z. Mohd Jenu, and A. Kazemipour
Center for Electromagnetic Compatibility, Faculty of Electrical and Electronic Engineering
Universiti Tun Hussein Onn Malaysia, 86400 Parit Raja, Batu Pahat, Johor, Malaysia

Abstract— Accurate measurement of electric field intensity is important in electromagnetic compatibility (EMC) field where the measured electric field emitted by an electrical or electronic product determines whether the product complies with regulation. To have valid measurement, the antennas used in the measurement must be calibrated accordingly. Both the measurement and calibration have to be done in a test site. Although there have been various alternative test sites available nowadays such as the anechoic chamber, legislative body such as the International Electrotechnical Commission (IEC) requires an open-area test site (OATS) as the reference for radiated emission measurement and antenna calibration. Therefore it is very important to understand the propagation mechanism in the OATS in order to design, evaluate and operate the OATS. This paper discusses the modeling and simulation of propagation mechanism in the OATS, starting with the basic propagation equation as a foundation, and the derivation of the electric field propagation model in an ideal OATS. The model uses a half wave dipole antenna as the transmitter. Simulations of the radiation of electromagnetic wave from a half-wave dipole antenna in the range of 30–1000 MHz have been performed in CST Microwave Studio® simulation software. The results of the calculation using the model were compared to the simulation. The average deviation was used to compare the result of the calculation using the theoretical model and the result of the simulation. The importance of height scanning of the receiving antenna was also elaborated. The results have proven that the theoretical model and the simulation are consistent and therefore the simulation validates the model.

Impact of Spacing and Number of Elements on Array Factor

S. F. Maharimi[1], **M. F. Abdul Malek**[2], **M. F. Jamlos**[1], **S. C. Neoh**[3], **and M. Jusoh**[1]

[1]School of Computer & Communication Engineering, University Malaysia Perlis, Malaysia
[2]School of Electrical System Engineering, University Malaysia Perlis, Malaysia
[3]School of Microelectronic Engineering, University Malaysia Perlis, Malaysia

Abstract— This paper is divided into two parts. The first part presents the impact of array factor according to the number of element and the element spacing. In designing a linear array antenna, few things need to be considered such as spacing elements, number of elements, phase and amplitude excitation, and others. When considering these parameters, the modified view of the array antenna design can be analysed through array factor. All these parameters are very important in order to optimize the side lobes level (SLL), gain, directivity and radiation pattern. The second part focuses on improvement of the array directivity in the linear antenna array. The directivity or radiation intensity of an antenna array depends on the array of factor. The number of elements and elements spacing have also a significant impact on the array directivity. Results are presented with a linear array antenna in the broadside array with the different spacing elements for the different number of antenna elements in the array factor and array directivity.

Analysis of Multi Turn 4-Arm Archimedean Spiral Antenna with Varying Spacing between Arms

Ashutosh Baheti[1], **Ali M. Mehrabani**[2], **and Lotfollah Shafai**[2]

[1]The LNM Institute of Information Technology, Jaipur, India
[2]The University of Manitoba, Winnipeg, Manitoba, Canada

Abstract— For so long Spiral Antennas are into work in various domains like in Aerospace, Missile Systems, GPS navigations Systems but the designing and complexity in understanding of this antenna is very high. Spiral antennas are circularly polarized and almost frequency independent, and can be used for broadband and/or multiband multipurpose applications, such as in mobile communication, early warning, and direction finding systems, Bluetooth applications, etc. Rumsey first summarized the features of such types of antenna systems. This antenna is four arm complex interleaved array antenna fed by four ports which regulates various Modes and Radiation Pattern with a Multiband and Broadband nature. The high Impedance of the antenna is very critical parameter which influences its high utility; this paper is too concerned with the Impedance effect when spacing is changed. Looking into more specifications of this antenna; Circular Polarization, Axial Ratio, Radiation Characteristics, Beamwidth and Impedance of the Antenna is observed and analyzed using Finite Element method with varying spacing between the two arms of the antenna. All the results were taken into account using HFSS Simulation tool. For this antenna simulation, Arlon DiClad 527 substrate with $\varepsilon_r = 2.5$ is chosen for enumerating all the parameters.

Results showed that as the Spacing between the two arms of the antenna is increased or width of Arm is reduced there will be less coupling between the arms of the antenna and thus it effects the Radiation Resistance (Impedance) of the Antenna as well as axial ratio degrades. The other properties like RHCP Gain, Radiation Pattern and Cross Polarization of Antenna are also observed over a frequency range. Such type of antenna is of prime importance in Mode forming system for Angle of Arrival estimation. With change in spacing between two arms the number of turns of the antenna is also observed which states that as the number of turns increases the active region in which the antenna should work expands and the frequency range increases keeping the fed point same but the gain of the antenna reduces as the number of turns becomes high. So we have to take care of optimization of number of turns where gain is maximum and antenna becomes more directive.

Some of the Images of the Design are shown below:

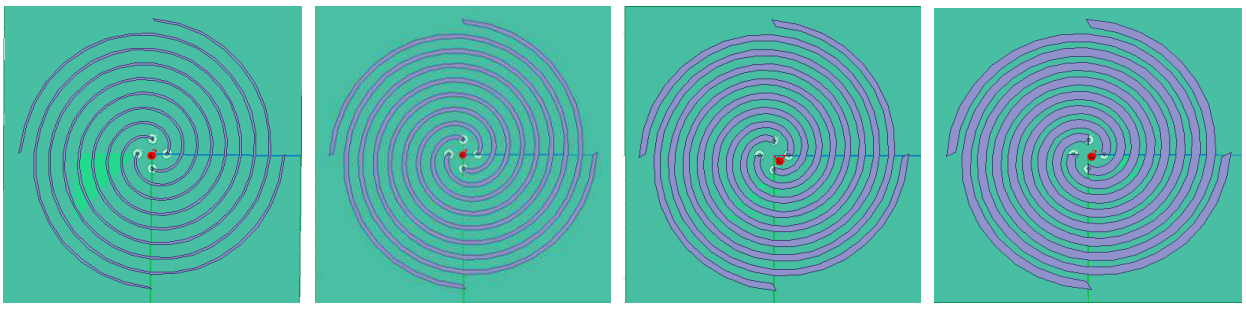

Reconfigurable Low-profile H-shaped Microstrip Antenna

A. F. A. Sheta, **W. M. A. Abdulkawi**, **and M. A. S. Alkanhal**
Department of Electrical Engineering, King Saud University
P. O. Box 800, Riyadh 11421, Kingdom of Saudi Arabia

Abstract— The paper presents a new compact microstrip reconfigurable low-profile H-shaped antenna for wireless applications. The proposed antenna has the ability reconfigure the beam into three different directions at the same resonant frequency. The antenna has been designed and fabricated on a Duroid substrate with a dielectric constant 2.2, thickness 1.5 mm, and loss tangent 0.004. Figure 1 shows the schematics of the proposed antenna. In the proposed antenna two artificial switches (PIN diodes) are used for reconfigurability of the maximum beam direction. The operation of the proposed antenna is based on ON and OFF states of PIN diodes in each side of H-shaped patch. It enables the antenna to change its beam in three directions, explained as case A, case B and case C. In case A switch 1 is ON and switch 2 is OFF. In case A proposed antenna has maximum beam directions of $\theta_{\max} = -75^\circ$ at $\phi = 0^\circ$. In case B switch 1 is OFF and switch 2 is ON, so the maximum beam direction tune to $\theta_{\max} = 75^\circ$ at $\phi = 0^\circ$. In case C both switches, switch 1 and switch 2 are in ON state, so the maximum beam direction tune to $\theta_{\max} = 5^\circ$ at $\phi = 90^\circ$. The proposed antenna is designed to operate at 1.8 GHz with peak gains of the antenna are 5.11 dBi, 5.11 dBi, and 2.68 dBi for case A, case B and case C respectively. The characteristics of the proposed antenna have been investigated using IE3D simulator. Antenna parameters such as gain, directivity, and return loss were measured using Network Analyzers and antenna test-bench. The proposed antenna has a great potential for modern wireless communications. This type of microstrip antennas has its maximum direction pattern presents in elevation plane. The proposed antenna is fed by a coaxial probe, 4.5 mm offset from the center of the ground plane in x direction. The proposed antenna consists of ground plane of dimension $17 \times 75\,\text{mm}^2$, and H-shaped patch of dimension $36.475 \times 67.5\,\text{mm}^2$, where the width of each side of H-shaped patch is 3 mm. The right side and left side are able to connect or disconnect by using two artificial switches (S_1 and S_2) on the patch (2 mm). The antenna frequency for $S_{11} < -10$ dB is closed to 1.8 GHz for two cases.

Recently, many techniques have been proposed to get good results and enhance the performance of the mobile antennas [1, 2].

ACKNOWLEDGMENT

This work is supported by the National Plan for Science and Technology Program, Kingdom of Saudi Arabia, Research Grant: 08-ADV210-2.

REFERENCES

1. Kim, J. Y., B. Lee, and C. W. Jung, "Reconfigurable beam-steering antenna using double loops," *Electronics Letters*, Vol. 47, No. 7, March 2011.
2. Islam, M. T., M. Naz, N. Misran, and B. Yati, "Modified E-H shaped microstrip antenna for wireless systems," *Proceedings of the 2009 IEEE International Conference on Networking, Sensing and Control*, Okayama, March 2009.

A Reconfigurable Antenna for Quad-band Mobile Handset Applications

Y. K. Park and Y. Sung
Department of Electronic Engineering, Kyonggi University
Yeongtong-Gu, Suwon-Si, Gyeonggi-Do, Republic Korea

Abstract— A reconfigurable antenna using two PIN diodes is presented for quad-band (GSM900 /GSM1800/GSM1900/UMTS) mobile handset applications. The proposed antenna has a size of $45 \times 11 \times 6\,\text{mm}^3$. By independently adjusting the on/off states of the two PIN diodes located on the radiating element, the proposed structure can be operated in the PIFA and loop mode, respectively. The PIN diodes are replaced by conducting tape in order to verify the concept. In regards to the fabricated reconfigurable antenna, when operating in the PIFA mode, the measured results show that the 7 dB bandwidth is 8.62%, which covers the GSM900 ($880 \sim 960\,\text{MHz}$) band. When operating in the loop mode, the measured results show that the 7 dB bandwidth is 26.36%, which covers the GSM1800 ($1710 \sim 1880\,\text{MHz}$), GSM1900 ($1850 \sim 1990\,\text{MHz}$), and UMTS ($1920 \sim 2170\,\text{MHz}$) bands, respectively. The measured 3D average gains are $-4.66\,\text{dBi} \sim -3.8\,\text{dBi}$, $-2.99\,\text{dBi} \sim -1.81\,\text{dBi}$, $-1.98\,\text{dBi} \sim -1.75\,\text{dBi}$, and $-2.31\,\text{dBi} \sim -1.75\,\text{dBi}$ for the GSM900, GSM1800, GSM1900 and UMTS bands, respectively.

Compatibility between Cognitive Radio and the Terrestrial Digital Broadcasting Services in the Digital Dividend Band

W. A. Hassan and T. A. Rahman
Wireless Communication Center, University Technology Malaysia (UTM), Malaysia

Abstract— The switching from analogue to digital broadcasting created newly freed spectrum in the band 470–862 MHz called Digital Dividend band. The sub-band 470–790 MHz is reserved for terrestrial digital broadcasting, however, the band is not fully utilized in many countries and the sharing of it is needed. The cognitive radio system gives the opportunity to share the licensed spectrum without causing interference to the primary service. In this paper, an overview of the compatibility between the cognitive radio system and the terrestrial digital broadcasting in the band 470–790 MHz is conducted. This is done based on the studies, results and recommendations conducted by the European Conference of Postal and telecommunication administration in 2011. Our study investigates the new proposed sensing methodologies for cognitive radio system. The study shows that sensing method is not efficient as a stand-alone technique for the compatibility between cognitive radio system and digital broadcasting systems, whereas the geolocation database is the current most efficient technique.

The Digital Dividend Spectrum in Asia

W. A. Hassan, **Y. Abdulrahman**, **and T. A. Rahman**
Wireless Communication Center, University Technology Malaysia (UTM), Malaysia

Abstract— The introduction of the digital broadcasting with high spectral efficiency forced the analogue terrestrial broadcasting to be phased out. The efficient spectrum usage by the digital broadcasting creates a freed spectrum in the Ultra High Frequency (UHF) band, which is called Digital Dividend Spectrum (DDS). In 2008, the European Communication Office (ERO) proposed the first frequency channel assignment (FCA) for mobile service operating in the DDS band for region 1. The second FCA was proposed by the Asian Pacific Telecommunity (APT) in 2010 for region 3. Because of the late submission of the APT FCA, some countries in region 3 follow the European FCA, the other the follows the APT FCA. Clearly, region 3 will not have a harmonized FAC, although the APT channel assignment approach is more favorable than European FAC. The study is conduced to review the non harmonized DDS issues in Asia. The study recommends the administration of region 3 to take a cooperative step in order to benefit maximally from the DDS.

Analytical Unit Pulse Propagation in an Active Single Resonance Lorentzian Medium

Ali Abdolali, **Maziar Hedayati**, **and Shahram Hedayati**
Department of Electrical Engineering, Iran University of Science and Technology, Iran

Abstract— In a causally dispersive medium the signal arrival appears in the dynamical field evolution as an increase in the field amplitude from that of the precursor fields to that of the steady-state signal. The classical theory of Sommerfeld and Brillouin of pulse propagation in a Lorentz medium is reexamined. While many rigorous studies of wave propagation in passive Lorentzian media have been performed, the corresponding problem in active media has remained theoretically unexplored. We use analytical approximations for describe the correct saddle-point .In this method used the refractive index for the determination of the response of an active Lorentzian medium .In this paper, illustrated that do not exist distance saddle points and then the near saddle points used for the determination of the response of an active Lorentzian medium to a step modulated pulse. There are Two types of wave dispersion, (Temporal dispersion and Spatial dispersion). Here used the time dispersion and surveyed in the frequency domain.

System Power Integrity Impact by Package Power/Ground Balls Assignment

C. H. Lin[1], **H. Y. Wang**[1], **and C. C. Wang**[2]

[1]Department of Electronic Engineering
National Kaohsiung University of Applied Sciences Kaohsiung, Taiwan
[2]R & D Electrical Laborary, Advanced Semiconductor Engineering, Inc., Taiwan

Abstract— Power integrity is one of the important issues of system design in present-day. Power and current levels are expected to increase with a corresponding to decrease in the voltage and increment of I/O number. Based on these factors, system designer has a novel challenge on power delivery network. Therefore, to design a power delivery network (PDN) becomes a major research topic.

The impact by power/ground ball assignment has been discussed in this paper. The power/ground ball is often used as a link between the package and printed circuit board (PCB). The resonance between the full planes will impact power stability. And it relates to the system power distribution from the voltage regulator module (VRM) to IC. In this investigation, the power signal propagation noise for different power/ground balls assignment has been pointed out.

For power/ground balls assignment, the preferred design is a power ball in the vicinity of a ground ball. But it is not always feasible for practical designs. When considering the PDN design, power/ground balls position is the key point for complete power delivery. That the power/ground balls position will affect the power delivery is demonstration. In this research, the VRM delivers energy to inner IC from PCB through power/ground balls to the package. The assignment of the power/ground balls at several places with different parasitic effects has been investigated for the impact of power integrity. The proposed arrangement of power/ground balls position is presented. The LC parasitic effects from different planes are extracted to perform s-parameter analysis of package system. The simulation results confirm with our theoretical analysis.

Metasurfaces for Ultracompact Base Stations

Xing Liu[1], **Shah Nawaz Burokur**[1], **André de Lustrac**[1], **G. Sabanowski**[2], **and Gérard-Pascal Piau**[2]

[1]IEF, University of Paris-Sud, CNRS, UMR 8622, Orsay Cedex 91405, France
[2]EADS IW, Suresnes 92000, France

Abstract— Metamaterials are intensely used for the design of directive antennas [1, 2]. In [1], Enoch et al. proposed to use the refractive properties of a low optical index material interface in order to achieve the directive emission. In [2], we have shown the possibility of using a novel composite metamaterial surface as a partially reflective surface in a Fabry-Perot (FP) cavity system to produce an ultrathin highly directive antenna. In this present paper, we present the design, implementation and characterization of a broadband compact base station antenna working in the [2 GHz–2.5 GHz] frequency range. The proposed antenna makes use of a controllable metasurface composed of metallic strips printed on a dielectric board. It is composed of a central isotropic conical broadband radiating element surrounded by a cylindrical metasurface. The centre frequency and the frequency band are determined by the length of the monopole and the ratio between the radius of its upper part and of its lower part [8]. This monopole feed has a working band extending from 1 GHz to 3 GHz. The metamaterial is composed of two layers of metallic strips placed on the outer face of the two cylindrical shape foam dielectric ($\varepsilon_r = 1.07$). These metallic strips on the foam cylinders can be continuous or discontinuous. The goal is to realize an antenna working between 2 GHz and 2.5 GHz and covering the UMTS and WIFI bands. It must be able to emit a directive lobe with an angular width $\leq 60°$ through 360° around the axis of the antenna and show overall dimensions of a few decimetres. Metamaterial made of metallic wires present very interesting features to be applied to directive antennas. A controllable electromagnetic band gap material with metallic wires incorporating PIN diodes as switching devices had been previously proposed [3]. This idea was developed and generalized in several works [4–7] to design smart screens, active frequency selective surfaces and metasurfaces. If the lattice is composed of electrically continuous wires, the structure acts as a reflector for EM waves with a frequency lower than the plasma frequency. If the lattice is made of electrically discontinuous wires the structure is transparent for these waves. The switching from a lattice made of electrically continuous wires to discontinuous wires can be realized if we incorporate switching elements like PIN diodes or MEMS.

REFERENCES

1. Enoch, S., G. Tayeb, P. Sabouroux, N. Guérin, and P. Vincent, "A metamaterial for directive emission," *Phys. Rev. Lett.*, Vol. 89, 213902, 2002.
2. Ourir, A., A. de Lustrac, and J.-M. Lourtioz, "Optimization of metamaterial based subwavelength cavities for ultracompact directive antennas," *Microwave Opt. Technol. Lett.*, Vol. 48, No. 12, 2573–2577, 2006.
3. De Lustrac, A., F. Gadot, S. Cabaret, J.-M. Lourtioz, T. Brillat, A. Priou, and E. Akmansoy, "Experimental demonstration of electrically controllable photonic crystals at centimeter wavelengths," *Appl. Phys. Lett.*, Vol. 75, 1625, 1999.
4. Tretyakov, S. A., S. Maslovski, and P. A. Belov, "An analytical model of metamaterials based on loaded wire dipoles," *IEEE Trans. Antennas Propag.*, Vol. 51, No. 10, 2652–2658, 2003.
5. Liu, L., S. Matitsine, and P. K. Tan, "Electromagnetic smart screen for tunable transmission applications," *Microwave Opt. Technol. Lett.*, Vol. 50, No. 6, 1510–1514, 2008.
6. Haché, S., S. N. Burokur, A. de Lustrac, F. Gadot, P. Cailleu, and G.-P. Piau, "Principles and applications of a controllable electromagnetic band gap material to a conformable spherical radome," *Eur. Phys. J. Appl. Phys.*, Vol. 46, 32611, 2009.
7. Burokur, S. N., J.-P. Daniel, P. Ratajczak, and A. de Lustrac, "Tunable bilayered metasurface for frequency reconfigurable directive emissions," *Appl. Phys. Lett.*, Vol. 97, 064101, 2010.
8. Balanis, C. A., *Antenna Theory: Analysis and Design*, 2nd Edition, Wiley, 1997.

Applicational Effects of an Atmospheric Pressure Plasma Device

Zhu-Wen Zhou[1], **Yan-Fen Huang**[2], **Si-Ze Yang**[3], **and De-Yong Xiong**[1]

[1]Institute of Applied Physics, Guizhou Normal College, Guiyang 550018, China
[2]School of Chemistry and Biology, Guizhou Normal College, Guiyang 550018, China
[3]Institute of Physics, Chinese Academy of Sciences, Beijing 100080, China

Abstract— We designed a atmospheric pressure plasma equipment, eggplant seeds were treated using the equipment with different voltage from 4420 to 6800 V. The results showed that the effects of different voltage plasma treatments on the seeds germination were not the same. The plant height, the plant extent, the root length, the root extent and the single fruit weight of the eight treatments from 4420 to 6800 V were increased distinctly. The eggplant yields of eight different voltage plasma treatments were increased than of the control (CK), the fruit yields of voltage treatments (5440 $\sim$ 6460 V) were better than of other voltages, the effects of fifth (5780 V) and sixth (6120 V) plasma treatments were best in most test indexes. The reasons may be that the treated seeds had been in different physical surroundings, the equipment is a dielectric barrier discharge (DPD), it creates a typical glow discharge free from filament and arc plasma, the acro-temperature of the plasma is nearly at room temperature, and plasma discharge gas pressure is atmospheric pressure. As the seeds were passed through the plasma on the carrier, the seeds were treated with uniform plasma discharge and were not burned. Test data were consistent with the similar estimating statistical analysis.

Design Curves of Microstrip Ring Resonator

Nafaa M. Shebani[1], **Amal E. Mohammed**[2], **and Bashir Moh. Khamoudi**[3]

[1]Office of Education Services, Surman, Libya
[2]Nasser International University, Tarhouna, Libya
[3]R&D Center, Tripoli, Libya

Abstract— To design a microstrip ring resonator that requires finding the mean radius of the resonator, the width and length of feed lines at a certain operating frequency.

This paper aims to give set of curves for designing a microstrip ring resonator with a simplest way, and to tabulate data for computing the width and length of the feed lines, these curves and tables are developed for different substrate materials.

The comparison of the produced results, curves and data, by the MATLAB softwares and results available in open literatures show a good agreement.

Session 4A1
Fiber Optics, Optical Sensors

Terahertz Emission by Atom in Multicolor Laser Field in Ionization-free Regime

A. V. Andreev[1], **S. Yu. Stremoukhov**[1, 2], **and O. A. Shoutova**[2]

[1]Physical Department, M. V. Lomonosov Moscow State University
119992 Leninskie Gory, 1, Build. 2, Moscow, Russia
[2]International Laser Center, M. V. Lomonosov Moscow State University
119992 Leninskie Gory, 1, Build. 62, Moscow, Russia

Abstract— Here we present the result of theoretical investigations of a single atom interaction with multicolor laser field formed by arbitrary number of the components with arbitrary orientation of polarization vectors. The developed theory is non-perturbative and valid in the whole subrelativistic region of laser field strength. The most specific feature is that the eigenfunctions of the cylindrically symmetric boundary value problem for atom in external field is used for wave function expansion (contrary to the traditional approaches where the free atom eigenfunctions are usually used as basis functions). It results in new mechanism of nonlinear atomic response which is mainly due to the light-induced anisotropy of electron wave function but not by electron transitions between the free atom eigenstates. As an example the terahertz (THz) emission in ionization-free regime is interpreted without exploiting the plasma nonlinearities (usually, four-wave mixing rectification process). Numerical results have a good agreement with the latest experimental results [1]. Numerical experiment simulates the argon atom interaction with fundamental and second harmonic of Ti:Sapphire laser. The parameters of the laser pulse can be easily achieved in modern lasers systems. It is shown that spectral width and efficiency of THz emission depend nonlinearly on the angle between the polarization vectors, delay time between the pulses, and chirp of the laser field components. Furthermore, relative amplitudes and widths of the laser pulses influences on the THz emission too. Numerical simulations shows that chirp of the fundamental frequency leads to the harmonic shifting, which is agree with the latest experimental data [2]. Optimization of the laser pulse parameters provides the THz emission in wide spectral region.

REFERENCES

1. Kim, K. Y., et al., *Nature Photonics*, Vol. 2, 605, 2008.
2. Ganeev, R. A., et al., *Phys. Rev. A*, Vol. 80, 033845, 2009.

Mode Field Diameters of Microstructured Optical Fibers: Estimation Using an Analytical Field Model

Dinesh Kumar Sharma and Anurag Sharma
Physics Department, Indian Institute of Technology Delhi, New Delhi 110016, India

Abstract— Microstructured optical fibers (MOF) have complex transverse dielectric cross-section which makes their electromagnetic analysis challenging. Maxwell's equations usually are solved numerically; however, simple analytical models serve a very useful purpose in understanding various characteristics and their estimation. We have recently developed an analytical field model for the fundamental mode of such fibers [1]. A special feature of our field model as compare to effective index method (EIM) is that it exhibits the required azimuthal variation of field and is better equipped to take into account the asymmetries of field around an air-hole. The parameters of the model are estimated using the variational principle. We have earlier used the model to estimate effective index and dispersion properties successfully. In this paper, we use the model for the estimation of the mode field diameter (MFD) of MOFs. There are a number of definitions of the MFDs that have been used in the literature. We have obtained various MFDs (Petermann-I, Petermann-II, Gaussian, etc.) using our model and have compared with the available experimental and numerical results. Significant differences in Petermann-I and Petermann-II MFDs show that the field is indeed non-Gaussian and the definitions based on Gaussian approximation of the field, which are often used, are not suitable for such fibers. Even the results of the experiments, which are usually in the form of the near field or the far field measurements are used to obtain the MFDs using the concepts based on the Gaussian field approximation and the values obtained for MFDs are thus not very accurate.

REFERENCES

1. *Opt. Quantum Electron.*, Vol. 41, 235–242, 2009.

Analysis of the Confinement Loss in Kagome Fibers

L. Vincetti, V. Setti, and M. Zoboli
Department of Information Engineering
University of Modena and Reggio Emilia, I-41125, Modena, Italy

Abstract— Hollow-core *Inhibited Coupling Fibers* (ICFs) have been widely analyzed in these years in order to minimize their *Confinement Loss* (CL) [1]. Their transmission spectra are composed by alternation of low loss and high loss regions. The latter are spectrally located at the cut-offs of the low spatially dependent cladding modes [2]. ICFs such as *Tube Lattice Fibers* (TLFs), *Kagome Fibers* (KFs), or their generalization *Polygonal Tube Fibers* (PTLFs) have a microstructured cladding composed by a lattice of *Tube Fibers* (TFs) with circular, hexagonal or N-sided polygonal cross sections, respectively, as highlighted in Fig. 1(a). Confinement loss (CL) characteristics of ICFs can be fruitfully described in terms of the modes of these TFs. Recently it has been shown that polygonal TFs are affected by Fano resonances which increases their CLs [3]. In this work it is shown that the same resonances can greatly affect also CLs of the ICF. Moreover CL can be substantially reduced by carefully choosing the shape of the cladding tubes. Here, for lack of space, only KF ($N = 6$), TLF ($N = \infty$) and a 24-PTLF ($N = 24$) will be considered. All the fibers have thickness $t = 500\,\text{nm}$, refraction index $n = 1.45$, and core size $R_{co} = 13.6\,upmu\text{m}$. The CL of the stand alone TFs taken from the ICFs claddings are shown on the bottom of Figs. 1(b) and (c) versus the normalized frequency $F = 2tf/c\sqrt{(n^2-1)}$; c and f are the speed of light and the frequency, respectively. Fano resonances (highlighted with blue lines), with their typical asymmetric shape, are well visible inside the low loss regions [3]. These resonances also cause higher CL in KF and 24-PTLF if compared to TLF, as shown at the bottom of Figs. 1(b) and (c). It has been proved that Fano resonances start from $F = (N+7)/31.8$ [3]. The higher N, the higher the spectral position of Fano resonances and, as a consequence, the higher the spectral window without Fano resonances. CL of KF is everywhere higher than TLF one, since the first resonance is at very low frequencies. In the 24-PTLF the first Fano-resonance appears at $F = 0.97$ very close to high loss region between the first and the second transmission windows. Indeed Fig. 1(c) shows that only the second transmission window is affected by Fano resonances, while the first one has CL comparable to those of the TLF. Thus, by properly choosing the number N of the polygon sides, CL can be reduced by shifting these resonances toward higher frequencies, outside the frequency range of interest.

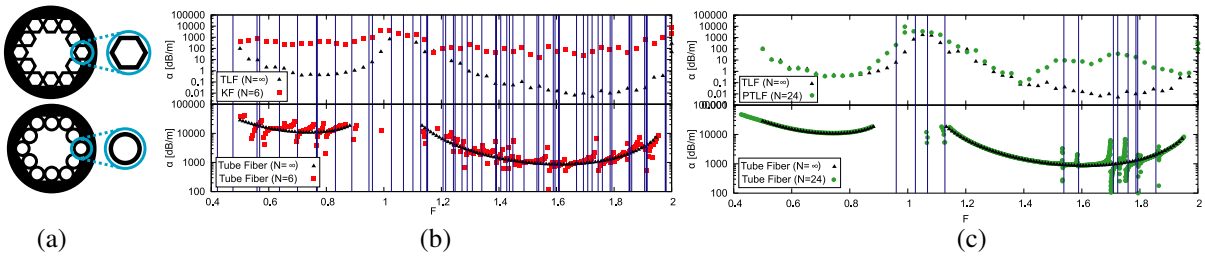

(a) (b) (c)

Figure 1: (a) KF (top) and TLF (bottom) cross sections. (b), (c) CL of KF (red squares), 24-PTLF (green dots) and TLF (black triangles). Blue solid lines highlight spectral position of Fano resonances.

REFERENCES

1. Wu, D. S., A. Argyros, and S. G. Leon-Saval, "Reducing the size of hollow core terahertz waveguides," *J. Lightw. Tech.*, Vol. 29, No. 1, 97–103, January 2011.
2. Vincetti, L. and V. Setti, "Waveguiding mechanism in tube lattice fibers," *Opt. Expr.*, Vol. 34, No. 10, 1064–1076, 1986.
3. Vincetti, L. and V. Setti, "Fano resonances in tube fibers," submitted to *J. Lightw. Tech.*, 2011.

Simultaneous Measurement of Stress, Temperature and Refractive Index Using an PMFBG Cascaded with an LPG

Jiang-Chiou Mau[1], **Pei-Ping Wu**[2], **Ming-Yue Fu**[3], **and Wen-Fung Liu**[2]

[1]Ph.D. Program in Electrical and Communications Engineering
Feng-Chia University, Taichung, Taiwan, R.O.C.
[2]Department of Electrical Engineering, Feng-Chia University, Taichung 40724, Taiwan, R.O.C.
[3]Department of Avionics Engineering, Air Force Academy, Kaohsiung, Taiwan, R.O.C.

Abstract— This study proposes a new fiber sensor based on the cascaded different types of fiber gratings for applying in the simultaneous measurement of stress, temperature, and refractive index. The fiber sensor is composed of a concatenated the fiber Bragg grating fabricated in polarization maintaining fiber (PMFBG) and the long period fiber grating (LPG) fabricated in photosensitive fibers. The sensing mechanism is based on the variation both of the reflection wavelength power and the Bragg wavelength corresponding to the Bragg peaks to be located on the positive or negative slope of the loss peak of LPG. Thus, this sensor can detect the changes of stress, refractive index, and temperature simultaneously by monitoring the wavelength shift and reflective power variation of PMFBG.

Because of PMFs to have different refractive indexes for the slow and fast axes, the FBG fabricated in the PMFs has two reflection grating wavelengths corresponding to the fast and slow axes. Moreover the light speed along the slow axis is lower than the fast axis, thus the refractive index of the slow axis is higher than that of the fast axis. The reflection peak at the longer Bragg wavelength belongs to the slow-axis grating and the shorter peak wavelength belongs to the fast-axis grating.

For the LPGs, the fundamental core modes are coupled to the cladding modes to generate several loss peaks in the transmission spectrum due to the phase match condition. Thus when the specific resonant wavelength of input light source passes through LPG in the core mode, it will be coupled to co-propagating cladding mode to result in the power loss of the wavelength.

Therefore, when an optical fiber sensor is based on the concatenated PMFBG and LPG, the stress, temperature, and index can be simultaneously obtained by means of the measurement of the Bragg wavelength shift ($\Delta\lambda$) of fast axis and the Bragg reflective power change of both slow and fast axes (ΔR_S, ΔR_F) on the slope region of the loss peak of LPG. It is expressed as the following matrix:

$$\begin{bmatrix} \Delta\lambda \\ \Delta R_F \\ \Delta R_S \end{bmatrix} = \begin{bmatrix} 1.519 & 0.0163 & 0 \\ 1.379 & 0.1445 & 42.975 \\ 1.0317 & 0.08 & 27.375 \end{bmatrix} \begin{bmatrix} \Delta S \\ \Delta T \\ \Delta index \end{bmatrix}, \quad (1)$$

where ΔS is the variation of stress, ΔT is the variation of temperature, Δn is the variation of index. The coefficients are determined by the Bragg wavelength shift and the Bragg reflective power variation of PMFBG in the separated experiment by applying various stress, temperature, and indexes to the sensor head.

By the transfer matrix, the measured the Bragg wavelength shift and Bragg reflective power variation of PMFBG can be used for obtaining the variation in stress, refractive index, and temperature. The proposed scheme of concatenating an PMFBG and an LPG is a highly promising and simple design for a wide range of sensing applications.

QoS-based Genetic Expression Programming Prediction Scheme in the EPONs

I-Shyan Hwang[1, 2], **Jhong-Yue Lee**[2], **and Andrew Tanny Liem**[2]

[1]Department of Information Communication, Yuan-Ze University, Chung-Li 32003, Taiwan
[2]Department of Computer Science and Engineering, Yuan-Ze University, Chung-Li 32003, Taiwan

Abstract— Ethernet Passive Optical Network (EPON) have been widely considered as one of the candidate to resolve the 'last mile' problem in the next generation broadband access networks due to its simplicity, cost-effectiveness and high data rate. As a time-division multiplexing PON (TDM-PON) technology, the transmission of EPON is shared among multiple subscribers. Therefore, the traffic prediction in the Dynamic Bandwidth Allocation (DBA) plays an important role in the EPON system to boost the Triple-Play-Services (data, video, voice) Quality-of-Service (QoS). However, nowadays, most literatures predict the unexpected incoming packet by adopting credit-prediction and linear-prediction scheme. In this paper, we propose an evolutionary algorithm — Genetic Expression Programming (GEP) prediction to solve the queue variation during waiting times as well as reducing the packet delay. We set the predictor in GEP based on cycle time, waiting time, bandwidth request and the mean bandwidth history request in every cycle time. Simulation results show that GEP prediction in DBA can avoid longer packet delay, reduce queue length, enhance QoS and effectively reduce high priority traffic delay and network performance degradation. Furthermore, we showed that our proposed prediction scheme can improve IPACT and has better system performance than well-known scheduling algorithm DBAM in terms of system throughput, queue length, end-to-end delay and jitter.

Performance and Confidentiality Comparison of Different Hybrid SAC/OCDMA-WDM Overlay Schemes

Isaac A. M. Ashour[1], **Sahbudin Shaari**[1], **Hossam M. H. Shalaby**[2], **and P Susthitha Menon**[1]

[1]Institute of Microengineering and Nanoelectronics (IMEN), Universiti Kebangsaan Malaysia
43600 UKM Bangi, Selangor, Malaysia
[2]Department of Electronics and Communications Engineering
School of Electronics, Communications, and Computer Engineering
Egypt-Japan University of Science and Technology (E-JUST), Alexandria 21934, Egypt

Abstract— Code pulses of a spectral amplitude coding/optical code division multiple-access (SAC/OCDMA) system are overlaid onto a multichannel wavelength division multiplexing (WDM) system. Modified quadratic congruence (MQC) codes are developed as the signature codes for the SAC/OCDMA system. The developed code is to avoid the overlapping between signals of both systems with no use of notch filters. In addition, performance and confidentiality results of this scheme are compared to our previous hybrid SAC/OCDMA-WDM overlay scheme which utilizes normal MQC codes with notch filters. The system performance and data confidentiality are evaluated in terms of bit-error rate (BER) and eye diagrams. The eavesdropper's interceptor that is based on a simple energy detector can scan all corresponding SAC/OCDMA wavelengths to detect an entire coded signal of an authorized user. Our results indicate that the performance and confidentiality have inverse relationship between the two hybrid systems. For a first hybrid scheme that does not adopt notch filters, the BER performance, when a data rate is 622 Mbps, for OCDMA users is about 10^{-15} at 4 dB of an optical attenuator, and BER for eavesdropper detection values vary from 10^{-6} to 10^{-15} due to different overlapping effects between WDM interferes and OCDMA pulses. On the second hand for a hybrid scheme that contains notch filters, the BER performance for OCDMA users is about 10^{-12} at 4 dB of an optical attenuator, and for eavesdropper detection values are mostly about 10^{-2}. However, it is concluded that an eavesdropper faces immunity from SAC/OCDMA system in both cases because WDM channels act as a partial masking over encoded signals in a hybrid scheme. Furthermore, the tradeoff between the performance and confidentiality for authorized SAC/OCDMA users is considered.

Birefringence in Elliptical Tube Fibers

L. Vincetti, V. Setti, and M. Zoboli
Department of Information Engineering
University of Modena and Reggio Emilia, I-41125, Modena, Italy

Abstract— Hollow core *Tube Fibers* (TFs) have recently been proposed as standalone *Terahertz* (THz) waveguides thanks to the great simplicity of their structures and to the low material absorption [1]. This waveguide consist of a hollow ring of dielectric material filled and surrounded by air. Light is mostly confined in the hollow core thus greatly reducing the absorption caused by the dielectric ring. Being the confinement mechanism based on the partial wave reflection on the dielectric ring, *Confinement Loss* (CL) and *Transmission Bandwidths* (TBWs) can be easily tuned by changing the internal ring size (R_{co}), the dielectric thickness (t) or refraction index of the dielectric ring (n) [1]. It has been shown that CL are almost bending insensible [2], while they are very sensible to the cladding shape variations due, for example, to fabrication process. Polygonal cladding shape has already been considered [3], while elliptical one has not. The goal of this paper is to analyze effects of the latter.

Reference circular TF is shown on Fig. 1(a) and it has $R_{co} = 1.71\,\mu\text{m}$, $t = 143\,\mu\text{m}$ and $n = 1.45$, that guarantees a transmission bandwidth of 1 THz with CL as low as 2 dB/m for the first TW. If this fiber is ideally compressed on the horizontal side and stretched on the vertical one, it gives rise to the elliptical shape of Fig. 1(a) which has the same core area and thickness of the initial circular TF, but a ratio between the internal semi-axes $\tau = a/b$. Fig. 1(b) compares dispersion curves and CL for the two *Fundamental Modes* (FM) polarizations for the circular and elliptical fibers with $\tau = \frac{1}{3}$.

It is clear that both dispersion curves and CL are very sensible to ring shape variations, but in different ways. When τ is decreased ($1 \rightarrow 0$) dispersion curves of both FMs polarizations shift to lower values, with very small birefringence, as shown on Fig. 1(c). Moreover, it is found that such birefringence is completely removed near the middle of the TW ($F \approx 1.5$). CL, on the contrary, strongly depend on the polarization. CL of the y-polarized FMs does not significantly depend on τ, while the x-polarized ones tend to higher CL. On one hand, this confirms that elliptical tube fibers can not be used as a polarization maintaining fibers for pulsed or broadband applications, since birefringence is zero inside the TWs. They can be used for polarization maintaining only at the sides of the TWs, although CL are higher than at the center. On the other side, great attention must be given to the fabrication process of the circular TF especially when they are used for randomly polarized optical beams: any elliptical defect in the ring shape will cause polarization dependent loss.

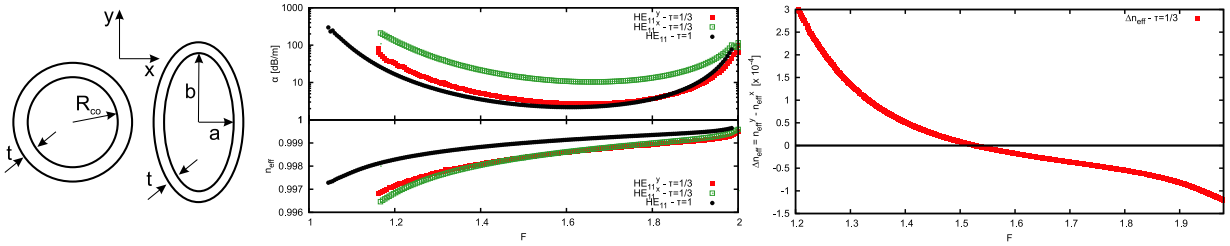

(a) (b) (c)

Figure 1: (a) Transverse cross sections of a circular (left) and an elliptical (right) TFs of the same core area. (b) Dispersion (bottom) and CL (top) curves for the two FMs polarizations in the circular and elliptical TFs with $\tau = \frac{1}{3}$. (c) Birefringence for the elliptical waveguide.

REFERENCES

1. Lai, C. H., B. You, J. Y. Lu, T. A. Liu, J. L. Peng, C. K. Sun, and H. C. Chang, "Modal characteristics of antiresonant waveguides for terahertz waveguiding," *Opt. Expr.*, Vol. 18, No. 1, 309–322, December 2009.
2. Lu, J. T., Y. C. Hsueh, Y. R. Huang, Y. J. Hwang, and C. K. Sun, "Bending loss of terahertz pipe waveguides," *Opt. Expr.*, Vol. 18, No. 25, 26332–26338, December 2010.
3. Vincetti, L. and V. Setti, "Fano resonances in tube fibers," submitted to *J. Lightw. Tech.*, 2011.

2D Fiberoptic Metal Profile Detector

Wei-Shu Hua[1], **Joshua Hooks**[2], **Nicholas Erwin**[2], **Wen-Jong Wu**[1], **Feng-Ju Hsieh**[2], **and Wei-Chih Wang**[2, 3, 4]

[1]Department of Engineering Science and Ocean Engineering, National Taiwan University, Taiwan
[2]Department of Mechanical Engineering, University of Washington, Seattle, WA, USA
[3]Department of Electrical Engineering, University of Washington, Seattle, WA, USA
[4]Medical Device Innovation Center, National Cheng Kung University, Taiwan

Abstract— Metal detector systems are widely using in current daily life. Nowadays, metal detectors operate on three basic technologies: very low frequency (VLF), pulse induction (PI), and beat-frequency oscillation (BFO). They are commonplace in libraries, airports, military camp, prisons, stores and shops. However, these devices share the common disadvantages of not being able to detect the profile of metal object and bulky in size. To overcomes these problems, we recently developed a compact metal detector capable of differentiate metal of different shapes and geometry using a fiber-optic magnetostriction sensor. This polymeric magnetostrictive metal detector system has many advantages, such as it is easy to fabricate and also resistant to RF interference (which is common in typical electromagnetic type metal detectors). The metal detector system utilizes a simple DC magnetic field detection scheme that integrated in magnetostriction material and interferometer to create the metal detection system. The basic concept of the metal detection is based on monitoring strain-induced optical path length change in the interferometer stems from the magnetic field induces magnetostriction effect on the ferromagnetic material which is coated on optic-fiber. The magnetostrictive device can produce polarized magnetic fields when applied magnetic field on the metal sensor, similarly generated from walk-through metal detectors system. Metal detection is made possible by disrupting the magnetic flux density present on the magnetostrictive sensor. In this paper, we will present our latest 3-D metal detection results. Several designs and their metal detection performance will be discussed and compared.

Gain Flattening in Erbium Doped Fiber Amplifiers by Use of a Coaxial Fiber

Jyoti Anand[1], **Jagneet Kaur Anand**[1], **and Enakshi K. Sharma**[2]

[1]Department of Electronics, Keshav Mahavidyalaya, University of Delhi, India
[2]Department of Electronic Science, University of Delhi South Campus, New Delhi 110021, India

Abstract— In this paper, we have proposed the use of a coaxial fiber configuration [1] for gain flattening in erbium doped fiber amplifiers. In coaxial fibers, the rod and tube form two independent waveguides, each supporting only one azimuthally symmetric mode. The two individual waveguides can be chosen to be synchronous at a phase matching wavelength $\lambda = \lambda_{ph}$. In the coaxial fiber, the rod and tube waveguide modes get evanescently coupled and hence coupled mode analysis [2] can be used to calculate the two supermodes of the coaxial configuration. We show that when such a coaxial fiber is spliced to a single mode fiber carrying a WDM signal, both the modes get excited in the coaxial fiber, each with its excitation coefficient strongly dependent on wavelength. Due to interference between the two modes, the coaxial fiber acts as a band reject filter at the phase matching wavelength, with attenuation and bandwidth depending on the fiber parameters. The fiber parameters are chosen such that the phase matching wavelength coincides with the peak of EDF spectrum, i.e., typically around ~ 1530 nm. This property can be employed for gain flattening at the end of an EDF. Alternatively, an erbium doped coaxial fiber with doping only in the inner core region (rod) can be used for inherent gain flattening. For such a configuration, the power at the phase matching wavelength couples back and forth between the inner doped core (which has amplification) and the outer undoped core as it propagates along the length of doped coaxial fiber. When a large number of wavelengths propagate through the EDF, the population inversion is reduced due to stimulated emission at each wavelength. The coaxial fiber couples in and out the wavelength corresponding to the gain peak which reduces the corresponding stimulated emissions around 1530 nm and hence, the population inversion is available to other wavelengths. This results in inherent gain flattening as well as increase in the average gain across the 1530–1560 nm band as in the case of long period grating in erbium doped fibers [3].

REFERENCES

1. Boucouvalas, A. C., *J. Lightwave Technol.*, Vol. LT-3, 1151, 1985.
2. Ghatak, A. K. and K. Thyagarajan, *Introduction to Fiber Optics*, Cambridge University Press, 1999.
3. Singh, R., Sunanda, and E. K. Sharma, *Optics Comm.*, Vol. 240, 123, 2004.

Rogue Waves Statistics in the Framework of One-dimensional Generalized Nonlinear Schrodinger Equation

D. Agafontsev[1] and V. Zakharov[2]

[1]Lebedev Institute of Physics, RAS, Moscow, Russia
[2]Department of Mathematics, University of Arizona, Tucson, USA

Abstract— We solve numerically the focusing generalized Nonlinear Schrodinger equation that takes into account the collapsing six-wave interactions term, as well as dumping terms (linear dissipation and three-photon absorption) and a general pumping term Φ,

$$i\Psi_t + (1-ia)\Psi_{xx} + |\Psi|^2\Psi + (1+ib)\alpha|\Psi|^4\,\Psi = i\Phi \tag{1}$$
$$\alpha > 0, \quad a, b \ll 1,$$

in the box with periodically boundary conditions. We start from the initial data

$$\Psi|_{t=0} = 1 + \epsilon(x),$$

where $\epsilon(x)$ is a stochastic noise. The development of modulation instability in (1) leads to formation of one-dimensional wave turbulence. In the integrable case $\alpha = a = b = \Phi = 0$ the turbulence is called integrable and relaxes to one of infinite possible stationary states. Addition of six-wave interactions term leads to appearance of collapses that eventually are regularized by the dumping terms, while the energy lost due to collapses is restored by the pumping term. In the latter case the system does not demonstrate relaxation-like behavior.

We measured evolution of spatial spectra $I_k = \langle|\Psi_k|^2\rangle$ and the PDF of $|\Psi|^2$, concentrating special attention on formation of "fat tails" in the PDF. Integrable turbulence appearing as a result of modulation instability of the stationary monochromatic wave leads to an almost Gaussian PDF. "Increase" of nonlinearity with six-wave interactions term leads to deviations from Gaussian-like PDF when higher waves appear more frequently. These deviations form power-law tails in the PDF and can be detected even when six-wave interactions term is small compared to terms of integrable NLS equation.

A Proposed Method for Sensitivity Analysis of Log-periodic Dipole Antenna Array-type Optical Electric Field Sensor

S. Tsujino[1], **H. Sugama**[2], **A. Tsuchiya**[1, 2], **K. Miyamoto**[1], **N. Hidaka**[2], **and O. Hashimoto**[1]

[1]Aoyama Gakuin University, Japan
[2]Kanagawa Industrial Technology Center, Japan

Abstract— In the microwave band, LPDA-type Optical Electric Field Sensor (LPDA-type OEFS) with high sensitivity and wideband (1.8 GHz to 6.0 GHz) characteristics has been proposed. It is difficult to analyze sensitivity characteristic of LPDA-type OEFS by electromagnetic field simulator because the OEFS has an optical modulator having micro and multiple electrodes. In this paper, we proposed an analysis method for LPDA-type OEFS which calculate phase shift of lightwave using analyzed modulation voltage by microwave. In addition, we investigated directional pattern by proposed method.

Figure 1 shows the analytical model of LPDA-type OEFS in a case. Antenna elements are arranged in 30 pairs on the substrate. The lengths of the elements are half wave and vary logperiodically. Optical waveguide ($LiNbO_3$) is positioned in the center of the OEFS. By using an electromagnetic field simulator, we analyzed amplitude and phase characteristics of modulation voltage by microwave between electrodes. Then, we obtained sensitivity characteristic of the OEFS by calculating the sum total of phase shifts of lightwave in each antenna elements.

Figure 2 shows the calculated and measured sensitivity characteristics in front of the OEFS. The calculated result corresponded to the measured one. Figure 3 shows the calculated and measured directional patterns in the horizontal plane at 1.8 and 6.0 GHz. The calculated results agreed with the measured results in ±60 degrees at 1.8 GHz and in ±30 degrees at 6.0 GHz. In another angle of the calculated results were similar to the measured ones.

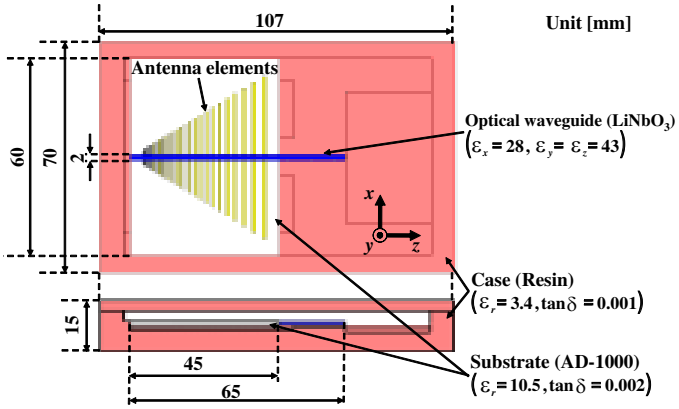

Figure 1: Analytical model of LPDA-type OEFS in a case.

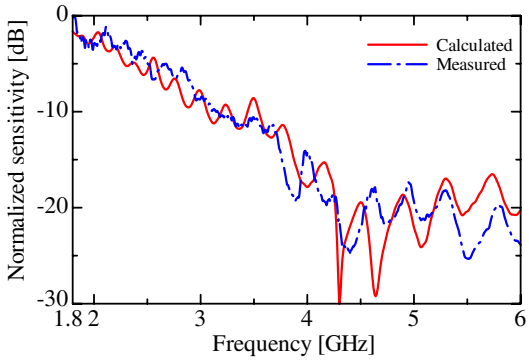

Figure 2: Normalized sensitivity characteristics.

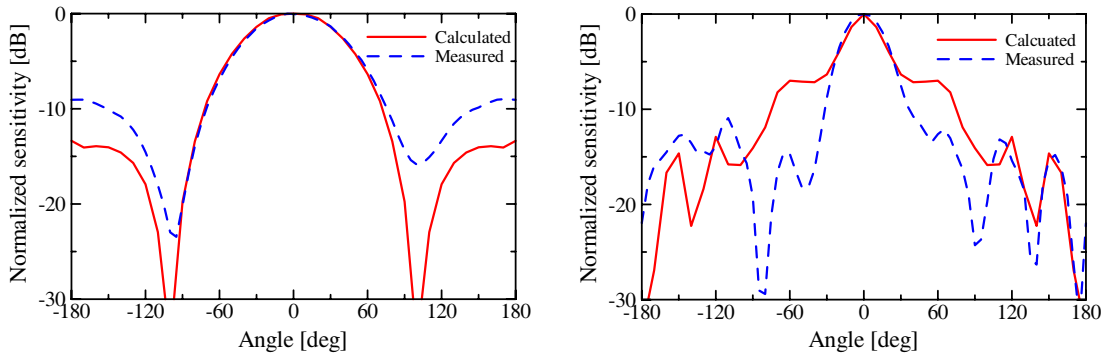

(a) 1.8 GHz (b) 6.0 GHz

Figure 3: Directional pattern in the horizontal plane.

Session 4A2
Fano Effect in Nanophotonics: Fundamentals and Applications

Nanoparticle Arrays with Narrow Fano-type Resonances and Their Application to Plasmonic Sensing

Arseniy I. Kuznetsov[1, 2], **Andrey B. Evlyukhin**[2], **Carsten Reinhardt**[2], **Manuel R. Gonçalves**[3], **Othmar Marti**[3], **Guillaume G. Vienne**[1], **Boris Luk'yanchuk**[1], **and Boris N. Chichkov**[2]

[1]Data Storage Institute, DSI Building 5, Engineering Drive 1, 117 608, Singapore
[2]Laser Zentrum Hannover e.V., Hollerithallee 8, D-30419, Hannover, Germany
[3]Institute of Experimental Physics, Ulm University, D-89069, Ulm, Germany

Abstract— Optical properties of large-scale arrays of spherical metal nanoparticles are studied experimentally and theoretically. These arrays are fabricated by a novel high-speed method, which is based on a combination of nanosphere lithography with laser-induced transfer (LIT) [1–3]. First, arrays of triangular prism-nanostructures are fabricated by the nanosphere lithography. Then these nanostructures are melted by femtosecond laser irradiation and transferred towards a different (receiver) substrate. Millions of identical nanoparticles can be transferred simultaneously by a single laser pulse. The transferred particles have spherical shape, which makes them suitable for plasmonic applications. They are arranged in high-quality hexagonal arrays corresponding to the template structures fabricated on the donor substrate by the nanosphere lithography (Fig. 1(a)). In such nanoparticle arrays, collective plasmonic modes with diffractive coupling between the nanoparticles can be excited. Excitation of these modes leads to the appearance of narrow Fano-type resonances in the optical transmission spectra. The spectral position of these Fano resonances is sensitive to the refractive index changes of the local environment which is promising for sensing applications (Fig. 1(b)). The sensitivity of 365 nm/RIU and the figure of merit (FOM) of 21.5 have been demonstrated in the visible spectral range using test waterglycerin solutions. This high sensing performance together with the fast and cheap fabrication procedure makes these nanoparticle array sensors promising for biomedical applications.

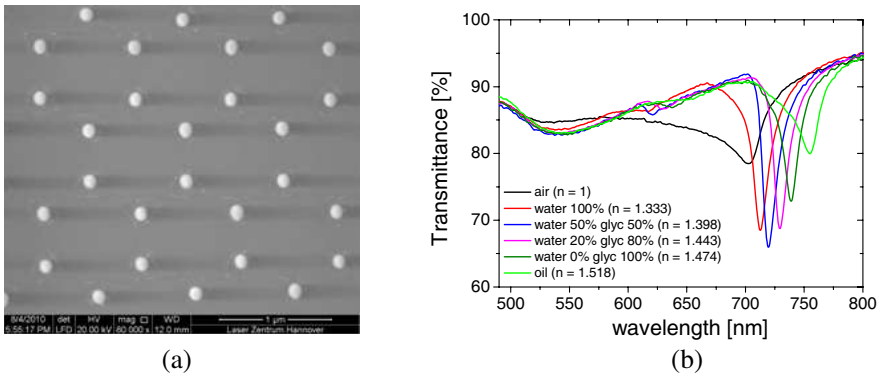

Figure 1: (a) An array of nanoparticles fabricated by a combination of the LIT approach and the nanosphere lithography [4]. (b) Optical transmission spectra of a nanoparticle array similar to that shown in Fig. 1(a) in liquid environments with different refractive index (n).

REFERENCES

1. Kuznetsov, A. I., J. Koch, and B. N. Chichkov, "Laser-induced backward transfer of gold nanodroplets," *Opt. Express*, Vol. 17, 18820, 2009.
2. Kuznetsov, A. I., A. B. Evlyukhin, C. Reinhardt, A. Seidel, R. Kiyan, W. Cheng, A. Ovsianikov, and B. N. Chichkov, "Laser-induced transfer of metallic nanodroplets for plasmonics and metamaterial applications," *J. Opt. Soc. Am. B*, Vol. 26, B130, 2009.
3. Kuznetsov, A. I., R. Kiyan, and B. N. Chichkov, "Laser fabrication of 2D and 3D metal nanoparticle structures and arrays," *Opt. Express*, Vol. 18, 21198, 2010.
4. Kuznetsov, A. I., A. B. Evlyukhin, M. R. Gonçalves, C. Reinhardt, A. Koroleva, M. L. Arnedillo, R. Kiyan, O. Marti, B. N. Chichkov, "Laser fabrication of large-scale nanoparticle arrays for sensing applications," *ACS Nano*, Vol. 5, 4843–4849, 2011.

Fano Resonance Tunable Plasmonic-photonic Nanoantennas

Ivan S. Maksymov and Andrey E. Miroshnichenko
Nonlinear Physics Centre and Centre for Ultrahigh Bandwidth Devices for Optical Systems (CUDOS)
Research School of Physics and Engineering, Australian National University, Canberra ACT 0200, Australia

Abstract— We suggest an all-optical spectral tuning mechanism over subwavelength light focusing with a photonic-plasmonic nanoantenna. The tunability originates from the manipulation of Fano resonances in a photonic crystal cavity that couples the nanoantenna with a far-field light source. Our approach presents a decisive step toward active spectral tuning of plasmonic nanoantennas without relying on nonlinear optical effects or mechanical reconfiguration.

We investigate a control mechanism over the line shape of Fano resonances [1, 2] in a gold plasmonic nanoantenna placed on the backbone of a dielectric photonic crystal cavity with a triangular lattice of air holes [Fig. 1(a)]. The fundamental cavity mode is excited by a laser beam focused on the bottom interface of the cavity. This mode is then coupled to a propagating surface plasmon mode of the nanoantenna. By means of 3D numerical simulations we demonstrate that a gradual defocusing of the laser beam leads to a change in the Fano line shape [3] accompanied by a shift in the resonance frequency [Fig. 1(b)]. Since the cavity is coupled to the nanoantenna, the change of the Fano line shapes also offers a spectral tuning of the energy focused into a subwavelength volume at the tip of the nanoantenna [4], as shown in Fig. 1(c).

Figure 1(c) shows that the maximum of the intensity at the nanoantenna apex can be shifted by $\sim 1.5\,\text{nm}$ by changing the spot radius R. The significance of this result achieved by simple defocusing can be better understood by comparing the efforts made to obtain this shift with the efforts in achieving a comparable shift with a 2D nonlinear PhC pumped by a high-intensity laser. In such a system a spectral shift of $\sim 1\,\text{nm}$ can be achieved by locally lowering the refractive index of the cavity by 0.2%, a value which is hardly attainable in practice. Therefore the investigated Fano resonance tuning can be suggested as an alternative to conventional tuning mechanisms exploiting nonlinear optical effects.

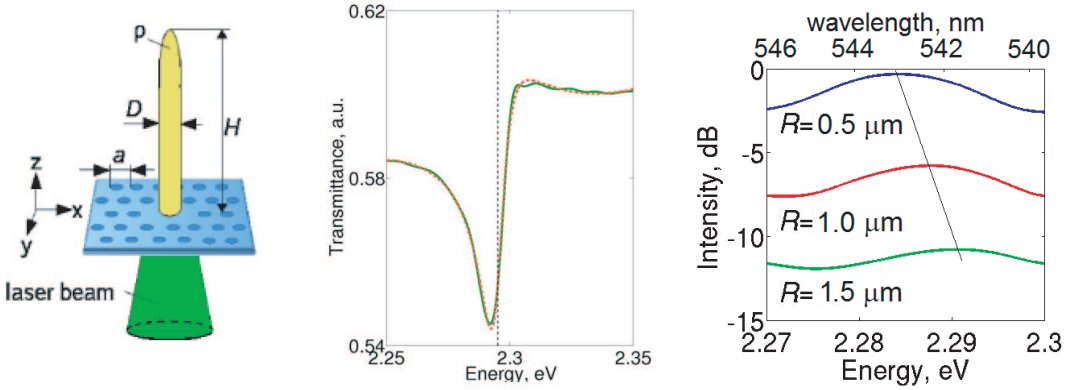

(a) (b) (c)

Figure 1: (a) Gold plasmonic nanorod antenna placed on the backbone of a photonic crystal cavity. (b) Transmission spectrum (green-solid lines) and best-fits to the Fano line shape (red-dashed line) of the isolated cavity. (c) Intensity of subwavelength focused light at the apex of the nanoantenna coupled to the cavity for different laser beam spot radii R.

REFERENCES

1. Fano, U., *Phys. Rev.*, Vol. 124, 1866–1878, 1961.
2. Miroshnichenko, A. E., S. Flach, and Yu. S. Kivshar, *Rev. Mod. Phys.*, Vol. 82, 2257–2298, 2010.
3. Galli, M., S. L. Portalupi, M. Belotti, L. C. Andreani, L. O'Faolain, and T. F. Krauss, *Appl. Phys. Lett.*, Vol. 94, 07101, 2009.
4. Maksymov, I. and A. Miroshnichenko, *Opt. Express*, Vol. 19, 5888, 2011.

Enhancement of the Nonlinear Response in Mach-Zehnder-Fano Interferometer

Yi Xu[1, 2] **and Andrey E. Miroshnichenko**[1]

[1]Nonlinear Physics Centre and Centre for Ultra-high Bandwidth Devices for Optical Systems (CUDOS)
Australian National University, Canberra ACT 0200, Australia
[2]Laboratory of Photonic Information Technology
School for Information and Optoelectronic Science and Engineering
South China Normal University, Guangzhou 510006, China

Abstract— By manipulating the resonance interaction in the Mach-Zehnder-Fano interferometer, we demonstrate the high-Q hybrid Fano resonance [1]. Enhancement of nonlinear response can be facilitated from such resonance hybridization which essentially increasing the phase sensitivity [2, 3]. It should be pointed out that the high-Q Fano resonances arising from resonances interference is the physical origin to release further degrees of freedom for advanced phase manipulation. Based on the introduced figure of merit the enhancement up to two orders of magnitude can be achieved compared to conventional geometries. The enhanced bistability benefited from nonlinear response enhancement which manifests itself as 100% extinction ration, large modulation depth and lowest threshold nonlinear switching [4, 5]. We further suggest a photonic crystal platform as one of possible applications.

REFERENCES

1. Xu, Y. and A. E. Miroshnichenko, *Phys. Rev. A*, Vol. 84, 033828, 2011.
2. Heebner, J. E. and R. W. Boyd, *Opt. Lett.*, Vol. 24, 847–849, 1999.
3. Heebner, J. E., N. N. Lepeshkin, A. Schweinsberg, G. W. Wicks, R. W. Boyd, R. Grover, and P.-T. Ho, *Opt. Lett.*, Vol. 29, 769–771, 2004.
4. Lu, Y., J. Q. Yao, X. F. Li, and P. Wang, *Opt. Lett.*, Vol. 30, 3069–3071, 2005.
5. Mario, L. Y., S. Darmawan, and M. K. Chin, *Opt. Express*, Vol. 14, 12770–12781, 2006.

Design and Tuning of Fano-shape Resonances in Planar Symmetric Coupled Oligomers

Mohsen Rahmani[1, 2], **Boris Lukiyanchuk**[1], **Yun Fook Thomas Liew**[1, 2], **and Minghui Hong**[2]

[1]Data Storage Institute, (A*STAR) Agency for Science, Technology and Research
DSI Building, 5 Engineering Drive 1, Singapore 117608, Singapore
[2]Department of Electrical and Computer Engineering, National University of Singapore
4 Engineering Drive 3, Singapore 117576, Singapore

Abstract— Arrays of planar symmetric coupled oligomers support higher sensitivity optical response than uncoupled plasmonic systems [1, 2]. Meanwhile, the mechanism of Fano resonance appearance in these structures is different from the asymmetric nano-structures. Previously, it has been shown that the asymmetric Fano resonance profile in nanoscale plasmonic systems can be obtained with symmetry breaking, breaking of time reversal symmetry, fabricating multiple metallic elements or tuning of incidence angle and light polarization [3]. These asymmetric conditions allow high-order multipolar modes to be excited with dipole mode, leading to exhibition of Fano resonance because of constructive and destructive interference between different eigenmodes. But in plasmonic planar oligomers Fano resonance appears due to excitation of different dipole modes arisen from a unique structure at the same time. Keeping in mind that dipole modes generally couple to incident light directly. This investigation can be used to design and tune the obtained Fano resonance under totally symmetric conditions due to the easiness of excitation of dipole modes [4]. It can improve potential applications of Fano resonance such as bio-chemical detection and switching and overcome the spatial restrictions of conventional optics [5]. In this work, the results of detailed study on different designed and fabricated quadrumers and pentamers consisting of a single central element and outer ring-like elements in nano-scales, is presented. It is shown experimentally that planar symmetric oligomers possess a good potential to design and tune the shape, intensity and figure of merit of Fano resonances. Highly precise theoretical calculations under inhomogeneous environment prove experimental results with high agreement.

REFERENCES

1. Rahmani, M., B. Lukiyanchuk, B. Ng, A. K. G. Tavakkoli, Y. F. Liew, and M. H. Hong, "Generation of pronounced Fano resonances and tuning of subwavelength spatial light distribution in plasmonic pentamers," *Opt. Exp.*, Vol. 19, 4949–4956, 2011.
2. Rahmani, M., T. Tahmasebi, Y. Lin, B. Lukiyanchuk, T. Y. F. Liew, and M. H. Hong, "Influence of plasmon destructive interferences on optical properties of gold planar quadrumers," *Nanotechnology*, Vol. 22, 245204, 2011.
3. Luk'yanchuk, B., N. I. Zheludev, S. A. Maier, N. J. Halas, P. Nordlander, H. Giessen, and C. T. Chong, "The Fano resonance in plasmonic nanostructures and metamaterials," *Nat. Mat.*, Vol. 9, 707–715, 2010.
4. Rahmani, M., T. Tahmasebi, B. Lukiyanchuk, Y. F. Liew, and M. H. Hong, "Polarization-controlled spatial localization of near-field energy in planar symmetric coupled oligomers," *App. Phys. A.*, Vol. 107, 23–30, 2011.
5. Rahmani, M., B. Lukiyanchuk, T. T. V. Nguyen, T. Tahmasebi, Y. Lin, T. Y. F. Liew, and M. H. Hong, "Influence of symmetry breaking in pentamers on Fano resonance and near-field energy localization," *Opt. Mat. Exp.*, Vol. 8, 1409–1415, 2011.

Fano Resonances in Complex Plasmonic Nanostructures for Novel Sensors

Harald Giessen[1], **Na Liu**[2], **Mario Hentschel**[1], **Andreas Tittl**[1], **Ralf Ameling**[1], **Nikolai Strohfeldt**[1], **Martin Mesch**[1], **Jun Zhao**[1], **Thomas Weiss**[1], **and Carsten Sönichsen**[3]

[1]4th Physics Institute, University of Stuttgart, Germany
[2]Rice University, Houston, TX, USA
[3]Department of Physical Chemistry, University of Mainz, Germany

Abstract— We engineer Fano resonances in complex plasmonic nanostructures to create novel plasmonic sensors. Among the structures are dipole-quadrupole coupled 2D and 3D plasmonic EIT structures, plasmonics oligomers, perfect plasmonic absorbers, plasmon-waveguide-polariton structures, as well as cavity enhanced plasmonic structures. Figures of merit that are comparable with the best localized surface plasmon resonance sensors can be obtained.

Fano resonances in plasmonic nanostructures have been a hot topic of research over the last few years [1]. Coherent coupling of a broad to a narrow resonance leads to interference phenomena in the spectrum. Engineering the resonances with regards to linewidth, spectral position, coupling strength, oscillator strength, and spectral phase allows for creation of very sharp and well modulated resonances which are suited for localized surface plasmon resonance sensing.

We are going to present 2D inverse [2] and 3D stacked dipole-quadrupole coupled structures [3] which give figures of merit of over 5 and sensitivities over 500 nm/RIU at attoliter volumes. These structures are demonstrated for glucose as well as for monomolecular layer biosensors. Stacking gold or palladium nanoparticles over a gold mirror with appropriate spacers allows for perfect plasmonic absorption, which can be used for glucose [4] as well as for gas sensing [5]. Gas sensing is also possible with very sharp Fano resonances in plasmon-waveguide structures [6]. Plasmonic oligomers such as septamers [7] or more complex structures [8] allow the generation of even multiple Fano resonances [9]. This can also be accomplished using multiple quadrupole coupling to a single dipole to create 3D plasmon rulers [10]. In combination with cavity enhancement, coupling of localized plasmon modes to microcavity modes [11, 12] or coupling of localized modes to surface plasmons [13] enhances the sensitivity even further. Plasmonic nanoantenna-enhanced sensing allows gas molecule detection down to a few hundred molecules [14].

REFERENCES

1. Lukyanchuk, B., N. I. Zheludev, S. A. Maier, N. J. Halas, P. Nordlander, H. Giessen, and C. T. Chong, "The Fano resonance in plasmonic nanostructures and metamaterials," *Nature Materials*, Vol. 9, 707, 2010.
2. Liu, N., T. Weiss, M. Mesch, L. Langguth, U. Eigenthaler, M. Hirscher, C. Sönichsen, and H. Giessen, "Planar metamaterial analog of electromagnetically induced transparency for plasmonic sensing," *Nano Lett.*, Vol. 10, 1103, 2010.
3. Liu, N., L. Langguth, T. Weiss, J. Kätel, M. Fleischhauer, T. Pfau, and H. Giessen, "Plasmonic analogue of electromagnetically induced transparency at the Drude damping limit," *Nature Materials*, Vol. 8, 758, 2009.
4. Liu, N., M. Mesch, T. Weiss, M. Hentschel, and H. Giessen, "Infrared perfect absorber and its application as plasmonic sensor," *Nano Lett.*, Vol. 10, 2342, 2010.
5. Tittl, A., P. Mai, R. Taubert, D. Dregely, N. Liu, and H. Giessen, "Palladium-based plasmonic perfect absorber in the visible wavelength range and its application to hydrogen sensing," *Nano Lett.*, Vol. 11, 4366, 2011.
6. Nau, D., A. Seidel, R. B. Orzekowsky, S.-H. Lee, S. Deb, and H. Giessen, "Hydrogen sensor based on metallic photonic crystal slabs," *Opt. Lett.*, Vol. 35, 3150, 2010.
7. Hentschel, M., M. Saliba, R. Vogelgesang, H. Giessen, A. P. Alivisatos, and N. Liu, "Transition from isolated to collective modes in plasmonic oligomers," *Nano Lett.*, Vol. 10, 2721, 2010.
8. Hentschel, M., D. Dregely, R. Vogelgesang, H. Giessen, and N. Liu, "Plasmonic oligomers: The role of individual particles in collective behavior," *ACS Nano*, Vol. 5, 2042, 2011.
9. Dregely, D., M. Hentschel, and H. Giessen, "Excitation and tuning of higher-order fano resonances in plasmonic oligomer clusters," *ACS Nano*, Vol. 5, 2011, DOI: 10.1021/nn202876k.

10. Liu, N., M. Hentschel, T. Weiss, A. P. Alivisatos, and H. Giessen, "Three-dimensional plasmon rulers," *Science*, Vol. 332, 1407, 2011.
11. Ameling, R. and H. Giessen, "Cavity plasmonics: Large normal mode splitting of electric and magnetic particle plasmons induced by a photonic microcavity," *Nano Lett.*, Vol. 10, 4394, 2010.
12. Ameling, R., L. Langguth, M. Hentschel, M. Mesch, P. V. Braun, and H. Giessen, "Cavity-enhanced localized plasmon resonance sensing," *Appl. Phys. Lett.*, Vol. 97, 253116, 2010.
13. Ameling, R., D. Dregely, and H. Giessen, "Strong coupling of localized and surface plasmons to microcavity modes," *Opt. Lett.*, Vol. 36, 2218, 2011.
14. Liu, N., M. L. Tang, M. Hentschel, H. Giessen, and A. P. Alivisatos, "Nanoantenna-enhanced gas sensing in a single tailored nanofocus," *Nature Materials*, Vol. 10, 631, 2011.

Optical Fano Vortex

Yi Xu[1, 2], **Anton S. Desyatnikov**[1], **and Andrey E. Miroshnichenko**[1]

[1]Nonlinear Physics Centre and Centre for Ultra-high Bandwidth Devices for Optical Systems (CUDOS)
Australian National University, Canberra ACT 0200, Australia
[2]Laboratory of Photonic Information Technology
School for Information and Optoelectronic Science and Engineering
South China Normal University, Guangzhou 510006, China

Abstract— We introduce the concept of optical Fano vortex in the context of Photonic crystal waveguide and coupled resonator system. The electromagnetic waves in the vicinity of the Fano resonance frequency manifest themselves as vortex like flows near the resonator. Based on the modified Fano-Anderson model [1], we outline the static and dynamic properties of this Fano vortex. The divergence of the scattering potential at the Fano resonance frequency is the analogue of the spatial singular point of electromagnetic wave' phase centered at a rotational flow [1, 2]. While the π phase jump at the resonance is also linked to the reversal of the current of vortex on each side of the resonant frequency. We further provide the pulse dynamics of this system which shows the potential for all-optical vortex switching.

REFERENCES

1. Miroshnichenko, A. E., S. Flach, and Yu. S. Kivshar, *Rev. Mod. Phys.*, Vol. 82, 2257, 2010.
2. Desyatnikov, A. S., Yu. S. Kivshar, and L. Torner, *Prog. Optics*, Vol. 47, 291–391, 2005.

ab Initio Electromagnetic Theory of Fano Resonances in Plasmonic Nanostructures

B. Gallinet and O. J. F. Martin
Nanophotonics and Metrology Laboratory, Swiss Federal Institute of Technology Lausanne, Switzerland

Abstract— We report on the derivation of an *ab initio* theory for Fano resonances in plasmonic nanostructures and metamaterials using the Feschbach formalism [1]. A general formula is obtained for the response of the system and general conclusions for the determination of the Fano resonance parameters are drawn, in particular on its modulation depth and asymmetry. Contrary to the original work of Fano, this theory includes losses in the materials composing the system. Analytical closed form expressions for the resonance parameters are obtained. This new resonance formula can also be derived from the classical model of two damped coupled oscillators, which demonstrates its applicability for a wide variety of non-conservative systems. Numerical calculations with a surface integral method [2] confirm the predictions of the electromagnetic theory and show in particular that the position and width of the Fano resonance can be extracted by fitting far-field spectra. This procedure is applicable not only for the interaction between radiative and non-radiative modes, but also for any continuum of radiative waves. We further show that specific features visible in the asymmetric lineshape far-field response of such structures originate from particular polarization distributions in their near-field. We relate the far-field spectrum to the near-field configuration of the radiative and non-radiative modes, and address the effect of their coupling on the frequency, width, asymmetry and modulation depth of the Fano resonance. This work presents a robust and consistent analysis of plasmonic Fano resonances and enables the control of their lineshape, based on Maxwell's equations. The insights into the physical understanding of Fano resonances gained this way will be of great interest for the design of plasmonic sensing platforms and metamaterials with tailored optical responses.

REFERENCES

1. Gallinet, B. and O. J. F. Martin, "*ab initio* theory of fano resonances in plasmonic nanostructures and metamaterials," *Phys. Rev. B*, Vol. 83, 235427, 2011.
2. Gallinet, B. and O. J. F. Martin, "Accurate and versatile modeling of electromagnetic scattering on periodic nanostructures with a surface integral approach," *J. Opt. Soc. Am. A*, Vol. 27, 2261–2271, 2010.

Fano Resonances in Disordered Systems at Bragg Wavelengths

A. N. Poddubny[1, 2], **M. V. Rybin**[1, 2], **M. F. Limonov**[1, 2], **and Yu. S. Kivshar**[1, 3]

[1]National Research University for Information Technology, Mechanics and Optics, Russia
[2]Ioffe Physical-Technical Institute, Russia
[3]Australian National University, Australia

Abstract— Fano resonance is a phenomenon, well-known across many different branches of physics [1]. Generally, the Fano resonance between continuum and discrete states manifests as an asymmetric profile of a narrow band in the spectrum. Here we demonstrate theoretically the novel type of Fano resonance, arising in the optical transmission spectra of the disordered photonic crystals at the Bragg wavelengths.

We consider one-dimensional photonic crystal consisting of alternating layers A and B. The structure is subjected to a specific type of disorder: the dielectric constants of the layers B fluctuate from layer to layer, different layers are statistically independent. All other parameters, i.e., layer thicknesses and dielectric constants of the layers A are not affected by the disorder. According to the general theory of one-dimensional disordered systems [2], transmission coefficient through such a structure decays exponentially with the number of layers and can be characterized by a certain localization length. Far from the Bragg wavelength the localization length weakly depends on the frequency and is determined by independent scattering from different layers B. At the Bragg condition one has to account for the multiple scattering events, leading to the quite unusual behaviour of the localization length.

Our rigorous theoretical analysis by means of the Fokker-Planck equation, confirmed by direct numberical simulations, reveals, that the frequency dependence of the inverse localization length near each Bragg resonance is given by a Fano-type expression. The Fano parameter, determining the shape of the spectrum, is controlled by the ratio of the thicknesses of the layers B and A. Depending on this ratio the localization can be either suppressed or enhanced at the Bragg condition. Fano-like resonances are also manifested in the transmission coefficient of the finite structure.

The microscopic origin of the effect is the interference between the fluctuations of the phase incursions of different layers B and the fluctuations of the reflection coefficients at the A/B boundaries. For the chosen type of the disorder, both these quantities stem from the same dielectric constants of the layers B, so they are correlated and can interfere. In particular, the suppression of the localization is a disordered counterpart of the Borrmann effect [3], well-known in the X-ray diffraction theory. Localization enhancement has another physical origin and is related to the fact, that the amplitude reflection coefficient of the B layers, averaged over disorder, is not zero. The interplay of these two effects leads to the asymmetrical Fano-like frequency dependence of the localization length.

Proposed theory explains recent experimental observations of Fano resonance in opals [4]. This type of Fano resonance has a general nature and can be manifested in a variety of the disordered systems, for instance, in the semiconductor superlattices with fluctuating carrier masses.

REFERENCES

1. Fano, U., "Effects of configuration interaction on intensities and phase shifts," *Phys. Rev. B*, Vol. 124, 1866, 1961.
2. Lifshits, I. M., S. A. Gredeskul, and L. A. Pastur, *Introduction to the Theory of Disordered Systems*, Wiley, New York, 1988.
3. Borrmann, G., "Die absorption von röntgenstrahlen im fall der interferenz," *Zeitschift für Physik*, Vol. 127, 297, 1950.
4. Rybin, M. V., et al., "Fano resonance between mie and bragg scattering in photonic crystals," *Phys. Rev. Lett.*, Vol. 103, 023901, 2009.

Investigation of Fano Resonance Induced by Higher-order Plasmon Modes on a Gold Disk with an Elongated Cavity

M. Amin and H. Bağcı
Division of Physical Sciences and Engineering King Abdullah
University of Science and Technology (KAUST), KAUST 4700, Thuwal 23955-6900, Saudi Arabia

Abstract— We demonstrate via simulations that a Fano resonance is observed in the extinction cross section spectrum of a gold nano-disk with an embedded non-concentric elongated cavity. The top view of the proposed designed and the plane wave incident on the device is shown in Fig. 1(a). The nonconcentric embedding of the cavity creates a thin wire on the narrower side between the disk and the cavity. According to plasmon hybridization theory, the strength of the coupling between the hybridized plasmon modes (of the disk and the cavity) depends on the thickness of this wire [1]. It has been shown previously that a gold disk with an embedded non-concentric circular cavity and a similar thin wire which allows for a strong hybridization, supports localized surface plasmon resonances over a band of frequency that includes visible and near infrared part of spectrum [2]. In this work, we extend the design of [2] to allow for the generation of a Fano resonance in the same region of the spectrum under normal incidence. The symmetry breaking non-concentric elongated cavity forces the otherwise dark higher order modes to brighten [3]. By tuning the parameters of the design, these narrow sub-radiant higher-order modes are moved closer to wide super-radiant dipole modes in the spectrum, which generates a Fano resonance dip. In Fig. 1, an example of this physical phenomenon is shown: The destructive interference between the hybridized dipole-dipole mode and the brightened quadruple-quadruple mode generates a Fano resonance in the visible range of the spectrum. An array of such device structure can be used to construct a highly dispersive medium, which might be useful in sensing and slow light applications [4].

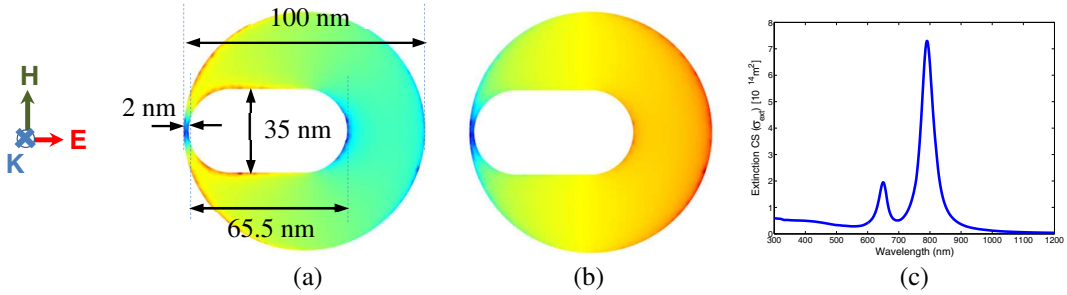

Figure 1: Device dimensions and the description of the plane-wave excitation are provided in (a). The thickness of the disk is 10 nm. The surface charge distributions at 642 nm (the peak where quadrupole modes hybridize) and 798 nm (at the peak where dipole modes hybridize) are shown in (a) and (b), respectively. (c) Extinction cross section spectrum of the device is presented in (a).

REFERENCES

1. Prodan, E., C. Radloff, N. J. Halas, and P. Nordlander, "A hybridization model for the plasmon response of complex nanostructures," *Science*, Vol. 302, 419–422, 2003.
2. Amin, M. and H. Bagci, "Scattering properties of vein induced localized surface plasmon resonances on a gold disk," *8th Int. Conf. High Speed Optical Network Enabling Tech.*, Riyadh, 2011.
3. Habteyes, T. G., S. Dhuey, S. Cabrini, P. J. Schuck, and S. R. Leone, "Theta-shaped plasmonic nanostructures: Bringing "dark" multipole plasmon resonances into action via conductive coupling," *Nano Lett.*, Vol. 11, 1819–1825, 2011.
4. Luk'yanchuk, B., N. Zheludev, S. Maier, N. Halas, P. Nordlander, H. Giessen, and C. Chong, "The Fano resonance in plasmonic nanostructures and metamaterials," *Nat. Mater.*, Vol. 9, 707–715, 2010.

Classical Analog of Electromagnetically Induced Absorption in Plasmonics

Harald Giessen[1], **Richard Taubert**[1], **Mario Hentschel**[1], **and Jürgen Kästel**[2]

[1]4th Physics Institute, University of Stuttgart, Germany
[2]DLR, Institute of Technical Physics, Stuttgart, Germany

Abstract— The ability to manipulate the phase shift between two coupled plasmonic resonances in a controlled fashion has been unavailable up to now. Here we present a strategy to overcome this limitation by employing the benefits of near-field coupling on the one hand and retardation effects due to far-field coupling on the other hand. We theoretically and experimentally demonstrate that in the intermediate regime the coupling of a broad dipolar to a narrow dark quadrupolar plasmon resonance is possible while simultaneously allowing for a retardation-induced phase shift. This leads to constructive interference and enhanced absorption. The observed phenomena can thus be termed classical analog of electromagnetically induced absorption.

Over the past decade, an extensive amount of research has been carried out on near-field coupling of noble metal nanoparticles. A plethora of intriguing coupling phenomena has been theoretically predicted and experimentally realized. One of the most exciting is the realization of the classical analog of electromagnetically induced transparency (EIT) in a plasmonic system [1]. EIT is an effect which originates from interference of two different excitation pathways. The coupling of a bright and a dark resonance can lead to destructive interference of the excitation pathways giving rise to a sharp peak of nearly perfect transmission within a broad transmittance dip.

One could, however, also change the phase of the interaction to realize constructive interference and, hence, achieve an enhancement of absorbance. Electromagnetically induced absorption (EIA) has been investigated in atomic physics. Instead of observing enhanced transmission like in the case of EIT, the coherent coupling to the dark state results in a narrow peak of enhanced absorbance on top of the broad dipolar absorbance feature.

Here, starting from the atomic physics concept of EIA, we introduce a plasmonic system which can be regarded as its classical analog [2]. In our plasmonic system, bright and dark transitions are realized by metallic nano-cut-wires: a dipole wire for the bright transition which is stacked on top of a quadrupole wire pair representing the dark transition.

By increasing the lateral displacement of the dipole, electromagnetic coupling between dipole and quadrupole is possible. This system is similar to the one that has been used to obtain the plasmonic analog of EIT [1], however, in that case the coupling between dipole and quadrupole was ccomplished solely by near-field coupling. Our coupling scheme relies on an intermediate coupling regime, where near-field effects still play a role, so that coupling to the quadrupole is still possible, but simultaneously retardation effects, which are characteristic for a travelling wave, are already relevant.

REFERENCES

1. Liu, N., L. Langguth, T. Weiss, J. Kätel, M. Fleischhauer, T. Pfau, and H. Giessen, "Plasmonic analogue of electromagnetically induced transparency at the Drude damping limit," *Nature Materials*, Vol. 8, 758, 2009.
2. Taubert, R., M. Hentschel, J. Kätel, and H. Giessen, "Classical analogue of electromagnetically induced absorption in plasmonics," 2011, submitted.

Session 4A3a
Imaging and Detection, Inverse Problem

Design of Undersampled Digitally Heterodyned SFGPR with Variable Sampling Frequency

D. Adirosi[1], **G. Alberti**[2], **and G. Galiero**[2]

[1]Thales Alenia Space Italia, Italy
[2]Consortium for Research on Advanced Remote Sensing Systems — CO.RI.S.T.A, Italy

Abstract— In [1] a new architecture of an Undersampled Digitally Heterodyned SFGPR with variable sampling frequency was presented. The key aspects and the advantages of the new architecture were presented and discussed: signal generation by means of DAC; undersampling of the echoes by means of a large bandwidth ADC with a planned step by step varying sampling frequency; digital quadrature demodulation of the undersampled echoes.

The SFGPR architecture presented had the following advantages:

- Absence of a synchronism chain, generally used in SFGPR to get a phase reference of the transmitted signal [3];
- Simplified RF front end: both Tx and Rx chains are substantially constituted by an amplifier and a filter; this is allowed by the undersampling of the received echoes;
- Simplified Frequency Generation Unit;
- Substantial reduction of the power consumption and weight due to the great simplification brought in the RF front end;

It was also remarked that the achievement of the mentioned goals had been possible by moving SFGPR complexities from the analog domain into the digital one.

In [2] the proposed SFGPR architecture was analysed for what concerns the aliased images. The necessity of the analysis performed was due to the wide bandwidth needed to be generated to achieve high resolution. The mentioned intrisic advantages achievable by moving GPR complexities from the analog domain into the digital one have the side effect to potentially "move" aliased images into the useful intermediate frequency band if a suitable frequency plan was not performed in advance. The analysis showed that a successful result is achievable with the aid of ad hoc software tools and that the characteristics of the filtering to be performed both in the analog domain (anti-aliasing LPF at DDS output) and in the digital one (LPF at the quadrature downconversion output) were easily achievable: results showed that the digital transition bandwidth can be increased from 0.5 MHz to 1.5 MHz.

In [1] were also showed the results of the simulations of a synchronism detector circuit to be implemented in a FPGA. This detector circuit was needed in that the sampling frequencies are different between them (on a step by step basis) and they are not integer multiple of the FPGA reference clock frequency; so it is necessary a circuit that determine when both are phase alligned. The mentioned synchronism detector circuit was designed by starting from phase detector circuits of digital PLLs [4] and adapted to the needs of the presented architecture.

In this paper, a preliminary design of a SFPGR based on the previously proposed architecture is shown. The whole set of parameters characterising the performances of a GPR (step frequency, first frequency to generate, number of steps,) is optimised by means of a "brute force" approach by using the software tools previously developed in a high level language (LabViewTM). The results of the simulations of the whole post-processing chain, from the undersampling of the step frequencies to their quadrature demodulation and processing to synthesize simulated target, are shown to fix the performances achievable with the chosen set of parameters.

Furthermore the design of the control logic of the whole SFPGR is made in VHDL and simulations have been performed in order to test its behaviour by means of standard VHDL simulation tools. Main results of these simulations will be presented.

These results show that the architecture proposed performs as foreseen.

REFERENCES

1. Adirosi, D., G. Alberti, and G. Galiero, "Undersampled digitally heterodyned SFGPR with variable sampling frequency," *PIERS Online*, Vol. 7, No. 1, 47–50, 2011.
2. Adirosi, D., G. Alberti, and G. Galiero, "'Spurious analysis of a wide bandwidth undersampled digitally heterodyned SFGPR," *Proc. 6th International Workshop on Advanced Ground Penetrating Radar, IWAGPR 2011*, Aachen, Germany, Jun. 2011.

3. Alberti, G., L. Ciofaniello, G. Galiero, R. Persico, and M. Sacchettino, "An Italian experience on stepped frequency GPR," *Progress In Electromagnetic Research Symposium*, PISA, Italy, Mar. 2004.
4. Best, R. E., *Phase-locked Loops: Design, Simulation and Aplications*, McGraw-Hill Professional, 2007.

Investigation on Passive Multi-channel Millimeter Wave Images for Concealed Object Detection

Seokwon Yeom and Dong-Su Lee
Division of Computer and Communication Engineering, Daegu University
15 Gyeongsan Gyeongbuk, 712-714, South Korea

Abstract— The use of millimeter wave imaging has been increased for military and security applications. Millimeter wave can penetrate clothing to detect the concealed metal or man-made objects. Moreover, passive millimeter wave imaging generates interpretable imagery under low-visibility conditions such as rain, fog, smoke, and dust. Passive millimeter wave imaging has advantages to operate as a stand-off type sensor in both indoor and outdoor open spaces. However, due to low signal level and resolution, the image analysis and processing are required to enhance the system capability. In this presentation, we investigate the effects of different wavelengths and polarization on passive millimeter wave imaging. The passive millimeter wave imaging system is equipped with a 500 mm diameter antenna and composed of four channels; 3 and 8 mm wavelengths with horizontal and vertical polarization for each. The imaging system captures various metal and man-made object concealed in a human subject as well as outdoor landscape. The histogram of images is analyzed and the normality is tested. The multivariate Gaussian mixture distribution is adopted to model the histogram of the images. It will be shown that the Gaussian mixture model is appropriate for image processing applications such as the segmentation of the concealed object and background.

Automatic Non-destructive Imagingsystem for Spot Welding Using a Magnetic Flux Leakage Method

Kenji Sakai[1], **Kosuke Miyake**[1], **Toshihiko Kiwa**[1], **Yoshinobu Hirano**[2], **and Keiji Tsukada**[1]

[1]Okayama University, Japan
[2]Ohashi engineering Co. Ltd., Japan

Abstract— Spot welding is widely used in various industrial fields, such as automobile industry, and its evaluation should be fast and visualizedfor a practical evaluation. However, the present evaluation system of spot welding is expensiveor required expertise. Therefore, a imaging system for spot welding evaluation with fast inspectiontime is required. In the previous study, we have reported that the spot welding can be evaluated using a magnetic flux leakage method. Thus, in this study, we developed automatic non-destructive imaging system of spot welding which enables fast inspection.

The developed system consists of sequencer and X-Y stage with a probe which applies the magnetic field to the spot welding and detects the leaked magnetic field automatically controlledby PC. The magnetic field is applied by coil wound on the probe, and the magnetic flux leakage is detected by a magneto resistance sensor (MR sensor) attached to the probe. The X-Y stage was moved by X- and Y-axis motor controlled by sequencer, and the probe moves to the position where the magnetic flux leakage is measured. Then, the magnetic field is applied and the detected magnetic flux leakage was recorded in the PC. This measurement process was repeatedautomatically at various points around the spot welding, and multipoint mapping of 11×11 points around spot welding was obtained.

The measured sample used in this study was two iron plates joined by spot welding and the welding time was varied to investigate the quality of spot welding. The detected magnetic field increased with increasing the welding time although the sample with short welding time had low magnetic field strength. This difference is caused by the difference of permeability at the spot welding and it was found that the permeability variation in spot welding could be visualizedand evaluated automatically using the developed system.

To clarify the correlation betweenthe detected magnetic field and the quality of spot welding, joint strength of spot welding was measured using tensilestrength tests. Consequently, the joint strength was high when the welding time was long.These results indicate that the detected magnetic field strength is correlated with the joint strength of spot welding.Therefore, the developed system can be used as a practical non-destructive inspection system, reducing the time and labor for spot welding evaluation.

Simulation Tool for the Error Estimation of the Probe Tilt in Eddy Current NDT Context

Laurent Santandrea[1], **Yann Le Bihan**[1], **Christophe Reboud**[2], **and Pierre Calmon**[2]

[1]Laboratoire de Génie Electrique de Paris, France
[2]CEA-LIST, France

Abstract— Finite Element Method (FEM) and Volume Integral Method (VIM) are two popular approaches for the simulation of Eddy Current (EC) Non-Destructive Testing problems. Modeling tool can provide information for design and characterization of EC probes. Particularly, they prove useful to evaluate the influence of probe tilt on the measurement. In this communication, we propose a comparison of two different approaches for probe tilt error estimation. The first one is the FEM solver DOLMEN using the two combined dual potential formulations, which is currently being connected to the CIVA simulation platform dedicated to NDT, within the CIVA 2012 project. The second one is a combination of Truncated Region Eigenfunctions expansions for the computation of electric field and the Volume Integral Method for the computation of the coil response to a flaw. After the comparison between simulated results and experimental data in the case of an air-cored coil, simulation of the effect of a ferrite core is presented with the DOLMEN code.

Checking of Combustion Chamber of Rocket Using ECT with AMR Sensor

D. F. He[1], **M. Shiwa**[1], **J. Takatsubo**[2], **and S. Moriya**[3]

[1]National Institute for Materials Science, Sengen 1-2-1, Tsukuba 305-0047, Japan
[2]Advanced Industrial Science and Technology, 1-2-1 Namiki, Tsukuba 305-8564, Japan
[3]Japan Aerospace Exploration Agency, Sengen 2-1-1, Tsukuba 305-8505, Japan

Abstract— Eddy current testing (ECT) system with high sensitive AMR sensor was developed. The magnetic field resolution of the AME sensor was about $12\,\mathrm{pT}/\sqrt{\mathrm{Hz}}$ at the frequencies above 1 kHz. A 20 turn circular coil with the diameter of 3 mm was used to produce the excitation field. A chamber type specimen made of copper alloy was prepared to simulate the cooling grooves of the combustion chamber of liquid rocket. Artificial defects with the depths of 30%, 50% and 70% of the wall thickness were made in the bottom of the cooling grooves. The width of the defects was 0.2 mm and the lengths of the defects were 3 mm, 5 mm and 10 mm respectively. The AMR sensor was located inside of the chamber and close to the inner surface of the chamber. The scanning was realized by rotating the chamber with a motor. To reduce the influence of lift off variance during scanning, a dual frequency excitation method was used. For the higher frequency (20 kHz) eddy-current signal, due to the smaller penetration depth, it only measured the surface condition and the variance of the lift off; for the lower frequency (2 kHz) eddy-current signal, due to the bigger penetration depth, it also measured the defect signals except of the surface condition and the lift of variance. By subtracting the eddy-current signals of the two frequencies and choosing a proper subtraction factor, the influence of the lift-off variance could be reduced. Using our dual frequency ECT system, all the artificial defects could be successfully detected and the influence of lift-off variance could also be reduced well.

Fast Numerical Shape Reconstruction of Highly Conductive Submicron Particles on Substrates

Mirza Karamehmedović[1], **Poul-Erik Hansen**[2], **and Thomas Wriedt**[3]

[1]Department of Process and Chemical Engineering, University of Bremen, Germany
[2]Danish Fundamental Metrology, Technical University of Denmark, Denmark
[3]Department of Process and Chemical Engineering, University of Bremen, Germany

Abstract— Optical characterisation of nano- and submicron structures often requires rapid numerical solution of inverse scattering problems. This is the case, e.g., in the production and quality control of functional nanomaterials. A commonly used approach in inverse scattering is the Kirsch-Kress Method (KKM). Here, the scattered near field is reconstructed from the given measurement data using a forward scattering model based on layer potentials, whereafter the position and shape of the scatterer are estimated by minimising a boundary condition error within a class of admissible boundaries.

In KKM, the radiation integrals representing the reconstructed scattered near field are used in the objective functional for the boundary-error minimisation, and they are therefore repeatedly evaluated during the inversion. Thus, the efficiency of the computation of these integrals greatly influences the overall efficiency of the inversion method. This is especially important in the shape estimation of structures *on substrates*, since the scattered near field in this case is given by radiation integrals that involve half-space Green's functions. Such Green's functions are namely given by Sommerfeld-type integrals, and are therefore computationally expensive.

We here present an efficient Kirsch-Kress type numerical method for shape reconstruction of highly conductive penetrable nano- and submicron particles on substrates. To speed up the inversion, the method eliminates or simplifies numerical integration wherever possible. First, to avoid integration of surface current densities, the forward model is based on the so-called Method of Auxiliary Sources (MAS). Here, the surface current densities in the radiation integrals are approximated by spatially impulsive sources: line currents in the 2D case and Hertzian dipoles in the 3D case. Next, matching of the sources with the measured scattered far field is done at discrete testing points, and finally, the relevant half-space Green's functions are approximated using Fresnel reflection and complex image theory. The particles to be reconstructed are either approximated as perfectly electrically conducting (PEC), or an appropriate Surface Impedance Boundary Condition (SIBC) is used.

We apply the inversion method to actual angular-resolved bistatic scatterometric data provided by the Danish Fundamental Metrology. Here, cross-sections of three platinum (Pt) submicron wires on silicon (Si) substrate are estimated based on the scattered far-field intensity measured in a narrow angular range. The samples are illuminated by a 325 nm HeCd laser. In addition, we present an analysis of the accuracy and efficiency of the inversion for families of circular PEC and silver (Ag) submicron wires on Si substrate, using numerically simulated measurement data. An example of shape estimation of a 3D Ag submicron particle on an Si substrate is also shown. Finally, we discuss the suitability of different approximations of the half-space Green's function in the forward model.

Session 4A3b
Innovative Instruments and Processing for Understanding Phenomenology through Remote Sensing

Designing for Science: Combining Geophysical and Engineering Models for Space Mission Design

Stephen D. Wall
Jet Propulsion Laboratory, California Institute of Technology
Mail Stop 202-204, 4800 Oak Grove Drive, Pasadena, CA 91101, USA

Abstract— Designers of scientific payloads for spaceborne remote-sensing missions typically design to engineering parameters such as mass, power, datarate and cost. Thus (in a highly simplified abstraction) the optimal mission is one that has minimum cost, mass and power, with maximum datarate. Payload requirements often are treated as constraints on the engineering design, largely because the connection between scientist/user need and spacecraft design has been somewhat vague. This situation makes it difficult to design missions with the scientist/user directly participating, and often creates animosity between engineers and scientists.

In the past few decades, the use of sophisticated models of target phenomenology in the remote sensing science community has emerged. Largely for the purpose of analyzing data, researchers model a target parametrically — for example, a natural surface might be modeled as having an RMS roughness and a related correlation length — and simulate the target's electromagnetic signature in a remote sensing instrument or instruments. Once validated, these models are used to predict the instruments' performance. They are also incorporated into predictive models such as those used for weather forecasting.

We have proposed to combine engineering design models with phenomenology models to allow designers to optimize spacecraft, payloads and missions to the target parameters of interest, as a logical next step in JPL's conceptual design process. Thus, a mission whose purpose is to measure atmospheric CO concentration in urban areas could be optimized to minimize uncertainty in that measurement, using both traditional and innovative optimizing algorithms. This would be made possible by merging the two model types and varying, in the above example, spacecraft design parameters (e.g., attitude control accuracy, lifetime) and payload design parameters (e.g., number of spectral channels, spectral bandwidth, signal-to-noise ratio) to directly minimize measurement error. Finally, measurement accuracy can be compared with total mission lifecycle cost and the appropriate design point chosen.

We will show some examples of this kind of model aggregation and some preliminary results, together with a vision showing how such a "supermodel" could be used in practice. The research described in this paper was carried out at the Jet Propulsion Laboratory, California Institute of Technology, under a contract with the National Aeronautics and Space Administration.

Interpreting Titan's Surface Geology from Cassini RADAR Observations

R. M. Lopes[1], **A. Le Gall**[2], **M. Janssen**[1], **R. Kirk**[3], **O. Aharonson**[4], **A. Hayes**[4], **K. L. Mitchell**[1], **E. R. Stofan**[5], **J. Radebaugh**[6], **S. Wall**[1], **C. Wood**[7], **and The Cassini RADAR Team**[1]

[1]Jet Propulsion Laboratory
California Institute of Technology, Pasadena, USA
[2]LATMOS, IPSL, Paris, France
[3]US Geological Survey, Flagstaff, USA
[4]California Institute of Technology, Pasadena, USA
[5]Proxemy Research, Bowie, USA
[6]Brigham Young University, Provo, USA
[7]Wheeling Jesuit University, Wheeling, USA

Abstract— The Cassini Titan Radar Mapper has been the prime instrument used to study Titan's surface geology, as it can penetrate Titan's haze and reveal underlying features. However, interpreting the data presents some unique challenges. The instrument acquires data in several modes including SAR, altimetry, radiometry, and scatterometry that have widely differing resolutions and respond to different surface characteristics. The SAR images, which have the highest resolution and provide the bulk of information about geologic units, can only distinguish between features if their backscatter characteristics or topographic slopes are sufficiently different from those of surrounding terrains. Structures are more easily recognized when oriented perpendicular to the radar's look direction. At Titan, the SAR mode of the RADAR instrument is used at altitudes under $\sim 4,000$ km, resulting in resolutions ranging from ~ 300 m to > 2 km, which is in some places insufficient to identify different geologic units on the surface. On Titan, the candidate surface materials (water ice, water-ammonia ice and other ice mixtures, hydrocarbons, and tholins) are different from the rocky surfaces more usually imaged with radars; in particular, scattering from the subsurface is thought to be significant. We have been able to identify a wide variety of geologic features on Titan's surface using SAR swaths, which now cover $\sim 47\%$ of the surface. The data are distributed over a wide latitudinal and longitudinal range, enabling some conclusions to be drawn about the global distribution and significance of processes. They reveal a geologically complex surface that has been modified by all the major geologic processes seen on Earth. In terms of global areal distribution, mountainous terrains (including the large Xanadu radar-bright region), dunes, and plains cover more area than other identified geologic units, $\sim 14\%$, 18%, and 14% respectively. In terms of latitudinal distribution, dunes and mountainous terrains are located mostly at low latitudes (less than 30 degrees), with almost no dunes being present above 60 degrees, while plains that appear bland at radar wavelengths are seen mostly at mid-latitudes. Channels formed by fluvial activity are present at all latitudes, but lakes filled with liquid are only found at high latitudes (above 60 degrees). Impact structures are mostly located at low latitudes, with no confidently identified craters poleward of 60 degrees, possibly indicating that more resurfacing has occurred at higher latitudes. Putative cryovolcanic features are not ubiquitous and some could actually be fluvial in origin. The Sotra Facula region is currently the best candidate for cryovolcanic terrain, consisting of a mountain with adjacent pit and flow-like features. We examine temporal relationships between units and conclude that aeolian and fluvial/pluvial/lacustrine processes are the most recent, while tectonic processes that led to the formation of mountainous terrains and Xanadu are likely the most ancient. Mountainous terrains, which along with Xanadu may have at least in part a tectonic origin, are radar-bright and radiometrically distinct from most other areas. They may have been washed clean of organic particulates by methane rains. Preliminary correlations between geologic units and surface properties derived from the radiometry measurements (brightness temperature, effective dielectric constant, and degree of volume scattering) will also be presented.

Generating Surface Fractal Dimension Maps from SAR Data

G. Di Martino[1], **G. Franceschetti**[1,2], **A. Iodice**[1], **D. Riccio**[1], **G. Ruello**[1], **and I. Zinno**[1]

[1]DIBET, Università di Napoli "Federico II", Via Claudio 21, Napoli 80125, Italy
[2]Jet Propulsion Laboratory, Pasadena, CA 91109, USA

Abstract— A huge amount of Synthetic Aperture Radar (SAR) images relevant to every part of the Earth and other solar system planets, are presently available, with various resolutions depending on the acquiring sensor. But models, techniques and tools to allow generating value added reliable products starting from SAR data are basically missing, in particular if single SAR images are analyzed. Concerning SAR images of natural areas, it is essentially possible to reliably identify only macroscopic deterministic topological features (i.e., shape of main reliefs) of the observed areas, also distinguishing superimposed man-made structures, whenever present.

In this paper, by exploiting the currently available SAR images, the extraction of meaningful stochastic parameters relevant to geomorphologic features of the observed surface (at different scales depending on the corresponding SAR resolution) is presented: fractal models and tools are adopted. The proposed technique is based on the inversion of the complete direct model that directly links stochastic fractal parameters of the natural surface to the stochastic parameters of the corresponding SAR image [1]. The observed natural surface is modeled via a fractional Brownian motion (fBm) twodimensional stochastic process [2, 3]. In this paper, the key parameter to be estimated directly from the SAR image is the fractal dimension D, that is strictly related to the roughness and the geomorphologic characteristics of the surface observed by the sensor [2, 3].

Let us consider the Power Spectral Density (PSD) of a range cut of the SAR image of a natural scene. We show that, in the small slope regime and in an appropriate range of spatial frequencies, this PSD presents a power-law behavior [1]. Consequently, in a log(wavenumbers)-log(|spectrum|) plane, a linear behavior is obtained, whose slope is related to the fractal dimension the scene under survey. Thus a linear regression technique on the range spectrum of homogeneous areas of the SAR image is implemented within a window sliding over the image: at each window position, the local fractal dimension is estimated. The Capon estimator is used for the spectral estimation [4]; several range cuts spectra are averaged to obtain the mean PSD; the linear regression is implemented to get the final fractal map of the surface.

In conclusion, we here present a processing technique that, starting from Single-Look-Complex (SLC) SAR data, generates valuable information, with precise physical meanings unveiled by the fractal geometry. The presented procedure is fully automatic, and makes use of only a single SAR image. It is then eligible for natural disasters monitoring, land-use applications and space exploration.

Full details, along with applications to SAR data, are provided during the conference presentation.

REFERENCES

1. Di Martino, G., D. Riccio, and I. Zinno, "SAR imaging of fractal surfaces," *IEEE Trans. Geosci. Remote Sens., IEEE Early Access*, in Print.
2. Mandelbrot, B. B., *The Fractal Geometry of Nature*, New York, Freeman, 1983.
3. Franceschetti, G. and D. Riccio, *Scattering, Natural Surfaces and Fractals*, Academic Press, Burlington, MA, USA, 2007.
4. Austin, T., A. W. England, and G. H. Wakefield, "Special problems in the estimation of power-law spectra as applied to topographical modeling," *IEEE Trans. Geosci. Remote Sens.*, Vol. 32, No. 4, 928–939, July 1994.

An Investigation into the Detection of Possible Gamma Rays from Lightning at Venus

Ralph D. Lorenz and David J. Lawrence
Applied Physics Laboratory, Johns Hopkins University, USA

Abstract— Venus lightning remains mysterious, with several claimed electromagnetic indications of discharges but predominantly negative optical searches. In the mid-1990s, earth-orbiting astrophysical observatories surprisingly discovered a new window on lightning — terrestrial gamma ray flashes (TGFs) produced by the bremmstrahlung of relativistic electrons accelerated upwards from the discharge. Could this phenomenon occur on Venus?

In fact, the Pioneer Venus Orbiter (PVO), in orbit at Venus for some 14 years, carried an Orbiter Gamma Ray Detector (OGBD) for astrophysical studies. Since PVO burned up on entry in 1992, before TGFs were discovered, we do not believe the OGBD data has been examined for Venusian flashes. We are now correlating the OGBD data from NSSDC with the ephemeris from the PDS Planetary Magnetospheres node to search for variations in count rate that may be associated with altitude, location and time of day.

Additionally, we have set up a gamma-ray propagation model for the Venus atmosphere using both pure CO_2 and full gas compositions and the full photon and electron physics in the MCNPX code (Monte Carlo Neutral Particle eXtended).

Whether or not the OGBD data (which is coarsely time-averaged, and shows variations associated with cosmic ray particle fluxes which correlate with those measured on the ground at Earth) shows evidence of flashes, the modelling results (covering source altitudes ranging from 65–90 km, and energies from 0.1–9 MeV) will indicate whether a gamma ray detector on a future mission may be useful for studying Venusian lightning. This exercise also highlights the lost information on binning and the importance of careful archiving of planetary datasets.

SWB: An Analysis and Visualization Tool for COSMO SkyMed

V. A. Loré[1], **G. Milillo**[2], **P. Milillo**[3], **A. Valentino**[1], **and G. Franceschetti**[4]

[1]INNOVA Consorzio per L'informatica e la Telematica s.r.l., Italy
[2]Agenzia Spaziale Italiana (ASI), Italy
[3]Facoltà di Scienze Matematiche, Fisiche e Naturali Dipartimento Interateneo di Fisica
Università Degli Studi di Bari, Italy
[4]Dipartimento di Ingegneria Elettronica e delle Telecomunicazioni
Università di Napoli "Federico II", Italy

Abstract— In recent years there has been a significant increase in the availability of data for Earth Observation (EO) and SAR in particular. The availability of high quality and low cost data will be further increased with the launch of SENTINEL missions.

It is important, therefore, to have advanced applications that can take advantage of this great amount of data and also have software (SW) tools that enable scientists and engineers to process and analyze data and to develop new and innovative applications.

The panorama of scientific SW for OT (commercial or not) had a great evolution in recent times as well and it is in this context that the "SAR WorkBench" (SWB) SW is placed.

SWB was initially developed in the framework of the Italian Space Agency (ASI) projects to overcome any lack of specific SW tools for COSMO SkyMed data in early stages of the mission when other SW on the market were still not ready to provide and adequate support.

SWB is an application for the analysis and post processing of multi-mission SAR data. It is modular and has a plug-in architecture. Core modules provide functionalities for ingestion/data exchange, QA (Quality Analysis) and basic data processing SWB also provides a powerful viewer for fast visualization and browsing of large sized products.

Currently already exists an extension module that enable SWB to exploit some of the features and processing capabilities of the powerful Orfeo ToolBox (http://orfeo-toolbox.org) and new extension modules for interferometry and polarimetry are planned.

One of the key features of SWB is that it is highly programmable and it can be extended writing new plug-ins in a high level programming language (www.python.org) that has good extensions for scientific programming (www.scipy.org). The resulting environment is very close to what scientists are used to but it do not requires expensive SW licenses.

Session 4A4
Antenna Theory and Radiation 1

High-gain and Light-weight Antenna for Radar System Using a Horn Covered with Curved Woodpile EBG

S. Kampeephat, **P. Krachodnok**, **and R. Wongsan**
School of Telecommunication Engineering, Institute of Engineering
Suranaree University of Technology, Nakhon Ratchasima, Thailand

Abstract— A high-gain and light-weight antenna using a horn covered with curved woodpile Electromagnetic Band Gap (EBG) is presented. The proposed antenna has the advantages of high gain, low profile, and low cost for fabrication. Moreover, it provides the moderately light weight compare to the other antennas in radar system at present. Because of, it can use the small mechanism system to rotate its antenna, as in the past. A Computer Simulation Technology (CST) software has been used to compute the return loss, VSWR, radiation pattern, elevation beamwidth (−3 dB), azimuth beamwidth (−3 dB) and gain of the antenna. The bandwidth, at S_{11} (−10 dB), is between 8 to 12 GHz with a gain more than 20 dB.

Gain Improvement of Curved Strip Dipole Using EBG Resonator

N. Fhafhiem, **P. Krachodnok**, **and R. Wongsan**
School of Telecommunication Engineering, Suranaree University of Technology
Nakhonratchasima 30000, Thailand

Abstract— In this work, the electromagnetic band gap (EBG) and metallic reflector plane are used for cavity wall of a curved strip dipole. The reflection phase of cavity walls is important for the cavity height (h) calculation, which has an effect on the antenna characteristic. The simulation results found that the cavity height of 0.63λ is most direction gain of 9.3 dB. The HPBW in E- and H-plane are 59.1° and 71.4°, respectively. Moreover, the patterns have low side lobe, so we can estimate that the structure volume is well designed. The proposed antenna covers bandwidth of 2.2 GHz–2.85 GHz that suitable for wireless communication and RFID system.

A New Feed for Reflector Based 100 Ω Impulse Radiating Antenna

Dhiraj K. Singh[1], **D. C. Pande**[1], **and A. Bhattacharya**[2]

[1]Electronics & Radar Development Establishment, Bangalore, India
[2]Indian institute of Technology, Kharagpur, West Bengal, India

Abstract— Improvement in the feeding structure of the reflector based impulse-radiating antenna (IRA) is attempted to reduce the input impedance of the conventional 200 Ω-conical plate-fed IRA. A novel feeding structure known as asymptotic conical dipole (ACD) was designed to get 100 Ω input impedance for reflector IRA. ACD-fed IRA has been analyzed using the Finite Difference Time Domain (FDTD) method and the result obtained shows better gain than a conventional conical taper-fed IRA. Moreover, a half ACD-fed IRA can give an input impedance of nearly 50 Ω which can be readily used with most of the single ended instrumentation without using a 50–200 Ω BALUN as commonly done with IRA.

A Dielectric Loaded HMSIW *H*-plane Horn Antenna

S. A. Razavi and M. H. Neshati
Department of Electrical Engineering, Ferdowsi University of Mashhad, Iran

Abstract— Recently the substrate integrated waveguide (SIW) technology has widely used in implementation of microwave devices and antennas. Horn antenna is one of the antennas implemented by this technology. In [1], an integrated H-plane horn antenna is proposed. In [2], we proposed a new scheme for H-plane horn antenna in order to reduce its size while its radiation characteristics remain unchanged and we called it "HMSIW H-plane horn antenna". This antenna has a wide beamwidth in E-plane. In this paper, a dielectric load is added to the proposed antenna in order to achieve narrow beamwidths both in E-plane and H-plane. A coaxial line is used as the feed to avoid parasitic radiation (witch may degrade the radiation pattern of the horn antenna in E-plane) and high conductor loss at high frequencies. A 1×4 array of the dielectric loaded antenna is also designed in order to investigate the usefulness of the presented antenna in an array. The antenna is designed for about 28 GHz and all the simulations are done with HFSS software.

REFERENCES

1. Li, Z. L. and K. Wu, "A new approach to integrated horn antennas," *Proceedings of International of Symposium on Antenna Technology and Applied Electromagnetics*, 535–538, Jul. 2004.
2. Razavi, S. A. and M. H. Neshati, "Coaxial line fed HMSIW H-plane horn antenna," *Progress In Electromagnetics Research Symposium Abstracts*, Suzhou, China, Sep. 12–16, 2011.

On the Radiation Fields of the Hyperbolic Helical Antenna

S. Adeniyi Adekola[1, 2], **A. Ike Mowete**[1], **and A. Ayotunde Ayorinde**[1]

[1]Department of Electrical and Electronics Engineering
Faculty of Engineering, University of Lagos, Lagos, Nigeria
[2]Department of Electrical and Electronics Engineering
Niger Delta University, Wilberforce Island, Yenegoa, Nigeria

Abstract— Cylindrical helical antenna structures of various cross-sections have received extensive analytical attention in the open literature, starting with the 1947 contributions of Kraus [1], through those of Wong and Loh [2], to Adekola et al. [3], to mention a few. One geometry that has yet, to the best of our knowledge, to be treated is that of the helix, wound on a hyperbolic cylinder, which is the focus of this presentation. Utilizing the circuit-geometric approach offered by the method of moments, the paper models the hyperbolic helical antenna as a configuration of two thin-wire elements, one or both of which may be excited. Analysis followed that described elsewhere [3], and the computational results obtained for the configuration in which only one of the two elements has a delta-gap excitation suggest that the hyperbolic helical antenna of this type should be particularly suitable for applications requiring multi-lobed radiation patterns.

REFERENCES

1. Kraus, J. D., "Helical beam antenna," *Electronics*, 109–111, 1947.
2. Wong, J. Y. and S. C. Loh, "Radiation field of an elliptical helical antenna," *IRE Trans. Ant. & Prop.*, Vol. 7, 46–52, 1959.
3. Adekola, S. A., A. I. Mowete, and A. A. Ayorinde, "Compact theory of the broadband elliptical helical antenna," *European Journal of Scientific Research*, Vol. 31, No. 3, 446–490, 2009.

Directivity Characteristics of a Circular-loop Zigzag Thin-wire Antenna

S. A. Adekola[1, 2], **A. Ike Mowete**[1], **and H. A. Muhammed**[1]

[1]Department of Electrical and Electronics Engineering, Faculty of Engineering
University of Lagos, Lagos, Nigeria
[2]Department of Electrical and Electronics Engineering, Niger Delta University
Wilberforce Island, Yenegoa, Nigeria

Abstract— This paper develops an analytical model, based on the Electric Field Integral Equation (EFIE) formulation, for the analysis of a circular-loop zigzag antenna excited by a current that is uniformly distributed along its axis. A closed-form expression is derived for the antenna's directivity, and computational results obtained from the expression suggest that the antenna's directivity is strongly dependent on the electrical length of the zigzag, particularly when the length is in the neighborhood of about 60% of the loop radius. The paper also discusses analytical and computational results concerning the antenna's radiation resistance, to characterize the efficiency of the circular-loop zigzag geometry as a radiator of radio-frequency energy.

Analysis of a Circular-loop Zigzag Thin-wire Antenna

S. A. Adekola[1, 2], **A. Ike Mowete**[1], **and H. A. Muhammed**[1]

[1] Department of Electrical and Electronics Engineering, Faculty of Engineering
University of Lagos, Lagos, Nigeria
[2]Department of Electrical and Electronics Engineering, Niger Delta University
Wilberforce Island, Yenegoa, Nigeria

Abstract— In this presentation, we develop an analytical model, using the electric field integral equation (EFIE) approach, for a folded zigzag thin-wire antenna, with the geometry of a circular-loop. Following a treatment described elsewhere [1], for the bi-elliptical torroidal helical antenna, the kernel of the integral expression for the magnetic vector potential for the problem is derived in a matrix format, through which distinct contributions to the radiation field by the circular-loop geometry and the zigzag emerge.

The computational results obtained for some input characteristics and the far-zone fields, for an assumed uniform current distribution, indicate that choice of number of zigzag sections provides the important possibilities of varying antenna's electrical length and controlling pattern directivity. Similar conclusions were arrived at by Zainud-Deen et al. [2], who investigated the performance features of zigzag antennas for portable radio equipment.

REFERENCES

1. Adekola, A., A. I. Mowete, and H. A. Muhammed, "A matrix-vector-potential analysis of the bi-elliptical toroidal helical antenna," *PIERS Proceedings*, to appear, Marrakesh, Morocco, 2011.
2. Zainud-Deen, S. H., K. H. Awadalla, A. L. Bahnacy, and H. A. Sharshar, "Performance analysis of zigzag antenna for portable radio equipment," *Antennas and Propagation Society International Symposium*, Vol. 1, 442–447, 1997.

On the Insulated Dipole Antenna in a Dissipative Non-conducting Medium

A. I. Mowete[1] and A. Ogunsola[2]

[1]Department of Electrical and Electronics Engineering, Faculty of Engineering
University of Lagos, Lagos, Nigeria
[2]Parsons Group International, Rail Transit Division, London, United Kingdom

Abstract— Using the quasi-static model earlier described elsewhere [1], this paper investigates the characteristics features of the fields radiated in the ambient medium, by the insulated thin-wire antenna, located in a dissipative dielectric medium. Accordingly, the dielectric insulation carried by the thin-wire dipole antenna is modelled by a volumetrically distributed polarization current, related to the distribution of current along the axis of the bare antenna, through the equation of continuity. Approximate expressions are subsequently derived for the axial and radial components of electric field intensity in the region occupied by the dielectric insulation, through which, by invoking boundary conditions appropriate to the material discontinuity, the fields in the ambient medium are characterized. As a test for the validity of the analytical results, computational results obtained from the expressions, for the case of the symmetric insulated antenna (half-wave dipole in an air-filled glass tube) are compared with those reported by Atlamazoglou and Uzonoglu [2], and the similarities in these results suggest that the quasi-static model is suitable for the use proposed by the paper.

REFERENCES

1. Mowete, I., A. Ogunsola, and L. Sandrolini, "A quasi-static theory for dielectric-coated thin-wire antenna structures," *Progress In Electromagnetics Research Letters*, Vol. 20, 45–54, 2011.
2. Atlamazoglou, P. E. and N. K. Uzonoglu, "A Galerkin moment method for the analysis of an insulated antenna in a dissipative dielectric medium," *IEEE Transactions on Microwave Theory and Techniques*, Vol. 46, No. 7, 988–997, 1998.

A Planar Resonator Antenna Using Folded Dipole with Reflective Walls

S. A-Sa, **P. Krachodnok**, **and R. Wongsan**
School of Telecommunication Engineering, Suranaree University of Technology
Nakhon Ratchasima 30000, Thailand

Abstract— A resonator antenna using a planar folded dipole with reflective walls is presented. A planar antenna comprising two back-to-back folded dipoles printed on a dielectric substrate and separated by a narrow rectangular ground plane is operated resonance frequency at 5.8 GHz. A highly directive radiation pattern is created due to the angle-dependent attenuation of the resonator antenna coupling to free space. The complete reflection phase for reflective walls is investigated through cavity height calculation. The simulation results found that the cavity height of 0.58λ is most direction gain of 12.97 dB. Effect of reflective walls length on the performance of the proposed antenna are also studied.

Reduction of EMI due to Antenna Radiation inside Complex PCB

Cheng-Wei Chen[2], **Dau-Chyrh Chang**[1], **Hsiao-Bin Liang**[2], **Chi-Hsiung Wang**[2], **and Tsan-Hung Wu**[2]

[1]Oriental Institute of Technology, Taiwan
[2]Climax Technology Co., Ltd., Taiwan

Abstract— In this paper, the reflector is adopted for changing the radiation pattern of a GSM PIFA antenna to reduce the environmental impact on radiation efficiency. The antenna passive and active parameters, efficiency and TIS/TRP (total isotropic sensitivity/total radiation power), of a wireless home security system panel with GSM module is measured to verify the improvement of this proposed solution. The simulation tool adopted in this paper is GEMS [1], which is applied to analysis the 3D EM environment and performance of antennas in the wireless communication product.

Introduction: In this paper, the compact size antenna shown in figure1 is designed for the purpose of high efficiency and this multi-band antenna (its operating frequency includes 900 MHz /1800 MHz) adopted GSM communication system. In this paper, the antenna adopts the concept of multi-band PIFA to design and to analyze whether the reflector can reduce the environmental effect on the antenna.

The PIFA antenna is mainly designed on FR4 board which dielectric constant is 4.4 and substrate thickness is 1.6 mm.

In this paper, in addition to measuring the performance of TRP/TIS of GSM antenna with the reflector and that without the reflector, we find that the result of the reflection loss and the simulative radiation pattern of the antenna in communication system is good.

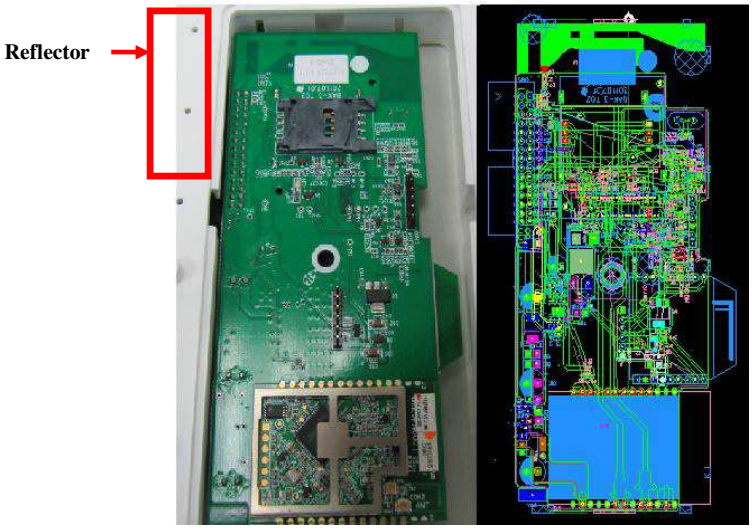

Figure 1: GSM PIFA antenna.

Effect of Attached Materials on Frequency Characteristics of UHF RFID Tag Antenna

P. Keowsawat[1] and P. Keowsawat[2]

[1]Department of Information and Communication Engineering, Faculty of Industrial Technology
Phetchaburi Rajabhat University, Phetchaburi 76000, Thailand
[2]Department of Physics, Faculty of Science and Technology
Phetchaburi Rajabhat University, Phetchaburi 76000, Thailand

Abstract— This paper studied the frequency characteristics of UHF RFID tag antenna attached on different materials. The simulation and measurement resonance frequency of tag antenna in free space were compared with those of tag antenna attached on the materials which have the different relative permittivity and loss tangent. The results showed the variation of resonance frequency when the relative permittivity and loss tangent of the materials were changed. The measurement radiation pattern also displayed the effect of attached materials on the UHF RFID tag antenna characteristics.

Introduction: Recently, the Radio Frequency Identification (RFID) was applied to use in many systems [1–3]. In practical, there are many types of materials that tag antenna would be attached. These materials have many varied relative permittivity (ε_r) and loss tangent ($\tan\delta$) that influence on the performance of the tag antenna such as antenna gain, resonance frequency and radiation pattern. Especially, the resonance frequency that changed from the design frequency caused the degradation of the overall RFID system efficiency. In this paper, the study of frequency characteristics of UHF tag antenna attached on different materials was presented by using the computer simulation and the validation of the simulation was confirmed by the measurement results.

Method and Results: The simulated UHF RFID tag antenna was half-wave planar folded dipole designed at 920 MHz. The frequency characteristics were studied by using Numerical Electromagnetic Code 2 (NEC2) [4]. The materials were modeled with width 20 cm, length 20 cm and height 20 cm. The permittivity and loss tangent were assigned to the materials according to the material properties. In this paper, the large range of permittivity from 1 to 100 and loss tangent from 0 to 0.1 that can cover all of the materials were studied. The difference of resonance frequency of the antenna attached on the materials was compared to that of the antenna in free space (design frequency). The result presented that the difference of resonance frequency was increased when the permittivity and loss tangent increased. The high permittivity and loss tangent materials have highly influence on the resonance frequency of tag antenna. In addition, the measured radiation pattern also exhibited the effect of attached material on the UHF RFID tag antenna.

Conclusions: The resonance frequency characteristics of UHF RFID tag antenna in free space and that attached on different materials were studied in this paper. The variation of operating frequency was showed when the permittivity and loss tangent of the materials were changed. It can conclude from the result that the high permittivity and loss tangent materials effectively have an affect on the UHF RFID tag antenna characteristics.

REFERENCES

1. Finkenzeller, K., *RFID Handbook: Fundamentals and Applications in Contactless Smart Cards and Identification*, J. Wiley & Sons, New York, 2003.
2. Rao, K. V. S., P. V. Nikitin, and S. F. Lam, "Antenna design for UHF RFID tags: A review and a practical application," *IEEE Trans. Antennas and Propagation*, Vol. 53, 3870–3876, 2005.
3. Griffin, J. D., G. D. Durgin, A. Haldi, and B. Kippelen, "RF tag antenna performance on various materials using radio link budgets," *IEEE Trans. Microwave Theory & Tech.*, Vol. 48, No. 12, 2397–2402, December 2000.
4. Burke, G. J. and A. J. Poggio, *Numerical Electromagnetics Code (NEC) — Method of Moments Parts I–III*, Lawrence Livermore Nat. Lab, Livermore, CA, 1981.

Fast Adaptive Least Mean Square Algorithm

S. Maity, **S. Dasgupta**, **and B. Gupta**
Department of Electronics and Tele-Communication Engineering, Jadavpur University, Kolkata, India

Abstract— Adaptive algorithms such as Least Mean Square (LMS), Normalized LMS (NLMS), Recursive Least square (RLS), Differential Steepest Descent (DSD), Accelerated Gradient Approach etc., take many iterations to give satisfactory result when the number of input elements (N) is too large, because they suffer from slow initial convergence. In Multi Split LMS (MS LMS) or VL-LMS No. of input elements (N) $= 2^p$ where p is any positive integer and N is also small. The system takes a long time to give the desired result for large No. of input elements (N).

In this work, an adaptive LMS is proposed with adaptive step size

$$\mu = A/g(N) \tag{1}$$

to fastest convergence with an accuracy of 10^{-10} where A is a constant and $g(N)$ is a polynomial of N. We update $\mu(n)$ [7–12] depending on the value of Mean Square Error (MSE) as given below.

$$\begin{cases} \mu(n) = \mu(n-1) - \Delta\mu; & \text{if MSE}(n) > \text{MSE}(n-1) \\ \mu(n) = \mu(n-1) + \Delta\mu; & \text{otherwise} \end{cases} \tag{2}$$

where $\Delta\mu$ is delta step size.

Algorithm:

1. Initialize input ($X(n)$) vector and initialize target ($d(n)$).
2. Initialize weight vector $W(n) = 0$.
3. Compute output ($Y(n)$) and error ($e(n)$) vector.
4. Compute μ using Equation (1).
5. Assign delta step size, $\Delta\mu = \mu$.
6. While (MSE > limiting error value (10^{-10})).
   a. Compute $\Delta W(n)$.
   b. Update $w(n)$.
   c. Compute error $e(n)$ and MSE(n).
   d. Update μ using Equation (2).

Table 1 shows the No. of iteration for MSE and RMSE case for small as well as large No. of input elements.

Table 2 compares the approximated values of MSE obtained by using various existing algorithms [1] and the new algorithm. From Table 2 it is readily seen that for $N = 32$, LMS, NLMS, VL-LMS converge after 380th iteration but MSE and $\sqrt{\text{MSE}}$ take 80 and 20 No. of iterations respectively.

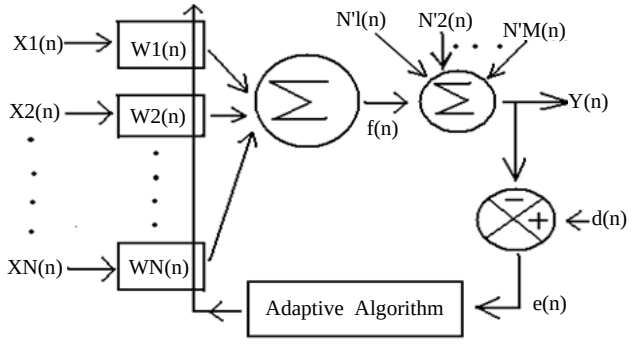

Figure 1: Block diagram of adaptive LMS algorithm.

Table 1: Comparison of MSE and $\sqrt{\text{MSE}}$ case.

No. of input elements (N)	No. of iterations for MSE < limiting error (10^{-10})	No. of iterations for $\sqrt{\text{MSE}}$ < limiting error (10^{-10})
12	77	21
64	68	24
247	21	23
1729	19	27
3892	16	26
6825	16	26
23456	16	21
79271	17	23
10^{10}	17	24
1234567	17	24
4×10^{10}	17	28

Table 2: Comparison of various existing algorithms and new algorithm.

Value of Mean Square Error (MSE) = $E\{e(n)^2\}$ for No. of Input elements (N) = 32					
ith Iteration	*LMS* [1]	*NLMS* [1]	*VL-LMS* [1]	*MSE as limit condition*	$\sqrt{MSE}$ *as limit condition*
3	3.25	3.25	1	214	14.63
8	2.125	2.125	0.8875	0.704	0.839
12	2.016	2.016	0.8341	4.1×10^{-9}	2.8×10^{-2}
20	1.062	1.362	0.60625	8.92×10^{-9}	8.2×10^{-11}
50	0.6625	0.6625	0.4375	3.1×10^{6}	0
75	0.4375	0.4375	0.0381	4.9×10^{6}	0
80	0.325	0.325	0.0325	6.1×10^{-11}	0
250	3.25×10^{-3}	1.56×10^{-3}	4.375×10^{-4}	0	0
350	5.5×10^{-4}	4.23×10^{-4}	3.81×10^{4}	0	0
380	3.81×10^{-4}	3.81×10^{-4}	3.81×10^{-4}	0	0
600	3.81×10^{-4}	3.81×10^{-4}	3.81×10^{-4}	0	0

In this new algorithm there is no constraint in choosing the value of N (even or odd, small or large) in contrast to the other methods such as VL-LMS, MS-LMS etc., the values of N can be an arbitrary number which is a salient feature of the proposed new algorithm.

Earlier works have been reported by taking limiting error in the order of 10^{-4} or 10^{-5}. But we have taken the limiting error as 10^{-10} to get better result. Hence this algorithm gives fast convergence for any positive real values of N.

REFERENCES

1. Nascimento, V. H., "Improving the initial convergence of adaptive filters: Variable-length LMS algorithm," *IEEE DSP, 14th International Conf. 2002*, Vol. 2, 667–670, 2002.

Session 4A5
Novel Mathematical Methods in Electromagnetics

Nonlinear Effects of Electromagnetic TM Wave Propagation in Anisotropic Layer with Kerr Nonlinearity

Yu. G. Smirnov and D. V. Valovik
Penza State University, 40 Krasnay Street, Penza 440026, Russia

Abstract— During many years problems of TE and TM waves propagation through nonlinear layers and circle cylindrical waveguides are intensively investigated. Such problems attract more and more attention due to their importance in different areas such as nonlinear optics, plasma physics, microelectronics etc. We consider electromagnetic waves propagating through a homogeneous isotropic nonmagnetic dielectric layer filled by media with Kerr nonlinearity. The layer is located between two half-spaces $x < 0$ and $x > h$ in Cartesian coordinate frame $Oxyz$. The layer is infinite along two directions: Oy and Oz. The half-spaces are filled with isotropic nonmagnetic medium containing no sources and with constant permittivities ε_1 and ε_3, respectively (ε_1 and ε_3 are arbitrary real values).

The permittivity inside the layer is described by the formula

$$\tilde{\varepsilon} = \varepsilon_2 + \alpha \left(|E_x|^2 + |E_z|^2 \right),$$

where ε_2 is a constant part of the permittivity in the layer, α is a coefficient of nonlinearity and both of them are arbitrary real constants.

We seek solutions to the Maxwell equations in the entire space.

This electromagnetic problem can be reduced to a nonlinear boundary eigenvalue problem for ordinary differential equations (nonlinearly depend on sought functions with transmission conditions nonlinearly depend on spectral parameter). Here we obtain a dispersion equation for TM waves propagating through such a layer with $\tilde{\varepsilon}$. The dispersion equation can be studied both analytical and numerical. From the dispersion equation constants of propagation can be numerically obtained. Having a value of the propagation constants (an eigenvalue) the fields (eigenfunctions) can be easily calculated. Using this dispersion equation nonlinear metamaterial can be studied as well.

We show that there are two types of solutions (eigenvalues and eigenmodes) of the nonlinear problem. First type is a solution (an eigenmode) that goes over to a linear eigenmode as $\alpha \to 0$. And also there is a new type of eigenmodes. These eigenmodes exist for any positive α and positive ε_2 and don't go over to linear eigenmodes as $\alpha \to 0$.

Electromagnetic TM Wave Propagation through a Nonlinear Metamaterial Layer with Arbitrary Nonlinearity

D. V. Valovik
Penza State University, 40 Krasnay Street, Penza 440026, Russia

Abstract— During many years problems of TE and TM waves propagation through nonlinear layers are intensively investigated. Such problems attract more and more attention due to their importance in different areas such as nonlinear optics, plasma physics, microelectronics etc. We consider electromagnetic waves propagating through a homogeneous anisotropic nonmagnetic dielectric layer filled by media with arbitrary nonlinearity. The layer is located between two half-spaces $x < 0$ and $x > h$ in Cartesian coordinate frame $Oxyz$. The layer is infinite along two directions: Oy and Oz. The half-spaces are filled with isotropic nonmagnetic medium containing no sources and with constant permittivities ε_1 and ε_3, respectively (ε_1 and ε_3 are arbitrary real values).

The permittivity inside the layer is described by the diagonal tensor

$$\tilde{\varepsilon} = \begin{pmatrix} \varepsilon_{xx} & 0 & 0 \\ 0 & \varepsilon_{yy} & 0 \\ 0 & 0 & \varepsilon_{zz} \end{pmatrix}$$

where $\varepsilon_{xx} = \varepsilon_f + \varepsilon_0 f\left(|E_x|^2, |E_z|^2\right)$, $\varepsilon_{zz} = \varepsilon_g + \varepsilon_0 g\left(|E_x|^2, |E_z|^2\right)$, where ε_f, ε_g are arbitrary real constant and ε_0 is the permittivity of free space. In the case of TM waves it does not matter what a form ε_{yy} has. The functions f, g are analytical functions of real variables and such that the relation $\frac{\partial f}{\partial(|E_z|^2)} = \frac{\partial g}{\partial(|E_x|^2)}$ is satisfied.

We seek solutions to the Maxwell equations in the entire space.

This electromagnetic problem can be reduced to a nonlinear boundary eigenvalue problem for ordinary differential equations (nonlinearly depend on sought functions with transmission conditions nonlinearly depend on spectral parameter). Here we obtain a dispersion equation for TM waves propagating through such a layer with $\tilde{\varepsilon}$. The dispersion equation can be studied both analytical and numerical. From the dispersion equation constants of propagation can be numerically obtained. Having a value of the propagation constants (an eigenvalue) the fields (eigenfunctions) can be easily calculated. Using this dispersion equation nonlinear metamaterial can be studied as well.

Wave Equation in the Electromagnetic Field with Velocity Curl

Zi-Hua Weng
School of Physics and Mechanical & Electrical Engineering
Xiamen University, Xiamen 361005, China

Abstract— The validity of wave equation is confined merely to one special condition that there exists only the electromagnetic field up to now. The people doubt whether the wave equation is still correct or not in the electromagnetic field in the presence of the velocity curl and gravitational fields. The existing theories do not explain why the wave equation should keep unchanged for the charged rotating objects, and then do not offer related compelling reasons.

The quaternion was invented by W. R. Hamilton in 1843, and then was first used by J. C. Maxwell to describe electromagnetic fields in 1861. H. Helmholtz in 1871 made clear the electromagnetic theory and some wave features effectively. O. Heaviside in 1884 recast Maxwell equation in terms of vector terminology deriving from the vectorial part of the quaternion. Later H. R. Hertz became famous as the first to demonstrate electromagnetic radiation in 1889.

The quaternion space for the gravitational field is independent of that for the electromagnetic field. Those two quaternion spaces can be combined together to become an octonion space, which was invented by A. Cayley etc. Further in the octonion space, the radius vector can be combined with the integral of the field potential to become the compounding physical quantity, which can be used to rephrase the electromagnetic field and the gravitational field simultaneously.

In terms of the compounding physical quantity, the study claim that there exist four kinds of 'weightlessness' states, two for the electromagnetic field, and other two for the gravitational field. It means that the field strength possesses stable magnitudes in the vacuum. On the other hand, the wave equation reveals that the compounding field strength is fluctuant periodically. Consequently the field strength is deviated from the velocity curl slightly and frequently.

ACKNOWLEDGMENT

The author is grateful for the financial support from the National Natural Science Foundation of China under grant number 60677039.

TE-like to TM-like Mode Conversion in a Finitely Conducting Periodically Corrugated Circular Waveguide

Omar R. Asfar and Nadiah H. Saba'neh
Department of Electrical Engineering
Jordan University of Science and Technology, Irbid, Jordan

Abstract— By relaxing the infinite conductivity assumption and using the perturbation method of multiple scales, it is shown that the hybrid TE_{11}-like (HE_{11}) mode can be effectively coupled to the TM_{11}-like (EH_{11}) mode by means of periodic corrugations in a circular cylindrical waveguide. Resonant coupling occurs when the wavenumbers of the two modes satisfy the resonance condition

$$\beta_{TE} - \beta_{TM} = k_w,$$

where k_w is the corrugation wavenumber. Evolution of the mode amplitudes shows energy exchange as the modes propagate down the guide. An approximation to the eigenfunctions of the HE_{11} and EH_{11} modes was found necessary to obtain a realistic mode conversion picture that nearly satisfies energy conservation when hybrid modes are used instead of TE and TM modes.

Optical Neural Router Consisting of Acousto-optic Waveguide-type Switches for Adaptive Network

N. Goto[1] and Y. Miyazaki[2]

[1]University of Tokushima, Japan
[2]Aichi University of Technology, Japan

Abstract— In packet transmission through broadband networks, the transmission efficiency decreases under heavy traffic if route selection is not properly carried out. We propose adaptive system using optical neural router.

As an algorithm to obtain the shortest path between routers, we propose a method using neural learning. There are dynamic routing and static routing. The dynamic routing exchanges routing information which may not necessarily be efficient. Memories and processing time increase when the control becomes complicated. On the other hand, the static routing is not necessarily efficient because routing tables have to be updated when the network configuration is changed or troubles occur in the network.

We consider a router consisting of neural devices and formularize it considering router performance and transmission speed. Output packets from the router are determined by controlling the neural devices to minimize time-of-arrival of the packets. Since neural network learns change of transmission capacity, flexible route selection can be expected in emergency. Optimum route selection algorithm considering various factors can be realized by adjusting coupling weights among neurons.

In this paper, we discuss optical neural router consisting of layered structure of acousto-optic (A-O) neural switches. The transmission route is controlled by applying r.f. electric signals for SAWs which were determined by learning. A-O switching device for optical neural router was analyzed by FDTD method. In this analysis, total analysis space is divided into small subdomains and each subdomain is calculated successively to simulate optical pulse propagation in long distance of hundreds times as long as wavelength.

Spatial Sampling Characteristics of Beam Wave Eigen Functions Representation for Optical CT

Yasumitsu Miyazaki
Department of Media Informatics, Aichi University of Technology
50-2 Manori, Nishihasama-cho, Gamagori 443-0047, Japan

Abstract— For medical image diagnosis assisted by computers, computer tomography technologies using X-ray, optic and electromagnetic beam waves as incident waves have been rapidly developed. Incident beam waves scan in transverse cross sections of biological organs to get interior medical image information. Wave CT technologies are developed by inverse Fourier transforms for beam wave attenuations along beam propagation axises. Beam transverse scanning is based on spatial sampling theorem for transversely scanning of incident beam waves. Similar principle in space as sampling theorem in time is expressed by eigen function expansions of beam fields.

When frequency characteristics of temporal function $x(t)$ has spectrum properties of band spectrums as $|f| \leq W$, $x(t)$ can be shown as superposition of local temporal sampling data, with index i

$$x(t) = \sum_{i=-\infty}^{\infty} x\left(\frac{i}{2W}\right) \varphi_i\left(t - \frac{i}{2W}\right)$$

using sinc function $\varphi_i\left(t - \frac{i}{2W}\right) = \frac{\sin 2\pi W(t-i\Delta t)}{2\pi W(t-i\Delta t)}$, where temporal unit element interval $\Delta t = \frac{1}{2W}$. In spatial case, electric field $\mathbf{E}(\mathbf{r})$ may be expressed as superposition of local field sampling data, with index $\bar{s}$

$$\mathbf{E}(\mathbf{r}) = \sum_{\bar{s}=-\infty}^{\infty} E^{(s)}(\mathbf{r}_s)\, \mathbf{\Psi}(\mathbf{r} - \bar{s}\Delta\mathbf{r}_s)$$

using local beam eigen functions, where $\mathbf{r}_s = \mathbf{r} - \bar{s}\Delta\mathbf{r}_s$ with spatial unit element distances $\Delta\mathbf{r}_s$.

Local beam eigen functions $\mathbf{\Psi}(\mathbf{r})$ at center $\mathbf{r}_t^{(s)} = \mathbf{r} - \bar{s}\Delta\mathbf{r}_s$ are given from local field functions satisfying vector wave equations derived by the Maxwell's equation. In free space, when the wave number is k, space position vector and space local coordinates $\mathbf{r}_t^{(s)} = t\mathbf{i}_t + s\mathbf{i}_s$, where transverse axis is s, and propagation axis is t coordinates, asymptotic Hermite Gaussian functions for rectangular coordinates can show local beam eigen functions.

Based spatial sampling theorem described in this paper, discussing scatterings and mode couplings in inhomogeneous guided modes in virtual waveguides corresponding to transversely divided sub-domains, precise image reconstruction theory of electromagnetic CT method is shown.

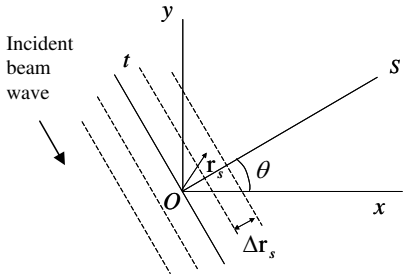

Figure 1: Projection coordinates (s,t) for spatial sampling and beam wave scanning.

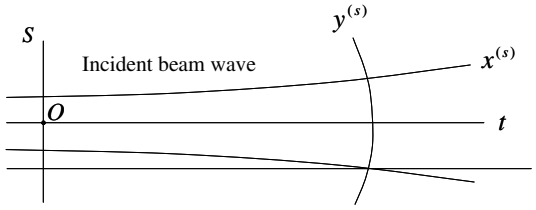

Figure 2: Beam coordinates $(x^{(s)}, y^{(s)})$ for incident beam wave scanning.

REFERENCES

1. Miyazaki, Y., *Proc. ISMOT, Electromagnetic theory Embedded Systems*, 4, Prague, 2011.
2. Miyazaki, Y. and K. Kouno, *Trans. IEE Japan, A*, Vol. 129, No. 10, 693–698, 2009.
3. Miyazaki, Y., *Opt. and Quantum Electron.*, Vol. 9, 153–165, 1977.

A Multi-dimensional CIP-BS Method for Electromagnetic Simulation

Yoshiaki Ando and Yusuke Takahashi
The University of Electro-Communications, 1-5-1 Chofugaoka, Chofu, Tokyo 182-8585, Japan

Abstract— The constrained interpolation profile (CIP) method is the numerical method using field values and their spatial derivatives, and is originally developed in the area of fluid dynamics. The application of the CIP method to electromagnetic dynamics acquires many attention, and related papers have been published [1, 2]. Recently, another CIP method, which is called as CIP-basis set (CIP-BS) method, is developed to solve general hyperbolic equations. In this paper, we develop a multi-dimensional CIP-BS method for electromagnetic simulation.

The basic methodology is as follows: First of all, we expand electromagnetic fields into a series of the CIP basis function set which consists of multiple basis functions in a subdomain. Then, the Galerkin method can be applied and we can obtain the solutions from the resulting linear equations.

We compute a rectangular cavity for a TE_{202} resonant mode. The developed CIP-BS method successfully works and their numerical results agree very well with analytical solutions. Then, we compare phase errors of the CIP-BS method with the one by the FDTD method, and the errors by the CIP-BS method are very small even for coarse grids.

Various schemes, such as the leap-frog time-stepping, the Crank-Nicolson method, etc., can be applied to the CIP-BS method. Of course, when choosing an implicit scheme, the stability condition can be removed.

Two types of absorbing boundary conditions (ABCs) for the CIP-BS methods are also developed in this study. The one is based on the one-way wave propagation, and the another is the perfectly matched layer (PML). The performance of the former ABC is close to the Mur's ABC in the FDTD method. For PML, we can improve the absorbing characteristics by increasing the number of layers.

REFERENCES

1. Ando, Y. and M. Hayakawa, "Implementation of the perfect matched layer for the CIP method," *IEICE Trans. Electron.*, Vol. E89-C, No. 5, 645–648, May 2006.
2. Ando, Y., H. Saito, and M. Hayakawa, "A nearly perfect total-field/scattered-field boundary for the one-dimensional CIP method," *IEICE Trans. Electron.*, Vol. E91-C, No. 10, 1677–1683, October 2008.

On the Implementation of a Discontinuous Galerkin Finite Element Method with Exact Absorbing Boundary Conditions

K. Sirenko, M. Liu, and H. Bağcı
Division of Physical Sciences and Engineering
King Abdullah University of Science and Technology (KAUST)
KAUST 4700, Thuwal, 23955-6900, Saudi Arabia

Abstract— Time domain discontinuous Galerkin finite element method (TD-DG) is becoming an alternative to the "traditional" finite element and the time domain finite difference methods for simulation of transient electromagnetic wave interactions on complex geometries. TD-DG owes its increasing popularity to several desired properties [1]: (i) Straightforward construction of high-order basis functions (localized to discretization elements); (ii) Smaller (easy-to-invert) mass matrices (localized to discretization elements); (iii) Explicit (more efficient) time integration schemes; (iv) Straightforward parallelization. It should be noted there that these properties are direct results of using numerical flux to realize the exchange of information between discretization elements [1].

TD-DG's intrinsic higher-order nature renders it a good candidate for solving Maxwell equations with high accuracy. However, like any other differential equation based methods, when applied to the characterization of wave interactions in open/unbounded domains, TD-DG's accuracy is limited by the accuracy of the method used for truncating the domain. Perfectly matched layers are the most widely accepted method used for this purpose [2]. Unfortunately, they are error-controllable up to only a certain degree, and thus they introduce non-negligible errors into the solution especially in long-duration simulations. On the other hand, mathematically rigorous exact absorbing boundary conditions (EACs) [3] can avoid these additional errors. There are several approaches to deriving EACs, but virtually none of those was implemented in a TD-DG framework. This work is intended to fill this gap.

The presentation will provide the implementation details of a higher-order TD-DG enhanced with EACs that are derived from the outgoing waves' radiation conditions. The EACs are introduced in the TD-DG framework via the use of numerical flux. The numerical flux, which is defined on the common edge of two neighboring discretization elements, relates the field values in those elements [1]. Since the region outside the EACs is not discretized, defining numerical flux on the boundary edges becomes a nontrivial task. The presentation will focus on the formulation of the numerical flux for this specific case as well as the implementation details such as the discretization of the differentiation and integration operators present in the expressions of the EACs.

The numerical results, which demonstrate the high accuracy of the TD-DG with EACs, will be presented. It will be shown that the use of EACs allows the demonstration of TD-DG's higher-order nature even when it is used for simulating wave interactions on open/unbounded domains.

REFERENCES

1. Hesthaven, J. S. and T. Warburton, *Nodal Discontinuous Galerkin Methods*, Springer, New York, 2008.
2. Gedney, S. D., C. Luo, J. A. Roden, R. D. Crawford, B. Guernsey, J. A. Miller, and E. W. Lucas, "A discontinuous Galerkin finite element time domain method with PML," *Proc. IEEE AP-S Int. Symp.*, 2008.
3. Sirenko, K., V. Pazynin, Y. Sirenko, and H. Bağcı, "An FFT-accelerated FDTD scheme with exact absorbing conditions for characterizing axially symmetric resonant structures," *Progress In Electromagnetics Research*, Vol. 111, 331–364, 2011.

Solution of Coupled Landau-Lifshitz-Gilbert and Volume Integral Equations for Characterizing Electromagnetic Wave Interactions on Composite Ferrite Structures

M. Furqan and H. Bağcı
Division of Physical Sciences and Engineering
King Abdullah University of Science and Technology (KAUST)
KAUST 4700, Thuwal 23955-6900, Saudi Arabia

Abstract— Recently, there has been an increasing interest in utilizing ferrite substrates in designs of microwave devices [1] mostly because ferrites' material properties can be tuned by adjusting the biasing DC magnetic field. This intriguing characteristic renders ferrites a good choice of substrate in reconfigurable designs, where, for example, an antenna pattern or a resonance frequency must be shifted electronically during the operation [2]. Therefore, simulation tools capable of accurately and efficiently characterizing wave interactions on composite ferrite structures are indispensable components of design frameworks.

The interactions of electromagnetic waves with ferrites are governed by the Landau-Lifshitz-Gilbert (LLG) equation. The existing numerical methods either directly discretize the LLG equation or incorporate a permeability tensor, which is derived from a small signal approximation of the LLG equation. Direct discretization method has been incorporated into time-domain finite-difference schemes [3] whereas tensor-approximation method has been used in finite element and volume integral equation (VIE) formulations [2, 4, 5]. So far, direct discretization of LLG equation has never been implemented in a VIE framework.

In this work, we develop a method-of-moment based discretization scheme for numerically solving the coupled LLG and VIE equations. Note that direct discretization of LLG equation requires approximation of both the magnetic flux density and magnetic field intensity. Magnetic flux density is discretized using the well-known SWG basis functions, which ensures the continuity of the normal component of the flux density [6]. On the other hand, boundary conditions might enforce a discontinuity on the magnetic field intensity's normal component, making the SWG basis functions not suitable for approximating it. To this end, we propose to use half-SWG basis functions; by this added degree of freedom, magnetic field intensity can be expanded consistently [7].

We will demonstrate the accuracy of the proposed discretization method by comparing numerical results with Mie series solutions. Additionally, the effectiveness of the method will be shown via its application to the characterization of electromagnetic wave interactions on realistic antenna designs loaded with ferrite substrates.

REFERENCES

1. Ustinov, A., G. Srinivasan, and B. Kalinikos, "Ferrite-ferroelectric hybrid wave phase shifters," *Appl. Phys. Lett.*, Vol. 90, 031913, 2007.
2. Kononov, V. G., C. A. Balanis, A. C. Polycarpou, and C. R. Birtcher, "Non-uniform field modeling of ferrite-loaded cavity-backed slot antennas," *IEEE Trans. Antennas Propag.*, Vol. 57, 3402–3405, 2009.
3. Dib, N. and A. Omar, "Dispersion analysis of multilayer cylindrical transmission lines containing magnetized ferrite substrates," *IEEE Trans. Microw. Theory Tech.*, Vol. 50, 1730–1736, 2002.
4. Kobidze, G. and B. Shanker, "Integral equation based analysis of scattering from 3-D inhomogeneous anisotropic bodies," *IEEE Trans. Antennas Propag.*, Vol. 52, 2650–2658, 2004.
5. Hu, L., L.-W. Li, and T. S. Yeo, "Analysis of scattering by large inhomogeneous bi-anisotropic objects using AIM," *Progress In Electromagnetics Research*, Vol. 99, 21–36, 2009.
6. Schaubert, D., D. Wilton, and A. Glisson, "A tetrahedral modeling method for electromagnetic scattering by arbitrarily shaped inhomogeneous dielectric bodies," *IEEE Trans. Antennas Propag.*, Vol. 32, 77–85, 1984.
7. Shanker, B., K. Aygün, and E. Michielssen, "Fast analysis of transient scattering from lossy inhomogeneous dielectric bodies," *Radio Sci.*, 39, 2004.

Axisymmetric Electric and Magnetic Field Calculations with Zonal Harmonic Expansion

F. Glück[1, 2]

[1]Karlsruhe Institute of Technology, IEKP, Karlsruhe 76021, P. O. Box 3640, Germany
[2]KFKI, RMKI, H-1525 Budapest, P. O. Box 49, Hungary

Abstract— The zonal harmonic expansion method is a special version of the spherical harmonic method, applied for axisymmetric systems. It can be 100–1000 times faster than the more widely known elliptic integral method and is more general than the similar radial series expansion. It has not only high speed, but also high accuracy, which makes the method especially appropriate for trajectory calculations of charged particles. Due to these properties, no interpolation is necessary when the electric and magnetic field during particle trajectories is computed with the aid of the zonal harmonic method.

The zonal harmonic field series formulas are convergent at field points within the central and remote regions, which have spherical boundaries, and their center, the source point, can be arbitrarily chosen on the symmetry axis. The rate of convergence of the field series depends on the distance of the field and the source point; smaller distance for central field points and larger distance for remote field points correspond to higher convergence rate. For a given field point, one can improve the convergence properties of the zonal harmonic method by optimal choice of the field expansion method (central or remote), of the source point, and of the source representation method. The zonal harmonic method is applicable also for special three-dimensional magnetic systems, whose components (coils or magnetic materials) are axially symmetric in their own local coordinate systems.

The charge density of axially symmetric electrodes can be computed by the boundary element method (BEM). The electric potential and field of the electrodes can be accurately calculated by elliptic integrals. Unfortunately, the Coulomb integration with summation over the many subelements of the discretized electrode surfaces is rather slow. The zonal harmonic expansion provides a much faster computation method, which at the same time keeps the high accuracy of the Coulomb integration. The electric field calculation using the zonal harmonic expansion method is similar to the magnetic field calculation, for example, the same Legendre polynomial and convergence formalism can be used in both cases.

To apply the zonal harmonic method for electric and magnetic field computations, we have written several FORTRAN and C codes that have been used for electromagnetic design studies and/or trajectory calculations connected with the aSPECT, WITCH, Nab, PERC and KATRIN experiments. The method has been included into the C++ simulation package KASSIOPEIA of the KATRIN experiment. A detailed overview of our method can be found in Refs. [1, 2].

REFERENCES

1. Glück, F., "Axisymmetric electric field calculation with zonal harmonic expansion," *Progress In Electromagnetics Research B*, Vol. 32, 319–350, 2011.
2. Glück, F., "Axisymmetric magnetic field calculation with zonal harmonic expansion," *Progress In Electromagnetics Research B*, Vol. 32, 351–388, 2011.

Propagation Characteristics of Dielectric Waveguides with Arbitrary Inhomogeneous Media along the Middle Layer (Part II)

Ryosuke Ozaki and Tsuneki Yamasaki
Department of Electrical Engineering, College of Science and Technology
Nihon University, Japan

Abstract— Light wave propagation in periodic structure waveguide is both theoretical and practical interest in many areas of physics and engineering. For example, applications include integrated optics, optical waveguide filter, and other optical devices. In periodic structures such as photonic crystal structures, it is known that a frequency stop band occurs. Consequently, in the design of photonic crystal structures with periodic constants same as optical wavelength, it is important to investigate the stop band region. On the one hand, it can be controlled optical constants by the development of manufacturing technology of semiconductor and optical devices. Thus, many analytical and numerical techniques have been proposed that are applicable to dielectric gratings having arbitrary structures. To deal with multilayered dielectric circular cylinder arrays such as photonic crystal structure, it is necessary to analyze the multilayered periodic arrays. In the multilayer method, as the inhomogeneous region is divided into an assembly of stratified thin layers with step index profile, the matrix size depends on the number of layers. In our method, the order of characteristic matrix equation depends on the modal truncation number, but it does not depend on the number of layers. Therefore the range of applicability for the periodic structures is much wider than that of the other method. In particular, our approach is effective method for the guiding problems such as multilayered periodic array. In guiding problem, it is necessary to analyze with high accuracy the complex propagation constants for both

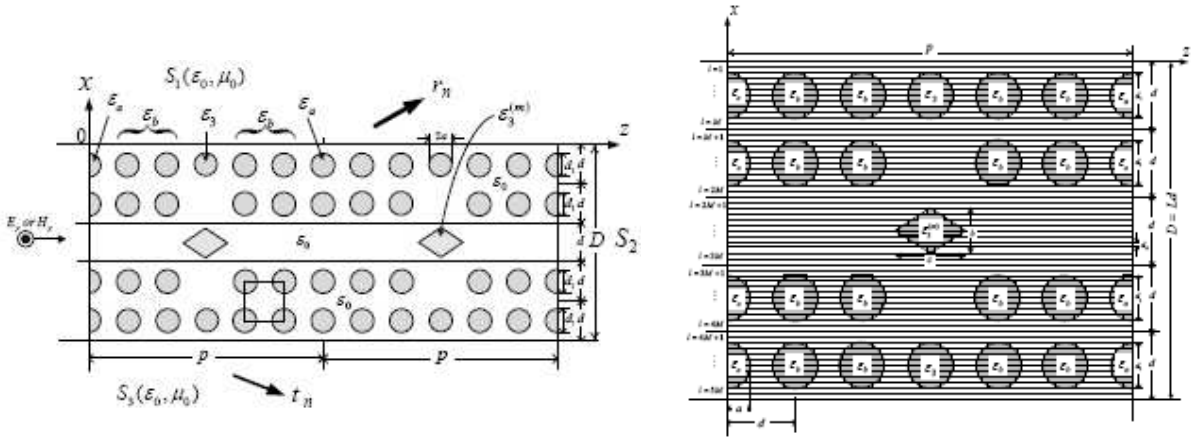

(a) Coordinate system (b) Approximated multilayer method

Figure 1: Structure of dielectric waveguides with arbitrary inhomogeneous media along the middle layer.

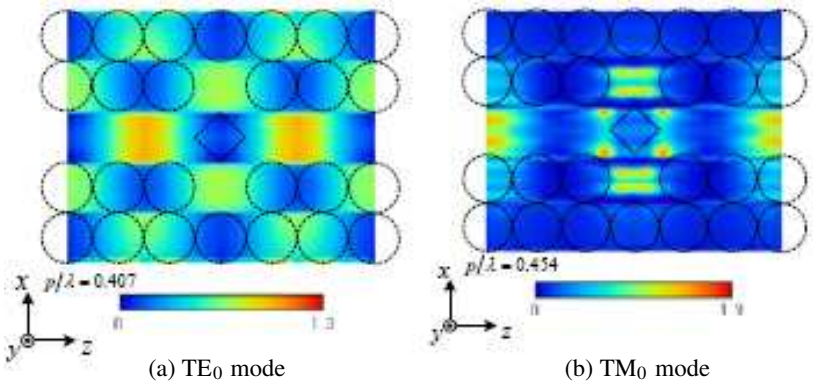

(a) TE_0 mode (b) TM_0 mode

Figure 2: Distribution of energy flow at the guided area.

stop band region and leaky wave region. However the guiding problem is reported by various numerical techniques, the propagation characteristic is not investigated in detailed in the Bragg region. In recent paper, we proposed an improved method to analyze the scattering problem of dielectric gratings with the dielectric rectangular cylinders in the middle layer.

In this paper, we apply an improved method for the guiding problem of dielectric waveguides with arbitrary inhomogeneous media along the middle layer introduced the defect layers, and analyzed the propagation characteristics of dielectric waveguide composed of dielectric circular cylinders and the arbitrary inhomogeneous media in the middle layer.

Numerical results are given for the complex propagation constants and the distribution of energy flow for the case of loaded with the rhombic dielectric structure as the inhomogeneous media in the middle layer for both TE_0 and TM_0 modes.

Dispersion Characteristics of Hyperbolic Waveguide for Weak-guidance

D. Kumar, **K. H. Mak**, **and H. Y. Wong**
Multimedia University, Malaysia

Abstract— This paper presents results on the electromagnetic wave propagation in a new type of dielectric optical waveguide of hyperbolic cross-section. This theoretical analysis essentially requires the use of an elliptical coordinate system. The Mathieu and modified Mathieu functions arise naturally in the representation of the electromagnetic field within a hyperbolic waveguide. In the context of non-circular guides, a hyperbolic cross-sectional guide structure would be rather interesting and unconventional. Field components in the different sections of the guide are deduced, and the eigenvalue equation for the system is derived. The small difference in the refractive index classifies this as a case of weak guidance.

Session 4A6
Microwave and Millimeter Wave Devices

Design of 120 GHz, 1 MW Gyrotron for Plasma Fusion Application

Anil Kumar, **Nitin Kumar**, **Udaybir Singh**, **R. Bhattacharya**,
Narendra K. Singh, **Hasina Khatun**, **M. K. Alaria**, **and A. K. Sinha**
Central Electronics Engineering Research Institute (CEERI, CSIR)
Pilani, Rajasthan-333031, India

Abstract— The gyrotron is a vacuum based device, generates very high power electromagnetic radiation in the millimeter wave band. 120 GHz gyrotron with 1 MW or more power is used in the Electron Cyclotron Resonance Heating (ECRH) in magnetically confined plasma. In this article a complete design of the gyrotron is presented. Considering the goal of 1 MW power and 120 GHz frequency, first the mode selection and the interaction cavity design are performed. The high order asymmetric mode $TE_{22,6}$ is selected as the operating mode by using the mode selection code GCOMS. The magnetic field (required for the gyration of electrons) at the cavity center is calculated on the basis of required frequency. The initial values of electron beam voltage and current are calculated considering the space charge effect and the normalized parameters (Δ, μ, F). The interaction cavity geometry is calculated on the basis of selected operating mode and Particle-in-Cell (PIC) code is used for the beam-wave interaction computation and power and frequency growth estimation. On the basis of the optimized beam parameters (beam current, beam voltage and velocity ratio), detuned magnetic field at cavity center and beam radius, the electron beam source (generally called Magnetron Injection Gun, MIG) is designed by using the EGUN and TRACK codes. The Gaussian type of magnetic field profile is also optimized for the adiabatic compression of the electron beam considering the minimum velocity spread (<5%) and the velocity ratio between 1.3 to 1.5. The electron beam transfer a friction of energy (30–40%) to the RF at the interaction cavity and rest of the electron beam energy is collected at the specially designed cylindrical waveguide type of structure called collector. For the 120 GHz gyrotron, single stage depressed collector is designed considering two major goals, one is maximum collector efficiency and second is the maximum beam spread at the collector wall. The electron beam data after the beam-wave interaction is used in the EGUN software to design the depressed collector. Finally, the RF window is designed for the effective transmission of the generated RF power. Good mechanical strength and stable dielectric properties are highly required properties of the window material. CVD diamond is an excellent material for the high power gyrotron window as it fulfills all the desired mechanical and dielectric properties. The thermal analysis is also performed for all the designed components to achieve the final tolerance, will be used during the actual fabrication of the device. The overall design data shows the 1 MW power generation at 120 GHz frequency.

Investigation of a Disc-Loaded Gyro-TWT Using Particle-In-Cell Simulation

R. K. Singh[1], **Ashutosh**[2], **and P. K. Jain**[2]

[1]Bharat Sanchar Nigam Limited, Ludhiana, India
[2]Center of Research in Microwave Tubes, Department of Electronics Engineering
Institute of Technology, Banaras Hindu University, Varanasi, India

Abstract— Among the gyrotron devices, the Gyro-TWT has the potential as high power wideband amplifier in the millimeter and sub-millimeter range. There has been a steady progress in the development of gyro-TWTs, both theory and experiment. Gyro-TWTs performance characteristics lead its use for a variety of application in myriad of areas, such as, high-resolution radar and high-information-density communication systems, high-gradient linear colliders, atmospheric sensing, etc. Gyro-TWTs incorporate interaction between electromagnetic waves and space charge cyclotron waves on the gyrating (periodic) electron beam in a smooth wall RF interaction structure supporting a fast waveguide mode.

The conventional gyro-TWT uses smooth wall cylindrical waveguide as its RF interaction structure, which limits the device bandwidth due to narrow band coalescence between the beam-mode line and the waveguide-mode dispersion hyperbola, at or near the cut-off of the waveguide. However, a disc-loaded waveguide, which is an all metal structure, does provide wider coalescence in comparison to conventional smooth wall guide. Hence, the use of a disc-loaded RF interaction structure, comprising annular metal discs at regular interval, in the gyro-TWT provides a wider device bandwidth with appreciable gain as well as high power handling capability.

In this paper, we have investigated the beam-wave interaction behavior of a disc-loaded gyro-TWT amplifier using PIC simulation with the help of a commercially available tool MAGIC. The MAGIC is a FDTD and PIC based code for plasma processes. Here, a 91 GHz single-stage second-harmonic disc-loaded gyro-TWT operating in the TE_{02} mode has been simulated. Second cyclotron harmonic operation is adapted to reduce the requirement of DC magnetic field. Simulations have been performed in the electron beam absent (cold) and electron beam present (hot) cases. In order to ensure the device operation at the desired mode and frequency, beam absent simulation is performed. Results obtained through the eigenvalue reveals its operating frequency and observing the field profile confirms the operating mode. The simulation is further extended in beam present case. The electrons are uniformly distributed in azimuthal direction in the form of beamlets and their evolution along the interaction length in the presence of RF is observed in the time domain. They start to bunch as they drift along the interaction region. Once the electrons are bunched, they transfer their energy to electric field which reverses its direction in each half cycle of the cyclotron frequency in synchronism with the Larmor gyration of the electrons. This makes possible amplification of an electromagnetic wave at the cyclotron frequency.

PIC simulation demonstrates a disc-loaded gyro-TWT of high output power and wideband along with appreciable gain. Beam-wave interaction and spatial power growth are validated using non-linear theory and found in fair agreement. An output power of 235 kW at 91.4 GHz with input power 450 W along with approximately 10% efficiency is achieved. The Fourier transform of time varying field confirms the exact frequency of operation in beam present case. Bunching phenomena in phase plot is explicitly observed along interaction length.

Design of Higher Harmonic Interaction Cavity for 0.3 THz Gyrotron

Anil Kumar[1, 2], **Nitin Kumar**[1], **Hasina Khatun**[1], **Udaybir Singh**[1], **V. Vyas**[2], **and A. K. Sinha**[1]

[1]Gyrotron Laboratory, Microwave Tube Division
CSIR-Central Electronics Engineering Research Institute (CEERI)
Pilani, Rajasthan 333031, India
[2]Department of Physics, Banasthali University, Banasthali, Rajasthan 304022, India

Abstract— The research in the field of THz radiation (300 GHz–3 THz) is getting big thrust due to the several remarkable and innovative applications in the field of fundamental material research, medical science, security, sensing, etc. There is a lack of efficient sources, detectors, transmission systems, etc., in the THz band, also called THz gap. Several applications, like NMR spectroscopy, material processing, etc., required high power (from tens of watt to few kW) in the THz band. The gyrotron is a perfect device as a radiation source to fulfill the demand of high power at THz band. The required magnetic field in the gyrotron operation directly depends on the frequency and inversely on the harmonic. In THz band, the magnetic field becomes very large at the fundamental harmonic operation of the device, so the higher harmonic operation ($s = 2$) is selected to reduce the magnetic field in the design of 0.3 THz gyrotron. The gyrotron is designed for the RF power more than 1 kW which is required in several applications like the high frequency ceramic sintering, high resolution spectroscopy, etc. The mode competition becomes severe at higher harmonic operation as the fundamental harmonic ($s = 1$) mode also compete due to the lower start oscillation current. A careful investigation of the start oscillation current and coupling coefficient is performed for several modes to avoid the high mode competition. The symmetric low order mode $TE_{0,6}$ is selected as the operating mode. The interaction cavity geometry and beam parameters are optimized for the operating mode. The beam-wave interaction simulations are performed for the higher harmonic operation by using the Particle-in-Cell code MAGIC. The results confirms more than 1 kW of power at 300 GHz frequency at second harmonic.

Study of Stagger-tuning in the Gyroklystrons

M. S. Chauhan and P. K. Jain
Center of Research in Microwave Tubes, Department of Electronics Engineering
Institute of Technology, Banaras Hindu University, Varanasi-221005, India

Abstract— Gyroklystrons find applications in the millimeter wave radars and linear supercolliders due to their capabilities to provide high-gain amplification with moderate bandwidth in the millimeter-wave band. The gyroklystron is a fast-wave electron-beam device which combines the multi-cavity klystron configuration with the cyclotron resonance maser instability energy extraction mechanism of gyrotron. The operation is similar to conventional klystron except that electron bunching occurs in the transverse direction rather than in the axial direction and larger overmoded TE cavities are used. This scheme makes them to be used at higher frequencies with larger cavity dimensions. Gyroklystrons under development have been designed to surpass both peak and average power limits of conventional microwave amplifiers. However, this device is having more complex fabrication difficulties, since several cavities have to be tuned properly and to maintain alignment of the cavities with the electron beam. Furthermore, the drift spaces, where ideally no field exists are susceptible to spurious oscillations due to leakage of electromagnetic fields from cavities.

One of the major limitations of gyroklystron is its limited bandwidth operation. To increase the bandwidth of a klystron, the resonant frequencies of its different RF interaction cavities are slightly detuned. This method is known as the stagger tuning and widely used to enhance the klystron bandwidth though at the cost of its gain. This technique of stagger tuning can also be applied to broadband the gyroklystron. The present paper aims to study a tradeoff in gain and bandwidth for the stagger tuned gyroklystrons. The present analysis is based on the point-gap model for gyroklystrons in which the size of the cavities assumed much smaller than the drift sections. Therefore, we can assume that the effect of electron ballistic phase bunching took place only in the long drift sections whereas only the electron energy modulation taking place in the short cavities. These assumptions along with the no space charge and zero velocity spread effects help us to obtain the necessary equations for calculating the susceptibility of gyroklystron that determines the interaction of electron beam with the cavity. This susceptibility helps us to write the balanced equations for calculating the field amplitude and phase in each cavity. Using these balanced equations, the gain of multicavity stagger tuned gyroklystron is calculated.

Here we have used a technique by which the device gain can be expressed as difference of two terms in which the first term is gain constant and independent of frequency detuning. The second term is dependent on frequency detuning and thus provides gain variation. This variable part is responsible for the stagger tuning in gyroklystrons. Here, we optimize this variable gain term simultaneously for the gain and bandwidth in terms of normalized frequency detuning parameter. The results obtained for two and three cavity gyroklystrons are analyzed. For the case of two cavity stagger tuned gyroklystron we have obtained maximum 5 times increase in bandwidth with approximately 17 dB reduction in gain as compared to the two cavity gyroklystron with no stagger tuning. The gain-bandwidth product is obtained nearly two times larger as compared to the two cavity 30 dB gain gyroklystron without stagger tuning. The results obtained for three cavity stagger tuned gyroklystron shows nearly 10 times more bandwidth with 32 dB decrease in gain as compared to the three cavity gyroklystron without stagger tuning. About 3.5 times increase in gain-bandwidth product is also observed as compared to three cavity 50 dB gain gyroklystron with no stagger tuning. The results obtained here demonstrate bandwidth enhancement, decrease in gain and the overall increase in the gain-bandwidth product due to stagger tuning. Therefore, this technique like in klystrons can be used for the performance improvement of gyroklystrons.

Power and Frequency Estimation for 0.67 THz Gyrotron for Radioactive Material Detection

Nitin Kumar, **Udaybir Singh**, **Anil Kumar**, **Hasina Khatun**, **and A. K. Sinha**
Central Electronics Engineering Research Institute (CEERI, CSIR)
Pilani, Rajasthan 333031, India

Abstract— Terahertz radiation (0.3 THz–3 THz) is emerging as a thrust research area due to its various remarkable applications. A new application of terahertz radiation for the detection of concealed radioactive materials is proposed by *Granatstein* and *Nusinovich* at 670 GHz frequency. The detection of radioactive materials is based on the phenomena of air breakdown by focused terahertz radiation. In the presence of radioactive material in a container, the density of electrons increases several folds in air and initiate the breakdown in the presence of electromagnetic radiation of terahertz frequency region, which is not possible in the absence of extra electrons produced by some radioactive material. In this article the results of beam-wave interaction and power and efficiency growth for 670 GHz, 300 kW gyrotron are presented. The beam parameters and the interaction cavity geometry calculations are performed for the selected operating mode $TE_{25,10}$. The detail of mode selection process is also presented. The mode competition is studied in terms of the start oscillation current and coupling coefficient. $TE_{22,11-}$ and $TE_{25,10-}$ are found as the most competing modes to the operating mode. The magnetic field at the cavity center is calculated directly from the frequency and detuned up to an optimum value to achieve the maximum efficiency. MAGIC code is used in the power and frequency calculations. The electron beam is launched at the first co-rotating maxima of the operating mode during the MAGIC simulations to obtain maximum beam-wave interaction efficiency. The results show more than 300 kW power at 670 GHz frequency at $TE_{25,10}$ mode.

Swarm Optimization of Raised Cosine Non-linear Cylindrical Waveguide Taper for High-power Applications

Rajeev Sharma[1], **Smrity Dwivedi**[2], **R. P. Gupta**[3], **and P. K. Jain**[2]

[1]Department of Scicence & Technology, TDT Division, New Delhi, India
[2]Department of Electronics Engineering, Institute of Technology
Banaras Hindu University, Varanasi, India
[3]Department of Electronics & Communication, Jaipur National University, Jaipur, India

Abstract— The requirement of non-linear taper arises at the output stage of high-power microwave/millimeter wave active devices, e.g., klystron, gyrotron, accelerator or any other system and act as the RF interface line between the device and system with maximum power transfer and minimum mode conversion. The presence of a taper section inevitably introduces unwanted parasitic modes. Taper should provide a good match at the input port and prescribed spurious mode suppression at the output port over a short length.

In the present paper, a non-linear cylindrical waveguide taper excited in the TE mode for its application in high-power CW gyrotron as a output taper connected at the end of RF interaction cavity has been analyzed using mode matching technique and optimized using an ANN technique. For the non-linear taper raised cosine profile has been taken since this function provides uniform contour at both the ends. This profile provides good impedance matching, low reflection as well as low mode conversion for a relatively smaller taper length.

The mode matching technique involves matching of the total modal field at each junction between uniform sections so that conservation of power is maintained. From this process, the amplitudes of the separate modes at the output of a junction have been deduced in terms of the amplitudes of the mode spectrum at the input to the junction. The power of the modal matching technique stems from the fact that the amplitudes of the modes have been expressed as the components of a scattering matrix. Each junction along the length has its own scattering matrix. The matrices for all junctions have been be cascaded and an overall scattering matrix has been formed. The overall scattering matrix contains the input reflection coefficient and the output transmission coefficient.

Then optimization of S-parameters for getting low mode conversion and high transmission has been done using an ANN technique. Particle swarm optimization (PSO) is a powerful ANN tool, which is used to solve continuous nonlinear function and optimizes multi variables at a time, for a given operating frequency and mode. PSO has been used here to achieve optimized tradeoff between matching of desired resonant frequency and minimizing the reflections in the desired mode of operation.

A raised cosine non-linear taper has been optimized for maximum transmission ($> 95\%$) and minimum mode conversion ($< 1\%$) at the desired mode for best fitness value. The design of a nonlinear taper for its application in a 42 GHz, 200 kW CW gyrotron operating in the $TE_{0,3}$ mode has been taken as a case study. The optimized results show the best matching obtained with the raised cosine taper which confirms effectiveness of this method for the design of the nonlinear cylindrical waveguide taper. Scattering parameters S_{11} and S_{21} have been achieved as 0.67% and 97.78%, respectively for the desired mode of operation. This design has been also validated using finite integration method based frequency domain commercial simulation code 'Microwave Studio' and the results are found in good agreement with the analytical values.

Investigation of New Material for Megawatt Power Gyrotron Collector

Hasina Khatun, Naveen K. Sahu, Sudeep Sharan, Ranojoy Bhattacharya, Uttam K. Goswami, Anil Kumar, Udaybir Singh, and A. K. Sinha
Gyrotron Laboratory, Microwave Tube Area, Central Electronics Engineering Research Institute (CEERI) Council of Scientific and Industrial Research (CSIR), Pilani, Rajasthan 333031, India

Abstract— Multi-megawatt power gyrotron needs lifelong collector. To overcome the problem of high thermal loading on the collector surface, the collector can be manufactured by copper alloys like aluminum oxide copper called Glidcop and zirconium chromium copper (ZrCrCu). The addition of small amount of zirconium chromium in copper increases the thermal and electrical conductivity whereas aluminium oxide decreases the thermal and electrical conductivity [1, 2]. But unlike OFHC copper, both the alloys of copper greatly resist the material softening even at alevated temperature. This is due to the high tensile strength of glidcop and ZrCrCu than OFHC copper as shown in Table 1. The paper presents the thermal analysis of single stage depressed collector of 120 GHz, 1 MW gyrotron. The simulation is carried out using ANSYS. A comparative analysis shows that the Glidcop and ZrCrCu can overcome the problem of thermal loading and able to operate the gyrotron for continuous wave (CW) pulse.

Table 1: Properties of OFHC copper and its alloy.

Properties	**OFHC Copper**	**ZrCrCu**	**Cu-Al_2O_3**
Electrical conductivity ($m/\Omega \cdot mm^2$)	58	50	50
Thermal conductivity (W/m·K)	391	330	344
Density (g/cm^3)	8.94	8.9	8.96
Specific heat (J/g·°C)	0.385	0.376	0.385
Thermal expansion coefficient (10^{-6}/K)	17.7	17	16.6
Tensile strength (MPa)	220	640	390
Young modulus (GPa)	115	120	130

REFERENCES

1. Beringer, M. H., "Design studies towards a 4 MW 170 GHz coaxial-cavity gyrotron," Dissertation, 191, Karlsruher Institut für Technologie, Fakultät für Elektrotechnik und Informationstechnik, 2010.
2. Thai-German Special Steel Center, www.thai-germansteel.com.

Eigenmode Analysis of Metal Photonic Band Gap Cavity for Gyrotron Operating in Higher Order Mode

Ashutosh and P. K. Jain
Center of Research in Microwave Tubes, Department of Electronics Engineering
Institute of Technology, Banaras Hindu University, Varanasi, India

Abstract— Photonic band gap (PBG) structures have proven wider research interest due to its fascinating frequency and mode selective property. The devices realized using PBG structures give promising performances. The PBG cavity have potential application in microwave, millimeter-wave and infrared devices, such as, antennas, waveguides, filters, resonators, planar reflectors, integrated circuits etc.

Approaching to higher frequency operation of the gyrotrons provide numerous new applications. In order to shift operating frequency to higher value, one needs higher DC magnetic field. Furthermore, higher frequency of operation also reduces the transverse dimension of the interaction structure for the fundamental cyclotron frequency. This results fabrication difficulties and expensive and also heating on resonator walls becomes excessive. Thereby, it reduces the power handling capability of the device. Beam interception also limits the performance of the small interaction structure device. To reduce the requirement of magnetic field, device must operate at higher cyclotron harmonic. In order to increase structure dimension, higher operating mode of RF structure is adapted but this causes overmoding of the structure due to the increase in mode density of nearby modes.These problems can be reduced by using photonic band gap structures which provide better mode selectivity. In comparison to conventional cylindrical cavity, higher transverse dimension of PBG cavity enables the high power handling capability for the same operating mode and frequency. Metal PBG structure is more suitable over dielectric for such high power devices. With the dielectric PBG, breakdown and charging are the unavoidable aspects. On the contrary, a metal PBG structure does not possess such problems due to their excellence conductibility and also reduces the absorption problem. Furthermore, vacuum grade composite dielectric materials presently available cannot sustain at very high operating temperature with sufficient mechanical strength.

In this paper, the eigenmode analysis of metal photonic band gap cavity operating in a higher order TE_{341} mode is presented. Band structure of the two dimensional photonic band-gap structure of triangular lattice is calculated using standard Yee's the finite difference time domain (FDTD) method for the TE mode of propagation. FDTD is used due to its various advantages over the other existing methods. The global band gap diagram of the structure has been calculated for the different value of rod radius to lattice constant ratio. Using this global band gap diagram, a proper design point is chosen for the PBG cavity to operate in a higher order mode. The designed PBG cavity is simulated using high frequency structure simulator (HFSS) for eigenmode analysis. A confined TE_{341} mode is observed at 35 GHz operating frequency. The reduced competing modes are observed in PBG cavity in comparison to cylindrical cavity. Comparison of transverse dimension of the PBG cavity and conventional cavity is also demonstrated.

Session 4A7a
Frequency Selective & Retarding Surfaces for Microwave and Millimetre-wave Applications

A Triple-bandgap Uni-planar EBG Structure for Antenna Applications

Huynh Nguyen Bao Phuong[1], **Dao Ngoc Chien**[1], **and Tran Minh Tuan**[2]

[1]School of Electronics and Telecommunications, Hanoi University of Technology
No. 1 Dai Co Viet Road, Hanoi, Vietnam
[2]National Institute of Information and Communications Strategy
No. 115 Tran Duy Hung Road, Hanoi, Vietnam

Abstract— A triple-band electromagnetic bandgap (EBG) structure for antenna applications is presented in this paper. This EBG structure is a kind of distorted uni-planar compact EBG (DUC-EBG). The idea proposed in this the paper is etching several properly shapes in the area of the UC-EBG cell to introduce three bandgaps separately. These bandgaps can be represented by three different equivalent circuits, from which the resonant frequencies can be estimated.

From the conventional UC-EBG structure as shown in Fig. 1(a), the straight lines are transformed into the meandered lines for connecting two adjacent cells. These lines introduce equivalent inductances, while the gaps between thee conductor edges of two contiguous lattices introduce equivalent capacitances. In this design, parasitical capacitances, which are produced by zigzags of the meandered lines, will allow to increase the total capacitance of the equivalent circuit, and hence move down the first bandgap of the structure to lower frequency region. This bandgap is formed similar as the principle of conventional UC-EBG. The other bandgaps are created by introducing moore equivalent capacitance C and inductance L in the proposed structure. In four pad corners, square split ring resonators (SSRR) are embedded to obtain the second bandgap. Thee total capacitance with SSRR consists of two parts, in which one part is the coupling capacitance between the outer and the inner rings, and the other one is produced by the electric chargees accumulates at the split (r). Thee current flowing along SSRR coil with width e produces the equivalent inductance. At last, two L-shaped slots are etching symmetry at the central pad of the structure. The slot width v introduces equivalent capacitance and the square pad connecting two slots can be resulted in equivalent inductance. As a result, it can be described by another equivalent circuit that defines the third bandgap independently with the other bandgaps. The formulas for investigating the central frequencies of the three bandgaps are also presented corresponding to the equivalent circuits.

Thee proposed EBG structure is printed on a FR4 dielectric slab with dielectric constant of 4.4 and thickness of 1.6 mm. The periodic spacing a $a = 12$ mm is chosen, and the gap g between conductor edges of two adjacent cells is 0.5 mm. The FDTD method based on in-house developed computational code was used to analysis the dispersion properties of the structure. Dispersion diagram of complete triple-bandgaps is numerically presented in Fig. 1(c).

In conclusion, the bandgaps of the DUC-EBG proposed in this paper include the frequency bands from 3.1125 to 4.65 GHz (39.2%)), from 4.9366 to 5.285 GHz (6.83%)), and from 6 to 7.42 GHz (21.16%). The structure is applicable to suppression of the surface wave propagating in all directions and can be used for multi-band applications such as dual/triple antennas.

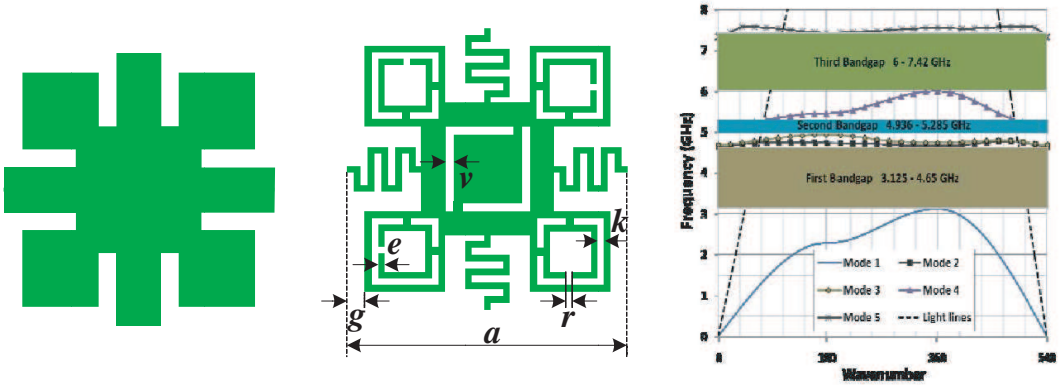

(a) (b) (c)

Figure 1: (a) Conventional UC-EBG, (b) Proposed triple-band EBG structure and (c) Dispersion diagram.

A Terahertz Meta Surface Filter Employing Sub-wavelength Metallic Apertures on a Thin Substrate

S. Hussain, **D. Kim**, **and J. H. Jang**
School of Information and Communication
WCU Department of Nano-Bio Materials and Electronics
Gwangju Institute of Science and Technology, Gwangju, South Korea

Abstract— In this paper, the design and simulation of a single layer meta-surface filter, having the simple geometry, has been demonstrated. The filter is made up of sub-wavelength metallic slot apertures which are periodic in a two dimensions, essentially forming a meta-surface. The filter is realized by fabricating the apertures using micro structured gold film on an ultra-thin silicon nitride substrate. Since, the substrate thickness is much smaller than the free space wavelength of the incident electromagnetic wave so there are no unwanted Fabry-Perot resonances which are inescapable in thick substrates. Ultra-thin substrate also facilitates achieving higher transmitted amplitude because of extremely low dielectric loss. The design of the filter was analyzed using finite element method (FEM) and was optimized for attaining the better out of band attenuation. Insertion loss of less than 0.5 dB has been achieved in the numerical simulation at the resonant frequency of the 1 THz.

A Broadband Photolithographic Polariser for Millimetre Wave Applications

G. Pisano, M. W. Ng, V. Haynes, and B. Maffei
Jodrell Bank Centre for Astrophysics, School of Physics and Astronomy
The University of Manchester, United Kingdom

Abstract— Circular polarisers are used to convert linear- into circular-polarisation, and vice versa. This is achieved by introducing a phase-shift of 90° between two orthogonal polarisations passing through the device. These devices can be designed for example using birefringent slabs with appropriate thicknesses (Quarter-Wave Plates). An interesting alternative solution consists of designing planar metallic grids with subwavelength geometries that exhibits different behaviour along two orthogonal axes. This technique was initially suggested by Lerner [1] and later adopted to build Half-Wave Plates [2].

In this work we present a broadband dielectrically embedded polariser (Quarter-Wave Plate) built using photo-lithographic techniques. The device was experimentally tested using a Vector Network Analyser working in W-band (75–110 GHz). The presented results are in excellent agreement with finite-element analysis simulations.

REFERENCES

1. Lerner, D. S., "A wave polarization converter for circular polarization," *IEEE Trans. Antennas Propag.*, Vol. 15, 3–7, 1964.
2. Pisano, G., et al., "A metal-mesh achromatic half-wave plate for use at submillimetre wavelengths," *Applied Optics*, Vol. 47, No. 33, 6251–6256, 2008.

Design and Characterization of a Dielectric Q-plate for Millimetre-wave Photon Orbital Angular Momentum Applications

S. Maccalli[1], **G. Pisano**[1], **M. W. R. Ng**[1],
B. Maffei[1], **Malcolm Gray**[1], **and S. Colafrancesco**[2]

[1]School of Physics and Astronomy, The University of Manchester, Manchester, UK
[2]School of Physics, University of the Witwatersrand, Johannesburg, South Africa

Abstract— Recent years have seen a growing interest in the research field of optical beams with complex wavefront structures [1] such as the Optical Vortices. These kind of beams can carry the well-known Spin Angular Momentum associated with the circular polarization of light (SAM) and an additional and different form of angular momentum: the so-called Orbital Angular Momentum (OAM) [2]. The OAM is the consequence of the phase-front not being parallel anymore to the transverse plane. When a wave has a vortex, optical parallel wavefront planes are no longer separated but connected through the helical wave front along the axis of the vortex. The existence of an optical vortex influences the distribution of phase over the whole space. It can be demonstrated that the accumulative phase difference around the axis of the vortex is $2\pi l$, where l is defined as the topological charge and can be any integer number going from $-\infty$ to $+\infty$ [2].

One way of producing beams carrying OAM is to use a device called q-plate. A q-plate can be imagined as an inhomogeneous birefringent plate where the ordinary and extraordinary axes, lying on the plate surface, change their orientation across it [3]. A material with such properties cannot be found in nature and it needs to be artificially designed. The usual way to generate birefringent materials starting from normal dielectrics is to cut sub-wavelength parallel grooves across it. Light crossing these materials will experience different refractive indices depending on its polarization being parallel or perpendicular to the grooves. Using this technique it is possible to design quasi-optical retarders cutting parallel grooves with appropriate geometries across the surfaces of dielectric slabs. The differential phase-shift introduced by the device will depend on the grooves depth. The device will be inherently narrow-band because the desired phase-shift is only achieved at a specific frequency (and its harmonics).

It is possible to use the above technique to also manufacture q-plates. Following the recipe given in [3], we designed a q-plate optimized to work at 100 GHz. Our $l = \pm 2$ q-plate is equivalent to an Half-Wave Plate with variable birefringent axes orientations: across the plate they follow directions parallel and perpendicular to concentric rings, as shown in Figure 1.

In this paper we present the design, fabrication and beam pattern characterization of a nylon-made q-plate that generates ± 2 charged OAM states at millimeter wavelengths. This q-plate is optimized to work around 100 GHz but the same design can be scaled to work at other frequencies in the millimeter-wave range. The designed plate can create a point defect on the phase front structure of a fundamental Gaussian beam with the associated optical vortex and annular intensity pattern: both phenomena have been accurately characterized by means of beam scanning. The simple manufacturing method used here allows cheap and fast q-plate production. Measurements collected using a millimeter wave VNA are compared with Finite-Element analysis (HFSS) simulation results. Our aim is to study and design new plates to improve the OAM manipulation possibilities in the millimeter spectrum.

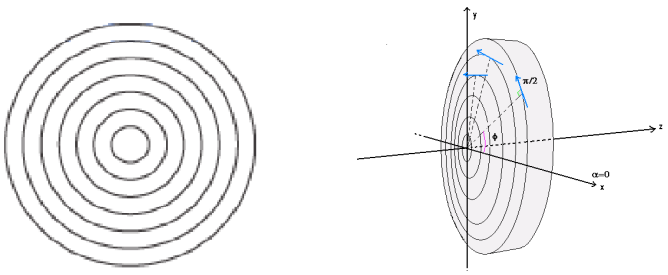

(a) (b)

Figure 1: Orientation of the optical axis in a q-plate built to produce a POAM mode ± 2 using formula given in [3] with $q = 1$ and $\alpha_0 = \pi/2$.

REFERENCES

1. Beijersbergen, M. W., L. Allen, et al., *Optics Commun.*, Vol. 96, 123, 1993.
2. Allen, L., et al., *Phys. Rev. A*, Vol. 45, 8185, 1992.
3. Marrucci, L., et al., *Phys. Rev. Lett.*, Vol. 96, 163905, 2006.

Dog Bone Triplet Metamaterial Wave Plate

I. Mohamed, **G. Pisano**, **M. W. Ng**, **V. Haynes**, **and B. Maffei**
Jodrell Bank Centre for Astrophysics, School of Physics and Astronomy
The University of Manchester, United Kingdom

Abstract— Metamaterials are artificially made sub-wavelength structures arranged in periodic arrays. These materials can be designed to interact with electromagnetic radiation in many different and interesting ways. For example, using periodic metallic grids it is possible to let the radiation experience a Negative Refractive Index (NRI): this was first demonstrated in 2000 [1].

We have used this technique to design and build a quasi-optical Half Wave Plate (HWP). Unusually large birefringences can be achieved by designing one axis with a NRI whilst leaving the other with a positive refractive index [2]. This allows for the fabrication of relatively thin waveplates, at sub-wavelength level.

However, due to their inherent requirement to achieve resonance to create the NRI band, the functional bandwidth of such NRI wave plate is of the order of 1–3% [2, 3]. We seek to increase the bandwidth by using the Pancharatnam theory [4] that has been successfully applied in the past with birefringent materials [5]. In this case different wave plates are rotated and cascaded with their axes oriented following specific angles. The HWP presented here is based on a 'dog bone triplet' geometry (image below). The dog bones are supported by polypropylene substrates.

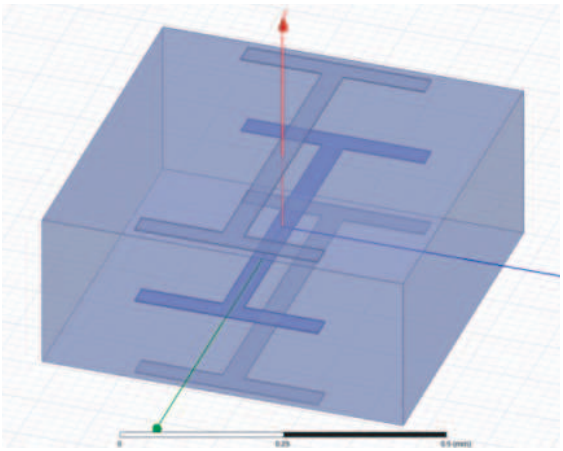

REFERENCES

1. Smith, D. R., et al., *Phys. Rev. Lett.*, Vol. 84, No. 18, 4184–4187, 2000.
2. Weis, P., et al., *Appl. Phys. Lett.*, Vol. 95, 171104, 2009.
3. Imhof, C. and R. Zengerle, *Opt. Comm.*, Vol. 280, 213–216, 2007.
4. Pancharatnam, S., *Proc. Indian Acad. Sci., Sec. A*, Vol. 41, No. 4, 137–144, 1955.
5. Pisano, G. P., et al., *App. Opt.*, Vol. 4527, No. 27, 6982–6989, 2006.

Millimetre Waves Photolithographic Polariser Beam Impact

B. Maffei, **G. Pisano**, **M. W. Ng**, **V. Haynes**, **and F. Ozturk**
Jodrell Bank Centre for Astrophysics, School of Physics and Astronomy
The University of Manchester, UK

Abstract— Quasi-optical polarisers can be used to create circularly polarised beams from linearly polarised fields. These devices can be designed using planar metallic grids with sub-wavelength structures that behave differently along two orthogonal axes. On the one hand, their design is usually based on transmission-line codes that implicitly assume plane waves and normal incidence conditions. On the other hand, in real practical situations, these devices are used with Gaussian beams.

In this work, we experimentally study the effects of a dielectrically embedded polariser made with photolithographic techniques on the Gaussian beam of a horn. The impact of the polariser on the beam is measured using a millimetre wave Vector Network Analyser working in the W-band.

Session 4A7b
Electromagnetic Theory

Energy Conservation in a Waveguide System with an Imperfection Core

Akira Komiyama
Osaka Electro-Communication University, Hatsu-cho, Neyagawa-shi 572-8530, Japan

Abstract— Mode waves in an ordered waveguide system composed of identical cores are extended over the entire system. When one of cores is illuminated at the input end of the waveguide system all extended modes are excited and propagate through the system. Mode waves in a disordered waveguide system composed of randomly different cores in size are localized and are concentrated into a narrow region of several cores [1]. When one of cores is illuminated at the input end of the waveguide system a number of localized modes are excited and only their modes propagate through the system. In a waveguide system with an imperfection core extended modes and a localized mode propagate through the system. Contributions of the extended modes to the light propagation can be divided into the direct wave, which is a wave propagating in an ordered waveguide system, and the scattered wave caused by an imperfection core. For fixed core number and $z \to \infty$ where z is the distance along the waveguide axis the asymptotic expansions of the amplitudes of the direct and scattered waves have been derived and it is shown that the direct wave is partially canceled by the scattered wave and a shadow takes place [2]. The amplitudes of the direct and scattered waves decrease in proportion to $z^{-\frac{1}{2}}$ and the amplitude of the sum of the both waves decreases in proportion to $z^{-\frac{3}{2}}$. So far, a physical meaning of the cancellation of the direct wave by the scattered wave is unclear.

In this paper, asymptotic expansions of the amplitudes of the direct and scattered waves in a waveguide system with an imperfection core are derived for large core number and the partial cancellation of the direct wave by the scattered wave is shown in detail. The total power of light in the cross section of a waveguide system is analytically derived and it is shown that the generation of the localized mode wave is balanced by the cancellation of the direct wave by the scattered wave.

REFERENCES

1. Komiyama, A., *Opt. Comm.*, Vol. 151, 25–30, 1998.
2. Komiyama, A., *IEICE Trans. Electron.*, Vol. E94-C, 59–62, 2011.

Maxwell's Transfer Functions

M. J. Underhill
Underhill Research Ltd., UK

Abstract— For antennas and propagation we require the total transfer function between the transmitter and the receiver over the operating band of frequencies. The classical EM equations need to be transformed into transfer functions conveniently defined by spatial and time domain Laplace Transforms. Transfer functions equations can define all the parameters of an antenna such as, near field stored energy and fields, coupling to other antennas and surfaces, and far-field array patterns.

Transfer functions are causal, contain explicit sources and sinks, may be partially reversible, may be defined to obey reciprocity, can embody power and energy continuity and conservation, and can contain all EM physics as observed. To be more readily acceptable the ElectroMagnetic (EM) transfer functions should appear as simple extensions to the well known Maxwell's equations.

"Maxwell's Equations" were created about six years after his death by FitzGerald, Heaviside, and Lodge-along with key contributions from Hertz [1]. In the same vein Maxwell's name is given to the proposed set of equations, "Maxwell's Transfer Functions" — MTFs.

The route to the transfer functions is through the "Physical EM (PEM) Model of Electromagnetism" put forward at PIERS 2011 in Marrakesh [2]. This model is based on coupled transmission lines for filaments in space following the direction of (primary) power flow. The variables are electric and magnetic vector potentials and bi-vector displacement currents. Such a model automatically has explicit sources and sinks and is causal in the same sense that waves on a transmission line are causal. This model contains, or relates to, seven new fundamental EM physics discoveries. 1. Local Ether with Ether Dragging, 2. EM Critical Frequency of 47.75 MHz, 3. EM Coupling with $1/f^{1/2}$ dependence and causing partial coupling of EM equations, 4. Process Capture and RSS Combining, 5. EM String Particle and Photon models, 6. EM explanations of Mass, Inertia, Ordinary Matter, Dark Matter and Particle Wave Diffraction, 7. Continuous Relativity (CR) that unites SR and GR, and allows superluminal (dense) particles.

Maxwell's equations cannot be solved without applying constraints. These can for example be, the application of an arbitrary gauge (such as the Lorentz gauge), the imposition of (real) boundary conditions as in waveguides, or the imposition of a spherical coordinates as is common for radiation from an antenna, or GTD (Geometrical Theory of Diffraction) constraints for reflector antennas. The PEM model contains a more flexible and versatile set of constraints. It contains the two new discoveries, *electromagnetic coupling* κ and *process capture*, which act as constraints, replacing all gauge, and coordinate constraints. Additional solutions of the EM equations, not necessarily requiring geometrical boundary conditions, are then possible.

We start with the six classical Maxwell equations and make them all reversible. The coupling factor κ is inserted in the two curl equations and the two constitutive relations. The two div equations are arguably not needed for the transfer functions. They represent a relationship between axial and radial div components. In any case the definition of div has to be redefined so that $\mathrm{div}|D| = 0$ or $\mathrm{div}|B| = 0$ to ensure local compliance with energy conservation. This gives a total of 10 equations of which two are optional and eight are essential. The eight essential equations are then, reassembled to give four equations defining contributions to each of the four fields as δE, δD, δH, and δB, each having two contributory terms combined together. We find that the terms for δD and δB have to be combined using the RSS (Root-Sum-of-the-Squares) process combination rule. We use the symbol $\oplus$ to signify this. The terms contributing to δE and δH, are combined conventionally. To obtain the final transfer functions, these four equations have to be integrated to combine the contributions from sources at all points in coupled space. The E and H contributions are integrated conventionally, and 'RSS integration' is used for the D and B contributions. The four resulting equations are the Maxwell Field Transfer Functions (MTFs).

The Physical EM (PEM) model is couched in terms of potentials and displacement currents. For completeness the MTFs can be rearranged into PEM transfer functions (PEMTFs).

REFERENCES

1. Hunt, B. J., *The Maxwellians*, Cornell University Press, 1991, ISBN 0-8014-8234-8.
2. Underhill, M. J., "A physical model of electro-magnetism for a theory of everything," *PIERS Online*, Vol. 7, No. 2, 196–200, 2011.

Novel Analytic EM Modelling of Antennas and Fields

M. J. Underhill
Underhill Research Ltd., UK

Abstract—

Summary: The Physical EM model [1] (Piers 2011, Marrakesh) and "Maxwell's Transfer functions" [2] are the basis for an analytic EM and antenna modelling method that requires no matrix inversion. *'Analytic Region Modelling'* is therefore very fast and efficient and scalable to problems of high complexity. A Mathcad implementation of the methodology is presented with some illustrative examples.

Process Capture: *Process Capture* is an observable fundamental law (originally seen in small tuned loop antennas). Overlapping distributed processes combine at any point according to the RSS (Root-Sum-of-the-Squares) law. The strongest process 'captures' and suppresses the weaker process. Over a short (coupling) distance the suppression is progressive. Process Capture is what makes Analytic Modelling possible. It allows *Process Regions* to be defined in which there is only one dominant process.

Electro-Magnetic Coupling: In free-space we find that the *co-local electro-magnetic (EM) coupling* between the fields H and D/ε, and between H and B/μ is not 100% but is $\kappa_0 = 1/2\pi$. This means that Process Regions of different processes can overlap, and the transfer of one process to another is progressive in the direction of power flow. Thus the positions of the process boundaries are not the same for transmission as for reception by the antenna. There is 'hysteresis'. EM coupling is found by experiment to be proportional to the inverse square root of the frequency. This means that antennas do not 'scale' perfectly in practice. Scale modelling is not always effective. This effect is most obvious in the estimation and measurement of the near-field. The far field is much less affected.

Evanescent Wave Profiles and Stored Energy: EM coupling also defines stored energy and evanescent wave profiles. Evanescent waves transport energy along wires and surfaces. Stored energy can be considered as an evanescent standing wave.

The Local Ether Four Transmission Line Model of EM: The chosen general purpose physical model is two low-pass and high-pass pairs of co-located transmission lines in a 'local ether'. One LP/HP pair represents conventional and electric displacement current, with electric vector potential. The other represents magnetic displacement current and magnetic vector potential. The local ether is the region of the stored energy of an antenna.

Multi-mode Antennas: For *Analytic Modelling* of antennas usually one transmission line per antenna element is sufficient. Multi-mode antennas such as the loop-monopole usually require additional (partially coupled) transmission lines for each operative mode.

The Theory of Transmission and Reception: A displacement current in a potential with an in-phase component will radiate power and the current attenuates in the direction away from the source of the current. A displacement current in an out-of-phase potential component will receive power, and the current increases in the direction towards the sink of the current. With these definitions the power transmitted or received at any point on an antenna surface may be calculated. Note that electric and magnetic quantities must be taken into account separately and together. And there can be conversion from one to the other.

Stored Energy in Space: Stored energy is the product of the displacement current and the quadrature potential. The stored energy of standing waves is found by separation into forward and reflected waves.

Stored Energy Capacity, Local Q and Antenna Q: The local Q is the stored energy in a small volume divided by the transported energy flowing through it. It is the *stored energy capacity*. The antenna Q is 2π times the total stored energy of an antenna divided by the transmitted or received energy per cycle.

Analytic Region Modelling: With the above definitions, three dimensional analytic expressions for all physical quantities surrounding an antenna, over a surface, in a waveguide, etc. may be obtained. The physical quantities can include, all fields, potentials, displacement currents, power flow (Poynting) vectors, spatial impedances and Qs, etc. Process capture allows finite regions to be represented in compact form with very few terms. No matrix inversion is required. The accuracy of the model can be improved by calibration by a few practical measurements.

Conclusion: "Analytic Region Modelling" could well be the future of most if not all EM modelling.

REFERENCES

1. Underhill, M. J., "A physical model of electro-magnetism for a theory of everything," *PIERS Online*, Vol. 7, No. 2, 196–200, 2011.
2. Underhill, M. J., "Novel analytic EM modelling of antennas and fields,".

Evanescent Fields Outside Weakly Deformed Optical Resonators

Stephen C. Creagh and Michael White
School of Mathematical Sciences, University of Nottingham, Nottingham NG7 2RD, UK

Abstract— Strongly directional emission may be achieved from whispering gallery modes in optical resonators which are only very slightly deformed from spherical or circular geometry. The ability to effect dramatic changes in the external field using very small geometry changes is potentially useful in applications such as lasers, sensors and filters, but an analytical description of this phenomenon is surprisingly challenging. A natural theoretical approach is to use short-wavelength approximations to treat the evanescent, external field, but this is complicated by the appearance of natural boundaries in the required complex ray data. In practice, one often finds that the external field cannot be extended far enough outside the resonator as long as the underlying ray family is computed exactly.

We exploit an approach which circumvents this problem by constructing approximate solutions of the eikonal equation for ray families which permit extension as far as required into the complex domain. The method successfully predicts the strong directionality seen in very weakly deformed resonators. An especially interesting regime occurs when the underlying ray family satisfies resonant conditions which put it near an island chain in the ray-dynamical phase space. Here one finds that the external and internal fields can differ in stark, counterintuitive ways. For example one may find that the directions of most intense emitted light seem to come from regions of the boundary where the internal field is least intense. A successful explanation of effects such as this is possible using an approximation of the ray family suitably modified to account for the resonance conditions. The explicit examples treated are two-dimensional but the overall approach generalises naturally to three-dimensional problems.

A New View of Spectral Analysis of Linear Systems

J. Heredia and E. Gago-Ribas
Electrical Engineering Department, University of Oviedo, Spain

Abstract— There are many scientific and technological areas where Signals & Systems Theory (SST) plays a fundamental role. There are also many references which treat this field, especially in connection with communication and circuit theory or with the important particular application concerning discrete signals and systems. While the usual point of view is perfectly valid for practical purposes, it uses to avoid many concepts which become fundamental in the generalization of the analysis of physical problems: a general representation different from the usual time-frequency domains, the description in terms of vector spaces and the algebra associated, the description of the Dirac delta and other generalized signals in terms of the distributions theory, etc. The most important aim of obtaining a Generalized Signals & Systems Theory (GSST) is to connect the usual Signals & Systems Theory with important mathematical representations that may be able to obtain more general representations that may be rigorously applied to model general physical problems (radiation and scattering problems in our particular case). This generalization is based on defining any problem under the infinite dimensional space of signals and systems analyses and the subsequent representations based on this algebra.

A particularly important analysis under the GSST is the so called *Generalized Spectral Analysis*. The description and development of this particular generalization will be the main goal of the present paper and can be summarized as follows. Once the infinite dimensional vector space algebra is defined-distance, vector spaces, norm and scalar product- each signal can be described as a *generalized linear combination*. By choosing a set of basis functions, it is possible to reconstruct the signal in terms of the generalized linear combination with the basis functions weighted by a set of coefficients which are obtained through the minimization of the *distance* between the original signal and this generalized linear combination. Usually, the calculation of each coefficient is just the scalar product between the original signal and each element of the base, that is, the projection of the signal over each element of the base-assuming that the set of infinite basis functions is orthogonal with respect to the scalar product-. Different convergence criteria usually appear from this particular analysis.

From this point of view, the selection of a specific set of basis functions leads to the description of a particular transformation and is able to define the concept of *generalized transformation*. For instance, if complex exponentials are chosen as the set of basis functions in continuous variable, therefore the generalized transform becomes the well known Fourier transform. These functions are eigenfunctions of any linear invariant system and their corresponding eigenvalues-spectrum of the system are the Fourier transform of the impulse response. The generalization of those concepts for linear non invariant systems where the sets of basis functions are not eigenfunctions of the systems together with the definition of a generalized transform leads to the concept of a generalized spectral analysis which widely open the scope of the traditional spectral analysis specially when dealing with time-space physical problems, usually invariant in time domain but non invariant in space domain-. The complete description of this generalization will be provided in the present paper.

Complex Parameterization of the Lossy Transmission Line Theory

E. Gago-Ribas and M. Carril-Campa
Electrical Engineering Department, University of Oviedo, Spain

Abstract— The usual transmission line theory (TLT) found in the specialized literature often deals with its analysis for the ideal case (lossless case) or the low losses approximation, the last one obtained from a mathematical point of view. The present paper deals with a rigorous methodology that allows confronting the TLT for the general lossy case in a very understanding and visual way. This methodology is based on analyzing the theory from the point of view of performing a rigorous analysis of the complex transformations (complex parameterization of the lossy transmission line theory, CTLT) which define the mathematical parameters involved in the physical description of the behavior of a transmission line with losses under time harmonic regime. From this point of view, the usual lossless case becomes a particularization of the general results in the CTLT analysis; besides, the low losses approximation may be fully understood under this generalization as well as other interesting particular cases such as the non dispersive lossy case.

One of the main important properties associated with the CTLT comes from the fact that they may be graphically represented by analytical curves which, in many cases, correspond to very interesting mathematical curves, ambling from basic circumferences to Cassini ovals, for instance. This leads to a set of graphs that may be summarized as follows:

- "Universal" characterizations of the behavior of both the basic parameters (characteristic impedance and propagation constant) as well as the wave parameters (impedance, admittance and reflection coefficient) involved in the transmission line theory, with all the parameterizations described by well-known analytical curves.
- "Graphical parameterizations of losses and important physical interpretations directly induced by the geometrical properties of these curves, many of them not easily available from the usual mathematical approach. The large number of physical interpretations appearing from the graphical analysis may be exemplified by the following examples: (i) the usual Smith Chart becomes a particular case (when losses become null) of the Generalized Smith Chart introduced in this paper. In fact, the new Generalized Smith Chart is only one of the several complex parameterizations that will be presented in this paper; (ii) the description of all the possible values of the characteristic impedance and propagation constant in terms of losses and the subsequent identification of all the transmission lines with a fixed value of a basic parameter (for instance, all the transmission lines with the phase of the characteristic impedance fixed to a specific value); (iii) from the practical and designing points of view it is possible to determine whether a solution is possible or not given some specific design constraints and, in case a solution is indeed possible, describing the range of transmission-line-wave-parameter values associated to such solution and the understanding of which parameters are susceptible of variation to resolve possible designing errors, allowing optimization approaches to their solution.

All these aspects are particularly relevant, both from the educational point of view, and from the standpoint of TL's based circuit design. Also, the difficulty of resolving some of the equations associated to the lossy TLT can be substantially reduced by using the geometrical properties associated to the CTLT methodology. In this sense, the paper will emphasize the concepts and physical interpretations that can be extracted from this methodology. This fully analytical methodology has also been implemented into a software tool that will be introduced also in the present paper.

Session 4P1
Physics and Applications of Structured Light

Shaping the Flow of Light in 4 Dimensions by Sub-cycle Switching of Ultrastrong Light-matter Coupling

Jean-Michel Ménard[1,2], **Michael Porer**[1,2], **Alfred Leitenstorfer,**[1,2], **Rupert Huber**[1,2], **Simone Zanotto**[3,4], **Riccardo Degl'Innocenti**[3,4], **Giorgio Biasiol**[3,4], **Lucia Sorba**[3,4], **and Alessandro Tredicucci**[3,4]

[1]Department of Physics, University of Konstanz, Konstanz 78457, Germany
[2]Department of Physics, University of Regensburg, Regensburg 93040, Germany
[3]Laboratorio NEST, Istituto Nanoscienze-CNR and Scuola Normale Superiore, Pisa I-56127, Italy
[4]Laboratorio TASC, CNR-IOM, Area Science Park, Trieste I-34149, Italy

Abstract— Patterning material properties on the sub-wavelength scale has opened exciting possibilities to shape the flow of light in all three spatial dimensions. Recently, nanostructured optical cavities have been used to enhance light-matter interaction and reach the ultrastrong coupling (USC) regime [1–4], where embedded quantum emitters absorb and re-emit virtual photons at a rate comparable to the frequency of the bare cavity mode. Here, we demonstrate, for the first time, spatial and temporal control of a light beam by combining a one-dimensional plasmon based photonic crystal (PC) with optically switchable light-matter interaction. More importantly, sub-cycle switching of the USC is achieved with an ultrafast pump-probe configuration paving the way towards nonadiabatic quantum electrodynamics (QED) phenomena.

A 12-fs near-infrared pump pulse photoinjects electrons into the lowest conduction subband of quantum wells (QWs) embedded inside 1D PC to activate mid-infrared transitions to the next higher subband. We use a phase-locked few-cycle multi-THz probe transient to monitor the dynamics on a femtosecond time scale by means of ultrabroadband electro-optic sampling [5, 6]. The full photonic dispersion is mapped out as light-matter interaction is activated and the bare cavity mode is found to abruptly convert into a light-matter mixed state over a time faster than a single cycle of light. The dynamics is characterized by a nonadiabatic opening of a pronounced anticrossing between a lower and upper polariton branch that reaches a minimum spectral separation of 3.4 THz, or 12% of the intersubband transition frequency. USC also induces a strong flattening of the photonic bands which generates a 20-fold slow-down of the group velocity inside the optical cavity. Finite difference frequency domain (FDFD) simulations reproduce well the measured bandstructure at late delay times ($\sim$ 1 ps) following the switch on of light-matter interaction, however an unexpected asymmetry of the ultrafast build-up dynamics suggests a novel class of nonadiabatic quantum interference. Finally, our scheme constitutes an ideal platform to study ultrafast cavity QED phenomena including the predicted emission of vacuum photons from nonadiabatic modulations of the USC regime [7, 8].

REFERENCES

1. Dini, D., R. Köhler, A. Tredicucci, G. Biasiol, and L. Sorba, "Microcavity polariton splitting of intersubband transitions," *PRL*, Vol. 90, 116401, 2003.
2. Günter, G., A. A. Anappara, J. Hees, A. Sell, G. Biasiol, L. Sorba, S. de Liberato, C. Ciuti, A. Tredicucci, A. Leitenstorfer, and R. Huber, "Sub-cycle switch-on of ultrastrong light-matter interaction," *Nature*, Vol. 458, 178, 2009.
3. Todorov, Y., A. M. Andrews, R. Colombelli, S. de Liberato, C. Ciuti, P. Klang, G. Strasser, and C. Sirtori, "Ultrastrong light-matter coupling regime with polariton dots," *PRL*, Vol. 105, 196402, 2010.
4. Zanotto, S., G. Biasiol, R. Degl'Innocenti, L. Sorba, and A. Tredicucci, "Intersubband polaritons in a one-dimensional surface plasmon photonic crystal," *APL*, Vol. 97, 231123, 2010.
5. Huber, R., F. Tauser, A. Brodschelm, M. Bichler, G. Abstreiter, and A. Leitenstorfer, "How many-particle interactions develop after ultrafast excitation of an electronChole plasma," *Nature*, Vol. 414, 286, 2001.
6. Sell, A., A. Leitenstorfer, and R. Huber, "Phase-locked generation and field-resolved detection of widely tunable terahertz pulses with amplitudes exceeding 100 MV/cm," *Opt. Lett.*, Vol. 33, 2767, 2008.
7. Ciuti, C., G. Bastard, and I. Carusotto, "Quantum vacuum properties of the intersubband cavity polariton field," *PRB*, Vol. 72, 115303, 2005.

8. De Liberato, S., C. Ciuti, and I. Carusotto, "Quantum vacuum radiation spectra from a semiconductor microcavity with a time-modulated vacuum Rabi frequency," *PRL*, Vol. 98, 103602, 2007.

Charge Carrier Dynamics in Nanostructures Driven by Ultrashort Light Pulses

A. S. Moskalenko, **J. Wätzel**, **and J. Berakdar**
Martin Luther University Halle-Wittenberg, Germany

Abstract— We investigate the charge carrier dynamics in nanostructures driven by ultrashort light pulses. In particular, we consider double quantum dots, semiconductor and graphene quantum rings, and nanoshells. Several types of pulses are considered: asymmetric half-cycle pulses, symmetric single-cycle pulses and few-cycle pulses. We show how to generate and eliminate currents as well as how to localize spatially spin and/or charge and then to maintain this localization in time. In the case of graphene quantum rings, conditions for the generation of pure charge and valley currents are determined.

Nanostructures containing many-particles may demonstrate fundamentally different responses to the external perturbing light pulses depending on the light spectral properties. The driving with frequencies close to the plasmon resonances lead to a strong collective response of the electronic system. This response is modelled by us using the single-particle properties of the nanostructure and the mean-field approximation. For a realistic description of the non-equilibrium dynamics we also investigate the scattering processes of the charge carriers leading to their relaxation. Electron-phonon and electron-photon interactions are taken into account. The effect of temperature leads to decoherence of the excited oscillations in the system, whereby they disappear and then revive in a some time interval unless the excitation decays due to the relaxation.

Finally, we can characterize the created non-equilibrium states in the nanostructures by investigating their time- and frequency-dependent emission properties applying the theory of the time-dependent spectra. We describe how to generalize this theory in order to measure the ultrafast changes of the polarization of the emitted light.

Optimal Control of Electron Dynamics with Shaped Laser Pulses

E. K. U. Gross
Max Planck Institute of Microstructure Physics
Weinberg 2, 06120 Halle (Saale), Germany

Abstract— With modern pulse-shaping facilities, the control of electronic motion has become feasible. In this lecture, quantum optimal control theory (OCT) [1] is combined with time-dependent density functional theory to calculate shaped laser pulses suitable to control the dynamics of electrons. Examples include the control of the chirality of currents in quantum rings [2], the location of electrons in double quantum dots [3], and the ionisation of molecules [4].

Two generalizations of the standard formulation [1] of optimal-control theory will be presented: The first generalization [5] allows the calculation of optimized pulses with frequency constraints. This generalization allows one to control electronic transitions by making them go through a chosen intermediate state. The figure below shows the density of the chosen intermediate state as a function of time.

The second generalization [6] achieves the optimization of **time-dependent** control targets. The latter allows one to control the path of a quantum system in Hilbert space, to drag the density of a quantum system along a given classical trajectory and, to maximize selected harmonic peaks in the high-harmonic-generation spectrum of atoms.

Finally, the control of nuclear (Ehrenfest) motion is included as well. To this end, the formalism of OCT is generalized to deal with mixed quantum-classical systems [7]. As an application, we will demonstrate selective bond-breaking on a single potential energy surface.

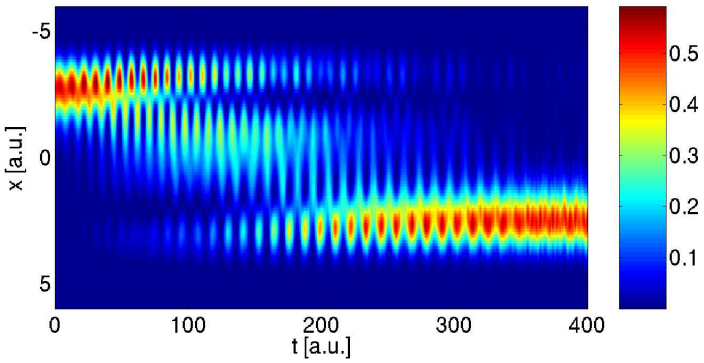

REFERENCES

1. Zhu, W., J. Botina, and H. Rabitz, *J. Chem. Phys.*, Vol. 108, 1953, 1998.
2. Räsänen, E., A. Castro, J. Werschnik, A. Rubio, and E. K. U. Gross, *PRL*, Vol. 98, 157404, 2007.
3. Räsänen, E., A. Castro, J. Werschnik, A. Rubio, and E. K. U. Gross, *PRB*, Vol. 77, 085324, 2008.
4. Castro, A., E. Räsänen, A. Rubio, and E. K. U. Gross, *EPL*, Vol. 87, 53001, 2009.
5. Werschnik, J. and E. K. U. Gross, *J. Opt. B*, Vol. 7, S300, 2005.
6. Serban, I., J. Werschnik, and E. K. U. Gross, *Phys. Rev. A*, Vol. 71, 053810, 2005.
7. Krieger, K., A. Castro, and E. K. U. Gross, *Chem. Phys.*, 2011.

Self-focusing of Structured Light

Anton S. Desyatnikov
Nonlinear Physics Centre, Research School of Physics and Engineering
The Australian National University, Canberra ACT 0200, Australia

Abstract— An overview of recent theoretical and experimental advances in nonlinear optics of structured light will be presented. In particular, the self-focusing dynamics of singular light beams carrying orbital angular momentum and optical vortices will be considered. We demonstrate theoretically that the vortex-free spiraling elliptic beams allow for a dramatic increase of the critical power of self-focusing in pure Kerr media, in contrast to the collapsing filaments with zero angular momentum. The collapse is fully suppressed in nonlocal nematic liquid crystals and we demonstrate experimentally the formation of stable spatial solitons carrying optical vortices, or vortex nematicons. Anisotropy of the liquid crystal media leads to the astigmatic deformation of vortex beams which, in its own turn, results in the formation of the so-called dipole azimuthons, i.e., a two-lobe rotating vortex beams. We show how the deformation of the soliton induced waveguide triggers the nontrivial topological reactions of optical vortices. These include charge flipping of vortices and the formation of three-dimensional vortex structures resembling pitchfork bifurcation diagrams. Several examples of more exotic vortex structures are presented, including the formation of DNA-like double helix structure by two vortex lines as well as the spontaneous knotting of waves, with the formation of localized loops, links, and knots. We search for common physical background for these phenomena in the internal vibrational modes of stable solitons and their interference patterns with the host self-trapped beam. We also discuss possible relation of these phenomena to the nonlinear dynamics of quantized vortices in atomic and exciton-polariton Bose-Einstein condensates.

Session 4P2
Lightning Electromagnetics

Channel Base Current Effects on the Magnetic Flux Density Waveshape Associated with Vertical Lightning Channel

M. Izadi, **M. Z. A Ab Kadir**, **C. Gomes**, **and W. F. Wan Ahmad**
Centre of Excellence on Lightning Protection (CELP), Faculty of Engineering
Universiti Putra Malaysia, UPM, Serdang, Selangor 43400, Malaysia

Abstract— The electromagnetic fields due to lightning channel are considered as effective factors to induce voltage on the power systems. The shape of electromagnetic wave associated with lightning channel depends highly on return stroke current wave shape and the parameters of lightning channel and its geometry. This paper is founded on the relation between channel base current parameters based on Heidler function as a realistic current function and the wave shapes of magnetic flux density. Further, some general functions were proposed by considering their effects. The results showed that the proposed equations are highly in agreement with the calculated values by using direct methods and that they could also predict the magnetic flux wave shapes versus different channel base current parameters under similar geometrical and lightning channel conditions. The estimated magnetic flux density wave shapes can be applied to Rachidi model to evaluate the induced voltage in the lightning.

Possible Relation between Lightning and Solitons

V. Skarka[1, 2]

[1]Laboratory of Photonics, University of Angers, 2, Bd Lavoisier, Angers 49000, France
[2]Institute of Physics, Pregrevica 118, Belgrade 11000, Serbia

Abstract— Far from the thermodynamic equilibrium, nonlinear systems open to the exchange of the energy and mater with outside world can reach steady states corresponding to self-organized spatiotemporal dissipative structures [1]. There are plenty of examples of self-organized systems in nature; the multicomponent lightning is one. Very strong electromagnetic ionizing wave is propagating through air from cloud to ground generating highly conductive plasma channel corresponding to a streamer. After contact of wave front with ground backward wave propagation occurs. In M-components stage current pulses propagate on background of quasi-stationary current [2]. Next component corresponds to a dart leader propagating through plasma channel from cloud to ground. Striking is that the streamer width is usually couple of meters while the lightning width is of order of magnitude of centimeter. The lightning is essentially an optical electromagnetic wave propagating in atmosphere [3]. As a consequence, such a wave will self-focus due to the Kerr nonlinear index of refraction of air. This self-focusing can explain why the lightning is narrower than the streamer itself. However, the self-focusing will necessarily lead to the wave collapse that would interrupt light stripe, in contrast with numerous photos showing stripes with constant width between two successive branching. Indeed, before field blow up, the intensity of the field is increasing and the plasma is generated due to multiphoton (or tunneling) ionization of neutral molecules. The plasma acts as a self-defocusing medium with higher order susceptibility of negative sign that saturates the Kerr nonlinearity suppressing field collapse [4]. In despite of inhomogeneous conditions and large energy dissipation, lightning maintains a constant width as a self-organized spatiotemporal dissipative soliton [5]. Such solitons appear due to a simultaneous balance of diffraction and dispersion with self-focusing and gain with loss, as it seems to happen in lightning too. Robustness of the lightning, which is never interrupted, in contrast to the unavoidable absorption of nonsolitonic laser beams, indicates its solitonic nature. In order to meet experimental conditions, we considered generation, evolution, and self-stabilization of optical dissipative light bullets from non-spherically symmetric inputs usual in inhomogeneous systems [6]. Numerical simulations confirm analytically established large domain of stability, useful for tuning experiments. In order to model lightning conditions, we studied the propagation in air of intense laser pulses with a phase singularity. Such pulses either filament in a controlled way or propagate as vortex solitons in a self-created plasma channel resisting to symmetry-breaking perturbations [4, 7]. These observations can be used for controlled triggering of lightning discharge, lightning protection, remote sensing, and long distance air communications.

REFERENCES

1. Nicolis, G. and I. Prigogine, *Self-organization in Nonequilibrium Systems*, John Wiley and Sons, New York, 1977.
2. Fisher, R. J., G. H. Schnetzer, R. Thottappillil, et al., *J. Geophys. Res.*, Vol. 98, 22887, 1993.
3. Bazelyan, E. M., *Plasma Physics Reports*, Vol. 21, 470, 1995.
4. Skarka, V., N. Aleksić, and V. I. Berezhiani, *Phys. Lett. A*, Vol. 319, 317, 2003.
5. Skarka, V. and N. Aleksić, *Phys. Rev. Lett.*, Vol. 96, 013903, 2006.
6. Aleksic, N. B., V. Skarka, D. V. Timotijevic, and D. Gauthier, *Phys. Rev. A*, Vol. 75, 061802(R), 2007.
7. Skarka, V., N. Aleksić, M. Derbazi, and V. I. Berezhiani, *Phys. Rev. B*, Vol. 81, 35202, 2010.

Physical Processes That Govern the Propagation of the Current Pulse along the Early Portions of the Lightning Return Stroke

Robert L. Gardner
6152 Manchester Park Circle, Alexandria, VA 22310-4957, USA

Abstract— The lightning return stroke begins when a downward propagating leader (stepped or dart) reaches within a few meters of the ground and connects with an upward propagating leader. This joining of non neutral plasma columns is an extremely energetic and complex event requiring an understanding of the behavior of several charged and uncharged species at temperatures up to a few electron volts, rapidly changing electric fields of several megavolts/meter and charge transfer of several coulombs in a few microseconds. This region is important in understanding lightning because it is the source of much of the high frequency content of the radio-frequency emission of the return stroke. The evolution of the plasma channel also governs the propagation of the return-stroke current as it moves up channel. Previous models have considered the plasma evolution but not considered the role of radiative transport in those early processes.

Longmire, et al. [1] proposed a propagation mechanism for streamer propagation in neutral plasma appropriate to a nuclear lightning environment. The model assumed a conducting streamer that formed when the enhanced fields around the streamer tip reached the air avalanche field. A three species air chemistry model was used along with thermal reservoirs for molecular heating along with neutral and ionized atoms representing oxygen and nitrogen. The model suggested a propagation velocity of 10^5 m/s, consistent with photographs of nuclear lightning, but substantially below that of natural lightning, so work began to understand the initial conditions for a similar model for the natural lightning environment. Radiative transport is key to predicting the propagation speed near c that is observed and predicted by Baum [2].

Natural lightning leader processes can lower several coulombs of charge into a column that eventually becomes the return-stroke channel. That charge has to wait while the full channel forms and the charges attach to air molecules under those low field conditions forming species like 0^2-. These heavy species are not very mobile and move at velocities much lower than the electron drift velocity of about 10^5 m/s. The like charges repel each other and spread the charge out first as free electrons then as charged molecules as the electric fields get lower than the air avalanche value. Analytic and numerical models were developed to show the charged-species channel expansion. This model showed a column of charge that expanded to about a meter in diameter and consisted of relatively evenly spaced charged species [3]. The hot gas at the tip also emits photons that travel forward in the low-density channel left from the leader processes. These photons scatter electrons and allow a substantial increase the propagation velocity. The velocity of the peak current slows because of the plasma channel losses confining the high frequency emission to the first few meters of the return stroke channel.

REFERENCES

1. Longmire, et al., *Phys. Fl.*, Vol. 27, 2694, 1984.
2. *Lightning Phenomenology Note 5*, EMP Note Series, www.ece.unm.edu/summa/notes.
3. *Proceedings, International Conference on Electromagnetics in Advanced Applications*, Sydney, September 2010.

Ground to Cloud and Cloud to Ground Lightning Flashes: A Comparative Study

S. Thirukumaran[1], **P. R. P. Hoole**[2], **R. Harikrishnan**[1], **K. Jeevan**[1], **and S. R. H. Hoole**[3]

[1]Department of Electrrical Engineering, University of Malaya, Malaysia
[2]School of Engineering, Taylor's University, Malaysia
[3]Department of Electrical and Computer Engineering, Michigan State University, USA

Abstract— Since cloud to ground lightning flashes are the most common type of earth flashes, it has received much attention with referecne to obtaining the engineering parameters such as the elctric charge moment (QL, where Q is the toal charge lowered by the lightning flash) rate of rise of current and peak electric current. Measurements made in various parts of the world were used to arrive at a standard that could be set for both land and airborne systems, devices and vehicles. In this paper we report the use of a well tested model of earth flash, namely the transmission line model, and explore the discharge process of the electric charges, as depicted in the voltage collapse shwon in Fig. 1(a) and Fig. 2(a) as well as the return stroke currents for cloud to ground flahses (e.g., Fig. 1(b)) and ground to cloud flashes (Fig. 2(b)).

Amongst the significant results we report are the much higher rate of rise of currents we observed for ground to cloud (upward) ligthning flash return stroke, and the much depper collapse of the electrostaic potential, and electric charges, in the case of ground to cloud retuen stroke. In contrast, the cloud to ground flash collapse of the electrostaic charge is not so severe, thus allowing for more subsequent flashes to occur over the same lightning channel.

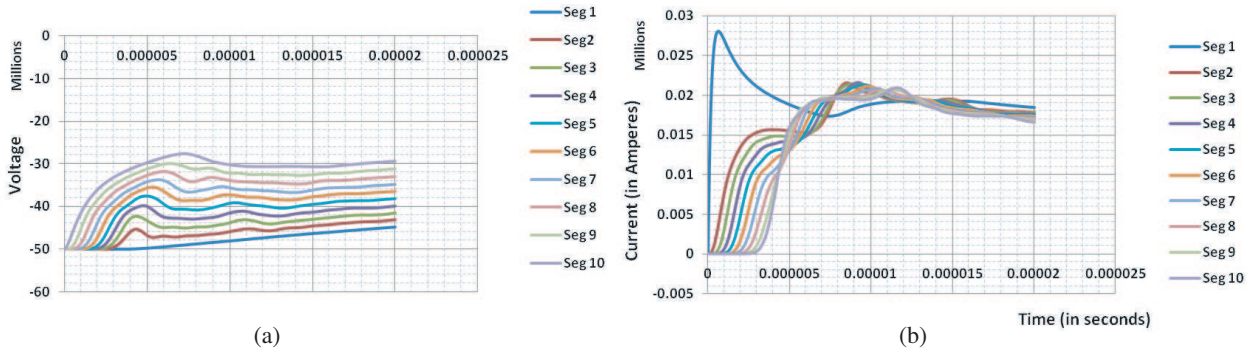

Figure 1: Cloud to Ground Lightning return stroke: (a) potential profiles along the channel, (b) return stroke electric currents along the channel.

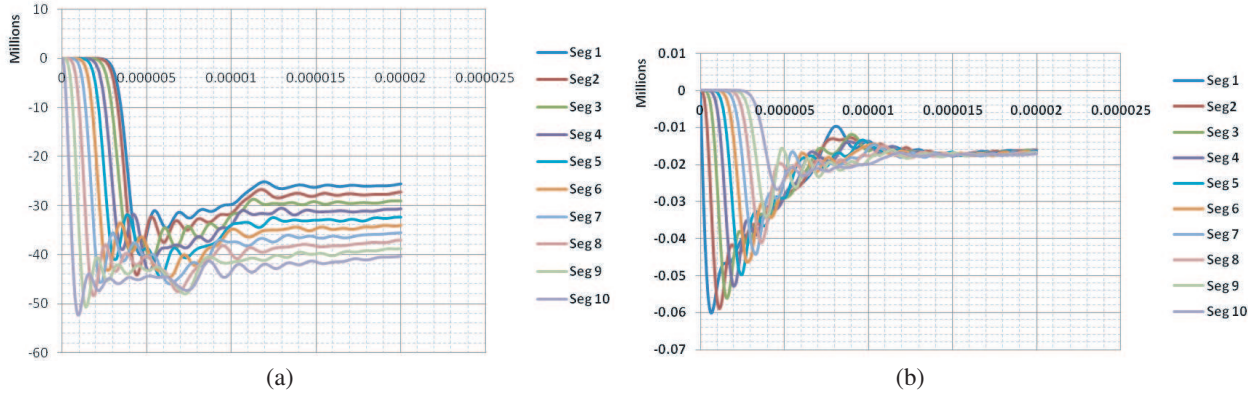

Figure 2: Ground to cloud lightning: (a) potential profile and (b) return stroke currents travelling from ground to cloud.

Electrostatic Discharges (ESD): Rate of Rise of Currents and Radiated Electric Fields

S. Thirukumaran[1], **P. R. P. Hoole**[2], **R. Harikrishnan**[1], **K. Jeevan**[1], **and S. R. H. Hoole**[3]

[1]Department of Electrrical Engineering, University of Malaya, Malaysia
[2]School of Engineering, Taylor's University, Malaysia
[3]Department of Electrical and Computer Engineering, Michigan State University, USA

Abstract— Electrostatic Discharge (ESD) is a major concern in Microelectromechanical Systems (MEMS) as well as in large systems such as in atmospheric electricity. We focus on ESD rate of rise of currents and the radiated electric fields, since both are directly connected to each other in that the radiated electric field is proportional to the rate of rise of ESD currents. In this paper we investigate two factors related to ESD and its indirect effects on electrical and electronic equipment and systems: (i) the shorter ESDs produce higher peak currents, while the waveshapes do not change much, and (ii) whether the ESD originates from the ground electrode, or from the live conductor, can make a significant difference to the resonances produced.

Furthermore, we show that ESDs that emanate from the ungrounded electrode may produce bipolar electric fields, and could pose a greater threat in indirect effects on electronic equipment.

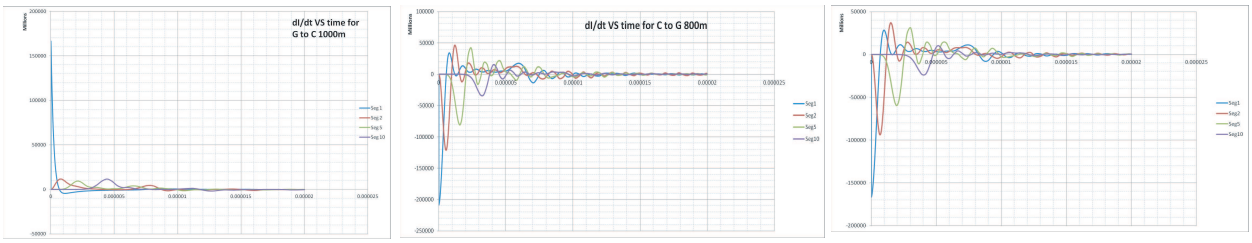

(a) (b) (c)

Figure 1: The dependence of rate of rise of currents (kA/microsecs) on whether the ESD emanates from the ground conductor or otherewise, as well as the length of the discharge channel.

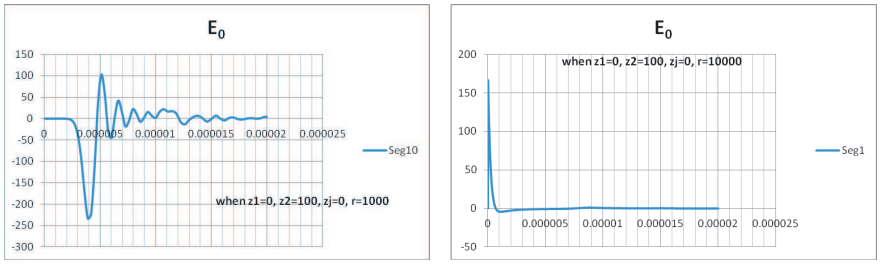

(a) (b)

Figure 2: Electric fields radiated by (a) an ESD that originates from an ungrounded electrode, and (b) that emanating from grounded electrode.

Session 4P3
Remote Sensing of the Earth, Ocean, and Atmosphere

Layover and Shadow Detection in Multi-baseline InSAR Based on Gerschgorin Disks

S. Li and H. Xu
School of Electronic and Information Engineering, Beihang University, Beijing, China

Abstract— As an optimal technology of terrain height measurement, InSAR has been widely discussed and rapidly improved, and the generation of world-wide, consistent, timely, high-precision digital elevation model (DEM) has always been the motive of InSAR technology development since its first introduction. However, InSAR technique suffers seriously from layover and shadow, which are general in SAR image because of the presence of complicated topographies containing abrupt slope and discontinuous surfaces, such as steep mountains and man-made building, etc.. The phase in layover and shadow region is distorted and difficult to be filtered and unwrapped correctly. Multi-baseline InSAR system and auxiliary input data are widely exploited to overcome the drawbacks of layover and shadow. In Multi-baseline InSAR technique, the height estimation in layover and shadow terrain is equivalent to the estimation of directions of arrival (DOA) of multiple signal components. In auxiliary input data technique, optical data and laser radar data are adopted. Whatever methods aforementioned, it would make sense to detect layover and shadow region.

In this paper, for multi-baseline InSAR system, source number estimation based on Gerschgorin disks is extended to detect layover and shadow region. The novel contribution of this paper relies mostly on the Gerschgorin disks application to distinguish layover and shadow from normal InSAR data, on the source number estimation without eigenvalue calculation, which is necessary for conventional layover and shadow detection. Firstly, for multi-baseline InSAR images, the geometric and signal models of layover and shadow are described. Then, the eigenvalue distribution of interferometric signal correlation matrix is analyzed. On the basis of it, Gerschgorin disks are proposed to estimate the position of eigenvalue and the source number. Consequently, the detection of layover and shadow is complemented according to the source number. Simulation results confirm the validity and efficiency of layover and shadow detection approach proposed in this paper.

Retrieval of Cloud Geometrical Properties Using ADEOS-II/GLI Data

Makoto Kuji
Nara Women's University, Japan

Abstract— It is of great interest to investigate the optical, microphysical, and geometrical properties of clouds that play crucial role in the earth climate system. Water clouds are generally optically thick and consequently have a great cooling effect on earth-atmosphere radiation budget. The water clouds usually exist in a lower troposphere where aerosol-cloud interaction occurs frequently, and then cloud droplet size variation influences reflection of solar radiation as well. Further, a cloud layer height is one of the key properties that determine downward longwave radiation and then surface radiation budget. In this study, top height, geometrical thickness and bottom height of a water cloud layer are investigated as cloud geometrical properties in particular.

Several studies show that observation data of some spectral regions including oxygen A-band, enables us to retrieve the cloud geometrical properties as well as the optical thickness, the effective particle radius. In this study, an algorithm was developed to retrieve simultaneously the cloud optical thickness, effective particle radius, top height, geometrical thickness and then bottom height of a cloud layer with the spectral observation of visible, near infrared, thermal infrared, and oxygen A-band channels.

This algorithm was applied to Advanced Earth Observing Satellite-II/Global Imager (ADEOS-II/GLI) dataset so as to retrieve global distribution of cloud geometrical properties. The retrieved results around Japan were compared with other observation such as ground-based active sensors, which suggests this algorithm work for cloud system over ocean at least. Based on this result, I further applied it to a global dataset and have obtained an initial result. I will continue the global analyses and their validation studies so as to contribute to surface radiation budget and cloud physics studies eventually. For example, the algorithm will be also applicable to dataset observed with the Global Change Observation Mission 1st-Cilmate/Second generation Global Imager (GCOM-C1/SGLI) that Japan Aerospace Exploration Agency (JAXA) has a plan to launch in a few year.

Optical Classification and the Absorption Character of Inland Entrophic Water in China

Yunmei Li[1], **Qiao Wang**[2], **Heng Lu**[1], **Jiazhu Huang**[1], **Chuanqing Wu**[2], **and Li Zhu**[2]

[1]Key Laboratory of Virtual Geographic Environment, Nanjing Normal University
Ministry of Education, Nanjing 210046, China
[2]Satellite Environment Application Center
Ministry of Environmental Protection, Beijing 100029, China

Abstract— Optical property of inland eutrophic water varies spatially and temporally corresponding to change of concentrations of water components. The same water type classified by optical property may have uniform character which may make water components deriving algorithm simpler and accuracy. Our purpose of this study is to elaborate water type classification scheme for inland eutrophic waters according above water reflectance, and compare the difference of absorption properties between different water types. Field measurements were carried out in August 2006, November 2006, 2007 and 2008, April, June, July and September 2009 in Taihu Lake, Chaohu Lake, Dianchi Lake and Sanxia Gorges Reservoir (China). The waters were classified into six optical water types (type A, B, C, D, E and F) by comparing peak and trough of remote sensing reflectance (R_{rs}) between 500–750 nm. All of the samples in Dianchi Lake belong to type A water, while other water bodies have several types at the same time. When parameterized a_{CDOM} and a_{NAP} by power function, the slope of CDOM S_{CDOM} could be clustered into two groups, i.e., one group for type A and one for type B, C, D, E and F; there is no significant difference of S_{NAP} between different water types. Absorption coefficients of phytoplankton were calculated by absorption coefficient of 440 nm and 675 nm using quadratic function and the coefficients varied in different water types.

Automatic Detection Algorithms for Oil Spill from Multisar Data

Maged Marghany and Mazlan Hashim
Institute for Science and Technology Geospatial (INSTeG)
Universiti Teknologi Malaysia, 81310 UTM, Skudai, Johore Bahru, Malaysia

Abstract— Oil spill or leakage into waterways and ocean spreads very rapidly due to the action of wind and currents. The study of the behavior and movement of these oil spills in sea had become imperative in describing a suitable management plan for mitigating the adverse impacts arising from such accidents. But the inherent difficulty of discriminating between oil spills and look-alikes is a main challenge with Synthetic Aperture Radar (SAR) satellite data and this is a drawback, which makes it difficult to develop a fully automated algorithm for detection of oil spill. As such, an automatic algorithm with a reliable confidence estimator of oil spill would be highly desirable. The main objective of this work is to develop comparative automatic detection procedures for oil spill pixels in multimode (Standard beam S_2, Wide beam W_1 and fine beam F_1) RADARSAT-1 SAR satellite data that were acquired in the Malacca Straits using three algorithms namely, textures using co-occurrence matrix, post supervised classification, and neural network (NN) for oil spill detection with window size 7×7.

Three steps are required for automatically detect oil spill from SAR images: dark spot detection, dark spot feature extraction and dark spot classification. In doing so, three algorithms are implemented: Co-occurrence textures; post supervised classification, and neural net work (NN). The co-occurrence textures involved: Mean; Homogeneity; Contrast; Dissimilarity; and Entropy algorithms. These texture algorithms are implemented to the different RADARSAT-1 SAR mode data with window Kernel size of 7×7 pixels and lines. In addition, the post supervised classification is applied to RADARSAT-1 SAR data using Mahalanobis classifier. Finally, Artificial Neural Net work technique (ANN) is also implemented to SAR data using back propagation algorithm.

In terms of texture analysis the mean-texture algorithm shows an excellent detection of oil spill in comparison to other texture algorithms. While entropy and contrast algorithms can be mainly used for look-alike detections. Furthermore, the mean-texture algorithm discriminates oil spill from surrounding environment such as look-alikes, sea surface and land. Kernel window sizes play an important role in implementation of mean-texture algorithm for oil spill detection. Kernel window size 7×7 pixels and lines provides excellent performance compared to 3×3, 5×5 and 11×11 pixels and lines, respectively. Blur images are produced when using 11×11 pixels and lines. Mahalanobis classifier algorithm provides information about the level of oil spill occurrences in RADARSAT SAR data with accuracy of 87.8%, and 92.7% using Mahalanobis regularized Mahalanobis classifier respectively. Finally, the results show that ANN distinguishes oil spill from surrounding sea surface features up to accuracy of about 96.46%.

In terms of ROC area, it could be inferred that oil spill, look-alikes and sea surface roughness were perfectly discriminated, as provided by area difference of 20% for oil spill, 35% look-alikes and 30% for sea roughness. Comparisons among the different three methods used, shows that ANN had a higher performance in detection of oil spill in RADARSAR SAR data, as evident in standard error deviation of 0.12. Kappa coefficient further indicates the performance of oil spill detection with ANN having an accuracy of 82.22% in comparison to Mean-texture algorithm and Mahalanobis classifier. The W_1 mode data has lower standard error of 15% in comparison to F_1 and S_2 mode data. This means that W_1 mode has better performance in detecting oil spills than F1and S_2 data modes. It can therefore be concluded that NN algorithm is an appropriate algorithm for oil spill automatic detection and W_1 beam mode is appropriate for oil spill and look-alikes discrimination and detection.

3-D Coastal Water Front Visualization Using RADARSAT-1 SAR Satellite Data

Maged Marghany and Mazlan Hashim
Institute for Science and Technology Geospatial (INSTeG)
Universiti Teknologi Malaysia, 81310 UTM, Skudai, Johor Bahru, Malaysia

Abstract— An ocean front is a boundary separating two masses into water of different densities, and is the primary cause of gradient change of physical ocean properties. The water masses separated by a front usually differ in temperature and salinity. Fronts occur on a wide range of scales, starting with those formed within an estuary between inflowing water and the estuary water. Other fronts are found on the continental shelf, separating a zone from coastal water from oceanic water or stratified water masse from one which is vertically mixed. Fronts also occur on a large-scale in the deep ocean, between water masses of different properties.

This paper presents work done to utilize RADARSAT-1 SAR data to reconstruct 3-D of coastal water front. Three algorithms of velocity bunching, Volterra and fuzzy B-spline are used to reconstruct 3-D coastal front. The veolocity bunching algorithm modeled significant wave height, Volterra algorithm simulated coastal current movement while fuzzy B-spline implemented the significant wave height to reconstruct 3-D coastal front. The study shows the signficant wave height varied bewteen 0.7 m to 1.3 m across the front. The front is dominated by strong tidal current that ranged between 0.9 m/s to 1.5 m/s. This front occurred in water depth of 20 m. Additionally, fuzzy B-spline reconstructed 3-D front with smooth graphic feature. Indeed, fuzzy B-spline tracked the smooth and rough surface. Finally, fuzzy B-spline algorithm can keep track of uncertainty with representing spatially clustered gradient of flow points across the front. In conclusion, the fuzzy B-spline algorithm can be used for 3-D front reconstruction with integeration of velocity bunching and Volterra algorithm.

Digital Elevation Model of Spit Using Dinsar of Radarsat-1 Fine Mode Data

Maged Marghany and Mazlan Hashim
Institute for Science and Technology Geospatial (INSTeG)
Universiti Teknologi Malaysia, 81310 UTM, Skudai, Johor Bahru, Malaysia

Abstract— Synthetic Aperture Radar interferometry (InSAR) is a relatively new technique for 3-D topography mapping. This work presents a new approach for 3-D object simulation using Differential synthetic aperture interferometry (DInSAR). In doing so, conventional DInSAR procedures are implemented to three repeat passes of RADARSAT-1 SAR fine mode data (F_1). Further, new approach of using fuzzy B-spline algorithm is implemented with phase unwrapping technique. Consequently, fuzzy B-spline is used to eliminate the phase decorrelation impact from the interferograms. The study shows the performance of DInSAR method using fuzzy B-spline is better than DInSAR technique which is validated by a lower range of error (0.02 ± 0.21 m) with 90% confidence intervals. In conclusion, integration of fuzzy B-spline with phase unwrapping produce accurate 3-D coastal geomorphology reconstruction.

Session 4P4
Microstrip and Printed Antennas, Array Antennas

Design of Reconfigurable Slot Antenna for Diverse Frequency Wireless Applications

C. Sulakshana and L. Anjaneyulu
Department of ECE, NIT Warangal, India

Abstract— In recent years, the topic of reconfigurability in an antenna system is a desired feature that has been the focus of much research. Miniaturization always indicates scientific progress. So efforts are always directed towards reducing the size of the antenna. Reconfigurable antennas helps in miniaturizing the entire device size since these antennas effectively allow the antenna volume to be reused as an antenna in a different form. This paper deals with design and simulated analysis of a novel and compact reconfigurable CPW fed slot antenna with frequency diversity. The basic antenna consists of CPW fed slot antenna which operates at 5.8 GHz. The frequency reconfigurability is obtained by connecting three slots through switches in basic antenna by using PIN diodes or RF MEMS. By controlling the switches the antenna can be operated at six different frequencies namely 5.65 GHz, 5.39 GHz, 6.64 GHz, 4.35 GHz, 3.95 GHz, 3.22 GHz and a dual band frequencies at 6.68 GHz and 7.29 GHz which are suitable for different wireless communication applications such as Wi-Fi, WiMAX, and WLAN, RFID and other C-band applications. The compact aperture area of the antenna is 35 mm × 30 mm × 1.5 mm and it is designed on a low cost FR4 substrate whose dielectric constant $\varepsilon_r = 4.3$. The effect of antenna length, size, substrate, thickness, shape has been evaluated and obtained good and acceptable 2D Radiation Pattern in elevation plane, gain, and efficiency. The simulated results are illustrated using Method of Moments based IE3D software.

Structure of Proposed Reconfigurable Antenna And Return Loss: The geometrical parameters are adjusted carefully and finally the antenna dimensions are obtained to be $L_1 = 30\,\text{mm}$, $L_2 = 2\,\text{mm}$, $L_3 = 1.5\,\text{mm}$, $L_4 = 5\,\text{mm}$, $L_5 = 6\,\text{mm}$, $W_1 = 15.3\,\text{mm}$, $W_1 = 3.6\,\text{mm}$, $W_1 = 10\,\text{mm}$, $W_1 = 6\,\text{mm}$, $\varepsilon_r = 4.3$. The gap spacing between ground plane and CPW feed line is $g = 0.4\,\text{mm}$. The substrate thickness $t = 1.5\,\text{mm}$. Three switches are introduced in the structure namely S_1, S_2 and S_3 which are connected between four slots.

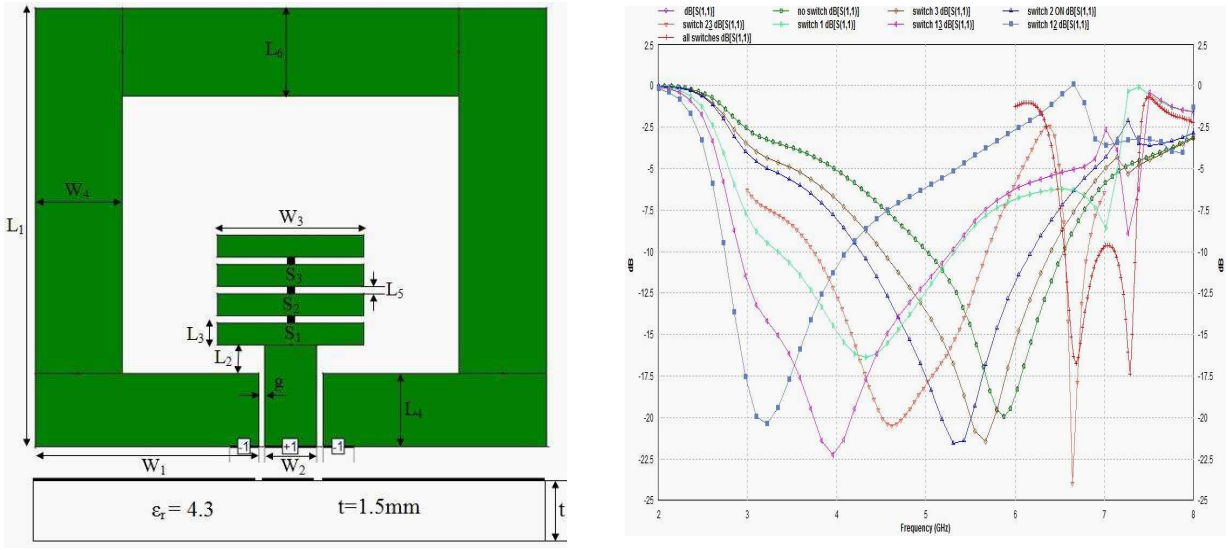

(a) (b)

Figure 1: (a) Geometry of the proposed reconfigurable antenna. (b) Comparison of return losses for various switch configurations.

A Single Feed Circularly Polarized Wallis Sieve Fractal Microstrip Antenna

V. Venkateshwar Reddy and N. V. S. N. Sarma
National Institute of Technology, Warangal, India

Abstract— A new type of compact circularly polarized single feed microstrip antenna is presented. In order to achieve specified characteristics wallis sieve fractal geometry is employed. Simulated results indicate that the proposed antenna gives a very good circular polarization with minimum axial ratio very close to 0 dB at the center frequency of 2430 MHz and −10 dB impedance bandwidth of 4.25%. The antenna provides almost constant gain of about 3.2 dBi over the frequency band of operation. This antenna can be used in WLAN, Bluetooth and WiMAX, Wi-Fi etc at ISM band.

Two cases have been studied in this context, first one is linearly polarized Wallis sieve fractal antenna and the second one is circularly polarized antenna. For linearly polarized case the antennas are with transmission line feeding. In this case the behavior of the antenna for three iterations is discussed. The resonant frequency of the antenna is changed from 2493 MHz to 2374 MHz when the iteration is changed from zero to two. For circular polarization the antenna is fed with probe feeding. The proposed antenna with iteration 2 gives axial ratio at the center frequency very close to 0 dB, the 3 dB axial ratio bandwidth of about 2%.

Fractal technologies allowed us to design miniature antennas and integrate multiple telecommunication services such as cellular (GSM 1800), wireless LAN, GPS and HiperLAN into a single device. The presented antenna is also proposed for a multiband operation and has the nature of giving linear polarization at certain resonant frequencies, circular polarization at other frequencies. The multiband antenna is operating at 1.9 GHz, 3.5 GHz, 4 GHz, 5.6 GHz, 6.3 GHz, 6.7 GHz, 7.2 GHz, 8.2 GHz, and 9.1 GHz respectively. In the multiband operation case antenna is giving linear polarization at 3.5 GHz, 4 GHz, 6.3 GHz, 6.7 GHz, 7.2 GHz, and 9.1 GHz. The antenna is giving circular polarization at 1.9 GHz, 5.6 GHz, and 8.2 GHz.

Flat Lens Based on Aperture-coupled-patch FSS with Four-pole Resonance Behavior

Yu Wang, Hiroyuki Deguchi, and Mikio Tsuji
Department of Electronics, Doshisha University, Kyotanabe, Kyoto 610-0321, Japan

Abstract— Reflectors and lens are the most commonly used high-gain antenna in many applications. They can transform the spherical wave illuminated from a primary source (such as horn) into plane wave. The traditional lens is similar to the lens used in optical fields. However, with the development of the PCB technology, flat lens with advantages of easier fabrication, thinner structure and lower profile are more possible to implement and can be a better alternative for the traditional ones.

In this paper, a novel multiple layered frequency selective surfaces (FSSs) element is proposed for flat lens use. The proposed structure consists of three screens of FSSs and two layers of substrate. The outside screens comprise four identical microstrip lines respectively, and the inside screen comprise four identical slots etched on the metal plane, as shown in Fig. 1. The proposed FSSs element is a kind of structure so-called "Antenna-filter-antenna (AFA)" which is a type of aperture-coupled patch actually. However, compared with the common used aperture-coupled patch which can just support two-pole resonance in the pass-band, this novel structure can expose a four-pole resonance behavior (see Fig. 2). Two poles are generated by the coupled microstrip lines while the third one is generated by the slot. As for the fourth pole, it is caused by the special thickness which is a similar phenomenon to the PF resonance. Ranging such elements homogeneously in array can make up a FSS with transmission characteristics. Scaling the geometry of the element can obtain the desired phase-delay.

Figure 3 shows the transmission phase on each cell of the flat lens. In order to transform the spherical wave into plane wave, such phase differences between each cell should be compensated. We can choose different geometry for each cell to realize the phase compensation. The detailed evaluation for the flat lens antenna will be presented at the talk.

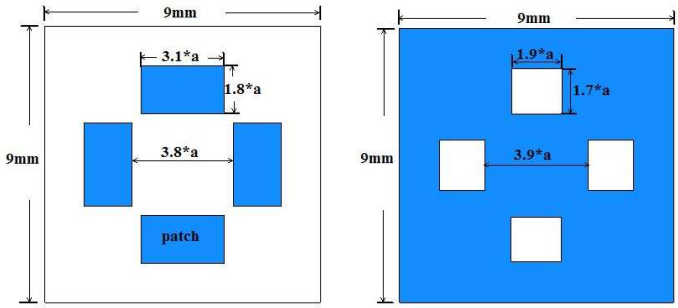

(a) (b)

Figure 1: Unit cell geometry for flat lens.

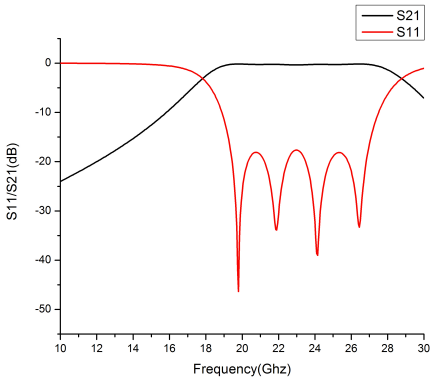

Figure 2: Frequency response with four-pole resonance behavior.

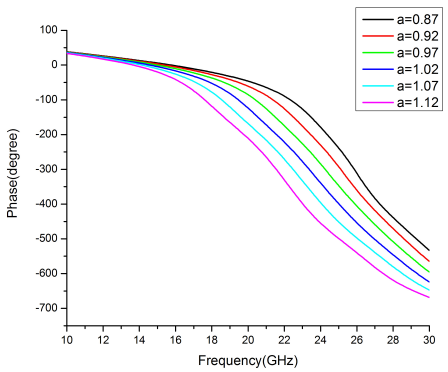

Figure 3: Transmission phase characteristics of proposed flat lens elements as a function of scale factor.

Analysis on Physical and Electromagnetic Parameter of a Concentric Split Ring Square Reflectarray Element

S. H. Yusop[1], **N. Misran**[1, 2], **M. T. Islam**[2], **and M. Y. Ismail**[3]

[1]Department of Electrical, Electronic and System Engineering
Universiti Kebangsaan Malaysia, Bangi, Selangor 43600, Malaysia
[2]Institute of Space Science (ANGKASA)
Universiti Kebangsaan Malaysia, Bangi, Selangor 43600, Malaysia
[3]Communication Engineering Department, Faculty of Electrical and Electronics Engineering
Universiti Tun Hussein Onn Malaysia (UTHM), Batu Pahat, Johor 86400, Malaysia

Abstract— A series of characterization studies of physical and electromagnetic parameters has been carried out and presented in this paper. This study is focused in improving the performance of the bandwidth of reflectarray antenna element. The physical parameter is considering investigation on a variation of gap sizes of the element while for electromagnetic parameters is considering investigation on a variation of substrate thickness and its permittivity. Figure of Merit used in this paper is the phase range and phase slope to analyze the practicality of the element and the bandwidth performance. The FoM is according to the analysis from reflection phase and return loss versus frequency responses graph. The element is designed using computer software CST Microstripes namely concentric split ring square element. This element is the combination of a conventional annular ring and a novel square ring element, with the introduction of a gap into the element at TE direction. As the results, both physical and electromagnetic parameters are affects the performance of both phase range and phase slope of the element.

A Novel Design of Dual-feed Single-element Antenna for 4G MIMO Terminals

Nguyen Khac Kiem, **Dang Nhu Dinh**, **Hoang The Viet**, **and Dao Ngoc Chien**
School of Electronics and Telecommunications, Hanoi University of Science and Technology
No. 1 Dai Co Viet Road, Hanoi, Vietnam

Abstract— This paper proposes a novel approach to design a dual-feed single element antenna for 4G MIMO terminals. The idea is to use isolated mode antenna technology — "iMAT" as mean of reducing dimension of antenna and mutual coupling between ports. Additionally, a crossover is implemented as feeding part of the antenna. With the presence of the crossover, the signal from the left port will excite for the right part of antenna and vice versa. As a result, the transmission between two ports of antenna is much below −15 dB level. The final design satisfies the return loss (RL) requirement of less than −10 dB in a frequency band ranging from 1.87 GHz to 2.25 GHz, which entirely covers the UMTS band for 3G/4G wireless communications. The model is designed on popular substrate FR4 with a dielectric constant of 4.4 and thickness of 1.6 mm. The simulated results are shown and discussed.

The work starts with design of radiating patch of antenna to operate in the band of UMTS from 1.92 GHz to 2.17 GHz. The technique using in this design refers to the isolated mode antenna technology — iMAT. By feeding antenna at two different locations, two different modes are excited, which are independent of each other. Each mode will produces separate radiation pattern, the diversity for the antenna was achieved. Thanks to this characteristic, the antenna is a promising candidate for MIMO systems. Moreover, the proposed antenna consists of a radiating patch with two broken lines at two ends which significantly reduce antenna size.

In the next step, the crossover coupler was embedded, as shown in Fig. 1(a). The crossover is a symmetrical four port network with two inputs and two outputs. Theoretically, the conventional crossover can be achieved by connecting two 90° hybrids; therefore, this crossover is designed by the two 50-Ω parallel arms and the middle of the structure is placed by a single 25-Ω line. The perfect design of crossover is accomplished if the adjacent ports are isolated. It means that when one input, i.e., port-1 is fed, the electric current flowing through crossover coupler will go out via port 3 and vice verse. Practical results, however, showed that it is difficult to achieve the desired requirements in all of frequency band of UMTS system with the conventional crossover. Because the structure of crossover includes some bends; therefore, the signal will be changed phase and magnitude when passing this bends. To overcome this limitation, a novel crossover with I-shaped Defected Ground Structure (DGS), as shown in Fig. 1(b), is introduced as the effective solution. The I-shaped DGS acts as a LC filter to collect energy, so when port-1 is fed, the signal will be cancelled at port-4 and vice versa, as plotted in Fig. 1(c). Finally, the crossover is placed with the radiating patch to form MIMO antenna with novel cross-fed method. The total dimension of antenna is 88.4 × 64.2 mm, allowing the antenna to be integrated into electronic devices, e.g., PDA, laptop.

Further measured results of S-parameters, and radiation patterns of antenna will be presented in full paper format which will detail the MIMO antenna features.

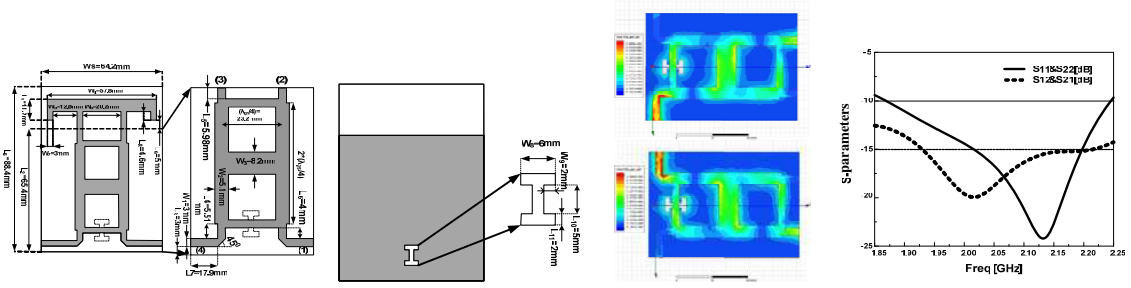

(a) (b) (c) (d)

Figure 1: (a) Top face of proposed antenna; (b) Bottom face of proposed antenna; (c) Surface current distributions on crossover coupler, and (d) S-parameters diagram.

Placement Effects on a Higher Order Mode Patch Antenna within HALE Aircraft Wing

Derek Gray
Faculty of Engineering, University of Nottingham, Malaysia Campus, Malaysia

Abstract— At present, there are 3 rival programs to improve upon NASA's ERAST UAVs; Aerovironment and Boeing are both testing H_2 powered aircraft for week long flights which resemble gliders, while Boeing is also working on a purely solar powered flying wing which more closely resembles the ERAST UAVs [1]. Irrespective of type, all 3 modern UAVs will have aerofoil shapes and wing structures generally resembling those of the ERAST UAVs due to the requirement for flight above the tropopause at low airspeeds [2]; the major difference will be the use of stiff wings [3]. As with the original ERAST UAVs, it will be preferable to place UHF and L-band antennas within the wings themselves where there will be no disruption to the flight dynamics of the aircraft. As long as the antennas are made from light weight materials such as thin metal sheeting and Styrofoam so there is minimal weight penalty. Thus, a 1.5 GHz higher order mode patch antenna on a 0.4 m square ground plane as described in [4] as an element of a Direction of Arrival array can be placed within the wing. However, such a broad radiation pattern may interact adversely with the solar panels and carbon fibre reinforced plastic main spar and ribs, and as such represents a worst case vehicle-antenna integration scenario. This paper investigates those interactions using the commercially available software FEKO^{TM}and builds on prior work [5]. It was found that the antenna interacted detrimentally with the spar, but had little or no interaction with the solar panels or ribs. This will be discussed in detail during the presentation.

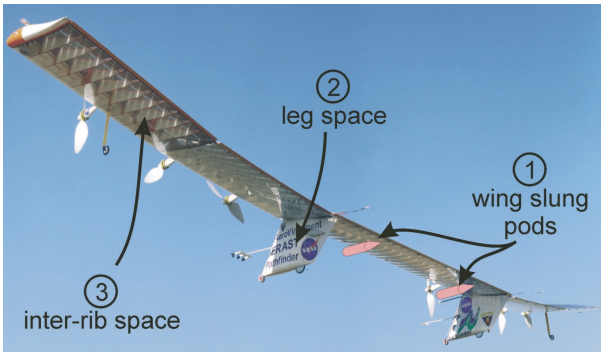

Figure 1: An ERAST UAV in flight with possible antenna installation positions marked.

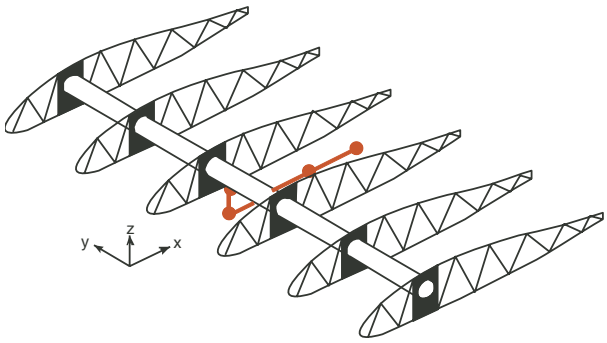

Figure 2: Structural sketch with antenna positions marked as red dots.

REFERENCES

1. Putrich, G., "Boeing aims for five-year flights after Vulture win," *Flight International*, September 16, 2010.
2. Hibbs, B. D., P. B. S. Lissaman, W. R. Morgan, and R. L. Radkey, "Aircraft," United States Patent 5,810,284, September 22, 1998.
3. Cox, E. C. and K. D. Swanson, "Aircraft control method," United States Patent 6,931,247, August 16, 2005.
4. Gray, D., H. Tsuji, M. Suzuki, and R. Miura, "Beacon microstrip patch antenna for DOA demonstration from prototype stratospheric aircraft," *IEEE Antennas and Propagation Symposium Digest*, 340-8, Honolulu, June 2007.
5. Gray, D., H. Tsuji, and R. Miura, "Investigation of dipole antennas embedded in wing of HALE aircraft," *IEICE Technical Report*, Vol. 105, No. 262, 91–96, Paper No. AP2005-81, September 2005.

Circularly Polarized Multiband Microstrip Antenna Using the Combination of Novel Fractals

Homayoon Oraizi and Shahram Hedayati
Electrical Engineering Department, Iran University of Science and Technology, Tehran, Iran

Abstract— In this paper, by computer simulation, it is demonstrated that multiband operation with circular polarization of radiation may be achieved by the combination of square and Giusepe Peano fractal geometries realized on a two layer microstrip antenna. The antenna feed is designed by an electromagnetic coupling system. The proposed antenna configuration also achieves some degree of miniaturization, which makes it suitable for wireless applications. The antenna characteristics, such as return loss, axial ratio and radiation patterns achieved by the proposed structure attest to its effectiveness as a mobile radiator.

An Equivalent Circuit of Microstrip Slot Coupled Rectangular Dielectric Resonator Antenna

M. F. Ain[1], **Y. M. Qasaymeh**[1], **Z. A. Ahmad**[2], **M. A. Zakariya**[1], **and Ubaid Ullah**[1]

[1]School of Electrical and Electronic Engineering
University Sains Malaysia, Pulau Pinang, Malaysia
[2]School of Materials and Mineral Resources Engineering
University Sains Malaysia, Pulau Pinang, Malaysia

Abstract— In this paper, an approximate model of the rectangular dielectric resonator antenna fed by microstrip slot coupled is presented. The equivalent model will be based on the input impedance of the antenna sub-elements. Since the antenna sub-elements impedances are functions of relative dimensions, the resonant frequency can be predicted using this model. The validity of the modeling is supported by comparing the values of the return losses measured of antenna geometry using computer simulation technology (CST) against those obtained by proposed model using Agilent advanced design system (ADS).

Low Cost, Efficient, High Gain and Wideband Microstrip Antenna Fed Yagi Array in Fabry-Perot Cavity

Avinash Ramnath Vaidya[1], **Rajiv Kumar Gupta**[2], **Sanjeev Kumar Mishra**[1], **and Jayanta Mukherjee**[1]

[1]Department of Electrical Engineering, IIT Bombay, Powai, Mumbai 400076, India
[2]Department of Electronics and Communication Engineering
Terna Engineering College, Nerul, New Mumbai 400706, India

Abstract— This article proposes an efficient, high gain and wideband antenna. Gain and bandwidth improvement using Fabry-Perot Cavity is demonstrated. The structure consists of Yagi array placed in $1.0\lambda_0$ Fabry-Perot Cavity (FPC) resonator. The structure is fed by a microstrip antenna that acts as a driven element, ground plane as a reflector and three metal patches above it act as directors. Gain as well as impedance and gain bandwidth is improved by fabricating third director on a FR4 superstrate. Bandwidth improvement is due to two near resonant frequencies and gain improvement is due to FPC formed by FR4 superstrate, which acts as PRS placed at about $1.0\lambda_0$ above the ground plane. Superstrate enhances the gain due to its phase smoothening effect and decreases the resonance frequency of third director fabricated on it. It results in two near resonance frequencies that leads to an improvement in impedance as well as gain bandwidth. The elements in the antenna are excited in space using a single feed microstrip patch. The array is easy to fabricate since the feed-lines network is completely avoided and air substrate is used, which results in good efficiency. Antenna offers 7.6% impedance bandwidth and maximum gain of 14.6 dBi with 3 dB gain bandwidth of 10.8%. Radiation patterns are symmetrical in broadside direction with little variation. SLL is less than -20 dB and F/B is about 20 dB with -26 dB cross polarization. The structure offers more than 90% antenna efficiency. The proposed structure can be packaged inside an application platform.

Parallel Metal Plated U-shape Ultra-wide Band Antenna with WLAN Band-notched Characteristics

Sanjeev Kumar Mishra[1], **Rajiv Kumar Gupta**[2], **Avinash R. Vaidya**[1], **and Jayanta Mukherjee**[1]

[1]Department of Electrical Engineering
Indian Institute of Technology (IIT), Bombay, Mumbai-400076, India
[2]Department of Electronics and Telecommunication Engineering
Terna Engineering College, Mumbai-400706, India

Abstract— In this article, a parallel metal plated ultra-wideband (UWB) antenna with band stop characteristics is proposed. The proposed antenna is a simple U-shaped monopole structure where a rectangular strip is placed on both sides at the top of semi annular ring monopole structure. The band-rejection characteristic is achieved by introducing a $\lambda/4$ open stub in the microstrip feeding line to prevent interference due to WLAN (wireless local area network) systems operating within ultra-wideband. To achieve the desired UWB response with WLAN band notched characteristics, the dimensions of rectangular strip, length and width of stub, and the gap between the ground plane and the radiating structure are optimized. Frequency rejection characteristics depend on the dimension of stub and can be fine controlled using other parameters. The proposed antenna is simulated, fabricated and tested. The antenna structure is designed using 0.5 mm thick copper metal plate for ground plane and radiating structure and 0.6 mm thick foam dielectric is placed between them. The relative permittivity (ε_r) 1.06 and loss tangent ($\tan\delta$) of foam are 1.06 and 0.0 respectively. The antenna structure is fed through a 50 Ω microstrip line using a SMA connector. The results show that the $S_{11} \leq -10$ dB from 3.09–11.1 GHz except 4.4–6.4 GHz frequency band. The proposed antenna provides more than 95% antenna efficiency and gain varies from 3–6 dB over the 3.09–11.1 GHz range except in 4.4–6.4 GHz notched band. The structure exhibits nearly omnidirectional radiation patterns, stable gain, and small group delay variation over the desired bands.

Performance Analysis of Reflectarray Antenna Elements printed on Non-linear Dielectric Materials

M. Hashim Dahri and M. Yusof Ismail
Radio Communications and Antenna Design Laboratory, Department of Communication Engineering
Faculty of Electrical & Electronic Engineering, University Tun Hussein Onn Malaysia
Parit Raja 86400, Johor, Malaysia

Abstract— Reflectarray antennas provide a low cost, low volume and low profile way for different type of applications. However due to limited phase range and narrow bandwidth performance their use is limited, particularly in the field of radar and satellite communications. This paper presents a thorough investigation of the relationship between phasing distribution characteristics and the bandwidth performance of two different reflectarray resonant elements. The gradient characteristics of dipole and rectangular patch elements printed on grounded non-linear dielectric anisotropic substrates have been investigated at X-band frequency range using CST computer model. A detailed analysis of static and dynamic phase distributions along with bandwidth performance with respect to dielectric anisotropy is presented for different anisotropic liquid crystal substrate materials. The preliminary analysis results show that dipole element offers maximum static and dynamic phase ranges of 210° and 290° respectively which offer a maximum Figure of Merit (FoM) value of 3.3°/MHz, compared to rectangular element which offers maximum static and dynamic phase ranges of 182° and 230° respectively which offer a maximum Figure of Merit (FoM) value of 0.225°/MHz. Further more the dipole element attains a maximum frequency tunability or dynamic bandwidth of 1.448 GHz compared to rectangular element which attains frequency tunability of 1.546 GHz. Moreover it has also been shown that an increase in dielectric anisotropy of non-linear materials affect FoM values and bandwidths of both resonant elements. The possibility of using different reflectarray elements with different non-linear dielectric materials presented in this work demonstrates a drastic effect on the phase range and bandwidth performance of reflectarray antenna which is required particularly for radar and earth observatory systems.

Session 4P5
Accelerated Computational Electromagnetics

Necessity of Quantitative Based Thermographic Inspection of Electrical Equipments

A. S. Nazmul Huda, **Soib Bin Taib**, **and Dahaman Bin Ishak**
School of Electrical and Electronic Engineering, Universiti Sains Malaysia
Nibong Tebal 14300, Pulau Pinang, Malaysia

Abstract— The paper discusses the necessity of automatic quantitative based infrared thermographic inspection of electrical equipments and also limitations of qualitative based temperature measurement. Infrared (IR) inspection is a non-touching and non-invasive diagnosis system. Power system consists of both indoor and outdoor electrical equipments such as circuit breaker, bushing, current transformer, different connectors, insulator, potential transformer, lighting arrester, capacitor, transformer and bus-bar etc can cause faults when the internal temperature within equipments reached the abnormality. Various reasons including contact problem, unbalanced current distribution, cracks in insulators, defective relays or terminal blocks etc produce unwanted heat within electrical equipments due to these abnormal behaviour. Thermographic inspection uses an IR camera for capturing and analyzing the thermal profile of faulty electrical equipment. Analysis of temperature distribution profile of target equipment can be performed by qualitatively or quantitatively. Qualitative based measurement is based on only image processing where the abnormal region is detected by the comparative evaluation between reference and hot spot temperature of the target equipment. But IR inspection in an uncovered environment can be strongly influenced by different environmental parameters such as ambient temperature, reflected or background temperature, wind speed, relative humidity of the object and precipitation etc. For this reasons accurate evaluation of equipment health can be interrupted and this can lead the inspection to the erroneous conclusion. So, the aim of this paper is to present the review of these effects on the IR temperature inspection and proposed an advanced quantitative based intelligent diagnosis system combining image processing and artificial neutral network.

Analysis and Prediction of Temperature of Electrical Equipment for Infrared Diagnosis Considering Emissivity and Object to Camera Distance Setting Effect

A. S. Nazmul Huda, **Soib Bin Taib**, **and Dahaman Bin Ishak**
School of Electrical and Electronic Engineering, Universiti Sains Malaysia
Nibong Tebal, Pulau Pinang 14300, Malaysia

Abstract— The paper presents the analysis and predictive model of infrared (IR) temperature with different emissivity and object to camera distance settings effect for obtaining accurate assessment of electrical equipment temperature using IR thermographic inspection. In recent years, IR thermography technology has gained more popularity than other fault diagnosis system of electrical equipments due to its non-contact and non-destructive properties. Abnormal behaviour of electrical equipment is occurred when current is diverted from its intended path due to overloading, load imbalance, corrosion and contact problems etc. As a result internal heat will begin to rise continuously until eventual failure. IR inspection is such a fast, reliable inspection system without interrupting the running operation of power system where fault diagnosis is performed through the analysis of thermal image captured by IR camera. Usually the emissivity values of camera are pre-defined by the thermal camera manufacturer. But emissivity value can be changed by object surface properties, angle of view and object to camera distance. So, incorrect emissivity settings can cause erroneous diagnosis of equipment and also interrupt actual abnormalities classifications to take automatic recommended actions. For conducting experiments, at first both effects were determined from the comparative evaluation of temperature measurement between thermocouple thermometer and infrared camera capturing pictures at different emissivities at a specific object to camera distance where the actual one implies the closest value to one another. For indirect measurement of IR temperature, the relationship between IR and thermocouple temperature for any given emissivity and distance was established. Furthermore prediction model of IR temperature and measurement error were also developed using response surface methodology. Experimental results conducted on 200 thermal images show that error of temperature measurement can be more than 15% for incorrect emissivity and distance settings. The comparison between predicted and experimental values describes that prediction model approach is appropriate.

Electric Field Calculations for the KATRIN Wire Electrodes

F. Glück[1, 2]

[1]Karlsruhe Institute of Technology, IEKP, 76021 Karlsruhe, P. O. Box 3640, Germany
[2]KFKI, RMKI, H-1525 Budapest, P. O. Box 49, Hungary

Abstract— The aim of the KATRIN experiment [1] is to determine the absolute neutrino mass scale in a model independent way, by measuring the electron energy spectrum shape near the endpoint of tritium beta decay. For this purpose, the KATRIN experiment uses two spectrometers: the pre-spectrometer (length: 4 m, diameter: 1.5 m), and the main spectrometer (length: 23 m, diameter: 10 m, surface: 650 m^2). Both of them are stainless steel vacuum tanks and contain a wire electrode system inside. The more negative potential of the wires, relative to the spectrometer tank, repels the small energy secondary electrons emitted on the inner tank surface, thus a substantial background reduction of the measurement is expected. The large main spectrometer tank is fully covered inside by a double-layered wire electrode system [2]: the wires have 0.2 and 0.3 mm diameter, and their total length is about 42 km. The 248 wire modules have been built by the group of Ch. Weinheimer at the University of Münster.

In order to make precise trajectory calculations of the signal and background electrons moving inside the spectrometers, one has to compute the electric potential and field of the wire electrodes. First, one can calculate the equivalent potential inside the wires by simple analytical formulas [3]. To get more precise potential and field maps, we used the boundary element method (BEM). With BEM, one has to discretize only the two-dimensional surface of the electrodes, not the whole three-dimensional space of the electrode system, as it is the case using the finite difference and finite element methods. BEM is especially advantageous for electrodes having small scale structures within large volumes.

In the past few years, we wrote 3 different C codes for the wire electrode simulations. In the first one (elcd31), only rectangles are used as discretization elements; the wire surfaces are discretized also by rectangles. In the second version (elcd32), axially symmetric conical elements and wire segment elements are used. In the third version (elcd33), the discretization is made by rectangles and wire segments. The charge density of each element is assumed to be constant over the element surface. The Coulomb matrix elements C_{ij}, defined as the potential at the centre of element i due to the element j with unit charge density, can be computed by some routines in these codes. The potential U_i of the element i is connected with the charge densities σ_j by the linear equation system: $U_i = \sum_{j=1}^{N} C_{ij}\sigma_j$. The N charge densities can then be computed by Gauss-Jordan elimination.

In order to get a sufficient discretization of the KATRIN wire electrode system, several hundred thousand elements are necessary. On the other hand, using the above scheme, the number of different charge densities N cannot be more than several 10 000, otherwise the Coulomb matrix does not fit into the computer main memory (and the computation time becomes also very large). In our codes, we solved this problem by using the approximate rotational symmetry of the wire electrodes. For example, in the cylindrical part of the KATRIN main spectrometer there are 1200 wires in the azimuthal direction, and all of them have approximately the same charge density. Using this symmetry, the number of geometrical elements can be much larger than the number of different charge densities.

REFERENCES

1. Angrik, J., et al., "KATRIN Design Report 2004," *Wissenschaftliche Berichte FZKA 7090*, KATRIN Collaboration, http://bibliothek.fzk.de/zb/berichte/FZKA7090.pdf.
2. Valerius, K., "The wire electrode system for the KATRIN main spectrometer," *Prog. Part. Nucl. Phys.*, Vol. 64, 291–293, 2010.
3. Read, F. H., et al., "Penetration of electrostatic fields and potentials through meshes, grids, or gauzes," *Rev. Sci. Instrum.*, Vol. 69, 2000–2006, 1998.

On the Construction of Dirac's Delta Functions from Poisson's and Maxwell's Equations

A. R. Baghai-Wadji[1, 2]

[1]School of Electrical and Computer Engineering, RMIT University, Australia
[2]Center for Electromagnetic Simulation CEMS, Beijing Institute of Technology, China

Abstract— A novel general concept for constructing one- and two dimensional Dirac's delta functions originating from Maxwell's equations has been introduced. Given a boundary value problem with an isolated dipole excitation, problem's Dyadic Green's functions are first constructed. The derived Green's are then used to establish integral representations for Dirac's delta functions. A plethora of novel representations for delta functions has been constructed for the first time, considering a large variety of materials. It is shown that every physically realizable (permissible) boundary value problem gives rise to a collection of delta functions. Formal proofs have been provided to establish the fact that the derived integral representations are genuine generalized functions. The new representations can be used for a systematic regularization of singular surface integrals appearing in the Method of Moments (MoM) applications. The customary arbitrarily-introduced epsilon-damping terms in divergent integrals have been made redundant and replaced by a transparent and systematic physics-based fundamental reasoning. The method promises to become an algorithmically sound way of regularizing divergent integrals and thus a sophisticated contribution to the summability and integrability of divergent series and integrals appearing in Electromagnetic (EM) simulations. In addition to numerous practical applications in accelerated EM computing, the underlying method has also been interpreted from a philosophical stand point, which involves Leibniz's Law of ontological identity, correlation and causation. It is also hoped that the proposed method contributes to propagating the powerful theory of generalized functions in the computational electromagnetic community.

On the Construction of a Hierarchy of Lower Dimensional Auxiliary Boundary Value Problems for Solving Real-life Problems in Engineering Applications

A. J. Smith and A. Baghai-Wadji
School of Electrical and Computer Engineering, RMIT University, Australia

Abstract— Solving two- and three-dimensional Boundary Value Problems (BVPs) in engineering practice can be computationally very demanding. Thereby, the proper choice of analysing and synthesizing functions plays a pivotal role. The primary ideas in this contribution are centred about designing tailored basis- and weighting functions for Galerkin-type methods by simultaneously reducing the order of the complexity of the problem (Model Order Reduction, MOR), based on physical considerations. The concept involves the following steps: (i) Given a higher (two or three) dimensional BVP, construct a hierarchy of lower dimensional (one or two) related auxiliary problems. (ii) Examine the hermiticity property of the differential operators involved in the auxiliary problems. (iii) If the auxiliary operators are already hermitian no change is necessary; otherwise (skilfully) modify the operators adequately so that they become hermitian. (iv) Determine the positive eigenvalues and the corresponding orthogonal eigenvectors of the (modified) auxiliary problems. (v) The eigenfunctions of each auxiliary operator, by definition, constitute a set of orthonormal functions. (vi) The tensor-product of the derived eigenfunctions, corresponding to one-dimensional operators, results in a set of higher-dimensional analysis functions. Since the onedimensional eigenfunctions inherit (incorporate) certain vital features of the original BVP only a few of the eigenfunctions suffice to produce higher quality problemtailored basis functions.

Since the differential operators involved in the Schroedinger equation are hermitian, in this paper, the above steps are explained in terms of suitably chosen and technically relevant problems in quantum mechanics. Quantum dot and quantum wire structures under realistic conditions have been analysed and the numerical results are compared against available data in literature. Excellent agreement has been achieved by simultaneously reducing the complexity of the model by order of magnitude.

On the Construction of Distributed Elementary Source Self-regularized Dyadic Green's Functions

H. A. Vagh and A. R. Baghai-Wadji
School of Electrical and Computer Engineering, RMIT University, Australia

Abstract— Complex structures built from rectangular and hexahedron elements are considered. The structures are decomposed into the constituent fundamental rectangular and hexahedron elements. The elements are affine transformed into the rectangular or hexahedron master elements. Even though both two dimensional and three dimensional structures are analysed in this paper, for the sake of simplifying the discussion, we shall limit the exposition in this abstract to the rectangular master element. Name the four surfaces of the master element the "south", "north", "east", and "west", surface. Select a surface, say, the north-surface. Assume N suitably chosen distributed (over the entire north-surface) elementary basis functions from a complete set of orthogonal functions. "Excite" the element by using the mentioned elementary sources. Find the responses of the rectangular master element to the chosen distributed elementary sources, which will be referred to as the dyadic Green's functions. Since the selected sources are distributed the Green's functions are by construction regularized; they are devoid of singularities, prompting the notion of distributed-source self-regularized Green's functions. Evaluate the Green's functions and their derivatives at all four surfaces (collapse of the data onto the boundary surfaces — data reduction). Proceed similarly with the remaining surfaces and construct and collapse the corresponding Green's functions.

In this contribution it will be shown that the created compact set of data fully suffice to analysis the master element, and consequently any element, subject to Dirichlet, Neumann, and interface (mixed) conditions. The treatment of each type of the constraints adds an intriguing nuance to the proposed method.

Since acoustic fields are bound to the domains of the rectangular and hexahedron elements, details of the method will be discussed in terms of the applications to micro-acoustic devices involving isotropic and anisotropic materials.

Session 4P6
Plasmas, Composite Media, Materials Science

Features of Magneto-optical Response in Multilayer Nanostructures Composite-silicon

E. Gan'shina[1], **V. Buravtsova**[1], **A. Novikov**[1], **and Y. Kalinin**[2], **and A. Sitnikov**[2]

[1]Moscow State Unversity, Faculty of Physics, Moscow 119991, Russia
[2]Voronezh State Technical University, Voronezh 394026, Russia

Abstract— One of the requests for successful development of materials for spintronics is a combination of semiconductor and magnetic properties in one material. From this perspective, there is a promising way to create multilayer systems on the basis of ferromagnetic metal and semiconductor layers. Nevertheless, the interpretation of results obtained for such structures is very difficult and the main complexities are related with their extremely high sensitivity to the quality of interfaces and diffusion processes between dissimilar phases, leading to the formation of metal–semiconductor compounds.

One of the effective methods to trace the formation of new phases at the interfaces is a magneto-optical (MO) spectroscopy, and, in particular, magneto-optical Kerr effect (MOKE) spectroscopy, which is very effective for studies of inhomogeneous magnetic materials. MO spectra are sensitive to the type and concentration of magnetic and nonmagnetic impurities, the presence of additional magnetic phases, magnetic and crystal microstructure, etc..

Here we present the results of magnetic and MO studies of $[(Co_{45}Fe_{45}Zr_{10})_Z(Al_2O_3)_{100-Z}(X)/\alpha\text{-}Si(Y)]_n$ multilayers (ML), where the granular composite based on $Co_{45}Fe_{45}Zr_{10}$ with concentrations before the percolation threshold was used as a magnetic layer. Three series with different thicknesses of magnetic (X) and non-magnetic (Y) layers and differnet X to Y ratio were studied. This made it possible to vary the relative contributions of interfaces into the total MO response of the ML. Magneto-optical properties were studied in the energy range of 0.5–4.2 eV in the Transversal Kerr Effect (TKE) geometry.

It was found that the TKE value depends nonlinearly on the Si thicknesses. The anomalous behavior of the magnetic and magneto-optical properties was observed for small thicknesses of Si layer for all series. Addition of Si layer thickness led to increasing of the magnetization and TKE magnitudes. The shape of TKE spectra measured in small and large magnetic fields were essentially different.

Measurements of the TKE field dependences $\delta(H)$ in the near IR range have shown their abnormal behavior that was considerably differ from $\delta(H)$ curves obtained in the visible range of spectra. The maximum of TKE was achieved at small fields ($H < 100$ Oe), and with following increasing of magnetic field H the sign of the effect changed with further saturation at fields ~ 2.5 kOe.

Results obtained allow to conclude that MO response in the studied ML is formed both by magnetic composite layer and new magnetic phase formed on the magnetic granule — semiconductor interface. The magneto-optical response of composite-silicon multilayer films is determined by sum of partial responses of two composites: $(Co_{45}Fe_{45}Zr_{10}) - Al_2O_3 + Si +$ silicides and $(Co_{45}Fe_{45}Zr_{10}) - Si +$ silicides. The contribution of each composite was identified since signs of TKE for these nanocomposite are different in the nearest IR spectrum. The magnetic states of both $(Co_{45}Fe_{45}Zr_{10}) - Al_2O_3 + Si +$ silicides and $(Co_{45}Fe_{45}Zr_{10}) - Si +$ silicides nanocomposite depend on the thicknesses of either semiconductor or composite layers. The thicknesses χ and Y at which the anomalous changes in magnetic and MO properties take place are well correlated with sharp changes in the electric properties of all series, and this fact is related to the intrinsic features of the formation process of $(Co_{45}Fe_{45}Zr_{10})$ composite on the interface in the (Si + silicides) matrix. To summarize, we used MO methods to trace the formation of two composites in magneto-semiconductor structures.

ACKNOWLEDGMENT

This research was supported by the Russian Foundation for Basic Researches.

Luminescence of Yttrium Niobium-tantalate Doubly Activated by Europium and/or Terbium under X-ray and Electron Beam Excitation

Iván D. Arellano[1], **Mihail Nazarov**[2], **and Jimmy A. Cortés**[1]

[1]Department of Physics, Technological University of Pereira, Vereda La Julita, Pereira, Colombia
[2]Institute of Applied Physics, Academy Sciences of Moldova, Republic of Moldova

Abstract— This paper reports the luminescence emission spectra of $Y(Ta,Nb)O_4$ activated by rare earth ions such as Eu^{3+} and Tb^{3+}. The influence of these rare earth ions on the luminescence of yttrium niobium-tantalate phosphors was investigated. The luminescent properties were studied under X-ray and electron beam excitations. Under these excitations, the emission centers of the rare earth activators (Eu^{3+},Tb^{3+}) were found to contribute efficiently to the overall luminescence. We can change the mol concentration of the incorporated activators to get a broad variation of visible photoluminescence. Color cathodoluminescence images showed clearly the dependence of chromaticity on the different activators. With their various luminescence chromaticities, these rare earth activated phosphors are promising materials for solid-state lighting applications as well as for X-ray intensifying screens in medical diagnosis, providing the broad variation of visible photoluminescence from blue to red.

Luminescence of Tantalate and Niobate Phosphors Excited from X-ray to THz Frequency Range

Mihail Nazarov[1, 2] **and Ahmad Fauzi Mohd Noor**[1]

[1]School of Materials and Mineral Resources Engineering
Universiti Sains Malaysia, 14300 Nibong Tebal, Penang, Malaysia
[2]Institute of Applied Physics, Academy Sciences of Moldova, Republic of Moldova

Abstract— Different types of excitation were used to better understand the luminescence and crystallographic data of yttrium tantalate and niobate phosphors.

The $YTaO_4$ and $YNbO_4$ systems are of great interest from fundamental scientific and also spectroscopic applications points of view. In these phosphors, activated by rare earth elements, the host-lattice emission centres and the rare earth emission centres contribute both to the overall luminescence. The growing interest toward luminescence spectroscopy in X-ray, vacuum ultraviolet (VUV) and the visible spectral range as well as in infrared and terahertz (THz) frequency range is due to industrial demands for new applications. The first reason to continue to investigate these phosphors is to study the luminescence mechanism of Eu^{3+} and Tb^{3+} ions in the tantalate and niobate host lattices. The other reason is to develop efficient luminescent materials that could be used not only in X-ray intensifying screens, but also in mercury-free fluorescent lamps or plasma display panels.

The crystalline structures of phosphors were determined by XRD measurements on the basis of Synchrotron X-ray Diffraction patterns (Pohang Accelerator Laboratory, Korea). The results show that the compound $YTaO_4$ has a fergusonite (distorted sheelite) structure with $I2\text{-}C_2^3$ space group symmetry and site symmetry C_2 for the molecular TaO_4. Monoclinic M' structure of $YTaO_4$ is differ from monoclinic M-structure of $YNbO_4$.

Photoluminescence (PL), cathodoluminescence (CL) and X-ray luminescence (XL) illustrate very high intensity of Eu emission in both matrixes, whereas Tb incorporation is effective only in $YTaO_4$. THz transmission spectra were measured for the first time for these phosphors; refraction indexes and absorption coefficients for the host lattices and doped phosphors were calculated. From THz measurements for $YNbO_4$ it is clear seen that the optical properties of host lattice changed with activator incorporation. Moreover, absorption coefficient increases with europium doping and decreases with terbium activation. The nature of this phenomenon is discussed and it maybe one of the reason of high Eu^{3+} emission and poor Tb^{3+} luminescence properties in $YNbO_4$.

However, to our knowledge, no result has been reported yet on application the frequency range from X-ray to THz for investigation $YTaO_4$ and $YNbO_4$ based phosphors. The advantage of every type of excitation is shown. We also discuss the interpretation of results in all types of spectroscopes with luminescence and crystallographic data.

Luminescence and Energy Transfer Mechanisms in $CaWO_4$

D. Spassky[1], **Mihail Nazarov**[2,3], **A. Zhbanov**[4], **and Ahmad Fauzi Mohd Noor**[2]

[1]Skobeltsyn Institute of Nuclear Physics, Moscow State University, Moscow 119991, Russia
[2]School of Materials and Mineral Resources Engineering, Universiti Sains Malaysia
Nibong Tebal, Penang 14300, Malaysia
[3]Institute of Applied Physics, Academy Sciences of Moldova, Republic of Moldova
[4]Department of Mechatronics, Gwangju Institute of Science and Technology
1 Oryong-dong, Buk-gu, Gwangju 500-712, Republic of Korea

Abstract— Development of the cryogenic phonon-scintillating detectors stimulates searching of the novel scintillating materials suitable for this application [1]. Calcium tungstate is a well-known wide-band-gap semiconductor commonly used as X-ray phosphor now attracts attention as a perspective cryogenic scintillator for the registration of weakly interacting massive particles [2]. Here the processes of the excitation energy transfer to the emission centers have been investigated for different samples of calcium tungstate crystals at low temperatures taking into account features of electronic structure of valence and conduction bands.

Two samples of $CaWO_4$ grown using Czochralski (cz) and hydrothermal (ht) methods were investigated. Spectra of luminescence, excitation and reflectivity were measured at the Superlumi station (DESY, Hamburg) and at the laboratory set-up as well. The electronic structure calculations of host lattice $CaWO_4$ were performed in the framework of density functional theory. The exchange correlation energy of electrons is described in the generalized gradient approximation within the scheme of Perdew GGA96 [1] [3] to calculate the total energy, band structure and DOS.

Intrinsic emission band related to self-trapped excitons on WO_4 complexes has been observed for the both of the samples while additional emission band related to the defects of crystal structure has been observed only for (ht) sample implying greater concentration of the defects in (ht) sample. It was shown for the (ht) sample that the features of DOS in conduction band are reproduced in the excitation spectrum of intrinsic luminescence while for (cz) sample the correlation is absent. The competition between excitation energy relaxation on intrinsic and extrinsic emission centers in (ht) sample is supposed to be the reason for the observed difference.

REFERENCES

1. Bavykina, I., G. Angloher, D. Hauff, M. Kiefer, F. Petricca, and F. Probst, *Opt. Mat.*, Vol. 31, 1382, 2009.
2. Mikhailik, V. B., H. Kraus, S. Henry, and A. J. B. Tolhurst, *Phys. Rev. B*, Vol. 75, 184308, 2007.
3. Perdew, J. P., K. Burke, and M. Ernzerhof, *Phys. Rev. Lett.*, Vol. 77, 3865, 1996.

Nonlinear Dynamics, Long-time Tails, and 1/F-noise in Simple Systems with Complex Hysteresis

Günter Radons, Sven Schubert, and Andreas Zienert
Institute of Physics, Chemnitz University of Technology, Chemnitz D-09107, Germany

Abstract— Hysteresis is a well-known phenomenon in many branches of science [1]. Complex hysteresis refers to situations, where for a given external parameter a huge number of internal system states are possible. Which one of these states is attained, depends on previous parameter variations and therefore on the history of the system. Correspondingly, in addition to a major hysteresis loop, sub-loops, sub-sub-loops, etc. are observed as the input is varied. Classical examples are magnetic materials, where magnetization and external magnetic field are related hysteretically. Similar behavior is found among others in piezo-electric materials, shape memory alloys, superconducting systems and other inhomogeneous or disordered systems. While the origin of the hysteretic behavior in these systems has been investigated quite extensively, not much is known about scenarios that may arise if hysteretic subsystems are coupled dynamically to its environment.

The Preisach operator provides one of the most prominent phenomenological models for describing the complex behavior of such hysteretic systems [1]. Here we consider two distinct situations for the dynamical coupling of hysteretic subsystems to its environment. In the first one the hysteretic nonlinearity simply acts as a transducer, which transforms input time series into output time-series. The case of i.i.d. random variables as input time series was considered by us previously in a series of papers and analytical results were obtained showing that under quite general circumstances the output time-series exhibits long-time tails and 1/f-noise [2–4]. In this contribution new and partially unexpected results for input with exponentially and algebraically decaying correlations are presented and compared with the corresponding white noise input cases. In the second scenario we treat systems, where the output of the hysteretic subsystem is fed back into the system after some interaction with the environment. In the continuous time case this results in operator-differential equations, which are solved numerically by a specialized integration algorithm. A concrete application, where a damped iron pendulum in a magnetic field is driven by a sinusoidally varying force is considered in detail. The possible dynamical scenarios are elucidated. We present evidence that such systems in general possess simultaneously infinitely many chaotic attractors. Which of these attractors is eventually reached depends in a complicated fractal manner on the initial conditions.

REFERENCES

1. Bertotti, G. and I. Mayergoyz, *The Science of Hysteresis*, Vol. 1–3, 2100, Academic Press, London, 2006.
2. Radons, G., *Phys. Rev. Lett.*, Vol. 100, 240602, 2008.
3. Radons, G., *Phys. Rev. E*, Vol. 77, 061133, 2008
4. Radons, G., *Phys. Rev. E*, Vol. 77, 061134, 2008.

Low Field Microwave Absorption, Giant Magnetoimpedance and Anisotropy Field in Soft Magnetic Materials

R. Valenzuela
Instituto de Investigaciones en Materiales
Universidad Nacional Autónoma de México, México 04510, México

Abstract— Microwave absorption at low magnetic fields (LFMA) has recently been observed [1] in a variety of magnetically ordered materials, such as multilayers, glass-coated microwires, amorphous ribbons, amorphous thin films, ferrites. It has been shown [2] that LFMA is similar to Giant Magnetoimpedance (GMI), and clearly different to ferromagnetic resonance (FMR). LFMA and GMI are both non-resonant absorption phenomena. LFMA occurs at magnetic fields significantly lower than the resonance field, and similarly to GMI, it has exhibited a strong dependence on the anisotropy field of the sample. In fact, a numerical derivation of GMI data leads [3] to the typical antisymmetrical plot typically observed in LFMA. In this work, we present a detailed study of LFMA in Ni-Zn ferrites. In particular, we compare the magnetic field separating the resulting antisymmetrical (maxima-minima) plot in the microwave absorption behavior ($\mathrm{d}P/\mathrm{d}H$ as a function of magnetic field H) of a ferrite of composition $Ni_{0.64}Zn_{0.36}Fe_2O_4$ at different temperatures in the 150–450 K range, with a calculation of the anisotropy field from direct measurements [4] of the magnetocrystalline anisotropy constant K_1 in a Ni-Zn ferrite single crystal of a very close composition ($Ni_{0.65}Zn_{0.35}Fe_2O_4$). A very good agreement is obtained.

REFERENCES

1. Medina, A. N., et al., *J. Appl. Phys.*, Vol. 79, 5462, 1999.
2. Montiel, H., et al., *Appl. Phys. Lett.*, Vol. 86, 072503, 2005.
3. Alvarez, G., et al., *Journal of Non-Crystalline Solids*, Vol. 353, 902, 2007.
4. Van Groenou, A. B., J. A. Schulkes, and D. A. Annis, *J. Appl. Phys.*, Vol. 38, 1133, 1967.

Numerical Experiments for Radial Dynamics and Opacity Effect in Argon Plasma Focus

Z. Ali[1, 2], **J. Ali**[1], **S. H. Saw**[3, 5], **and S. Lee**[4, 5]

[1]Institute of Advanced Photonics Science, Nanotechnology Research Alliance
Universiti Teknologi Malaysia (UTM), Johor Bahru 81310, Malaysia
[2]Karachi Institute of Power Engineering, P. O. Box 3183, Karachi, Pakistan
[3]INTI University College, Nilai 71800, Malaysia
[4]Nanyang Technological University, National Institute of Education, Singapore
[5]Institute for Plasma Focus Studies, 32 Oakpark Drive, Chadstone VIC3148, Australia

Abstract— A z-pinch in its simplest form is a column of plasma in which current (J) is driven in the axial direction (z) by an electric power source producing an azimuthal (θ) direction magnetic field (B) that tends to confine plasma by ($J \times B$) force. One application of this configuration is Plasma Focus. Dense plasma focus (DPF) is essentially a pulsed electric gas discharge between coaxially arranged electrodes. DPF devices belong to the family of dynamic Z-pinches which are self-constricted plasma configurations. The Lee model code was developed to simulate the plasma dynamics in a DPF. The model incorporates the energy and mass balances equivalent, at least in the gross sense, with radiation-coupled dynamics to all the processes which are not even specifically modeled. It is a well known fact that radiation loss is an inevitable phenomenon in the final stage of pinch compression. The most obvious one is that of a focus or a Z-pinch. Plasma self-absorption is an important factor during the pinch compression. In this paper the effect of self absorption of line radiation was investigated in argon plasma by a series of numerical experiment considering both aspects, i.e., by including and excluding the self absorption term in Lee code. The results were compared for various parameters, i.e., Radial trajectories, pinch duration, pinch current, line radiation yield while changing pressure. The effect of radiation self absorption was observed in last few fractions of seconds (200–300 ns). Considering self absorption, the compression shows a value of radius of about 0.2 mm while a collapse (radiative collapse) was observed otherwise. The results illustrated that the radiation cooling becomes significant when the plasma is dense and turn to be opaque for radiation. Hence in real case we do not see a radiative collapse in argon PF as self absorption plays in real experiments. The results of pinch duration and pinch current also indicated that self absorption is essentially enhancing the pinch.

Three-dimensional Analysis of a Surface Plasmon Resonance Waveguide Sensor for Detecting Material Absorption

J. Shibayama, **A. Yokomizo**, **J. Yamauchi**, **and H. Nakano**
Faculty of Science and Engineering, Hosei University, Tokyo 184-8584, Japan

Abstract— A surface plasmon resonance (SPR) sensor has been intensively studied, because of its high sensitivity for detecting a change in the refractive index of an analyte [1]. In addition to conventional Kretschmann-type SPR sensors composed of a prism coated with a thin metal, waveguide-type SPR sensors have also received growing attention due to the advantages such as small size, ruggedness and multi-channel sensing [2]. Unfortunately, the theoretical investigations of the waveguide-type sensors were based on the two-dimensional (2-D) analyses. Therefore, we have studied three-dimensional (3-D) models of the sensor using the beam-propagation method (BPM) [3, 4]. Note that the studies of the waveguide-type sensors have focused on detecting a change in the real part of the refractive index.

Recently, the SPR sensors have also been utilized to detect a change in the imaginary part of the refractive index [5, 6]. That is, for an analyte with absorption, the surface plasmon resonance becomes weak, leading to a detectable change of the reflection or the output power. Notice that all the absorption-based sensors studied so far have been based on the conventional Kretschmann-type structures, except for our 2-D investigation of the Kretschmann-type waveguide sensor [6]. We are therefore motivated to investigate the 3-D model of an absorption-based waveguide-type sensor.

In this presentation, we numerically study the waveguide-type sensor for detecting material absorption, i.e., a change in the imaginary part of the refractive index. We first present the basic equation of the 3-D BPM and the dielectric function of the metal expressed by the Drude-critical points (D-CP) model. We next analyze the sensor with a single mode waveguide, in which only the imaginary part of the refractive index of the analyte is varied with the real part being fixed. We finally improve the sensitivity of the sensor with a modification to the light guiding structure.

REFERENCES

1. Homola, J., "Present and future of surface plasmon resonance boisensors," *Analytical and Bioanalytical Chemistry*, Vol. 377, No. 3, 528–539, 2003.
2. Harris, R. D. and J. S. Wilkinson, "Waveguide surface plasmon resonance sensors," *Sens. Actuators B*, Vol. 29, 261–267, 1995.
3. Shibayama, J., S. Takagi, T. Yamazaki, J. Yamauchi, and H. Nakano, "Numerical analysis of waveguide-based surface plasmon resonance sensor with adsobed layer using two- and three-dimensional beam-propagation methods," *IEICE Trans. Electron.* Vol. E90-C, No. 1, 95–101,2007.
4. Shibayama, J., "Three-dimensional numerical investigation of an improved surface plasmon resonance waveguide sensor," *IEEE Photon. Technol. Lett.*, Vol. 22, No. 9, 643–645, 2010.
5. Kano, H. and S. Kawata, "Surface-plasmon sensor for absorption-sensitivity enhancement," *Appl. Opt.*, Vol. 33, No. 22, 5166–5170, 1994.
6. Shibayama, J., "A Kretschmann-type absorption-based surface plasmon resonance waveguide sensor," *Microwave Opt. Technol. Lett.*, Vol. 50, No. 10, 2497–2500, 2008.

Microwave Characterization of Expanded Graphite/Phenolic Resin Composite for Strategic Applications

Jyoti Prasad Gogoi and Nidhi Saxena Bhattacharyya
Microwave Engineering Laboratory, Department of Physics
Tezpur University, Tezpur-784028, India

Abstract— Light weight expanded graphite (EG) flakes are synthesized from natural graphite flakes of size $\sim 2\,\mu$m employing chemical oxidation and thermal treatment method. Scanning electron microscope investigation shows that EG flakes consist of numerous graphite sheets of nanometers thickness and micrometer in diameter. EG flakes are mechanically mixed with novolac phenolic resin (NPR) in different weight ratios (30 wt.%, 40 wt.% & 50 wt.%) and compressed with thermal treatment to develop expanded graphite/novolac phenolic resin (EG/NPR) composites. Nicolson-Ross method is used to determined the complex permittivity ($\varepsilon_r = \varepsilon_r' - j\varepsilon_r''$) of the developed composites using Agilent E8362C vector network analyzer. A high value of dielectric loss tangent ($\varepsilon_r''/\varepsilon_r' > 1$ has been observed for the three compositions in the entire X band. Shielding effectiveness of developed composites of thickness 3.7 mm measured in the frequency range of 8 to 12 GHz shows a maximum value of -48 dB for 50 wt.% EG/NPR composites. The material production is simple and cost effective, and the absorbing material is light weight and thus, is beneficial for installation in some strategic components.

Session 4P7
Electromagnetic, Electronics and Signal Processing Research in Biomedical Engineering

Investigation of AC Effects in Planar Spiral Coils for Powering Implantable Electronics

Gordana K. Felic[1, 2], **David C. Ng**[1, 2], **and Efstration Skafidas**[1, 2]

[1]National ICT Australia, VRL, Melbourne 3010, Australia
[2]The University of Melbourne, Melbourne 3010, Australia

Abstract— Flat spiral coils can be used for transferring electrical power into implantable electronics via magnetic induction. We studied different flat spiral coil topologies and aspect ratios by varying track widths, spacing and thicknesses. Using numerical simulation, electrical and electromagnetic characteristics such as impedance, current density, and proximity effect at various frequencies were investigated. In particular, we look into the interrelation between spiral topology and proximity effects. A clear understanding of these effects will allow us to predict the behaviour of any spiral coil topologies and allow a simplified circuit model to be built. In this study, we focused on 3-turn spiral coils of a fixed dimension as a basis for elucidating how changes in geometry affect key figures-of-merit of the spiral coils when used as inductive coils. We observed that coil geometry contributes considerably to AC effects at higher frequencies. Based on the result from this work, we have gained a clearer understanding of coil designs for enabling high efficiency power transfer and also transmit and receive circuit matching requirement.

REFERENCES

1. Kuhn, W. B. and N. M. Ibrahim, "Analysis of current crowding effects in multiturn spiral inductors," *IEEE Trans. Microwave Theory and Techniques*, Vol. 49, No. 1, 31–38, 2001.
2. Orlando, B., A. S. Royet, and B. Viala, "Fast analysis of proximity effects in integrated inductors with high-permeability magnetic materials," *IEEE Trans. Magnetic*, Vol. 42, No. 10, 3371–3373, 2006.

Kalman Filter for ABR Signal Analysis

M. Hafizi Omar, **Sh-Hussain Salleh**, **Ting Chee Ming**,
R. Ariffi Suraya, **Kamarulafizam**, **and Tan Tian Swee**
Center for Biomedical Engineering (CBE), Transportation Research Alliance (TRA)
Universiti Teknologi Malaysia, Skudai, Johor 81310, Malaysia

Abstract— Auditory brainstem response (ABR) is an electrophysiological response in the electroencephalogram (EEG) reading which generated by the brainstem in response to auditory stimulus. ABR is very useful in determination of hearing threshold especially for uncooperative subject's and newborn infants. However, due to several factors, particularly on the technical aspects, including noise interference and other brain activities, the screening consumes a large portion of time to obtain the meaningful result. Conventional method to retrieve the underlying wave V using averaging technique requires more trials. Because of this, screening cannot be performed in a large scale. Based on this issue, this paper purposes a method for ABR denoising and detection of wave V by using Kalman Filter. This technique estimates the potential being analyzed sequentially by referring the previous sweeps information. By implementing this technique, the unwanted signal can be filtered out from every sweeps of ABR recorded. The system has been tested on 20 normal adult subjects with no history of hearing impairment. The ABR signal is collected using high accuracy biosignal data acquisition and processing system (high-end 24 bit biosignal amplifier, gUSBamp, gTec, Austria). From the analyzed result, wave V can be detected by less number of sweeps and still preserving the morphology of ABR signal. This approach shows better capability of estimating ABR signal by detecting wave V in minimum number of sweeps compared to conventional averaging technique. Therefore, our results show that the time of recording can be reduced for each screening.

Wave V Detection Using Continuous Wavelet Transform of Auditory Brainstem Response Signal

M. M. Rushaidin, **Sh.-Hussain Salleh**, **O. Hafizi**, **H. Mahyar**, **C. M. Ting**, **and A. K. Ariff**
Centre for Biomedical Engineering, Transport Research Alliance
Universiti Teknologi Malaysia, UTM Skudai, Johor 81310, Malaysia

Abstract— Auditory brainstem response (ABR) audiometry is well known tools for detection of hearing loss. It is a neurologic test of ABR in response to the stimuli such as click sound, tone burst or chirp. The non-invasive electrodes are used to obtain the ABR signals. In ABR, wave V of the ABR signals is used as indicator of hearing loss because it is the most dominant and robust peak wave. In current device, there are about 2000 sweeps of the ABR signals have to be averaged in order to get the meaningful signal which required about 4 minutes for one single stimulation level, which is consumed a lot of time. Therefore it is compulsory to have a fast detection method to reduce the recording time. Several types of signal processing techniques have been introduced by researchers to obtain the best technique to detect the ABR signals such as Fast Fourier Transform (FFT) and discrete wavelet transform (DWT). In this study, the continuous wavelet transform (CWT) of ABR signal had been introduced as a marker to identify the ABR waves. Study showed that the CWT of auditory brainstem response can be used a marker to identify the ABR waves with the sensitivity, 0.63 and the specificity, 0.83.

Adaptive Discrimination Filters for TMS-electroencephalographic Feature Extraction

Arief R. Harris[1], **Daniel J. Strauss**[2], **and Sh-Hussain Salleh**[1]

[1]Center for Biomedical Engieneering, Transport Research Alliance
Universiti Teknologi Malaysia, Johor, Malaysia
[2]Computational Diagnostics and Biocybernetics Unit at Saarland University Hospital and Saarland University of Applied Sciences, Homburg/Saarbruecken, Germany

Abstract— We introduce a new scheme to obtain an optimal discriminant filter (ODF) for Transcranial magnetic stimulation (TMS) evoked potentials. The proposed discriminant feature extraction schemes are parts of decision support systems to provide physicians with more practical, fast, accurate and objective diagnoses or therapies. The ODF is optimally designed to illuminate the discriminant features so that the filtered EEG signals from any classes can be further classified much faster and easier. Even the computational time of the feature extraction is relatively fast since it only involves a single filtration for each feature. This supervised feature extraction technique has the advantage of the well-known fisher criterion as a distance measure. This scheme is used to analyze the time course of the impact of single-pulse TMS to the auditory ERPs. The proposed schemes were able to extract even the slightest impacts of TMS, making it a promising tool for the extraction of weak ERPs components, particularly in hybrid TMS-EEG/ERP setups.

Malay Speech Digit Recognition for Speech Therapy Application

Tan Tian Swee, **Sh-Hussain Salleh**, **Ahmad Kamarul Arif**, **Cheng Wei Lip**, **and Lau Chee Yong**
Center for Biomedical Engineering (CBE), Transportation Research Alliance (TRA)
Universiti Teknologi Malaysia, Skudai 81310, Johor, Malaysia

Abstract— Disorder of speech is defined by the American Speech-Language-Hearing Association (ASHA) as one type of communication disorder. The most difficult task in speech language pathologist is to diagnose the speech disorder. This diagnostician looks on aspect of an individual's communication ability rather than their communication. It required involvement of speech-language pathologists (SLPs) who provide an assortment of service that relate to communication disorder. Therefore, research on applications of speech recognition to speech and language development has been widely conducted since 1990. The improvement in technology has replaced the traditional speech therapy with more attractive tools for diagnostic and training of speech disorder. This paper proposes a method for detecting speech stuttering using speech recognition technique. Stuttering shows break in the usual time sequence of utterance where the usual flow is interrupted. There also conspicuous oscillations and fixations, repetitions and prolongations of sounds and syllables. Stuttering always varies with emotional stress where stuttered increase as in situations invest with fear and shame. Stuttered people may speak perfectly when they are alone and start to stutter when talking to listener. This paper focuses on all Malay digits from kosong (zero) through sembilan (nine). The system is tested using speech data recorded in word-based unit and syllable-based unit. Two experiments on monophones-based and syllable-based have been conducted to find the optimum setting for phoneme recognition. The overall results show that monophones-based unit system is able to do recognition with 90.18% accuracy for monophones-based network and 100% accuracy for word-based network, while syllable-based unit system is able to do recognition with 63.89% accuracy for syllable-based network. Through this paper it can be concluded that this system able to be used as diagnostic software for speech disorder.

Comparison of Different Time-domain Feature Extraction Methods on Facial Gestures' EMGs

M. Hamedi, **Sh-H. Salleh**, **A. M. Noor**, **T. T. Swee**, **and I. K. Afizam**
Center for Biomedical Engineering, Transportation Research Alliance
Universiti Teknologi Malaysia, Skudai, Malaysia

Abstract— Electromyography is a bio-signal which is applied in various fields of study such as motor control, neuromuscular physiology, movement disorders, postural control, human machine/robot interaction and so on. Processing of these bio-signals is the essential fact during each application and there still can be seen many challenges among researchers in this area. This paper is focused on the comparison between the classification performances by using different well known feature extraction methods on facial EMGs. Totally ten facial gestures namely smiling with both side of lips, smiling with left side of lips, smiling with right side of lips, opening the mouth like saying 'a' in apple word, clenching the molar teeth, gesturing 'notch' by pulling up the eyebrows, frowning, closing the both eyes, closing the right eye and closing the left eye are recorded from 6 participants through 3 bi-polar recording channels. In the first step, the signals are filtered to get prepared for better processing.Then, time-domain feature extraction methods INT, MAV, MAVS, RMS, VAR, and WL are applied to signals. Finally, the features are classified by Fuzzy C-Means in order to achieve the recognition accuracy and evaluate the performance of each feature extraction method. This work is carried out by revealing that, RMS gives the most probability amplitude approximation in a steady power and non-tiring contraction when the signal is modelled as Gaussian random process. In contrary, WL proved its weakness in estimating the value of facial EMGs.

Determination of Optimal Auscultation Point on the Chest Walls for Personal Identification Using Heart Sounds

Sh-Hussain Salleh, **I. Nur Fariza**, **I. Kamarulafizam**, **A. K. Ariff**, **and Ting Chee Ming**
Center for Biomedical Engineering (CBE), Transportation Research Alliance (TRA)
Universiti Teknologi Malaysia, Skudai, Johor 81310, Malaysia

Abstract— This paper propose an optimal auscultation point of heart sounds for personal identification using heart sounds. The four typical auscultation points were aortic, pulmonary, Lower Left Sternal Border (LLSB) and mitral. These four views of heart sounds have been recorded for each participant who seated in a relaxed position. Several experiments were conducted using 2,314 cycles from 30 participants to find the highest recognition rate among the four locations of heart sounds. The system is developed by a combination of data analysis methods Mel Frequency Cepstrum Coefficients (MFCC) and Gaussian Mixture Model (GMM). Preliminary results from the experiments showed the highest recognition is at location tricuspid with 94.35% when the GMM has 1 state and 32 mixtures. So, it can be concluded that the values of heart sounds at LLSB point is better than other point.It is also might be due to right ventricle walls are thinner than the left ventricle walls which has to pump for longer distances and greater cross-pressures.

Standalone ECG Monitoring System Using Digital Signal Processing Hardware

Goh Chun Seng, **Sh-Hussain Salleh**, **Arief R. Harris**, **J. M. Najeb**, **and I. Kamarulafizam**
Center for Biomedical Engineering, Transport Research Alliance
Universiti Teknologi Malaysia, Johor, Malaysia

Abstract— The electrocardiogram (ECG) is a demanded and popular tool for non-invasive method to evaluate patients' heart condition in clinical environment. Automated QT interval against the manual method studied by European medicines agency (EMEA) in 2008 shows more focus on healthy subject. Traditionally, QT interval measurements of patients are interpreted manually from ECG strip paper printed by ECG recording machines. The QT interval shown to be important indicator prior to Myocardial Infarction (MI) and it is important to observe and monitor any changes in the period of the QT interval. ECG interval parameter measurements are found in small sized ECG monitoring equipment which is used by physicians and cardiologists to monitor heart condition but it is non-reconfigurable and provides no analytical results for research purposes and it is costly. Therefore, a low cost standalone Digital Signal Processing (DSP) prototype for ECG monitoring is developed in order to assist physician and cardiologist in carrying out their measurement on QT interval for ECG monitoring. The design of the DSP hardware based stand alone system are divided into three hardware units, first the Digital signal processor with memory unit, second is the signal monitoring displays unit and third is analog front end unit. Firmware development in this system design is to attach each hardware unit to perform specific functions in carrying out operation on the stand alone system. The advantages of this stand alone system design are able to run in stand-alone operation and as well as eligibility of on board pre-program algorithm for ECG analysis which existing ECG monitoring equipment are lacking.

Heart Sound Analysis Using Hidden Markov Models

Hadrina Sh-Hussain, **Sh-Hussain Salleh**, **Tan Tian Swee**,
Ting Chee Ming, **Ahmad Kamarul Ariff**, **and I. Kamarulafizam**
Center for Biomedical Engineering (CBE), Transportation Research Alliance (TRA)
Universiti Teknologi Malaysia, Skudai, Johor 81310, Malaysia

Abstract— Auscultation of the heart is accompanied by both electrical activity and sound. This auscultation of the heart provides clues to the diagnosis of many cardiac abnormalities. Unfortunately, detecting relevant symptoms and forming a diagnosis based on heart sounds through stethoscope is difficult. The reason why General Practioners find it difficult is that the duration of heart sounds are often short and being separated from one another by less than 30 ms. In addition, the monetary cost for false positives constitute waste of time and emotional anxiety for both patients and GPs. Through such reason, this research addressed the need for accurate dependable equipment and heart sound analysis. This work is aimed to design a Heart Murmur Analysis System For Detection Abnormalities in Heart Sound (HMA System) which can reduce the learning period, low-cost and easy to use. The system use complex mathematical digital signal processing algorithm to address the above problem. The mel-frequency cepstrum features were used as the features for the heart sound. Finally Markov model was used to train and recognize the murmurs that later can be used by general practioners (GPs) to help in their decision on detecting heart murmurs. The proposed system was tested with 26 patients from medical school uitm selayang. The number of recruited patients in this study consisted 20 normal and 6 abnormal patients with various murmurs firmed by cardiologist. From this, classification rate of 99.71% accuracy was achieved using the HMM has 1 states, and 1 mixtures.

Author Index